PROCEEDINGS OF
THE PHYSICAL SOCIETY

VOL 73, PART 1 1 January 1959 No 469

Domain Configurations on Ferrites

BY D. J. CRAIK† AND P. M. GRIFFITHS
Department of Physics, University of Nottingham

Communicated by L. F. Bates; MS. received 14*th July* 1958, *in final form* 28*th August* 1958

Abstract. The domain structures of Mn, Mn Zn, Ni, Cu and Ba ferrite crystals have been examined by the conventional and modified Bitter figure techniques.

In the cases of Mn, Ni and Ba ferrites the patterns observed are in accordance with the nature of their magnetic constants.

The Mn Zn ferrite crystal examined gave anomalous patterns considered to be due to a strain induced uniaxial anisotropy.

§ 1. INTRODUCTION

THE ferrimagnetic ferrites generally belong to the spinel group with a formula $MO.Fe_2O_3$. They have low magnetic saturation, of the order 3000–4000 gauss and, generally, have a low negative anisotropy, implying that their easy directions of magnetization lie in the [111] directions. Barium ferrite is an exception, its crystal structure being hexagonal, and it should therefore have two easy directions of magnetization parallel to the hexagonal axis, as in cobalt. Its anisotropy is of the order of 10^6 erg cm^{-3}, which is considerably higher than that for most cubic-spinel ferrites.

Extensive study has been made of their magnetic constants and behaviour, especially in the field of ferromagnetic resonance. Some theoretical treatments, e.g. Smit and Wijn (1954), have been based on hypothetical domain wall structures, but until recently experimental observations of their domain structures were not available. Galt (1954) correlated the domain wall movement in a picture frame of nickel ferrite with its magnetization. Sixtus, Kronenberg and Tenzer (1956) showed domain structures on barium ferrite which were very similar to the structures observed by Roberts and Bean (1954) using polarized light microscopy on MnBi. Paulus (1957) obtained a cleaved (100) surface on a Ni–Co ferrite and obtained patterns characteristic of a positive anisotropy, i.e. with the four easy directions of magnetization in the cleaved (100) surface. Bates, Craik and Griffiths (1958) found patterns on a cleaved (100) surface of a Mn ferrite specimen. Bates, Clow, Craik and Griffiths (1958) examined a large-grain polycrystalline specimen of composition $Mn_{0.7}Zn_{0.3}Fe_2O_4$, and found domain structures due to surface strain only.

In this paper domain configurations on single crystals of Mn, Mn Zn, Ni, Cu and Ba ferrites are described, and an attempt is made to analyse them. The Mn and Ni ferrites appear to have the expected domain structures, i.e. corresponding to negative anisotropy: the Ba ferrite corresponds to a normal uniaxial magnetic material, in this case electron microscopy has been able to elaborate on the patterns previously obtained. The Mn Zn specimen has an anomalous structure.

---

† Now at Boots Pure Drug Co Ltd., Nottingham.

§ 2. EXPERIMENTAL TECHNIQUE

Craik (1956) published a method by which domain structures could be studied by electron microscopy, using a Bitter figure technique. It was subsequently found (Craik and Griffiths 1957, 1958) that an extension of this method enabled figures to be studied to greater advantage by optical microscopy. A film of a special magnetite colloid is dried on the specimen surface. The colloid is prepared so that it dries without aggregation of the individual particles; these are set in a solid matrix of a water soluble plastic (sodium carboxy methyl cellulose) and this plastic film may either be removed for examination by the electron microscope or examined, while still on the surface, by a metallurgical microscope.

It was found, by many comparisons between this method and the conventional Bitter figure technique, that patterns could be observed in greater detail; in some cases patterns were actually observed in the dried film which were not seen with a wet colloid, e.g. on the cleaved surface of a Mn ferrite specimen (Bates, Craik and Griffiths 1958).

§ 3. SPECIMEN PREPARATION

The specimen surfaces observed were of three types: those obtained by cleavage (Mn, Mn Zn and Ba), those obtained by grinding, polishing and etching (Mn, Mn Zn, Ni and Ba), and lastly, those having natural growth facets requiring no further preparation (Ni and Cu).

The Mn Zn ferrite crystal specimen cleaved spontaneously on cooling after preparation. Further faces were obtained both on this, and on the Mn ferrite, by cleaving with a small chisel. These cleavage faces are known to be (100) planes. The surfaces obtained were never perfectly flat, but showed slight undulations and ridges, as well as fine cracks present in the original crystal.

To obtain faces containing easy directions, the ferrites were mounted in plastic blocks and their faces ground at calculated angles. The orientating cut was performed on a standard surface grinder, after which the surfaces were polished on a series of emery cloths and finished with 6 μ and $\frac{1}{4}$ μ diamond polishing compound. To obtain a strain free surface the specimens were then etched. This technique was used successfully on a Ni ferrite single crystal of overall dimension of less than a millimetre.

§ 4. RESULTS

4.1. *Manganese Ferrite*

Nickel has a face-centred cubic structure and negative anisotropy; its domain structure has been fully investigated and found to consist of 180°, 109° and 71° domain walls, with associated fir trees, closure formations and Néel spikes (Stephan 1955, Yamamoto and Iwata 1953). Manganese ferrite has been found by microwave resonance experiments to have negative anisotropy and was expected, considering the magnitude of the anisotropy, to exhibit a similar domain structure to nickel.

As already reported (Bates, Craik and Griffiths 1958) a manganese ferrite single crystal, prepared at the Mullard Research Laboratories by the flame fusion technique, was cleaved to a (100) surface on which two types of pattern were observed by the Bitter figure technique; a very fine surface structure of parallel bands of spacing 0·3 μ and a coarser structure formed by regular intensification of these fine bands. The fine structure was considered to be a strained surface effect due to cleavage, while the coarse structure was one of free poles, expected on a surface containing no easy direction of magnetization.

Since it was not possible to obtain a (110) plane by cleavage, it had to be obtained by grinding. After the final ¼ μ diamond polish a clean scratch-free surface was obtained. Figure 1† shows a typical strain pattern on this surface consisting of 'wriggly' domain walls which have a wall thickness, measured by electron microscopy, of 0·5 μ. This and other considerations suggested that the specimen surface was still strained, and it was therefore etched in boiling concentrated HCl for 2 minutes. The etch gave a very bright surface, broken by a few large etch pits which were generally long, narrow and ellipsoidal, with their major axes in [110] directions. A number of deep cracks, which lay in both the [100] and [110] directions were enlarged by the etching, and these served to give the crystallographic directions with respect to the patterns. It was also found that the ferrite etched to a (110) surface, producing large, flat, strain-free areas.

A colloid film was dried on the surface but no structure was observed; however, when a small normal field was applied, a clear pattern of domain walls was observed, figure 2. Running horizontally across the figure is a pair of 109° walls A with smaller 71° walls B branching away towards the lower edge. At both ends of this figure lie etch pits; that on the right has spike closure domains at its outside edge. On the left hand side a double Néel spike has been formed, presumably at either a small etch pit or an inclusion. In two places, the wall doubling has broken down into a more normal 'fir tree' type of surface closure. At one point one wall has divided to give a pair, giving a further fir tree pattern and also a 'stepped' wall, which consists of alternate 180° and 109° domain walls. When a small horizontal field was applied to this specimen, very complicated patterns were found. Figure 3 shows an intricate system of fir tree patterns similar to the arabesque pattern observed by Yamamoto and Iwata (1953) on a (110) plane of Ni.

Figure 4 shows a portion of a system of slab domains near an edge of the specimen; in this region the lower edge of the print approaches the edge of the specimen where it curved due to grinding, and a progressive increase in the size of the 'fir tree' closure branches is noted towards the top of the figure. At the lower edge is a simple 180° domain wall which continued to the edge of the specimen.

In a (110) plane there are four easy directions of magnetization parallel to the [111] directions, see figure 27 (*b*). In the demagnetized state the specimen is composed of domains in which the magnetic vectors lie in one of these easy directions. These domains will be bounded by three types of domain wall, viz. 180°, 109° and 71° walls, and will be arranged to give complete flux closure in the specimen. 'Fir tree' patterns were obtained on all types of wall. These were observed by Williams, Bozorth and Shockley (1949) on the (100) surface of a single crystal of silicon iron and were interpreted as surface flux closure domains, resulting from a misorientation of the specimen surface with respect to the true crystallographic plane. 'Fir tree' patterns were later observed by Yamamoto and Iwata (1953) on the (110) plane of a single crystal of nickel. The 'fir tree' patterns found on Mn ferrite are in all ways analogous to those observed on nickel and were used to estimate the degree and direction of the surface with respect to the true (110) plane.

---

† Figures 1–26, see Plates I–VI.

An orientating cut was then made, and a small well orientated region was obtained in the centre of the specimen surface. Figures 5 and 6 show typical patterns obtained in this region. A 180° domain wall crosses the left hand corner of figure 5 and only two diminutive 'fir tree' branches are formed along a considerable length of the wall. Towards the centre is a well defined Néel spike; the arrows give the directions of magnetization. A series of single spikes have also been formed at small etch pits. These Néel (1944) spikes have been previously observed on iron and nickel and we now see that they occur at non-ferromagnetic inclusions in ferrites also.

Figure 6 gives a typical example of the closure system found on the specimen. It occurs at a deep crack which has been enlarged by etching. The crack runs vertically in the figure and is parallel to a [110] direction. Two 180° domains terminate in an echelon type of closure similar to that found by Martin (1957) on a (100) surface of silicon–iron bounded by a (111) surface. Here, a single 180° domain wall A is terminated at the crack by a system of 180°, 109° and 71° domain walls which form the echelon. Striations have been formed on either side of the main 180° wall and lie perpendicular to it, indicating the direction of magnetization (Kittel 1949). A 71° wall B is parallel to the crack and a 109° wall C joins it towards the top of the figure. In the main 71° domain are closure spikes in which the magnetization is antiparallel to that in the domain enclosing them.

There are important differences between manganese ferrite and nickel in domain sizes and spacings. These depend, theoretically, on the crystal size and the square root of the ratio of the wall energy to the crystalline anisotropy. The wall energy for manganese ferrite can be calculated (Smit and Wijn 1954) to be

$$\gamma = 3\,(AK_1)^{1/2}$$

where γ is the wall energy, A the exchange coupling energy ($=10^{-6}\,\mathrm{erg\,cm^{-1}}$, Smit and Wijn 1954) and K_1 the crystalline anisotropy ($= -3 \times 10^4\,\mathrm{erg\,cm^{-3}}$, Bozorth, Tilden and Williams 1955), whence

$$\gamma = 3(10^{-6} \times 3 \times 10^4)^{1/2}\,\mathrm{erg\,cm^{-2}} = 0{\cdot}5\,\mathrm{erg\,cm^{-2}},$$

compared with 1 erg cm^{-2} for nickel.

Since the anisotropy and wall energies are comparable and the size of the specimen of manganese ferrite compares with the specimen of nickel used by Yamamoto and Iwata, similar domain spacings were expected. It was, however, found that the structure on manganese ferrite was approximately $\frac{1}{2}$ the size of that on the nickel. The theoretical spacings cannot be calculated unless the type of closure structure involved is known. The ferrite patterns described were not found in the absence of an applied magnetic field and this may be due to the low intensity of magnetization I_s. However, I_s for nickel is of the same order, and patterns can apparently be observed on this material without an applied magnetic field.

The domain structures have been found to show two unusual features, not observed on nickel. The first is the pronounced curvature of some of the domain walls, and the second the formation of 'stepped' walls unaccompanied by 'fir tree' closure. The curvature of the walls (figures 2, 5 and 6) is a true effect not due to distortion of the colloid film. Two possible explanations of this curvature are suggested. Firstly, the presence of small varying stresses in the crystal and secondly, the presence of excess ferrous iron. The first would cause the anisotropy to vary from place to place, e.g. a region in which the stress has increased the

V.
19

anisotropy locally will tend to repel a domain wall, since in that region the wall energy will be increased, and vice versa. Secondly, when ferrous iron is diffused through the lattice an alteration of the exchange energy and crystalline anisotropy energy will result. This would have a similar effect as in the former case. If these explanations are valid, then the volumes affected will not have sharp boundaries, but will be surrounded by gradual transitional regions to the normal ferrite.

A 180° domain wall is normally straight, and magnetostatic energy must be balanced against the change in wall energy in a curved wall. Where the curvature of the wall is greatest a 'stepped' wall is formed, possibly due to decrease in magnetostatic energy compared with that of a greatly curved wall which does not follow any easy direction of magnetization.

The wall doubling, apparent in many of the figures here, has been observed on nickel, both by Stephan and by Yamamoto and Iwata. The latter workers considered it to be an extension of normal fir tree closure.

4.2. *Manganese–Zinc Ferrite*

This specimen, obtained from the G.E.C. Research Laboratories, was grown by the flame fusion technique and had a nominal 50–50 manganese–zinc composition. When received it was in two portions, having spontaneously cleaved on cooling. The cleaved surfaces were examined both by electron and optical microscopy. They had bright (100) faces with an array of perpendicular cracks. A film of colloid was dried on one of them in the presence of a small normal field. The surface was covered with a fine structure, figure 7, roughly similar to that on the cleaved surface of the magnanese ferrite. In the latter case (Bates, Craik and Griffiths 1958), the patterns on a similar crystallographic surface were of two distinct types, viz. a fine system of parallel bands of spacing 0·3 μ and an underlying coarser pattern representing closure of the internal domain structure. The fine pattern was interpreted as due to a very shallow, intensely and uniformly strained layer caused by cleavage.

The fine patterns on the manganese–zinc ferrite are basically similar to those on manganese ferrite, particularly in their regularity and spacing. Due to their close spacing, from magnetostatic considerations they cannot represent the internal domain structure, and they probably represent a shallow surface domain structure enclosing a cleavage strain. In manganese–zinc ferrite, the fine patterns are formed by zigzag bands which are most clearly seen by electron microscopy (figure 8). The zigzag angles are approximately 120° and 60°, and the band formation generally lies at either 90° and 45° to the array of perpendicular cracks in the surface (figure 10). The majority of the cleaved surfaces showed this fine structure. Figure 9 is a micrograph of a region of the surface near a surface crack. The zigzag bands are modified in the neighbourhood of the crack to form a simpler structure. This consists of a row of minute domains running perpendicular to the crack and is similar to some types of maze patterns found on the strained surface of silicon-iron (Chikazumi and Suzuki 1955, Stephan 1957), but the spacing is considerably smaller.

Figure 10 is a low magnification picture of the original cleaved surface; it shows large scale patterns of spacing approximately 50 μ, superimposed on the fine structure. The fine structure lies almost parallel to the large pattern. The coarse structure is typical of uniaxial magnetic crystal, since it is formed of parallel light and dark bands in the presence of a small normal field and shows closure consisting of reverse spikes. Where a crack occurs the configuration of the bands, with apparent reverse spikes, is analogous to those in cobalt. The coarse structure could be moved by the application of a field applied parallel to the apparent direction of magnetization, but a similar magnetic field applied perpendicular to this direction did not alter the pattern.

The cubic nature of the crystal lattice of manganese–zinc ferrite would normally preclude the uniaxial domain structure which has been found. A uniaxial structure could, however, arise when one of the crystal directions is favoured above the others due to a bulk strain. This implies that the strain anisotropy is the governing factor in the domain formation. Assuming that the strain anisotropy must be equal to or greater than the crystalline anisotropy, then $\frac{2}{3}\lambda\epsilon \geqslant K_1$, where λ is the coefficient of magnetostriction, ϵ is the stress and K_1 is the crystalline anisotropy. This would require a stress of approximately 10^7 dyn mm^{-2}.

Since the crystal had cleaved spontaneously on cooling, stresses must have existed which exceeded its tensile strength, i.e. of the order of 10^{10} dyn mm^{-2}. It is therefore not unreasonable that smaller stresses should have remained.

A (110) surface was ground on the specimen, polished and etched in boiling concentrated HCl. It again etched to a (110) plane and showed large clear areas. The patterns showed closed loops and a branching pattern of lines, figure 11. The spacings of the main branches were generally of the order of 20 μ and are much smaller than would be expected for this plane. However, they are much larger in scale than the cleavage strain pattern found on the (100) plane. They are known not to be a surface strain effect, since the crystal was later etched for ten minutes in boiling concentrated HCl and the patterns persisted. Electron microscopic examination showed no underlying structure.

The patterns obtained on the (110) surface are compatible with the uniaxial patterns observed on the (100) surface, in that they are formed of incomplete loops of very irregular spacing, such as are found on a plane set at an angle to the basal plane of a uniaxial crystal, e.g. cobalt, see figure 12. The close similarity of these patterns reinforces the above argument as to the formation of a uniaxial structure due to bulk strain effects.

In this particular case, it is suggested that a completely anomalous domain structure has arisen due to bulk strain, and thus for any ferrite in a similar strained condition the magnetic behaviour will be anomalous and measurements unreliable.

4.3. *Nickel Ferrite*

Several small crystals of nickel ferrite were grown from a borax melt. In contrast to the flame fusion specimens they had 8 well defined growth facets, identically triangular with angles of 60°. The general shape of the crystals was octahedral. This shape can be obtained by eight (111) planes in the eight segments of a system of orthogonal axes, figure 27 (*a*), and hence it is assumed that the facets were indeed (111) planes, purely from crystallographic considerations. These facets should therefore be bounded by three [110] directions inclined at 60° to each other, and the perpendiculars from each side will be [112] directions, as was later verified by the patterns obtained on the calculated (110) plane.

The crystals were cemented to a brass plate with 'Durofix', and to obtain a thin liquid layer of colloid a large drop of colloid was placed over and around the crystal. A small piece of microscope coverslip was then allowed to float on the colloid and was held horizontally against the crystal by surface tension. The patterns obtained consisted of a series of closed loops and heavy colloidal deposits, characteristic of a surface with no easy direction of magnetization, figure 13. Very similar patterns were obtained on a number of the natural facets with no normal field. However, when such a field was applied, and reversed, the pattern reversed, the heavy and fine deposits switching across alternate regions (figures 14 (*a*) and (*b*)).

These patterns are very similar to those obtained on a corresponding plane of a nickel single crystal (Yamamoto and Iwata 1953, Stephan 1954) and are again typical of a material with a negative crystalline anisotropy. The dense bands towards the left-hand edge of figure 13 are parallel to the [112] directions in the surface and suggest an internal domain structure of 180° and 109° walls. Between the heavy bands very fine parallel domains are formed, presumably to effect surface closure within the larger domains. The fine structure over the rest of the crystal is due to a more complicated internal closure system. By reversing a normal field (figures 14 (*a*) and (*b*)) these bands are shown to have large components alternatively into and out of the surface.

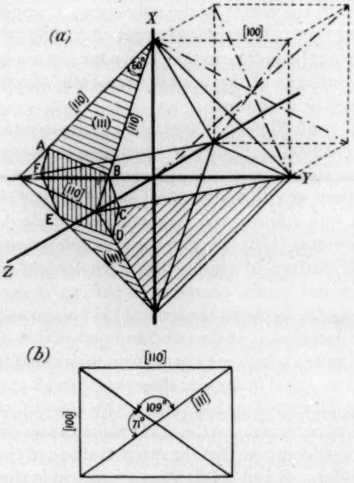

Figure 27.

In order to grind a (110) plane, e.g. like ABCDEF of fig. 27 (*a*), a small crystal was mounted in a plastic block with one of its facets parallel to the surface. The crystal was first placed with the selected face downwards on a glass slide and a drop of polystrene glue was gently poured over it. When the glue was set, it was peeled from the slide, taking the crystal with it, and laid flat on the base of the mounting press before adding the polystrene granules. The interface angle between a (111) plane and a (110) plane is 35° 18′, and a flat was ground on the face of the plastic block containing the crystal at this angle and parallel to one of the facet sides. The cut was sufficiently deep to be within ½ mm of the specimen. Further grinding was then performed entirely by hand with 6 μ and ¼ μ diamond compound. When a scratch-free surface had been obtained, the specimen was etched in boiling 50% HCl, 50% concentrated HNO_3 for varying periods. After several minutes, deep grooves were etched into the surface, where the strained regions around coarse scratches, which had subsequently been polished out, were preferably etched away. These deep grooves persisted throughout the etch and were never removed. Since the etching loosened the crystal from the plastic block, it was not possible to repolish the surface with fine powders between etching. Some traces of structure appeared after 5 hours etching and the specimen was eventually etched for 10 hours. After this prolonged etching the undulations in the surface were so deep as to obscure any clear configurations which might otherwise have formed.

However, when a normal field was applied to the newly ground and etched surface an arabesque pattern of domains, similar to that observed on manganese ferrite, was formed. When a horizontal field was applied parallel to the (110) direction a system of closure spikes was formed, figure 15. These spikes are 'fir tree' closure domains, indicating that the surface was slightly misorientated during the grinding operation. They point in [100] directions and their bases lie along a 71° wall, i.e. in the centre of the specimen; it appears that the domains run parallel to its long axis. Towards the upper edge of figure 15 is a series of 180° domain walls, enclosing the surface to the [110] edge just above the top of the print. The original (111) surfaces of the crystal were little affected by the prolonged etching and could still be examined.

It was possible to apply films to all surfaces simultaneously, so that the patterns on them could be correlated. Figure 16 illustrates such a case. It is composed of three prints taken from contiguous regions of the three surfaces, i.e. a (110) plane with (111) planes at either side of it, joined along [110] directions. The figure was obtained with a horizontal magnetic field applied parallel to the [110] direction. On the central (110) face there is a complex series of spikes. On the (111) faces a simple pattern of closure has been formed, consisting mainly of parallel straight lines and a more complicated pattern in one region of the upper (111) plane. At the edge between the lower (111) plane and the (110) plane are two types of closure domains. At the left-hand part of this boundary of the (110) surface is a series of spikes which are continuous with small triangular closure, on the (111) plane. More usual triangular closure is formed at the right-hand part of this boundary where it is closed in the (111) face by a system of parallel bands. In one case the small closure triangle on the (111) plane has no domain wall associated with it and hence it would appear that the internal shape of the closure spike in the (110) plane is triangular. Small Néel spikes are ringed in the figure.

The patterns on the (111) surfaces in figure 16 are very different from those in figures 13 and 14, due both to the altered shape of the specimen and to the presence of the applied field, and indicate a much simpler closure structure which corresponds to the pattern on the (110) face. Both the (111) planes appear to have alternature wall and chain-like arrays of free poles. This structure may be compared with patterns obtained by Bates and Wilson (1951) on the (111) surface of a nickel single crystal, with a field applied parallel to the [110] direction in the (111) plane. Throughout the specimen domains in which the vectors of magnetization are alternatively inclined at 109° to each other are formed, as may be verified by following the wall and chain-like structures, on either (111) plane, which are seen to be continuous with the 109° domain walls on the (110) plane. This situation is most readily seen towards the right-hand side. It is difficult to interpret the complex structure towards the left-hand side; it consists a of complicated mixture of surface closure, seen both on the upper (111) plane and the (110) plane, due to a slight misorientation, and also normal domain closure at the specimen edge. In the centre of the (110) plane 71° domains may exist to give more complete flux closure. Their existence, however, is difficult to decide upon, since any such wall will tend to become attached to the bases of the deep scratches. They will not be expected to be shown on the surface, since the scratches will obscure colloidal deposits over them.

4.4. *Copper Ferrite*

The specimens were grown from a borax melt and were not well formed externally, and little of their crystallographic structure and form could be determined by inspection. They were of somewhat smaller dimensions than the nickel ferrite, of the order of 0·4 mm. A crystal with fairly well-defined triangular faces, presumed to be (111), was found and patterns were obtained on one of them, both by optical and electron microscopy, using the dried film technique. In order to apply a film to these tiny crystals, they were first mounted on small brass blocks with 'Durofix', flooded with colloid and the excess removed by careful blotting.

Several different types of pattern were obtained; figure 17 shows a structure which may be compared with that found on the (111) surface of nickel ferrite. However, other regions of the same surface were covered with parallel walls, of which figure 18 is an electron micrograph. The dark bands have sharp boundaries which are unlike the diffuse deposits generally found over a domain wall. The curvature of the bands is artificial, and due to distortion of the colloid film while sited on the electron microscope specimen grid, as the film stretched across only a few squares of the grid and was incompletely supported. Figure 19 shows a second type of fine structure of a most unusual nature. It appears as rows of discrete ellipsoidal structures.

No data on the anisotropy of this ferrite are known and owing to the uncertainty concerning the orientation of the crystallite surfaces and the easy directions of magnetization, the patterns obtained cannot be interpreted exactly. It is clear, at least, that these small crystals have a well defined and complicated domain structure. The pattern in figure 18 appears to represent a system of slab domains. If the heavy bands are domain walls, then a very approximate value for the crystalline anisotropy will be 2×10^4 erg cm^{-3}, assuming that the exchange coupling energy is similar to that for the other ferrites, but no indication of the sign of the anisotropy can be inferred. The possibility of cleavage strain must not be neglected since the crystal might at some time have been broken. A second interpretation is that the dark bands are complete domains, of a similar type to those found on the cleaved face of manganese ferrite, which they resemble closely. They are unusual in that the width of the light and dark areas are greatly dissimilar.

The second type of fine structure, figure 19, is very similar to arrays of 'lozenges' observed by various workers (Paxton and Nilan 1955, Bates and Hart 1953, Bates and Davis 1956) on the (110) face of silicon–iron. It differs from them in its extreme fineness, the long axis being of the order of 5 μ.

4.5. *Barium Ferrite*

Barium ferrite has two easy directions of magnetization parallel to the hexagonal axis. The domain structure would therefore be expected to give 180° domain walls parallel to this axis. The specimen, obtained from the G.E.C. Research Laboratories, was grown by the flame fusion technique. It was not a single crystal, but consisted of very large grains some millimetres in diameter. The specimen was originally a cylinder some 0·7 cm in diameter and approximately 2 cm long. Barium ferrite has a single cleavage plane, the basal plane of the hexagonal structure, and this was parallel to the long axis of the cylinder. Several such planes were exposed by cleavage. The surfaces were examined using the dried film technique both by optical and electron microscopy.

Four main types of pattern were found. Where the crystals were thinnest a maze pattern existed, similar to that recorded by Sixtus, Kronenberg and Tenzer (1956). On somewhat thicker crystals a second pattern of undulatory walls was found, as in figure 20; alternate light and dark bands indicate that the domains which these patterns enclose are magnetized in antiparallel directions in the bulk of the crystal. The third type of pattern, figure 21, found on the thickest crystal, consisted of an array of star like structures enclosed by undulatory walls; an electron micrograph, figure 22, shows that the star surfaces are of opposite polarity to the surrounding regions. The fourth type, figure 23, was a network of enclosed loops 0·6 μ to 0·3 μ in diameter.

Some of these patterns obtained on the basal plane are similar to those of Roberts and Bean (1954) on MnBi which were discussed by Goodenough (1956) who considered the wall energy densities and the surface pole closures of the different types of array of undulatory wall structures. The patterns shown in figure 20 are considered to represent small, approximately circular, spike terminations lying in a roughly parallel array of undulatory walls, and are similar to the patterns on MnBi.

The electron microscope shows that the patterns can have an even more complicated form. Figure 22 consists of rosette-like closures having any number of elongated branches from two to eight, differing from the hexagonal ones on MnBi. Moreover, these were at times completely surrounded by closed undulatory walls of very great amplitude. Large portions of the closed walls shown in figure 22 were continuous outside the range of the figure. The patterns in figure 23 differ greatly from any previously observed in their exceptional fineness and regularity, the diameter of the loops being 1/10 of that of the rings or rosettes in the other patterns. They differ in a most important manner, in that on the application of a normal field, neither the small loops nor the larger loops enclosing them tended to attract colloid. This suggests that they do not represent the bases of reverse spikes but are minute closure domains. The complete closure structure could contain reverse spikes inside the material, i.e. it could correspond with the uniaxial closure structure postulated by Lifshitz (1944).

The domain walls in figure 20 were the finest continuous lines of particles obtained by progressively diluting the colloid; assuming them to be approximately equal to the wall width, direct measurement gives the wall width to be approximately 1×10^{-5} cm. The wall width, according to Smit and Wijn (1954), is equal to $7\,(A/K_1)^{1/2}$, where A is the exchange coupling energy, approximately 10^6 erg cm^{-1}, and K_1 the crystalline anisotropy energy, 10^6 erg cm^{-3}, giving a calculated value of $0{\cdot}7 \times 10^{-5}$ cm, in reasonable agreement with the above measurement.

It is to be noted that no anomalous structures have been obtained on the cleaved basal planes, the structures shown being compatible with what may be expected from a knowledge of the anisotropy. This implies that there is no cleavage strain comparable with the anisotropy as far as this plane is concerned, which is in marked contrast to the ferrites considered above.

An axial plane was obtained by grinding perpendicular to the crystal basal plane. Due to the very high crystalline anisotropy, approximately 10^6 erg cm^{-3} compared with 10^4 erg cm^{-3} for the ferrites previously considered, it was only necessary to obtain a clean scratch-free surface by careful grinding and polishing. Surface strain does not appreciably alter the form of the underlying domain structure.

Figure 24 shows patterns obtained by the wet colloid technique on a typical crystal face in the ground surface. Running horizontally and completely across the crystal is a pattern of 180° domain walls parallel to the hexagonal axis. Several reverse domains are formed at the crystal boundary, and in one case a reverse domain arises from a surface pit or inclusion sited near the left-hand boundary. This plays a similar role to the Néel spikes on the manganese ferrite, in that it reduces the surface pole energy. Figures 26 (*a*) and (*b*) were obtained in the presence of an applied field normal to the surface. In figure 26 (*a*) a boundary between two crystals extends horizontally across the figure. The domain walls running across the lower grain are not exactly parallel, due to a slight misorientation of the surface from the crystallographic plane containing the easy directions of magnetization, which causes the components of the magnetic vectors normal to the surface in alternate domains to attract colloid, thus giving the pattern of alternate light and dark bands instead of the walls seen in figure 24. When the normal field is reversed, figure 26 (*b*), the pattern is reversed. In figure 26 the hexagonal axes in the two crystals are in close alignment and there is considerable interaction between their domain structures; in particular, three walls are continuous across the crystal boundary, although there is a considerable difference in the domain spacings.

Not all the crystals were so closely aligned. Figure 25 shows four crystals in which both the orientation of the plane and the hexagonal axis differs. In the left hand crystal the surface is presumably very nearly correctly orientated to the hexagonal axis, the walls being straight and parallel, while in the largest crystal the walls are curved and branched, and the surface presumably makes a considerable angle with the hexagonal axis. Even where there is a difference of direction between the hexagonal axes, in the two largest crystals, of 33°, there is still considerable interaction between the domain structures. At the boundary an array of reverse spikes has been formed and other spikes can be seen arising from grinding pits. These patterns of 180° domains and dagger shaped spikes of reverse magnetization on the axial planes are fully analogous to the patterns on the corresponding plane of cobalt and also to the configuration on MnBi revealed by polarization microscopy by Roberts and Bean (1954).

Examination, by electron microscopy, of the axial planes of cobalt and barium ferrite demonstrated one noticeable difference: if this plane of cobalt is scratched, chains of minute domains are formed along the scratch due to the localized strain (Bates 1957). When barium ferrite was examined, immediately after grinding, similar strain patterns were not observed accompanying the scratches, although the latter were readily visible due to the replica effect of the colloid film. This difference is probably due to the very different mechanical properties of the two materials and indicates that the barium ferrite is much less strain sensitive than cobalt.

The pronounced interaction (figures 25 and 26) of the domains in adjacent crystals, even at high angles of incidence, conforms to the view that no perpendicular closure is present at the crystal boundaries. This interaction arises from a high surface pole density which is largely counteracted by the corresponding pattern of the surface pole density on the adjacent grain.

§ 5. CONCLUSIONS

The above investigations have demonstrated domain structures in most of the simple ferrites. Some of these are easily explained and are, in fact, expected from a knowledge of the crystal structure and the magnetic properties of the materials; others are anomalous structures.

From the technical point of view it was expected that difficulty would be experienced in obtaining clear patterns by the Bitter figure technique. The intensity of magnetization is low in all cases, and for most of the materials a low crystalline anisotropy tended to give poorly defined domain walls.

The impossibility of electropolishing the surfaces created difficulty in the removal of polishing strain. A well electropolished surface is practically certain to be strain free, and etching must be performed very carefully, with frequent inspection to achieve the same result, the appearance of the pattern being the main criterion of the surface state. In the case of many ferrites various clear patterns may be caused by strain in the surface layer, and these will bear little relation to the underlying domain configuration, e.g. manganese ferrite and manganese–zinc ferrite (Bates *et al.* 1958).

It is rarely possible to obtain a smooth flat surface by etching, since there is always a tendency to form etch pits, which on some surfaces may be continuous, and as etching is selective in strained regions an initially smooth surface may appear scratched when lightly etched. Cleavage can produce smooth surfaces, but in some cases these have a strained layer which gives rise to special kinds of pattern and surfaces which can be obtained in this way are always limited, e.g. to (100) planes of manganese ferrite or the basal plane of barium ferrite.

The patterns obtained are in accordance with expectation in the cases of nickel, magnanese and barium ferrites. The first two, cubic spinel ferrites, showed configurations on the (110) plane consisting of 180°, 109° and 71° domain walls. Barium ferrite, hexagonal, whose axial plane contains two easy directions of magnetization, showed a typical uniaxial configuration of 180° domains and reverse spikes. On the basal plane, containing no easy direction of magnetization, a system of reverse spike terminations of variable configuration was found.

The manganese–zinc ferrite crystal showed anomalous patterns, considered to be due to strains set up during its preparation.

The cubic spinel ferrites showed marked surface structures of very fine spacing due either to cleavage or grinding strain. That such were not observed for the barium ferrite is probably due to its high magnetic anisotropy. The fine structures on all the cubic spinel ferrites, and the anomalous structure on the manganese–zinc ferrite showed that these ferrites are very strain sensitive, despite their physical hardness.

ACKNOWLEDGMENTS

The authors wish to thank Professor L. F. Bates, who suggested this work, for his encouragement and valuable suggestions in the preparation of the manuscript. The manganese ferrite crystal was kindly supplied by Dr. K. Hoselitz of the Mullard Research Laboratories. The MnZn and barium ferrites were kindly supplied by Mr. L. A. Thomas of the G.E.C. Research Laboratories. D. J. C. thanks Mr. O. W. Trigg for technical assistance and P. M. G. thanks the Department of Scientific and Industrial Research for a maintenance grant.

REFERENCES

BATES, L. F., 1957, *Endeavour*, **16,** 151.
BATES, L. F., CLOW, H., CRAIK, D. J., and GRIFFITHS, P. M., 1958, *Proc. Phys. Soc.*, **72,** 224.
BATES, L. F., CRAIK, D. J., and GRIFFITHS, P. M., 1958, *Proc. Phys. Soc.*, **71,** 789.
BATES, L. F., and DAVIS, P. F., 1956, *Proc. Phys. Soc.* B, **69,** 1109.
BATES, L. F., and HART, A., 1953, *Proc. Phys. Soc.* A, **66,** 813.
BATES, L. F., and WILSON, G. W., 1951, *Proc. Phys. Soc.* A, **64,** 691.
BOZORTH, R. M., TILDEN, E. F., and WILLIAMS, A. J., 1955, *Phys. Rev.*, **99,** 1788.
CHIKAZUMI, S., and SUSUKI, K., 1955, *J. Phys. Soc. Japan*, **10,** No. 7.
CRAIK, D. J., 1956, *Proc. Phys. Soc.* B, **69,** 647.
CRAIK, D. J., and GRIFFITHS, P. M., 1957, *Proc. Phys. Soc.* B, **70,** 1000.
—— 1958, *Brit. J. Appl. Phys.*, **9,** 276.
GALT, J. K., 1954, *Bell Syst. Tech. J.*, **33,** 1023.
GOODENOUGH, J. B., 1956, *Phys. Rev.*, **102,** 356.
KITTEL, C., 1949, *Rev. Mod. Phys.*, **21,** 541.
LIFSHITZ, E., 1944, *J. Phys., Moscow*, **8,** 337.
MARTIN, D. H., 1957, *Proc. Phys. Soc.* B, **70,** 77.
NÉEL, L., 1944, *Cah. Phys.*, **25,** 21.
PAULUS, M., 1957, *C.R. Acad. Sci., Paris*, **245,** 2227.
PAXTON, W. S., and NILAN, T. G., 1955, *J. Appl. Phys.*, **26,** 994.
ROBERTS, R. W., and BEAN, C. P., 1954, *Phys. Rev.*, **96,** 1494.
SIXTUS, K. J., KRONENBERG, K. J., and TENZER, R. K., 1956, *J. Appl. Phys.*, **27,** 1051.
SMIT, J., and WIJN, H. P. J., 1954, *Advances in Electronics and Electron Physics*, Vol. VI, Ed. L. Morton (New York: Academic Press).
STEPHAN, W., 1955, *Exp. Tech. Phys.*, **1,** 1.
—— 1957, *Ibid.*, **4,** 145.
WILLIAMS, H. J., BOZORTH, R. M., and SHOCKLEY, W., 1949, *Phys. Rev.*, **75,** 155.
YAMAMOTO, M., and IWATA, T., 1953, *Sci. Rep. Res. Insts Tôhoku Univ.*, A, **5,** No. 5.

A Bitter Figure Examination of Some Polycrystalline Nickel–Cobalt Alloys

By L. F. BATES and E. D. ISAAC
Department of Physics, University of Nottingham

MS. received 5th September 1958

Abstract. A Bitter figure examination of polycrystalline Ni–Co alloys of compositions 21, 29, 46 and 59% Co, respectively, showed wall movements to occur in the last three alloys, the field limits being in reasonable agreement with the results of a study of the heat changes accompanying magnetization processes in the alloys.

The Bitter figure technique has been used to study domain wall movements in a series of polycrystalline Ni–Co alloys. Four alloys of compositions 21, 29, 46 and 59% Co, respectively, were studied. In the course of a study of the heat changes accompanying magnetization processes in these alloys Bates and Clow found evidence in favour of the disperse field theory of coercivity; the present investigation was therefore undertaken to obtain confirmation or otherwise of these results.

At room temperature Ni–Co alloys have a face-centred cubic crystal structure. The magnetic anisotropy, which changes sign at the compositions 19% Co and 68% Co, is negative within that range. Approximate values of the anisotropy constant are (Yamamoto and Taniguchi 1956)

Composition (% Co)	21	29	46	59
Anisotropy (10^3 ergs cm^{-3})	−2	−30	−70	−130

Thus, in all the alloys studied, the easy directions of magnetization lie in [111] directions.

The specimens were obtained in the form of long, cylindrical rods of diameter approximately 4 mm. These were annealed for 8 hours at 1200°c in a hydrogen atmosphere and subsequently cooled at 150 deg hr^{-1}. The alloys are sensitive to cooling in a magnetic field (Masumoto, Inoue and Ukaji 1954), and although the cooling was carried out in the earth's field, it appeared to have very little effect on their properties.

Thermal measurements previously made on the specimen rods (Bates and Clow 1958) showed that domain wall movements occur below the values of the effective field as tabulated,

Composition (% Co)	21	29	46	59
Field limit for wall movements (Oe)	30	50	120	200

For the powder pattern examinations rods approximately 2·5 cm in length of each alloy were prepared. On each a flat surface was ground along its length. This surface was then ground down to grade 0000 emery and electropolished for 20 minutes at 22 volts in a bath of chromic and acetic acids.

Figure 1 (for all figures see Plate) shows a typical pattern as seen on the surface of the freshly prepared specimen containing 59% Co, in the absence of an applied horizontal magnetic field. The dotted lines indicate the approximate positions of grain boundaries. The domains remained stationary even on the application of a horizontal field and, as can be seen, a large proportion of the domain magnetic vectors are orientated in one direction, the grinding direction, which runs vertically in the photograph. The domains appear to lie wholly parallel to the surface, indicating an excess, strain-induced anisotropy. Hence the domains shown in figure 1 were assumed to be due to grinding strain.

In an attempt to remove the strained surface layer, the specimens were re-electropolished for a further ten minutes. However, on examination, similar patterns were again seen. It was therefore concluded that bulk strain was present throughout the specimens. In order to remove this strain, the specimens were given a further anneal for five hours at 1050°c and, since the anneal was carried out in hydrogen, no extra surface preparation was necessary.

Each specimen was examined between the pole-pieces of a small electromagnet, and chosen horizontal fields were applied along the long axis of the specimen. The effective fields were measured with a magnetic potentiometer in conjunction with a galvanometer amplifier.

Figures 2–6 show one region of the surface of the specimen containing 59% Co in different horizontal fields throughout a magnetization cycle. The fields were applied in directions indicated by the arrows and the dotted lines again mark the positions of grain boundaries, where necessary.

Figure 2 shows the specimen in the saturated state with an effective field of some −200 Oe. In figure 3 the field has been reduced to −30 Oe and domain nucleation has taken place from grain boundaries. Further nucleation has taken place in figure 4 where the field was reduced to −5 Oe. Figure 5 shows the pattern in a field of −1 Oe; here the domains are fully formed and we see them as alternate light and dark bands. In figure 6 a reverse field of 3 Oe, slightly larger than the coercive field of the specimen, was applied. On comparison of figures 5 and 6 it is seen that the light bands in figure 5 have become the dark bands in figure 6. The explanation of this effect was given by Mee (1950). From the formation of bands of colloid, it is apparent that the magnetic vectors of the domains do not lie exactly in the surface of the grains, since, if this were the case, then a simple pattern of domain walls would be observed. Where the magnetic vector makes an angle with the crystallite surface a magnetic field applied in the same sense as the vector will increase the component of the vector normal to the surface; when, however, a field is applied in the opposite sense it will tend to decrease this normal component. Where the vector is increased colloid will lie thickly over the surface and vice versa.

The direction of magnetization in a domain can be determined since any undulations in the specimen surface at right angles to the direction of magnetization cause striations of colloid to be produced. Thus the direction of magnetization is always at right angles to the direction of the striations. On several of the grains of the specimen containing 59% Co rotation of the direction of magnetization was observed while domain nucleation was taking place, as may be seen by comparing figures 3 and 4.

In the centre of figure 6 are seen two grains having vastly different domain configurations. On the lower grain is observed a system of alternate light and dark domains together with a system of spikes growing from the lower boundary of the crystallite, presumably to effect more complete flux closure at the boundary. On this grain, the direction of magnetization may be assumed to lie within a few degrees of the specimen surface. However, in the case of the upper grain, a complex pattern has been formed, caused by free poles situated over a complicated closure system below the surface. This will be the case if the direction of magnetization makes a large angle with the specimen surface.

The patterns obtained on the specimens containing 46% and 29% Co showed similar characteristics. However, in these two cases, while it was possible to decide visually between what limits of field domain wall movement occurred, the patterns were not so well defined, presumably due to the progressive decrease of the crystalline anisotropy, and will not be reproduced here.

On the surface of the 21% Co specimen, no evidence of domains was observed, presumably because the anisotropy is small in this region of composition. For the other three alloys, wall movements were recorded as follows:

Composition (% Co)	29	46	59
Field limit for wall movements (Oe)	30	75	140
Bates and Clow (Oe)	50	120	200

We may assume that wall movements took place to a lesser extent at fields higher than those recorded, and therefore the figures quoted show fair agreement with the fields estimated for the same specimens by Bates and Clow, which are given in the third line of the above table. It was found impracticable to record any figures for change in magnetization by domain vector rotation.

ACKNOWLEDGMENTS

We wish to thank the Electrical and Allied Industries Research Association for support which made this work possible and for permission to publish.

REFERENCES

BATES, L. F., and CLOW, H., 1958, *Report of the International Conference on Magnetism, Grenoble*, 1958, to be published in *J. Phys. Radium*.
MASUMOTO, H., INOUE, S., and UKAJI, I., 1954, *Sci. Rep. Res. Insts, Tôhoku*, A, **6**, 375.
MEE, C. D., 1950, *Proc. Phys. Soc.* A, **63**, 922.
YAMAMOTO, M., and TANIGUCHI, S., 1956, *Sci. Rep. Res. Insts, Tôhoku*, A, **8**, 280.

V.7
195

Energy Loss Processes in Ferroelectric Ceramics

By B. LEWIS

Communication from the Staff of the Research Laboratories of The General Electric Company Limited, Wembley, England

MS. received 29th July 1958, in final form 23rd September 1958

Abstract. By a study of ageing effects in which permittivity, elastic compliance and the electrical and mechanical loss coefficients decrease with time, the principal ferroelectric loss process in low fields is identified as microhysteresis associated with small-amplitude domain boundary movement. Larger fields produce macrohysteresis effects due to large-scale boundary movement, and the permittivity, compliance and loss coefficients are increased. Although boundary movement is responsible for almost all the energy loss, its contribution to permittivity and compliance is usually small compared with induced effects within each domain. Thus a change in the magnitude of boundary movement alters the permittivity and compliance only slightly, but changes the loss coefficients considerably.

§ 1. Introduction

An outstanding problem in connection with the behaviour of ferroelectric materials is the identification of the processes responsible for energy loss and an explanation of the variations observed with amplitude, time and composition, as described, for example, by Schofield and Brown (1957), Gray and Herbert (1956) and Mason (1955). Excluding variation with temperature, which will not be discussed here, the electrical and mechanical loss coefficients vary over a wide range. For example, tan δ for barium titanate may vary from 0·2 to 0·01 according to the conditions of measurement, and may be reduced to 0·002 by the incorporation of a small amount of nickel, with only minor associated changes of permittivity and Curie temperature. The mechanical loss coefficient $1/Q$ shows a similar range of variation.

An obvious source of energy loss in ferroelectric materials lies in their characteristic hysteresis. This arises from the existence of spontaneous polarization which can be switched from one crystallographic axis to another by an external field. Thus, in an applied field, domain boundaries move so that favourably oriented domains grow at the expense of those which are less favourably oriented and if this movement is impeded hysteresis loss is observed.

Macrohysteresis effects, which are manifest in the familiar (P, E) hysteresis loops, commence when the applied field is sufficient to make a boundary jump irreversibly from one position of stability to another. With larger fields the magnitude of each jump is correspondingly greater and the macrohysteresis process thus contributes an amplitude-dependent term to the permittivity and the dielectric loss. Experimental results reported in this paper show that there is a fairly well defined threshold field below which the amplitude-dependent macrohysteresis effects are negligibly small.

Below this threshold field the domain boundaries are constrained at positions of maximum stability associated with the presence of impurities, dislocations and internal stress. Under the action of an applied field, however, they are able to move against the restoring force of their constraints and so make a contribution to the permittivity. This boundary movement component of permittivity has been discussed by McQuarrie and Buessem (1955), McQuarrie (1956) and Plessner (1956) and identified by them as the process concerned in ageing effects in which permittivity decreases with time. The ageing mechanism is the migration of domain boundaries to positions of greater stability.

Since dielectric loss also decreases with time, even with fields well below the macrohysteresis threshold, there must be energy loss associated with the low field boundary movement process. This loss, which will be called microhysteresis loss, may be associated with the switching of individual atomic moments in successive lattice planes traversed by the moving boundary.

In addition to the boundary movement contributions to permittivity there is, of course, a substantial intrinsic component due to induced polarization within each domain. The intrinsic permittivity of each domain depends on the orientation of the polar axis and thus for the specimen as a whole it varies with the state of over-all polarization. This variation is small, however, compared with the contributions to permittivity arising from the direct changes of polarization associated with boundary movement in an applied field.

Spontaneous polarization in ferroelectric materials is accompanied by spontaneous deformation. Consequently an applied stress brings about strains due to domain boundary movement and induced strain within each domain, giving components of compliance which are analogous to the three components of permittivity discussed above. The ferroelectric loss processes controlling the value of the mechanical loss coefficient $1/Q$ are also analogous to those which determine the dielectric loss.

This paper describes an attempt to separate the three components of permittivity and compliance, making use of the amplitude dependence of macro boundary movement and the time dependence of micro boundary movement, and to determine the loss coefficients associated with each of these processes. A particular object of this analysis is to discover the physical differences accounting for the extreme variability of losses with composition and measurements have, therefore, been made on both high and low loss materials.

§ 2. EXPERIMENTAL

Measurements of loss coefficients as a function of amplitude and of time have been made on specimens with compositions based on barium titanate, $BaTiO_3$. The ceramics were prepared following the usual methods.

As a high-loss material a barium titanate–zirconate of the composition $Ba(Ti_{0\cdot95}Zr_{0\cdot05})O_3$ (Kell and Hellicar 1956) was used. This has a somewhat higher electro-mechanical activity than $BaTiO_3$ with similar, or slightly higher, values of loss coefficients.

A barium-nickel titanate $(Ba_{0\cdot98}Ni_{0\cdot02})TiO_3$ was chosen as a typical low-loss material. The loss coefficients after ageing are about one tenth that of $BaTiO_3$ and the electromechanical activity is only slightly reduced.

Permittivity and loss tangent were obtained by bridge measurements of capacitance and equivalent parallel resistance. The measurements were made at

1 kc/s except for those at high amplitudes which were made at 50 c/s. Both the materials had d.c. resistivities of the order 10^{12} ohm cm, and energy loss due to conductivity was negligibly small at these frequencies.

Compliance was found by measuring the radial mode resonant frequency of a disc or the length mode resonance of a bar. The variation with temperature shows peaks near the Curie temperature and the lower transition temperatures. At 60°c above the Curie temperature the compliance drops to about two-thirds of its room temperature value, showing that there is a substantial component of compliance of ferroelectric origin. The measurement of compliance above the Curie temperature was made using a quartz-ceramic composite oscillator. At lower temperatures disc specimens were poled with a unidirectional field and their electrical characteristics measured with a variable frequency bridge near the radial mode resonant frequency. The frequency f_r and the equivalent parallel resistance R_m at resonance were measured, and also the bandwidth Δf between the half power points, from which the mechanical $Q=f_r/\Delta f$ was calculated.

At high amplitudes the bridge method became impracticable because of the power required and because the heat generated in the specimen necessitated rapid measurements. A 30w amplifier was used to supply an admittance network and R_m was measured by substitution. $1/Q$ was then obtained by extrapolating the linear relation between R_m and $1/Q$ observed at low and moderate amplitudes. This amounts to an assumption that the electromechanical activity is independent of driving amplitude

§ 3. RESULTS

It is convenient, in analysing experimental results, to consider the complex permittivity ϵ and the complex compliance s, where

$$\epsilon=\epsilon'-j\epsilon'', \qquad \ldots\ldots(1)$$

$$s=s'-js''. \qquad \ldots\ldots(2)$$

The electrical and mechanical loss coefficients are then defined as

$$\frac{\epsilon''}{\epsilon'}=\tan\delta, \qquad \ldots\ldots(3)$$

and

$$\frac{s''}{s'}=\frac{1}{Q}. \qquad \ldots\ldots(4)$$

As already discussed the observed permittivity ϵ_{At}, at amplitude A and time t, is the sum of three terms:

$$\epsilon_{At}=\epsilon_{\mathrm{H}}+\epsilon_{\mathrm{h}}+\epsilon_{\mathrm{i}}. \qquad \ldots\ldots(5)$$

ϵ_{H} is the amplitude dependent macrohysteresis complex permittivity at amplitude A, ϵ_{h} is the time dependent microhysteresis component at time t, and ϵ_{i} is the intrinsic component which is assumed to be independent of A and t.

Similarly the observed compliance s_{At} can be written

$$s_{At}=s_{\mathrm{H}}+s_{\mathrm{h}}+s_{\mathrm{i}}. \qquad \ldots\ldots(6)$$

3.1. *Macrohysteresis Effects*

The variation with field of permittivity and loss tangent for $\mathrm{Ba(Ti_{0.95}Zr_{0.05})O_3}$ and for $\mathrm{(Ba_{0.98}Ni_{0.02})TiO_3}$ is given in figure 1. These results show quite clearly the threshold field beyond which permittivity and loss increase with amplitude.

Comparing the two materials, the threshold field is greater, and tan δ below the threshold field smaller, for the specimen containing nickel.

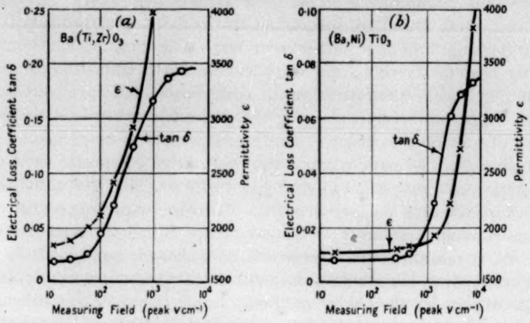

Figure 1. Increase of permittivity and loss tangent due to macrohysteresis effects in moderate fields; (*a*) for $Ba(Ti_{0\cdot95}Zr_{0\cdot05})O_3$, (*b*) for $(Ba_{0\cdot98}Ni_{0\cdot02})TiO_3$.

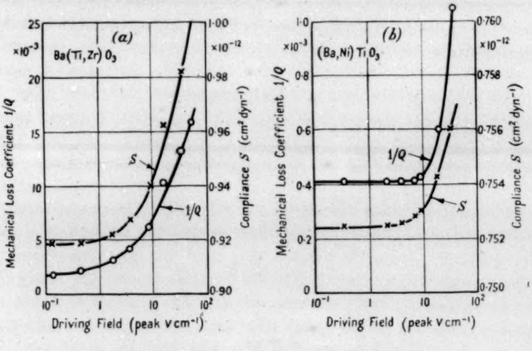

Figure 2. Increase of compliance and mechanical loss coefficient due to macrohysteresis effects at moderate amplitudes; (*a*) for $Ba(Ti_{0.95}Zr_{0.05})O_3$, (*b*) for $(Ba_{0.98}Ni_{0.02})TiO_3$.

In an analogous experiment compliance and mechanical loss factor were measured over a range of stress amplitude. The results are shown in figure 2 plotted against the driving field. No attempt has been made to determine the actual values of strain or stress amplitude. Again there is a threshold amplitude beyond which macrohysteresis effects appear and which is higher for $(Ba,Ni)TiO_3$. Below the threshold, the loss factor for $(Ba,Ni)TiO_3$ is only about one fifth that for $Ba(Ti,Zr)O_3$.

Since in equation (5) ϵ_h and ϵ_l are independent of amplitude it follows that at amplitude *A* the permittivity due to macrohysteresis is

$$\epsilon_H = \epsilon_{At} - \epsilon_{0t}, \qquad \ldots\ldots(7)$$

where ϵ_{0t} is the permittivity below the threshold field where $\epsilon_H = 0$. Considering real and imaginary parts it follows from equations (3) and (4) that the electrical loss coefficient associated with the macrohysteresis process is

$$(\tan\delta)_{\mathrm{H}} = \frac{\epsilon_{\mathrm{H}}''}{\epsilon_{\mathrm{H}}'} = \frac{\epsilon_{At}'' - \epsilon_{0t}''}{\epsilon'_{At} - \epsilon_{0t}'}, \qquad \ldots\ldots(8)$$

and that the mechanical macrohysteresis loss coefficient is

$$\left(\frac{1}{Q}\right)_{\mathrm{H}} = \frac{s_{\mathrm{H}}''}{s_{\mathrm{H}}'} = \frac{s_{At}'' - s_{0t}''}{s_{At}' - s_{0t}'}. \qquad \ldots\ldots(9)$$

Substituting data derived from figures 1 and 2 into equations (8) and (9) we find for $Ba(Ti_{0.95}Zr_{0.05})O_3$

$$(\tan\delta)_{\mathrm{H}} = 0{\cdot}29, \quad (1/Q)_{\mathrm{H}} = 0{\cdot}18,$$

and for $(Ba_{0.98}Ni_{0.02})TiO_3$

$$(\tan\delta)_{\mathrm{H}} = 0{\cdot}21, \quad (1/Q)_{\mathrm{H}} = 0{\cdot}14.$$

The pairs of values for the two materials are very similar in spite of the differences between the directly observed losses. This indicates that the form of the potential function which controls the macrohysteresis process is similar in each case although the amplitude must be greater for $(Ba,Ni)TiO_3$, to give the higher value of threshold field. Comparing the values of $(\tan\delta)_{\mathrm{H}}$ and $(1/Q)_{\mathrm{H}}$ it may be significant that whereas both 180° and 90° boundary movement can contribute to permittivity only 90° changes affect compliance.

3.2. *Microhysteresis Effects*

Experimental ageing data for $Ba(Ti,Zr)O_3$ and $(Ba,Ni)TiO_3$ are given in figures 3 and 4. The failure of the $Ba(Ti,Zr)O_3$ specimens to show any further ageing after about eight hours is probably due to the effect of small temperature changes. The specimens were protected from draughts and were not handled during the course of an experiment but their temperature was not thermostatically controlled. Deliberate temperature changes of a few degrees temporarily reversed the ageing of $Ba(Ti,Zr)O_3$ but had no effect on $(Ba,Ni)TiO_3$ which continues to age for many months at room temperature, giving ultimate values $\tan\delta \sim 10^{-3}$ and $1/Q \sim 4\times10^{-4}$.

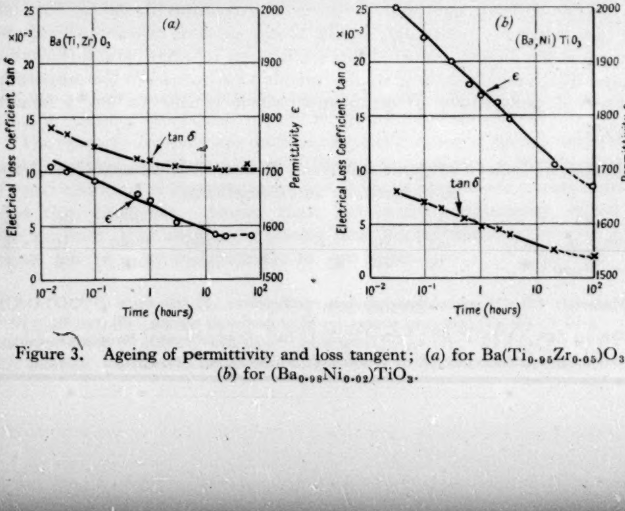

Figure 3. Ageing of permittivity and loss tangent; (*a*) for $Ba(Ti_{0.95}Zr_{0.05})O_3$, (*b*) for $(Ba_{0.98}Ni_{0.02})TiO_3$.

If we assume that the variation in properties with time is entirely due to a change in the micro boundary movement terms then, for a pair of measurements separated by a suitable time interval,

$$\Delta\epsilon_{0t} = \Delta\epsilon_{\mathrm{h}}, \qquad \ldots\ldots (10)$$

where Δ indicates the change in value over the time interval.

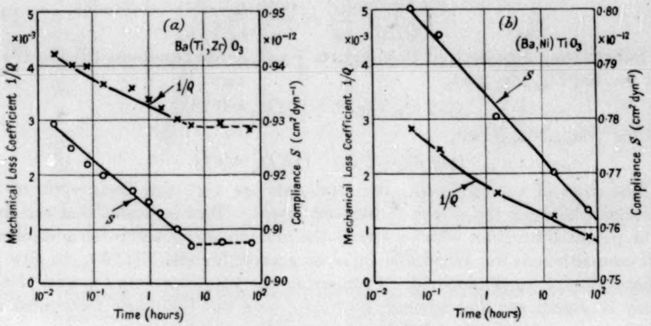

Figure 4. Ageing of compliance and mechanical loss coefficient; (*a*) for $Ba(Ti_{0\cdot95}Zr_{0\cdot05})O_3$, (*b*) for $(Ba_{0\cdot98}Ni_{0\cdot02})TiO_3$.

The loss coefficients associated with the microhysteresis process are then

$$(\tan\delta)_{\mathrm{h}} = \frac{\Delta\epsilon_{\mathrm{h}}''}{\Delta\epsilon_{\mathrm{h}}'} = \frac{\Delta\epsilon''_{0t}}{\Delta\epsilon_{0t}'}, \qquad \ldots\ldots (11)$$

and

$$\left(\frac{1}{Q}\right)_{\mathrm{h}} = \frac{\Delta s_{\mathrm{h}}''}{\Delta s_{\mathrm{h}}'} = \frac{\Delta s_{0t}''}{\Delta s_{0t}'}. \qquad \ldots\ldots (12)$$

The values of $(\tan\delta)_{\mathrm{h}}$ and $(1/Q)_{\mathrm{h}}$ found in this way are not quite independent of the time interval concerned. They are usually somewhat higher for the initial period of ageing than for the later part. Average values over the period of the full line curves in figures 3 and 4 are given in columns (2) and (3) of the table. These four values are remarkably similar to one another, in contrast to the wide differences in the directly observed loss coefficients, columns (4) and (5), and it is suggested that these differences are due mainly to variations in the proportion of the observed permittivity or compliance which is due to micro boundary movement.

Microhysteresis Loss Coefficients and Micro Boundary Movement Contributions to Permittivity and Compliance

(1)	(2)	(3)	(4)	(5)	(6)	(7)	(8)	(9)
$Ba(Ti_{0\cdot95}Zr_{0\cdot05})O_3$	63	56	10	3	1580	0·907	16	5
$(Ba_{0\cdot98}Ni_{0\cdot02})TiO_3$	38	44	2	0·8	1670	0·763	5	2

(1) Material; (2), (3) microhysteresis loss coefficients: (2) $(\tan\delta)_{\mathrm{h}} \times 10^{-3}$, (3) $(1/Q)_{\mathrm{h}} \times 10^{-3}$; (4)–(7) observed properties after moderate ageing: (4) $(\tan\delta)_{0t} \times 10^{-3}$, (5) $(1/Q)_{0t} \times 10^{-3}$, (6) ϵ_{0t}', (7) $s_{0t}' \times 10^{-12}$ (cm dyn^{-1}); (8), (9) micro boundary movement contribution to ϵ' and s' (%): (8) $\epsilon_{\mathrm{h}}'/\epsilon_{0t}'$, (9) s_{h}'/s_{0t}'.

In any ferroelectric material containing domain boundaries, even when fully aged, ϵ_{h} and s_{h} do not become zero, so that the intrinsic components of permittivity and compliance ϵ_{i} and s_{i} can never be isolated. There are circumstances however, in which boundary movement cannot occur, and energy losses are then found to be very small. For example, in antiferroelectric materials such as sodium niobate or lead zirconate, and in ferroelectrics above the Curie point, spontaneous polarization is zero and in both cases $\tan\delta$ is about 10^{-3}; when values higher than this are observed the additional loss is usually due to conductivity. Measurements with a quartz–ceramic composite oscillator show that above the Curie temperature $1/Q$ for $BaTiO_3$ also drops to about 10^{-3}. It therefore seems reasonable to suppose that in most ferroelectric materials the energy loss associated with intrinsic processes is small compared with microhysteresis loss.

If we assume $\epsilon''_{\mathrm{i}} \ll \epsilon''_{\mathrm{h}}$ then equation (5), for low fields with $\epsilon_H = 0$ and $\epsilon_{At} = \epsilon_{0t}$, becomes

$$\epsilon_{0t}' = \epsilon_{\mathrm{h}}' + \epsilon_{\mathrm{i}}', \quad \epsilon_{0t}'' = \epsilon_{\mathrm{h}}''. \qquad \ldots\ldots(13)$$

Hence

$$\frac{(\tan\delta)_{0t}}{(\tan\delta)_{\mathrm{h}}} = \frac{\epsilon_{0t}''}{\epsilon_{0t}'}\frac{\epsilon_{\mathrm{h}}'}{\epsilon_{\mathrm{h}}''} = \frac{\epsilon_{\mathrm{h}}'}{\epsilon_{0t}'}, \qquad \ldots\ldots(14)$$

and similarly

$$\frac{(1/Q)_{0t}}{(1/Q)_{\mathrm{h}}} = \frac{s_{\mathrm{h}}'}{s_{0t}'}. \qquad \ldots\ldots(15)$$

The observed loss coefficient is thus the microhysteresis loss coefficient multiplied by the ratio of the micro-boundary movement contribution to the total observed permittivity or compliance. Values of this ratio, calculated from the loss coefficients in columns (4) and (5), are given in columns (8) and (9) of the table. These figures indicate that in $Ba(Ti, Zr)O_3$ the micro boundary movement contribution, after ageing, is about three times as large as in $(Ba,Ni)TiO_3$.

In comparing the figures for permittivity with those for compliance, one reason why the micro-boundary movement contribution to compliance is lower, is that less than half of the observed compliance is of ferroelectric origin, as can be seen from its variation through the Curie temperature. Taking this point into account and remembering that only 90° boundary movement contributes to compliance, the figures suggest that the microhysteresis contribution to permittivity is principally by movement of 90° boundaries and that any contribution from 180° boundary movement is small. This is in agreement with evidence that 180° domains require more energy for growth than for nucleation (Little 1955) and are thus expected to contribute only to macrohysteresis effects.

The ultimate values of loss coefficients, after prolonged ageing, are determined by the curvature of the deepest available energy minima, by the de-ageing effect of small temperature changes or applied fields, and by losses arising from causes other than hysteresis. Among these factors are conductivity, either of the ceramic itself or of absorbed moisture, and normal anelastic losses. On both counts low porosity is favourable to low losses.

§ 4. CONCLUSIONS

The observed losses in both $Ba(Ti, Zr)O_3$ and $(Ba,Ni)TiO_3$ can be accounted for entirely as macro- and micro-hysteresis loss associated with movement of domain boundaries. The lower losses in (Ba,Ni)TiO_3 indicate that boundary movement is more difficult in this material and that domain boundaries are strongly held in their equilibrium positions.

The particular composition $(Ba_{0.98}Ni_{0.02})TiO_3$ represents the limit of solid solubility of nickel in the $BaTiO_3$ lattice. There is a progressive change in properties, including the Curie temperature, up to 2% Ni. Beyond this proportion the Curie temperature remains constant and changes in other properties indicate dilution by a non-ferroelectric phase. Presumably the presence of Ni ions on Ba sites presents an obstacle to the movement of domain boundaries. This could be due to lattice strain arising from the small size of $Ni^{2+} = 0{\cdot}78$ Å compared with $Ba^{2+} = 1{\cdot}34$ Å. Alternatively the foreign ions may interrupt the ferroelectric coupling, forming isolated non-ferroelectric centres in the ferroelectric lattice.

References

Gray, A. L., and Herbert, J. M., 1956, *Acustica*, **6**, 229.

Kell, R. C., and Hellicar, N. J., 1956, *Acustica*, **6**, 235.

Little, E. A., 1955, *Phys. Rev.*, **98**, 978.

Mason, W. P., 1955, *J. Acoust. Soc. Amer.*, **27**, 73.

McQuarrie, M. C., 1956, *J. Amer. Ceram. Soc.*, **39**, 54.

McQuarrie, M. C., and Buessem, W. R., 1955, *Bull. Amer. Ceram. Soc.*, **34**, 402.

Plessner, K. W., 1956, *Proc. Phys. Soc.* B, **69**, 1261.

Schofield, D., and Brown, R. F., 1957, *Canad. J. Phys.*, **35**, 594; *J. Acoust. Soc. Amer.*, **29**, 394.

Some Equilibrium and Non-Equilibrium Properties of an $(n+1)$-state Ideal Solution

By R. O. DAVIES
Physics Department, Queen Mary College, London

MS. received 1st *September* 1958

Abstract. The properties of an assembly of $n+1$ reacting isomers in ideal solution is examined with reference to the thermodynamic theory of relaxation. It is shown explicitly how the equilibrium properties of the system can be related to the chemical reaction coefficients and to what extent the formalism of statistical mechanics can be used in this context. The matrix of relaxation times is obtained in terms of the 'transition probabilities' together with their derivatives with respect to concentration. The latter terms give rise to a condition (additional to the well-known condition for microscopic reversibility) which must be satisfied if the Onsager reciprocity relations are to be valid. There is no obvious physical interpretation for this extra condition.

---

§ 1. Introduction

In recent years there has been renewed interest in thermo-mechanical relaxation processes in liquids and gases. This has given rise to extensive experimental studies (such as the measurement of sound absorption in relaxing fluids) whose ultimate aim is to obtain microscopic information about the system being studied (McCoubrey and McGrath 1957, Davies and Lamb 1957). Unfortunately it is not quite easy to realize this aim. In part this is because of well-known difficulties in producing a viable microscopic theory of irreversible processes. However, just as important—at least at the present time—is the fact that the macroscopic theory is not yet in a form which enables us to see clearly how the macroscopic, observable quantities are to be interpreted. Thus, we may measure relaxation strengths and relaxation times of one sort or another and still be quite uncertain about how these are to be interpreted.

In many cases the only hope of progress lies in assigning to the process mechanisms of 'chemical' type in which the elementary constituents of the system combine or change their state in a surveyably small number of ways. In this case we have available the relaxation theory of coupled chemical reactions (see Prigogine and Defay 1954, Meixner 1953, Davies 1956). Whereas the principles of this theory are clear enough (they are summarized in § 2), there are certain detailed calculations needed before the theory can be applied to particular cases. At this stage it does not seem to be possible to give a really general treatment, even in the case of ideal solutions. The purpose of this paper is to derive the principal theorems needed for the special case of an $(n+1)$-state ideal solution. That is, we consider a system of $n+1$ reacting isomers, each of which can change into all of the others. There are n independent reactions such a system.

In § 3 we derive the main results concerning the diagonalization and inversion of the matrix of ordering coefficients, $\beta_{rs} = (\partial A_r/\partial z^s)$ (where A_r is the r^{th} affinity and z^s the s^{th} degree of reaction). In § 4 we use the results of § 3 to prove that the relaxing specific heat in a many-state process is in fact that which would be obtained by equilibrium calculations. (This result has been used frequently by workers concerned with relaxation of the vibrational degrees of freedom, see, for example, Andreae, Heasell and Lamb 1956). In § 5 we obtain general matrices which represent the relaxation time operator (or, rather, its inverse) in terms of transition probabilities and the derivatives. Finally, we discuss the self adjoint nature of this operator in relation to Onsager reciprocity and the principle of microscopic reversibility.

§ 2. SUMMARY OF THE GENERAL THEORY

In terms of a notation used elsewhere (Davies 1956) the theory of relaxation considers ν independent thermodynamic variables x^α (such as p, T, ...), their conjugate dependent variables X_α (such as $-V$, S) which depend also on n ordering variables z^r. The affinities A_r are conjugate to the ordering variables and the condition for thermodynamic equilibrium is that the A_r vanish.

Expanding linearly about an equilibrium point one has the basic thermostatic equations

$$\begin{aligned} X_\alpha &= c_{\alpha\beta} x^\beta + \lambda_{\alpha s} z^s \\ A_r &= \lambda_{r\beta} x^\beta + \beta_{rs} z^s \end{aligned} \qquad \ldots\ldots(1)$$

Here (and later) we use the summation convention; Greek affixes run from 1 to ν and Latin affixes from the *second* half of the alphabet from 1 to n. The second law or rather the assumed existence of a free energy $F(x, z)$ tells us that $c_{\alpha\beta} = c_{\beta\alpha}$, $\lambda_{r\alpha} = \lambda_{\alpha r}$ and $\beta_{rs} = \beta_{sr}$. The $c_{\alpha\beta}$ are 'frozen' thermodynamic coefficients, the $\lambda_{r\alpha}$ are 'reaction' coefficients which tell us how the ordering processes effect the thermodynamic quantities and β_{rs} is a set of ordering coefficients defined by $\beta_{rs} = \partial A_r/\partial z^s$. Since the free energy is a minimum at equilibrium, β_{rs} is a negative definite.

The time-dependent behaviour of the system is assumed to be given by

$$\mathscr{D} z^r = L^{rs} A_s \qquad \ldots\ldots(2)$$

where $\mathscr{D} \equiv d/dt$ and the Onsager symmetry principle requires

$$L^{rs} = L^{sr}. \qquad \ldots\ldots(3)$$

Eliminating A_r and z^s between equations (1) and (2) we find the (observable) time-dependent behaviour of the thermodynamic variables given by

$$X_\alpha = \{c_{\alpha\beta} - \lambda_{\alpha r}(I + \tau\mathscr{D})^{-1r}{}_s \beta^{-1st} \lambda_{t\beta}\} x^\beta \qquad \ldots\ldots(4)$$

with

$$\tau_s{}^r = -\beta^{-1rt} L^{-1}{}_{ts}. \qquad \ldots\ldots(5)$$

Putting $\mathscr{D} = 0$ in equation (4) shows that the equilibrium values of the thermodynamic coefficients are given by

$$\bar{c}_{\alpha\beta} = c_{\alpha\beta} - \lambda_{\alpha r} \beta^{-1rs} \lambda_{s\beta}. \qquad \ldots\ldots(6)$$

The transformation rules for the various quantities are those suggested by the position of affixes, e.g. the z^r are components of a contravariant vector and the A_r are those of a covariant vector. The two separate parts of

$$-dF = X_\alpha dx^\alpha + A_r dz^r$$

should be regarded as invariant differential forms.

The notation strongly suggests the advantage of using the Dirac language and notation with β_{rs} as the fundamental, or metric, tensor. Define $\beta^{rs} = \beta^{-1rs}$ and represent contravariant vectors by 'kets' ($|\rangle$) and covariant vectors by 'bras' ($\langle|$), the correspondence between them being, as usual, given by the metric: $\lambda_\alpha{}^r = \beta^{rs}\lambda_{\alpha s}$, etc. τ can now be regarded as the linear operator $-L^{-1}$ and equations (4) and (6) can be expressed without explicit reference to the representation

$$X_\alpha = \{c_{\alpha\beta} - \langle\lambda_\alpha|(I+\tau\mathscr{D})^{-1}|\lambda_\beta\rangle\}x^\beta \qquad \ldots\ldots(7)$$

with

$$\bar{c}_{\alpha\beta} = c_{\alpha\beta} - \langle\lambda_\alpha|\lambda_\beta\rangle. \qquad \ldots\ldots(8)$$

If we choose as basis the normalized eigenkets $|\tau_r\rangle$ of τ (whose existence and orthogonality are assured by the Onsager symmetry condition (3) and the negative definite nature of the metric) we may write

$$X_\alpha = \left\{c_{\alpha\beta} - \sum_{r=1}^{n} \frac{\langle\lambda_\alpha|\tau_r\rangle\langle\tau_r|\lambda_\beta\rangle}{1+\tau_r\mathscr{D}}\right\}x^\beta \qquad \ldots\ldots(9)$$

and

$$\bar{c}_{\alpha\beta} = c_{\alpha\beta} - \sum_r \langle\lambda_\alpha|\tau_r\rangle\langle\tau_r|\lambda_\beta\rangle \qquad \ldots\ldots(10)$$

where

$$\tau|\tau_r\rangle = \tau_r|\tau_r\rangle. \qquad \ldots\ldots(11)$$

The observable properties of the system are therefore the relaxation times τ_r and the products of 'principal' or 'proper' reaction coefficients, given by the matrix elements appearing in (9) and (10).

In order to make further progress towards a microscopic description it is necessary to specify the z^r as the degress of n independent chemical reactions such that the change in mole number of species i in the system is given by

$$dN^i = \nu_r{}^i dz^r. \qquad \ldots\ldots(12)$$

Specification of the $\nu_r{}^i$ in (12) can be considered as fixing the base vectors of the system, since the changes in mole numbers are of course invariant physical properties. The affinities are

$$\mathrm{A}_r = -\sum_i \nu_r{}^i\mu_i \qquad \ldots\ldots(13)$$

(where μ_i are the chemical potentials) and hence the metric tensor with (p, T) as the thermodynamic variables is

$$\beta_{rs} = -\sum_i\sum_j \nu_r{}^i\nu_s{}^j\partial\mu_i/\partial N^j. \qquad \ldots\ldots(14)$$

It is a solution property of system and as such should come from the equilibrium theory.

The specification of τ depends of course on rate assumptions; we shall consider a special case in § 4. Before discussing this we must settle the question of inverting the β matrix of (14). This is essential because the calculation of any scalar product of given covariant vectors such as $(\lambda_{\alpha r})$ requires it.

§ 3. Inversion of the β-matrix for an $(n+1)$-state Ideal Solution

We now consider the special case of $n+1$ reacting isomers in an ideal solution defined by

$$\mu_i = \mu_i{}^0(p, T) + RT\ln(N^i/N) \quad (N = \sum N^i). \qquad \ldots\ldots(15)$$

(From here on we define $\Sigma_i = 1$ and let Latin letters from the first half of the alphabet run from 1 to $n+1$. The suppression of summation is indicated by brackets.)

Case 1.

For the reaction system

$$\nu_r{}^i = \delta_r{}^i - \delta_{r+1}{}^i \quad \begin{pmatrix} r = 1 \ldots n \\ i = 1 \ldots n+1 \end{pmatrix} \qquad \ldots\ldots (16)$$

we may obtain β from equations (14)–(16):

$$\beta_{1rs} \equiv -\beta_{1rs}/RT = \delta_{rs}/N^{(r)} + \delta_{r+1,\,s+1}/N^{(r+1)} - \delta_{r,\,s+1}/N^{(s+1)} - \delta_{r+1,\,s}/N^{(r+1)}. \qquad \ldots\ldots (17)$$

The matrix B_1 of equation (17) can be inverted by elementary methods if it is observed that

$$|B_1| = \begin{vmatrix} (N^1)^{-1} + (N^2)^{-1} & -(N^2)^{-1} & \cdot & \cdot \\ -(N^2)^{-1} & (N^2)^{-1} + (N^3)^{-1} & -(N^3)^{-1} & \cdot \\ \cdot & -(N^3)^{-1} & \ddots & \ddots \\ & \ddots & \ddots & -(N^n)^{-1} \\ \cdot & \cdot & -(N^n)^{-1} & (N^n)^{-1} + (N^{n+1})^{-1} \end{vmatrix}$$

$$= (N^1 + N^2 + \ldots N^{n+1})/(N^1 N^2 \ldots N^{n+1}), \qquad \ldots\ldots (18)$$

a formula which may be proved by induction. The result is, for Case 1,

$$(B_1{}^{-1})^{rs} = -RT\beta_1{}^{rs} = \begin{cases} N\sigma_r(1-\sigma_s) & r \leqslant s \\ N\sigma_s(1-\sigma_r) & r \geqslant s \end{cases} \qquad \ldots\ldots (19)$$

where $\quad N = N^1 + N^2 + \ldots + N^{n+1}$

and $\quad \sigma_r = (N^1 + N^2 + \ldots + N^r)/N.$

Case 2.

Consider now an alternative reaction system defined by

$$\nu_r{}^i = \delta_r{}^i - \delta_{n+1}{}^i \sum_r \begin{pmatrix} r = 1 \ldots n \\ i = 1 \ldots n+1 \end{pmatrix}. \qquad \ldots\ldots (20)$$

Using equations (14), (15) and (20) we may again form the ordering coefficients, which we now distinguish with the subscript 2 from those of Case 1:

$$\beta_{2rs} \equiv -\beta_{2rs}/RT = \sum_r \sum_s /N^{n+1} + \delta_{rs}/N^{(r)} \qquad \ldots\ldots (21)$$

In order to invert B_2 we can make use of the result already obtained in equation (19) for B_1. Comparing the reaction systems defined by (16) and (20) we see that the change in basis involves the linear transformation of the contravariant degree of reaction defined by the matrix T:

$$z_2 = Tz_1$$
$$T_s{}^r = \delta_s{}^r - \delta_s{}^{r-1}. \qquad \ldots\ldots (22)$$

The inverse of T is easily seen to be

$$(T^{-1})^r{}_s = \begin{cases} 1 & r \geqslant s \\ 0 & r \leqslant s \end{cases} \qquad \ldots\ldots (23)$$

and one may check that the matrices of (17) and (21) are related, as they should be, by

$$B_2 = T'^{-1} B_1 T^{-1}. \qquad \ldots\ldots (24)$$

Using now the transformation rules for the inverse B matrices, we must have

$$B_2{}^{-1} = TB_1{}^{-1}T' \qquad \ldots\ldots (25)$$

so that the use of (22) and (19) yields, for Case 2,

$$(B_2{}^{-1})^{rs} = -RT\beta_2{}^{rs} = N^{(r)}\delta_{rs} - \frac{N^rN^s}{N}. \qquad \ldots\ldots(26)$$

The very simple result of equation (26) can be checked independently by using a matrix formula proved by Bodewig (1956, p. 32) and attributed by him to Bartlett. It is:

$$(A+xy')^{-1} = A^{-1} - \left(\frac{1}{1+y'A^{-1}x}\right) A^{-1}xy'A^{-1}. \qquad \ldots\ldots(27)$$

Set $A = -\operatorname{diag}(NN^r)$, $x = y = [N^r]$. Then the left side of equation (27) becomes $(NB_2{}^{-1})^{-1}$ while the right side reduces to $(B_2)/N$ thus verifying that equation (26) inverts to equation (21).

§ 4. CALCULATION OF THE RELAXING SPECIFIC HEAT

We shall now illustrate the use of § 3 to calculate the incremental heat capacity of an ideal solution from the relaxation formula (6) and show that it agrees with that obtained from thermodynamics and, in a certain limit, from statistical mechanics.

In order to do this we require a mathematical Lemma.

With $B_1{}^{-1}$ defined by equation (19) and η_i a set of $(n+1)$ numbers, the following identity is satisfied:

$$\sum_{s=1}^{n} (-\eta_s + \eta_{s+1})(B_1{}^{-1})^{st} = \frac{1}{N} \sum_{u=1}^{n+1} \sum_{s=1}^{t} N^sN^u(\eta_u - \eta_s). \qquad \ldots\ldots(28)$$

(Here, for the sake of clarity, we indicate summation explicitly.) Equation (28) is proved in the Appendix.

To calculate the incremental specific heat by equation (6) we need the reaction coefficient $\lambda_{S_r} = \partial S/\partial z^r = (1/T)(\partial H/\partial z^r) = \Sigma_i \nu^i{}_r h_i/T$. Introducing $\nu^i{}_r$ from equation (16) we find equation (6) takes the form

$$\delta C_p = T\delta(\partial S/\partial T) = -\frac{1}{RT^2} \sum_{s=1}^{n} \sum_{t=1}^{n} (h_s - h_{s+1})B^{-1st}(h_t - h_{t+1}). \qquad \ldots\ldots(29)$$

Making use of the identity (28) in (29) this becomes

$$\delta C_p = \frac{1}{RT^2} \sum_{i=1}^{n+1} (h_i - h)^2 \qquad \ldots\ldots(30)$$

where $h \equiv H/N$ is the mean molar enthalpy and h_i are the partial enthalpies.

Let us now verify this by thermodynamics. From the conditions of chemical equilibrium $(A_r = 0)$ we have

$$N^i = (N/z)\exp(-\mu_i{}^0/RT) \qquad \ldots\ldots(31)$$

where $\quad z = \sum_i \exp(-\mu_i{}^0/RT) = \exp(-\mu/RT).$

Now the incremental specific heat can be calculated from $H = \sum_i N^ih_i$:

$$\delta C_p = \sum_i h_i \frac{\partial N_i}{\partial T}. \qquad \ldots\ldots(32)$$

Evaluate the derivative $\partial N^i/\partial T$ by the use of (31) and substitute in (32). Equation (30) is recovered. In the special case in which all the species present have the same partial volume, the quantities $h_i - h$ appearing in (30) become $u_i - u$. Equation (30) is then just the formula which would be found by applying elementary statistical mechanics to a system consisting of independent, localized particles each having molar energy level u_i open to it. This is what is done (without justification) by Andreae, Heasell and Lamb (1956).

Equation (30) can of course be recovered by using the representation of Case 2 in § 3 (equations (20) and (26)); indeed the work is somewhat simpler, but it is worth while to use Case 1 so as to have access to the identity of equation (28).

The importance of this section is that it justifies the naïve use of formulae drawn from statistical mechanics in dealing with isomeric reactions in ideal solution.

§ 5. The Connection between Transition Probabilities and Relaxation Times, Onsager Reciprocity

The macroscopic rate constants L^{rs} introduced in equation (2) have no very obvious microscopic interpretation. It is therefore convenient to consider an alternative set of constants $P_i^{\,j}$ $(i, j=1 \ldots n+1)$ which are to be interpreted as transition probabilities per unit time, on a pseudo-microscopic footing. Call $P_i^{\,j} (i \neq j)$ the 'probability per unit time' that a molecule in state i goes over to state j. Let $P_i^{\,i}$ be defined by the relation

$$P_i^{\,i} = -\sum_j{}' P_i^{\,j} \text{ or } \sum_j P_i^{\,j} = 0 \qquad \ldots\ldots (33)$$

and assume that the kinetics of the system is governed by

$$\frac{dN^i}{dt} = N^j P_j^{\,i} \qquad \ldots\ldots (34)$$

in which the $P_j^{\,i}$ must be considered as functions of state depending on the thermodynamic variables (x^α) and degrees of reaction (z^r). Expand equation (34) about an equilibrium state for which

$$N^j P_j^{\,i} = 0 \qquad \ldots\ldots (35)$$

and we find (using the definition of z^r in equation (12)) that

$$\frac{d\Delta N^i}{dt} = \left\{ N^j \frac{\partial P_j^{\,i}}{\partial z^s} + \sum_j P_j^{\,i} \nu^j{}_s \right\} z^s + N^j \frac{\partial P_j^{\,i}}{\partial x^\alpha} x^\alpha. \qquad \ldots\ldots (36)$$

On the other hand, the earlier rate parameters appear in the following consequence of (1) and (2):

$$\frac{dz^r}{dt} = -W^r{}_s z^s - W^r{}_\alpha x^\alpha \qquad \ldots\ldots (37)$$

with $\qquad W^r{}_s = (\tau^{-1})^r{}_s = -L^{rt}\beta_{ts}$

and $\qquad W^r{}_\alpha = L^{rs}\lambda_{s\alpha}.$

Comparing equations (36) and (37) we find (with the help of (12)) that

$$-\nu^i{}_t W^t{}_s = N^j \frac{\partial P_j^{\,i}}{\partial z^s} + \nu^j{}_s P_j^{\,i} \qquad \ldots\ldots (38)$$

$$-\nu^i{}_t W^t{}_\alpha = N^j \frac{\partial P_j^{\,i}}{\partial x^\alpha}. \qquad \ldots\ldots (39)$$

Let us now use the second representation (Case 2) of § 3 and we find from equation (38) that the mixed matrix of inverse relaxation times is given by

$$(\tau^{-1})^r{}_s = W^r{}_s = -N^j \frac{\partial P_j^{\,r}}{\partial z^s} - P_s^{\,r} + P^r{}_{n+1} \sum_s. \qquad \ldots\ldots (40)$$

In dealing with this equation it should be remembered that the transition probabilities $P_i^{\,j}$ are intensive properties of the system. Therefore one has a set of relations, analogous to the Gibbs–Duhem formulae, expressing homogeneity:

$$N^k \frac{\partial P_i^j}{\partial N^k} = 0. \qquad \ldots\ldots (41)$$

To illustrate the meaning and importance of these general results, we consider two special problems.

(*a*) Consider the simplest and most popular case with $n=1$: the two-state mechanism. There is only a single relaxation time. According to equations (33), (40) and (41) it is given by

$$\tau^{-1} = W = P_1{}^2 + P_2{}^1 + x\frac{\partial P_2{}^1}{\partial x} - (1-x)\frac{\partial P_1{}^2}{\partial x} \qquad \ldots\ldots (42)$$

where $x = N^2/N$ is mole fraction of species 2.

This is a special case of a much more obscure formula given by Davies and Lamb (1956). The first two terms in (42) are of course well known and often used. The second two terms are written so as to make it obvious that any exact theory of these simple relaxation mechanisms needs to establish the dependence of 'transition probabilities' on concentration.

(*b*) The formal theory built up in § 2 rests heavily on the Onsager reciprocity principle of equation (3). Without it the reality of the relaxation times τ_r and the orthogonality of the eigenvectors $|\tau_r\rangle$ are not assured. Now that we have an expression for the τ-matrix in terms of 'transition probabilities' it is important to see what is needed in order for the reciprocity principle to be valid.

The easiest way of doing this is to use equations (21) and (40) to form $W_{ts} = B_{2tr} W^r{}_s$. The required condition is then $W_{ts} - W_{st} = 0$. With the help of equation (33), this condition can be written in the form

$$\begin{aligned}\sum_t \left(\frac{P_s{}^{n+1}}{N^{(n+1)}} - \frac{P_{n+1}{}^s}{N^{(s)}}\right) + \sum_s \left(\frac{P_{n+1}{}^t}{N^{(t)}} - \frac{P_t{}^{n+1}}{N^{(n+1)}}\right) + \frac{P_t{}^s}{N^{(s)}} - \frac{P_s{}^t}{N^{(t)}} \\ + N^j\left\{\sum_t \left(\frac{\partial P_j{}^{n+1}/\partial N^s}{N^{(n+1)}} - \frac{\partial P_j{}^s/\partial N^{n+1}}{N^{(s)}}\right) + \sum_s \left(\frac{\partial P_j{}^t/\partial N^{n+1}}{N^{(t)}} - \frac{\partial P_j{}^{n+1}/\partial N^t}{N^{(n+1)}}\right)\right. \\ \left. + \frac{\partial P_j{}^s/\partial N^t}{N^{(s)}} - \frac{\partial P_j{}^t/\partial N^s}{N^{(t)}}\right\} = 0 \qquad \ldots\ldots (43)\end{aligned}$$

for all $s,\ t \leqslant n$.

The structure of this equation shows immediately that there are two *sufficient* conditions which will assure Onsager symmetry. They are

$$\frac{P_i^j}{N^{(j)}} - \frac{P_i^j}{N^{(i)}} = 0 \qquad \ldots\ldots (44)$$

and

$$N^k\left(\frac{\partial P_k{}^i/\partial N^i}{N^{(j)}} - \frac{\partial P_k{}^i/\partial N^i}{N^{(i)}}\right) = 0. \qquad \ldots\ldots (45)$$

The first of these (44) is the usual form of the condition for 'microscopic reversibility'. It simply says that, in equilibrium, the average number of transitions $i \to j$ is equal to the average number $j \to i$. It is of course the basis of Onsager's original argument (1931) and has also been discussed by many later writers (e.g. Prigogine 1947, Denbigh 1951).

The second condition (45) does not seem to admit any obvious physical interpretation. It is to be hoped that it is true because one is naturally anxious to keep the pleasing, symmetric formalism of the general theory. If equation (45) *is* satisfied then the derivative terms appearing in (42) will vanish.

§ 6. CONCLUSION

The detailed theory of the thermodynamics of relaxation has here been applied to the simple but important case of an $(n+1)$-state isomeric mechanism in ideal solution. It is shown how relaxing components of any thermodynamic variable can be calculated; the process justifies the use of a quasi statistical mechanics with a 'partition function' for the Gibbs energy given by

$$\sum_i \exp(-\mu_i^0/RT).$$

The matrix of relaxation times is related to a set of 'transition probabilities' together with their dependence on concentrations; because of this last fact, the conditions for Onsager reciprocity include not only the well-known 'microscopic reversibility' principle, but also a new restriction involving the dependence of transition probabilities on concentration.

ACKNOWLEDGMENT

I wish to thank Dr. John Lamb for many stimulating discussions and helpful comments on the subject of this paper.

APPENDIX

PROOF OF THE LEMMA OF § 4 (EQUATION (28))

Define $(B^{-1})^{0t}=0$ and the left side of equation (28) can be rewritten in a form suitable for the substitution of (19). Thus:

$$\begin{aligned}\sum_{s=1}^{n}(-\eta_s+\eta_{s+1})(B^{-1})^{st} &= -\sum_{s=1}^{n}\eta_s[(B^{-1})^{st}-(B^{-1})^{(s-1)t}]+\eta_{n+1}[B^{-1}]^{nt}\\ &= -N\sum_{s=1}^{t}\eta_s[\sigma_s-\sigma_s\sigma_t-\sigma_{s-1}+\sigma_{s-1}\sigma_s]\\ &\quad -N\sum_{s=t}^{n}{}_{+1}\eta_s[\sigma_t-\sigma_s\sigma_t-\sigma_t+\sigma_{s-1}\sigma_t]\\ &\qquad +N\eta_{n+1}\sigma_t(\sigma_{n+1}-\sigma_n)\\ &= -\sum_{s=1}^{t}\eta_s N^s+\sigma_t\sum_{s=1}^{n}{}^{+1}\eta_s N^s.\end{aligned}$$

The right side of this equation reduces to the right side of equation (28), viz.,

$$\frac{1}{N}\sum_{u=1}^{n+1}\sum_{s=1}^{t}N^s N^u(\eta_u-\eta_s).$$

REFERENCES

ANDREAE, J. H., HEASELL, E. L., and LAMB, J., 1956, *Proc. Phys. Soc.* B, **69**, 625.
BODEWIG, E., 1956, *Matrix Calculus* (Amsterdam: North-Holland).
DAVIES, R. O., 1956, *Rep. Progr. Phys.*, **19**, 326 (London: Physical Society).
DAVIES, R. O., and LAMB, J., 1956, *Proc. Phys. Soc.* B, **64**, 293.
—— 1957, *Quart. Rev.* **11**, 134 (London: Chemical Society).
DENBIGH, K. G., 1951, *The Thermodynamics of the Steady State* (London: Methuen).
McCOUBREY, J. C., and McGRATH, W. D., 1957, *Quart. Rev.* **11**, 87 (London: Chemical Society).
MEIXNER, J., 1953, *Kolloidzschr.*, **134**, 3.
ONSAGER, L., 1931, *Phys. Rev.*, **37**, 405; **38**, 2265.
PRIGOGINE, I., 1947, *Étude Thermodynamique des Phénomènes irréversibles* (Liège: Desoer).
PRIGOGINE, I., and DEFAY, R., 1954, *Chemical Thermodynamics* (London: Longmans Green).

The Evaporation Theory of Photonuclear Reactions

By J. A. EVANS
Department of Mathematical Physics, University of Birmingham

MS. received 13*th August* 1958, *in final form* 8*th September* 1958

Abstract. There is considerable disagreement between the predictions of the evaporation (or statistical) theory, and the experimental results for the ratio of emission probabilities of protons and neutrons from a heavy nucleus excited by γ-ray absorption. This investigation deals with refinements which can be made to the evaporation theory; namely, the use of accurate experimental nucleon separation energies, and the assumption of a realistic, diffuse nuclear surface. Penetrabilities are calculated for the nucleus ^{118}Sn, assuming a diffuse nuclear surface, and it is found that proton emission is enhanced by a factor of about 4. Finally, the effects of shell structure are discussed in connection with the densities of levels in the residual nuclei.

It is found that the theory still predicts far less proton emission than is actually observed.

§ 1. INTRODUCTION

The simple statistical theory of nuclear reactions was worked out by Weisskopf and Ewing (1940), and is based on the Bohr assumption that the decay of an excited nucleus is independent of the mode of formation. The emission width Γ_b of a particle b is related to the capture cross section σ_b of the inverse process by

$$\omega_c \Gamma_b = \pi^{-2} k^2 \sigma_b \omega_r$$

where ω_c, ω_r are the densities of levels in the compound and residual nuclei respectively. Here k is the wave number, and ϵ the kinetic energy of the particle b.

Expanding the cross section as a sum of partial wave contributions, we have

$$\sigma_b = \pi k^{-2} \sum_l (2l+1) T_l$$

and for the emission width,

$$\omega_c(E)\Gamma_b(\epsilon) = \pi^{-1} T(\epsilon)\omega_r(E - E_b - \epsilon),$$

where the transmission coefficient T is given by $T(\epsilon) = (2l+1)T_l(\epsilon)$.

E is the excitation energy of the compound nucleus and E_b is the separation energy of the particle b in this nucleus. The excitation function F_b is now defined as

$$F_b(E - E_b) = \pi \int_0^{E - E_b} T(\epsilon)\omega_r(E - E_b - \epsilon)\,d\epsilon.$$

The ratio of emission probabilities of protons to neutrons is

$$\eta(E) = F_p/F_n$$

a function of the incident γ-ray energy.

Theoretical ratios, so calculated, are compared with the experimental ones obtained by Hirzel and Wäffler (1947), for a wide range of nuclei excited by the γ-rays from the ^{7}Li(p, γ) reaction.

§ 2. CALCULATION OF η FOR PROTONS INCIDENT ON A SQUARE WELL

If a square nuclear well is assumed, exact calculations can be made for $T(\epsilon)$. For protons, these involve tabulated Coulomb wave functions (Bloch *et al.* 1951). The relevant theory is given by Blatt and Weisskopf (1952), who give graphs of the excitation functions against energy for nuclei with $Z=30$, 50, 70 and 90. For the purpose of this work experimental neutron and proton separation energies accurate to 300 kev (N. Zeldes, private communication†) are used. From the Blatt and Weisskopf graphs (and interpolations between them) the ratio η is calculated for various nuclei investigated by Hirzel and Wäffler. The results for $E=17{\cdot}6$ MEV are shown in table 3. Also shown are some results originally quoted by Hirzel and Wäffler, which they calculated from the excitation curves of Weisskopf and Ewing. Although they had experimental values of the energy difference $(E_{\mathrm{p}}-E_{\mathrm{n}})$ they had to use two extreme values, 7·5 and 10 MEV, for the neutron separation energy E_{n}.

2.1. *The Effect of the Surface Diffuseness*

This problem has been considered by Scott (1954), and Kikuchi (1957), who calculated penetrabilities for s-wave protons on various target nuclei. (However, Kikuchi's Coulomb barriers seem to be inconsistent with his choice of nuclear radius parameter r_0). Scott discussed the possibility of describing the effect of the diffuse surface by using a larger square well, and gave a prescription for calculating the appropriate radius. This will be considered in more detail later.

The present work is concerned with the nucleus ^{118}Sn, for which a diffuse well,

$$V=-V_0\{1+\exp(r-R_0)/a\}^{-1}$$

with parameters suggested by Melkanoff, Moszkowski, Nodvik and Saxon (1956) is assumed. These are given in table 1.

Table 1. Diffuse Well Parameters

Radius parameter r_0	$1{\cdot}33\times10^{-13}$ cm
Nuclear radius R_0	$6{\cdot}5\times10^{-13}$ cm
V_0	50 MEV
a	$0{\cdot}5\times10^{-13}$ cm

The resulting barriers, for a few orders of l, are shown in figure 1 and it is seen that the 'tail' of the nuclear potential has the effect of pulling down the barrier, and will therefore enhance proton emission.

In calculating a barrier penetrability, we ignore the boundary condition at $r=0$, and consider a static flow problem with a current impinging from infinity on one side of the barrier, and a pure outgoing transmitted wave on the other. This problem is most conveniently solved using the W.K.B. method which, however, breaks down near the top of the barrier. As the lowest barrier is at approximately 8 MEV, the approximation is probably reliable up to about 6 MEV, but not higher. This method in fact overestimates the penetrability. Phase integrals

$$G_l(\epsilon)=\hbar^{-1}\int\{2m(V_l(r)-\epsilon)\}^{1/2}dr$$

---

† Dr. Zeldes gives many references for binding energies, of which the ones numbered 19, 22, 23, 24, 25, 26, 27, 28, 73 are relevant (see Zeldes 1958).

were calculated for various energies by numerical integration. The partial wave penetrabilities are given by

$$T_l(\epsilon)=\exp[-2G_l(\epsilon)].$$

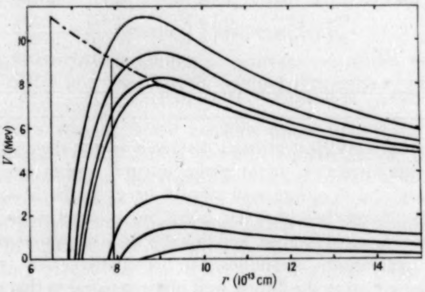

Figure 1. Resultant nuclear, centrifugal and Coulomb barriers for protons (upper group) and neutrons. Also shown (chain line) is the pure Coulomb barrier for s-wave protons, and the modified square well, Coulomb barrier of radius $7{\cdot}9\times10^{-13}$ cm with which an approximation to the diffuse penetrability can be made. This corresponds to $r_0=1{\cdot}62$.

The results are given in table 2, and $T(\epsilon)$ is plotted in figure 2. Also shown is the result of a W.K.B. calculation of $T(\epsilon)$ with a square well of radius $R_0=6{\cdot}5\times10^{-13}$ cm.

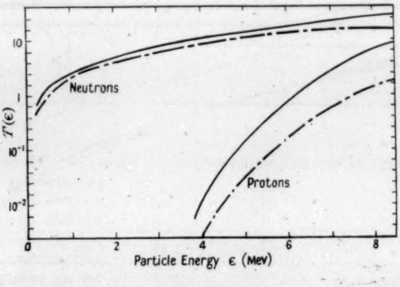

Figure 2. Penetrability $T(\epsilon)$ plotted against energy ϵ for protons and neutrons for a tin nucleus. The full lines pertain to the diffuse nuclear boundary, the chain lines to the sharp (square) boundary of radius $6{\cdot}5\times10^{-13}$ cm.

2.2. *The Enlarged Square Well Approximation*

It is a simple matter to extend Scott's analysis to include a centrifugal barrier. The method replaces the quantity

$$\frac{Ze^2}{r}+\frac{\hbar^2 l(l+1)}{2mr^2}-\epsilon$$

in the phase integral by an exponential which touches it at the inner turning point ($r=\rho$) of the integration. This clearly has the wrong ($r\rightarrow\infty$) asymptotic form,

Table 2. Diffuse Well Penetrabilities for Protons

ϵ (MeV)	3	4	5	6	7	8	9
T_0	$1{\cdot}0\times10^{-4}$	$4{\cdot}2\times10^{-3}$	$4{\cdot}8\times10^{-2}$	0·190	0·530	1·0	1·0
T_1	$0{\cdot}6\times10^{-4}$	$2{\cdot}0\times10^{-3}$	$2{\cdot}5\times10^{-2}$	0·111	0·296	0·84	1·0
T_2	—	$0{\cdot}4\times10^{-3}$	$0{\cdot}5\times10^{-2}$	0·037	0·152	0·38	0·85
T_3	—	$0{\cdot}1\times10^{-3}$	$0{\cdot}1\times10^{-2}$	0·007	0·037	0·11	0·37
T_4	—	—	—	0·002	0·009	0·03	0·08
T_5	—	—	—	—	0·001	0·003	0·01
$T(\epsilon)$	$2{\cdot}8\times10^{-4}$	$12{\cdot}9\times10^{-3}$	$15{\cdot}5\times10^{-2}$	0·775	2·53	6·5	11·6

but the error is only manifest at large distances where the nuclear potential is negligible. So the correction to the phase integral arising from the difference between a diffuse and a square well should be given fairly accurately. It is assumed that the Saxon potential has taken on its asymptotic form of a pure exponential in the region of interest, and this should be a quite reasonable approximation. This assumption simplifies the calculation, but is by no means necessary. After equating the diffuse well phase integral to that of a square well of radius r_1, one again obtains Scott's equation $r_1 = \rho + 0{\cdot}62a$. In deducing this result, one has to assume that the quantity $(a/\rho)(x+2y)(x+y+1)^{-1}$ is less than and not too near unity. Here $x = Ze^2/\rho$, $y = \hbar^2 l(l+1)/2m\rho^2$.

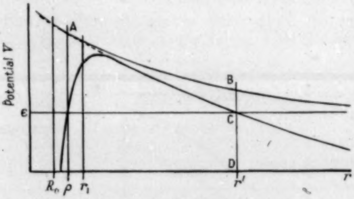

Figure 3. Details of Scott's approximation.

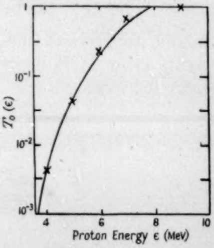

Figure 4. The curve represents the penetrability $T_0(\epsilon)$ for s-wave protons incident on the diffuse nuclear surface (^{118}Sn). The points are the results of an approximate calculation based on an enlarged square well, of radius $7{\cdot}9\times10^{-13}$ cm.

From figure 3 it is clear that the ratio BC/DC is a measure of the accuracy of replacing the Coulomb and centrifugal tail AC by the exponential AB. This ratio is given by

$$\mathrm{BC}/\mathrm{DC} = (x+y-1)\exp[-(x+2y)(x+y-1)^{-1}\{2y[(x^2+4y)^{-1/2}-x]-1\}].$$

An examination of this function indicates that the ratio BC/DC is never likely to be greater than 20%. ρ is obviously energy dependent, and dependent on l to an unimportant extent; so to make the approximation useful for computing penetrability against energy curves, one has to choose some value of ϵ (say half the barrier height) and take the corresponding value of ρ in the formula for r_1.

In figure 4 Scott's approximation of using a square well of radius r_1 is compared with the diffuse well calculation for s-wave protons. It fails only near the top of the barrier where the W.K.B. method is itself unreliable. The accuracy of the approximation will increase with l.

§ 3. NEUTRON PENETRABILITIES

The centrifugal barriers pertaining to neutrons are shown in figure 1. As the barriers are rather low, the W.K.B. method of calculating penetrabilities is unreliable even at low energies.

However, at Los Alamos, some machine calculations have been done on neutron penetrabilities with a Saxon potential (Beyster *et al.* 1957). A small imaginary part is included in the potential, and the resulting absorption lowers the penetrabilities by about 10%. This error is not critical for the present purpose, so these penetrabilities have been assumed. The appropriate quantity $T(\epsilon)$ is plotted in figure 2 together with the corresponding exact square well ($R=6{\cdot}5\times10^{-13}$cm) result, calculated from expressions given by Blatt and Weisskopf.

§ 4. CALCULATION OF EXCITATION FUNCTIONS AND DISCUSSION OF SHELL EFFECTS

The values of the functions F_n, F_p were calculated using $E=17{\cdot}6$ Mev and the separation energies $E_p=10{\cdot}0\pm0{\cdot}2$ Mev and $E_n=9{\cdot}2\pm0{\cdot}2$ Mev. For the level densities in the residual nuclei, the empirical formula

$$w(U)=0{\cdot}015\exp(5{\cdot}1U^{1/2})$$

was used in agreement with Blatt and Weisskopf. The question naturally arises whether this is the best one can do. The residual nuclei in the two emission processes must be given the same level densities because the parameters of the empirical formula vary smoothly with A and Z. This is compatible with a complete neglect of shell effects. Newton (1956) has developed a formula for level density which includes shell effects. This is used in conjunction with a pairing energy which essentially re-defines the ground states of even–even, and even–odd nuclei to bring them into line with a smooth curve through the ground

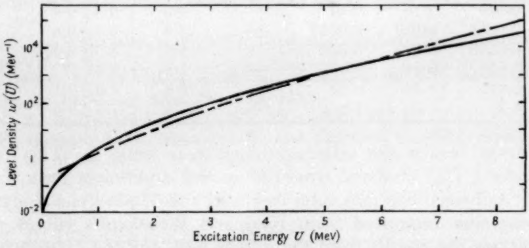

Figure 5. A plot of $w(U)$, the nuclear level density against excitation energy U. The full line represents the empirical formula of Blatt and Weisskopf. The chain line represents the formula of Newton. The curves refer to both $^{117}_{50}$Sn and $^{117}_{49}$In.

states of odd–odd nuclei. Theoretically, the reason for doing this is that the pairing energy is a co-operative phenomenon which cannot be included in a Fermi gas model of non-interacting particles.

For the two residual nuclei (^{117}Sn, ^{117}In) under consideration, the Newton formulae turn out to be almost identical. The resulting level density is plotted against excitation energy U in figure 5, with the above mentioned empirical formula for comparison. In addition, as they are both even–odd type nuclei, they have approximately the same pairing energy of 1·2 Mev. To obtain a rough orientation on the effect the pairing energy has on the ratio η, we can consider the maximum values of the integrands of F_n and F_p. The effect on these indicates that the ratio η would be decreased by at most a factor 3.

Except for shell effects, the theory is slowly varying with nuclear parameters such as A and Z. It follows that in order to obtain information about photo-disintegration of the nucleus ^{117}Sn, we can use the figures so far obtained, and merely substitute in the appropriate binding and pairing energies. This nucleus is a more critical case, since the residual nucleus (^{116}In) after proton emission is odd–odd, and has no pairing energy. That after neutron emission (^{116}Sn) is even–even, and has a pairing energy of about 2 Mev. By using a method similar to the previous case we obtain an overall enhancement of proton emission by a factor of about 10.

Table 3. The Ratio η as a Percentage

Nucleus	H.W. $E_n = 10$	H.W. $E_n = 75$	B.W. theory	Revised theory	H.W. expt.	Expt. E_p	Expt. E_n
$^{118}_{50}$Sn	0·0021	0·018	0·0063	0·02	1·1	10·0 ± 0·2	9·2 ± 0·2
$^{117}_{50}$Sn	0·0008	0·014	0·0013	~0·05	2·2	9·6 ± 0·2	7·1 ± 0·2
$^{113}_{48}$Cd	0·0046	0·054	0·0015	—	4·6	9·5	6·4
$^{112}_{48}$Cd	0·019	0·10	0·47	—	4·0	9·8 ± 0·4	9·5 ± 0·4
$^{111}_{48}$Cd	0·0018	0·029	0·0055	—	3·4	8·8 ± 0·6	6·7 ± 0·6
$^{105}_{46}$Id	0·0078	0·077	0·022	—	5·5	8·5 ± 0·35	6·8 ± 0·35
$^{98}_{42}$Mo	0·026	0·14	0·050	—	2·8	9·4	8·3
$^{77}_{34}$Se	0·021	0·20	0·20	—	4·8	9·6 ± 0·1	7·4 ± 0·1
$^{53}_{24}$Cr	4·7	—	1·3	—	32·4	11·3 ± 0·6	7·9 ± 0·6

All relevant results are collected together in table 3. This table shows values of ratio η (%) obtained from theory and experiment for various nuclei. The second and third columns refer to Hirzel and Wäffler as already explained. Column four was computed from Blatt and Weisskopf's curves. The fifth column contains the results from the diffuse well, and the experimental results of Hirzel and Wäffler are in column six. The last two columns contain experimental separation energies.

§ 5. Conclusion

It is clear from figure 2 that the penetrability of the diffuse nuclear surface to protons is greater than that of the corresponding sharp surface by a factor of about 5. At the same time, the factor by which neutron penetrability is so enhanced is less than 2. This is understandable, as figure 1 shows. In the important region, the pure Coulomb barrier is much steeper than the centrifugal barriers and consequently is pulled down much more by the effect of the nuclear potential. This enhancement of proton emission is not in itself sufficient to clear up the discrepancy between theory and experiment. As already explained, we may obtain a further factor from a consideration of the shell effects in the residual nuclei, and in the case of the nucleus ^{117}Sn a factor of 10 came from this cause. But as table 3 shows, the final ratio η for this latter nucleus is still too small by a factor 40.

There have been more recent experiments, mainly using bremsstrahlung, and these appear to confirm the order of magnitude of Hirzel and Wäffler's results (e.g. Butler and Almy 1953, Ferrero *et al.* 1957). The fact that the theory continues to disagree significantly with experiment is good evidence that there is a competing direct interaction process, which provides most of the observed protons.

The increase in penetrability, arising from the nuclear surface diffuseness, is obviously not a very important effect, and one is quite justified in using an approximation to allow for it. In so far as the W.K.B. method is reliable this may be done simply by using an enlarged square well. Whether this approximation is good independently of the W.K.B. method is not clear, but it does not seem an unreasonable supposition.

ACKNOWLEDGMENTS

I would like to thank Professors J. S. Levinger and R. E. Peierls for much helpful discussion and criticism. Dr. Zeldes supplied some valuable information, for which I am very grateful.

I am also grateful to the Department of Scientific and Industrial Research for their award of a maintenance grant.

REFERENCES

BEYSTER, J. R., SCHRANDT, R. G., WATT, M., and SALMI, E. W., 1957, *Los Alamos Report*, LA-2099.

BLATT, J. M., and WEISSKOPF, V. F., 1952, *Theoretical Nuclear Physics* (New York: Wiley), chap. VII, 5, 6.

BLOCH, I., HULL, M. M., BROYLES, A. A., BOURICIUS, W. G., FREEMAN, B. E., and BREIT, G., 1951, *Rev. Mod. Phys.*, **23**, 147.

BUTLER, W. A., and ALMY, G. M., 1953, *Phys. Rev.*, **91**, 58.

FERRERO, F., HANSON, A. O., MALVANO, R., and TRIBUNO, C., 1957, *Nuovo Cim.*, **6**, 585.

HIRZEL, O., and WÄFFLER, H., 1947, *Helv. Phys. Acta*, **20**, 373.

KIKUCHI, K., 1957, *Prog. Theor. Physics*, **17**, 643.

MELKANOFF, M. A., MOSZKOWSKI, S. A., NODVIK, J., and SAXON, D. S., 1956, *Phys. Rev.*, **101**, 507 (L).

NEWTON, T. D., 1956, *Canad. J. Phys.*, **34**, 807.

SCOTT, J. M. C., 1954, *Phil. Mag.*, Ser. 7, **45**, 441.

WEISSKOPF, V. F., and EWING, D. H., 1940, *Phys. Rev.*, **57**, 472.

ZELDES, N., 1958, *Nuclear Physics*, **7**, 27.

Complete Absorption of Light by Thin Metal Films

BY T. TURBADAR
University of Damascus, Syria, U.A.R.†

Communicated by W. T. Welford; MS. received 3rd *July* 1958,
in revised form 4*th September* 1958

Abstract. Reflectances of non-opaque aluminium films were measured from the substrate side as a function of angle of incidence. For the p-polarization there is a maximum reflectance near the critical angle for the substrate; for a certain range of Al thicknesses this is followed by a sudden drop which can be to zero reflectance giving complete absorption. This effect can be predicted from thin film theory but has not previously been noted.

§ 1. INTRODUCTION

IT is well known that a metallic film deposited on a glass plate has two different reflectances, one at the air side R, and the other at the substrate side R', this being always smaller than R for any thickness of the film in the case of normal incidence (Faust 1950, Rouard, Malé and Trompette 1953). The variation of R' with the angle of incidence ϕ was investigated theoretically by Abelès (1957), but no experimental results were given. The author has chosen Al film in his investigation of the variation of R' with ϕ, because of its increasing use in beam splitters.

The aluminium films were deposited on glass by evaporation from tungsten loops after pre-fusing in vacuum. The source-substrate distance was 20 cm. The pressure during evaporation was about 10^{-5} mm Hg. The evaporation time was not strictly controlled but was usually less than 30 seconds. The substrate, polished optical glass, was chemically cleaned and then cleaned by ionic bombardment immediately before evaporation. Its temperature during evaporation was not measured but was certainly less than 50 °C. The substrate was made of a prismatic shape of about 2° 30′ to avoid multiple reflections, but this put a limit of about 39° to the angle of incidence from glass to Al, due to total internal reflection at the interface glass–air. This limit could be extended to about 42° if a parallel glass plate were used. To extend the limit of ϕ further, a right angle prism was used with the Al film deposited on its hypotenuse. In this way, the reflectance R' of the Al film at the glass side could be investigated beyond the critical angle of total reflection of glass.

§ 2. METHOD OF MEASUREMENT

The reflectance R' was measured for both planes of polarization, **E** vector parallel to the plane of incidence (p) and perpendicular (s). Both R_p' and R_s' were calculated from the following relation allowing for two reflections at glass–air interfaces:

$$R' = \frac{I'}{I}\frac{1}{(1-r_\phi)^2}$$

---

† This work was carried out while the author was a guest worker at the Technical Optics Section, Imperial College of Science and Technology, London.

where I and I' represent respectively the intensities of the incident and reflected light. They were measured with the Wright spectrophotometer (Wright 1954). The reflectance r_ϕ of the glass of the prism at the angle of incidence in air ϕ was obtained from experimental curves (r, ϕ) which were plotted for both planes of polarization.

§ 3. EXPERIMENTAL RESULTS

Figures 1*a*, *b*, *c*, and *d* show the curves giving R_p' and R_s' as functions of the angle of incidence in glass ϕ_g for Al films of different thicknesses. The

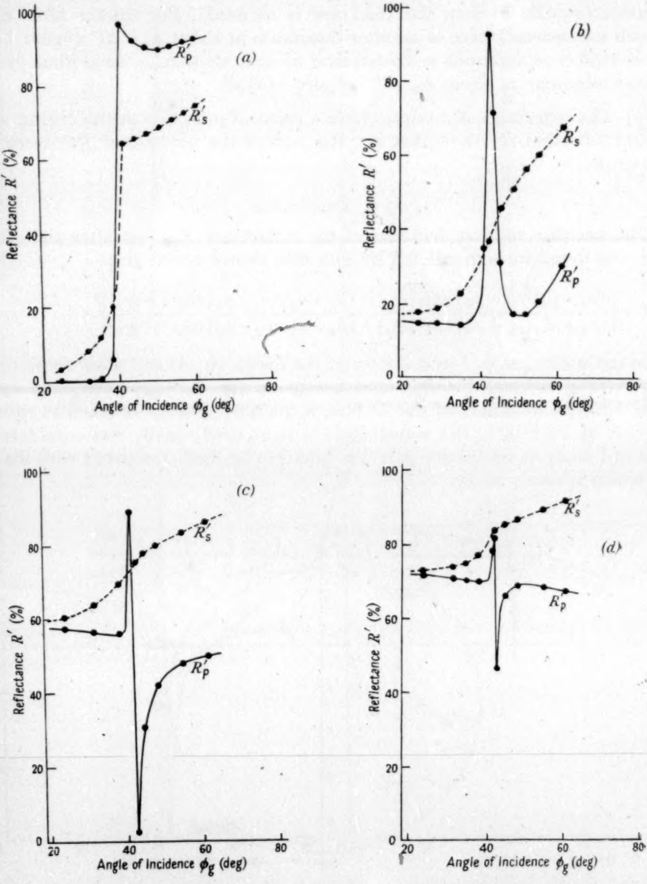

Figure 1. (*a*) Al film $\simeq 25$ Å; (*b*) Al film $\simeq 80$ Å; (*c*) Al film $\simeq 125$ Å; (*d*) Al film $\simeq 190$ Å.

conclusions which may be drawn from these experimental results are the following:

(*a*) The reflectance R_p' reaches a maximum value just after the critical angle of total reflection for glass has been reached. This maximum value decreases as the thickness of the Al film increases. R_p' decreases from its maximum very rapidly to a minimum whose value depends also on the thickness of the Al film. It is only 0·028 for a film whose transmittance at normal incidence is about 0·10 (figure 1(*c*)), and increases when the film is thinner or thicker, as shown in figures 1 (*a*), (*b*), (*d*). For thinner films the minimum broadens and its value increases towards 1 when the thickness is reduced. For thicker films which are still transparent there is another maximum at about $\phi_g = 50°$ (figure 1 (*d*)). Theoretical considerations as shown later on indicate that for such films there is a broad minimum at about $\phi_g = 70°$ (figure 3 (*d*)).

(*b*) The reflectance R_s' curves have a point of inflection at the critical angle of total reflection for the substrate, the rate of the increase of R_s' decreasing afterwards.

§ 4. Discussion

The peculiar sudden decrease of the reflectance R_p' just after the critical angle was found to be predicted by thin film theory which gives

$$R' = \left| \frac{(\mu_2 - \mu_1)(\mu_1 + \mu_0)\exp(ig_1) + (\mu_2 + \mu_1)(\mu_1 - \mu_0)\exp(-ig_1)}{(\mu_2 + \mu_1)(\mu_1 + \mu_0)\exp(ig_1) + (\mu_2 - \mu_1)(\mu_1 - \mu_0)\exp(-ig_1)} \right|^2 \quad \ldots\ldots (1)$$

where the subscripts 0, 1 and 2 refer to the media air, Al and glass respectively, and where $\mu = n/\cos\phi$ for R_p', and $\mu = n\cos\phi$ for R_s' ; $g_1 = (2\pi/\lambda)n_1h_1\cos\phi_1$, where h_1 is the thickness of the Al film, n_1 its refractive index taken as equal to $0{\cdot}79 - 5{\cdot}3i$ at $\lambda = 5500$ Å, the wavelength of light used; $\cos\phi_1$ was considered as equal to 1 since its imaginary part was found to be small compared with the real part which is nearly unity.

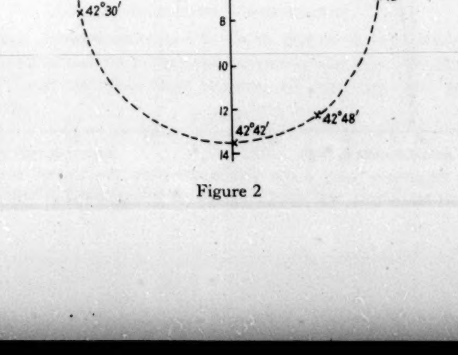

Figure 2

By dividing equation (1) by $(\mu_2+\mu_1)(\mu_1+\mu_0)\exp(ig_1)$ we get:

$$\mathrm{R}' = \left| \frac{\dfrac{\mu_2-\mu_1}{\mu_2+\mu_1} + \dfrac{\mu_1-\mu_0}{\mu_1+\mu_0}\exp(-2ig_1)}{1 + \dfrac{\mu_2-\mu_1}{\mu_2+\mu_1}\dfrac{\mu_1-\mu_0}{\mu_1+\mu_0}\exp(-2ig_1)} \right|^2 \quad \ldots\ldots(2)$$

In the range $\phi_g = 42° \rightarrow 44°$, the first term of the numerator in equation (2) is very nearly constant in the case of R_p'; its average value $-0{\cdot}668+0{\cdot}601i$ is represented on the Argand diagram as OA (figure 2). In the same range of ϕ_g

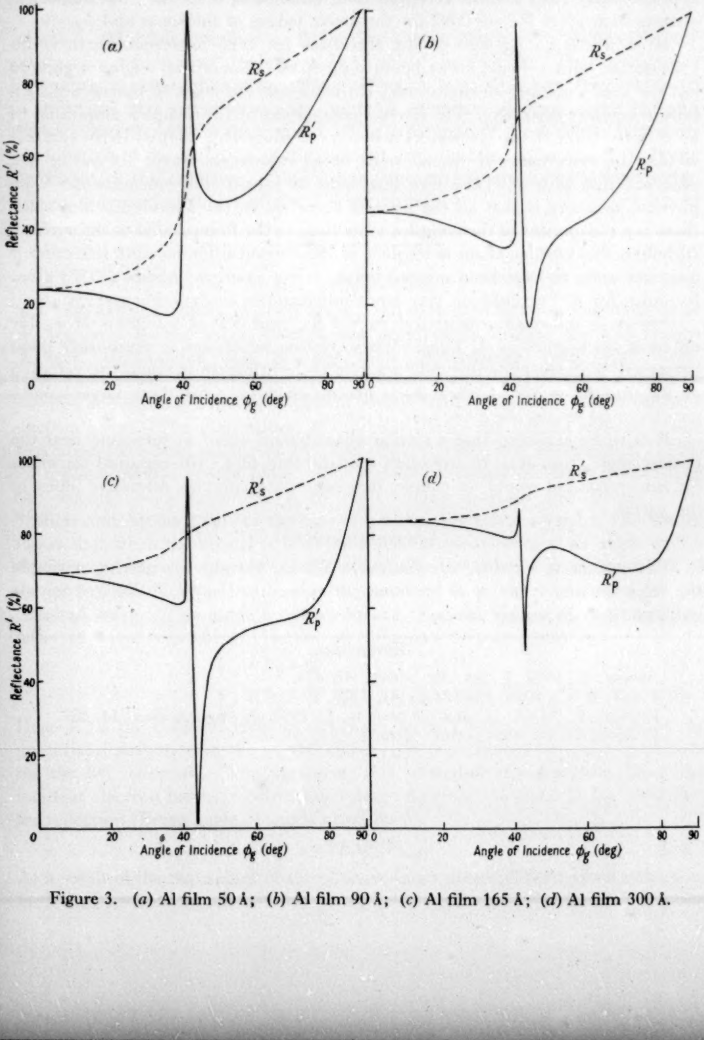

Figure 3. (*a*) Al film 50 Å; (*b*) Al film 90 Å; (*c*) Al film 165 Å; (*d*) Al film 300 Å.

the term $(\mu_1-\mu_0)/(\mu_1+\mu_0)$ varies rapidly as can be seen in the diagram; its vector OB_m describes the dotted circle of diameter approximately 13·5. The quantity $\exp(-2ig_1)$ has a slowly varying argument but its modulus can range from unity to zero according to the thickness chosen for the Al film. Thus it can be seen that for a given g_1 there will be a certain angle of incidence at which the numerator in equation (2) is a minimum in the case of R_p', this angle being approximately that for which OB_m points in the opposite direction to OA. Furthermore, there will be one particular value of thickness at which the minimum value of R_p' is actually zero. Graphically we find that this value is approximately 165 Å and the corresponding value of ϕ_g is 43° 25′; but numerical computation gives $R_p'=0{\cdot}0092$ for the above values of thickness and ϕ_g.

It is worth noting that at the thickness for zero reflection, there is no transmitted light. This follows because ϕ_g exceeds the critical angle for glass to air, the final medium, so that $\cos\phi_a$, the cosine of the angle of emergence, is a pure imaginary quantity. The normal component of the complex amplitude in air is of the form $A\exp(i\cos\phi_g z)$, where z is a coordinate normal to the surface, so that the disturbance in the air must be an evanescent wave. It was in fact observed that with the 125 Å film there was no measurable transmission. The physical meaning is that all the light is absorbed in the aluminium film since there is a component of the complex amplitude in the film parallel to the surface. Although this curious effect is implicit in the formulae for metallic reflection it does not seem to have been noticed before. For example, Abelès (1957) gives formulae for R' but does not give any computational or experimental results.

Figure 3 shows the theoretical curves R_p' and R_s' as functions of ϕ_g for different thicknesses of Al films. These results which are in reasonably good agreement with the experimental ones give more information about the variation of R_p' and R_s' with ϕ_g when ϕ_g is greater than 60°; for these larger angles experimental results were not easy to obtain.

It is to be expected that a similar effect would occur at reflection near the critical angle from glass to any other metallic thin film; the required thickness for zero reflection would, of course, depend on the complex refractive index of the metal.

ACKNOWLEDGMENTS

The author is indebted to Professor W. D. Wright for making available the experimental facilities of his laboratories, and to Dr. W. T Welford for his guidance and invaluable advice.

REFERENCES

ABELES, F., 1957, *J. Opt. Soc. Amer.*, **47,** 473.
FAUST, R. C., 1950, *Phil. Mag.*, **41,** 1238.
ROUARD, P., MALÉ, D., and TROMPETTE, J., 1953, *J. Phys. Radium*, **14,** 587.
WRIGHT, W. D., 1954, *Optica Acta*, **1,** 102.

Multiple Interference Fringes in Electron Micrographs of Wedge-Shaped Single Crystals

By R. E. BURGE

Wheatstone Physics Laboratory, University of London, King's College

Communicated by J. T. Randall; MS. received 7th August 1958,
in final form 26th September 1958

Abstract. Multiple interference fringes have been observed in electron micrographs of wedge-shaped single crystals of poly-L-proline II. The interference fringes which occur when strong Bragg reflection is possible have been observed to split into two components as a result of secondary electron scattering and double refraction within the crystals. The separation of the fringe components is a function of the deviation of the incident electron beam from the exact Bragg condition for the reflection. The fringe contours are qualitatively interpreted using the dynamical theory of electron scattering.

---

§ 1. INTRODUCTION

INTERFERENCE effects in both bright and dark field electron micrographs of regularly shaped single crystals and polycrystalline films are well known (e.g. Heidenreich and Sturkey 1945, Heidenreich 1949, Hall 1948, Hashimoto 1954). Interference fringes occur when strong Bragg reflection is possible and represent lines of constant crystal thickness parallel to the incident electron beam. The distribution of intensity within the fringes and the fringe separation have been calculated by MacGillavry (1940) and Heidenreich (1949) for a plane-parallel crystal plate. The dynamical theory of electron scattering has recently been extended (Kato 1949, 1952 a, b, Kato and Uyeda 1951, Molière and Niehrs 1954) to the case of a finite polyhedral crystal. The theory shows that when the crystal is oriented to the incident beam at an angle within the range where a given reflection is observable the effective inner potential of the crystal assumes two values for the primary wave and two values for the reflected wave. The inner potential values, V_{p} and V_{r}, for the primary and reflected waves respectively (Honjo and Mihama 1954), are given by

$$V_{\mathrm{p}} = V_0 + |V_{hkl}|[\epsilon \pm (1+\epsilon^2)^{1/2}] \qquad \ldots\ldots(1)$$

$$V_{\mathrm{r}} = V_0 + |V_{hkl}|[-\epsilon \pm (1+\epsilon^2)^{1/2}]. \qquad \ldots\ldots(2)$$

Here V_0 is the constant term in the usual Fourier series representation of the potential distribution in the crystal and V_{hkl} is the relevant structure amplitude for the *hkl* reflection. The parameter ϵ is related to the deviation $\Delta\theta$ of the incident electron beam (accelerating voltage E) from the exact Bragg condition for reflection (Bragg angle θ) and is given by

$$\epsilon = 2E\Delta\theta / |V_{hkl}|. \qquad \ldots\ldots(3)$$

As a result of the two values of the effective inner potential for a given reflection, both the incident and reflected waves are doubly refracted; the double refraction is conveniently represented by assuming four refractive indices for the crystal given by the expressions (excluding the relativity correction)

$$n_{\mathrm{p}}=1+V_{\mathrm{p}}/2E, \quad \text{and} \quad n_{\mathrm{r}}=1+V_{\mathrm{r}}/2E,$$

where V_{p} and V_{r} are given by equations (1) and (2).

As the deviation from the Bragg angle increases the refractions of the two components of the primary waves arising on passing through a wedge-shaped single crystal also increase; strong diffraction has been observed for the (220) reflection of MgO for ϵ in the range from $+2{\cdot}0$ to $-1{\cdot}5$, and smaller ranges have been observed for other reflections (Honjo and Mihama 1954, Molière and Niehrs 1955, Cowley, Goodman and Rees 1957).

In this work interference fringes are reported in electron micrographs of crystals of poly-L-proline II. The molecule of this poly-amino acid has a helical configuration (Cowan and McGavin 1955) and the crystals to be described here are monoclinic, space group $P2_1$, $a=11{\cdot}00\,\text{Å}$, $b=6{\cdot}94\,\text{Å}$, $c=9{\cdot}36\,\text{Å}$, $\beta=90^{\circ}$ as determined by electron diffraction (Burge 1957), chain axis along c.

The fringes are found to split into two components (an observation which has not been made before) under suitable conditions which depend on the crystal thickness and the deviation from the Bragg angle for the (101) reflection.

§ 2. THE ELECTRON MICROSCOPY OF POLY-L-PROLINE II

Specimens were prepared by slow evaporation of aqueous solutions of the polymer (average degree of polymerization 20, average chain length 60 Å) and nucleation of the crystals directly on stainless steel specimen grids without specimen films. The chain axes of the helical molecules are perpendicular to the fibre axis.

Typical bright and dark field electron micrographs of the fibrous crystals (taken using a Metropolitan-Vickers E.M.3 electron microscope, accelerating voltage 75 kv, angular aperture of objective lens 3×10^{-3} radian) are shown in figures 1 and 2 (Plate I).

Under the conditions of figure 1 reflected electrons from all possible lattice planes within the crystal were intercepted by the objective aperture. The dark field image was formed entirely by reflected electrons and incoherently scattered electrons. The incoherent scattering gave rise to the density defining the fibre outline and the reflected electrons to the sharp lines of increased density adjacent to and parallel to one edge of the main fibre and attached spines. The observation of Bragg fringes on one side of the fibre only is due to the fact that the dark field image was produced by displacement of the objective aperture. Reflected electrons on one side of the symmetry axis of the incident electron beam were intercepted by the aperture; the transmitted electrons were reflected by planes separated by a minimum of 6 Å ($d_{101}=7{\cdot}13\,\text{Å}$).

All the spines growing from the main fibre axis are in a similar orientation to the incident beam and typical higher magnification micrographs of single spines are shown in figures 3 (*a*), (*b*), and (*c*) (Plate II).

Longitudinal interference fringes (the dark fringes represent lines of minimum electron transmission) are clearly visible running along the spines though the fringe contours differ in the three cases; the fringes represent lines of constant crystal thickness.

The splitting of fringes into doublets of equal density is shown to a greater or lesser extent in figures 3 (*a*), (*b*), and (*c*) and both the inter-fringe and intra-fringe separations vary along the lengths of the spines. Spines (*a*) and (*b*) are very similar in thickness and shape and in both cases the inter-fringe separation varies from zero to about 300 Å in a continuous manner. The splitting of the fringes into doublets is observed for (*a*) only near the base of the spine, but in (*b*) the separation appears along almost the entire spine length and the intra-fringe separation varies from zero to about 170 Å. In (*c*) the thickness of the spine is roughly constant along its length and the inter- and intra-fringe separations are approximately 360 Å and 140 Å respectively. The disposition of the fringes observed along other spines was of the same general type as that shown in figure 3 though the separations of the doublets were very variable.

§ 3. DISCUSSION

The theory developed by MacGillavry (1940) and Heidenreich (1949) predicts that diffraction maxima occur for electrons reflected from a crystal plate of thickness D when the following relation is satisfied:

$$\left[\frac{V^2_{hkl}}{E^2} + \Delta\theta^2 \sin^2 2\theta\right]^{1/2} = \frac{m\lambda}{2D}, \quad m = 1, 3, 5. \qquad \ldots\ldots (4)$$

For electrons incident at the Bragg angle on plane-parallel crystals of different thicknesses transmission minima in electron micrographs may be expected for crystals with thicknesses D_m where $D_m = mE\lambda/2V_{hkl}$.

The theory, without modification, cannot be quantitatively applied to a crystal of varying thickness although a periodic dependence of the intensity of the transmitted electrons on the crystal thickness may be expected. (Equation 4 predicts that the increment of crystal thickness between successive fringes for the (101) reflection ($V_0 = 8{\cdot}1$ volts, $V_{101} = 1{\cdot}70$ volts) is 1900 Å which is in considerable error as judged by the resolution in the micrographs shown in figure 3). The general features of the changes of inter-fringe separation may, however, be qualitatively explained on the basis of a periodic dependence of the intensity of the transmitted electrons on crystal thickness if a continuous decrease in thickness gradient across spine cross sections as the distance from the tip increases is assumed. The inter- and intra-fringe separations increase at the same rate along a given spine and the observed fringe systems may be considered as two superimposed single fringe systems with slightly different values of the thickness increment between adjacent fringes.

The differences in intra-fringe separation between figures 3 (*a*), (*b*) and (*c*) correspond to differences in the values of the deviations from the Bragg angle appropriate to the three cases. In figure 3 (*a*) the high fringe contrast and the small degree of splitting of the fringes into two components indicates a small value of $\Delta\theta$ while larger values are applicable to figures 3 (*b*) and (*c*); it was not possible to measure $\Delta\theta$ with the specimen stage used. At the Bragg angle the effective inner potential values in the crystal are $V_0 \pm V_{hkl}$ (a result first deduced by Sturkey (1948)) and the separation between the transmitted waves in the crystal is a minimum.

Two superimposed fringe systems of the type observed may be explained in one of two ways, depending on whether the crystal is perfect or contains discontinuities (though it is difficult to understand why the observed fringe components are of the same density). For a perfect crystal the fringes might be ascribed to dynamical interaction and for a discontinuous crystal to secondary scattering. The first explanation has been advanced by Renninger (1937) and Heidenreich (1950) to explain the appearance of the ' forbidden ' (222) and (002) reflections in both x-ray and electron diffraction patterns from diamond and the second by many authors, e.g. Cowley, Rees and Spink (1951), to explain similar reflections in electron diffraction patterns from disordered or mosaic crystals. The (101) reflection in poly-L-proline II can arise both in the normal manner and as a multiple reflection from two sets of suitable lattice planes by either of these processes, but, in the crystals considered, which are made up of discontinuous lengths of polymer chain, the second process appears to be the more likely. The path lengths of the multiply reflected electrons in the wedge-shaped crystals will differ from those only reflected once and the separations of the doubly refracted components will differ. The separations of the doubly refracted transmitted wave components and the magnitudes of the beat wave vectors between them (which govern the dimensions of the interference fringes) will increase with deviation from the exact Bragg condition for reflection.

Acknowledgments

I wish to thank Professor J. T. Randall for encouragement and the provision of facilities, and Dr. E. Katchalski for the sample of poly-L-proline II.

References

Burge, R. E., 1957, *Ph.D. Thesis*, University of London.
Cowan, P. M., and McGavin, S., 1955, *Nature, Lond.*, **176**, 501.
Cowley, J. M., Goodman, P., and Rees, A. L. G., 1957, *Acta Cryst., Camb.*, **10**, 19.
Cowley, J. M., Rees, A. L. G., and Spink, J. A., 1951, *Proc. Phys. Soc.* A, **64**, 609.
Hall, C. E., 1948, *J. Appl. Phys.*, **19**, 198.
Hashimoto, H., 1954, *J. Phys. Soc. Japan*, **9**, 150.
Heidenreich, R. D., 1949, *J. Appl. Phys.*, **20**, 993.
—— 1950, *Phys. Rev.*, **77**, 271.
Heidenreich, R. D., and Sturkey, L., 1945, *J. Appl. Phys.*, **16**, 97.
Honjo, G., and Mihama, K., 1954, *J. Phys. Soc. Japan*, **9**, 184.
Kato, N., 1949, *Proc. Imp. Acad. Japan*, **25**, 41.
—— 1952 a, *J. Phys. Soc. Japan*, **7**, 397.
—— 1952 b, *Ibid.*, **7**, 406.
Kato, N., and Uyeda, R., 1951, *Acta Cryst.*, **4**, 227.
MacGillavry, C. H., 1940, *Physica*, **7**, 329.
Molière, K., and Niehrs, H., 1954, *Z. Phys.*, **137**, 445.
—— 1955, *Ibid.*, **140**, 581.
Renninger, M., 1937, *Z. Phys.*, **106**, 141.
Sturkey, L., 1948, *Phys. Rev.*, **73**, 183.

Thermoelectric Measurements on Natural Galena at Low Temperatures

By D. M. FINLAYSON and D. GREIG[†]

Department of Natural Philosophy, University of Aberdeen

MS. received 4th September 1958

Abstract. The thermoelectric power of n-type single crystals of natural galena has been measured down to liquid hydrogen temperatures. The theory developed by Howarth and Sondheimer fits the experimental results fairly well. An electron effective mass ratio in the range 0·11–0·19 was obtained. No evidence of phonon drag effects was observed.

---

§ 1. INTRODUCTION

THE thermoelectric power of lead sulphide has been measured at low temperatures by Devyatkova *et al.* (1941) but only samples of high electron density were used. Since we had available natural single crystals covering a fairly wide range of electron densities (Finlayson and Greig 1956, to be referred to as I), it seemed worth while to carry out thermoelectric measurements and compare them with recent theories especially that developed by Howarth and Sondheimer (1953) which considers the behaviour of polar semiconductors. It was hoped that thermoelectric measurements might indicate the relative importance of the optical modes in the carrier scattering processes.

§ 2. EXPERIMENTAL METHODS

The rectangular samples were similar to those discussed in I. They were held between two copper blocks enclosed in a copper can, the upper block being in good thermal contact with the can which in turn was soldered to the hydrogen or helium bath. The upper block was drilled to form a 1 cm^3 cavity which served as the bulb of a gas thermometer. This block carried a bakelite platform on which rode the lower block, insulated electrically and thermally from the upper, and carrying a 100Ω heating coil. The lower block was lightly sprung to allow for thermal contraction. Copper–constantan thermocouples were attached to the crystals which were kept in good thermal and electrical contact with the copper blocks.

The thermocouple e.m.f's and the thermoelectric e.m.f. between the two probes were measured on a Tinsley No. 3184 potentiometer. The thermocouples were calibrated against the gas thermometer with helium gas in the copper can to ensure equilibrium.

Experimental difficulties were encountered in attaching the crystals to the copper blocks and the thermojunctions to the crystals. For the former, three methods were used: (*a*) a 34 s.w.g. platinum wire was welded to the end of the crystal and the wire then soldered to the block, (*b*) the crystal was cemented under pressure to the block by ‘ Araldite ’ or ‘ Elargol W4 ’ conducting cement, (*c*) the ends of the crystal were copper plated and then soldered to the block. The 46 s.w.g. thermojunctions were welded directly to the crystal as described in I.

[†] Now at the National Research Council, Ottawa.

The following tests were employed to check the effectiveness of these arrangements (cf. Geballe and Hull 1954). (i) When the temperature gradient between the ends of the sample was changed by a factor of 5, no systematic change was observed in the thermoelectric power Q. (ii) When Q was measured in helium and then under vacuum, differences were sometimes observed. If this difference was greater than 10%, the crystal was remounted. The final measurements were taken under vacuum. (iii) Q did not change by more than a few per cent when a crystal was remounted, provided it passed tests (i) and (ii). In addition, a number of crystals, having the same electron density as those described, were measured at room temperature and found to have the same value of Q.

It was estimated that the relative error of a single value of Q was about 7%, but since the curves represent values taken over several runs, the final error in Q will be somewhat less.

The values of electron density quoted were obtained from Hall effect measurements which, as observed in I, remained approximately constant over the whole temperature range.

§ 3. DISCUSSION

In a polar semiconductor the high frequency optical modes may be at least as important as the acoustic modes in scattering the carriers. This has been discussed at length by Howarth and Sondheimer (1953, to be referred to as HS). They point out that at low temperatures it is not possible to define a time of relaxation and hence the conventional expressions for thermoelectric power cannot be obtained. Their calculations lead directly to rather complex formulae covering all ranges of temperature and degeneracy. In our temperature range the HS theory must be used when discussing optical scattering, but one must still determine, if possible from the experimental results, whether optical, acoustic or some other form of scattering is predominant at any particular temperature. Considering for the moment only optical and acoustic scattering, at sufficiently low temperatures the acoustic waves will predominate (Ehrenberg 1958, p. 186). Accordingly, we have fitted an ' acoustic ' curve to each of our experimental plots at the lowest available temperature.

3.1. *Non-Degenerate Range. Acoustic Scattering*

If we assume a simple scattering process in which the mean free path is proportional to ϵ^{s} where ϵ is the energy of the electrons, then (Johnson 1956)

$$Q = -\frac{k}{e}[(2+S) - \mathscr{J}^{*}] \qquad \ldots\ldots(1)$$

where $\mathscr{J}^{*}$ is the reduced Fermi level.

For acoustic scattering $S=0$ and the thermoelectric power is then given by

$$Q = -\frac{k}{e}[\ln RT^{3/2} - \ln r - 5\cdot16 + 1\cdot5 \ln m^{*}/m_0]. \qquad \ldots\ldots(2)$$

This equation was fitted to the experimental curve for Q shown in figure 1 at 30° K by assuming a suitable value of the effective mass ($m^{*}/m_0 = 0\cdot13$). Using this value of the effective mass, the curve of Q appropriate to acoustic scattering was plotted from equation (2) as shown and found to deviate considerably from the experimental values.

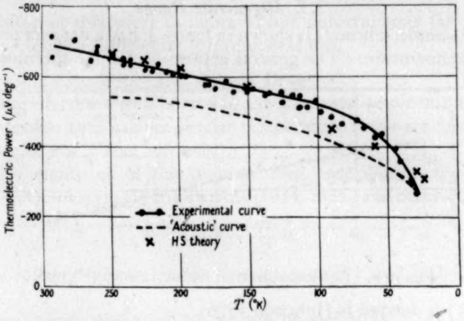

Figure 1. Extrinsic electron density $1{\cdot}4 \times 10^{16}$ cm^{-3}.

3.2. *Non-Degenerate Range. HS theory of optical scattering*

The HS expression for the thermoelectric power due to optical scattering in the non-degenerate range gives

$$Q = -\frac{k}{e}[\ln RT^{3/2} - \ln r - 7{\cdot}16 + 1{\cdot}5 \ln m^*/m_0 + \zeta] \qquad \ldots\ldots (3)$$

where ζ varies with temperature and is presented as a plot against Θ/T where Θ is the Debye temperature (194° K for PbS). We assumed that at fairly high temperatures optical scattering would predominate and fitted equation (3) to the experimental curve of figure 1 at 250° K (at higher temperatures this sample moves into the intrinsic range). The effective mass required at 250° K was $m^*/m_0 = 0{\cdot}19$. The curve then obtained from equation (3) agreed fairly well with the experimental values.

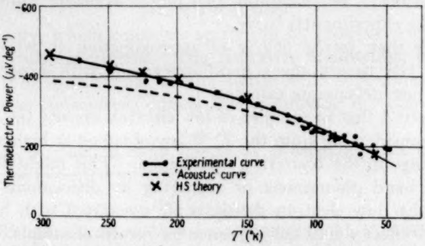

Figure 2. Extrinsic electron density $1{\cdot}4 \times 10^{17}$ cm^{-3}.

A similar process was applied to the curve shown in figure 2. This sample, having a higher electron concentration, had a degeneracy temperature near 60° K and the acoustic curve was fitted at this point while the HS curve was fitted at room temperature. The effective masses required were $m^*/m_0 = 0{\cdot}16$ and $0{\cdot}17$ respectively. Again the acoustic curve fits poorly while the HS theory fits the experimental points very well.

3.3. *Degenerate Range*

The third sample, whose Q is shown in figure 3, had a degeneracy temperature above room temperature. The general expression for the thermoelectric power from which (1) is derived is (Johnson 1956)

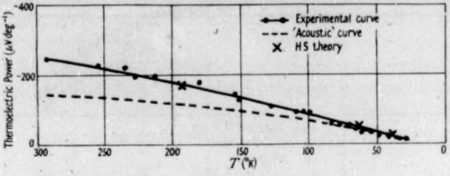

Figure 3. Extrinsic electron density $1{\cdot}4 \times 10^{18}$ cm^{-3}.

$$Q = -\frac{k}{e}\left[\frac{(2+S)F_{1+S}(\mathscr{J}^*)}{(1+S)F_S(\mathscr{J}^*)} - \mathscr{J}^*\right] \qquad \ldots\ldots (4)$$

where $F_S(\mathscr{J}^*)$ is a Fermi–Dirac integral.

$$\mathscr{J}^* = \mathscr{J}_0^*[1 - \pi^2/12\mathscr{J}_0^{*2}] \qquad \ldots\ldots (5)$$

and

$$\mathscr{J}_0^* = \frac{h^2}{2m^*kT}\left(\frac{3n}{8\pi}\right)^{3/2}. \qquad \ldots\ldots (6)$$

Taking $S=0$ for acoustic scattering, and using equations (4) and (6), the acoustic curve was fitted at low temperatures by an effective mass ratio of 0·11. Once more the agreement with experiment was poor. An attempt was made to fit the HS high degeneracy approximation but this deviated considerably from the experimental points at higher temperature so the HS arbitrary degeneracy approximation was used instead. HS give curves of what is effectively Q against $\mathscr{J}^*$ for a few values of Θ/T. When this was fitted to the experimental curve at 194°K ($\Theta/T=1$ being the lowest value of this ratio calculated by HS) by an effective mass of 0·11, the remaining two points available from the HS paper fell exactly on the experimental curve.

We conclude that, to the degree of approximation to which it has been developed, the HS theory gives good agreement with experiment both in degenerate and non-degenerate samples.

In I we observed that in samples of low electron density the mobility below 70°K departed considerably from the $T^{-5/2}$ law obtained at higher temperatures, indicating a change in the scattering mechanism. This might be attributed to either impurity band phenomena or scattering by dislocations since there is some evidence that low electron densities are associated with high dislocation densities†. This effect would not influence the results of sample 3 or of sample 2 in the temperature range considered but we might have expected a mechanism which had a dominant effect on the mobility to be apparent in the Q values of sample 1 below 70°K. The scattering mechanism affects the thermoelectric power formulae via the energy dependence of the mean free path. If dislocation scattering is independent of electron energy then the equation for Q should be formally the same as for acoustic scattering. We might then expect the experimental points to fall below those of the HS theory in this region and there is some indication of this effect in figure 1, but unfortunately the experimental points do not extend to sufficiently low temperatures.

---

† We are grateful to Dr. R. S. Allgaier for this suggestion.

3.4. *Phonon Drag*

Phonon drag effects are well known in the elemental semiconductors (see, for example, Frederikse 1953). In a similar temperature range we find no evidence of phonon drag effects in lead sulphide.

Quantitative estimates of the phonon drag contribution Q_P obtained by Frederikse (1953), Johnson (1956), Parrott (1954, 1957) and others, can be written

$$Q_P = -\frac{ul\phi}{\mu T} \qquad \ldots\ldots(7)$$

where u is the velocity of sound, μ the electron mobility, and $l\phi$ the phonon mean free path.

The thermal conductivity can be written (Kittel 1953, p. 81)

$$K = \tfrac{1}{3} C_V u l_K \qquad \ldots\ldots(8)$$

where C_V is the specific heat per unit volume and l_K the mean free path relating to the thermal conduction process. Parrott (1954) has shown that $l\phi \sim 40 l_K$ in germanium and a similar calculation gives $l\phi \sim 30 l_K$ in lead sulphide. Equations (7) and (8) then give

$$Q_P \sim \frac{100K}{C_V \mu T}.$$

The specific heat of lead sulphide is of the same order of magnitude as that of germanium and if we consider samples containing 10^{16} electrons cm^{-3} the mobility is also similar. Hence since no Q_P contribution is observed in lead sulphide, this implies that the thermal conductivity is of the order of 100 times less than that of germanium. We do not know of any low temperature measurements of the thermal conductivity of lead sulphide, but Joffe (1957) reports the thermal conductivity of lead telluride at 50°K to be nearly 200 times less than that of germanium at the same temperature.

§ 4. CONCLUSION

A simple theory, which considers scattering by acoustic modes only, fails to give agreement with experiment. The Howarth–Sondheimer theory of optical scattering fits the experimental results fairly well, suggesting that, over the temperature range considered, optical modes provide the dominant scattering mechanism.

The absence of phonon drag effects is consistent with the low thermal conductivity to be expected in lead sulphide.

REFERENCES

DEVJATKOVA, E. D., MASLAKOVETS, U. P., and SOMINSKII, M. S., 1941, *Bull. Acad. Sci. U.R.S.S.*, **5**, 409.
EHRENBERG, W., 1958, *Electric Conduction in Semiconductors and Metals* (Oxford: University Press).
FINLAYSON, D. M., and GREIG, D., 1956, *Proc. Phys. Soc.* B, **69**, 796.
FREDERIKSE, H. P. R., 1953, *Phys. Rev.*, **92**, 248.
GEBALLE, T. H., and HULL, G. W., 1954, *Phys. Rev.*, **94**, 1134.
HOWARTH, D. J., and SONDHEIMER, E. H., 1953, *Proc. Roy. Soc.* A, **219**, 53.
JOFFE, A., 1957, *J. Phys. Radium*, **18**, 209.
JOHNSON, V. A., 1956, *Progress in Semiconductors*, **1** (London: Heywood).
KITTEL, C., 1953, *Introduction to Solid State Physics* (New York: Wiley).
PARROTT, J. E., 1954, *Proc. Phys. Soc.* B, **67**, 587.
—— 1957, *Ibid.*, **70**, 590.

Time Dependent Changes in Excess Carrier Concentrations in the Presence of Surface Recombination

By J. D. NIXON† and P. C. BANBURY
Physics Department, University of Reading

MS. received 24th July 1958, in final form 15th September 1958

Abstract. A system is considered in which a thin slab of semiconductor, of infinite bulk lifetime, is initially in equilibrium and is then subjected to a uniform excitation throughout the bulk. The case in which surface recombination takes place via Shockley–Read centres has been treated, and the time dependence of the transient change in carrier concentrations has been evaluated under certain approximations for the case of germanium, as a function of surface potential. The time constants differ from the steady-state lifetime except in the case of low trap densities.

§ 1. Introduction

The study of the decay of excess carriers in semiconductors is often carried out with reference to rectangular filaments. The decay of carriers at the surface was first treated by Shockley (1950) for an extrinsic material in which the rate of recombination at the surface was taken to be proportional to the surface excess of the minority carrier concentration, barriers on the free surface not being considered. It was shown that the decay of the longitudinal conductance of a uniformly excited specimen could be described by a number of time constants, of which the longest, being of chief interest, was shown to be the same as the steady state filament lifetime. Provided that $sB/D \ll 1$, where s is the surface recombination velocity, B the half-thickness of a wide slab and D the diffusion constant for minority carriers, the longest time constant is independent of the diffusion constant; the same value of time constant is obtained if the carrier concentrations are assumed to be uniform throughout the specimen (Shockley 1950, p. 351).

Subsequently Shockley and Read (1952) have discussed the statistics of recombination in the bulk via recombination centres; in these circumstances the rate may not be simply proportional to the excess carrier concentration, since the occupancy of the centres is also relevant. They have defined lifetimes *in the steady state* as the ratio of the excess carrier concentration to the net rate of recombination. The transient behaviour of such a system upon the introduction of a disturbance has been discussed by Sandiford (1957). The time constant of this transient is not in general the same as the steady state lifetime.

The analysis by Shockley and Read has been transposed by Stevenson and Keyes (1954) to surface recombination, in the steady state, through surface recombination centres. These authors have obtained a relationship between surface recombination velocity and surface potential. It is often more convenient to measure a transient time constant, and in the following analysis we have considered transient conductance changes in the presence of surface recombination centres, similar to the centres discussed by Shockley and Read. A condition such as obtains in the low *s* approximation referred to above is assumed, in which the gradient of the quasi Fermi level may be neglected through the thickness of the slab. The assumption that the quasi Fermi levels are flat throughout the barrier region was made by Stevenson and Keyes; we have estimated this to be satisfactory for a reasonably wide range of the values of surface recombination velocity and barrier height obtained experimentally on etched specimens. Bulk recombination will be neglected. The results will thus be relevant to specimens in the form of thin slabs. This shape is in any case experimentally desirable if the surface potential is to be determined from conductance measurements, as in field effect experiments.

---

† Now at the Department of Physics, Western Reserve University, Cleveland, U.S.A.

§ 2. FORMULATION OF THE PROBLEM

In the following analysis we shall assume that recombination takes place through centres at a single energy u_t (in units of $\boldsymbol{k}T$) measured from the mid-gap energy at the surface, this energy being taken as positive if the levels are between the middle of the gap and the conduction band. The notation of Shockley and Read and Stevenson and Keyes will be followed. The former authors have shown (1952, Appendix A) that for small disturbances the net capture rates for electrons and holes may be written

$$U_{\mathrm{cn}}=C_{\mathrm{n}}[(1-f)\delta n_{\mathrm{s}}-(n_{\mathrm{s}}+n_1)\delta f] \qquad \ldots\ldots(1)$$

$$U_{\mathrm{cp}}=C_{\mathrm{p}}[f\delta p_{\mathrm{s}}+(p_{\mathrm{s}}+p_1)\delta f] \qquad \ldots\ldots(2)$$

where $n_1=n_i\exp u_t$, $p_1=n_i\exp -u_t$, n_s and p_s are the equilibrium concentrations of electrons and holes in the surface, and δn_s and δp_s are the disturbances in these quantities. The probability that the centres are occupied by electrons in the equilibrium condition is f. Since the specimen is a slab whose large faces are assumed to have symmetrical properties, the carrier concentrations within the specimen will be symmetrical. It is therefore sufficient to confine the argument to one half of the specimen. We shall suppose that the system is initially in equilibrium, and that carrier pairs are subsequently added at a uniform rate throughout the bulk. In the ensuing transient the capture rates for electrons and holes heed not be equal, but an overall continuity condition may be imposed, namely

$$\Delta P-\Delta N=N_t\delta f \qquad \ldots\ldots(3)$$

where ΔP is the number of excess holes in the specimen per unit area of surface and ΔN the number of excess electrons. N_t is the density of surface centres and δf the change in their occupancy.

In equilibrium the number of holes in the half-specimen per square centimetre of surface is

$$P_{\mathrm{tot}}=\int_{\mathrm{bulk}}^{\mathrm{surface}} n_i\exp(-u)dx.$$

In the excited condition

$$P_{\mathrm{tot}}+\Delta P=\int_{\mathrm{bulk}}^{\mathrm{surface}} n_i\exp(-u)\exp w_{\mathrm{p}}dx,$$

$$=P_{\mathrm{tot}}\exp w_{\mathrm{p}}$$

where w_p is the departure of the quasi Fermi level for holes from the Fermi level (figure 1). Changes in u are here assumed negligible.

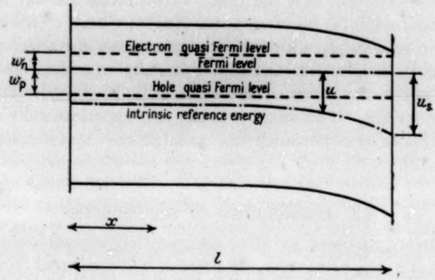

Figure 1. Schematic energy band diagram showing notation used in text.

Hence $\Delta P = \dfrac{\delta p_s}{p_s} P_{\text{tot}}$ and similarly $\Delta N = \dfrac{\delta n_s}{n_s} N_{\text{tot}}$.

Equation (3) now becomes

$$\delta f = \frac{1}{N_t}\left[\frac{\delta p_s}{p_s} P_{\text{tot}} - \frac{\delta n_s}{n_s} N_{\text{tot}}\right]. \qquad \ldots\ldots(4)$$

Since $U_{\text{cn}} = -\dfrac{d}{dt}(N_{\text{tot}} + \Delta N) + U$, where U is the external generation rate, there follows from equations (1) and (4)

$$\frac{n_s}{N_{\text{tot}}} U - \frac{d}{dt}(\delta n_s) = \frac{n_s}{N_{\text{tot}}} C_n \left[\frac{p_s \delta n_s}{p_1 + p_s} - \frac{n_s + n_1}{N_t}\left(\frac{\delta p_s}{p_s} P_{\text{tot}} - \frac{\delta n_s}{n_s} N_{\text{tot}}\right)\right].$$

Similarly

$$\frac{p_s}{P_{\text{tot}}} U - \frac{d}{dt}(\delta p_s) = \frac{p_s}{P_{\text{tot}}} C_p \left[\frac{n_s \delta p_s}{n_1 + n_s} + \frac{p_s + p_1}{N_t}\left(\frac{\delta p_s}{p_s} P_{\text{tot}} - \frac{\delta n_s}{n_s} N_{\text{tot}}\right)\right].$$

§ 3. DISCUSSION OF SOLUTIONS

The assumption of transient solutions of the form $A \exp -\alpha t$ leads to a quadratic equation in α, the roots of which may be evaluated. If the discriminant of this equation is $b^2 - 4c$, it is found that $b^2 \gg 4c$ in many cases. The two solutions then become b and c/b, where b is large compared with c/b. In circumstances where the above inequality is not valid the equation must be solved in full; it has been found in almost all cases considered that one solution is small compared with the other. The larger root gives a much shorter time constant than the smaller root, and will not be considered further. The smaller root (longer time constant) corresponds to the transient that will be observed experimentally. In those cases in which the simple form of solution is valid this time constant is

$$\tau = \frac{C_n\left[\frac{1}{(S_-+T_-)N_{tot}} + \frac{S_++T_+}{N_t}\right] + C_p\left[\frac{1}{(S_++T_+)P_{tot}} + \frac{S_-+T_-}{N_t}\right]}{\frac{C_pC_nn_i}{N_{tot}P_{tot}}\left[\frac{1}{(S_++T_+)(S_-+T_-)} + \frac{P_{tot}+N_{tot}}{N_t}\right]}. \qquad \ldots\ldots(5)$$

where $S_- = \exp - u_s$, $S_+ = \exp u_s$, $T_- = \exp - u_t$, $T_+ = \exp u_t$.

In figure 2 the value of the time constant in the case of n-type germanium ($n_0 = 2 \times 10^{14}\,\mathrm{cm}^{-3}$, $p_0 = 2{\cdot}5 \times 10^{12}\mathrm{cm}^{-3}$) is plotted as a function of u_s for $N_t = 10^{14}$ and 10^{12}, $u_t = +10$, 0, -10 and $C_p/C_n = 100$, 1 and 0·01, for a specimen of half-thickness of 1 mm. In the calculation of these values of time constant the full solution has been employed where necessary. It is of interest to examine the behaviour of this time constant in two particular cases.

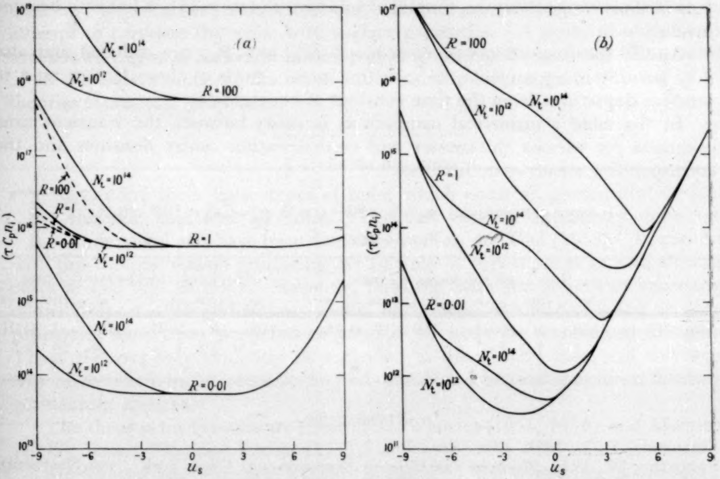

Figure 2. The quantity $\tau C_p n_i$ plotted as a function of u_s for $N_t = 10^{12}$ and 10^{14}, and for $C_p/C_n \equiv R = 10^2$, 1 and 10^{-2}. (*a*) Continuous line: $u_t = -10$ for the indicated values of N_t; broken line: $u_t = +10$ for $N_t = 10^{12}$ and 10^{14}. (*b*) $u_t = 0$.

(i) *Low Density of Centres*

In the case where $N_t \to 0$ the approximate solution is clearly valid. The time constant is given by equation (5) which reduces to

$$\tau = \frac{C_n(\exp u_s + \exp u_t) + C_p(\exp - u_s + \exp - u_t)}{C_nC_pn_i\left(\frac{1}{N_{tot}} + \frac{1}{P_{tot}}\right)} \qquad \ldots\ldots(6)$$

As indicated in § 1 the analysis has been made for low values of surface recombination rate, in which circumstances the surface recombination velocity *s* is related to the steady-state lifetime τ_s by $s=l/\tau_s$. On this basis an expression for τ_s may be obtained from the Stevenson and Keyes analysis and compared with equation (6). The two are identical in the case when the specimen is sufficiently thick or the barrier height sufficiently low to allow that $N_{\text{tot}}=n_i l \exp u_b$ and $P_{\text{tot}}=n_i l \exp -u_b$ where $n_i \exp u_b$, $n_i \exp -u_b$ are the bulk equilibrium concentrations of electrons and holes.

(ii) *Finite Density of Centres*

In the section above only those terms of equation (5) in $1/N_t$ have been retained. As N_t approaches either N_{tot} or P_{tot}, whichever is smaller, other terms in the expression are liable to become significant, in the first place when $u_s \simeq u_t$, and over a progressively increasing range of u_s as N_t becomes greater. It is in these ranges that the simplified solution, equation (5), is liable to become invalid.

As the specimen thickness is reduced N_{tot} and P_{tot} are reduced and also they become more sensitive to variation in u_s. Both of these factors tend to produce departures from the time constant of equation (6).

In the table a numerical comparison is made between the transient time constants for various thicknesses and recombination centre densities and the corresponding steady-state lifetimes.

n-type germanium, $n_0=2\times10^{14}$ cm^{-3}, $p_0=2{\cdot}5\times10^{12}$ cm^{-3},
$u_t=0$, $u_s=-3$

	Specimen thickness = 2 mm						Specimen thickness = 0·2 mm					
	$N_t=10^{12}$ cm^{-2}			$N_t=10^{14}$ cm^{-2}			$N_t=10^{12}$ cm^{-2}			$N_t=10^{14}$cm^{-2}		
C_p/C_n	100	1	0·01	100	1	0·01	100	1	0·01	100	1	0·01
τ_t/τ_s	1·2	1·2	1·0	15	15	2·7	2·9	2·8	1·2	56	54	9·5

REFERENCES

SANDIFORD, D. J., 1957, *Phys. Rev.*, **105,** 2.

SHOCKLEY, W., 1950, *Electrons and Holes in Semiconductors* (New York: van Nostrand).

SHOCKLEY, W., and READ, W. T., 1952, *Phys. Rev.*, **87,** 835.

STEVENSON, D. T., and KEYES, R. J., 1954, *Physica*, **20,** 1041.

1/*f* Noise in Germanium Devices

By T. B. WATKINS
Mullard Research Laboratories, Salfords, Redhill, Surrey

MS. received 26th June 1958, *in revised form 20th August* 1958

Abstract. A number of theories have recently been proposed to explain 1/*f* noise in germanium filaments. These theories may be extended to germanium devices and suggest experiments which may be performed to give evidence of their validity. Specially made diodes with a free surface opposite the junction were used and simultaneous field effect and noise measurements were made in an attempt to correlate the noise with surface properties. A study of noise in the breakdown region of a reverse biased p–n junction was carried out. The results of all the experiments are discussed and a noise model suggested by one of the theories tentatively proposed.

---

§ 1. INTRODUCTION

THERE are three basic types of noise which occur in germanium devices, thermal, shot and 1/*f* noise. The first two are apparently quite well understood and have been discussed by Van der Ziel (1955). In contrast with this the mechanism producing the 1/*f* noise is very obscure as with all other cases of this type of noise. Recently, however, with the growth of knowledge of the properties of germanium several fairly detailed theories based on these properties have been proposed to explain 1/*f* noise in germanium filaments. These theories may evidently be extended to the devices case, and this work was undertaken in an attempt to find which mechanism was most likely in germanium devices.

The three main theories are those of McWhorter (1955, 1956), and Morrison (1955), Bess (1956) and Petritz (1956).

McWhorter and Morrison's theory is based on the properties of the surface states of the germanium which have been reviewed by Kingston (1956). The noise is attributed to the trapping of charge carriers in the slow states. Measurements by McWhorter on a germanium filament of the time constants of these states carried out in conjunction with Kingston (1956) showed that they have a range and distribution suitable for an explanation of the 1/*f* spectrum. McWhorter has calculated the magnitude of the fluctuations of the number of carriers in the slow states. This will give rise to fluctuations in the surface barrier height so that the conductance of a filament will be modulated and noise produced. The magnitude of this noise is in good agreement with the measured values.

In Bess' theory the basic noise event is the diffusion of an impurity atom along a dislocation pipe on to the surface of the germanium filament. In n-type germanium the diffusion of donor atoms is considered. While the atom is on the surface there is one less donor in the bulk so that the Fermi level is changed which modulates the conductivity. Bess calculates the probability that the diffusing atom is captured by the dislocation from which it emerged or a neighbouring one and shows that a $1/f$ spectrum may be obtained under certain conditions.

Petritz criticizes McWhorter's theory on the grounds that most workers have found that the time constants of the slow states are very dependent on temperature, whereas the $1/f$ noise is known to show little variation with temperature. In addition it is difficult to see how McWhorter's theory can give the very large values of noise encountered in metal–semiconductor contacts or point contact diodes. Petritz proposes a mechanism which involves the local breakdown of barriers. In the case of the diode the current from the metal flows through the germanium oxide layer where the high field causes breakdowns. They may be initiated by thermal fluctuations and healed by increases in local ohmic heating. The varying thickness of the oxide layer may give rise to a $1/f$ spectrum. In the case of a filament microscopic irregularities on the surface may cause the oxide layer to penetrate into the surface channel causing a local point of high resistivity where the field will be higher than average. Breakdown of this region will give an increase in channel current.

§ 2. EXPERIMENTAL METHOD

Although the above theories refer mainly to germanium filaments it is evident that their principles can be extended to the case when excess carriers are present as in germanium devices. Basically we may say that McWhorter's theory postulates that the noise is caused by fluctuations of the surface height. Bess' theory depends on fluctuations of the Fermi level and Petritz's theory proposes high fields at the surface. In order to obtain evidence for and against these theories a series of experiments was carried out on an arrangement using specially made diodes which permitted simultaneous measurements of noise and surface properties. The diodes were made from 2 Ω cm n-type germanium with normal indium alloy junctions about 0·5 cm in diameter. There was a free surface opposite the junction and the base thickness was about 100 μ. A ring-type base connection was made and the diode was fitted in a holder so that the junction side was hermetically sealed from the free surface and the ambients on each side could be changed independently. A field electrode of 0·7 cm diameter insulated by a thin sheet of mica was placed on the free surface opposite the junction.

The diode was used in the forward bias condition and supplied from a constant current source. Holes are injected at the junction and diffuse across the base to recombine on the free surface. Taking typical values for the parameters, it may be shown that under the experimental conditions the mean excess hole concentration is sufficiently high to enable the diffusion gradient to be neglected. A uniform hole concentration may therefore be assumed throughout the base under the junction. Further, the equilibrium hole concentration may be neglected in comparison with the total hole concentration.

The voltage drop V across the diode is the sum of the voltage drops across the junction V_j and that across the base resistance V_b.

Assuming that the current I is carried entirely by holes and recombines only on the free surface area opposite the junction A_s we may write the following equations

$$V = V_\mathrm{j} + V_\mathrm{b}; \qquad V_\mathrm{j} = \frac{kT}{q}\ln\frac{p}{p_\mathrm{n}}; \qquad V_\mathrm{b} = I\left(\frac{1}{G_\mathrm{l}} + \frac{1}{G_\mathrm{m}}\right)$$

$$I = A_\mathrm{s} q s p$$

where p = total hole concentration, p_n = equilibrium hole concentration, s = surface recombination velocity, G_l = unmodulated part of base resistance, G_m = modulated part of base resistance $= K_1 + K_2 q(\mu_n + \mu_p)p$; K_1 and K_2 are constants, μ_n and μ_p are the electron and hole mobilities respectively and all other symbols have their usual significance.

We now consider the application of a transverse field to the free surface. This type of experiment has been reviewed by Kingston (1956). A variation of barrier height occurs and providing the frequency is high enough only the fast states are involved. This changes s in accordance with the theory of Stevenson and Keyes (1954). The change in s varies p so that V_j and V_b are also changed. For a change in s of δs the change of voltage across the diode δV is given by

$$\delta V = -\frac{\boldsymbol{k}T}{q}\frac{\delta s}{s} + \frac{I^2}{G_m}\frac{K_2(\mu_n + \mu_p)}{A_s}\frac{\delta s}{s^2}. \qquad \ldots\ldots (1)$$

The first term arises from V_j and is independent of current while the second is from the modulated part of the base resistance and is proportional to I^2. We see that at some value of current a change in s will produce no change in V. In the case of low currents when the first term is dominant we have

$$\delta V = -\frac{\boldsymbol{k}T}{q}\frac{qp}{I}A_s\delta s.$$

If it is assumed that p remains constant δV is directly proportional to δs. Following Thomas and Rediker (1956) who used a similar arrangement with a reverse bias, it was found that curves resembling the (s, ϕ_s) barrier height curves of Stevenson and Keyes (1954) could be constructed. Traces were produced on an oscilloscope by the application of a field of about 120 c/s. Varying the barrier height by Bardeen–Brattain ambient cycle (1953) gave different traces and the complete curve was constructed by fitting the traces together. With a constant current s varies so that p does not remain constant. The curves may be corrected by noting that

$$\delta V = \frac{\boldsymbol{k}T}{q}\frac{\delta p}{p}. \qquad \ldots\ldots (2)$$

A measurement of the change of d.c. voltage across the diode with change of ambient gave the relative increase in hole concentration.

The horizontal axes of the curves traced on the oscilloscope are actually produced by the applied field F. In later experiments these curves will be used mainly as an indication of the position of the surface barrier and will not be corrected for variations in p.

The noise voltage across the diode was measured by a harmonic wave analyser in conjunction with a pre-amplifier and square law detector. The harmonic wave analyser had a bandwidth of about 10 c/s and a frequency range 20 c/s–16 kc/s. The square law detector had a time constant of 18 seconds.

§ 3. SURFACE STATES AND NOISE MEASUREMENTS

3.1. *Measurements of Field Effect and Noise for varying Current and constant Ambient*

This experiment was performed to see whether there was any correlation between fluctuations of s and the noise. The ambient on the free surface side was chosen so that the field effect measurement gave a trace on the oscilloscope corresponding to fairly steep slope on the (s, F) curve. The forward bias current was then set to a series of fixed values between 0 and 10 mA and at each value measurements were taken of the slope of the trace and the noise level at 125 c/s on the harmonic wave analyser The slope of the trace is a measure of dV/dF which is directly proportional to dV/ds since ds/dF remains the same throughout the experiment.

According to equation (1) the slope of the trace should become zero and then reverse as the current is increased. Zero slope occurs at about 4·5 mA. It was found that minimum noise occurred also at this current.

The results are shown in figure 1. The ambient used was dry nitrogen. The vertical scale of the (slope)^2 curve was chosen to give the best agreement between the two curves. Similar agreement was also found using wet ambients.

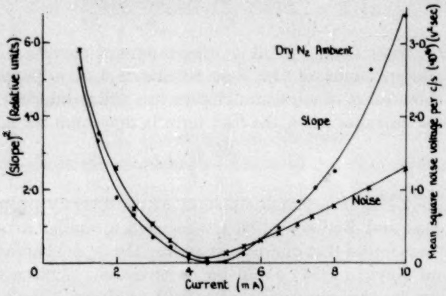

Figure 1. Noise and (slope)^2 plotted against current. Specimen No. 3, aged surface.

The interpretation of these results is that noise is associated with fluctuations in s. The slope of the line gives a measure of how a constant change of s affects the voltage across the diode over the current range. If the noise is associated with fluctuations of s then the mean square noise voltage should vary as the square of the change of the diode voltage produced by a change of s as the bias current is varied.

Noise measurement on transistors used as diodes with emitter and collector strapped together have been made by Fonger (1956). A decrease in the noise level at a certain current was found and this was explained in terms of the noise being due to fluctuation in s. The experiments described above give direct corroboration of this.

3.2. *Measurements of Fast States and Noise for varying Ambients and constant Current*

An attempt was made to correlate the noise level and the height of the surface barrier. According to McWhorter's theory there should be a minimum at the top of the (s, ϕ_s) curve as in this region fluctuations of the barrier height produce no changes in s. Bess' theory also predicts a minimum at this point as variations in the Fermi level at the surface are equivalent in their effect on s to variations in barrier height.

The current was set to 0·5 mA in which case the first term in equation (1) is dominant. It was found that changes in ambient produced changes in noise level as well as altering the barrier height. Great difficulty was experienced in obtaining a surface which would give reproducible changes in noise level with ambient. Finally, after a large number of experiments two types of surface giving different reproducible noise behaviours were recognized. The first, which we call the aged surface, was formed by repeated treatments of changing ambients on a freshly etched surface over a period of several weeks and the second, called the etched surface, was formed from an aged surface by very lightly etching. Fresh thoroughly etched surfaces were very unstable. Three specimens were used for the experiments. No difference was found between superoxol and C.P.4 etching.

Typical results for each surface are shown in figures 2 and 3. Here the (s, F) curves are plotted together with the noise at the various ambients. $F = 0$ is arbitrarily taken to coincide with the top of the curve. The noise levels are corrected by using equation (2) and are referred to the value of p obtaining at the top of the (s, F) curve. It appears that with the aged surface the noise increases as the surface goes from the n-type side (wet ambients) to the p-type side (ozone). This was indicated by results obtained with dry nitrogen. With this ambient it was found that the barrier height depended on the previous ambient. After

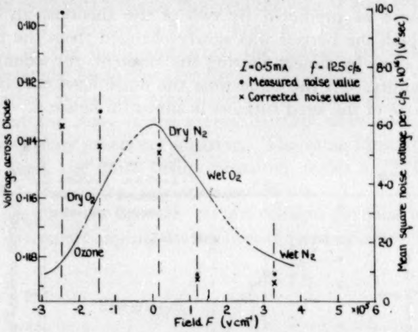

Figure 2. Measurement of noise and barrier height. Specimen No. 1, aged surface.

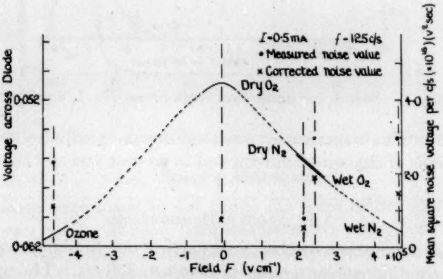

Figure 3. Measurement of noise and barrier height. Specimen No. 1, etched surface.

oxygen it gave a more p-type barrier than after wet nitrogen. In the former case the noise was greater.

With the etched surface it appears that the noise level may be a function of the type of adsorbed molecule rather than the barrier height. This is illustrated in figure 3, where it is seen that although dry nitrogen and wet oxygen produce very nearly the same barrier height the noise level is considerably different.

All these results were repeatable with each of the three specimens with one exception. On one aged surface ozone gave decreased noise although the surface became more p-type.

3.3. *The Search for the Minimum*

In order to see whether there was any sign of a dip in the noise level at the top of the (s, F) curve as predicted by two of the theories, an experiment was performed in which the barrier was slowly changed from the p- to the n-type side. This was done by slowly altering the ambient, for example by changing the relative humidity. At the same time the noise level was closely observed. The results for one of the aged surfaces is shown in figure 4. It is seen that no dip was found. This experiment was performed on all the specimens under various conditions of changing ambient and in no case was any sign at a minimum indicated.

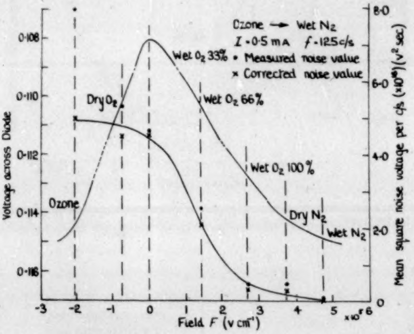

Figure 4. Search for minimum. Specimen No. 1, aged surface.

3.4. *Spectra Measurements*

Measurements of noise spectra were carried out for both types of surfaces under various conditions over a range of 20 c/s to 500 c/s. The upper frequency limit was determined by the $1/f$ noise falling below the background noise. In the case of the aged surface the ambient was controlled so that the barrier was kept at the top of the (s, F) curve and the spectrum measured. This was repeated for a barrier height on the p-type side and on the n-type side. In each case the spectrum was of the form $1/f^{1\cdot 15}$ and the more p-type the barrier the greater the noise.

For the etched surface wet and dry nitrogen ambients were used and similar results to the above obtained. The wet ambient always gave the greater noise.

3.5. *Slow State Measurements*

The sudden application of a voltage to the electrode gave a slow change of voltage across the diode which may be attributed to the slow states. The aged surfaces gave a slow decay with wet ambients and a fast decay with dry ambients. With the etched surfaces the reverse was true. Ozone gave fast decays with both types of surface.

§ 4. BREAKDOWN NOISE

4.1. *Measurements of Noise and Reverse Current*

Because of the failure to obtain any definite link between the surface states and the $1/f$ noise it was decided to make a study of breakdown phenomena as a source of noise as Petritz's theory suggests the idea of high fields at the surface. When a reverse bias is applied to a p–n junction a high field is produced along the surface and in the bulk, and when the voltage exceeds a certain value ionization or avalanche breakdown occurs.

To see whether avalanche breakdown was a noisy process measurements of reverse current and noise in the reverse current were made on the collector diode of an p–n–p alloy junction transistor. The same form of noise measuring apparatus was used, the noise being measured across a 220 Ω resistor in the collector circuit. The centre frequency was 85 c/s.

The results are shown in figure 5. At low voltages the noise was immeasurably small but rose extremely rapidly in the breakdown region.

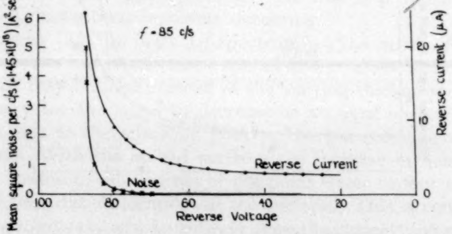

Figure 5. Reverse current and noise plotted against reverse voltage.

4.2. *Spectra Measurements*

Measurements were made to determine the form of the spectrum produced by the breakdown noise. At room temperature with a voltage of 77·5 v a spectrum with a law $1/f^{0\cdot75}$ was found. At temperatures below about 0°c the form changed and the spectrum became composed of a $1/f$ component and a shot noise component. The shot noise component was associated with spikes which appeared on an oscilloscope monitoring the broad band noise. These spikes only appeared below about 0°c. It is tempting to associate the $1/f$ component with breakdown on the surface and the shot noise component with breakdown in the bulk.

4.3. *The Law for the Breakdown Noise*

This was derived from a consideration of what fluctuating quantities can produce the noise.

We may write for the reverse current in the breakdown region $I_R = A_{\text{eff}} s p_n M$ where A_{eff} is the effective surface area over which the generation of hole–electron pairs producing the reverse current takes place. M is the multiplication factor. If it is assumed that independent fluctuations of M and s occur we have

$$[\delta I_R^2]_{\text{av}} \Delta f = \frac{[\delta s^2]_{\text{av}}}{s^2} I_R^2 \Delta f + \frac{[\delta M^2]_{\text{av}}}{M^2} I_R^2 \Delta f.$$

$[\delta s^2]_{\text{av}}$ and $[\delta M^2]_{\text{av}}$ are the mean square fluctuations per unit bandwidth in s and M respectively.

The first term is just M^2 times the noise in the reverse current at low voltages and for values of M used in the experiments is negligibly small compared with the second term.

To test this equation we must measure the noise with varying I_R while keeping M constant. This may not be done by changing the voltage which alters M. I_R may be varied by changing the temperature and assuming that $[\delta M^2]_{\text{av}}$ is independent of temperature which is a characteristic of $1/f$ noise. M, however, for a given voltage is a function of temperature as may be seen from figure 6. Here the normalized reverse current is plotted as a function of reverse voltage for three different temperatures.

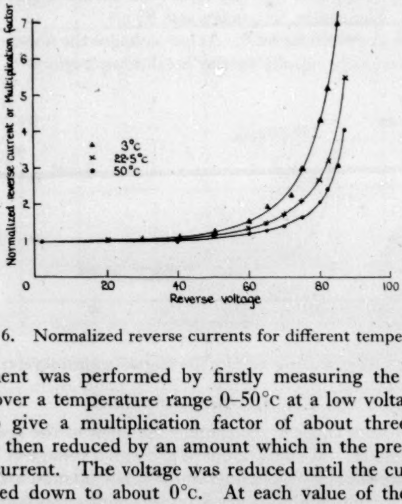

Figure 6. Normalized reverse currents for different temperatures.

The experiment was performed by firstly measuring the variation of the reverse current over a temperature range 0–50°c at a low voltage. The voltage was then set to give a multiplication factor of about three at 50°c. The temperature was then reduced by an amount which in the previous experiment had halved the current. The voltage was reduced until the current was halved. This was repeated down to about 0°c. At each value of the current a noise measurement at 85 c/s was made. The results showed that, over the temperature range, the mean square noise current varied exactly as I_R^2.

§ 5. Discussion of Results

To sum up we may say that the following points have been brought out by the experiments:

(*a*) $1/f$ noise in devices is associated with fluctuations of the surface recombination velocity s.

(*b*) No evidence has been found to show that the fluctuations in s are due to variations in the barrier height nor has any definite link been established between them and the normal surface recombination centres.

(*c*) With an aged surface there appears to be a tendency for the noise to decrease as the surface becomes more n-type.

(*d*) With etched surfaces wet ambients give increased noise.

(*e*) Avalanche breakdown is a noisy process which can produce a spectrum of $1/f$ form and obeys a law

$$[\delta I_R^2]_{av}\Delta f = \frac{[\delta M^2]_{av}}{M^2} I_R^2 \Delta f.$$

It appears that a great deal more work is required to establish definitely the implications of the results, particularly the very critical one in (*b*). However, in an attempt to find some explanation for them the following noise model based on Petritz's theory is very tentatively proposed.

We consider localized regions on the surface where there is a high field. Such points may occur when an edge dislocation meets the surface where there may be a highly p-type region and the energy gap may be smaller (Morrison 1956, Allen 1956). Recombination centres at these regions of area δA will have hole current flowing to them $qsp\delta A$. If the potential drop is comparable with the energy gap ionization may occur especially as the hole gives up its energy when captured by a recombination centre. An additional hole current $(M-1)qsp\delta A$ will be injected into the germanium and will produce a mean square noise current $[\delta M^2]_{av}q^2s^2p^2\delta A^2\Delta f$. As this is proportional to p^2 it is very nearly as if fluctuations in s were occurring.

To explain why $[\delta M^2]_{av}$ has a $1/f$ spectrum we can invoke Petritz's starting and healing processes but in this case a spread in the values of the potential drops and energy gaps may be used instead of the varying thicknesses of oxide layer.

The tendency for the noise to decrease as an aged surface becomes more n-type may be due to the adsorbed positive charges reducing the fields at the localized points. With the etched surfaces the increase in noise with the wet ambients may be due to movements of the polar water vapour molecules in the fringe fields of the edge dislocations at the surface. This is consistent with the slow state measurements which indicate that the water vapour molecules are nearer the germanium–germanium oxide interface with the etched surface than with the aged surface. In the former case the time constants with wet ambients are much shorter than in the latter case.

ACKNOWLEDGMENTS

The author wishes to acknowledge the assistance of many members of the Solid State Physics Division in this work. In particular, Mr. S. Thomson, Mr. P. Moore and Mr. R. Whillier have greatly helped with the measurements and apparatus, and Dr. K. Hoselitz has given constant encouragement.

REFERENCES

ALLEN, J. W., 1956, *J. Electronics*, **1**, 580.
BARDEEN, J., and BRATTAIN, W. H., 1953, *Bell Syst. Tech. J.*, **32**, 1.
BESS, L., 1956, *Phys. Rev.*, **103**, 72.
FONGER, W. H., 1956, *Transistors I* (New York: R.C.A. Labs.), p. 239.
KINGSTON, R. H., 1956, *J. Appl. Phys.*, **27**, 101.

McWHORTER, A., 1955, *Thesis: 1/f Noise and Related Surface Effects in Germanium* (Massachusetts Institute of Technology).

—— 1956, *Semiconductor Surface Physics*, Ed. R. H. Kingston (University of Pennsylvania Press), p. 207.

MORRISON, S. R., 1955, *Phys. Rev.*, **99**, 1904.

—— 1956, *Ibid.*, **104**, 619.

PETRITZ, R. L., 1956, *Semiconductor Surface Physics*, Ed. R. H. Kingston (University of Pennsylvania Press), p. 226.

STEVENSON, D. T., and KEYES, R. J., 1954, *Proc. International Conferences in Semiconductors, Amsterdam*, p. 1041.

THOMAS, J. E., and REDIKER, R. H., 1956, *Phys. Rev.*, **101**, 984.

VAN DER ZIEL, A., 1955, *Proc. Inst. Radio Engrs, N.Y.*, **43**, 1634.

Nuclear Deformation and the Photodisintegration Giant Resonances

By J. H. CARVER and W. TURCHINETZ
Research School of Physical Sciences, Australian National University, Canberra

MS. received 19th June 1958, in final form 10th September 1958

Abstract. The effects of nuclear deformation and shell closure upon the photodisintegration giant resonances have been investigated by measuring the (γ,n) cross sections for seven isotopes with $82 \leqslant N \leqslant 108$ using the bremsstrahlung from the 33 MeV Canberra electron synchrotron. The induced radioactivities were measured with a NaI(Tl) scintillation spectrometer. The most accurate results were obtained for the ^{181}Ta (γ,n) reaction leading to the 8·15 hour isomeric level of ^{180}Ta, the yield of which was measured to $\frac{1}{2}\%$ statistical accuracy at 250 kev intervals over the rising part of the activation curve. The giant resonance for the reaction measured in this way has a width of 5·3 MeV and shows no evidence for the splitting into two components predicted by recent calculations on the photodisintegration of spheroidal nuclei. In qualitative agreement with these calculations, it was found that the (γ,n) cross sections for the other distorted nuclei investigated, ^{150}Nd, ^{154}Sm and ^{160}Gd, have widths of 5·7, 6·5 and 5·3 MeV respectively, while for the closed-shell nuclei ^{141}Pr, ^{142}Nd and ^{144}Sm, the corresponding (γ,n) cross sections have widths of 4·3, less than 5·0 and 4·0 MeV. In addition, it was found that the (γ,n) cross sections for closed-shell nuclei have substantially larger high-energy tails than do those for spheroidal nuclei.

---

§ 1. Introduction

The hydrodynamical model (e.g. Goldhaber and Teller 1948, Jensen and Steinwedel 1950) and the single-particle shell model (Wilkinson 1956) have been successful in explaining many of the general features of the giant resonances of nuclear photodisintegration. A connection between these two apparently opposite points of view has been pointed out by Brink (1957) for the special case of oscillator wave functions, and both models are consistent with the general limits imposed by the sum-rule calculations of Levinger and Bethe (1950) for nuclear electric dipole absorption.

According to the single-particle model, narrower giant resonances are to be expected for closed-shell nuclei, and this is supported by the observations of, for example, Nathans and Halpern (1954). Recently Okamoto (1956, 1958) and, independently, Danos (1958) have elaborated the hydrodynamical model and have suggested a detailed correlation between nuclear deformation and the widths of the giant resonances. In the case of highly deformed nuclei (i.e. those with large quadrupole moments), the giant resonance is expected to split into two peaks corresponding to absorption along the major and minor axes of the nuclear spheroid. Soga and Fujita (1957) and Wilkinson (1958) have suggested that this effect is not peculiar to the hydrodynamical model, and have investigated a single-particle model in which the nucleons move freely in a spheroidal potential well. Their conclusions about the splitting are similar to those of Okamoto (1958) and Danos (1958).

The widths of the two peaks are difficult to estimate and, if the splitting is less than the half-widths, only one broadened peak will be observed. Both the hydrodynamical and single-particle calculations take the nuclear shape from the ground-state properties, and it is not certain that this shape is retained for the highly excited states to which the absorption leads. Coupling between the two modes may cause further overlapping of the peaks. Nevertheless, for highly distorted nuclei there should be a broadening of the giant resonance produced by the deformation in addition to those factors considered by Wilkinson (1956).

The largest nuclear deformations occur in the neighbourhood of the rare earth nuclei. In the present experiments the effects of nuclear deformation and of shell closure have been studied in this region with neutron numbers $82 \leqslant N \leqslant 108$.

§ 2. EXPERIMENTAL METHOD

Residual activity methods have been used to study the (γ,n) reactions in ^{141}Pr, ^{142}Nd, ^{144}Sm, ^{150}Nd, ^{154}Sm, ^{160}Gd and ^{181}Ta. The tantalum samples were in the form of 175 mg cm^{-2} metal foils. Oxide powders of each of the rare earth elements were used in their natural isotopic abundance. These powders were contained in 120 mg cm^{-2} aluminium cans, the thickness of the samples being approximately 500 mg cm^{-2}.

Samples were irradiated with the bremsstrahlung from the 33 Mev Canberra electron synchrotron and the induced gamma-ray activities were measured with a 1¾ in. diameter × 2 in. thick NaI(Tl) scintillation spectrometer, the resolution of which was 9% for the 662 kev line of ^{137}Cs. The crystal was enclosed in a 3 in. thick lead castle with a graded shield of cadmium, brass and aluminium to absorb the lead X-rays. The data were recorded on a multi-channel kicksorter of the Hutchinson–Scarrott type. The methods used to calculate the relative efficiency of the spectrometer for different gamma-ray energies have been described previously (Carver and Turchinetz 1958). Since for most of the activities studied the intensities of the various rare earth X-ray lines were being measured, the relative yields did not depend greatly on the energy response of the spectrometer. All the absolute yields reported here have been related to the ^{63}Cu(γ,n) results of Berman and Brown (1954) by measuring the annihilation radiation from 9·8 min ^{62}Cu induced in copper foils. The decay scheme for ^{140}Pr is well known (Browne *et al.* 1952), and measurement of the X-rays and annihilation radiation for this isotope† provided a direct check of the relative efficiency of the spectrometer for the rare earth X-rays and annihilation radiation.

The (γ,n) reactions studied in this work are listed in table 1. Only the more important gamma-ray lines are given in the table but further details of the decay schemes are discussed below for each particular case. The (γ,n) and $(\gamma,2n)$ thresholds B(n) and B(2n) have been obtained from measured atomic masses, where possible, and otherwise from the semi-empirical mass tables of Cameron (1957). The nuclear eccentricities $e=(a-b)/R$ (where a and b are the major and minor radii of the nuclear spheroid and R the radius of a sphere of the same volume) as computed by Okamoto (1958) from quadrupole moments and Coulomb excitation data are also given in table 1.

By measuring the induced activities in this way, it is possible, with one exception (^{142}Nd, see below) to sort out the (γ,n) reactions in particular isotopes

---

† Produced in the ^{141}Pr(γ,n) reaction by irradiating praseodymium oxide below the ^{16}O(γ,n) threshold (15·6 Mev).

Table 1

	%			B(n)	B(2n)	(γ,n) product nucleus	
Isotope	abundance	N	e	(MeV)	(MeV)	Half-life	Principal γ-rays
^{141}Pr	100	82	~0	9·99	18·28	3·4 min	K x-ray, γ^+
^{142}Nd	27·13	82	0·04	10·47	19·3	2·5 hr	K x-ray, γ^+
^{144}Sm	3·16	82	—	10·2†	19·7†	8·5 min	K x-ray, γ^+
^{150}Nd	5·60	90	0·24	7·87	12·97	1·8 hr	2 groups: at 118 & 212 kev
^{154}Sm	22·53	92	0·32	8·2	14·77	47 hr	K x-ray, 102 kev
^{160}Gd	21·90	96	0·44	7·6†	12·70	18 hr	K x-ray, 362 kev
^{181}Ta	99·988	108	0·22	7·72	13·8†	8·15 hr	K x-ray

† Threshold determined from semi-empirical mass tables (Cameron 1957). The other thresholds are based on measured values (Johnson and Nier 1957, Wapstra 1955).

unambiguously, without the use of separated isotopes. This was one reason for choosing this method in preference to a total neutron yield measurement. The activity method has the further advantage of being completely independent of the spectrum of the emitted neutrons. The (γ,n) cross section σ_1 will make the greatest contribution to the total absorption and, for these heavy nuclei, the (γ,2n) cross section σ_2 will be next in importance.‡ For the closed-shell nuclei ($N=82$) σ_2 will not be very important since B(2n) is well above the peak in the absorption.

In the remaining cases σ_2 must be estimated from other data and added to the measured σ_1 to obtain the total cross section. A similar complication exists for the total neutron yield measurements where to obtain the total cross section an estimated σ_2 must be subtracted from the measured $\sigma_1+2\sigma_2$.

§ 3. THE REACTION ^{181}Ta (γ,n) ($N=108$)

^{181}Ta is a highly distorted nucleus with $e=0{\cdot}22$, and according to the theory of Okamoto (1958) and Danos (1958) the giant resonance at 14 MeV is expected to split into two peaks with a separation, calculated from e, of approximately 2 MeV. The quadrupole moment is positive and the integrated cross section for the higher energy peak is expected to be twice that for the lower energy peak. The single-particle calculations of Soga and Fujita (1957) and Wilkinson (1958) lead to similar conclusions.

This cross section has been measured previously in this laboratory at 1 MeV intervals (Carver, Edge and Lokan 1957). The measurement of the (γ,n) cross section has now been repeated at closer energy intervals in a search for the suggested double peak. The 8·15 hr ^{180}Ta activity induced in tantalum foils (175 mg cm^{-2}) was determined by counting the 55 kev x-rays. The induced activity was measured with $\frac{1}{2}$% statistical accuracy at 250 kev intervals over the rising portion of the activation curve, the bremsstrahlung being monitored with a Victoreen r-meter in a Perspex block. These measurements extended over several days and before commencing a series of runs the synchrotron was ' warmed up ' for at least half an hour. Runs on successive days were interlaced and it was found that, after the initial warming-up period, there was no difficulty in reproducing previous measurements. The duration of the runs varied from 1 hour to a quarter-hour, depending on the energy.

---

‡ Other multiple reactions, e.g. (γ,3n), (γ,p), (γ,α), do not contribute significantly to the giant resonance region with which these remarks are chiefly concerned (see Carver and Turchinetz 1958).

The yield per röntgen was measured as a function of the maximum bremsstrahlung energy k_0, and these results were then corrected for the r-meter response to obtain the yield per electron $A(k_0)$ shown in figure 1. A zero-order approximation to the cross section was obtained by means of the relation

$$\sigma_0(k_0)=\frac{A'(k_0)}{S(k_0, T)}$$

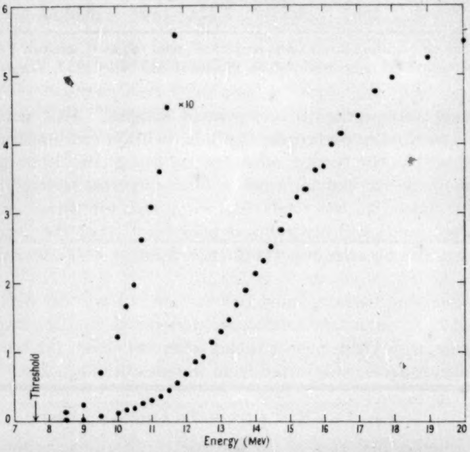

Figure 1. Activation curve for ^{181}Ta(γ,n) leading to the 8·15 hr level of ^{180}Ta. Statistical errors are smaller than experimental points.

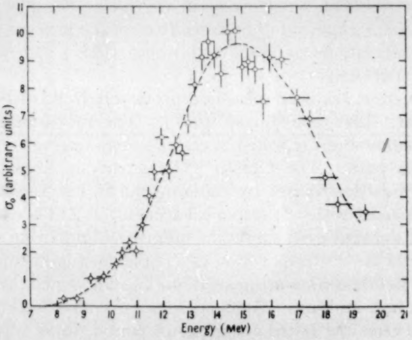

Figure 2. Zero-order approximation (see text) obtained using unsmoothed points from the activation curve (figure 1). The horizontal bars indicate the energy intervals over which the activation differences were determined.

where the prime denotes differentiation with respect to k_0 and $S(k_0, T)$ is the normalizing function defined by Carver and Lokan (1957). The derived values of σ_0 are given in figure 2. The points have been obtained by taking for $A'(k_0)$ the unsmoothed point differences of the measured activation yield points. The probable errors shown in figure 2 have been estimated from the statistical accuracy of the measured yield points; the horizontal bars indicate the energy intervals over which the activation differences were determined.

It is seen that the difference points are consistent with the smooth curve obtained from a smoothed derivative $A'(k_0)$. The results were analysed by an iterative method (Carver and Lokan 1957) to obtain the (γ,n) cross section σ_1 (figure 3, curve A) which has a width of 5·3 MeV and peaks at 13·5 MeV.

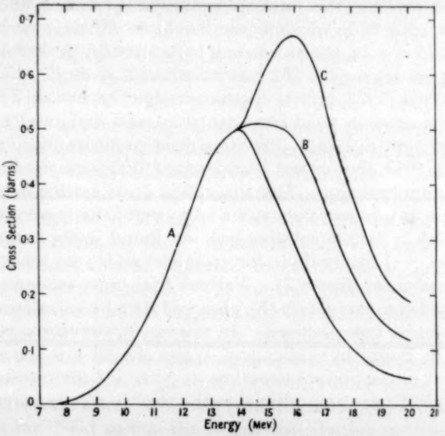

Figure 3. A, derived cross section for ^{181}Ta(γ,n), σ_1; B, total cross section, $\sigma_1 + \sigma_2$ where σ_2 has been taken from the data of Carver and Turchinetz (1958); C, $\sigma_1 + 2\sigma_2$.

Below the $(\gamma,2n)$ threshold (13·8 MeV), σ_1 represents the shape of the total γ-ray absorption if it can be assumed that transitions to the 8·15 hr isomeric level of ^{180}Ta are proportional to transitions to the ^{180}Ta stable ground state and hence to the total (γ,n) cross section.† That this assumption is probably true, apart from differences near the threshold, is shown by direct measurements of the relative photo-production of two isomers (e.g. Goldemberg and Katz 1953, Katz, Baker and Montalbetti 1953).

The 8·15 hr level of ^{180}Ta is known to have $I = 1^{\pm}$ (Brown *et al.* 1951), and the ground state is assumed to be the other member of the $I = 1,8$ doublet predicted by the collective model (Nilsson 1955) with higher (unknown) rotational levels built on this basis. Near the ^{181}Ta (γ,n) threshold the relative cross sections leading to the two levels may vary owing to fluctuations in the densities and properties of the excited states from which they may be populated, but at higher energies these fluctuations are expected to be unimportant (Ericson 1958). The approximately equal yield of these two levels in the ^{181}Ta (γ,n) reaction (Carver and Turchinetz 1958) implies that at high excitation there are no great differences in the densities of the levels from which they may be reached.

---

† The absolute cross section scale of figure 3 has been determined by the methods previously described (Carver and Turchinetz 1958) and refers to the total (γ,n) cross section, not the fraction decaying via the 8·15 hr isomer.

In the region below the (γ,2n) threshold and below the known peak in the absorption cross section, the present results show no second maximum. At higher energies the contribution of the (γ,2n) cross section σ_2 to the total cross section has been obtained from previous measurements (Carver, Edge and Lokan 1957) of the relative values of σ_1 and σ_2. It is found that $\sigma_1+\sigma_2$ (figure 3, curve B) is smooth and peaks at 14·5 Mev with a width of 6·3 Mev. Although there is no evidence for two peaks in this total absorption cross section, the present results imply that the cross section which would be obtained from a measurement of the total neutron yield $\sigma_1+2\sigma_2$ shows a strong higher energy peak at 16 Mev (figure 3, curve C).

Fuller and Weiss (1958, private communication) have made a careful measurement of the total neutron yield from tantalum and find two peaks in the total neutron cross section $\sigma_1+2\sigma_2$. Previous measurements of σ_1 and σ_2 (Carver, Edge and Lokan 1957, Carver and Turchinetz 1958) were used to correct these data for neutron multiplicity. The absorption cross section $\sigma_1+\sigma_2$ obtained by Fuller and Weiss in this way indicates a splitting of the resonance with peaks at 12·5 and 15·5 Mev. Such a splitting was not found in the present work. The presence or absence of two peaks in the cross section is very sensitive to the shape of σ_0 near its maximum (figure 2). Various trial cross sections with two peaks were assumed and compared with the observed data by calculating the activation curves and zero-order cross sections. In this way it was estimated that a splitting of the magnitude found by Fuller and Weiss should just have been observed with the accuracy of the present experiments provided the transitions to the 8 hr isomeric state of ^{180}Ta are proportional to the total (γ,n) cross section as has been assumed.

§ 4. THE (γ,n) REACTIONS IN ^{150}Nd, ^{154}Sm AND ^{160}Gd ($N=90$, 92 AND 96)

These nuclei are all highly deformed (see table 1). The (γ,n) activation curves have been determined at 0·5 Mev intervals from the thresholds to 18 Mev and at 1 Mev intervals from 18 Mev to 32 Mev. The samples were enclosed in cadmium to minimize slow neutron reactions. Tantalum foils were irradiated at the same time and used to monitor† the irradiations which were for periods of three hours. An ionization chamber was used for continuous monitoring of the radiation during each run. Above the ^{16}O (γ,n) threshold (15·6 Mev) the samples were allowed to decay for at least one hour before being counted, so that the 2 min ^{15}O activity had completely decayed.

The rare earth (γ,n) yields were determined as follows:

^{150}Nd (γ,n)^{149}Nd. ^{149}Nd decays by negatron emission with a half-life of 1·8 hr. A complex γ-ray spectrum follows the β^- decay and to date no satisfactory decay scheme has been proposed (Rutledge, Cork and Burson 1952). The relative yields at the different bremsstrahlung energies were determined by counting two broad γ-ray groups centred at 118 and 212 kev. An estimate of the absolute yield for this reaction awaits further data.

---

† The ^{181}Ta(γ,n) yield curve was taken from the results of Carver, Edge and Lokan (1957), at high energies, and the more accurate results of the present paper below 20 Mev.

^{154}Sm $(\gamma,n)^{153}$Sm. The 47 hr ^{153}Sm activity has been studied by a number of groups and most of the recent data appear to be in agreement with the decay scheme proposed by Dubey, Mandeville and Rothman (1956). Relative yields were determined from the intensities of the K x-rays and the 102 kev line. The absolute yields were obtained from the intensity of the K x-radiation. There is disagreement in the literature on the magnitude of the K shell conversion coefficient α_K for the abundant 102 kev transition, with one group of workers giving $\alpha_K \simeq 0{\cdot}65$ (Lee and Katz 1954, Siegbahn 1951, Joshi, Subbarao and Thosar 1957) and the other giving $\alpha_K \simeq 1{\cdot}2$ (McGowan 1954, Marty 1955, Dubey, Mandeville and Rothman 1956). This discrepancy introduces an uncertainty of only 2% in the yield estimated from the K x-ray intensity but one of 25% in that estimated from the intensity of the 102 kev line.

^{160}Gd $(\gamma,n)^{159}$Gd. Both K x-radiation and 362 kev γ-rays are prominent in the spectrum of 18 hr ^{159}Gd. The absolute yields were obtained from the intensity of the 362 kev line adopting the decay scheme proposed by Ballini and Barloutand (1956). It is estimated that the uncertainties in this decay scheme contributed about 15% to the probable error in the yield of the ^{161}Gd (γ,n) reaction.

The measured ratios of the rare earth activities to the ^{181}Ta(γ,n) monitor are shown in curves A of figures 4, 5, and 6. The activation curves (per electron) and the derived cross sections are shown in curves B and C of figures 4, 5, and 6. The $(\gamma,2n)$ cross sections can be expected to contribute significantly to the total cross sections for these isotopes. The general similarity of the (γ,n) cross sections for all the spheroidal nuclei suggests that the $(\gamma,2n)$ contribution may be comparable with that for ^{181}Ta, so that the widths of the resonances will be increased by about 1 Mev. The broadening produced by the $(\gamma,2n)$ reactions is expected to be least for ^{154}Sm and greatest for ^{160}Gd owing to the differences in the $(\gamma,2n)$ thresholds (table 1). Conversely, the observed (γ,n) widths are greatest for ^{154}Sm and least for ^{160}Gd so that the $(\gamma,2n)$ contribution is expected to make the total widths more nearly equal.

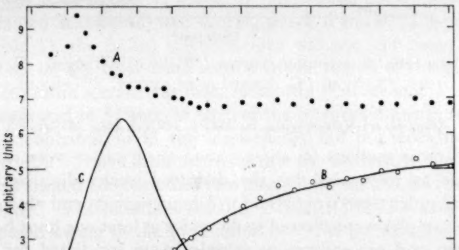

Figure 4. A, the ratio of activation curves ^{150}Nd$(\gamma,n)/^{181}$Ta(γ,n); B, activation curve for ^{150}Nd(γ,n); C, derived cross section: ^{150}Nd(γ,n).

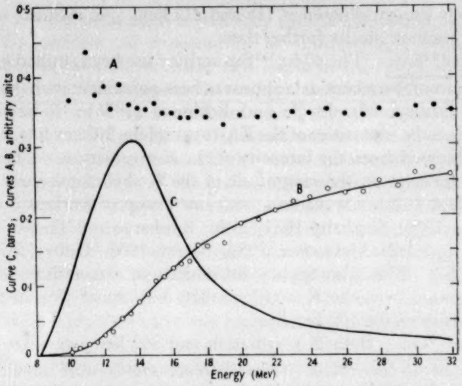

Figure 5. A, the ratio of activation curves ^{154}Sm(γ,n)/^{181}Ta(γ,n); B, activation curve for ^{154}Sm(γ,n); C, derived cross section: ^{154}Sm(γ,n).

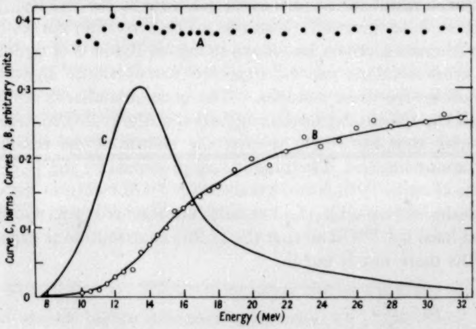

Figure 6. A, the ratio of activation curves ^{160}Gd(γ,n)/^{181}Ta(γ,n); B, activation curve for ^{160}Gd(γ,n); C, derived cross section: ^{160}Gd(γ,n).

§ 5. THE (γ,n) REACTIONS IN ^{141}Pr, ^{142}Nd AND ^{144}Sm ($N=82$)

The (γ,n) cross sections for these closed-shell nuclei were measured by the same methods as were used for the distorted nuclei discussed above. The neodymium samples were irradiated for 2-hour periods and above the ^{16}O (γ,n) threshold the samples were allowed to decay for at least one hour before counting. The samarium and praseodymium samples were irradiated for periods of 10 minutes and 5 minutes respectively and owing to the short half-lives involved (8·5 min and 3·4 min) it was not possible to wait for the ^{15}O activity to decay completely. Above the ^{16}O (γ,n) threshold the yields of ^{140}Pr and ^{143}Sm were determined from the intensities of the X-ray lines after subtracting the contribution from the low-energy tail of the Compton distribution due to the combined oxygen and rare-earth annihilation radiation.

The yields were determined as follows:
^{141}Pr(γ,n)^{140}Pr, ^{142}Nd(γ,n)^{141}Nd†, ^{144}Sm(γ,n)^{143}Sm. Each of these reactions leads to a particularly simple radio-isotope which decays mainly by positron emission and electron capture in a ground-to-ground state transition. The relative yields at different bremsstrahlung energies were determined by counting the x-rays. In the case of ^{141}Nd a complication arises due to the presence of ^{149}Nd which has a complex γ-ray spectrum and a similar half-life to ^{141}Nd. The fraction of x-rays in the total Nd γ-ray spectrum due to internal conversion of the γ-rays in the decay of ^{149}Nd was measured by determining the spectrum of substantially pure ^{149}Nd produced by neutron capture in natural Nd. The result so obtained was in good agreement with that found by Schmid and Burson (private communication). Absolute yields were obtained from the x-ray intensities after making the following corrections:—

(i) K-capture/β^+: determined from the measured disintegration energy and the tables of Feenberg and Trigg (1950) for ^{143}Sm; in the case of ^{141}Nd see Polak *et al.* (1958), and for ^{140}Pr Browne *et al.* (1952).

(ii) K-capture/total capture obtained from the work of Brysk and Rose (1955) and the disintegration energies W_0.

(iii) K shell fluorescence yield W_K taken from the compilation by Bergstrom (1955). The pertinent data for each isotope are collected in table 2.

Table 2

Activity	$T_{\frac{1}{2}}$ (min)	W_0 (Mev)	K/β^+	$\dfrac{\text{K-capture}}{\text{Total capture}}$	W_K
^{140}Pr	3·4	3·25	0·63	0·89	0·89
^{141}Nd	150	1·80	48	0·89	0·90
^{143}Sm	8·5	3·47	0·60	0·89	0·91

The measured ratios of the rare-earth activities to the ^{181}Ta(γ,n) activity are shown in curves A of figures 7, 8 and 9. Activation curves and derived cross sections are shown in curves B and C of figures 7, 8 and 9. Owing to their high threshold (table 1), the (γ,2n) cross sections will not, for these nuclei, have a significant effect on the total cross section in the region of the giant resonance. The ^{141}Pr(γ,2n) cross section has been measured (Carver and Turchinetz 1959) and, when integrated to 31 Mev, is 18% of the integrated (γ,n) cross section and makes a large contribution to the high-energy tail but does not significantly increase the width. It has been assumed that the contribution of σ_2 to the total cross section is similar for the other closed-shell nuclei and no corrections for σ_2 have been made. The situation for the ^{142}Nd(γ,n)^{141}Nd reaction is somewhat more complicated owing to the production of ^{141}Nd by means of the (γ,2n) and (γ,3n) reactions discussed above. Neither of these reactions affects the cross section near the peak. The contribution from the (γ,3n) reaction will almost certainly be very small (<1% of the total yield at 32 Mev). The reaction ^{143}Nd

---

† This activity can also be produced by means of the reactions ^{143}Nd(γ,2n) and ^{144}Nd(γ,3n). The abundances of ^{142}Nd, ^{143}Nd and ^{144}Nd are 23·1%, 12·2% and 23·9%, and the reaction thresholds (Johnson and Nier 1957) leading to ^{141}Nd are 10·5, 17·0 and 25·5 Mev respectively.

(γ,2n) will contribute to the high-energy tail in the cross section curve C of figure 8 above 17 MeV. The abundance of ^{143}Nd is 0·51 times that of ^{142}Nd and the yield of the ^{143}Nd(γ,2n) reaction may amount to as much as 5% of the total yield at 32 MeV. It is not, however, possible to estimate these effects with any accuracy, other than to indicate that they are probably small; and no corrections have been made to the data of figure 8, curve C.

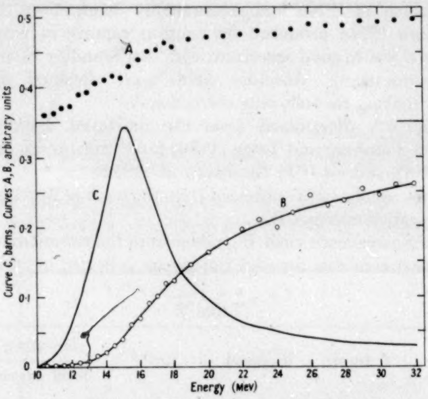

Figure 7. A, the ratio of activation curves ^{141}Pr(γ,n)/^{181}Ta(γ,n); B, activation curve for ^{141}Pr(γ,n); C, derived cross section: ^{141}Pr(γ,n).

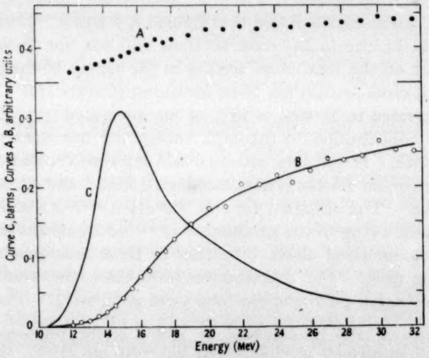

Figure 8. A, the ratio of activation curves ^{142}Nd(γ,n)/^{181}Ta(γ,n); **B,** activation curve for ^{142}Nd(γ,n); C, derived cross section: ^{142}Nd(γ,n).

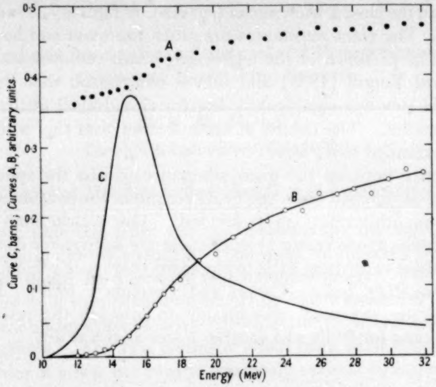

Figure 9. A, the ratio of activation curves ^{144}Sm(γ,n)/^{181}Ta(γ,n); B, activation curve for ^{144}Sm(γ,n); C, derived cross section: ^{144}Sm(γ,n).

§ 6. DISCUSSION

The widths, peak energies and integrated cross sections for the reactions studied are listed in table 3.

Table 3. Summary of Results

Isotope	N	Peak energy (Mev)	Width (Mev)	$\int\sigma\, dE$ (Mev barns)
^{141}Pr	82	15·3	4·3	$2{\cdot}2 \pm 0{\cdot}3$
^{142}Nd	82	14·8	$< 5{\cdot}0$	$< 2{\cdot}3 \pm 0{\cdot}3$
^{144}Sm	82	15·3	4·0	$2{\cdot}5 \pm 0{\cdot}4$
^{150}Nd	90	13·2	5·7	—
^{154}Sm	92	13·6	6·5	$2{\cdot}4 \pm 0{\cdot}4$
^{160}Gd	96	13·5	5·3	$2{\cdot}2 \pm 0{\cdot}4$
^{181}Ta	108	13·5 14·5 (total)	5·3 6·3 (total)	$2{\cdot}4 \pm 0{\cdot}8$ $3{\cdot}3 \pm 1{\cdot}2$ (total)

The observed broadening of the giant resonances for the distorted nuclei is in qualitative agreement with the predictions of the theories of Okamoto (1958), Danos (1958) and Soga and Fujita (1957). However, the more distinctive feature of these theories—namely, the predicted splitting of the resonance into two components—was not observed for ^{181}Ta, the most carefully investigated case.

The absence of splitting in the ^{181}Ta(γ,n) reaction leading to the spin 1, 8·15 hr level ^{180}Ta may possibly be explained by Wilkinson's (1958) observation that on the single-particle model of photon absorption there is a tendency for the low-energy component of the giant resonance doublet to be associated with higher angular momentum transitions than the high-energy component. The present results differ most markedly from the total neutron yield data of Fuller and Weiss (private communication) in the energy region, from threshold up to about 14 Mev, where the neutron yield data exhibit the lower peak which, according to Wilkinson, will involve high angular momentum transitions and possibly a preferential population of the high spin, stable state of ^{180}Ta.

Curves C of figures 4, 5 and 6 show that the shapes of the resonances are very similar for all the highly distorted nuclei investigated in this work. The gamma-ray absorption in the closed-shell nuclei (curves C of figures 7, 8 and 9) is, however, very different. The giant resonances are much narrower and have a large high-energy tail. The presence of the high-energy tails removes an anomaly noted by Nathans and Yergin (1955) and others who found that the cross section integrated to 22 MEV was significantly less for closed-shell nuclei than for other neighbouring nuclei. The results of table 3 show that this is not so when the integration is extended to 31 MEV.

The difference between the giant resonance widths for spherical and non-spherical nuclei as inferred from the (γ,n) reactions above is increased when the contribution from other reactions is included. This is clear from a consideration of $(\gamma,2n)$ thresholds above (table 1) since these are so high for closed-shell nuclei that these reactions contribute little to the giant resonance region, as is borne out by the results for ^{141}Pr $(\gamma,2n)$ (Carver and Turchinetz 1959). In contrast, the $(\gamma,2n)$ reactions are expected considerably to broaden the resonances for the distorted nuclei and for ^{181}Ta add another 1 MEV to the width.

REFERENCES

BALLINI, R., and BARLOUTAND, R., 1956, *J. Phys. Radium*, **17**, 534.
BERGSTROM, I., 1955, *Beta- and Gamma-Ray Spectroscopy*, editor K. Siegbahn (Amsterdam: North-Holland Publishing Co.).
BERMAN, A. J., and BROWN, K. L., 1954, *Phys. Rev.*, **96**, 83.
BRINK, D. M., 1957, *Nuclear Physics*, **4**, 215.
BROWN, H. N., BENDEL, W. L., SHORE, F. J., and BECKER, R. A., 1951, *Phys. Rev.*, **84**, 292.
BROWNE, C. I., RASMUSSEN, J. O., SURLS, J. P., and MARTIN, D., 1952, *Phys. Rev.*, **85**, 146.
BRYSK, H., and ROSE, M. E., 1955, *U.S.A.E.C. Report* O.R.N.L.-1830 and corrigendum.
CAMERON, A. G. W., 1957, *A.E.C.L. Report* C.R.P.-690.
CARVER, J. H., EDGE, R. D., and LOKAN, K. H., 1957, *Proc. Phys. Soc.* **A**, **70**, 415.
CARVER, J. H., and LOKAN, K. H., 1957, *Aust. J. Phys.*, **10**, 312.
CARVER, J. H., and TURCHINETZ, W., 1958, *Proc. Phys. Soc.*, **71**, 618.
—— 1959, *Ibid.*, **73**, 110.
DANOS, M., 1958, *Nuclear Physics*, **5**, 23.
DUBEY, V. S., MANDEVILLE, C. E., and ROTHMAN, M. A., 1956, *Phys. Rev.*, **103**, 1430.
ERICSON, T., 1958, *Nuclear Physics*, **6**, 62.
FEENBERG, E., and TRIGG, G., 1950, *Rev. Mod. Phys.*, **22**, 399.
GOLDEMBERG, J., and KATZ, L., 1953, *Phys. Rev.*, **90**, 308.
GOLDHABER, M., and TELLER, E., 1948, *Phys. Rev.*, **74**, 1046.
JENSEN, J. H. D., and STEINWEDEL, H., 1950, *Z. Naturfor.*, **5a**, 413.
JOHNSON, W. H., and NIER, A. O., 1957, *Phys. Rev.*, **105**, 1014.
JOSHI, M. C., SUBBARAO, B. N., and THOSAR, B. V., 1957, *Proc. Ind. Acad. Sci.*, **45a**, 390.
KATZ, L., BAKER, R. G., and MONTALBETTI, R., 1953, *Canad. J. Phys.*, **31**, 250.
LEE, M. R., and KATZ, R., 1954, *Phys. Rev.*, **93**, 155.
LEVINGER, J. S., and BETHE, H., 1950, *Phys. Rev.*, **78**, 115.
MCGOWAN, F. K., 1954, *Phys. Rev.*, **93**, 163.
MARTY, N., 1955, *J. Phys. Radium*, **16**, 458.
NATHANS, R., and HALPERN, J., 1954, *Phys. Rev.*, **93**, 437.
NATHANS, R., and YERGIN, P. F., 1955, *Phys. Rev.*, **98**, 1296.
NILSSON, S. G., 1955, *K. Danske Vidensk. Selskab, Mat. Fys. Medd.*, **29**, No. 16.
OKAMOTO, K., 1956, *Prog. Theor. Phys.*, **15**, 75.
—— 1958, *Phys. Rev.*, **110**, 143.
POLAK, H. L., SCHOO, W., SCHRAM, B. L., GIRGIS, R. K., and VAN LIESHOUT, R., 1958, *Nuclear Physics*, **5**, 271.
RUTLEDGE, W. C., CORK, J. M., and BURSON, S. B., 1952, *Phys. Rev.*, **86**, 775.
SIEGBAHN, K., 1951, *M. Siegbahn Memorial Volume*, Uppsala, p. 237.
SOGA, M., and FUJITA, J., 1957, *Nuovo Cim.*, **6**, Series 10, 1494.
WAPSTRA, A. H., 1955, *Physica*, **21**, 367.
WILKINSON, D. H., 1956, *Physica*, **22**, 1039.
—— 1958, *Phil. Mag.*, **3**, 567.

Some Methods for analysing unresolved Proportional Counter Curves of X-ray Line Spectra

BY R. M. DOLBY

Cavendish Laboratory, Cambridge

MS. received 27th June 1958, in final form 18th September 1958

Abstract. Three different pulse analysis methods are described by which the intensities of several closely spaced spectral lines, as detected by a proportional counter, may be determined quickly and unambiguously. The techniques are applicable where each significant line occurring in the spectrum can be obtained separately for calibration procedures; x-ray emission microanalysis, for example, fulfils this condition. The two methods which have been tested gave absolute errors in the order of a few per cent in analysing various mixtures of copper and nickel. An important application of such techniques is in the analysis of characteristic x-rays having long wavelengths and low intensity, since maintenance of an adequate counting rate under these conditions is difficult if a crystal or ruled grating spectrometer is used.

§ 1. INTRODUCTION

PROPORTIONAL counters are attractive for wavelength discrimination in x-ray work because of their wide angle of acceptance and consequent high counting rate, in contrast to the inefficient use of available photons by crystal and ruled grating spectrometers. Owing to their intrinsically poor energy resolution, however, proportional counters have been employed hitherto only for harmonic elimination or, if used alone, for such tasks as determining the Kα intensities of elements which differ by at least three in atomic number.

In x-ray emission microanalysis (Castaing 1951) of the low atomic numbered elements it becomes necessary to dispense as far as possible with crystals, gratings and filters, particularly when scanning techniques (Cosslett and Duncumb 1957, Melford and Duncumb 1958) are applied. Low beam current, low x-ray generation efficiency, absorption effects, and low spectrometer efficiency combine to make reasonable counting rates very difficult to obtain. While detection of the x-rays directly in a wide angle thin window proportional counter gives an adequate counting rate, it is at the expense of overlapping pulse height distributions when neighbouring elements in the periodic table are present. This difficulty is illustrated in general terms by Maeder (1958), who has derived a family of curves showing the count rate contamination of a desired peak by an adjacent undesired peak.

As the performance of proportional counters is already high relative to theoretical predictions (Bisi and Zappa 1955), attention in the present investigation has been given to pulse analysis rather than to improvement of the detector itself. In particular, the height, position and shape of the composite pulse height distribution curve has been examined on the assumption that the component curves, each arising from a separate Kα line, are fully and uniquely represented in the composite curve.

As might be expected, such an investigation is a special case of a more general problem. For a Gaussian curve

$$y = A\exp\left[-\frac{(x-b)^2}{2\sigma^2}\right]$$

there are three parameters, peak amplitude, position of the mean, and standard deviation σ. The most general problem is that of deducing all the parameters of each Gaussian component in a composite curve which has resulted from linear addition of an unspecified number of components with unspecified parameters. There appears to be no discussion of this case in the literature, and the lack of a sufficiently selective orthogonality (i.e. one which will select one Gaussian curve with specified parameters and reject all others) between given Gaussian components and convenient reference functions makes the prospect of an easy solution seem rather remote. This is in contrast to Fourier analysis, in which the periodic orthogonality of sines and cosines readily leads to a unique series of sines and cosines for any given function.

Removing only one of the unknowns, however, seems to permit a practical solution. Anderson (1956), for example, studying the radial distribution functions of electron diffraction in gases, has resolved composite curves containing as many as six components, with exact knowledge only of the correct number of components. Using an iterative process in conjunction with an IBM 650 electronic computor, Anderson was able to deduce all the parameters with three guesses in less than an hour.

Many special methods have been devised to cope with problems in which certain parameters are known and one or more of the remainder are desired. In the analysis of X-ray diffraction patterns, for example, an overlapping Kα doublet often obscures essential information. The line spacing and ratio of intensities are known. Working from this basis, Dumond and Kirkpatrick (1931) obtained an infinite series which expressed ordinate points on the component lines in terms of a set of ordinate measurements on the experimental curve, whiie Rachinger (1948) employed a wholly graphical resolution procedure. Finch (1949), in determining the correct diameters of overlapping diffraction rings, derived a family of curves giving the deviation of the composite peak from the true position of the stronger line as a function of overall half-width. The literature contains many other methods and references in connection with the case of unresolved doublets (e.g. Anantharaman and Christian 1953, Canty and Franklin 1958, Richtmeyer and Barnes 1934).

In general terms, the way in which an instrumental weighting (smearing) function acts upon an undistorted curve to form the observed (smeared) function can be described by a convolution integral. If this integral equation can be solved explicitly, which it usually cannot, an exact expression for the undistorted function is obtained. Morton (1952) pointed out that certain approximations can be made where a great improvement in resolution is not required, as in the correction of pulse height distributions due to continuous radiation. Lidén and Starfelt (1954) used Morton's simplified solutions to correct scintillation counter pulse height distribution curves of continuous γ-ray spectra but also solved the integral equation numerically by a series of approximations in cases where more improvement in resolution was necessary.

A particularly convenient way of handling the convolution integral uses Fourier analysis. This technique, the Fourier transformation, was suggested by Smith

(1934) to determine the correct widths of X-ray lines, free from all instrumental broadening. Shull (1946) and Stokes (1948) have employed the idea to solve for the weighting functions which characterize the line broadening effect of small diffraction particles (< 1000 Å) in a Debye–Scherrer apparatus. A more general treatment of instrumental distortion of line shapes and of the appropriate Fourier correction processes is outlined by Alexander (1950, 1954).

While study of the convolution integral either directly or by the Fourier transformation is indeed appropriate in theory for the proportional counter and its response to characteristic line spectra, certain practical difficulties lead to very inaccurate results. A significant improvement in resolution is needed, and in this situation the information requirements for a solution of the integral equation are different from that which is available: (i) accurate knowledge of composite curve shape is required, particularly of any small, sharp details, features in which proportional counter curves are singularly lacking; (ii) part of the data is wasted (the known positions of the constituent peaks).

Nevertheless, there being no fundamental obstacle to resolving such curves, methods can be devised which utilize the available data to good advantage. The techniques outlined in this paper are based on and employ these main features of the X-ray microanalysis situation:

(*a*) All parameters of the component curves are known except the amplitudes; each constituent pulse height distribution can be obtained readily in pure form for calibration, so that its position, height, and shape can be established fully.

(*b*) The given composite specimen curve is formed by linear addition of the component curves (neglecting space charge, dead time in the electronics, or other effects which can usually be avoided).

Utilizing the above principles, the following methods for obtaining the component curve amplitudes are discussed:

(i) The simultaneous equations method, which requires linearly independent ordinate or area measurements, equal in number to the unknowns, to be made on the observed composite pulse height distribution. Equations describing these measurements in terms of contributions from the constituent curves are established, from which the amplitudes of the constituents can be solved.

(ii) The peak shift method, which employs the relationship between observed peak position and ratio of components in a composite pulse height distribution, the ratio being a unique one when there are only two components.

(iii) The waveform analysis method, which utilizes the linear independence between different Fourier components in a composite pulse height distribution to establish simultaneous equations describing these components in terms of the constituent Fourier components in the contributing curves. The pulse height distribution amplitudes are obtained from the solutions of these equations.

The main emphasis is on techniques which seemed readily adaptable to high speed electronic processes rather than on those requiring detailed graphical procedures, although the peak shift method, in requiring reference to a graph, does not give an analogue output. While only the first two schemes have been tested, the untried waveform analysis method has been included, as it illustrates a strong possibility in the use of orthogonality or curve shape discrimination principles as a means of effecting resolution.

The presence of background radiation will be neglected in the following discussions. The effects of background near the wavelengths of interest have not been fully investigated, but it appears that spurious radiations, the intensities of which are either constant or proportional to one of the unknowns, are not a serious practical difficulty.

§ 2. SIMULTANEOUS EQUATIONS METHOD

Consider several superimposed and unresolved Gaussian shaped pulse height distribution curves with known positions, known standard deviations, and unknown peak heights, *A*, *B*, *C*, etc. Under these conditions, ordinate or area measurements *M* of the composite curve can be expressed in terms of contributions from the component curves:

$$\left.\begin{aligned} M_1 &= K_1A + K_2B + K_3C \ldots \\ M_2 &= K_4A + K_5B + K_6C \ldots \\ M_3 &= K_7A + K_8B + K_9C \ldots \\ &\ldots \end{aligned}\right\} \quad \ldots\ldots (1)$$

If each component curve is represented by an equation which is linearly independent of the others, the equations are soluble and the solutions will be of the form

$$\left.\begin{aligned} A &= k_1M_1 + k_2M_2 + k_3M_3 \ldots \\ B &= k_4M_1 + k_5M_2 + k_6M_3 \ldots \\ C &= k_7M_1 + k_8M_2 + k_9M_3 \ldots \\ &\ldots \end{aligned}\right\} \quad \ldots\ldots (2)$$

in which the *k*'s are functions only of the constants in equations (1).

In the microanalysis–proportional counter situation, the Kα pulse height distribution curves of neighbouring elements in the periodic table have standard deviations σ which are of the same order as the curve spacings (Bisi and Zappa 1955, Hendee and Fine 1954). Then in an example, if ordinate measurements are made at positions corresponding to the component peaks, the separations of which are exactly σ, equations describing a composite pulse height distribution due to three elements can be written

$$\begin{aligned} y_A &= A + 0{\cdot}607B + 0{\cdot}135C \\ y_B &= 0{\cdot}607A + B + 0{\cdot}607C \\ y_C &= 0{\cdot}135A + 0{\cdot}607B + C \end{aligned}$$

By the usual methods, the solutions are

$$\begin{aligned} A &= 1{\cdot}83y_A - 1{\cdot}52y_B + 0{\cdot}68y_C \\ B &= -1{\cdot}52y_A + 2{\cdot}85y_B - 1{\cdot}52y_C \\ C &= 0{\cdot}68y_A - 1{\cdot}52y_B + 1{\cdot}83y_C \end{aligned}$$

2.1. *Practical Techniques*

For practical microanalysis, a differential pulse height analyser and ratemeter are required for each element whose presence is suspected in the specimen. The analyser channels may be centred on the peaks of the component pulse height distribution curves or may be arranged in any other way, using any channel width, which gives the required linearly independent measurements. Optimum channel widths and positions can be found from signal-to-noise ratio considerations. In the case of two elements, for example, centring the channels exactly on the two component peaks may not give the best ratio of desired to undesired element in the output of each analyser.

All analysers are connected simultaneously to the common proportional counter and pulse amplifier, the ratemeter outputs then furnishing d.c. voltages which correspond to M_1, M_2, M_3 . . of equations (1). These signals, combined in a resistor or operational amplifier matrix according to equations (2), are registered on separate d.c. meters or other indicating devices for each of the elements.

While in principle it should be possible to extend the technique to include as many elements as is desired, thus far separation of only the adjacent elements nickel–copper and copper–zinc has been attempted. The matrixing operation was obtained simply by connecting the terminals of each meter (Ni and Cu or Cu and Zn) between the two ratemeter outputs, with suitably arranged voltage dividers to establish coefficients.

Calibration in the Ni–Cu case, for example, is accomplished by placing pure copper under the electron beam, the appropriate voltage divider being adjusted to give a null reading on the meter indicating nickel. Then with pure nickel pulses, the nickel meter can be calibrated for 100% reading. A similar procedure is followed for the other meter.

2.2. *Specimen Synthesis*

To check the linearity of the method in separating two test wavelengths, a scanning x-ray microanalyser (Cosslett and Duncumb 1957) was arranged to give only a horizontal sweep, the electron beam moving in linear sawtooth fashion across the edge of a thin copper sheet on a nickel background. Controlling the relative time the beam spends on each element gives a convenient method of synthesizing known proportions of copper and nickel. Calibration is straightforward, since time is proportional to distance on a monitor screen, the monitor being scanned in synchronism with the electron beam. The sweep rate was about 200 c/s, considerably faster than the ratemeter time constants.

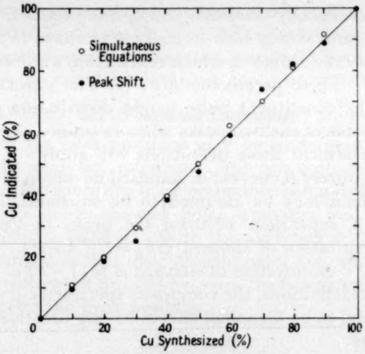

Figure 1. Experimental points in separating synthesized mixture of copper and nickel by the simultaneous equations and peak shift methods.

2.3. *Results*

In the observations (figure 1) by the simultaneous equations method a beam current of 0·15 μA at 25 kv was used, giving a total count rate of 8000 pulses per second with about 800 pulses per second appearing at the output of each pulse height analyser. The analyser channel widths were 0·5 volt, centred on the pulse height distribution peaks. The mean pulse height was about 20 volts, this height giving a separation of nearly 1·5 volts between the component peaks of copper and nickel.

Under substantially the same conditions as in the above experiment, a brass specimen also was analysed. The composition was measured by the simultaneous equations method and checked with a crystal spectrometer. Indicated concentrations were as follows: for the simultaneous equations method, Cu $0{\cdot}58 \pm 0{\cdot}04$, Zn $0{\cdot}40 \pm 0{\cdot}04$; for the crystal method, Cu $0{\cdot}60 \pm 0{\cdot}01$, Zn $0{\cdot}40 \pm 0{\cdot}01$.

§ 3. PEAK SHIFT METHOD

It has long been noticed that the peak of an unresolved or partially resolved x-ray doublet deviates slightly from the position of the stronger component. This effect causes some difficulty in determining the true diameters of diffraction rings, but the shift can be obtained from the known doublet parameters and the true diameter found (Finch 1949). By similar techniques the process can essentially be reversed for proportional counter curves, the observed shift of a two component composite peak being employed to determine the amplitudes of the constituents.

The shape of the curve which relates fractional concentration of the constituents to peak position is determined by several factors: x-ray generation efficiency of the elements in the specimen at the operating voltage; β lines; background radiation; transmission characteristics of the path between the specimen and the counter; spacing between the constituent pulse height distribution curves; standard deviation, escape peak, and other characteristics of the counter; and the means of pulse height discrimination itself. An empirically obtained curve automatically takes everything into account, but it is nevertheless helpful to see in a general way how overall curve shape is affected by two main parameters, the observed values of which result from a combination of previously mentioned factors. These parameters are: (i) The standard deviation relative to the spacing of the constituent pulse height distribution peaks, (ii) The ratio of observed count rates of the two peaks when examined separately in pure form. In the following treatment these definitions will apply: α, β, peak count rates of the purely A and purely B curves; σ, standard deviation of the two proportional counter curves, which may be assumed to be substantially identical (Hendee and Fine 1954); b, separation between the peaks of the two distributions; F_B, fractional concentration of element $BF_B = B/(A+B)$. From the definition of F_B, the fractional concentration of element A is $(1-F_B)$.

Using the above definitions, the composite specimen curve S, the constituents of which are assumed to be Gaussian curves having identical standard deviation, can be expressed as

$$y_S = \alpha(1-F_B)\exp\left[-\frac{x^2}{2\sigma^2}\right] + \beta F_B \exp\left[-\frac{(x-b)^2}{2\sigma^2}\right].$$

To establish the appropriate relationships at the peak, differentiate and set the derivative to zero.

$$\frac{dy_S}{dx}=0=-\alpha(1-F_B)\frac{x}{\sigma^2}\exp\left[-\frac{x^2}{2\sigma^2}\right]+\frac{\beta F_B(b-x)}{\sigma^2}\exp\left[-\frac{(x-b)^2}{2\sigma^2}\right].$$

The value of x which satisfies this equation is x_p, the position of the composite peak. Next solve for F_B, the fractional concentration of element B.

$$F_B=\left\{1+\frac{\beta}{\alpha}\left(\frac{b}{x_p}-1\right)\exp\left[\frac{2bx_p-b^2}{2\sigma^2}\right]\right\}^{-1}. \qquad \ldots\ldots(3)$$

Figure 2 shows a plot of F_B against x_p/b with β/α and σ as parameters. The graph shows that the proportional counter has favourable characteristics for application of the peak shift method to resolution of neighbouring elements in the periodic table (when $\Delta Z=1$, $\sigma\simeq b$). For $\Delta Z=2$, the imminence of two peaks gives the curve a pronounced non-linearity, seriously limiting its usefulness in this situation unless the standard deviation could be suitably increased.

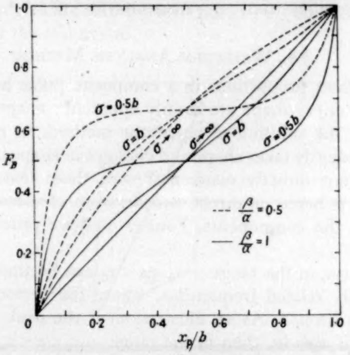

Figure 2. Graph of equation (3), showing relationship between x_p/b the shift of the composite peak towards the position of element B, and F_B, the fractional concentration of element B. The standard deviation σ of the constituent curves is expressed in terms of b, the spacing between the curves. The count rate ratio of pure elements A and B is designated β/α.

3.1. *Practical Techniques*

Determination of the peak positions may be made graphically with a single channel pulse height analyser, ratemeter, and pen recorder, the pure element calibration peaks and the specimen trace preferably being combined on one graph.

Alternatively, two single channel pulse analysers and ratemeters may be arranged in a null bridge fashion. With the analysers staggered on both sides of the peak, but arranged so that their discriminator biases are jointly controlled, a d.c. meter can be connected directly between the two ratemeter outputs, so that a null reading indicates the peak position.

3.2. *Results*

The curves in figure 2 were derived only to show the main features of the peak shift mechanism. Nevertheless, direct application of such curves to an experimental situation yielded the results shown in figure 1. The null bridge method was employed to find the specimen peak, while other conditions, including the method of nickel–copper synthesis, were the same as in the simultaneous equations tests. The proportional counter and other equipment were characterized by the parameters $\sigma = 1{\cdot}2b$ and $\beta/\alpha = 0{\cdot}8$, where β is the peak count rate for pure Cu and α for pure Ni. Voltage readings for the peak positions were put in the form x_p/b for use with figure 2.

As in the experiments with the simultaneous equations method, a piece of brass was also analysed. The indicated fractional concentration of the constituents, copper and zinc, by the peak shift method and by a crystal spectrometer were in good agreement: peak shift method, Cu $0{\cdot}59 \pm 0{\cdot}04$, Zn $0{\cdot}41 \pm 0{\cdot}04$; crystal method, Cu $0{\cdot}60 \pm 0{\cdot}01$, Zn $0{\cdot}40 \pm 0{\cdot}01$.

§ 4. WAVEFORM ANALYSIS METHOD

As the constituent proportions in a composite pulse height distribution are varied, changes in curve shape are readily apparent; shape is directly related to content. Indeed, the solution of equations method, in requiring several area measurements, evidently takes shape and changes in shape into account, although the analysis was not directly concerned with these features. The following method, however, is based on direct consideration of overall curve shape and of its relationship to the components, Fourier analysis providing the mechanism for such a study.

A Gaussian curve in the range $-x_0 < x < x_0$ can be thought of as a synthesis of several integrally related frequencies, where the period of the fundamental is specified by the limits. As an illustration, if the peak height of a Gaussian curve S is 1, and if $x_0 = 4\sigma$, then in the range $-x_0 < x < x_0$

$$\begin{aligned} y_S = {} & 0{\cdot}313 + 0{\cdot}461 \cos \pi x/x_0 + 0{\cdot}182 \cos 2\pi x/x_0 \\ & + 0{\cdot}039 \cos 3\pi x/x_0 + 0{\cdot}004 \cos 4\pi x/x_0 + \ldots \qquad \ldots\ldots (4) \end{aligned}$$

A similar Fourier analysis can be performed in the case of two or more unresolved pulse height distribution curves in one composite curve, the limits, as in the above example, having been chosen to lie well off the tails of the curve. The resulting wave at each frequency will be related to its components due to the individual elements by the usual principles of phasor addition, the proportionality between phase shift and frequency being taken into consideration.

The composite wave at each frequency contains two linearly independent facts about the composite curve: amplitude and phase angle (or the amplitudes of two different, but known, phases). Furthermore, information contributed by a composite wave at a given frequency is linearly independent of that contributed by a composite wave at any other frequency. This is evident in a simple way when it is appreciated that the amplitudes and phases of the various frequencies must vary with respect to each other to account for the observed differences in pulse height distribution waveform as the proportions of the various constituents are changed.

In view of the above discussion, it is reasonable to expect that the fundamental frequency alone should in principle be able to yield information about two unknowns; the fundamental and second harmonic, four unknowns, etc. Against this expectation, however, should be weighed the decreasing amplitudes of the higher harmonics. Signal-to-noise ratio considerations will probably limit analysis to the fundamental and second harmonic. (Widening the limits x_0 has the effect of increasing the higher harmonics relative to the fundamental, however, all frequencies ultimately approaching the same amplitude, albeit infinitesimal, as $x_0 \rightarrow \infty$.)

The observed amplitudes and phases of the appropriate frequencies in the composite pulse height distribution curve, together with the known spectrum of each component curve, are sufficient to enable a set of linear equations to be written, the simultaneous solutions of which yield the amplitudes of the component frequencies. The peak height of a pulse height distribution curve and the amplitudes of its frequency components being proportional, the component curve-heights are readily solved. The phases and amplitudes of the constituent curve spectra are ascertained by separate calibration analyses with pure samples of each of the unknowns.

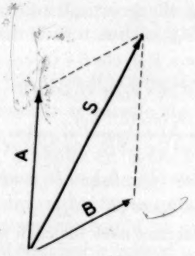

Figure 3. If the length of S and the angular relationships between A, B and S are known, then there is a unique solution for the lengths of A and B.

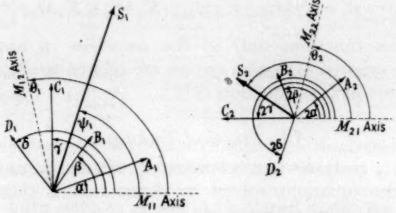

Fundamental Second Harmonic

Figure 4. Fourier components representing elements A, B, C and D, with respect to arbitrary reference axes. Angle between M_{21} axis and S_2 is ψ_2.

To illustrate these principles in the simplest significant case, that of two unknowns, only the fundamental frequency is required and a graphical construction gives the unknown quantities, as in figure 3.

In the case of a composite curve representing three or four X-ray wavelengths in unknown proportions, both the fundamental and second harmonic must be utilized. Referring to figure 4, S_1 and S_2 are the amplitudes of phasors representing the two selected Fourier components of the composite curve. In addition, the phases of all component waves at each frequency and the ratios A_2/A_1, B_2/B_1, . . . are known, having been determined in calibration analyses. The individual amplitudes A_1, B_1, C_1, D_1 are unknown. From figure 4, by phasor summation

$$\left.\begin{aligned}\mathbf{S}_1&=\mathbf{A}_1+\mathbf{B}_1+\mathbf{C}_1+\mathbf{D}_1\\ \mathbf{S}_2&=\mathbf{A}_2+\mathbf{B}_2+\mathbf{C}_2+\mathbf{D}_2\end{aligned}\right\}\qquad\ldots\ldots(5)$$

From the spectrum calibration analyses

$$\frac{A_2}{A_1}=a;\quad \frac{B_2}{B_1}=b;\quad \frac{C_2}{C_1}=c;\quad \frac{D_2}{D_1}=d.\qquad\ldots\ldots(6)$$

With reference to figure 4, equations (5) are rewritten in trigonometric form and combined with equations (6). S_1 and S_2 are resolved into components in the directions of any two convenient reference or measurement axes and expressed in terms of the constituent phasors at the fundamental frequency, M_{11}, M_{12}, M_{21}, M_{22} then representing the practical measurement of these components. To simplify notation, axis M_{21} is chosen such that the angle $A_2M_{21}=2\alpha$.

$$\begin{aligned}\mathrm{M}_{11}=S_1\cos\psi_1 &= A_1\cos\alpha+B_1\cos\beta+C_1\cos\gamma+D_1\cos\delta\\ M_{12}=S_1\cos(\psi_1-\theta_1) &= A_1\cos(\alpha-\theta_1)+B_1\cos(\beta-\theta_1)+C_1\cos(\gamma-\theta_1)\\ &\quad +D_1\cos(\delta-\theta_1)\\ M_{21}=S_2\cos\psi_2 &= aA_1\cos 2\alpha+bB_1\cos 2\beta+cC_1\cos 2\gamma+dD_1\cos 2\delta\\ M_{22}=S_2\cos(\psi_2-\theta_2) &= aA_1\cos(2\alpha-\theta_2)+bB_1\cos(2\beta-\theta_2)+cC_1\cos(2\gamma-\theta_2)\\ &\quad +dD_1\cos(2\delta-\theta_2).\qquad\ldots\ldots(7)\end{aligned}$$

A judicious choice of reference axes for each measurement will eliminate one term from each equation.

Since equations (7) are linear with respect to the unknowns, the answers appear in the form

$$\left.\begin{aligned}A_1&=K_1M_{11}+K_2M_{12}+K_3M_{21}+K_4M_{22}\\ B_1&=K_5M_{11}+K_6M_{12}+K_7M_{21}+K_8M_{22}\\ &\cdots\end{aligned}\right\}\qquad\ldots\ldots(8)$$

where the K's are functions only of the constants in equations (7). The amplitudes of the original Gaussian curves are related to A_1, B_1, C_1, D_1 by the spectrum equations (such as equation (4)).

4.1. *Practical Techniques*

While Fourier analysis and component resolving can be carried out graphically and the equations solved by determinants, these operations lend themselves well to electronic treatment.

Before an electronic Fourier analysis can be performed, however, the incoming proportional counter pulses must be put in a convenient form for such an operation. If the pulses are first squared up and suitably lengthened, the pulse height spectrum can be scanned at a rate substantially faster than the incoming pulse rate, a technique which wastes few pulses, as in the Hutchinson–Scarrott (1951) pulse height analyser. In such an operation pulse height information appears as time or phase information in the form of short pulses of uniform amplitude appropriately positioned relative to the sawtooth controlling the sweeping operation. The pulse height distribution is then a time probability distribution of these pulses over the period of the sweep.

The next step in the process, extraction of the various frequency components from the pulses in the sweep analyser output, is accomplished by separate bandpass filters for the fundamental and each harmonic.

As shown in equations (7), resolution of the sine waves S_1 and S_2, each into two components, may then be carried out, a process which can be handled electronically by a phase demodulation scheme (Hirsch 1953) or by a sampler or clamper which in effect measures the ordinate of the wave in question once in each cycle (McGregor 1952), both common techniques in colour television receivers. With such resolvers or demodulators operating on two different phases for each frequency, the resulting d.c. components correspond to M_{11}, M_{12}, M_{21}, M_{22} of equations (7). Spurious demodulation products are removed by low pass filters.

The d.c. components are next fed into a resistor or operational amplifier matrix which solves for the amplitudes of the various pulse height distribution curves according to equations (8). Finally, the output, in analogue form, may be used to energize scanning cathode-ray tubes, meters or other indicating devices.

4.2. *Two Wavelengths*

A block diagram of equipment to handle the simplest case, in which one unknown is detected and the other is rejected by each demodulator (there thus being no need for a matrix), is shown in figure 5. A sweep frequency in the order of 100 kc/s represents a compromise between pulse circuit design limitations and a high maximum rate of input pulses.

Calibration of such an instrument would be as follows : The sweep width would be set to include the full composite pulse distribution curve of wavelengths

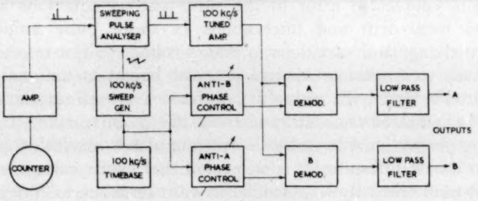

Figure 5. **Block diagram of pulse analysis method for simultaneous resolution of two closely spaced spectral lines.**

A and *B*. Then pure element *A* would be placed under the electron beam, the resulting characteristic x-rays being used to adjust the anti-*A* phase control for zero output from the *B* channel. Similarly, pulses from pure element *B* would establish the condition for zero output from the *A* channel, the indicating means in the *B* channel at the same time being set to 100%. Finally, a return to element *A* would allow calibration of the *A* channel indicator.

4.3. *Three or Four Wavelengths*

Extension of the two wavelength technique to resolve three adjacent wavelengths follows the pattern of figure 6, which shows two demodulations being carried out on the fundamental and one on the second harmonic. If the demodulation axes are chosen such that one unknown term is eliminated by each demodulator, then a simplified matrix can be designed which allows a straightforward calibration procedure.

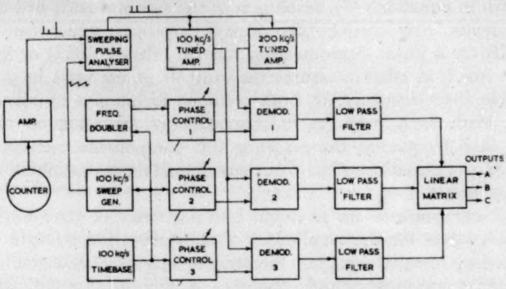
SWEEPING PULSE ANALYSER
100 kc/s TUNED AMP.
200 kc/s TUNED AMP.
AMP.
FREQ. DOUBLER
PHASE CONTROL 1
DEMOD. 1
LOW PASS FILTER
COUNTER
100 kc/s SWEEP GEN.
PHASE CONTROL 2
DEMOD. 2
LOW PASS FILTER
LINEAR MATRIX
OUTPUTS
A
B
C
100 kc/s TIMEBASE
PHASE CONTROL 3
DEMOD. 3
LOW PASS FILTER

Figure 6. Block diagram of pulse analysis method for simultaneous resolution of three closely spaced spectral lines.

Setting up a four-wavelength matrix is likely to be more difficult, but with the aid of approximate solutions of equations (7), empirical trimming of the K coefficients of equations (8) should be possible.

§ 5. DISCUSSION

5.1. *Errors*

The main sources of error in the simultaneous equations and peak shift experiments were drift and fluctuations in mean pulse amplitude due to temperature change and variations in mains voltage. The sensitivity of any of these methods to a spurious change in pulse height at the analyser input can be appreciated by noting that only a 7% decrease in overall amplification is needed to switch the indicated concentration from 100% Zn to 100% Cu, mean pulse height being proportional to energy. In spite of h.t. regulation and a moderate degree of mains stabilization, it is suspected that mains voltage variations (filaments, etc.) were primarily responsible for short term (up to 20 seconds) fluctuations of ±5% in indicated concentrations, although statistical fluctuations were not far below this.

These relatively fast changes were superimposed on a long-term drift largely due to temperature change of the proportional counter. Pulse height drifts amounting to a 30% change in the indicated concentrations were observed in the space of 30 minutes. Such drifts can usually be corrected by frequent calibration.

While drift was a problem in the experiments, it should be remembered that the main advantage of these pulse analysis methods is not at the relatively short wavelengths of the K lines of nickel, copper, and zinc, which were examined here only for test purposes. In a more appropriate region of wavelengths, up to 44 Å for the Kα line of carbon, the effect of pulse amplification drift would be much less serious. A 29% decrease in mean pulse height would be required to shift the indicated concentration from 100% nitrogen to 100% carbon. This represents an improvement by a factor of four over the situation in the neighbourhood of copper. Nevertheless, of course, drift should be minimized at its sources by proper stabilization of the significant parameters.

5.2. *System Comparisons*

While the peak shift method, although fundamentally inefficient and slow, has been included in these discussions as a matter of interest, the main purpose has been to increase the overall efficiency and speed of long wavelength X-ray microanalysis. Lower beam currents mean better spatial resolution and greater flexibility in the preparation of specimens; a higher useful speed of analysis means better scanning pictures. In connection with these desirable characteristics, any complete system of analysis must be assessed from an information point of view. Although such an assessment is beyond the scope of the present paper, it may be useful to indicate the lines it should follow.

For purposes of comparing various systems, an arbitrary but very general quality factor Q can be defined from signal-to-noise ratio and bandwidth considerations. There will be a fundamental $(Q_\lambda)_{\max}$ which characterizes the information which emerges from the specimen at a given wavelength λ. When this signal, together with other wavelengths, is fed into an imperfect system of analysis, information will be wasted, and the several wavelengths will interact in a way which makes the Q_λ quality factor of the emergent information necessarily lower than $(Q_\lambda)_{\max}$.

Consider the simultaneous equations method, for example. The proportional counter will not collect all of the available photons. Also, the information is degraded by the additive nature of random noise even though the signals derived from the pulses may be combined subtractively according to the signs in equations (2).

A similar situation prevails in the waveform analysis method. But an advantage of the more complex scheme is that very high pulse utilization efficiency can be achieved; all pulses, irrespective of their place in the height distribution, contribute in establishing the amplitudes and phases of the Fourier components. Furthermore, it is likely that signal-to-noise degradation would be less than in the simultaneous equations method. Each pulse exerts an influence which is appropriate for its position in the distribution; in the simultaneous equations method all pulses lying within certain prescribed limits are endowed arbitrarily with a given influence.

It is clear that the techniques outlined in this paper, together with the classical methods of spectrometry, should be evaluated as complete information handling *systems*, from specimen to output, each with characteristic capacities for information collection and sorting under the given X-ray microanalysis conditions of operation.

§ 6. CONCLUSION

Poor energy resolution has been the chief factor limiting the usefulness of the proportional counter as the main agent of dispersion in the study of X-ray spectra. Because of the disadvantages of ancilliary means of dispersion at long wavelengths, several pulse analysis methods have been suggested by which the

Kα lines of two or more adjacent elements in the periodic table may, in effect, be resolved completely. These methods should be instrumental in extending present microanalysis techniques to include the elements of very great interest and importance, oxygen, nitrogen, and carbon.

ACKNOWLEDGMENTS

The author is indebted to Dr. N. C. Nixon, Dr. P. Duncumb, and to his supervisor, Dr. V. E. Cosslett, for many helpful discussions and suggestions. Thanks are also due to Dr. Duncumb for the use of his scanning microanalysis equipment, on which the experimental runs were made.

Financial assistance from a scholarship given by the Marshall Aid Commemoration Commission is gratefully acknowledged.

REFERENCES

ALEXANDER, L., 1950, *J. Appl. Phys.*, **21**, 126; 1954, *Ibid.*, **25**, 413.
ANANTHARAMAN, T. R., and CHRISTIAN, J. W., 1953, *Brit. J. Appl. Phys.*, **4**, 155.
ANDERSON, R. E., 1956, *Ph.D. Dissertation*, University of Michigan.
BISI, A., and ZAPPA, L., 1955, *Nuovo Cim.* 2, 988.
CANTY, B. F., and FRANKLIN, A. D., 1958, *J. Appl. Phys.*, **29**, 870.
CASTAING, R., 1951, *Ph.D. Dissertation*, Paris.
COSSLETT, V. E., and DUNCUMB, P., 1957, *Nature, Lond.*, **177**, 1172.
DUMOND, J. W. M., and KIRKPATRICK, H. A., 1931, *Phys. Rev.*, **37**, 136.
FINCH, L. G., 1949, *Nature, Lond.*, **163**, 402.
HENDEE, C. F., and FINE, S., 1954, *Phys. Rev.*, **95**, 281.
HIRSCH, C. J., 1953, *Advanc. Electron.*, **5**, 291.
HUTCHINSON, G. W., and SCARROTT, G. G., 1951, *Phil. Mag.*, **42**, 792.
LIDÉN, K., and STARFELT, N., 1954, *Ark. Fys.*, **7**, 448.
MCGREGOR, R. B., 1952, *Electronics*, **25**, 214.
MAEDER, D., 1958, *Nuclear Instrum.*, **2**, 324.
MELFORD, D. A., and DUNCUMB, P., 1958, *Metallurgia Manchr*, **57**, 159.
MORTON, G. A., 1952, *Advanc. Electron.*, **4**, 69.
RACHINGER, W. A., 1948, *J. Sci. Instrum.*, **25**, 254.
RICHTMEYER, F. K., and BARNES, S. W., 1934, *Phys. Rev.*, **46**, 352.
SHULL, C. G., 1946, *Phys. Rev.*, **70**, 679.
SMITH, L. P., 1934, *Phys. Rev.*, **46**, 343.
STOKES, A. R., 1948, *Proc. Phys. Soc.*, **61**, 382.

The Internal Friction of Annealed Copper at Low Temperatures

By D. H. NIBLETT and J. WILKS
Clarendon Laboratory, Oxford

MS. received 5th August 1958

Abstract. The internal friction of annealed polycrystalline copper has been measured as a function of strain amplitude in the temperature range 20° to 300°K. Both the amplitude-dependent and the amplitude-independent contributions to the decrement increase with increasing temperature over the whole range. Current theories are inadequate to account for the observed dependence of the friction on both strain amplitude and temperature.

§ 1. Introduction

Although many measurements of internal friction have been made at room temperature and above, there is still a scarcity of information at lower temperatures, particularly about the behaviour of pure annealed metals. In previous experiments on the internal friction of polycrystalline copper subjected to varying degrees of cold work (Niblett and Wilks 1957), at temperatures down to 20°K, the friction appeared to arise from at least two components. One component gives rise to a characteristic peak (Bordoni 1949) which is associated with cold work, and the other is a background friction which is quite high in annealed specimens and which is somewhat modified by cold work. Although the behaviour of the Bordoni peak is now fairly well understood in terms of a relaxation mechanism (Seeger, Donth and Pfaff 1957), much less is known about the mechanism responsible for the background and we are at present investigating this friction in some detail. Measurements are being made on polycrystalline copper as we find that values obtained for the friction are much more reproducible than is the case for single crystals, while viscous grain boundary effects should be negligible at these temperatures. So far only preliminary results have been obtained but these are of interest as they are not consistent with any of the current theories.

§ 2. Experimental

The apparatus and method used were similar to those we have described previously, the specimen being in the form of a beam vibrating transversely at a frequency of about 1150 c/s. The 99·999% oxygen-free copper was kindly supplied by the British Non-Ferrous Metals Research Association; it was given a preliminary anneal in argon at 600°K and had a mean grain size of about 0·2 mm. The results are shown in figure 1; the friction, less a small correction term arising from thermoelastic damping, is given as a function of the maximum strain amplitude used in making the measurements. These results were quite reproducible, the state of the material being not much affected by the measurements. For example, the first points obtained in figure 1 were those at 90°K marked by a cross; after measurements at all the other temperatures had been made, a second run was taken at 90°K and this gave the points marked by a diamond. Although consistent results are obtained on a given specimen there is of course no reason to suppose that specimens prepared from different samples of copper will give exactly similar results. For example, although the general behaviour of the friction in the present experiments is similar to that of a specimen reported previously (Niblett and Wilks 1957), its magnitude is considerably higher. This difference almost certainly arises from small differences in structure and impurity content, to which internal friction is very sensitive.

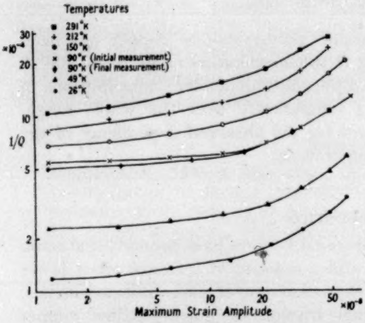

Figure 1. The internal friction of annealed polycrystalline copper as a function of strain amplitude.

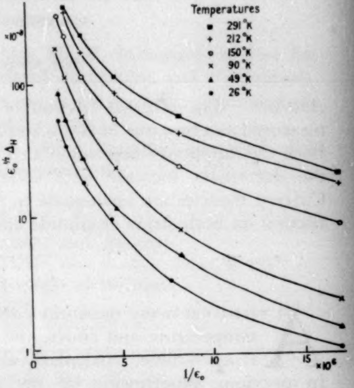

Figure 2. The strain amplitude dependen friction Δ_H plotted according to the theor of Granato and Lücke. ϵ_0 is the maximum strain amplitude.

§ 3. Discussion

Assuming that the friction arises from the motion of dislocations, the marked dependence on temperature and strain amplitude suggests that under the action of a sufficient applied stress a dislocation suddenly moves over a potential barrier. As a result of such motion, the stress-strain curve exhibits hysteresis and there is an associated internal friction. The only extensive treatment of such behaviour has been given by Granato and Lücke (1956), who consider that friction arises from the irreversibility when dislocations are torn away from impurity atoms. The authors argue that for a large number of measurements at room temperature and above, the friction may be resolved into two components: one component Δ_I independent of the strain amplitude and one Δ_H that varies with strain amplitude. It appears from figure 1 that our results might also be discussed in this way.

According to the theory of Granato and Lücke the dependence of the part Δ_H on the strain amplitude ϵ_0 is such that a plot of $\log \epsilon_0^{1/2}\Delta_H$ against $1/\epsilon_0$ should give a straight line, whose slope is proportional to the concentration of impurity atoms on the dislocations†. None of our results give a straight line when plotted in this way, as is illustrated in figure 2, although the form of the curves is similar to that obtained by Granato and Lücke from the data of Noggle and Baker. As Granato and Lücke remark, this type of plot is rather sensitive to the lower values of the friction, so that small errors in determining Δ_H from the total observed friction will be exaggerated. Nevertheless similar behaviour may also be observed in the values of the internal friction of copper at room temperature reported by Barnes, Hancock and Silk (1958), by Nowick (1950) and by Thompson and Holmes (1956).

---

† See Granato and Lücke (1956), p. 805.

The above discrepancy is such that the observed friction at low amplitudes is greater than the theory predicts, and this may perhaps be associated with the comparatively large component of the friction which remains at the lowest strain amplitudes. This contribution is hardly understood at all. One would expect that lengths of dislocation lying between pinning points would vibrate as stretched strings and give rise to a viscous damping (Koehler 1952). Both estimated values and recent results on germanium at megacycle frequencies (Granato and Truell 1956) suggest that such effects will be very small at the frequencies used in the present experiments. Moreover, damping arising in this way should also be proportional to the frequency of the vibrations; evidence on this point is hard to obtain, but it appears likely that the frequency dependence is small.

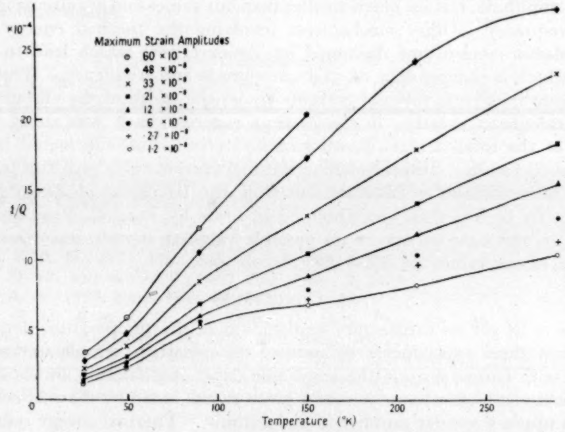

Figure 3. The internal friction of annealed polycrystalline copper as a function of temperature.

In figure 3 our values of the internal friction are shown as a function of temperature for different strain amplitudes. The friction is roughly proportional to the temperature, the slight bulge in most of the curves at the lower end being probably due to a small contribution from the Bordoni mechanism. Granato and Lücke do not discuss the temperature dependence to be expected on their model in any detail. Nevertheless, they remark that if the temperatures are sufficiently high that the impurities reach their equilibrium values along the dislocations, then the lengths on the dislocation loops will vary with temperature in such a way that the logarithms of the slopes of the lines in figure 2 should vary linearly with $1/T$ (Lücke and Granato 1957). However, it is impossible to assign a definite slope to the curves obtained from our results. In any case, one would not expect the concentration of impurities on the dislocation lines to change much during the few hours when the specimen was cooled below room temperature during an experiment.

For low amplitudes of oscillation the observed friction depends only slightly on the strain, so that the lowest curve in figure 3 gives approximate values for the strain independent friction Δ_I. This is roughly proportional to the temperature, while the general form of the curves implies that the component Δ_H also varies with temperature in a similar way. Although one might expect the friction to decrease steadily with falling temperature, as the motions of defects in the crystal become frozen up, there is no adequate theoretical account of this behaviour.

The only theories of internal friction which lead to this type of temperature dependence are those in which the damping is proportional to the thermal energy of the crystal (which to a rough approximation varies as the temperature). Eshelby (1949), Leibfried (1950) and Nabarro (1951) have calculated the damping of vibrating lengths of dislocations by the thermal motion of the crystal. Their values have the right sort of temperature dependence and are independent of strain amplitude, but are much smaller than our values and are also proportional to the frequency. Other mechanisms involving the thermal energy are the thermo-elastic mechanisms discussed by Zener (1948) which lead to internal friction which is independent of strain amplitude and frequency. The friction arising from transverse thermal currents across the width of the vibrating beam may be calculated exactly; in the present experiments it was always a small fraction of the total, and as mentioned above has been subtracted from our experimental results. Intercrystalline thermal currents also give rise to friction which is more difficult to calculate, but from the discussion of Zener (1948) it will probably be less than was observed in brass by Randall, Rose and Zener (1939). In this case its maximum possible value at room temperature is less than 10% of our values for Δ_I.

§4. CONCLUSION

There is as yet no satisfactory explanation of the temperature dependence observed in these experiments in spite of its essentially simple nature. The variation with temperature of the amplitude dependent friction almost certainly arises because at higher temperatures a given strain, aided by thermal activation, is able to unpin a greater number of dislocations. Thermal energy reduces the activation energy required to unpin a dislocation (for example, Seeger 1954) but the exact dependence of the friction on temperature will be a sensitive and complicated function of the distribution of loop lengths in the crystal. It will therefore be difficult to extend Granato and Lücke's treatment to include the effect of temperature. In this connection an earlier result is of interest; a specimen of polycrystalline copper, pre-strained 0·5%, exhibited an amplitude dependent friction which *decreased* as the temperature *increased* in the region between 200° and 300°K (Niblett and Wilks 1957). These temperatures are so far distant from that of the Bordoni maximum that this behaviour cannot be associated with the peak. At low temperatures the amount of unpinning produced by a given strain amplitude will increase with rising temperature and in general the friction will also increase. Ultimately, however, the effect of increasing temperature must be to free the dislocation from all the pinning points; there is then no hysteresis, and Δ_H is zero. Hence, one might expect that under certain conditions the friction should fall with rising temperature.

Since it seems probable that the amplitude dependent friction arises in the manner discussed by Granato and Lücke, it is of interest to consider why the plots of figure 2 are not straight lines. Granato and Lücke resolve the observed friction into two components Δ_I and Δ_H, and assume that Δ_I remains constant at all amplitudes, even though the mean loop length must increase as unpinning proceeds. They justify this assumption on the grounds that only long loops contribute much to Δ_I and that the unpinning processes are concerned with other much shorter loops. However, it is possible that Δ_I also increases with strain amplitude on account of the increase in loop lengths and that some of the rise in the friction–amplitude curves should be associated with Δ_I rather than with Δ_H. The revised values of Δ_H might then give a linear plot.

ACKNOWLEDGMENTS

One of the authors (D. H. N.) wishes to thank the Pressed Steel Company, and the other (J. W.) the Metropolitan-Vickers Electrical Company, for their Research Fellowships.

REFERENCES

BARNES, R. S., HANCOCK, N. H., and SILK, E. C. H., 1958, *Phil. Mag.*, **3**, 519.
BORDONI, P. G., 1949, *Ric. Sci.*, **19**, 851.
ESHELBY, J. D., 1949, *Proc. Roy. Soc.* A, **197**, 396.
GRANATO, A., and LÜCKE, K., 1956, *J. Appl. Phys.*, **27**, 583, 789.
GRANATO, A., and TRUELL, R., 1956, *J. Appl. Phys.*, **27**, 1219.
KOEHLER, J. S., 1952, *Imperfections in Nearly Perfect Crystals* (New York: Wiley), p. 197.
LEIBFRIED, G., 1950, *Z. Phys.*, **127**, 344.
LÜCKE, K., and GRANATO, A., 1957, *Dislocations and Mechanical Properties of Crystals* (New York: Wiley), p. 425.
NABARRO, F. R. N., 1951, *Proc. Roy. Soc.* A, **209**, 278.
NIBLETT, D. H., and WILKS, J., 1957, *Phil. Mag.*, **2**, 1427.
NOWICK, A. S., 1950, *Phys. Rev.*, **80**, 249.
RANDALL, R. H., ROSE, F. C., and ZENER, C., 1939, *Phys. Rev.*, **56**, 343.
SEEGER, A., 1954, *Z. Naturf.*, **9a**, 870; *Phil. Mag.*, **45**, 771.
SEEGER, A., DONTH, H., and PFAFF, F., 1957, *Farad. Soc. Disc.* No. 23, p. 19.
THOMPSON, D. O., and HOLMES, D. K., 1956, *J. Appl. Phys.*, **27**, 713.
ZENER, C., 1948, *Elasticity and Anelasticity of Metals* (Chicago: University Press).

The Small Angle Scattering of 970 Mev Protons by Carbon

By C. J. BATTY†, W. O. LOCK† and P. V. MARCH‡

† Department of Physics, University of Birmingham
‡ Department of Natural Philosophy, University of Glasgow

MS. received 25*th August* 1958, *in final form* 17*th October* 1958

Abstract. The differential cross section for the scattering of 970 Mev protons by carbon through laboratory angles of 1½° to 5° has been measured using nuclear emulsions to detect the scattered particles. The results show a sharp rise at small angles due to the onset of Coulomb scattering and have been fitted at the larger angles (greater than 2°) in terms of a simple model in which the nucleus is represented by a purely imaginary central potential. Values for the diffraction and total cross sections are then derived. Preliminary results of a more detailed analysis, which includes a spin–orbit potential, shows that a fit can be obtained at all angles if a small negative real part to the central potential is included. Further evidence is found for polarization effects at these energies.

§ 1. Introduction

In the study of the scattering of protons by complex nuclei, the small angle region is of particular interest. The interference effects between the Coulomb and the nuclear scattering enable one to learn something of the real and imaginary parts of the central potential. Measurements at small angles present many experimental problems but they have the advantage that in general the contamination due to inelastic scattering is small. This has been shown by work at lower energies in which the energy spectra of protons from various elements have been studied as a function of the scattering angle (Tyren and Maris 1957). Detailed data at the energies considered in this paper are not available, but preliminary results (Huq *et al.*, to be published) suggest that the amount of inelastic scattering for angles less than 5° is of the order of a few per cent of the elastic scattering. The small angle scattering of protons by carbon has been studied by Dickson and Salter (1957) at 95 and 135 Mev, by Gerstein, Niederer and Strauch (1957) at 96 Mev, and by Chamberlain *et al.* (1956) at 300 Mev. The first two sets of experiments showed a dip in the differential cross section at the small angles due to the interference between the Coulomb and the nuclear scattering. At 310 Mev the interference is not quite so marked but is nevertheless significant. It seemed of interest to investigate this problem at a considerably higher energy, and this paper describes a study of the scattering of 970 Mev protons from carbon at angles between 1½° and 5° (laboratory system). The results of preliminary experiments have been reported at the Rochester and Padua–Venice Conferences in 1957. The results presented in this paper are based on a set of exposures made subsequent to these experiments, using an improved beam normalization method.

§ 2. Experimental Arrangement

The high energy protons were obtained from the Birmingham synchrotron operated at full energy. The protons circulating in the internal beam were scattered at $5\frac{1}{2}$° from a carbon target inside the vacuum box, and emerged into the atmosphere through a thin steel window (see figure 1). After passing through the focusing shims (van der Raay 1957) necessary to focus the beam into the experimental room, the height of the beam was defined by a slit-shaped channel of tungsten alloy, $\frac{3}{4}$ in. high by 3 in. wide and about 15 in. long. The beam then passed down an iron channel 30 in. long, $1\frac{1}{4}$ in. wide and 2 in. high, which removed protons not travelling parallel to the main beam, and then through a wide channel in a concrete shielding wall into the experimental room. The beam incident on the second target (hereafter called the scatterer) was well collimated and had a total divergence in the horizontal direction of approximately 0·1°. The profile of the intensity distribution in the horizontal plane was gaussian with a standard deviation of 0·8 cm. In the vertical direction the beam was roughly rectangular in shape with a mean height of 4·4 cm. The collimation system was aligned to the beam direction by the use of x-ray films.

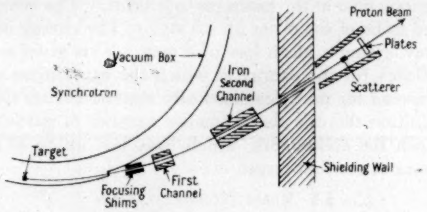

Figure 1. Plan view of the experimental arrangement.

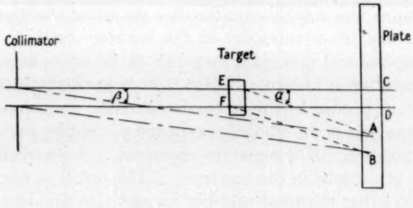

Figure 2. Diagram of the geometry of the target and plate arrangement.

The carbon scatterer was placed in the beam at a distance of about 1 metre from the shielding wall, while the emulsions, to detect the scattered protons, were at a distance of 1 metre beyond the scatterer (see figure 2). Additional shielding was used to protect the emulsions from the background of protons originating from the machine. The scatterer used was a carbon pillar $1\frac{1}{2}$ in. wide and 2 in. thick. The plates used were 7 in. × 1 in. × 200 μ G5 Ilford emulsions, which were held in position horizontally on a bakelite scattering table. Two main exposures, each using eight plates, were made, one with and one without the scatterer in position. Each exposure consisted of a run of 1000 machine pulses, with subsidiary exposures of 100 pulses before, and after, the main exposure. During these subsidiary exposures, $200\,\mu$ thick G5 stripped emulsions were exposed at the scatterer position, normal to the beam. This was done for beam normalization purposes.

§ 3. BEAM ENERGY

The energy of the beam circulating inside the synchrotron under the conditions used in this experiment was (980 ± 10) Mev. The protons in the beam lose energy as they make multiple traversals of the carbon target which scatters them out of the machine, and they also transfer some energy to carbon nuclei when they scatter through $5\frac{1}{2}^\circ$ to be accepted by the collimation system. Therefore, the energy of the protons emerging from the synchrotron is (975 ± 10) Mev, where the 10 Mev uncertainty arises from the lack of precise knowledge of the value of the magnetic field at the mean particle orbit. The energy spread in the beam is estimated to be of the order of ± 5 Mev. The energy loss in the carbon scatterer is 16 Mev, giving a mean loss of 8 Mev. This gives an effective mean value of 967 ± 10 Mev for the energy at which the experiment was carried out, with an energy spread for particles elastically scattered from the first target, of ± 5 Mev. In addition there is also a smaller number of particles, in the beam which passes down the collimators, which have lost up to 40 Mev in inelastic scattering processes at the first target.

§ 4. BEAM NORMALIZATION

The emulsions exposed at the scatterer position, for the runs before and after the main exposure, enabled the beam distribution over the scatterer to be determined. The beam intensity in the plates used to detect the scattered protons in the main exposure was simply obtained by counting the track density in the emulsions. Thus the beam intensity at the carbon scatterer can be obtained provided the horizontal and vertical divergence of the beam between the scatterer and the detector position is known. These factors were obtained from a detailed analysis of the beam profile in the normal incidence emulsions exposed at the target, and from analysis of an emulsion exposed vertically, parallel to the beam, at the scatterer position, in a separate exposure. A correction was applied for the absorption of protons in the scatterer. The result of these measurements and calculations was that the total number of particles incident on the scatterer within ± 12 mm of the centre of the Gaussian for the horizontal distribution of the beam, was $(3{\cdot}58 \pm 0{\cdot}22) \times 10^7$ protons.

§ 5. SCANNING PROCEDURE

A plan of the scatterer and plate arrangement is given in figure 2. The incident beam is taken to be 24 mm in horizontal width, that is $EF = 24$ mm, because the beam intensity was calculated for the limits of ± 12 mm about the beam centre. The emulsions were exposed with the plane of the emulsion horizontal.

Protons scattered through an angle α from the scatterer (see figure 2) will give rise to tracks over the region AB in the plates. Protons scattered through an angle β by the edge of the iron collimator can also reach the region AB. Thus in searching the region AB it is necessary to measure the angle of all tracks which are found in order to distinguish between protons from these two sources.

The angle measurement technique employed was suggested by Dr. S. J. Goldsack and is the following. Each plate being searched was placed on the stage of a Cooke, Troughton and Simms type 4000 microscope, fitted with a coarse movement superstage, and was so arranged that the direction of the main beam in the plates was nominally parallel to the y movement of the stage. One eyepiece of the microscope contained a graticule scale divided into 120 divisions, which corresponded to a length of 100 μ at the magnification used (× 45 objective, × 15 eyepieces). The length of the scale was placed perpendicular to the direction of the beam. As each track was observed in the field of view its position A where it crossed the graticule was recorded. The plate was then moved through a distance of 191 microns in the y direction, and the position of the track B where it crossed the graticule was again recorded. The distance D in microns between A and B is related to the angle θ between the track and the stage y motion by

$$\tan \theta = D/191. \qquad \ldots\ldots(1)$$

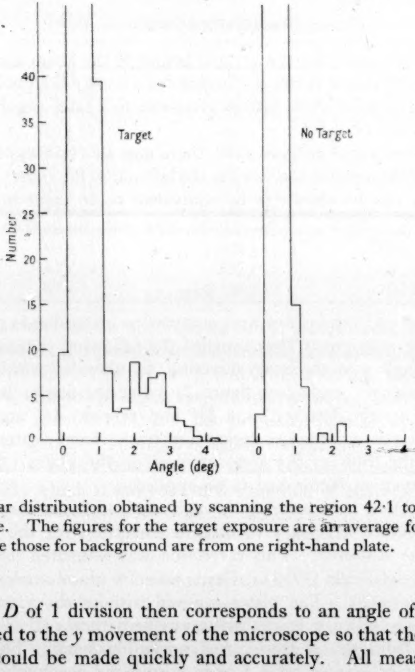

Figure 3. Angular distribution obtained by scanning the region 42·1 to 45 mm from the beam centre. The figures for the target exposure are an average for four right-hand plates, while those for background are from one right-hand plate.

A displacement D of 1 division then corresponds to an angle of $\frac{1}{4}°$. A system of stops was fitted to the y movement of the microscope so that the desired movement of 191 μ could be made quickly and accurately. All measurements were made to the nearest graticule division, giving a a resolution of $\pm\frac{1}{8}°$.

Figure 3 shows an angular distribution of the tracks observed in a region of a plate corresponding to a mean scattering angle of $2\frac{1}{2}°$. The two peaks correspond to the tracks of protons scattered through the angles α and β and are seen to be well resolved. It is also clear that the background of protons scattered from the collimator is large, and this background increases as the angle β becomes smaller. A search of the plates exposed without any scatterer in position shows that all the tracks in the right-hand peak do in fact correspond to protons scattered from the target.

§ 6. ANGULAR ERRORS

Three factors contribute to a spread in the scattering angle to which observations refer. First, the angular divergence of the beam in the horizontal direction was measured directly in the plates, and was found to be approximately $\frac{1}{10}°$ per cm. Secondly, from measurements in the central beam region on the angles of all the tracks in the beam, the angular spread in the beam was found to be $\pm 0{\cdot}4°$. Thirdly, the measurement technique employed only measures the projected angle of scatter, θ in the horizontal plane, undergone by a proton at the target. If this corresponds to a true angle of scatter ϕ where the angle of scatter in the vertical plane is δ, then

$$\cos\phi = \cos\theta\cos\delta. \qquad \ldots\ldots (2)$$

In fact δ is always small, for the vertical height of the beam is only 4·4 cm, and the target to plate distance is 100 cm, so that $\cos\phi = \cos\theta$ to a good approximation. A consideration of these three factors gives rise to a total angular spread on the experimental points of $\pm 0{\cdot}5°$.

Due to the method of analysis used, there may also be a systematic difference in the angles for the protons scattered to the left and to the right. For the present experiment this can be shown to be equivalent to an error in the beam angle determination of $\pm 0{\cdot}12°$. This would give rise to a systematic left–right asymmetry of $\pm 0{\cdot}05$.

§ 7. RESULTS

Tracks observed in the plates were accepted as being due to protons scattered from the carbon scatterer if they satisfied the following criteria: (i) they were at the correct angle α to the beam direction, (ii) they lay within the region AB for a given scattering angle (see figure 2). For the angles between $1\frac{1}{2}°$ (the lowest angle of scatter detected) and $2\frac{1}{4}°$ and between $4\frac{1}{2}°$ and 5° (the largest angle detected) the acceptance region for tracks from scattered protons lay partly outside the limit of the area searched on the plates. In these cases a geometrical correction factor had to be applied.

The cross section for scattering through small angles is observed to be large, and it was therefore necessary to make a correction for the plural Coulomb scattering in the scatterer. This correction was estimated using the multiple scattering theory of Bethe (1953). Corrections for plural nuclear scattering may be shown to be small. The plates exposed without the scatterer in position showed that the number of tracks which satisfied criteria (i) and (ii), but which did not come from the scatterer, was negligibly small. The cross sections given in the last column of table 1 were normalized absolutely using the beam intensity given in § 4. The normalization error, including the error in the beam intensity, is estimated to be $\pm 10\%$.

Table 1

(1)	(2)	(3)	(4)	(5)
1½	348 ± 19	5·47	1·09	10·21 ± 0·55
1¾	464 ± 22	2·60	1·04	6·78 ± 0·32
2	613 ± 25	1·49	1·02	5·23 ± 0·21
2¼	619 ± 25	1·17	1·01	4·19 ± 0·17
2½	724 ± 27	1·02	1·01	4·27 ± 0·16
2¾	679 ± 26	1·00	1·00	3·97 ± 0·15
3	596 ± 25	1·00	1·00	3·48 ± 0·15
3¼	572 ± 24	1·00		3·34 ± 0·14
3½	463 ± 21	1·08		2·92 ± 0·13
3¾	409 ± 20	1·05		2·50 ± 0·12
4	418 ± 20	1·00		2·44 ± 0·12
4¼	374 ± 19	1·02		2·23 ± 0·11
4½	227 ± 15	1·40		1·86 ± 0·12
4¾	165 ± 13	1·63		1·56 ± 0·12
5	92 ± 10	3·13		1·68 ± 0·18

(1) Laboratory angle (°); (2) total number of tracks; (3) geometrical correction factor; (4) plural scattering correction factor; (5) $d\sigma/d\Omega$ (barn sterad^{-1}).

Table 2. Asymmetry Measurements

Lab. angle (°)	No. of tracks Left	 Right	Corrected asymmetry
2	307 ± 18	306 ± 18	−0·02 ± 0·04
2¼	310 ± 18	309 ± 18	−0·02 ± 0·04
2½	300 ± 17	424 ± 21	0·15 ± 0·04
2¾	292 ± 17	387 ± 20	0·12 ± 0·04
3	235 ± 15	361 ± 19	0·18 ± 0·04
3¼	236 ± 15	336 ± 18	0·12 ± 0·04
3½	177 ± 13	286 ± 17	0·20 ± 0·05
3¾	152 ± 12	257 ± 16	0·23 ± 0·05
4	180 ± 13	238 ± 15	0·11 ± 0·05
4¼	143 ± 12	231 ± 15	0·20 ± 0·05
4½	89 ± 9	138 ± 12	0·19 ± 0·07

Separating the results for the observations in the plates to the left, and to the right, of the beam centre, it is possible to calculate the asymmetry, ϵ, as a function of angle, where $\epsilon(\theta) = (R-L)/(R+L)$. L and R refer to the number of tracks scattered to the left, and to the right, respectively, at an angle θ. The results of this calculation are given in table 2. The estimated possible systematic error in the asymmetry is ±0·05. The figures for the asymmetry given in the last column of table 2 have been corrected for a small systematic asymmetry (of the order of 0·02 to 0·03) which is inherent in the method of analysis used.

§ 6. DISCUSSION

(*a*) *Simple model.*

The results plotted in figure 4 show a sharp rise in the differential cross section at the small angles associated with the onset of Coulomb scattering. At the larger angles (> 2½°) the scattering is predominantly nuclear scattering. The curves shown in the figure have been calculated on the basis of the following assumptions.

The differential cross section at an angle θ, $\sigma(\theta)$, may be written as

$$\sigma(\theta) = (\mathscr{R}I_c + \mathscr{R}_0 I_n)^2 + (\mathscr{I}I_c + \mathscr{I}I_n)^2 \qquad \ldots\ldots(3)$$

where I_c and I_n represent the scattering amplitudes for Coulomb and nuclear scattering respectively, and where $\mathscr{R}$ and $\mathscr{I}$ denote real and imaginary parts. The real and imaginary parts of the amplitude I_c, were calculated using the formula given by Mott and Massey (1949), for the scattering of protons by a point charge, modified to allow for relativistic effects. The effect on the differential cross section for Coulomb scattering of replacing a point charge by a charge distribution of finite size is very small in the angular region of interest. To calculate the nuclear scattering amplitude, two assumptions were made: (i) that the scattering nucleus may be represented by a region of potential, which was taken to be imaginary and (ii) spin dependent potentials were neglected. With these assumptions $\mathscr{R}I_n = 0$, and $\mathscr{I}I_n$ was calculated using the formula of Fernbach Serber and Taylor (1949) for the scattering of nucleons by a 'black-disc', normalized to a total diffraction scattering cross section σ_d, so that

$$\mathscr{I}I_n(\theta) = i\sqrt{\left(\frac{\sigma_d}{\pi}\right)}\left[\frac{J_1(kR\sin\theta)}{\sin\theta}\right] \qquad \ldots\ldots(4)$$

where k is the wave number of the incident proton (in the laboratory system) R is the radius of the carbon nucleus, J_1 is a first order Bessel function and θ is the scattering angle in the laboratory system.

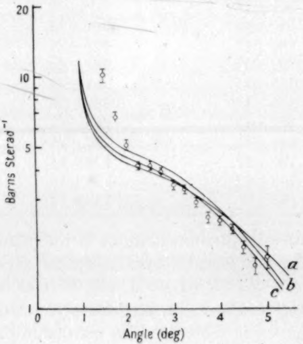

Figure 4. The differential cross sections for the scattering of 970 MeV protons from carbon as a function of laboratory angle of scatter. Curve *a* is calculated for $\sigma_d = 130$ mbn, $R = 2{\cdot}80 \times 10^{-13}$ cm; curve *b* for $\sigma_d = 130$ mbn, $R = 3{\cdot}0 \times 10^{-13}$ cm; and curve *c* for $\sigma_d = 120$ mbn, $R = 3{\cdot}0 \times 10^{-13}$ cm.

The calculations of $I_n(\theta)$ and thus of $\sigma(\theta)$, were carried out for various values of R and σ_d. Some of the curves obtained are shown in figure 4. Allowing for the normalization error of ± 10% and the statistical error in the results, the estimated best values of R and σ_d are $R = 3{\cdot}0 \pm 0{\cdot}1 \times 10^{-13}$ cm, $\sigma_d = 120 \pm 15$ mbn. The value for R is to be compared with that of $3{\cdot}04 \times 10^{-13}$ cm obtained by Fregeau (1956) for the radius of the carbon nucleus, using a uniform density distribution. The value of σ_d agrees well with those determined directly by other workers (see table 3).

Table 3. Cross Sections for Carbon

Reference	Energy	σ_t (mbn)	σ_a (mbn)	σ_d (mbn)
Booth *et al.* (1958)	765 MeV Neutrons	$342{\cdot}1 \pm 3{\cdot}7$	197 ± 25	145 ± 25
Chen *et al.* (1955)	860 MeV Protons	405 ± 23	209 ± 22	196 ± 31
Booth *et al.* (1957)	900 MeV Protons	392 ± 24	230 ± 20	162 ± 31
Coor *et al.* (1955)	1·4 GeV Neutrons	378 ± 10	201 ± 13	177 ± 17
Law (1958, private communication)	910 MeV Protons	$362{\cdot}0 \pm 2{\cdot}4$	$231{\cdot}4 \pm 6{\cdot}5$	$130{\cdot}6 \pm 6{\cdot}0$
Present work	970 MeV Protons	374 ± 34	254 ± 37	120 ± 15

A value of the total cross section σ_t can be obtained for these values of σ_d and R by using (4) and the optical theorem

$$\sigma_t = \frac{4\pi}{k} \mathscr{I} I_n(\theta) \qquad \ldots\ldots(5)$$

where $\mathscr{I} I_n(0)$ is the imaginary part of the forward ($\theta = 0°$) amplitude for nuclear scattering, which is obtained from equation (4). This gives a value of $\sigma_t = 374 \pm 34$ mbn. This is compared in table 3 with the values obtained by direct measurements by other workers; the absorption and diffraction cross sections corresponding to each quoted total cross section are also given.

(*b*) *More detailed calculations.*

It is clear that the simple model described above gives a good representation of the small angle scattering data at 970 MeV, for angles greater than 2°. Below 2° the measured cross section is greater than the cross section predicted by the model we have employed. There are at least three factors, which the model neglects, which may account for this discrepancy. Firstly, the expression (3) is not completely correct. It may be shown that the presence of both nuclear absorption and Coulomb scattering does not allow the two sets of scattering amplitudes to be added directly (Batty 1959) but effectively increases the amount of Coulomb scattering at small angles; in the present case this effect is very marked and accounts almost entirely for the discrepancy between the theoretical curves and experimental points at angles of less than 2°. Secondly, we have ignored the possible presence of a spin orbit potential, and thirdly we have assumed the real part of the central potential to be zero. One might expect the effects of any spin dependent potential on the shape of the differential cross section to be small, although the magnitude of the absolute cross sections will change. A real part to the central potential could also make appreciable difference to the calculated cross sections.

A detailed analysis of the effects of these factors has been made by Batty (1959) for an energy of 310 MeV. A potential of the form

$$V(r) = V_c \rho'(r) + V_n \rho(r) + \frac{C|V_n|}{r} \frac{d\rho(r)}{dr} \boldsymbol{\sigma} . \mathbf{L}, \qquad \ldots\ldots(6)$$

was used, where V_c is the Coulomb and V_n the nuclear potential, $\rho'(r)$ and $\rho(r)$ the charge and density distributions and C the spin–orbit coupling parameter.

We have used this method to make a preliminary analysis of our results at 970 MeV, using a value for $\mathscr{I} V_n$ given directly by the nucleon–nucleon total cross sections (Brown, Ashmore and Nordhagen 1958). In the majority of experiments the beam intensity used and thus the absolute values of the differential cross sections, are not well determined. It is necessary, therefore, to introduce into the analysis a normalization constant N (Batty 1959). This is the number by which the observed values of the differential cross section must be multiplied in order to give a good fit to the theoretical curves. It is not possible to apply the analysis to the asymmetry measurements due to the presence of inelastic contamination, particularly at the larger angles. A fit to the experimental differential and total cross section data then gives $\lambda=-0{\cdot}4$, $C=1{\cdot}0\times10^{-27}\,\mathrm{cm}^2$, $N=1{\cdot}22$ where $\lambda=\mathscr{R}V_{\mathrm{n}}/\mathscr{I}V_{\mathrm{n}}$.

The theoretical curve obtained for the differential cross section using the above parameters is plotted in figure 5. The agreement with the experimental points (which have been multiplied by the factor N) is seen to be much better than that shown in figure 4, especially at angles smaller than 2°. The value obtained for N is rather high as the accuracy of the normalization of the experimental results was estimated to be to $\pm10\%$ (i.e. we expect N to lie between 0·9 and 1·1). However, it is possible that there may be some unknown systematic error in the method of beam monitoring used which could have caused the beam intensity to be overestimated and hence given rise to low values for the experimental cross section.

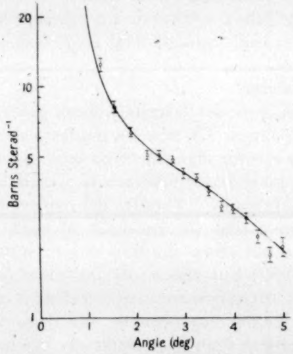

Figure 5. The differential cross sections for the scattering of 970 MeV protons from carbon as a function of laboratory angle of scatter. The full line is that calculated using $\lambda=-0{\cdot}40$ and $C=1{\cdot}0\times10^{-27}\,\mathrm{cm}^2$ (see text). The experimental points at the smallest angles have been corrected for the finite angular resolution of the apparatus.

The fit to the experimental data is not completely unique since fits to the data which are not much worse can be obtained with values of N closer to 1, which correspond to smaller absolute values of λ. However, in all of these λ is found to be negative. To obtain more definite information about the values of λ and C, it is necessary either to perform experiments of increased accuracy at small angles, or to measure other quantities which contain these two parameters.

The present analysis shows that the real part of the central potential is of opposite sign to the imaginary part. This is in contrast to the situation at lower energies where, although the real part is small and decreasing with increasing incident nucleon energy, it has the same sign as the imaginary part. Our value for C is similar to that obtained by Booth, Hutchinson and Ledley (1958) in an analysis of the total cross section for 765 MeV neutrons in which they assumed the central potential to be purely imaginary. No other optical model analyses using realistic density distributions for the nucleus have been made at energies above 350 MeV.

(*c*) *Polarization effects.*

The asymmetries given in table 2 are similar to those obtained in other emulsion experiments in this laboratory (Batty and Goldsack 1957, 1958) and by the counter group of this laboratory (Huq *et al.*, to be published) after adjustment for different angles for the first scattering. It should be emphasized, however, that the experiment described in this paper was not designed to measure small asymmetries, and possible systematic errors may be larger than the value of ± 0·05 stated in § 6. Since the energy detection threshold for protons counted in the plates is only 400 MeV, the asymmetry calculated is based on observations of both elastically and inelastically scattered protons. The asymmetry corresponding to elastically scattered protons only may well be higher. It is possible, therefore, that the marked polarization effects found at lower energies still exist at energies of the order of 1 GeV. This statement is in agreement with the data obtained by Huq *et al.* (1959) using Čerenkov counters with a high energy detection threshold.

ACKNOWLEDGMENTS

Our thanks are due to Dr. S. J. Goldsack who contributed greatly to this work in its early stages and with whom we have had the benefit of many fruitful discussions; to Dr. P. J. Duke and Dr. H. B. van der Raay who also gave us considerable assistance in the early stages of the experiments; to the scanners at Birmingham (Miss J. Kendrick, Miss H. Sismey and Miss M. Whittle) and at Glasgow (Miss O. Archibald, Mrs. K. Burton and Miss M. Thomson) and to the synchrotron staff for their efficient operation of the machine.

P. V. M. wishes to thank Professor P. I. Dee for permission to collaborate in this work. C. J. B. wishes to thank the Department of Scientific and Industrial Research for a Maintenance Grant.

REFERENCES

BATTY, C. J., 1959, *Proc. Phys. Soc.*, **73**, in the press.
BATTY, C. J., and GOLDSACK, S. J., 1957, *Proc. Phys. Soc.* A, **70**, 165.
—— 1958, *Ibid.* **72**, 1130.
BETHE, H. A., 1953, *Phys. Rev.*, **89**, 1256.
BOOTH, N. E., HUTCHINSON, G. W., and LEDLEY, B., 1958, *Proc. Phys. Soc.*, **71**, 293.
BOOTH, N. E., LEDLEY, B., WALKER, D., and WHITE, D. H., 1957, *Proc. Phys. Soc.* A, **70**, 209.
BROWN, G. E., ASHMORE, A., and NORDHAGEN, R., 1958, *Proc. Phys. Soc.*, **71**, 565.
CHAMBERLAIN, O., SEGRE, E., TRIPP, R., WIEGAND, C., and YPSILANTIS, T., 1956, *Phys. Rev.*, **102**, 1659.
CHEN, F. F., LEAVITT, C. P., and SHAPIRO, A. M., 1955, *Phys. Rev.*, **99**, 857.
COOR, T., HILL, D. A., HORNYAK, W. F., SMITH, L. W., and SNOW, G., 1955, *Phys. Rev.*, **98**, 1369.
DICKSON, J. M., and SALTER, D. C., 1957, *Nuovo Cim.*, **6**, 235.
FERNBACH, S., SERBER, R., and TAYLOR, T. B., 1949, *Phys. Rev.*, **85**, 1132.
FREGEAU, J. H., 1956, *Phys. Rev.*, **104**, 225.
GERSTEIN, G., NIEDERER, J., and STRAUCH, K., 1957, *Phys. Rev.*, **108**, 427.
MOTT, N. F., and MASSEY, H. S. W., 1949, The theory of atomic collisions, 2nd Edn (Oxford: Clarendon Press), p. 48.
VAN DER RAAY, H. B., 1957, *Nucl. Instrum.*, **1**, 351.
TYREN, H., and MARIS, TH. A. J., 1957, *Nucl. Phys*., **3**, 52; **4**, 662.

RESEARCH NOTES

The (γ, n) and (γ, 2n) Reactions in ^{141}Pr

By J. H. Carver and W. Turchinetz
Research School of Physical Sciences, Australian National University, Canberra

MS. received 19*th June* 1958

There are few measurements of the competition between single and multiple emission in nuclear photodisintegration. Such measurements can give information about the relative importance of direct emission and compound nucleus formation. Among the heavy elements the (γ, n), (γ, 2n) and (γ, 3n) reactions in ^{181}Ta have been investigated previously by a combination of induced radioactivity and total neutron yield measurements (Carver, Edge and Lokan 1957, Carver and Turchinetz 1958). It was found that direct interactions accounted for a large part of the photon absorption in the high-energy tail above the giant resonance.

Praseodymium is particularly suitable for this type of measurement. It is monoisotopic and both the (γ, n) and (γ, 2n) reactions can be studied by activation methods. Since ^{141}Pr has a closed neutron shell ($N=82$), it is interesting to compare these results with those for ^{181}Ta ($N=108$) which is midway between shells.

Samples of praseodymium oxide were irradiated with the bremsstrahlung from the Canberra 33 MeV electron synchrotron and the induced activities were measured with a scintillation spectrometer. The measurement of the 3·4 min ^{140}Pr produced in the (γ, n) reaction is described above (Carver and Turchinetz 1959). A similar method was used to determine the (γ, 2n) cross section by measuring the yield of 4·5 hr ^{139}Pr.

The decay of ^{139}Pr is similar to that of ^{140}Pr in that the majority of transitions involve β^+ emission or electron capture between ground states (Stover 1951, Browne *et al.* 1952, Handley and Olson 1954). As a result, the relative yields can be estimated from the x-ray intensities with fair accuracy ($\sim 10\%$ at 30 MeV), the major uncertainty being that in the ratio of K capture to β^+ emission as discussed below. The quantities needed to evaluate the absolute yields were as follows:

(i) The K-shell fluorescence yield $W_K=0{\cdot}89$ in both cases (Bergstrom 1955). (ii) The ratio of K-capture to total capture equal to 0·89 in both cases (Brysk and Rose 1955). (iii) The ratio of K-capture to positron emission, K/β^+: For ^{140}Pr this is given by Browne *et al.* (1952) as $K/\beta^+=0{\cdot}63$, which is in good agreement with the theoretical value obtained from the graphs of Feenberg and Trigg (1950) for a distintegration energy of 3·25 MeV. For ^{139}Pr Stover (1951) has estimated the ratio $K/\beta^+ \simeq 16$ on the basis of absorption measurements. During the course of this work a comparison was made of the ratio of K x-ray intensity to annihilation radiation intensity from ^{140}Pr and ^{139}Pr. It was found that for ^{139}Pr $K/\beta^+=5{\cdot}2$, assuming the result quoted by Browne *et al.* (1952) of $K/\beta^+=0{\cdot}63$ for ^{140} Pr. In view of the uncertainties inherent in the use of absorption measurements with Geiger counters for the determination of intensities, the value of $K/\beta^+ = 5{\cdot}2$ was adopted for ^{139}Pr rather than the larger value quoted by Stover (1951). It may be noted that this amounts to using a value of $f_K = 0{\cdot}76$ for the probability of K-capture rather than $f_K = 0{\cdot}85$ which follows from Stover's data.

The ^{141}Pr (γ, n) and $(\gamma, 2n)$ cross sections (σ_1 and σ_2) derived from the measured activation curves are shown in the figure. Also shown is the activation curve for the reaction ^{141}Pr $(\gamma, 2n)$; that for ^{141}Pr (γ, n) has been published above (Carver and Turchinetz 1959). The $(\gamma, 2n)$ threshold is at 18·3 MeV (Johnson and Nier 1957), which is about 3 MeV above the peak in σ_1 and consequently σ_2 takes up a much smaller fraction of the total integrated cross section than is the case for ^{181}Ta. The total integrated cross sections for ^{141}Pr are

$$\int_0^{31} \sigma_1 \, dE = 2{\cdot}2 \pm 0{\cdot}3 \text{ MeV barns, and } \int_0^{31} \sigma_2 \, dE = 0{\cdot}4 \pm 0{\cdot}06 \text{ MeV barns}$$

with the ratio

$$\int_0^{31} \sigma_1 \, dE \bigg/ \int_0^{31} \sigma_2 \, dE = 5{\cdot}5 \pm 0{\cdot}6,$$

whereas for ^{181}Ta the corresponding ratio is $2{\cdot}7 \pm 0{\cdot}3$.

It should be noted that σ_2 does not alter the conclusion concerning the narrowing of the giant resonance at closed shells as inferred from the measurements of σ_1 (Carver and Turchinetz 1959).

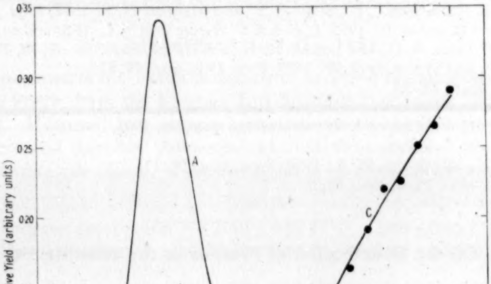

Cross sections for the reactions: A, ^{141}Pr (γ, n); B, ^{141}Pr $(\gamma, 2n)$; C, the activation curve for ^{141}Pr $(\gamma, 2n)$.

As in the ^{181}Ta case, σ_1 is still finite well beyond the $(\gamma, 2n)$ threshold where, if the statistical conditions were satisfied, σ_2 should be the predominant process.

In this higher energy region, σ_1 must be due to direct emission and only σ_2 will involve the formation of a compound nucleus at some stage. The relative integrated cross sections for the high-energy tail are

$$\int_{21}^{31} \sigma_1\,dE \Big/ \int_{21}^{31} \sigma_2\,dE = 1{\cdot}5 \pm 0{\cdot}25,$$

which is even higher than the corresponding ratio ($0{\cdot}86 \pm 0{\cdot}15$) for ^{181}Ta. These results suggest that direct emission may occur with greater probability in the case of closed shell nuclei.

Other reactions are unlikely to contribute greatly to the total absorption. The coulomb barrier has a height of about 12 MeV, and reactions involving proton emission are expected to have small yields and are most likely to follow direct interactions. The threshold for the (γ, 3n) reaction is 29 MeV (Johnson and Nier 1957). The total integrated cross section

$$\int_{0}^{31} (\sigma_1 + \sigma_2)\,dE = 2{\cdot}6 \pm 0{\cdot}4 \text{ MeV barns}$$

agrees moderately well with the value of 2·88 obtained from the dipole sum rule with an exchange force parameter $x = 0{\cdot}5$ (Levinger and Bethe 1950).

REFERENCES

BERGSTROM, I., 1955, *Beta- and Gamma-Ray Spectroscopy* (Amsterdam: North-Holland Publishing Co.).

BROWNE, C. I., RASMUSSEN, J. O., SURLS, J. P., and MARTEN, D. F., 1952, *Phys. Rev.*, **85**, 146.

BRYSK, H., and ROSE, M. E., 1955, *U.S.A.E.C. Report* O.R.N.L.-1830 and corrigendum.

CARVER, J. H., EDGE, R. D., and LOKAN, K. H., 1957, *Proc. Phys. Soc.* A, **70**, 415.

CARVER, J. H., and TURCHINETZ, W., 1958, *Proc. Phys. Soc.*, **71**, 613.

—— 1959, *Ibid.*, **73**, 69.

FEENBERG, E., and TRIGG, G., 1950, *Rev. Mod. Phys.*, **22**, 399.

HANDLEY, T. H., and OLSON, E. L., 1954, *Phys. Rev.*, **96**, 1003.

JOHNSON, W. H., and NIER, A. O., 1957, *Phys. Rev.*, **105**, 1014.

LEVINGER, J. S., and BETHE, H. A., 1950, *Phys. Rev.*, **78**, 115.

STOVER, B. J., 1951, *Phys. Rev.*, **81**, 8.

On the Distribution of Protons in the Nuclide ^{12}C

BY L. R. B. ELTON†, B. J. HILEY‡ AND R. PRICE‡

† Department of Physics, Battersea College of Technology, London
‡ Wheatstone Laboratory, King's College, London

MS. received 1*st October* 1958

THE scattering of high energy electrons from ^{12}C has been analysed for a large variety of possible nuclear form factors (Fregeau 1956), and in particular for the density distribution given by the form factor

$$\rho(r) = \rho_0\left(1 + \frac{4}{3}\frac{r^2}{a_0^{\,2}}\right)\exp\left(-\frac{r^2}{a_0^{\,2}}\right) \qquad \ldots\ldots(1)$$

which is based on shell model considerations. The analysis has not, however, been performed in terms of the so-called Fermi form factor (Yennie, Ravenhall and Wilson 1954)

$$\rho(r) = \frac{\rho_{\mathrm{F}}}{1 + \exp\left[4{\cdot}4(r-c)/t\right]} \qquad \ldots\ldots(2)$$

which has been used for the analysis of electron scattering by heavier nuclides (Hofstadter 1956). In order to be able to systematize the work on electron scattering over the whole range of elements this calculation has now been performed by means of the Born approximation, which for such a light nuclide is valid except at the largest scattering angles. Such a calculation was first done by Advani, Harihar and Gatha (1956), but, as we shall see below, the choice of parameters by these authors is open to serious criticism.

The differential cross section in the Born approximation can be written (Hofstadter 1956)

$$\frac{d\sigma}{d\Omega}=\left(\frac{Ze^2}{2E}\right)^2\frac{\cos^2\frac{1}{2}\theta}{\sin^4\frac{1}{2}\theta}\left[\int_0^\infty 4\pi r^2\rho(r)\,\frac{\sin qr}{qr}\,dr\right]^2 \qquad \ldots\ldots(3)$$

where $k=E/\hbar c$ is the wave number of the incident electron, $q=2k\sin\frac{1}{2}\theta$ is the magnitude of the momentum transfer and θ is the scattering angle in the centre-of-mass system. The integral was performed by means of a formula due to Blankenbecler (1956), valid for $c \gg z$, which is the case here,

$$\int_0^\infty \frac{r\sin qr}{1+\exp[(r-c)/z]}\,dr=\pi cz\left\{\frac{\pi z}{c}\sin(qc)\cosh(\pi qz)\,\mathrm{cosech}^2(\pi qz)\right.$$
$$\left.-\cos(qc)\,\mathrm{cosech}(\pi qz)\right\}. \qquad \ldots\ldots(4)$$

The parameters c and t in (1) were varied independently and a best fit was obtained with

$$c=2\cdot35\pm0\cdot05\,\mathrm{f},\quad t=1\cdot85\pm0\cdot15\,\mathrm{f}. \qquad \ldots\ldots(5)$$

With these parameters the Fermi distribution is almost indistinguishable when plotted on a graph, from the Fregeau distribution that gives the best fit to the experiments. However, past experience has shown this to be a poor criterion of equivalence and therefore the second and fourth moments of the respective distributions were calculated. They are found to be in excellent agreement:

	$[\langle r^2\rangle]^{1/2}$	$[\langle r^4\rangle]^{1/4}$
Fregeau distribution	2·40 ± 0·05 f	2·66 ± 0·05 f
Fermi distribution	2·39 ± 0·05 f	2·68 ± 0·05 f.

The comparison has of course been made with the results obtained by Fregeau using the Born approximation. Exact calculations should reduce these values by about 0·03 f.

Although it is not possible to give an exact meaning to the concepts of half-density radius c and skin thickness t for distribution (1), a reasonable estimate can be made and is in complete agreement with (5) (Hofstadter 1957, table IV). The same table shows the skin thickness of ^{16}O to be equally small, while those of heavier nuclides lie in the neighbourhood of $t\sim 2\cdot5$ f. It would be most interesting to see whether other light nuclides, that are not even–even, have larger t or whether all light nuclides have small t. The small skin thicknesses result in the r.m.s. radii $[\langle r^2\rangle]^{1/2}$ of both ^{12}C and ^{16}O being about 10% below the values obtained from the semi-empirical formula of Elton (1958), which fits the heavier nuclides†.

---

† There is a mistake in this paper, the correction of which slightly changes the coefficients of the semi-empirical formula. The change is negligible for heavier nuclides, but leads to an r.m.s. radius of 2·60f for ^{12}C.

A truly remarkable fact is that the central density of nuclear matter found for the Fermi distribution is only 2% below the average found for heavier nuclides (Elton 1958). For a light nuclide such as ^{12}C, which has a very small core of constant density, the scattering experiments determine the central density rather closely and it can be concluded that nuclear matter is in a state of saturation at the centre of the carbon nucleus.

Lastly, it must be pointed out that the conclusion drawn by Advani *et al.* from the ^{12}C data, namely that it is possible to distinguish between different functional forms of the density, is not correct. This conclusion was based on the assumption of a strict proportionality of c to $A^{1/3}$ and a strictly constant value of t. As we now know, neither of these assumptions is valid.

REFERENCES

ADVANI, M. K., HARIHAR, P., and GATHA, K. M., 1956, *Proc. Phys. Soc.* A, **69**, 650.
BLANKENBECLER, R., 1956, *Amer. J. Phys.*, **25**, 279.
ELTON, L. R .B., 1958, *Nucl. Phys.*, **5**, 173; **8**, 396.
FREGEAU, J. H., 1956, *Phys. Rev.*, **104**, 225.
HOFSTADTER, R., 1956, *Rev. Mod. Phys.*, **28**, 214.
—— 1957, *Ann. Rev. Nuclear Sci.*, **7**, 231.
YENNIE, D. R., RAVENHALL, D. G., and WILSON, R. N., 1954, *Phys. Rev.*, **95**, 500.

Pair Production in the Field of the Electron

BY J. MOFFATT AND G. C. WEEKS†
Clarendon Laboratory, Oxford

MS. received 12*th September* 1958

IN a recent review article Joseph and Rohrlich (1958) have discussed the theory of pair production and Bremsstrahlung in the field of free and bound electrons. Because of mathematical complexity, no exact calculations of the cross sections for these processes have been made to date, but the authors discuss the errors inherent in the approximate calculations of Borsellino and Votruba. In particular, they conclude that for pair production from free electrons at extreme relativistic energies Borsellino's approximation gives an upper limit and Votruba's a lower limit to the exact theory. The calculations of Votruba have been improved by Joseph and Rohrlich who give the lower limit to the total cross section as:

$$\sigma_{\min}=\left(\frac{28}{9}\ln\frac{2k}{\mu}-\frac{100}{9}\right)\bar{\phi}$$

where k is the photon energy, μ the rest energy of the electron, and $\bar{\phi}=r_0^2/137$ is the usual cross section unit.

Measurements of the total absorption cross section of liquid hydrogen for 94 MeV photons previously made in this laboratory (Moffatt, Thresher, Weeks and Wilson 1958) gave a cross section of 4·7 millibarns for incoherent pair production, which at 94 MeV should be almost equal to the pair production cross section for a free electron. Unfortunately, when this result was published, the experimental measurement was compared with an earlier calculation by Rohrlich and Joseph which was slightly in error. We have since extended our measurements on liquid hydrogen to two lower energies, and it is of interest to compare the experimental data with the upper and lower limits referred to above.

---

† Now at Atomic Energy Research Establishment, Harwell, Berks.

The experimental method was similar to that used at 94 MeV except that the peak energy of the synchroton and the counter bias were reduced, so that the mean energy of the photons detected was 68·5 MeV for one set of runs and 42·5 MeV for the other. Normalized counting rates were measured with the liquid hydrogen absorber in and out of the beam, and from the measured transmission, total absorption coefficients were deduced. Because of the more rapid variation of cross section with energy at the lower energies, the counter threshold was set nearer to the peak energy of the synchroton, and this involved a somewhat larger correction for pile up of pulses, but even at 42·5 MeV, the correction was only 1·2%.

(1)	(2)	(3)	(4)	(5)
42·5 ± 1·0	23·93 ± 0·40	16·64	4·58	2·71 ± 0·40
68·5 ± 1·2	20·73 ± 0·42	11·25	5·41	4·07 ± 0·42
94·0 ± 1·5	19·24 ± 0·32	8·64	5·96	4·64 ± 0·32

(1) Energy (MeV) ; (2) total cross section (mbn) (experimental) ; (3) Compton cross section (mbn) (calculated) ; (4) coherent pair cross section (mbn) (calculated) ; (5) incoherent pair cross section (mbn).

The total experimental cross sections per atom are shown in column (2) of the table, the errors quoted being standard deviations. Columns (3) and (4) give the calculated cross sections for Compton scattering and coherent pair production by the screened nuclear field. The screening correction for molecular hydrogen was taken as one half that for atomic hydrogen. Bernstein and Panofsky (1956) have shown that at 500 MeV, the effect of molecular binding is to reduce the screening correction, and since the screening correction for atomic hydrogen is only about 1% at 94 MeV, the error due to the uncertainty in the effect of binding is not likely to exceed 0·03 mbn. Column (5) lists the values of the incoherent pair production cross sections deduced by subtracting columns (3) and (4) from column (2).

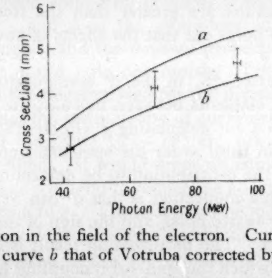

Pair production cross section in the field of the electron. Curve *a* is the theoretical cross section of Borsellino, curve *b* that of Votruba corrected by Joseph and Rohrlich.

The effect of screening on incoherent pair production in atomic hydrogen has been calculated by Wheeler and Lamb (1939) and at energies below 100 MeV the correction is extremely small. As the correction for molecular hydrogen is likely to be equally small the data of column (5) may be taken as pair cross sections for a free electron. Wheeler and Lamb took no account of exchange effects, but these are negligible for small momentum transfers where screening is most significant. The experimental data are compared with the Borsellino and Votruba approximations shown in the figure. The results are in agreement with the conclusion of Joseph and Rohrlich that the correct cross section is intermediate between the two curves.

Joseph and Rohrlich also show that Votruba's approximation is correct at very low energies and is probably more nearly correct at high energies. In assessing the experimental data it must be borne in mind that in columns (3) and (4) of the table no account has been taken of small effects such as radiative corrections and double Compton processes. There is some evidence (Moffatt *et al.* 1958) that the coherent pair cross sections of Bethe and Heitler may be too small at 94 MeV by approximately 1%, and the corrections to Compton scattering are probably of about the same magnitude. The effect of such correction, would be to decrease our estimates of the pair cross section for a free electrons bringing them closer to the lower curve of the figure.

REFERENCES

BERNSTEIN, D., and PANOFSKY, W. K. H., 1956, *Phys. Rev.*, **102**, 522.

JOSEPH, J., and ROHRLICH, F., 1958, *Rev. Mod. Phys.*, **30**, 354.

MOFFATT, J., THRESHER, J. J., WEEKS, G. C., and WILSON, R., 1958, *Proc. Roy. Soc.* A, **244**, 245.

WHEELER, J. A., and LAMB, W. E., 1939, *Phys. Rev.*, **55**, 858.

The *g*-value of S-state Ions

By I. FIDONE[†] AND K. W. H. STEVENS[‡]

MS. received 1*st October* 1958

In a recent letter (Watkins 1958) attention is drawn to the fact that, whereas the crystal field theory of the *g*-value of S-state ions predicts that their *g*'s will always be less than the free electron value, a number of cases are known in which the observed values are greater than the free electron value. The purpose of this note is to point out that the effects of covalent bonding can give positive contributions to *g*.

There is only one sextet, ^{6}S, in the d^5 configuration, and the spin–orbit coupling only has matrix elements between this and the ^{4}P term. Thus in the usual perturbation method for calculating *g* (Pryce 1950) there is no second order contribution, and in third order the spin–orbit coupling occurs squared, which allows the sign of the contribution to be determined unambiguously. A relevant observation in this connection is that d^5 can be regarded either as five electrons in the d-shell or as five holes, and the sign of the spin–orbit coupling is reversed for the two cases. The perturbation result is changed significantly if there are other sextets to which the spin–orbit coupling has matrix elements, for there is then a second order contribution to *g*, the sign of which depends on whether the excited state is obtained by promoting an electron or a hole from the ground state.

[†] University of Palermo, Sicily.

[‡] Department of Physics, University of Nottingham.

Suppose then that the ion is in a cubic environment and that there is an appreciable amount of covalent bonding. The ground term will be described as $(t_{2g})^3\,(e_g)^2\,{}^6A_{1g}$, where the one-electron states approximate to d-states. That is, we suppose that the states may be taken in the forms:

$$|xy\rangle \equiv p|\mathrm{d}, xy\rangle + q|\phi\rangle$$
$$|x^2-y^2\rangle = r|\mathrm{d}, x^2-y^2\rangle + s|\psi\rangle$$

where $|\phi\rangle$ and $|\psi\rangle$ denote the states of the surrounding ions, which are admixed with amounts q and s. It is now important to note that there will be states orthogonal to these, which contain d-functions, approximately:

$$|XY\rangle \equiv q|\mathrm{d}, xy\rangle - p|\phi\rangle$$
$$|X^2-Y^2\rangle \equiv s|\mathrm{d}, x^2-y^2\rangle - r|\psi\rangle.$$

They may either contain no electrons or two. In the former case excited sextets can be obtained by promoting an electron from the ground configuration into one of these states. In the latter case a hole can be similarly excited, which is the same as exciting an electron into the ground configuration from one of the filled levels. The spin–orbit coupling will only have matrix elements from the ground term with such an excited sextet if it has symmetry type ${}^6T_{1g}$. Such sextets are readily constructed by operating on the ground configuration with L_z. For example, a state of one such sextet (having $S_z = 5/2$) is obtained from the particular ground state

$$\left\{\overset{+}{xy},\ \overset{+}{yz},\ \overset{+}{zx},\ \overset{+}{x^2-y^2},\ \overset{+}{3z^2-r^2}\right\}$$

by promoting the electron (or hole) in xy into X^2-Y^2, giving

$$\left\{\overset{+}{X^2-Y^2},\ \overset{+}{yz},\ \overset{+}{zx},\ \overset{+}{x^2-y^2},\ \overset{+}{3z^2-r^2}\right\}.$$

A quantitative calculation shows that this sextet gives a contribution to g of approximately

$$\pm\ \frac{2}{5}\,\frac{\zeta}{\Delta}\,|\langle xy|l_z|X^2-Y^2\rangle|^2,$$

where ζ is the one-electron spin–orbit coupling constant, approximately equal to $+400\,\mathrm{cm}^{-1}$ in Mn^{2+}, and Δ is the promotion energy. $|\langle xy|l_z|X^2-Y^2\rangle|^2$ depends on overlap integrals and the detailed properties of $|\phi\rangle$ and $|\psi\rangle$, and is non-zero provided that q and s do not vanish. The positive sign is for the promotion of holes and the negative sign for the promotion of electrons.

It may be noticed that the introduction of covalence tends to bring electrons on to the central ion if the $|XY\rangle$, $|X^2-Y^2\rangle$ etc. orbits are filled, and remove electrons if they are unfilled. It would seem plausible in the case of Mn^{2+} to suppose that the covalence will tend to reduce the positive charge on the ion, and give a positive contribution to g. The effect may be more pronounced with Fe^{3+} ions, and may be strongly dependent on the environment of the ion.

This type of contribution to g is not confined to S-state ions, but may be small compared with other contributions in the general cases and thus less easily recognized.

REFERENCES

PRYCE, M. H. L., 1950, *Proc. Phys. Soc.* A, **63**, 25.
WATKINS, G. D., 1958, *Phys. Rev.*, **110**, 986.

Many-Body Problem with One-Body Forces

By J. S. BELL
Atomic Energy Research Establishment, Harwell, Berks.

Communicated by B. H. Flowers; MS. received 29*th September* 1958

In the many fermion problem with two-body forces a number of authors (Cooper 1956, Goldstone, unpublished, Gottfried, preprint, Bohr, Mottelson and Pines 1958) have found singularities associated with the interaction of two particles near the Fermi surface. While these may be of physical significance, they may alternatively be merely artificial products of unfortunate choices of approximation sequence. To illustrate the latter possibility we consider here the simple problem of the ground state of a Fermi gas in which is embedded a one-particle scattering centre; the latter is supposed not strong enough to have bound states in the usual sense. The accurate solution can of course be found by determining the single-particle eigenstates of the potential, subject to the conventional periodic boundary conditions, and forming a determinantal wave function of the appropriate number. It is clear that the single-particle wave functions exhibit no peculiarities near the arbitrarily chosen Fermi surface. The total energy of the system is the sum of the eigenvalues of the occupied states.

Suppose now we tackle the problem along the lines currently used with two-body forces. In lowest order perturbation theory the energy shift is the expectation value of the scattering potential in the unperturbed state:

$$\Delta E = \sum_{|\mathbf{k}|<k_F} \langle \mathbf{k}|v|\mathbf{k}\rangle .$$

A group of higher order terms is included when v is here replaced by the reaction matrix t given by

$$\langle \mathbf{k}''|t|\mathbf{k}\rangle = \langle \mathbf{k}''|v|\mathbf{k}\rangle + \sum_{\mathbf{k}'} \langle \mathbf{k}''|v|\mathbf{k}'\rangle \frac{Q(k')}{E-E'} \langle \mathbf{k}'|t|\mathbf{k}\rangle$$

where $Q(k)=0$ for $k<k_F$, and otherwise unity, while $E=k^2/2m$, $E'=k'^2/2m$. The resulting expression can be written

$$\Delta E = \sum_{|\mathbf{k}|<k_F} (\psi_{\mathbf{k}}{}^0, v\psi_{\mathbf{k}})$$

where in momentum space the one particle wave function $\psi_{\mathbf{k}}$ is given by

$$\psi_{\mathbf{k}}(\mathbf{k}') = \psi_{\mathbf{k}}{}^0(\mathbf{k}') + \sum_{\mathbf{k}''} \frac{Q(k')}{E-E'} \langle \mathbf{k}'|v|\mathbf{k}''\rangle \psi_{\mathbf{k}}(\mathbf{k}'')$$

and

$$\psi_{\mathbf{k}}{}^0(\mathbf{k}') = \delta_{\mathbf{k},\mathbf{k}'}.$$

Consider for simplicity a separate potential, and take it to be attractive:

$$\langle \mathbf{k}'|v|\mathbf{k}''\rangle = -g(k')g^*(k'')/V$$

where V is the quantization volume. The solution is then

$$\psi_{\mathbf{k}}(\mathbf{k}') = \psi_{\mathbf{k}}{}^0(\mathbf{k}') + \frac{Q(k')g(k')}{V(E-E')}\phi_{\mathbf{k}}$$

with

$$\phi_{\mathbf{k}} = -g^*(k)\left\{1 + \int_{|\mathbf{k}'|>k_F} \frac{d\mathbf{k}'}{(2\pi)^3}\frac{|g(k')|^2}{E-E'}\right\}^{-1}$$

where in the last line the limit $V \to \infty$ has been taken. The integrand is negative and logarithmically divergent at $k=k_F$. Thus for small g, $\psi_{\mathbf{k}}$ is singular just below the Fermi surface—indicating bound states of the potential as modified here by the exclusion principle.

All this is quite similar to what happens with two-body forces for particles of equal and opposite momenta. In the present case it seems clear that the singularity has no significance whatever, arising simply from an unfortunate selection of higher order terms to be included in the first approximation.

References

Bohr, A., Mottelson, B. R., and Pines, D., 1958, *Phys. Rev.*, **110**, 936.
Cooper, L. N., 1956, *Phys. Rev.*, **104**, 1189.

On the Wu–Yang Potential Energy Function

By Y. P. VARSHNI

Department of Physics, Allahabad University, Allahabad, India

MS. received 25th August 1958

§ 1. Introduction

Quite a large number of potential energy functions have been suggested for diatomic molecules. Recently Varshni (1957) has made a comparative study of the various functions.

In the present note we investigate the consequences of certain assumptions regarding the constants in the function proposed by Wu and Yang (1944) who have suggested the following:

$$U = a\,\mathrm{e}^{-mr} - \frac{b}{r^n} \qquad \ldots\ldots(1)$$

where a, b, m and n are constants. Except for the region near $r=0$, it gives the conventional potential energy curve. This satisfies the first and second criteria of a suitable function given in Varshni (1957). This does not satisfy the third criteria and gives $U=-\infty$ at $r=0$.

It may be added that a similar function with negative exponential term and positive inverse power term has been investigated by Linnett (1940, 1942).

Conditions (8*a*, *b*, *c*) of Varshni (1957) provide

$$ma\,\mathrm{e}^{-mr} = bn/r_\mathrm{e}^{\,n+1} \qquad \ldots\ldots(2)$$

$$k_\mathrm{e} r_\mathrm{e}^{\,n+1} = -bn(n+1)/r_\mathrm{e} + bnm. \qquad \ldots\ldots(3)$$

For different values of n, Wu and Yang plotted $k_\mathrm{e} r_\mathrm{e}^{\,n+1}$ against $1/r_\mathrm{e}$ for different states (ground as well as excited) of various diatomic molecules of a molecular *period* (e.g. KK, KL, LL etc). They obtained a straight line for a certain value of n, whence they concluded that n, m and b are constant in each period. On numerical calculation they obtained not unsatisfactory values of the force constant k_e.

If the conclusion that n, m and b are constant in each period is correct, we should be able to deduce the values of α_e and $\omega_\mathrm{e} x_\mathrm{e}$.

We can easily deduce that

$$X = \frac{U'''(r_e)}{U''(r_e)} = -\frac{m^2 r_e^2 - (n+1)(n+2)}{m r_e^2 - (n+1) r_e} \qquad \ldots\ldots(4)$$

$$Y = \frac{U^{\mathrm{IV}}(r_e)}{U''(r_e)} = \frac{m^3 r_e^3 - (n+1)(n+2)(n+3)}{m r_e^3 - (n+1) r_e^2} \qquad \ldots\ldots(5)$$

whence α_e and $\omega_e x_e$ can be obtained from (Varshni 1957):

$$\alpha_e = -\left(\frac{X r_e}{3} + 1\right) \frac{6B^2}{\omega_e} \qquad \ldots\ldots(6)$$

$$\omega_e x_e = \left[\frac{5}{3} X^2 - Y\right] \frac{2{\cdot}108 \times 10^{-16}}{\mu_A}. \qquad \ldots\ldots(7)$$

Wu and Yang have applied their relation to HH, KH, LH, KK, KL and LL periods. Calculations of α_e and $\omega_e x_e$ are lengthy and hence we have taken only one period KK for our investigation. We have chosen this period because a good number of states were available for this period. Amongst the states of neutral diatomic molecules examined by Wu and Yang, such states have been left out for which α_e and $\omega_e x_e$ are not available, or whose constants were inaccurate. It may be pointed out that some of the ω_e and r_e values as given here (taken from Herzberg 1950) are slightly different from the old values used by Wu and Yang. However, the differences are insignificant for our purposes.

For KK period, Wu and Yang give the following values of the constants: $n = 4$, $m = 3{\cdot}0303 \times 10^8$.

Table 1

Molecule	ω_e (cm^{-1})	r_e (10^{-8} cm)	B_e (cm^{-1})	% error in k_e
Li_2	269·69	2·936	0·5572	+2·1
	255·45	3·108	0·4975	−14·4
	351·43	2·672	0·6727	−5·8
BeO	1370·82	1·362	1·5758	0
	1144·24	1·463	1·366	+1·2
	1487·3	1·331	1·651	−5·2
C_2	1788·2	1·266	1·753	−10·7
	1608·3	1·318	1·617	−18·9
	1641·3	1·312	1·633	−19·6
BeF	1172·6	1·394	1·418	+14·2
	1265·6	1·361	1·488	+10·6
BO	1280·3	(1·311)	(1·503)	+24·6
	1260·7	1·352	1·413	+ 9·9
	1885·4	1·205	1·7803	−14·6
CN	2164·1	1·151	1·970	−19·0
	2068·7	1·172	1·899	−19·3
CO	1515·6	1·235	1·612	+9·6
N_2	1460·4	1·293	1·44	−7·2
	2359·6	1·094	2·010	−20·6
NO	2373·6	1·066	1·986	−11·7
	1904·0	1·151	1·705	−11·5
O_2	700·36	1·604	0·819	+21·2
	1432·7	1·227	1·400	+9·1
	1580·4	1·207	1·446	−3·4
F_2	1139·8	1·282	1·080	+17·8
			Average (regardless of sign)	12·1

Table 1 gives the required data, together with the percentage errors in calculation of k_e, as given by Wu and Yang. Results for α_e and $\omega_e x_e$ are given in table 2.

Table 2

Molecule	α_e obs. (cm^{-1})	α_e calc. (cm^{-1})	$\omega_e x_e$ obs. (cm^{-1})	$\omega_e x_e$ calc. (cm^{-1})
Li_2	0·0080	0·0221	2·744	9·64
	0·0054	0·0199	1·574	9·49
	0·0070	0·0218	2·592	9·77
BeO	0·0154	0·0429	7·745	40·95
	0·0163	0·0498	8·414	57·85
	0·0190	0·0411	11·83	38·58
C_2	0·0161	0·0348	16·44	34·08
	0·0172	0·0357	12·14	36·31
	0·0168	0·0353	11·67	35·99
BeF	0·0161	0·0435	8·78	41·81
	0·01685	0·0414	9·12	38·53
BO	—	0·0383	10·07	33·06
	0·0196	0·0368	11·157	35·45
	0·01648	0·0315	11·769	30·04
CN	0·02215	0·0315	20·25	29·79
	0·01735	0·0314	13·144	29·93
CO	0·02229	0·0333	17·25	29·08
N_2	0·013	0·0299	13·891	30·07
	0·0187	0·0286	14·456	27·45
NO	0·0182	0·0268	15·85	25·85
	0·0178	0·0268	13·97	25·78
O_2	0·011	0·0818	8·002	287·03
	0·01817	0·0263	13·95	24·79
	0·0158	0·0248	12·07	24·52
F_2	0·014	0·0212	9·7	21·88

§ 2. DISCUSSION

It will be noticed from table 2 that the calculated values, both of α_e and $\omega_e x_e$, are usually much larger than the experimental ones. A plot of calculated against observed values shows that there is no connection between the observed and the calculated values. Results for force constant are also not very inspiring, the average percentage error for these states being 12·1. Similar results for α_e and $\omega_e x_e$ can be expected for other molecular groups.

From their failure to derive correct dissociation energies, it was realized by Wu and Yang themselves that their assumptions did not apply in regions far from $r = r_e$. Our investigations clearly show that even at $r = r_e$ the assumption that the values of the constants remain the same for the various states of different diatomic molecules of a molecular period is not true.

ACKNOWLEDGMENT

The author is grateful to the Ministry of Scientific Research of the Government of India for a Fundamental Research Grant.

REFERENCES

HERZBERG, G., 1950, *Spectra of Diatomic Molecules* (New York: Van Nostrand).
LINNETT, J. W., 1940, *Trans. Faraday Soc.*, **36,** 1123.
—— 1942, *Ibid.*, **38,** 1.
VARSHNI, Y. P., 1957, *Rev. Mod. Phys.*, **29,** 664.
WU, C. K., and YANG, C. T., 1944, *J. Phys. Chem.*, **48,** 295.

Ionization and Dissociation by Electron Impact in Fluorine, Hydrogen Fluoride, Chlorine and Hydrogen Chloride

By R. THORBURN[†]
Research and Development Branch, United Kingdom Atomic Energy Authority
(Industrial Group), Capenhurst, Chester

MS. received 24th September 1958

§ 1. INTRODUCTION

THE great amount of data available in the literature for ionization and dissociation produced in gases by electron impact has been reviewed by Field and Franklin (1957).

It would seem that, until more knowledge of such chemical parameters as bond energies and ionization potentials of free radicals are obtained by methods other than electron impact, the data of most general use obtained by electron impact methods would be on diatomic molecules.

There is a great lack of experimental data on the diatomic molecules F_2, HF and Cl_2, because of the experimental difficulties arising from the introduction of these molecules into the mass spectrometer. The results given in this note constitute the first complete study of the appearance potentials of both positive and negative ions formed in F_2, HF, Cl_2 and HCl by electron impact.

The processes which lead to the formation of positive and negative ions when a diatomic molecule XY is bombarded by electrons are:

$$XY + e \rightarrow XY^+ + 2e \qquad \ldots\ldots (1)$$

$$XY + e \rightarrow X^+ + Y + 2e \qquad \ldots\ldots (2)$$

$$XY + e \rightarrow XY^{-*} \rightarrow X + Y^- \qquad \ldots\ldots (3)$$

$$XY + e \rightarrow X^+ + Y^- + e. \qquad \ldots\ldots (4)$$

The energy balances for these reactions are, respectively:

$$A(XY^+) = I(XY) \qquad \ldots\ldots (\mathrm{i})$$

$$A(X^+) = I(X) + D(X-Y) + K + E \qquad \ldots\ldots (\mathrm{ii})$$

$$A(Y^-) = D(X-Y) - EA(Y) + K + E \qquad \ldots\ldots (\mathrm{iii})$$

$$A(Y^-) = A(X^+) = I(X) + D(X-Y) - EA(Y) + K + E \qquad \ldots\ldots (\mathrm{iv})$$

where $A(XY^+)$, $A(X^+)$ and $A(Y^-)$ denote the appearance potentials of XY^+, X^+ and Y^- ions; and $D(X-Y)$, $I(XY)$, $I(X)$ and $EA(Y)$ denote the dissociation energy of XY, the ionization potential of XY and X, and the electron affinity of Y, respectively. The terms K and E represent the kinetic and excitation energies of the fragments formed in each of the processes. If K and E are zero for any particular process, the sum of the quantities on the right-hand side of the appropriate energy equation represents the minimum energy required for the reaction, and is denoted by A_0.

§ 2. APPARATUS AND EXPERIMENTAL TECHNIQUES

The mass spectrometer used was a Metropolitan-Vickers M.S.2 modified for corrosive gas analysis, with a high-pressure nickel inlet system and a stainless-steel source.

[†] Now at Birkenhead Technical College, Cheshire.

The appearance potentials of the positive ions were measured using the method of extrapolated voltage intercepts (Warren 1950), the standard for calibrating the electron-energy scale being $A(A^+)$ from argon (15·76 ev). The negative-ion appearance potentials were measured by the method of linear intercepts using $A(O^-)$ from O_2 as the standard, the values of $A(O^-)$ being $4{\cdot}7 \pm 0{\cdot}1$ ev and $17{\cdot}1 \pm 0{\cdot}2$ ev (Thorburn 1953). The presence of O_2 in the spectrometer at the same time as the gases being studied did not produce any interference in the negative-ion ionization efficiency curves for the F^- and Cl^- ions from F_2, HF, Cl_2 and HCl; the shapes of the curves were the same whether O_2 was in the spectrometer or not.

§ 3. RESULTS AND DISCUSSION

3.1. *Fluorine*

The appearance potentials of the positive and negative ions formed in F_2 are given in table 1. The values $D(F_2) = 1{\cdot}6$ ev (Cottrell 1954), $I(F) = 17{\cdot}42$ ev (Moore 1949) and $EA(F) = 3{\cdot}62$ ev (Pritchard 1953) have been used to determine the values of A_0 for the various processes suggested.

Table 1. Appearance Potentials of Ions Formed in F_2

Ion	Appearance potential (ev)	Process of formation	A_0(ev)
F_2^+	$16{\cdot}6 \pm 0{\cdot}2$	$F_2 + e \rightarrow F_2^+ + 2e$	$I(F_2)$
F^+	$15{\cdot}5 \pm 0{\cdot}2$	$F_2 + e \rightarrow F^+ + F^- + e$	15·40
	$19{\cdot}2 \pm 0{\cdot}3$	$F_2 + e \rightarrow F^+ + F + 2e$	19·02
F^-	< 2	$F_2 + e \rightarrow F^- + F$	0
	$15{\cdot}7 \pm 0{\cdot}3$	$F_2 + e \rightarrow F^+ + F^- + e$	15·40

The value of $I(F_2) = 16{\cdot}6 \pm 0{\cdot}2$ ev is in favourable agreement with that of 16·5 ev measured by Burns (1954). The occurrence of ion-pair formation $F^+ + F^-$ is shown by the equality of the appearance potentials for F^+ and F^-. The ratio of the ion currents due to F^+ and F^- for 18-volt electrons was about 1·3. Because of the source design, no electrons with energies less than 2 ev reached the trap. At this energy F^- ions were observed, but since only the high-energy side of the resonance capture peak could be measured, the appearance potentials of the F^- in this process could not be determined. Burns (1954) has shown that some F^- ions are formed by electrons with zero energy, and this is consistent with the minimum energy value for such a process.

3.2. *Hydrogen Fluoride*

Previous studies of the ions formed in HF by electron impact have been made by Burns (1954), who measured the appearance potentials of HF^+ and F^-, and by Coope, Frost and McDowell (1957), who measured the appearance potential of the HF^+ ions. The appearance potentials of both positive and negative ions were measured in this work and the values are given in table 2. The A_0 values are calculated by using $D(HF) = 5{\cdot}8$ ev (Cottrell 1954) and $I(H) = 13{\cdot}6$ev (Moore 1949) in conjunction with the values of EA (F) and I(F) given in § 3.1.

The ionization potential of HF determined in this work is $16{\cdot}0 \pm 0{\cdot}2$ ev. The values given in the literature for $I(HF)$ are $16{\cdot}38 \pm 0{\cdot}05$ ev (Burns 1954) and 15·77 ev and 16·97 ev (Coope, Frost and McDowell 1957). The value of 15·77 ev refers to formation of HF^+ ions in their ${}^2\Pi_i$ state, and that of 16·97 ev to the

Table 2. Appearance Potentials of Ions formed in HF

Ion	Appearance potential (ev)	Process of formation	A_0(ev)
HF^+	16·0 ± 0·2	$HF + e \rightarrow HF^+ + 2e$	$I(HF)$
F^+	23·6 ± 0·2	$HF + e \rightarrow H + F^+ + 2e$	23·22
H^+	20·2 ± 0·4	$HF + e \rightarrow H^+ + F + 2e$	19·40
F^-	3·1 ± 0·4 3·7 ± 0·3	See text	

formation of HF^+ ions in the $A^2\Sigma^+$ state. The value of $I(HF)$ measured in this work agrees more with the values of Coope *et al.*, but, although a careful search was made to detect a break in the HF^+ ionization efficiency curve, none could be identified with certainty because of the electron energy spread in the conventional ion source used.

The appearance potentials for F^- ions differ by about 0·6 ev. The values obtained by Burns (1954) were 8·85 ev and 9·55 ev, a difference of 0·7 ev. Burns suggests that the lower value corresponds with the formation of F^- and H^- ions simultaneously. This is an unsatisfactory explanation, and the processes producing F^- ions in the low-energy capture processes can still not be explained. The values obtained in the present work cannot be reconciled with those obtained by Burns. As the electron energy scales were carefully calibrated in both cases, the difference between the two sets of appearance potential values cannot be due to a difference in experimental techniques.

3.3. *Chlorine*

Apart from the measurement of $I(Cl_2)$ by electron impact methods (Morrison and Nicholson 1952) no complete studies of the ions formed by electron impact in Cl_2 have been reported. Table 3 gives the appearance potentials for positive and negative ions, and the A_0 values are calculated using $D(Cl_2) = 2{\cdot}48$ ev (Cottrell 1954), $EA(Cl) = 3{\cdot}82$ ev (Pritchard 1953) and $I(Cl) = 13{\cdot}01$ ev (Moore 1949).

Table 3. Appearance Potentials of Ions Formed in Cl_2

Ion	Appearance potential (ev)	Process of formation	A_0(ev)
Cl_2^+	11·8 ± 0·1	$Cl_2 + e \rightarrow Cl_2^+ + 2e$	$I(Cl_2)$
Cl^+	11·9 ± 0·2	$Cl_2 + e \rightarrow Cl^+ + Cl^- + e$	11·67
	15·7 ± 0·3	$Cl_2 + e \rightarrow Cl^+ + Cl + 2e$	15·49
Cl^-	< 2	$Cl_2 + e \rightarrow Cl^- + Cl$	0
	4·4 ± 0·2		
	12·0 ± 0·2	$Cl_2 + e \rightarrow Cl^+ + Cl^- + e$	15·49

The value of $I(Cl_2) = 11{\cdot}8 \pm 0{\cdot}1$ ev agrees with the value of 11·8 ev measured by Morrison and Nicholson (1952). Recently Watanabe (1957) has obtained a value of 11·48 ± 0·01 by photoionization measurements. As in the case of F_2, ion-pair formation $Cl^+ + Cl^-$ occurs. The process producing Cl^- ions at 4·4 ± 0·2 ev is not easily understood without postulating the existence either of an excited state of the neutral fragment Cl or of the negative ion Cl^-.

3.4. *Hydrogen Chloride*

Of the four gases F_2, HF, Cl_2 and HCl, the largest amount of electron impact work has been done with HCl. Data on the formation of both positive and negative ions have been given by Nier and Hanson (1936), Morrison and Nicholson (1952), Gutbier and Neuert (1954), Reese, Dibeler and Mohler (1956) and Fox

(1957). The main discrepancies in the literature have been in the values given for the appearance potential of Cl^- ions. The appearance potentials of the positive and negative ions formed in HCl measured in the present work are given in table 4. The A_0 values for the processes are calculated from $D(\mathrm{HCl}) = 4{\cdot}43$ ev (Cottrell 1954) in conjunction with the values of $I(\mathrm{Cl})$, $I(\mathrm{H})$ and $EA(\mathrm{Cl})$ given in the preceding sub-sections.

Table 4. Appearance Potentials of Ions Formed in HCl

Ion	Appearance potential (ev)	Process of formation	A_0 (ev)
HCl^+	12·8 ± 0·1	$\mathrm{HCl} + e \rightarrow \mathrm{HCl}^+ + 2e$	I (HCl)
HCl^{2+}	36·0 ± 0·8	$\mathrm{HCl}^+ + e \rightarrow \mathrm{HCl}^{2+} + 2e$	
	17·6 ± 0·2	$\mathrm{HCl} + e \rightarrow \mathrm{H} + \mathrm{Cl}^+ + 2e$	17·44
Cl^+	20·8 ± 0·3		
	22·6 ± 0·3		
Cl^{2+}	50 ± 2		
H^+	18·4 ± 0·3	$\mathrm{HCl} + e \rightarrow \mathrm{H}^+ + \mathrm{Cl} + 2e$	18·03
	28·2 ± 0·5		
Cl^-	< 2	$\mathrm{HCl} + e \rightarrow \mathrm{H} + \mathrm{Cl}^-$	0·61

The ionization potential measured for HCl is in agreement with the value of 12·78 ev obtained by Morrison and Nicholson (1952) using the electron impact method. Watanabe (1957) has obtained the value of $I(\mathrm{HCl}) = 12{\cdot}74 \pm 0{\cdot}01$ ev by photoionization methods, while the spectroscopic value is 12·85 ev.

No Cl^- ions were found for electron energies above 3 ev. This agrees with the results of Reese, Dibeler and Mohler (1956), but disagrees with those of Gutbier and Neuert (1954) and of Fox (1957) who found evidence for ion-pair formation $\mathrm{H}^+ + \mathrm{Cl}^-$. The values of $A(\mathrm{Cl}^-)$ given by these authors are $0{\cdot}8 \pm 0{\cdot}3$ ev, 4 ± 1 ev and $13{\cdot}6 \pm 0{\cdot}5$ ev; and $0{\cdot}66 \pm 0{\cdot}02$ ev and $14{\cdot}5 \pm 0{\cdot}1$ ev, respectively.

§ 4. CONCLUSIONS

The positive and negative ions formed by electron impact in F_2, HF, Cl_2 and HCl have been studied. Only in F_2 and Cl_2 was evidence found for a continuous pair-formation process. The results for positive ions are in agreement with those in the literature where such data are available.

ACKNOWLEDGMENTS

This Note is published by permission of Sir Leonard Owen, Managing Director, and Dr. H. Kronberger, Director of Research and Development of the United Kingdom Atomic Energy Authority (Industrial Group). Messrs. J. Bishop and E. A. Billett, of the Research and Development Branch, Capenhurst, were responsible for the design of the mass-spectrometer system, and gave much assistance during the work described.

REFERENCES

BURNS, J. F., 1954, *Carbide and Carbon Chemicals Co., K-25 Plant, Report K*-1147.

COOPE, J. A. R., FROST, D. C., and MCDOWELL, C. A., 1957, *Nature, Lond.*, **179,** 1186.

COTTRELL, T. L., 1954, *The Strength of Chemical Bonds* (London : Butterworths Scientific Publications).

FIELD, J. L., and FRANKLIN, F. H., 1957, *Electron Impact Phenomena* (New York : Academic Press).

Fox, R. E., 1957, *J. Chem. Phys.*, **26**, 1281.
Gutbier, H., and Neuert, H., 1954, *Z. Naturf.*, **9 (a)**, 335.
Moore, C. E., 1949, *Circ. Nat. Bur. Stand.*, *no.* 467.
Morrison, J. D., and Nicholson, A. J. C., 1952, *J. Chem. Phys.*, **20**, 1021.
Nier, A. O., and Hanson, E. E., 1936, *Phys. Rev.*, **50**, 722.
Pritchard, H. O., 1953, *Chem. Rev.*, **52**, 529.
Reese, R. H., Dibeler, V. H., and Mohler, F. L., 1956, *J. Res. Nat. Bur. Stand.*, **57**, *Research Paper* 2725.
Thorburn, R., 1953, *Conference on Applied Mass Spectroscopy* (London : Institute of Petroleum).
Warren, J. W., 1950, *Nature, Lond.* **165**, 811.
Watanabe, K., 1957, *J. Chem. Phys.*, **26**, 542.

Polarization of Light from the Cathode Glow

By R. S. SHEPHERD†
Physics Department, Queen's University, Belfast

Communicated by K. G. Emeléus ; MS. received 22nd September 1958

Seeliger and Handt (1929) reported that the HgI line 4347Å emitted from the cathode glow (' Erste Kathodenschicht ') in a number of gases containing mercury vapour as a contaminant was partially polarized with the electric vector perpendicular to the cathode. This result appeared to be in accord with the facts that the light from the cathode glow is excited either by slow electrons coming from the cathode surface, or by positive rays moving in the opposing direction, and that both kinds of particles have a marked directed component of velocity parallel to the axis of the discharge. The present note describes briefly some experiments done with more modern optical techniques applied to the study of a line emitted by the main gas present in the tube. A discharge through hydrogen has been used, and the Balmer line H_β, which is prominent in the spectrum of the cathode glow (Emeléus and Hall 1931), investigated. The line was isolated by an interference filter, and polarization searched for with polaroid discs and a photomultiplier.

Preliminary experiments showed, as would be expected, that spurious polarization resulted unless great care was taken to avoid reflection from the cathode and tube walls and oblique transmission through windows. The main part of the apparatus finally used is shown in the figure.

The anode of the discharge A was a fixed disc 2·5 cm in diameter. The cathode C was a second disc tilted away from the line of observation (vertical in the figure) at 2°, to prevent light being reflected from it into the viewing system. It could be moved axially in the discharge tube without turning by rotating the glass tube B, and was connected by a flexible lead to a terminal fused through the main tube wall. A side arm level with the cathode (below in the figure) had a B29 ground glass socket, whose mating cone extended for several centimetres before widening into 60 mm bore tubing M which carried the entire viewing system. The neck had fused to its inner wall one end of a narrower tube H which extended back to the discharge tube, and was terminated by a glass disc K, attached lightly by a film of vacuum grease, and across which the pressure was equalized by means of a hole J. A second window N, which was vacuum tight, was fused into the neck of M near the shoulder, and beyond this M was at atmospheric pressure. It contained, in order, (*a*) a movable frame holding polaroid discs, (*b*) an interference filter transmitting H_β with a half band width of about 25Å, (*c*) a No. 6094C EMI photomultiplier, all arranged for normal incidence.

---

† Now at Atomic Weapons Research Establishment, Aldermaston, Berks.

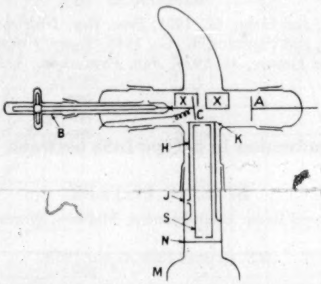

Discharge tube for studying polarization. Some details are omitted (see text). The tilt of the cathode, actually 2°, is exaggerated for clarity.

The rim of the cathode was shaped to accommodate K. The cross section of the beam of light from the discharge to the photomultiplier was defined by a metal tube S, 20 mm in diameter and 150 mm long, closed at both ends by plates with 1 mm × 15 mm parallel slits perpendicular to the axis of the discharge tube.

Directly opposite the side-arm carrying the viewing apparatus there was a light-trap, consisting of a horn-shaped side-arm painted dead-black on the outside. To prevent the discharge from distorting into this two glass half-cylinders XX (not shown in detail) were spot-fused on to the inside wall of the discharge tube in such a way as to block most of the entrance to the horn, leaving only a slit in the line of sight of the viewing system which was too narrow to allow the discharge to enter the horn, but sufficiently wide to prevent reflection from the half cylinders to the photomultiplier.

The discharge was moved past K by moving the cathode. Since the latter had only to be changed in position by about 5 mm to scan the whole of the cathode glow, and the inter-electrode distance was about 150 mm, the discharge was not appreciably affected by the alteration in its total length. For each position of the cathode, the photomultiplier current was measured for various orientations of the polaroid.

The results were entirely negative. Employing cathode falls of up to 1500 v, with currents of order of 1 mA and pressures of order of 0·1 mm Hg, no polarization of H_β was found from any part of the cathode glow. It is estimated from calibration of the viewing system as a unit that a ratio of 0·05, for $(J_1-J_2)/(J_1+J_2)$ could have been detected, where J_1 and J_2 denote the intensity of the light with electric vector perpendicular and parallel to the tube axis. Seeliger and Handt (1929) obtained ratios as large as 0·25 for the mercury line studied by them.

The origin of the difference between Seeliger and Handt's results and ours is not clear, and like other properties of the cathode glow (Stewart and Emeléus 1955) requires further investigation.

ACKNOWLEDGMENT

The author wishes to thank Professor K. G. Emeléus for suggesting this work and for his interest in its progress.

REFERENCES

EMELÉUS, K. G., and HALL, O., 1931, *Proc. Roy. Irish Acad.*, **40,** 1.
STEWART, D. T., and EMELÉUS, K. G., 1955, *Trans. Faraday Soc.*, **51,** 491.
SEELIGER, R., and HANDT, T., 1929, *Ann. Phys.*, *Lpz.*, **3,** 575.

Electrical Conduction in p-Type InSb between 100° and 2°K

BY E. H. PUTLEY
Royal Radar Establishment, Malvern, Worcs.

MS. received 18*th August* 1958

MEASUREMENT of the Hall coefficient R and conductivity σ of p-type InSb from about 100°K down to 2°K has indicated a number of features not previously reported.

Metallurgical evidence indicated that in the majority of the material the dominant impurities were zinc or cadmium (Hulme and Mullin 1957) and when steps were taken to remove these impurities n-type material was produced, the residual impurity being so far unidentified. If this n-type material were subjected to a treatment consisting of heating in a vacuum at two or three hundred degrees centigrade for a few hours and then quenching to room or liquid air temperatures it became p-type. Hulme has found that by carefully controlling the conditions, n-type material containing electron concentrations in the region of $5 \times 10^{14}\,\mathrm{cm}^{-3}$ could be converted to p-type with hole concentrations ranging between $1{\cdot}5 \times 10^{14}$ and $1{\cdot}2 \times 10^{16}\,\mathrm{cm}^{-3}$ and that the process was a reproducible one. The nature of the impurity responsible has not yet been identified.

Figures 1 and 2 show respectively the Hall coefficient and conductivity of a number of specimens between 20°K and 100°K. It is seen that two types of behaviour are present. The group of specimens with the shallower activation energy is that in which it is believed that the residual impurity is zinc or cadmium, while the specimens (the C58 group) with the deeper energy levels were those from which the group II impurities had been removed and which had then been re-converted to p-type by the heat treatment.

The value obtained for the shallower level was about 0·0075 ev while that for the deeper one was about 0·018 ev. Values corresponding to the shallower level have been reported by Hrostowski *et al.* (1955) and Fritzsche and Lark-Horovitz (1955). The extrinsic carrier concentration in the purest material was about $5 \times 10^{13}\,\mathrm{cm}^{-3}$ and while in this material the shallower level was the dominant one, analysis of the variation of carrier concentration with temperature indicated that some of the deeper lying impurities were also present. This analysis (made in

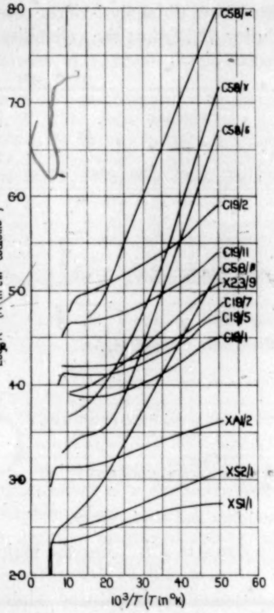

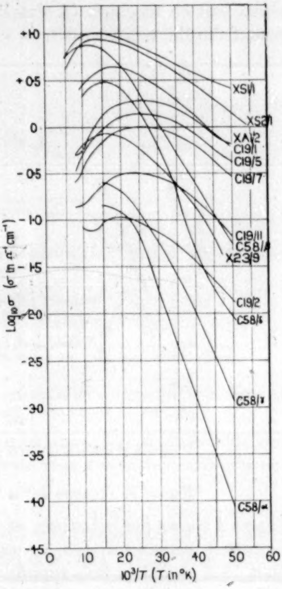

Figure 1. Hall coefficient for p-type InSb. Figure 2. Conductivity of p-type InSb.

a similar way to that for silicon by Putley and Mitchell 1958) indicated that the total impurity concentration was about $2 \times 10^{15}\,\mathrm{cm}^{-3}$.

Above about 30°K the Hall mobility $R\sigma$ decreased as the temperature rose. From these results an empirical expression was derived for the lattice mobility

$$\mu_{\mathrm{L}} = 5{\cdot}40 \times 10^{6} T^{-1{\cdot}45}\,\mathrm{cm^2\,sec^{-1}\,v^{-1}}.$$

This expression is based upon experimental data up to 100°K, and it predicts a room temperature mobility of about 1400, which is higher than the usually accepted value (~ 800). It is possible that other scattering mechanisms, such as electron–hole scattering, play a part at room temperature, but are not important at or below 100°K.

Below 30°K the mobility falls as the temperature is lowered. While it is thought that ionized impurity scattering is responsible for this, it is difficult to estimate its effect because below 20°K impurity band conduction becomes important, which also causes the mobility to fall. Assuming that at 20°K ionized impurity scattering is the dominant mechanism and calculating the concentration of scattering centres from the Brooks–Herring expression gives a concentration for the best material of about $5 \times 10^{14}\,\mathrm{cm}^{-3}$. This is somewhat smaller than the concentration of impurity centres ($\sim 2 \times 10^{15}\,\mathrm{cm}^{-3}$) obtained from the analysis of the hole concentration data. If the structure of the acceptor centre is similar to that found in silicon then the value obtained from the analysis of the concentration data will be too high (Kohn 1957, Putley 1958) but the reliability of the estimate from the mobility data is somewhat dubious.

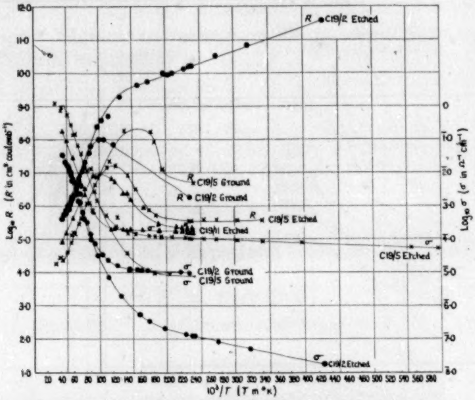

Figure 3. p-type InSb Hall coefficient and conductivity.

Figure 3 shows the behaviour of R and σ down to 2°K. For the majority of specimens R passes through a maximum value of 10^6 to $10^8\,\mathrm{cm^3\,coulomb^{-1}}$ at about 10°K and then falls rapidly as the temperature is reduced while below 10°K the conductivity is practically independent of temperature. This type of behaviour has been described earlier (Fritzsche and Lark-Horovitz 1955) and has been attributed to impurity band conduction. It was found that the results obtained depended upon the nature of the surface. Measurements were made with lightly ground surfaces and with surfaces etched with a CP4 etch. In the majority of cases etching reduced the value of the maximum in R by about a factor of ten and produced a corresponding increase in σ. The value of $R\sigma$ ($\simeq 10\,\mathrm{cm^2\,v^{-1}}$ at 4°K) was not very dependent upon the surface treatment. When the purest specimen (C19/2) was etched, however, R continued to rise steadily as the temperature fell and σ fell at a similar rate. At 2°K, R had reached about $10^{11}\,\mathrm{cm^3\,coulomb^{-1}}$ and the corresponding value of σ was about $10^{-8}\,\Omega^{-1}\,\mathrm{cm^{-1}}$. The resistance of the specimen was about 2000 megohms, necessitating the use of a cryostat designed for measurement of high resistivity material (Mitchell and Putley 1959). These values for R and σ indicate a mobility of about $1000\,\mathrm{cm^2\,v^{-1}sec^{-1}}$ which is of the order expected for holes in the valence band. Thus it appears that in the purest material (extrinsic hole concentration $\sim 5\times 10^{13}\,\mathrm{cm^{-3}}$) impurity band conduction is not observed. The behaviour below 10°K can be accounted for by conduction in the valence band and the presence of an acceptor level at about 0·001 ev above the band.

ACKNOWLEDGMENT

This note is published by permission of the Controller, H.M. Stationery Office.

REFERENCES

FRITZSCHE, H., and LARK-HOROVITZ, K., 1955, *Phys. Rev.*, **99**, 400.
HROSTOWSKI, H. J., MORIN, F. J., GEBALLE, T. H., and WHEATLEY, G. H., 1955, *Phys. Rev.*, **100**, 1672.
HULME, K. F., and MULLIN, J. B., 1957, *J. Electron. and Control*, **3**, 160.
KOHN, W., 1957, *Solid State Physics*, **5**, 527 (New York: Academic Press).
MITCHELL, W. H., and PUTLEY, E. H., 1959, *J. Sci. Instrum.*, in the press.
PUTLEY, E. H., and MITCHELL, W. H., 1958, *Proc. Phys. Soc.*, **72**, 193.
PUTLEY, E. H., 1958, *Proc. Phys. Soc.*, **72**, 917.

An Oscillatory Transverse Magnetoresistance Effect in n-type InSb

BY E. H. PUTLEY
Royal Radar Establishment, Malvern, Worcs.

MS. received 30*th July* 1958, *in revised form* 2*nd September* 1958

OBSERVATIONS on a number of specimens of n-type InSb having electron concentrations between 5×10^{13} and $5\times10^{14}\,\mathrm{cm}^{-3}$ have shown in the helium temperature range evidence of an oscillatory transverse magnetoresistance effect of a character different from that associated with the de Hass–van Alphen effect.

A negative magnetoresistance effect at low induction B has previously been observed (Fritzsche and Lark-Horovitz 1955, Frederikse and Hosler 1956, 1957). Broom (1958) has recently shown that this is a 'size effect' dependent on the dislocation density in the specimen.

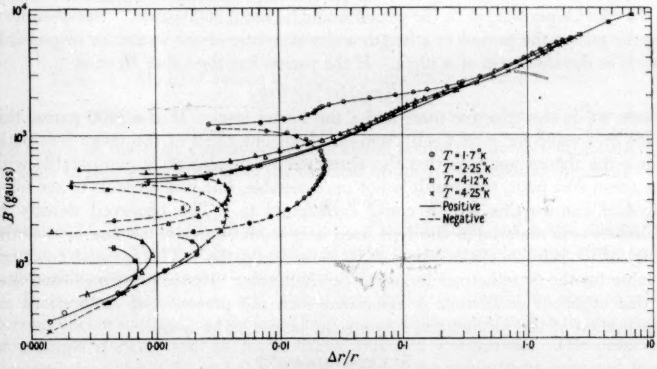

Transverse magnetoresistance effect in n-type InSb C19/3.

The figure shows results obtained in a typical specimen with $5\times10^{14}\,\mathrm{cm}^{-3}$ electron concentration at a number of temperatures. The measurements were made using a reversing procedure to eliminate any contribution from the Hall effect. The results were recorded using a Kipp Micrograph Recording Potentiometer. The results show that below 4·25°K this negative magnetoresistance is preceded at very low fields by a small positive magnetoresistance. Thus these results suggest a single period of an oscillation which is very rapidly damped. Now such behaviour can be produced by the de Haas–van Alphen effect (Davydov and Pomeranchuk 1940) and for this material the first minimum should occur at an induction of about 4000 gauss, but this oscillation is periodic in $1/B$ and we should expect to see about twenty periods between 1000 and 100 gauss. Since only one is observed it is concluded that this behaviour cannot be accounted for by the de Haas–van Alphen effect of the main group of carriers. The similarity of the behaviour at higher temperatures with that found by Broom (1958) and the fact that this effect is not observed in all specimens of similar electron concentration, suggest rather that it is a structure sensitive effect.

Sondheimer (1950) has shown that an oscillatory effect periodic in B can occur in thin metal films of thickness comparable with the mean free path. This effect has recently been observed in sodium wires (Babiskin and Siebenmann 1957). It has been pointed out (see for example MacDonald and Sarginson 1952) that an internal size effect is possible where dislocations form a regular pattern of layers. Since this type of pattern is found in InSb it is of interest to see whether Sondheimer's theory can account for this effect. In the specimen studied here the electron gas is degenerate below 4°K so that it is valid to apply a theory developed for metals.

It is rather difficult to determine the precise period of the oscillation since the non-oscillatory component is very large. It is seen that at about 4000 gauss the resistance is roughly double the value at zero field and that above 4000 gauss the increase of resistance varies as B^2 and is practically independent of temperature. If this behaviour is used to subtract empirically the B^2 dependence from the behaviour at the lower inductions, it is found that the first maximum occurs at about 100 gauss while the minimum is at about 1900 gauss. Hence if the effect is periodic in B, the period would be about 3600 gauss. Sondheimer's theory relates the period to a length a characteristic of the structure responsible (such as the thickness of a film). If the period has the value B, then

$$B = 6(2m^*\zeta)^{1/2}/ea$$

where m^* is the effective mass and ζ the Fermi level. If $B = 3600$ gauss, this leads to a value for a of 4×10^{-6} cm, or about one third of the mean free path. Since the theory assumes that the characteristic dimension is comparable with the mean free path, this result is not unreasonable, but it is difficult to see what physical feature this length could correspond to. The observed density of dislocations in material of the type used here would indicate a value of a of the order of 10^{-3} cm, or of the order of 100 mean free paths. This is much too large a value for the Sondheimer model to be applicable. Hence it is concluded that if this apparent oscillation is associated with the presence of dislocations an explanation of the mechanism responsible has yet to be found.

ACKNOWLEDGMENT

The note is published by permission of the Controller, H.M. Stationery Office.

REFERENCES

BABISKIN, J., and SIEBENMANN, P. G., 1957, *Phys. Rev.*, **107**, 1249.
BROOM, R. F., 1958, *Proc. Phys. Soc.*, **71**, 470.
DAVYDOV, B., and POMERANCHUK, I., 1940, *J. Phys. U.S.S.R.*, **2**, 147.

FREDERIKSE, H. P. R., and HOSLER, W. R., 1956, *Canad. J. Phys.*, **34**, 1377; 1957, *Phys. Rev.*, **108**, 1136.
FRITZSCHE, H., and LARK-HOROVITZ, K., 1955, *Phys. Rev.*, **99**, 400.
MACDONALD, D. K. C., and SARGINSON, K., 1952, *Rep. Progr. Phys.*, **15**, 249 (London: Physical Society).
SONDHEIMER, E. H., 1950, *Phys. Rev.*, **80**, 401.

Eddy Current Losses in 65/35 Nickel-Iron

BY E. W. LEE, A. G. H. TROUGHTON† AND D. R. CALLABY
Department of Physics, University of Nottingham

Communicated by L. F. Bates; *MS. received 5th June* 1958

IN 1950 Williams, Shockley and Kittel pointed out that in a ferromagnetic material possessing large domains and few domain walls the effective permeability associated with a domain wall must be very high since it is unity within the domain itself. They showed that in consequence the extremely non-uniform permeability associated with a domain-and-wall structure would give rise to eddy-current losses far greater than those calculated assuming the material to be characterized by a uniform permeability. It may be shown (Lee 1959) that in a material in which the domain structure is that depicted in figure 1 the ratio η of the eddy current losses calculated taking the domain structure into account to that calculated from the classical uniform permeability model is

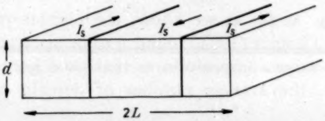

Figure 1. Model of domain structure in magnetically annealed Perminvar and 65/35 nickel–iron.

$$\eta \simeq 3L/pd \qquad \ldots\ldots(1)$$

in which $2L$ is the width of the specimen, d its thickness and p the number of domain walls. This fact is now believed to be the basic explanation of the well-known eddy-current anomaly in electrical sheet steels.

In a recent paper (Lee and Troughton 1958) we sought to observe eddy current effects arising from the large local permeability associated with movement of a single domain wall in magnetically annealed Perminvar. The observed loss ratio was about 12 and this fell far short of the value to be expected from equation (1), which for a single wall in a specimen of the dimensions used should have been about 60. It was concluded that although the specimen contained one circular wall, this was not sufficiently mobile to contribute significantly to the total loss.

† Now at Services Electronics Research Laboratory, Baldock, Herts.

For reasons which have not yet been elucidated, although the domain structure in magnetically annealed 65/35 nickel–iron is precisely similar to that in Perminvar, the walls are held much more loosely and, consequently, we were able to observe loss ratios much nearer the anticipated values. An apparatus for investigating domain structure in materials of this type has recently been developed (Lee, Callaby and Lynch 1958) thus enabling us to find the number of domain walls in each specimen.

The specimens of 65/35 nickel–iron were stamped rings, 1 in. external and 11/16 in. internal diameter, prepared by powder metallurgy and magnetically annealed by the Post Office Research Station. They were available in five different thicknesses, nominally, 8, 10, 15, 30 and 100 microns. Measurements were made on a stack of specimens, as received, using an a.c. bridge as described previously, care being taken to ensure that the exciting field was sufficiently low to avoid hysteresis loss and errors due to non-linearity. In practice the maximum r.m.s. exciting field was 3 milli-oersteds, and in all cases the final results were obtained by extrapolating to zero field. The results are shown in the table.

d (microns)	η	μ	p	μ/p
99	12·2	524	5	105
57	21	398	5	80
32	60	432	3	140
16	52	660	7	93
10	40	1050	15	70
8	64	881	12	73

The loss ratios are, as far as we know, the highest yet observed although Buckley, Jackson and Thomas (1953) found η to be as large as 46 in a 50 micron thick specimen of the same composition as that used here. Also shown in the table are values of p, the average number of domain walls calculated from equation (1), and the permeability per wall; there are signs that p varies systematically with specimen thickness; in addition, measurements at different temperatures indicated quite clearly that the number of walls changes, often abruptly, with temperature. Figure 2 shows a characteristic result. In the

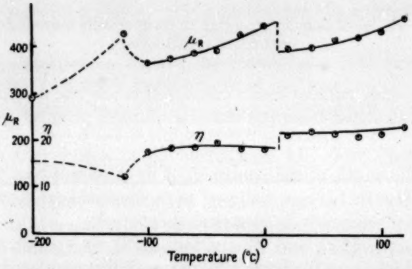

Figure 2. Permeability and loss ratio for specimen of thickness 50 microns as a function of temperature. A change in domain structure appears to take place between 0°c and 20°c.

range -100 to $+100$°c both μ and η increase slightly due to a slight increase with temperature in the mobility of the circular walls. Between 0 and 20°c μ decreases suddenly and η increases, corresponding to a sudden decrease in the number of domain walls.

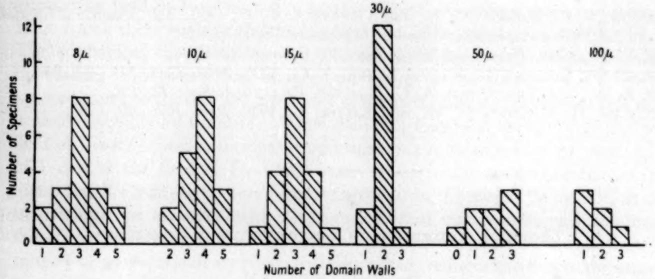

Figure 3. Distribution of the number of domain walls for specimens of differing thicknesses.

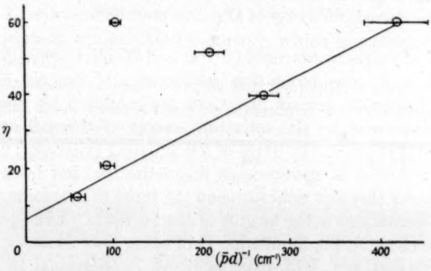

Figure 4. Observed loss ratio η as a function of $(pd)^{-1}$. The horizontal lines give an indication of the uncertainty in $\bar{p}$.

To investigate the above-mentioned variation of p with thickness, the domain structure in these specimens was observed using the Kerr-effect technique described previously. It was established that the domain walls were essentially circular and the number of domain walls per specimen was measured. The results obtained for the specimens of various thicknesses are shown in figure 3, from which $\bar{p}$, the mean value of p, was obtained. The observed loss ratio η is plotted in figure 4 against the quantity $(\bar{p}d)^{-1}$. Apart from two values for the 32 and 57 micron specimens the experimental points lie in a straight line, as anticipated. The line does not appear to pass through the origin and, moreover, its slope is considerably less than that given by equation (1). This indicates, as with Perminvar, that a considerable contribution to the permeability arises from processes other than movement of the circular domain walls. Nevertheless the slope of the experimental line is sufficiently great to be regarded as confirmation of the domain-and-wall eddy current calculations.

ACKNOWLEDGMENT

We wish to express our thanks to Professor L. F. Bates for his interest and useful suggestions made during the course of this work.

REFERENCES

BUCKLEY, S. E., JACKSON, G. A., and THOMAS, A. G. F., 1953, *Soft Magnetic Materials for Telecommunications* (London: Pergamon Press), p. 313.
LEE, E. W., 1959, *Proc. Instn Elect. Engrs*, Pt. C, in the press.
LEE, E. W., CALLABY, D. R., and LYNCH, A. C., 1958, *Proc. Phys. Soc.*, **72**, 233.
LEE, E. W., and TROUGHTON, A. G. H., 1958, *Proc. Phys. Soc.*, **72**, 596.
WILLIAMS, H. J., SHOCKLEY, W., and KITTEL, C., 1950, *Phys. Rev.*, **80**, 1090.

Thermal Activation of Ferromagnetic Domains

BY F. D. STACEY
Department of Geophysics, Australian National University, Canberra, Australia

MS. received 15*th September* 1958

IN the theory of magnetic viscosity (Street and Woolley 1949, 1950, Néel 1950, 1951, 1955) it is considered that movements of domain walls and discontinuous jumps in domain directions are inhibited by potential barriers which can be overcome by the activation energy of thermal agitation. Néel (1955) described this process in terms of a fluctuating (viscosity) field which was caused by the agitation of spontaneous magnetization, but he was not certain whether to consider that this field supplied the force to overcome the barriers or simply caused fluctuations in the heights of the barriers. The energy of thermal agitation is fundamental, the fluctuating field being only a consequence, and the barriers are potential, not field, barriers being proportional to the square of spontaneous magnetization. This applies both to the barriers inhibiting domain rotations, which are due to magnetocrystalline and shape anisotropies and to barriers inhibiting domain wall movements. When the latter are due to crystal defects or internal strains they appear as distortions of the patterns of spontaneous magnetization σ which may be considered as the superposition of distortion fields on undistorted patterns. The distortion fields interact with σ, the interaction energy being proportional to σ^2. Therefore the second alternative, in which fluctuations of energy rather than field are considered, should be regarded as more correct.

This is equivalent to the approach of Street and Woolley (1949, 1950) who considered the probability P of energy E being available to overcome a potential barrier to be given by

$$P = C\,\mathrm{e}^{-E/\boldsymbol{k}T} \qquad \ldots\ldots (1)$$

$\boldsymbol{k}$ being Boltzmann's constant and T the absolute temperature. The factor C in equation (1) is a characteristic frequency of the fluctuation and has been regarded as a constant, independent of temperature; the purpose of this note is to derive a numerical value of C which is shown to be proportional to T.

The argument is similar to that of Nyquist (1928), who made a thermodynamic analysis of electrical noise due to thermal agitation of electrons in resistances. Consider two identical volumes, I and II, of any ferromagnetic material at the same temperature T, to be connected in a common magnetic circuit by means of a material of infinite permeability. Then the spontaneous fluctuating field of I causes a flux in this circuit, imparting magnetic energy to II in which there is also a fluctuating field but quite uncorrelated with that in I. The probability that I will be in a state in which the instantaneous value of its fluctuating field gives a flux, of magnetic energy E, in the circuit is $e^{-E/\boldsymbol{k}T}$, and by continuity of the flux and similarity of the two volumes considered this energy is shared equally by I and II. Thus the mean magnetic energy of II due to the field of I is $\boldsymbol{k}T/2$ and in thermal equilibrium this is balanced by the mean energy of I due to the field of II. This state of thermodynamic balance cannot be disturbed if a non-dissipative filter is included in the magnetic circuit, as could in principle be arranged with a system of ideal search coils and condensers; therefore the inclusion of a filter which blocks all frequencies except those in a range ν to $\nu + d\nu$, which are perfectly transmitted, reduces the flux in the circuit to an oscillation of frequency ν and a changing envelope such that its energy has a probability $e^{-E/\boldsymbol{k}T}$ of having a value E. (The fluctuating field of I, being proportional to $\sqrt{E}$ has a Gaussian probability distribution.) The mean energy of the flux is $\boldsymbol{k}T$, independently of ν or the range of frequency of the filter, which therefore implies an equipartition of energy, which is uniformly spread over the frequency spectrum.

The equipartition is valid only at low frequencies and for a general consideration of all frequencies it must be replaced by the Planck expression for the energy of the oscillation at any frequency ν, which is

$$\frac{\boldsymbol{h}\nu}{e^{\boldsymbol{h}\nu/\boldsymbol{k}T}-1},$$

where $\boldsymbol{h}$ is Planck's constant. This spectrum is not continuous but cuts off at $\boldsymbol{h}\nu/\boldsymbol{k}T \sim 1$. Although the cut-off is not sharp and the spectrum extends to indefinitely high frequencies with an exponential decrease, an effective cut-off frequency f may be found by taking the area of the spectral curve of energy plotted against frequency, which is

$$f\boldsymbol{k}T = \int_0^\infty \frac{\boldsymbol{h}\nu d\nu}{e^{\boldsymbol{h}\nu/\boldsymbol{k}T}-1} = \frac{(\boldsymbol{k}T)^2}{\boldsymbol{h}}\frac{\pi^2}{6},$$

so that

$$f = \frac{\pi^2}{6}\frac{\boldsymbol{k}T}{\boldsymbol{h}}. \qquad \ldots\ldots(2)$$

We may therefore consider the fluctuating magnetic viscosity field to have a spectrum of frequencies from zero to f, as given by equation (2).

Use is now made of the mathematical analysis of random fluctuations which has been given by Rice (1944, 1945), who showed that if electrical noise current has a frequency range from zero to f then the number of current peaks per second which exceed a value I is

$$\frac{f}{\sqrt{3}} \exp(-I^2/I_0^2),$$

where I_0 is the r.m.s. value of noise current. I and I_0 could express equally well the instantaneous and r.m.s. values of the viscosity field H. Thus the probability of a fluctuating field peak of amplitude H or greater occurring in one second is

$$P=\frac{f}{\sqrt{3}}\exp(-H^2/H_0^2)=\frac{f}{\sqrt{3}}e^{-E/kT}, \qquad \ldots\ldots(3)$$

where E is the energy of field H. Just as Nyquist (1928) showed that electrical noise power is independent of the resistance and its physical size and shape (assuming no reactance), so equation (3) applies to any volume of a ferromagnetic which we care to consider, including any selected region of a domain or domain wall. It expresses the probability that, in one second, a domain or domain wall will acquire thermally a peak value of the viscosity field in the required direction with sufficient energy to overcome a potential barrier of energy E. Equations (1) and (3) may therefore be identified and, as f is given by equation (2), we have

$$C=\frac{\pi^2}{6\sqrt{3}}\frac{\boldsymbol{k}T}{\boldsymbol{h}}. \qquad \ldots\ldots(4)$$

This result is independent of the nature of the barrier.

At room temperature $C\sim 6\times 10^{12}\,\mathrm{sec}^{-1}$. This is the reciprocal of the 'reorganization time' of the fluctuating field which Néel (1951, 1955) roughly estimated to be about 10^{-10} second. The absolute difference is not important because only the logarithm of C affects magnetic viscosity, but the proportionality of C to T appears to be significant. It is possible that the variation of magnetic viscosity with temperature could be measured with sufficient accuracy to test this dependence of C upon T, which may help to resolve the theoretical doubt (Lawson and Uhlenbeck 1950, p. 78) about the upper frequency limit which is experimentally inaccessible in the case of electrical noise.

REFERENCES

LAWSON, J. L., and UHLENBECK, G. E., 1950, *Threshold Signals*, M.I.T. Radiation Laboratory Series No. 24 (New York: McGraw-Hill).
NÉEL, L., 1950, *J. Phys. Radium*, **11**, 49.
—— 1951, *Ibid.*, **12**, 339.
—— 1955, *Advanc. Phys.* (*Phil.Mag.* Suppl.), **4**, 191.
NYQUIST, H., 1928, *Phys. Rev.*, **32**, 110.
RICE, S. O., 1944, *Bell Syst. Tech. J.*, **23**, 282.
—— 1945, *Ibid.*, **24**, 46.
STREET, R., and WOOLLEY, J. C., 1949, *Proc. Phys. Soc.* A, **62**, 562.
—— 1950, *Ibid.*, B, **63**, 509,

Spin of ^{103}Ru by Deuteron Stripping

BY P. MASON†, F. C. FLACK† AND G. PARRY‡
† Washington Singer Laboratories, University of Exeter
‡ Nuclear Physics Research Laboratory, University of Liverpool

MS. received 3rd October 1958

THE ground state of the β-emitter ^{103}Ru is predicted by the shell model to have a spin of 7/2 or 5/2 with even parity. Investigators of the daughter nucleus ^{103}Rh (see for example Flack and Mason 1958) have accordingly been left with several spin possibilities in assigning excited states at 538 kev and 650 kev. A direct measurement of the spin of ^{103}Ru seemed desirable and deuteron stripping with the even–even ^{102}Ru nucleus as target appeared feasible. Because of the variety of isotopes in natural Ru it was necessary to use enriched ^{102}Ru (97·2%) which was obtained from Oak Ridge National Laboratory, U.S.A.

Targets of both natural and enriched black oxides of ruthenium were prepared by allowing a slurry of fine powder and water to dry on thin gold foils. Targets were bombarded in the Liverpool 37-inch cyclotron by deuterons of about 8·9 Mev, using the magnetic spectrograph and target chamber described previously (Green and Middleton 1956, Dalton, Hinds and Parry 1957). The photographic plates were covered with thin Al foil of sufficient thickness to absorb deuterons from the target. Angular distributions were measured only for proton groups from the separated isotope.

The spectrum of protons emitted by an enriched target at an angle of observation of 30° to the incident deuterons is shown in figure 1. The peak of main interest is marked P_0 and is attributed to ^{103}Ru formed in its ground state for the following reasons. The measured Q-value of $4{\cdot}11 \pm 0{\cdot}06$ Mev is in good agreement with that of $4{\cdot}06 \pm 0{\cdot}7$ Mev obtained from the masses of ^{102}Ru, ^{103}Rh (Duckworth 1957) and the known β-endpoint of ^{103}Ru (de Raad *et al.* 1954). The recent semi-empirical mass formula of Cameron (1957), which had to be used to compute Q-values for other Ru isotopes, predicts 4·1 Mev for this reaction. Also a comparison was made between the relative intensities of groups on the 30° spectra obtained from the natural and enriched targets. The relative abundances of the isotopes in the two targets were known. Agreement was obtained between the experimental and computed variation of intensities if P_0 was due to the transition to the ground state in ^{103}Ru and if the other groups were identified as shown in figure 1. Thus P_1 changed in intensity by the same factor as P_0 between the two targets and is identified as corresponding to an excited state of ^{103}Ru at 220 ± 60 kev. Similarly peaks marked ^{102}Ru(0) and ^{102}Ru(1·94) correspond to ^{101}Ru (d, p) ^{102}Ru transitions to the ground and 1·94 Mev states. A gamma ray of energy 1·98 Mev following β-decay of ^{102}Tc has been reported (Seelmann-Eggebert, private communication to *Nuclear Data Sheets*, National Research Council, Washington). The expected Q-value for ^{101}Ru (d, p) ^{102}Ru, from Cameron's tables, is 6·8 Mev, the measured value being $6{\cdot}22 \pm 0{\cdot}06$ Mev. Other Ru isotopes in the enriched material, whose calculated Q-values lay within 1 Mev of that measured, existed only to 0·03% or

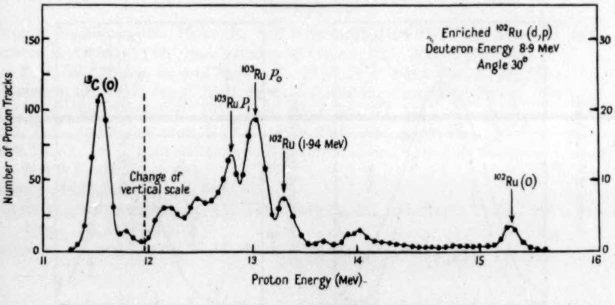

Figure 1. Proton energy spectrum at an angle of observation of 30° resulting from the deuteron bombardment of a gold leaf supported target of enriched ^{102}Ru.

less, compared with ^{101}Ru which was 1·8% abundant. The peaks at lower energies than P_1, being broad and probably compound, were not analysed.

Angular distributions of the groups P_0 and ^{102}Ru(0) are shown in figure 2. The experimental distribution for the group P_0 peaks at about 29°. To fit this with theoretical stripping curves there are several possibilities depending on the radius chosen. The Gamow Critchfield radius is 7·4 fermis. Using this radius and Butler theory the curve for $l_n=2$ peaks below 29° while the curves for $l_n>2$ peak above. A theoretical curve peaking at 29° requires for $l_n=2$, $R=5·3$ fermis; for $l_n=3$, $R=8·0$ fermis and for $l_n=4$, $R=10·6$ fermis. Similar curves are obtained using the theory of Bhatia *et al.* (1952) with higher values of the radius. The Coulomb effect displaces the peak of the experimental distribution to larger angles, and if this effect only were present the results would undoubtedly be attributed to an $l_n=2$ transition. However, nuclear scattering of the incident deuterons and outgoing protons tends to counteract the angular shift due to the Coulomb effect (Tobocman and Kalos 1955). Thus while the possibility of the transition being $l_n=4$ seems very unlikely, it is not possible to decide between $l_n=2$ and $l_n=3$ on the goodness of fit to simple stripping curves. The ordering of states in the shell model suggests that the chance of the 59th neutron going into an f shell ($l_n=3$ transition) is remote and, taking this into account, a strong indication is given that the angular distribution corresponds to an $l_n=2$ transition.

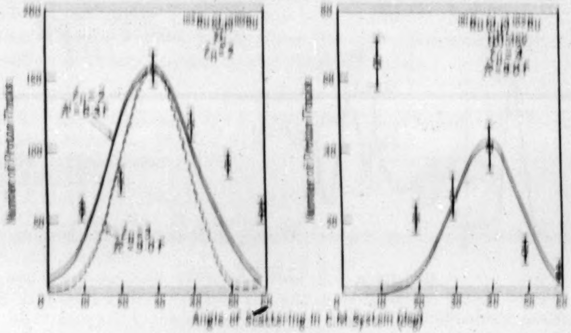

Figure 2. Angular distribution of the proton groups from the reactions ^{102}Ru (d, p) ^{103}Ru and ^{101}Ru (d, p) ^{102}Ru. The theoretical curves were computed using the theory of Bhatia *et al.* (1952).

The angular distribution corresponding to the formation of ^{102}Ru(0) is complex. The forward peak indicates the presence of an $l_n=0$ component, while the experimental curve at larger angles could include a contribution from $l_n=4$. The angular distribution for P_1 was found to be almost isotropic while that for ^{102}Ru (1·94) suggests l_n values of 2 or more.

If the ground state of ^{103}Ru is formed by an $l_n=2$ transition from an even-even nucleus (0$^+$ state) it follows that ^{103}Ru must have spin and parity 3/2$^+$ or 5/2$^+$, while an $l_n=3$ transition gives corresponding values 5/2$^-$ and 7/2$^-$. The value 5/2$^+$ is to be preferred from the point of view of the shell model. Additional experimental evidence for this view is obtained as follows. A level in ^{103}Rh at 538 kev has been shown (Flack andMason 1958) to have spin 7/2 or 9/2 with even parity. This level is produced from ^{103}Ru by an allowed β-transition (Mayer 1955) with $\log ft = 5{\cdot}7$, thus ruling out suggestions for odd parity in the ground state of ^{103}Ru. The only consistent arrangement, considering the remaining alternatives, is that ^{103}Ru has a ground state condition $5/2^+$, the 538 kev level in ^{103}Rh has spin and parity $7/2^+$ and the allowed β-transition between these states has $\Delta I = 1$, No. One of the suggested spins, 9/2, for the level in ^{103}Rh at 650 kev, also reached by an allowed β-transition, is now ruled out leaving the alternatives $7/2^+$ or $5/2^+$.

In the case of the reaction forming the ground state of ^{102}Ru, since ^{101}Ru has spin and parity $5/2+$ (Orring 1952) and ^{102}Ru is an even–even nucleus, the selection rules require at least an $l_n = 2$ transition. The complex nature of the corresponding angular distribution suggests the presence of low-lying excited levels giving proton groups not resolved from the ground state group.

ACKNOWLEDGMENT

One of us (P. M.) wishes to acknowledge the receipt of a maintenance grant and other financial assistance from the Department of Scientific and Industrial Research during the course of this work.

REFERENCES

BHATIA, A. B., HUANG, K., HUBY, R., and NEWNS, H. C., 1952, *Phil. Mag.*, **43**, 485.

CAMERON, A. G. W., 1957, *Atomic Energy of Canada Ltd., Report No.* 433.

DALTON, A. W., HINDS, S., and PARRY, G., 1957, *Proc. Phys. Soc.* A, **70**, 586.

DUCKWORTH, G., 1957, *Progr. Nucl. Phys.*, 6 (London: Pergamon Press).

FLACK, F. C., and MASON, P., 1958, *Proc. Phys. Soc.*, **71**, 247.

GREEN, T. S., and MIDDLETON, R., 1956, *Proc. Phys. Soc.* A, **69**, 16.

MAYER, M. G., 1955, *Beta and Gamma Ray Spectroscopy*, edited by Siegbahn (Amsterdam: North Holland), p. 433.

ORRING, J., 1952, *Ark. Fys.*, **4**, 469.

DE RAAD, B., MIDDLEKOOP, W. C., VAN NOOYEN, B., and ENDT, P. M., 1954, *Physica, 's Grav.*, **20**, 1278.

TOBOCMAN, W., and KELOS, M. H., 1955, *Phys. Rev.*, **97**, 132.

LETTERS TO THE EDITOR

A Simple Method of Calculating Moiré Patterns

The use of moiré patterns between two grids is becoming more and more important in modern technology and it is therefore valuable to develop a simple treatment. Guild (1956) has grasped clearly that moiré patterns are essentially diffractive effects, but it is by no means clear how he arrives at the often complex formulae in his book. A simple derivation of the main formulae which brings out the essential physical processes behind them may not be out of place.

It has long been known to crystallographers (Ewald 1913) that problems in three-dimensional diffraction can be solved by the use of reciprocal space. Diffraction by a single plane grating is normally so simple that use of reciprocal space is an unnecessary complication, but successive diffraction by two plane gratings, as in the formation of moiré patterns, often justifies its use. Moreover, the technically important case where the planes of the two gratings are parallel and relatively close together can be solved with great simplicity. It is readily seen, either by reference to the original geometrical definition of reciprocation or by use of the modern vector definition, that a system of parallel equidistant straight lines ruled on a plane will give rise in reciprocal space to a system of parallel equidistant straight lines in a plane perpendicular to the physical rulings. The lines in reciprocal space are perpendicular to the plane of the grating. The spacings of the two systems of lines are, of course, reciprocal. The lines in reciprocal space should be 'weighted' with the complex Fourier coefficients of the waveform of the plane grating ruling. Since the reciprocal lines extend indefinitely, they will always cut the 'sphere of reflection' of any incident wavelength short enough to be diffracted, and hence a plane grating always gives spectra for any angle of incidence when $\lambda < d$. The angle of diffraction is easily derived by the usual Ewald construction. Consider next a system of two gratings substantially in contact. To obtain a two-dimensional diagram in reciprocal space, take the two rulings parallel but of slightly different spacings. Let OA (figure 1) represent the common plane of the gratings, and let P_1Q_1 be the first reciprocal line from the first grating, situated a distance a^* from O. Let a collimated beam fall normally on the gratings along T_1C_1O, then the first order diffraction spectrum from the first grating will travel out along C_1P_1 by the Ewald construction.

Let T_2C_2O represent this first diffracted ray falling on the second grating. Let P_2Q_2 represent the reciprocal line of the grating, distance $-b^*$ from O. Then the ray T_2C_2O will give a diffracted beam along the line C_2P_2. Since a^* and b^* are very nearly equal C_2P_2 is not far from the original ray $T_1C_1O_1$ and generates the moiré pattern by interfering with it. The spacing of the moiré pattern is inversely proportional to the angle between C_2P_2 and T_1C_1O. It will be seen that there will be a reciprocal line P_3Q_3 due to the first grating and at a distance $-a^*$ from O, which passes very close to the reciprocal line P_2Q_2 and cuts the Ewald sphere in a point P_3 so close to P_2 that the sphere may be regarded as plane in this region. The diffracting angle of the moiré pattern is $P_2C_2P_3$ and may be calculated by projecting a^* and b^* on to the sphere of reflection, regarded as plane, and picking off the angle from a point C_2 unit distance away. It is however more convenient to project a^* and b^* on to the plane of the gratings and work from unit distance, and it will be seen at once that the moiré pattern represents a difference vector between $\mathbf{a}^*$ and $\mathbf{b}^*$ calculated in this plane. This construction is valid as long as the spacing of the moiré pattern is very long compared with the wavelength; the spacing of the original gratings need not be very long compared with the wavelength.

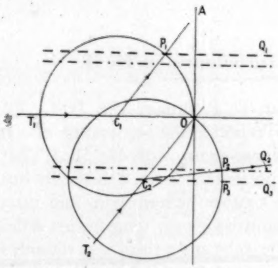

Figure 1.

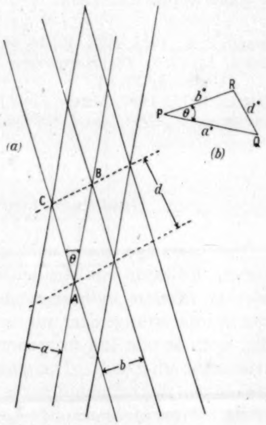

Figure 2.

If one of the gratings, say the second, is rotated in its own plane, the Ewald diagram can no longer be drawn in two dimensions as the reciprocal line P_2Q_2 is not now in the plane of the paper but is parallel to the plane of the paper and above or below it. All the essential features of the diffraction can be inferred from another two-dimensional diagram obtained by projecting P_2Q_2 and P_3Q_3 on to the plane of the gratings. In figure 2 (*a*) are shown the original gratings and in figure 2 (*b*) the equivalent diagram in what may be called the 'reciprocal plane'.

It is readily shown that if $\mathbf{a}^*$ and $\mathbf{b}^*$ are the reciprocal vectors corresponding to the gratings of spacings $\mathbf{a}$ and $\mathbf{b}$ respectively, then $\mathbf{d}^*$ is reciprocal to the moiré spacing $\mathbf{d}$ and gives it in magnitude and direction.

Thus in the triangle ABC $2 \times \text{area} = \text{AB}.a = \text{AC}.b = \text{BC}.d$, whence $\text{AB} = K.a^*$; $\text{AC} = K.b^*$; $\text{BC} = K.d^*$. Moreover $\text{BAC} = \theta$ is the angle between the gratings and RPQ, the angle between the reciprocal vectors, is equal to the angle between the gratings, i.e. θ. Hence the triangles PQR and ABC are similar and $\mathbf{d}$ may be inferred in magnitude and direction from $\mathbf{d}^*$.

This type of calculation may obviously be extended to more complex line gratings (such as half-tone screens) and gratings with imperfections or irregularities (Menter 1957). It is clearly related to the Abbe theory of microscopic vision (Rogers 1954). For gratings not in parallel planes, the full three-dimensional Ewald construction must be used.

By the use of Ewald's reciprocal space any particular problem in moiré production may be solved. In the case of gratings lying in parallel planes, the reciprocal space may be condensed into a reciprocal plane and the moiré patterns developed as difference vectors in this reciprocal plane.

College of Technology,
Gosta Green,
Birmingham, 4.
22nd September 1958.

G. L. Rogers.

Ewald, P. P., 1913, *Phys. Z.*, **14**, 465.
Guild, J., 1956, *The Interference Systems of Crossed Diffraction Gratings* (Oxford : University Press).
Menter, J. W., 1957, *Nature, Lond.*, **179**, 752.
Rogers, G. L., 1954, *Amer. J. Phys.*, **22**, 384.

Quantized Growth of Turbulence in He II

Two years ago one of us, together with D. F. Brewer and D. O. Edwards (Brewer, Edwards and Mendelssohn 1956) reported the observation of a sudden onset of friction in heat conductivity experiments with He II. The same experimental arrangement was used in the present work, i.e. a thermally insulated tube, open at one end to a constant temperature helium bath, and carrying a heater at the other end. The measured quantities are the temperature differences between two thermometers at the ends of the tube and a third one, roughly in the middle. Most of the results were obtained on a tube of 0·1 cm internal diameter and 150 cm length. Tubes of 0·05 and 0·17 cm diameter yielded similar data. The main features of the observations can be summarized as follows:

(i) At low rates of heat input Q the thermal resistance $\Delta T/Q$ has a value W_0, essentially independent of Q (figure 1). This state of the liquid can be identified with the viscous outflow of the normal fluid, since its viscosity derived from these data agrees with other measurements (cf. Brewer and Edwards 1958).

(ii) At a critical rate of heat input Q_c' this state of flow becomes unstable and changes discontinuously into another with higher thermal resistance W'. This onset is subject to velocity hysteresis and may only occur at higher heating rates Q_c'', Q_c''', etc., leading to W'', W''', etc. The hysteresis is more pronounced at lower temperatures but can be decreased by mechanical shock (e.g. tapping the cryostat).

(iii) The rise of thermal resistance at a *fixed* value of Q_c requires time (up to twenty minutes) and is slowest near Q_c'. ΔT always changed linearly with time and this behaviour was interpreted as a steady progress of the state of high thermal resistance through the tube. That this is actually the case could be demonstrated by readings of the centre thermometer. It seems reasonable to assume that the state of high thermal resistance is connected with turbulence in the superfluid.

(iv) The growth of turbulence was found to proceed in various ways. The simplest is a gradual filling of the tube with the turbulent state, starting from the cold end only (figure 2 (*a*)), which is the most common pattern close to Q_c'. At higher heat currents, turbulence may start simultaneously at both ends (figure 2 (*b*)) or in the middle of the tube as well as at one end (figure 2 (*c*)). Various other patterns have been observed, becoming more complicated as the transition proceeds at higher values of Q_c. At the highest heat currents short linear portions appear to merge into an exponential curve.

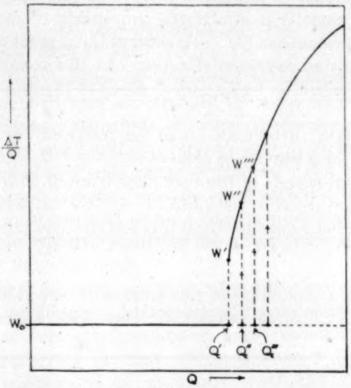

Figure 1. Thermal resistance $\Delta T/Q$ plotted against heat input Q.

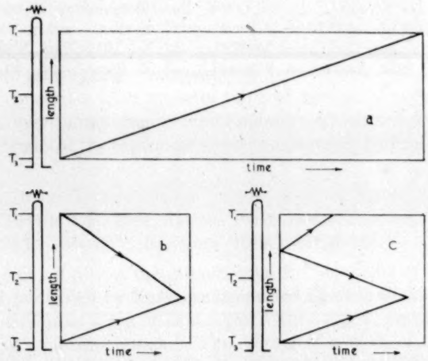

Figure 2. Progression of the turbulent front with time through the length of the tube. T_1, T_2 and T_3 indicate the positions of the three thermometers.

(v) The various speeds of the turbulent front (within the experimental error of 5–15%) seem to be always simple multiples of the lowest speed. The quantal aspect of the speeds could further be demonstrated by slightly reducing the heat current for part of a transition, such as shown in figure 2 (*a*). It was found that the speed of the front was unaffected by this.

(vi) Once turbulence had progressed through the whole tube no further time effects occurred. For instance, if, after *W'* had been reached, the heat input was raised to Q_c'', then W'' was attained in about 1 minute by an exponential increase in ΔT.

(vii) Decrease of the heat input from any value of W', W'', etc., either to a lower Q_c or to zero, also occurred within less than 1 minute by exponential decay.

(viii) *Sudden* decrease of Q from above Q_c' to zero did not seem to remove existing turbulence since it is afterwards impossible to maintain the value of W_0 at heating rates greater than Q_c'. As soon as Q_c' is reached the heat resistance rises rapidly to W' by an exponential curve. In this manner we observed the persistance of turbulence after waiting for as much as 15 minutes (cf. Mendelssohn 1958).

(ix) This persistent turbulence could be removed by maintaining a heat flow just below Q_c' for a minute or less.

(x) The minimum speeds of the turbulent front at different experiments at any given temperature stood in the ratio $2x:3x:4x$, etc. where x (in the 0·1 cm tube) was of the order of 4 cm min^{-1} and was not strongly temperature dependent between 1·1° and 1·3°K.

A full report and a discussion of this work will be published later. We are grateful to Dr. D. O. Edwards and Mr. G. Davey for their help in this work.

Clarendon Laboratory,
Oxford.
27th November 1958.

K. Mendelssohn.
W. A. Steele.

Brewer, D. F., and Edwards, D. O., 1958, *Low Temperature Physics and Chemistry* (Wisconsin: Univ. of Wisconsin Press), p. 12.
Brewer, D. F., Edwards, D. O., and Mendelssohn, K., 1956, *Phil. Mag.*, **1**, 1130.
Mendelssohn, K., 1958, *Nuovo Cim.* **9** (suppl.), 228, *Z. Phys. Chem.*, **16**, 322.

REVIEWS OF BOOKS

Mass Spectroscopy, by H. E. Duckworth. Pp. xvi+206. (Cambridge : University Press, 1958.) 35*s*.

The author of this volume in the series of Cambridge Monographs on Physics has accomplished very successfully the aims set out in his preface, to describe the operational principles of mass spectroscopes and their many applications in nuclear and molecular physics, and in geology. The result is a book which will appeal to a wide range of readers. Not only to those actively engaged in fundamental research in mass spectroscopy and in the applications discussed, but also to others who would like to acquire a general knowledge of a fascinating branch of physics which is becoming increasingly important as a technique in many fields of study.

Concise descriptive accounts are given of positive ion optics and methods of producing positive ion beams. Mathematical formulae relevant to such fundamental properties as focussing conditions, mass resolution and dispersion are given without encumbering the text with derivations. The performance and special design considerations of particular instruments are then discussed with reference to these formulae.

Applications of mass spectroscopy to pure physics are described under the headings isotope abundance and atomic mass determinations, nuclear physics and molecules under electron impact. In the final chapter on geological applications, the emphasis is on age determination and studies of isotope fractionation in geophysical processes.

The book concludes with a useful table of isotope abundances and atomic masses, and a very comprehensive bibliography which will lead the inquiring reader to full details of the topics surveyed so admirably by Professor Duckworth.

D. H. TOMLIN.

Handbuch der Physik, Vol. XVI, *Electric Fields and Waves*, edited by S. Flügge. Pp. vii+753. (Berlin : Springer, 1958.) DM 158.

The sixteenth volume of the monumental Encyclopedia of Physics edited by S. Flügge and published by Springer is entitled Electric Fields and Waves, and although this title may seem at first sight a little vague, perusal of the volume shows that it is accurate enough. The editing of a work of this kind must be a difficult matter ; the various contributions must be written simultaneously by specialists who can have little opportunity of knowing what line is being followed in parts other than their own, and Dr. Flügge has done well to get together in this volume five well balanced monographs which together form a very useful survey of the principles of electromagnetic fields and waves as applied in modern techniques of telecommunication and the like. The first four sections are almost entirely mathematical though their authors have obviously kept in mind the problems arising in practical applications. The last article, being mainly experimental, seems a little out of character with the others but it is complementary to them and makes the whole volume fairly representative of the physics of that portion of the spectrum that can be loosely described as radio.

The sections are arranged systematically in an order that to the experimentalist is one of increasing frequency. Dr. G. Wendt develops the theory of static fields and stationary currents. The mathematical evaluation of typical field-systems in both two and three dimensions is presented in considerable detail and this is followed by a brief review of numerical, graphical and experimental methods such as the electrolytic tank, rubber sheet etc. (This article is in German and the others in English). Dr. Ronold W. P. King follows with the principles of quasi-stationary and non-stationary currents in electric circuits and carries the reader in a manner well known from his books as far as the region of the transmission line and the radiating antenna. Professor F. E. Borgnis and Dr. C. H. Papas deal with the theory of waveguides and cavity-resonators and Dr. H. Bremmer with the propagation of electromagnetic waves through free space. In each case there is a detailed mathematical discussion of a selection of typical problems chosen so as to cover the field of present day practice. In the last section Dr. L. Hartshorn and Dr. J. A. Saxton discuss the experimental techniques for determining the dispersion and absorption of electromagnetic waves in the frequency ranges associated with the other sections. This article amounts to a broad survey of the methods of measuring the complex permittivity or dielectric constant and absorption coefficients of materials with a brief discussion of the significance of the results so far available. One might perhaps have expected this article to appear in a volume which included a detailed discussion of the theory of dielectric behaviour but this merely emphasizes the difficulties of editing previously mentioned. The present volume constitutes a convenient and authoritative survey of modern knowledge in the field which it covers and as such it is a most useful contribution to the literature of physics.

L. H.

Handbuch der Physik, Vol. XXXIV, *Corpuscles and Radiation in Matter* II, edited by S. Flügge. Pp. viii + 316. (Berlin : Springer, 1958.) DM 78.

This volume cannot be regarded as a more or less self-contained entity since much of the complete topic is considered in another volume of this series. We have six topics brought together here, viz. The Passage of Slow Electrons and Ions in Gases (in German) by R. Kollath, pp. 1–52 ; The Passage of Fast Electrons through Matter (English) by R. D. Birkhoff, pp. 53–138 ; Positronium (German) by L. Simons, pp. 139–165 ; X-ray Production by Heavy Charged Particles (English) by E. Merzbacher, pp. 166–192 ; The Energy Loss of Charged Particles in Matter (English) by W. Whaling, pp. 193–217 ; Compton Effect (English), by R. D. Evans, pp. 218–298, together with the Subject Index in both languages.

As can be seen at a glance, the separate topics do not link closely together but as separate contributions to the field they are one and all of an exceedingly high standard. In every case the contributions show clearly the fact that a real expert on the topic is at work on a subject in which he is thoroughly well versed. The reader is brought up to date in his knowledge after a smooth sweep through the field. There is nowhere a feeling of being enmeshed in detail as can so easily be the case in exhaustive authoritative works. Expert summarizing and ready reference to earlier review articles on more detailed aspects makes for a well-rounded treatment in all cases.

The total of 213 figures, many of them packed with useful information in readily appreciated form, helps to make the volume one which can be read with pleasure and yet one which will become a reference book in many ways. It may not be out of place, even where all have done a very good job indeed, to single out for special mention the article on The Compton Effect by R. D. Evans. This contribution is properly the longest of the present volume and it fills a real gap in the literature. It is packed with many curves and much useful data, sometimes derived with the help of the I.B.M. computer at M.I.T. It is a pleasure to welcome this article and indeed the complete volume. It will prove a most valuable source book for many years to come.

The standard of work of the publishers is first class. The volume can be warmly commended to the attention of all physicists. S. C. CURRAN.

Numerical Analysis, by D. R. HARTREE. 2nd Edn. Pp. xvi + 302. (London : Clarendon Press, 1958.) 42*s*.

This is the second edition of a very successful book, by the late Professor D. R. Hartree, first published in 1952. It was stated in the original preface that the purpose of the book was to give an introduction to numerical analysis to workers in various fields of pure or applied science who may have to carry out calculations of a non-trivial magnitude. The main changes in the new edition are in the chapter on the numerical integration of ordinary differential equations which has been largely rearranged and somewhat extended, particularly as regards the treatment of equations with two-point boundary conditions. There is also a new section on Whittaker's cardinal function and various changes in the sections on the solution of linear equations and quadrature. The chapter on the organization of calculations for an automatic digital computer has been slightly shortened by omitting the sections concerned with details of programming ; these no longer seemed necessary in view of the fact that so much more has now been published on this subject.

The book carries evidence on every page of the author's long experience and feeling for the practical aspects of the subject. It is, in my opinion, the best available introductory handbook for anyone who is primarily interested in getting results and only secondarily interested in the formal aspects of the subject. M. V. WILKES.

A Treastise on Photo-elasticity, by E. G. COKER and L. N. G. FILON. 2nd Edn, revised with an introduction and bibliography by H. T. Jessop. Pp. xxxii + 720. (Cambridge : University Press, 1957.) 70*s*.

Photo-elasticity, discovered by Brewster in 1816 and studied by the great classical physicists Biot, Fresnel, Neumann, Maxwell, Mach and many others, was turned to practical use by Coker from 1909 onward in the Engineering Laboratories of University College, London, to which many research workers, including some from American industry, were attracted during the second and third decades of the century. By 1931 when Coker and Filon published their *Treatise on Photo-elasticity* which was in effect a complete manual of theory and practice, there were centres of active work in France, Switzerland, Germany and Japan as well as in the U.S.A. Since then there has been a continuous stream, interrupted only by the second world war, of original publications dealing for the most part with developments in technique, but although thirteen textbooks have appeared, including one by Jessop and Harris in 1949, Colonel Jessop himself says that none can replace that of Coker and Filon which remains the most comprehensive and authoritative work on the theory of the subject and on the principles of its application to stress analysis. Jessop and Harris dedicated their book to the memory of Filon and this act of grateful piety is now supplemented by the issue of a revised edition of the *Treatise* by Coker and Filon, substantially unchanged, but augmented by a valuable introduction by the reviser Colonel Jessop, Senior Lecturer in Photoelasticity in the Department of Civil and Municipal Engineering in University College, London. He reviews the developments of the subject since 1931, which are numerous, the most important being the application of the methods of frozen-stress and of observations in scattered light to explore stress distribution in three dimensions. Papers on both these methods have been published by him, and are listed in the complete bibliography of 97 original papers which concludes the additional matter of this new edition. It is regrettable that the beautiful colour plates of the first edition have had to be omitted but doubtless the cost was prohibitive. At seventy shillings the second edition will be welcome indeed to those workers who have had no access to the original save from the shelves of a library not their own, while those possessing the original will be glad to bring their knowledge and their bibliography up to date. A. M. TAYLOR.

An Introduction to Fourier Analysis and Generalised Functions, by M. J. LIGHTHILL. Pp. viii + 79. (Cambridge : University Press, 1958.) 17*s*. 6*d*.

Dirac's delta function was first introduced into mathematical physics as a purely heuristic device. A proper mathematical interpretation of it was first provided by Schwartz's theory of distributions, and then by Temple's theory of generalized functions. Schwartz's theory lies closer to the original conception, but rests on some rather abstract mathematical notions. Temple's theory, on the other hand, involves only the commonplaces of mathematical analysis ; it is therefore the natural approach for this book, which grew out of a course on Fourier series given to undergraduates in their third year. The climax of the book is the theorem that every generalized function is uniquely represented by its Fourier series. A theory which can, without loss of rigour, be so excitingly simple should surely be a part of the equipment of every mathematical physicist.

Besides the main topic the book also treats of Fourier transforms, and of their asymptotic behaviour. It is intended as a collection of *proofs* rather than of results, and the intention is beautifully carried out. The theorems are straightforward and memorable, the proofs are clear and concise ; there are a fair number of examples and exercises ; and there is just the right amount of explanation of what is being done. R. O. GANDY.

Mikrowellen-Messtechnik, by F. J. TISCHER. Pp. xi + 310. (Berlin, Göttingen, Heidelberg : Springer, 1958.) DM 54.

This book deals entirely with the art of microwave measurements, the reader being assumed familiar with microwave theory and techniques. Emphasis is placed on the errors which occur in the various types of measurement, and the theory is kept to the minimum sufficient for the understanding of the measurement involved.

Basic questions of frequency measurement and frequency stability are considered first, the discussion ranging over the use of cavity resonators and other frequency measuring techniques. Frequency stabilization of microwave oscillators, and microwave frequency stabilization by atomic and molecular resonances, such as the caesium atomic beam, and the Maser are also included. Microwave power measurements with calorimeters, bolometers, thermisters, and crystals are considered, and also methods involving radiation pressure. Measurements of pulsed power are also discussed, and estimates are given of the accuracy possible with the various methods.

Matching devices and impedance measurements are discussed very comprehensively, the author having made significant contributions in this field. Two novel methods mentioned are the use of a rotating inductive probe in a waveguide, and a vibrating capacitive probe for impedance measurements. A discussion of waveguide components follows, including ferrite devices.

Methods for measuring the *Q* of cavity resonators are presented in detail, and also measurements on the electric properties of materials, including tensor permeabilities. Finally, there are useful chapters on antenna measurements, and on noise in microwave receivers.

The book is to be recommended for the many novel and interesting ideas it contains, and for its accent on the accuracy of microwave measurements. In general the coverage of the various topics is good, though in some instances it could be improved. This is so in the chapters on microwave power measurements, and on cavity *Q* measurements, where some consideration of coupling losses would be beneficial. Also some consideration of the use of optical techniques, such as interferometers, could with advantage have been included, both for microwave measurements and for the shorter wavelengths.

However, within its 300 pages the book contains a wealth of information on microwave measurements, and this coupled with a very extensive bibliography makes the book a valuable addition to the literature on the subject.

W. CULSHAW.

Atmospheric Electricity, by A. J. CHALMERS. Pp. vii + 327. (London : Pergamon Press, 1957.) 63*s*.

The ground covered is that conventionally associated with the words atmospheric electricity—the earth's potential gradient in fine weather, the ionization of the lower atmosphere, the electrification of clouds and precipitation, corona discharge in the earth's field, and the lightning discharge. It expands and brings up to date (mid 1956) the same author's text published in 1948. The treatment is elementary and didactic—a sixth form student will find few difficulties.

One tenth part of the printed matter is given over to a list of references, each of which has been mentioned at least once, and some many times, in the text. Very few of them are the subject of any critical comment, and many of them cover only very trivial points. These citations clog the text, sometimes to the extent of obscuring the argument, often to the extent of hiding the essential interest in a mass of detail. Atmospheric electricity was a favoured study of such men as Franklin and Kelvin ; in this century it has been advanced by the beautiful observations of Schonland and the fertile speculations of Simpson. It is not one of the duller corners of physics, but this book makes it appear so. It is a useful compendium for the specialist, but will make no converts to the subject.

The arrangement is convenient for quick reference and the book is pleasant to look at and to handle, but there are far too many printer's (or proof-reader's) errors. G. D. ROBINSON.

Effects of Radiation on Materials, edited by J. J. HARWOOD, H. H. HAUSNER, J. J. MORSE, and W. G. RAUCH. (Report of a Colloquium Sponsored by the U.S. Office of Naval Research and the Martin Company of America, March 1957.) Pp. v + 355. (New York : Reinhold Publishing Corporation, 1958.) 84*s*.

Eleven papers delivered at a three-day colloquium at the Johns Hopkins University, Baltimore (March 1957) are here published as separate chapters of a book.

Most of the book consists of studies of the electrical, magnetic, mechanical and optical changes induced in solids by irradiation. The book opens with a chapter which describes the current theoretical concepts used in connection with the effects of radiation in solids. There are chapters on the irradiation of semiconductors, of surfaces and of metals and alloys. Considerable space is given to the study of irradiation in organic substances, particularly in regard to polymer chemistry. Because of its importance in producing a high yield of atomic displacements, the effect of neutron irradiation is chiefly considered, although radiation from charged particle accelerators and γ-ray sources are also treated in some detail. Randomly spaced amongst these papers is a group of chapters dealing with reactor technology. These concern reactor design, dose measurement, auxiliary reactor equipment and the problems associated with shielding. The chapters seem somewhat out of place in this book especially as no corresponding detail concerning particle accelerators is given. The information is unlikley to be sufficient for those concerned with reactor design, but it should be of considerable use both for those planning reactor experiments and those indirectly concerned with reactor operation. Extensive lists of references are given at the end of every chapter and the book ends with a bibliography containing nearly eight hundred references.

The scope of the book is too wide for it to be either comprehensive, or of use to specialists in their own particular field. However, when, as often happens, technical or research workers require information about closely allied subjects, this book should prove of considerable use. Although it contains rather too much technical jargon, the book is, in the main, well written. J. A. BASTIN.

Fig. 1

Fig. 2

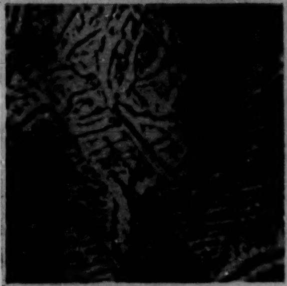

Fig. 3

Fig. 4

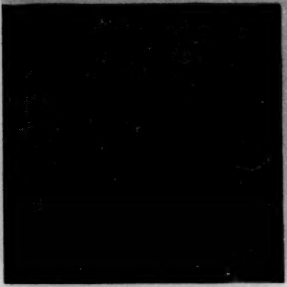

Fig. 5

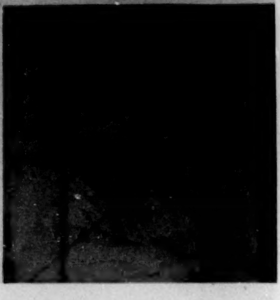

Fig. 6

Figure 1. Strain pattern on approximate (110) surface of manganese ferrite (×67).

Figure 2. 109° domain walls and fir tree patterns on approximate (110) surface of manganese ferrite (×193).

Figure 3. Intricate system of fir trees on approximate (110) manganese ferrite surface, small horizontal field (×333).

Figure 4. Fir tree patterns on 180° wall on approximate (110) manganese ferrite surface (×333).

Figure 5. Spikes arising from pits in (110) manganese ferrite surface. Néel spike ringed. Arrows give directions of magnetization (×333).

Figure 6. Echelon-type closure at crack parallel to [110] direction in (110) manganese ferrite surface (×333).

PLATE I.

Fig. 7

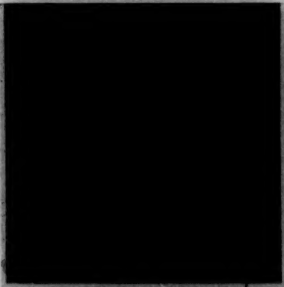

Fig. 8

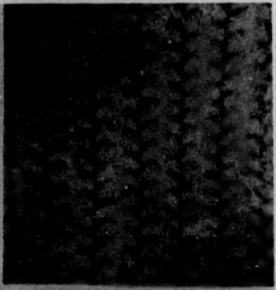

Fig. 9

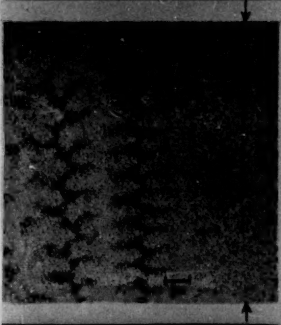

Fig. 10

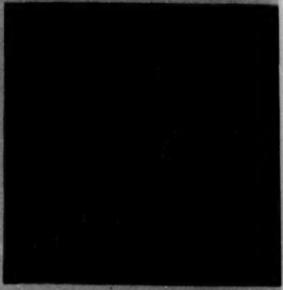

V.
19

Fig. 11

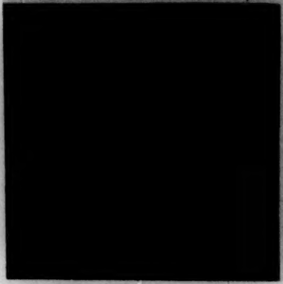

Fig. 12

Figure 7. Fine structure on cleaved (100) surface of MnZn ferrite (× 667).
Figure 8. Electron micrograph of fine structure, as figure 7.
Figure 9. Electron micrograph of fine structure near a crack (arrowed).
Figure 10. Coarse structure on cleaved (100) surface (× 333).
Figure 11. Branching pattern observed on (110) surface of MnZn ferrite (× 333).
Figure 12. Electron micrograph of structure on approximate basal plane of cobalt, cf. figure 11.

PLATE II.

Fig. 13

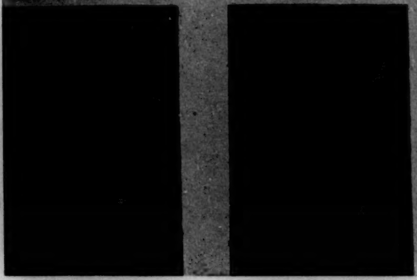

Fig. 14 (*a*)

Fig. 14 (*b*)

Fig. 15

Figure 13. Pattern observed on a natural (111) facet of Ni ferrite (× 100).

Figure 14 (*a*) and (*b*). Part of pattern of figure 12, showing effect of the reversal of a normally applied field (× 333).

Figure 15. Closure domains on (110) faces of Ni ferrite (× 267).

PLATE III.

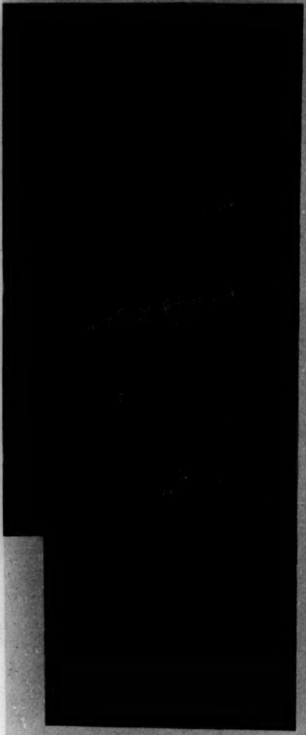

Fig. 16

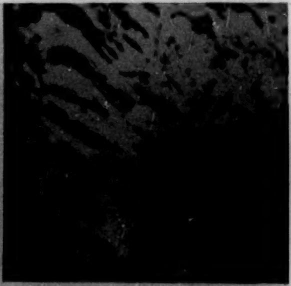

Fig. 17

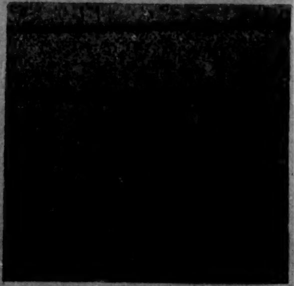

Fig. 18

Fig. 19

Figure 16. Composite print of patterns on three contiguous faces, i.e. (111), (110) and (111), of Ni ferrite. Néel spike ringed. (×187.)

Figure 17. Pattern obtained on natural facet of Cu ferrite (×333).

Figure 18. Electron micrograph of apparent domain walls on Cu ferrite facet.

Figure 19. Electron micrograph of lozenge-type pattern on Cu ferrite facet.

Plate IV.

PROC. PHYS. SOC. VOL. 73, PT. I (D. J. CRAIK AND P. M. GRIFFITHS)

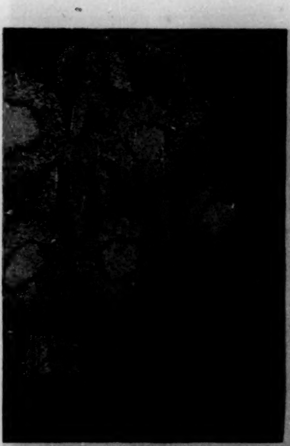

Fig. 20

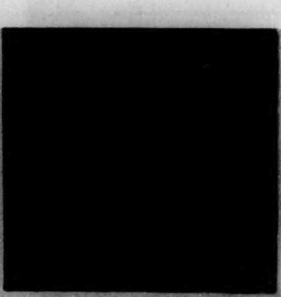

Fig. 21

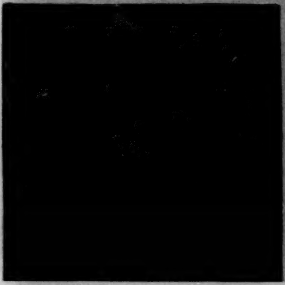

Fig. 22

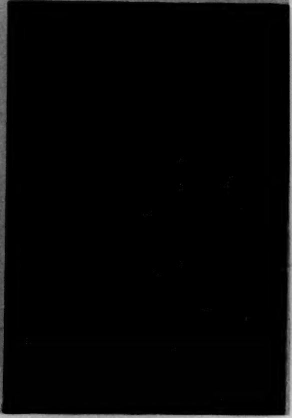

Fig. 23

Figure 20. Electron micrograph of undulatory wall structure on cleaved basal plane of barium ferrite.

Figure 21. Intricate pattern on cleaved basal plane of barium ferrite (×267).

Figure 22. Electron micrograph of structure of figure 21.

Figure 23. Electron micrograph of pattern on cleaved basal plane of barium ferrite, with 1 μ spacing.

PLATE V.

Fig. 24

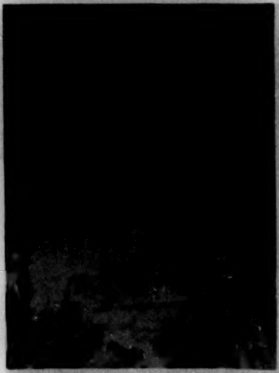

Fig. 25

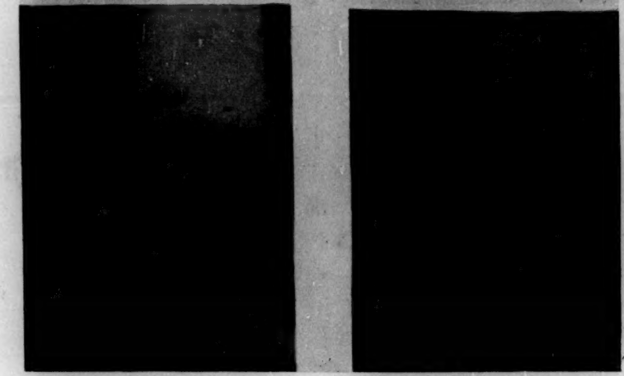

Fig. 26 (*a*) **Fig. 26 (*b*)**

Figure 24. Pattern on axial planes of barium ferrite crystals (× 107).

Figure 25. Patterns showing interaction of domains at boundaries on axial planes of barium ferrite crystals (× 107).

Figure 26 (*a*) and (*b*). Effect of reversal of normally applied field on axial planes of barium ferrite crystal (× 333).

PLATE VI.

Fig. 1

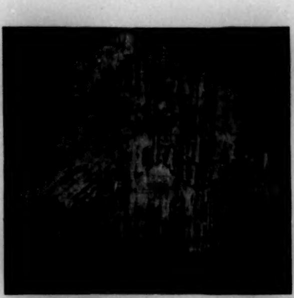

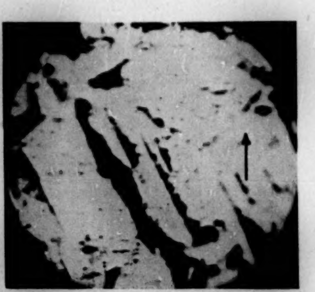

Fig. 2

Fig. 3

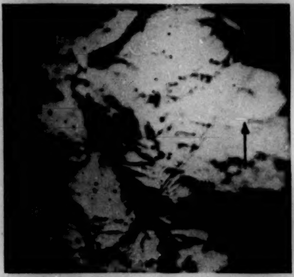

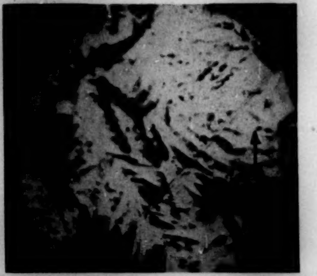

Fig. 4

Fig. 5

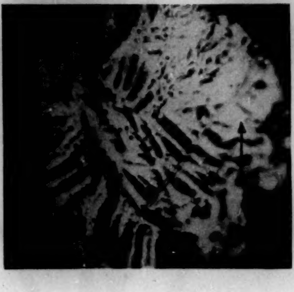

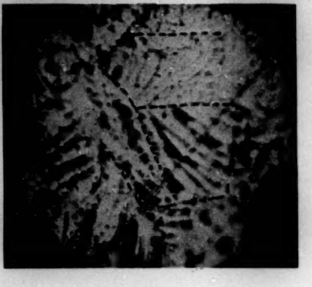

Fig. 6

0·1mm

Figure 1. Typical pattern on 59% Co alloy; – – – approximate grain boundaries; $H=0$ (weak vertical field).
Figure 2. 59% Co alloy, $H=200$ Oe along arrow. Specimen saturated.
Figure 3. 59% Co alloy, $H=30$ Oe along arrow.
Figure 4. 59% Co alloy, $H=5$ Oe along arrow.
Figure 5. 59% Co alloy, $H=1$ Oe along arrow.
Figure 6. 59% Co alloy, H, reversed, $=3$ Oe at arrow. Note reversal of bands.

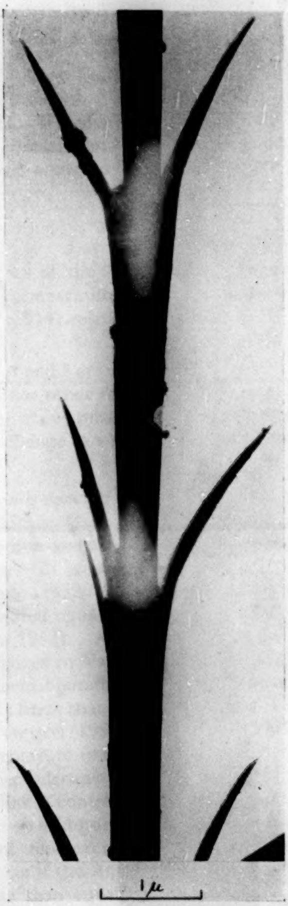

Figure 1. Typical bright field electron micrograph of crystals of poly-L-proline II.

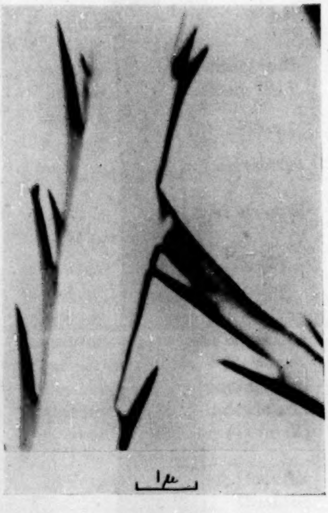

Figure 2. Typical dark field electron micrograph of crystals of poly-L-proline II. (Printed negatively.)

PLATE I.

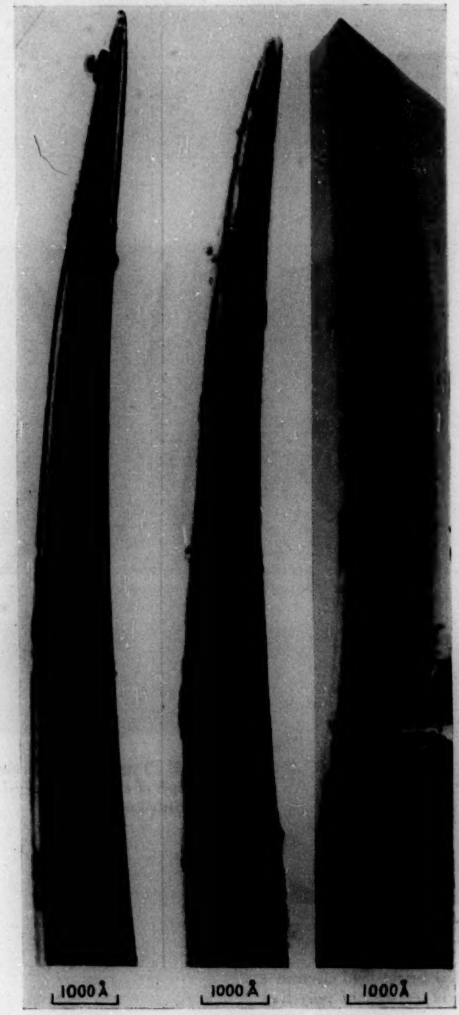

(a) (b) (c)

Figure 3. Electron micrographs of single crystal spines. Spines (a) and (b) are shown at lower magnification in the centre of figure 1. Spine (c) grew from a similar main fibre to that shown in figure 1.

Plate II.

Viscosity of Normal Paraffins

By Y. P. VARSHNI and S. N. SRIVASTAVA
Department of Physics, Allahabad University, Allahabad, India

MS. received 28th July 1958, in revised form 30th September 1958

Abstract. It is shown that the Andrade–Guzman relation $\eta = Ae^{b/T}$ for the variation of viscosity with temperature is adequate for normal paraffins. Andrade's improved equation $\eta v^{1/3} = Be^{c/vT}$ gives less satisfactory results.

---

§ 1. Introduction

One of the well-known equations for the variation of the viscosity with temperature is the Andrade–Guzman (Andrade 1930, Guzman 1913, 1914) relation

$$\eta = Ae^{b/T} \qquad \ldots\ldots(1)$$

where A and b are constants. Reference may be made to Varshni and Srivastava (1958) for other references in the field.

The above relation (1) was later modified by Andrade (1934) to take account of the change in volume which accompanies change of temperature:

$$\eta v^{1/3} = Be^{c/vT} \qquad \ldots\ldots(2)$$

where v is specific volume and B and c are constants.

Andrade–Guzman (AG) relation (1) is known to be satisfactory for many of the non-associated liquids. Usually the accuracy of results from equations (1) and (2) is of the same order (Srinivasan and Prasad 1942). However, Andrade (1952, 1954) has shown from the behaviour of b and c for liquid alkali metals that equation (2) is theoretically more satisfactory (see also Andrade and Dobbs 1952). Associated liquids do not conform to either equation (1) or (2) (references in Varshni and Srivastava 1958).

Normal paraffins are known to be non-associated liquids. However, Doolittle (1951) finds that the AG equation is not fully satisfactory for them. Doolittle and Peterson (1951) and Doolittle (1951) have drawn ($\ln \eta$, $1/T$) diagrams showing the departure from linearity. But detailed calculations have been reported only for heptadecane by Doolittle (1951). This abnormal behaviour of normal paraffins is contrary to expectations. The present investigation was undertaken with two fold purpose: firstly, to examine how far the AG equation (1) can or cannot represent the (η, T) relation for normal paraffins; and secondly, to examine if the Andrade relation (2), which is theoretically sounder, gives better results than equation (1).

Fortunately, accurate data on viscosity and specific-volume at the same temperatures for normal paraffins are available from the studies of Doolittle and Peterson (1951) and Doolittle (1951). Making use of these data we have evaluated the constants in equations (1) and (2) by the method of least squares for seven normal paraffins (for which more than four points are available.) These are given in table 1 for η in poises and T in degrees Kelvin.

Table 1

No. of C atoms	Liquid	*A*	*b*	*B*	*c*
9	C_9H_{20}	0·13468	1168·051	0·45962	1172·56
11	$C_{11}H_{24}$	0·10847	1383·937	0·41668	1376·84
13	$C_{13}H_{28}$	0·10493	1515·35	0·41928	1499·28
17	$C_{17}H_{36}$	0·08888	1788·61	0·41793	1739·00
28	$C_{28}H_{58}$	0·11604	2053·01	0·5568	1986·07
36	$C_{36}H_{74}$	0·12514	2219·37	0·62698	2150·43
64	$C_{64}H_{130}$	0·15460	2614·84	0·87630	2534·79

Observed and calculated values by the two equations together with the percentage errors are recorded in table 2 opposite.

§ 2. Discussion

The average percentage errors for the seven paraffins are summarized in table 3.

Srinivasan and Prasad (1942) showed that for a number of organic liquids equation (1) was as good as equation (2). Andrade and Dobbs found that equation (2) gives a 'slightly closer fit' than equation (1) for liquid alkali metals. For the liquids under investigation we see that errors by (1) are less than those by equation (2), indicating that for normal paraffins equation (1) is slightly better than equation (2).

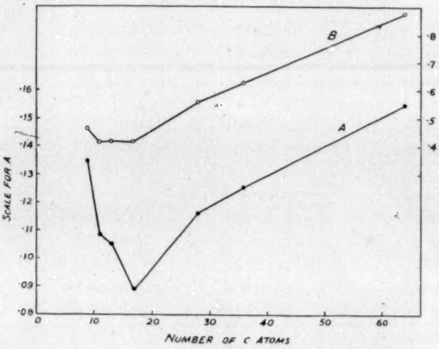

Figure 1.

Figure 1 shows the variation of *A* and *B* and figure 2 that of *b* and *c* with the number of carbon atoms. The behaviour of *A* and *B* is somewhat similar ; both show an initial decrease followed by an approximately linear increase. Values of *b* and *c* are very close to each other (table 1) and the corresponding behaviour is shown in figure 2. To avoid overlapping the two curves have been displaced by 100 units.

For liquid alkali metals, Andrade (1952) has shown that *c* varies regularly with increase in atomic weight, but *b* shows erratic behaviour. This indicates

Table 2

Liquid	Temp. (°K)	η obs. (10^{-2} poise)	Equation (1) η calc (10^{-2} P)	Equation (1) % Error	Equation (2) η calc (10^{-2} P)	Equation (2) % Error
C_9H_{20}	263·2	1·150	1·140	−0·8	1·128	−1·9
	293·2	0·7165	0·7235	+0·9	0·7259	+1·3
	323·2	0·4968	0·4996	+0·5	0·5051	+1·7
	373·2	0·3087	0·3080	−0·02	0·3105	+0·5
	423·2	0·2136	0·2127	−0·04	0·2103	−1·5
$C_{11}H_{24}$	263·2	2·1670	2·084	−3·8	2·052	−5·3
	293·2	1·1860	1·217	+2·5	1·219	+2·7
	323·2	0·7609	0·7850	+3·1	0·7947	+4·4
	373·2	0·4384	0·4424	+0·9	0·4503	+2·7
	423·2	0·2894	0·2854	−1·3	0·2874	−0·7
	473·2	0·2048	0·2020	−1·3	0·1977	−3·5
$C_{13}H_{28}$	293·2	1·883	1·843	−2·1	1·827	−3·0
	323·2	1·118	1·140	+2·0	1·144	+2·3
	373·2	0·6001	0·6085	+1·4	0·6155	+2·5
	423·2	0·3765	0·3767	+0·1	0.3788	+0·6
	473·2	0·2615	0·2580	−1·3	0·2550	−2·5
$C_{17}H_{36}$	293.2	4·209	3·965	−5·8	3·880	−7·8
	323·2	2·170	2·251	+3·7	2·244	+3·4
	373·2	1·018	1·072	+5·3	1·091	+7·1
	423·2	0·5984	0·6085	+1·7	0·6234	+4·2
	473·2	0·3938	0·3894	−1·1	0·3966	+0·7
	523·2	0·2785	0·2713	−2·6	0·2712	−0·3
	573·2	0·2030	0·2014	−0·8	0·1944	−0·4
$C_{28}H_{58}$	373·2	2·872	2·842	−1·0	2·826	−1·6
	423·2	1·460	1·484	+1·6	1·491	+2·1
	473·2	0·8856	0·8888	+0·3	0·8948	+1·0
	523·2	0·5920	0·5870	−0·8	0·5882	−0·6
	573·2	0·4173	0·4170	−0·1	0·4143	−0·7
$C_{36}H_{74}$	373·2	4·884	4·787	−2·0	4·894	+0·2
	423·2	2·315	2·371	+2·4	2·379	+2·8
	473·2	1·344	1·362	+1·3	1·373	+2·2
	523·2	0·8749	0·8702	−0·5	0·8732	−0·2
	573·2	0·6083	0·6012	−1·2	0·5961	−2·0
$C_{64}H_{130}$	373·2	17·85	17·07	−4·4	17·06	−4·4
	423·2	7·144	7·427	+4·4	7·484	+4·8
	473·2	3·757	3·883	+3·4	3·900	+3·8
	523·2	2·292	2·290	−0·1	2·289	−0·1
	573·2	1·525	1·480	−2·9	1·470	−3·6

that *c* is of greater theoretical importance. However, in the present case the values of *b* and *c* are quite close to each other and their variation with the number of carbon atoms (figure 2) does not show any sharp difference.

Table 3

Liquid	C_9H_{20}	$C_{11}H_{24}$	$C_{13}H_{28}$	$C_{17}H_{36}$	$C_{28}H_{58}$	$C_{36}H_{74}$	$C_{64}H_{130}$	Average (for all)
Average % error by eqn. (1)	±0·4	±2·2	±1·4	±3·0	±0·8	±1·5	±3·0	±1·8
Average % error by eqn. (2)	±1·4	±3·2	±2·2	±3·4	±1·2	±1·5	±3·3	±2·4

It will be noticed that most of the paraffins considered here have high molecular weights. These higher paraffins are rarely pure, usually some of the neighbouring paraffins being also present. Doolittle and Peterson (1951) give the following possible percentages of impurities: $C_{17}H_{36}$ 0·2%, $C_{28}H_{58}$ 5%, $C_{36}H_{74}$ 5%, $C_{64}H_{130}$ 10%.

The conclusions of this paper are subject to this important limitation. Values of the constants change with the number of carbon atoms, and impurities may affect them to a noticeable extent.

Next we discuss the applicability of the two equations separately.

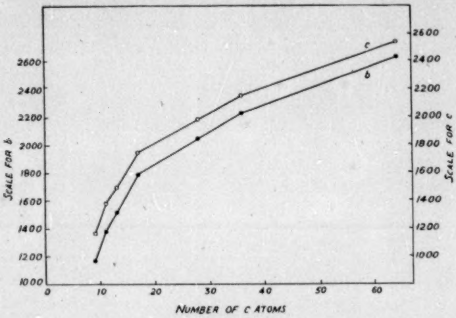

Figure 2.

Andrade equation.

It may be emphasized that the lesser success of Andrade equation (2) does not indicate its shortcoming. Andrade's equation was derived from a consideration of spherical or approximately spherical molecules. The structure of the paraffins under consideration is very far from this picture.

As is well known, as the number of carbon atoms increases, the physical constants of the normal paraffins show increasing deviation from the values expected from the law of corresponding states. It seems reasonable to consider that the deviation of this kind mainly originates in the change of molecular shape from the sphere to rod. It is plausible that these molecules might be represented as chains of segments which interact as point centres of force. The use of the lattice model, in which the molecules occupy groups of consecutive lattice sites, was first suggested by Fowler and Rushbrooke (1937); it has been used widely in connection with the theory of high polymer solutions. In this model there are non-ideal entropy effects even in the absence of interactions, due to interference between different chain molecules.

Kurata and Isida (1955) have employed a modified lattice model of the hole theory of liquids for normal paraffins and discussed effects which arise as a result of the deviation from the sphere in the shape of the molecule. Simha and Hadden (1956, 1957) have also discussed the theory of liquid hydrocarbon in relation to their structure.

It is very reasonable to consider that the viscosity will depend on the type of the intermolecular force. With metals, the particles are spherical with an isotropic intermolecular force falling off slowly with distance, whereas the n-hydrocarbons have intermolecular forces falling off perpendicular to the chain axis as the sixth power of the distance (Wake 1947).

The relation of viscosity to the length of the molecule and branching has been treated by Nederbragt and Boelhouwer (1947).

On the whole the fit of the Andrade equation is satisfactory, "the maximum percentage error depending in general as would be expected on the range of viscosity, defined as the ratio of the viscosity at the lowest temperature of the experimental range to that at the highest temperature" (Andrade 1934). For example in the case of $C_{28}H_{58}$ the range is 7 and the maximum error 2%, while in case of $C_{17}H_{36}$ the range is 21 and the maximum error 7%. It may be noted that the fit for $C_{17}H_{36}$ can be improved (see below).

It may be added that Andrade (1934) found his equation very satisfactory for some of the lower paraffins, viz. pentane, hexane, heptane and octane.

Andrade–Guzman equation.

The average percentage errors in the case of the Andrade–Guzman equation are of the order of 1·8 (except heptadecane). This is of the same order as the errors found for many other liquids (e.g. Srinivasan and Prasad 1942, Prasad 1933). Hence it is as adequate for normal paraffins as for other non-associated liquids.

The case of heptadecane needs special mention. If we omit the point for 293·2°K (which is an extrapolated point) and recalculate A and b from the remaining points, better results are obtained as shown in table 4.

Table 4. Heptadecane $A = 0{\cdot}099132$; $b = 1737{\cdot}23$

Temperature (°K)	323·2	373·2	423·2	473·2	523·2	573·2
η calc (10^{-2} P)	2·140	1·042	0·6010	0·3895	0·2743	0·2053
% error	−1·38	+2·36	+0·43	−1·45	−1·51	+1·13
Average error 1·38						

It appears probable that the reported value of η at 293·2°K is in error.

The new value of A also makes the A curve (figure 1) smoother. In later discussion we shall use these new values of A and b.

The exponent b/T is often written as E_{vis}/RT, where E_{vis} is called 'energy of activation for viscous flow'.

A number of workers (Ewell and Eyring 1937, Kierstead and Turkevich 1944, Waring and Becher 1947, Wake 1947) have investigated the applicability of the AG equation to normal paraffin liquids and attempted to interpret the values of A and b on theoretical grounds.

The trend of our values of E_{vis} with those determined by earlier workers has been compared in table 5.

Our results are somewhat lower than the previous values.

A number of attempts have been made to connect E_{vis} with other properties of liquids.

Ewell and Eyring (1937) have suggested that the ratio of $E_{\text{vap}}/E_{\text{vis}}$ can be taken as an index of the size and the shape of the molecule, or more precisely, of the unit of flow in the liquid (see also Eyring and Hirschfelder 1937). Hirschfelder, Stevenson and Eyring (1937) have pictured the process of flow in a liquid as involving the rotation of a pair of molecules about a common centre of mass and movement into a hole in the liquid. The energy of activation of viscosity is therefore related to the energy of hole formation which is related to the energy of vaporization.

Following the above considerations, Simons and Wilson (1955) have shown that E_{vis} is related to the boiling point T_b by the following equation (for the n-paraffins below $n=19$)

$$E_{\text{vis}} = 1{\cdot}212\ T_b^{1{\cdot}2} - 1000.$$

Table 5. E_{vis} (cal mol^{-1}) for Normal Paraffins

No. of C atoms	EE	KT	VS
8	2140	2088	
9	2440	2394	2320
10	2600	2565	
11	3060	2778	2749
12		3010	
13			3010
14	3600	3203	
16	4010	3652	
17			3451
18	4150	3891	
28			4078
32		4922	
36			4409
64			5194

EE = Ewell and Eyring; KT = Kierstead and Turkevich; VS = present work.

It is not possible to test the relation for higher paraffins, as boiling points are known only up to nonadecane; n-paraffins with $n > 19$ break up before boiling.

It may be considered that the energy of activation of viscous flow of a normal paraffin is proportional to the number of carbon atoms, if the chain moves rigidly as a whole, since the volume of the hole to receive it and any work function involved in entering the hole will vary directly as the number of carbon atoms. But it is found that this linearity does not hold. We can interpret the departure from linearity in either of two ways: (i) that only part of the molecule moves (Kauzmann and Eyring 1940) or (ii) that the number of segments is not equal to n (here the term 'segment' means an element of the hydrocarbon chain, the size of which is equal to that of a cell).

Instead, Wake (1947) finds that E_{vis} is linear with log n. The relation is shown in figure 3 for the paraffins under consideration. It is seen that the relation is well obeyed.

While the workers have paid considerable attention to the constant b, the other constant A has received much less attention. Kierstead and Turkevich (1944) found that $1/A$ increases linearly with n up to $n=18$ (note their equation is for fluidity; thus their A is our $1/A$). However, their point for $C_{32}H_{66}$ was abnormal, being much lower than the expected value from the linear relation. Our results (figure 1) show that A does not decrease uniformly but there appears to be a minimum at about $n=17$. Later on there is uniform increase. Waring and Becher (1947) found that for similar substances log A is linear with E_{vis}. However, in our case (figure 4) this is not true for the whole range, but beyond $n=17$ it is well followed. The regular variation of A and b with n makes it possible to estimate their values for the paraffins for which no data is available.

It may be added that Gutmann and Simmons (1952, 1953) have found Vogel's (1921) equation, viz. $\log\eta = A + B/(T+C)$ satisfactory for five lower paraffins.

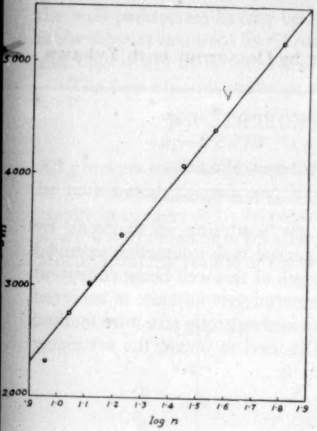

Figure 3.

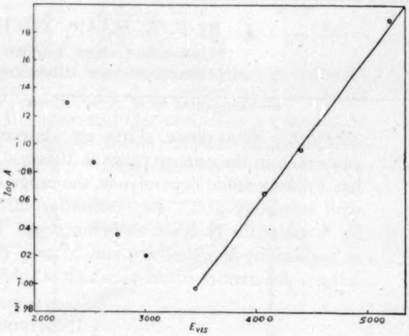

Figure 4.

ACKNOWLEDGMENT

The authors are grateful to Prof. K. Banerjee for his kind interest in the work.

REFERENCES

ANDRADE, E. N. DA C., 1930, *Nature, Lond.*, **125,** 309, 582.
—— 1934, *Phil. Mag.*, **17,** 497, 698.
—— 1952, *Proc. Roy. Soc.* A, **215,** 40.
—— 1954, *Endeavour*, **13,** 117.
ANDRADE, E. N. DA C., and DOBBS, E. R., 1952, *Proc. Roy. Soc.* A, **211,** 12.
DOOLITTLE, A. K., 1951, *J. Appl. Phys.*, **22,** 1031.
DOOLITTLE, A. K., and PETERSON, R. H., 1951, *J. Amer. Chem. Soc.*, **73,** 2145.
EWELL, R. H., and EYRING, H., 1937, *J. Chem. Phys.*, **5,** 726.
EYRING, H., and HIRSCHFELDER, J., 1937, *J. Phys. Chem.*, **41,** 249.
FOWLER, R. H., and RUSHBROOKE, G. S., 1937, *Trans. Faraday Soc.*, **33,** 1272.
GUTMANN, F., and SIMMONS, L. M., 1952, *J. Appl. Phys.*, **23,** 977.
—— 1953, *Ibid.*, **24,** 1067.
DE GUZMAN, J., 1913, *An. Soc. Esp. Fis. Quim.*, **11,** 353; 1914, *Ibid.*, **12,** 432.
HIRSCHFELDER, J., STEVENSON, D., and EYRING, H., 1937, *J. Chem. Phys.*, **5,** 896.
KAUZMANN, W., and EYRING, H., 1940, *J. Amer. Chem. Soc.*, **62,** 3113.
KIERSTEAD, H. A., and TURKEVICH, J., 1944, *J. Chem. Phys.*, **12,** 24.
KURATA, M., and ISIDA, S., 1955, *J. Chem. Phys.*, **23,** 1126.
NEDERBRAGT, G. W., and BOELHOUWER, J. W. M., 1947, *Physica*, **13,** 305.
PRASAD, B., 1933, *J. Indian Chem. Soc.*, **10,** 143.
SIMHA, R., and HADDEN, S. T., 1956, *J. Chem. Phys.*, **25,** 702.
—— 1957, *Ibid.*, **26,** 425.
SIMONS, J., and WILSON, W. H., 1955, *J. Chem. Phys.*, **23,** 613.
SRINIVASAN, M. K., and PRASAD, B., 1942, *Phil. Mag.*, **33,** 258.
VARSHNI, Y. P., and SRIVASTAVA, S. N., 1958, *J. Phys. Chem.*, **62,** 706.
VOGEL, H., 1921, *Phys. Z.*, **22,** 645.
WAKE, W. C., 1947, *Trans. Faraday Soc.*, **43,** 708.
WARING, C. E., and BECHER, P., 1947, *J. Chem. Phys.*, **15,** 488

Low Energy Elastic Scattering of Neutrons by Deuterons with Yukawa Interaction

By F. A. HAAS† and H. H. ROBERTSON‡
†University College, London
‡National Physical Laboratory, Teddington, Middlesex

Communicated by H. S. W. Massey; MS. received 11th September 1958

Abstract. Five phase shifts are determined for scattering of neutrons by deuterons in the energy range 0–10 Mev. The central type interaction assumed has Yukawa radial dependence, the range and depth of this well being consistent with two-body data. Representation of the deuteron ground state is achieved by means of the Hulthén wave function. The resonating group structure method as applied by Buckingham and Massey (1941) is used to obtain the scattering integro-differential equation which is solved exactly.

---

§ 1. INTRODUCTION

SINCE at low energies the non-central force between nucleons can be adequately represented by an equivalent central component, previous workers have shown justifiable interest in determining the relative merits of differently shaped central interactions with their various associated ranges and depths. The present work may be regarded as a continuance of this trend.

Buckingham and Massey (1941) formulated the n–d problem upon the basis of resonating group structure assuming charge–independent two-body forces with an internucleonic interaction energy of the form

$$V(r) = V(r)(mM + hH + bMH + w), \qquad \ldots\ldots(1)$$

where M and H are the Majorana and Heisenberg operators respectively. They adopted an exponential shape for the radial dependence $V(r)$ and solved the scattering integro-differential equation by exact methods. These calculations were subsequently extended to neutron energies of 16 Mev (Buckingham, Hubbard and Massey 1952).

Christian and Gammel (1953) derived n–d phase shifts in Born approximation for orbital angular momenta $l \geqslant 1$ assuming gaussian and Yukawa shaped radial wells. Using the Yukawa shape, zero-order phase shifts in the low-energy limit were evaluated by accurate solution of the integro-differential equations. For higher energies the zero-order phase shifts were evaluated using the less accurate 'zero-range' approximation. The well parameters used and the results obtained in the above computations have been conveniently summarized by de Borde and Massey (1955).

The original formulation of Buckingham and Massey has recently been revised by Burke and Robertson (1957) and calculations carried through for five different ranges of gaussian shape. The latter workers solved the scattering integro-differential equation using both exact and variational methods.

In this paper the formulation of Burke and Robertson is adopted and their work extended to the Yukawa interaction

$$V(r) = V_0 \frac{\exp[-r/\lambda]}{r/\lambda}, \quad V_0 = -68{\cdot}01\,\text{Mev}, \quad \lambda = 1{\cdot}18 \times 10^{-13}\,\text{cm}, \qquad \ldots\ldots(2)$$

V.7
195

the well parameters having been determined by Burke (1956). This potential is the same as that used by Christian and Gammel in their zero-order phase work and thus it will be of interest to compare the Blatt–Jackson curves arising.

The two experimentally permissible sets of scattering lengths are:

$$\left.\begin{array}{lll} a_4 = 2{\cdot}4 \times 10^{-13}\ \text{cm}, & a_2 = 8{\cdot}3 \times 10^{-13}\ \text{cm}, & \text{I} \\ a_4 = 6{\cdot}2 \times 10^{-13}\ \text{cm}, & a_2 = 0{\cdot}8 \times 10^{-13}\ \text{cm}, & \text{II.} \end{array}\right\} \quad \ldots\ldots (3)$$

All previous work mentioned indicates II to be the correct set although it should be added that Troesch and Verde (1951) and Gordon (1950) have produced results in support of I. In particular, Christian and Gammel obtained the values $a_4 = 5{\cdot}9 \times 10^{-13}$ cm, $a_2 = 1{\cdot}5 \times 10^{-13}$ cm. Figure 1 shows the Blatt–Jackson curves arising from the results of the relevant work previously quoted.

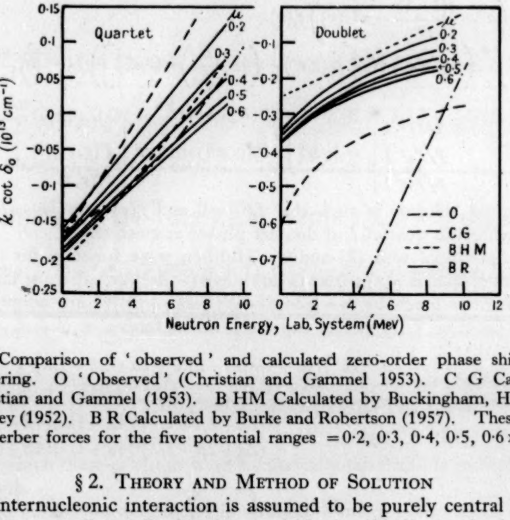

Figure 1. Comparison of 'observed' and calculated zero-order phase shifts for n-d scattering. O 'Observed' (Christian and Gammel 1953). C G Calculated by Christian and Gammel (1953). B HM Calculated by Buckingham, Hubbard and Massey (1952). B R Calculated by Burke and Robertson (1957). These curves are for Serber forces for the five potential ranges $= 0{\cdot}2,\ 0{\cdot}3,\ 0{\cdot}4,\ 0{\cdot}5,\ 0{\cdot}6 \times 10^{26}\ \text{cm}^{-2}$.

§ 2. THEORY AND METHOD OF SOLUTION

If the internucleonic interaction is assumed to be purely central and of the form (1) then, according to Buckingham and Massey (1941), the elastic scattering is described by the integro-differential equation:

$$(\nabla_r^2 + k^2)F(\mathbf{r})$$

$$= \alpha U(\mathbf{r})F(\mathbf{r}) + \int \{Q(\mathbf{r},\mathbf{r}') + [P(\mathbf{r},\mathbf{r}') + (1 + E_{\mathrm{n}}/E_{\mathrm{d}})N(\mathbf{r},\mathbf{r}')]\}F(\mathbf{r}')\,d\mathbf{r}',$$

where $U(r) = \dfrac{4M}{3\hbar^2}\displaystyle\int \chi^2(R)V(|\mathbf{r} + \tfrac{1}{2}\mathbf{R}|)\,d\mathbf{R}$

$$Q(\mathbf{r},\mathbf{r}') = \left(\frac{4}{3}\right)^3 \frac{4M}{3\hbar^2}\chi(u)V(t)\chi(v) \qquad N(\mathbf{r},\mathbf{r}') = \left(\frac{4}{3}\right)^3 \frac{4M}{3\hbar^2}E_{\mathrm{d}}\chi(u)\chi(v)$$

and according to Burke and Robertson (1957)

$$P(\mathbf{r},\mathbf{r}') = \left(\frac{4}{3}\right)^3 \frac{4M}{3\hbar^2}[\chi(u)\{-V(u) - V(v)\}\chi(v)]$$

$$+ \left(\frac{4}{3}\right)^5 \left[\chi(u)\nabla_v^2\chi(v) + \chi(v)\nabla_u^2\chi(u) + \chi'(u)\chi'(v)\frac{\mathbf{u}\cdot\mathbf{v}}{uv}\right]. \quad \ldots\ldots (4)$$

The vectors **r**, **r**′, **u**, **v** and **t** are defined as in the earlier work. α, β and γ depend on the spin state of the system and are given in table 1.

Table 1

	Quartet	Doublet
α	$2w+2b-m-h$	$2w-b+\frac{1}{2}m-h$
β	$2m+2h-w-b$	$2m-h+\frac{1}{2}w-b$
γ	1	$-\frac{1}{2}$

Expanding $F(\mathbf{r})$, $Q(\mathbf{r},\mathbf{r}')$, $N(\mathbf{r},\mathbf{r}')$ and $P(\mathbf{r},\mathbf{r}')$ in terms of Legendre polynomials the following integro-differential equation for the radial function $f_l(r)$ can be derived:

$$\frac{d^2f_l(r)}{dr^2}+\left(k^2-\frac{l(l+1)}{r^2}-\alpha U(r)\right)f_l(r)$$
$$=\int_0^\infty\left(\beta q_l(r,r')+\gamma\left[p_l(r,r')+\left(1+\frac{E_{\mathrm{n}}}{E_{\mathrm{d}}}\right)n_l(r,r')\right]\right)f_l(r')\,dr', \quad\ldots\ldots(5)$$

where

$$\left.\begin{matrix}q_l(r,r')\\p_l(r,r')\\n_l(r,r')\end{matrix}\right\}=2\pi rr'\int_0^\pi P_l(\cos\theta)\sin\theta\,d\theta\left\{\begin{matrix}Q(\mathbf{r},\mathbf{r}'),\\P(\mathbf{r},\mathbf{r}'),\\N(\mathbf{r},\mathbf{r}').\end{matrix}\right. \quad\ldots\ldots(6)$$

The required solution is such that $f_l(0)=0$ and $f_l(r)\sim\sin(kr-\frac{1}{2}l\pi+\delta_l^{\mathrm{q,d}})$, δ_l^{q} and δ_l^{d} being the quartet and doublet phases respectively.

If the potential well (2) and the Hulthén wave function for the deuteron ground state, that is $\chi(r)=[\exp(-\alpha r)-\exp(-\beta r)]/\eta r$, where η the normalization constant is given by $\eta=[\{2\pi(\beta-\alpha)^2\}/\{\alpha\beta(\alpha+\beta)\}]^{1/2}$ are adopted then the potential function $U(r)$ can be expressed in the form

$$U(r)=\frac{16\pi\lambda^2MV_0}{3\hbar^2\eta^2}\cdot\frac{1}{r}\Big\{\mathrm{e}^{r/\lambda}[\mathrm{Ei}^*((4\alpha+1/\lambda)r)-2\mathrm{Ei}^*((2\alpha+2\beta+1/\lambda)r)$$
$$+\mathrm{Ei}^*((4\beta+1/\lambda)r)]+\mathrm{e}^{-r/\lambda}[-\mathrm{Ei}^*((4\alpha-1/\lambda)r)+2\mathrm{Ei}^*((2\alpha+2\beta-1/\lambda)r)$$
$$-\mathrm{Ei}^*((4\beta-1/\lambda)r)]-\mathrm{e}^{-r/\lambda}\ln\left[\frac{(2\alpha+2\beta+1/\lambda)^2(4\alpha-1/\lambda)(4\beta-1/\lambda)}{(2\alpha+2\beta-1/\lambda)^2(4\alpha+1/\lambda)(4\beta+1/\lambda)}\right]\Big\}, \quad\ldots\ldots(7)$$

where

$$\mathrm{Ei}^*(y)=\int_y^\infty \mathrm{e}^{-t}\frac{dt}{t}.$$

Again, using the chosen explicit forms for $\chi(r)$ and $V(r)$ the kernels $q_l(r,r')$, $n_l(r,r')$ and $p_l(r,r')$ can be appropriately rewritten. Thus

$$q_l(r,r')=\frac{27}{4}\left(\frac{4}{3}\right)^4\frac{MV_0\lambda\pi10^{13}}{\eta^2\hbar^2}\{E(\alpha,\alpha)-E(\beta,\alpha)-E(\alpha,\beta)+E(\beta,\beta)\}, \quad\ldots\ldots(8)$$

where $E(a,b)=rr'$

$$\int_{-1}^{+1}\frac{\exp[-\frac{2}{3}a(r^2+4r'^2+4rr'x)^{1/2}-\frac{2}{3}b(r'^2+4r^2+4rr'x)^{1/2}-\frac{2}{3}(r^2+r'^2-2rr'x)^{1/2}/\lambda]}{(r^2+4r'^2+4rr'x)^{1/2}(r'^2+4r^2+4rr'x)^{1/2}(r^2+r'^2-2rr'x)^{1/2}}$$
$$\times P_l(x)\,dx,$$

x being such that $x=\mathbf{r}\,.\,\mathbf{r}'/rr'$ and r, r' are measured in units of 10^{-13} cm. Similarly,

$$n_l(r,r')=\frac{9}{2}\left(\frac{4}{3}\right)^4\frac{ME_{\mathrm{d}}}{\hbar^2\eta^2}\{F(\alpha,\alpha,1,1)-F(\beta,\alpha,1,1)-F(\alpha,\beta,1,1)+F(\beta,\beta,1,1\}, \quad\ldots\ldots(9)$$

where $F(a,b,n,m) =$

$$rr' \int_{-1}^{+1} \frac{\exp\left[-\tfrac{2}{3}a(r^2+4r'^2+4rr'x)^{1/2} - \tfrac{2}{3}b(r'^2+4r^2+4rr'x)^{1/2}\right]}{(r^2+4r'^2+4rr'x)^{n/2}(r'^2+4r^2+4rr'x)^{m/2}} P_l(x)\,dx.$$

If the kernel $p_l(r,r')$ is split into the components $p_l^1(r,r')$ and $p_l^2(r,r')$ then $p_l^1(r,r')$ is given by

$$\begin{aligned} p_l^1(r,r') = \frac{27}{4}\left(\frac{4}{3}\right)^4 \frac{\pi V_0 \lambda M}{\eta^2 \hbar^2} \Big\{ & F\left(\alpha+\frac{1}{\lambda}, \alpha, 2, 1\right) - F\left(\beta+\frac{1}{\lambda}, \alpha, 2, 1\right) \\ & - F\left(\alpha+\frac{1}{\lambda}, \beta, 2, 1\right) + F\left(\beta+\frac{1}{\lambda}, \beta, 2, 1\right) + F\left(\alpha, \alpha+\frac{1}{\lambda}, 1, 2\right) \\ & - F\left(\alpha, \beta+\frac{1}{\lambda}, 1, 2\right) - F\left(\beta, \alpha+\frac{1}{\lambda}, 1, 2\right) + F\left(\beta, \beta+\frac{1}{\lambda}, 1, 2\right)\Big\} 10^{13}, \end{aligned} \quad \ldots\ldots(10)$$

and

$$\begin{aligned} p_l^2(r,r') = \frac{9}{2}\frac{\pi}{\eta^2}\left(\frac{4}{3}\right)^5 . \, 10^{26} \Big\{ & 2\alpha^2 F(\alpha,\alpha,1,1) + \frac{9}{4}G(\alpha,\alpha,3,3) + \alpha^2 G(\alpha,\alpha,2,2) \\ & + \frac{3\alpha}{2}G(\alpha,\alpha,2,3) + \frac{3\alpha}{2}G(\alpha,\alpha,3,2) + 2\beta^2 F(\beta,\beta,1,1) + \frac{9}{4}G(\beta,\beta,3,3) \\ & + \beta^2 G(\beta,\beta,2,2) + \frac{3\beta}{2}G(\beta,\beta,2,3) + \frac{3\beta}{2}G(\beta,\beta,3,2) \\ - \Big[& (\alpha^2+\beta^2)F(\beta,\alpha,1,1) + \frac{9}{4}G(\beta,\alpha,3,3) + \alpha\beta G(\beta,\alpha,2,2) + \frac{3\alpha}{2}G(\beta,\alpha,2,3) \\ + & \frac{3\beta}{2}G(\beta,\alpha,3,2) + (\alpha^2+\beta^2)F(\alpha,\beta,1,1) + \frac{9}{4}G(\alpha,\beta,3,3) + \alpha\beta G(\alpha,\beta,2,2) \\ + & \frac{3\beta}{2}G(\alpha,\beta,2,3) + \frac{3\alpha}{2}G(\alpha,\beta,3,2)\Big]\Big\}, \end{aligned} \quad \ldots\ldots(11)$$

where

$$G(a,b,n,m) = rr' \int_{-1}^{+1} \frac{\exp\left[-\tfrac{2}{3}a(r^2+4r'^2+4rr'x)^{1/2} - \tfrac{2}{3}b(r'^2+4r^2+4rr'x)^{1/2}\right]}{(r^2+4r'^2+4rr'x)^{n/2}(r'^2+4r^2+4rr'x)^{m/2}} \times (2r'^2+2r^2+5rr'x)P_l(x)\,dx.$$

The way in which these integrals were numerically tabulated is indicated in the next paragraph.

Robertson (1956) has described the solution of integro-differential equations of the general form

$$\frac{d^2 f_l(r)}{dr^2} + \left(k^2 - \frac{l(l+1)}{r^2} - U(r)\right) f_l(r) = \int_0^\infty k_l(r,r') f_l(r')\,dr' \equiv g_l(r), \text{ say,} \quad \ldots\ldots(12)$$

by a simultaneous equation method. If the kernel function dies off with sufficient rapidity then the upper limit may be replaced by a suitable finite value R'. The range of integration is now split by a convenient number of points r_0', r_1', $r_2' \ldots R' = Nh$, all equally spaced. Equation (12) can now be written

$$\frac{d^2 f_l(r)}{dr^2} + u_l(r) f_l(r) = \int_0^{R'} k_l(r,r') f_l(r')\,dr', \quad \ldots\ldots(13)$$

and the right-hand side reduces to

$$\int_0^{R'} k(r,r') f(r')\,dr' = \sum_{m=0}^{N} T_m k(r_n, r_m') f(r_m') = \sum_{m=0}^{N} T_m k_{nm} f_m,$$

where the coefficients T_m are the integrating factors appropriate to the method of integration. Replacing the derivative by its central difference representation equation (13) becomes

$$f_{n-1} - (2 - h^2 u_n) f_{n+1} = h^2 \sum_{m=0}^{N} T_m k_{nm} f_m + C_n, \qquad \ldots\ldots(14)$$

where $C_n = (\frac{1}{12}\delta^4 - \frac{1}{90}\delta^6 + \ldots) f_n$. Following Fox and Goodwin (1949) we can reduce the order of the difference correction C_n by operating upon (14) with $(1 + \frac{1}{12}\delta^2)$ obtaining

$$(1 + \tfrac{1}{12} h^2 u_{n-1}) f_{n-1} - (2 - \tfrac{10}{12} h^2 u_n) f_n + (1 + \tfrac{1}{12} h^2 u_{n+1}) f_{n+1}$$
$$= \tfrac{1}{12} h^2 \sum_{m=0}^{N} (k_{n-1,m} + 10 k_{nm} + k_{n+1,m}) T_m f_m + C_n, \qquad \ldots\ldots(15)$$

where $C_n = (-\frac{1}{240}\delta^6 + \ldots) f_n$. Equation (15) can be written in the alternative form

$$\sum_{m=0}^{N} B_{nm} f_m = C_n. \qquad \ldots\ldots(16)$$

Thus by this method, assuming the boundary conditions $f(0) = f_0 = 0$ and $f(h) = f_1 = 1$, it is possible to determine some multiple of the desired solution of the original integro-differential equation.

§ 3. NUMERICAL WORK

The kernel integrals given in the previous paragraph have been evaluated numerically and owing to the magnitude of this task, work has been confined to the S-state. For the parameters α and β occurring in the Hulthén wave function, the values $\alpha = +0{\cdot}22315 \times 10^{13}\ \mathrm{cm}^{-1}$, $\beta = 1{\cdot}615 \times 10^{13}\ \mathrm{cm}^{-1}$ were taken which Burke (1956) has justified by a minimization of the deuteron binding energy.

The electronic computer DEUCE has been extensively used throughout and this required the construction of a programme and suitable sub-routines to enable the x integration at each of a selected number of points in a grid of r versus r'. The integration formula used was that of Gauss and it was necessary to tabulate at the points $r' = 0, h, 2h \ldots 29h$ for $r = 0, h, \ldots 29h$ (900 points) in order to comply with the simultaneous equations programme.

Trial runs for the intervals $h = \frac{1}{4}, \frac{1}{2}, 1{\cdot}0$ showed a wide difference in the rates at which the integrals died away. Referring to figure 2, we see that $q_0(r, r')$ is a short-range, rapidly varying kernel, whereas $n_0(r, r')$ and $p_0(r, r')$ vary more slowly and have significant values for larger r and r'. We can split up the total kernel into a long-range and a short-range part, viz.

$$\int k(r, r') f(r')\, dr' = \int k^{(\mathrm{L})}(r, r') f(r')\, dr' + \int k^{(\mathrm{S})}(r, r') f(r')\, dr' \qquad \ldots\ldots(17)$$

or

$$g(r) = g^{(\mathrm{L})}(r) + g^{(\mathrm{S})}(r).$$

The programme we use to solve the integro-differential equation has a fixed number of 30 points in the range of integration. Upon examination, it becomes evident that an interval $h = 0{\cdot}4$ is required to represent $k^{(\mathrm{S})}$ adequately because of its rapid variation in the range. On the other hand, $k^{(\mathrm{L})}$ does not become negligibly small until r' exceeds 20, thus requiring an interval of about $h = 0{\cdot}8$ to cover the range in 30 points. However, the problem can be solved by making use of the properties of $g(r)$ and $f(r)$. It turns out that $g(r)$ and $f(r)$ are smooth functions at interval $h=0{\cdot}8$. Hence it is possible to interpolate in a table of $f(r)$ at interval $2h$ to obtain the values at interval h. That is to say, the function at interval h can be written as a linear combination of the function values at interval $2h$. Thus, the integral $g^{(S)}(r)$ is obtained by integrating $k^{(S)}(r,r')f(r')$ at interval h and writing $f\{(2h+1)h\}$ in terms of $f(2nh)$, and so the integro-differential equation can be solved at interval $2h$. With the notation of (13)

$$g^{(S)}(r)=\int_0^{R'} k^{(S)}(r,r')f(r')\,dr' = \sum_{m=0}^{N} T(mh)k^{(S)}(2nh,mh)f(mh), \qquad \ldots\ldots(18)$$

where $r=2nh$.

We now write $f(mh)$ in terms of $f(2mh)$ by means of the interpolation formula,

$$f(mh)=\sum_{p=0}^{N}\beta_{mp}f(2ph),$$

and obtain

$$g^{(S)}(2nh)=\sum_{m=0}^{N}\sum_{p=0}^{N}T(mh)k^{(S)}(2nh,mh)\beta_{mp}f(2ph). \qquad \ldots\ldots(19)$$

The matrix of coefficients β_{mp} was calculated using a four-point Lagrangian interpolation formula. The equation (19) can be written entirely in matrix notation and the process of finding $g^{(S)}(2nh)$ can be given as a set of matrix operations on the kernel $k(nh,mh)$. This is, of course, the method which was used in the machine computations.

It may be thought that equation (12) could be solved more easily by an iterative method, which would give successive approximations to $f(r)$ by using previous approximations on the right-hand side of the equation.

For example, we might find approximations $f^{(1)}, f^{(2)}, \ldots f^{(t)}$ to f, where

$$\frac{d^2f^{(t)}}{dr^2}+\left(k^2-\frac{l(l+1)}{r^2}-U(r)\right)f^{(t)}=\lambda^{(t)}\int_0^\infty k^{(S)}(r,r')f^{(t-1)}(r')\,dr' + \int_0^\infty k^{(L)}(r,r')f^{(t)}(r')\,dr'.$$

An interval of $2h$ would be used to find $f^{(t)}$ from this equation by a method similar to that described earlier; the first integral on the right-hand side would be evaluated at an interval h, the values of $f^{(t-1)}$ having been interpolated to halves.

The $\lambda^{(t)}$ is merely a scaling factor, chosen to equalize the amplitudes of $f^{(t)}$ and $f^{(t-1)}$ for a value of r at which the corresponding integrals are reasonably large; it should clearly tend to unity as t increases.

In practice, however, this method is unsatisfactory. The sequence of approximations $f^{(t)}$ is not convergent. The reason for this is not difficult to find and the problem is similar to that considered by Bückner (1948), of successive approximations for Fredholm integral equations. The simpler case of iterative solution of matrix equations has been investigated by Plunkett (1950).

In order to economize on DEUCE time, all integrals were tabulated as triangular matrices and advantage taken of the symmetry of the complete kernel to form the final square matrix. Even so, about 55 DEUCE hours were spent in tabulating and assembling the kernel integrals.

All integrands become infinite along the lines $r=2r'$ and $r'=2r$ at the lower limit of integration and in addition $E(a,b)$ shows similar behaviour along $r=r'$ at the upper limit of integration. For these particular lines the correct finite

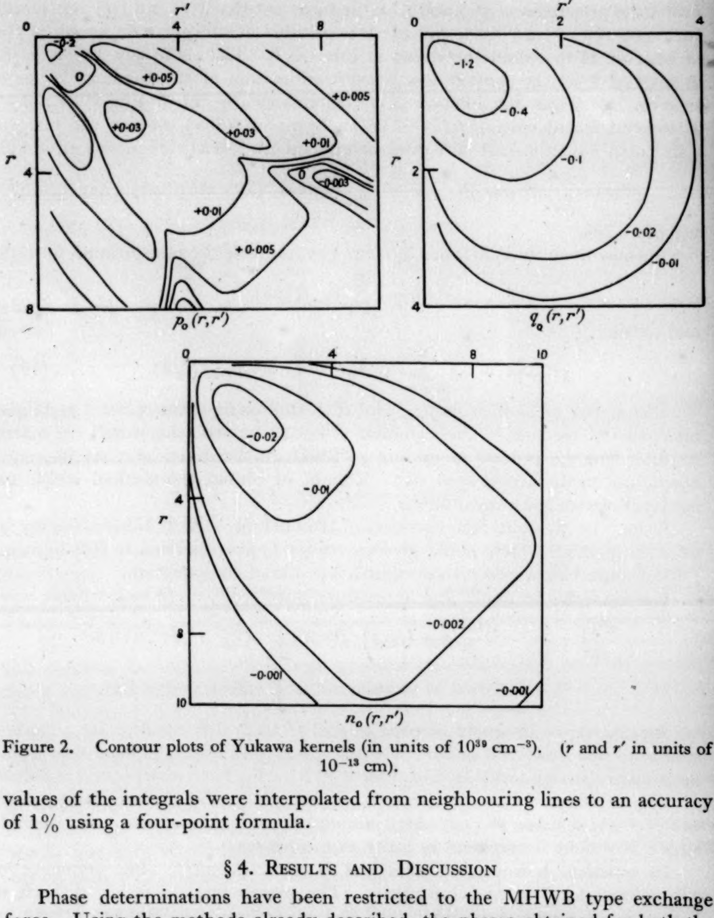

Figure 2. Contour plots of Yukawa kernels (in units of 10^{39} cm^{-3}). (r and r' in units of 10^{-13} cm).

values of the integrals were interpolated from neighbouring lines to an accuracy of 1% using a four-point formula.

§ 4. RESULTS AND DISCUSSION

Phase determinations have been restricted to the MHWB type exchange force. Using the methods already described, the phases obtained for both the quartet and doublet spin states are given in table 2. The Blatt–Jackson curves

Table 2. S-phases Evaluated with Kernels Tabulated at Both 0·4 and 0·8 × 10^{-13} cm

$k \times 10^{13}$(cm^{-1})	Quartet	Doublet
0·4	+75·868°	−60·038°
0·2	−63·173°	−28·594°
0·12	−43·206°	−13·596°
0·075	−28·498°	− 6·467°

(figure 3) corresponding to these phases are seen to agree quite well with those of Christian and Gammel. From these curves the following values for the quartet and doublet scattering lengths are obtained:

$$a_q = 6{\cdot}9 \times 10^{-13}\text{ cm}, \qquad a_d = 1{\cdot}4 \times 10^{-13}\text{ cm}. \qquad \ldots\ldots(20)$$

The doublet value is in good agreement with that of the earlier work but a_q is considerably larger.

It is well-known that the kernels in the n–d scattering can be divided into those of long and short range and that the small, slowly decreasing tail of the long-range kernels can make an appreciable contribution to the scattering (see for instance Burke and Robertson 1957). The serious effect of neglecting the tail is amply demonstrated by the phases of table 3, obtained by solution at interval $h = 0{\cdot}4$ and with the upper limit of integration taken to be 11·6. The appropriate Blatt–Jackson curves are shown in figure 3, from which the following estimates are obtained:

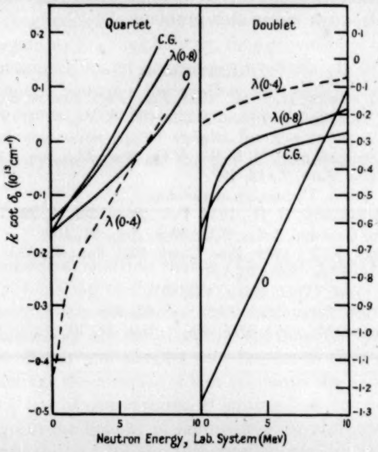

Figure 3. Comparison of ' observed ' and calculated zero-order phase shifts.
O ' Observed ' (Christian and Gammel 1953)
C G Calculated by Christian and Gammel (1953)
(0·4) Calculated using an interval $h = 0{\cdot}4$
(0·8) Calculated using an interval $h = 0{\cdot}8$

$$a_q = 2{\cdot}6 \times 10^{-13}\text{ cm}, \qquad a_d = 4{\cdot}2 \times 10^{-13}\text{ cm}. \qquad \ldots\ldots(21)$$

It is a coincidence that these are in some agreement with the experimental set I, equation (3). The largest discrepancy between the values of tables 2 and 3

Table 3. S-phases evaluated with all Kernels tabulated at $0{\cdot}4 \times 10^{-13}$ cm

$k \times 10^{13}(\text{cm}^{-1})$	Quartet	Doublet
0·4	+87·953°	−75·591°
0·2	−38·371°	−47·250°
0·12	−19·220°	−30·341°
0·075	−10·741°	−19·427°

is 25° and this is due to neglect of a tail which is less than 0·001 in magnitude. This shows the large effect which the long-range kernel has upon the scattering and it is confirmed by a solution of the equations at $h = 0{\cdot}8$ in which the phases differ from those in table 2 by less than 3°.

ACKNOWLEDGMENTS

Thanks are due to Professor H. S. W. Massey and to Dr. R. A. Buckingham for their help and interest in this work, to the Director of the National Physical Laboratory and to the Superintendent of its Mathematics Division for the use of DEUCE, to the English Electric Company also for the use of DEUCE and to the Ministry of Education and the University of London for awards which enabled one of us (F. A. H.) to work on this problem.

REFERENCES

de Borde, A. H., and Massey, H. S. W., 1955, *Proc. Phys. Soc.* A, **68**, 769.

Buckingham, R. A., Hubbard, S. J., and Massey, H. S. W., 1952, *Proc. Roy. Soc.* A, **211**, 183.

Buckingham, R. A., and Massey, H. S. W., 1941, *Proc. Roy. Soc.* A, **179**, 123.

Bücker, H., 1948, *Duke Math. J.*, **15**, 197.

Burke, P. G., 1956, *Thesis*, University of London.

Burke, P. G., and Robertson, H. H., 1957, *Proc. Phys. Soc.* A, **70**, 777.

Christian, R. S., and Gammel, J. L., 1953, *Phys. Rev.*, **91**, 100.

Fox, L., and Goodwin, E. T., 1949, *Proc. Camb. Phil. Soc.*, **45**, 373.

Gordon, M. M., 1950, *Phys. Rev.*, **80**, 111.

Plunkett, R., 1950, *Quart. Appl. Math.*, **VII**, 419.

Robertson, H. H., 1956, *Proc. Camb. Phil. Soc.*, **52**, 538.

Troesch, A., and Verde, M., 1951, *Helv. Phys. Acta*, **24**, 39.

Longitudinal Polarization of the Electrons from the Decay of Unpolarized Positive and Negative Muons

BY G. CULLIGAN, S. G. F. FRANK AND J. R. HOLT
Nuclear Physics Research Laboratory, University of Liverpool

Communicated by H. W. B. Skinner; *MS. received 14th August* 1958

Abstract. The polarization of electrons from the decay of unpolarized positive and negative muons has been detected by the method of transmission of bremsstrahlung through magnetized iron. It is shown that the positrons have positive helicity and the negatrons negative helicity, thus providing a clear demonstration of violation of invariance under charge conjugation. It follows on the basis of the two component neutrino theory that the neutrino associated with the decay of the pion has negative helicity and the anti-neutrino positive helicity. The agreement of this with recent results for the neutrino in β-decay lends support to this theory and confirms the law of conservation of leptons.

---

§ 1. INTRODUCTION

THE two component neutrino theory (Lee and Yang 1957 a, Salam 1957, Landau 1957) has, up to the present, been very successful in accounting for experimental data concerning the weak interactions between fermions. At the basis of this theory are the ideas that the neutrino and anti-neutrino are fully polarized parallel or anti-parallel with respect to their direction of motion and that in all reactions the number of leptons minus the number of anti-leptons remains constant ('law of conservation of leptons').

The actual sign of the helicity of the neutrino or anti-neutrino, which is $+1$ for the parallel case and -1 for the anti-parallel case, has to be decided experimentally and the leptonic assignment of the particles $e^{\pm}$, $\mu^{\pm}$, ν and $\bar{\nu}$ by definition and experiment.

The lepton conservation law requires that the processes of positive and negative β-decay should be associated uniquely with neutrinos of opposite kind. The processes are then $p \rightarrow n + e^{+} + \nu$ or $p + e^{-} \rightarrow n + \nu$ and $n \rightarrow p + e^{-} + \bar{\nu}$, where in the first two cases the particle is defined to be a neutrino and in the last case an anti-neutrino. The negatron is by definition a lepton, so it follows that the neutrino also is a lepton and the positron and anti-neutrino are anti-leptons.

The experiments described below are concerned with the fixing of the neutrino and anti-neutrino helicities and with the applicability of the lepton conservation law to the decay processes of the pion and muon.

We have shown that the positrons from the decay of unpolarized positive muons have positive helicity and that the negatrons from the decay of negative muons have negative helicity. The result for positive muons has already been published in brief form (Culligan *et al.* 1957) and we have recently learned that similar results for both particles have been obtained elsewhere (Crowe, private communication). The following argument is based on the two component theory.

The pion decay process $\pi \rightarrow \mu + \nu$ involves a single neutrino or anti-neutrino. The muon decay is known to be predominantly $\mu \rightarrow e + \nu + \bar{\nu}$ involving one neutrino of each kind, because of the shape of the energy spectrum of the decay electrons (Lee and Yang 1957 a). Experiments have shown that the muon in the first process is polarized (Garwin, Lederman and Weinrich 1957, Friedman and Telegdi 1957, Cassels *et al.* 1957), the electrons in the subsequent decay of both positive and negative muons being emitted predominantly backwards relative to the direction of emission of the muon from the pion.

Using the above information we can, in a simple way, connect the sign of the helicity of the neutrinos or anti-neutrinos emitted in the pion decay with that of the electrons emitted in the subsequent muon decay. Figure 1 illustrates the argument; the pion may be either positive or negative and the electron helicity has been arbitrarily taken to be positive.

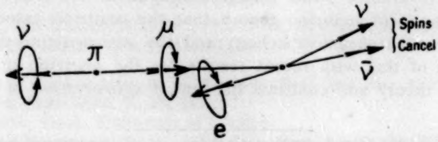

Figure 1. To illustrate the connection between the helicities of the electron, muon and first neutrino in the π, μ, e decay chain. The electron helicity has been taken to be positive but otherwise the diagram applies equally to positively charged and negatively charged particles.

The two particles emitted in the pion decay must spin in opposite directions to conserve angular momentum since the pion has zero spin; they move in opposite directions and thus have the same helicity. In the subsequent decay of the muon, since the electron energy spectrum is peaked towards the upper limit, most of the electrons are associated with neutrinos moving into the opposite hemisphere. As these neutrinos, of opposite kind, have opposite helicities, their spins will tend to cancel and the electrons and muons will spin in the same sense. The latter two are known to move in opposite directions so they must have opposite helicities. Thus we conclude that the electrons associated with the muon decay and the neutrinos associated with the pion decay have opposite helicities.

On the basis of the two component theory the results of our experiment thus fix the helicities of the muons of both signs (negative for positive muons and positive for negative muons) and show that the neutral particle emitted in positive pion decay has negative helicity while that emitted in negative pion decay has positive helicity. Applying lepton conservation to the decay processes of the muon and pion it can be seen that the positive muon is an anti-lepton and the particle emitted with it in the positive pion decay is a lepton, i.e. a neutrino rather than an anti-neutrino. So we conclude that the neutrino has negative helicity.

Recent work on nuclear β-decay (Goldhaber *et al.* 1958) has led to the same conclusion regarding the neutrino involved in this process. Since both conclusions are dependent on the law of conservation of leptons their agreement provides confirmation of this law as applied to the processes of β-decay, pion decay and muon decay and also supports the two component theory.

The sign of the neutrino helicity together with that of the positrons emitted with them in β-decay, which is known to be positive (Rehovoth Conference Proceedings 1958) enables the type of angular correlation between the directions of emission of the two particles in this process to be determined. Thus in a $0 \to 0$ allowed transition the particles must be emitted predominantly in the same direction to conserve angular momentum, whereas in a $\Delta J = \pm 1$ allowed transition they must be emitted predominantly in opposite directions. These correlations are characteristic of the vector V and axial vector A types of coupling respectively. This argument provides an important part of the evidence for the V and A types of coupling in β-decay as opposed to the scalar S and tensor T types which were favoured until recently (Culligan *et al.* 1957, Sudarshan and Marshak 1958).

Calculations of the electron polarization in muon decay have been carried out by Lee and Yang (1957 b), by Uberall (1957) and by Kinoshita and Sirlin (1957). These show on the basis of the two component theory, that electrons of all energies from the decay of unpolarized muons have the same polarization. The value of the polarization is proportional to the parameter ξ of the theory, which depends on the type of coupling between the particles and can take a value between -1 and $+1$. The extreme values correspond to 100% polarization of the electrons. The magnitude of ξ can be determined also from measurements of the asymmetry of electron emission from polarized muons, a combination of earlier results leading to a value of $0{\cdot}87 \pm 0{\cdot}12$ (Wilkinson 1957) and a recent experiment to the value $0{\cdot}91 \pm 0{\cdot}14$ (Swanson 1958). Our measurements of the polarization are considerably less accurate than these, but certainly require a value greater than 0·6.

Finally, the result that the electrons from the decay of unpolarized positive and negative muons at rest have opposite polarization provides a clear demonstration of the violation of invariance under charge conjugation.

§ 2. Apparatus

To detect longitudinal polarization of the electrons from muon decay we have made use of the fact that such polarization persists in the bremsstrahlung quanta produced by them (McVoy and Dyson 1957). The polarization of the quanta can be detected by comparing their transmission through iron magnetized either parallel or anti-parallel to their direction of motion. There is a difference due to the Compton cross section being dependent on the relative directions of the spins of quantum and scattering electron (Gunst and Page 1953).

Above 0·6 Mev the total Compton cross section is greater when the spins are anti-parallel. The difference between the cross sections for the anti-parallel and parallel cases increases from a negative value at low energies through zero at 0·6 Mev to a broad maximum at about 3 Mev and then decreases slowly at higher energies. Over the energy region with which we are concerned (10 Mev to 50 Mev) the difference in transmission through the 16 cm thickness of iron used in the experiment, when the direction of magnetization is reversed, is expected to be about 5% if the γ-radiation is fully polarized.

The experimental details were different in the work with positive and negative muons. In the first case the pion beam was brought to rest in a carbon target in which the muons were produced by decay. In the second it was necessary to use the muons present as a 3% contamination of the negative pion beam. The latter experiment was the more difficult of the two because the muon intensity was smaller by a factor of 4 and also because of a 12% contamination of 200 Mev electrons in the negative pion beam. Special arrangements had to be made to eliminate the background produced by these electrons.

Figure 2 shows the general arrangement of the apparatus with the counters used in the negative beam, while figure 3 shows the details of the polarization detector with the counters used in the positive beam. From counter number 2 onwards the apparatus was essentially the same in both cases.

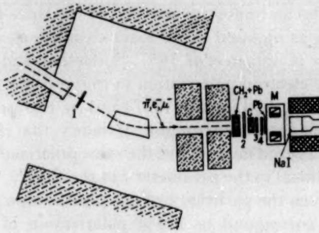

Figure 2. General arrangement of apparatus and counters used in the negative pion beam.

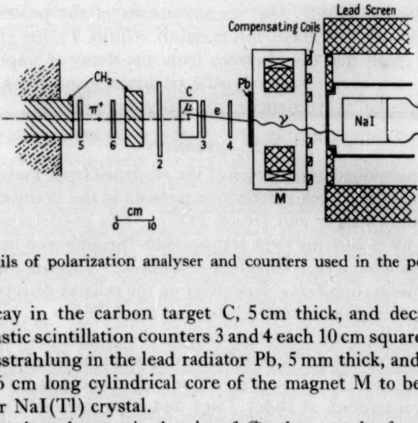

Figure 3. Details of polarization analyser and counters used in the positive pion beam.

Muons decay in the carbon target C, 5 cm thick, and decay electrons are detected by plastic scintillation counters 3 and 4 each 10 cm square. The electrons produce bremsstrahlung in the lead radiator Pb, 5 mm thick, and this then passes through the 16 cm long cylindrical core of the magnet M to be detected in the 5 inch diameter NaI(Tl) crystal.

In order to select the required pulses from the crystal a fast coincidence was arranged between the electron counters 3, 4 and pulses greater than about 2 MEV from the crystal. This coincidence pulse operated a gate through which the linear pulses from the crystal passed to a pulse height analyser.

The main sources of background were random coincidences between single pulses from the crystal and double coincidences 3, 4 and in the case of the negative muon experiment, real triple coincidences produced by the high energy electron contamination of the beam.

The double coincidence rate 3, 4 was reduced by placing counter number 2, 20 cm in diameter, in anti-coincidence. In the positive beam the main function of this was to reduce the rate in these counters due to pions. In the negative beam it helped to eliminate the effect of the electron contamination.

However, it was not very efficient in doing this because of the presence in the beam of bremsstrahlung produced where the electrons impinged on the various collimators and absorbers. A considerable improvement was made by placing 4 cm of lead directly before the veto counter to convert the bremsstrahlung to showers, but final elimination was achieved only by taking additional veto pulses from counter number 1, placed before the beam focusing magnet (figure 2).

Monitoring of the beam was carried out with the combination of counters $562\bar{3}$ in the positive beam and with $\bar{1}234$ in the negative beam, the bar above a number indicating a veto counter.

§ 3. ELECTRONICS

A block diagram of the electronics used with the negative muon experiment is shown in figure 4. The difference in the case of positive muons was the absence of counter number 1 and the different monitoring arrangement. The coincidence units were of the Garwin type, the resolving time being 40 mμsec. Scintillators number 2, 3 and 4 were mounted on EMI 6260B photo-electron multipliers followed by simple EFP 60 head amplifiers. Number 1, which counted at a mean rate of about 2×10^5 per second, was used with an EMI 6097B feeding a 130 ohm cable directly. The sodium iodide crystal was mounted on an EMI 6099 5 inch multiplier.

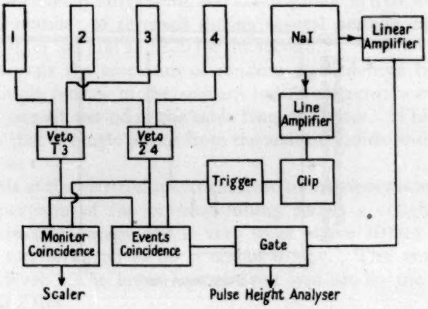

Figure 4. Block diagram of the electronics used in the negative pion beam.

Pulses from the crystal to operate the coincidence circuit were taken from dynode number 9 of the multiplier and after passing through a line amplifier clipped to a total width of about 30 mμsec. They were then used to operate a trigger circuit which fed pulses of standard size, 40 mμsec wide, to the coincidence circuit.

The linear pulses from the crystal were taken from dynode number 7 and after amplification passed through the gate to a 50 channel pulse height analyser.

§ 4. Tests and Adjustments

One of the principle concerns in this investigation was to make sure that there were no direct magnetic effects on any of the counters. All the multipliers were well shielded with soft iron and mu-metal and the stray field of the magnet in the neighbourhood of the 5 inch multiplier was neutralized with compensating coils (figure 3).

To check the counters for residual effects pulses were taken linearly from each counter in turn, a discriminator set on a steep part of the pulse spectrum and the counting rate measured with the magnetic field in opposite directions. In this way it was shown that the change in pulse height from counters 2, 3, 4 and NaI was less than 0·1%.

An overall check was made in the negative pion beam by switching off the veto counters and examining the gated spectrum of the bremsstrahlung from the electron contamination. When the magnetic field was reversed there was no change in the number of pulses greater than 5 Mev within the statistical accuracy of ± 0·25% and no change above 12 Mev within an accuracy of ± 1%. The above tests were carried out at the beginning of every run with the cyclotron.

The arrangement was checked as an analyser by using the bremsstrahlung from the ^{90}Y β-radiation, which is known to be highly polarized (Goldhaber *et al.* 1957). A 150 mc source enclosed in a silver capsule was placed in the position of the carbon target and the electron counters removed. Spectra of pulses from the sodium iodide crystal were recorded for the two directions of magnetization. The difference of these is plotted in figure 5 and shows the expected increase in analysing power with energy.

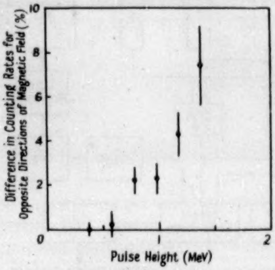

Figure 5. Test of analyser with bremsstrahlung from ^{90}Y β-radiation.

The procedure at the start of each run with the cyclotron was as follows. All the counters were mounted in position, but the magnet was absent. A beam of positrons was provided by placing a lead radiator in the vacuum pipe between the cyclotron and bending magnet to convert some of the electrons in the negative pion beam. The field direction in the magnet was such as to focus the positrons and not the negative particles. The energy of the positrons at the focus could be varied by altering the strength of the magnetic field.

The pulses from the 'events' coincidence unit (figure 4) were taken directly to the pulse height analyser. Then the delays in the cables from counters 3 and 4 and the trigger circuit were adjusted so that the pulses from the coincidence unit formed a well-defined peak with positrons of energies within the range 10 Mev to 50 Mev.

The linear output from the sodium iodide crystal was then connected to the gate circuit and the gated spectrum viewed on the pulse height analyser. The energy scale was then calibrated by varying the positron energy through the above range.

The magnet was next placed in position and, in the full pion beam, the vetoed double coincidence rate $\bar{1}\bar{2}34$ was measured for various thicknesses of absorber to enable this to be set to give the maximum rate. The performance of the veto counters was checked at this stage.

Finally, in the case of the negative beam, the gated linear spectrum from the crystal was examined both with optimum absorber thickness and with a sufficiently increased thickness that no muons could reach the carbon target. The number of beam contamination electrons reaching the lead radiator was practically the same in both cases and the spectrum in the second case then revealed any residual effect due to them. This effect was difficult to measure because of the small counting rate, but was less than 10% of the pulses greater than 12 Mev due to the muon decay electrons.

§ 5. MEASUREMENTS AND RESULTS

The spectrum of pulses from the sodium iodide detector was recorded for a certain number of monitor counts with the magnetic field alternately in one direction and the other. There was an interval of about 1 hour between reversals in the experiment with the positive beam and about ½ hour in that with the negative beam. The total number of reversals during several periods on the cyclotron in each case was 110 for the first and 220 for the second.

At regular intervals the spectrum of random coincidences between double counts 3, 4 and single counts in the sodium iodide detector was measured by putting a delay of one r.f. period in the cable from the latter. This spectrum had the same shape as that of single pulses from the sodium iodide and increased very rapidly below 10 Mev.

The upper limit of the electron spectrum from muon decay is at about 53 Mev. As the energy spectrum of the bremsstrahlung shows a roughly logarithmic increase with decreasing energy and is very weak above 30 Mev the saturation level of the gate was arranged to be at about 40 Mev. The amplification was linear up to this level. The lower energy limit was set by the trigger circuit (figure 4) at about 2 Mev.

The following are the chief counting rates for the two experiments:

In the case of positive muons the electron rate $\bar{2}34$ was about 300 per second. The rate in the gated spectrum between 12 Mev and 30 Mev was 5 per minute. The random coincidence rate was about 3% of this, but the proportion increased to about 20% at 6 Mev.

In the case of negative muons the electron rate $\bar{1}\bar{2}34$ was about 80 per second. The rate in the gated spectrum between 12 Mev and 30 Mev was 4 per minute with the random rate accounting for half this.

The results for both cases are displayed in figure 6, in which the difference between the total spectra for the two directions of magnetization is plotted as a percentage of the mean. The errors shown are the statistical standard deviations.

Corrections have been made to the experimental points to allow for the effect of the random coincidence component in diluting the percentage difference.

It is clear that there is a magnetic effect which is considerably greater than the errors and in opposite directions for positive and negative muons. The integrated experimental effect above 12 MEV is $+4{\cdot}7 \pm 1{\cdot}2\%$ for positive muons and $-5{\cdot}6 \pm 2{\cdot}3\%$ for negative muons. In the positive case the transmission of the magnet was greater when the north pole was towards the source and since the Compton cross section is least when the spins of quantum and electron are in the same direction this means that the quanta, and hence the positrons, have positive helicity. Likewise the electrons from negative muon decay have negative helicity.

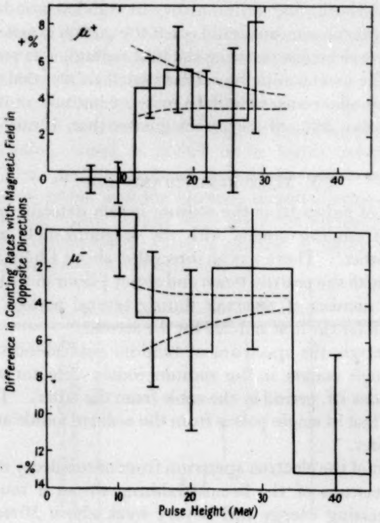

Figure 6. Difference in counting rates for the two directions of magnetization with positive muons (above) and negative muons (below). The broken curves represent attempts to fit the measurements on the assumption of 100% electron polarization.

The broken curves in figure 6 represent an attempt to set limits between which the experimental points should lie assuming the electrons to be fully polarized. The curves showing the greater effect for both positive and negative muons were calculated on the assumption that the bremsstrahlung radiation also was fully polarized. The formula of Gunst and Page (1953) for the spin dependence of the Compton cross section as a function of energy was used, putting in the thickness of the iron and its degree of saturation.

The curves showing the smaller effect were calculated by considering 50 MEV fully polarized electrons to be incident on the lead radiator and carrying through a Monte Carlo calculation on the showers produced, using the formulae given by

Dyson (1957) for the polarization of the secondary quanta and electrons. The calculations were not carried below 12 MEV. It can be seen from Dyson's formulae that incident electrons of lower energy give rise to a greater effect for a given quantum energy.

The experimental points are in satisfactory agreement with some curve between the estimated limits in both cases. The integrated difference above 12 MEV from the theoretical upper limit is ± 6%, which is to be compared with a figure of 4·9 ± 1·1% obtained by combining the results for positive and negative muons and ignoring the difference in sign. From a consideration of the errors we feel justified in saying that the results point to a degree of polarization between 60 and 100%.

ACKNOWLEDGMENTS

We wish to record our thanks to Professor H. W. B. Skinner for his close interest in this work and to Professor J. M. Cassels, Dr. H. Uberall and Dr. H. P. Noyes for valuable discussions. We are indebted to Dr. J. C. Kluyver for his collaboration during the first stage of the experiment. Messrs. T. Massam and S. Rodgers have rendered much useful assistance. The work with the cyclotron was greatly facilitated by the co-operation of the operating crew under Mr. B. Halliday. G. C. wishes to acknowledge the receipt of a grant from the Department of Scientific and Industrial Research.

REFERENCES

CASSELS, J. M., O'KEEFFE, T. W., RIGBY, M., WETHERELL, H. M., and WORMALD, J. R., 1957, *Proc. Phys. Soc.* A, **70,** 543.
CULLIGAN, G., FRANK, S. G. F., HOLT, J. R., KLUYVER, J. C., and MASSAM, T., 1957, *Nature, Lond.*, **180,** 751.
DYSON, F. J., 1957, *Proceedings 7th Rochester Conference* (New York: Interscience).
FRIEDMAN, J. I., and TELEGDI, V. L., 1957, *Phys. Rev.*, **106,** 1290.
GARWIN, R. L., LEDERMAN, L M., and WEINRICH, M., 1957, *Phys. Rev.*, **105,** 1415.
GOLDHABER, M., GRODZINS, L., and SUNYAR, A. W., 1957, *Phys. Rev.*, **106,** 826.
—— 1958, *Ibid.*, **109,** 1015,
GUNST, S. B., and PAGE, L. A., 1953, *Phys. Rev.*, **92,** 970.
KINOSHITA, T., and SIRLIN, A., 1957, *Phys. Rev.*, **108,** 844.
LANDAU L., 1957, *Nuclear Physics*, **3,** 127.
LEE, T. D., and YANG, C. N., 1957 a, *Phys. Rev.*, **105,** 1671.
—— 1957 b, *Elementary Particles and Weak Interactions* (Brookhaven National Laboratory).
MCYOY, K. M., and DYSON, F. J., 1957, *Phys. Rev.*, **106,** 1360.
REHOVOTH CONFERENCE PROCEEDINGS 1958 (Amsterdam: North Holland Publishing Co.), p. 346.
SALAM, A., 1957, *Nuovo Cim.*, **5,** 299.
SUDARSHAN, E. C. G., and MARSHAK, R. E., 1958, *Phys. Rev.*, **109,** 1860.
SWANSON, R. A., 1958, *Phys. Rev.*, **112,** 580.
UBERALL, H., 1957, *Nuovo Cim.*, **6,** 376.
WILKINSON, D. H., 1957, *Nuovo Cim.*, **6,** 516.

Knock-on Electrons from Cosmic-Ray μ-Mesons

By J. L. LLOYD and A. W. WOLFENDALE
Department of Physics, Durham Colleges in the University of Durham

Communicated by G. D. Rochester; MS. received 17th September 1958

Abstract. A cloud chamber study has been made of the electron secondaries produced by fast μ-mesons in iron and lead plates and cloud chamber gas.

The mean probability of a meson emerging from a plate accompanied by a single electron has been accurately determined for mesons in the momentum range 0·5–200 GeV/c. This probability is $9\cdot 0 \pm 0\cdot 4\%$ for $55\,\mathrm{g\,cm^{-2}}$ iron and $5\cdot 80 \pm 0\cdot 15\%$ for $11\cdot 5\,\mathrm{g\,cm^{-2}}$ lead. A search has been made for any anomalous dependence of electron production upon primary momentum or sign of charge but none has been detected.

---

§ 1. INTRODUCTION

A STUDY of the interaction of the μ-meson with electrons is important in that it can give information about the nature of the μ-meson. Some information on the properties of very slow μ-mesons has been found from experiments on μ-mesic atoms but it is possible that the fast μ-meson behaves in a somewhat different manner from the slow μ-meson.

Probably the direct μ-meson–electron interaction can best be investigated by measuring the energy spectrum of the electrons knocked-on in a gas by μ-mesons as a function of the momentum and sign of the μ-meson. It is, however, difficult to determine the absolute ranges of the slow knock-on electrons (δ-rays) in the region of a few tens of kev, and at higher energies, in the region of a few MeV, the cross section for interaction is too low for results of any statistical accuracy to be obtained. In the experiment reported here the production of low energy δ-rays in the gas and higher energy electrons ($\gtrsim 1$ MeV) in metal plates has been investigated. In neither case has an absolute cross section been measured.

§ 2. THE EXPERIMENTAL ARRANGEMENTS

A large cloud chamber of illuminated volume 60 cm × 60 cm × 11 cm was operated under the Manchester Cosmic Ray Spectrograph. The chamber contained argon (80% by volume) and oxygen with a 50–50% water–alcohol condensant, at a total pressure of about 110 cm Hg. Two arrangements were used:

(*a*) The chamber contained one plate of iron and one of lead of thickness 54·7 and $50\cdot 9\,\mathrm{g\,cm^{-2}}$ respectively. The spectrograph was operated with Geiger counters as detecting elements (Hyams *et al.* 1950) and the maximum detectable momentum of the instrument was about 20 GeV/c.

(*b*) The chamber contained nine 1 cm lead plates, each of mass $11\cdot 47\,\mathrm{g\,cm^{-2}}$, the spectrograph being operated with flat cloud chambers (Holmes *et al.* 1956).

The maximum detectable momentum was then about 300 GeV/c. The momenta of the μ-mesons were determined using the data from the flat chambers whenever possible.

In both arrangements stereoscopic photographs of the cloud chamber were taken.

§ 3. THE EXPERIMENTAL RESULTS AND THEIR ANALYSIS

3.1. *The δ-rays*

In arrangement (*a*), § 2, the track segments in the three parts of the cloud chamber were long and the illumination conditions good enough for δ-rays to be detected with high efficiency. Each meson track was scanned carefully, the stereo-pair of photographs being used to exclude spurious events, and δ-rays having ranges greater than 1·23 mm were measured. The range was defined as the distance from the origin of the δ-ray to its end-point, as projected on to the plane of the photograph.

For the few tracks whose end-points lay outside the illuminated volume the lengths were estimated from scattering and ionization.

A length of 1·56 km of meson track was scanned, equivalent to 363 g cm^{-2}.

The differential range spectrum of δ-rays for all primaries is shown in figure 1. Distinction has been made between positive and negative primaries for each range group. It is clear that there is no significant difference between the production of δ-rays by positive and negative primary particles.

The χ^2-test has been applied to the results to search for any deviation from the expected number with variation in the momentum and sign of the primary, for a number of δ-ray ranges. No χ^2 is unusually high and the distribution in χ^2

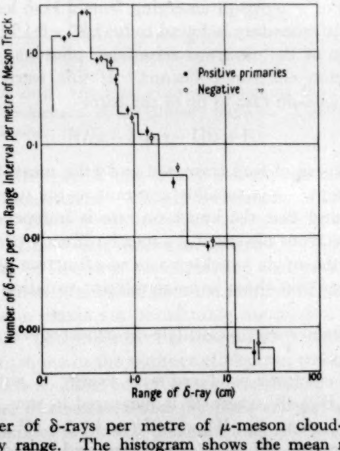

Figure 1. The number of δ-rays per metre of μ-meson cloud-chamber track, as a function of δ-ray range. The histogram shows the mean rate for both positive and negative mesons. The deficiency of δ-rays of lowest energy is due to a somewhat variable acceptance criterion based upon visual estimation of the range. The experimental points have been separated laterally.

is as expected for a good fit. The overall value would be exceeded by chance once in three occasions.

3.2. *The Production of Knock-on Electrons from Metal Plates*

(*a*) *Production from iron.*

In arrangement (*a*), §2, a study was made of the number of single knock-on electrons emerging from the iron plate, a knock-on electron being defined as one producing a track in the cloud chamber leaving the plate within one radiation length of the primary. Since the statistical accuracy of the second arrangement, with many lead plates, was so much higher only the frequency of knock-on electrons in iron was measured here.

The result for iron is $9{\cdot}0 \pm 0{\cdot}4\%$ for the whole of the incident primary spectrum of μ-mesons of both signs. No significant variation with momentum of primary was detected.

(*b*) *Production from lead.*

Knock-on electrons from the 1 cm lead plates in arrangement (*b*), §2, were examined in detail. A strict criterion of visibility of the μ-meson track was applied to minimize any loss of particles, the criterion for acceptance of knock-on electron tracks being identical with that for the arrangement (*a*) mentioned above. The number of cases of single and multiple knock-on electrons was noted. Some nineteen thousand traversals were observed. Personal bias towards a particular momentum or sign was avoided by scanning for electron tracks before the spectrograph records were examined.

3.3. *Single Knock-on Electrons*

The probability of a μ-meson emerging from a 1 cm lead plate accompanied by a single electronic secondary is found to be $5{\cdot}80 \pm 0{\cdot}15\%$. It is possible that a significant fraction of the electrons arise from photons, which are themselves secondary to μ-meson–electron collisions. If this were the case one would expect the single knock-on rate to be of the form

$$A + B[1 - \exp(-x/\lambda)]$$

where x is the thickness of lead traversed and λ the mean free path for electron production by photons. λ is sensibly constant in the important energy region 1–10 Mev. It is found that the knock-on rate is independent of plate number showing that the electrons observed are mostly directly produced.

Figure 2 shows the single knock-on rate as a function of primary momentum and sign. It is clear that there is no significant variation with the sign of the meson.

An attempt has been made to calculate the expected rate of knock-on electrons in the following way:

The number of electrons produced with energy W within dW in 1 cm lead is $0{\cdot}684\,W^{-2}(1-W/W_0)\,dW$ where W is measured in Mev. W_0 is the maximum transferable energy, given by $W_0 = (pc)^2/(pc + 1{\cdot}1 \times 10^4\,\text{Mev})$. Neglecting the effect of the ejection angle of the electron, the lead thickness which is effective in producing electrons which will be seen is the mean range R of electrons of energy W.

The range-energy relation has been determined as follows. Katz and Penfold (1952) have given a formula for the practical range R_p in aluminium and Hereford and Swann (1950) have published absorption curves from which the relation between R_p and R in aluminium has been determined. These results have been taken over to the case of lead using the effect of Z upon R given by Husain and Putman (1957). Finally the theory (modified because this is a first passage problem) and Monte Carlo results of Wilson (1951, 1952) have been used. The resulting relation is $R = 6{\cdot}6 \times 10^{-3} W^{1{\cdot}61}$ cm, $W \leqslant 25$ MeV. In view of the uncertainties in the derivation it is estimated that the relation is only accurate to about 20%.

The resulting knock-on rate is

$$0{\cdot}684 \left\{ \frac{1}{0{\cdot}61 W_{\text{max}}} - \frac{1}{1{\cdot}61 W_0} \right\} R_{\text{max}}.$$

There is no sharp cut-off in range but an effective upper limit is found by writing $R_{\text{max}} = 0{\cdot}0066 W_{\text{max}}^{1{\cdot}61} = 1$ cm, from which $W_{\text{max}} = 22{\cdot}5$ MeV. The justification for this value is that although secondaries will be formed within a 1 cm plate with $W > 22{\cdot}5$ MeV their number will be small because (*a*) the production rate decreases rapidly with increasing W and there is no compensating increase in R, and (*b*) multiplication becomes important.

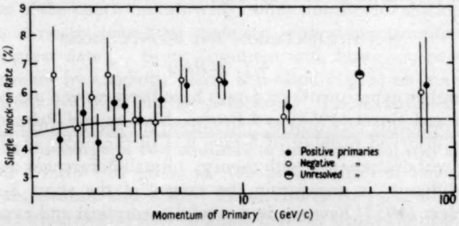

Figure 2. The rate of single knock-on electrons emerging from a 1 cm lead plate as a function of the momentum of the primary particle. The curve is a rough estimate of the expected rate.

It will be seen from figure 2 that theory and experiment fit as well as can be expected without normalization. Clearly no anomaly of any appreciable magnitude exists.

3.4. *Knock-on Showers*

The total number of electrons accompanying each μ-meson in lead depends more strongly upon momentum than does the number of single electrons because of the rapid increase in maximum transferable energy and the consequent effect of energetic showers. The presence or absence of high-energy showers produces large statistical fluctuations in the number of electron tracks, making it desirable to exclude these events by some cut-off procedure when counting.

The total number of electron tracks per plate and per μ-meson produced by collisions in the chamber is plotted in figure 3 against the meson momentum. Four showers initiated by electrons of energy estimated to be above 500 MeV were excluded from the analysis. The smooth curve is a rough estimate of the number expected. It has been derived by adding to the theoretical number of single knock-on electrons the effect of energy transfers between 22·5 MeV and 500 MeV. For this computation Wilson's shower curves have been used, and the fact that some showers will emerge from the lowest plate before completely developing has been allowed for. The resultant curve is not to be regarded as showing more than the expected trend. The standard errors shown are underestimates since they are the square roots of total numbers. It will be seen that there is no evidence of any large anomaly.

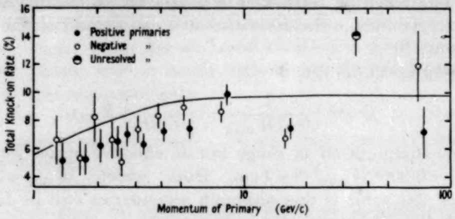

Figure 3. The rate of total number of knock-on electrons from a 1 cm lead plate. The curve is a rough estimate of the expected rate. The errors indicated are underestimates for reasons given in the text.

§ 4. DISCUSSION AND CONCLUSIONS

4.1. *δ-Rays*

Cloud chamber experiments on δ-rays have been carried out by Seren (1942), Lovati, Mura and Succi (1954) and Brown, McKay and Palmatier (1949). In each case the observed number of δ-rays was of the order of 100. In no case was there any real discrepancy with theory. Small differences are easily explainable by the difficulty in measuring the ranges of the short δ-rays. Tidman, George and Herz (1953) have made a careful theoretical and experimental study of δ-ray production in nuclear emulsions. δ-ray counts were made on stopping protons and stopping μ-mesons (mainly positive) with $\beta < 0{\cdot}4$. Counts were also made on tracks of fast particles, with plateau grain density. The results, with a low energy cut-off of about 20 kev, are in excellent agreement with theory.

These experiments do not overlap the present work. They show that there is good agreement with theory with respect to absolute number of δ-rays, distribution in energy of δ-rays and to the velocity of the primary particle except for very high velocities. At high velocities there had been no measurements on the dependence upon momentum and charge of primary. The present experiment has tested this dependence and found none.

4.2. *Knock-on Electrons*

A number of experiments have been made on μ-meson–electron interactions of higher energy.

Earlier workers with cloud chambers have usually given little more than the knock-on rate for the total meson spectrum. Their results vary widely, from the 3·6% of Johnson, Shutt and Barry (1940) to 17% found by Trumpy (1938). It seems likely that the spread in values arises from poor track visibility in some experiments and the inclusion of occasional dense knock-on showers in others.

Wilson (1938) has carried out a magnet cloud chamber experiment using a gold plate and finds the rate of knock-on production to be 4·8% and 0·8% for μ-mesons of momenta above and below 3 GeV/c respectively. Above 3 GeV/c Wilson's results are not inconsistent with the results presented here: below 3 GeV/c there is an unexplained discrepancy.

The use of nuclear emulsion permits a study of the dynamics of the μ-meson–electron interaction, in so far as the angle of ejection and energy of the knock-on electron can be determined for a wide range of electron energies. Kannangara and Zivkovic (1953) have studied the cross section for production of knock-on electrons in nuclear emulsion underground. Above 100 MeV the ratio of experimental to theoretical rate is $1·1 \pm 0·2$ and the distribution of energies and angles of ejection are as expected. No measurements of the momenta of the primary μ-mesons were made in this experiment.

Walker *et al.* (1951) and Walker (1953), using successively a multiplate cloud chamber and a magnet cloud chamber, also find agreement between experiment and theory.

It is clear from these experiments that the number and energy spectrum of knock-on electrons, of energy in the range 50–500 MeV at least, is as given by theory. The present experiment shows that the dependence on sign and momentum of primary is also consistent with theory.

The variation of the knock-on rate with atomic number for thick plates depends on the variation of range, scattering angle etc. with atomic number and will not be discussed in great detail. Some comment will, however, be made here on a counter experiment by Caglioti, Sciuti and Gigli (1955) on the production of secondary electrons by high energy μ-mesons. These authors used counter arrangements to study knock-on production in lead and aluminium. From the measured rates of discharge of two counters in one detecting tray Caglioti, Scuiti and Gigli found a ratio $1·21 \pm 0·03$ for the probabilities of recorded knock-on production in aluminium and lead. This ratio is in agreement with that of Z/A for the two elements and may indicate that the numbers of g cm^{-2} effective in the production of measured knock-on electrons is the same in both cases. It must be pointed out however that this result is not of general application since the total number of electronic secondaries emerging from a plate varies quite rapidly with Z and primary momentum, and the number recorded by a counter array depends critically on the geometrical arrangement of the counters and the energy of the knock-on electrons.

In the experiment reported here the ratio of knock-on electron probabilities for iron and lead is 1·55 compared with a ratio 1·17 for Z/A for the two elements.

Some information on the variation of knock-on electron probability with primary energy at high energies, $\gtrsim 10$ GeV, can, in principle, be derived from a study of the variation of knock-on rate or the ratio of soft to hard component with depth underground. That there is an increase with depth is clear but the rate of increase is uncertain on account of the differing experimental arrangements used. As yet no experiment has been performed with the same well designed arrangement at a wide range of depths underground.

In conclusion it appears that there is no significant anomaly in the production of knock-on electrons with energies between about 20 kev and a few hundred MeV by primaries having momentum below 200 GeV/c.

ACKNOWLEDGMENTS

The authors are grateful to Professor G. D. Rochester for generous support successively as Acting Head of Department at the University of Manchester when the basic data were collected, and as Head of the Department at Durham where the authors carried out the analysis. Mr. A. L. Rodgers is thanked for his assistance in operating the Manchester spectrograph and Dr. E. Rössle for his co-operation in running the cloud chambers.

REFERENCES

BROWN, W. W., MCKAY, A. S., and PALMATIER, E.D., 1949, *Phys. Rev.*, **76,** 506.
CAGLIOTTI, G., SCIUTI, S., and GIGLI, A., 1955, *Nuovo Cim.*, **1,** 851.
HEREFORD, F. L., and SWANN, C. P., 1950, *Phys. Rev.*, **78,** 727.
HOLMES, J. E. R., OWEN, B. G., RODGERS, A. L., and WILSON, J. G., 1956, *Report on the Conference on Recent Developments in Cloud Chamber and Associated Techniques* (London : University College), p. 177.
HUSAIN, S. A., and PUTMAN, J. L., 1957, *Proc. Phys. Soc.* A, **70,** 304.
HYAMS, B. D., MYLROI, M. G., OWEN, B. G., and WILSON, J. G., 1950, *Proc. Phys. Soc.* A, **63,** 1053.
JOHNSON, T. H., SHUTT, R. P., and BARRY, J. G., 1940, *Phys. Rev.*, **57,** 1062.
KANNANGARA, M. L. T., and ZIVKOVIC, M., 1953, *Phil. Mag.*, **44,** 797.
KATZ, L., and PENFOLD, A. S., 1952, *Rev. Mod. Phys.*, **24,** 28.
LOVATI, A., MURA, S., and SUCCI, C., 1954, *Nuovo Cim.*, **11,** 92.
SEREN, L., 1942, *Phys. Rev.*, **62,** 204.
TIDMAN, D. A., GEORGE, E. P., and HERZ, A. J., 1953, *Proc. Phys. Soc.* A, **66,** 1019.
TRUMPY, B., 1938, *Z. Phys.*, **111,** 338.
WALKER, W. D., HAMMEL, J. E., SINCLAIR, R. M., and SORREL, J. D., 1951, *Phys. Rev.*, **83,** 655.
WALKER, W. D., 1953, *Phys. Rev.*, **90,** 234.
WILSON, J. G., 1938, *Nature, Lond.*, **142,** 73.
WILSON, R. R., 1951, *Phys. Rev.*, **84,** 100 ; 1952, *Ibid.*, **86,** 261.

Optical Model Analysis of the Scattering of 310 MeV Protons by Carbon

By C. J. BATTY
Physics Department, University of Birmingham

Communicated by R. E. Peierls; MS. received 25th September 1958

Abstract. The optical model parameters for the scattering of 310 MeV protons by carbon are obtained in an analysis using the semi-classical approximation. The results are compared with those obtained by other analyses in this energy region. The modification of the Coulomb scattering by the absorption of protons in the nucleus is also considered in some detail.

---

§ 1. INTRODUCTION

RECENTLY several analyses have appeared of the scattering of high energy nucleons by complex nuclei (Bethe 1958, Bjorklund, Blandford and Fernbach 1957) in terms of the optical model. However the situation is still unsatisfactory in that widely varying values for the various parameters have been obtained. Bethe's analysis concentrated on the small angle points, where inelastic scattering is small and spin-dependent effects are relatively unimportant. However, he obtained the various terms in the scattering amplitude coming from interference between the Coulomb and nuclear scattering separately, and did not allow for renormalization of the experimental points, the absolute magnitude of which is quoted as accurate only to ± 20%.

We have therefore recalculated the problem in a unified way, evaluating all amplitudes in the semi-classical approximation (Shapiro 1955) which is accurate for small angle scattering. In the course of this, we have found that the way in which the Coulomb scattering amplitude is usually obtained, by multiplying the point nucleus amplitude by a form factor to allow for the finite size of the nucleus, gives an extremely bad approximation. The absorption of protons in the nucleus actually leads to an enhancement of the Coulomb amplitude at small angles, rather than a diminution.

We therefore evaluate all of the amplitudes arising from the nuclear scattering, Coulomb scattering and interference between the two, directly. We can then determine both the real part of the nuclear potential and the normalization of the experimental results (Chamberlain *et al.* 1956). Later the introduction of spin-dependent effects shows that the determination of the real part of the nuclear potential is relatively insensitive to specific assumptions about the spin–orbit force. Comparison of theoretical results for the polarization with the experiments gives a best fit for a value of the spin–orbit coupling parameter somewhat higher than that obtained by Bethe (1958).

§ 2. METHOD

2.1. *The Optical Model*

The optical model as a description of the interaction between a nucleon and a nucleus at high energies has been extensively used in the analysis of scattering experiments. In this model the nucleus is replaced by a complex spin-dependent potential of the form

$$V(r) = V_{\mathrm{n}}(r) + V_{\mathrm{s}}(r)\boldsymbol{\sigma}.\mathbf{L} \qquad \ldots\ldots(1)$$

where $V_{\mathrm{n}}(r)$ is the central and $V_{\mathrm{s}}(r)$ the spin–orbit potential at a point distant r from the centre of the nucleus. $\boldsymbol{\sigma}$ is the spin of the incident nucleon and $\mathbf{L}$ its angular momentum. It can be shown (Fernbach, Heckrotte and Lepore 1955, Brown 1957) that $V_{\mathrm{s}}(r)$ is related to $V_{\mathrm{n}}(r)$ by the equation

$$V_{\mathrm{s}}(r) \propto \frac{1}{r}\frac{dV_{\mathrm{n}}}{dr}. \qquad \ldots\ldots(2)$$

Alternatively if $\rho(r)$ is the density distribution of nucleons in the nucleus then we can write the equation in the form

$$V(r) = V_{\mathrm{n}}\rho(r) + \frac{C|V_{\mathrm{n}}|}{r}\frac{d\rho(r)}{dr}\boldsymbol{\sigma}.\mathbf{L} \qquad \ldots\ldots(3)$$

where C is the spin–orbit coupling constant which may be complex ($C = ce^{i\alpha}$). The expression of the optical model potential in the above form has involved an expansion in which the range of the nucleon–nucleon force has been taken to be small compared with the radius of the nucleus.

In the case where protons are the incident particles then we must add a further term $V_{\mathrm{c}}\rho'(r)$ to allow for the Coulomb forces. Here $\rho'(r)$ is the charge density in the nucleus. In recent analyses (Bethe 1958) the tendency has been to assume that $\rho(r)$ is given by the charge distribution for the nucleus as determined by electron scattering experiments. This is equivalent to assuming that the density of protons and neutrons throughout the nucleus is the same and for light nuclei such as carbon this would seem to be justified. In this case $\rho(r)$ and $\rho'(r)$ are identical. In the present case slightly different forms have been taken for these two functions; this was merely to give convenient forms for various terms in the analysis and the difference should not be important numerically.

In an analysis of the scattering of 350 MEV neutrons Ashmore, Mather and Sen (1958) and Brown, Ashmore and Nordhagen (1958) show that the real part of V_{n} is small. Bethe (1958) and Bjorklund, Blandford and Fernbach (1957) also obtain small values for this parameter and in the subsequent analysis we shall assume that this is so.

Brown, Ashmore and Nordhagen (1958) further show how the imaginary part of V_{n} can be related to the nucleon–nucleon forward scattering amplitudes and hence to the total cross sections for nucleon–nucleon scattering. In the following analysis we shall use the value given for the imaginary part of V_{n} by their method.

2.2. *The Semi-Classical Approximation*

The amplitude for the scattering of a nucleon through an angle θ by the potential given in (1) is

$$f(\theta) = A(\theta) + B(\theta)\boldsymbol{\sigma}.\mathbf{n} \qquad \ldots\ldots(4)$$

where $\mathbf{n}$ is a unit vector perpendicular to the scattering plane.

Simple expressions for $A(\theta)$ and $B(\theta)$ can be obtained in terms of the semi-classical approximation (Shapiro 1955). The final expressions obtained for $A(\theta)$ and $B(\theta)$ are then

$$\left.\begin{aligned} A(\theta) &= \frac{k}{i}\int_0^\infty \mathrm{J}_0(kb\sin\theta)\{\tfrac{1}{2}[\exp(i\chi^+)+\exp(i\chi^-)]-1\}\,b\,db \\ B(\theta) &= -\frac{k}{2}\int_0^\infty \mathrm{J}_1(kb\sin\theta)\{\exp(i\chi^+)-\exp(i\chi^-)\}\,b\,db \end{aligned}\right\} \quad \ldots\ldots(5)$$

where

$$\chi^\pm = \chi_1 \pm \chi_2 = -\frac{E}{k}\int_{-\infty}^{\infty}\{V_\mathrm{n}(r) \pm kbV_\mathrm{s}(r)\}\,dz$$

$$r^2 = z^2 + b^2 \quad \ldots\ldots(6)$$

and we have used the units $\hbar = c = 1$.

Here b is the impact parameter of the incident nucleon and J_0 and J_1 are zero and first order Bessel functions. θ and k, the scattering angle and wave number of the incident nucleon, are in the centre-of-mass system.

The differential scattering cross section at an angle θ is then given by

$$\frac{d\sigma}{d\Omega} = |A(\theta)|^2 + |B(\theta)|^2 \quad \ldots\ldots(7)$$

while the polarization is

$$P(\theta) = \frac{2\mathscr{R}(A^*B)}{|A|^2 + |B|^2} \quad \ldots\ldots(8)$$

§ 3. Analysis

3.1. *No Spin–Orbit Force*

We shall first perform the analysis neglecting spin-dependent forces. In the case where protons are incident equation (3) then becomes

$$V(r) = V_\mathrm{c}\rho'(r) + V_\mathrm{n}\rho(r) \quad \ldots\ldots(8)$$

and

$$\chi_1(b) = \chi_\mathrm{c}(b) + \chi_\mathrm{n}(b)$$

where

$$\chi_\mathrm{c}(b) = -\frac{E}{k}\int_{-\infty}^{\infty} V_\mathrm{c}(r)\,dz, \quad \chi_\mathrm{n}(b) = -\frac{E}{k}\int_{-\infty}^{\infty} V_\mathrm{n}(r)\,dz.$$

If we now assume that the nucleus has a radius R, then for $r > R$,

$$\rho(r) = \rho'(r) = 0,$$

$$V_\mathrm{n} = 0, \quad \chi_\mathrm{n}(b) = 0, \quad V_\mathrm{c}(r) = V_\mathrm{p}(r)$$

and

$$\chi_\mathrm{c}(b) = \chi_\mathrm{p}(b) = -\frac{E}{k}\int_{-\infty}^{\infty} V_\mathrm{p}(r)\,dz \quad \ldots\ldots(9)$$

where $V_\mathrm{p}(r)$ is the potential at a distance r from a point charge.

The scattering amplitude $A(\theta)$ is next split into three parts as follows. (*a*) A term A_n depending purely on the nuclear potential V_n and hence a function of χ_n only. (*b*) A term A_p, the point charge scattering amplitude, a function of χ_p only. (*c*) A term δA depending on χ_n, χ_c and χ_p. In the absence of Coulomb scattering this term is zero. In the absence of nuclear scattering it acts purely as a correction to A_p to give the correct distribution from a nucleus of finite size. Then

$$A(\theta) = A_\mathrm{n} + A_\mathrm{p} + \delta A. \quad \ldots\ldots(10)$$

where

$$A_\mathrm{n} = \frac{k}{i}\int_0^R \mathrm{J}_0(kb\sin\theta)\{\exp(i\chi_\mathrm{n}) - 1\}\,b\,db.$$

$$A_\mathrm{p} = \frac{k}{i}\int_0^\infty \mathrm{J}_0(kb\sin\theta)\{\exp(i\chi_\mathrm{p}) - 1\}\,b\,db.$$

$$\delta A = \frac{k}{i}\int_0^R \mathrm{J}_0(kb\sin\theta)\,[\exp(i\chi_\mathrm{n})\{\exp(i\chi_\mathrm{c}) - 1\} - (\exp(i\chi_\mathrm{p}) - 1)].$$

If now we define $\lambda = \mathscr{R}V_{\rm n}(r)/\mathscr{I}V_{\rm n}(r)$ then the terms involving $\chi_{\rm n}$ and hence $V_{\rm n}(r)$ can be split into two parts.

Let $\chi_{\rm n} = \chi_{{\rm n}_{\rm R}} + i\chi_{{\rm n}_{\rm I}}$ where the subscripts R and I refer to the real and imaginary parts respectively. Then since λ is small and $\chi_{{\rm n}_{\rm I}}$ never greater than 1 in the cases considered, to first order in λ

$$\exp(i\chi_{\rm n}) \simeq (1 + i\lambda\chi_{{\rm n}_{\rm I}})\exp(-\chi_{{\rm n}_{\rm I}}). \qquad \ldots\ldots(11)$$

Substituting (11) into (10) we finally obtain

$$A(\theta) = A_{\rm p} + A_{\rm n}' + \delta A_1' - I + \lambda\{A_{\rm n}'' + \delta A_1''\} \qquad \ldots\ldots(12)$$

with $A_{\rm p}$ defined previously

and

$$\left.\begin{aligned}
A_{\rm n}' &= \frac{k}{i}\int_0^R {\rm J}_0(kb\sin\theta)\{\exp(-\chi_{\rm nI}) - 1\}b\,db.\\
A_{\rm n}'' &= k\int_0^R {\rm J}_0(kb\sin\theta)\chi_{\rm nI}\exp(-\chi_{\rm nI})b\,db.\\
\delta A_1' &= \frac{k}{i}\int_0^R {\rm J}_0(kb\sin\theta)\exp(-\chi_{\rm nI})\{\exp(i\chi_{\rm c}) - 1\}b\,db.\\
\delta A_1'' &= k\int_0^R {\rm J}_0(kb\sin\theta)\chi_{\rm nI}\exp(-\chi_{\rm nI})\{\exp(i\chi_{\rm c}) - 1\}b\,db.\\
I &= \frac{k}{i}\int_0^R {\rm J}_0(kb\sin\theta)\{\exp(i\chi_{\rm p}) - 1\}b\,db.
\end{aligned}\right\} \qquad \ldots\ldots(13)$$

Now $\chi_{\rm p}$ and $\chi_{\rm c}$ can be directly calculated for a nucleus of given shape and charge whilst $\chi_{\rm nI}$ is a function of the imaginary part of the central potential. This can be calculated from the total cross sections for nucleon–nucleon scattering following the treatment of Brown, Ashmore and Nordhagen (1958).

In calculating $\chi_{\rm c}(r)$ the charge distribution $\rho'(r) = \pi^{-3/2}a^{-3}\exp\{-(r/a)^2\}$, with $a = 1{\cdot}965$ fermi was used. This distribution has the advantage that the Coulomb potential in the nucleus (charge $Z\alpha$) has the simple form

$$V_{\rm c}(r) = \frac{Z\alpha}{r}\,{\rm erf}\left(\frac{r}{a}\right). \qquad \ldots\ldots(15)$$

In calculating $\chi_{\rm nI}$ the distribution of nucleons in the nucleus was taken as

$$\rho(r) = \frac{1}{3\pi^{3/2}a_1^{\,3}}\left(1 + \frac{4}{3}\frac{r^2}{a_1^{\,2}}\right)\exp\left(-\frac{r^2}{a_1^{\,2}}\right) \qquad \ldots\ldots(16)$$

with $a_1 = 1{\cdot}635$ fermis.

The distributions for $\rho(r)$ and $\rho'(r)$ both give a good fit to the electron scattering data of Fregeau (1956).

3.2. *Including Spin–Orbit Force*

If we now introduce the term $V_{\rm s}(r)$ into equation (8) then the effect is to modify $A(\theta)$ in (4) and to introduce the further term $B(\theta)$. Taking $A(\theta)$ in the form given by equation (12) the terms affected are $A_{\rm n}''$, $\delta A_1'$, $\delta A_1''$ and $A_{\rm n}'$. The corrections to the first three terms are small and can be neglected. The term $A_{\rm n}'$, which is effectively the nuclear scattering amplitude for neutrons by an imaginary potential will be changed. However Brown, Ashmore and Nordhagen (1958) have shown that the spin–orbit potential does not alter the shape of the curve of $A_{\rm n}'$ as a function of angle markedly, but increases its value. By normalizing $A_{\rm n}'$ at zero angle to the value given by the optical theorem and the value of the total cross section, the effect of spin–orbit forces on $A(\theta)$ is allowed for automatically.

$B(\theta)$ can be calculated for a given value of C using (5). In these calculations it was assumed that the nuclear potential $V_n(r)$ was purely imaginary. It can be shown that to a good approximation $B(\theta) \propto C$ so that the effect of various values for C is easily calculated.

The procedure therefore was to evaluate equation (12), treating λ as an unknown, as described in the previous section. $B(\theta)$ was also evaluated for various values of C.

Hence by fitting the calculated to the observed cross sections a value could be obtained for λ. Since in the data of Chamberlain *et al.* (1956) the absolute values of the cross section are only known to $\pm 20\%$ it is necessary to introduce a normalization constant N. This is the number by which the observed values of the cross section must be multiplied in order to give a good fit to the theoretical curves. We expect N to lie between 0·8 and 1·2. N was usually determined by fitting the data at 7° where the term depending on λ in (12) is small.

§ 4. RESULTS

The analysis was first performed using a real value of the coupling parameter $C = 2{\cdot}0 \times 10^{-27}\,\text{cm}^2$. A good fit to the data was obtained with $\lambda = 0{\cdot}23$ and $N = 1{\cdot}07$ and the curve obtained is plotted in figure 1 together with the experimental data. In order to determine the sensitivity of the value of λ to the value chosen for C, the calculations were next repeated using $C = 1{\cdot}4 \times 10^{-27}\,\text{cm}^2$. Using $N = 1{\cdot}00$ gave $\lambda = 0{\cdot}30$. Changing N to 1·05 keeping C at the same value gave $\lambda = 0{\cdot}24$. Hence we seen that λ is relatively insensitive to the values chosen for C and N. In all cases there is good agreement between the theoretical and experimental curves. In the subsequent calculations we have taken $\lambda = 0{\cdot}23$.

The polarization was calculated using (8) and the predicted curves for $C = 2{\cdot}0$ and 1·4 (in units of $10^{-27}\,\text{cm}^2$) are plotted in figure 2 together with the experimental points of Chamberlain *et al.* (1956). The agreement is seen to be best for the value $C = 2{\cdot}0 \times 10^{-27}\,\text{cm}^2$.

The effect of a complex value for C was next investigated and in figure 2 polarization curves with $C = 2{\cdot}0$ and $C = 2{\cdot}0 - 0{\cdot}5i$ are plotted. Because of possible systematic errors in the polarization results of Chamberlain *et al.* (1956) of the order of $\pm 0{\cdot}04$, it is not possible to distinguish experimentally between these two curves. However, larger imaginary parts to C would probably not fit the data.

We have neglected spin-dependent potentials arising from Coulomb forces. The effect of these has been considered by Heckrotte (1956) and Eriksson(1956). These results show that the value for $P(\theta)$ should be increased slightly. However, the correction is not large and we have neglected such effects in our calculations.

§ 5. COMPARISON WITH OTHER RESULTS

5.1. *Central Potential*

The imaginary part of the central potential at the centre of the nucleus, V_n in equation (3), can be calculated directly from the nucleon–nucleon cross sections. Using $\sigma_{pp} = 24$ mbn, $\sigma_{np} = 35$ mbn and the radial distribution of (16) gives a value of 31·5 MeV for $\mathscr{I} V_n(0)$. Hence the real part corresponds to a potential of 7·25 MeV at the origin. It is difficult to compare these values with those of other workers who may have used different density distributions and radii. However, the product of the potential and nuclear volume is much less dependent on the exact choice of density distribution and radius. If Ω is the volume of the nucleus then for the present analysis $\Omega = 73{\cdot}9$ fermi^3 giving a value for $\Omega\mathscr{I}V_n(0) = 2{\cdot}330 \times 10^{-36}$ Mev cm^3 and $\Omega\mathscr{R}V_n(0) = 0{\cdot}54 \times 10^{-36}$ Mev cm^3. These values are compared in table 1 with those of other workers.

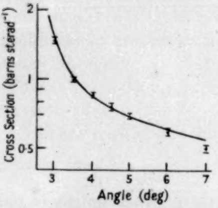

Figure 1. Comparison of the theoretical curve obtained using $C = 2{\cdot}0 \times 10^{-27}$cm^2, $\lambda = 0{\cdot}23$ and $N = 1{\cdot}07$ with the cross section data of Chamberlain *et al.* (1956).

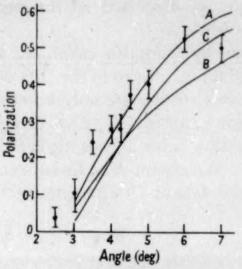

Figure 2. Theoretical curves for the polarization calculated with
A, $C = 2{\cdot}0 \times 10^{-27}$ cm^2,
B, $C = 1{\cdot}4 \times 10^{-27}$ cm^2,
C, $C = (2{\cdot}0 - 0{\cdot}5i) \times 10^{-27}$ cm^2.
The experimental points are those of Chamberlain *et al.* (1956).

The present results, together with those of Bethe (1958) and Bjorklund, Blandford and Fernbach (1957) have been obtained by an analysis of nucleon–nucleus scattering data using realistic density distributions for the nucleus. However, Riesenfeld and Watson (1956) calculated the optical model potentials directly from the nucleon–nucleon phase-shift data of Feshbach and Lomon (1956). The two sets of results (A and B) refer to the two sets of phase-shifts. More recently Ohnuma (1958) has performed a similar analysis using the phase-shift data of Signell and Marshak (1957, 1958) (SM) and of Gammel and Thaler (1957) (GT). These sets of phase-shifts have given good fits to the available nucleon–nucleon scattering data.

Table 1. Values of the Real and Imaginary Parts of the Central Potential

Reference	Energy	$\mathscr{I}V_n(0)$	$\mathscr{R}V_n(0)$	$\lambda = \dfrac{\mathscr{R}V_n(0)}{\mathscr{I}V_n(0)}$	$10^{36}\Omega\mathscr{I}V_n$	$10^{36}\Omega\mathscr{R}V_n$
Present work	310	31·5	7·25	0·23	2·33	0·54
Bethe (1958)	310	46	12	0·26	2·30	0·60
Bjorklund, Blandford and Fernbach (1957)	300	16	0	0	2·37	0
Riesenfeld and Watson (1956)	274	A 15·9	2·23	0·14	2·24	0·31
		B 15·9	−8·19	−0·52	2·24	−1·16
Ohnuma (1958)	300	(GT) 20·41	8·56	0·42	2·43	1·02
		(SM) 20·23	7·06	0·35	2·41	0·84

Values in Mev; last two columns Mev cm^3.

It is seen from table 1 that although the absolute magnitudes of $\mathscr{R}V_n$ and $\mathscr{I}V_n$ vary considerably, the values of the volume potentials and λ are much more constant. There is also qualitative agreement between the sets of parameters obtained from the nucleon–nucleon and nucleon–nucleus scattering data.

5.2. *Spin–Orbit Potential*

The value of the spin orbit coupling parameter obtained in this analysis is purely real with $C = 2{\cdot}0 \times 10^{-27}\,\text{cm}^2$, although a negative imaginary part of $0{\cdot}5 \times 10^{-27}\,\text{cm}^2$ could not be excluded. These values are compared with those obtained by other workers in table 2.

Table 2. Spin–Orbit Coupling Constant

Reference	Energy (MeV)		$\mathscr{R}C$ (10^{-27} cm²)	$\mathscr{I}C$ (10^{-27} cm²)	$\lvert C \rvert = c$ (10^{-27} cm²)
Present work	310		2·0	—	2·0
			2·0	−0·5	2·06
Bethe (1958)	310		1·28	−0·4	1·35
Bjorklund, Blandford and Fernbach (1957)	300		1·35	−1·63	2·1
Riesenfeld and Watson (1956)	274	A	0·59	−1·48	1·58
		B	1·14	−1·37	1·79
Ohnuma (1958)	300 (SM)		2·02	−0·50	2·08
	(GT)		1·50	−0·27	1·52

Our value of C agrees with that obtained by Ohnuma (1958) using the Signell and Marshak (1957) phase-shifts. It is rather larger than that obtained by Bethe (1958).

§ 6. COULOMB SCATTERING

In figure 3 we have plotted the cross sections for the Coulomb scattering from a point charge, also that from a distributed charge of the form given by (14).

If we next consider equation (10), then

$$A = A_n + A_p + \delta A$$

where the symbols have been defined previously. In the absence of nuclear scattering $A_n = 0$ and δA acts purely as a correction to A_p to give the correct scattering from a nucleus of finite size. If now the nucleus absorbs some of the incident protons, that is we introduce an imaginary part to V_n in (8), then not only does A_n become finite but δA is changed considerably. In the present

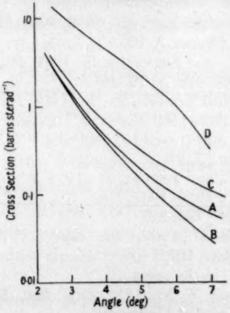

Figure 3. Coulomb scattering calculated for A, point charge, B, extended nucleus, C, partially absorbing nucleus, D, totally absorbing nucleus.

calculations this can be done for two cases, a partially and a totally absorbing sphere. We then have

$$A_{\mathrm{c}}\ (\text{total}) = \int_R^\infty \mathrm{J}_0(kb\sin\theta)\{\exp(i\chi_{\mathrm{p}})-1\}bdb = A_{\mathrm{p}} - I \qquad \ldots\ldots(17)$$

$$A_{\mathrm{c}}\ (\text{partial}) = \int_0^\infty \mathrm{J}_0(kb\sin\theta)\{\exp(-\chi_{\mathrm{nI}})[\exp(i\chi_{\mathrm{c}})-1]\}bdb = A_{\mathrm{p}} - I + \delta A_1'. \qquad \ldots\ldots(18)$$

In both cases the purely nuclear scattering A_{n}, which would remain in the absence of Coulomb forces has been subtracted. This division of the scattering into nuclear and Coulomb is not unambiguous since it is just the interference between the two which produces the effect we are discussing. The cross sections calculated for the two cases (17) and (18) are also plotted in figure 3. It is seen that the amount of Coulomb scattering at small angles is considerably increased by absorption in the nucleus. Hence the cross section for combined nuclear and Coulomb scattering cannot be obtained by directly adding the amplitudes together, but must be calculated exactly.

§ 7. CONCLUSIONS

Using the semi-classical approximation the data of Chamberlain *et al.* (1956) have been analysed to give a ratio of the real to imaginary parts of the central potential equal to 0·23 at an incident energy of 310 MEV. The spin–orbit coupling parameter is found to be real and equal to $2{\cdot}0 \times 10^{-27}\,\mathrm{cm}^2$ although a negative imaginary part of $0{\cdot}5 \times 10^{-27}\,\mathrm{cm}^2$ could not be excluded.

The Coulomb scattering from an extended nucleus has been calculated and it is shown that absorption of the incident protons by the nucleus actually increases the amount of Coulomb scattering at small angles.

ACKNOWLEDGMENTS

The author is indebted to Dr. G. E. Brown, who initially suggested the problem, for his continued guidance and help throughout the course of this work. This work was done whilst the author was in receipt of a Department of Scientific and Industrial Research maintenance grant.

REFERENCES

ASHMORE, A., MATHER, D. S., and SEN, S. K., 1958, *Proc. Phys. Soc.*, **71**, 552.
BETHE, H. A., 1958, *Annals of Physics*, **3**, 190.
BJORKLUND, F., BLANDFORD, I., and FERNBACH, S., 1957, *Phys. Rev.*, **108**, 795.
BROWN, G. E., 1957, *Proc. Phys. Soc.* A, **70**, 361.
BROWN, G. E., ASHMORE, A., and NORDHAGEN, R., 1958, *Proc. Phys. Soc.*, **71**, 765.
CHAMBERLAIN, O., SEGRÈ, E., TRIPP, R., WIEGAND, C., and YPSILANTIS, T., 1956, *Phys. Rev.*, **102**, 1659.
ERIKSSON, T., 1956, *Nucl. Phys.*, **2**, 91.
FERNBACH, S., HECKROTTE, W., and LEPORE, H., 1955, *Phys. Rev.*, **97**, 1059.
FESHBACH, H., and LOMON, E., 1956, *Phys. Rev.*, **102**, 891.
FREGEAU, J. H., 1956, *Phys. Rev.*, **104**, 225.
GAMMEL, J. L., and THALER, R. M., 1957, *Phys. Rev.*, **107**, 291, 1337.
HECKROTTE, W., 1956, *Phys. Rev.*, **101**, 1406.
OHNUMA, S., 1958, *Phys. Rev.*, in the press.
RIESENFELD, W. B., and WATSON, K. M., 1956, *Phys. Rev.*, **102**, 1157.
SHAPIRO, I. I., 1955, *Thesis*, Harvard University.
SIGNELL, P. S., and MARSHAK, R. E., 1957, *Phys. Rev.*, **106**, 832.
—— 1958, *Ibid.*, **109**, 1229.

V.
19

Inelastic Scattering of Neutrons by Thorium

By R. BATCHELOR and J. H. TOWLE
Atomic Weapons Research Establishment, Aldermaston, Berks.

Communicated by K. W. Allen; MS. received 9th September 1958, in final form 22nd October 1958

Abstract. The inelastic scattering of neutrons of up to 1·6 MeV energy by natural thorium and uranium has been studied using the millimicrosecond time of flight technique. Scattering has been observed to levels in ^{232}Th at ~0·05, 0·150 ± 0·015, (0·30 + 0·02), 0·79 (two levels) and 1·09 ± 0·02 MeV. The data obtained for ^{238}U are in agreement with previous work. Differential cross sections measured at 90° are also reported.

§ 1. Introduction

Inelastic neutron scattering is well known to be a useful technique for investigating the level structure of heavy nuclei. Using a ^{3}He neutron spectrometer, Batchelor (1956) has studied inelastic scattering by ^{238}U. The observed spectrum was consistent with ^{238}U having levels forming a ground-state rotational band, though individual levels could not be resolved. There was evidence also for a level or group of levels at about 700 kev. Scattering to levels of excitation higher than 1 MeV cannot be studied with this spectrometer. R. C. Allen (1957) has observed inelastic scattering to levels in ^{238}U at 50 ± 20 and 140 ± 25 kev, using a hydrogen-filled recoil counter. The resolving power of this instrument is very limited since the recoil spectrum is a continuous one, and information on scattering to higher levels could not easily be obtained.

Considerable progress has recently been made by the development of the millimicrosecond (mμsec) time of flight spectrometer, which is capable of much better resolution than preceding neutron spectrometers, and can be used over a wider range of energy. Using the time of flight technique in conjunction with the large Van de Graaff accelerator at Los Alamos, Cranberg and Levin (1956, 1958) have followed up their general survey of inelastic scattering at 2·45 MeV with a more detailed study of scattering by ^{238}U at lower energies. In this latter work† levels in ^{238}U were located at 0·044 ± 0·004, 0·146 ± 0·006, 0·30 ± 0·03, 0·73 ± 0·03, 0·98 ± 0·02, 1·06 ± 0·03 and 1·26 ± 0·04 MeV, the first three of which together with the ground state form a rotational band.

We report here results on the inelastic scattering of neutrons by ^{232}Th obtained at Aldermaston using apparatus similar to that at Los Alamos. The interest in ^{232}Th was stimulated by its close similarity to ^{238}U, both being heavy even–even nuclei, and well removed from closed shells. In consequence similar level schemes might reasonably be expected.

---

† Dr. Cranberg has kindly informed us of the following correction to his paper. The level reported at 0·73 MeV, should now be at 0·70 ± 0·02 MeV, owing to a recent change in the accepted position of a level in niobium used for calibration purposes. This value is in better agreement with our measurement of 0·71 ± 0·02 MeV (§3·2).

Some information on the levels of these nuclei is available from Coulomb excitation studies. Davis *et al.* (1956) identified the first levels at 45 ± 3 and 50 ± 5 kev in ^{238}U and ^{232}Th respectively. Moore *et al.* (1957) report a level in thorium at 719 kev excitation, and McGowan and Stelson (1957) observed γ-rays of 790, 740 and 613 kev energy from thorium which they showed to be consistent with a direct excitation of a 2^+ state at 790 kev decaying by E2 transitions to the $J = 0^+$, 2^+ and possibly 4^+ members of the ground state rotational band.

§ 2. TIME OF FLIGHT APPARATUS

Although the technique has been previously described in detail by Cranberg (1955), a brief description of the Aldermaston apparatus will be made since this is the first reported work using it. A schematic diagram of the apparatus is shown in figure 1.

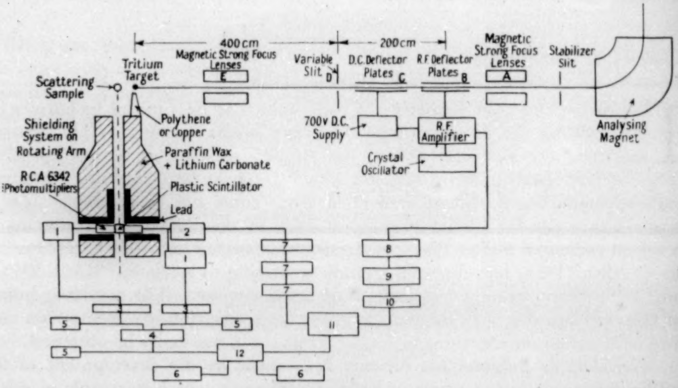
400 cm
200 cm
Magnetic Strong Focus Lenses
E
Tritium Target
Scattering Sample
Variable Slit
D
D.C. Deflector Plates
C
R.F. Deflector Plates
B
Magnetic Strong Focus Lenses
A
Stabilizer Slit
Analysing Magnet
Polythene or Copper
Shielding System on Rotating Arm
Paraffin Wax + Lithium Carbonate
RCA 6342 Photomultipliers
Plastic Scintillator
Lead
700v D.C. Supply
R.F. Amplifier
Crystal Oscillator
1
2
1
7
7
7
8
9
10
3
3
5
5
4
11
5
12
6
6

Figure 1. Schematic diagram of time of flight apparatus; 1, slow head amplifier; 2, fast head amplifier; 3, slow amplifier; 4, slow coincidence unit; 5, scaler; 6, 100 channel kicksorter; 7, line amplifier; 8, pulse shaping unit; 9, variable delay unit; 10, line amplifier; 11, time to pulse height converter; 12, gate.

The analysed proton beam from the 6 Mev Van de Graaff accelerator is pulsed by deflecting it at a high frequency across an aperture D. A sinusoidal potential of frequency 2·5 Mc/s and amplitude variable up to 10 kv is applied to the deflector plates B. These plates are 60 cm long, spaced 1 cm apart, and form part of a tuned circuit of an r.f. power amplifier which is driven by a crystal controlled oscillator. The plates are water-cooled to avoid drifts in tuning due to heating by bombardment with the deflected beam. The beam passes next through another set of deflector plates C, at right angles to B, to which a d.c. potential is automatically applied in the event of a failure of the r.f. voltage. This protects the target from a continuous beam of up to 50 μA. Such a safety system is very important in the case of a gaseous tritium target using a thin entrance foil. The magnetic lenses A are used to obtain a well-focused beam at the slit position before the r.f. voltage is applied. Focusing of the pulsed beam, which is normally between 1 and 2% of the unpulsed beam, is accomplished with another set of lenses E.

An interesting effect which has been noticed is that the focused beam at the target produces two spots spaced a few millimetres apart. The effect is due to the finite transit time of the beam through the deflector plates and to the fact that in one r.f. cycle the beam is swept across the slit in two directions. The spacing depends on the geometry of the system, the r.f. voltage and the beam energy. The relative intensity of the two spots depends critically on the beam tube alignment and the focusing conditions, and in general it has not been possible to reproduce the conditions from one run to another.

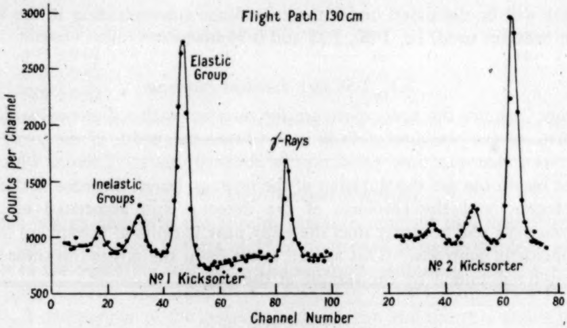

Figure 2. Complete time spectrum for thorium at 1·58 Mev incident neutron energy.

The general scheme of the electronics is the same as that used at Los Alamos, but the individual units differ in detail. The line amplifiers are those developed commercially by Rhode and Schwartz and have a bandwidth of 280 Mc/s and a gain variable up to 10. The time to pulse height converter (time-sorter) has been developed at Aldermaston by Mr. W. Gore from an original design by Dr. P. Orman of Atomic Energy Research Establishment, Harwell, and will be described elsewhere. When checked with a pulse generator the output was found to be linear with delay. In these experiments the output was adjusted to correspond to 2 $m\mu$sec per channel of a 100-channel kicksorter. Two kicksorters were used to obtain a complete representation of one r.f. cycle which lasts for 400 $m\mu$sec. As seen in figure 2 there are two presentations of the neutron spectrum since there are two neutron bursts, but only one timing pulse, per r.f. cycle. The relative intensity of the two presentations is directly proportional to that of the two beam spots at the target.

The neutron detector consisted of a 1 in. thick plastic scintillator viewed by two R.C.A. 6342 photomultipliers with the outputs connected in coincidence. With this arrangement neutrons down to about 250 kev energy could be detected with a background coincidence rate of 2 per second.

Neutrons were produced by the $^3H(p, n)^3He$ reaction using a tritium gas cell 1 in. long, and were monitored by a long counter placed 250 cm away at 30° to the proton beam.

The scattering samples were in the form of hollow cylinders 2·5 cm o.d., 1·0 cm i.d. and 5 cm long made from natural elements. They were placed in a vertical position in line with the proton beam 9 cm from the tritium target. Measurements were made at 90° only. In order to obtain the differential cross sections, measurements were also made of the scattering from a polythene sample, since the n–p cross section is known. The polythene sample had dimensions 0·5 cm i.d., 0·9 cm o.d., 5 cm long. The variation of detector efficiency with neutron energy was obtained by measuring the amount of n–p scattering at suitable angles.

§ 3. RESULTS

These will be discussed under three headings corresponding to the incident neutron energies used, i.e. 1·58, 1·35 and 0·74 MeV.

3.1. 1·58 *MeV Incident Neutrons*

Figure 2 shows the time spectrum for thorium with a flight path of 130 cm and a tritium gas pressure of 14 lb in^{-2}. From the width of the γ-ray peak it can be seen that the time resolution is about 6 mμsec. Factors which affect the time resolution are the duration of the neutron burst, the sizes of the sample and detector, and the response of the detector and associated electronics. A neutron peak will be wider than the γ-ray peak because of the spread in energy of the incident neutrons. This spread arises from the target thickness and the finite angle subtended by the sample at the target.

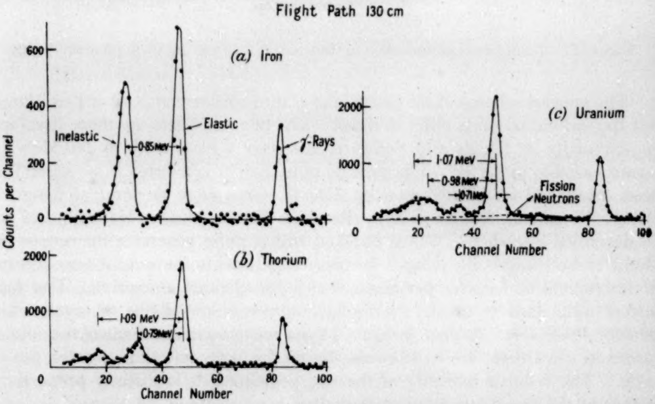

Figure 3. Time spectra with background subtracted for 1·58 MeV incident neutron energy.

In figure 3 the time spectra are presented for iron, thorium and uranium, after subtraction of the background obtained with no sample present. The spectrum for iron is a useful check on the energy calibration since the first excited state of ^{56}Fe is known to lie at 0·85 Mev (Day 1956). With this resolution there appear to be two inelastic groups from thorium corresponding to levels at 0·79 and 1·09 Mev. The values for the level energies and differential cross sections are summarized in table 1. For uranium, the results are in good agreement with those obtained by Cranberg and Levin (1958), see Introduction.

Table 1

		$\sigma(90°)$ (mbn sterad^{-1})	
	Level (Mev)	$E_n = 1{\cdot}58$ Mev	$E_n = 1{\cdot}35$ Mev
^{232}Th			
	Ground state + rotational levels	260	240
	0·79	93	100
	1·09 ± 0·2	62	—
^{238}U			
	Ground state + rotational levels	240	220
	0·71 ± 0·02	30	44
	0·98 ± 0·02	50	—
	1·07 ± 0·02	50	—

The errors in $\sigma(90°)$ arise mainly from uncertainties in the effect of multiple scattering and are estimated to be about ±20%.

3.2. 1·35 *Mev Incident Neutrons*

At this energy and with the tritium pressure reduced to 7 lb in^{-2} (thereby reducing the energy spread of the incident neutrons), it was possible to examine the levels in the region 0·7 to 1 Mev with improved resolution. The time spectra for thorium, uranium and iron, after subtraction of background, are shown in figure 4. A comparison of the inelastic peaks of iron and thorium shows that the

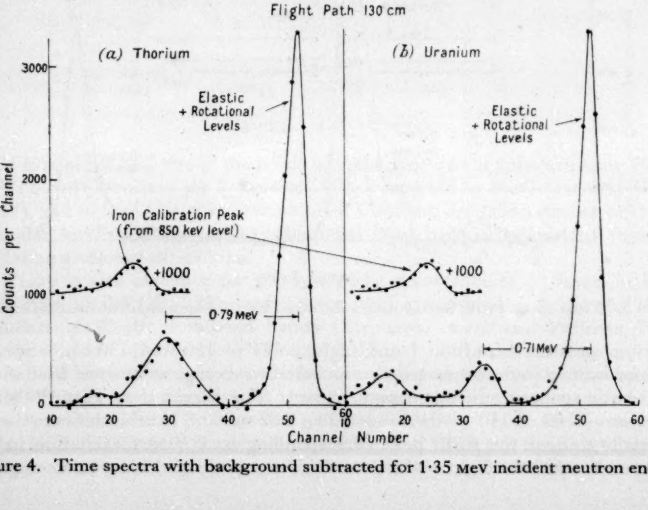

Figure 4. Time spectra with background subtracted for 1·35 Mev incident neutron energy.

thorium peak corresponding to a level of excitation at 0·79 Mev is much broader than that expected for scattering from a single level. An analysis of the peak shows that if there are two levels present, approximately equally excited (this is a reasonable assumption since the composite peak is fairly symmetrical) then the levels are separated by approximately 60 kev. Thus we tentatively suggest that there are levels at $0{\cdot}76 \pm 0{\cdot}03$ and $0{\cdot}82 \pm 0{\cdot}03$ Mev in ^{232}Th. In table 1, these levels are referred to collectively as '0·79' Mev. It may be noted that within the resolution the first inelastic group from ^{238}U corresponds to one level at $0{\cdot}71 \pm 0{\cdot}02$ Mev.

Where possible the energies of the inelastic groups have been calculated by two methods which have yielded the same answers within the experimental error. In the first method the γ-ray peak is used to establish time zero, and the neutron energies are calculated from the known calibration of the time-sorter. In the second method the reference time is obtained from the peak due to elastic neutrons, the energy of which is calculated from the bombarding proton energy, the thickness of the entrance foil of the tritium cell, and the tritium pressure. A value of $0{\cdot}85 \pm 0{\cdot}01$ Mev is obtained for the excitation of the first level in ^{56}Fe.

3.3. 0·74 *Mev Incident Neutrons*

These measurements were made to ascertain if scattering to a ground state rotational band as reported by Cranberg for ^{238}U could be observed with ^{232}Th. Figure 5 shows the time spectra, after subtraction of background, obtained with a tritium pressure of 4 lb in^{-2} and flight paths of 180 and 130 cm. Spectra obtained with a lead sample are also included for comparison since lead shows only elastic scattering in this energy region. The curves show that ^{232}Th has levels at $\sim 0{\cdot}05$, $0{\cdot}150 \pm 0{\cdot}015$ and $0{\cdot}30 \pm 0{\cdot}02$ Mev. There is however some uncertainty about the small peak corresponding to 0·30 Mev excitation in the spectrum for 180 cm flight path, since the γ-ray peak of the next presentation,

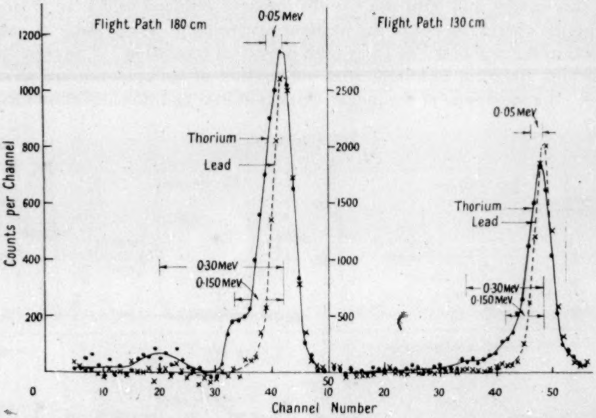

Figure 5. Time spectra with background subtracted for 0·74 Mev incident neutron energy.

if detected, should be at the same place. This doubt is partially removed by the spectrum obtained with the 130 cm flight path, since in this case the γ-ray peaks are well removed from the neutron peaks, but the statistics are not good. Unfortunately, neither γ-ray peak could be observed since that in the first presentation was outside the range of the time-sorter, and the number of counts in the second presentation was small. The yield of the inelastic scattering to the 0·05, 0·15 and 0·30 Mev levels relative to elastic scattering, with 0·74 Mev neutrons, is given in table 2.

Table 2

Level in ^{232}Th (Mev)	Ground state	~0·05	0·150 ± 0·015	0·30 ± 0·02
†Relative yield at 90° $E_n = 0{\cdot}74$ Mev	100	43	10	$\lesssim 11$

†Yields relative to ground state group = 100 units.

§ 4. Discussion

We conclude from this work that the nuclei ^{232}Th and ^{238}U have similar level schemes at low excitation (figure 6), and show similar behaviour in the scattering of fast neutrons at 90°.

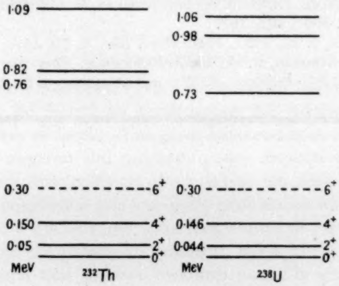

Figure 6. Level schemes.

It is possible that one of the levels we have observed at approximately 790 kev in ^{232}Th corresponds to the 2^+ level at 790 kev reported by McGowan and Stelson (1957), and it would be of interest to see if Coulomb excitation studies can reveal a similar level in ^{238}U. A 2^+ vibrational level is expected in this region of excitation (Alder *et al.* 1956).

There is also evidence for the systematic occurrence of 1^- levels in heavy even–even nuclei ($A > 222$), which have been interpreted as being the lowest members of $K = 0^-$ rotational bands (Stephens, Asaro and Perlman 1955). Levels we have observed in ^{232}Th and ^{238}U may fall into this category.

It is of interest to note that the location and properties of the excited states in these nuclei have a bearing on their neutron capture cross sections, owing to the competition of this process with inelastic scattering. Lane and Lynn (1957) have calculated the (n, γ) cross sections of ^{238}U and ^{232}Th as a function of neutron energy. Reasonable agreement with the experimental results was obtained by assuming, in addition to the ground state rotational bands, levels at 700 and 775 kev in ^{238}U (1^- and 3^- respectively) and a similar pair of levels at 425 and 500 kev in ^{232}Th. However, we have no evidence for levels between 300 and 750 kev excitation in ^{232}Th. In view of this apparent discrepancy it is of interest to obtain more experimental data on the neutron capture cross section in the energy range 0·2 to 1·2 MEV. These measurements are now in hand at Aldermaston.

ACKNOWLEDGMENTS

We wish to thank Mr. E. J. Frewin for his help in this work, Mr. R. J. Brooker who supplied the electronics for the deflection system, and the operating crew of the Van de Graaff for their excellent cooperation.

REFERENCES

ALDER, K., BOHR, A., HUUS, T., MOTTELSON, B., and WINTHER, A., 1956, *Rev. Mod. Phys.*, **28,** 432.

ALLEN, R. C., 1957, *Phys. Rev.*, **105,** 1796.

BATCHELOR, R., 1956, *Proc. Phys. Soc.* A, **69,** 214.

CRANBERG, L., 1955, Proceedings of the International Conference on the Peaceful Uses of Atomic Energy. Vol. **4,** Paper P/577. (New York: United Nations.)

CRANBERG, L., and LEVIN, J. S., 1956, *Phys. Rev.*, **103,** 343.

—— 1958, *Ibid.*, **109,** 2063.

DAVIS, R. H., DIVATIA, A. S., LIND, D. A., and MOFFAT, R. D., 1956, *Phys. Rev.*, **103,** 1801.

DAY, R. B., 1956, *Phys. Rev.*, **102,** 767.

LANE, A. M., and LYNN, J. E., 1957, *Proc. Phys. Soc.* A, **70,** 557.

McGOWAN, F. K., and STELSON, P. H., 1957, *Bull. Amer. Phys. Soc.* [II], **2,** 207.

MOORE, A. S., CLASS, C. M., PROSSER, F. W., and SCHIFFER, J. P., 1957, *Bull. Amer. Phys. Soc.* [II], **1,** 88.

STEPHENS, F. S., ASARO, F., and PERLMAN, I., 1955, *Phys. Rev.*, **100,** 1543.

The Electron Capture Cross Sections for Protons in Helium

By C. A. HAYWOOD

Physics Department, The University, Leicester

MS. received 27th May 1958, in revised form 6th October 1958

Abstract. The impact parameter formulation of the method of perturbed stationary states is used to calculate the cross section for electron capture by protons in helium. The σ–σ transition from ground state to ground state is investigated. A one-body formulation is used in which the captured electron moves initially in the combined field of the other electron, the helium nucleus and the incident proton.

The presence of the passive electron is allowed for by using as the initial wave function before the collision, an approximation to that calculated from the self-consistent field for the helium atom. During the collision this initial wave function is modified by the introduction of a variational parameter which is determined by a minimization condition for the energy.

The possibility of using the one-body formulation for more complex systems is demonstrated by calculations of the electron-capture cross section for protons in argon and neon.

§ 1. INTRODUCTION

BORN and OPPENHEIMER (1927) have shown that the energy levels of a molecule may be found by considering the nuclei as fixed or slowly vibrating centres of force. The error involved is of the order of $(m/M)^{1/2}$ where m, M are the electron and nuclear masses respectively. Thus it should be justifiable to treat a slow collision of a positive ion with an atom in a similar way. We can either consider it as a one-body problem in which the electron is in the combined field of a nucleus and a moving centre of force, or as a two-body problem in which both the proton and electron move in the field of the nucleus. Mott (1931) has shown that the two methods formally give the same result if $(m/M)^{1/2}$ be neglected. Similarly Frame (1931) has considered the special case of excitation of an atom by a fast α-particle. This problem had been considered as a one-body problem by Gaunt (1927) and Bethe (1930). If the velocity of the α-particle is greater than the orbital velocities of the electrons in the atom, the well-known Born approximation may be made in the two-body formulation. The two methods give formally very different formulae for the excitation probabilities but Frame shows that they are in fact identical, provided once again that $(m/M)^{1/2}$ may be neglected. Thus it would appear that the restriction of the one-body method to *slow* impacts is not necessary. No general solution of the two-body problem has been given but the one-body problem can be solved for both fast and slow collisions.

§ 2. THE CAPTURE CROSS SECTION FORMULAE

Bates, Massey and Stewart (1953) have deduced a formula which may be used to compute the cross section for electron capture by protons in helium which includes the effect of ' distortion '. Distortion refers to the deviation of the incident proton from a straight line trajectory and its variation in speed along the path. The expression obtained is

$$a_n(\infty)=\int_{R>}^{\infty} M_{0n}(R)\exp\left\{i\frac{2\pi}{h}\int_{R>}^{R}\frac{\delta E_{0n}(R')}{\bar{v}_{0n}(R')}\left(1-\frac{\bar{v}_{0n}(\infty)^2\Delta^2}{\bar{v}_{0n}(R')^2R'^2}\right)^{-1/2}dR'\right\}dR \qquad \ldots\ldots(1)$$

$a_n(\infty)$ may be called the ' probability amplitude ', as $|a_n(\infty)|^2$ is the probability that after an infinite time (i.e. after the collision) the electron will be in the nth state of the field in which it moves.

$\delta E_{0n}(R')$ stands for $W_n(R')-W_0(R')$, the difference between the final and initial energy eigenvalues of an electron moving in the combined field of the helium nucleus and the colliding proton, when the latter are separated by a distance R'.

Δ is the initial impact parameter for the collision and is related to the proton coordinate Z in the direction of the initial proton approach by $R^2=\Delta^2+Z^2$

$$M_{0n}(R)=\frac{\int\psi_n^*(\partial V/\partial Z)\psi_0\,d\tau}{\delta E_{0n}(R)}.$$

$\bar{v}_{0n}(R)$ is the mean of the relative velocity before and after the collision when the particles are a distance R apart and ψ_0, ψ_n are the initial and final electron wave functions. V is the potential energy of the electron in the proton field.

If the distortion is neglected, and we imagine the proton to move in a straight line past the helium nucleus with a velocity v:

$$\delta E_{0n}(R') \to W_n(\infty)-W_0(\infty)$$

and

$$\bar{v}_{0n}(R') \to v.$$

Substitution in equation (1) then gives

$$a_n(\infty)=\int_{-\infty}^{+\infty} M_{0n}(Z)\exp\left[\frac{2\pi i}{hv}(W_n(\infty)-W_0(\infty))Z\right]dZ \qquad \ldots\ldots(2)$$

with

$$M_{0n}(R)=\frac{\int\psi_n^*(\partial V/\partial Z)\psi_0\,d\tau}{W_n(\infty)-W_0(\infty)}.$$

This formula was first deduced by Mott (1931). If ψ_0 and ψ_n are replaced by the atomic functions then the Born approximation is obtained. The cross section Q for electron capture is then obtained by integrating over all impact parameters:

$$Q=2\pi\int_0^{\infty}|a_n(\infty)|^2\Delta\,d\Delta. \qquad \ldots\ldots(3)$$

It is a less drastic simplification however if we regard W_0 still as a function of R while taking the simple form for $W_n(\infty)$. In the deduction of equation (1) although only the initial and final states occur explicitly, the effect of the intervening states is still partially included, because the general wave function is expanded in terms of the perturbed stationary state wave functions and the perturbations need not be small. As the simplifying assumption is made that a_0 is much greater than a_j, $a_n(\infty)$ ceases to be bounded at ± 1 and in fact it will be shown that it greatly exceeds unity in some cases.

The direction in which inclusion of distortion effects will affect the value of the capture cross section has been considered by Bates, Massey and Stewart. If $W_n(R)-W_0(R)$ is effectively greater numerically than $W_n(\infty)-W_0(\infty)$, inclusion of distortion effects will result in a smaller value of the cross section, and vice versa. The same will be true but to a lesser extent, if $W_n(R) - W_0(R)$ is greater than $W_n(\infty) - W_0(R)$ which we use in the computation that follows. These considerations are important as they enable a theoretical upper limit to be assigned to the cross section. It will be shown that this upper limit is *below* the experimental values.

The present method consists of regarding the electron which is eventually captured, as moving in the combined field of the helium nucleus, incident proton and the other uncaptured electron. As a zero order approximation, the presence of the second electron could be ignored, this corresponding to the case of electron capture from ionized helium. In this case the initial wave function of the target electron may be taken as the product of two hydrogen-like wave functions, with the introduction of a variational parameter:

$$\psi_0(r, R) = A \exp(-z_1 r) \exp(-f z_2 p) \qquad \ldots\ldots(4)$$

where A is a normalizing factor, z_1 is the atomic number of the helium nucleus, z_2 is the atomic number of the hydrogen nucleus and f is the variational parameter. Both A and f are functions of the separation R of the proton and helium nucleus, r and p being the distances of the electron from the helium nucleus and proton respectively, in atomic units.

In order to take into account the presence of the second electron, z_1 may be replaced by z, the 'effective' helium nuclear charge, allowing for the shielding effect of the second electron. More properly the entire term $e^{-z_1 r}$ should be replaced by the electron wave function for the helium atom as calculated by the self-consistent field method of Hartree (1927). The extent to which a constant value of z approximates to this is discussed below. This is still an approximation because the presence of the proton modifies the field in which the 'shielding' electron moves. The true wave function for the target electron could only be obtained by a method of successive approximation, in effect a self-consistent field calculation for the helium–proton complex. If however z is a function of r which is not known in analytical form, the problem can only be solved by extremely lengthy numerical quadratures. The main difficulty lies in the determination of the variational parameter f. However, in view of the success of the variational treatment of the normal helium atom (Hylleraas 1929) in which even a simple treatment gives good agreement with experiment for the ionization potential for a constant value of z equal to about 1·69, it may be expected that the appropriate z would be a slowly varying function of r. It is therefore of interest to solve the problem for z constant to see if the capture cross section is sensitive to the value chosen. The use of a constant value of z has the great advantage that the problem can be solved analytically to a large extent and can in fact be then applied to any impact system provided that a proper choice of z can be made.

The identity of the two electrons in the helium atom must of course be considered but this may be done at a later stage.

§ 3. CHOICE OF THE EFFECTIVE HELIUM NUCLEAR CHARGE (z)

The self-consistent field wave function for a 1s electron of the configuration $1s^2$ for helium has been calculated by Wilson and Lindsay (1935). Writing

$$\psi(r) = a\, e^{-zr} \qquad \ldots\ldots(5)$$

we require values of z and a which give a good fit to the wave function and which satisfy the normalization condition. It is found that $z = 1{\cdot}6$ gives a reasonably good fit. a is then found from the usual normalization condition. This function, together with the Hylleraas approximation $z=1{\cdot}69$, is shown graphically in figure 1. Naturally the ionization potential calculated from $z=1{\cdot}6$ is not as good as the Hylleraas value; in fact the best value of z in this respect is 1·7042. It will be noticed that the curve for $z=1{\cdot}6$ is a better fit at large values of r than that for $z=1{\cdot}69$.

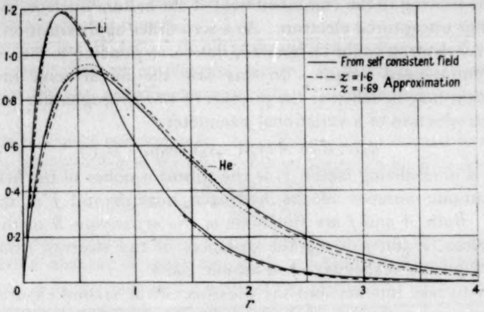

Figure 1.

When the separation R of the helium nucleus and the proton tends to infinity the electron wave function is of the form given by equation (5). In general the form will be as given by equation (4).

As R tends to zero, f tends to unity and p tends to r. Equation (4) then becomes

$$\psi(r,0)=A(0)\,e^{-(z+1)r}. \qquad \ldots\ldots(6)$$

This corresponds to the case of ionized lithium, for which the self-consistent field has been calculated by Fock and Petrashen (1935). This wave function together with the approximation given by equation (6) for $z=1{\cdot}6$ is also included in figure 1. The agreement remains good therefore at each end of the range of R and will be presumed to be reasonable for intermediate values.

§ 4. Analysis of the Capture Cross Section Formulae

We regard the helium nucleus has having a constant effective charge z which will be set equal to 2, 1·69 and 1·6 to give cross sections to the various degrees of approximation already considered.

The Mott formula has been used by Frame (1937) to calculate the cross section for excitation of lithium by α-particles.

4.1. *The Initial Wave Function* $\psi_0(r, R)$

The initial wave function $\psi_0(r, R)$ is given by equation (4). The parameter f is found from the condition that the energy shall be stationary. We write f' for the arbitrary value of f and ψ_0' for the corresponding value of ψ_0. Thus for a given value of D, the modulus of R, we need to find the value of f' which makes the energy stationary. The value so found is then $f(D)$. The notation is such that

$$E(D,f')\to W_0(D)\equiv W_0(R) \text{ as } f'\to f.$$

The expectation value of the energy is $\int \psi_0{}' H \psi_0{}^{*\prime} d\tau$ where H is the total Hamiltonian for the system i.e. $\frac{1}{2}\nabla^2 + V'$; V' is the potential energy of the electron in the combined field of the helium nucleus, second electron and proton:

$$V' = -\left(\frac{z}{r} + \frac{1}{p}\right).$$

One form of Green's theorem may be written:

$$\int \psi' \nabla^2 \psi^{*\prime} d\tau = \int_s \psi' \nabla \psi^{*\prime} dS - \int \nabla \psi' \nabla \psi^{*\prime} d\tau.$$

As $\psi_0 \to 0$ as $r \to \infty$, the surface integral over the bounding surface of the range of integration vanishes. Thus the expectation value of the energy may be written:

$$E(D, f') = \int (\tfrac{1}{2} \operatorname{grad} \psi_0{}' \cdot \operatorname{grad} \psi_0{}^{*\prime} + \psi_0{}' V' \psi_0{}^{*\prime})\, d\tau. \qquad \ldots\ldots (7)$$

The normalizing condition to determine $A(D, f')$ is:

$$\int \psi_0{}' \psi_0{}^{*\prime} d\tau = 1. \qquad \ldots\ldots (8)$$

$A(D, f')$ is eliminated explicitly from equation (7) by dividing formally by equation (8) and the resulting expression may be now reduced to a function of D and f' by the method adopted by Frame (1937). The result, expressed in continued fraction form, convenient for numerical computation is

$$E(D, f') = -\tfrac{1}{2}(z^2 - f'^2)\left[1 - \cfrac{1/f'}{1 + \cfrac{(1/f') \exp[2D(z-f')] - 1/z}{2/z - \cfrac{2(\exp[2D(z-f')] - 1)}{D(z^2 - f'^2)}}}\right] \qquad \ldots\ldots (9)$$

Direct location of the turning points involves a prohibitive number of computations as the energy minima are relatively 'flat' and so it is necessary to resort to direct differentiation of equation (9).

We require the condition that $\left(\frac{\partial E}{\partial f'}\right) = 0$ and obtain:

$$\begin{aligned}\frac{(2bf' + Dacf')^2}{Da^2 \exp[2D(z-f')]}\left(\frac{\partial E}{\partial f'}\right)_D &= 2f'^2 \exp[-2D(z-f')] \\ &\quad \times \left[\left(cf' - \frac{2}{z}\right)\left(\frac{4b}{a} + Dc\right) - \frac{4b^2}{Da^2}(1 - f')\right] \\ &\quad + 4Df'\left(c - \frac{2}{z}\right) + \left(2D + \frac{1}{f'}\right)\left(2b + \frac{2Da}{z}\right) \\ &\quad + \exp[-2D(z-f')]\left[-\frac{4b^2}{Da} - 2b\left(\frac{2}{z} + c\right) - \frac{2Dac}{z}\right]\end{aligned} \qquad \ldots\ldots (10)$$

where $a = z^2 - f'^2$, $b = 1 - \exp[2D(z-f')]$, $c = 1/z + \exp[2D(z-f')]/f'$.

The normalizing factor $A(D)$ is found from the condition that

$$\int \psi_0{}'^2 \, d\tau = 1.$$

We obtain

$$\pi A^2(D) = \frac{(z^2 - f^2)^3 \exp(2fD)}{2zf/D(\exp[-2D(z-f)] - 1) + (z^2 - f^2)(f \exp[-2D(z-f)] + z)} \qquad \ldots\ldots (11)$$

which may be computed when $f(D)$ is known. Also $\pi A^2(D) \to (z+1)^3$ as $D \to 0$. This completes the analysis required to compute $\psi_0(r, R)$ and $W_0(R)$.

4.2. *The Function* M_{0n} (R)

In equation (2) V is the potential of the electron in the proton field. In atomic units: $V = -1/p$ and $\partial V/\partial Z = (1/p^2)\,\partial p/\partial Z$. ψ_n is the normalized wave function of the electron after capture into the ground state of the incident proton

$$\psi_n(r, R) = \frac{1}{\sqrt{\pi}} \exp(-p).$$

Writing M_{0n}' for $M_{0n}(R) \,.\, (W_n - W_0(R))$ we have from equation (2)

$$M_{0n}' = \frac{1}{\sqrt{\pi}} \int \frac{\exp(-p)}{p^2} \frac{\partial p}{\partial Z} \,.\, A(D) \exp(-zr - fp) \,.\, d\tau. \qquad \ldots\ldots(12)$$

Here for simplicity the unperturbed form for the final state wave function is taken. The perturbed form would be $B(D) \exp(-p - l(D)r)$ where $l(D)$ is a variational parameter and $B(D)$ is a normalizing factor. The effect of taking the simple form is discussed later. Again following the argument given by Frame (1937) we obtain:

$$M_{0n}' = \frac{A(\pi)^{1/2} \cos\lambda}{D^2} \int_0^\infty \int_{|D-r|}^{D+r} \exp(-zr - \alpha p) \frac{r}{p^2} (D^2 - r^2 + p^2)\, dp\, dr$$

or

$$\frac{D^2 M_{0n}'}{A(\pi)^{1/2} \cos\lambda} = \int_0^D \frac{\exp(-\alpha p)}{p^2} \int_{D-p}^{D+p} g(r, p)\, dr\, dp$$
$$+ \int_D^\infty \frac{\exp(-\alpha p)}{p^2} \int_{p-D}^{p+D} g(r, p)\, dr\, dp, \qquad \ldots\ldots(13)$$

where

$$g(r, p) = r \exp(-zr)(D^2 + p^2 - r^2); \quad \alpha = f + 1 \text{ and } \lambda = \cos^{-1}(Z/D).$$

The inner integrations with respect to r are straightforward, and so are 7 of the resulting outer integrals. After considerable manipulation we obtain, writing $J \equiv 3 + 3zD + z^2D^2$, $K \equiv 3 - 3zD + z^2D^2$,

$$\begin{aligned}
\frac{D^2 M_{0n}'}{A(\pi)^{1/2} \cos\lambda} = \\
&- \frac{2 \exp(-zD)}{z^4 D} J(\exp[-(z+\alpha)D] - \exp[+(z-\alpha)D]) \\
&- \frac{8 \exp(-zD)}{z^4} J + \frac{4 \exp(-zD)}{z^4} J\alpha \int_0^D \exp(-\alpha p) \frac{\sinh zp}{p}\, dp \\
&+ \frac{2 \exp(-zD)}{z^2} (1 + zD) \Big[\frac{1}{z^2 - \alpha^2} (2z - \exp(-\alpha D)\{(z-\alpha)\exp(-zD) \\
&\qquad\qquad + (z+\alpha)\exp(+zD)\}) \Big] \\
&+ \frac{2 \exp[-(z+\alpha)D]}{z^4 D} [J \exp(-zD) - K \exp(+zD)] \\
&- \frac{2\alpha}{z^4} [J \exp(-zD) - K \exp(+zD)] \int_D^\infty \frac{1}{p} \exp[-(z+\alpha)p]\, dp \\
&+ \frac{2}{z^2} ((1 + zD) \exp(-zD) - (1 - zD) \exp(+zD)) \frac{\exp[-(z+\alpha)D]}{z+\alpha}
\end{aligned}$$

$$\ldots\ldots(14)$$

The first remaining integral may be shown to be, for all the cases relevant to this investigation, i.e. $D>0$; $1<\alpha<2$:

$$\int_0^D \exp(-\alpha p)\frac{\sinh zp}{p}\,dp = 1{\cdot}55725\,\ldots - \tfrac{1}{2}\int_{zD}^{1}\left(\frac{\exp(x)}{x}-\frac{\exp(-x)}{x}\right)dx$$

$$+\tfrac{1}{2}\ln\left(\frac{z+\alpha}{|z-\alpha|}\right)-\int_{zD}^{(z+\alpha)D}\frac{\exp(-y)}{y}\,dy-\int_{(z-\alpha)D}^{zD}\frac{\exp(y)}{y}\,dy.$$

This, and the second of the remaining integrals in equation (14) may be expressed in terms of the exponential integrals in the notation of Jahnke and Emde (1938).

Combining these results we then obtain after further reduction

$$M_{0n}'(D)=\frac{A(D)(\pi)^{1/2}\cos\lambda}{z^4D^2}\exp(-zD)\Bigg[\exp[(z-\alpha)\mathrm{D}]\left\{12z-\frac{4z^3(1+\alpha D)}{(z^2-\alpha^2)}\right\}$$

$$-8(3+3zD+z^2D^2)+\frac{4z^3(1+zD)}{(z^2-\alpha^2)}$$

$$+2\alpha(3+3zD+z^2D^2)\left\{\ln\left(\frac{z+\alpha}{|z-\alpha|}\right)+\overline{\mathrm{Ei}}[(z-\alpha)D]\right\}$$

$$+2\alpha(3-3zD+z^2D^2)\exp(2zD)\{-\mathrm{Ei}[-(z+\alpha)D]\}\Bigg]. \qquad \ldots\ldots(15)$$

If $\alpha\geqslant z$, the term $\overline{\mathrm{Ei}}[(z-\alpha)D]$ must be replaced by $\mathrm{Ei}[(z-\alpha)D]$. We write for convenience

$$M'_{0n}=\frac{A(\pi)^{1/2}\cos\lambda}{z^4D^2}\exp(-zD)F(D). \qquad \ldots\ldots(16)$$

Now for small x, $\overline{\mathrm{Ei}}(x)\simeq\mathrm{Ei}(-x)\simeq-\ln(1/\gamma x)$. Where $\gamma=\exp(c)=1{\cdot}781072$, c being Euler's constant. Thus as $D\to0$, $\alpha\to2$ and $F(D)\to0$.

4.3. *The Probability Amplitude* $a_n(\infty)$

From equation (2) we have, using the result of equation (16),

$$a_n(\infty)=\int_{-\infty}^{+\infty}\frac{A(\pi)^{1/2}\cos\lambda\exp(-zD)}{z^4D^2\{W_n-W_0(R)\}}F(D)\exp\left[\frac{2\pi i}{hv}\{W_n-W_0(R)\}Z\right]dZ.$$

Now when the proton is at the point of closest approach to the helium nucleus, $\cos\lambda=0$. A, $W_0(R)$ and the function $F(D)$ are only functions of D and as Z goes through zero from negative to positive values $\cos\lambda$ changes sign. Thus a graph of $M_{0n}(Z)$ against Z has a centre of symmetry at the origin. On the other hand, $\cos[(2\pi/hv)\{W_n-W_0(R)\}]$ has the line $Z=0$ as a line of symmetry and consequently this term vanishes on integration from $-\infty$ to $+\infty$. We are left with

$$a_n(\infty)=i\int_{-\infty}^{+\infty}M_{0n}(Z)\sin[(2\pi/hv)\{W_n-W_0(R)\}Z]\,dZ.$$

But $D^2 = Z^2 + \Delta^2$ which gives, on changing the variable of integration from Z to D:

$$a_n(\infty) = 2i \int_\Delta^\infty \frac{A(D)(\pi)^{1/2} \exp(-zD) F(D)}{z^4 D^2 \{W_n - W_0(D)\}} \sin \frac{\{W_n - W_0(D)\}(D^2 - \Delta^2)^{1/2}}{v} \, dD \qquad \ldots\ldots (17)$$

as $h/2\pi = 1$ in atomic units. The value of $a_n(\infty)$ for $\Delta = 0$ is specifically required

$$|a_n(\infty)|_0 = \frac{2i\sqrt{\pi}}{z^4 v} \int_0^\infty \frac{\Theta}{D} \frac{\sin x}{x} \, dD$$

where

$$\Theta = A(D) \exp(-zD) F(D) \qquad \ldots\ldots (18)$$

$$x = \{W_n - W_0(D)\} D / v.$$

§ 5. THE CAPTURE CROSS SECTION

The helium electrons are indistinguishable and the specification of one of them as being the 'target' electron has been merely a matter of convenience. Denoting the electrons by I and II, the probability $|a_n(\infty)|^2$ is the probability that one particular electron will be captured at a given impact parameter while the other one is not captured. If this probability is denoted by P and if P' is the probability that the proton will capture the other electron after having already captured a particular one, then the expression

$$2P - P^2(1 + P')^2 \qquad \ldots\ldots (19)$$

is the probability that only one unspecified electron will be captured. This expression must be used to calculate the cross section.

5.1. *The Calculations*

The variational parameter $f(D)$ is found from equation (10). The method adopted in solving this equation numerically was to compute the values of $(\partial E/\partial f')_D$ for a given value of D and for trial values of f' until it changed sign. The value of f' to make $(\partial E/\partial f')_D$ equal to zero was then found by a Lagrangian interpolation.

The functions $W_0(D)$, $A(D)$ and $M_{0n}'(D)$ were then computed directly from equations (9), (11) and (15) respectively. The probability amplitudes are given by equation (17) which may be written

$$a_n(\infty) = i \int_\Delta^\infty M(D) \sin\left(\frac{\phi(D, \Delta)}{v}\right) dD$$

where

$$M(D) = \frac{2M_{0n}(D)}{\cos \lambda}$$

$$\phi(D, \Delta) = \{W_n - W_0(D)\}(D^2 - \Delta^2)^{1/2}.$$

These integrals were computed for a range of values of Δ for different proton energies, on a mechanical differential analyser.

The results obtained for $a_n(\infty)$ are given in figures 2 and 3 and illustrate graphically the variation of $a_n(\infty)$ with impact parameter and energy for $z = 2$ and $z = 1{\cdot}69$ respectively. The results for $z = 1{\cdot}6$ are not plotted as the general form of the results is similar to that for $z = 1{\cdot}69$.

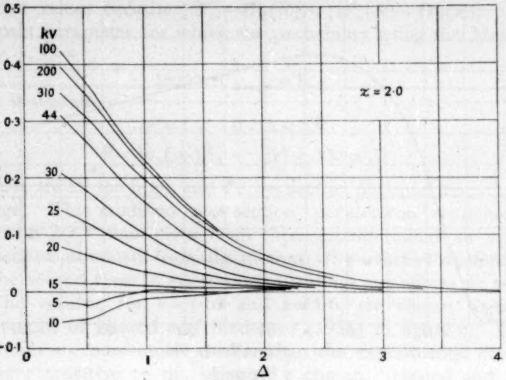

Figure 2.

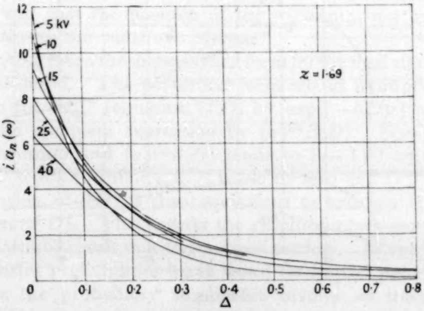

Figure 3.

5.2. *The Cross Section* $Q(v)$

It is customary to express these cross sections in units of $\pi a_0{}^2$, the area of the first Bohr orbit in hydrogen. We have therefore to evaluate the integral

$$Q(v)=2\int_0^\infty |a_n(\infty)|^2\Delta\, d\Delta.$$

The final results obtained are shown graphically in figures 4 and 5. In figure 5 $2Q(v)$ is plotted against impact energy and the experimental results of Hasted and Stedeford (1955) are also shown for comparison. The cross sections refer to the capture of the 'target' electron by the proton, the other electron remaining in the ground state of the ionized helium atom. This cross section will now be referred to as $Q_1(v)$. In order to obtain the cross section for the capture of either, but only one electron the expression (19) must be used. Numerical results taking this into account were not obtained for reasons to be given in the next section.

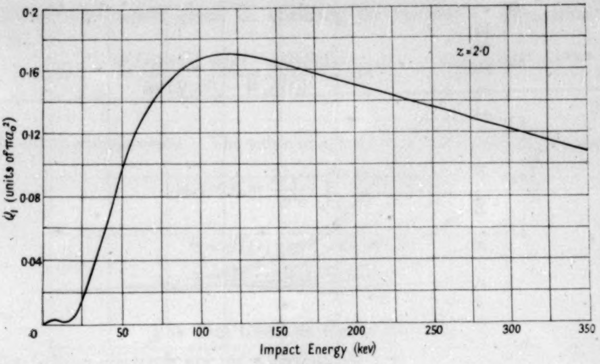

Figure 4.

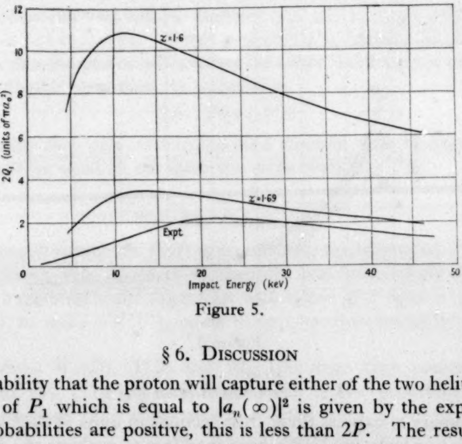

Figure 5.

§ 6. Discussion

The probability that the proton will capture either of the two helium electrons, in the terms of P_1 which is equal to $|a_n(\infty)|^2$ is given by the expression (19). As all the probabilities are positive, this is less than $2P$. The results shown in figure 5 are the cross sections $2Q_1$ obtained by using the first term in the above expression for $z = 1{\cdot}69$ and $1{\cdot}6$. The agreement with experiment is not good, either as regards magnitude or energy for maximum cross section. The shapes of the curves however are similar. If the second term in the above expression is included, the cross sections become negative in some cases and inclusion of the third term increases this effect. The cross section Q_1 however can have no physical significance because many of the probabilities are greater than unity, as was anticipated. However when the $a_n(t)$ are small, the neglect of the effect of intermediate states becomes less important. This is true for large values of the impact parameter Δ. Under these conditions the effects of distortion also become less. Thus the probabilities here calculated should become more exact the larger the value of Δ. Due to the effect of distortion they will always exceed the exact values because $\{W_n - W_0(R)\} < \{W_n(R) - W_0(R)\}$. Denoting by Δ^* the impact parameter for which the probability using the Mott formula becomes unity,

$$|a_n(\infty)|^2{}_{\Delta=\Delta^*} = 1.$$

It follows that if we take

$$P = 1 \qquad 0 < \Delta < \Delta^*$$

$$P = |a_n(\infty)|^2{}_{\Delta} \qquad \Delta^* < \Delta < \infty,$$

then these values are all too high, and a cross section obtained from these values will be too large. This modified cross section 'per electron' we denote by Q_1^*. The cross section $2Q_1^*$ thus gives from these considerations an upper limit to the cross section obtained from the method of perturbed stationary states. Inclusion of the second term in expression (19) in no way affects the subsequent argument. The results, for $z = 1{\cdot}69$ and $z = 1{\cdot}6$, are shown together with experimental results of Hasted and Stedeford (1955) in figure 6. The calculated upper limits are now much smaller than the experimental cross section and remain very sensitive to the value of z chosen. Hasted and Stedeford consider that their results represent a lower limit to the true cross section. It should be noted that all cross section curves approach each other as the proton energy decreases and that the position of the maximum not only agrees very well but is *insensitive* to the value of z chosen.

The effect of having taken the unperturbed form for the final state wave function must now be considered. The perturbed form would multiply the integrand in the expression for M_{0n}' (equation (12)) by $\exp(-l(D)r)$ and in addition would multiply the complete expression by $(\pi)^{1/2}B(D)$. Now as D tends to zero $l(D)$ tends to unity and $(\pi)^{1/2}B(D)$ tends to $(z+1)^{3/2}$ which for $z = 1{\cdot}69$ equals $4{\cdot}4$. As D tends to infinity $l(D)$ tends to zero and $(\pi)^{1/2}B(D)$ tends to unity. The inclusion of $l(D)$ is thus equivalent to taking a larger value of z (now as a function of D). This *reduces* the resulting cross section. Inclusion of the term $B(D)$ would result in a *larger* cross section. As explained however, the calculated transfer probabilities break down for impact parameters less than Δ^*. Furthermore the probability amplitudes involve an integration over D (equation (17)). Consequently, inclusion of the perturbed form for the final state wave function may increase the cross section by a factor which must be less than $4{\cdot}4$. A very rough estimate, by considering the forms of the functions involved, would indicate a factor of not more than two. This by itself would bring the calculated values more into line with experiment. This however is not necessarily significant as all the other approximations tend to give values too high. Work is proceeding to establish the extent to which the various approximations affect the cross sections.

It is not established that the cross section–energy curves approach the origin monotonically outside the range investigated. In view of the subsidiary maximum at low energies for the ionized helium case ($z = 2$) it is possible that a similar effect will occur.

From figure 2 it will be observed that there are certain impact parameters at which $a_n(\infty)$ changes sign. Thus at some impact parameters there is zero probability of capture. At larger distances the probability becomes finite again although the contribution to the cross section from this region is very small. The magnitude of the contribution is however greater than the order of inaccuracy of the computations, so cannot be accounted for in that way. There would seem to be little physical significance in the effect.

Bransden, Dalgarno and King (1954) have calculated the capture cross section for protons in helium using a modified Born approximation. Their results are also shown in figure 6. A rough extrapolation would seem to indicate agreement at high energies with the results obtained here.

The possibility of using the one-body formulation for the determination of capture cross section for more complicated atoms has been mentioned. We still assume that the initial wave function for the target electron in the atom is obtained from the self-consistent field and furthermore that a reasonably accurate approximation is obtained with a constant value of the effective nuclear charge z. In order to obtain an upper limit to the value of the cross section it is only necessary to approximate at large r. The energy at which the maximum cross section occurs, being insensitive to z, will therefore be expected to agree with experiment.

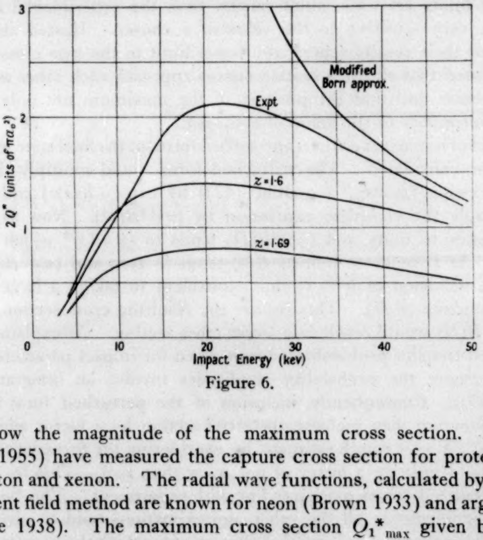

Figure 6.

Consider now the magnitude of the maximum cross section. Hasted and Stedeford (1955) have measured the capture cross section for protons in neon, argon, krypton and xenon. The radial wave functions, calculated by the Hartree self-consistent field method are known for neon (Brown 1933) and argon (Hartree and Hartree 1938). The maximum cross section $Q_1{}^*{}_{\max}$ given by the three values of z chosen for helium may be plotted against z. If now approximations for the effective nuclear charge for neon and argon are made, they may be plotted on the same graph against the experimental maximum cross sections. The approximations are to be made at large r and the observed cross sections are to be divided by the atomic number in each case to give the maximum cross section 'per electron', $Q_{1\max}$. It is assumed that the experiments measure σ–σ transitions. It is found that $z=1{\cdot}58$ gives a reasonably good approximation to the 3s-electron wave function for argon and $z=1{\cdot}77$ gives a good approximation to the 2s-electron wave function for neon. The graph is shown in figure 7. The full line is the theoretical plot obtained from the values of $z=2$, $1{\cdot}69$ and $1{\cdot}6$. The points marked by small circles, refer to the above approximation for argon and neon. The point for helium is similarly obtained by estimating the appropriate value of z to agree with the wave function obtained from the Hartree field at large r. Also shown for comparison are the points, denoted by small triangles, obtained by using the values of z which give the observed ionization energies of the inert gases considered. As expected from the helium results, these latter points do not lie on the theoretical curve. The positions of the other points (circles) for argon and neon however mean that calculations of exactly the same type as used in this investigation would predict accurately the observed cross section as regards magnitude and energy for the maximum and of course as regards the general shape of the energy variation curve which is similar for all the inert gases. This represents better success for the theory in the case of the more complicated atoms argon and neon than in the case of the more simple helium atom.

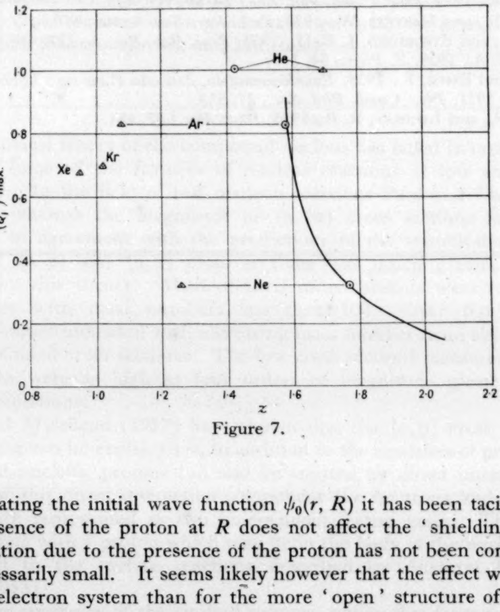

Figure 7.

In calculating the initial wave function $\psi_0(r, R)$ it has been tacitly assumed that the presence of the proton at R does not affect the 'shielding' electron. The polarization due to the presence of the proton has not been considered but it is not necessarily small. It seems likely however that the effect would be less for a many-electron system than for the more 'open' structure of the helium atom.

In order to obtain precise cross sections it would be necessary to use initial and final wave functions which are accurate over the whole collision region, distortion should be taken into account and all the intermediate states should be considered specifically. However the results shown in figure 7 indicate the consistency of the theoretical argument and a reasonable agreement with experiment and demonstrate the possibility of using the one-body formulation of the method of perturbed stationary states, for many-electron systems.

ACKNOWLEDGMENTS

The author wishes to thank Professor E. A. Stewardson for the facilities for carrying out this investigation and Dr. R. O. Davies for helpful discussions about the mathematical analysis.

REFERENCES

BATES, D. R., MASSEY, H. S. W., and STEWART, A. L., 1953, *Proc. Roy. Soc.* A, **216,** 437.
BETHE, H., 1930, *Ann. Phys., Lpz.,* **5,** 325.
BORN, M., and OPPENHEIMER, J. R., 1927, *Ann. Phys., Lpz.,* **84,** 457.
BRANSDEN, B. H., DALGARNO, A., and KING, N. M., 1954, *Proc. Phys. Soc.* A, **67,** 1075.
BROWN, F. W., 1933, *Phys. Rev.,* **44,** 214.
FRAME, J. W., 1931, *Proc. Camb. Phil. Soc.,* **27,** 511.
—— 1937, *Ibid.,* **33,** 115.
FOCK, V., and PETRASHEN, M. J., 1935, *Phys. Z. Sowjet,* **8,** 547.
GAUNT, J. A., 1927, *Proc. Camb. Phil. Soc.,* **23,** 732.
HARTREE, D. R., 1927, *Proc. Camb. Phil. Soc.,* **24,** 89, 111, 426.
HARTREE, D. R., and HARTREE, W., 1938, *Proc. Roy. Soc.* A, **166,** 450.
HASTED, J. B., and STEDEFORD, J. B. H., 1955, *Proc. Roy. Soc.* A, **227,** 466.
HYLLERAAS, E. A., 1929, *Z. Phys.,* **54,** 347.
JAHNKE, E., and EMDE, F., 1938, *Funktionentafeln,* 3rd edn (Leipzig: Teubner), p. 1.
MOTT, N. F., 1931, *Proc. Camb. Phil. Soc.,* **27,** 553.
WILSON, W. S., and LINDSAY, R. B., 1935, *Phys. Rev.,* **47,** 681.

Cross Sections for (n, p) and (n, α) Reactions with 14·5 MeV Neutrons

By R. F. COLEMAN, B. E. HAWKER, L. P. O'CONNOR
AND J. L. PERKIN
Atomic Weapons Research Establishment, Aldermaston, Berks.

Communicated by K. W. Allen; *MS. received* 15*th October* 1958

Abstract. Activation methods have been used to measure twenty-seven (n, p) and twenty-two (n, α) cross sections at 14·5 MeV for target nuclides in the mass range $100 < A < 250$. Radiochemical separations were made in every case.

The (n, p) cross sections fell gradually from 10 to 1 mbn over the mass range examined. No trend was apparent for the (n, α) cross sections measured, which were all of the order of 0·3 to 3·0 mbn.

The (n, p) cross sections are in good agreement with the predictions of the direct interaction theory of Brown and Muirhead.

§ 1. INTRODUCTION

THE statistical theory of the compound nucleus has failed in recent years to explain some of the features of nuclear reactions at low and medium energies. In the field of fast neutron reactions Paul and Clarke (1953) showed that, whereas the magnitude of (n, 2n) cross sections for 14·5 MeV neutrons was in agreement with the predictions of the statistical theory, the magnitude of (n, p) and (n, α) cross sections was much greater than that calculated from this theory. Most of their measurements were restricted to target nuclides with mass numbers less than 100. Over this range the experimental values increased with increasing mass number from about 1 to 100 times the calculated cross sections. The few cross sections measured for heavy target nuclides were as high as four orders of magnitude greater than the theoretical predictions.

Brown and Muirhead (1957) have shown that the (n, p) cross sections of Paul and Clarke can be explained if, in addition to the emission of protons from the compound nucleus, protons can also be emitted by direct interaction. In their theory of this direct interaction component the neutrons and protons in the nucleus are represented as two independent Fermi gases. The incident neutron interacts with a proton which may be in the body of the nucleus. This is in contrast to the surface reactions described by Austern, Butler and McManus (1953).

The energy spectrum of the emitted protons, unlike that from a compound nucleus, consists of a high-energy peak with a maximum energy of $E_n + Q$ where E_n is the energy of the incident neutron and Q is the energy released in the reaction. To calculate the direct (n, p) activation cross sections observed, a low energy cut-off to magnitude $E_n - q$ must be imposed, where q is the binding energy of the last proton in the target nucleus. This ensures that the residual nucleus after proton emission is not left with sufficient excitation to emit a further neutron either directly or later on from a compound nucleus if formed.

For target elements with mass numbers greater than 100 the increasing height of the Coulomb barrier has relatively little effect on the emission of the high energy protons from direct interactions with 14·5 MeV neutrons.

The emission of protons from compound nucleus reactions will, however, be strongly inhibited by the Coulomb barrier and any contribution that these reactions will make to the total (n, p) cross section will be insignificant. We have chosen this target mass region, therefore, to make a survey of (n, p) cross sections at 14·5 MeV and to compare the results obtained with the predictions of Brown and Muirhead's direct interaction theory.

A similar survey of (n, α) cross sections was also made but as yet no direct interaction theory for this reaction is available which will predict precise values for the cross sections.

§ 2. GENERAL METHOD

Only a brief outline of the experimental methods will be given here as most of the procedures used have been described in greater detail in a previous paper concerning radiative capture cross sections for 14·5 MeV neutrons (Perkin, O'Connor and Coleman 1958).

2.1. *Neutron Irradiation*

Fast neutrons were obtained by bombarding a tritiated titanium target with 500 kev deuterons. Neutron emission from the target was maintained at about 10^{10} per second during the course of the experiments. Samples for irradiation were sandwiched between two thin aluminium discs and were placed close to the back of the tritium target.

The ^{27}Al (n, α) ^{24}Na reaction was used to monitor the neutron flux in this close position. In order to calibrate the ^{24}Na activity of the aluminium discs in terms of neutron flux, a separate experiment was performed in which aluminium discs were irradiated in positions of known geometry with respect to a tritium target. The neutron output from this target was found by counting the associated α particles from the (D, T) reaction in a known geometry and at an angle of 135° to the beam. The accuracy of the flux determined in this way was estimated to be about $\pm 3\%$.

2.2. *Chemical Separations*

Because of the variety of other reactions possible, it was essential to separate chemically every (n, p) and (n, α) product.

In general about 100 mg of spectroscopically pure material was used for each irradiation. After irradiation this was dissolved in a suitable solvent and 1 mg of an inactive carrier was added. The desired reaction product was isolated in a pure state using ion exchange, solvent extraction and precipitation reactions. The final solution containing the separated reaction product was divided into two portions, one for the measurement of activity and the other for the determination of the chemical yield of the process. This yield was determined by a suitable colorimetric or microtitration method. In a few cases where no stable carrier was available, tracer amounts of an α-emitting isotope were added. The chemical yield was then determined by measuring the α-activity at the beginning and end of the separation scheme.

2.3. *Counting Techniques*

Counting was usually carried out by mounting the separated reaction product on a $20\,\mu g\,cm^{-2}$ foil and placing in a 4π proportional counter. Since the source weighed only about 0·5 mg the correction for the self-absorption of β particles was in all the cases examined negligible.

In the five cases where α-particle emitting tracers were employed, the 4π proportional counter was not used because of spurious counts caused by the overloading of the counter amplifier by α-particle pulses. An end-window geiger counter with an aluminium foil to prevent the counting of α-particles was used instead. The efficiency of the geiger counter was found with β-particle sources of various energies which had previously been standardized by counting in a 4π proportional counter.

§ 3. POSSIBLE ERRORS

3.1. *Low Energy Neutrons*

Errors in the observed cross sections for 14·5 MeV neutrons due to activation by low energy neutrons present during the irraidation will depend on the intensity of these neutrons and the magnitude of the cross sections at this lower energy. In an earlier paper (Perkin, O'Connor and Coleman 1958) it was concluded that low-energy neutrons of approximately 2 MeV, i.e. (D,D) and lineastically scattered (D,T) neutrons, were present to the extent of approximately 1% of the 14·5 MeV flux. This figure is also valid for the present work as the same irradiation geometry was used. Because of the thresholds of the (n, p) reactions examined (~2 MeV; see Q values in the table), and the height of the Coulomb barrier for heavy elements, it can be concluded that the cross sections measured at 14·5 MeV will be of the same order or greater than the corresponding cross sections in the region of 2 MeV. Thus the correction required to the measured (n, p) cross sections at 14·5 MeV to account for low-energy neutron activation will be approximately 1%, i.e. negligible compared with the other experimental errors.

The same reasoning concerning the low energy neutron corrections for the (n, p) cross sections can be applied to the (n, α) cross sections measured, due account being taken of the increased barrier height for α-particles.

3.2. *(n, pn) Reactions*

The residual activity from an (n, p) reaction with a nuclide (A, Z) can also be produced by an (n, pn) reaction with a nuclide $(A+1, Z)$ if this nuclide is present. This was the case in some 30% of the (n, p) cross sections measured. In order to estimate the possible errors incurred in the (n, p) cross sections, theoretical calculations were made of the magnitude of (n, pn) cross sections for heavy target nuclides. This was done by calculating the number of protons emitted from a nucleus with energies less than $E_n - q$, the low energy cut-off mentioned in the Introduction. Values of the order of 3% of the corresponding (n, p) cross section were obtained. This was confirmed experimentally in one case.

In view of these results it was assumed generally that the activity resulting from (n, pn) reactions was too small to cause any significant errors in the (n, p) cross sections measured.

3.3. *(n, pp) Reactions*

In some 60% of the (n, α) cross section experiments with a target nuclide (A, Z) the residual activity measured could also have resulted from (n, pp) reactions with a target nuclide $(A-2, Z)$. However, the direct ejection of a proton from the nucleus will leave it with such a low excitation energy that the probability that a second proton will penetrate the Coulomb barrier is very small. The cross section for the (n, pp) reaction will certainly be much less than that for the (n, pn) reaction which is itself small relative to either the (n, p) or (n, α) cross sections observed. No corrections were made therefore to the (n, α) cross sections as measured to allow for (n, pp) reactions.

§ 4. RESULTS AND DISCUSSION

4.1. *(n, p) Cross Sections*

The results obtained are shown in the table and figure 1. The standard deviation errors quoted are due mainly to the counting statistics of the residual activity and the uncertainties in the neutron flux and chemical yield determinations. In figure 1 the cross sections are plotted as a function of the neutron number of the target nuclide. Cross sections reported in the literature for lighter elements are also included for comparison.

(n, p) cross sections						(n, α) cross sections			
(1)	(2)	(3)	(4)	(5)	(6)	(1)	(2)	(3)	(4)
^{109}Ag	12·5[1]	15	−0·31	21·8	0·57	^{115}In	2·89[7]	10	2·94
^{115}In	15·5	25	−0·67	19·0	0·82	^{130}Te	0·37	15	1·25
^{127}I	11·7[2]	15	−0·02	18·5	0·63	^{133}Cs	1·9[8]	10	4·19
^{136}Ba	38·3	10	−1·51	9·3	4·1	^{139}La	1·87	10	4·97
^{138}Ba	2·2[3]	15	−4·06	3·0	0·73	^{142}Ce	7·04	10	5·65
^{139}La	2·33[4]	15	−1·6	9·3	0·25	^{146}Nd	2·6	15	6·67
^{140}Ce	12·1	10	−3·01	4·8	2·5	^{156}Gd	3·22	15	5·48
^{142}Ce	9·4	10	−4·19	2·35	4·0	^{162}Dy	3·56	10	5·15
^{142}Nd	13·5	20	−1·38	9·5	1·42	^{178}Hf	2·0	10	6·73
^{143}Nd	11·5	20	−0·15	13·7	0·84	^{187}Re	0·94	15	7·40
^{153}Eu	7·4	10	−0·25	12·1	0·61	^{190}Os	0·57	15	9·36
^{157}Gd	11·3	15	−0·92	5·1	2·2	^{191}Ir	2·43	15	9·43
^{175}Lu	3·42	15	−0·31	7·4	0·46	^{194}Pt	1·26	20	7·09
^{184}W	4·75	20	−2·59	2·2	2·2	^{196}Pt	0·55	20	5·24
^{186}W	2·9	20	−3·44	1·4	2·1	^{197}Au	0·43	10	6·69
^{187}Re	3·93	10	−0·53	5·3	0·74	^{200}Hg	1·77	20	7·21
^{193}Ir	2·7	20	−0·31	6·8	0·40	^{202}Hg	1·01	10	4·07
^{194}Pt	3·92	10	−1·32	3·4	1·15	^{203}Tl	0·37	10	6·22
^{195}Pt	2·91	10	−1·45	2·9	1·0	^{208}Pb	1·58	15	5·95
^{197}Au	2·42[5]	10	+0·03	6·4	0·38	^{209}Bi	0·52[9]	15	9·74
^{200}Hg	3·63	10	−1·52	3·0	1·21	^{230}Th	4·6	25	9·15
^{201}Hg	2·12	15	−0·71	3·9	0·55	^{238}U	1·5	20	8·76
^{205}Tl	6·8[6]	10	−0·97	2·6	2·6				
^{209}Bi	1·33	20	+0·15	7·2	0·19				
^{235}U	1·86	20	−0·62	5·1	0·37				
^{237}Np	1·3	25	+0·27	3·3	0·4				
^{239}Pu	3·0	15	+0·07	3·3	0·91				

(1) Target nuclide; (2) observed cross section (mbn); (3) standard deviation (%); (4) Q-value (MEV); (5) calculated cross section (mbn); (6) ratio $\sigma_{\text{obs}}/\sigma_{\text{calc.}}$

Previous determinations of (n, p) and (n, α) cross sections in the present target mass range

[1]	10·5 ± 2·0 mbn	Dvantiev *et al.* (1957)	[5]	20·5 ± 8 mbn	Peck (1957)
[2]	> 230 ± 140 mbn	Paul and Clarke (1953)	[6]	3·05 ± 1·5 mbn	Paul and Clarke (1953)
[3]	6·3 ± 2 mbn	Paul and Clarke (1953)	[7]	2·5 ± 0·4	Blosser *et al.* (1955)
[4]	5·7 ± 2·5 mbn	Paul and Clarke (1953)	[8]	1·0 ± 0·3	Blosser *et al.* (1955)
			[9]	1·2 ± 1	Paul and Clarke (1953)

The outstanding feature of the (n, p) cross sections for heavy nuclides is the relatively smooth downward trend from 10 mbn to 1 mbn over the mass range 100 to 250. This is in marked contrast to the cross sections in the mass range 0 to 100 where there is no general trend and the individual values are scattered over the range of approximately 10 to 400 mbn. A few cross sections lie well away from the general trend of values for heavy nuclides. These occur near the closed neutron shells of 82 and 126. Relatively high values are found just before the closed shells and low values at the closed shells.

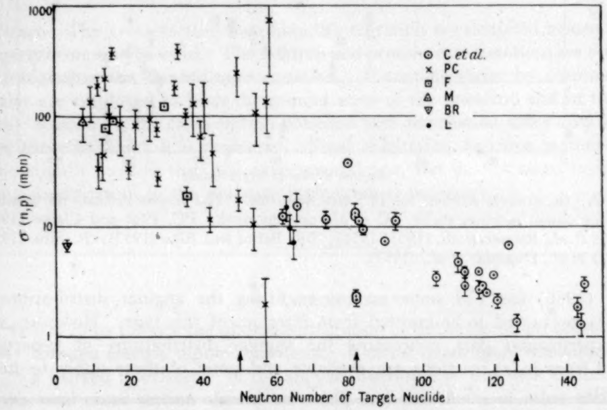

Figure 1. (n,p) cross sections for 14·5 MeV neutrons. The arrows indicate the positions for closed neutron shells. C *et al.*, present work; PC, Paul and Clarke (1953); F, Forbes (1952); M, Martin (1954); BR, Battat and Ribe (1953); L, Levkovskii (1957).

We have calculated for each experimentally observed (n, p) reaction the cross section predicted by the direct interaction theory of Brown and Muirhead. The result of these calculations are given in the table. The observed and calculated cross sections agree to within a factor of two for most of the reactions examined. In addition there does not appear to be any systematic change in the agreement over the mass range measured. These facts can be considered as good evidence for the type of direct mechanism that Brown and Muirhead envisage.

4.2. (*n*, α) *Cross Sections*

The results obtained are shown in the table and figure 2. Practically all the (n, α) sections measured lie between the limits 0·3 to 3·0 mbn. No obvious trend in the values is apparent, nor is it possible to state definitely whether or not shell structure has any effect on the cross sections.

The evidence of Paul and Clarke for the failure of the statistical theory of the compound nucleus to account for the (n, α) cross sections observed for 14·5 MeV neutrons and heavy elements implies that these reactions proceed via a direct process. The exact nature of this mechanism is at the moment unknown.

As the mean free path of a fast α-particle in nuclear matter is smaller than that of a proton, the (n, α) reactions observed will originate in the nuclear surface.

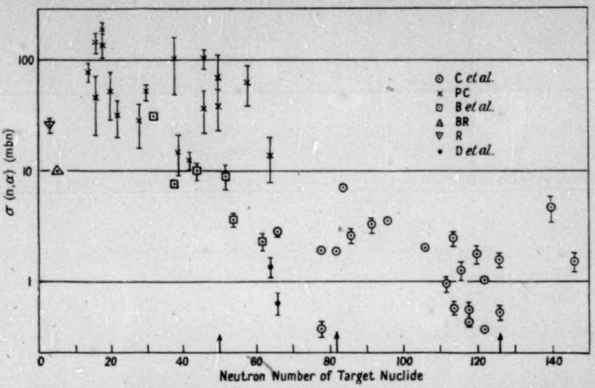

Figure 2. (n, α) cross sections for 14·5 MeV neutrons. The arrows indicate the positions for closed neutron shells. C *et al.*, present work; PC, Paul and Clarke (1953); B *et al.*, Blosser *et al.*, (1955, 1958); BR, Battat and Ribe (1953); R, Ribe (1956); D *et al.*, Dvantiev *et al.*, (1957).

Butler (1956) has had some success in fitting the angular distributions of particles presumed to be emitted from reactions of this type. However, very few experimental data concerning the angular distributions of α-particles emitted from (n, α) reactions are available and none of these apply to heavy elements.

ACKNOWLEDGMENTS

We are indebted to Dr. G. Brown and Dr. H. M. Muirhead for making available to us their direct interaction computations. These greatly facilitated our own calculations. We are especially grateful to Dr. H. M. Muirhead for helpful discussion and correspondence.

We also wish to thank Messrs. J. Prosser, A. L. Garraway and B. Smith who assisted in the irradiation and counting of the samples, and the operators of the A.W.R.E. 800 kv Cockcroft–Walton Accelerator.

REFERENCES

AUSTERN, N., BUTLER, S. T., and MCMANUS, H., 1953, *Phys. Rev.*, **92,** 351.

BATTAT, M. E., and RIBE, F. L., 1953, *Phys. Rev.*, **89,** 80.

BLOSSER, H. G., GOODMAN, C. D., and HANDLEY, T. H., 1958, *Phys. Rev.*, **110,** 531.

BLOSSER, H. G., GOODMAN, C. D., HANDLEY, T. H., and RANDOLPH, M. L., 1955, *Phys. Rev.*, **100,** 429.

BROWN, G., and MUIRHEAD, H., 1957, *Phil. Mag.*, 2, **16,** 472.

BUTLER, S. T., 1956, *Phys. Rev.*, **106,** 272.

DVANTIEV, B. G., LEVKOSSKII, V. N., and MALIEVSKII, A. D., 1957, *Proc. Acad. Sci. U.S.S.R.*, **113,** 537.

FORBES, S. G., 1952, *Phys. Rev.*, **88,** 1309.

LEVKOVSKII, V. N., 1957, *Proc. Acad. Sci. U.S.S.R.*, **113,** 1032.

MARTIN, H. G., 1954, *Phys. Rev.*, **93,** 498.

PAUL, E. B., and CLARKE, R. L., 1953, *Canad. J. Phys.*, **31,** 267.

PECK, R. A., 1957, *Phys. Rev.*, **106,** 965.

PERKIN, J. L., O'CONNOR, L. P., and COLEMAN, R. F., 1958, *Proc. Phys. Soc.*, **72,** 505.

RIBE, F. L., 1956, *Phys. Rev.*, **103,** 741.

Photodisintegration of the Deuteron at 130 MeV

By A. F. NICHOLSON† and G. E. BROWN

Department of Mathematical Physics, University of Birmingham

Communicated by R. E. Peierls; MS. received 12th September 1958

Abstract. The cross section for photodisintegration is calculated assuming the Siegert theorem to be valid. The neutron and proton wave functions are obtained by integrating the Schrödinger equation. Potentials given by Gammel and Thaler are employed in both the ground state of the deuteron and in the final state. Results for the cross section obtained with retardation differ only slightly from those in which it is neglected. Final results for the cross section give a value slightly smaller than the experimental one, but do not seem to indicate that a modification in the radiative interaction is necessary.

§ 1. INTRODUCTION

FROM 20 to 150 MeV the photodisintegration of the deuteron proceeds mainly through electric dipole transitions. Electric quadrupole transitions cause a marked interference in the angular distributions but their contributions to the total cross section should be small, and the effects of other transitions should be negligible (Schiff 1950, Marshall and Guth 1950). If the observed angular distribution is folded about 90° in the centre-of-mass system, the cross section takes the form

$$\frac{d\sigma(\theta)}{d\Omega}=a+b\sin^2(\theta) \qquad \ldots\ldots(1)$$

so that

$$\sigma_{\mathrm{T}}=4\pi a+\frac{8\pi}{3}b=A+B. \qquad \ldots\ldots(2)$$

It is well known that A would vanish if the forces acting between neutron and proton were purely central. Experimentally, A is found to be nearly constant at about 50 μbn from 20 MeV to 250 MeV, while B decreases from about 500 μbn for 20 MeV photons to 10 μbn at 150 MeV and remains near that value to 250 MeV. Above 60 MeV, A is dominant (Keck and Tollestrup 1956, Whalin, Schriever and Hanson 1956). Earlier attempts to account for this behaviour (e.g. Austern 1952, Fujimura 1953, Yamaguchi and Yamaguchi 1954, 1955, Zachariasen 1956, Bernstein 1957) were not very successful and led Wilson (1952, 1956) to suggest a specific model in which part of the photodisintegration goes by way of production and annihilation of virtual s-wave mesons. Austern (1957) argued that such a model is necessary and that the Siegert theorem is inapplicable above 20 MeV.

It is, however, clear that in the static limit, the process required by these authors is taken completely into account by the renormalized mass and static interaction between the proton and neutron,† since it is part of the self-interaction of the two-particle system. Work of Gammel and Thaler (1957 a, b) indicated that the nucleon–nucleon scattering could be fitted up to 300 Mev by a static potential plus spin–orbit interaction. Since previous qualitative arguments from the Born expansion indicated that the final state interaction between neutron and proton was of great importance, and calculations with simple forces by one of us (A. F. N.) bore out this conclusion, we decided to calculate the photo-disintegration of the deuteron using wave functions for both initial and final states which are solutions in the Gammel–Thaler potentials.

---

† Now at Weapons Research Establishment, South Australia.

We carried out calculations of $d\sigma(\theta)/d\Omega$ for a centre-of-mass energy of 120 Mev, which corresponds to a photon energy of 130 Mev in the laboratory system, and to nucleon–nucleon scattering with a laboratory energy of 248 Mev (240 Mev if the transformation is made non-relativistically).

While this work was in process, we received results obtained by de Swart and Marshak (1958), who have been able to fit the experimental photo-disintegration data very nicely within the above framework for photon energies of 22, 54 and 80 Mev, employing the potentials of Signell and Marshak (1957, 1958). Further results obtained by de Swart (private communication) indicate that calculations at an energy of 150 Mev give too low a cross section.

§ 2. Method of Calculation

The triplet even-parity potential for the initial state was taken to be

$$\begin{aligned} {}^3V^+(r) &= \infty \qquad r<r_0^+, &\ldots\ldots(3)\\ &= -\frac{V_{\rm C}^+\exp(-\mu_{\rm C}^+ r)}{\mu_{\rm C}^+ r} - S_{12}\frac{V_{\rm T}^+\exp(-\mu_{\rm T}^+ r)}{\mu_{\rm T}^+ r}, \quad r>r_0^+, \end{aligned}$$

where

$$r_0^+ = 0{\cdot}4\ \mathrm{f},$$
$$V_{\rm C}^+ = 100{\cdot}7\ \mathrm{Mev}, \qquad \mu_{\rm C}^+ = 1{\cdot}230\ \mathrm{f}^{-1},$$
$$V_{\rm T}^+ = 257\ \mathrm{Mev}, \qquad \mu_{\rm T}^+ = 1{\cdot}203\ \mathrm{f}^{-1},$$

and S_{12} is the tensor force operator. This potential is No. 4 of a set of possible ground-state potentials given by Gammel, Christian and Thaler (1957), and was chosen from that set for the present calculations because of its consistency with the results of the later analyses by Gammel and Thaler (1957 a, b) of nucleon–nucleon scattering up to 310 Mev. However, the high-energy analyses led to the inclusion of spin–orbit forces in all states. The presence of such a strong short-range spin–orbit interaction in even $T=0$ states does not, however, seem to be clearly indicated (de Swart, Signell and Marshak 1957) and, in any case, would have little influence, since it acts only in the d-state‡ and even here would be partially masked by the centrifugal barrier.

With the potential of equation (3) the deuteron wave function has the form

$$\psi_{\rm D} = \frac{N}{r\sqrt{(4\pi)}}\left(u(r)+\tfrac{1}{4}w(r)S_{12}\right)\chi_1^{\,m} \qquad \ldots\ldots(4)$$

---

†Recently, L. D. Pearlstein and A. Klein (private communication) have shown that in a consistent formulation of the problem in field theory, another process, not considered by Wilson and Austern, just cancels the contribution they consider, in the static limit.

‡ To avoid confusion we employ small letters (s and d) when referring to the initial state, and capital ones (P and F) when referring to the final state.

with N chosen so that u is asymptotically $\exp(-\gamma r)$. (This definition of w differs trivially from the usual one.)

The triplet odd-parity potential for the final state is taken to be (Gammel and Thaler 1957 a)

$$
\begin{aligned}
3V^-(r) &= \infty, \quad r < r_0 \\
&= -S_{12}V_T^-\left(1-\frac{r_0^-}{r}\right)\frac{\exp(-\mu_T^- r)}{\mu_T^- r} - \mathbf{L}.\mathbf{S}V_{LS}^-\exp(-\mu_{LS}^- r), \qquad r > r_0
\end{aligned}
\qquad \ldots\ldots(5)
$$

where

$$
\begin{gathered}
r_0^- = 0{\cdot}4125\,\text{f}, \\
V_T^- = -26\,\text{Mev}, \qquad \mu_T^- = 0{\cdot}80\,\text{f}^{-1}, \\
V_{LS}^- = 7122{\cdot}5\,\text{Mev}, \; \mu_{LS}^- = 3{\cdot}70\,\text{f}^{-1},
\end{gathered}
$$

and **L . S** is the spin–orbit operator.

For electric dipole transitions with these forces, the final state will be a sum of $^3P_0$, $^3P_1$ and coupled $^3P_2$ and $^3F_2$ waves, for which the radial wave functions (multiplied by kr) are asymptotically

$$
\left.
\begin{aligned}
v_{0,1}(r) &= \sin\left(kr-\frac{\pi}{2}+\delta_{0,1}\right) \\
v_{2\alpha}(r) &= \cos\epsilon\sin\left(kr-\frac{\pi}{2}+\delta_\alpha\right) \\
v_{F\alpha}(r) &= \sin\epsilon\sin\left(kr-\frac{3\pi}{2}+\delta_\alpha\right) \\
v_{2\beta}(r) &= -\sin\epsilon\sin\left(kr-\frac{\pi}{2}+\delta_\beta\right) \\
v_{F\beta}(r) &= \cos\epsilon\sin\left(kr-\frac{3\pi}{2}+\delta_\beta\right)
\end{aligned}
\right\} \qquad \ldots\ldots(6)
$$

where δ_α and δ_β are the eigenphase shifts and ϵ is the mixing parameter for the $^3P_2$ and $^3F_2$ waves (Blatt and Biedenharn 1952).

The cross section parameters A and B are given by the expressions (Czyz and Sawicki, to be published):

$$
\begin{aligned}
A = C(k)\{&\tfrac{2}{3}L_0^2+\tfrac{3}{2}L_1^2+J_\alpha^2+J_\beta^2+2J_\alpha J_\beta\cos(\delta_\alpha-\delta_\beta)+Z_\alpha^2+Z_\beta^2 \\
&+2Z_\alpha Z_\beta\cos(\delta_\alpha-\delta_\beta)+\sqrt{6}L_1[J_\alpha\cos(\delta_1-\delta_\alpha)+J_\beta\cos(\delta_1-\delta_\beta)] \\
&+\tfrac{2}{3}\sqrt{6}L_0[Z_\alpha\cos(\delta_0-\delta_\alpha)+Z_\beta\cos(\delta_0-\delta_\beta)]\},
\end{aligned}
\qquad \ldots\ldots(7)
$$

$$
\begin{aligned}
B = C(k)\{&\tfrac{1}{2}L_1^2+\tfrac{1}{3}[J_\alpha^2+J_\beta^2+2J_\alpha J_\beta\cos(\delta_\alpha-\delta_\beta)]+Z_\alpha^2+Z_\beta^2 \\
&+2Z_\alpha Z_\beta\cos(\delta_\alpha-\delta_\beta)-\sqrt{6}L_1[J_\alpha\cos(\delta_1-\delta_\alpha)+J_\beta\cos(\delta_1-\delta_\beta)] \\
&-\tfrac{2}{3}\sqrt{6}L_0[Z_\alpha\cos(\delta_0-\delta_\alpha)+Z_\beta\cos(\delta_0-\delta_\beta)]\},
\end{aligned}
\qquad \ldots\ldots(8)
$$

where

$$
C(k) = \frac{1}{72}\frac{e^2}{\hbar c}\frac{kE_\gamma}{(E_\gamma-E_B)}N^2, \qquad \ldots\ldots(9)
$$

E_γ being the photon energy and k, the relative final-state momentum, both in the centre-of-mass system, and E_{B} the deuteron binding energy. The other quantities are defined by

$$\left.\begin{aligned}
J_{\alpha} &= (-\sqrt{\tfrac{3}{2}}\cos\epsilon+\sin\epsilon)(L_{2\alpha}+\sqrt{\tfrac{3}{2}}L_{\mathrm{F}\alpha}) \\
J_{\beta} &= (\cos\epsilon+\sqrt{\tfrac{3}{2}}\sin\epsilon)(L_{2\beta}+\sqrt{\tfrac{3}{2}}L_{\mathrm{F}\beta}) \\
Z_{\alpha} &= -(\cos\epsilon+\sqrt{\tfrac{3}{2}}\sin\epsilon)(\sqrt{\tfrac{2}{3}}L_{2\alpha}+L_{\mathrm{F}\alpha}) \\
Z_{\beta} &= (-\sqrt{\tfrac{3}{2}}\cos\epsilon+\sin\epsilon)(\sqrt{\tfrac{2}{3}}L_{2\beta}+L_{\mathrm{F}\beta})
\end{aligned}\right\} \qquad \ldots\ldots(10)$$

where, assuming the Siegert theorem to be valid,

$$\left.\begin{aligned}
L_0 &= \int_0^\infty (u-w)v_0 f(pr)r\,dr \\
L_1 &= \int_0^\infty (u+\tfrac{1}{2}w)v_1 f(pr)r\,dr \\
L_{2\alpha,\,2\beta} &= \int_0^\infty (u-\tfrac{1}{10}w)v_{2\alpha,\,2\beta} f(pr)r\,dr \\
L_{\mathrm{F}\alpha,\,\mathrm{F}\beta} &= \tfrac{3}{5}\int_0^\infty wv_{\mathrm{F}\alpha,\,\mathrm{F}\beta} f(pr)r\,dr
\end{aligned}\right\} \qquad \ldots\ldots(11)$$

where the function $f(pr)$ describes the effect of retardation in electric transitions. Using the general formulae for electric transitions given by Austern and Sachs† (1951) one easily finds that the appropriate form of f is

$$f(pr)=\int_0^1 dy\,\mathrm{j}_0(ypr) \qquad \ldots\ldots(11.1)$$

where j_0 is the spherical Bessel function. Although pr is rather small over the region of the main contribution in equation (11), it is not clear that one can expand $f(pr)$ in a power series in pr, keeping only the first terms, without substantial errors because of contributions from large distances. We have evaluated the integrals, equation (11), for two cases, taking $f(pr)=1$ and $f(pr)=\mathrm{j}_0(pr)$, i.e. for the two end points of the integration, equation (11.1). The former choice corresponds to neglect of retardation; the values coming from the latter will be referred to as 'retarded' in inverted commas, because to obtain the true retarded values, one should evaluate the integrals for several values of y lying between 0 and 1 and then average over these. Since, however, with the extreme value of y the results differed only little from the unretarded ones, we have not bothered to do this, since it is clear that the effect of retardation is not important.

§ 3. RESULTS AND DISCUSSION

The wave functions were found by numerical integration of the wave equations. The ground state was found to contain 6·6% of d-state, and the phase shifts were found to check with those of Gammel and Thaler.

The table displays the values of the transition amplitudes which were obtained using these wave functions in equations (10) and (11). The amplitudes are shown split into their s- and d-parts, which arise from the u and w functions, respectively, in the definitions (11).

---

† See Sachs (1953), p. 239, for a simple discussion of this.

	‘Retarded’			Unretarded		
	Total	s-part	d-part	Total	s-part	d-part
100 L_0	1·86	6·04	−4·19	1·72	5·80	−4·08
100 L_1	11·40	8·68	2·72	11·10	8·46	2·64
100 $L_{2\alpha}$	2·87	3·18	−0·31	2·56	2·89	−0·33
100 $L_{F\alpha}$	−0·91	—	−0·91	−0·96	—	−0·96
100 $L_{2\beta}$	1·57	1·66	−0·09	1·94	1·83	0·11
100 L_{F_β}	5·87	—	5·87	6·20	—	6·20
100 J_α	−2·31	−4·18	1·87	−1·82		
100 J_β	7·72	1·46	6·25	8·39		
100 Z_α	−1·26	−2·29	1·02	−1·00		
100 Z_β	−9·40	−1·78	−7·62	−10·22		

When these values are inserted in equations (7) and (8), the ‘retarded’ cross section parameters are found to have the values $A=36{\cdot}6\,\mu$bn, $B=5{\cdot}8\,\mu$bn, whereas if retardation is ignored the results are only slightly different, viz. $A=39{\cdot}8\,\mu$bn, $B=5{\cdot}0\,\mu$bn. These figures should be compared with the experimental values of about $A=44\,\mu$bn, $B=13\,\mu$bn (Whalin, Schriever and Hanson 1956, Keck and Tollestrup 1956).

It can be seen that the predicted cross section at 120 MEV is somewhat smaller than the experimental value. This is not surprising, since effects from virtual p-wave meson production, although small, are not negligible at this energy (Zachariasen 1956) and should be included before comparison with experiment is made. Our cross section is, however, more than double that obtained by Marshall and Guth (1950) and Schiff (1950) and we obtain a large isotropic term, indicating that the neutron–proton interaction in the final state is of primary importance in determining the form and magnitude of the cross section. It is also clear that it is not necessary to modify the dipole radiative interaction, at least not as drastically as proposed by Austern and Wilson.

The importance of including all of the electric dipole transitions has been stressed by de Swart and Marshak (1958). We can illustrate this in our case by giving results which would be obtained in two special cases if certain transitions were left out:

(1) Transitions to F-states omitted: $A=13{\cdot}0\,\mu$bn, $B=10{\cdot}9\,\mu$bn.

(2) Transitions from the d-state omitted: $A=5{\cdot}1\,\mu$bn, $B=11{\cdot}1\,\mu$bn.

We note, finally, that our calculations have shown the effect of retardation to be relatively unimportant, even at this high energy.

ACKNOWLEDGMENTS

We would like to thank Professor R. E. Peierls for encouragement and advice. We are grateful to Mr. J. Stuttard for assistance with the numerical work. One of us (A. F. N.) would like to thank the Australian National University for the award of a scholarship. The other author (G. E. B.) is grateful to the Institute for Theoretical Physics, University of Copenhagen, for hospitality and support during his stay there.

References

Austern, N., 1952, *Phys. Rev.*, **85**, 283; 1957, *Ibid.*, **108**, 973.

Austern, N., and Sachs, R. G., 1951, *Phys. Rev.*, **81**, 705.

Bernstein, J., 1957, *Phys. Rev.*, **106**, 791.

Blatt, J. M., and Biedenharn, L. C., 1952, *Phys. Rev.*, **86**, 399.

Fujimura, J., 1953, *Progr. Theor. Phys.*, **9**, 132.

Gammel, J. L., Christian, R. S., and Thaler, R. M., 1957, *Phys. Rev.*, **105**, 311.

Gammel, J. L., and Thaler, R. M., 1957 a, *Phys. Rev.*, **107**, 291; 1957 b, *Ibid.*, **107**, 1337.

Keck, J. C., and Tollestrup, A. V., 1956, *Phys. Rev.*, **101**, 360.

Marshall, J. F., and Guth, E., 1950, *Phys. Rev.*, **78**, 738.

Sachs, R. G., 1953, *Nuclear Theory*, (Cambridge, Mass.: Addison-Wesley).

Schiff, L. I., 1950, *Phys. Rev.*, **78**, 733.

Signell, P. S., and Marshak, R. E., 1957, *Phys. Rev.*, **106**, 832; 1958, *Ibid.*, **109**, 1229.

de Swart, J. J., and Marshak, R. E., 1958, *Phys. Rev.*, **111**, 272.

de Swart, J. J., Signell, P. S., and Marshak, R. E., 1957, *Nuovo Cim.*, **6**, 1189.

Whalin, E. A., Schriever, B. D., and Hanson, A. O., 1956, *Phys. Rev.*, **101**, 377.

Wilson, R. R., 1952, *Phys. Rev.*, **86**, 125; 1956, *Ibid.*, **104**, 218.

Yamaguchi, Y., and Yamaguchi, Y., 1954, *Phys. Rev.*, **95**, 1635; 1955, *Ibid.*, **98**, 69.

Zachariasen, F., 1956, *Phys. Rev.*, **101**, 371.

Importance of Distortion in Inelastic Encounters Between Heavy Systems

By D. R. BATES

Department of Applied Mathematics, The Queen's University of Belfast

MS. received 11*th September* 1958

Abstract. It is shown that distortion may have a considerable influence on excitation and ionization cross sections even at quite high energies. Using an impact parameter treatment detailed calculations are carried out on the collision processes $H^+ + H(1s) \rightarrow H^+ + H(2s)$ and $He^{2+} + H(1s) \rightarrow He^{2+} + H(2s)$. The introduction of allowance for distortion is found to lead to much smaller cross sections at low and moderate energies.

§ 1. Introduction

It was originally hoped that collisions between atoms and ions at low and moderate energies could in principle be satisfactorily treated by means of the perturbed stationary state approximation in which the complete wave function of the colliding systems is expanded in terms of the electronic wave functions these systems would have if the nuclei were held fixed in position. (Mott and Massey 1949, Bates, Massey and Stewart 1953). Recent work (Bates 1957, 1958) has, however, revealed that the perturbed stationary state approximation has very serious defects which make the realization of the original hopes impossible. At present there is no alternative general approximation designed for low and moderate energies. Consequently, it is desirable to attempt to refine the standard high energy approximation of Born so as to extend its range of validity. With this aim in view the introduction of allowance for distortion will be examined.

§ 2. Theory†

The impact energy below which Born's approximation is unreliable naturally depends on the particular collision process concerned and cannot be specified simply, but its value is likely to be of the order of 100 kev in the case of excitation or ionization of atoms by incident protons (and proportionally larger if the incident particles are more massive). It might be thought at first that the distortion arising from an interaction potential of perhaps only about 10 ev could not have an appreciable effect at the impact energy mentioned, and therefore that the failure must be due to some other cause. However, the effect of distortion cannot be dismissed so readily. In Born's approximation the integrand of the transition matrix element contains a term of the form $\exp[i\mathbf{R} . (K_i\mathbf{n}_i - K_f\mathbf{n}_f)]$ where $\mathbf{R}$ is the relative position vector of the nuclei, K_i and K_f are the magnitudes of the wave numbers of the relative motion before and after the transition and $\mathbf{n}_i$ and $\mathbf{n}_f$ are unit vectors in the directions of incidence and of scattering respectively. Since K_i and K_f are extremely large compared with unity and since the difference between them is minute, the main contribution to the transition matrix element arises when $\mathbf{n}_f$ is almost parallel to $\mathbf{n}_i$, that is from encounters in which very little deviation occurs. Approximate account may be taken of distortion by replacing K_i by an almost equal quantity $\kappa_i(\mathbf{R})$ which depends on the initial interaction potential, and by replacing K_f by an almost equal quantity $\kappa_f(\mathbf{R})$ which depends on the final interaction potential. In spite of these very close equalities it is clear that $[\kappa_i(\mathbf{R})-\kappa_f(\mathbf{R})]$ may differ considerably from $[K_i-K_f]$ so that distortion may greatly influence the transition matrix element.

---

† Atomic units are used except where otherwise stated.

The detailed study of the problem can most conveniently be carried out in the impact parameter formulation.

Let the target system be located at the origin of coordinates and let the incident system move with constant velocity v in the positive direction along a line distant ρ from the Z axis. The electronic wave function may be represented by the exapansion

$$\Psi(\mathbf{r},t)=\sum_n a_n(t)\phi_n(\mathbf{r})\exp(-i\epsilon_n t) \qquad \ldots\ldots(1)$$

in which $\mathbf{r}$ denotes the position vector of the active electron and t the time, and in which $\phi_n(\mathbf{r})$ and ϵ_n are the unperturbed eigenfunctions and eigenenergies of the target system in the state indicated by the subscript, so that

$$\mathscr{H}\ \phi_n(\mathbf{r})=\epsilon_n\phi_n(\mathbf{r}) \qquad \ldots\ldots(2)$$

where $\mathscr{H}$ is the Hamiltonian. Reminders of the dependence of the coefficients $a_n(t)$ on ρ and v are omitted. If $v(\mathbf{r},\mathbf{R})$ is the instantaneous interaction potential when the position vector of the incident system is $\mathbf{R}$ then

$$\{\mathscr{H}+v(\mathbf{r},\mathbf{R})\}\Psi(\mathbf{r},t)=i\frac{\partial}{\partial t}\Psi(\mathbf{r},t). \qquad \ldots\ldots(3)$$

Proceeding in the customary manner by substituting (1) in (3) and using (2) and the orthonormal property of the ϕ_n's it may be shown that

$$i\frac{\partial}{\partial Z}a_n(Z)=\frac{1}{v}\sum_s a_s(Z)V_{ns}\exp[-i\alpha_{sn}Z], \qquad \ldots\ldots(4)$$

with

$$V_{ns}=\int\phi_n{}^*(\mathbf{r})v(\mathbf{r},\mathbf{R})\phi_s(\mathbf{r})d\mathbf{r} \qquad \ldots\ldots(5)$$

$$\alpha_{sn}=(\epsilon_s-\epsilon_n)/v \qquad \ldots\ldots(6)$$

and with the zero of time chosen so that

$$Z=vt. \qquad \ldots\ldots(7)$$

If the initial conditions in (4) are taken to be

$$a_0(-\infty)=1,\quad a_s(-\infty)=0\quad (s\neq 0), \qquad \ldots\ldots(8)$$

the cross section describing excitation from state 0 to state n is (Mott 1931)

$$Q_{0n}=2\pi\int_0^\infty |a_n(\infty)|^2\rho d\rho \qquad (a_0{}^2). \qquad \ldots\ldots(9)$$

A first approximation to the required solution of (4) may be obtained by assuming that $a_0(Z)$ is unity and that the other coefficients $a_s(Z)$ $(s\neq 0)$ are so small that terms involving them may be neglected. This yields

$$ia_n(\infty)=\frac{1}{v}\int_{-\infty}^{\infty}V_{n0}\exp[-i\alpha_{0n}Z]dZ, \qquad \ldots\ldots(10)$$

which is the impact parameter version of the Born approximation (Frame 1931).

Two related improvements can readily be made. Instead of taking $a_0(Z)$ equal to unity, it is clearly better to take

$$a_0(Z) = \exp\left[-\frac{i}{v}\int_0^Z V_{00}\,dZ \right] \qquad \ldots\ldots(11)$$

since when terms involving $a_s(Z)$ $(s \neq 0)$ are neglected the relevant differential equation reduces to

$$i\frac{\partial}{\partial Z}a_0(Z) = \frac{1}{v}a_0(Z)V_{00}. \qquad \ldots\ldots(12)$$

Further, the term $a_n(Z)V_{nn}/v$ on the right-hand side of (4) does not, like the the other terms, contain a complex oscillatory factor and therefore may be important even though $a_n(Z)$ is very small (cf. Kramers 1957). Retaining this term (which allows for distortion in state n) and substituting from (11) (which allows for distortion in state 0) it is seen that (4) becomes

$$i\frac{\partial}{\partial Z}a_n(Z) = \frac{1}{v}\left\{ V_{nn}a_n(Z) + V_{n0}\exp\left[-i\alpha_{0n}Z - \frac{i}{v}\int_0^Z V_{00}\,dZ \right] \right\}. \qquad \ldots\ldots(13)$$

On solving (13) it is found that

$$ia_n(\infty) = \frac{1}{v}\int_{-\infty}^{\infty} V_{n0}\exp\left[-i\alpha_{0n}Z - i\beta_{0n} \right]dZ \qquad \ldots\ldots(14)$$

where

$$\beta_{0n} = \frac{1}{v}\int_0^Z (V_{00} - V_{nn})\,dZ. \qquad \ldots\ldots(15)$$

Detailed balancing is, of course, satisfied. This *distortion approximation* differs appreciably from the Born approximation unless β_{0n} is much less than a radian. If the mass M and energy $\mathscr{E}$ of the incident particle are in units of the mass of the proton and in kev respectively, then

$$1/v = 4{\cdot}997(M/\mathscr{E})^{1/2}. \qquad \ldots\ldots(16)$$

Noting that the integral in (15) is likely to be of the order of unity, it is apparent that distortion must in general remain important up to quite high impact energies, as suggested at the beginning of this section.

§ 3. CALCULATIONS AND RESULTS

To illustrate the effect of distortion detailed calculations have been carried out on

$$\mathrm{H^+ + H(1s) \rightarrow H^+ + H(2s)}, \qquad \ldots\ldots(17)$$

and on

$$\mathrm{He^{2+} + H(1s) \rightarrow He^{2+} + H(2s)}. \qquad \ldots\ldots(18)$$

Elementary algebra gives that

$$V_{2s,\,1s} = \mathscr{Z}(2\sqrt{2}/27)\,(2+3R)\exp(-3R/2), \qquad \ldots\ldots(19)$$

and that

$$V_{1s,\,1s} - V_{2s,\,2s} = \frac{\mathscr{Z}}{R}\left[(1+R)\exp(-2R) - \tfrac{1}{8}(8+6R+2R^2+R^3)\exp(-R)\right], \qquad \ldots\ldots(20)$$

in which

$$R = (\rho^2 + Z^2)^{1/2} \qquad \ldots\ldots(21)$$

and $\mathscr{Z}$ is the nuclear charge on the incident particle. Substituting these expressions in (15) and (14), the asymptotic coefficients $a_{2s}(\infty)$ were computed and thence from (9) the cross sections $Q_{1s,\,2s}$ were also computed. Much labour was entailed as the main integrations had to be carried out by numerical methods.

Figure 1 shows the derived $(a_{2s}(\infty), \rho)$ curves at several impact energies $\mathscr{E}$ together with the curves obtained earlier, using the Born approximation (Bates 1958). It is apparent that distortion greatly reduces $a_{2s}(\infty)$ when ρ is small and $\mathscr{E}$ is low or moderate. The reduction is more pronounced for process (18) then for process (17) because of the stronger interaction.

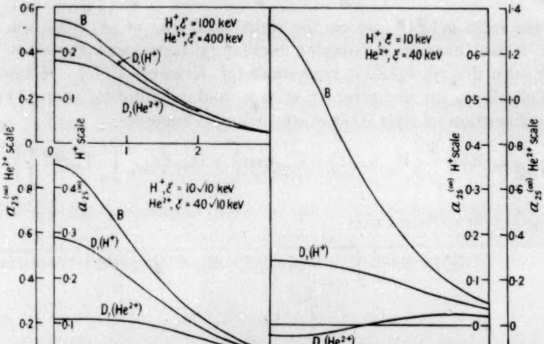

Figure 1. Asymptotic coefficients $a_{2s}(\infty)$ (vertical scale) plotted against impact parameter ρ (horizontal scale). Curve B of each set of three gives the Born approximation for H^+ impact and for He^{2+} impact ; one of the two curves D gives the distortion approximation for H^+ impact and the other the distortion approximation for He^{2+} impact. In each case the inner vertical scale is for H^+ impact and the outer for He^{2+} impact. The energy $\mathscr{E}$ of the incident H^+ or He^{2+} ion is indicated.

In figure 2 the corresponding $(\log Q_{1s,\,2s}, \log \mathscr{E})$ curves are compared with the curves based on the Born approximation (Bates and Griffing 1953). Distortion is seen to lead to a marked diminution in $Q_{1s,\,2s}$ except when $\mathscr{E}$ is high. It even causes (18) to be *less* effective than (17) at equal low velocities of relative motion, though the fact that the charge on the alpha particle is twice that on the proton makes (18) four times *more* effective than (17) at equal high velocities of relative motion.

The distortion approximation cannot be valid in the early part of the impact energy range covered in figure 2. Various corrections are likely to be needed. For example, coupling due to transitions to the 2p state doubtless has to be taken into account. Further, in the case of (17) allowance must be made for the effect of the resonance capture processes

$$H^+ + H(1s) \rightarrow H(1s) + H^+ \qquad \ldots\ldots(22)$$

and

$$H^+ + H(2s) \rightarrow H(2s) + H^+ \qquad \ldots\ldots(23)$$

which must be very great at the lower impact energies. It is worth noting that because of these resonance capture processes, the cross section for (17) must be less close to the cross section for

$$\mathrm{He}^+(1s)+\mathrm{H}(1s)\rightarrow\mathrm{He}^+(1s)+\mathrm{H}(2s) \qquad \ldots\ldots(24)$$

(at the same velocity of relative motion) than the slight difference between the fields of H^+ and $He^+(1s)$ would lead one to expect†. Similar remarks apply to other H^+–$H(1s)$ and $He^+(1s)$–$H(1s)$ collisions.

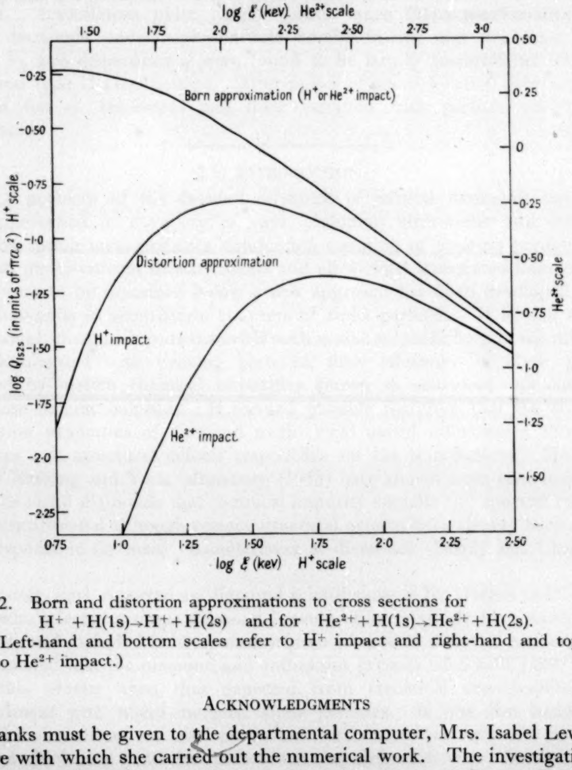

Figure 2. Born and distortion approximations to cross sections for $H^+ + H(1s) \rightarrow H^+ + H(2s)$ and for $He^{2+} + H(1s) \rightarrow He^{2+} + H(2s)$. (Left-hand and bottom scales refer to H^+ impact and right-hand and top scales to He^{2+} impact.)

ACKNOWLEDGMENTS

Thanks must be given to the departmental computer, Mrs. Isabel Lewis, for the care with which she carried out the numerical work. The investigation has been supported in part by the Air Force Cambridge Research Center, Geophysics Research Directorate, of the Air Research and Development Command, United States Air Force, through its European Office, under Contract No. AF 61(052)–131.

---

† Incidentally, the distortion approximation to the cross section for (17) may differ more from the true cross section for this process than it does from the cross section for (24) (again at the same velocity of relative motion).

REFERENCES

BATES, D. R., 1957, *Proc. Roy. Soc.* A, **243,** 15.

—— 1958, *Ibid.*, **245,** 299.

BATES, D. R., and GRIFFING, G. W., 1953, *Proc. Phys. Soc.* A, **66,** 961.

BATES, D. R., MASSEY, H. S. W., and STEWART, A. L., 1953, *Proc. Roy. Soc.* A, **216,** 437.

FRAME, J. W., 1931, *Proc. Camb. Phil. Soc.*, **27,** 511.

KRAMERS, H. A., 1957, *Quantum Mechanics* (Amsterdam : North Holland Publishing Company), p. 211.

MOTT, N. F., 1931, *Proc. Camb. Phil. Soc.*, **27,** 553.

MOTT, N. F., and MASSEY, H. S. W., 1949, *Theory of Atomic Collisions*, 2nd Edn (Oxford: Clarendon Press), p. 153.

Some Scintillation Characteristics of Diamond under Alpha Particle Bombardment

By J. E. RALPH
Department of Physics, King's College, London

Communicated by J. T. Randall; *MS. received* 5*th September* 1958

Abstract. Scintillation pulse height spectra were examined for thirty-five natural diamonds under alpha-particle bombardment, and the mean pulse heights V_0 and dispersions η were found to be largely uncorrelated with the type I and type II classification. After-pulses of about 50 msec duration were observed for all specimens and their variation with particle energy was investigated.

---

§ 1. Introduction

The problem of the detailed structure of natural diamonds has been approached in a variety of ways, including ultra-violet and infra-red absorption measurements, conduction counting of ionizing particles and radiation, photo-current measurements and ultra-violet stimulated fluorescence. In the work to be described below a new approach has been developed using single diamonds as scintillation counters of alpha particles. It is well known that although chemically pure materials such as zinc sulphide do give scintillations when bombarded with ionizing particles, their efficiency is often greatly increased by certain chemical impurities known as activators—for instance, manganese in zinc sulphide. It seemed possible therefore that the study of scintillation properties of diamond might yield useful information about the impurities and structural defects responsible for the scintillations. However, recently Bunting and Von Valkenburg (1958) have shown from examination of over a thousand diamonds that chemical impurity content and spectral type are largely uncorrelated although certain structural defects have already been shown to be responsible for many characteristics of diamonds (Benny and Champion 1956).

The only work reported on diamond scintillations is by Wright and Garlick (1954) who selected a single diamond because of its relatively high scintillation efficiency, and included it in an examination of several different materials. It was concluded that the diamond and anthracene crystals used gave pulse height dispersions greater than that expected from statistical considerations for bombardment with mono-energetic alpha particles. It was also found that diamond and thallium activated potassium iodide were the only two materials examined which gave small after-pulses following each main pulse. Belcher (1950) has also reported these after-pulses in thallium activated potassium iodide using gamma-ray excitation.

§ 2. Experimental

The apparatus used was in the form of a conventional scintillation spectrometer. The diamond and the polonium alpha-particle source were contained in an evacuated chamber with the crystal in contact with a glass window. The photomultiplier (E.M.I. 6094) had its cathode in contact with the other side of this window to give a light collection solid angle of a little less than 2π. The output of the photomultiplier was fed through a cathode follower to a wide-band amplifier and the output of this was passed to a pulse-height analyser and a scaler. Facilities were provided for varying the alpha-particle energy, a series of aluminium foils being used as absorbers. A moving collimating hole was arranged to allow bombardment of limited regions of the crystal surface. Sharp-cut-off filters were used to estimate the wavelength range of the emitted light. A neon lamp pulsed by a flip-flop circuit replaced the alpha source in the determination of the pulse height disperson due to the photomultiplier.

Specimens of both type I and II were examined in a preliminary experiment. Pulse height spectra were obtained for each specimen, those shown in figure 1 being representative of good and poor resolution crystals. Considerable variations in response were observed from one part of the crystal surfaces to another and a holder was designed to enable the crystal position to be exactly repeated.

Three larger specimens were included in the above examination and one of these, S_5, was used for the more specific experiments described later. Thirty-five diamonds were examined under the same conditions. For each a pulse height distribution curve was obtained and the mean pulse height V_0 and the pulse height dispersion η were found from this. The large variation found for η_0 the intrinsic pulse height dispersion (Wright and Garlick 1954) is shown in figure 2. The type I and II classification has been determined for these crystals by ultra-violet absorption and conduction counting by other workers, and no correlation was found between this and the magnitude of V_0 or η_0.

Pulse height distribution curves were also obtained for a range of different irradiated areas on the surface of S_5 and on some smaller crystals. Little change was observed for S_5 except at the edges, but large variations were found for the smaller ones. These may have been due to changes in the light collection efficiency with the region in which the light was produced. Pulse height spectra were obtained before and after several days of alpha bombardment and also before and after thirty minutes of neutron irradiation in a nuclear reactor. No change was observed in either case, but this treatment was only carried out for one crystal. The neutron dosage was insufficient to produce the green coloration which results from large doses.

Using S_5 the values of V_0 for a range of alpha-particle energies between 0 and 5·3 MeV were found and the intrinsic pulse height dispersion η_0 was obtained for each energy.

An examination of the nature of the variation of the after-pulse spectrum with alpha-particle energy was also carried out. The after-pulses were amplified to cover the range of the pulse height analyser and a pulse height spectrum obtained for each of several values of energy. From these a series of graphs were obtained by plotting the counting rate in fixed analyser channels against particle energy and this was repeated for several values of channel height. A set of divergent straight lines was obtained which when extrapolated cut the energy axis at 1·5 MeV.

To determine the wavelength range of the emitted light the mean photomultiplier current was measured for each of the set of sharp-cut-off filters and this was repeated for each of a range of particle energies. The photomultiplier current was plotted against energy for each filter as shown in figure 4.

§ 3. RESULTS

From the preliminary examination of a number of crystals the following general characteristics were observed. The crystals were all of about the same size, 1 to 2 mm, and it was found that all gave detectable scintillations although the magnitude of pulse height varied by a factor of about twenty from the best to the poorest scintillator. The best specimens gave pulses of the same order as those from an anthracene crystal of approximately the same dimensions and under the same conditions. A large number of after-pulses were observed following each main pulse for all specimens, although for some it was difficult to distinguish between the main and after-pulses as indicated by figure 1. The duration of the after-pulses was about 50 msec. The pulse height dispersion was frequently greater than 50% although for one or two diamonds it was as low as

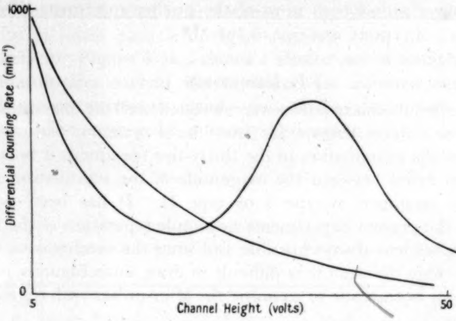

Figure 1. Approximate limits of range of pulse height distribution curves for scintillations from diamond.

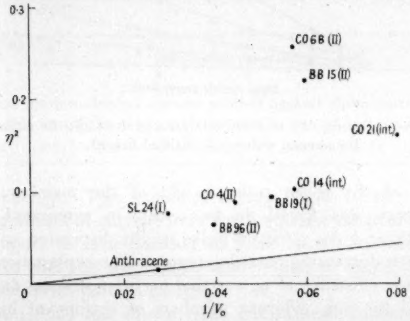

Figure 2. Values of the square of the pulse height dispersion plotted against $1/V_0$ for several diamonds, together with the line $\eta^2=K/V_0$ for the photomultiplier.

25% compared with about 15% for anthracene. The pulse height dispersions η for a number of crystals are plotted in figure 2 together with the straight line $\eta^2 = K/V_0$ representing the variation with the mean pulse height V_0 of the dispersion due to the photomultiplier. The heights of the points above this line are the corresponding values of η_0^2, the intrinsic dispersion due to the crystal itself (Wright and Garlick 1954).

Of the thirty-five diamonds examined three were much larger than the rest and each gave larger pulses than most of the smaller specimens. Two of these large crystals were of type II and one of type I.

§ 4. DISCUSSION

Since after-pulses and main pulses were detected in all the diamonds examined, the mechanism or defects responsible must be a common feature of natural diamonds. From the examination of the thirty-five specimens it is clear that no strong correlation exists between the magnitude of the scintillation main pulse and whether the specimen is type I or type II. It has been pointed out, however, that in the present experiments no simple separation of the main pulse from the after-pulses was always possible and since the mechanisms of each are probably considerably different it is difficult to draw unambiguous conclusions. No attempt has yet been made to examine the after-pulses with regard to crystal type classification.

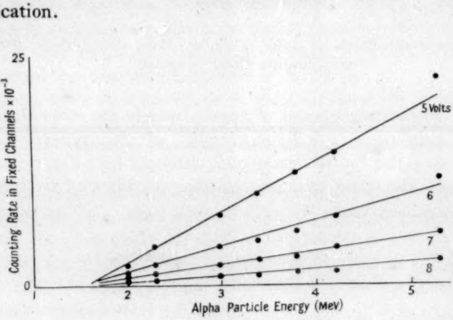

Figure 3. After-pulse counting rate in fixed channels plotted against alpha-particle energy for several values of channel height.

The variation of the mean pulse height of the main pulses V_0 with alpha-particle energy was found to be linear, in agreement with Wright and Garlick (1954), and the intrinsic pulse height dispersion η_0 was found to increase rapidly with decreasing particle energy. The explanation suggested by these workers for the existence of η_0 was that particles striking different parts of the surface passed through different numbers of regions of high conversion efficiency of alpha-particle energy into radiation. Thus as this energy is reduced the number of events making up each pulse decreases and so the dispersion would increase. This explanation also indicates that no correlation would be expected between η_0 and type I or type II. The effect on the after-pulses of varying the particle energy is shown in figure 3. As the bombardment energy was reduced so the heights of the after-pulses were reduced in overall magnitude. Energies below 2·0 MeV were not used in this experiment, due to the small pulse size produced, and channel heights below 5·0 volts were not possible. However, these graphs indicate that the after-pulses are very small below 1·5 MeV. The linearity of the portions above 1·5 MeV is a function both of the light decay characteristics and of the amplifier time constants which convert this decay into a pulse system, and detailed interpretation is therefore difficult. However, the non-linearity at lower particle energies suggests some difference in structure near the surface. Figure 4 also shows a similar set of straight lines when the main photomultiplier current was measured for different energies, indicating that the measured current is mainly due to the after-pulses, rather than the main pulses. The main pulse intensity also varies linearly with energy but is zero at zero energy. Two values of energy below 1·5 MeV were used but the corresponding values of current were small and the range of these for each filter is shown in figure 4. The linearity of these curves for different sharp-cut-off filters indicates that the wavelength distribution of the emitted light does not vary appreciably with particle energy.

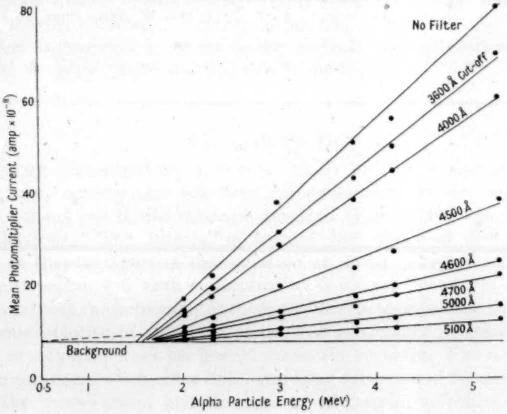

Figure 4. Mean photomultiplier current plotted against alpha particle energy for various values of sharp-cut-off filters placed between the crystal and the multiplier cathode.

Champion (1953) has shown from conduction counting experiments that often electron trap density increases towards the natural growth surface of diamonds and this behaviour may arise from gross defects which would be more common near the surface. These may simply give rise to optical inefficiency due to light scattering or they may be associated with deep traps which could be responsible for a much longer, lower intensity after-pulse system for low energies.

§ 5. CONCLUSION

These experiments show that no strong correlation exists between the efficiency of a diamond scintillation counter and its type I or type II classification. Such behaviour therefore contrasts markedly with its efficiency as a conduction counter which is strongly dependent on this classification.

ACKNOWLEDGMENTS

I wish to thank Dr. F. C. Champion for his interest and support during the course of this work, and the Kent Education Committee for providing a grant.

REFERENCES

BELCHER, E. H., 1950, *Nature, Lond.*, (a) **166,** 826.
BENNY, A. B. H., and CHAMPION, F. C., 1956, *Proc. Roy. Soc.* A, **234,** 432.
BUNTING, E. N., and VON VALKENBURG, A., 1958, *Amer. Min.*, **43,** 102.
CHAMPION, F. C., 1953, *Proc. Roy. Soc.* A, **220,** 485.
WRIGHT, G. T., and GARLICK, G. F. J., 1954, *Brit. J. Appl. Phys.*, **5,** 13.

Investigation of Ultrasonic Velocities in Organic Solutions

By B. RAMACHANDRA RAO and K. SUBBA RAO
Ultrasonic Laboratories, Andhra University, Waltair, India

Communicated by E. G. Richardson; MS. received 14*th May* 1958, *in revised form* 27*th October* 1958

Abstract. This paper embodies the results of the investigation of ultrasonic velocity, adiabatic compressibility and molar sound velocity R in solutions of benzoic acid, phthalic acid and salicylic acid in some organic liquids and its variation with concentration. Measurements of ultrasonic velocity were made by a precision double crystal interferometer method. Molar sound velocity of the three solutes obtained by extrapolating the R against molar concentration graphs were interpreted in terms of the method of bond and atomic velocity increments given by Lagemann and Rao respectively.

---

§ 1. INTRODUCTION

EARLIER investigations (Nomoto 1952) on the variation of ultrasonic velocity, density and adiabatic compressibility versus concentration in several organic liquid mixtures revealed significant deviations from ideal linear behaviour. The interesting feature was observed that whatever the deviation of these properties the variation of molar sound velocity R and the molar compressibility B with concentration is always linear. It is mainly with a view to studying the behaviour of these physical properties that the investigation of ultrasonic velocity in solutions of organic substances in organic solvents is taken up, as very little work has been done on the variation of ultrasonic velocities in organic solutions. Schaaffs (1937) and later Sibaiya and Narasimhaiya (1941) took up the investigation and determined ultrasonic velocities and adiabatic compressibilities of solutions of naphthalene in different organic liquids. In every one of these solutions they observed a definite increase of velocity and a decrease of adiabatic compressibility with concentration. More recently Lal (1950, 1951) has investigated the effect of dissolving benzoic acid in different organic liquids on the ultrasonic velocity and adiabatic compressibility and concluded that in every case there is a definite decrease in the velocity and increase in the compressibility of the solvent. This unusual observation of Lal in the case of benzoic acid solutions is contrary to the results of the earlier investigations. Using the diffraction method for determining ultrasonic velocities at ordinary frequencies, it is surprising that Lal could establish a definite decrease in velocity though the observed decrease in most of the solutions is as small as 10 m sec^{-1} for the highest concentration. As the results obtained by Lal appeared to be rather inaccurate, this investigation has been taken up afresh using the more accurate method of determining ultrasonic velocities recently developed by Rao and Rao (1957) which enables velocity measurements with an accuracy to 0·1% to be made.

§ 2. RESULTS

Ultrasonic velocities are thus determined in different concentrations of solutions obtained by dissolving known quantities of the solute weighed accurately in a precision balance in known volumes of the solvent. The density of each solution is determined with an accuracy to 0·1% by using a specific gravity bottle. The average molecular weight of the solution $\overline{M}$ is calculated for each concentration by using the relation $\overline{M}=(n_1M_1+n_2M_2)/(n_1+n_2)$ where M_1 and M_2 are the molecular weights of the solute and solvent, and n_1 and n_2 are the number of gramme molecules of the solute and solvent. The molar fraction of the solute is given by the relation $C=n_1/(n_1+n_2)$ and is expressed as a percentage. The molar sound velocity R is calculated for each concentration by Rao's formula $R=\overline{M}v^{1/3}/\rho$, where ρ is the density and v is the ultrasonic velocity in the solution. The molar sound compressibility values are also obtained by using the relation $B=\overline{M}\beta^{1/7}/\rho$, where $\beta=1/v^2\rho$ is the adiabatic compressibility.

Solutions of benzoic acid in chloroform, benzene and ethyl alcohol, phthalic acid in methyl alcohol, ethyl alcohol and acetone, and salicylic acid in methyl alcohol were investigated. The variation of all these physical properties with concentration expressed as molar fraction for all the solutions are studied and the results are presented in graphical form in figures 1 to 5. Of these only the benzoic–ethyl alcohol solution has already been studied by Lal but a fresh investigation of this has been undertaken with a view to verifying the decrease in velocity with concentration reported by him.

Figures 1, 2 and 3 show the variation of v, ρ and β for benzoic acid solutions. In all the cases, the curves show a progressive increase of velocity and decrease of compressibility with concentration. For this particular combination, Lal has observed a decrease of velocity 56 m sec^{-1} for a concentration of 0·2 mole per litre while for the same concentration, which is equivalent to 1·13 molar fraction, we find a definite increase of velocity by 8 m sec^{-1}. It is interesting to note that even for the highest concentration possible the increase in velocity observed is only 28 m sec^{-1}. There are slight departures from strict linearity in almost all the curves showing variation of v, ρ and β with concentration. An interesting case is that of benzoic acid–chloroform solution wherein we observed a decrease of density with increase of concentration. In spite of this decrease in density the compressibility showed only a decrease with increase of concentration. The variation of R and B with molar fraction is found to be strictly linear in all three cases and the data given in table 1 show the linear variation of R with concentration in three solutions.

Figure 4 shows the variation of v and β for solutions of phthalic acid in three different solvents. The curves are found to be accurately linear for solutions in ethyl alcohol and acetone. In all cases an increase of velocity and a decrease of compressibility are noticed with increase of concentration. The variation of R and B with concentration is again found to be strictly linear. The linear variation of R with concentration for the phthalic acid solutions can be judged from the data given in table 1.

Another substance which belongs to the same series as benzoic and phthalic acids is salicylic acid and solutions of this in methyl alcohol are studied. The variations of v, ρ and β with concentration presented in figure 5 show very slight

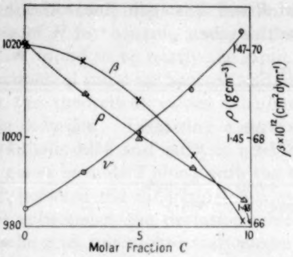

Figure 1. Variation of ultrasonic velocity, density and adiabatic compressibility with molar concentration in benzoic acid–chloroform solution.

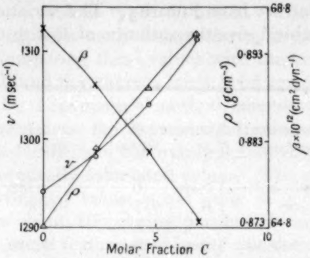

Figure 2. Variation of ultrasonic velocity, density and adiabatic compressibility with molar concentration in benzoic acid–benzene solution.

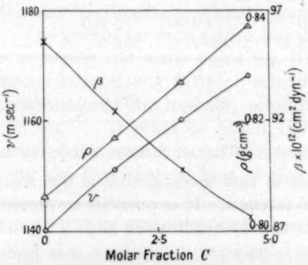

Figure 3. Variation of ultrasonic velocity, density and adiabatic compressibility with molar concentration in benzoic acid–ethyl alcohol solution.

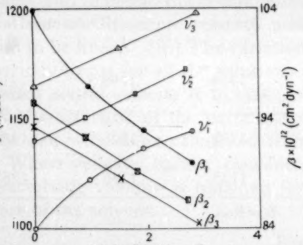

Figure 4. Variation of ultrasonic velocity and adiabatic compressibility in

1. phthalic acid–methyl alcohol solution.
2. phthalic acid–ethyl alcohol solution.
3. phthalic acid–acetone solution.

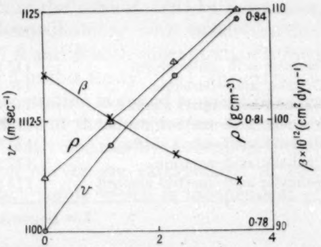

Figure 5. Variation of ultrasonic velocity, density and adiabatic compressibility with molar concentration in salicylic acid–methyl alcohol solution.

departure from linearity. The variation of R and B is again linear and the data in table 1 give the variation of R with C for this case.

Table 1

Solution							
Benzoic acid–	conc.	0	2·595	5·051	7·401	9·618	100
chloroform	R	807·6	816·0	823·5	831·6	841·0	1151
Benzoic acid–	conc.	0	2·388	4·660	6·829	—	100
benzene	R	975·2	978·8	984·5	991·7	—	1261
Benzoic acid–	conc.	0	1·540	3·031	4·479	—	100
ethyl alcohol	R	597·3	606·1	614·6	622·6	—	1154
Phthalic acid–	conc.	0	0·965	1·907	2·834	—	100
methyl alcohol	R	416·5	424·7	433·5	441·1	—	1284
Phthalic acid–	conc.	0	0·909	1·806	2·681	—	100
ethyl alcohol	R	597·3	603·6	610·2	616·5	—	1313
Phthalic acid–	conc.	0	1·458	2·869	—	—	100
acetone	R	773·6	780·7	788·0	—	—	1275
Salicylic acid–	conc.	0	1·158	2·288	3·394	—	100
methyl alcohol	R	416·5	425·5	433·0	440·9	—	1135

§ 3. ESTIMATION OF MOLAR SOUND VELOCITY OF THE SOLUTE

An interesting result of this investigation is the remarkable linear variation of R and B with molar fraction. It is possible to obtain the value of R for the pure solute by extrapolating the readings in table 1 up to a molar fraction of 100. In the case of the three benzoic acid solutions, it is found, by extrapolating the results to 100 molar fraction, that the final value is approximately the same. The values thus obtained are given in table 2.

Table 2. Values of R

Solution	Extrapolated	Average	Theoretical	
			L	R
Benzoic acid–chloroform	1151			
Benzoic acid–benzene	1261	1174	1198·8	1213
Benzoic acid–ethyl alcohol	1154			
Phthalic acid–methyl alcohol	1284			
Phthalic acid–ethyl alcohol	1313	1291	1426	1481
Phthalic acid–acetone	1275			
Salicylic acid–methyl alcohol	1135	1135	1236	1287

L = Lagemann; R = Rao.

It will be interesting to compare this value of R with the theoretical value that can be deduced for this solute by following the methods given by Lagemann and Rao for calculating the value of R of any organic molecule whose chemical formula is known. Rao considered that R for any organic molecule can be estimated by taking into consideration the contributions due to atoms and bonds. Lagemann has followed an entirely different method of estimating R by taking into account only the contribution due to various types of bonds. The final values of R for benzoic acid calculated by both methods are shown in table 2 and are found to be nearly the same. Comparing these values with the average experimental value for benzoic acid, it is found that there is fairly good agreement with the theoretical values calculated by Lagemann's method, the deviation being only 2%. Following a similar procedure the experimental values of R for phthalic acid and salicylic acid as deduced from the extrapolation of R are also given in table 2 along with the theoretically calculated values. The agreement between the theoretical and experimental values is not quite so good for these substances, the deviation which is about 10% being particularly high in phthalic acid, but such deviations are a normal feature even in the calculations of atomic or bond increments from a homologous series of organic compounds. In general, it may be said that the agreement is satisfactory when we consider the fact that R values for the solutes are obtained by a large extrapolation of the experimental results which could be obtained only up to a mole fraction of 3/10 because of the low solubility of the solutes investigated.

It is interesting to see what value for the velocity is obtained for each solute by extrapolating to 100 molar fraction those velocity against molar fraction graphs which are fairly linear. The graphs for each solute dissolved in different solutions are found to intersect at nearly the same point for 100% concentration, thus giving an average characteristic velocity for each solute in the liquid condition. The average values thus obtained for benzoic, phthalic and salicylic acid are 1657, 2278 and 1778 m sec^{-1}. It must be noted that these velocities do not correspond to the velocity of the solutes in the solid state but that they give the characteristic velocity for the hypothetical case of the solute in liquid form at 100% concentration.

§ 4. Conclusions

The following are the main conclusions drawn from the ultrasonic studies of some of the physical properties of solutions of organic substances in organic solvents. (i) Contrary to some of the previous observations by Lal, it is found that the effect of an addition of the organic solute is invariably to increase the velocity and decrease the compressibility of the solvent. (ii) In most cases, the variations of ultrasonic velocity and compressibility with molar fraction are found to be linear. (iii) The variation of R and B with concentration is found to be strictly linear for all the solutions used in this study. (iv) The extrapolation of molar sound velocity R to 100% concentration is found to yield fixed values of R characteristic of the particular solute and those values are found to agree fairly well with those calculated from bond velocities by Lagemann's method. (v) When velocity against concentration curves are extrapolated to 100% a characteristic velocity is obtained for each solute which is independent of the nature of the solvent.

References

Lal, K. C., 1950, *Indian J. Phys.*, **24,** 461.
—— 1951, *Ibid.*, **25,** 73.
Nomoto, O., 1952, *Bull. Kobayasi Inst. Phys. Res.*, **2,** 137.
Rao, B. R., and Rao, K. S., 1957, *J. Sci. Industr. Res.*, **16-B,** 483.
Schaaffs, W., 1937, *Z. Phys.* **105,** 658.
Sibaiya, L., and Narasimhaiya, R. L., 1941, *J. Mysore University*, **1-B,** 133.

Band Spectra of Magnesium Oxide and Hydroxide between 4000 and 3600 Å

By D. PESIC† and A. G. GAYDON
Chemical Engineering Department, Imperial College, London

MS. received 9th October 1958

Abstract. Band systems in the extreme violet have been excited in 'vacuum' arcs in oxygen, ordinary water vapour and heavy-water vapour, and also in a flame. Wavelengths of MgOH and MgOD bands are listed. An oxide system in the same region has been studied under large dispersion but is too complicated to analyse; it is attributed to a polyatomic emitter, possibly Mg_2O_2.

§ 1. Introduction

When magnesium is excited in an arc or flame, a complex band structure is observed in the extreme violet, between 4000 and 3600 Å, in addition to the well-known MgO bands at 5211 Å. These extreme violet bands have been known for a long time. Eder (1903) obtained them when Mg salts were introduced into a flame, and he and other early workers (see Kayser 1910) suggested MgO as the emitter. Verhaeghe (1935) attempted to analyse the bands and formed two Deslandres arrays with (0, 0) bands at 3799 and 3766 Å. However, Barrow and Crawford (1954) found that the structure of the system obtained from burning Mg ribbon was very complex and concluded that the carrier was doubtful; they also obtained the bands in absorption and gave new data. Brewer and Porter (1954) used very large dispersion (0·67 Å mm^{-1}) to study the bands; they attributed them to MgO on grounds of variation of intensity with temperature and composition and gave some fragmentary vibrational analysis, but were unable fully to resolve the rotational structure and appear to think that several electronic states of triplet multiplicity might be involved. Recently, Gaydon and Guénebaut (see Gaydon 1957) obtained bands in an oxy-hydrogen flame and in a vacuum arc in ordinary and heavy-water vapour (H_2O and D_2O) and suggested the possibility of overlapping bands of MgOH and perhaps a polyatomic oxide.

The assignment of the bands is important in connection with the determination of the species present in the gas in contact with magnesium oxide and the determination of the dissociation energy of MgO and of other thermochemical data. In the present investigation, the bands have been studied using sources developed in this laboratory for investigations of other alkaline earth oxides and hydroxide spectra (Gaydon 1955, Charton and Gaydon 1956).

§ 2. Experimental

Two sources were used, a vacuum arc and an oxyhydrogen flame. The vacuum arc was the same as that described by Gaydon (1955). Magnesium metal electrodes were used and the arc was run in oxgyen and in an atmosphere of ordinary or heavy-water vapour. Most of the work has been done with flowing oxygen at about 10 mm Hg, or with a few mm Hg water vapour controlled by slow continuous pumping. Preliminary investigation showed that this pressure was best for stability of the arc and consumption of the electrodes. The arc was operated on 220 v d.c. with current between 0·7 and 1·0 ampere.

---

† Usual address, Institute of Nuclear Science, Bikidrich, Belgrade.

The spectrum excited in an approximately stoichiometric oxy-hydrogen premixed flame was examined, using the burner described by Charton and Gaydon (1956). A solution of chloride was used.

For preliminary work and for the flame spectrum, medium quartz and glass spectrographs were used. The main part of the work has been undertaken with a 10 ft concave grating (disper. 2·7 Å mm^{-1} in 2nd order) and a 30 000 lines per inch 21 ft concave grating (disper. 1·28 Å mm^{-1} in 1st and 0·59 Å mm^{-1} in 2nd order). An iron arc comparison spectrum was used. The spectra were taken on Ilford Astra III, Zenith, HP3 and R.P. Panchromatic plates. The exposure times, depending on the spectrograph, varied from 10 seconds to several hours.

§ 3. COMPLEX SPECTRUM OF AN OXIDE OF MAGNESIUM

The spectrum of the vacuum arc in oxygen (see Plate, strip (*b*)) consists of four main groups which are different in appearance and contain bands degraded in different directions. The first group centred at 3640 Å is very weak and consists of bands degraded to the red. It starts with one very weak band showing open rotational structure, and finishes with a group of bands, the successive stronger heads of which are separated by about 3 Å. The second group is the most intense feature of the whole spectrum and consists of the shorter wavelength side of very diffuse bands which are followed by very fine rotational structure. In the central part, the bands either degrade to the violet or have only a maximum. Toward the red, the structure of the group becomes more definite, and it finally shows fine rotational structure. This part of the spectrum is shown in strip (*f*). The bands of the third group (3766–3840 Å, strip (*c*)) are degraded to the red. They have a very regular appearance and show clear regularly spaced heads. A few bands start with a single head, while the majority are double headed. On plates taken with the 21 ft grating, all these bands show fine rotational structure. However, although the dispersion was 0·59 Å mm^{-1} (strip (*g*)), none of these bands is completely resolved. The end of this group is undefined due to the presence of the strong magnesium triplet. This third group merges into the weaker fourth group which extends to 3989 Å. Some of these bands are degraded to longer wavelengths, while some are not clearly degraded either way.

Attempts at vibrational analysis have had little success. There are two strong sequences of red-degraded bands commencing at 3766 and 3799 Å, these being the (0, 0) sequences of Verhaeghe's systems I and II. Most of the bands of Verhaeghe's four other sequences are observed, but they are weak and our wavelengths differ rather from his, so that the reality of the complete arrays is not convincing. Most of the strong diffuse bands of our second main group are not included in these arrays.

Even with the largest dispersion, the rotational structure appears too complex to enable the analysis of any single band.

For purposes of identification, we list the most prominent features which we feel are certainly attributable to an oxide of magnesium in table 1. Many less strong bands are not included, especially in the congested second group where overlapping of complex structure makes it difficult to isolate true band heads. In the table, visual estimates of intensity are given on a scale of 10 for the strongest band. Letters R, V or M indicate that the band is degraded to the red, to the violet, or has only a headless maximum.

Table 1. Wavelengths of Outstanding Bands of Magnesium Oxide (Mg_2O_2 ?)

λ	I	Deg.	λ	I	Deg.	λ	I	Deg.	λ	I	Deg.
3639·45	3	M	3724·9	6	V	3804·16	6	R	3887·12	4	R
72·11	4	R	66·10	7	R	04·31	6	R	95·47	4	M
74·77	3	R	71·80	6	R	05·28	8	R	3902·60	4	M
77·63	3	R	72·33	8	R	10·30	8	R	06·82	3	R
80·92	3	R	77·40	7	R	15·70	9	R	11·38	3	R
84·46	3	R	77·81	8	R	17·53	6	R	16·39	3	R
88·39	3	M	82·65	5	R	21·51	7	R	21·95	2	R
95·98	4	M	84·20	6	R	24·4	7	V	28·83	3	R
98·53	5	R	88·47	5	R	54·80	3	M	36·58	2	R
3720·66	10	V	90·96	6	M	55·21	4	R	44·00	2	M
20·96	9	V	98·24	7	R	59·54	4	V	45·11	3	M
21·40	9	V	98·36	7	R	74·19	5	M	53·70	4	M
									61·48	3	M

§ 4. BANDS OF MgOH AND MgOD

Spectrum with the oxy-hydrogen flame. This has only been photographed with the medium-quartz instrument ; the general appearance is shown in strip (*a*) of the Plate. There are two main groups of diffuse bands, but no definite heads. The main features are listed in table 2, but owing to diffuseness and the limited dispersion wavelengths are only accurate to ± 2 Å.

Table 2. Wavelengths of Outstanding Bands of Magnesium in Oxy-hydrogen Flame

λ	I	Deg.	λ	I	Deg.	λ	I	Deg.	λ	I	Deg.
3627	0	V	3719	7	V	3810	9	V	3855	3	V
3645	1	M	3731	5	V	3815	7	M	3859	3	V
3696	8	V	3751	3	M	3822	7	M	3882	3	V
3703	10	V	3801	5	V	3834	10	M	3914	2	M
3707	7	M	3807	9	M	3848	4	V	3942	1	V
									3969	1	V

Spectrum of the arc in H_2O. The emission covers the same region of the spectrum as the arc in oxygen, but the positions of individual bands are quite different. This is shown in the enlargement of a portion of the spectrum in strip (*d*) of the Plate. A few of the strongest oxide heads occur on some plates. The bands of the arc in H_2O are mostly diffuse, but show a number of heads degraded to the violet. Some of these band heads are separated by about 70 cm^{-1}, but no vibrational scheme has been obtained. The lines, grouped around the maxima, are separated by between 4 and 6 cm^{-1}, this spacing being presumably connected with the rotational structure. The strongest of these arc bands are listed in table 3, from measurements of large dispersion. Many weak features and some of the moderately strong features from the central regions are omitted.

The flame bands all appear to be present in the arc, although perhaps with somewhat modified intensity distribution, but some of the arc bands, especially the violet degraded bands at 3783·3 and 3770·6 do not occur in the flame.

Table 3. Wavelengths of Outstanding Bands of MgOH

λ	I	Deg.	λ	I	Deg.	λ	I	Deg.	λ	I	Deg.
3660·1	4	V	3724·8	4	M	3784·52	5	V	3848·56	8	M
76·0	4	V	31·76	8	V	92·78	5	V	49·68	8	V
84·06	4	V	32·37	4	M	97·44	3	V	54·9	7	V
86·4	8	V	42·19	5	M	3802·40	8	M	59·7	6	V
95·09	7	V	47·07	4	M	08·82	8	V	76·82	6	V
3703·25	6	V	51·34	4	M	10·17	8	V	80·16	6	V
04·09	8	V	59·37	2	M	19·23	6	V	82·5	6	V
07·9	8	V	70·63	7	V	26·41	5	V	3901·16	5	V
08·80	8	V	72·9	5	M	34·80	6	M	14·64	4	M
09·38	6	M	82·0	5	V	45·08	5	M	19·1	5	V
19·60	10	V	83·36	8	V	46·93	6	M	36·2	4	V

The arc in D_2O. The spectrum of the vacuum arc in heavy water vapour has a similar general appearance (see strip (*e*)) to the arc in H_2O, but the bands are displaced. The isotope shift is so large that it is not, unfortunately, possible to relate the bands of the arcs in D_2O and in H_2O. A selection of the outstanding heads is given in table 4.

Table 4. Wavelengths of Outstanding Bands of MgOD

λ	I	Deg.	λ	I	Deg.	λ	I	Deg.	λ	I	Deg.
3650·23	3	M	3701·1	3	V	3756·21	4	V	3878·6	3	M
56·2	3	V	11·05	4	V	82·84	3	V	79·38	5	M
65·52	5	V	13·51	4	V	94·5	2	V	80·0	3	M
68·44	4	V	33	3	M	97·33	3	M	92·7	6	V
71·76	6	V	36·60	4	V	97·79	3	R	3903·90	5	M
76·22	3	V	37·81	3	V	99·92	4	V	09·8	8	M
79·64	4	V	38·5	3	R	3807·46	3	M	11·3	4	V
82·85	4	V	40·6	3	M	52·8	4	V	15·20	4	R
98·3	6	V	41·3	3	M	70·1	8	M	20·04	3	V
3700·08	6	V	46·2	4	V	78·32	5	M			

The undoubted isotope shift clearly shows the presence of hydrogen in the emitter, but the structure is not sufficiently open for a hydride. Assignment of the bands to the triatomic hydroxides MgOH and MgOD seems fairly safe.

§ 5. COMPARISON WITH PREVIOUS WORK

Verhaeghe shows a microphotometer trace of his spectrum, but lists only the bands which he has analysed into Systems I and II, and Sequence A. All the strong bands in this list appear to be due to the oxide. The sequences formed by the weak bands are, however, rather uncertain.

Barrow and Crawford stress the complexity of the system and express doubt about the emitter. Their photograph shows bands of MgH, indicating that hydrogen was present. Comparison of their wavelengths shows that both the oxide bands and the MgOH bands occurred under these conditions. Considering the diffuse nature of the bands, the agreement with our wavelengths is very good.

Of the 27 heads recorded by Brewer and Porter, eight seem to be due to the oxide alone, 12 can definitely be identified with our MgOH and four coincide with both oxide and MgOH; the remaining three are unobserved by us. Since their attempt at analysis includes both oxide and hydroxide heads, it can have little meaning, and their conclusions about the dissociation energy may be affected by the undoubted presence of the hydroxide. Indirect determination of the dissociation energy of the oxide by observation of the Mg lines in flames (e.g. Veits and Gurvich 1956) may also be affected by existence of the hydroxide.

§ 6. Discussion

The flame bands, and those in the arc in water vapour, have a very similar general appearance to bands of the analogous hydroxide of calcium (Gaydon 1955). The slight difference between the flame and arc spectra is difficult to account for, but it is possible that the higher temperature of the arc modifies the rotational intensity distribution and favours heads of bands formed from lines of high rotational quantum number. The general halation around the strong, wide Mg lines at 3829, 3832 and 3838 Å and the Rowland Ghosts of these lines modify the appearance of the arc spectrum. The flame shows less continuous background and is better for observation of weaker groups of bands, but because of the low light intensity is not suitable for work at high dispersion.

The bands of the arc in oxygen are only just detectable in the arc in water vapour, and disappear in an arc in hydrogen. This appears to rule out Mg_2 as emitter. Since no vibrational scheme can be obtained for the whole mass of bands, these must either be due to a polyatomic emitter, or must consist of a number of overlapping systems. Brewer (1953), Brewer and Porter (1954) and Gaydon (1955) have discussed the possibility of a polyatomic emitter and of systems of MgO of triplet multiplicity. Even if triplet states were involved, a rotational analysis for a molecule as light as MgO should be possible; even heavier molecules, such as TiO and ZrO, give systems amenable to analysis. Triplet systems of molecules of comparable weight, such as N_2 and CO, would appear to have quite open structure under this dispersion of 0·59 Å mm^{-1}. We must therefore conclude that a polyatomic emitter is responsible, at any rate for the main second group of bands. The species which can be expected are MgO_2, Mg_2O and Mg_2O_2. Although occurrence of these molecules in an arc at high temperature might appear unlikely (Brewer and Mastick 1951), similar molecules of the alkaline earth metals were found by a mass spectrometric method by Aldrich (1951) and Inghram and Chupka (1955).

The sharp-headed red-degraded bands of our third group (3766–3840 Å) look simpler than those of the second group. It is unlikely, but just possible, that these bands could belong to a diatomic emitter. We think it more probable, however, that they form part of the main system. If the emitter is Mg_2O_2, Mg_2O or MgO_2, it is likely to possess some symmetry (unlike MgOH) and could then form perpendicular-type and parallel-type bands; in this case, the second group may be perpendicular-type and the third group could be simpler parallel-type bands. The occurrence of some heads shaded to the red and some to the violet frequently takes place in polyatomic spectra.

James and Sugden (1955) pointed out that the hydroxides and fluorides of Ca, Sr and Ba lay in similar spectral regions, and Gaydon (1957) and Charton and Gaydon (1956) noted that the complex oxides of these metals lay in similar regions to the fluorides and hydroxides. This is also largely true for magnesium: hydroxide, MgOH, 3969–3627; complex oxide, Mg_2O_2?, 3922–3639; fluoride, MgF, 3685–3507. The close parallelism of band systems of the hydroxides and the isoelectronic fluorides is not surprising, but the reason why the bands of the oxide should occur in a similar region is less obvious. Magnesium, unlike the other metals of the group, does not possess an unfilled inner shell, so we cannot attribute the correspondence to excitation of an electron in a shielded inner shell.

REFERENCES

ALDRICH, L. T., 1951, *J. Appl. Phys.*, **22,** 1168.
BARROW, R. F., and CRAWFORD, D. V., 1945, *Proc. Phys. Soc.*, **57,** 12.
BREWER, L., 1953, *Phys. Rev.*, **52,** 48.
BREWER, L., and MASTICK, D. F., 1951, *J. Amer. Chem. Soc.*, **73,** 2045.
BREWER, L., and PORTER, R., 1954, *J. Chem. Phys.*, **22,** 1874.
CHARTON, M., and GAYDON, A. G., 1956, *Proc. Phys. Soc.*, **69,** 520.
EDER, J. M., 1903, *Denkschr. Akad. Wiss. Wien.*, **74,** 45.
GAYDON, A. G., 1955, *Proc. Roy. Soc.* A, **231,** 437.
—— 1957, *Mém. Soc. Sci. Liège*, **18,** 507.
INGHRAM, M. O., and CHUPKA, W. A., 1955, *J. Chem. Phys.*, **23,** 2159.
JAMES, C. G., and SUGDEN, T. M., 1955, *Nature, Lond.*, **175,** 333.
KAYSER, H., 1910, *Handbuch der Spektroskopie* (Leipzig: Hirzel), **5,** 717.
VERHAEGHE, J., 1935, *Wis-en Natuurk. Tijdschr.*, **7,** 224.
VEITS, I. V., and GURVICH, L. V., 1956, *Optika i. Spektrosk.*, **1,** 22.

Vacancy Diffusion in Ordered Alloys

By E. W. ELCOCK

Department of Natural Philosophy, University of Aberdeen

MS. received 19*th September* 1958

Abstract. A mechanism of vacancy diffusion in ordered alloys is examined in some detail for the stoichiometric simple cubic binary alloy. Upper and lower bounds for the ratio G of the self-diffusion coefficients of the two components of the alloy are calculated as functions of the temperature in the reduced temperature range $0 \leqslant T/T_c \leqslant 0{\cdot}5$, where T_c is the critical temperature of ordering. In this temperature range it is found that $1/a \leqslant G \leqslant a$ where $a \simeq 2$ and only slightly temperature dependent. Such experimental evidence as there is bears out this simple yet striking result.

---

§ 1. Introduction

It has been shown (Elcock and McCombie 1958) that it is possible to discuss vacancy diffusion in ordered binary alloys in terms of certain unit processes, each of which consists of a highly correlated series of vacancy jumps. It was shown that, in the low temperature limit, all unit processes other than what was called the six-jump process may be ignored, when it is possible to obtain numerical values for the upper and lower bounds for the ratio of the self-diffusion coefficients G for the two components of the ordered alloy. It is the aim of the present paper to obtain an expression for G valid over a range of temperature and, in particular, at temperatures at which measurements of self-diffusion coefficients become a practicable possibility.

It will be assumed that (1) the lattice of the alloy is simple cubic, the state of perfect order of the AB alloy being such that if a site on the lattice is occupied by an atom of one kind, the nearest neighbour sites of this site are all occupied by atoms of the other kind; (2) the configuration energy of the alloy may be written in terms of nearest neighbour pair interaction energies E_{AA}, E_{BB} and E_{AB}; (3) the only mechanism for atom interchange is by vacancy jumps from a site to a nearest neighbour site; (4) correlated motion of vacancy pairs may be ignored; (5) in a vacancy jump involving a change in configuration energy ΔE of the local environment of the vacancy, the local environment passes through an energy barrier $\Delta E + U$ for $\Delta E > 0$ and U for $\Delta E < 0$. It is assumed that differences in U for different vacancy jumps are small compared with the ordering energy

$$E_{AA} + E_{BB} - 2E_{AB} = \epsilon \text{ say.}$$

Consider a vacancy supposed initially to be at an a site in the otherwise perfectly ordered AB crystal. A jump of the vacancy into one of the nearest neighbour b sites disorders a B atom with consequent increase in configuration energy and, for temperatures low compared with the critical temperature, will almost always be followed by a jump of the vacancy back to its original position. Two successive jumps of the vacancy away from its initial position, involving the disordering of two atoms and consequently a greater increase in configuration energy, will occur much less frequently and such jumps also will tend to be immediately retraced: the vacancy is strongly bound to its initial position. It follows that a configuration in which a vacancy has a perfectly ordered local environment is, at sufficiently low temperatures, very stable.

Eventually the vacancy will, in some series of jumps, either return to its initial stable position by a process not depending on retracing of jumps, or escape to a different stable position. Either process will result, in general, in net displacements of the atoms of the alloy; such processes will be called 'unit processes'. In fact, at sufficiently low temperatures, the escape to a different stable position is the more probable unit process. Starting with the local environment of the vacancy perfectly ordered, the vacancy will be in a position to escape if it makes three successive jumps round a square of four nearest neighbour sites in a (100) plane: the vacancy then lies on a (011) mirror plane of symmetry and is just as likely to make a further forward jump round the square as to retrace the last jump. If the vacancy makes the forward jump, however, it will then be bound to a *new* stable position at the site on the square diagonally opposite to the initial site of the vacancy. In going from the initial to the final stable configuration the vacancy makes six jumps round the square. The net result so far as self diffusion is concerned is that if the initial stable vacancy site was an a(b) site, two B(A) atoms will have interchanged places, so that each has been displaced a distance equal to the diagonal of the square, and one A(B) atom will have moved the same distance. *No net disordering occurs.*

In order to execute any other non-trivial series of jumps starting and ending in a stable state, the vacancy and its local environment must pass through a configuration of higher energy than any occurring in the six-jump process described. Moreover, the increase in the number of equivalent processes will not compensate for this increase in configurational energy at sufficiently low temperatures. At sufficiently low temperatures then, we may regard diffusion as taking place solely by the six jump unit process described. As the temperature increases, more and more complicated unit processes come into play until finally a temperature is reached at which correlations between successive vacancy jumps become relatively unimportant and the present point of view ceases to be useful. The present paper will not be concerned with this 'high' temperature range. In the low temperature range then, it is necessary to classify and estimate the relative contributions to self-diffusion of the different possible unit processes. In the following sections this problem will be discussed for the stoichiometric AB alloy: before going on to the actual details of the calculation, however, it is useful to consider, in quite general terms, the form that the calculation will take.

In principle the self-diffusion in the alloy could be examined in the following way. Suppose that at a given temperature and a given time, $t=0$, all the atoms of an equilibrium configuration of the alloy are labelled: by examination of the positions of the labelled atoms at a later time t, where t is very large compared with the mean jump time of a vacancy, the self-diffusion could be evaluated. Suppose that the jump history of every vacancy (and so of every atom) in the time interval t has been followed in detail. Suppose also that the density of vacancies and any other relevant factors are such that correlated motions of groups of vacancies play a negligible part in the process of atomic rearrangement. Fix attention for the moment on just one of the vacancies. In general, and in a way already discussed, two successive jumps of the vacancy will be highly correlated. The jump history of the vacancy in the time t will break up naturally into a sum of shorter histories in each of which the vacancy makes a passage between successive stable states. In a single short history successive vacancy jumps will be highly correlated: successive short histories, on the other hand, will be largely independent of one another, i.e. a short history is independent of the—at least immediate—past history of the vacancy. These short histories are the unit processes already mentioned: each may be characterized by the nature of the atom displacements to which it gives rise, and the frequency with which unit processes of this kind occur in the complete jump history of the vacancy in the time t.

It must be remembered that, although it is convenient to fix attention on the vacancy jump process, what is really of interest is the displacements of the atoms. In a vacancy jump process atoms along the track of the vacancy are moved. For clarity and simplicity in this general description, it will now be assumed that each successive unit process, in the complete history of each vacancy in the time t, moves a fresh set of atoms, i.e. correlations in the successive displacements of a particular atom other than those occurring in a single unit process will be ignored. (The slight modification necessary when this assumption is not made is examined in the detailed calculations to follow.) Let the unit processes be classified into their various groups i, such that a unit process of group i gives rise to net atom displacements $\Sigma d_A^2 = d_{A,i}^2$, $\Sigma d_B^2 = d_{B,i}^2$ say, and unit processes of group i occur with frequency ν_i in the complete history of a vacancy, now taken as typical of all the vacancies. With these suppositions then, the sum of the squares of the displacements of A and B atoms in the time interval t may be written as

$$\left.\begin{aligned}\sum d_A^2 &= \Big(\sum_i d_{A,i}^2 \nu_i\Big) n_V \\ \sum d_B^2 &= \Big(\sum_i d_{B,i}^2 \nu_i\Big) n_V\end{aligned}\right\} \qquad \ldots\ldots(1)$$

where n_V is the equilibrium number of vacancies in the alloy at the given temperature.

It is now apparent from (1) that Σd_A^2 and Σd_B^2 may be calculated by (*a*) considering the various possible unit processes that can take place in an alloy of the given composition and lattice; (*b*) assessing the net displacements to which each of these unit processes, considered in isolation, gives rise; (*c*) assigning appropriate frequencies to each of these processes. The required ratio G of the self-diffusion coefficients may then be obtained by taking the ratio of Σd_A^2 to Σd_B^2: it should be noted that, for the calculation of G, all that is required is the estimation of frequency ratios. In the detailed calculations which follow it is convenient to begin, after some preliminary definitions, with the discussion of the method of assigning frequency ratios since these frequency ratios determine which unit processes need detailed examination: this is done in § 3. In § 4 the required unit processes are classified and the atom displacements to which each gives rise are evaluated. Finally, in § 5, the ratio of the self-diffusion coefficients is calculated and the result discussed in relation to available experimental data.

§ 2. PRELIMINARY DEFINITIONS

It is necessary now to give greater precision to the terms 'local environment of a vacancy' and 'unit process'. The definitions of these terms are framed with the needs of the subsequent analysis in mind.

A ***unit process*** is defined as a vacancy jump process starting and ending with the local environment of the vacancy perfectly ordered, and giving rise to net displacements of atoms.

The *local environment of a vacancy* is defined as the smallest region surrounding the vacancy such that, when this region is perfectly ordered and independently of the state of order of the rest of the crystal, (1) any six-jump unit process of the vacancy displaces only atoms of the original local environment of the vacancy; (2) all possible six-jump unit processes of the vacancy are equally probable. For the simple cubic lattice this definition makes the local environment of a vacancy on a particular lattice site consist of the first to the fifth nearest neighbour shells of atoms of the site.

These definitions have the consequence that successive unit processes are largely independent of one another, with the result that correlations between unit processes will not play an important part in the analysis: this is the property required of the 'short histories' in the general discussion at the end of § 1, where the present definition of unit processes was anticipated.

Finally, it is useful to define the 'neighbourhood' of the local environment of a given vacancy, with respect to a particular unit process for the vacancy. This is defined as that region surrounding the local environment of the vacancy such that, at every stage of the unit process, the local environment of the vacancy lies within the region defined by the initial local environment of the vacancy and its neighbourhood.

§ 3. FREQUENCY RATIOS FOR UNIT PROCESSES

During a particular unit process the region of the crystal lying within the outer boundary of the neighbourhood of the initial local environment of the vacancy will pass through a configuration of maximum energy: the difference ΔE between this maximum configuration energy and the energy of the initial configuration is characteristic of the particular unit process and will in part determine the energy barrier to be surmounted in the course of the unit process. Suppose that unit processes i and j, say, are characterized by energy barriers $\Delta E_i + U_i$ and $\Delta E_j + U_j$ with associated entropy factors n_i and n_j respectively. The entropy factors are just the number of distinct configurations of the characteristic maximum energy available to the vacancy at the start of the given unit process. It will be assumed that the relative probability of unit processes i and j, i.e. the frequency factor ν_i/ν_j, is given by

$$\frac{\nu_i}{\nu_j} = \frac{P_i n_i \exp\left[-(\Delta E_i + U_i)/kT\right]}{P_j n_j \exp\left[-(\Delta E_j + U_j)/kT\right]}, \qquad \ldots\ldots (3.1)$$

where P_i is the probability of finding the perfectly ordered local environment of the given vacancy in a neighbourhood appropriate to the ith unit process. Remembering $|U_i - U_j| \ll \epsilon$, to a good approximation

$$\frac{\nu_i}{\nu_j} = \frac{P_i n_i}{P_j n_j} \exp\left[-(\Delta E_i - \Delta E_j)kT\right]. \qquad \ldots\ldots (3.2)$$

It remains to evaluate P_i/P_j. A good approximation to P_i/P_j may be obtained by methods similar to those used by Bethe (cf. Fowler and Guggenheim 1939) in evaluating the partition function for a binary alloy. In the temperature range of immediate interest, $0 \leqslant T/T_c \leqslant 0{\cdot}5$ where T_c is the critical temperature of long range ordering, the equilibrium configuration of the crystal is essentially perfectly ordered ($1-s \leqslant \mathrm{O}e^{-6}$ where s is the usual long range order parameter) and the application of the Bethe method becomes trivial, giving

$$\frac{P_i}{P_j} = \frac{N_i}{N_j}\exp\left[-(\Delta\mathscr{E}_i-\Delta\mathscr{E}_j)/kT\right], \qquad \ldots\ldots(3.3)$$

where (1) $\Delta\mathscr{E}_i$ is the difference between the configuration energy of the crystal with the neighbourhood of the perfectly ordered local environment of the vacancy appropriate to the ith unit process, and the configuration energy of the crystal with this neighbourhood perfectly ordered; and (2) N_i is the associated entropy factor. From (3.2) and (3.3)

$$\frac{\nu_i}{\nu_j} = \frac{n_iN_i}{n_jN_j}\exp\left[-\{(\Delta E_i+\Delta\mathscr{E}_i)-(\Delta E_j+\Delta\mathscr{E}_j)\}/kT\right]. \qquad \ldots\ldots(3.4)$$

From (3.4) it is seen that it will be convenient to classify the various unit processes into groups, each group being characterizied by a particular value of $(\Delta E+\Delta\mathscr{E})$. In the next section these groups will be discussed in detail in order of increasing $(\Delta E+\Delta\mathscr{E})$, i.e. in order of decreasing frequency.

It is necessary, for this discussion, to distinguish between vacancies which initially occupy an a site (a vacancies) and a b site (b vacancies) respectively. In order to make the classification of the groups of unit processes easier, and to ensure that a and b vacancies executing geometrically the same kind of unit process belong to the same group in the classification, it is convenient to assume that $|E_{\mathrm{AA}}-E_{\mathrm{BB}}| \leqslant |\bar{E}-E_{\mathrm{AB}}| = \epsilon$ where $2\bar{E}=E_{\mathrm{AA}}+E_{\mathrm{BB}}$: the main body of the results to be obtained, however, will be seen to be largely independent of this assumption.

§ 4. Unit Processes

We begin by classifying those unit processes for which the neighbourhood of the initial local environment of the vacancy is perfectly ordered. It will be taken, unless explicitly stated otherwise, that all the unit processes discussed in this section have this characteristic.

4.1. *Unit Processes for which* $\Delta E \sim 12\epsilon$

The only processes in this group are the six-jump processes already discussed in which the vacancy makes six successive jumps round a square of four nearest neighbour sites in a (100) plane: an a(b) vacancy moves to the a(b) site of the square diagonally opposite its initial site; two B(A) atoms and one A(B) atom each move a distance $a\sqrt{2}$ where a is the lattice parameter. The values of ΔE for the two kinds of vacancy are given by

$$\left.\begin{aligned}\Delta E_{\mathrm{a}} &= 8E_{\mathrm{BB}}+4E_{\mathrm{AA}}-12E_{\mathrm{AB}}\\ \Delta E_{\mathrm{b}} &= 8E_{\mathrm{AA}}+4E_{\mathrm{BB}}-12E_{\mathrm{AB}}\end{aligned}\right\}, \qquad \ldots\ldots(4.1)$$

and, for a given vacancy, twenty-four distinct configurations of maximum energy may be reached in three successive vacancy jumps.

4.2. *Unit Processes for which $\Delta E \sim 16\epsilon$*

It is convenient to discuss separately those processes taking place entirely in one (100) plane and those processes taking place entirely in one unit cell of eight nearest neighbour sites: there are no other unit processes in this group.

4.2.1. *Unit processes taking place in one unit cell.*

The eight sites of the unit cell are supposed labelled with the numbers zero to seven (see figure) and the initial configuration is supposed to be that in which the lattice sites are occupied by atoms bearing the same label as the site with zero labelling the vacancy. Any configuration of the labelled atoms can be written as a permutation operator of the kind, symbolized by a Roman capital,

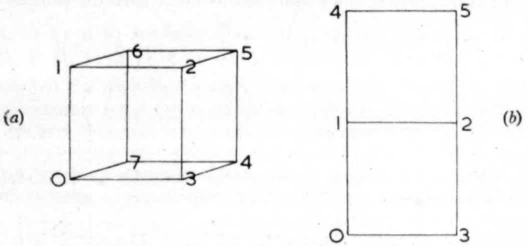

Figure 1. (*a*) The labelling of the sites of the unit cell. (*b*) The labelling of the sites in a (100) plane.

$$\mathrm{P} = \begin{pmatrix} 0 & 1 & 2 & 3 & 4 & 5 & 6 & 7 \\ x_0 & x_1 & x_2 & x_3 & x_4 & x_5 & x_6 & x_7 \end{pmatrix},$$

where $x_i \neq x_j$ for all i and j and $0 \leqslant x_i \leqslant 7$ for all i. This operator is to be read as "the atom which was on site 0 is now on site x_0; the atom which was on site 1 is now on site x_1" etc. The operator may also be regarded as representing the vacancy jump process or processes by which the final configuration is obtained from the initial configuration. In all operators, columns of the same number will be omitted. It is also convenient to have permutation operators acting on the sites themselves: these will be represented by bold face capitals. In particular, the symmetry operators which take the cube into itselt and leave the site 0 invariant will be needed: they are, the rotation operators about the line $0-5$

$$\left.\begin{aligned} \mathbf{C}_3 &= \begin{pmatrix} 1 & 2 & 3 & 4 & 6 & 7 \\ 3 & 4 & 7 & 6 & 2 & 1 \end{pmatrix} \\ \mathbf{C}_3^2 &= \begin{pmatrix} 1 & 2 & 3 & 4 & 6 & 7 \\ 7 & 6 & 1 & 2 & 4 & 3 \end{pmatrix} \end{aligned}\right\}, \qquad \ldots\ldots(4.2)$$

and the reflection operators

$$\left.\begin{aligned} \mathbf{R}_1 &= \begin{pmatrix} 1 & 2 & 4 & 7 \\ 7 & 4 & 2 & 1 \end{pmatrix} \\ \mathbf{R}_2 &= \begin{pmatrix} 1 & 3 & 4 & 6 \\ 3 & 1 & 6 & 4 \end{pmatrix} \\ \mathbf{R}_3 &= \begin{pmatrix} 2 & 3 & 6 & 7 \\ 6 & 7 & 2 & 3 \end{pmatrix} \end{aligned}\right\}, \qquad \ldots\ldots(4.3)$$

corresponding to reflections in the planes 0653, 0752, 0154 respectively. The group of operators (4.2) and (4.3), together with the identity operator, will be referred to as the group $\mathscr{G}$.

Consider first those unit processes in the cube for which the first two successive vacancy jumps are from site 0 to site 1 and then to site 6. The configuration of maximum energy for these processes can now be reached in two further vacancy jumps, first to site 5 and then to site 2. The vacancy is now equally likely to make a further forward jump to site 1 as to retrace the last jump. If the vacancy makes the forward jump, two further forward jumps in each of which the configuration energy is decreased, first to site 6 and then to site 5, give the process

$$\mathrm{P}_1=\begin{pmatrix}5&6\\6&5\end{pmatrix}\begin{pmatrix}1&6\\6&1\end{pmatrix}\begin{pmatrix}1&2\\2&1\end{pmatrix}\begin{pmatrix}2&5\\5&2\end{pmatrix}\begin{pmatrix}5&6\\6&5\end{pmatrix}\begin{pmatrix}1&6\\6&1\end{pmatrix}\begin{pmatrix}0&1\\1&0\end{pmatrix}$$
$$=\begin{pmatrix}0&1&2&5&6\\5&0&6&1&2\end{pmatrix}, \quad \ldots\ldots (4.4)$$

where the seven operators in (4.4) are to be read from right to left, and disordered atoms are indicated by columns in the final configuration operator containing an odd and an even number, zero for this purpose being counted as even. This is a metastable configuration in which the vacancy is on site 5 with its nearest and next nearest neighbours ordered but the site 0 occupied by a wrong atom. The vacancy is in some degree bound to the site 5. The process so far, however, is not a complete unit process in that the local environment of the vacancy (site 0) is not perfectly ordered.

Before going on to discuss 'completion' processes, however, it is convenient to enumerate those jump processes which, starting from the metastable configuration, return to the metastable position leaving some of the atoms of the cube interchanged in position, i.e. those processes which generate different metastable configurations of the same type as P_1. Such processes must not pass through a configuration for which $\Delta E \geqslant 16\epsilon$. If $\Delta E > 16\epsilon$ for some configuration of the process, the process belongs to another group. If $\Delta E = 16\epsilon$ for some configuration then the process is either a completion process, which will be discussed below, or it is effectively *two* unit processes taking place one after the other: this last point will become clearer in what follows. Two processes satisfying these conditions are the six-jump processses

$$\left.\begin{aligned}\mathrm{L}_1&=\begin{pmatrix}5&6\\6&5\end{pmatrix}\begin{pmatrix}1&6\\6&1\end{pmatrix}\begin{pmatrix}0&1\\1&0\end{pmatrix}\begin{pmatrix}0&7\\7&0\end{pmatrix}\begin{pmatrix}6&7\\7&6\end{pmatrix}\begin{pmatrix}5&6\\6&5\end{pmatrix}\\&=\begin{pmatrix}0&1&7\\7&0&1\end{pmatrix}\\\mathrm{L}_1^1&=\begin{pmatrix}5&6\\6&5\end{pmatrix}\begin{pmatrix}6&7\\7&6\end{pmatrix}\begin{pmatrix}0&7\\7&0\end{pmatrix}\begin{pmatrix}0&1\\1&0\end{pmatrix}\begin{pmatrix}6&1\\1&6\end{pmatrix}\begin{pmatrix}5&6\\6&5\end{pmatrix}\\&=\begin{pmatrix}0&1&7\\1&7&0\end{pmatrix}\end{aligned}\right\} \quad (4.5)$$

It is to be noted that $\mathrm{L}_1' = \mathrm{L}_1^{-1} = \mathrm{L}_1^2$. Either of the operators L_1 or L_1^{-1} acting on the configuration P_1 generate new configurations $\mathrm{L}_1\mathrm{P}_1$, $\mathrm{L}_1^{-1}\mathrm{P}_1$ of the same kind.

From L_1 and L_1^{-1} it is possible to generate four more operators of the same kind by operating on L_1 and L_1^{-1} by the symmetry operators of the group $\mathscr{G}$. Thus:

$$\left.\begin{aligned} L_2 &= \mathbf{R}_2 L_1 \mathbf{R}_2^{-1} &&= \begin{pmatrix} 0 & 3 & 7 \\ 7 & 0 & 3 \end{pmatrix} \\ L_2^{-1} &= \mathbf{R}_2 L_1^{-1} \mathbf{R}_2^{-1} &&= \begin{pmatrix} 0 & 3 & 7 \\ 3 & 7 & 0 \end{pmatrix} \\ L_3 &= \mathbf{R}_3 L_1 \mathbf{R}_3^{-1} &&= \begin{pmatrix} 0 & 1 & 3 \\ 3 & 0 & 1 \end{pmatrix} \\ L_3^{-1} &= \mathbf{R}_3 L_1^{-1} \mathbf{R}_3^{-1} &&= \begin{pmatrix} 0 & 1 & 3 \\ 1 & 3 & 0 \end{pmatrix} \end{aligned}\right\} . \qquad \ldots\ldots(4.6)$$

It is to be noted that $\mathbf{R}_1 L_1 \mathbf{R}_1^{-1} = L_1^{-1}$ when $\mathbf{R}_1 L_1^{-1} \mathbf{R}_1^{-1} = (\mathbf{R}_1 L_1 \mathbf{R}_1^{-1})^{-1} = L_1$. It follows immediately from the multiplication table of the group $\mathscr{G}$ that (5) gives the only distinct operators which can be generated from L_1 and L_1^{-1} by the operators of $\mathscr{G}$: thus, for example, $\mathbf{C}_3 L_1 \mathbf{C}_3^{-1} = \mathbf{R}_3 \mathbf{R}_1 L_1 \mathbf{R}_1^{-1} \mathbf{R}_3^{-1} = \mathbf{R}_3 L_1^{-1} \mathbf{R}_3^{-1}$. Further operators of this kind may now be generated by taking all possible products among the operators (4.5) and (4.6). It is again readily verified that the only new operators generated in this way are:

$$\left.\begin{aligned} M_1 &= L_1 L_3^{-1} &&= \begin{pmatrix} 1 & 3 & 7 \\ 3 & 7 & 1 \end{pmatrix} \\ M_1^{-1} &= L_3 L_1^{-1} &&= \begin{pmatrix} 1 & 3 & 7 \\ 7 & 1 & 3 \end{pmatrix} \\ N_1 = N_1^{-1} &= L_1 L_3 &&= \begin{pmatrix} 0 & 1 & 3 & 7 \\ 3 & 7 & 0 & 1 \end{pmatrix} \\ N_2 = N_2^{-1} &= L_1 L_2 &&= \begin{pmatrix} 0 & 1 & 3 & 7 \\ 1 & 0 & 7 & 3 \end{pmatrix} \\ N_3 = N_3^{-1} &= L_2^{-1} L_3 &&= \begin{pmatrix} 0 & 1 & 3 & 7 \\ 7 & 3 & 1 & 0 \end{pmatrix} \end{aligned}\right\} . \qquad \ldots\ldots(4.7)$$

The set of operators (4.5), (4.6) and (4.7) together with the identity operator form a group, $\mathscr{L}$, say: it follows that no new operators of this kind can be formed from products of the operators of $\mathscr{L}$ among themselves. Further, the group $\mathscr{L}$ is invariant under operations of the group $\mathscr{G}$: i.e. no new operators can be generated by subjecting the operators of $\mathscr{L}$ to the operations of $\mathscr{G}$.

We have the result then that if L is any operator of $\mathscr{L}$, the configurations LP_1 have the following properties: (1) LP_1 represents a metastable configuration in which the vacancy is at site 5; a single disordered atom is at site 0 and all other atoms are ordered; (2) the configuration is capable of being generated by a vacancy jump process starting with the vacancy jumping from site 0 to site 1; (3) all the configurations LP_1 are distinct.

So far we have considered only processes starting with the vacancy jump from site 0 to site 1. To each of these processes there will correspond two other processes, one starting with the vacancy jump from site 0 to site 3 and the other starting with the vacancy jump from site 0 to site 7. These processes will be generated by the totality of operators of the form $\mathbf{G}(LP_1)\mathbf{G}^{-1}$ where $\mathbf{G} = \mathbf{R}_2$

(or $\mathbf{C}_3$), $\mathbf{G}=\mathbf{R}_1$ (or $\mathbf{C}_3{}^2$) respectively. Each of these operators generates a metastable configuration of the same kind as before. It is convenient to write these last configurations in a slightly different way: we have

$$\mathbf{G}\mathrm{LP}_1\mathbf{G}^{-1}=\mathbf{G}\mathrm{L}\mathbf{G}^{-1}\mathbf{G}\mathrm{P}_1\mathbf{G}^{-1}=\mathrm{L}'\mathbf{G}\mathrm{P}_1\mathbf{G}^{-1} \qquad \ldots\ldots(4.8)$$

i.e.

$$\mathbf{G}\mathrm{LP}_1\mathbf{G}^{-1}=\mathrm{L}'\mathrm{Q}_G\mathrm{P}_1,$$

where $\mathrm{Q}_G=\mathbf{G}\mathrm{P}_1\mathbf{G}^{-1}\mathrm{P}_1{}^{-1}$. From (2) and (3):

$$\left.\begin{aligned} \mathrm{Q}_{\mathrm{R}_1} &= \mathrm{L}_1{}^{-1}\begin{pmatrix} 2 & 4 & 6 \\ 4 & 6 & 2 \end{pmatrix}=\mathrm{L}_1{}^{-1}\mathrm{Q} \text{ say,} \\ \mathrm{Q}_{\mathrm{R}_3} &= \mathrm{L}_3{}^{-1}\begin{pmatrix} 2 & 4 & 6 \\ 6 & 2 & 4 \end{pmatrix}=\mathrm{L}_3{}^{-1}\mathrm{Q}^{-1} \end{aligned}\right\}, \qquad \ldots\ldots(4.9)$$

and the operators Q and Q^{-1}, which only involve even numbers, commute with the operators of the group $\mathscr{L}$, which only involve odd numbers. It follows from (4.8) and (4.9) that we may write the operators generating the processes having 0 to 3 or 0 to 7 as their initial jumps and giving rise to the metastable position, in the general form $\mathrm{Q}^\alpha\mathrm{LP}$, where $\alpha=\pm 1$ and L is any operator of $\mathscr{L}$. It also follows immediately from (4.8) that no new operators of this kind may be obtained by operating again on $\mathrm{Q}^\alpha\mathrm{LP}_1$ with any of the operators of $\mathscr{L}$.

We are now in a position to discuss completion processes, i.e. those processes which, starting from the metastable configuration, complete a unit process of which the first vacancy jump was from site 0 to site 1. Such processes are certainly given by the reverse of any of the processes leading *to* the metastable position. It follows that the operators representing unit processes starting with a first vacancy jump from site 0 to site 1 have the general form $[\mathrm{Q}^\alpha\mathrm{L}'\mathrm{P}_1]^{-1}\mathrm{LP}_1$ where $\alpha=0,\ \pm 1$ and L′ and L are operators of $\mathscr{L}$. Now Q^α commutes with L′ and so

$$\begin{aligned}[\mathrm{Q}^\alpha\mathrm{L}'\mathrm{P}_1]^{-1}\mathrm{LP}_1=\mathrm{P}_1{}^{-1}\mathrm{L}'^{-1}\mathrm{Q}^{-\alpha}\mathrm{LP}_1&=\mathrm{P}_1{}^{-1}\mathrm{Q}^{-\alpha}\mathrm{L}'^{-1}\mathrm{LP}_1\\ &=\mathrm{P}_1{}^{-1}\mathrm{Q}^{-\alpha}\mathrm{L}''\mathrm{P}_1. \end{aligned} \qquad \ldots\ldots(4.10)$$

Now, from (4.4), we can write

$$\mathrm{P}_1=\begin{pmatrix} 0 & 1 & 5 \\ 5 & 0 & 1 \end{pmatrix}\begin{pmatrix} 2 & 6 \\ 6 & 2 \end{pmatrix}=\mathrm{UV} \text{ say,} \qquad \ldots\ldots(4.11)$$

where V is self-reciprocal and commutes with U and L, and U commutes with Q^α. It follows that

$$\mathrm{P}_1{}^{-1}\mathrm{Q}^{-\alpha}\mathrm{LP}_1=\mathrm{V}^{-1}\mathrm{U}^{-1}\mathrm{Q}^{-\alpha}\mathrm{LUV}=(\mathrm{VQ}^{-\alpha}\mathrm{V})(\mathrm{U}^{-1}\mathrm{LU}). \qquad \ldots\ldots(4.12)$$

But from (4.9) and (4.11),

$$\mathrm{VQ}^{-\alpha}\mathrm{V}=\mathrm{Q}^\alpha. \qquad \ldots\ldots(4.13)$$

Substituting from (4.13) in (4.12):

$$\mathrm{P}_1{}^{-1}\mathrm{Q}^{-\alpha}\mathrm{LP}_1=\mathrm{Q}^\alpha(\mathrm{U}^{-1}\mathrm{LU}). \qquad \ldots\ldots(4.14)$$

For $\alpha=0$, L the identity operator, the unit processes represented by the operator (4.14) are the trivial ones involving a process giving rise to the metastable configuration followed by what is effectively the retracing of the same process. In all other cases the operators (4.14) represent distinct sets of unit processes giving rise to distinct end configurations involving net displacements of the atoms of the cube. By comparison of (4.10) and (4.14) it is seen that the number of distinct unit processes leading to the same end configuration, represented by a particular operator (4.14), is the number of ways in which the particular L can be written as a binary product L′L″: this number is the same for all L. It remains to evaluate the net atom displacements involved in the thirty-six distinct sets of unit processes. This is readily done by writing out the operators (4.14) explicitly. It is found that there are six different classes of unit processes from the point of view of net displacements. These are:

Class 0: 1 set of processes: $\Sigma d_{\mathrm{e}}^2=0$; $\Sigma d_{\mathrm{o}}^2=0$;
Class 1: 2 sets of processes: $\Sigma d_{\mathrm{e}}^2=6a^2$; $\Sigma d_{\mathrm{o}}^2=0$;
Class 2: 8 sets of processes: $\Sigma d_{\mathrm{e}}^2=0$; $\Sigma d_{\mathrm{o}}^2=6a^2$;
Class 3: 3 sets of processes: $\Sigma d_{\mathrm{e}}^2=0$; $\Sigma d_{\mathrm{o}}^2=8a^2$; ......(4.15)
Class 4: 16 sets of processes: $\Sigma d_{\mathrm{e}}^2=6a^2$; $\Sigma d_{\mathrm{o}}^2=6a^2$;
Class 5: 6 sets of processes: $\Sigma d_{\mathrm{e}}^2=6a^2$; $\Sigma d_{\mathrm{o}}^2=8a^2$;

where Σd_{e}^2 and Σd_{o}^2 are the sums of the squares of the displacements of odd and even atoms respectively, and it is to be remembered that these processes are appropriate to a vacancy initially on an even site.

As already mentioned, each of these sets of processes is to be given an equal weight: it follows that the mean displacements per unit even vacancy process of this kind taking place in the cube are

$$\left.\begin{aligned}\overline{\sum d_{\mathrm{e}}^2} &= \frac{2\times 6+16\times 6+6\times 6}{36}\,a^2=4a^2\\ \overline{\sum d_{\mathrm{o}}^2} &= \frac{8\times 6+3\times 8+16\times 6+6\times 8}{36}\,a^2=6a^2\end{aligned}\right\} \quad \text{......(4.16)}$$

The question now arises as to whether these processes discussed above constitute the *only* unit processes taking place in the unit cell. The answer is ‘ no ’ in the sense that we have so far restricted ourselves to unit processes beginning with the vacancy jump 0 to 1. We can generate new unit processes in the same unit cell by operating on any of the unit processes above with $\mathbf{R}_1$ and $\mathbf{R}_2$: these will correspond to unit processes beginning with the jumps 0 to 3 and 0 to 7 respectively. Similarly, we can generate unit processes in the other unit cells sharing the site 0 by operating on the unit processes already obtained with the symmetry operators which take the original unit cell into one of these other unit cells. However, none of the sets of unit processes obtained in these ways need be considered explicitly since it is clear that their inclusion would not affect the result embodied in (4.16). Apart from these processes then, are there still others? Careful examination of the various possibilities for the next vacancy jump at each stage of the ‘prototype’ process P_1 shows that there are no unit processes in the cube still uncounted. It is undesirable to go through this examination in detail here: a single example of the kind of analysis necessary will have to suffice. For example, after the fifth jump of P_1, a possible sixth jump of the vacancy is to site 0 giving rise to the configuration

$$\begin{aligned}P_2&=\begin{pmatrix}0&1\\1&0\end{pmatrix}\begin{pmatrix}1&2\\2&1\end{pmatrix}\begin{pmatrix}2&5\\5&2\end{pmatrix}\begin{pmatrix}5&6\\6&5\end{pmatrix}\begin{pmatrix}1&6\\6&1\end{pmatrix}\begin{pmatrix}0&1\\1&0\end{pmatrix}\\ &=\begin{pmatrix}2&5&6\\5&6&2\end{pmatrix},\end{aligned}$$

in which the vacancy is back at site 0, there is a pair of disordered atoms on sites 5 and 2 and all other atoms are ordered. The vacancy could now make a four jump process, 0 to 7 to 6 to 1 to 0 again, followed by the inverse of the process P_2: this would re-order all the atoms and complete a unit process. However, if, after the sixth and tenth jumps in this process, we were to insert the jump process 0 to 1 to 6 to 5 and back again, which clearly leaves the complete process effectively unchanged, we merely have a unit process, $P_1^{-1}L_1^{-1}P_1$, which has already been counted. It is also by similar considerations to these that a point already mentioned can be clarified, that if $\Delta E = 16\epsilon$ for a second time in some jump process, then that process is either a completion process or is effectively *two* unit processes taking place one after the other.

4.2.2. *Unit processes taking place in one* (100) *plane.*

It is convenient now to label the sites and initial configuration of atoms in a (100) plane as in figure 1 (*b*). Consider first those unit processes in this (100) plane for which the configuration of maximum energy is reached by the four successive vacancy jumps 0 to 1 to 4 to 5 to 2. The vacancy is now equally likely to make a further forward jump to site 1 as to retrace the last jump. If the vacancy makes the forward jump, two further forward jumps, in each of which the configuration energy is decreased, first to site 4 and then to site 5, give the process

$$
\begin{aligned}
P_1' &= \begin{pmatrix} 4 & 5 \\ 5 & 4 \end{pmatrix}\begin{pmatrix} 1 & 4 \\ 4 & 1 \end{pmatrix}\begin{pmatrix} 1 & 2 \\ 2 & 1 \end{pmatrix}\begin{pmatrix} 2 & 5 \\ 5 & 2 \end{pmatrix}\begin{pmatrix} 4 & 5 \\ 5 & 4 \end{pmatrix}\begin{pmatrix} 1 & 4 \\ 4 & 1 \end{pmatrix}\begin{pmatrix} 0 & 1 \\ 1 & 0 \end{pmatrix} \\
&= \begin{pmatrix} 0 & 1 & 2 & 4 & 5 \\ 5 & 0 & 4 & 2 & 1 \end{pmatrix}, \qquad \ldots\ldots(4.17)
\end{aligned}
$$

giving rise to a metastable state with the vacancy on site 5 and a single disordered atom on site 0. As before, it is convenient now to enumerate those processes which start and finish with the metastable configuration, and which satisfy similar conditions to those imposed on the corresponding processes in the previous section. Examination shows that all these processes are restricted to the (100) plane itself and, in particular, that none of the processes discussed in the preceding section play a part here. By similar methods to those already discussed, it is found that the only two processes satisfying the appropriate conditions are

$$
\left.\begin{aligned}
S_1 &= \begin{pmatrix} 2 & 5 \\ 5 & 2 \end{pmatrix}\begin{pmatrix} 1 & 2 \\ 2 & 1 \end{pmatrix}\begin{pmatrix} 0 & 1 \\ 1 & 0 \end{pmatrix}\begin{pmatrix} 0 & 3 \\ 3 & 0 \end{pmatrix}\begin{pmatrix} 2 & 3 \\ 3 & 2 \end{pmatrix}\begin{pmatrix} 2 & 5 \\ 5 & 2 \end{pmatrix} \\
&= \begin{pmatrix} 0 & 1 & 3 \\ 3 & 0 & 1 \end{pmatrix} \\
S_1' &= \begin{pmatrix} 2 & 5 \\ 5 & 2 \end{pmatrix}\begin{pmatrix} 2 & 3 \\ 3 & 2 \end{pmatrix}\begin{pmatrix} 0 & 3 \\ 3 & 0 \end{pmatrix}\begin{pmatrix} 0 & 1 \\ 1 & 0 \end{pmatrix}\begin{pmatrix} 1 & 2 \\ 2 & 1 \end{pmatrix}\begin{pmatrix} 2 & 5 \\ 5 & 2 \end{pmatrix} \\
&= \begin{pmatrix} 0 & 1 & 3 \\ 1 & 3 & 0 \end{pmatrix}
\end{aligned}\right\} \qquad \ldots\ldots(4.18)
$$

and $S_1' = S_1^2 = S_1^{-1}$. Either of the operators S_1 or S_1^{-1} acting on the configuration P_1' generate a new configuration of the same kind. Since these are the only operators of this kind, it follows that we can write down immediately the operators representing unit processes taking place in the (100) plane and starting with the vacancy jumps 0 to 1 to 4 to 5 (or, equivalently, 0 to 1 to 2 to 5): they are of the general form

$$[S_1^{\beta}P_1']^{-1}S_1^{\alpha}P_1 = P_1'^{-1}S_1^{\gamma}P_1', \qquad \ldots\ldots(4.19)$$

where $\gamma=0$, ± 1. The set of unit processes given by $\gamma=0$ are trivial: the remaining two sets of processes belong to the same class of diffusion process and each gives

$$\Sigma d_e^2 = 0; \qquad \Sigma d_o^2 = 8a^2. \qquad \ldots\ldots(4.20)$$

Each of the sets of processes has to be given an equal weight: it follows that we may write the mean displacement per unit even vacancy process of this kind taking place in the (100) plane as

$$\overline{\Sigma d_e}^2 = 0; \qquad \overline{\Sigma d_o}^2 = 5\cdot\dot{3}a^2. \qquad \ldots\ldots(4.21)$$

Finally, we can generate other unit processes by operating on the unit processes already obtained with those symmetry operators of the cubic lattice which leave the site 0 unchanged. These processes need not be considered explicitly, however, since their inclusion would not affect the result (4.21). There are no other unit processes in this group taking place in a (100) plane. Further, the unit processes considered in this and the preceding section exhaust this group completely.

4.3. *Unit Processes for which* $\Delta E \sim 18\epsilon$

This group of unit processes comprises, amongst others, processes in which, by a six jump process, the vacancy escapes from one or other of the metastable configurations of the processes discussed in the preceding section, leaving behind a semi-permanent region of local disorder. As will be seen in the next section, the frequencies of unit processes in this, and groups with higher values of ΔE, are sufficiently low in the temperature range of immediate interest to allow the contribution to the ratio of the self-diffusion coefficients from such unit processes to be ignored. This then completes the discussion of unit processes with the characteristics, (1) the neighbourhood of the initial local environment of the vacancy is perfectly ordered and (2) the frequency is sufficiently high for the process to be included in the present approximation.

For the same reason, all unit processes for which the neighbourhood of the initial local environment of the vacancy is disordered may be ignored. Examination shows that there are no such processes for which $\Delta E + \Delta\mathscr{E} < 18\epsilon$.

§ 5. THE RATIO OF THE SELF-DIFFUSION COEFFICIENTS

Ignoring for the moment then, (*a*) unit processes for which $\Delta E + \Delta\mathscr{E} \gtrsim 18\epsilon$, and (*b*) all correlations in successive displacements of a particular atom except those occurring in a single unit process, the results of the preceding sections make possible the calculation of the ratio G of the self-diffusion coefficients of the two components of the alloy. We introduce frequencies ν_{a1}, ν_{b1}, ν_{a2} and ν_{b2} for the unit processes for a and b vacancies respectively: subscript 1 refers to the group $\Delta E \sim 12\epsilon$; subscript 2 to the group $\Delta E \sim 16\epsilon$, and to save notational complexity we have anticipated the result that the frequencies for 'plane' and 'cube' unit processes of group 2 are the same. Let n_a and n_b be the concentrations of a and b vacancies respectively. It follows from § 4 and the general description at the end of § 1 that

$$G = \Sigma d_A{}^2 / \Sigma d_B{}^2$$

$$= \frac{2n_a\nu_{a1} + 4n_b\nu_{b1} + 4n_a\nu_{a2} + 11\cdot\dot{3}n_b\nu_{b2}}{4n_a\nu_{a1} + 2n_b\nu_{b1} + 11\cdot\dot{3}n_a\nu_{a2} + 4n_b\nu_{b2}}. \qquad \ldots\ldots (5.1)$$

Introducing $r = n_b/n_a$; $\alpha_1 = \nu_{b1}/\nu_{a1}$; $\alpha_2 = \nu_{b2}/\nu_{a2}$ and $\delta = \nu_{a2}/\nu_{a1}$, we may write

$$G = \frac{(2 + 4r\alpha_1) + \delta(4 + 11\cdot\dot{3}r\alpha_2)}{(4 + 2r\alpha_1) + \delta(11\cdot\dot{3} + 4r\alpha_2)}. \qquad \ldots\ldots (5.2)$$

From (3.2),

$$\delta = \frac{\nu_{a2}}{\nu_{a1}} = \frac{48e^{-16\epsilon/kT}}{24e^{-12\epsilon/kT}} = 2e^{-4\epsilon/kT} = 2\theta \text{ say}, \qquad \ldots\ldots (5.3)$$

where the numerical factors are the entropy factors n_i and n_j for the two unit processes (this entropy factor is the same for both 'plane' and 'cube' processes of group 2, justifying the introduction of a single frequency for these processes). Similarly,

$$\alpha_1 = \alpha_2{}^2 = \exp\left[-4(E_{AA} - E_{BB})/kT\right] = \theta^{2\beta} \text{ say},$$

where

$$\beta = (E_{AA} - E_{BB})/(E_{AA} + E_{BB} - 2E_{AB}) = (E_{AA} - E_{BB})/2\epsilon. \qquad \ldots\ldots (5.4)$$

Finally, using the value for kT_c given by the quasi-chemical approximation,

$$\epsilon = kT_c \ln(3/2) = 0\cdot4055kT_c. \qquad \ldots\ldots (5.5)$$

Substituting from (5.3), (5.4) and (5.5) in (5.2):

$$G = \frac{(2 + 4r\theta^{2\beta}) + 2\theta(4 + 11\cdot\dot{3}r\theta^{\beta})}{(4 + 2r\theta^{2\beta}) + 2\theta(11\cdot\dot{3} + 4r\theta^{\beta})}, \qquad \ldots\ldots (5.6)$$

where $\theta = \exp(-1\cdot622T_c/T)$.

In general it is to be expected that r will be a function of the temperature, its precise form depending on the formation energies for the two different kinds of vacancy. For given $\theta(T/T_c)$ and β, however, G is a monotonically increasing function of r: it follows, that, for given θ and β, and *independently of any temperature variation of r*,

$$\frac{1 + 4\theta}{2 + 11\cdot\dot{3}\theta} \leqslant G \leqslant \frac{2 + 11\cdot\dot{3}\theta^{1-\beta}}{1 + 4\theta^{1-\beta}} \qquad \ldots\ldots (5.7)$$

or, for $\theta \ll 1$, $|\beta| \ll 1$,

$$\tfrac{1}{2} - 0\cdot8\dot{3}\theta \leqslant G \leqslant 2 + 3\cdot\dot{3}\theta, \qquad \ldots\ldots (5.8)$$

where the constant terms represent the effects of processes of group 1 (the six-jump processes), and the terms in θ represent the effects of processes of group 2.

The extension of the discussion to include unit processes involving higher values of ΔE would lead to the appearance of terms in higher powers of θ in (5.7) and (5.8). For $0 \leqslant T/T_c \leqslant 0\cdot5$, however, $0 \leqslant \theta \leqslant 0\cdot04$ and it is likely that (5.8) gives a good approximation to upper and lower bounds for G in this reduced temperature range. The value $T/T_c \sim 0\cdot5$ may be taken as being the reduced temperature at which, under favourable circumstances, diffusion measurements just become practicable. It is seen from (5.6) that although group 2 processes may, particularly for $r \gg 1$ or $r \ll 1$, make an appreciable contribution to the temperature variation of G in the higher part of this reduced temperature range, the upper and lower bounds for G are, by (5.8), substantially unaffected by these processes.

§ 6. DISCUSSION

The calculation of G in the preceding section was made with the neglect of all correlations in successive displacements of a particular atom except those occurring in a single unit process. The definition of a unit process (§ 2), however, was framed in such a way as to make correlations between successive unit processes small. The only residual correlations are, in fact, a property solely of the geometry of the lattice, and are of essentially the same nature as the Bardeen–Herring correlations for vacancy diffusion in a pure metal.

A detailed calculation of the effect of these residual correlations on the ratio G would be very difficult and has not been done. The order of magnitude of the effect, however, may be estimated by a step by step examination of the effects of residual correlation between two, three, four ... successive six-jump unit processes (the processes giving the dominant contribution to G) of a particular vacancy. Such a calculation indicates that, in fact, the correlation correction to G will be negligible. Certainly the inclusion of the effects of these residual correlations will leave unaffected the main conclusion of § 5, namely that in the temperature range $0 \leqslant T/T_c \leqslant 0{\cdot}5$, $1/a \leqslant G \leqslant a$ where $a \simeq 2$ and is only slightly temperature dependent.

The calculations of the present paper have also been concerned solely with the stoichiometric simple cubic binary alloy. This is because unit processes for this alloy are geometrically relatively simple to visualize and analyse. The available results of experimental measurements of self-diffusion are for the body-centred cubic alloy Cu–Zn with a composition slightly away from exact stoichiometry. A corresponding analysis for the body-centred cubic alloy to that given in the preceding sections would, however, be considerably more tedious owing to the greater diversity and complexity of the unit processes other than those of group 1. In view of the meagreness of the experimental data available, it has not seemed worth while to carry this analysis through in detail. The processes of group 1 (the six-jump unit processes, but now round the sides of a rhombus or folded rhombus of nearest neighbour sites rather than a square as in the simple cubic lattice) are again simple, however, and it is readily shown that, ignoring all unit processes other than these (the low temperature limit), $2/3 \leqslant G \leqslant 3/2$. Further, there is little doubt that a more detailed analysis would lead to a similar result to that for the simple cubic lattice, namely that in the temperature range $0 \leqslant T/T_c \leqslant 0{\cdot}5$, $1/a \leqslant G \leqslant a$ where $a \simeq 3/2$ and is only slightly temperature dependent. Such experimental evidence as there is (Kuper *et al.* 1956) is in agreement with this simple and yet very striking result.

In conclusion, it is perhaps noteworthy that if, as has been assumed in the preceding discussion, the only mechanism of atom interchange in these alloys is by vacancy jumps from a site to a nearest neighbour site, then it would be expected that self-diffusion in face-centred cubic alloys would be markedly different in character from that for simple and body-centred cubic alloys discussed above.

In particular, there would seem to be no reason to expect the ratio G to be severely restricted by ordering effects in face-centred cubic alloys, in marked contrast to the result obtained above for simple and body-centred cubic alloys. In consequence an experimental study of face-centred and body-centred cubic alloys from this point of view might prove rewarding.

ACKNOWLEDGMENTS

The author would like to thank Dr. C. W. McCombie for his interest and advice at all stages of the investigation and Dr. A. B. Lidiard for some very interesting correspondence.

REFERENCES

ELCOCK, E. W., and MCCOMBIE, C. W., 1958, *Phys. Rev.*, **109**, 605.

FOWLER, R. H., and GUGGENHEIM, E. A., 1939, *Statistical Thermodynamics* (Cambridge: University Press).

KUPER, A. B., LAZARUS, D., MANNING, J. R., and TOMIZUKA, C. T., 1956, *Phys. Rev.*, **104**, 1536.

Lattice Absorption Bands in Silicon

By F. A. JOHNSON
Royal Radar Establishment, Great Malvern, Worcs.

MS. received 19*th August* 1958, *in revised form* 29*th September* 1958

Abstract. A series of detailed measurements have been made of the absorption spectrum of pure vacuum grown crystals of silicon in the wavelength range 2μ to 30μ, and over the temperature range 20°K to 365°K.

Some new absorption bands have been found, and an explanation is offered for the positions and temperature dependence of all the principal absorption peaks in terms of multiple phonon interactions involving phonons with energies corresponding to temperatures of 200, 480, 595 and 695°K.

---

§ 1. Introduction

The lattice absorption bands of silicon, which extend from about 5 to 6μ to at least 30μ, have been investigated by a number of workers in the past, notably by Collins and Fan (1954). They showed that these bands were characteristic of the bulk material, largely independent of impurities or dislocations, and had a temperature dependence which suggested that they were connected with thermal vibrations. They were not able, however, to suggest any satisfactory explanation for the presence of these bands.

Lax and Burstein (1955) showed theoretically that although there could be no interaction between a single phonon and infra-red radiation in a homopolar crystal, the simultaneous interaction of two phonons would produce an electric moment with which the radiation could interact. Two distinct types of interaction are possible, firstly the absorption of a photon and the emission of two phonons (summation bands), and secondly the absorption of a photon and a low-energy phonon and the emission of a high-energy phonon (difference bands). These two mechanisms are readily distinguished by the different temperature dependences. Summation bands involving the emission of two phonons of wave number ν_1 and ν_2 will have a temperature dependence of the form $(1+F_1)(1+F_2)-F_1F_2$, where $F=1/[(\exp(\boldsymbol{hc}\nu/\boldsymbol{k}T)-1]$, and difference bands involving the absorption of a phonon of wave number ν_1 and the emission of a phonon of wave number ν_2 will have a temperature dependence of the form $F_1(1+F_2)-F_2(1+F_1)$. In each case the first term is proportional to the probability of absorption of a photon and the second term is proportional to the probability of induced emission of a photon; thus the difference is proportional to the nett absorption. Since F is approximately unity when $\boldsymbol{hc}\nu/\boldsymbol{k}T=0{\cdot}6$, and decreases exponentially with decreasing temperature, summation bands only would be observed at the lowest temperatures, and these would not become markedly temperature dependent until the thermal energy became comparable with the energy of one of the phonons involved in the summation band.

The position of any absorption band is determined by the energy transferred to the lattice by the two phonons, and to conserve momentum the two phonons must have equal but opposite wave vectors. Lax and Burstein (1955) also investigated the selection rules for the diamond lattice and showed that the two phonons must come from distinct branches of the vibration spectrum. Now the absorption due to the interaction of radiation with phonons from a particular pair of distinct branches of the vibration spectrum must spread over an appreciable energy range since the vibration spectrum is not a line spectrum, but the maxima in the absorption must be closely associated with the maxima in the density of states for the two branches: sharply defined maxima in the density of states will result in sharper absorption peaks, and conversely less sharply defined maxima will result in boarder peaks. It must also follow that the more sharply defined the maxima in the density of states becomes, the more nearly the *energies* of the phonons producing the peak absorption become characteristic of the two branches† and consequently the temperature dependent factors F also become characteristic of the branches.

In general, the maxima in the density of states tend to occur for wave vectors nearer the edge of the reduced zone and consequently the characteristic energies of the phonons associated with lattice absorption peaks will tend to be close to the energies of phonons at the edge of the reduced zone. On this basis there should be a close correlation between the lattice absorption bands and the vibration spectrum.

Previous data on the lattice absorption bands in silicon are insufficiently detailed to form the basis of an unambiguous interpretation in terms of a vibration spectrum and are further complicated by the presence of a strong band at 9μ and a weaker band at 19μ due to oxygen impurities. More recent techniques have resulted in the preparation of silicon crystals which have much smaller concentrations of dissolved oxygen, and it therefore seemed desirable to undertake a careful redetermination of the positions and temperature dependence of the lattice bands in silicon using the purer material now available.

§ 2. EXPERIMENTAL

Three silicon specimens of thickness approximately 18, 4 and 1 mm were cut from pure high quality single crystals grown *in vacuo*. These were mechanically polished and their transmissions were measured as a function of wavelength over the range 2 to 30μ.

The optical system used consisted of a Nernst filament lamp as a source, a Leiss double monochromator and two mirror systems, one for focusing the radiation from the monochromator on to the specimen, and the other for focusing the radiation transmitted by the specimen on to a Golay detector. In addition a mask that could be moved into or out of the beam of radiation as required was incorporated for checking the zero response of the detector. The output from the Golay detector was fed into a narrow band Barr and Stroud amplifier via a calibrated attenuator. The amplified signal was rectified by an electromechanical phase sensitive rectifier and, after passing through a simple low pass filter having a time constant of 5 seconds, was measured in a Honeywell Brown recording potentiometer.

The cryostat was essentially the same as that described by Roberts (1954) but incorporating the improved window seals described by Roberts (1958).

---

† In the hypothetical limit of a line vibration spectrum, the density of states is infinite and the phonon energies are characteristic of the branches being of course the line energies.

The monochromator was calibrated by determining the positions of known absorption bands using the method described by Downie, Magoon, Purcell and Crawford (1953). High resolution was achieved by the use of four sets of prisms: CaF_2, NaCl, KBr, and CsBr for the appropriate parts of the wavelength range.

The maximum gain of the detection system was adjusted until the noise level was approximately 2 to 3% of the signal. The method used for determining the transmission of the specimen at each particular wavelength was a follows. The wavelength was fixed by setting the prism angle to the appropriate value, the attenuator gain was reduced by a suitable amount, and the slit widths of the monochromator were then adjusted by a servo loop to give an approximately constant output signal. The servo loop was disconnected and measurements were made in the order shown in table 1. The intervals between measurements were to allow the amplifier transients to decay. The purpose of using the calibrated attenuator was to make the recorder deflection with and without the specimen comparable. This greatly reduces the dependence of the transmission measurements on the linearity of the amplifier and increases the accuracy of the measurements particularly for small transmissions.

Table 1

Measured Quantity	Attenuator Gain	Specimen Position	Mask Position	Time Interval (sec)
Detector signal	G	Out	Out	36
—	Maximum	In	Out	36
Detector signal	Maximum	In	Out	72
—	G	Out	Out	36
Detector signal	G	Out	Out	36
—	G	Out	In	36
Detector signal	G	Out	In	18
—	Maximum	Out	In	18
Detector signal	Maximum	Out	In	18
Thermocouple e.m.f.	—	—	—	18

The entire measuring sequence was carried out automatically. A uniselector was used to control the various stages of the experiment and readings of the recorder deflection were made at regular intervals by a Hilger and Watts digitizer during the time periods shown in table 1 and automatically punched out on tape by a standard Creed high speed punch. After each complete set of readings had been taken, the prisms of the monochromator were rotated through an angle of 30 seconds to select a new wavelength for the next set. This process was continued until the whole useful wavelength range of the particular prisms had been covered.

The absorption coefficient α at each wavelength was computed from the equation

$$t=\frac{16n^2\exp(-\alpha d)}{(n+1)^4-(n-1)^4\exp(-2\alpha d)} \qquad \ldots\ldots(1)$$

where d is the specimen thickness in millimetres and n is the refractive index. The refractive index of silicon has been measured by Briggs (1950) and the results can be represented by the empirical equation

$$n^2=1+A/[1-(\nu/\nu_0)^2] \qquad \ldots\ldots(2)$$

where $A = 10{\cdot}695$ and $\nu_0 = 3226\,\text{mm}^{-1}$. It was found that in the region of lowest absorption between 2 and $4\,\mu$, the measured transmissions of the three samples were very nearly the same, but exceeded the theoretical limit of $2n/(n^2+1)$ calculated from Brigg's data by 1 to 2%. It therefore seemed reasonable to modify the value of A in formula (2) in each case to make these two figures agree.

A short punched tape containing the necessary auxiliary data giving the constants of formulae (1) and (2) and the calibration curves of the monochromator was added to the main tape containing the readings taken during the experiment. The entire data was then processed by the laboratory's electronic computer. The computer was programmed to type out the results in seven columns giving respectively: the prism angle, the transmission, the absorption coefficient, the wave number, the wavelength, the thermocouple e.m.f., and finally any comments such as the number of readings rejected in the detailed statistical analysis of the data or comments on any other feature likely to reduce the accuracy of a particular result.

The four curves giving the absorption coefficient as a function of wave number for the four fixed temperatures are the best values obtained from approximately 400 000 readings taken in the course of the experiment.

§ 3. Results

The absorption coefficient was plotted against wave number for the four temperatures and the results are shown in the figure. The 20° and 77° curves

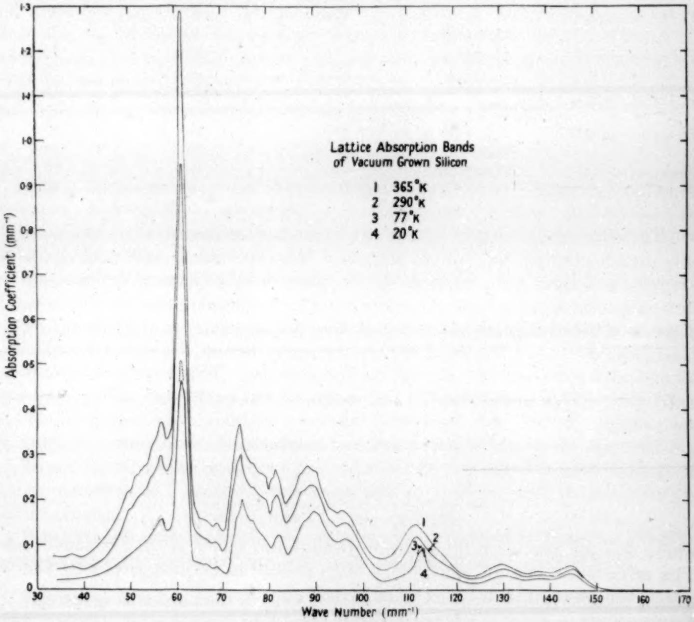

were almost identical, the only significant difference being in the height of the two peaks at 61 and 56 mm^{-1}.

The new features that have been found in this more detailed investigation are a very weak absorption tail extending from 150 to 190 mm^{-1}, a number of weak absorption bands in the range 100 to 150 mm^{-1} overlaid by the residual oxygen band at 110 mm^{-1}, and small absorption peaks at approximately 76, 69 and 38 mm^{-1}. The residual oxygen band at 110 mm^{-1} is approximately five times smaller than that usually found in gas-pulled crystals, and the oxygen band at 51·5 mm^{-1} has disappeared. The main absorption peaks below 100 mm^{-1} have been reported previously.

With the exception of the weak band at 38 mm^{-1}, all the bands are evidently summation bands. The key to the identification of this spectrum in terms of characteristic phonon energies is to be found in the three well-defined high energy bands. The shapes of these bands are very definite, and consequently the temperature dependence can be measured with a much greater certainty than is possible for the more complex bands below 100 mm^{-1}. Further, these high energy bands must clearly be due to combinations of optical modes. The analysis of these bands in terms of two-phonon summation bands proved to be impossible: no correlation between the observed position and temperature dependence could be established. However, a logical extension of Lax and Burstein's theory suggests the possibility of interactions between the infra-red radiation and three or more phonons. It would be expected that for such higher order interactions the matrix elements for the transitions would be considerably smaller than the matrix elements for two-phonon processes, and further that the simple selection rule for the two-phonon processes would not be applicable to the three-phonon case. It would thus be reasonable to attribute the very weak absorption tail running from 150 to 190 mm^{-1} to four-phonon summation bands, the weak bands between 100 and 150 mm^{-1} to three-phonon summation bands, and the main bands below 100 mm^{-1} to two-phonon summation bands. The evidence for this general interpretation will now be discussed in detail.

§ 4. DISCUSSION

One would expect the highest energy band to be a summation band of three transverse optic phonons. This would require the characteristic temperature for each phonon to be 695°K, and the characteristic temperature dependence of the band to be $(1+F_1)^3-F_1^3$, where $F_1=[\exp(695/T)-1]^{-1}$. The relevant information is set out in the first row of table 2 and it will be seen that the characteristic temperature dependence calculated as described above agrees well with the observed temperature dependence.

The next band is presumably due to a combination of two transverse optic phonons and one longitudinal optic phonon. This would require a characteristic temperature for the longitudinal phonon of 595°K, and the characteristic temperature dependence of the band to be $(1+F_1)^2(1+F_2)-F_1^2F_2$, where $F_2=[\exp(595/T)-1]^{-1}$. It will be seen from the second row of table 2 that the calculated temperature dependence agrees well with the observed temperature dependence.

The third band may be either a combination of one transverse optic phonon and two longitudinal optic phonons or a combination of two transverse optic phonons and one longitudinal acoustic phonon, provided a characteristic

Table 2. Assignment of Absorption Peaks and Comparison of Theoretical and Experimental Values for Temperature Dependence

(1)		(2)				(3)	(4)			
ν(mm^{-1})	(**hc**ν/**k**)(°K)	20°	77°	290°	365°		20°	77°	290°	365°
144·8	2085	1	1	1·3	1·6	TO+TO+TO				
						695+695+695	1	1	1·33	1·64
137·8	1985	1	1	1·4	1·7	TO+TO+LO				
						695+695+595	1	1	1·41	1·72
130·2	1875	1	1	1·45	1·9	TO+LO+LO				
						695+595+595	1	1	1·45	1·85
						or TO+TO+LA				
						695+695+485	1	1	1·49	1·93
96·4	1388	1	1	1·3	1·5	TO+TO				
						695+695	1	1	1·22	1·40
89·6	1290	1	1	1·3	1·5	TO+LO				
						695+595	1	1	1·27	1·46
81·9	1180	1	1	1·3	1·6	TO+LA				
						695+485	1	1	1·35	1·62
76·6	1103					TO+TA+TA				
						695+204+204				
74·0	1065	1	1	1·5	1·8	LO+LA				
						595+470	1	1	1·44	1·74
68·9	992					LO+TA+TA				
						595+198+198				
61·0	880	1	1·1	2·05	2·65	TO+TA				
						695+185	1	1·10	2·25	2·72
						or 680+200	or 1	1·08	2·21	2·56
56·6	815	1	1·1	2·0	2·6	LO+TA				
						595+220	1	1·06	2·02	2·46
						or 575+200	or 1	1·08	2·28	2·63

(1) Position ; (2) relative intensity (observed) ; (3) suggested assignment and characteristic temperatures ; (4) corresponding relative intensity (calculated). T = transverse, L = longitudinal, O = optic, A = acoustic.

Three-phonon cut-off 2200°K = 3 × 733°K ; two-phonon cut-off 1470°K = 2 × 735°K.

temperature of 485°K is assigned to the longitudinal acoustic phonon. Again it will be seen that in either case the calculated temperature dependence agrees well with the observed temperature dependence.

The region between 124 and 104 mm^{-1} is largely obscured by the residual oxygen band, but in the case of the 20°K curve the oxygen band is fairly narrow and an examination of the shape of the absorption curve in this region indicates that there are probably unresolved absorption bands at 123, 116, 108 and 103 mm^{-1} corresponding to equivalent temperatures of 1780, 1670, 1555 and 1480°K respectively. These bands could well be due to three phonon summation bands.

The probable assignment of the main bands below 100 mm^{-1} is shown in table 2 and the agreement between the calculated and observed temperature dependences is reasonably good. There is some uncertainty in the figures quoted for the observed temperature dependence for these bands due to the difficulty in estimating the background absorption in each case. The values assigned to the characteristic temperature dependence for the transverse acoustic branch range from 185 to 220°K, the most probable value being about 200°K. It will be seen from table 2 that this value gives a slightly better agreement between the observed and calculated temperature dependence of the strongest band at 61 mm^{-1}.

Additional evidence for the correctness of this general interpretation is provided by the selection rules for two-phonon processes which, it will be recalled, require the two phonons to come from distinct branches. Thus the following combinations of two phonons would be forbidden: two longitudinal optic or acoustic phonons in all directions; two transverse optic phonons in the 100 and 111 directions; and a longitudinal optic and longitudinal acoustic phonon near the zone boundary in the 100 direction. The forbidden combinations of two longitudinal optic or acoustic phonons would be expected to produce minima in the absorption curves at about 83 mm^{-1} and 67 mm^{-1} respectively, and it will be seen from figure 1 that there is a pronounced minimum at 84 mm^{-1} and a large gap in the curves between 70 and 64 mm^{-1}. Further it would be expected that the band at 96·4 mm^{-1} attributed to two transverse optic phonons would be markedly weaker than the other two phonon bands since this combination is forbidden in two symmetry directions, and again it will be seen from figure 1 that this is the case. The minimum at 80 mm^{-1} on the high energy side of the band at 74 mm^{-1} attributed to longitudinal optic and acoustic phonons may be due to the fact that this combination is forbidden near the zone boundary in the 100 direction.

The summation band of phonons from the longitudinal acoustic and transverse acoustic branches which would be expected to appear somewhere between 47·5 mm^{-1} and 50·5 mm^{-1} is evidently unresolved. It is possible that the small hump appearing at 49·3 mm^{-1} in the two higher temperature curves may be due to this combination. The weak band at 68·9 mm^{-1} is presumably a combination of a longitudinal optic and two transverse acoustic phonons. This assignment would suggest a characteristic temperature of 198°K for the transverse acoustic phonons, in good agreement with previous estimates. Further it would be expected that the combination of a transverse optic and two transverse acoustic phonons would produce an absorption peak at approximately 76 mm^{-1} and the very small hump in the absorption curves at 76·6 mm^{-1} may be due to this combination. The very weak band at 37·2 mm^{-1} would appear to be a difference band, possibly due to the absorption of a transverse acoustic phonon and the emission of a longitudinal and a transverse acoustic phonon.

The estimated position for the cut-off for the three-phonon processes is 153 mm^{-1} and for the two-phonon processes is 102 mm^{-1}. These two figures suggest that the equivalent temperature of the fundamental Raman frequency is 734°K. External evidence for the general correctness of this value is provided by the known values of the Debye temperatures. The high temperature θ_D values have been measured for diamond, silicon, germanium, and grey tin, and are 1960, 660, 390 and 240°K respectively (Hill and Parkinson 1952). The θ_D values should provide a reasonable indication of the order of magnitude of the Raman equivalent temperature which, in the case of diamond, has been measured directly, and has a value of 1920°K. Recently the Raman equivalent temperature has been measured for germanium by Brockhouse and Iyengar (1958) and has a value of 435°K. Thus the value of 734°K assigned to the Raman equivalent temperature for silicon is evidently of the right order.

The results obtained in this analysis of the lattice bands of silicon can be compared with the values of the equivalent temperatures of phonons in the 100 direction deduced from the analysis of the fine structure in the absorption edge of silicon (Macfarlane, McLean, Quarrington and Roberts 1958). This structure is interpreted in terms of indirect transitions involving single phonons with equivalent temperatures of 212, 670, 1050 and 1420°K. These are interpreted as transverse acoustic, longitudinal acoustic, longitudinal optic, and transverse optic phonons respectively. The lowest energy phonon has an energy close to that assigned to transverse acoustic phonons in this paper, but the other three do not agree and the two high energy phonons have equivalent temperatures well above that estimated for the Raman equivalent temperature. The explanation for this large discrepancy may be that the indirect transitions are assisted by more than one phonon. Obviously, however, one must await the results of neutron scattering experiments before one can be certain about the correctness of this interpretation of the lattice bands of silicon.

ACKNOWLEDGMENTS

It is a pleasure to acknowledge the advice and assistance received from colleagues in this laboratory. In particular I should like to thank Dr. D. J. Howarth for programming the computer and Miss M. G. Harrison for carrying out the computations and graph plotting.

This paper is published by permission of the Controller, H.M. Stationery Office.

REFERENCES

BRIGGS, H. B., 1950, *Phys. Rev.*, **77,** 727.
BROCKHOUSE, B. N., and IYENGAR, P. K., 1958, *Phys. Rev.*, **111,** 745.
COLLINS, R. J., and FAN, H. Y., 1954, *Phys. Rev.*, **93,** 674.
DOWNIE, A. R., MAGOON, M. C., PURCELL, T., and CRAWFORD, B., 1953, *J. Opt. Soc. Amer.*, **43,** 941.
HILL, R. W., and PARKINSON, D. H., 1952, *Phil. Mag.*, **63,** 309.
LAX, M., and BURSTEIN, E. B., 1955, *Phys. Rev.*, **97,** 39.
MACFARLANE, G. G., MCLEAN, T. P., QUARRINGTON, J. E., and ROBERTS, V., 1958, *Phys. Rev.*, **111,** 1245.
ROBERTS, V., 1954, *J. Sci. Instrum.*, **31,** 251.
—— 1959, *Ibid.*, in the press.

Thermal Relaxation in Gases: A New Method of Analysing the Experimental Data

By A. C. J. JOHNSON

Sub-department of Acoustics, Department of Physics, University of Liverpool

Communicated by H. D. Parbrook; MS. received 17th September 1958, in final form 7th November 1958

Abstract. It is shown that in the case of a single relaxation in a gas the relaxation time can be found in a simple manner if measurements are made of *both* the velocity dispersion and the absorption per wavelength. The problem is reduced to one of fitting circles and straight lines to the data. In the case of a multiple relaxation it is shown how the individual relaxation times can be found. The method is applied to some published results in a few gases to show the working of the method in practice.

§ 1. Introduction

The most commonly used method for finding the relaxation time for a thermal relaxation process in a gas is to plot the velocity of sound or the excess absorption per wavelength over that due to viscosity and heat conduction, against the logarithm of the ratio of frequency to pressure. Both of these graphs should be symmetrical curves. From the peak in the absorption graph or the point of inflection of the velocity graph, the relaxation time can be calculated. Quite often neither of these points can be reached experimentally and the points have to be fixed by extrapolation. As neither of the curves has a simple shape such as a straight line or circle, it becomes necessary to use templates, or some such device to find the wanted point. It is the aim of this paper to show that, by making use of both velocity and absorption measurements, it is possible to reduce the problem to one of fitting circles and straight lines. As a consequence of this method of presenting the data it becomes possible to decide, not only the amount of the relaxing specific heat and the relaxation time, for a single time constant process, but also the nature of the relaxation processes if there is more than one time constant. A further advantage of the method is that not only is use made of all the experimental data, but also it is possible to obtain information on the viscothermal absorption, provided that this can be satisfactorily represented by the Stokes–Kirchhoff equation. The method is related to that used in the analysis of dielectric constant measurements by Cole and Cole (1941).

§ 2. Equations for a Single Relaxation Process

The basic equation from which the usual expressions for the velocity dispersion and excess absorption are derived is obtained by writing (Kneser 1931)

$$C_V = C_\infty + \frac{C_i}{1+i\omega\tau} \qquad \ldots\ldots(1)$$

where $\omega = 2\pi f$, τ is the relaxation time, C_V the effective specific heat, C_∞ its value at infinite frequency, and C_i is the specific heat contribution of the mode of oscillation that is relaxing.

Making use of the relations $C_p - C_V = R$, and $C_p/C_V = \gamma$ and putting $C_0 = C_i + C_\infty$ we find

$$\gamma = \frac{C_0(C_0+R) + (\omega\tau)^2 C_\infty(C_\infty+R)}{C_0{}^2 + \omega^2\tau^2 C_\infty{}^2} + \frac{i\omega\tau R C_i}{C_0{}^2 + \omega^2\tau^2 C_\infty{}^2} \qquad \ldots\ldots(2)$$

$$= A + iB. \qquad \ldots\ldots(3)$$

Eliminating $\omega\tau$ from these equations and writing

$$\gamma_0 = (C_0 + R)/C_0, \ \gamma_\infty = (C_\infty + R)/C_\infty$$

we find

$$B^2 + A^2 - A(\gamma_0 + \gamma_\infty) + \gamma_0\gamma_\infty = 0. \qquad \ldots\ldots(4)$$

This is the equation of a circle with centre at $B = 0$, $A = \gamma_0 + \frac{1}{2}\gamma_\infty$ and diameter $\gamma_\infty - \gamma_0$. It now remains to determine the quantities A and B and show how the relaxation time can be found from the circle.

The propagation constant in an absorbing medium can be written as $k + i\alpha$ where $k = 2\pi/\lambda$ and α is the absorption coefficient per unit length. From this we find the velocity $c = \omega/(k + i\alpha) \simeq \omega/k - i\alpha/k^2$ provided that $\alpha \ll k$. (In a typical gas α/k is about 0·01). Now $\gamma = c^2 M/RT$. Hence $\gamma = (c^2 - i\alpha\lambda c^2/\pi)M/RT$, putting $\omega/k = c$ as α/k^2 is small. Comparing this with the equation above we see that

$$A = c^2 M/RT, \text{ and } B = -\alpha\lambda c^2 M/RT\pi$$

where $\alpha\lambda$ is equal to the measured $\alpha\lambda$ less the contribution calculated from the Stokes–Kirchhoff relation. This is the procedure normally followed. As these quantities differ from c^2 and $\alpha\lambda c^2/\pi$ by a factor which is normally constant a plot of c^2 against $c^2\alpha\lambda/\pi$ should give a semicircle (α is always a positive quantity). The points of intersection of this circle with the axis of c^2 give the values of the squares of the low and high frequency velocities.

2.1. *Determination of the Relaxation Time*

The equations above have been worked out in terms of $\omega\tau$, i.e. ω is the independent variable. In most experiments however this is not the case. The relaxation time is usually controlled by some collision process and is therefore inversely proportional to the pressure, so it is usual to use the pressure as the independent variable. Making use of this information we can write $\omega K/P$ in place of $\omega\tau$ where K is the quantity to be determined.

If m is the slope of the line joining any experimentally determined point to the point of intersection of the semicircle and the axis of A (or c^2) nearest the origin, it can be shown that

$$1/m = \omega\,(C_\infty/C_0)(K/P). \qquad \ldots\ldots(5)$$

A graph of $1/m$ against $1/P$ should therefore be a straight line through the origin from whose slope the value of K can be found. Some experiments have been done in which the frequency was variable and in this case the corresponding graph is one of $1/m$ against frequency.

2.2. *Application to Published Results*

Although many papers exist in which either velocity or absorption measurements can be found, there are very few in which a combined homogeneous set of results is given in a form suitable for the present analysis.

To show how the method works out in practice some results have been plotted in figures 1 to 4.

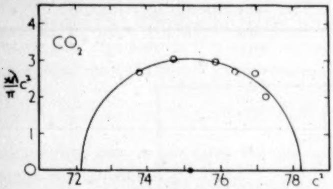

Figure 1 (*a*). Semicircular plot for carbon dioxide (units for ordinate and abscissa m^2 sec^{-2} × 10^{-3}).

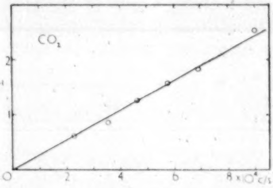

Figure 1 (*b*). Straight line graph for the determination of the relaxation time in carbon dioxide.

The CO_2 results (figure 1) are taken from Leonard's paper (1940); they have been obtained from the graphs in the paper and in consequence are not very reliable. However they show that the results are in good agreement with the hypothesis that the relaxing specific heat is 0·984*R* which is the value quoted by Vigoureux (1950).

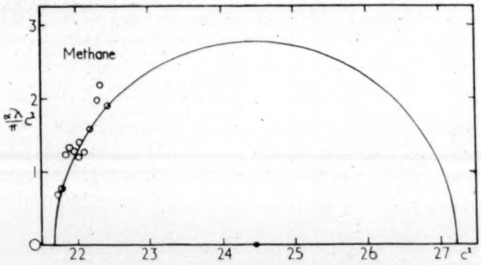

Figure 2 (*a*). Semicircular plot for methane (units for ordinate and abscissa m^2 sec^{-2} × 10^{-4}).

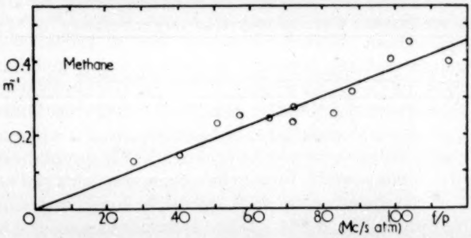

Figure 2 (*b*). Straight line graph for the determination of the relaxation time in methane.

The methane results (figure 2) are taken from a paper by Kelly (1957). The absorption values are the ones in his table II and the velocities were found by plotting the values given in his table I, drawing a smooth curve through the points, and finding from this curve the velocities at the pressures at which the absorption had been measured. From the straight line graph the frequency to pressure ratio of the point of inflection of the velocity squared graph is 263 Mc/s atm compared with his value of 300 Mc/s atm. The corresponding relaxation time is $1{\cdot}21 \times 10^{-9}$ sec at 1 atm pressure, which compares with his value of between 1·06 and $1{\cdot}29 \times 10^{-9}$ sec.

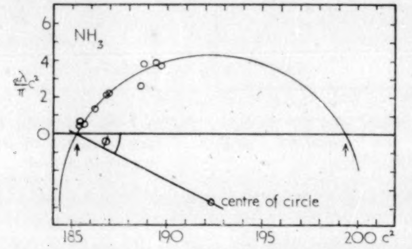

Figure 3. Arc plot for ammonia (units for ordinate and abscissa $m^2\ sec^{-2} \times 10^{-3}$).

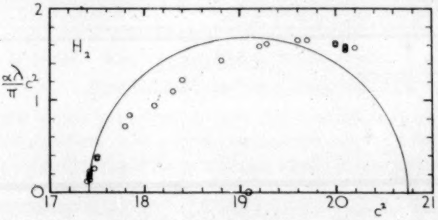

Figure 4. Arc plot for hydrogen (units for ordinate and abscissa $m^2\ sec^{-2} \times 10^{-5}$).

The results in ammonia (figure 3) which are taken from some measurements by Petralia (1953), are obviously not in agreement with the hypothesis of a single relaxation time, nor are the results in hydrogen (figure 4). These latter however are a mixed set, in that the velocities used are those obtained by Rhodes (1946) and the absorption coefficients were measured in this laboratory by Parbrook and Tempest (1958).

§ 3. MULTIPLE RELAXATION PROCESSES

3.1. *Distribution of Relaxation Times with Independent Processes*

In the study of losses in dielectrics the equation giving the effective dielectric constant is of exactly the same form as the equation for the specific heat used above. It can be shown that this equation leads to the conclusion that a plot of the real and complex parts of the dielectric constant against each other should be a circle (see for example Smyth 1955, p. 56). When these plots are made it is quite often found that the points do not lie on the expected circle but on one with its centre below the real axis. From such graphs Cole and Cole (1941), developed an empirical relation for the distribution of relaxation times necessary to give the observed results. This distribution is

$$f(S)dS = \frac{1}{2\pi} \frac{\sin \beta\pi}{\cosh (1-\beta) S - \cos \beta\pi}$$

where $S = \log(\tau_0/\tau)$ in which τ_0 is the most probable relaxation time. $f(S)dS$ is the probability of finding a relaxation time such that $\log(\tau_0/\tau)$ lies between S and $S+dS$.

Applying this distribution to the acoustic case is equivalent to modifying the specific heat equation in the same way as the dielectric equations are altered. If this is done the equation (1) above becomes

$$C_V = C_\infty + \frac{C_i}{1+(i\omega\tau_0)^{1-\beta}}.$$

Substituting this in the equation for γ and eliminating $(\omega\tau_0)^{1-\beta}$ as before, we obtain the result:—

$$A^2 + B^2 - A(\gamma_0+\gamma_\infty) + B(\tan\phi)(\gamma_\infty-\gamma_0) + \gamma_0\gamma_\infty = 0 \qquad \ldots\ldots (6)$$

which is the equation of a circle with centre at

$$A = \tfrac{1}{2}(\gamma_0+\gamma_\infty), \quad B = -(\gamma_\infty-\gamma_0)\tan\tfrac{1}{2}\phi.$$

The circle intersects the A axis at γ_0 and γ_∞ as before. It can also be shown that the angle between the A axis and the diameter through γ_0 is given by $\phi = \tfrac{1}{2}\beta\pi$.

The determination of the relaxation time in this case is more difficult than in the previous one. If, as before, we let m be the slope of the line joining any experimental point to the point of intersection of the circle and the axis of A nearest the origin, the following equation can be found:

$$\frac{1}{m} = \tan\phi + \left(\frac{\omega K}{P}\right)^{1-\beta} \frac{C_\infty/C_0}{\cos\phi}. \qquad \ldots\ldots (7)$$

In order to find the constant K it is therefore necessary to plot a graph of $\log(1/m - \tan\phi)$ against $\log(1/P)$.

From the intercept of this line on the axis of $\log(1/m - \tan\phi)$ the value K can be found. The intercept is given by

$$I = (1-\beta)\log(\omega K) + \log(C_\infty/C_0) - \log(\cos\phi).$$

As the value of ϕ and hence β can be found from the graph of A against B as shown above, and as C_∞/C_0 is usually known, all the quantities in the equation for I are known except K which can therefore be found. In the case of NH_3 quoted above this log graph is not a good line which suggests that a more detailed experimental investigation is needed to find the actual relaxation mechanism acting. The method of analysing results in this way, however, may have applications in some other cases of multiple relaxation. A distribution of relaxation times similar to that used in dielectric experiments has been found to give reasonably good agreement in the case of the propagation of compressional waves in liquid glycerol (Piccirelli and Litovitz 1957).

3.2. *Independent Relaxation Processes*

If a significant contribution to the specific heat is made by excited states other than the lowest, it is reasonable to suppose that there may be more than one time constant for the relaxation process. Experimental evidence that this is the case is provided in several cases. There are now two ways in which the molecules may be de-excited. Either they may go from each excited state directly to the ground state, or they may go from the highest excited state to the next lower and so to the ground state. In the first case the equation for the specific heat, corresponding to equation (1) becomes (Buschmann and Schäfer 1941)

$$C_V = C_\infty + \frac{C_1}{1+i\omega\tau_1} + \frac{C_2}{1+i\omega\tau_2} \qquad \ldots\ldots(8)$$

where C_1 and C_2 are the contributions to the specific heat of the states 1 and 2 which relax with times τ_1 and τ_2. In the second case the equation for the specific heat is not readily modified (Beyer 1957).

It is obvious from equation (8) that the quantities A and B for the two modes cannot simply be added to find the total A and B values. However this case can be dealt with by calculating the real and complex parts of the specific heat from the experimental results. If A and B have the same meanings as before, then the real and complex parts of the specific heat are given by $(A-1)R/\{(A-1)^2+B^2\}$ and $BR/\{(A-1)^2+B^2\}$ respectively.

In the special case of a single relaxation time, plotting these functions against each other will again give a semicircle. In general however this is not the case and the shape of the graph enables some further deductions to be made. If the processes are such that equation (8) is obeyed, then whatever the relative relaxation times, the resultant curve should lie inside a semicircle with a diameter equal to the total specific heat that is affected by the relaxation process. If the experimental points are found to lie outside this semicircle then the possibilities are that interacting modes of decay exist, or that the observed propagation constants are due to some other mechanism.

The results in hydrogen (figure 4) are of interest in that they lie, over part of their range, outside the semicircle, which suggests that coupled modes of decay may exist. However as the results are a mixed set a further analysis awaits a complete homogeneous set of results. It may be of interest to note that if the fact that the curve lies outside the semicircle is disregarded as being an error (it is more difficult to make accurate measurements in this region) it turns out that the ratio of the relaxation times for the two modes making the largest contribution to the specific heat is about 10, the mode making the larger contribution having the shorter relaxation time. This may be compared with the results obtained in SO_2 by Lambert and Salter (1957) for a vibrational relaxation where the mode making the larger contribution also has the shorter relaxation time.

§ 4. SINGLE RELAXATION PROCESS WHERE THE STOKES–KIRCHHOFF ABSORPTION IS NOT KNOWN

It may happen that measurements are made in a gas for which the Stokes–Kirchhoff absorption is not known. In this case the following method may be helpful.

By rearrangement of the equations (2) and (3) for A and B in terms of $\omega\tau$ and by writing, as before, $\tau = K/P$ it can be shown that

$$PC_0B = \omega KAC_\infty - \omega K(C_\infty + R). \qquad \ldots\ldots(9)$$

On substituting the values of A and B this becomes:

$$[P(\alpha\lambda)_R/\pi]\,c^2C_0 = -\omega Kc^2C_\infty + \omega K(C_\infty + R)\,RT/M \qquad \ldots\ldots(10)$$

where $(\alpha\lambda)_R$ is written to indicate that this part is due to relaxation. Now the Stokes–Kirchhoff absorption equation can be rearranged to give the relation

$$\frac{(\alpha\lambda)_{SK}}{\pi} = \frac{\omega}{Pc^2}K_1$$

where K_1 is the unknown part of the Stokes–Kirchhoff equation. If we put $(\alpha\lambda)_m/\pi$ for the measured coefficient, then $(\alpha\lambda)_m = (\alpha\lambda)_{SK} + (\alpha\lambda)_R$. Substituting this in equation (10) and rearranging:

$$\frac{(\alpha\lambda)_m}{\pi} P = \frac{-\omega K C_\infty}{C_0} + \frac{\omega}{c^2}\left[\frac{KRT(C_\infty + R) + K_1 M C_0}{MC_0}\right]. \quad \ldots\ldots(11)$$

A plot of $(\alpha\lambda)_m P/\pi$ against $1/c^2$ should therefore be a straight line from which both K and K_1 can be found.

This method is only likely to prove useful if a fairly large part of the dispersion region is available to experiment, as otherwise the precision needed in measurement is too high for any accuracy to be achieved.

Another error may arise if the frequency/pressure ratio is very high due to the invalidity of the Stokes–Kirchhoff equation. As has been pointed out by Truesdell (1953) among others, this equation is an approximation to the viscothermal absorption, and is valid only at low frequency/pressure ratios and for perfect gases. It is of course valid for much of the published work to date.

REFERENCES

BEYER, R. T., 1957, *J. Acoust. Soc. Amer.*, **29**, 243.
BUSCHMANN, K. F., and SCHÄFER, K., 1941, *Z. Phys. Chem.* B, **50**, 73.
COLE, K. S., and COLE, R. H., 1941, *J. Chem. Phys.*, **9**, 341.
KELLY, B. J., 1957, *J. Acoust. Soc. Amer.*, **29**, 1005.
KNESER, H. O., 1931, *Ann. Phys., Lpz.*, [V], **11**, 761.
LAMBERT, J. D., and SALTER, R., 1957, *Proc. Roy. Soc.* A, **243**, 78.
LEONARD, R. W., 1940, *J. Acoust. Soc. Amer.*, **12**, 241.
PARBROOK, H. D., and TEMPEST, W., 1958, *J. Acoust. Soc. Amer.*, **30**, 985.
PETRALIA, S., 1953, *Nuovo Cim.*, Ser. 9, **10**, 817.
PICCIRELLI, R., and LITOVITZ, T. A., 1957, *J. Acoust. Soc. Amer.*, **29**, 1009.
RHODES, J. E., 1946, *Phys. Rev.*, **70**, 932.
SMYTH, C. P., 1955, *Dielectric Behaviour and Structure* (New York: McGraw-Hill).
TRUESDELL, C., 1953, *J. Rat. Mech. and Analysis*, **2**, 643.
VIGOUREUX, P., 1950, *Ultrasonics* (London: Chapman and Hall).

Electrical Conduction in n-Type InSb between 2°K and 300°K

By E. H. PUTLEY

Royal Radar Establishment, Malvern, Worcs.

MS. received 30th July 1958, in revised form 5th September 1958

Abstract. Using a digital recording technique the electrical conductivity and Hall coefficient have been measured between 2°K and 300°K for samples of InSb containing from 10^{18} down to 5×10^{13} conduction electrons cm^{-3}. The behaviour of the Hall mobility has been accounted for by a combination of acoustic lattice and ionized impurity scattering and the concentration of scattering centres estimated.

The intrinsic carrier concentration has been calculated from the results obtained above 180°K while the results below 20°K show no evidence of a donor activation energy even in the purest material. At 4°K deviations from ohmic behaviour were observed for fields above 0·1 v cm^{-1}.

§ 1. Introduction

The electrical conductivity and the Hall coefficient have been measured between 2°K and 300°K of single crystals of n-type InSb in which the extrinsic carrier concentration ranged from 5×10^{13} cm^{-3} up to 10^{18} cm^{-3}.

From the results obtained between 300°K and 180°K the intrinsic carrier concentration has been calculated.

The behaviour of the mobility between 20°K and 100°K was compared with that expected from a combination of acoustic lattice scattering and ionized impurity scattering. From this comparison the concentration of scattering centres may be estimated. For the best material this concentration is comparable with the carrier concentration.

Measurements below 20°K showed no evidence of a donor ionization energy even in the purest specimens. The mobility at 4°K was smaller than the value expected from the concentration of scattering centres estimated from measurements at higher temperatures.

Deviations from ohmic behaviour at 4°K were observed for electric fields above 0·1 v cm^{-1}, but these could be accounted for by the change in mobility with effective electron temperature.

§ 2. Experimental Details

The measurements were made on single crystal specimens of dimension about $1·5 \times 0·2 \times 0·1$ cm cut from plates perpendicularly to the direction of crystal growth. Unless otherwise stated, the surfaces were lightly ground to true up the dimensions. This grinding was done with the specimen stuck to a glass plate. Current and potential leads were attached using indium solder. Temperatures above 20°K were measured by means of platinum resistance thermometers, and below 20°K by carbon resistance thermometers. The conductivity and Hall

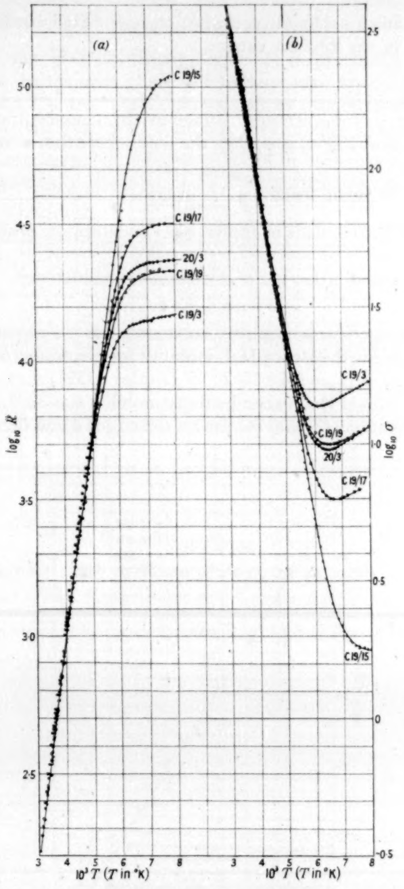

Figure 1. (*a*) Intrinsic Hall coefficient; (*b*) intrinsic conductivity. Abscissae should read $10^3/T$.

coefficient were measured using the standard potentiometric procedures, but above 20°K the majority of measurements were made using a digital recording technique (Carter, Howarth and Putley 1958). The magnetic induction used for measuring the Hall coefficient was about 2000 gauss.

§ 3. INTRINSIC CONDUCTIVITY

Figure 1 shows the results for log σ and log R in the intrinsic range for a number of the purer specimens. The intrinsic carrier concentration n_i was calculated by two methods. First it was assumed that because of the high mobility ratio the holes made a negligible contribution to the Hall coefficient. Hence at any temperature in the intrinsic range

$$R = -\frac{3\pi}{8}\frac{1}{ne} \qquad \ldots\ldots(1)$$

giving n the electron concentration. If the extrinsic concentration (determined from the value of R at 100°K) is m, then the hole concentration will be

$$p = n - m \qquad \ldots\ldots(2)$$

and hence n_i can be found using

$$n_i = (np)^{1/2}. \qquad \ldots\ldots(3)$$

Some of the assumptions made in applying (1) to determine m and n are discussed in the Appendix.

The second method makes use of the intrinsic conductivity

$$\sigma = ne\mu_n + pe\mu_p. \qquad \ldots\ldots(4)$$

In these intrinsic specimens impurity scattering can be neglected, so that the empirical formulae for the lattice Hall mobility for electrons (6) and the corresponding one for holes ($\mu_p = 5{\cdot}4 \times 10^6 T^{-1{\cdot}45}$ (Putley 1959)) may be used. It was assumed that the ratio of Hall to conductivity mobility was $3\pi/8$. Then inserting the value of m, equations (2) and (4) can be solved for n and hence n_i found from (3).

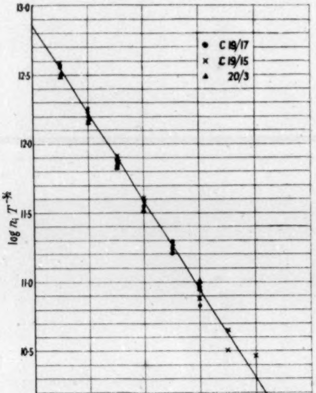

Figure 2. InSb intrinsic carrier concentration log $n_i T^{-3/2}$ plotted against $10^3/T$.

The results of these two calculations were consistent with themselves and with each other to within ±10% over the temperature range 300°K to 180°K. They are shown plotted in figure 2 as log $n_i T^{-3/2}$ against $1/T$. n_i can be represented by the expression

$$n_i = 5{\cdot}70 \times 10^{14}\, T^{3/2} \exp(-0{\cdot}125/kT). \qquad \ldots\ldots(5)$$

Values of n_i calculated from this expression agree, within the experimental error, with those given by the formula found by Hrostowski *et al.* (1955).

§ 4. THE EXTRINSIC RANGE

Below 100°K the Hall coefficient (figure 3) is practically independent of temperature. In the majority of cases R does not vary by more than 10 or 20% between 100°K and 2°K and it often shows a slight maximum at about 20°K. At 100°K the conductivity (figure 4) of all but very impure specimens rises as the temperature falls, passing through a maximum at about 50°K and then falling as the temperature is lowered further. None of the specimens showed any evidence of an impurity ionization energy. The largest variation of Hall coefficient at

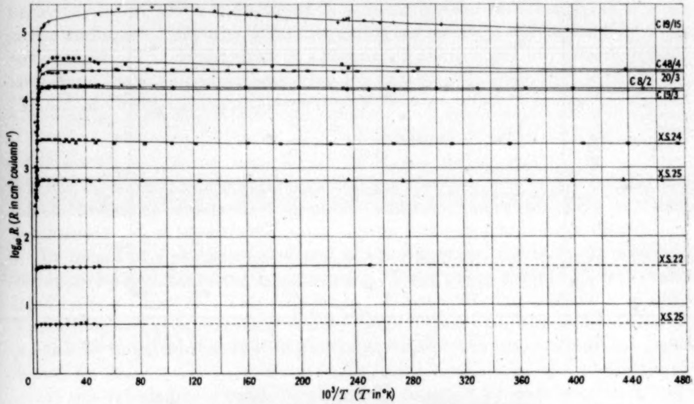

Figure 3. Hall coefficient of n-type indium antimonide.

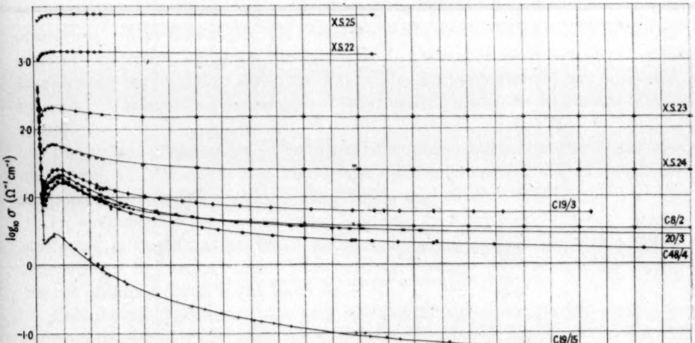

Figure 4. Conductivity of n-type indium antimonide.

low temperatures was found in the specimen with the smallest electron concentration (C19/15, figure 5), but in this specimen the Hall coefficient fell appreciably below 3 °K, rather than rose. In view of the small changes in the Hall coefficient with temperature, it is clear that below 100 °K the dominant factor responsible for the variation of conductivity with temperature is the variation of electron mobility.

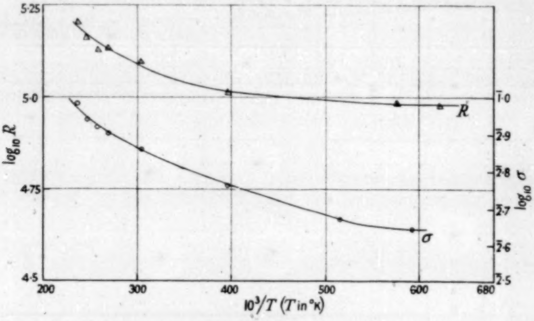

Figure 5. Behaviour of Hall coefficient and conductivity of InSb C19/15 below 4°K.

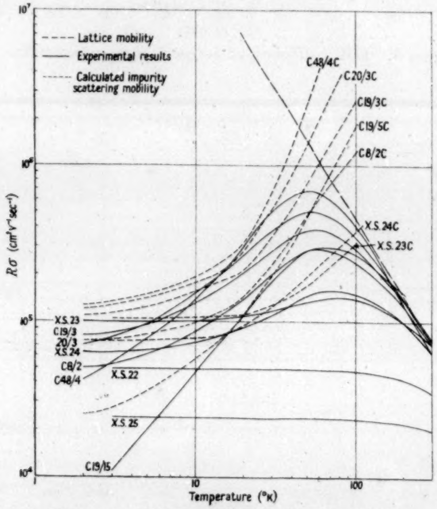

Figure 6. Hall mobility of electrons in InSb.

Figure 6 shows the behaviour of the Hall mobility $R\sigma$ for a number of specimens in which the electron concentration ranged between 10^{18} cm^{-3} down to 5×10^{13} cm^{-3} and for temperatures from below 2 °K up to 300 °K. In an attempt to analyse these results the lattice scattering below 100°K was estimated by fitting an envelope to the curves between 100°K and 300°K and extrapolating it downwards. It was found that this could be represented by the expression

$$R\sigma = 1{\cdot}04 \times 10^{9}\, T^{-1{\cdot}68} \qquad \ldots\ldots(6)$$

which is in close agreement with that quoted by Hrostowski *et al.* (1955). The behaviour below 100°K is discussed by considering the combination of acoustic lattice and ionized impurity scattering taking into account the degeneracy of the electron gas. The conductivity of a degenerate electron gas where both acoustic lattice and ionized impurity scattering are important is given by the expression (Mansfield 1956)

$$\sigma = \frac{\sigma_L}{\ln(1+\exp\eta)} F(\eta, \alpha) \qquad \ldots\ldots(7)$$

where η is the reduced chemical potential and $\alpha = \sigma_L/\sigma_I$. σ_I is the conductivity which would be observed if impurity scattering were the only scattering mechanism. σ_L is the lattice conductivity for a degenerate semiconductor.

By means of a procedure outlined in the Appendix, the impurity scattering conductivity and hence the concentration of scattering centres N_I was calculated using (6) and (7). This calculation was made over the range 20°K to 100°K. In addition to the experimental results, figure 6 shows the extrapolated lines for μ_L and an impurity mobility defined as $\mu_I = \sigma_I R$. The table gives the values found for N_I.

If this calculation is valid, N_I should be constant for each specimen. It is seen that for specimens with 10^{15} or more carriers this is reasonably true. For the purer specimens N_I is fairly constant above 50°K. but increases rapidly at lower temperatures. At 20°K lattice scattering is small compared with impurity scattering. A further check was therefore made on the validity of the theory of impurity scattering by taking the values of N_I estimated at 20°K and using them to calculate the mobility down to 2°K. The curves obtained are included in figure 6. It is seen that the calculated results tend roughly to double the observed values.

The values obtained for N_I near 100°K would indicate that the better specimens such as 20/3 and C48/4 are virtually uncompensated. This deduction is supported by metallurgical evidence (Hulme and Mullin 1957).

In specimens with carrier concentrations greater than $10^{16}\,\mathrm{cm}^{-3}$ impurity scattering is important at 300°K and at low temperatures the conductivity is independent of temperature. This is in agreement with the metallic approximation obtained for σ_I in the limit $\eta \to +\infty$.

Calculating N_I for the two very degenerate specimens (with carrier concentrations of $1{\cdot}72 \times 10^{17}$ and $1{\cdot}15 \times 10^{18}$ respectively) taking the value $1{\cdot}5 \times 10^{-2}$ for the effective mass ratio, gave a concentration of impurity centres of about twice that of the free carriers. In these very impure specimens it is thought unlikely that the concentration of ionized impurity centres should greatly exceed the free carrier concentration, but it has been suggested that the value of the effective mass should increase at energies above the bottom of the band. If we assume that the number of scattering centres equals the number of free carriers, then values are obtained for the effective mass ratio between 2 and $2{\cdot}5 \times 10^{-2}$. Since the carrier concentration in these very degenerate specimens is more than an order of magnitude greater than that in the most impure of the specimens

Fermi Level and Concentration of Impurity Scattering Centres for n-Type InSb

Specimen No.	Electron Concentration (cm^{-3})		T(°K) 20	30	40	50	60	70	80	90	100	
XS23	$1\cdot09\times10^{16}$	η	6·8	4·4	3·2	2·4	1·9	1·5	1·1	0·9	0·6	
		$N_{\mathrm{I}}(\mathrm{cm}^{-3})$	1·41	1·35	1·27	1·21	1·17	1·11	1·05	1·05	1·02	$\times10^{16}$
XS24	$2\cdot83\times10^{15}$	η	2·5	1·3	0·7	0·2	−0·1	−0·4	−0·7	−0·9	−1·0	
		N_{I}	6·98	6·58	6·32	5·41	5·20	5·10	5·12	5·42	5·27	$\times10^{15}$
C19/3	$4\cdot90\times10^{14}$	η	−0·3	−1·0	−1·4	−1·8	−2·1	−2·3	−2·5	−2·7	−2·9	
		N_{I}	12·3	9·95	8·51	7·46	6·46	5·95	5·69	5·30	5·05	$\times10^{14}$
C8/2	$4\cdot74\times10^{14}$	η	−0·3	−1·0	−1·5	−1·8	−2·1	−2·4	−2·6	−2·8	−2·9	
		N_{I}	17·9	16·5	13·0	11·7	11·4	11·1	10·7	10·4	8·3	$\times10^{14}$
20/3	$2\cdot8\times10^{14}$	η	−0·9	−1·6	−2·0	−2·4	−2·7	−2·9	−3·1	−3·3	−3·4	
		N_{I}	7·45	5·62	4·60	3·61	3·03	2·7	2·37	—	—	$\times10^{14}$
C48/4	$2\cdot07\times10^{14}$	η	−1·2	−1·9	−2·4	−2·7	−3·0	−3·2	−3·4	−3·6	−3·8	
		N_{I}	6·02	3·71	2·68	1·80	1·08	—	—	—	—	$\times10^{14}$
C19/15	$5\cdot25\times10^{13}$	η	−2·7	−3·3	−3·7	−4·1	−4·4	−4·6	−4·8	−5·0	−5·1	
		N_{I}	11·7	10·3	8·12	6·94	6·30	5·84	5·50	4·95	4·24	$\times10^{14}$

considered in the table, the assumption of $m^*/m = 1\cdot5\times10^{-2}$ for those specimens does not seem unreasonable.

In conclusion, it appears that the combination of acoustic lattice scattering and ionized impurity scattering gives a fair description of the behaviour of the conductivity in the neighbourhood of the conductivity maximum (40°K to 100°K) and indicates that the best specimens are only slightly compensated. There is a serious discrepancy between the predictions of this model and the observed results at lower temperatures. The reasons for this have not yet been clarified but two possibilities must be considered. First, there may be additional scattering mechanisms operating at low temperatures. If so, these scattering mechanisms must increase in importance as the temperature falls. If they were independent of temperature as, for example, neutral impurity scattering, then they would be most important where the mobility is a maximum and not at the lowest temperatures. The recent work of Sladek (1958) has shown the existence of impurity band conduction in n-type InSb at 4°K. It is possible that even at zero magnetic fields the electrons are mainly in impurity states at the foot of the conduction band and therefore their mobility is considerably reduced. The behaviour of the Hall coefficient of specimen C19/15 (figure 5) measured at 2300 gauss is consistent with this picture. The second possibility is that the theory of impurity scattering is seriously in error at low temperatures. Both Blatt (1957) and Sclar (1956) have recently pointed out this possibility, but their work indicates that the theory used here predicts too low a mobility, not too high a value, as we have found. Again this difficulty may be resolved by using a more exact band model. This has been done by Ehrenreich (1957) in considering lattice scattering. Ehrenreich's work suggests that our use of a formula based on acoustic lattice scattering is incorrect. What is required is a combination of polar scattering with impurity scattering, but this has not yet been developed. It will be of great interest to see if such a combination gives better agreement in the 40°K to 100°K range than the combination we have used here.

§ 5. THE DEPENDENCE OF THE HALL EFFECT AND CONDUCTIVITY ON ELECTRIC FIELDS AT HELIUM TEMPERATURES

In carrying out these measurements routine checks were made to ensure that the electric fields applied were not excessively high. In one case the results obtained were of sufficient interest to warrant discussion.

Measurements at 4·2°K and 1·7°K on specimen C19/15 indicated ohmic behaviour for fields up to about 0·1 v cm^{-1} and a very rapid fall in resistance for fields between 0·2 and 0·3 v cm^{-1} (figure 7). As the field was increased, the Hall effect increased slightly at first and then tended to fall, but in the range of fields used the maximum change was not more than 50%. The Hall mobility increased with the field. At these temperatures impurity scattering is dominant, therefore if the effective electron temperature is raised by the field, the mobility would be expected to rise. Gunn (1957) has obtained an approximate expression for the variation of mobility with field

$$\mu = \frac{\mu_{L_0}}{x}\,\frac{(3\,ax^{-4}+1)}{(ax^{-4}+1)^2} \qquad \ldots\ldots(8)$$

where x is given by

$$\frac{3\mu_{L_0}}{8c^2}E^2 = x^2(x^2-1)\,\frac{(ax^{-4}+1)^2}{(3\,ax^{-4}+1)}$$

where $a = 3\mu_{L_0}/\mu_{I_0}$. Here c is the velocity of sound ($2{\cdot}25\times10^5$ cm sec^{-1} at 0°K (Potter 1956)) and μ_{I_0} is the impurity mobility at zero field. To apply these expressions to the results one needs to know a value for μ_{L_0}. μ_{I_0} can be taken as the measured mobility at low fields. If the empirical formula (6) for μ_L is extrapolated to 4°K it yields a value $\mu_{L_0} = 10^{10}$ cm^2 v^{-1} sec^{-1}. This value can hardly be realistic, because it implies a mean free path of the order of 10 metres and therefore even in a crystal free from all defects and impurities the mobility would be limited by the size of the crystal. In view of this a value for μ_{L_0} was estimated by fitting equation (8) to the results at the lowest field to give a measurable change in mobility. μ was then calculated for the higher fields. In figure 8 the results of these calculations are compared with experiments. At 4.2°K, taking $\mu_{L_0} = 8.6 \times 10^7$ cm^2 v^{-1} sec^{-1} the agreement is fairly good, but at 1.7°K, with $\mu_{L_0} = 9.2 \times 10^8$, the calculated results rise more rapidly than the observed values.

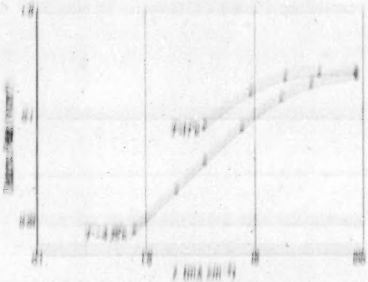

Figure 7. Variation of electric field with current density for n-type sample C19/15.

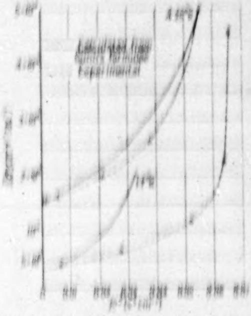

Figure 8. Variation of mobility with field squared for InSb C19/15.

The maximum field which can be applied is limited by Joule heating. While it is believed that the fields applied were not too large to introduce serious errors here, that may be the reason for the big discrepancy at 1.7°K. On the other hand, the theory used assumes a non-degenerate and mono-energetic electron gas, both doubtful assumptions in this case. It does appear, however, that the order of magnitude of the changes in conductivity can be accounted for by the expected change in electron mobility with effective electron temperature.

§ 6. CONCLUSION

A considerable amount of detailed investigation is needed to elucidate the behaviour of InSb below 10°K. The preparation of specimens containing known impurities in concentrations of less than 10^{12} cm^{-3} is required, together with further study of surface effects and the effects of dislocations. It will then become worthwhile to make detailed studies of the dependence of the galvanomagnetic effects upon induction. Further work on the dependence of the conductivity upon electric fields would be well worthwhile, using pulsed techniques.

ACKNOWLEDGMENTS

It is a great pleasure to acknowledge the help given by Dr. Avery and his team who supplied the samples of indium antimonide.

I would also like to thank Mr. C. Wright and the liquefier staff for supplying the liquid hydrogen and helium.

I wish to thank the many colleagues at the Royal Radar Establishment with whom I have discussed various aspects of these results.

Finally, I am deeply indebted to Mr. W. H. Mitchell, Mr. P. Herman, Miss M. Stallard, Miss S. Lucas, Miss P. Baker and Mrs. Y. Edwards, for their various contributions to the experimental work and the computation of the results.

This paper is published by permission of the Controller, H.M. Stationery Office.

APPENDIX

The conductivity of a degenerate electron gas where both acoustic lattice and ionized impurity scattering are important is given by the expression (7) quoted above

$$\sigma = \frac{\sigma_L}{\ln(1+\exp\eta)} F(\eta, \alpha) \qquad \ldots\ldots(\mathrm{A}\ 1)$$

where η is the reduced chemical potential, $\alpha = \sigma_L/\sigma_I$, and σ_I is the conductivity which would be observed if impurity scattering were the only scattering mechanism.

σ_L is the lattice conductivity for a degenerate semiconductor, i.e.

$$\sigma_L = \frac{16\,(2\pi m^* \boldsymbol{k}T)^{3/2}}{3\pi h^3}\,\mu_L\,\boldsymbol{e}\ln(1+\exp\eta) \qquad \ldots\ldots(\mathrm{A}\ 2)$$

where m^* is the effective mass, μ_L is the lattice Hall mobility in a non-degenerate specimen; $F(\eta, \alpha)$ denotes the function

$$F(\eta, \alpha) = \int_0^\infty \frac{x^3 \exp(x-\eta)\,dx}{[x^2 + 3F_2(\eta)\alpha/\ln(1+\exp\eta)][\exp(x-\eta)+1]^2} \ldots\ldots(\mathrm{A}\ 3)$$

which has been tabulated by Howarth (private communication).

Furthermore, the impurity conductivity σ_I is related to the concentration of scattering centres N_I by the expression

$$\begin{aligned}\sigma_I &= \frac{32K^2 m^* (\boldsymbol{k}T)^3 F_2(\eta)}{N_I\,\boldsymbol{e}^2 h^3 f(x)} \\ &= 2{\cdot}496 \times 10^{14} \left(\frac{m^*}{m}\right) \frac{T^3 F_2(\eta)}{N_I f(x)} \qquad \ldots\ldots(\mathrm{A}\ 4)\end{aligned}$$

(assuming for InSb the dielectric constant $K = 14$). Here $F_2(\eta)$ is the Fermi–Dirac integral of order 2 and $f(x) = \ln(1+x) - x/(1+x)$ with

$$\begin{aligned}x &= \frac{\bar{\eta}(\boldsymbol{k}T)^{1/2} K h}{\mathrm{e}^2 (2m^*)^{1/2} F_{1/2}'(\eta)} \\ &= 0{\cdot}1105\,\frac{\bar{\eta} T^{1/2}}{(m^*/m)^{1/2} F_{1/2}'(\eta)} \qquad \ldots\ldots(\mathrm{A}\ 5)\end{aligned}$$

Here $F_{1/2}(\eta)$ is the $\frac{1}{2}$ order Fermi–Dirac integral. $\bar{\eta}$ is given by

$$\frac{\bar{\eta}^2 + 3\alpha_1}{\bar{\eta}^3 + \alpha_1\bar{\eta}} = \tanh\left(\frac{\bar{\eta}-\eta}{2}\right)$$

where

$$\alpha_1 = \frac{3F_2(\eta)}{\ln(1+\exp\eta)}\,\alpha. \qquad \ldots\ldots(\mathrm{A}\ 6)$$

The solution of (A 6) has been tabulated by Mansfield (1956). In these calculations, the values for the Fermi–Dirac integrals were obtained from the tabulations of McDougall and Stoner (1938) and of Rhodes (1950). From the empirical expression (6) for the lattice mobility and (A 2) σ_L was found. η was found using the relation

$$\begin{aligned}\eta &= \frac{4\pi(2m^*\mathbf{k}T)^{3/2}}{h^3}F_{1/2}(\eta)\\ &= 5{\cdot}45\times10^{15}\,(m^*/m)^{3/2}\,T^{3/2}\,F_{1/2}\,(\eta). \qquad \text{......(A 7)}\end{aligned}$$

In these calculations the value $1{\cdot}5\times10^{-2}$ was used for (m^*/m).

In using (A 7) to find η the value of n was obtained by using the Hall coefficient at 100°K in equation (1). This implies that classical statistics are valid at this temperature and that the low magnetic field approximation is valid. Examination of the table shows that for the majority of cases considered the first assumption is not unreasonable. There is some doubt however whether on account of the high mobility the low field factor $3\pi/8$ is correct. According to theory the limiting value for infinite field is unity, but the observed variation of Hall effect with field appears to be smaller than the theory predicts. In view of this uncertainty the factor $3\pi/8$ was used. The error should not be greater than 20% which is not large compared with other uncertainties involved. Knowing σ_L and η, (A 1) can be solved to find α and hence σ_I. Then, using (A 4), N_I can be found.

REFERENCES

BLATT, F. J., 1957, *J. Phys. Chem. Solids*, **1,** 262.

CARTER, R. H. A., HOWARTH, D. J., and PUTLEY, E. H., 1958, *J. Sci. Instrum.*, **35,** 115.

EHRENREICH, H., 1957, *J. Phys. Chem. Solids*, **2,** 131.

GUNN, J. B., 1957, *Progress in Semiconductors*, **2,** 211.

HROSTOWSKI, H. J., MORIN, F. J., GEBALLE, T. H., and WHEATLEY, G. H., 1955, *Phys. Rev.*, **100,** 1672.

HULME, K. F., and MULLIN, J. B., 1957, *J. Electronics and Control*, **3,** 160.

MCDOUGALL, J., and STONER, E. C., 1938, *Phil. Trans. Roy. Soc.* A, **237,** 67.

MANSFIELD, R., 1956, *Proc. Phys. Soc.* B, **69,** 76.

POTTER, R. F., 1956, *Phys. Rev.*, **103,** 47.

PUTLEY, E. H., 1959, *Proc. Phys. Soc.*, **73,** 128.

RHODES, P., 1950, *Proc. Roy. Soc.* A, **204,** 396.

SCLAR, N., 1956, *Phys. Rev.*, **104,** 1548.

SLADEK, R. J., 1958, *J. Phys. Chem. Solids*, **5,** 157.

Ultrasonic Attenuation in Superconducting and Normal Mercury

By L. MACKINNON and A. MYERS
Department of Physics, The University, Leeds

MS. received 21*st August* 1958, *in revised form* 16*th October* 1958

Abstract. The relative attenuation of 10 Mc/s longitudinal ultrasonic waves has been studied in superconducting and normal mercury over the temperature range 1·17°K to 4·2°K. The marked difference in the attenuation for the two states, previously noted for other superconductors, is also observed here, and is not inconsistent with energy-gap theory. In the normal metal, the attenuation increases rapidly as the temperature decreases, but it is difficult to estimate its 'zero-field' value as there is a marked magnetic field dependence; in particular, an unusual increase in attenuation has been observed at the lower temperature with a transverse field. There is no theory of this last effect.

§ 1. INTRODUCTION

ULTRASONIC attenuation studies in superconductors have so far been confined to the elements lead, tin and indium. Mercury has not previously been studied because it is relatively difficult to handle; it was decided however that this difficulty should not be insuperable and that it would be worth while to study the absorption of ultrasonic waves in it, in order to compare the behaviour with that of other superconductors. Mercury is readily available in a very pure state, so that a marked electronic absorption was to be expected.

Experiment showed that the absorption of waves of frequencies of 30 Mc/s or more was very heavy in a polycrystalline specimen, presumably largely as a result of grain-boundary scattering, etc. As single crystals were not available, it was therefore necessary to work at a lower frequency. The frequency chosen was 10 Mc/s (at which the wavelength of the sound in solid mercury is $1/(60 \pm 5)$ cm) and the work has also been confined to longitudinal waves; however, the results obtained, especially with the normal metal in a magnetic field, seem sufficiently new and unusual to be worth reporting at this stage.

§ 2. EXPERIMENTAL ARRANGEMENT

Figure 1 is a block diagram of the electronic circuit. Short (3–5 μsec) pulses of 10 Mc/s oscillations are fed (at a rate of about 2000 per second) to two X-cut quartz plates, one on the end of a mercury specimen in a cryostat and the other on the end of a comparison specimen kept at constant (room) temperature. The pulses are converted into ultrasonic waves by the quartz plates; the waves then travel down the two specimens to be reconverted into electrical oscillations by quartz plates at the other ends; then the emerging electrical oscillations are amplified and detected and their rectified envelope is displayed on a cathode ray oscilloscope (Solartron type CD 513).

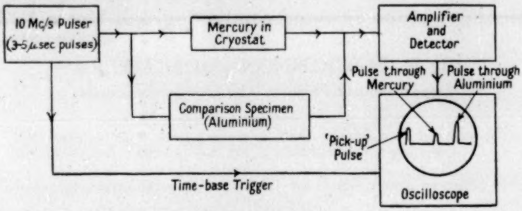
10 Mc/s Pulser
(3-5 μsec pulses)
Mercury in Cryostat
Amplifier and Detector
Pulse through Mercury
Pulse through Aluminium
Comparison Specimen (Aluminium)
'Pick-up' Pulse
Time-base Trigger
Oscilloscope

Figure 1. Block diagram of apparatus.

As absorption in the mercury is heavy, no pulses arising from multiple reflections were observed. Therefore only relative attenuation studies could be carried out. This is done by measuring the height of the transmitted pulse as displayed on the oscilloscope. So that correction could be made for variations in input pulse, this height was compared with the height of the pulse received through the comparison specimen, in which the attenuation was presumed to be constant. The amplifying circuits were checked with a calibrated attenuator (Standard Telephones types 74600 A and B) so that the pulse height could be converted to units of attenuation.

The cryostat assembly was conventional. Liquid helium was supplied by the National Physical Laboratory, Teddington.

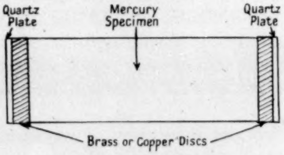
Quartz Plate
Mercury Specimen
Quartz Plate
Brass or Copper Discs

Figure 2. Method of fixing quartz plates to the mercury specimen.

Experiments were carried out on two mercury specimens. These were cast as cylindrical rods. It was found that the high viscosity silicone fluid (Dow Corning 200 fluid, viscosity $2{\cdot}5 \times 10^6$ centistokes) normally used for quartz–metal bonding at liquid helium temperatures (McSkimin 1953) would not wet the ends of the mercury rods (necesarily kept cold). The arrangement shown in figure 2 was therefore adopted. The quartz plates were attached, using the silicone fluid, to brass or copper discs (of sufficient impurity to ensure negligible electronic absorption in them). The other side of each disc was then amalgamated with a little mercury and then the discs, at room temperature, were brought into contact with the mercury rod, at solid carbon-dioxide temperature. The resulting local melting and refreezing made the necessary join.

The assembly of mercury rod and transducers was then mounted vertically in the cryostat, much as described in an earlier paper (Mackinnon 1955). Magnetic fields could be applied externally to the cryostat either along the specimen, with a solenoid producing up to 1000 oersteds, or across the specimen, with an electromagnet producing up to rather over 4000 oersteds.

§ 3. Experimental Results

3.1. *The First Specimen*

The first specimen was made from redistilled mercury, as supplied by Johnson, Matthey and Co. The purity was not specified but appears from the results to have been very high. When mounted, the specimen was 2·5 cm in diameter and 3·1 cm long; the end-plates were of brass of the same diameter as the specimen and the quartz plates were ½ in. in diameter. The experiments carried out on this were of an exploratory nature. The results are shown in figure 3, the values for the attenuation in the normal metal below the transition temperature being those obtained when a field of just over 400 oersteds was applied along the length of the specimen. (It will be noted that the reference point for the attenuation has been arbitrarily taken as the value at the transition temperature in both figures 3 and 5; there is no significance in this.)

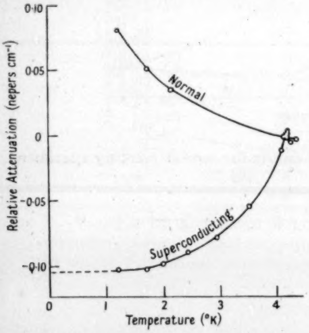

Figure 3. Relative attenuation–temperature curves for first mercury specimen.

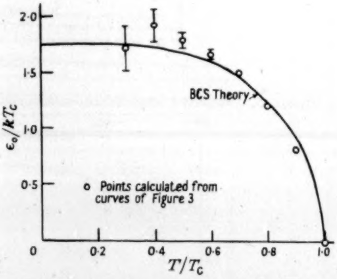

Figure 4. Comparison of the results of figure 3 with the BCS theory.

Although there is no reason to suppose that the relative absorption in the superconducting and normal states is simply a matter of the relative number of absorbers (electron or holes), the simple Fermi function, giving the ratio of the two attenuation coefficients as $2/\{1-\exp(\epsilon_0/\boldsymbol{k}T)\}$ and used by Morse and Bohm (1957) in interpreting their results for tin and indium, was applied to the results shown in figure 3 to obtain values of $\epsilon_0/\boldsymbol{k}T_c$ as a function of T/T_c; here ϵ_0 is half the (variable) energy gap in an energy-gap model, $\boldsymbol{k}$ is Boltzmann's constant, T the absolute temperature and T_c the transition temperature for mercury in zero field (4·15°K). These results are shown as points in figure 4, where the solid line represents the variation of $\epsilon_0/\boldsymbol{k}T_c$ predicted by the Bardeen, Cooper and Schrieffer (1957) (BCS) theory of superconductivity.

These exploratory results were satisfactory and work was therefore started on some spectroscopically standardized mercury.

3.2. *The Second Specimen*

The second specimen was made from spectroscopically standardized mercury, of purity in excess of 99·999% (Johnson, Matthey and Co., Laboratory No. 11621, Catalogue No. J.M. 190). It was cast *in vacuo*, after degassing, as a cylindrical rod, which had a diameter of ½ in. and a length of 2·8 cm after mounting. The end plates were of copper and the quartz plates were again ½ in. in diameter.

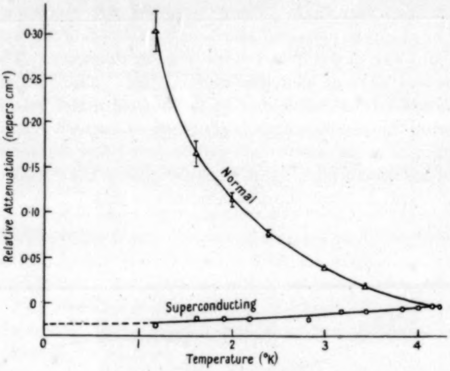

Figure 5. Relative attenuation–temperature curves for second mercury specimen.

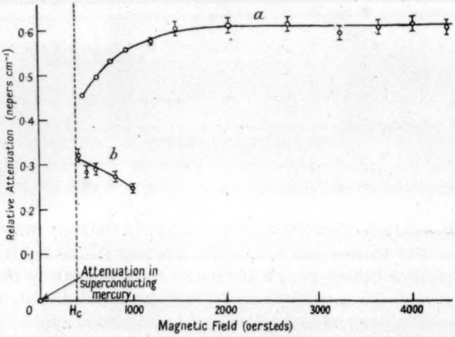

Figure 6. Variation of attenuation in normal mercury (relative to attenuation in superconducting mercury) at 1·17°K with magnetic field applied, *a* at right angles to the direction of the sound, *b* along the direction of the sound.

Results are shown in figure 5. The curve shown here for the absorption in the normal metal is an estimate of what it might be in zero magnetic field were such a state realizable. This estimate is made uncertain by the marked magnetic field dependence of the absorption, which varies with the direction of the field as shown in figure 6; this variation is most marked at the lowest temperatures reached, and figure 6 shows it at 1·17 °K.

It will be noted that the absorption is decreased on longitudinal application of the field (i.e., along the length of the specimen in the same direction as the sound). On the other hand, if the field is applied transversely, then the absorption is very much enhanced. Figure 7 shows the temperature dependence of this effect; by 1·90 °K and at higher temperatures, there is a decrease in absorption with magnetic field application, and by 3·33 °K there is relatively little effect.

Therefore to estimate the zero-field attenuation, it is necessary to extrapolate curves such as those of figure 6 to zero field: hence the relatively large possible error shown on the 'normal' curve of figure 5.

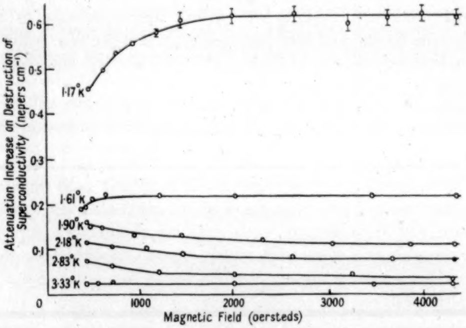

Figure 7. Variation of attenuation in normal mercury (relative to attenuation in superconducting mercury) with magnetic field applied at right angles to the direction of the sound, for various temperatures between 1·17 °K and 3·33 °K.

§ 4. Discussion of Results

It would be unwise to attach too much significance to the agreement between the set of results obtained with the first specimen and the BCS theory as shown in figure 4; it might though be argued that, if the BCS theory (or a similar energy-gap theory) is valid, then the ratio of the electronic absorptions in the superconducting and normal states is simply that of the number of absorbers; this would probably imply no change in mean-free-path for 'normal' electrons on change in state. A more detailed theory of the effect is needed for a satisfactory interpretation.

There is an additional possible objection to drawing too many conclusions from the first results, namely that dependence of the absorption on magnetic field in the normal metal has not been studied for this case. However, the experiments on the second specimen show that longitudinal field variation is not always very great; as the results are not too sensitive to the value chosen for the normal attenuation coefficient, this objection may not be too serious.

The uncertainty shown in figure 4 for the calculated points represents the difficulty of extrapolating the curve for the superconducting attenuation to the absolute zero of temperature; this extrapolation gives the zero of the electronic component of attenuation and is therefore most important in any interpretation of the results.

In the case of the results from the second specimen, the difficulty associated with this extrapolation combined with the very small change in attenuation for the superconducting state over the whole temperature range make it very difficult indeed to estimate the superconducting attenuation coefficient reliability. It is, in fact, too difficult to do so to allow any comparison such as that of figure 4 to be made.

The results obtained on the magnetic field dependence of the absorption are interesting and merit further study. While it has previously been observed that in superconductors part but not all of the electronic absorption can be removed by a magnetic field (Morse, Bohm and Gavenda 1958), such an increase in absorption as is here noted at 1·61°K and below has not previously been recorded†.

The higher electronic absorption in the first specimen at the transition temperature seems to suggest that this specimen is more free from the combined effect of lattice imperfections and chemical impurities but the explanation of this fact may be less simple than this.

§ 5. CONCLUSIONS

This investigation into the attenuation of ultrasound in mercury has shown interesting effects, particularly as regards the magnetic field dependence, which are worth further study both from the experimental and the theoretical aspect. The results are not inconsistent with existing theories of superconductivity. It is hoped to carry on this work with single crystals where improved propagation of the ultrasound may allow higher frequencies to be used and in this way fuller data may be obtained.

ACKNOWLEDGMENTS

The authors are grateful to Professor E. C. Stoner and to Dr. F. E. Hoare for their encouragement and helpful comments. The apparatus was built with the help of a grant from the Royal Society. One of us (A. M.) is indebted to the Department of Scientific and Industrial Research for a maintenance grant.

REFERENCES

BARDEEN, J., COOPER, L. N., and SCHRIEFFER, J. R., 1957, *Phys. Rev.*, **108,** 1175.
MACKINNON, L., 1955, *Phys. Rev.*, **100,** 655.
McSKIMIN, H. J., 1953, *J. Appl. Phys.*, **29,** 988.
MORSE, R. W., and BOHM, H. V., 1957, *Phys. Rev.*, **108,** 1094.
MORSE, R. W., BOHM, H. V., and GAVENDA, J. D., 1958, *Phys. Rev.*, **109,** 1394.

---

† Since this was written R. W. Morse (private communication) has drawn our attention to an earlier discovery of rising attenuation in tin, the sound being propagated along a particular crystal direction ; this is incompletely reported by Morse *et al.* (*Bull. Amer. Phys. Soc.*, 1958, **3,** 45) and no temperature dependence of the effect is recorded.

A Note on the Theory of Diffusion of Copper in Germanium

By M. D. STURGE†
Mullard Research Laboratories, Salfords, Surrey

MS. received 17th October 1958

Abstract. The theory of Frank and Turnbull of the diffusion of copper in germanium is extended to take into account the finite rate of generation of vacancies in the bulk, and the finite reaction rate in the postulated dissociation of a substitutional copper atom into an interstitial and a vacancy. Comparison of the extended theory with experiment yields an order of magnitude estimate of 10^{-8} cm for the effective radius of a dislocation for annihilation of a vacancy. It is shown that this result is consistent with the view that vacancy generation and annihilation occurs at dislocation jogs, provided that the attraction of an edge dislocation for a vacancy is taken into account.

§ 1. INTRODUCTION

THE anomalous diffusion of copper in germanium (van der Maesen and Brenkman 1955, Tweet and Gallagher 1956, Fuller and Ditzenberger 1957) has been explained by Frank and Turnbull (1956). They assume that there are two states of a copper atom in the germanium lattice: a slowly diffusing substitutional state which shows the characteristic electrical activity of copper (as an acceptor and recombination centre), and a rapidly diffusing interstitial state. In jumping from a substitutional site to an interstitial site the copper atom leaves behind it a lattice vacancy, which diffuses independently. Frank and Turnbull are able to explain in order of magnitude the high diffusion constant of copper in germanium, and explain its strong dependence on dislocation density by assuming that the rate of equilibration of the vacancy concentration, though not the equilibrium vacancy concentration itself, depends on dislocation density. In order to simplify their argument they assume that this rate of equilibration is either very fast or very slow; they also assume that the dissociation and recombination reaction proceeds rapidly, so that there is always local equilibrium between the reacting species. Experiments by Tweet (1957) on the kinetics of precipitation of copper in germanium have cast doubt on the validity of the latter assumption at temperatures below 600°C.

In the present paper we set up, and solve where possible, general diffusion and reaction equations describing the Frank–Turnbull model, in which the operation of vacancy generation and annihilation appears explicitly, and in which the finite rate of the dissociation–recombination reaction is allowed for. The theoretical solutions are compared with experiment and the cross section of a dislocation for vacancy capture deduced. In the final section the atomistic interpretation of this cross section is considered.

---

† Now at the Royal Radar Establishment, Great Malvern, Worcs.

Some of the theoretical results have been derived independently by Penning (private communication).

§ 2. The Generalized Frank–Turnbull Theory

The theory of Frank and Turnbull identifies the electrically active state of copper in germanium as a slowly diffusing substitutional atom Cu_S, and assumes that this can dissociate into a rapidly diffusing interstitial atom Cu_I and a vacancy V, thus:

$$Cu_S \rightleftharpoons Cu_I + V.$$

The progress of this bimolecular reaction can be described by the equation

$$\tau \frac{\partial c_S}{\partial t} = K c_I c_V - c_S \qquad \ldots\ldots(1)$$

where c_S, c_I, c_V are the atomic concentrations of substitutional copper, interstitial copper and vacancies respectively, and $K = c_S'/c_I' c_V'$, where primes refer to equilibrium solubilities. The equilibrium concentrations and the time constant τ are assumed to be functions of temperature only. The diffusion constant of substitutional copper is assumed to be small, so (confining our attention to a one-dimensional system) the conservation of copper atoms gives

$$\frac{\partial}{\partial t}(c_I + c_S) = D_I \frac{\partial^2 c_I}{\partial x^2} \qquad \ldots\ldots(2)$$

where D_I is the diffusion coefficient of interstitial copper. Similarly, conservation of lattice sites gives

$$\frac{\partial}{\partial t}(c_V + c_S) = D_V \frac{\partial^2 c_V}{\partial x^2} + k(c_V' - c_V) \qquad \ldots\ldots(3)$$

where D_V is the diffusion coefficient of the vacancies, and k is a rate constant describing the production of vacancies in the bulk, which is assumed to be a monomolecular process. The principal mechanism for vacancy generation and annihilation in the bulk is dislocation climb, so k is strongly structure dependent.

Equations (1), (2) and (3) are too complicated to solve without further approximations. Let us first consider the case where there is instantaneous local equilibrium in the reaction $Cu_S \rightleftharpoons Cu_I + V$, so that $\tau = 0$. Two limiting cases are considered by Frank and Turnbull. If k is very large, the vacancy concentration cannot deviate appreciably from its equilibrium value c_V', and diffusion of interstitial copper is the limiting process. On the other hand, if k is very small, all vacancies have to diffuse from the surface and as this is a slow process compared to the interstitial diffusion the interstitial concentration can be put equal to its equilibrium value c_I'. In both cases equations (1), (2) and (3) reduce to a normal diffusion equation, but with different effective diffusion coefficients, respectively given by

$$\left.\begin{aligned} D_1 &= \frac{c_I' D_I}{c_I' + c_S'} \\ D_2 &= \frac{c_V' D_V}{c_V' + c_S'} \simeq \frac{D_{Ge}}{c_S'} \end{aligned}\right\} \qquad \ldots\ldots(4)$$

as $c_V' \ll c_S'$, where D_{Ge} is the self-diffusion coefficient of germanium. Experimentally $D_1 = 2{\cdot}8 \times 10^{-5}\,\mathrm{cm^2\,sec^{-1}}$ (Fuller, Struthers, Ditzenberger and Wolfstirn 1954) while, according to (4), D_2 is $10^{-6}\,\mathrm{cm^2\,sec^{-1}}$ at 875°c and falls to less than

$10^{-8}\,\mathrm{cm^2\,sec^{-1}}$ at 600°c. Equation (4) for D_2 has been confirmed by Penning (1958 b).

Let us now consider the case of intermediate k. If k is small, we can still put $c_I = c_I'$. Combining equations (1) and (3) we have

$$\frac{\partial c_S}{\partial t} = D_2 \frac{\partial^2 c_S}{\partial x^2} + \frac{c_S' - c_S}{\theta} \qquad \ldots\ldots(5)$$

where $\theta = (c_V' + c_S')/kc_V'$ and τ has been put equal to zero. Consider a semi-infinite crystal bounded by the plane $x=0$, where the copper concentration is maintained at c_S'. Equation (5) can be solved by a straightforward application of the Laplace transformation, giving†

$$c_S/c_S' = 1 - e^{-t/\theta}\,\mathrm{erf}\,\frac{x}{2\,(D_2 t)^{1/2}}. \qquad \ldots\ldots(6)$$

Similarly, we find for the fractional uptake f of substitutional copper in a sheet of thickness $2d$:

$$f = 1 - e^{-t/\theta} + \frac{2\,(D_2 t)^{1/2}\,e^{-t/\theta}}{d}\left[\pi^{-1/2} + 2\sum_{n=1}^{\infty}(-1)^n\,\mathrm{ierfc}\,\frac{nd}{(D_2 t)^{1/2}}\right]. \qquad \ldots\ldots(7)$$

If $\theta \gg d^2/4D_2$ the surface is the principal source of vacancies and equations (6) and (7) reduce to the solutions of the normal diffusion equation with the effective diffusion coefficient D_2; if $\theta \ll d^2/4D_2$ diffusion of vacancies can be neglected and (6) and (7) reduce to

$$f = c_S/c_S' = 1 - e^{-t/\theta}, \qquad \ldots\ldots(8)$$

so long as $\theta \gg d^2/4D_1$, so that $c_I = c_I'$. Equation (8) was first derived by Penning (private communication).

Now consider the case of large k (small θ). If k is so large that the vacancy concentration is always at its equilibrium value c_V', we have for a semi-infinite body with its boundary at $x=0$:

$$c_S/c_S' = c_I/c_I' = \mathrm{erfc}\,\mu$$

where $\mu = x/2(D_1 t)^{1/2}$. If k is not quite so large it can be shown that to a first approximation c_I/c_I' is unchanged. Substituting $c_I = c_I'\,\mathrm{erfc}\,\mu$ into (1), and combining with (3), we obtain

$$\theta\frac{\partial c_S}{\partial t} = c_S' - \frac{c_S}{\mathrm{erfc}\,\mu}$$

with the approximate solution

$$c_S = c_S'\,\mathrm{erfc}\,\mu\left[1 - \exp\left(\frac{-t}{\theta\,\mathrm{erfc}\,\mu}\right)\right] \qquad \ldots\ldots(9)$$

(the terms neglected in regarding μ as constant can be shown to be small except in the region $t/\theta \sim 10\,\mathrm{erfc}\,\mu$). Equation (9), although only derived for the case of small θ, reduces to (8) when $\theta \gg x^2/4D_1$, and therefore provides a convenient interpolation formula in a region where an exact solution is unobtainable owing to the non-linearity of the equations.

---

† The conventions $\mathrm{erf}\,u = \dfrac{2}{\sqrt{\pi}}\displaystyle\int_0^u \exp(-t^2)\,dt$, $\mathrm{erfc}\,u = 1 - \mathrm{erf}\,u$, $\mathrm{ierfc}\,u = \displaystyle\int_u^\infty \mathrm{erfc}\,t\,dt$ are used.

Now let us drop the assumption of infinite reaction rate ($\tau = 0$). If k is large, we have $c_V = c_V'$. Differentiating equation (1) twice we have

$$\frac{\partial^2 c_S}{\partial x^2} + \tau \frac{\partial^3 c_S}{\partial x^2 \partial t} = K c_V' \frac{\partial^2 c_i}{\partial x^2} \simeq \frac{1}{D_1} \frac{\partial c_S}{\partial t} \qquad \ldots\ldots(10)$$

from (3), as $c_i' \ll c_S'$. Again considering a semi-infinite crystal bounded by the plane $x = 0$, we can solve (10) by a straightforward sine transformation, which gives us two alternative solutions, useful in the limits of large and small t/τ respectively:

$$\frac{c_S}{c_S'} = \operatorname{erfc} \mu + \frac{1}{\sqrt{\pi}} \frac{\tau}{t} (\tfrac{3}{2}\mu - \mu^3) \exp(-\mu^2) + \ldots \qquad \ldots\ldots(11)$$

$$\frac{c_S}{c_S'} = e^{-\lambda} \left[\frac{t}{\tau} - \frac{1}{2!} f_1(\lambda) \left(\frac{t}{\tau}\right)^2 + \frac{1}{3!} f_2(\lambda) \left(\frac{t}{\tau}\right)^3 - \frac{1}{4!} f_3(\lambda) \left(\frac{t}{\tau}\right)^4 + \ldots \right] \qquad \ldots\ldots(12)$$

Here $\lambda = \dfrac{x}{(D_1 \tau)^{1/2}}$, and $f_1(\lambda) = 1 - \tfrac{1}{2}\lambda$,

$$f_2(\lambda) = 1 - \frac{7\lambda}{8} + \frac{\lambda^2}{8}, \quad f_3(\lambda) = 1 - \frac{19\lambda}{16} + \frac{5\lambda^2}{16} - \frac{\lambda^3}{48}.$$

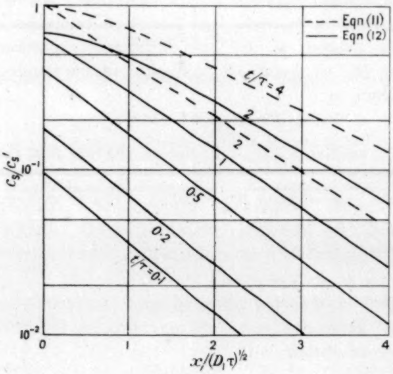

Figure 1. Concentration as a function of depth, at various times, deduced from equations (11) and (12).

Figure 1 shows c_S/c_S' as a function of λ and t/τ according to equations (11) and (12). A useful analytic approximation to (12), valid for small λ, is

$$c_S/c_S' = e^{-\lambda}(1 - e^{-t/\tau}), \quad c_i/c_i' = e^{-\lambda}.$$

This relation illustrates the physical situation; interstitial atoms diffuse from the surface a mean distance $(D_1 \tau)^{1/2}$ before combining with a vacancy, and the substitutional copper concentration builds up to its local equilibrium value $c_S' c_i / c_i'$ with the time constant τ. The fractional uptake in a plane sheet under these conditions is

$$f = 1 - e^{-t/\tau}. \qquad \ldots\ldots(13)$$

Equation (13) was derived independently by Penning (private communication).

If k is very small, so that $\theta \ll \tau$, $c_i = c_i'$. A similar argument to that above leads to equations (11), (12) and (13) in which D_1 is now replaced by D_2. If $x^2/4D_1 \ll \theta \ll x^2/4D_2$ (intermediate k) it is easy to show that (13) is replaced by

$$f = 1 - e^{-t/(\tau+\theta)}. \qquad \ldots\ldots(14)$$

We now summarize the theoretical conclusions. There are four processes involved in the Frank–Turnbull theory; diffusion of interstitial copper from the surface, diffusion of vacancies from the surface, production of vacancies in the bulk, and the reaction $\mathrm{Cu_s} \rightleftharpoons \mathrm{Cu_i} + \mathrm{V}$. The time constants of these processes are respectively $x^2/4D_1$, $x^2/4D_2$, θ, τ, where x is the distance from the point of interest to the nearest supply of copper. If any one of these processes is rate-limiting the situation is simple; the normal diffusion equation, with effective diffusion coefficient D_1 and D_2 respectively, in the first two cases; exponential build-up independent of position in the second two cases. In many experimental situations, however, one process cannot be regarded as rate-limiting, and the more complicated solutions derived in this paper have to be used.

If τ can be neglected and if $\theta \ll x^2/4D_2$, equation (9) applies, while if $\theta \gg x^2/4D_1$, equations (6) and (7) apply. In the intermediate case,

$$x^2/4D_1 \ll \theta \ll x^2/4D_2,$$

(6), (7) and (9) all reduce to equation (8). In the case of finite τ, if $\theta \ll \tau$ equations (11) and (12) apply as written, whereas if $\theta \gg \tau \gg x^2/4D_1$, they apply with D_2 replacing D_1. If $x^2/4D_1 \ll \theta \ll x^2/4D_2$ equation (14) applies. We have only considered cases which can be described by two of the four parameters $x^2/4D_1$, $x^2/4D_2$, θ, τ; more complicated cases could in principle be dealt with but are unlikely to be of practical importance.

§ 3. COMPARISON OF THEORY WITH EXPERIMENT

Fuller and Ditzenberger (1957) measured the total quantity of radioactive copper and the total number of acceptors taken up during diffusion of copper into germanium slices of approximately known etch pit count. They attributed the difference between the radioactive and acceptor concentrations to the presence of interstitial copper atoms.[†] They observed that whereas the acceptor concentration tends to the equilibrium value, the interstitial concentration decreases during heating, with a time constant of the order of θ. This decrease is not consistent with the theory. It cannot be attributed to there being only a finite supply of copper at the surface, as the acceptor concentration would then tend to a value lower than the thermal equilibrium concentration, dependent on the amount of copper available. Nor can it be a precipitation effect, as the specimen never reached a temperature higher than the diffusion temperature. It is possible that there is a systematic error in the interstitial concentration which is the small difference between two comparatively large quantities. Systematic errors of 10% in either quantity, due to the presence of radioactive or electrically active impurities, seem to be quite possible. However, it must be borne in mind that c_i', the 'equilibrium' concentration of interstitial copper, may be a less definite quantity than has been assumed in the theory.

[†] Fuller and Ditzenberger suppose the interstitial copper to be a donor, so that the observed hole concentration is equal to $c_s - c_i$. However, Penning (1958 a) has shown that interstitial copper is probably not ionized at room temperature, and we therefore assume here that the observed hole concentration is equal to c_s.

If we ignore this difficulty, we can compare the observed acceptor concentration with the theory. In most of these specimens $d^2/4D_1t$ is small and equation (7) should describe the rate of uptake of substitutional copper. This equation is compared with experiment in figure 2, and the parameters from which the theoretical curves are calculated are given in the table. Of these parameters θ is adjustable, while D_2 is calculated from equation (4), D_{Ge} being taken from the results of Letaw, Portnoy and Slifkin (1956) and c_s' from those of Woodbury and Tyler (1957). The theory fits the results within experimental error.

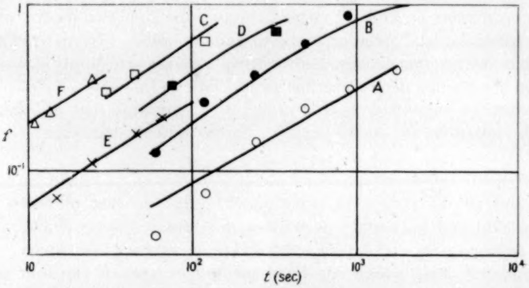

Figure 2. Comparison of Fuller and Ditzenberger's results with equation (7); fractional uptake of substitutional copper against time. The parameters describing the theroetical curves are given in the table.

Parameters for the Theoretical Curves in figure 2

(1)	(2)	(3)	(4)	(5)	(6)	(7)
A	800	0·4–1	2·5	5600	10^4	1·3–3
B	800	2·3–4·2	2·5	5600	750	0·5–1
C	810	50	2·8	2250	120	1·5
D	810	50	2·8	2250	280	3·5
E	760	50	1·2	1300	800†	5
F	875	50	13	120	300†	20

(1) Curve; (2) T(°c); (3) $10^{-3}N_D$ (cm^{-2}) (N_D is the mean etch pit count and is assumed to represent the density of edge dislocations); (4) 10^7D_2 (calc)(cm^2 sec^{-1}); (5) $d^2/4D_2$(sec); (6) θ (fitted) (sec); (7) $N_D\theta D_2$.

† These values for θ are probably overestimates as $d^2/4D_1\,t$ is not small in these specimens.

Van der Maesen and Brenkman (1955) measured the acceptor concentration as a function of depth in large germanium specimens into which copper or nickel† had been diffused at 800°c. The crystals were grown in a horizontal boat and probably had dislocation densities in the range 2×10^4 to $10^5\,\mathrm{cm}^{-2}$ (Penning, private communication). The results (corrected for the multiple acceptor nature of copper and nickel) are shown in figures 3 and 4, in which the ratio of copper or nickel concentration to its saturation value is plotted against $x/t^{1/2}$, where x is the depth in centimetres and t the time of diffusion in seconds. As $x^2/4D_2t$ is large except near the surface, the curves are calculated from equation (9), D_1 being taken as $2\times10^{-5}\,\mathrm{cm^2\,sec^{-1}}$ for copper and $2{\cdot}5\times10^{-5}\,\mathrm{cm^2\,sec^{-1}}$ for nickel. The results for copper agree quite well with theory, taking $\theta=1{\cdot}5\times10^3$ sec. The results for nickel are not consistent with a single value for θ. It is not impossible that θ should vary, as the dislocation density might be different in different specimens; θ could even be lower near the surface than it is in the bulk, as is suggested by the curve for $t=10{\cdot}5$ min. The values of θ we get from the three curves in figure 4 are 2×10^3, 4×10^3, 2×10^4 sec. However, as experiments on nickel are difficult owing to its low solubility and to the confusing effects of copper impurity, it seems best to take the value of θ from the copper data, in order to derive the quantity $N_D\theta D_2$. This lies between 7 and 40, in poor agreement with the results of Fuller and Ditzenberger at the same temperature. This discrepancy could be due to an overestimate of the dislocation density in the specimens of van der Maesen and Brenkman.

---

† Apart from the work of van der Maesen and Brenkman described here, qualitative evidence for the applicability of the Frank–Turnbull theory to nickel in germanium is provided by the work of Penning (1958 a).

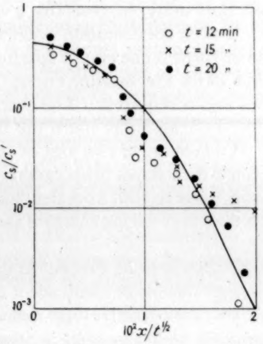

Figure 3. Comparison of van der Maesen and Brenkman's results for copper with equation (9). $D_1=2\times10^{-5}\,\mathrm{cm^2\,sec^{-1}}$, $t/\theta=0{\cdot}6$.

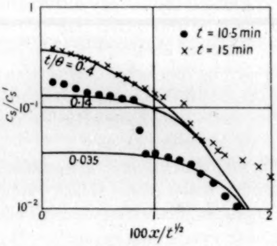

Figure 4. Comparison of van der Maesen and Brenkman's results for nickel with equation (9).

§ 4. INTERPRETATION OF THE VACANCY GENERATION–ANNIHILATION RATE CONSTANT

Suppose there are in a germanium crystal n sites per cubic centimetre at which a vacancy can be generated or annihilated, assume these sites to be randomly distributed, and neglect for the moment any long range interaction between such a site and a vacancy. In unit time the vacancy makes $2D_V/a^2$ jumps, where a is the atomic spacing, so the probability of annihilation is $2nD_V/Na^2$, where N is the number of lattice sites per cubic centimetre. This probability is the reciprocal vacancy lifetime k, so

$$\theta \simeq \frac{c_S'}{kc_V'} = \frac{Na^2}{2nD_2} = \frac{1{\cdot}2\times 10^7}{nD_2}.$$

The number n_D of lattice sites per cubic centimetre which lie on the core of a dislocation is $2{\cdot}5\times 10^7 N_D$, so $n/n_D \simeq (2N_D\theta D_2)^{-1} = 0{\cdot}1$ to 1 at 800°c (see table). We can define an effective radius of the dislocation for annihilation of a vacancy as an/n_D, which is about 10^{-8} cm, but this quantity has only mathematical significance.

Let us now consider possible atomistic interpretations of the quantity n/n_D. We suppose that all n sites lie on or near a dislocation and at first neglect the long range interaction between the dislocation and the vacancy. It is generally believed that a dislocation in a metal can only create or annihilate vacancies by the non-conservative motion ('climb') of a jog, and it is probable that this is also true in germanium and silicon. Dash (1958) has observed trails left by moving dislocations in silicon, and his results show that if, as is probable, these trails are lines of vacancy clusters left by moving jogs, the number of jogs on a grown-in dislocation in silicon is of the order of 500 per centimetre. We would expect the same order in germanium, so n/n_D should be of the order of 2×10^{-5} (though very variable, as the jogs are presumably formed by slip during cooling,) which is quite inconsistent with the experimental value.

The experimental value of n/n_D, rather less than unity, suggests that a vacancy can condense at any point on a dislocation. If such condensation occurred, the vacancy would disappear, but two jogs would be formed one atomic spacing apart (actually two vacancies are required). While twice the vacancy energy (about 4 ev) is gained, the energy of formation of two jogs is required. The energy of a single jog is of the order $\frac{1}{2}Gb^3$ where G is the shear modulus and $\mathbf{b}$ the Burgers vector, which is about 14 ev in germanium. The energy of two jogs of opposite sign close together is much less than this, because their strain fields cancel at large distances, but the core energy (which is probably quite large in a covalent material) remains, and would have to be less than one tenth of the total jog energy if vacancies are to condense in this way.†

The fact that vacancy generation and annihilation appears to occur preferentially at edge dislocations (Dash 1956) whereas jogs capable of climb occur equally on all types, suggests that we must take into account the attractive force that an edge dislocation exerts on a vacancy. If the energy gain when a vacancy is close to the dislocation is U, the vacancy concentration there is raised by the factor $e^{U/kT}$; a vacancy moving at random in the lattice will spend that much more time in the vicinity of the dislocation, so its probability of annihilation by a jog might be expected to be raised by this factor. This argument is not strictly correct, however, as the jogs can no longer be regarded as randomly distributed. Penning (private communication) has made a calculation using the normal diffusion equation, in which vacancies are assumed to diffuse radially towards the dislocation, which is treated as a cylinder of radius R_s within which the vacancy concentration is raised by the factor $e^{U/kT}$. Subsequently the vacancy diffuses along the cylinder to a jog, where it is instantaneously annihilated. Penning finds

---

† Hornstra (1958) shows that whereas in the diamond lattice two vacancies are required to form a double jog on a dislocation, a single vacancy can condense on certain types of dislocation without forming a jog, and dangling bonds can be taken up in the process. Thus it might, after all, be energetically possible for vacancies to condense on an unjogged dislocation.

$$(N_D D_2 \theta)^{-1} \simeq 4\pi\{-\ln(\pi N_D R_s^2)\}^{1/2}(R_s/p)\,e^{U/2kT} \qquad \ldots\ldots(15)$$

where p is the mean distance between jogs ($p \gg R_s$). As the number of jogs per cubic centimetre is $n_D a/p$, Penning's result differs from that assuming a random distribution of jogs throughout the crystal by the slowly varying pre-exponential factor (of order 10 if we take $R_s = 10^{-7}$ cm) and by replacing U/kT in the exponential by $U/2kT$.

If we take p to be 2×10^{-3} cm we can explain the observed value of n/n_D at 800°c if we assume $U = 1{\cdot}4$ to $1{\cdot}8$ ev. An estimate of U can be made from linear elasticity theory, though this breaks down in the immediate region of the dislocation. According to this theory, U is zero for a screw dislocation, but if there is an edge dislocation at the origin of polar coordinates the gain in energy of an impurity atom at the point (R, θ) is

$$U(R,\theta) = \frac{1}{3\pi}\frac{1+\nu}{1-\nu}Gb\,\delta V\frac{\sin\theta}{R}$$

where ν is Poisson's ratio, and δV is the change in volume of the rest of the lattice due to relaxation around the impurity (Cottrell 1953). For a vacancy δV is unknown, but if we suppose it to be two-thirds the atomic volume, the maximum value of U at one atomic spacing from the centre of the dislocation is 1·7 ev. This is probably an overestimate, as we have used linear elasticity theory in a region where it is certainly invalid, but it shows that the discrepancy noted above can reasonably be attributed to the attraction of the dislocation for the vacancy.

This calculation rests on the assumption that any excess or deficit of vacancies in the bulk is reproduced proportionally in the 'Cottrell atmosphere' of vacancies near the dislocation; in other words, the Cottrell atmosphere is in equilibrium with the bulk rather than in thermal equilibrium. So long as n/n_D is less than one, the probability of a vacancy jump taking it out of the Cottrell atmosphere (which is $e^{-U/kT}$) is greater than the probability of it meeting a jog, so this assumption is justified as a crude approximation. If n/n_D is greater than one, on the other hand, the Cottrell atmosphere, by interaction with jogs, will tend to remain in thermal equilibrium, providing a source or sink for vacancies as their bulk concentration varies.

§ 5. CONCLUSIONS

The Frank–Turnbull theory as here generalized gives a reasonably good account of the diffusion of copper in germanium. Applying the theory to the experimental results, we find the effective radius of a dislocation for capture of a vacancy to be of the order 10^{-8} cm. This result is consistent with a model of vacancy capture by jog climb, if the interaction energy of a vacancy with an edge dislocation is assumed to be about 1·6 ev, a value consistent with the theoretical estimate.

ACKNOWLEDGMENTS

The author thanks Messrs P. D. Southgate and T. B. Watkins for helpful discussions, and Mr. P. Penning for communicating his unpublished work and for detailed criticism of a preliminary draft.

REFERENCES

COTTRELL, A. H., 1953, *Dislocations and Plastic Flow in Crystals* (Oxford: University Press) p. 57.

DASH, W. C., 1956, *J. Appl. Phys.*, **27**, 1193.

—— 1958, *Ibid.*, **29**, 705.

FRANK, F. C., and TURNBULL, D., 1956, *Phys. Rev.*, **104**, 617.

FULLER, C. S., and DITZENBERGER, J. A., 1957, *J. Appl. Phys.*, **28**, 40.

FULLER, C. S., STRUTHERS, J. D., DITZENBERGER, J. A., and WOLFSTIRN, K. B., 1954, *Phys. Rev.*, **93**, 1182.

HORNSTRA, J., 1958, *Phys. Chem. Solids*, **5**, 129.

LETAW, H., PORTNOY, W. M., and SLIFKIN, L., 1956, *Phys. Rev.*, **102**, 636.

VAN DER MAESEN, F., and BRENKMAN, J. A., 1955, *Trans. Electrochem. Soc.*, **102**, 229.

PENNING, P., 1958 a, *Philips Res. Rep.*, **13**, 17.

—— 1958 b, *Phys. Rev.*, **110**, 586.

TWEET, A. G., 1957, *Phys. Rev.*, **106**, 221.

TWEET, A. G., and GALLAGHER, C. J., 1956, *Phys. Rev.*, **103**, 828.

WOODBURY, H., and TYLER, W., 1957, *Phys. Rev.*, **105**, 84.

Note added in proof. Equation (15) only holds in the limit $p \gg R_S$. If $p \ll R_S$, we have $N_D \theta D_2 = -(1/4\pi) \ln (\pi N_D R_S^2) \simeq 1{\cdot}5$. This result, which corresponds to rate-limitation by the diffusion of vacancies to dislocations rather than by the subsequent annihilation process is consistent with the experimental data (Penning, private communication).

RESEARCH NOTES

Neutron Spectra and Differential Cross Sections of the Reactions $^{19}F(\alpha, n)^{22}Na$ and $^{27}Al(\alpha, n)^{30}P$

By R. BATCHELOR and J. H. TOWLE
Atomic Weapons Research Establishment, Aldermaston, Berks.

MS. received 23rd October 1958

A TIME-OF-FLIGHT spectrometer (Batchelor and Towle 1959) has been used to measure the spectrum of neutrons from the reactions $^{19}F(\alpha, n)^{22}Na$ and $^{27}Al(\alpha, n)^{30}P$ at the angles of 0, 30, 60, 90 and 135° to the incident particles. Targets of CaF_2 and Al, $100\,\mu g\,cm^{-2}$ thick were bombarded with helium ions at several energies between 3 and 6 Mev. Throughout the measurements the yield of γ-rays was monitored using a NaI(Tl) scintillation counter, this facility providing a check on the stability of the targets. The efficiency of the neutron detector was obtained by comparison with a long counter.

Two typical examples of neutron time-spectra for the $^{19}F(\alpha, n)^{22}Na$ reaction are shown in figure 1. The neutron peaks are labelled by the corresponding levels in ^{22}Na. The zero of the time scale was obtained from the position of the γ-ray peak, and the time scale was calibrated using a double pulse generator. The measured differential cross sections are summarized in figures 2 and 3 and the table. The errors on these measurements are estimated to be ±20% and are due mainly to uncertainties in the efficiency of the neutron detector. Two curves, namely those for the group to the 0·59 Mev level in ^{22}Na at $E_\alpha = 4{\cdot}64$ Mev and for the group to the ground state of ^{30}P at $E_\alpha = 5{\cdot}4$ Mev are not symmetrical about 90° in the centre-of-mass system. If the reaction proceeds mainly through the formation of a compound nucleus, this indicates interference between levels of differing parity in the compound nucleus. The levels in the compound nucleus at this excitation (about 15 Mev) are very closely spaced (Endt and Braams 1957).

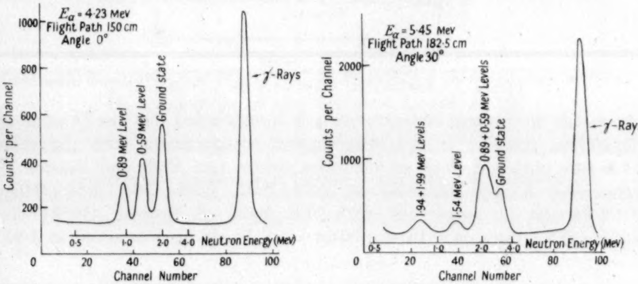

Figure 1. Time-spectra of neutrons from $^{19}F(\alpha,n)^{22}Na$.

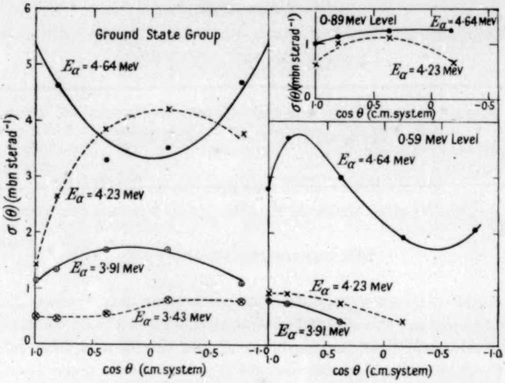

Figure 2. Differential cross sections for ^{19}F(α,n)^{22}Na.

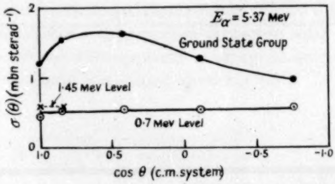

Figure 3. Differential cross sections for ^{27}Al(α,n)^{30}P.

From all the present measurements it is concluded that the *Q* value of the ^{19}F(α, n)^{22}Na reaction is $-1{\cdot}94 \pm 0{\cdot}03$ Mev in agreement with the value of $-1{\cdot}928$ Mev obtained from atomic mass values (see Endt and Braams 1957). Levels were located in ^{22}Na at $0{\cdot}59 \pm 0{\cdot}02$, $0{\cdot}89 \pm 0{\cdot}02$, $1{\cdot}54 \pm 0{\cdot}03$ and $1{\cdot}97 \pm 0{\cdot}04$ Mev in agreement with the work of Browne (1955) on the ^{24}Mg(d, α)^{22}Na reaction. In the latter work levels were resolved at 1·94 and 1·99 Mev.

$E\alpha$	Corresponding levels in ^{22}Na	σ(θ) at 0° (mbn sterad⁻¹)
4·93	g.s. + 0·59 + 0·89	6·3
	1·54	0·3
5·31	g.s. + 0·59 + 0·89	16
	1·54	0·4
	1·97	1·5

Energies are in Mev.

At one of the bombarding energies used, $E_\alpha = 3{\cdot}91$ Mev, the second neutron group corresponds to a level at $0{\cdot}62 \pm 0{\cdot}02$ Mev rather than $0{\cdot}59 \pm 0{\cdot}02$ Mev as found with $E_\alpha = 4{\cdot}23$ and 4·64 Mev, and the width of the corresponding peak in the time spectrum is not noticeably greater than one due to the excitation of a single level. This may be due to the contamination of the group leading to the 0·59 Mev level by one leading to a level at a slightly higher energy (not higher than 0·69 Mev).

A state having $T=1$, $J=0^+$ is expected at about 0·6 Mev in ^{22}Na (see Endt and Braams 1957, for references). It is thought that neither the 0·59 nor the 0·89 Mev level has $T=1$ since they are both strongly excited in the ^{24}Mg(d, α)^{22}Na reaction. It is of interest to note that a level at 0·666 Mev has recently been reported from observations on the γ-rays in the ^{19}F(α, n)^{22}Na reaction (Temmer and Heydenburg 1958). There is also some unconfirmed evidence for a level between those at 0·59 and 0·89 Mev from the ^{25}Mg(p, α)^{22}Na reaction (Browne 1955).

The Q value of the ^{27}Al(α, n)^{30}P reaction was estimated to be $-2·67 \pm 0·03$ Mev in agreement with the value 2·671 Mev obtained from atomic mass values (Endt and Braams 1957). Levels in ^{30}P were found at $0·70 \pm 0·03$ and $1·45 \pm 0·03$ Mev, in agreement with values obtained from the ^{32}S(d, α)^{30}P reaction (Paris, Van der Leun and Endt 1957). The doublet 0·680 Mev $T=1$, and 0·708 Mev $T=0$ reported in the latter work would appear unresolved in our experiment.

REFERENCES

BATCHELOR, R., and TOWLE, J. H., 1959, *Proc. Phys. Soc.*, **73**, 193.
BROWNE, C. P., 1955, *M.I.T. Laboratory for Nuclear Science Progress Report*, May 31st, 1955.
ENDT, P. M., and BRAAMS, C. M., 1957, *Rev. Mod. Phys.*, **29**, 683.
PARIS, C. H., VAN DER LEUN, C., and ENDT, P. M., 1957, *Bull. Amer. Phys. Soc.* II, **2**, No. 4, 179.
TEMMER, G. M., and HEYDENBURG, N. P., 1958, *Bull. Amer. Phys. Soc.* II, **3**, No. 3, 200.

Inelastic Scattering of High Energy Nucleons by Complex Nuclei II: Excitation of the 4·4 MeV Level of ^{12}C

BY G. P. McCAULEY
Department of Mathematical Physics, University of Birmingham

Communicated by R. E. Peierls; MS. received 23rd October 1958

§ 1. INTRODUCTION

IN part I (McCauley and Brown 1958) we used a semi-classical formalism to derive an expression for the scattered amplitude in the excitation of particular low-lying levels of complex nuclei by high energy nucleons. This gave the amplitude for small angle scattering in terms of the forward part of the free nucleon–nucleon scattering matrix, and was seen to be equivalent to a direct interaction with distorted waves. The distorting potential was similar to the optical potential for elastic scattering as derived by Riesenfeld and Watson (1956) and Brown (1957).

As a particular example we consider here the excitation of the first excited level of ^{12}C by 160 Mev protons. This reaction has been studied experimentally by Tyrén and co-workers (Tyrén, Hillman and Johansson 1957, Tyrén and Maris 1957, Maris and Tyrén 1957) and theoretically, using the direct interaction picture, by Benoist, Marty and Meyer (1957) and Squires (1958). These authors take into account the distortion of the incident and scattered waves due to a purely absorptive central potential. However, we know from the polarization effects in elastic scattering (see for example Alphonce, Johansson and Tibell 1957) that the optical potential should also contain a spin-orbit part, and would expect theoretically (Riesenfeld and Watson 1956, Ohnuma 1958) that the real central part should be large for energies up to about 200 MeV. In the present paper it is shown that the inclusion of these additional terms in the optical potential does not appreciably alter the results obtained by Squires, either for cross sections or polarizations. This is true for both the *LS* and *jj* coupling assignments of the nuclear levels, so we give detailed results only for the case of *LS* coupling which is both simpler and more nearly in agreement with experiment.

We also consider in some detail the matrix element for the case where the transfer of angular momentum (2 units) has component zero along the beam direction. This term is small at the main peak of the differential cross section, but appears to become dominant at very small angles. It is a large part of the contribution, neglected by Squires, for the case where the transfer of angular momentum has component ± 2 along the direction of the momentum transfer. The small forward peak arising from this term has not been observed at energies in the region of 160 MeV, though very large forward peaking is familiar at much lower energies, 12 to 20 MeV (Sherr 1957).

§ 2. EXPRESSION FOR SCATTERED AMPLITUDE

Before applying the results of part I to the case of 160 MeV protons scattering from ^{12}C, we make one modification which extends the angular range of validity. We allow the two particle scattering matrix for the particular collision inside the nucleus which is responsible for the excitation to vary with the final scattering angle. The coherent scattering of the wave before and after the inelastic event is still mainly small angle scattering, for which the forward part of the two particle scattering matrix is used. Most of the momentum transfer to the nucleus as a whole goes via the excited particle.

With this modification the formulae of part I, § 5, for the scattered amplitude when the nucleus is left in state M may be written in the form

$$\left.\begin{aligned} f_M(\theta) &\equiv A_M(\theta) + \boldsymbol{\sigma}_0 . \mathbf{n} N_M(\theta) + \boldsymbol{\sigma}_0 . \mathbf{c} C_M(\theta) + \boldsymbol{\sigma}_0 . \hat{\mathbf{k}} K_M(\theta) \\ &= \frac{k}{2\pi i} \int \mathrm{e}^{-ikb \sin\theta \cos\phi} G_M(b, \phi; \theta) b \, db \, d\phi \end{aligned}\right\} \quad \ldots\ldots (2.1)$$

where

$$G_M(b, \phi; \theta) = \tfrac{1}{2}\{A(b) + \boldsymbol{\sigma}_0 . \hat{\mathbf{k}} \times \hat{\mathbf{b}} B(b), \langle M | G(\theta) | 0 \rangle\}_+ . \quad \ldots\ldots (2.2)$$

The first part of the anti-commutator (which is necessary because of the occurrence of different components of the spin operator $\boldsymbol{\sigma}_0$) represents the distortion due to the unexcited nucleons, and the second the inelastic event. If a Gaussian shape is assumed for the density distribution of the nucleus we have (I, 4.9)

$$A(b) + \boldsymbol{\sigma}_0 . \hat{\mathbf{k}} \times \hat{\mathbf{b}} B(b) = \exp\left[V \mathrm{e}^{-b^2/a^2} + \boldsymbol{\sigma}_0 . \hat{\mathbf{k}} \times \hat{\mathbf{b}} W(b/a) \mathrm{e}^{-b^2/a^2}\right] \quad \ldots\ldots (2.3)$$

where

$$\left.\begin{aligned} V &= (A-1) \frac{2i}{a^2 k} \bar{\alpha}(0) \\ W &= (A-1) \frac{4}{a^3 k^2} \bar{\beta}(0). \end{aligned}\right\} \quad \ldots\ldots (2.4)$$

The coefficients $\bar{\alpha}(0)$ and $\bar{\beta}(0)$ come from the two particle scattering amplitude, averaged for protons and neutrons as in I, § 3, taken in the laboratory system in the form

$$\bar{f}(\theta) \equiv \bar{\alpha}(\theta) + (\boldsymbol{\sigma}_0 + \boldsymbol{\sigma}_1) \,.\, \mathbf{n} \sin\theta \bar{\beta}(\theta) + \text{other spin terms} \quad \ldots\ldots (2.5)$$

where $\mathbf{n} = \hat{\mathbf{k}} \times \hat{\mathbf{k}}'$ is the normal to the scattering plane. The second part of (2.2) is given explicitly as

$$\langle M | G(\theta) | 0 \rangle = \left[\frac{2\pi i}{k} \bar{\alpha}(\theta) + \frac{2\pi}{k^2} \bar{\beta}(\theta) \boldsymbol{\sigma}_0 \,.\, \hat{\mathbf{k}} \times \nabla \right] \left\langle M \left| \sum_{i=1}^{A} \delta(\mathbf{b} - \mathbf{b}_i) \right| 0 \right\rangle \quad \ldots\ldots (2.6)$$

$\mathbf{b}_i$ being the projection of the position vector of the *i*th nucleon of the nucleus.

We consider the *LS* coupling assignments for the ground state and first excited (2^+) state of ^{12}C. Both are $p^8[44]$ states with $S = 0$. We take M as the component of angular momentum of the final nuclear state along the beam direction and use oscillator wave functions. These are chosen to give the same root-mean-square radius, 2·45 fermis (see Fregeau and Hofstadter 1955), as the previous Gaussian distribution with $a = 2{\cdot}0$ fermis. These choices lead to

$$\left.\begin{aligned} \left\langle \pm 2 \left| \sum_i \delta(\mathbf{b} - \mathbf{b}_i) \right| 0 \right\rangle &= \frac{4}{3} \sqrt{\frac{21}{10}} g_1(b) \mathrm{e}^{\mp 2i\phi} \\ \left\langle 0 \left| \sum_i \delta(\mathbf{b} - \mathbf{b}_i) \right| 0 \right\rangle &= \frac{4}{3} \sqrt{\frac{7}{5}} (g_0(b) - g_1(b)) \end{aligned}\right\} \quad \ldots\ldots (2.7)$$

where

$$\left.\begin{aligned} g_0(b) &= \frac{\gamma}{\pi a^2} \exp\left(-\gamma \frac{b^2}{a^2} \right), \\ g_1(b) &= \frac{\gamma^2 b^2}{\pi a^4} \exp\left(-\gamma \frac{b^2}{a^2} \right), \qquad \gamma = \frac{13}{9}. \end{aligned}\right\} \quad \ldots\ldots (2.8)$$

The functions $g_0(b)$ and $g_1(b)$ are obtained by integrating the *p*-wave densities along the beam direction for each impact parameter *b*.

The choice of the beam direction as axis of quantization is convenient in enabling us to do the ϕ-integration of (2.1) explicitly for each term; this gives rise to expressions containing Bessel functions. For example the term $A_0(\theta)$ discussed below becomes, to zero order in W,

$$A_0(\theta) = \bar{\alpha}(\theta) \frac{4}{3} \sqrt{\frac{7}{5}} \, 2\pi \int_0^\infty \mathrm{J}_0(kb \sin\theta) \exp\left[V \exp\left(-\frac{b^2}{a^2} \right) \right] [g_0(b) - g_1(b)] b \, db. \quad \ldots\ldots (2.9)$$

The alternative choice of the direction of the momentum transfer as axis of quantization is simpler in the absence of a distorting potential, but is not so useful here since it destroys the cylindrical symmetry which leads to the Bessel functions. The final results are of course independent of this choice of axis.

The remaining integrals can be evaluated numerically, or can be converted into double series in V and $x = \frac{1}{2} ak \sin\theta$, which can be summed in part algebraically to give rapid convergence. The series method was found to be more convenient for dealing with the large number of similar integrals, and complex values of V. In considering the effect of the spin-orbit part of the potential it was found to be sufficient to include terms of first order in W.

Antisymmetrization of the nuclear wave functions introduces a correction to the multiple scattering terms due to the possibility of interchanging the states of two of the nuclear particles. For small values of b, where multiple scattering is most important, this effect introduces a coefficient 0·87 in the V^2 term in the expansion of (2.3) for a carbon nucleus in the LS coupling limit.

The values of $\bar{\alpha}(\theta)$ and $\bar{\beta}(\theta)$ were obtained from the potentials of Gammel and Thaler (1957), and are given in the table. These potentials have been used successfully in relating the elastic scattering from nuclei to nucleon–nucleon scattering by M^c^Manus and Thaler (1958).

Values of $\bar{\alpha}(\theta)$ and $\bar{\beta}(\theta)$ in fermis calculated from Gammel–Thaler nucleon–nucleon potentials, $\bar{\beta}(0)$ being defined as $\lim_{\theta\to 0}\bar{\beta}(\theta)$

	$\theta=0°$	$\theta=10°$	$\theta=22{\cdot}5°$
$\bar{\alpha}(\theta)$	$0{\cdot}857+0{\cdot}820i$	$0{\cdot}779+0{\cdot}711i$	$0{\cdot}440+0{\cdot}381i$
$\bar{\beta}(\theta)$	$0{\cdot}395+1{\cdot}28i$	$0{\cdot}359+1{\cdot}33i$	$0{\cdot}240+1{\cdot}35i$

§ 3. Results and Discussion

With these values of $\bar{\alpha}$ and $\bar{\beta}$ we find $V=-1{\cdot}64-1{\cdot}72i$ and $W=-0{\cdot}29-0{\cdot}94i$. This corresponds to an optical potential whose imaginary central part reaches a maximum of 72 MeV at the centre of the nucleus. This number is very sensitive to the shape assumed for the density distribution of the nucleus; if the Gaussian is replaced by a square distribution giving the same root-mean-square radius it is reduced to 25 MeV (this point is discussed in some detail by Bethe 1958).

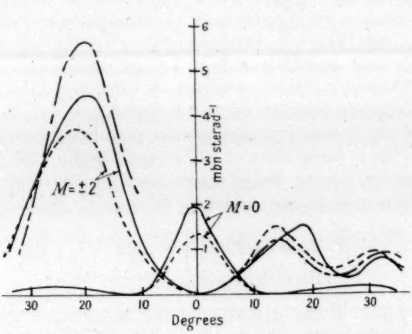

Asymmetric cross section for inelastic scattering of polarized protons exciting the 4·43 MeV level of ^{12}C. The full lines show results using complex values for V and W, the dashed lines are for real V alone, i.e. pure absorption.

The chain line shows the experimental results of Tyrén scaled down by a factor *two* (see text).

Calculations were performed with two different values of V, one using only the real part, pure absorption, and the other using both the real and imaginary parts quoted above. Results were also obtained with and without the inclusion of the spin-orbit term W. In the figure we give the results for the case of pure absorption only, and for the case where all of V and W were included. We have plotted the asymmetric cross section for the scattering of a completely polarized incident beam with spin up†, showing separate cross sections for the final nuclear states $M = \pm 2$ and $M = 0$. The additional terms in the optical potential have remarkably little effect on the results for $M = \pm 2$; the real central part reduces the asymmetry slightly, but this is compensated by the spin-orbit part, which also increases the cross section by about 15% at the peak. This still leaves the theoretical cross section at about half the experimental value. If *jj* coupling wave functions are used for the nuclear states the situation is even worse. The matrix element for producing the excitation without flipping the spin of one of the nuclear particles is reduced by a factor $\sqrt{(5/14)}$; the spin flip term is too small to compensate for this reduction. It has been suggested by Squires that the agreement with experiment could be considerably improved by adding a small collective admixture to the *LS* wave function for the excited state, in analogy with the case of electron scattering studied by Ferrell and Visscher (1956). The matrix elements for the pure collective case are several times as large as those for the *LS* case, so even a small admixture can double the cross section. The general trend of the polarization results would be unaltered, but a detailed evaluation with the matrix elements would be very lengthy.

The curve shown in the figure for the case $M = 0$ indicates the possibility of a forward peak in the cross section. (The two curves should be added to give the full cross section for the 2^+ state.) This is entirely due to the distortion as can be seen from the integral (2.9). For θ and V both zero, the first two factors of the integrand are unity, and the integrals of g_0 and g_1 cancel. As θ is increased less weight is given to large values of b where g_1 is larger, so the integral becomes positive. However, a negative real V gives less weight to small b, so that the actual integral is negative for $\theta = 0$ and changes sign as θ increases, producing what is essentially a diffraction pattern for the $M = 0$ cross section. This effect is clearly sensitive to the shape of well assumed for the distorting potential. Replacing the Gaussian well by a square well reduces the width of the peak by a quarter and its height by almost a half; the height of the main $M = \pm 2$ peak is increased by about 10%. We see therefore that this forward peak occurs at angles of less than 5°, which are difficult to observe experimentally. It is interesting to note that at lower energies the forward peak due to the distortion of the incident and scattered waves dominated the inelastic scattering from this level (Banerjee and Levinson 1957). This forward peak is found to be slightly larger when the suggested collective admixture is added. More experimental information on the small angle cross sections would provide a good test of the present theoretical approach.

ACKNOWLEDGMENTS

My thanks are due to Dr. G. E. Brown for suggesting this problem, and to Professor R. E. Peierls and Mr. L. Castillejo for several helpful discussions. I should also like to acknowledge a Research Studentship from the Ministry of Education for Northern Ireland.

---

† Note: The graphs of the asymmetric cross section contain the same information as the cross section and polarization for scattering of an unpolarized incident beam, as no asymmetry–polarization difference is indicated by either the present theory or experiments (cf. Squires).

REFERENCES

ALPHONCE, R., JOHANSSON, A., and TIBELL, G., 1957, *Nucl. Phys.*, **3**, 185.
BANERJEE, M. K., and LEVINSON, C. A., 1957, *Annals of Physics*, **2**, 499.
BENOIST, P., MARTY, C., and MEYER, P., 1957, *C.R. Acad. Sci., Paris*, **245**, 1389.
BETHE, H. A., 1958, *Annals of Physics*, **3**, 190.
BROWN, G. E., 1957, *Proc. Phys. Soc.* A, **70**, 361.
FERRELL, R. A., and VISSCHER, W. M., 1956, *Phys. Rev.*, **104**, 475.
FREGEAU, J. H., and HOFSTADTER, R., 1955, *Phys. Rev.*, **99**, 1503.
GAMMEL, J. L., and THALER, R. M., 1957, *Phys. Rev.*, **107**, 291, 1337.
MARIS, Th. A. J., and TYRÉN, H., 1957, *Nucl. Phys.*, **4**, 662.
McCAULEY, G. P., and BROWN, G. E., 1958, *Proc. Phys. Soc.*, **71**, 893.
McMANUS, H., and THALER, R. M., 1958, *Phys. Rev.*, **110**, 590.
OHNUMA, S., 1958, *Phys. Rev.*, **111**, 1173.
RIESENFELD, W. B., and WATSON, K. M., 1956, *Phys. Rev.*, **102**, 1157.
SHERR, R., 1957, *Proc. of Pittsburgh Conference.*
SQUIRES, E. J., 1958, *Nucl. Phys.*, **6**, 504.
TYRÉN, H., HILLMAN, P., and JOHANSSON, A., 1957, *Nucl. Phys.*, **3**, 336.
TYRÉN, H., and MARIS, Th. A. J., 1957, *Nucl. Phys.*, **3**, 52; **4**, 637.

A Measurement of the Effect of the Coulomb Field of a Nucleus on the Decay Rate of Negative Muons

BY A. ASTBURY, M. HUSSAIN, M. A. R. KEMP, N. H. LIPMAN†,
H. MUIRHEAD, R. G. P. VOSS AND A. KIRK‡
Nuclear Physics Research Laboratory, University of Liverpool
‡ Department of Applied Mathematics, University of Liverpool

MS. received 7*th October* 1958

NEGATIVE muons brought to rest in matter disappear as a result of two processes, decay and nuclear capture. The rate of loss in a material of atomic number Z is $\lambda_L(Z)$, given by

$$\lambda_L(Z)=\lambda_D(Z)+\lambda_C(Z)$$

where $\lambda_D(Z)$ and $\lambda_C(Z)$ are the decay and capture rates respectively. Measurements of $\lambda_L(Z)$ have been made for a number of materials; for recent determinations see for example Sens *et al.* (1957), and Astbury *et al.* (1958).

The main object in these experiments has been the determination of $\lambda_C(Z)$, but in evaluating this quantity it has previously been necessary to assume that $\lambda_D(Z)$ was equal to the decay rate of the positive muon. This assumption can only be an approximation since (*a*) distortion of phase space, (*b*) time dilatation, and (*c*) the Coulomb distortion of the outgoing electron spectrum can modify $\lambda_D(Z)$ for a bound negative muon.

Calculations on effects (*a*) and (*b*) indicate that they give a decrease in the decay rate, in accordance with the equation

$$\lambda_D(Z)=\lambda_D(0)[1-\beta(Z_{\text{eff}}/137)^2] \qquad ......(1)$$

where $\lambda_D(Z)$ and $\lambda_D(0)$ are the decay rates for a muon bound to a nucleus of atomic number Z and for a free muon respectively, and β is a constant having an estimated value between 3 and 5 (Khuri and Wightman 1958, Huby and Newns 1958, private communication). Z_{eff} is the effective atomic number of the nucelus in question (Wheeler 1949). The effect of the distortion of the wave function of the electron by the Coulomb field (*c*) is more difficult to evaluate but should be of opposite sign to effects (*a*) and (*b*) and probably a smaller magnitude than that observed in β-decay, since the muon may be outside the nucleus when it decays. The rates $\lambda_{\mathrm{C}}(Z)$ and $\lambda_{\mathrm{D}}(Z)$ may be obtained separately by making a further measurement, that of the fraction of stopped muons which emit an electron, $f=\lambda_{\mathrm{D}}(Z)/\lambda_{\mathrm{L}}(Z)$. Experimental difficulties make an absolute measurement of f difficult for a single material. However, it is possible to find relative values for f under identical physical conditions for two materials one of which is of low atomic number. Thus for two nuclei with atomic numbers Z_1 and Z_2 (the latter assumed small), the effect $R(Z_1)$ of the Coulomb field on the decay rate of the bound muon will be given by

---

† Now at C.E.R.N., Geneva, Switzerland.

$$R(Z_1)=\frac{\lambda_{\mathrm{D}}(Z_1)}{\lambda_{\mathrm{D}}(0)}\simeq\frac{\lambda_{\mathrm{D}}(Z_1)}{\lambda_{\mathrm{D}}(Z_2)}=\frac{f(Z_1)}{f(Z_2)}\,\frac{\lambda_{\mathrm{L}}(Z_1)}{\lambda_{\mathrm{L}}(Z_2)}.$$

The authors have measured R for two pairs of elements, copper–aluminium and copper–polythene. In each case the target was a sandwich of alternate layers of the two elements in question (it was assumed that the polythene was effectively equivalent to carbon). Several factors determined the thickness of each sheet. The sheets had to be sufficiently thick to give confidence in the calculation of the relative numbers of muons stopping in each element. These were calculated using range–energy tables (Rich and Madey 1954). On the other hand, if the sheets were too thick, decay electrons originating in one element would be detected with higher efficiency than those from the other. By using thin sheets any errors due to different decay electron spectra and uncertainty in the muon spectrum were minimized. Details of the targets used are given in the table.

The arrival of muons was indicated by coincidence $12\bar{3}$ in a counter telescope, the target being placed between counters 2 and 3, and the appearance of a decay electron by a further coincidence $\bar{2}34$. (Further experimental details are given in the paper by Astbury *et al.* 1958). The time intervals between the occurrence of events $12\bar{3}$ and $\bar{2}34$ were measured electronically and displayed on a pulse height analyser. This yielded data in the form of a curve

$$y=A\exp\left[-\lambda_{\mathrm{L}}(Z_1)t\right]+\mathrm{B}\exp\left[-\lambda_{\mathrm{L}}(Z_2)t\right]+C$$

where A and B are related to $f(Z_1)$ and $f(Z_2)$ respectively, t is the time between the arrival of a muon and the appearance of its decay electron, and C is the constant random background. The values of $\lambda_{\mathrm{L}}(Z_1)$ and $\lambda_{\mathrm{L}}(Z_2)$ were obtained by Astbury *et al.* (1958). In order to obtain reliable values for A and B, the position of zero time on the pulse height analyser had to be stable and accurately known. During runs this position was frequently checked, and found to be stable to within 7 mμsec. This corresponds to an uncertainty of 1% in the final value of R.

The experimental data were analysed with the aid of the Manchester electronic computer and the ratio R determined. A correction was applied to the experimental data for the γ-rays arising from the decay of excited nuclei produced by muon capture, which could cause coincidences in counters 3 and 4, thereby simulating electrons; this was done by placing an anti-coincidence counter 5 immediately after the target and measuring the ratio of events obtained with counter 5 on to those with this counter off, viz. the ratio (number of γ-rays)/(number of γ-rays + electrons). The non-conservation of parity in muon decay also made necessary the introduction of a small correction for the anisotropy of the electrons emitted when the muons stopped in polythene.

The results for R are presented in the table. The errors quoted cover uncertainties in statistics, zero time effects, values for $\lambda_L(Z)$, range–energy calculations, and non-conservation of parity. The values for R calculated from equation (1), R_{calc}, are also shown. Values of Z_{eff} were obtained from Wheeler (1949), and β was taken to be 4.

Target	$\left(\frac{Z_1}{Z_2}\right)_{\text{eff}}$	Thickness (g cm^{-2})	Number of sheets	R_{calc}	R
Copper–Polythene	$\frac{20\cdot7}{5\cdot8}$	10	32/32	0·91	$1\cdot03 \pm 0\cdot05$
Copper–Aluminium	$\frac{20\cdot7}{11\cdot7}$	11	30/30	0·94	$1\cdot015 \pm 0\cdot055$

It can be seen from the table that the change in decay rate of a negative muon due to atomic binding is small, and could not seriously affect published results for $\lambda_C(Z)$, since for light nuclei $\lambda_D(Z)$ is close to $\lambda_D(0)$, and for heavy nuclei $\lambda_C(Z) \gg \lambda_D(Z)$ so that a small correction to $\lambda_D(Z)$ would leave $\lambda_C(Z)$ virtually unchanged; for example a correction of 3% to $\lambda_D(Z)$ alters our published result (Astbury *et al.* 1958) of $\lambda_C(Z)$ for copper by 0·2%.

Similar data have been obtained by Lundy *et al.* (1958), to whom we are grateful for the communication of results prior to publication. We should also like to thank Drs. Doniach, Huby and Newns of this University for stimulating theoretical discussions.

References

Astbury, A., Kemp, M. A. R., Lipman, N. H., Muirhead, H., Voss, R. G. P., Zangger, C., and Kirk, A., 1958, *Proc. Phys. Soc.*, **72**, 494.

Khuri, N. D., and Wightman, A. J., quoted by Sens, J. C., Lundy, R. A., Swanson, R. A., Telegdi, V. L., and Yovanovitch, D. D., 1958, *Bull. Amer. Phys. Soc., Ser.* II, **3**, 198.

Lundy, R. A., Sens, J. C., Swanson, R. A., Telegdi, V. L., and Yovanovitch, D. D., 1958, *Phys. Rev. Letters*, **1**, 102.

Rich, M., and Madey, R., 1954, UCRL Report No. 2301.

Sens, J. C., Swanson, R. A., Telegdi, V. L., and Yovanovitch, D. D., 1957, *Phys. Rev.*, **107**, 1464,.

Wheeler, J. A., 1949, *Rev. Mod. Phys.*, **21**, 133.

Some Observations on the Spectra of the Diatomic Fluorides of Silicon, Germanium, Tin, and Lead

BY R. F. BARROW, D. BUTLER, J. W. C. JOHNS
AND J. L. POWELL
Physical Chemistry Laboratory, University of Oxford

MS. received 2nd October 1958

THERE has been little systematic study of the spectroscopic properties of the diatomic halides of the typical elements of group IV. In a recent paper (Johns and Barrow 1958) some progress in the elucidation of the spectrum of SiF was reported: in the present note are given the results of further observations of this spectrum and of the spectra of GeF, SnF and PbF. The spectra were studied in emission, using hollow cathode discharges, with helium as carrier gas.

SiF

Rotational analyses have been made of the 0, 0, 0, 1 and 0, 2 bands of the green ε-system, and of the 1, 0 and 0, 0 bands of the ultra-violet ε-system. These systems arise from transitions $\mathrm{C}'^2\Pi - \mathrm{A}^2\Sigma^+$ and $\mathrm{D}'^2\Pi - \mathrm{A}^2\Sigma^+$ respectively. In addition, bands of the systems C′–X, D′–B and D′–X have also been observed. Constants for the new states are given in table 1. The δ-bands are now believed to arise from SiF_2 (Johns, Chantry and Barrow 1958).

Table 1. Constants for SiF

State	$\nu_{0,0}$ for D′, C′ –A	T_e	A	ω_e	$x_e\omega_e$
$\mathrm{D}'^2\Pi$	23912·6	46606·7	~0	1032·9	5·28
$\mathrm{C}'^2\Pi$	$19264{\cdot}4_6$	41964·9	$16{\cdot}5_4$	1031·8	4·45

State	B_e	α_e	p[b]	q[b]
$\mathrm{D}'^2\Pi$	0·6329[a]	0·0044[a]		−0·0037
$\mathrm{C}'^2\Pi$	0·6376	0·0039	$-0{\cdot}0086_6$	$-0{\cdot}0002_7$

Notes: [a] α_e for D′ was estimated, using the Pekeris relation.
[b] p, q are the Λ-type doubling constants (Mulliken and Christy 1931).

GeF

A number of new bands have been photographed in the region 1900 to 2450 Å which are assigned to six systems, each with the ground state as lower state. Bands of the system $\mathrm{B}(^2\Sigma) - \mathrm{A}(^2\Sigma)$ have also been observed between 7400 and 8500 Å: the earlier analyses of systems A, B–X (Andrews and Barrow 1950) have been confirmed. However, the strongest feature of the infra-red spectrum consists of a complex band at 8550 to 8700 Å. This has intensity minima at $11617{\cdot}_5$ and $11580{\cdot}_3$, a red-degraded head at $11589{\cdot}_2$ and a line-like branch with an edge at 11585·$_6$ cm^{-1}. The appearance is thus of a doublet 0, 0 band, in which the shorter-wavelength sub-band is degraded to the violet and the longer-wavelength sub-band degraded to the red. It is assigned provisionally to the transition E($^2\Pi$)–B($^2\Sigma$).

Table 2. Constants for GeF

State	T_e	A	ω_e	$x_e\omega_e$	ω'/ω''
G	49428·7 49389·7	39	719·$_3$	3·5$_5$	1·08
F	(47325) (47318)	?7	(804)		1·22
E ($^2\Pi$)	(46693) (46655)	38	(812)		1·23
D	(45101) (45063)	38	(789)		1·20
C	(44005·0) (43979·5)	25·5	(682)		1·03
C'	(43484) (43455)	29	(829)		1·26
B ($^2\Sigma^+$)	35007·4	—	800·4	4·1$_5$	1·20
A ($^2\Sigma^+$)	23316·8	—	413·5	1·0$_5$	0·62
X ($^2\Pi_r$)	935 0	935	665·8 664·5	2·85 2·75	1·00

Notes: 1. Figures in parentheses are of T_0 and $\Delta G_{1/2}$ respectively.

2. The transitions A, B, C, G–X are strong and the constants for these states are in consequence more reliable than for the other states.

SnF

Yuasa (1939) has observed the visible system, now called A$^2\Sigma$ – X$^2\Pi$, in emission: otherwise observations are confined to the study of the spectrum in absorption (Jenkins and Rochester 1937). We have found that the spectrum is excited very strongly in the present source, and have measured all the bands between about 2000 and 9000 Å. Eight excited states have been recognized in transitions to the ground state, and bands of the systems B, F–A have also been observed. It has thus been possible to amplify, and in several cases, to correct, the earlier analyses based on absorption from the sub-level X$^2\Pi_{1/2}$. The results are given in table 3.

PbF

The hollow cathode source proved rather unsatisfactory in this case, and many atomic lines were excited; bands which may perhaps arise from FeF at 3100 to 3400 Å were also excited rather strongly. However, several bands of the transition A–X$^2\Pi$ were observed. The multiplet intervals are found to be the same in the systems A, B–X (table 4) and the presumption is therefore strong that state A, like B, is $^2\Sigma$, and not $^2\Delta$, as has been believed hitherto.

Table 3. Constants for SnF

State	T_e	A	ω_e	$x_e\omega_e$	ω'/ω''
G	(46438·8) (46351·8)	87	(609·9)		1·05
F ($^2\Sigma^+$)	45552·6	–	688·2	$4{\cdot}6_5$	1·17
E	42137·1 41856·1	281·0	677·0	3·0	1·16
D	(41361·4)	~0	(622)		1·07
C (?$^2\Delta$)	(40841·6) (40772·8)	69·3	(600)		$1{\cdot}0_3$
B $^2\Sigma^+$	34107·9		677·6	2·74	1·16
B$'$	(33039·8)				>1·0
A $^2\Sigma^+$	20137·8		420·0	$2{\cdot}20_6$	0·72
X $^2\Pi_{3/2}$	2316·9	2316·9	588·8	2·82	1·00
X $^2\Pi_{1/2}$	0		583·3	2·69	

Notes: 1. Figures in parentheses are of T_0 and $\Delta G_{1/2}$ respectively.
2. The transition B$'$–X is weak, and there are visible only the two 0, 0 sub-bands, which show the correct ground-state multiplet separation.

Table 4. Multiplet Intervals ($X^2\Pi_{3/2} - X^2\Pi_{1/2}$), cm^{-1}

	System	
	A–X	B–X†
$v''=0$	—	8278·8
1	8303·5	8303·3
2	8326·8	8330·0
3	8354·4	8357·5
4	8382·4	—

† from Rochester (1938).

In considering possible electron configurations for the excited states of SiF (Johns and Barrow 1958), it was suggested that state $A^2\Sigma^+$ was

$$\ldots\,(w\pi)^4(x\sigma)(v\pi)^2.$$

However, the present work shows that all four molecules possess similar first excited states, and, in the case of PbF it seems most likely that state A gives Pb($^3P_1$) + F(^2P) on dissociation (Wieland and Newburgh 1952). If this is accepted, considerations of detailed electron correlation (see, for example, Durie and Ramsay 1958) suggest that a more probable configuration is

$$\ldots\,(w\pi)^4(x\sigma)^2(u\sigma),$$

where ($u\sigma$) is antibonding.

Apart from PbF, in which the information about state C is incomplete and conflicting (Wieland and Newburgh 1952), the lowest four states of the four fluorides may be summarized as follows:

	T_e (ev)	ω'/ω''
C(?$^2\Delta$)—$(w\pi)^4(x\sigma)^2(\delta)$	$5{\cdot}18 \pm 0{\cdot}56$	$1{\cdot}03 \pm 0{\cdot}01$
$B^2\Sigma^+$ —$(w\pi)^4(x\sigma)^2(\sigma)$	$4{\cdot}32 \pm 0{\cdot}19$	$1{\cdot}18 \pm 0{\cdot}02$
$A^2\Sigma^+$ —$(w\pi)^4(x\sigma)^2(u\sigma)$	$2{\cdot}69 \pm 0{\cdot}20$	$0{\cdot}73 \pm 0{\cdot}11$
$X^2\Pi_r$ —$(w\pi)^4(x\sigma)^2(v\pi)$	0	1·00

This situation does not hold for some of the other halides of the group, notably for GeCl, GeBr, SnCl, SnBr, where the first excited states are case-*a*, possibly $^2\Delta$, states, correlating most probably with $\mathrm{M}(^1\mathrm{D}) + \mathrm{X}(^2\mathrm{P})$. The configurations may be . . . . . $(w\pi)^4(x\sigma)(v\pi)^2$, $\mathrm{A}(^2\Delta)$.

The hope that Rydberg series might be obvious features of the short-wavelength spectra of these molecules has not been fulfilled. All that can be said at the moment is that the ionization potentials estimated earlier (Johns and Barrow 1958) are likely to be not far wrong, and that the vibration frequencies for the ground states of the ions are probably close to the limiting value, about $1{\cdot}2\omega''$, shown by many of the excited states of the molecules.

One of us (J. W. C. J.) is indebted to the Department of Scientific and Industrial Research for the award of a Studentship.

REFERENCES

ANDREWS, E. B., and BARROW, R. F., 1950, *Proc. Phys. Soc.* A, **63**, 185.
DURIE, R. A., and RAMSAY, D. A., 1958, *Canad. J. Phys.*, **36**, 35.
JENKINS, F. A., and ROCHESTER, G. D., 1937, *Phys. Rev.*, **52**, 1135.
JOHNS, J. W. C., and BARROW, R. F., 1958, *Proc. Phys. Soc.*, **71**, 476.
JOHNS, J. W. C., CHANTRY, G. W., and BARROW, R. F., 1958, *Trans. Faraday Soc.*, **54**, 1589.
MULLIKEN, R. S., and CHRISTY, A., 1931, *Phys. Rev.*, **38**, 87.
ROCHESTER, G. D., 1938, *Proc. Roy. Soc.* A, **167**, 567.
WIELAND, K., and NEWBURGH, R., 1952, *Helv. Phys. Acta*, **25**, 87.
YUASA, T., 1939, *Proc. Phys. Math. Soc., Japan*, **21**, 497.

The Diffusion of Boron in Germanium

By M. D. STURGE†
Mullard Research Laboratories, Salfords, Surrey

MS. received 17th *October* 1958, *in final form* 8th *December* 1958

DUNLAP (1954) found the diffusion coefficient of boron in germanium to be given by

$$D = D_0 \exp(-Q/RT)$$

with $D_0 = 10^9$ cm² sec⁻¹, $Q = 105$ kcal mol⁻¹. These values are quite inconsistent with those for the other group III acceptors; for instance, Dunlap found that for gallium $D_0 = 40$ cm² sec⁻¹, $Q = 70$ kcal mol⁻¹. Dunlap suggested that the difficulty of alloying boron with germanium led to a spuriously low diffusion coefficient at low temperatures. This note describes measurements which suggest that the diffusion coefficient of boron in germanium is close to that of gallium, and less than Dunlap's values by a factor of up to ten.

Boron is deposited on antimony doped germanium (about 1 ohm cm n-type) by heating the germanium in redistilled boron tribromide vapour at 850°c. It is found that boron deposited in this manner will not diffuse into the germanium. To overcome this difficulty a lead pellet is alloyed to the germanium in hydrogen at 850–900°c. The lead dissolves some of the boron as well as the germanium and on cooling a p-type recrystallized region is produced, with an acceptor

---

[†] Now at the Royal Radar Establishment, Malvern, Worcs.

density in the region of 10^{18} cm^{-3}. The lead by itself produces no change in type. The specimen is then heated in helium at the diffusion temperature (less than the alloying temperature) for a few days. The p–n junction, initially coincident with the boundary of the recrystallized region, advances into the germanium at a rate determined by the diffusion coefficient of boron, which is the only acceptor present. After slow cooling the specimen is sectioned and mechanically polished. Etching (in 4 parts of nitric acid, 1 part of hydrofluoric acid, and 2 parts of hydrogen peroxide) shows up the boundary of the recrystallized region as a sharp ridge. Subsequent electroplating with copper or nickel, with the junction biased in reverse, shows the p–n junction as the limit of plating. The thickness of the diffused layer can then be measured under the microscope with an accuracy to ± 2 microns. The identification of the boundaries revealed by these methods has been confirmed by observations on impurities of known diffusion coefficient. The resistivity of the recrystallized region is found by a four-probe measurement, and the carrier density is deduced from the resistivity with the aid of the mobility data of Trumbore and Tartaglia (1958), the effect of the lead impurity on the mobility being neglected.

It is reasonable to assume the initial boron concentration $c(x, 0)$ to be given by the step-function $c = c_1$, $x < 0$, $c = 0$, $x > 0$, where x is the distance from the boundary of the recrystallized region. If we assume the diffusion coefficient of boron to be constant throughout the system, and that diffusion is one-dimensional, the concentration at any subsequent time $c(x, t)$ is the solution of the diffusion equation

$$D\frac{\partial^2 c}{\partial x^2} = \frac{\partial c}{\partial t} \qquad \ldots\ldots (1)$$

subject to the above initial condition, and to the conservation law

$$\int_{-\infty}^{\infty} c(x, t)dx = \int_{-\infty}^{0} c_1 dx.$$

The appropriate solution of (1) is

$$c(x, t) = \tfrac{1}{2}c_1 \operatorname{erfc}\{x/2(Dt)^{1/2}\}.$$

The antimony concentration c_0 is constant, so the p–n junction occurs at $x = x_0$, where

$$c_0 = \tfrac{1}{2}c_1 \operatorname{erfc}\{x_0/2(Dt)^{1/2}\}. \qquad \ldots\ldots (2)$$

In practice $c_1/2c_0$ is a large number, so for a given x_0 and t, D is slowly varying, and an error of a factor of two in $c_1/2c_0$ produces an error in D less than that due to experimental error in x_0. For this reason any difference in D in the recrystallized region is of little importance, and we can also neglect errors due to the identification of the observed p–n junction with the point at which $c = c_0$, and to the rough and ready method of finding c_1.

Diffusion temp. (°c)	$10^{-5}t$ (sec)	$10^{-15}c_0$ (cm^{-3})	$10^{-18}c_1$ (cm^{-3})	10^4x_0 (cm)	$10^{13}D$ (cm^2 sec^{-1})	Dunlap's results Boron	Dunlap's results Gallium
890	4·1	1	1	32	12 ± 2	100	15
846	2·0	2	2	11	3 ± 1	20	5
790	8·4	5	0·2	8	0·9 ± 0·3	2·5	0·9

The experimental results are given in the table, D being calculated from equation (2). For comparison Dunlap's results for boron and for gallium are included.

In this experiment boron diffuses in the presence of lead impurity. There is some evidence (Logan 1956) that the presence of tin in germanium raises the equilibrium concentration of vacancies. We might expect lead to have a similar effect, and therefore to enhance diffusion coefficients of substitutional impurities. However, unless the diffusion coefficient of lead is much greater than that of boron the concentration of lead in most of the diffusion zone will be too small to have an appreciable effect. If it does have an effect, the measured value D will be an upper limit for the diffusion coefficient of boron in pure germanium. A lower limit is presumably provided by the self-diffusion coefficient of germanium, and this differs very little from D (Letaw *et al.* 1956). It appears therefore, that the diffusion constant of boron in germanium differs little from that of the other group III acceptors.

ACKNOWLEDGMENTS

The author's thanks are due to Mr. W. B. Johnson, Mr. E. J. Millett and Mr. J. Dale for helpful discussions, to Mr. J. Dale and Mr. J. Sewell for providing the junctions, and to Mr. F. E. Roberts for help with the resistivity measurements.

REFERENCES

DUNLAP, W. C., 1954, *Phys. Rev.*, **94**, 1531.
LETAW, H., PORTNOY, W. M., and SLIFKIN, L., 1956, *Phys. Rev.*, **102**, 636.
LOGAN, R. A., 1956, *Phys. Rev.*, **101**, 1455.
TRUMBORE, F. A., and TARTAGLIA, A. A., 1958, *J. Appl. Phys.*, **29**, 1511.

LETTERS TO THE EDITOR

Comment on T. B. Grimley's Paper " The Molecular Orbital Theory of the Interaction between an Atom and a Crystal Surface "

With regard to Grimley's (1958) article it appears proper to point to some papers on the quantum mechanical theory of chemisorption, dealing with the same problems and applying the same methods.

The chemisorption of an atom on a one-dimensional chain of atoms of another kind was thoroughly studied by Volkenstein (1947, 1952) and Bontsch-Brujevitsch (1951) who used the LCAO MO method. In order to study the interaction with the surface of a three-dimensional crystal a method analogous to that of Koster and Slater (1954), Baldock (1952) and Lifshic (1947) was used (Koutecký 1956, 1958). The application of Wannier functions makes it possible to formulate the problem very generally so that we can derive general theorems on the localization of electronic states that are being created during the chemisorption. This method of studying chemisorption on the three-dimensional crystals succeeded preparatory studies on chemisorption on two-dimensional crystals (Koutecký 1955, 1957 a, b), which used Dewar's modification of the MO method (Dewar 1949). This modification is very similar to the method applied by Koster and Slater and Baldock. Recently a thorough and systematic investigation was carried out on necessary and sufficient conditions for the existence of localized states in various models of interaction between an atom and crystals of various types (Koutecký and Fingerland). The results agree partly with those of Grimley (1958) and have been discussed in their relation to the localized surface states of Tamm type, by using the paper generalizing the theory of surface states (Koutecký 1957 c), in which the method of Koster, Slater, Baldock and Lifshic was also used.

Institute of Physical Chemistry,
Czechoslovak Academy of Sciences,
Prague.
4th November 1958.

J. Koutecký.

Baldock, G. R., 1952, *Proc. Camb. Phil. Soc.*, **48**, 457.
Bontsch-Brujevitsch, V. L., 1951, *J. Phys. Chem., Moscow*, **25**, 1033.
Dewar, M. J. S., 1949, *Proc. Camb. Phil. Soc.*, **45**, 638.
Grimley, T. B., 1958, *Proc. Phys. Soc.*, **72**, 103.
Koster, G. F., and Slater, J. C., 1954, *Phys. Rev.*, **95**, 1167.
Koutecký, J., 1955, *Doklady Akad. Nauk SSSR*, **101**, 1194.
—— 1956, *Z. Elektrochem.*, **60**, 835.
—— 1957 a, *Coll. Czech. Chem. Comm.*, **22**, 669.
—— 1957 b, *Ibid.*, **22**, 683.
—— 1957 c, *Phys. Rev.*, **108**, 13.
—— 1958, *Trans. Faraday Soc.*, **54**, 1038.
Koutecký, J., and Fingerland, A., *Coll. Czech. Chem. Comm.* (in the press).
Lifshic, J. M., 1947, *J. Exp. Theor. Phys.*, **11**, 1017.
Volkenstein, F. F., 1947, *J. Phys. Chem., Moscow*, **21**, 1317.
—— 1952, *Ibid.*, **26**, 1462.

Probability of Freezing

It has been established experimentally that the chance of water freezing is dependent upon its volume and the duration and depth of supercooling. Bigg (1953 a) has derived useful relationships between these variables and the probability of freezing by applying probability theory to freezing in general. The relationships can be derived in a much more straightforward manner than Bigg used.

The probability of freezing taking place in volume V within the time interval t to $t+dt$ may be written as $Vf(T_s)\,dt$ where $f(T_s)$ is a function of the supercooling T_s. Suppose we have a large number N of identical but isolated drops of volume V, the temperature of any one drop always being the same as that of any other drop. If $P(V,t)$ is the probability of freezing having taken place in volume V during the time interval 0 to t, then

$$P(V,t)=N_t/N$$

where N_t = number of drops frozen at time t. The number frozen during the time interval 0 to $t+dt$ will therefore be

$$N_{t+dt}=N_t+(N-N_t)Vf(T_s)\,dt$$

which, on dividing both sides by N, becomes

$$P(V,t+dt)=P(V,t)+\{1-P(V,t)\}Vf(T_s)\,dt.$$

Now since

$$P(V,t+dt)=P(V,t)+dt\frac{\partial}{\partial t}P(V,t)$$

it follows that

$$\frac{\partial}{\partial t}P(V,t)=\{1-P(V,t)\}Vf(T_s)$$

and

$$\ln\{1-P(V,t)\}=-\int_0^t Vf(T_s)\,dt. \qquad \ldots\ldots(1)$$

If the temperature remains fixed, then

$$\ln\{1-P(V,t)\}=-Vtf(T_s). \qquad \ldots\ldots(2)$$

If cooling takes place at a steady rate c, $c=dT_s/dt$ and

$$\ln\{1-P(V,t)\}=-\int_0^{T_s}\frac{V}{c}f(T_s)\,dT_s. \qquad \ldots\ldots(3)$$

Equations (1), (2) and (3) are equivalent to the results obtained by Bigg.

Equations (2) and (3) have found application in conjunction with experimental results for the freezing of water. They have been used to compute curves of probability of freezing against temperature for a given volume of water and a given cooling rate, and to make an estimate of the number of water drops that will freeze under various conditions in natural clouds (Bigg 1953 b, Carte 1956).

My thanks are due to Dr. A. P. Burger of this Laboratory for his mathematical advice. This letter is published with permission of the South African Council for Scientific and Industrial Research.

National Physical Research Laboratory, A. E. CARTE.
S.A. Council for Scientific and Industrial Research,
Pretoria,
South Africa.

30th October 1958.

BIGG, E. K., 1953 a, *Proc. Phys. Soc.* B, **66**, 688.
—— 1953 b, *Quart. J. R. Met. Soc.*, **79**, 510.
CARTE, A. E., 1956, *Proc. Phys. Soc.* B, **69**,1028.

CORRIGENDUM

The Demagnetizing Energy and Domain Structure of a Uniaxial Single Crystal, by M. Fox and R. S. Tebble (*Proc. Phys. Soc.*, 1958, **72,** 765).

Equation (2) on p. 767 *should read*

$$\mu_{ij}' = \begin{pmatrix} 1+(\mu^*-1)\cos^2\theta & 0 & (\mu^*-1)\sin\theta\cos\theta \\ 0 & \mu^* & 0 \\ (\mu^*-1)\sin\theta\cos\theta & 0 & 1+(\mu^*-1)\sin^2\theta \end{pmatrix}$$

REVIEWS OF BOOKS

Kontinuumstheorie der Versetzungen und Eigenspannungen, by Dr. Ekkehart Kroner. Pp. vii + 179. (Berlin: Springer, 1958.) DM 32.

Imperfections in crystals, particularly dislocations and foreign atoms, provide sources of locked-up internal stresses. Within the realm of linear elasticity, such stresses have the same status, and are handled by the same methods, as those of thermal origin. As was recognized by Duhamel and von Neumann, the main feature of the latter (in simply connected bodies) concerns their failure to satisfy St. Venant's compatibility conditions. Modern work has thrown much further light on the 'incompatibility' tensor, above all its significance in relation to continuous distributions of dislocations. The concept of the latter as the unit source of locked-up stress has proved exceedingly fruitful in various directions, and now dominates current ideas.

A compact account of these matters is provided in the present monograph by Dr. Kroner, a member of the German school at Stuttgart and an important original contributor to the field. The section headings are Continuum Theory of Dislocations (Geometry); Continuum Theory of Dislocations (Statics); Dislocations in Crystals; Non-Riemannian Geometry of Dislocations; Applications; together with a useful introduction, a list of up-to-date references, and an index. The text does not, for the most part, make easy reading, and is severely mathematical, but will prove an indispensable instrument for those seriously interested in the subject. M. A. JASWON.

Les Semiconducteurs, by P. Aigrain and F. Englert. Pp. x + 203. (Paris: Dunod, 1958.) 980 *fr.*

This modest volume is an advanced text on semiconductor physics and a fascinating, profound, and sometimes controversial analysis of the structure of semiconductor theory. It is written in an extremely condensed but lucid manner with many original ideas and insights in the connection between different aspects of semiconductor physics.

The book should be available wherever semiconductor theory is studied, but it is too concise to be taken as an introduction; it makes considerable demands on the reader. Beginners may also feel irritated by the absence of references, the lack of index, the considerable number of misprints and, in some instances, a poor correlation between text and diagrams.

W. EHRENBERG.

Progress in Semiconductors, Vol. 3, edited by A. F. Gibson, P. Aigrain and R. E. Burgess. Pp. vii + 210. (London: Heywood, 1958.) 55*s*.

This volume contains the following reviews: The Magnetoresistivity of Germanium and Silicon by M. Glicksman; The Chemical Purification of Germanium and Silicon by J. M. Wilson; Electronic Conductivity of Silver Halide Crystals by J. W. Mitchell; Silicon Junction Diodes by D. E. Mason and D. F. Taylor; Lifetime of Excess Carriers in Semiconductors by A. Many and R. Bray; Scattering and Drift Mobility of Carriers in Germanium by M. S. Sodha; Electronic Processes in Cadmium Sulphide by J. Lambe and C. C. Klick.

None of the subjects reviewed is of very recent origin, or has seen spectacular developments during the last few years, so that the authors lack any clear guidance about what they should assume the reader to know; but all contain references up to 1957.

The articles are of very different merit, the best ones being notable achievements, the less fortunate ones appear more difficult to digest than a collection of relevant abstracts. All the articles will be of value to workers with particular interest in the fields covered. W. EHRENBERG.

Physikalische Abhandlungen und Vorträge, Vols. I–III, by Max Planck. Pp. xv + 776, xi + 716, xii + 426. (Braunschweig: Vieweg, 1958.) DM 150.

The three volumes of the discussions and lectures of Professor Max Planck are published appropriately during the year of the celebration of the centenary of his birth by the Union of German Physical Societies and by the Max Planck Society for the Promotion of Science. In the foreword to these volumes Max von Laue explains how they came into being with the intention that they should be a memorial to his memory. " For the memory of a scholar is faithfully preserved by making it easy for future generations to read in the original text what he has written rather than by statue or bust ". With few exceptions, where the shape of the original was too far from that of the present publication, this design has been carried out.

The individual original papers are arranged in chronological order in volumes I and II. The first is dated 1879, when Planck was twenty-one years old, and the volume presents a remarkable sequence of original thought and work on the fundamental principles of thermodynamics. There are papers on other topics such as an early one on the theory of liquid rays, but these seem like intrusions into the main theme and the author appears to slip back quickly to his chief motif.

In this series Planck is seen clarifying for himself and for the world of science some of the obscurities of thermodynamics and at the same time adding to the knowledge of it by means of fundamental papers and the solution of special problems. About half-way through this volume a paper appears on electric oscillations excited by resonance and damped by radiation, followed by five papers on irreversible processes of radiation. The investigations described in them were begun with the intention of obtaining a closer examination of the processes of emission and absorption of heat rays and the resulting state of temperature equilibrium, from the point of view of the electromagnetic theory. There follows a paper on Maxwell's theory of electricity and then another on irreversible processes of radiation. The reader feels that in these papers Planck is coming close to his great discovery and this is indeed the case. He does in fact obtain Wien's law of radiation in the course of the work. But the great result appears almost casually in a short paper read on October 19th 1900 entitled ' On an Improvement of Wien's spectral Equation '. Kurlbaum had, on the same occasion, reported the experimental results obtained by himself and Rubens in the region of long waves and had shown the breakdown of Wien's law in this region. Planck rose to explain how his electromagnetic theory of radiation stood with respect to the experimental facts. By a partly empirical process, which appeared to him to be a natural modification of a result he had previously obtained, he was able to derive a formula containing two constants and to show that it agreed with experiment. Shortly afterwards a work appears in which he establishes the law of radiation, not by means of the laws of electromagnetic radiation or thermodynamics, but on the basis of a quite new elementary process. Here his formula appears in its well-known orm containing the constants $\boldsymbol{k}$ and $\boldsymbol{h}$.

Volume II reveals Planck's interest in many other subjects than thermodynamics and contains his contributions to them. It contains, for example, papers on the theory of Kaufmann's measurements of the deviation of β-rays, on the theory of relativity and on general dynamics. But the main theme is still thermodynamics and the theory of radiation, with increasing emphasis on the quantum theory and applications of it until in the latter half this is the chief subject of the various contributions. This volume is of interest from a historical point of view. It covers the period 1902–1941, during the early part of which the quantum theory was almost struggling to keep its head above water. It is a period of adverse criticism, of attempts at alternative explanations and of Planck's firm conviction, in spite of opposition, of the inadequacy of the classical theory.

Towards the end of this period there appears a notable paper on Henri Poincaré and the quantum theory from which much can be learned both of Poincaré and Planck. In spite of his revolutionary discovery Planck always hoped to find some unifying principle valid throughout the physical world or, at least, to live to see it discovered. For this reason he welcomed Schrödinger's form of the quantum theory and his last papers showed his interest in it. The volume ends with three works entitled ' An Attempt at a Synthesis between Wave Mechanics and Corpuscular Mechanics ' the last appearing in 1941 when Planck was eighty-three years old. It brings to an end the rich yield of an incomparable Master.

Volume III is divided into three parts. The first is devoted to articles and lectures of an original character such as ' unity in the physical World-picture ', ' New Paths of Physical Knowledge ' and Planck's Nobel lecture on the origin and development of the quantum theory. These are all of interest on account of their subject matter and of their revelation of Planck's scientific and philosophical insight and points of view. The second part is devoted to orations made on various occasions and ends with Planck's scientific autobiography. It contains tributes to Heinrich Hertz, Paul Drude, Hendrick Antoon Lorentz and to Arnold Sommerfeld. There are also tributes to Max von Laue, who has done so much to bring these volumes into being, on the occasions of the celebration of his sixtieth and seventieth birthdays and for whom Planck expresses his warm regard. The appreciations of the personal qualities of these great physicists and of the scope and value of the work done by them are of great interest. The final pages are devoted to speeches and reminiscences on the occasion of Planck's eightieth birthday celebration, to the funeral oration and to some personal recollections of him. H. T. FLINT.

Atomic Physics and Human Knowledge, by Niels Bohr. Pp. viii + 101. (New York: John Wiley; London: Chapman and Hall, 1958.) $ 3.95.

The philosophical attitude of the great majority of physicists is mainly due to Niels Bohr. His doctrine has spread through personal contact. A young theoretical physicist who did not spend some time at Copenhagen was not considered properly trained. But we of the older generation who are of about the same age as Bohr and in responsible positions could not learn his ideas at the source and were dependent on his publications, apart from occasional discussions at scientific conferences. But Bohr's papers are not numerous and are scattered over different periodicals and congress reports which are not easily accessible.

Therefore this collection is a most welcome gift. It contains seven articles, mostly addresses delivered at various congresses. For the physicist they centre around the article " Discussions with Einstein on Epistemological Problems in Atomic Physics ", reprinted from the book *Albert Einstein, Philosopher—Scientist* (The Library of Living Philosophers, vol. 7, 1949, p. 199). It is a remarkable document, a model of the way dissentions between scientists should be argued out. And it is a most complete and satisfactory account of Bohr's principle of complementarity in physics.

All the other articles go far beyond the restricted domain of physics. Most of them begin with a condensed account of the story how the physicists were confronted with a new stituation which compelled them to reconsider the logical principles applied in describing their activities and their results. But then Bohr compares the ideas thus developed with those used in other branches of human knowledge and shows that everywhere apparent contradictions can be avoided by using the concept of complementarity. The first two addresses delivered in the years 1932 and 1937 deal with the problems of life, and the same theme is taken up in the last article of 1949. The third article is of particular interest; there different branches of human culture and civilization are considered from the standpoint of complementarity. The fifth and the sixth articles endeavour to show how the epistemological lesson learned from atomic theory has influenced our thinking in general and helped in establishing a unity of human knowledge.

It is unavoidable that in such a book overlapping takes place. But as each article regards the problems from another angle these repetitions are not at all tedious.

At present the doctrine of the Copenhagen school is again under attack, mainly from Marxistic philosophers. Therefore the new access to Bohr's authentic presentations of his philosophy is most welcome though it may be doubted whether his careful and cautious analysis will have any effect on those who are accustomed to the blunt weapons of dialectical materialism. All those who approach the problem unbiased, with open mind, will consider Bohr's book as a precious gift. M. BORN.

G. I. Taylor's Scientific Papers, Vol. 1, edited by G. K. Batchelor. Pp. x + 593. (Cambridge: University Press, 1958.) 75*s*.

The editor Dr. Batchelor and the Cambridge University Press are to be congratulated along with their backers the Ministry of Supply (through the Aeronautical Research Council) and the Master and Fellows of Trinity College, Cambridge, in making available the collected works to date of Sir Geoffrey Taylor.

In the past few years the number of collections of scientific papers which have been published has become almost vanishingly small, perhaps largely due to the increasing availability of the original papers. However, with a writer as exceptional as Sir Geoffrey Taylor, whose works cover such a large field that even the best informed of his colleagues may not be aware of them all, the need remains. With the knowledge that there are three more volumes to follow devoted to the mechanics of fluids one cannot fail to comment on the contrast Sir Geoffrey provides to the ever-increasing tendency to specialization in research. When, as here, the contributions are so basic to their subjects and so far-reaching they stamp him as unique as he has, fortunately, long been recognized to be.

The volume under review, volume 1, is concerned with the mechanics of solids and it is almost impossible in the space of a short review to give anything like a summary of the contents. There are forty-one papers reproduced ranging from contributions to classical dynamics and classical elasticity through plasticity to faults and dislocations. It is really an intresting commentary on the volume as a whole that the contribution to classical dynamics " a relation between Bertrand's and Kelvin's theorems on impulses " should have been made years after the subject was thought to have become a closed book.

Interest in the volume will probably centre around the work on dislocations and plasticity where the contributions he has made are of fundamental importance. As long ago as 1934 he was blazing the trail for present-day thought; indeed some of his work at that time might almost have been written yesterday.

Dr. Batchelor notes that the present volumes have been prepared with as little change as possible of the original forms of the papers; printing errors and small mathematical slips have been rectified without comment but any substantial change in the text as originally published has been disclosed in a footnote. All the figures have been redrawn in a uniform style and the whole presentation and format is most attractive.

In short your reviewer cannot give too great a welcome to the appearance of this volume which will quite certainly provide the stimulus for much thought and research.

L. HOWARTH.

Sound Pulses, by F. G. Friedlander. Pp. xi + 202. (Cambridge: University Press, 1958.) 40*s*.

A sound pulse is a small aperiodic disturbance with a clearly defined front, and under certain assumptions its propagation in a fluid is described by the scalar wave equation. Dr. Friedlander demonstrates that such a phenomenon (which has analogues in optics and electromagnetic wave theory) is readily discussed in terms of the theory of linear partial differential equations of hyperbolic type: the properties of pulse fronts as wave fronts in the sense of geometrical optics are established by considering them as hypersurfaces in space–time which are characteristics of the wave equation. The first three chapters of his book are devoted to a detailed exposition of this approach, and the remainder concern its application to topics in reflection and diffraction. Some hitherto unpublished material is presented and there is an extensive up-to-date bibliography.

The book will interest workers already established in the field, for it makes available in a single short volume a unified treatment of the subject using a variety of mathematical techniques. In particular it provides an introduction to the theory of distributions and its application to Green's functions. For these same reasons, a good graduate student of applied mathematics would profit by working through the book, and noting the contents of Dr. Friedlander's mathematical arsenal.

This valuable addition to the Cambridge Monographs is marred by a multitude of printing errors. The corrections to some are obvious, but others will require the reader's close attention and are liable to undermine his confidence in subsequent pieces of difficult reasoning. Further, although the author of such a volume has to compress his arguments, a reader's time is valuable, and wherever it can be saved by an extra phrase this should be supplied. These shortcomings combine in the proof concerning the propagation of diffracted fronts in shadow (pp. 28, 29), where the reading would also be improved by a clearer figure and the introduction of a separate vector symbol for the general point in shadow. D. W. MARTIN.

Handbuch der Physik, Vol. VI, *Elasticity and Plasticity*, edited by S. FLÜGGE. Pp. vii + 642. (Berlin: Springer, 1958.) DM 116.

This volume of the *Handbuch der Physik* has six articles, all in English, dealing with elasticity, plasticity, photoelasticity, rheology, fracture and fatigue. The first article, entitled The Classical Theory of Elasticity, is by I. N. Sneddon and D. S. Berry, and the classical theory for infinitesimal strains is here, as in Green and Zerna's book, derived from the general treatment for large deformations. Problems of flexure and torsion and two-dimensional and three-dimensional elastic problems are then discussed. This article concludes with short sections on dynamical problems and on thermoelasticity. The second article, by H. T. Jessop, is on photoelasticity. After short summaries of the theories of classical elasticity and crystal optics, an account is given of the well-established methods of two-dimensional photoelastic stress analysis and of the more recent ' frozen stress ' and other three-dimensional techniques. Some practical applications and a very brief review of photoplasticity and dynamic photoelasticity conclude this article.

The third article, entitled The Mathematical Theories of the Inelastic Continuum, by A. M. Freudenthal and Hilda Geiringer, is by far the longest in this volume. The first half of this article considers continuum mechanics of viscoelastic, plastic and viscoplastic materials, whilst the second half is concerned with the behaviour of ideally plastic solids and treats both the general theory and specific boundary value problems in this field.

Rheology, by M. Reiner, is the fourth article and a number of aspects of this somewhat controversial subject are here discussed. This article includes descriptions of different types of ideal rheological solids, second-order phenomena and methods of measurement.

The last two articles, Fracture, by G. R. Irwin, and Fatigue, by A. M. Freudenthal, are both quite short. They are largely concerned with recent advances in particular aspects of these two rather wide subjects.

The volume contains subject indexes in English and German and is very well produced. The articles, all by well-known authorities, are excellent within their scope and extremely welcome as short monographs within their respective fields. The usefulness of the whole volume as a unit in an *Encyclopaedia of Physics* is less certain. There is considerable overlap between articles, whilst many aspects of the subjects are dealt with very briefly or not at all. Some of the gaps will perhaps be filled by articles in later volumes. H. KOLSKY.

The Calculation of Atomic Structures, by D. R. HARTREE. Pp. xiv + 182. (New York: Wiley; London: Chapman and Hall, 1957.) 40*s*.

While this review was being written the sad news of the death of Professor Hartree reached the reviewer. It was but a small consolation to consider how fortunate we are that Professor Hartree was persuaded to write this book. Almost everyone who has computed a self-consistent field has had to draw on Hartree's personal experience, either through correspondence or personal contact. His neat, handwritten letters, full of practical details of the method and of unpublished data, helped many through their calculations. Much of this information, fortunately, has been preserved in Hartree's book, which fulfils extremely well its purpose to provide both a compilation of calculating techniques and a source of practical advice on how best to carry out the computation of atomic structures by the self-consistent field method.

The book starts from the very beginning, though, of course, some familiarity with elementary results of quantum mechanics is assumed. Thus, the first chapter reviews central-field wave functions and chapter 2 contains an elementary and very clear account of the variation principle. The real subject of the book is first tackled in chapter 3, where both Slater's method for complex atoms and the Hartree–Fock equations are discussed. This is followed in chapter 4 by a survey of the numerical procedures necessary for the computation of atomic structures, such as the solution of second-order differential equations.

Chapter 5 will probably be essential reference for every future computer of atomic fields. It shows in detail how to apply the numerical procedures of chapter 4 to the solution of an atomic problem. Many examples are included and it provides a thorough background for all phases of the work required in the numerical solution of the radial wave equation.

In the five remaining chapters incomplete groups, interpolation procedures, energy relations, relativistic equations and further approximations are treated. The chapter on interpolation procedures should be particularly noted. It provides a badly needed review of the methods of obtaining starting approximations for the atomic wave functions. Also, both here and in an appendix many important numerical results are listed, some for the first time.

In considering the book as a whole it is worth reminding ourselves that it is essentially a monograph. It is therefore not unexpected that some subjects that one would have liked to have seen discussed more fully are only briefly considered. Self-consistent field equations are nowadays much used in molecular problems and a more comprehensive treatment than the one provided here would have been useful. On the numerical side, the days of computation of atomic fields on desk calculators are surely numbered, and an account is needed of methods of computation suitable for electronic computers. As it is, however, the book will continue to be an essential reference for a long time.

S. L. ALTMANN.

Progress in Elementary Particles and Cosmic Ray Physics, edited by J. G. WILSON and S. A. WOUTHUYSEN. Pp. xii + 470. (Amsterdam : North Holland Publishing Company, 1958.) 45 guilders.

Progress in Elementary Particles and Cosmic Ray Physics is the fourth volume in a series which originally carried the title " Progress in Cosmic Ray Physics ". The latest volume contains five articles of varying length, all written by authors with international reputations in their respective fields of study.

The first article (66 pages) by B. D'Espagnat and J. Prentki is a theoretical discussion of the strong interactions of the strange particles, the hyperons and the K-meson. The treatment will be of considerable value to theoretical physicists interested in high-energy phenomena, but will not be of great value to the young experimentalist seeking some insight into the theoretical problems posed by the discovery of the strange particles. The second article is a very short review of the properties and production of strange particles by W. D. Walker. This subject has grown tremendously during the last three years and only a somewhat superficial review can be given in the space of 30 pages. Walker's article is, however, very clearly and concisely written and provides a useful introduction to the experimental material available up to the early months of 1957. Very little space is devoted to some of the more subtle aspects of the subject ; for example, the short-lived and long-lived neutral K-decays are dealt with in a brief paragraph of half a page.

The third article is concerned with the interaction of μ-mesons with matter. G. N. Fowler and A. W. Wolfendale have written a long chapter (90 pages) which is a very excellent and authoritative review of the subject. Classical electromagnetic interactions, the scattering of μ-mesons by nuclei, non-classical electromagnetic interactions and the universal Fermi interaction are all dealt with in detail. The writers show very clearly the importance of high energy μ-meson interactions, particularly for investigations on the validity of electromagnetic theory at extremely high energies.

The fourth and fifth articles concern the origin and nature of the cosmic radiation itself. S. F. Singer has written an excellent review (130 pages) of the properties of the primary cosmic radiation and its time variations. Although the writer is not an expert in the field he found parts of the article to be of great interest. The last chapter is a review (60 pages) of theories of the origin of cosmic radiation by V. L. Ginzburg. This article discusses data on the primary cosmic radiation near the earth, the distribution of cosmic radiation in the galaxy, the motion of cosmic ray particles in interstellar space, and finally possible sources of cosmic radiation.

All the articles in the present volume, with the possible exception of the second, are written for the information of the expert or would-be expert in the particular field. A considerable previous knowledge of the subject is necessary in order to understand these review articles. Thus they are not likely to be of value to the scientist who wishes to widen his general knowledge. It has now become clear that the fields covered in the book are very diverse. In fact high-energy physics, both experimental and theoretical work, is largely divorced from almost all of the cosmic ray problems discussed by Singer and Ginzburg. The number of physicists seriously interested in both fields is probably dwindling rapidly. After reading the book the writer feels, therefore, that the decision the editors have reached to combine review articles on these two fields into one annual volume was unwise. If it is worthwile doing at all then the reviews should be written for the non-expert in order to give them a wide appeal among the large number of nuclear physicists and the much smaller number of cosmic ray physicists. If the present level of writing is to be maintained, then it would surely be wise to publish separate bi-annual volumes on ultra-high-energy nuclear physics and cosmic radiation. C. C. BUTLER.

A Dictionary of Named Effects and Laws in Chemistry, Physics, and Mathematics, by D. W. G. BALLENTYNE and L. E. Q. WALKER. Pp. v + 206. (London : Chapman and Hall, 1958.) 30*s*.

Admirable in intention, and amateurish in execution, this dictionary fails to meet a very real need. The effects bearing personal names, for example in photography, are such common currency with those to whom they *are* common currency, that their lack of meaning to workers in a neighbouring field can easily be overlooked. The same applies to mathematical functions and chemical tests or reactions. But ' amateurish ', as regards lexicography, is the only word for a work which mentions Stefan's Law under Boltzmann, but not directly. Omissions from a dictionary are less serious than errors : there are far too many of these—Debye and Sherrer method, Gneisen constant (with Gruneisen constant as well), Larmour's Formula, Misterlich Law of Isomorphism, Van Kleck Paramagnetism, are examples. Meanings, as well as names, are also untrustworthy, above all in a disgraceful Appendix of Units (eighteen entries) including : " Oersted—The oersted is the unit of magnetic reluctance (resistance) . . . ", and " Weber—A name formerly given to the Coulomb "—with no alternative in either case. Subtleties of definition are for the most part completely missed.

The book appears to be stronger on chemistry and mathematics than on physics. Some of the entries are admirable. Libraries may be advised to acquire the work but to paste a large warning label on it : " Useful, but not to be trusted ". It is sad that this poor carrying out of a good intention may hinder it from being done better. F. C. FRANK.

The Measurement of Colour, by W. D. WRIGHT. Pp. ix + 263. (London : Hilger, 1958.) 52*s*.

During recent years there has been a considerable increase of interest in the subject of colour measurement, and consequently the second edition of this book has appeared at a most appropriate time. It has been largely re-written, and provides a clear, concise, and up-to-date account of many aspects of the subject. The first four chapters are devoted to visible radiation, the eye, the theory of colour-measurement systems, and the international (C.I.E.) system now in use ; other chapters deal with colorimetric instruments, colour atlases, three-colour reproduction systems, and a large array of practical applications.

The book is written in Professor Wright's usual clear and straightforward style, and contains excellent summaries of work done in many fields, especially that of colour vision ; a large number of recent references are given. Although the physiological and psychological aspects of colour problems are treated with due regard, the reader is never allowed to overlook the fundamental physics. The chapters are set out in the most logical order, but some colorimetrists might feel that this is not necessarily the best order ; however it is undoubtedly the best order for a reader who is unfamiliar with the subject. In some chapters, particularly the one on instruments, the subject matter has very wisely been limited in order to give a proper treatment of the essentials of the subject. In short, this book is excellent, and is to be thoroughly recommended.

A. W. S. TARRANT.

Electric Conduction in Semiconductors and Metals, by W. EHRENBERG. Pp. x + 389. 1st Edn. (Oxford : Clarendon Press, 1958.) 63*s*.

Ten years ago it could be said that the broad features of many semiconductors were qualitatively understood in terms of the energy band theory of solids. Great advances have been made in the meantime and we now have a quantitative understanding of the high-mobility semiconductors which surpasses that of any other class of systems studied in solid state physics. One attractive example may be quoted to illustrate this; Kohn's theory of optical absorption by electrons bound to impurity atoms in Ge and Si, using as the only parameters the bulk dielectric constant and the effective mass values derived from cyclotron resonance experiments, is in beautiful and striking agreement with the absorption spectra observed by Burstein, Fan and others. Other examples might be quoted; all would illustrate the exactness and unity of the description which the one-electron theory provides of diverse semiconductor properties, optical, electrical and magnetic. The field is still expanding rapidly and provides stimulus and excitement for both experimenters and theoreticians—separately and in close collaboration. This means that we look eagerly at new books on semiconductors, but also that we judge them by high standards.

Dr. Ehrenberg has chosen to review principally the *electrical* properties of semiconductors. The initial chapters carefully set out the basic one-electron theory; that is to say, the quantum mechanics of electrons moving in periodic lattices and the employment of the Boltzmann transport equation to calculate their statistical behaviour as observed when we measure conductivities, Hall constants, etc. This part includes also a discussion of lattice vibrations and the deduction of the times of relaxation of electron distributions as brought about through electron–lattice interactions. Later chapters then show how the observed properties of semiconductors are interpreted by the theory. It is pleasant to find here discussions not only of the elemental and the intermetallic semiconductors, but also of ionic compounds and of the fascinating transition metal oxides. The final three chapters deal with the important subject of contacts between semiconductors and metals and junctions between n-type and p-type semiconductors. No detailed application of the theory developed in this book is made to metals.

The author's discussion of the topics he has selected is full and he has carefully written into his text much detail that will be of value to experienced workers in the field. In the opinion of the reviewer, however, the book is not a book for beginners. They may be confused by the detail and, by the restriction of the principal subject to electrical properties, they will probably miss that feeling of excitement which the present theory of semiconductors should rightly generate. In this connection it is not unjust to draw attention to the existence of a number of misleading statements; " the rigorous proof of Bloch's theorem is extremely difficult ", is one such. The Hamiltonian operator for an electron in a crystal lattice and the translational symmetry operators of the lattice commute among themselves; it is not particularly difficult to derive Bloch wave functions as the simultaneous eigenfunctions of all these operators. And it is important for the understanding of the theory to see this close connection between Bloch wave functions and translational symmetry. The significance of Brillouin zones, for example, is difficult to grasp otherwise. To say that the proof of Bloch's theorem is extremely difficult frightens the reader into thinking he will not understand what it is about, for how can he if he is not given the opportunity to see it proved ?

In summary the book may well be useful to experienced semiconductor physicists, but is not recommended for beginners. To the reviewer it does not succeed in portraying the elegance and attractiveness of the subject of semiconductors. A. B. LIDIARD.

Three Dimensional Dynamics—a Vectorial Treatment, by C. E. EASTHOPE. Pp. viii + 277. (London : Butterworths Scientific Publications, 1958.) 42*s*.

It might be expected that there would already be a wealth of suitable students' textbooks on Three Dimensional Dynamics—a subject in which no great development can have occurred since the publication of Routh's famous treatise on *Rigid Body Dynamics* nearly 100 years ago. However, as all who have taught the subject know, this is far from the case. There are many admirable treatises on various aspects of mechanics. However, there has been a real lack of a reasonably short but at the same time systematic and comprehensive book which, starting from fundamental principles, will conduct the student safely to the level at which he can handle the problems of rolling bodies or of gyrostatics so familiar to examination candidates since Routh's day. Dr. Easthope's is certainly such a book and can be warmly recommended to those students of mathematics and physics whose curriculum is still framed to demand the full rigour of vectorial mechanics without an immediate easy escape to Lagrange's equations.

The subject matter covered within the book coincides with what is more or less conventionally agreed to be the reasonable limit of dynamics in an Honours curriculum. After introductory chapters on vector algebra and on the motion of a particle, the kinematics of a rigid body in three dimensions and the theory of rotating reference frames are developed. The general equations of motion of a system of particles are then derived and their application to a rigid body is illustrated by several examples. The use of Euler's equations is developed, and a chapter is devoted to gyrostats and precessional motion. The treatment is clear and simple throughout. The only criticism I might mention is the possibly excessively mathematical character of the book. There is very little in the way of practical illustration which is, I believe, a pity, for the student deserves some proof that the dynamics he is made to learn is not only an excellent form of mental exercise but also a practical and important subject. J. C. G.

BOOK NOTICES

Fundamentals of Gas Dynamics, edited by H. W. EMMONS. High Speed Aerodynamics and Jet Propulsion, Vol. III. Pp. xiii + 749. (London: Oxford University Press, 1958.) £7.

Dynamical Analogies, 2nd Edn, by H. F. OLSON. Pp. xi + 278. (Princeton, New Jersey, Toronto, New York, London: Van Nostrand, 1958.) 51*s*.

Handbook of Automation, Computation and Control, Vol. 1, edited by E. M. GRABBE, S. RAMO and D. E. WOOLRIDGE. (New York: John Wiley; London: Chapman and Hall, 1958.) 136*s*.

The Universe, A Scientific American Book. Pp. xxxii + 142. (London: George Bell, 1958.) 13*s*. 6*d*.

Microwave Propagation in Snowy Districts, edited by Y. ASAMI. Pp. viii + 198. (Sapporo, Japan: Research Institute of Applied Electricity, Hokkaido University, 1958.)

Abhandlungen aus dem Fritz-Haber-Institut der Max-Planck-Gesellschaft in Berlin-Dahlem, Band XXXIV, 1957. Pp. vi + 614. (Berlin-Dahlem, 1958.)

Science Students' Guide to the German Language, by A. F. CUNNINGHAM. Pp. xiv + 186. (London: Oxford University Press, 1958.) 12*s*. 6*d*.

The Rheology of Elastomers, edited by P. MASON and N. WOOKEY. Pp. viii + 202. (London: Pergamon Press, 1958.) 50*s*.

The Theory of Dielectrics, by H. FRÖHLICH. 2nd Edn. Monographs on the Physics and Chemistry of Materials. Pp. vii + 192. (Oxford: Clarendon Press, 1958.) 30*s*.

Royal Society Mathematical Tables: 4, Tables of Partitions, by HANSRAJ GUPTA, C. E. GWYTHER and J. C. P. MILLER. Pp. xxxix + 132. (London: Cambridge University Press, 1958.) 63*s*.

Tables of Natural Logarithms for Arguments between Five and Ten to Sixteen Decimal Places, U.S. Department of Commerce, National Bureau of Standards. Pp. xii + 506. (Washington: U.S. Government Printing Office, 1958.) $4.00.

Energy Loss and Range of Electrons and Positrons, by A. T. NELMS. Suppt. to NBS Circular 577. Pp. 31. (Washington: U.S. Government Office, 1958.) 30 cents.

Tables of Transport Integrals $J_n(x) \equiv \int_0^x \frac{e^z z^n \, dz}{(e^z - 1)^2}$, by W. M. ROGERS and R. L. POWELL. NBS Circular 595. Pp. 46. (Washington: U.S. Government Office, 1958.) 40 cents.

The Physics of Metals and Metallography, Vol. 4, No. 1. Pp. 159. (London, New York, Paris, Los Angeles: Pergamon Press, 1957.) £10 10*s*. per annum (2 volumes).

Conference on Extremely High Temperatures, Boston, Mass., 18–19 *March*, 1958, edited by H. FISCHER and L. C. MANSUR. Pp. xi + 258. (New York: John Wiley; London: Chapman and Hall, 1958.) 78*s*.

PARIS: PUBLICATIONS SCIENTIFIQUES ET TECHNIQUES DU MINISTÈRE DE L'AIR:

Cinétique du développement d'un gros cristal dans la méthode de l'allongement critique, par H. LATIÈRE. Pp. xx + 118. No. 342, 1958. 1950 *fr*.

Sur quelques nouvelles généralisations de la théorie des nombres complexes et leurs applications, par D. RIABOUCHINSKY. Pp. xxiv + 166. No. 343, 1958. 2750 *fr*.

Contribution à l'analyse de la turbulence associée à des vitesses moyennes, par A. CRAYA. Pp. xx + 111. No. 345, 1958. 1480 *fr*.

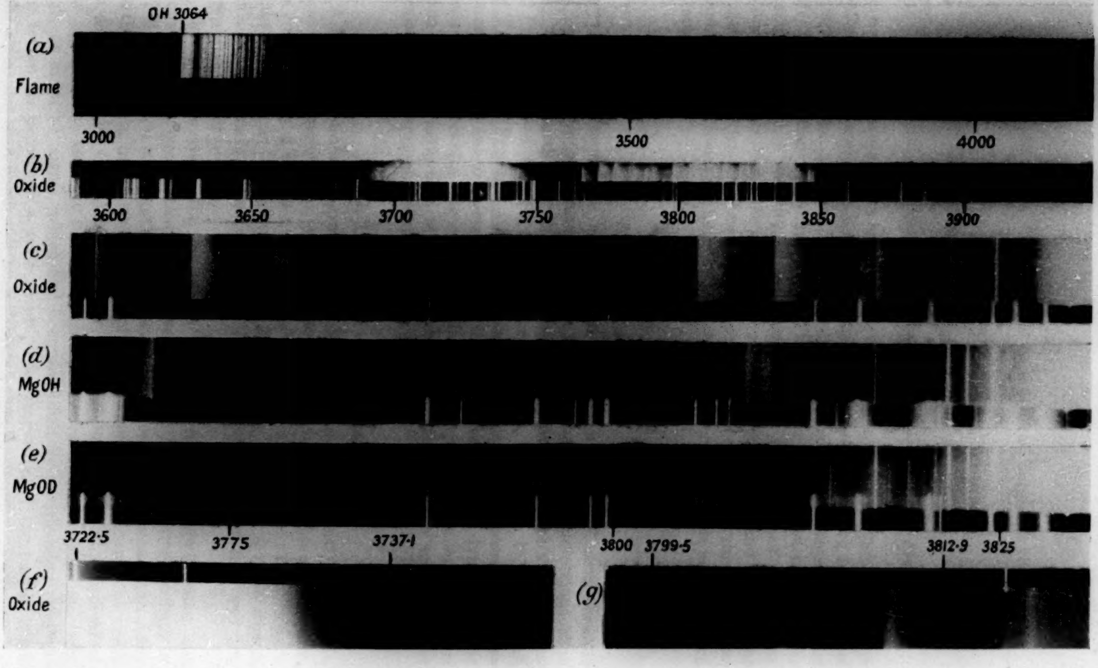

(*a*) Oxy-hydrogen flame containing magnesium chloride. Medium quartz spectrograph. (*b*) and (*c*) Mg arc in O_2. 1st order, 21 ft grating. (*d*) Mg arc in H_2O vapour. 1st order, 21 ft grating. (*e*) Mg arc in D_2O vapour. 1st order, 21 ft grating. (*f*) and (*g*) Mg arc in O_2. 2nd order, 21 ft grating.

Iron arc comparison spectra are shown below the main spectra in (*a*), (*b*), (*c*), (*d*) and (*e*), and above in (*f*) and (*g*).

Ultrasonic Wave Propagation in a Nickel Single Crystal

By J. de KLERK†
Imperial College of Science and Technology, London

MS. received 2nd October 1957, *in revised form 4th September* 1958

Abstract. The propagation of ultrasonic energy in a nickel single crystal by an improved pulse technique has been employed to investigate the behaviour of the dynamic elastic constants of, and the energy losses in the specimen, with and without an applied magnetic field. The dynamic elastic constants behave according to Zener's theory of anelasticity in the test range of frequencies. Values of the relaxation time for internal atomic rearrangement and ratios of the relaxation strengths for shear and compressional waves are evaluated for the sample. Energy losses are substantially reduced when the sample is magnetized to saturation.

§ 1. Introduction

The pulse technique employed in the present series of measurements permitted more accurate velocity and attenuation determinations than those obtained from techniques employed by previous workers (Firestone and Frederick 1946, Huntington 1947, Lazarus 1949, McSkimin 1950, Roderick and Truell 1952, Bradfield 1952) in this field. The resultant increased accuracy of measurements led to a detailed study of the behaviour of the dynamic elastic constants of a nickel single crystal at ultrasonic frequencies, as well as to the effects of a magnetic field upon the dynamic elastic constants and upon the attenuation of ultrasonic energy in the crystal.

§ 2. Experimental Equipment

A block functional diagram of the electronic equipment used is shown in figure 1. The synchronizer, which initiated and synchronized all timing circuits, was controlled by a 1 Mc/s quartz crystal oscillator. Phantastron circuits were employed to select every sixth and 1200th pulse from the 1 Mc/s quartz oscillator, and these pulses were used in the electronic delay unit and the transmitter trigger unit.

The electronic delay unit, by means of time-variable electronic gates, was able to select any one of the first 65 pulses from the 1 Mc/s quartz oscillator in a 1200 μsec interval to trigger the oscilloscope time base. By means of this delay unit the start of the time base could be delayed in 1 μsec steps, accuracy of which was determined by the quartz oscillator, in order to examine each individual echo and hence to measure the time interval between echoes. Each echo was displayed as an r.f. signal, which had been amplified by a wide-band receiver. This technique permitted a more accurate determination of the leading edge of the echo that than obtainable with detected signals.

---

† Now at Brown University, Providence, Rhode Island, U.S.A.

The Miller time base generator provided extremely linear sweep voltages to the dual beam cathode-ray tube display unit. One trace of the cathode-ray tube displayed the r.f. echo signals while the second trace which was displayed above and below the first trace provided 1 μsec time calibration signals. Photographic records were made of the cathode-ray tube display which, when projected on to a screen, permitted time measurement correct to ± 5 millimicroseconds.

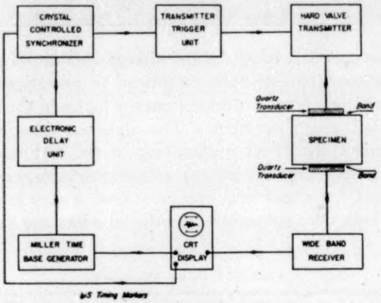

Figure 1. Block functional diagram of electronic circuit.

Every 1200th pulse from the 1 Mc/s quartz oscillator was used to trigger both the electronic delay unit and the transmitter trigger unit. This latter unit provided large amplitude negative going signals which were used to trigger the hard valve transmitter. By this technique it was possible to produce an r.f. pulse in which the first half-cycle rose to full amplitude thus permitting accurate determinations of the start of the transmitter pulse and the succeeding echoes.

§ 3. Results of Measurements

3.1. *Velocity*

The velocities of propagation of compressional and shear ultrasonic waves in a nickel single crystal were measured in the [001] and [111] directions in the frequency range 2 to 15 Mc/s. Similar measurements were made with the nickel single crystal magnetically saturated in the hard, medium and easy directions of magnetization. These measurements show the velocities to be frequency dependent due to the ΔM effect discussed by Nowick (1953). In the demagnetized state the velocities increase with increasing frequency and tend to maximum values determined by the unrelaxed values of the appropriate dynamic moduli. In the magnetically saturated state the velocities show a slight decrease with increasing frequency and tend to minimum values determined by the unrelaxed values of their appropriate dynamic moduli. With each type of wave the velocity showed an increase for the magnetically saturated state over the demagnetized state. The largest increase in velocity of approximately 4% was obtained for shear waves at 2 Mc/s propagated in the $[1\bar{1}0]$ direction with particle motion in the [110] direction with saturation induction in the [001] direction. The smallest increase in velocity of approximately 0·2% was obtained for compressional waves at 15 Mc/s in the $[1\bar{1}0]$ with saturation induction in the [111] direction.

Figure 2, curve A, shows a plot of the fractional velocity change $\Delta v/v$ against increasing and decreasing magnetic field for shear waves in the $[1\bar{1}0]$ direction with particle motion in the [110] direction and the magnetic field along the [001] direction. The curve obtained for increasing field is of the same shape as the initial curve of magnetization for nickel and reaches a maximum value of 3·34% at values of field greater than 3200 oersteds. If the $(\Delta v/v, H)$ curve can be correlated with the (B, H) curve for the specimen it would be expected that the remanent $\Delta v/v$ value should have been approximately 80% of the maximum value instead of the low observed value. The following suggested explanation of this behaviour is based on the behaviour of the magnetic domains during a cycle of magnetization. On reducing the field from saturation value 180° magnetic domain boundary movements can only occur if an external agency can produce perturbations of the crystal lattice of sufficient amplitude. It would seem therefore that the ultrasonic radiation supplied the necessary energy for this to take place, but a reversal of the direction of the applied magnetic field would be required to complete the 180° boundary movements.

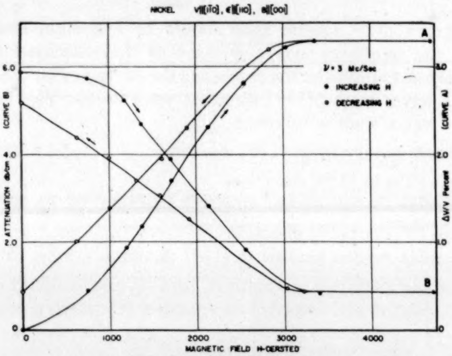

Figure 2. Percentage: Curve A—Change of velocity with magnetic field. Curve B—Change of attenuation with magnetic field.

Curve A in figure 2 is not in agreement with those obtained by Bozorth, Mason and McSkimin (1951) who show negative values of $\Delta v/v$ at low magnetic field strengths on reducing the magnetic field to zero. These workers suggested that the free energy of the crystal was lower in some ordered arrangements of the domains than for the demagnetized state. The author questions the validity of this argument, as the presence of an applied magnetic field would increase the internal energy of the specimen, and suggests that either their specimen or their magnetic pole pieces had not been completely demagnetized before their measurements were made.

Levy and Truell (1953), who made measurements on a nickel single crystal between 10 and 100 Mc/s, reported that no $\Delta v/v$ was observed. Their failure to observe a change in velocity with applied magnetic field was due to the limitations of their equipment in detecting small velocity changes.

The velocity equations for stress waves in a solid can be written in the form

$$v^2 = AM \qquad \ldots\ldots(1)$$

where A is a constant and M the elastic modulus. It follows that a small change ΔM in M will produce a small change Δv in the velocity as given by

$$2\frac{\Delta v}{v} = \frac{\Delta M}{M}. \qquad \ldots\ldots(2)$$

It can be shown (Nowick 1953) that

$$\frac{\Delta M}{M} = \frac{\Delta_M}{1+\omega^2\tau^2} \qquad \ldots\ldots(3)$$

where Δ_M is the relaxation strength and τ is the relaxation time.

Combining (2) and (3)

$$2\frac{\Delta v}{v} = \frac{\Delta_M}{1+\omega^2\tau^2} \qquad \ldots\ldots(4)$$

i.e.

$$1+4\pi^2 f^2\tau^2 = \frac{v\Delta_M}{2\Delta v}. \qquad \ldots\ldots(5)$$

Hence a graph of f^2 against $1/\Delta v$ should be a straight line, from whose intercepts on the frequency axis a measure of the relaxation time τ can be attained. This was found to be the case when the Δv values for the compressional and two shear waves in the $[1\bar{1}0]$ direction were used. The relaxation times for these three waves were as follows:

Compressional waves (L) in $[1\bar{1}0]$ direction	$2{\cdot}3\times10^{-8}\,\mathrm{sec} = \tau_L$,
Shear waves (T_1) in $[1\bar{1}0]$ direction with particle motion parallel to [001] direction	$2{\cdot}7\times10^{-8}\,\mathrm{sec} = \tau_{T_1}$,
Shear waves (T_2) in $[1\bar{1}0]$ direction with particle motion parallel to [110] direction	$3{\cdot}2\times10^{-8}\,\mathrm{sec} = \tau_{T_2}$.

The ratio of the relaxation strengths Δ_G and Δ_E can be found by substituting the appropriate moduli and velocities in equation (4) which gives

$$\frac{\Delta_G}{\Delta_E} = \frac{v_L \Delta v_T}{v_T \Delta v_L}\,\frac{1+\omega^2{\tau_T}^2}{1+\omega^2{\tau_L}^2}. \qquad \ldots\ldots(6)$$

From the appropriate values of v, Δv, ω and τ the following values of Δ_G/Δ_E were calculated:

Frequency (Mc/s)	5	10	15
Δ_G/Δ_E, L and T_1 waves	1·22	1·12	1·08
Δ_G/Δ_E, L and T_2 waves	1·42	1·24	1·15

For the usual values of G/E for metals Δ_G is approximately 15% to 20% greater than Δ_E (Nowick 1953).

3.2. *Elastic Constants*

The values of the elastic constants c_{11}, c_{12} and c_{44} were computed using the velocity equations for propagation of plane elastic waves in the $[1\bar{1}0]$ direction, taking ρ as $8{\cdot}90\,\mathrm{g\,cm^{-3}}$, for compressional waves (L)

$$\rho v^2 = \tfrac{1}{2}(c_{11}+c_{12}+2c_{44}) \qquad \ldots\ldots(7)$$

for shear waves with particle motion in the [001] direction (T_1)

$$\rho v^2 = c_{44} \qquad \ldots\ldots(8)$$

and for shear waves with particle motion in the [110] direction (T_2)

$$\rho v^2 = \tfrac{1}{2}(c_{11} - c_{12}). \qquad \ldots\ldots(9)$$

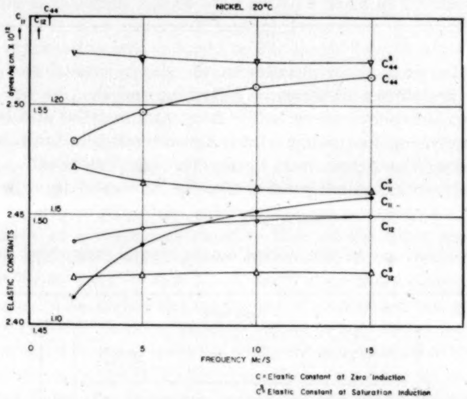

Figure 3. Change of elastic constant with frequency for zero and saturation induction {B||[001]}.

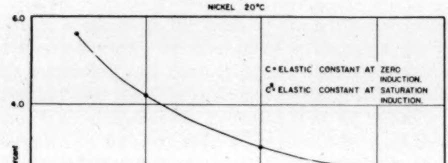

Figure 4. Change of elastic constants with frequency at saturation induction {B||[001]}.

Figure 3 shows the changes in the elastic constants with both frequency and magnetic field in the [001] direction. For the demagnetized state, all three elastic constants increase with increasing frequency and tend to maximum values which are the unrelaxed elastic constants. For the magnetically saturated state, $c_{11}{}^{s}$ and $c_{44}{}^{s}$ show a slight decrease with frequency while $c_{12}{}^{s}$ shows a slight increase. All three values remain constant at frequencies higher than 10 Mc/s.

The fractional differences

$$\frac{c^{s}-c}{c}=\frac{\Delta c}{c} \qquad \ldots\ldots(10)$$

with frequency between the constants in the demagnetized and magnetically saturated states are shown in figure 4. $\Delta c_{11}/c_{11}$ and $\Delta c_{44}/c_{44}$ are positive and decrease with increasing frequency, while $\Delta c_{12}/c_{12}$ is negative and becomes more negative with increasing frequency. Each curve tends to a limit, which at very high frequencies will be determined by the unrelaxed constants.

The anisotropy of a cubic crystal is usually expressed as

$$c=c_{11}-c_{12}-2c_{44}. \qquad \ldots\ldots(11)$$

The change of anisotropy of the nickel single crystal employed in the present series of measurements is shown in figure 5. The anisotropy for the demagnetized state shows an increase with frequency, whereas that at saturation induction in the [001] direction remained constant between 2 and 15 Mc/s.

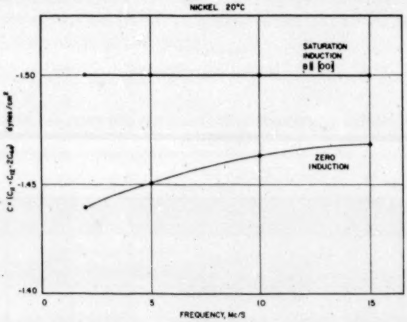

Figure 5. Change of anisotropy with frequency at zero and saturation induction {B‖[001]}. Units of ordinates should be × 10^{12}.

3.3. *Attenuation*

Individual echoes were photographed and their amplitudes measured by projecting the records on a screen. After corrections were made for the width of the oscilloscope trace, a graph of $\log_{10}$ (amplitude) against echo number was drawn, from the slope of which the attenuation was obtained. This technique provided an accuracy to $\pm 0{\cdot}002$ dB cm^{-1}.

The attenuation of both types of shear waves and compressional waves in the [1$\bar{1}$0] direction changes linearly with frequency between 2 and 15 Mc/s, each increasing with increasing frequency for both zero and saturation induction. The application of a magnetic field to the nickel single crystal reduced the attenuation, the extent of the change varying with the type of wave and the direction of magnetization; the greatest reduction was found in each case when the magnetic field was parallel to the [001] direction. With each type of wave the reduction in attenuation increased with increasing frequency, the greatest changes occurring for shear waves with particle motion in the [110] direction. In this case the attenuation was so high above 3 Mc/s in the demagnetized state that one echo only was observed, but at saturation induction in the [001] direction the attenuation was reduced to 2·3 dB cm^{-1} at 15 Mc/s.

The attenuation observed was mainly due to micro-eddy currents caused by the vibration of the magnetic domain boundaries or 'Bloch walls' and the observed reduction in attenuation to the alignment of the domains in the direction of magnetization with the consequent reduction in number of domain boundaries. If one assumes Kittel's (1956) explanation of a 'Bloch wall', when an ultrasonic wave passes through one of these walls, where the spin directions change from atomic plane to atomic plane, the spin vectors are forced to oscillate about their normal positions at a frequency close to that of the ultrasonic wave. These oscillations of the spin vectors cause micro-eddy currents to flow in opposite directions on either side of the Bloch wall, thus absorbing energy from the ultrasonic wave. The higher the frequency of oscillation the greater the values of micro-eddy currents become, causing higher energy losses from the ultrasonic wave. The attenuation measurements made for propagation of the compressional and two shear waves in the [1$\bar{1}$0] direction show that different amounts of energy were extracted from the ultrasonic waves for the three different directions of particle motion as the same number of Bloch walls were traversed by each type of wave. The greatest amount of energy was absorbed from the shear wave with particle motion in the [110] direction, and this wave also showed the greatest reduction in attenuation when the sample was magnetized to saturation, thereby removing the Bloch walls from the path of the ultrasonic wave.

Curve B of figure 2 shows the change of attenuation with applied magnetic field H for both increasing and decreasing H, while propagating shear waves in the [1$\bar{1}$0] direction with particle motion in the [110] direction. This curve follows the same type of hysteresis curve as that for velocity (curve A). The residual attenuation at saturation field strengths, where all the Bloch walls have been removed, would be due to such mechanisms as dislocation damping (Granato and Lücke 1956) and thermoelastic heat flow (Lücke 1956).

ACKNOWLEDGMENTS

The author wishes to express his gratitude to Dr. R. W. B. Stephens of the Physics Department at Imperial College for his helpful advice and encouragement, to Dr. H. Wilman of the Chemical Engineering Department for his help in checking the orientation of the axes of the nickel single crystal, to Professor R. Truell of Brown University, Providence, Rhode Island, U.S.A., for his kindness in providing the nickel ingot from which the single crystal was cut, and to Mr. M. Markham of the National Physical Laboratory, Teddington, for useful discussions and advice regarding the design of part of the equipment.

References

Bradfield, G., 1952, *Nuovo Cim.*, Ser. 9, **7,** 162.

Bozorth, R. M., Mason, W. P., and McSkimin, H. J., 1951, *Bell Syst. Tech. J.*, **30,** 970.

Firestone, F. A., and Frederick, J. R., 1946, *J. Acoust. Soc. Amer.*, **18,** 200.

Granato, A., and Lücke, K., 1956, *J. Appl. Phys.*, **27,** 583.

Huntingdon, H. B., 1947, *Phys. Rev.*, **72,** 321.

Kittel, C., 1956, *Introduction to Solid State Physics*, 2nd Edn. (New York: Wiley), p. 432.

Lazarus, D., 1949, *Phys. Rev.*, **76,** 545.

Levy, S., and Truell, R., 1953, *Rev. Mod. Phys.*, **25,** 140.

Lücke, K., 1956, *J. Appl. Phys.*, **27,** 1433.

McSkimin, H. J., 1950, *J. Acoust. Soc. Amer.*, **22,** 413.

Nowick, A. S., 1953, *Progress in Metal Physics*, Vol. 4 (London: Butterworths Scientific Publications).

Roderick, R. L., and Truell, R., 1952, *J. Appl. Phys.*, **23,** 267.

Phenomenological Theory of Ultrasonic Vibration Potentials in Liquids and Electrolytes

By A. WEINMANN
Mathematics Department, University of Leicester

Communicated by A. N. Hunter; MS. received 8th April 1958, *in revised form* 22*nd September* 1958

Abstract. A macroscopic phenomenological relationship is proposed, which takes into account the electric polarization produced in a liquid when density gradients are present. This is used to calculate the ultrasonic vibration potentials in an electrolyte, thus generalizing the Debye formula for this effect, to the case where the pure solvent produces its own potentials. The formula is in agreement with the few available experimental observations for reasonable values of the parameters. A calculation is also made of the disturbing effect of the measuring electrodes, and a simple equivalent circuit is derived under certain reasonably general conditions, from which the effect of an arbitrary impedance of the measuring apparatus can be allowed for.

§ 1. Introduction

In 1933 Debye proposed a method of estimating the effective masses of ions in solution by measurement of the potentials produced by the passage of ultrasonic waves through an electrolyte. Owing to experimental difficulties such measurements have only recently been made by Hunter (1950, 1958), Rutgers (1938), Rutgers and Vidts (1946, 1950), Rutgers and Rigole (1958), Yeager, Dietrick and Hovorka (1953), Yeager *et al.* (1949). In disagreement with Debye's formula the potentials measured increase at very low concentrations so as to be greatest in pure water and certain other solvents.

It is possible to explain the existence of these potentials in pure liquids as being due to density gradients producing an electric polarization (Weinmann, to be published). The present treatment accepts the existence of these potentials in a similar way to the method of Huang (Born and Huang 1954, § 7) for the theory of lattice vibrations in crystals.

The notation, with slight modifications, is that used by Debye (1933).

§ 2. Basic Equations

The equation proposed for the electric polarization $\mathbf{P}$ in a fluid in which there is an electric field $\mathbf{E}$ and a density gradient ∇d is

$$\mathbf{P} = \frac{\epsilon-1}{4\pi}\mathbf{E} + \alpha\nabla d. \qquad \ldots\ldots(1)$$

In this equation the changes in ϵ with density are neglected so that $\mathbf{E}$ shall be of the first order in $\mathbf{a}_0$, the velocity of the fluid particles. (This is justifiable when external fields are absent as in the present application.) The factor $(\epsilon-1)/4\pi$ is introduced so that the formula reduces to the usual form

$\mathbf{P}=(\epsilon-1)\mathbf{E}/4\pi$ when $\nabla d=0$. The constant α can be identified in terms of the maximum potential $\phi_{\max}$ produced in the pure liquid when plane ultrasonic waves are propagated through it. If

$$d=d_0+d_1\cos(kz-\omega t), \qquad \ldots\ldots(2)$$

in which $k=2\pi/\lambda$ and $\omega=2\pi f$, is supplemented by the Maxwell equations

$$\mathbf{D}=\mathbf{E}+4\pi\mathbf{P}, \qquad \ldots\ldots(3)$$

$$\nabla\,.\,\mathbf{D}=4\pi\rho, \qquad \ldots\ldots(4)$$

$$\nabla\times\mathbf{E}=0, \qquad \ldots\ldots(5)$$

$$\nabla\,.\,\mathbf{j}+\partial\rho/\partial t=0, \qquad \ldots\ldots(6)$$

together with the relation

$$\mathbf{E}=-\nabla\phi, \qquad \ldots\ldots(7)$$

the solution for the electric potential is

$$\phi=\frac{4\pi\alpha d_1}{\epsilon}\cos(kz-\omega t). \qquad \ldots\ldots(8)$$

Further, since

$$a_0\simeq\frac{\omega}{k}\frac{d_1}{d_0}=c\frac{d_1}{d_0},$$

it follows that

$$\alpha=\frac{\epsilon c|\phi_{\max}|}{4\pi d_0 a_0}. \qquad \ldots\ldots(9)$$

§ 3. APPLICATION TO THE VIBRATION POTENTIALS IN AN ELECTROLYTE

The following result can be obtained by the method used by Debye (1933), except that equations (1) and (3) replace Debye's $\mathbf{D}=\epsilon\mathbf{E}$ and the forces due to pressure gradients are included (Hermans 1938). It is simpler to solve the equations by the method used in § 4 in which the result is generalized to allow for the disturbing effects of the electrodes. If these disturbing effects are neglected the expression for the peak potential, for either progressive or standing waves, reduces to

$$|\phi_{\max}|=\frac{a_0[(Sc\nu M_{\mathrm{H}}/e)^2+(\phi_\infty/a_0)^2]^{1/2}}{[1+S^2]^{1/2}},\ S=\frac{4\pi L}{\epsilon\omega}, \qquad \ldots\ldots(10)$$

(see equations (32) and (42)) in which

$$L=\sum e_j{}^2\hat{n}_j/\rho_j,\ \nu=\frac{\sum\hat{n}_j e_j|e|(m_j-m_j')/(M_{\mathrm{H}}\rho_j)}{\sum\hat{n}e_{jj}{}^2/\rho_j}, \qquad \ldots\ldots(11)$$

and e_j, $\hat{n}_j$, ρ_j, m_j are the charge, equilibrium concentration (in number of ions/cm³), friction constant, and mass of the ions of species j; m_j' is the mass of solvent which would occupy the same volume as the ions; M_{H} is the mass of a hydrogen atom, and e the electronic charge. L is approximately equal to the specific conductivity of the electrolyte and ν is a quantity characteristic of the pure Debye effect. ϕ_∞ denotes the peak potential at infinite dilution given by equation (9).

Equation (10) differs only in the term $(\phi_\infty/a_0)^2$ from Debye's formula with Hermans' pressure gradient modification. The dependence on concentration is contained in L, which is directly proportional to the concentration of solute. (If the solvent has appreciable conductivity of its own, both L and ν contain contributions from the solvent ions independent of the concentration of the electrolyte.)

If the parameters are suitably chosen equation (10) can reproduce the observed experimental results with the increase in alternating potential with decreasing concentration of solute, and fits the results of Hunter (1958) after allowance has been made for the effect of his input circuit. This is not a good test of the theory because the input impedance is not yet accurately known and absolute values are not yet available. The number of free constants can be reduced by taking ϕ_∞/a_0 for water as 15μv for unit particle velocity as was found experimentally by Rutgers and Rigole (1958). For a solution of a typical binary electrolyte, such as KCl, the conductivity may be used for L thus leaving ν as an unknown parameter. The table shows the results for several possible values of ν, and for a wide range of concentrations.

Peak potentials as given by equation (10). L is taken as the known specific conductivity of a solution of KCl (at 18°c). $\epsilon = 80$ and $c = 1{\cdot}5 \times 10^5$ cm sec^{-1} for water; $\omega = 3 \times 10^6$ sec^{-1} as in the experiments of Hunter (1958). $|\phi_\infty/a_0|$ has been taken as 15×10^{-6} volts cm^{-1} sec^{-1}, as observed by Rutgers and Rigole (1958). The results have been converted from e.s.u. to microvolts, and the columns refer to the following values of ν: (I) $\nu = 2$; (II) $\nu = 6$; (III) $\nu = 12$; (IV) $\nu = 24$. The concentration τ is in moles/litre. For comparison column (V) gives the observed potentials of Yeager, Dietrick and Hovorka (1953), and (VI) those of Hunter (1958) (partially corrected, see text).

τ (mole/litre)	(I)	(II)	(III)	(IV)	(V)†	(VI)
0	15	15	15	15		15
0·000 01	14·8	14·8	14·8	14·8		15
0·000 1	12·8	12·8	12·8	12·9		10
0·000 2	9·6	9·6	9·7	10·0		8
0·000 5	4·7	4·8	5·0	5·9		
0·001	2·49	2·66	3·08	4·43	6	
0·002	1·29	1·57	2·24	3·93	—	
0·005	0·61	1·07	1·94	3·78	5	
0·01	0·40	0·98	1·90	3·75	3	
0·02	0·34	0·95	1·88	3·75		
0·05	0·32	0·94	1·88	3·75		
0·1	0·31	0·94	1·87	3·75		

† Experimental values at 200 kc/s (see text).

Although the table refers to a frequency of 480 kc/s (approximately that used by Hunter 1958), approximate values for the frequencies used by Rutgers and Rigole (1958) (1 Mc/s) and by Yeager, Dietrick and Hovorka (1953)

(200 kc/s) can be obtained by respectively doubling and halving the numbers in the τ column. The results of Yeager, Dietrick and Hovorka (1953) would be consistent with a value of ν between 2 and 6. Hunter's (1958) results do not go to sufficiently high concentrations for the effects of different ν's to be appreciable.

§ 4. DISTURBING EFFECT OF THE MEASURING ELECTRODES

To allow for the disturbing influence of the electrodes and associated external circuit the actual system is idealized by dividing it into three non-interacting parts. These parts are the electrolyte, the electrodes (which are assumed not to disturb the ultrasonic waves, to be good conductors and to be inserted into planes which would in their absence be equipotential surfaces) and a two-terminal external circuit assumed to act as a linear impedance Z.

Equations (3) to (7) must be supplemented by suitable boundary conditions at the surfaces of separation of the three components. It is convenient to define these boundary conditions by replacing abrupt changes with rapid but continuously varying ones in which the derivatives are continuous to all orders occurring. Consider separately the three parts of the system.

(i) *Electrolyte.*

Equation (1) holds with

$$\rho=\sum n_j e_j, \quad \mathbf{j}=\sum n_j e_j \mathbf{v}_j, \qquad \ldots\ldots(12)$$

where n_j, $\mathbf{v}_j$ are the particle density and velocity of ions of species j. Further the equations of motion and continuity of the ions of species j are (see Debye 1933, Hermans 1938)

$$m_j \frac{d\mathbf{v}_j}{dt} = e_j \mathbf{E} - \rho_j(\mathbf{v}_j - \mathbf{v}_0) + m_j' \frac{d\mathbf{v}_0}{dt}, \qquad \ldots\ldots(13)$$

$$\nabla . (n_j \mathbf{v}_j) + \frac{\partial n_j}{\partial t} = 0. \qquad \ldots\ldots(14)$$

Equation (14) holds also for the solvent which is labelled with $j=0$.

(ii) *Electrodes.*

$$\mathbf{j}=\sigma_c \mathbf{E}, \quad \sigma_c \text{ large}, \qquad \ldots\ldots(15)$$

$$\mathbf{D}=\epsilon_c \mathbf{E}. \qquad \ldots\ldots(16)$$

(iii) *External impedance.*

If the terminal potentials are ϕ_0 and ϕ_1, then the current I satisfies

$$-\phi_0+\phi_1=ZI. \qquad \ldots\ldots(17)$$

(Time factors $e^{-i\omega t}$ are used for the alternating potentials.)

In addition to the above equations we have the equation for the velocity of the longitudinal progressive waves in the solvent

$$\mathbf{v}_0=\mathbf{a}_0 \exp[i(\mathbf{k} . \mathbf{r}-\omega t)], \quad \mathbf{a}_0 \times \mathbf{k}=0. \qquad \ldots\ldots(18)$$

Let S_0' and S_1' be two surfaces drawn in the electrolyte and just touching the electrodes as in figure 1. If contact potentials between electrolyte and electrodes are neglected then

$$\phi \text{ is continuous across } S_0' \text{ and } S_1'. \qquad \ldots\ldots(19)$$

By (15) and (16) $\mathbf{E}$ and $\mathbf{D}$ are negligibly small in the electrodes, except in any equation in which they occur multiplied by σ_c. Thus from (3) and (5), neglecting $\mathbf{D}\cdot\mathbf{n}$ in the electrodes with respect to $\mathbf{D}\cdot\mathbf{n}$ in the electrolyte,

$$\mathbf{j}\cdot\mathbf{n}-\mathbf{j}_c\cdot\mathbf{n}=-\frac{1}{4\pi}\frac{\partial}{\partial t}\mathbf{D}\cdot\mathbf{n},\quad \text{on } S_0', \text{ and on } S_1', \qquad \ldots\ldots(20)$$

the suffix c denoting quantities referring to the conducting electrodes. (ϕ is approximately constant in the electrodes.)

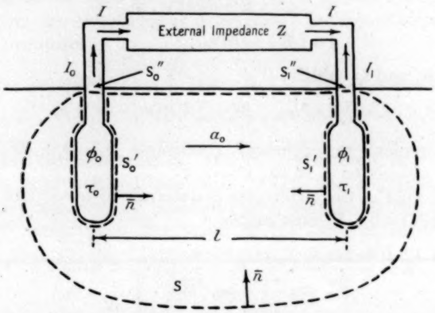

Figure 1. Idealized form of cell, electrodes and external circuit. The surfaces are shown dashed and the direction of the normal as $\mathbf{n}$.

It is convenient to express the currents leaving the electrodes and entering the external impedance in terms not involving the conductors. This can be done by applying the divergence theorem to the volume τ_0 enclosed by the surface $S_0'+S_0''$ and using equations (3) and (6)

$$\begin{aligned} I_0+\int_{S_0'}\mathbf{j}\cdot d\mathbf{S} &= \int_{(S_0'+S_0'')}\mathbf{j}\cdot d\mathbf{S}=\int_{\tau_0}\nabla\cdot\mathbf{j}\,d\tau \\ &= -\frac{1}{4\pi}\frac{\partial}{\partial t}\int_{\tau_0}\nabla\cdot\mathbf{D}\,d\tau=-\frac{1}{4\pi}\frac{\partial}{\partial t}\int_{(S_0'+S_0'')}\mathbf{D}\cdot d\mathbf{S}. \qquad \ldots\ldots(21)\end{aligned}$$

With the same approximations as lead to equation (20)

$$I_0=-\int_{S_0'}\mathbf{j}\cdot d\mathbf{S}-\frac{1}{4\pi}\frac{\partial}{\partial t}\int_{S_0'}\mathbf{D}\cdot d\mathbf{S}. \qquad \ldots\ldots(22)$$

Equation (20) will determine the normal component of the currents on S_0' and on S_1', and the currents are known on S_0'' and S_1'', so that the problem is determinate.

Let the particle density of ions of species j be

$$n_j=\hat{n}_j+\nu_j, \qquad \ldots\ldots(23)$$

where $\hat{n}_j$ denotes the equilibrium density (see equation (11)) and treat ν_j, $\mathbf{v}_j$ as being of the first order of small quantities, considering only the solutions for which

$$\nu_j,\ \mathbf{v}_j,\ \mathbf{E},\ \phi,\ I \text{ depend on time by a factor } e^{-i\omega t}. \qquad \ldots\ldots(24)$$

Then equation (14) gives

$$v_j = \hat{n}_j \nabla \cdot \mathbf{v}_j / i\omega. \qquad \ldots\ldots(25)$$

In equation (13) to the same order $d\mathbf{v}_j/dt$ can be replaced by $\partial \mathbf{v}_j/\partial t$, when

$$\mathbf{v}_j = (\rho_j - i\omega m_j)^{-1}[e_j \mathbf{E} + (\rho_j - i\omega m_j')\mathbf{v}_0]. \qquad \ldots\ldots(26)$$

Equations (23), (25), (26) can be inserted into (12) to give expressions for ρ and $\mathbf{j}$. Using the condition of neutrality $\Sigma \hat{n}_j e_j = 0$

$$\rho = [L\nabla \cdot \mathbf{E} + i\omega M \nabla \cdot \mathbf{v}_0]/i\omega, \qquad \ldots\ldots(27)$$

$$\mathbf{j} = L\mathbf{E} + i\omega M \mathbf{v}_0, \qquad \ldots\ldots(28)$$

to the first order, and in which

$$L = \sum \hat{n}_j e_j^2/\rho_j, \quad M = \sum \hat{n}_j e_j (m_j - m_j')/\rho_j. \qquad \ldots\ldots(29)$$

(Since under typical experimental conditions $\rho_j/\omega m_j \simeq 10^7$, ωm_j has been neglected with respect to ρ_j in the above.)

The electric field in the electrolyte is determined by equations (1), (4), (27), (7) and (25) with $j = 0$. $\mathbf{E}$ must satisfy

$$\epsilon \nabla \cdot \mathbf{E} + \frac{4\pi\alpha m_0 \hat{n}_0}{i\omega} \nabla^2 \nabla \cdot \bar{v}_0 = \frac{4\pi}{i\omega}[L\nabla \cdot \mathbf{E} + i\omega M \nabla \cdot \mathbf{v}_0], \qquad \ldots\ldots(30)$$

where $d = m_0 n_0$.

To solve these with the appropriate boundary conditions it is convenient to divide $\mathbf{E}$ into two parts

$$\mathbf{E} = \mathbf{E}^{(1)} + \mathbf{E}^{(2)}, \quad \phi = \phi^{(1)} + \phi^{(2)}, \qquad \ldots\ldots(31)$$

where $\mathbf{E}^{(1)}$ is the solution which neglects the effects of the electrodes, and is given by the particular solution of equations (30) and (18)

$$\mathbf{E}^{(1)} = \mathbf{A} \exp[i(\mathbf{k} \cdot \mathbf{r} - \omega t)],$$

$$\mathbf{A} = -(L - i\omega\epsilon/4\pi)^{-1}[\alpha m_0 \hat{n}_0 k^2 + i\omega M]\mathbf{a}_0. \qquad \ldots\ldots(32)$$

When the electrodes are inserted in planes of constant $\phi^{(1)}$ (planes of constant $\mathbf{k} \cdot \mathbf{r}$), $\mathbf{E}^{(2)}$ must be a solution of the homogenous part of equation (30), thus

$$\nabla \cdot \mathbf{E}^{(2)} = 0, \quad \mathbf{E}^{(2)} = -\nabla \phi^{(2)}, \qquad \ldots\ldots(33)$$

and $\phi^{(2)}$ must also be constant over the electrodes. The values of these constants are determined by the requirement that the total field given by equation (31) must satisfy equation (17) where

$$I = I_0 = -I_1, \qquad \ldots\ldots(34)$$

and I_0 and I_1 are given by equation (22) and the similar equation.

The right-hand side of equation (22) can be computed with the aid of equations (1), (3), (18), (25), (28) and (31): $\mathbf{E}^{(1)}$ drops out because of equation (32) and there remains only

$$I_0 = -(L - i\omega\epsilon/4\pi) \int_{S_0'} \mathbf{E}^{(2)} \cdot d\mathbf{S}, \qquad \ldots\ldots(35)$$

$$I_1 = -(L - i\omega\epsilon/4\pi) \int_{S_1'} \mathbf{E}^{(2)} \cdot d\mathbf{S}. \qquad \ldots\ldots(36)$$

It would appear that equations (34), (35), (36) together with a constant value of $\phi^{(2)}$ on S_0' and S_1' would overdetermine $\phi^{(2)}$. This is not the case for applying the divergence theorem to the volume enclosed by S_0', S_1' and S, and using equation (33) shows that equation (34) will be satisfied providing

$$\int_S \mathbf{E}^{(2)} \cdot d\mathbf{S} = 0.$$

This is possible since the value of $\nabla\phi^{(2)} \cdot \bar{n}$ on S can still be specified. It appears possible to choose $\phi^{(2)}$ to satisfy equation (37) and also so that $\phi^{(2)}$ decreases at large distances from the electrodes as is necessary for a sensible solution.

Equation (17) requires

$$\frac{A}{ik}\exp\,[i(\mathbf{k}\cdot\mathbf{r}_0-\omega t)](e^{ikl}-1)+\int_{\mathbf{r}_0}^{\mathbf{r}_1}\mathbf{E}^{(2)}\cdot d\mathbf{r}=-Z(L-i\omega\epsilon/4\pi)\int_{S_0'}\mathbf{E}^{(2)}\cdot d\mathbf{S}, \qquad \ldots\ldots(37)$$

where $\mathbf{r}_0$ and $\mathbf{r}_1$ are two points on S_0' and S_1' respectively and l is the distance between the two equipotential planes in which the electrodes are situated. Given an arbitrary solution of equation (33), subject to the same boundary conditions as $\phi^{(2)}$, and using the value of the specific conductivity of the electrolyte for L, the capacity C and resistance R of the cell are given by

$$C=\frac{\epsilon}{4\pi}\int_{S_0'}\mathbf{E}^{(2)}\cdot d\mathbf{S}\bigg/\int_{\mathbf{r}_0}^{\mathbf{r}_1}\mathbf{E}^{(2)}\cdot d\mathbf{r}, \qquad \ldots\ldots(38)$$

$$R=\frac{1}{L}\int_{\mathbf{r}_0}^{\mathbf{r}_1}\mathbf{E}^{(2)}\cdot d\mathbf{r}\bigg/\int_{S_0'}\mathbf{E}^{(2)}\cdot d\mathbf{S}. \qquad \ldots\ldots(39)$$

(The change in dielectric constant with concentration of electrolyte has been neglected.)

Any conductivity of the solvent itself can be allowed for by including the ions of the solvent with those of the solute so that its contribution appears in the expression for L. This necessitates the inclusion of the solvent ions in the expression for M. Alternatively the right-hand sides of equations (12) can be modified by adding the solvent charge density ρ_s and current density $\mathbf{j}_s$ and adding the equation

$$\mathbf{j}_s=\sigma_s\mathbf{E},$$

where σ_s is the conductivity of the pure solvent. This results merely in L being replaced by $L+\sigma_s$ in equations (27), (29) and (39) without change in M.

C and R are the actual capacity and resistance of the cell as measured externally in the convential way. (A simple case for which the solution for $\phi^{(2)}$ can be written down explicitly is that in which the electrolyte is contained between the plates of a parallel plate condenser.)

Using equation (38) in (37) and solving

$$\int_{\mathbf{r}_0}^{\mathbf{r}_1}\mathbf{E}^{(2)}\cdot d\mathbf{r}=-\frac{A\exp[i(\mathbf{k}\cdot\mathbf{r}_0-\omega t)]\cdot(e^{ikl}-1)}{ik[1+(L-i\omega\epsilon/4\pi)4\pi CZ/\epsilon]}, \qquad \ldots\ldots(40)$$

which fixes the scale of $\mathbf{E}^{(2)}$. The final solution for the current through the external impedence follows from equations (34), (35), (38) and (40)

$$I=\frac{\exp\,[i(\mathbf{k}\cdot\mathbf{r}_0-\omega t)](e^{ikl}-1)(L-i\omega\epsilon/4\pi)4\pi CA}{ik\epsilon[1+(L-i\omega\epsilon/4\pi)4\pi CZ/\epsilon]}. \qquad \ldots\ldots(41)$$

This can be written

$$I=\{(A/k)\exp[i(\mathbf{k}\,.\,\mathbf{r}_0-\omega t+kl/2)]\,.\,2\sin(kl/2)\}/Z_{\text{tot}}, \qquad \ldots\ldots (42)$$

where

$$Z_{\text{tot}}=Z+R/(1-i\omega CR), \qquad \ldots\ldots (43)$$

by means of equations (38) and (39). This form shows that the cell acts as a constant voltage generator in series with the parallel connected combination of C and R, and gives rise to the equivalent circuit of figure 2.

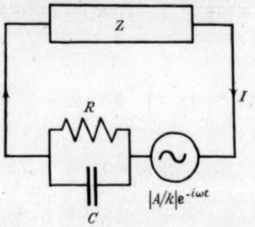

Figure 2. Equivalent circuit of the cell showing external impedance Z connected.

The peak potential is given by $|A/k|$ and this is reduced to the form given in equation (10) by means of equation (32). If the electrodes are placed a half wavelength apart then the peak to peak value is measured so giving twice the result of equation (10). Minor modifications to the analysis are necessary for standing waves, giving the same peak potential of equation (10) with a phase change and with a_0 the maximum particle velocity for the solvent occurring at the antinodes : the equivalent circuit of figure 2 still applies.

It is worth noting that the influence of the leads to the electrodes has been neglected. The theory could be modified to allow for this but a suitable design of cell may minimize their effect.

§ 5. Conclusion

The suggested phenomenological relation of equation (1) has been used to derive the modifications to the Debye formula, with Hermans' pressure gradient corrections, for the vibration potentials in an electrolyte, when the pure solvent itself produces potentials. The peak potentials produced are the same for progressive and stationary waves and the formula is in qualitative agreement with experimental observations. Quantitative agreement can be obtained if the parameters are suitably chosen and this leads to reasonable values of the parameters, but no definite conclusions are possible without more accurate experimental results. It would be especially useful to have values of the potentials over a wide range of concentration of electrolyte in order to find the two limits of zero and large concentration. For electrolytes of fairly large concentration the effect of temperature changes would be mainly to alter the dielectric constant and experiments at different temperatures could be used to verify this.

For conditions which can be satisfied fairly well in actual experiments the effect of the measuring electrodes can be allowed for by means of a simple equivalent circuit. These conditions are approximately satisfied by the experimental arrangements of Hunter (1958) and Yeager, Dietrick and Hovorka (1953), but not by those employed by Rutgers and Rigole (1958) : in the latter case the electrode arrangement will disturb the electric field, although the amount of this disturbance would probably not be large if the external circuit is of high impedance.

ACKNOWLEDGMENT

It is a pleasure to thank Dr. A. N. Hunter for first interesting us in this work and for many helpful and stimulating conversations.

REFERENCES

BORN, M., and HUANG, K., 1954, *Dynamical Theory of Crystal Lattices* (Oxford: University Press).
DEBYE, P., 1933, *J. Chem. Phys.*, **1**, 13.
HERMANS, J. J., 1938, *Phil. Mag.*, **25**, 426; **26**, 674.
HUNTER, A. N., 1950, *Proc. Phys. Soc.* B, **63**, 58.
—— 1958, *Ibid.*, **71**, 847.
RUTGERS, A. J., 1938, *Physica*, **5**, 46.
RUTGERS, A. J., and RIGOLE, W., 1958, *Trans. Faraday Soc.*, **54**, 139.
RUTGERS, A. J., and VIDTS, J., 1946 *Nature, Lond.*, **157**, 74.
—— 1950, *Ibid.*, **165**, 109.
YEAGER, E., BOGOSH, J., HOVORKA, F., and McCARTHY, J., 1949, *J. Chem. Phys.*, **17**, 411.
YEAGER, E., DIETRICK, H., and HOVORKA, F., 1953, *J. Acoust. Soc. Amer.*, **25**, 456.

Measurement of Ultrasonic Absorption in Liquids by the Observations of Acoustic Streaming

By D. N. HALL and J. LAMB
Electrical Engineering Department, Imperial College, London

MS. received 26*th August* 1958, *in revised form* 4*th November* 1958

Abstract. Propagation of an ultrasonic wave through an absorbing liquid contained in a tube gives rise to a gradient of pressure along the axis which is determined by observing the velocity of flow of the liquid through a side tube connected in parallel with the main tube. The intensity of the ultrasonic wave is found by recording the voltage applied to the exciting transducer, the parameters of which are measured in the vicinity of resonance. Obstruction of the sound field by the intensity measurement is thus avoided. The observations are used to evaluate the absorption coefficients of liquids over the range 130 kc/s to 1560 kc/s.

The limits and accuracy of the technique are discussed and a new theoretical approach enables the pressure gradient to be derived from second-order acoustic variables without recourse to the concept of radiation pressure.

§ 1. Introduction

Measurements of ultrasonic absorption in liquids over wide ranges of frequency and temperature have revealed the existence of relaxation processes to many of which can be given a direct molecular interpretation. In providing a new approach to the study of fast reactions, these investigations have led to a better understanding of molecular behaviour in liquids (Davies and Lamb 1957, de Groot and Lamb 1957, Bass and Lamb 1957, 1958). In order to evaluate the energy parameters associated with a molecular reaction, which gives rise to observed relaxational behaviour, it is desirable to be able to make measurements of ultrasonic absorption over the widest possible ranges of frequency and temperature.

Pulse techniques have been employed for absorption measurements over the frequency range 1 to 200 Mc/s but at the lower end of this range it is only possible to obtain accurate results for liquids having high absorption coefficients α in excess of about 0·06 cm^{-1} (Andreae, Bass, Heasell and Lamb 1958). Otherwise an accuracy to $\pm 2\%$ can, in general, be obtained. The lower limit of frequency imposed upon these measurements is due principally to diffraction effects associated with a source of finite diameter. Measurements at frequencies below 1 Mc/s have been made by reverberation techniques (Karpovich 1954, Lawley and Reed 1955) but in the present stage of development these methods do not yield an accuracy comparable with that of the pulse technique used at higher frequencies.

Propagation of an ultrasonic wave through an absorbing fluid medium causes a pressure gradient to exist along the direction of propagation which, in an unbounded medium, is responsible for steady flow. This streaming phenomenon was first analysed in detail by Eckart (1948). Later work showed that the streaming velocity is a function of the ultrasonic absorption and led to the development of an apparatus which, in principle, enabled this absorption to be determined from a measurement of the pressure gradient in a tube completely filled with the sound beam (Piercy and Lamb 1954, Piercy 1956). This system proved satisfactory for operation in the frequency range 1 to 10 Mc/s with liquids having absorption coefficients between 2×10^{-4} and 0·1 cm^{-1}.

The aim of the present work has been to develop a system for the measurement of ultrasonic absorption in liquids over the frequency range 100 kc/s to 2 Mc/s, based on the previous technique. In the process, improvements have been made in both the experimental and theoretical aspects of this problem. It should be emphasized that the difficulties encountered in extending the minimum frequency of measurement from 1 Mc/s to 100 kc/s are comparable with those associated with an increase from 100 Mc/s to 1000 Mc/s.

In the former experimental arrangement the pressure gradient in the tube filled with the sound beam was determined by direct observation of the velocity of the return flow of liquid through a small side tube connected in parallel with the main tube.† The ultrasonic intensity was measured by means of a radiation pressure paddle which itself imposed restrictions on the frequency range over which the system could be employed.

A description is given in § 2 of an improved 'side tube' technique for which the theory is developed later in § 3 showing that the pressure gradient can be derived directly from second-order variables without recourse to the concept of radiation pressure, as hitherto. § 2 contains a description of the method which has now been developed for the necessary measurement of the intensity of the ultrasonic wave, and consideration is given to the accuracy and limits of the present system in § 4.

§ 2. AN IMPROVED SIDE TUBE TECHNIQUE FOR THE MEASUREMENT OF THE PRESSURE GRADIENT

2.1. *Description of the Experimental System*

A functional sketch of the assembly is shown in figure 1. A transducer T either of quartz or of barium titanate, of 6 cm diameter radiates directly into the main tube M containing the test liquid. The transducer housing H is bolted on to the main tube via the flanges F, between which is placed an annular polythene gasket. After passing through the test liquid in M the ultrasonic wave is finally absorbed in the long tube A which contains a highly absorbing liquid such as acetic acid or methyl cyclohexane. A polythene diaphragm of 0·007 in. thickness is clamped between the flanges G, and separates the liquid in the absorbing termination from the test liquid.

Since reflections from the absorber can be neglected the time-average of the first-order acoustic variables associated with the travelling wave in the test liquid is zero. The time-average of the second-order pressure, however, is non-zero and a pressure gradient exists in the main tube, the value of which depends upon the absorption coefficient α of the test liquid. The pressure gradient causes liquid to flow through a glass side tube S in the sense indicated on figure 1. If z_1 and z_2 are distances measured from the transducer face to the points of entry of the side tube into the main tube, and E is the energy density of the (assumed) plane sound wave, then it is shown in § 4 that the difference in pressure between the ends of the side tube is given by:

---

† The term 'acoustic streaming' is therefore a misnomer although its use is retained owing to the lack of a suitable alternative.

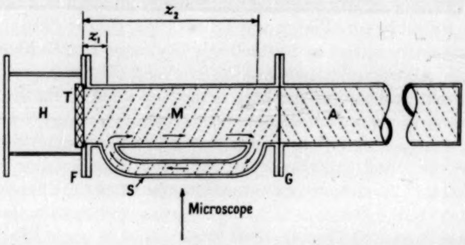

Figure 1. Schematic diagram of acoustic system: H, transducer housing (air filled); T, barium titanate or quartz transducer; M, main tube containing test liquid; S, side tube; A, non-reflecting absorber containing a highly absorbing liquid; F, flange connection with polythene gasket; G, flange connection with polythene diaphragm.

$$\Delta p = E[\exp(-2\alpha z_1) - \exp(-2\alpha z_2)]. \qquad \text{......(1)}$$

The velocity of fluid flow along the axis of a tube of radius r and of length l with this difference in pressure across its ends is given from Poisseuille's law as:

$$v = \Delta p r^2/4\eta l \qquad \text{......(2)}$$

where η is the shear viscosity of the liquid in question. In practice this equation must be modified to include end effects associated with the connection of the side tube into the main tube: these and other factors are taken into account by the following combination of equations (1) and (2) involving a calibration constant, k:

$$k\eta v/E = \exp(-2\alpha z_1) - \exp(-2\alpha z_2). \qquad \text{......(3)}$$

k is determined by measurements of v and E for a number of liquids of known absorption coefficient and shear viscosity. As in the previous work, v is measured by observing through a microscope the velocity of flow of aluminium particles suspended in the liquid.

Choice of dimensions of the system is governed by consideration of the lowest frequency at which it is to operate. In the present arrangement this minimum frequency is set at 130 kc/s: the main tube is 5·4 cm in diameter and 21 cm long whilst the internal diameter of the side tube is 0·7 cm and the distance $z_2 - z_1$ between the points at which it enters the main tube is 16·1 cm.

Barium titanate discs are used as transducers at frequencies of 130 kc/s and 290 kc/s and an X-cut quartz disc is employed at 520 kc/s and at its third harmonic of 1560 kc/s.

2.2. *Measurement of the Intensity of the Ultrasonic Wave*

Since standing waves generate unwanted streaming it is essential that the terminating absorber shall be sensibly non-reflecting and that the means adopted for the measurement of the intensity of the wave shall produce a minimum of disturbance to the sound field. The radiation paddle used by Piercy and Lamb (1954) introduced standing waves into the system particularly at frequencies below a few Mc/s. In the present arrangement disturbance of the sound field by measurement of its intensity has been completely avoided by measuring the radiation resistance, applied voltage and efficiency of the transducer. The energy density is obtained from equation (A 17) of the Appendix and is given by

$$E = \frac{I}{c} = \frac{(D_V - D_L) D_L V^2}{D_V A c} \qquad \ldots\ldots(4)$$

where D_V is the diameter of the admittance loop about resonance when vibrating in vacuum, D_L is the corresponding value when radiating into a liquid, V is the applied voltage, A is the area of cross section and c is the velocity of sound in the liquid.

D_V is found for each transducer in its housing by a preliminary measurement. At each subsequent measurement of D_L the necessary associated measurement of clamped conductance of the transducer is found by recording the conductances G_A and G_B at frequencies f_A and f_B remote and equidistant from the frequency of resonance, f_C (figures 2 and 3). The maximum conductance at C (figure 3) is found by a systematic frequency scan. D_L is then the difference between G_C and the arithmetic mean of G_A and G_B. The admittance measurements are made using a Wayne Kerr r.f. bridge type B601, the balance point being detected by an oscilloscope used in conjunction with a radio receiver.

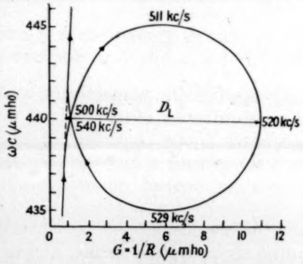

Figure 2. Representative admittance loop for a quartz transducer radiating into benzene. The directions of the arrows show frequency increasing. 520 kc/s is the resonant frequency. $Q=29$. As explained in the text it is not usual in practice to plot the full loop.

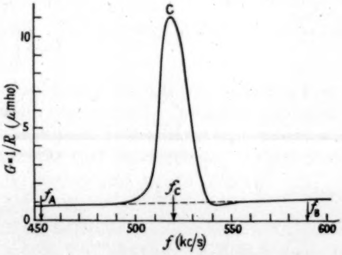

Figure 3. The conductance against frequency plot corresponding to the admittance loop of figure 2. A, B and C are points to which reference is made in the text.

§ 3. THEORY OF THE SIDE TUBE CONFIGURATION

Equation (1) of § 2 was derived intuitively in a previous paper (Piercy and Lamb 1954) by assuming that the cause of the liquid flow in the side tube was a gradient of radiation pressure in the main tube, and by equating the radiation pressure with the energy density. In the following derivation the pressure gradient is obtained directly from second-order variables without recourse to the concept of radiation pressure.

The excess pressure, density and particle velocity due to the sound wave can be represented by

$$\left.\begin{aligned} p-p_0&=p_1+p_2+\dots \\ \rho-\rho_0&=\rho_1+\rho_2+\dots \\ u&=u_1+u_2+\dots \end{aligned}\right\} \qquad \dots\dots(5)$$

where the suffix 0 refers to equilibrium conditions in the absence of the sound wave, the suffix 1 signifies the first-order terms depending only on the angular frequency ω, whilst the second-order terms are represented by the suffix 2. The amplitudes p_2, ρ_2 and u_2 are time-independent and are those which influence the steady streaming. u_2 is the streaming velocity which occurs in an unbounded medium and p_2 the associated static pressure, the gradient of which causes the flow of fluid in the side tube of the present arrangement.

The force f acting on a small element of fluid can be expressed (Nyborg 1953) by

$$f=-\nabla p+\left(\mu'+\frac{4\mu}{3}\right)\nabla\nabla\,.\,u-\mu\nabla\times\nabla\times u \qquad \dots\dots(6)$$

where

$$f=\rho\left[\frac{\partial u}{\partial t}+(u\,.\,\nabla)u\right]$$

and μ and μ' are the shear and bulk viscosity coefficients, respectively, and are assumed constant. Using the equation of continuity we obtain:

$$\frac{\partial}{\partial t}(\rho u)+F'=-\nabla p+\left(\mu'+\frac{4\mu}{3}\right)\nabla\nabla\,.\,u-\mu\nabla\times\nabla\times u \qquad \dots\dots(7)$$

where

$$F'=\rho(u\,.\,\nabla)u+u\,.\,\nabla(\rho u). \qquad \dots\dots(8)$$

Take now the time-average of (7) including second-order terms, noting that $\partial(\rho_1 u_1)/\partial t=0$ in the steady state. Thus

$$F=-\nabla p_2+(\mu'+4\mu/3)\nabla\nabla\,.\,u_2-\mu\nabla\times\nabla\times u_2 \qquad \dots\dots(9)$$

where

$$F=\rho_0\langle(u_1\,.\,\nabla)u_1\rangle+\rho_0\langle u_1(\nabla\,.\,u_1)\rangle. \qquad \dots\dots(10)$$

If we assume that u_2 is irrotational then it follows that

$$\mu\nabla^2 u_2=\nabla p_2+F. \qquad \dots\dots(11)$$

Most of the measurements made with the streaming equipment lie in the Fresnel zone of the transducer, under which conditions it is a reasonable approximation to put

$$u_1=u_0\exp(-\alpha z)\exp[j(\omega t-kz)] \qquad \dots\dots(12)$$

for a transducer radiating in the z direction. Substituting (12) into (10) we get

$$F=-\rho_0\alpha u_0^2\exp(-2\alpha z). \qquad \dots\dots(13)$$

In cylindrical coordinates

$$\nabla^2 u_2=\frac{1}{r}\frac{\partial}{\partial r}\left(\frac{r\partial u_2}{\partial r}\right)+\frac{1}{r^2}\frac{\partial^2 u_2}{\partial\theta^2}+\frac{\partial^2 u_2}{\partial z^2}. \qquad \dots\dots(14)$$

Now $\partial u_2/\partial\theta=0$ since circular symmetry is assumed, and $\partial u_2/\partial z=0$ in the steady state; hence

$$\nabla^2 u_2=\frac{1}{r}\frac{\partial}{\partial r}\left(r\frac{\partial u_2}{\partial r}\right). \qquad \ldots\ldots(15)$$

Now p_2 is independent of r and θ and so

$$\nabla p_2=\partial p_2/\partial z. \qquad \ldots\ldots(16)$$

Substituting (15) and (16) in (11):

$$\mu\nabla^2 u_2=\frac{\mu}{r}\frac{\partial}{\partial r}\left(r\frac{\partial u_2}{\partial r}\right)=\frac{\partial p_2}{\partial z}+F. \qquad \ldots\ldots(17)$$

It is shown in Appendix 1 that u_2 is zero in a tube completely filled with a sound beam.

Thus under these conditions (17) becomes

$$\frac{\partial p_2}{\partial z}+F=0$$

and therefore

$$\begin{aligned}\frac{\partial p_2}{\partial z}&=\rho_0\alpha u_0^2\exp(-2\alpha z)\\ &=2\alpha E\exp(-2\alpha z) \qquad \ldots\ldots(18)\end{aligned}$$

where E is the energy density at the source. The pressure difference between the two points z_1 and z_2 is thus given by

$$\Delta p_2=\int_{z_1}^{z_2}\frac{\partial p}{\partial z}dz=E\{\exp(-2\alpha z_1)-\exp(-2\alpha z_2)\}. \qquad \ldots\ldots(19)$$

Δp_2 is the pressure which gives rise to the liquid flow when the side-tube is connected between z_1 and z_2. It should be noted that equation (19) is equivalent to the expression derived less rigorously by Piercy and Lamb (1954).

§ 4. ACCURACY AND LIMITS

The results at 520 kc/s and 1560 kc/s in table 1 show that although k depends upon frequency there is good agreement at each frequency between the measurements using benzene and carbon tetrachloride.

A further indication of the accuracy of the technique is given by the agreement between the values of α/f^2 found for various liquids by this and by other methods as is shown in table 2. Some of the liquids referred to exhibit a relaxation due to the perturbation by the sound wave of a molecular equilibrium. In such cases the values of α/f^2 quoted from the results of other workers have been deduced from the equation (see, for example, Lamb and Pinkerton 1949):

$$\frac{\alpha}{f^2}=B+\frac{A}{1+(f/f_c)^2}. \qquad \ldots\ldots(20)$$

The term B represents the absorption at frequencies much greater than the characteristic frequency f_c and A is the contribution of the relaxation. In all cases exhibiting relaxation the parameters A, B and f_c have been evaluated from the results of measurements over a wide range of frequencies using pulse techniques which yield an accuracy to about $\pm 2\%$ in α/f^2.

The lowest absorption value which can be measured reliably at any frequency is determined by two factors: the intensity level above which turbulence occurs

Table 1. Evaluation of the Constant k (equation (3)) at 25° C

Frequency (kc/s)	Liquid	Accepted value of $\alpha/f^2 (\times 10^{17}\ \mathrm{sec^2\ cm^{-1}})$	Values and sources of information (α/f^2, A and B, $\times 10^{17}\ \mathrm{sec^2\ cm^{-1}}$)	Measured value of $Q = \eta v/E$ (cm)	Deduced value of k (cm^{-1})	Mean value of k(cm^{-1})
1560	Carbon tetrachloride	545	545 (*a*), 533 (*b*), 560 (*c*), 570 (*d*), 556 (*e*).	$2{\cdot}25 \times 10^{-3}$	143	149
	Benzene	845	849 (*a*), 845 (*f*), 875 (*g*), 900 (*c*), 800 (*b*).	$2{\cdot}77 \times 10^{-3}$	154	
520	Carbon tetrachloride	545	as for carbon tetrachloride above	$3{\cdot}36 \times 10^{-4}$	139	139
	Benzene	845	as for benzene above	$5{\cdot}01 \times 10^{-4}$	139	
130	Acetic acid	128 000	128 000 [$A = 132\,000$, $f_c = 725$ kc/s, $B = 140$] (*h*)	$1{\cdot}97 \times 10^{-3}$	222	222

(*a*) Heasell and Lamb 1956. (*b*) Pellam and Galt 1946. (*c*) Rapuano 1947. (*d*) Willard 1941. (*e*) Bazulin 1938. (*f*) Andreae 1955. (*g*) Piercy and Lamb 1954. (*h*) Lamb and Pinkerton 1949.

Table 2. Results of Experiments using the Side-tube Technique (25°c)

Frequency (kc/s)	Liquid	Measured value of Q (cm)	$\alpha/f^2 \times 10^{17}\ \mathrm{sec^2\ cm^{-1}}$ (from Q)	Values from other techniques. $\alpha/f^2 \times 10^{17}\ \mathrm{sec^2\ cm^{-1}}$ (A and B, $\times 10^{17}\ \mathrm{sec^2\ cm^{-1}}$)
520	Propionic acid	$3{\cdot}56 \times 10^{-3}$	10 000	9660 ($A = 10\,000$, $f_c = 2{\cdot}44$ Mc/s, $B = 127$) (*j*)
130	Propionic acid	$2{\cdot}28 \times 10^{-3}$	9650	10 100 ($A = 10\,000$, $f_c = 2{\cdot}44$ Mc/s, $B = 127$) (*j*)
1560	Ethyl alcohol	$2{\cdot}68 \times 10^{-4}$	51·3	50·2 (*k*), 53·7 (*c*), 51 (*g*)
130	Carbon disulphide	$1{\cdot}5 \times 10^{-4}$	6400	5870 ($A = 5870$, $f_c = 78$ Mc/s, B [illegible]0) (*m*)
1560	Propylene chloride	$23{\cdot}5 \times 10^{-4}$	609	597 ($A = 475$, $f_c = 51{\cdot}4$ Mc/s, $B = 122$) (*n*)
520	Propylene chloride	$3{\cdot}59 \times 10^{-4}$	592	

(*j*) Lamb and Huddart 1950. (*k*) Pinkerton 1949. (*m*) Andreae, Heasell and Lamb 1956. (*n*) R. A. Padmanabhan, private communication. α/f^2 in column 4 has been deduced from Q using equation (3) and the appropriate value of k from table 1.

and the fluid velocity in the side tube below which the flow in non-axial. In practice this lower limit is $\alpha = 1{\cdot}4 \times 10^{-4}\,\mathrm{cm}^{-1}$ at 520 kc/s and above, and $4 \times 10^{-4}\,\mathrm{cm}^{-1}$ at 130 kc/s.

The highest absorption value which can be accommodated is governed by the following considerations. α is evaluated from equation (3) in which all other quantities are either measured directly or are known from other data. The right-hand side of equation (3) reaches a maximum as a function of α at $\alpha_0 = 0{\cdot}0575$ for the values of z_1 and z_2 set by the dimensions of the present apparatus. In order to avoid ambiguity in determining the absorption coefficient it is desirable to restrict the measurements to liquids having values of α below α_0. If necessary check measurements are made at higher frequencies using a pulse apparatus (Andreae *et al.* 1958). Further, owing to the absorption of the wave in travelling the distance z_1 from the source, represented by the term $\exp(-2\alpha z_1)$ in equation (3), increasing values of α eventually lead to a flow velocity in the side tube which is too small to measure reliably. It is considered that the upper value of α which can be measured is $\alpha = 0{\cdot}02\,\mathrm{cm}^{-1}$ at 130 kc/s rising to $0{\cdot}04\,\mathrm{cm}^{-1}$ at 1560 kc/s.

It is estimated that for values of α within the ranges stated above it is possible to measure the absorption coefficients of liquids with accuracies to within $\pm 5\%$ at 1560 kc/s, $\pm 6\%$ at 520 kc/s and $\pm 11\%$ at 130 kc/s. In all experiments the energy density radiated from the source is less than $0{\cdot}08\,\mathrm{w\,cm}^{-2}$.

ACKNOWLEDGMENTS

Financial assistance in support of this work and a research bursary for D. N. H were kindly provided by the Worshipful Company of Clothworkers to whom the authors thanks are due.

APPENDIX I

TO SHOW THAT $u_2 = 0$ IN A TUBE COMPLETELY FILLED WITH SOUND

We have

$$\mu \nabla^2 u_2 = \frac{\partial p_2}{\partial z} + F = \frac{\mu}{r}\frac{\partial}{\partial r}\left(r\frac{\partial u_2}{\partial r}\right) \qquad \ldots\ldots (\mathrm{A}\,1)$$

and $\partial p_2/\partial z = \text{constant} = A$ for small values of α such that $\exp(-2\alpha z) \simeq 1 - 2\alpha z$. Hence

$$\frac{d}{dr}\left(r\frac{du_2}{dr}\right) = \frac{r}{\mu}F + \frac{Ar}{\mu}, \qquad \ldots\ldots (\mathrm{A}\,2)$$

$$\frac{du_2}{dr} = \frac{Ar}{2\mu} + \frac{1}{\mu r}\int_0^r rF(r)\,dr + \frac{B}{r}. \qquad \ldots\ldots (\mathrm{A}\,3)$$

The integration constant B must be zero as otherwise the velocity gradient on the axis would be infinite. Let $r_0 = \text{tube diameter} = \text{sound beam diameter}$; then $F(r) = F$ between $r = 0$ and $r = r_0$ and

$$\frac{du_2}{dr} = \frac{Ar}{2\mu} + \frac{F}{\mu r}\int_0^r r\,dr = \frac{1}{2\mu}(A+F)r \qquad \ldots\ldots (\mathrm{A}\,4)$$

therefore

$$u_2 = \frac{1}{2\mu}(A+F)\int_{r_0}^r r\,dr = \frac{1}{4\mu}(A+F)(r^2 - r_0^2). \qquad \ldots\ldots (\mathrm{A}\,5)$$

The constant A is found by applying the boundary condition that the net flow is zero, i.e.

$$\int_0^{r_0} u_2(r)\,r\,dr = \left[u_2(r)\frac{r^2}{2}\right]_0^{r_0} - \int_0^{r_0}\frac{r^2}{2}\frac{d}{dr}u_2(r)\,dr = 0$$

therefore

$$\int_0^{r_0}\frac{r^2}{2}\frac{d}{dr}\,u_2(r)\,dr = 0. \qquad \ldots\ldots(\mathrm{A}6)$$

Hence from (A 4) and (A 6)

$$\int_0^{r_0}\frac{r^2}{2}\frac{d}{dr}u_2(r)\,dr = \int_0^{r_0}\frac{r^2}{2}\frac{1}{2\mu}\,(A+F)r\,dr = \frac{1}{4\mu}\,(A+F)\frac{r_0^4}{4} = 0$$

and

$$A = -F. \qquad \ldots\ldots(\mathrm{A}7)$$

Thus, substituting (A 7) in (A 5), $u_2 = 0$, which is the required condition.

Experiments with glass tubes have shown that due to a non-ideal source streaming occurs in a tube completely filled with a sound beam. Some of this unwanted streaming is diverted into the side-tube and is taken into account by the value of k which is nevertheless independent of α for a given frequency.

APPENDIX 2

INTENSITY MEASUREMENT

The following admittance analysis is for a piezoelectric transducer. The corresponding impedance analysis for a magnetostrictive transducer is given by Hunt (1954).

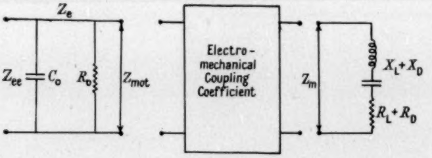

Figure 4. Impedance diagram for a piezoelectric transducer.

Referring to figure 4, the subscripts for the impedances Z $(=R+jX)$ are: ee, input; e, clamped electrical; mot, motional; m, mechanical; L, load; D, effective loss; $Z_m = Z_D + Z_L$.

The coupling coefficients are defined by

$$T_{\mathrm{em}} = \frac{\text{input voltage}}{\text{output velocity}} = \frac{iZ_{\mathrm{mot}}}{v}\,; \quad T_{\mathrm{me}} = \frac{-\text{output force}}{\text{input current}} = \frac{-vZ_{\mathrm{m}}}{i} \qquad (\mathrm{A}8)$$

where v = the velocity of the driving face, V = voltage, i = current. Now

$$Z_{\mathrm{ee}} = Z_{\mathrm{e}} + Z_{\mathrm{mot}} = Z_{\mathrm{e}} - \frac{T_{\mathrm{em}}T_{\mathrm{me}}}{Z_{\mathrm{m}}} \qquad \ldots\ldots(\mathrm{A}9)$$

and $|-T_{\mathrm{em}}T_{\mathrm{me}}| = |T_{\mathrm{em}}|^2 = |T_{\mathrm{me}}|^2 = T^2$. The efficiency N is given by

$$N = \frac{W_0}{W_1} = \frac{R_{\mathrm{L}}|v|^2}{R_{\mathrm{ee}}|i|^2} = \frac{R_{\mathrm{L}}}{R_{\mathrm{ee}}}\,\frac{|Z_{\mathrm{mot}}|}{|Z_{\mathrm{D}}+Z_{\mathrm{L}}|} \qquad \ldots\ldots(\mathrm{A}10)$$

where W_1 = electrical power input, W_0 = acoustical power output. The relevant admittances Y are defined

$$Y_{ee} = \frac{1}{Z_{ee}}, \quad Y_e = \frac{1}{Z_e}, \quad Y_{mot} = Y_{ee} - Y_e. \qquad \ldots\ldots(A\,11)$$

Substituting from (A9),

$$Y_{mot} = \frac{-T^2/Z_e{}^2}{Z_D + Z_L + T^2/Z_e}. \qquad \ldots\ldots(A\,12)$$

From (A 10) and (A 12) we get

$$N = \frac{R_L|Y_{mot}|Z_{ee}{}^2}{R_{ee}|Z_D + Z_L + T^2/Z_e|}.$$

Now at resonance, having tuned out C_0, $Z_{ee} = R_{ee}$, and thus

$$N = \frac{R_L}{G_{ee}} \frac{|Y_{mot}|}{|Z_D + Z_L + T^2/Z_e|}.$$

Also, at resonance, Y_{mot} is the diameter of the admittance loop D, and $X_D + X_L = 0$, therefore

$$N = \frac{D_L}{G_{ee}} \frac{R_L}{R_D + R_L + T^2/Z_e}. \qquad \ldots\ldots(A\,13)$$

where G is the conductance. Now

$$D_L = Y_{mot} = \frac{-T^2/Z_e{}^2}{R_D + R_L + T^2/Z_e}$$

from (A 12). Hence *in vacuo*, when $R_L = 0$,

$$D_V = \frac{-T^2/Z_e{}^2}{R_D + T^2/Z_e}, \qquad \ldots\ldots(A\,14)$$

and

$$\frac{D_V - D_L}{D_V} = \frac{R_L}{R_D + R_L + T^2/Z_e}. \qquad \ldots\ldots(A\,15)$$

Substituting (A 15) in (A 13)

$$N = \frac{D_L}{G_{ee}} \frac{(D_V - D_L)}{D_V} = \frac{W_0}{W_1} \qquad \ldots\ldots(A\,16)$$

and

$$W_1 = \frac{(V)^2}{R_{ee}},$$

the intensity I (= power flow per unit area averaged over the cross section of the tube) is

$$I = \frac{W_0}{A} = \frac{(D_V - D_L)D_L}{D_V} \frac{V^2}{A} \qquad \ldots\ldots(A\,17)$$

where A is the area of the transducer.

REFERENCES

ANDREAE, J. H., 1955, *Ph.D. Thesis*, University of London.

ANDREAE, J. H., BASS, R., HEASELL, E. L., and LAMB, J., 1958, *Acustica*, **8**, 131.

ANDREAE, J. H., HEASELL, E. L., and LAMB, J., 1956, *Proc. Phys. Soc.* B, **69**, 625.

BASS, R., and LAMB, J., 1957, *Proc. Roy. Soc.* A, **243**, 94.

—— 1958, *Ibid.*, **247**, 168.

BAZULIN, P., 1938, *J. Expt. Theor. Phys.*, **8**, 457.

DAVIES, R. O., and LAMB, J., 1957, *Quart. Rev. Chem. Soc.*, **11**, 134.

ECKART, C., 1948, *Phys. Rev.*, **73**, 68.

de Groot, M. S., and Lamb, J., 1957, *Proc. Roy. Soc.* A, **242,** 36.
Heasell, E. L., and Lamb, J., 1956, *Proc. Phys. Soc.* B, **69,** 869.
Hunt, F. V., 1954, *Electroacoustics* (New York: Harvard University Press.)
Karpovich, J., 1954, *J. Acoust. Soc. Amer.*, **26,** 819.
Lamb, J., and Huddart, D. H. A., 1950, *Trans. Faraday Soc.*, **46,** 540.
Lamb, J., and Pinkerton, J. M. M., 1949, *Proc. Roy. Soc.* A, **199,** 114.
Lawley, L. E., and Reed, R. D. C., 1955, *Acustica*, **5,** 316.
Nyborg, W. L., 1953, *J. Acoust. Soc. Amer.*, **25,** 68.
Pellam, J. R., and Galt, J. K., 1946, *J. Chem. Phys.*, **14,** 608.
Piercy, J. E., 1956, *J. Phys. Radium*, **17,** 405.
Piercy, J. E., and Lamb, J., 1954, *Proc. Roy. Soc.* A, **226,** 43.
Pinkerton, J. M. M., 1949, *Proc. Phys. Soc.* B, **62,** 129.
Rapuano, R. A., 1947, *Phys. Rev.*, **72,** 78.
Willard, G. W., 1941, *J. Acoust. Soc. Amer.*, **14,** 438.

Guided Propagation in a slowly varying Medium

By D. E. WESTON

Admiralty Research Laboratory, Teddington, Middlesex

MS. received 17*th July* 1958, *in revised form* 30*th September* 1958

Abstract. Some simple formulae are derived, which are useful in investigating wave propagation in a variable stratified medium. It is shown that the rays in a two-dimensional medium with slowly varying thickness and structure may be described by a characteristic time. From this time the ray angles at any horizontal position may be calculated. The characteristic time formula is also derived from considerations of normal modes, and then from considerations of energy flux. The formula still applies when there are slow bends or twists in the medium, with no limits on final amplitude. The extension to three-dimensional guides is discussed. Some formulae for intensity in slowly varying media are also obtained. The ideas are applied to the propagation of sound (especially underwater), shear wave, and electromagnetic radiation, and the present limitations of the method indicated.

---

§ 1. Introduction

THE problem of long distance sound propagation in the sea, where there is an arbitrary bottom profile and the water structure may vary horizontally, is one for which no rigorous solution is possible using wave methods. The usual approach is to approximate by tracing a series of individual rays out from the source. The work is long and tedious and is therefore often carried out with the aid of an electronic computer. It is difficult to appreciate what is happening, e.g. which of the bottom characteristics are important, and difficult to judge the accuracy of computation necessary. A new approach is described here which shows up the general relations involved and is sufficiently simple in application to be useful in many practical cases. It has been found possible, using equation (1) below, to determine what on the average happens to a ray, or rather a beam of rays, within a small angle.

The generalizations on ray tracing in stratified media are made here specifically for layer thicknesses of many wavelengths, but many of the conclusions still apply at relatively low frequencies (but not to the zero-order mode). The results are applicable to sound waves in any medium and to electromagnetic waves, and hold over a wide range of frequencies. The recent book by Ewing, Jardetzky and Press (1957) may be cited as a general reference on the propagation of elastic waves in layered media; the present treatment is concerned with media having a structure and depth which *vary slowly with horizontal position.* As suggested above, underwater acoustics has many problems in which the above ideas are useful, especially those in which rays are bottom-reflected rather than refracted above the bottom.

For conditions in a bounded stratified medium varying sufficiently slowly, a given ray is shown to obey the relation

$$\int_0^H \frac{\sin\phi dh}{c} = T. \qquad \ldots\ldots(1)$$

Here H is the total depth (of water), h the measurement depth, ϕ the angle the ray makes with the boundaries (often horizontal), and c the local sound velocity. The sign of ϕ is taken positive for both downgoing and upgoing rays. The integral is found to have the dimensions of a time T, which may be called the characteristic time for the ray. By its use the ray angles at one locality may be found from those at another locality, a detailed *knowledge of the intermediate conditions being unnecessary*. Because of the restriction to slow changes it is possible to have a region small enough for changes in depth and structure to be negligible, and yet large enough for the rays considered to suffer many bottom reflections (or refractions), and the term 'locality' is used here and elsewhere with this special meaning. The equation may be derived in any one of three ways, as set out in §§2, 3 and 4. First the straightforward but somewhat clumsy ray-tracing proof is given, since it provides a good physical picture of the meaning behind the equation. Secondly, there is an account of the relation between equation(1) and the eigenvalue equation in mode analysis. Thirdly, the characteristic time formula (equation (1)) is derived, rather more elegantly, from considerations of energy flux. The last approach leads on to some important formulae for calculating intensity, and the limitations and applications of the various equations are also described.

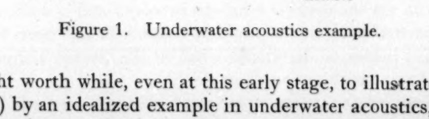

Figure 1. Underwater acoustics example.

It is thought worth while, even at this early stage, to illustrate the usefulness of equation (1) by an idealized example in underwater acoustics, with geometry and velocities as shown in figure 1. Before posing the problem it is necessary to describe the propagation conditions qualitatively. The three layers are assumed fluid, with sound velocities such that $c_3 > c_1 > c_2$. The source is at any depth in isovelocity water of depth H_a, and at this locality all rays having $\cos\phi > c_1/c_3$ suffer total internal reflection at the bottom. Conversely all rays at locality a having $\cos\phi < c_1/c_3$ suffer some loss of amplitude on reflection and after repeated reflections virtually all their energy will be transmitted into the bottom. Thus there is a critical angle defined by $\cos\phi_{\mathrm{crit}} = c_1/c_3$. The sound is supposed to propagate downslope into a layered region having a boundary or 'thermocline' at depth D. In this region the shallower rays in stratum 2 are unable to return to the higher-velocity stratum 1, and the limit for such rays occurs at a critical refraction angle defined by $\cos\phi_{\rm refr}=c_2/c_1$.

Rays leaving the source and propagating into deeper water undergo a series of reflections at the sloping bottom, at each of which the ray angles become shallower (compare figure 3). Detailed ray tracing calculations may be used to show that even the steepest effective ray at the source (angle $\phi_{\rm crit}$) eventually becomes so shallow that in the layered region its angle in stratum 2 is less than $\phi_{\rm refr}$. At this range all the energy will be trapped below the thermocline and there will be no rays in stratum 1, i.e. *zero intensity* for a receiver in the upper layer. The problem posed here is to find the range at which this first occurs. The only conventional method available involves lengthy ray-tracing and a detailed knowledge of the bottom profile.

However, equation (1) shows that the ray angles are controlled primarily by the water depth, and the critical depth corresponding to the critical range is simply found by equating the characteristic times at source and receiver:

$$\frac{H_{\rm a}\sin\phi_{\rm crit}}{c_1}=\frac{(H_{\rm b,\,crit}-D)\sin\phi_{\rm refr}}{c_2} \qquad \ldots\ldots(2)$$

or

$$H_{\rm b,\,crit}=D+H_{\rm a}\sin\phi_{\rm crit}\operatorname{cotan}\phi_{\rm refr}. \qquad \ldots\ldots(3)$$

For, say, $H_{\rm a}=5$ units, $D=6$ units, $\phi_{\rm crit}=0{\cdot}4$ (23°), $\phi_{\rm refr}=0{\cdot}2$ (11°), one has $H_{\rm b,\,crit}=15{\cdot}6$ units. If the critical depth is known the critical range may be read off from the depth profile. It may be shown that a critical distance as short as 200 units would approximately satisfy the condition for slow depth change. This calculation could be applied to water a few fathoms deep for frequencies of a few kilocycles per second, or to water a few thousand fathoms deep for very low frequencies. The method may still be used in more complicated circumstances, when T has to be found by numerical integration.

§ 2. Ray Tracing Derivation of the Characteristic Time Formula

2.1. *The Model*

The model indicated in § 1 is assumed here, i.e. a stratified medium (fluid for acoustic waves) with perfectly reflecting boundaries, the stratification and depth varying only very slowly with position. It is necessary to assume as very small the second as well as the first range derivatives, so that models with corrugated surfaces are ruled out. The stratification is taken not to be so abrupt that there is an appreciable reflected as well as refracted ray. This is justified if the impedance changes occur over a distance of several wavelengths, since the waves reflected from the succesive parts of the region of change interfere with one another and the total reflection is negligible. This restriction to gentle impedance or velocity changes is removed in § 6.2. Completely random density variations, both vertical and horizontal, are allowable provided the changes occupy several wavelengths. The usual ray theory assumptions are made and the medium is assumed to be at rest. The method of derivation is first illustrated by working out the isovelocity case, then the general case is tackled. One of the bounding surfaces is initially assumed plane, like the surface of the sea, but it is shown in § 2.4 that the formula still holds when all the surfaces are curved.

2.2. *Isovelocity Medium*

Consider first the simplest case of an isovelocity medium with plane boundaries, a ray undergoing successive reflections at surface and bottom as in figure 2. From the triangle OPQ

$$\frac{\mathrm{OP}}{\sin\angle\mathrm{OQP}}=\frac{\mathrm{OQ}}{\sin\angle\mathrm{OPQ}} \qquad \ldots\ldots(4)$$

and from the triangle OQP′

$$\frac{\mathrm{OQ}}{\sin\angle\mathrm{OP'Q}}=\frac{\mathrm{OP'}}{\sin\angle\mathrm{OQP'}}. \qquad \ldots\ldots(5)$$

Thus

$$\mathrm{OP}\sin\phi=\mathrm{OQ}\sin\phi=\mathrm{OP'}\sin\phi'. \qquad \ldots\ldots(6)$$

If the depths H and H' are measured along any parallel lines through P and P′ this gives

$$H\sin\phi=H'\sin\phi'=cT,\ \text{a constant} \qquad \ldots\ldots(7)$$

and the relation is preserved along the ray. For *plane* boundaries with this definition of H the relation is thus geometrically exact for *any* bottom slope. This ray approach may be compared with the wave solution for the electromagnetic sectoral horn (Barrow and Chu 1939).

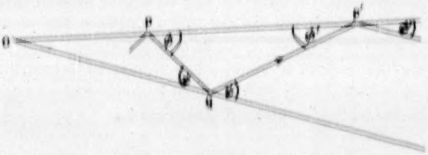

Figure 2. Isovelocity medium with plane boundaries.

Consider now the isovelocity case where bottom curvature is allowed, as in figure 3. The ray is deflected through an angle equal to twice the bottom slope at every bounce on the bottom. For sufficiently small bottom slopes the interbounce distance is very small in comparison with the distance necessary for an appreciable change in depth and a differential equation may be written

$$\frac{d\phi}{dr}=\frac{\text{twice bottom slope}}{\text{interbounce distance}}$$

$$=-\frac{2dH/dr}{2H/\tan\phi} \qquad \ldots\ldots(8)$$

or

$$H\cos\phi\,d\phi+\sin\phi\,dH=0 \qquad \ldots\ldots(9)$$

$$d(H\sin\phi)=0 \qquad \ldots\ldots(10)$$

$$H\sin\phi=cT,\ \text{a constant}. \qquad \ldots\ldots(11)$$

The constant cT could be called the characteristic length for the ray. It may be noted that the bottom slope is supposed always very much less than the ray angle, so that in applying equation (11) ϕ may be measured with respect to either the surface or bottom as convenient.

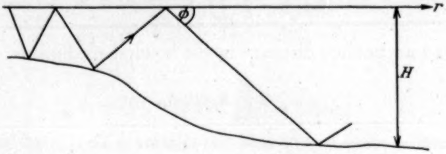

Figure 3. Isovelocity medium with bottom curvature.

2.3. *General Case*

Let there be m strata, a typical one having thickness h_j, sound velocity c_j and ray angle ϕ_j. It may be noted that (ignoring the small distinction between upgoing and downgoing rays), ϕ is now a function of the measurement depth (i.e. the nearest distance h to the upper boundary), the horizontal measurement range r and the source angle or T value. Two kinds of $d\phi$ are used in this paper. First, in this section a ray with a given source angle or T value is assumed and $d\phi$ refers to the changes with vertical and horizontal position, e.g. over the elementary range dr, which range though small must nevertheless be supposed to include a large number of interbounce distances. Secondly, in later sections a given point is taken, and $d\phi$ refers to the beam width corresponding to a small range of source angles or element dT of characteristic time.

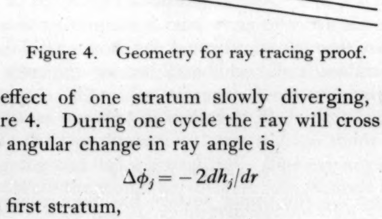

Figure 4. Geometry for ray tracing proof.

Consider the effect of one stratum slowly diverging, the rest remaining parallel, as in figure 4. During one cycle the ray will cross this stratum twice, as shown, and the angular change in ray angle is

$$\Delta\phi_j = -2dh_j/dr \qquad \ldots\ldots(12)$$

or, referred to the first stratum,

$$\Delta\phi_1 = -2\frac{dh_j}{dr}\frac{d\phi_1}{d\phi_j}. \qquad \ldots\ldots(13)$$

If all the strata are now allowed to diverge, the total effect referred to the first stratum is

$$\Delta\phi_1 = -2\frac{d\phi_1}{dr}\sum_{j=1}^{m}\frac{dh_j}{d\phi_j}. \qquad \ldots\ldots(14)$$

The cycle or interbounce distance in the layered medium is

$$2\sum_{j=1}^{m} h_j \cot\phi_j. \qquad \ldots\ldots(15)$$

The differential equation may now be written as in the last subsection

$$\frac{d\phi_1}{dr} = -\frac{(2d\phi_1/dr)\sum_{j=1}^{m} dh_j/d\phi_j}{2\sum_{j=1}^{m} h_j \cot\phi_j} \qquad \ldots\ldots(16)$$

or

$$\sum_{j=1}^{m}\left(h_j\cot\phi_j + \frac{dh_j}{d\phi_j}\right) = 0. \qquad \ldots\ldots(17)$$

Now since all the changes are very slow Snell's law is applicable:

$$\cos\phi/c = K, \text{ a constant for the ray} \qquad \ldots\ldots(18)$$

and

$$-\sin\phi\, d\phi/c = dK, \text{ a constant for the beam.} \qquad \ldots\ldots(19)$$

Equation (7) may be multiplied through by (19), using the appropriate subscripts

$$\sum_{j=1}^{m}\left(\frac{h_j\cos\phi_j d\phi_j}{c_j} + \frac{\sin\phi_j dh_j}{c_j}\right) = 0. \qquad \ldots\ldots(20)$$

On integration this gives

$$\sum_{j=1}^{m}\frac{h_j\sin\phi_j}{c_j} = T, \text{ a constant.} \qquad \ldots\ldots(21)$$

It is necessary to add that T is continuous at any position where a stratum appears or disappears at the surface or bottom. Thus equation (21) may be generalized, the summation always extending over all strata present. If the strata are now supposed to become very thin the summation may be replaced by an integration, giving the desired equation for the characteristic time:

$$\int_0^H \frac{\sin\phi dh}{c} = T. \qquad \ldots\ldots(22)$$

It may be noted that in order to carry out an integration along a ray as in (22) it is necessary to move through a horizontal distance equal to half an interbounce distance. This procedure is allowable only because the cycle distance has been assumed small compared to the distance necessary for an appreciable change in conditions (compare definition of 'locality' in § 1).

2.4. *Curved Surface*

Now in §§ 2.2 and 2.3 the upper surface has been assumed plane, but this restriction is not necessary. Consider an isovelocity medium in which the surface is curved and the angle is θ at any point, causing a typical ray to be turned through the additional angle ψ. If θ and ψ are both initially zero, the successive values at each bounce will be:

$$
\begin{aligned}
\psi_1 &= 2\theta_1 \\
\psi_2 &= 2\theta_1 + 2(\theta_2 - 2\theta_1) = 2(\theta_2 - \theta_1) \\
&\vdots \\
\psi_j &= 2(\theta_j - \theta_{j-1}) + 2(\theta_{j-3} - \theta_{j-4}) + \dots
\end{aligned}
$$

For very gradual bends ($d\theta/dj$ small) the value of ψ_j may be written in the integral form

$$\psi_j \to \int_0^j \to \frac{2d\theta}{2dj}\, dj = \theta_j. \qquad \ldots\ldots(23)$$

Thus if the ray angles are measured with respect to the boundary slope, small curvature of the boundaries may be neglected. In the more general layered medium it is possible to refer the changes in ψ at the bottom to their equivalents at the surface and it is found that the above proof still holds, but the additional changes in slope of the layers cannot be considered in this way. The best procedure is to regard the surface curvature as split into a series of linear segments, one for each interbounce distance. The change from one segment to the next may be considered to occur just before each reflection at the *surface*. Thus for each journey to the bottom and back the rays will be travelling within plane parallel layers where θ does not change. The changes in θ occur only at each surface bounce, and the proof above is valid. It may be noted that with the restriction to *slow* variation it is permissible to consider separately the effects of changes in water structure and in surface slope. In general the characteristic time formula holds for surface slope changes without restriction, provided the changes are slow.

An identical proof may be given if the third dimension is considered and the whole plane twisted. θ is now the angle of twist and can attain any value if the variation is slow.

§ 3. MODE TRANSMISSION DERIVATION OF THE CHARACTERISTIC TIME FORMULA

Now at long ranges from the source a given ray plus its immediate neighbours may be regarded as illuminating the whole layer depth and the idea of rays may usefully give way to the wave concept of modes. For a stratified medium with no horizontal variation the normal modes may be calculated by the 'rays with phase' method. This method is not usually exact, since the reflected waves at small impedance changes are neglected, as described in § 2.1 (compare the WKB approximation). The idea of synthesizing modes by adding together interfering plane waves was first described by Brillouin (1936) and by Page and Adams (1937). In the two-dimensional case a given mode is equivalent to the sum of one downgoing and one upgoing ray. The ray angle is usually different for each mode, and since the modes are discrete only discrete equivalent ray angles are allowed. In a medium which can be represented by a manageable number of homogeneous layers it is possible to take all the various reflected waves into account and make the method exact (Tolstoy 1955).

In its simplest form it is only necessary to calculate the difference in the phase changes along two paths. Any paths which start together and end together may be used, provided that the one path visits both the surface and bottom once more than the other. Thus one path could be chosen to coincide with the ray path from surface to bottom and back, whilst the other lies along the surface. It is easiest however to assume a vertical path to the bottom and back, with zero phase change for the second path. The total phase change along such a vertical path is

$$2\int_0^H \frac{2\pi \sin\phi\, dh}{\lambda} + \Theta_B + \Theta_S = 2\pi N. \qquad \ldots\ldots(24)$$

Here λ is the local value of wavelength, Θ_B and Θ_S are the phase changes on reflection at bottom and surface, and $2\pi N$ is the total phase difference. The condition for reinforcement, i.e. for allowed modes or allowed angles, is that N be an integer. N is in fact the mode number.

The equation may be rewritten (using the pulsatance ω):

$$\int_0^H \frac{\sin\phi\, dh}{c} = \frac{\pi N - \frac{1}{2}(\Theta_B + \Theta_S)}{\omega} = T. \qquad \ldots\ldots(25)$$

This is the same as equation (1), and shows that T is approximately equal to N times the half-period of the wave.

If a mode is transmitted through slow horizontal changes in depth and structure the positions of the nodes (of acoustic pressure) will change, but the dispersion should be small and the *number* of nodes is unlikely to change. Thus a mode may be assumed to keep its identity (and energy content) for slow changes and the constancy of the characteristic time may be considered proved. This is usually true but an exception occurs when there is mode degeneracy (see § 7). Thus there may be more than one type of mode with the same value for N, the same phase velocity, the same equivalent ray angles, and the same T. There may be an interchange of energy between these modes however slowly the horizontal changes occur, but T should always remain constant.

It may be noted that the effects of bends and twists are automatically included in the discussion above.

This derivation shows too that strictly the characteristic time T may only assume discrete values, but for large mode numbers this point is academic. In practice there is always sufficient scattering or energy loss for the higher modes to spread in angle and merge into one another. It is interesting to see that because of this, 'mode' concepts can be applied in unusual places, e.g. for relatively high frequencies in deep water. In addition Θ_B and Θ_S are not in general constant, but will change when the depth and structure change, since the grazing angles at the boundaries change. It is of course N and not T which is really constant, but the distinction is usually unimportant. The lack of strict constancy in T is explained by the fact that neither the incident wave nor the reflecting surface are really plane and, since phase change is a function of angle, the angles of incidence and reflection are *not* in general equal. The concept of the problem is simplified by replacing the real bounding surfaces by neighbouring equivalent surfaces which have no phase change on reflection and if the integration range is extended to these surfaces T becomes once more strictly constant.

Associated with a given mode there is a phase velocity equal to $c \sec\phi$, and according to Snell's law this expression is independent of depth at a given position.

There is also a mean sound velocity for the ray, resolved in a horizontal direction, and equal to

$$\frac{\text{distance along ray for one cycle}}{\text{time along ray for one cycle}} = \int_0^H \cot\phi \, dh \bigg/ \int_0^H \frac{\operatorname{cosec}\phi \, dh}{c}. \qquad \ldots\ldots(26)$$

The velocity of equation (26) also follows from the expression for the mean horizontal velocity with which energy travels in the medium, when wave effects are ignored. It is not the same as the group velocity (defined as $d\omega/dk$ where $k=2\pi/\lambda$) because of the variable phase change at the boundaries, but may often be a very good approximation to it (e.g. at high frequencies far from the mode 'cut off'). Near the 'cut off' frequency of an acoustic mode associated with a real bottom the group velocity is quite different, since Θ_B changes rapidly with glancing angle, corresponding to a large proportion of the energy being carried in the evanescent wave in the bottom.

§ 4. ENERGY FLUX DERIVATION OF THE CHARACTERISTIC TIME FORMULA

It is possible to derive the formula for the characteristic time associated with a ray in yet a third way, from considerations of energy flux. Thus when the total depth *increases* the intensity must *decrease*, in order to keep the total energy flux rate constant. This method assumes for a given ray only that the angle with respect to the boundary surface can be expressed uniquely in terms of the thickness or depth H (structure is a function of H) and the measurement depth h, again for slow variations. It is necessary first to find from ray theory an equation for the intensity, by making use of the reciprocity theorem. The intensity is calculated for the acoustic case and there is a parallel proof for electromagnetic radiation.

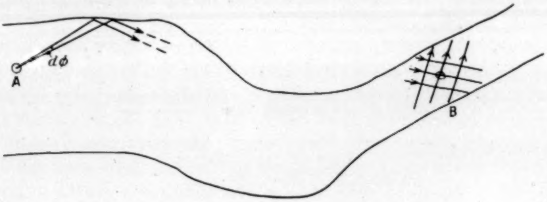

Figure 5. Geometry for energy flux proof.

Consider the propagation between distant points A and B for the two-dimensional model described above. An acoustic line source at A has a power output which may be shown to be proportional to $\rho_A A_A^2$ and independent of c_A. Here A_A is the area velocity of the source (i.e. rate of flow of area, or integral of normal particle velocity along a line enclosing the point A), and ρ_A and c_A are the local values of density and sound velocity. Consider the power per unit length dS which is radiated into the small angle $d\phi$ (between ϕ and $\phi+d\phi$), as in figure 5. This may be written

$$dS = \alpha\rho_A A_A^2 \, d\phi \qquad \ldots\ldots(27)$$

where α is a constant. All this power must flow through the locality near position B, so that

$$dS = \beta p_B^2. \qquad \ldots\ldots(28)$$

Here p_B is the acoustic pressure at B and β is a factor depending only on the local conditions near B (total depth, measurement depth, and structure). This equation will apply if the distance between (A) and (B) is much greater than the distance necessary for the angle range $d\phi$ to illuminate the whole thickness or depth of the medium, so that any focusing effects will have averaged out. Equating (27) and (28) gives

$$\alpha\rho_A A_A^2\, d\phi = \beta p_B^2. \qquad \ldots\ldots(29)$$

Now for a source at B and receiver at A it follows from reciprocity considerations that

$$p_A^2 = \left(\frac{A_B p_B}{A_A}\right)^2 = \frac{A_B^2 \alpha \rho_A d\phi}{\beta}. \qquad \ldots\ldots(30)$$

The intensity at A associated with the angle $d\phi$ is thus

$$dI_A = \frac{p_A^2}{\rho_A c_A} = \left(\frac{\alpha A_B^2}{\beta}\right)\frac{d\phi}{c_A} = \gamma\frac{d\phi}{c_A}. \qquad \ldots\ldots(31)$$

The intensity for the beam thus varies simply as $d\phi/c$. This is an important result which is discussed fully in § 6.

Now the two-dimensional model above gives the correct answer ($d\phi/c$) for variation with both range and measurement depth. Consideration of a three-dimensional medium gives an answer ($\cos\phi d\phi/c^2$) which shows correctly how intensity varies with measurement depth at a given position, but has the wrong range dependence. This arises because depth or structure changes tend to cause a horizontal focusing or defocusing of the beam, so that there is no single value for β. The trouble cannot be overcome by assuming circular symmetry, since in the reciprocity argument this assumption would be separately necessary for both positions A and B (see also § 6.4).

Consider now the rate of energy flux dE through a vertical line near position A, which flux rate must be a constant independent of the horizontal position of A.

$$dE = \int_0^H dI\cos\phi dh = \int_0^H \frac{\gamma d\sin\phi dh}{c} \qquad \ldots\ldots(32)$$

On integration this gives

$$\int_0^H \frac{\sin\phi dh}{c} = \frac{E}{\gamma} = T, \text{ a constant}. \qquad \ldots\ldots(33)$$

The final result holds even if the boundaries are not lossless, and automatically includes the possibility of bends in the medium.

§ 5. THREE-DIMENSIONAL GUIDES

So far the discussion has mainly concerned two-dimensional guides and it is interesting to see what changes may be necessary in three dimensions. In one type of problem there is guiding in one dimension and spreading in the other two, such as for sound propagation between sea surface and sea bed. Hardly any modifications to the arguments are necessary here, as discussed in § 6.4. In the second type of problem there is guiding in two dimensions, as in waveguide tubing, and the application of the above ideas is not so straightforward. It is interesting to digress briefly and explore the limitations of the method.

One special case is the rectangular guide, with walls parallel to the x and y axes. The field within the guide may be regarded as due to the superposition of four almost plane waves, instead of the two waves in the two-dimensional case. Variations of the local velocity within the guide may be treated if they can be expressed in the separable form

$$c = f(x)g(y). \qquad \ldots\ldots(34)$$

For a given mode or equivalent set of rays it is then possible to define two different values of the characteristic time, T_x and T_y, which will each be unchanged for any slow variations in f or g or for slow bends or twists.

A value of T may also be defined for the radially symmetrical modes in a radially symmetrical circular guide, since any mode may be considered as the sum of an infinite number of plane waves by using Sommerfeld's integral.

For a quite general change in cross-sectional shape and velocity structure the energy in a given mode will be transmitted without loss, provided the change is slow enough. It is, of course, necessary that there should be a possible mode in the new guide shape that corresponds to the mode considered in the old shape. For example, consider the illustrated change in section (figure 6) for a rectangular guide, with a half wavelength as the unit of length.

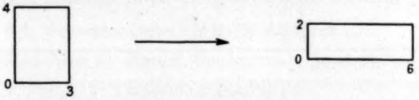

Figure 6. Example of changing guide section.

In the first case there are 3 × 4 possible modes (neglecting the possibility of a zero-order mode) and in the second case 6 × 2 modes. Only six modes are common to both shapes, however, so for equal initial excitation per mode only half the total energy will be transmitted. In general it may be difficult to decide what are the corresponding modes in the new guide shape and this may even depend on the intermediate forms. A theorem due to Weyl (1912) is of interest here; this states that the number of modes in an (isovelocity) enclosed space of arbitrary shape is asymptotically proportional to the volume, when the number is large. It has been used in deriving the radiation formulae of Rayleigh and of Planck and in Debye's theory of the specific heats of solids, as well as in room acoustics. It means that the number of travelling modes possible in a guide is asymptotically proportional to the cross-sectional area (compare the example above), or to the thickness for a two-dimensional medium.

§ 6. INTENSITY FORMULAE

6.1. *Intensity in an Isovelocity Medium*

It was shown in § 4 that the intensity due to a small range of initial ray angles varies as $d\phi/c$ (for a given range of starting angle, or dT). This is for two-dimensional propagation between two nearly parallel perfectly reflecting boundaries, and for the three-dimensional problem with two surfaces a cylindrical spreading term must be added. This varies slowly at long ranges and is neglected in the first three sub-sections of § 6.

Consider now an isovelocity medium, where

$$H \sin\phi = cT. \qquad \ldots\ldots(35)$$

The angular width of the ' beam ' is found by differentiation

$$H\cos\phi d\phi = cdT\,; \qquad \ldots\ldots (36)$$

hence

$$d\phi = \frac{cdT}{H\cos\phi} = \tan\phi\frac{dT}{T} = \frac{cdT}{(H^2 - c^2T^2)^{1/2}}. \qquad \ldots\ldots (37)$$

The beam intensity will therefore vary as $\tan\phi$, or inversely as $(H^2 - c^2T^2)^{1/2}$. Thus, as expected, it is greatest for large angles and small depths. For an omnidirectional source the total integrated intensity is proportional to the local maximum value of ϕ. It may be noted that the steeper source angles contribute as much as the shallower ones, even though there will be a $\cos\phi$ term in the energy flux from the source. This is because intensity is here proportional to energy density and not to energy flux density, so that the ratio of energy flux through unit area in a vertical plane to the intensity produced is also $\cos\phi$.

6.2 *Intensity in a Stratified Medium with No Horizontal Variation*

In a stratified medium Snell's law gives, as in equation (19),

$$\sin\phi d\phi/c = -dK, \text{ a constant}. \qquad \ldots\ldots (38)$$

The intensity due to the beam

$$dI \propto d\phi/c \propto \operatorname{cosec}\phi. \qquad \ldots\ldots (39)$$

An intensity proportional to $\operatorname{cosec}\phi$ may be alternatively stated as an energy density inversely proportional to the normal velocity component, i.e. the total energy in a layer is proportional to the time a ray takes to cross it.

This result may also be derived from first principles, for a model consisting of any number of discrete parallel layers. A particular stratum at one of its boundaries will lose energy at a rate $dI_k \sin\phi_k T_k$ per unit area, where dI_k is the intensity of the wave travelling towards the boundary and T_k is the intensity transmission coefficient. In equilibrium this must be balanced by the incoming energy $dI_{k+1}\sin\phi_{k+1}T_k$ from the neighbouring stratum, the transmission coefficient being the same. In equilibrium, too, the intensities of the wave components travelling towards and away from a boundary in any one stratum must be the same. Thus $dI \propto \operatorname{cosec}\phi$, even where there is imperfect transmission between layers. This result holds down to the lowest frequencies, but it should be remembered that it applies to the ' intensities ' of the component plane waves which for thin layers may differ appreciably from the mean intensities. The equipartition of normal energy flux in the above conditions may be compared with the commonly occurring principle of equipartition of energy. In § 7.2 the relationship is extended to include the case where there are many wave types.

The discussion above removes the restriction of the characteristic time formula to gradual vertical changes, though with abrupt vertical changes the distribution of energy amongst the layers may take longer to reach equilibrium, and stricter interpretation of slowness of horizontal change may therefore be needed.

6.3. *Intensity in the General Two-Dimensional Case*

Now if there are no losses the general formula $d\phi/c$ predicts the relative intensity due to a beam of rays, and reduces to $\operatorname{cosec}\phi$ for the local intensity.

The intensity integrated over all allowed ray angles is proportional to $\phi_{\max}/c$, and to $\phi_{\max}\sec\phi_{\max}$ locally.

If the ray angle considered is allowed to become shallower, or if the measurement position is supposed to change suitably, the value of ϕ in a given stratum will decrease. As $\phi \to 0$ so $d\phi \to \infty$ (or better $d\phi/dT \to \infty$) and $\operatorname{cosec}\phi \to \infty$, i.e. the relative intensity tends to become infinite (according to the ray approximation). If the rays become still shallower they will not be able to penetrate at all into the given stratum. The angle ϕ then becomes imaginary, and only the wave theory 'evanescent' acoustic field is present. It may be noted that as a general ray angle or mode number decreases, so ϕ may become zero and then imaginary in successive strata, which need not even lie next to one another. Thus it is possible for the maximum of intensity to move about in depth in quite a complicated manner. All this occurs, of course, for only one ray, corresponding to infinitesimal total energy. If the intensity due to all rays is considered the effects are somewhat smoothed over. Further limits are placed by wave theory.

6.4. *Intensity in the Three-Dimensional Case*

It is not intended here to discuss the intensity in guides, but rather the intensity for propagation from a point source between two nearly parallel planes. Before considering this it is necessary to look at the extra problem involved in having a component of bottom slope at right angles to the ray direction. This produces a horizontal deflection of the ray towards the thicker part of the layer (or towards the deeper water), which for small slopes may be shown to be equal to the orthogonal component of slope times $2\tan\phi$. The change in the vertical ray angle is still controlled mainly by the parallel slope component, the orthogonal component having only a second order effect. Thus a unique characteristic time still exists, and the values of T (or rather dT) in (42) and (43) below are the same.

For a source A producing unit intensity at unit range the flux through $d\phi_A$ (for ϕ_A both positive and negative) is $4\pi\cos\phi_A d\phi_A$. This may be equated with the total flux at range r that is associated with $d\phi_A$, but to make this calculation it is necessary to assume circular symmetry about the source. At a given range the intensity may be taken as proportional to either $\operatorname{cosec}\phi_B$ or to $d\phi_B/c_B$, say

$$dI_B = \gamma_B d\phi_B/c_B. \qquad \ldots\ldots(40)$$

(Note: ϕ_B is a function of h.) The flux is then

$$2\pi r\int_0^H \gamma_B \frac{d\phi_B}{c_B}\cos\phi_B\, dh = 2\pi r\gamma_B\, dT \qquad \ldots\ldots(41)$$

where T is the characteristic time. If this is solved for γ_B and the results substituted in (40) we find

$$dI_B = \frac{2d\phi_A d\phi_B}{rdT}\frac{\cos\phi_A}{c_B}. \qquad \ldots\ldots(42)$$

Similarly for a source at position B and receiver at A, assuming circular symmetry about B,

$$dI_A = \frac{2d\phi_A d\phi_B}{rdT}\frac{\cos\phi_B}{c_A}. \qquad \ldots\ldots(43)$$

The departure from reciprocity is due to the differences in the shapes of the contours in the two cases and will usually be small, so that either (42) or (43) may be used. The total intensity is of course found by integration over all allowed angles, this integrated intensity being approximately proportional to the maximum local value of ϕ_B.

If an isovelocity medium is supposed, $\cos\phi$ will be greater for the region of greater depth. Thus in an underwater acoustics example consider the propagation from near the top of a seamount at 500 fathoms depth to the surrounding plain at 2000 fathoms depth. It will be slightly worse than that from a basin of 2000 fathoms depth to the surrounding plain at 500 fathoms.

It is also possible to make up examples where the horizontal focusing could be quite important, as in figure 7 (compare a lens). Note how the rays are bent towards the deeper water. This focusing will occur for only one value of ϕ, however, and the overall effect would probably not be significant.

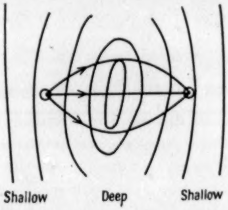

Figure 7. Example of horizontal focusing.

To illustrate the use of the above intensity formulae, consider the example already described in § 1. Take the formula which assumes circular symmetry about the source A (equation 42) and assume loss-free boundaries. Because the water is isovelocity near the source this simplifies to

$$dI_B = 2c_A d\phi_B / c_B r H_A \qquad \text{......(44)}$$

or for the total intensity

$$I_B = 2c_A \phi_{B,\max} / c_B r H_A \qquad \text{......(45)}$$

where $\phi_{B,\max}$ is the steepest ray at the receiver and corresponds to ϕ_{crit} at the source.

For $H_B < D$ the water is isovelocity throughout and

$$I_B = \frac{2}{rH_A} \sin^{-1}\left(\frac{H_A \sin\phi_{\mathrm{crit}}}{H_B}\right). \qquad \text{......(46)}$$

For $H_B = H_A = 5$, $r = 200$, and other values as in § 1, $I_B = 0{\cdot}0008$ or -31 dB. For small depth changes the spreading is of course cylindrical.

Since $\phi_{\max}$ may be found from the characteristic time equation (1) plus Snell's law (18), equation (45) gives immediately the intensity in the general case. For example, in the top layer

$$I_{B1} = \frac{2}{rH_A} \times \sin^{-1}\left[\frac{-D(H_{B,\mathrm{crit}} - D) + (H_B - D)\{(H_{B,\mathrm{crit}} - D)^2 - H_B(H_B - 2D)\}^{1/2}}{H_B(H_B - D)} \tan\phi_{\mathrm{refr}}\right]. \qquad \text{......(47)}$$

This formula confirms that as the critical distance is approached ($H_B \to H_{B,\text{crit}}$) so the intensity falls to zero, since $\phi_{\text{max}} \to 0$.

§ 7. APPLICATIONS

7.1. *Occurrence of Guided Transmission*

The ideas on slowly varying media presented above may be useful wherever there is guided propagation, so the commoner applications in various branches of physics are introduced in this sub-section. In some cases only the qualitative idea of a mode travelling in a bent or changing guide is useful, in others the theory may be applied quantitatively. The applications are mainly to mechanical vibrations and electromagnetic waves and two of the special effects arising are considered in the sub-section following this one. The range of wavelengths is very large : from a fraction of a micron (light waves) or a fraction of a centimetre (ultrasonics) up to several miles (radio waves and seismic waves). Zero-order modes are specifically excluded from the discussion.

In the laboratory gas-filled, liquid-filled and solid (i.e. rod or plate) acoustic waveguides have all been investigated. For example the lowest mode which will propagate in a liquid-filled circular cylinder with compliant walls (' hosepipe ') corresponds to the electromagnetic type H_0 or E_1. Such a hosepipe may be bent or even tied in knots without appreciably affecting its transmission properties. The plane of polarization of ultrasonic shear waves in a sodium chloride crystal has been shown to follow twists in the general crystal structure (Aleksandrov and Khaĭmov-Mal'kov 1956).

In underwater acoustics the problem is essentially two-dimensional, and a wide range of depths is encountered. Guiding may occur (i) due to successive reflections at the surface and bottom of the sea, the detailed theory of the two-layer model being given by Pekeris (1948), (ii) due to refraction in the water keeping the energy within a natural sound channel, such as the SOFAR channel (Ewing and Worzel 1948), (iii) due to a combination of reflection and refraction. In sufficiently shallow water or in shallow sound channels frequencies of several kilocycles per second (wavelengths of several inches) may be effectively trapped and spread cylindrically. At the other extreme in the deep ocean basins very low frequency modes may be excited by shallow-focus earthquakes: the T-phase at 2 c/s and above travelling with the velocity of sound (Tolstoy and Ewing 1950) and the Airy phase at about 0.1 c/s (Press, Ewing and Tolstoy 1950). Waves can also propagate in the bottom material and may be of the longitudinal or shear type. The general theory for elastic waves in layered media has been given by Ewing, Jardetzky and Press (1957) who also describe its application to seismology and geophysical prospecting. In the atmosphere shallow sound channels trapping high frequencies are perhaps less common than in the sea, but they occur for example with temperature inversions. The whispering gallery phenomenon is really of the same nature. At the other end of the scale the atmosphere is able to trap waves of several seconds period and the atmospheric tidal waves (such as those excited by the Krakatoa eruption) are an extreme example. It may be noted that the low frequency waves in both the atmosphere and the sea are propagating in a medium with curved boundaries.

Now light rays may be transmitted without loss down a rod of transparent material, undergoing total internal reflection at each boundary. This has recently been applied (Hopkins and Kapany 1955) in the fibrescope, consisting of a bundle of glass fibres each of which may be 25μ in diameter (about 50 wavelengths) and up to 75 cm long. A picture thrown on one end of the bundle is reproduced at the other end, so that the device may be used as a bronchoscope, or gastroscope, etc., for the examination of lungs or stomach. The point of interest here is that such bundles of fibres are flexible and may be bent through large angles without their optical properties being changed.

Transmission of electromagnetic waves in artificial waveguides for the centimetre wavelength region has become increasingly important since the late 1930's. This has led to theoretical work on propagation in special forms having a variable cross section, such as conical and sectoral horns, starting with Barrow and Chu in 1939 (see Lamont 1950). Bent waveguides are very common in practice and many theoretical papers have been written, usually starting from the wave equation in a guide with circular curvature (Buchholz 1939 etc., see Lamont 1950). Inhomogeneous and anisotropic guides have also been examined.

In the atmosphere anomalous propagation sometimes occurs for radio waves of frequency above about 1000 Mc/s (30 cm), the energy travelling with little loss in quite shallow ducts (of the order of hundreds of feet). In addition, for frequencies roughly 20 kc/s to 30 Mc/s (15 km to 10 m) the waves may be guided to long distances between the surface of the earth and the ionosphere, the latter extending upwards from about 60 km.

7.2. *Applicability of the Formulae*

The possibility of waves with transverse vibrations, as discussed in § 7.1, leads to some new effects. These are divided into two groups in the discussion below. It is not intended here to treat the case of the zero-order mode. Thus modes associated essentially with only one interface are excluded from treatment, such modes being possible when there is rigidity, absorption, surface roughness, a gravitational field etc.

First note that transverse vibrations may be polarized in two orthogonal directions. This means it is possible to have degenerate modes, i.e. different modes having the same phase velocity. This sometimes occurs in electromagnetic guides, but is not usual for shear waves since the waves of different polarization will normally be coupled through the longitudinal wave. If there is true degeneracy there is liable to be an interchange of energy between the modes; on a slow bend, for example, this interchange may be independent of the slowness and depend only on the total angle of turn. The characteristic time formula still applies to degenerate modes, but intensity formulae should be used with great care. It may be noted that any slight distortion in the guide is likely to remove the degeneracy and for such almost-degenerate modes there will be no interchange if all guide variatons occur sufficiently slowly.

Secondly, observe that different wave or ray types may be present in the same mode. In a rod for example the shear waves are coupled to the longitudinal waves by reflection at the boundaries. In the two-dimensional case a shear wave with displacements parallel to a boundary (the SH wave in seismological notation) is reflected without change of type at the boundaries and a purely shear wave mode is possible, but this is an exception. In the general case of a layered elastic medium it is possible to find the mode eigenvalues etc. by a development of the rays with phase method (Tolstoy and Usdin 1953). In an anisotropic elastic medium there is more than one shear wave ray, these rays having different velocities and angles, and all being coupled together in the one mode, through interface effects. This is similar to the phenomenon of double refraction or birefringence in electromagnetic waves, which leads to sets of ordinary *and* extraordinary rays for light modes travelling in crystal rods or for electromagnetic waves travelling in guides filled with anisotropic material. It is shown in the next paragraphs that the intensities of each ray type in each stratum are proportional to cosec ϕ, by an extension of the argument in § 6.2. The additional ray types may be regarded as travelling separately in additional strata and the expression which remains constant in changing conditions is therefore the *sum* of the characteristic time integrals for all the different ray types. However, after a disturbance, some time or distance may be needed for the appropriate equilibrium distribution of intensities to be attained, so that a stricter interpretation of slowness of variation will again be needed. A further modification is needed if *all* the ray types are *not* present in *all* the strata, as indicated below (equation (53)).

Consider a layered medium having no horizontal variation, with n ray types possible in a given stratum. The subscripts 1 to n refer to the ray type, u and d to upgoing and downgoing rays, and F_j is the rate of arrival or departure of energy per unit area of interface. In equilibrium conditions the upper boundary of the stratum may be regarded as totally reflecting, with intensity conversion coefficient from $F_{k\mathrm{u}}$ to $F_{j\mathrm{d}}$ equal to T_{kj}. There are n equations for the downgoing rays, a typical one being

$$F_{j\mathrm{d}} = \sum_{k=1}^{n} T_{kj} F_{k\mathrm{u}}. \qquad \ldots\ldots (48)$$

The typical equation at the lower boundary is

$$F_{j\mathrm{u}} = \sum_{k=1}^{n} T'_{kj} F_{k\mathrm{d}}. \qquad \ldots\ldots (49)$$

Also the mean rate of energy transport across the stratum must be zero:

$$\sum_{j=1}^{n} F_{j\mathrm{u}} = \sum_{j=1}^{n} F_{j\mathrm{d}}. \qquad \ldots\ldots (50)$$

If all equations of type (48) are added together one obtains

$$\sum_{j=1}^{n} F_{j\mathrm{d}} = \sum_{k=1}^{n} F_{k\mathrm{u}} \sum_{j=1}^{n} T_{kj}, \qquad \ldots\ldots (51)$$

but since $\sum_{j=1}^{n} T_{kj} = 1$ this reduces to (50), as does the sum of all type (49) equations. Thus there are $2n-1$ linear independent equations and $2n$ unknown values of F (the values of T and T' are ' given '). The obvious solution, which must also be unique, is

$$F = \text{constant for stratum.} \qquad \ldots\ldots (52)$$

Thus F is independent of both ray type and direction and is equal to intensity multiplied by $\sin\phi$.

As an example it may be seen that the ratios of the intensities for the longitudinal and shear wave components of the coupled mode in a plate are equal to the ratio of their cosec ϕ values, provided the intensities are averaged over a number of neighbouring modes to get rid of wave effects.

If all the ray types in a stratum are lumped together the argument of § 6.2 shows that ΣF is constant from stratum to stratum. If n is constant (including the case where the same ray types are present in each stratum, but different types are possible provided the total number per stratum is constant) the intensities are proportional to cosec ϕ, independent of ray type, direction, and stratum. In general, at a given horizontal position intensity is proportional to cosec ϕ/n, and the characteristic time must be replaced by a sum of the integrals for all wave types:

$$\Sigma\int_0^H \frac{\sin\phi\, dh}{nc} = T. \qquad \ldots\ldots(53)$$

The completely general statement for the intensity is now that it is proportional to $d\phi/nc$. These formulae cover the case where strata, in which extra wave types can propagate, slowly appear or disappear.

§ 8. LIMITATIONS

Some of the limitations to the characteristic time and intensity equations have already been touched on above. The most important is the requirement for infinitesimally slow horizontal changes. For too fast a change there will be dispersion in the value of the characteristic time T, energy passing into neighbouring modes. It should be noted that the slope of the boundaries and interfaces is not the only criterion, and rate of change of slope (i.e. curvature) plus even higher derivatives are of importance.

In a simple case, such as an isovelocity medium with changing depth, the interpretation of ' slow ' may not be very strict. For a 2 to 1 depth variation there should be sufficient distance for several reflections of a typical ray, say three cycle distances, each equal to four times the water depth for a ray with $\tan\phi = \frac{1}{2}$. Thus at least 12 times the mean water depth is the distance necessary for the formulae to hold approximately, corresponding to about 2° bottom slope. It is possible to extend this approach to find out what the spread in the value of T actually is. Thus in the present example suppose there are two regions of constant depth connected by one of constant slope. Some of the rays will undergo one more slope reflection than the rest, so the spread in the final angle will be twice the bottom slope or 4°.

It was pointed out in § 6 that the changes must be rather slower for layered media having sharp interfaces, and in § 7 that they must be slower still where several ray types are possible. Slow changes are also necessary for near-degenerate modes, where the intensity formulae must also be used carefully (§ 7). Consider what happens, too, when there develops at about mid-depth a high-velocity layer which the rays cannot penetrate. This splits the illuminated field into two parts, between which there can still be an interchange of energy by the ' tunnel ' effect due to the evanescent wave field. The limit of what can be accepted as a slow horizontal change will now be so strict as to make the applicability of the theory of academic interest only.

Great care must be taken in applying the theory when the total layer thickness is reduced between two measurement points. As the layer becomes thinner so all the rays become steeper and for a large reduction some of the rays may become vertical (i.e. normal to the boundaries). These rays will then be reflected back along their original horizontal path, the value of T still remaining constant. In practice, with boundaries that are not completely loss-free there is likely to be almost complete absorption of such rays, due to the large number of high-angle reflections.

Besides the slowness limitation the following points should be borne in mind:

(*a*) When the ray angles are correct the mean intensity *along* a layer is predictable, but the local intensity may vary rapidly with range. Such effects arise when there is vertical focusing due to the velocity structure and bottom shape. They are most important at short distances but may sometimes persist to long ranges.

(*b*) Wave effects, such as interference near boundaries and diffraction into shadow zones, may occur.

(*c*) Scattering may take place in the body of the medium and at either boundary, dispersing the energy amongst the different modes. For a boundary the term ' scattering ' may be used to describe the effects of roughnesses or irregularities varying in scale from a wavelength to several interbounce distances.

(*d*) In calculating intensity an allowance must in general be made for the absorption in the medium and the reflection losses at the boundaries.

(*e*) The possibility of energy travelling outside the layers considered (e.g. in the sea-bed) must be remembered.

(*f*) If there is no loss for rays beneath a certain critical angle the usual intensity calculations would consider only such rays, steeper rays being greatly attenuated after a few reflections. For a finite slope this critical angle will be slightly changed and there may also be a significant contribution from rays beyond the critical angle.

§ 9. CONCLUSIONS

(*a*) Some equations have been developed which are useful in describing the propagation of elastic or electromagnetic waves in a variable stratified medium. There is particular application to underwater sound transmission in water of variable depth.

(*b*) The characteristic time formula (equation (1)) makes it possible to calculate ray angles knowing only the local velocity structure, provided the horizontal changes in structure have been sufficiently slow. The formula holds for abrupt vertical changes in velocity and density (assuming elastic waves), for random slow changes in density, for slow bends and twists, and in both two- and three-dimensional layered media. Equation (53) shows the form when any number of different ray types is permitted.

(*c*) The intensity due to a set of rays in such a slowly varying medium is in general proportional to $d\phi/nc$, where n is the number of ray types in the stratum. If there is no horizontal variation, intensity is proportional to $\operatorname{cosec}\phi/n$. Specific formulae for the transmission loss in three dimensions are given in equations (42) and (43).

ACKNOWLEDGMENTS

The writer is indebted to Mr. A. G. D. Watson for many helpful discussions.

REFERENCES

ALEKSANDROV, K. S., and KHAĬMOV-MAL'KOV, V. YA., 1956, *Kristallografiya*, **1**, No. 3, 373–4.
BARROW, W. L., and CHU, L. J., 1939, *Proc. Inst. Radio Engrs, N.Y.*, **27**, 51.
BRILLOUIN, L., 1936, *Rev. Gén. Élect.*, **40**, 227.
BUCHHOLZ, H., 1939, *Elekt. Nachr. Tech.*, **16**, 73.

Ewing, M., Jardetzky, W. S., and Press, F., 1957, *Elastic Waves in Layered Media* (New York: McGraw-Hill).
Ewing, M., and Worzel, J. L., 1948, *Geol. Soc. Amer. Mem.* 27.
Hopkins, H. H., and Kapany, N. S., 1955, *Optica Acta*, **1**, 164.
Lamont, H. R. L., 1950, *Wave Guides* (3rd edn) (London: Methuen).
Page, L., and Adams, N. I., 1937, *Phys. Rev.*, **52**, 647.
Pekeris, C. L., 1948, *Geol. Amer. Soc. Mem.* 27.
Press, F., Ewing, M., and Tolstoy, I., 1950, *Bull. Seismol. Soc. Amer.*, **40**, 111.
Tolstoy, I., 1955, *J. Acoust. Soc. Amer.*, **27**, 274.
Tolstoy, I., and Ewing, M., 1950, *Bull. Seismol. Soc. Amer.*, **40**, 25.
Tolstoy, I., and Usdin, E., 1953, *Geophysics*, **18**, 844.
Weyl, H., 1912, *Math. Ann.*, **71**, 441.

Diamond Conduction Counters with Small Electrode Separations

By F. C. CHAMPION and S. B. WRIGHT

Department of Physics, University of London, King's College

MS. received 15*th September* 1958

Abstract. Using good diamond counters and variable electrode separations from $10\,\mu$ up to 1 mm, a survey of the surfaces of several specimens allowed the selection of crystals with the most uniform behaviour. The variation of the characteristics of the (pulse height, field) curve with electrode separation, could not be explained for these crystals simply in terms of trapping distribution or field distortion due to dark current. There is evidence that recombination of charge carriers at recombination centres close to the site of ionization is the dominating feature and dislocations are probably the defects responsible.

---

§ 1. INTRODUCTION

THE variation of the counting properties of diamonds at different electroed separations has been studied in an attempt to explain the magnitude of the charge pulse produced by ionizing radiations such as α-particles; the gap widths have been varied from $10\,\mu$ up to 1 mm. The best counting diamonds were used and a survey of the surfaces of the specimens was carried out in order to select crystals with counting properties which were as uniform as possible across the surface. No perfectly uniform crystal was found but allowance could be made for small variations. A polonium source provided α-particles of homogeneous energy 5·3 Mev but the introduction of aluminium absorbing foils also allowed lower energies to be used.

§ 2. EXPERIMENTAL

The apparatus used in these experiments is shown in figure 1. It enabled the position of each electrode on the surface of the diamond to be adjusted quickly and easily. The diamond was mounted on a Perspex insulator which could be raised or lowered by means of three levelling screws to bring the surface of the crystal into the plane of the electrodes. The Perspex insulator could be rotated through 360°. On either side of the diamond mount was a steel trolley kinematically mounted so that it was free to move only in the direction towards the diamond mounting. Each trolley carried a Perspex insulator about 1 in. thick to which was fixed an electrode consisting of a small piece of razor blade spot welded to a steel needle held in a pin chuck. Screws pressing against the needle in the horizontal direction enabled the needle to be flexed slightly to bring the edges of the electrodes parallel to each other, and perpendicular to the direction of motion of the electrode trolleys. The electrodes could thus be changed quickly when they became chipped by rubbing on the diamond surface. A kinematic lever with a 5 to 1 reduction ratio driven by a micrometer was used to drive each electrode trolley. In this way it was possible to move the electrodes accurately $1\,\mu$ at a time. There was no observable backlash in the system. Coil springs were used to hold the electrode trolleys and levers firmly on the baseplate of the instrument, and also to act as return springs for the system.

In order to use the diamond for the detection of α-particles it was necessary to evacuate the system to eliminate gas discharge. The electrode system was therefore enclosed in a vacuum tight brass cylinder, which also acted as an electrical screen. The micrometers were mounted in the wall of the vacuum can through O-ring seals so that the position of the electrodes could be altered without releasing the vacuum. A small quartz window was fixed in the wall of the vacuum chamber to enable the crystal to be irradiated with either visible or ultra-violet light. This was necessary in order to depolarize the diamonds after a period of counting. The polonium source was mounted directly above the diamond, and was provided with a brass shutter operated from outside the can through an O-ring seal. Aluminium foils of varying thicknesses were mounted on a disc arranged so that each foil could be brought between the source and the crystal. In this way α-particles with energies ranging from 5·3 MeV down to approximately 0·7 MeV were available.

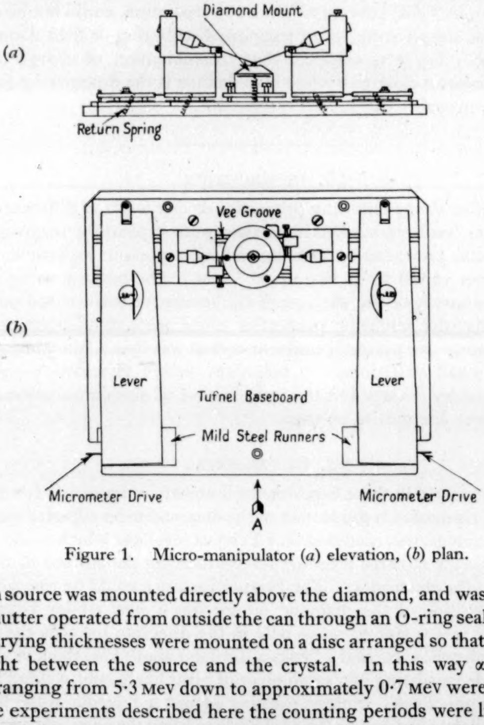

Figure 1. Micro-manipulator (*a*) elevation, (*b*) plan.

In the experiments described here the counting periods were limited to a few seconds and the crystal could be depolarized by irradiation with white light for about 1 minute. In this way it was found that repeatable results could be obtained without polarization fields building up in the crystal.

The variation of the counting properties across the surface of several specimens was examined. This was done by moving the electrode separation 5–100 μ and plotting the maximum pulse height observed against the applied field. The slope of the (maximum pulse height, field) curve at low fields, and also the saturation value reached at high fields were used as measures of the counting properties of the diamond at that particular part of the crystal surface. As the depth of penetration of 5 MeV α-particles in diamond is only of the order of 15 μ the ionization is confined to the surface layers of the crystal. The effect of distortion of the field along the length of the α-particle track on the pulse height was investigated using α-particles of different energies, and comparing the pulse heights observed. Any field distortion present would be shown as a reduced field effect on the ions, as the α-particle moves farther into the crystal. Thus if field distortion is present the pulses observed will not be proportional to the α-particle energy.

The most uniform crystals found in the tests outlined above were used to investigate the effect of variation of the electrode separation on the counting properties of the crystal. Again the curve of maximum pulse height against field was plotted at each electrode separation ; the initial slope at low fields and the maximum saturation value reached at high fields were used as measures of the counting properties. On the crystal specimens available, and with the apparatus described, it was possible to use electrode separations from 10 μ up to 1 mm. Again the effects of field distortion on the results was investigated by the use of α-particles of different energies.

§ 3. RESULTS

The results of the scan of a crystal surface for three diamonds are shown in figure 2. In this diagram the initial slope of the (maximum pulse height, field saturation) curve is used as the measure of the counting properties, and is plotted

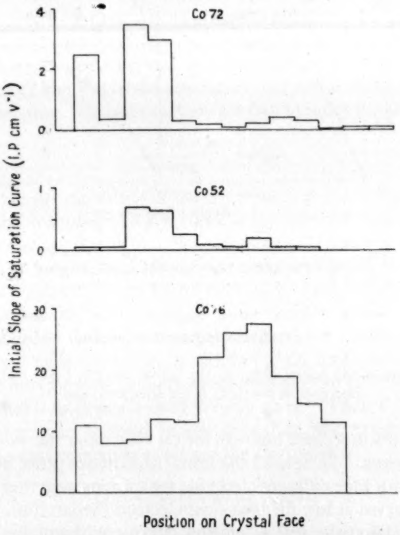

Figure 2. Variation of initial slope of (pulse height, field) curve with position on crystal face.

against the position on the crystal surface. Crystals Co 52 and Co 72 are typical of most of the diamonds tested, giving quite good counting pulses on one part of the crystal surface, and few or no counts on the remainder of the surface. With Co 52 the largest pulses obtained on the best portion of the crystal were equivalent to 60 000 ion pairs, and with Co 72 the largest pulses corresponded to 160 000 ion pairs.

The third crystal, Co 76, was most uniform, giving maximum pulses of the order of 250 000 ion pairs on all parts of the surfaces tested. The initial slope of the saturation curve was found to vary from 7·5 ion pairs cm per volt up to a maximum of 30 ion pairs cm per volt. On the part of the crystal which gave the highest initial slope to the saturation curve, breakdown or multiplication pulses could be obtained much more readily than on other parts of the surface. As already described by Taylor (1956), these pulses are very much larger than the normal counting pulses, sometimes reaching several million ion pairs in height, and they are usually only observed after counting has been in progress for several seconds.

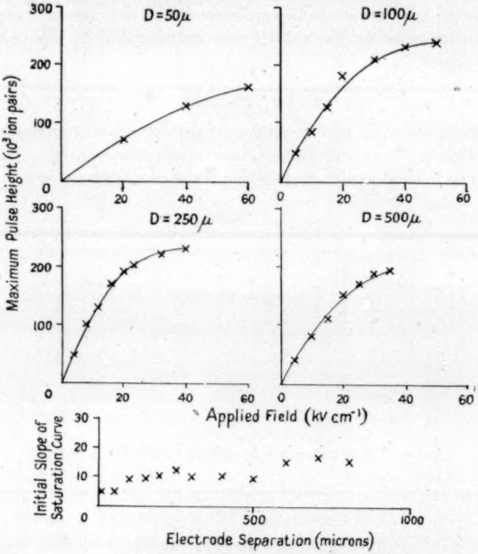

Figure 3. Variation of the initial slope of the (pulse height, field) curve as a function of electrode separation D for specimen Co 76.

Although results described here are for Co 76, similar behaviour was observed with other specimens. In figure 3 the initial (maximum pulse height, saturation) curves are shown for four different electrode separations, together with a plot of the slopes of these curves at low fields against electrode separation. At the smallest separation used ($10\,\mu$) the full saturation curve could not be obtained due to electrical breakdown at high fields. It was found that for separations of $50\,\mu$ and over the maximum value reached by the saturation curve lay between 200 000 and 300 000 ion pairs, and did not vary systematically with electrode separation. Also the initial slope of the saturation curve was found to be approximately constant over a wide range of electrode separations. At an electrode separation of 1 mm the very good counting region of Co 76 found in the previous test was beginning to appear between the electrodes, and this could account for the rise on the slope of the saturation curve at this separation.

The maximum pulse height was also plotted against α-particle energy at various electrode separations. These results were not all taken at the same field, but they were all taken towards the top of the linear portion of the saturation curves. The fact that these are consistently straight lines indicates that any field distortion in the crystal is not significantly affecting the observed pulses. Full saturation curves for the various energy α-particles were plotted at some electrode separations, and these were found to be proportional to the α-particle energy within the experimental error right down to the smallest field strengths used.

§ 4. DISCUSSION

The theory usually used for the treatment of conduction pulses in crystals is that developed by Hecht (1932) for photocurrents. This was applied to the case of charges released by ionizing particles in crystal counters by Hofstadter (1949). In this theory it is assumed that the crystal contains uniformly distributed trapping sites. Under these conditions the expression obtained for the charge pulse induced on the electrodes is of the form

$$Q=\frac{N\mathbf{e}\,\delta}{D}\,[1-\exp(-D/\delta)] \qquad \ldots\ldots(1)$$

where Q is the charge pulse observed, N is the number of ion pairs released, $\mathbf{e}$ the electronic charge, D the electrode separation and δ the mean separation of the charges before trapping. If both carriers are free to move in the crystal then

$$\delta=\frac{E}{nsu}\,(\mu_{\mathrm{e}}+\mu_{\mathrm{h}}) \qquad \ldots\ldots(2)$$

where μ_{e} and μ_{h} are the mobilities of the electrons and holes respectively, n is the trap density, s the trapping cross section, u the thermal velocity of the charge carriers, and E is the applied field. An expression of this form can be made to fit the observed (pulse height, field saturation) curve very well.

It has, however, already been found necessary to modify the simple theory in order to account for the wide range of pulse heights which is observed when crystals are bombarded with monoenergetic α-particles. The simplest modification to the theory is to assume that, in addition to the uniform trapping density in the crystal, there are trapping barriers which stop most or all of the charge carriers, dividing the crystal into crystallites of varying sizes. Then if S is the maximum distance the charges can separate in any crystallite, the equation for the charge pulse produced in that crystallite as seen at the electrodes is

$$Q=\frac{N\mathbf{e}\,\delta}{D}\,[1-\exp(-S/\delta)]. \qquad \ldots\ldots(3)$$

Trapping barriers of this kind have been proposed by Freeman and van der Velden (1951) and by Champion (1953).

At low fields, before saturation of the pulse height begins, both equations (1) and (3) give a slope

$$\frac{dQ}{dE} = \frac{Ne\mu}{nsuD}. \qquad \ldots\ldots(4)$$

The initial slope of the (pulse height, field) curve should therefore be inversely proportional to D, independent of whether the motion of the charges is restricted by trapping barriers or not. Since the present experiment shows the initial slope to be independent of the gap width D, the theory is inadequate. Again, equation (3) indicates that for S less than D, the maximum pulse height should be proportional to S/D while for S greater than D it should be independent of D. Actually it is found that the saturation pulse height is consistently independent of D and hence the suggestion that barrier layers might be the cause of the wide range of pulse heights observed with monoenergetic α-particles cannot be correct.

Hecht's theory as outlined above depends on two basic postulates, firstly that the trap density in the crystal is uniform, and secondly that when the charges are released by ionization no recombination occurs. A non-uniform trap distribution carried to the limit passes over into the barrier layers postulated by Champion and while these are probably responsible for various polarization phenomena and certain electroluminescent effects, such barriers have just been shown to be inadequate to explain the wide distribution of pulse heights given by monoenergetic α-particles. It therefore seems that the second assumption that no recombination occurs must be modified. Before considering recombination, however, it must first be demonstrated that the non-uniform electric field distribution, emphasized by Taylor (1956), cannot account for the spread of pulse heights. Taylor showed that in diamonds conveying appreciable dark current a non-uniform field may be set up across the diamond which, because of resulting space charge phenomena, would give a non-uniform distribution of pulse heights for monoenergetic particles. A direct test was made of this theory on the present specimens by fixing the electrodes and then scanning various regions of the crystal with finely collimated α-ray beams. No appreciable variation in pulse height was found with changing position of bombardment relative to the electrodes either in a direction perpendicular or parallel to them. A similar result had already been observed with other specimens by Stratton (1957). All these experiments therefore indicated that the basic feature governing the size of the α-ray pulse height was some intrinsic property of the crystal itself at the position of the ionizing process.

It is therefore suggested that this intrinsic property gives rise to recombination centres and it will now be shown that on this assumption it is possible to give an explanation of both the pulse height spectrum and the behaviour at saturation. If it is supposed that recombination can take place only when carriers of both signs are close to recombination centres and, conversely, that once the carriers have moved away from these centres they are then free (apart from trapping) to move to the electrodes, then the amount of recombination which occurs at any ionizing event will depend on the density or proximity of recombination centres in the region of ionization and on the time which the charge carriers spend close to that region. The relative values of S and D will be almost irrelevant since the possible maximum pulse height is no longer primarily dependent on trapping phenomena but depends basically on the recombination probability in the vicinity of the ionization process.

With this assumption, the pulse height spectrum may be explained in two ways, either by assuming that the density of recombination centres varies from place to place in the crystal, or that the crystal contains extended regions of recombination centres separated by regions where little or no recombination takes place. There is reason to believe that both situations occur; in the second case an ionizing particle striking close to a recombination region will produce a small pulse and one striking further away gives a correspondingly larger pulse.

Before discussing the nature of the defects which act as the recombination centres we recall that when counting diamonds are bombarded with neutrons or electrons of sufficiently high energy, irradiation damage occurs and the counting rate and pulse height decrease (Benny and Champion 1956, Dolphin and Stratton 1957). The defects produced by irradiation damage must certainly consist of single or multiple vacant sites and complementary interstitial atoms. If the irradiated specimens are heated to about 500°C, partial annealing occurs as shown by partial restoration of the pulse height. No such annealing occurs in non-irradiated specimens and hence it is concluded that the natural defects primarily responsible for the pulse spectrum must be either (*a*) quite different from the defects produced by irradiation or (*b*) the same as the residual defects produced by irradiation which resist annealing. However, these residual defects cause a permanent yellow discoloration of initially water-white specimens at a concentration which produces a reduction in pulse height of much less than 50% of its original value. It is therefore clear that the natural defects in non-irradiated water-white specimens, while playing a dominant role in controlling the pulse height spectrum, do not show accompanying optical effects in the absorption spectrum in the visible range of wavelengths.

It is therefore reasonable to suppose that these natural defects must be of such a nature that they are more spatially extensive yet less individually powerful in their optical effects than vacant sites or interstitial atoms. Now van Heerden (1957) has suggested that when highly perfect crystals of cadmium sulphide are used as counters, the applied electric field is only of the same order as the recombination field of the ions along the track of an α-particle. A relatively weak imperfection may therefore be sufficient to distort the applied electric field sufficiently to tip the balance in favour of recombination. It is suggested that these extended recombination centres in diamond, where they are even weaker optically than single vacant sites, are relatively small but spatially extensive displacements of planes of atoms, that is, dislocations. Such defects could not be produced by radiation damage but they would be expected to be produced in plenty in the conditions of high temperature and pressure demanded for diamond growth.

The amount of charge eventually able to form a conduction pulse is the amount remaining after recombination has occurred in the vicinity of extended dislocations in the region close to the α-particle track. As fluorescent recombination is the cause of the scintillations observed when α-particles impinge on diamonds there may be a close connection between the behaviour of a diamond as a scintillation counter and as a conduction counter. Such experiments are in progress and will be reported later. Meanwhile it should be further pointed out that the pulse height falls steadily as irradiation damage increases, even for pulses formed at saturation fields. This would be difficult to explain if simple trapping of charges by the effects induced by irradiation were entirely responsible for the progressive reduction in pulse height. If, however, the vacant sites and interstitial defects act not only as trapping sites but also as further agents to distort and reduce the applied electric field, their presence will increase the effective range of action of the dislocations already present as recombination centres and hence the pulse height, even at maximum field strength will decrease with bombardment dosage as observed.

§ 5. CONCLUSION

The experiments described show that the trapping barrier model for diamond counters is not sufficient to explain the observed (pulse height, field) curves. Recombination of charge carriers at recombination centres close to the site of ionization does, however, afford a qualitative explanation of the saturation curve and pulse height spectra observed for α-particles incident on diamonds. It is still necessary however, to assume some trapping of charges in the crystal to account for polarization effects, glow curves and various other electrical and optical phenomena.

ACKNOWLEDGMENTS

We should like to thank Mr. Cotty of the Diamond Corporation for supplying suitable diamonds for these experiments. One of us (S. B. W.) is indebted to the Department of Scientific and Industrial Research for a maintenance grant.

REFERENCES

BENNY, A. H. B., and CHAMPION, F. C., 1956, *Proc. Roy. Soc.* A, **234,** 432.
CHAMPION, F. C.. 1953, *Proc. Roy. Soc.* A, **220,** 485.
DOLPHIN, G. W., and STRATTON, K., 1957, *Proc. Roy. Soc.* A, **244,** 424.
FREEMAN, G. P., and VAN DER VELDEN, H. A., 1951, *Physica,* **17,** 565.
HECHT, K., 1932, *Z. Phys.* **77,** 235.
VAN HEERDEN, P. J., 1957, *Phys. Rev.,* **106,** 468.
HOFSTADTER, R., 1949, *Nucleonics,* **4,** 2, **5,** 29.
STRATTON, K., 1957, *Ph.D. Thesis,* University of London.
TAYLOR, K. W., 1956, *Ph.D. Thesis,* University of London.

The Thermoelectric Power of a Semiconducting Diamond

By H. J. GOLDSMID, C. C. JENNS and D. A. WRIGHT
Communication from the Staff of the Research Laboratories of
The General Electric Company Limited, Wembley, England

MS. received 14*th November* 1958, *in final form* 23*rd December* 1958.

Abstract. The thermoelectric power of a p-type semiconducting diamond has been measured in the temperature range 220°K to 700°K. After subtracting an electronic component, estimated from the previous Hall effect measurements on the sample, it has been possible to determine the phonon-drag component of the thermoelectric power. This component has been found to vary with temperature approximately as $T^{-3\cdot6}$, with a value of about 2·5 mv $\deg^{-1}$ at room temperature. The magnitude of the effect is of the order to be expected from the known behaviour of germanium and silicon.

---

§ 1. Introduction

It was found by Frederikse (1953) and by Geballe and Hull (1954) that the thermoelectric power of germanium at low temperatures rises to much higher values than are expected from the usual electron theory. Herring (1954) and Frederikse were able to explain these observations by showing that when there is a temperature gradient, the flow of phonons from the hot to the cold region of a crystal results in preferential scattering of electrons in the same direction. An additional thermoelectric voltage results from this flow of electrons; the phenomenon is called the phonon-drag effect.

Geballe and Hull (1955) found that the same effect occurs in silicon, in which case it is more marked,—thermoelectric powers of more than 50 mv $\deg^{-1}$ have been observed—and it is appreciable at higher temperatures than in germanium. It was, therefore, thought that, if it could be measured in diamond, the thermoelectric power should show a phonon-drag component at room temperature and above. Usually, the resistivity of diamond is between 10^{14} and 10^{16} Ω cm, so that the determination of the thermoelectric power is not possible, but recently several type II diamonds having a much lower resistivity have been discovered (Custers 1952, 1954). In particular, one diamond of this class (Type IIb) was found by Austin and Wolfe (1956) to have a resistivity of only 270 Ω cm at 20°c, falling to little more than than 1 Ω cm at about 400°c. It was, therefore, decided to make thermoelectric power measurements on this same sample.

§ 2. Experimental Procedure

The thermoelectric power of a semiconductor with a low thermal conductivity may be determined by clamping a sample between two metal blocks and measuring the differences in potential and temperature between them. However, the thermal conductivity of diamond is higher than for any metal (Berman *et al.* 1953) so that, if such a method were used, the temperature gradients in the metal blocks would be greater than in the sample. The presence of unknown thermal resistances at the contacts would be a further source of error. In the case of diamond, therefore, it is necessary to determine the potential, and temperature, gradients using probes on the faces of the sample. Some difficulty was experienced in devising probes which would make reasonably good electrical contact with the diamond. The short length, 3 mm, of the sample posed a further problem.

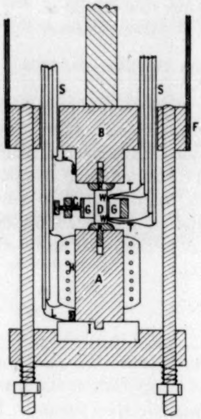

Figure 1. Apparatus for measurement of thermoelectric power.

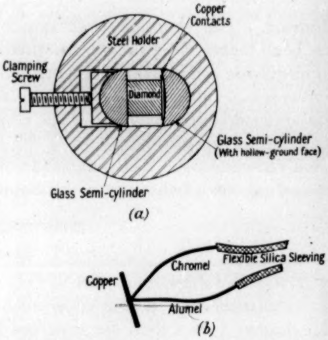

Figure 2. Method of applying electrical and thermal contacts.

A temperature gradient was applied to the diamond using the apparatus shown in figure 1. The diamond D, after being cleaned in a saturated solution of potassium dichromate in phosphoric acid at 100°c, was pressed between two annealed copper rivets R, attached to the copper blocks A and B. Block A was heated electrically by means of the nichrome coil H, while block B formed the heat sink. The copper wires L were used in measuring the potential difference between A and B at low temperatures as described below. The thermocouple wires T, the wires L and the heater leads were introduced through flexible silica sleeving S. A and B were electrically insulated from one another by the ceramic disc I. The apparatus was mounted in an evacuated silica enclosure. For measurements at the lower temperatures, this enclosure was dipped into liquid air, while, for higher temperature measurements, it was allowed to stand in air at room temperature or it was electrically heated. Heat was transferred between the block B and the surrounding vessel by means of the long copper cylinder F.

The problem of making electrical and thermal contact to the diamond was solved by using the steel clamp C, the glass blocks G and the copper probes W, which are shown in more detail in figure 2 (*a*). The probes were made from pieces of 40 s.w.g. copper wire, slightly longer than the width of the diamond. They were clamped in position between two glass semi-cylinders. The face of the glass block touching the copper probes was hollow ground, since previous experience had shown that electrical contact could best be made at the edges of the diamond. By this means pressure was applied at the edges of the sample.

The temperature of those portions of the diamond in contact with the probes was determined using 46 s.w.g. chromel–alumel thermocouples welded to the copper wires as shown in figure 2 (*b*). Since the copper probes were much softer than either the diamond or the glass block, it was expected that equal areas of contact with both would be made. Since the thermal conductivity of diamond is more than a thousand times that of glass, the probes took up the temperature of the former. The chromel–alumel thermocouples were welded to thicker wires of the same materials before leaving the enclosure. The junctions between these wires and the copper leads to the potentiometer were held in a water bath at room temperature. The thermoelectric potential difference between the probes was determined, using the two chromel wires to complete the circuit. In calculating the absolute thermoelectric power of diamond from the results, a small correction, corresponding to the thermoelectric power of chromel, was applied. In view of the high resistance of the contacts, a galvanometer with a rather high resistance, 535 Ω, was used.

Below room temperature it was found that the resistance between the probes became too great for the thermoelectric voltage between them to be measured with any degree of precision. It was, however, possible to determine the thermoelectric voltage between the blocks A and B, because the electrical resistance between the rivets R was much less than that between the probes W. In the range above room temperature, where the voltages between the rivets and between the probes could both be determined accurately, it was found that the ratio between these voltages remained constant. Thus, the thermoelectric power below room temperature was determined by assuming that the ratio between the voltages remained constant in this range also. It was noted that this ratio was close to that between the length of the sample and the distance between the probes. This suggests that the copper rivets made good thermal contact over the whole of the end faces of the diamond.

§ 3. EXPERIMENTAL RESULTS

The experimental results are shown in figure 3. These were obtained from thermoelectric voltages of between 5 and 10 mv in all cases. The uppermost curve represents the observed thermoelectric power in the temperature range 220°K to 700°K. It was not possible to extend the measurements to lower temperatures because the electrical resistance, even between the ends of the sample, became too great (i.e. more than a few megohms).

It was found that, if the diamond were removed and then the apparatus reassembled, the experimental results were not exactly reproduced. The variation of thermoelectric power with temperature always remained the same, i.e. on the log–log plot shown in figure 3, the curve always had the same slope at a given temperature. However, the absolute values of the thermoelectric power were sometimes found to differ by as much as ± 20% from those illustrated. It is thought that this rather poor reproducibility is connected with the difficulty in making good electrical contact to the diamond. It is suspected that the copper probes made electrical contact at one or two points, rather than over the whole tangential area. On the other hand, it is thought that thermal contact was made over the whole of this area. It is, therefore, possible that the thermoelectric potential difference and the temperature difference were sometimes measured between different planes. The results shown in figure 3 were obtained with an assembly giving intermediate values between the extremes, and it is probable that their absolute values are in error by no more than ± 10%.

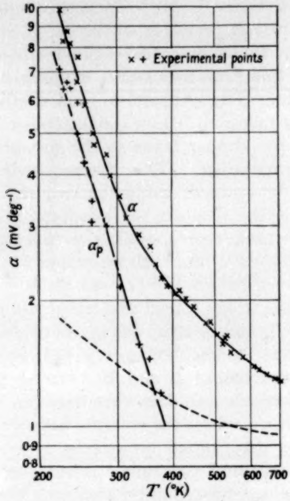

Figure 3. Thermoelectric power as a function of temperature for a type IIb diamond Broken curve represents $\alpha_e - \frac{3}{2}\frac{\boldsymbol{k}}{\boldsymbol{e}}\ln\frac{m^*}{m}$ calculated from Hall effect data.

§ 4. DISCUSSION

The electronic component of the thermoelectric power α_e for a non-degenerate p-type semiconductor is given (Wilson 1953) in terms of the reduced Fermi potential η by

$$\alpha_e = \frac{\boldsymbol{k}}{\boldsymbol{e}}\left(\frac{5}{2} + \lambda - \eta\right) \qquad \ldots\ldots(1)$$

where it is assumed that the relaxation time τ of charge carriers of energy E may be expressed in the form

$$\tau \propto E^{\lambda}$$

The hole concentration p is given in terms of η by

$$p = 2\left(\frac{2\pi m \boldsymbol{k} T}{h^2}\right)^{3/2}\left(\frac{m^*}{m}\right)^{3/2} \exp\eta \qquad \ldots\ldots(2)$$

where m^* is the density-of-states effective mass of a hole, and m the mass of a free electron. Thus

$$\alpha_e = \frac{\boldsymbol{k}}{\boldsymbol{e}}\left\{\frac{5}{2} + \lambda - \ln\frac{p}{2} + \frac{3}{2}\ln\left(\frac{2\pi m \boldsymbol{k} T}{h^2}\right) + \frac{3}{2}\ln\frac{m^*}{m}\right\}. \qquad \ldots\ldots(3)$$

Austin and Wolfe showed that the mobility is approximately proportional to $T^{-3/2}$ in the range of temperature over which the measurements were made, so it is reasonable to use a value of λ equal to $-\frac{1}{2}$, corresponding to acoustical-mode lattice scattering in a covalent crystal.[†] It is, therefore, possible to calculate the value of

$$\alpha_e - \frac{3}{2}\frac{\boldsymbol{k}}{\boldsymbol{e}}\ln\left(\frac{m^*}{m}\right)$$

using equation (3) and the values of the hole concentration p determined by Austin and Wolfe from their Hall effect measurements. The results of this calculation are shown by the lower broken curve of figure 3. It is seen that the experimental values of the thermoelectric power α lie well above this curve, over the whole range of temperature. In order to make α equal to α_e it would be necessary to assume absurdly high values for the effective mass or for λ, even at the higher temperatures. It is clear that the results can only be explained if it is assumed that there is a very appreciable phonon-drag effect. Strictly speaking the phonon-drag component of the thermoelectric power α_p is equal to $\alpha - \alpha_e$ but, below 400°K, α_e is so much less than α_p that it is a reasonable approximation to put

$$\alpha_p \simeq \alpha - \alpha_e + \frac{3}{2}\frac{\boldsymbol{k}}{\boldsymbol{e}}\ln\frac{m^*}{m} \qquad \ldots\ldots(4)$$

For reasonable values of m^*/m the last term cannot amount to more than about ± 100 μv deg^{-1} compared with α greater than 2 mv deg^{-1}.

A straight line (on the log–log plot shown in figure 3) may be drawn through the values of α_p calculated from equation (4). The slope of this line, obtained by the method of mean squares, indicates that α_p is proportional to $T^{-3\cdot6}$ with a possible error in the exponent of $\pm 0\cdot3$.

It is interesting to compare the phonon-drag effect in diamond with the effects observed in p-type germanium and silicon. Geballe and Hull found that α_p is proportional to $T^{-3\cdot2}$ in the purer samples of germanium, and to $T^{-2\cdot3}$ in silicon. Herring pointed out that α_p should be proportional to $T^{-3\cdot5}$ in the ideal case of a sample with a low carrier concentration, the carriers being scattered by longitudinal modes of vibration at low temperatures and boundary scattering of phonons being neglected. He showed that with more complex scattering laws an exponent of temperature numerically less than 3·5 would be expected.

Herring also found, by dimensional analysis, that

$$\alpha_p \propto \frac{\rho c^5 f}{\mu m_1^*} \qquad \ldots\ldots(5)$$

where ρ is the density, c the velocity of sound and f the fraction of the scattering of the carriers which is due to low energy, longitudinal mode, phonons. m_1^* is the inertial effective mass and μ the mobility of the charge carriers. If it is supposed that f is equal to unity and m_1^* is approximately the same for diamond, silicon and germanium, relation (5) should enable the relative values of α_p in these materials to be predicted.

The table shows the values of the relevant quantities and also the experimental values of α_p extrapolated to 200°K. $\alpha_p\mu/\rho c^5$, shown in the last column of the table, is of the same order for all three materials, in spite of a ratio of about 200 : 1 between the values of α_p for diamond and germanium. It seems,

---

[†] Wedepohl's (1957) observations of the mobility variation for a number of other diamonds throw some doubt on the validity of setting $\lambda = -\frac{1}{2}$. However, any consequent error in the calculated value of α_e is likely to be no more than that arising from the uncertainty in effective mass.

Comparison of α_p in Diamond, Silicon and Germanium

(1)	(2)	(3)	(4)	(5)	(6)	(7)
Diamond	3·51	$17{\cdot}7\times10^{5}$ a	$2{\cdot}2\times10^{3}$ d	$2{\cdot}77\times10^{28}$	$1{\cdot}1\times10^{-2}$	$4{\cdot}0\times10^{-31}$
Silicon	2·33	$9{\cdot}16\times10^{5}$ b	$1{\cdot}5\times10^{3}$ e	$1{\cdot}00\times10^{27}$	$1{\cdot}2\times10^{-3}$ g	$12\ \times10^{-31}$
Germanium	5·33	$5{\cdot}41\times10^{5}$ c	$4{\cdot}5\times10^{3}$ f	$5{\cdot}49\times10^{25}$	$5\ \times10^{-5}$ h	$9{\cdot}1\times10^{-31}$

(1) Element ; (2) density ρ (g cm^{-3}) ; (3) sound velocity c (cm sec^{-1}) ; (4) hole mobility at 200°K, μ (cm^{2} v^{-1}) ; (5) $\rho c^{5}/\mu$ (gm v sec^{-4}) ; (6) experimental α_p (v deg^{-1}) ; (7) $\alpha_p\mu/\rho c^{5}$ (g^{-1} deg^{-1} sec^{4}).

Notes : a, Bhagavantam and Bhimasenachar 1946 ; b, Bridgman 1949 ; c, Bond *et al.* 1950 ; d, Austin and Wolfe 1956 ; e, Ludwig and Watters 1956 ; f, Morin and Maita 1954 ; g, Geballe and Hull 1955 ; h, Geballe and Hull 1954.

therefore, that relation (5) is a reasonably good guide to the relative magnitudes of the phonon components of the thermoelectric power.

§ 5. CONCLUSIONS

It is concluded that the presence of the phonon-drag effect on the thermoelectric power of diamond has been definitely established. Its magnitude, in comparison with that for silicon or germanium, is of the order predicted by Herring and its variation with temperature is close to that expected in the ideal case of scattering of electrons by longitudinal modes of vibration, at temperatures well below the Debye temperature.

Because of errors inherent in the experimental measurements it has been impossible to establish the absolute magnitude of the thermoelectric power to within about ±10%, so it is not possible to use the results to determine the effective mass of the carriers. In order to do this it would be necessary to extend the Hall and thermoelectric measurements to rather higher temperatures, using a considerably longer sample with, preferably, a higher carrier concentration.

ACKNOWLEDGMENT

The authors wish to thank Dr. J. F. H. Custers of the Diamond Research Laboratory, Johannesburg, for the loan of the diamond.

REFERENCES

AUSTIN, I. G., and WOLFE, R., 1956, *Proc. Phys. Soc.* B, **69**, 329.
BERMAN, R., SIMON, F. E., and ZIMAN, J. M., 1953, *Proc. Roy. Soc.* A, **220**, 171.
BHAGAVANTAM, S., and BHIMASENACHAR, J., 1946, *Proc. Roy. Soc.* A, **187**, 381.
BOND, W. L., *et al.*, 1950, *Phys. Rev.*, **78**, 176.
BRIDGMAN, P. W., 1949, *Proc. Amer. Acad. Arts and Sci.*, **77**, 187.
CUSTERS, J. F. H., 1952, *Physica*, **18**, 489.
—— 1954, *Ibid.*, **20**, 183.
FREDERIKSE, H. P. R., 1953, *Phys. Rev.*, **92**, 248.
GEBALLE, T. H., and HULL, G. W., 1954, *Phys. Rev.*, **94**, 134.
—— 1955, *Ibid.*, **98**, 940.
HERRING, C., 1954, *Phys. Rev.*, **96**, 1163.
LUDWIG, G. W., and WATTERS, R. L., 1956, *Phys. Rev.*, **101**, 1699.
MORIN, F. J., and MAITA, J. P., 1954, *Phys. Rev.*, **94**, 1525.
WEDEPOHL, P. T., 1957, *Proc. Phys Soc.* B, **70**, 177.
WILSON, A. H., 1953, *The Theory of Metals*, 2nd Edn. (Cambridge : University Press).

The Theory of Electrical and Photoelectric Effects for Three Carriers in a Magnetic Field

By A. K. WALTON and T. S. MOSS
Royal Aircraft Establishment, Farnborough, Hants

MS. received 18*th September* 1958, *in revised form* 14*th November* 1958

Abstract. Formulae for the Hall, magnetoresistance, photoelectromagnetic and Dember effects due to electrons and slow and fast holes are derived for the cases of energy independent relaxation time and lattice scattering. The expressions given are evaluated as far as the third order in magnetic fields for small magnetic fields and as far as the first order for large magnetic fields. They readily reduce to formulae which agree with those expressions which have so far been published. The results are discussed for the particular case of germanium.

§ 1. Introduction

The presence of three types of charge carrier in germanium has been indicated by cyclotron resonance experiments (Dresselhaus *et al.* 1955) and by conductivity, magnetoresistance and Hall effect measurements (Willardson *et al.* 1954). There appear to be, in addition to the conduction band electrons, two types of holes in the valence band. Hall effect and conductivity measurements on p-type germanium indicate that about 2% of the holes present have a mobility of about eight times that of the more abundant type of hole. Attempts to detect these high mobility holes by using drift techniques (Harrick 1955) have failed and Rittner (1956) has given theoretical reasons to show why the fast holes cannot be detected in this way. A magnetic field is necessary to reveal the presence of the fast holes.

It is the purpose of this paper to develop theoretical expressions for electrical transport phenomena in semiconductors in the presence of magnetic fields, taking into account the presence of the third carrier. We shall see that the third carrier has a profound quantitative effect on terms in powers of magnetic field higher than the first.

Materials with multiple but simple energy bands will be considered. This treatment may well be applicable to many of the most interesting semiconductors and in particular to the III–V compounds, but will not be applicable in general to germanium and silicon. However, the analysis will apply in strongly p-type germanium and silicon for galvanomagnetic effects and even in photomagnetic effects, where electrons are always involved, our preliminary experiments show quite negligible anisotropy in some cases.

The Hall and magnetoresistance effects will be treated first, followed by the photoelectromagnetic and Dember effects.

§ 2. THE HALL AND MAGNETORESISTANCE EFFECTS

2.1. *General Theory*

In these effects a magnetic field is applied at right angles to the length l and thickness r of a specimen as shown in the figure. An external voltage is applied between the soldered end contacts. The current carriers, accelerated in the resulting field E_x, are deflected by the magnetic field H and the surface is charged until a field E_y is produced which, in equilibrium, results in zero current in the y direction.

The assumptions made in the following analysis are:

(*a*) The energy surfaces in k-space are spherical.

(*b*) The effective masses are energy independent.

(*c*) Any changes of carrier concentration from their thermal equilibrium values are relatively small, i.e. $\Delta q/q$, $\Delta n/n$, $\Delta p/p \ll 1$, where q, n, p refer to fast holes, electrons and slow holes respectively.

(*d*) Carrier lifetimes and diffusion constants have their equilibrium values.

(*e*) End effects are negligible, i.e. a specimen long and wide compared with its thickness is considered.

(*f*) Negligible space charge exists, i.e. $\Delta n = \Delta p + \Delta q$ everywhere.

(*g*) Classical statistics may be used.

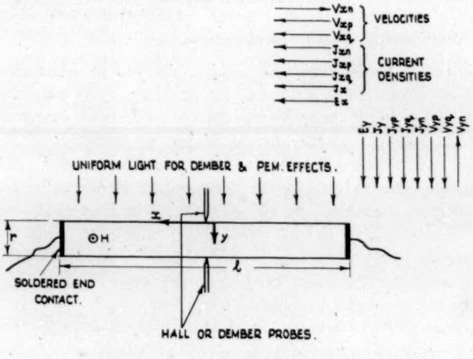

Definition of field and current directions.

Now, referring to the figure, a long thin specimen implies $\partial J_x/\partial x = 0$ and $\partial E_y/\partial x = 0$. But since div $\mathbf{J} = 0$, $\partial J_y/\partial y = 0$. Further, for open circuit Hall probes, which is the case we shall consider, $J_y = 0$ at the surface. Hence $J_y = 0$ over all y and we may write

$$J_{yn} + J_{yp} + J_{yq} = 0 . \qquad \ldots\ldots (1a)$$

The condition (Van Roosbroeck 1956) curl $\mathbf{E} = 0$ together with $\partial E_y/\partial x = 0$ yields the relation

$$\partial E_x/\partial y = 0 . \qquad \ldots\ldots (1b)$$

In the treatment of the Hall and magnetoresistance effects we shall assume that the specimen thickness in the y direction is very large compared with the diffusion length or that the surface recombination is sufficiently high for diffusion currents to be neglected. Two-carrier Hall and magnetoresistance theory, including the effect of diffusion currents, has been treated by Landauer and Swanson (1953).

The equations of motion of the three carriers are seen from the figure to be

$$\frac{dV_{xp}}{dt}=\frac{e}{M_p}E_x+\omega_p V_{yp}; \quad \frac{dV_{xq}}{dt}=\frac{e}{M_q}E_x+\omega_q V_{yq}; \quad \frac{dV_{xn}}{dt}=\frac{e}{M_n}E_x-\omega_n V_{yn};$$

$$\frac{dV_{yp}}{dt}=\frac{e}{M_p}E_y-\omega_p V_{xp}; \quad \frac{dV_{yq}}{dt}=\frac{e}{M_q}E_y-\omega_q V_{xq}; \quad \frac{dV_{yn}}{dt}=\frac{e}{M_n}E_y+\omega_n V_{xn}; \qquad \ldots\ldots(2)$$

where for each carrier M is the effective mass and $\omega=eH/M$.

Since we are only concerned with acquired motion, $V_{xn}+iV_{yn}=0$ when $t=0$, assuming each collision completely randomizes the motion. Using this boundary condition the solution for electrons is found to be

$$V_{xn}+iV_{yn}=\frac{-(E_x+iE_y)}{iH}[1-\exp(i\omega_n t)] \qquad \ldots\ldots(3)$$

with similar expressions for $V_{xp}+iV_{yp}$, and $V_{xq}+iV_{yq}$.

Equation (3) gives the velocities V of the carriers at any time t between collisions. It may be shown that the probability that a carrier suffers a collision in an interval of time dt is dt/τ where τ is the mean free time which is dependent only on the material and the thermal energy of the particular carrier. It readily follows that the mean velocity of carriers is given by

$$\bar{V}=\left[\frac{1}{\tau}\int_0^\infty e^{-T/\tau}V(T)dT\right]_{av} \qquad \ldots\ldots(4)$$

where the average over τ is taken with respect to the energy distribution $f(\epsilon)$ at temperature θ°K (Brooks 1955) of the carriers

$$f(\epsilon)d\epsilon=\frac{4}{3\sqrt{\pi}}\left(\frac{\epsilon}{k\theta}\right)^{3/2}e^{-\epsilon/k\theta}d\left(\frac{\epsilon}{k\theta}\right). \qquad \ldots\ldots(5)$$

Thus from equations (3) and (4) the current density produced by the electrons is

$$J_{xn}+iJ_{yn}=-\left\{\frac{ne(E_x+iE_y)}{i\tau_n H}\int_0^\infty \exp(-T/\tau_n)[1-\exp(i\omega_n T)]dT\right\}_{av}. \qquad \ldots\ldots(6)$$

Thus

$$\left.\begin{aligned} J_{xn}&=\frac{ne^2}{M_n}\left\{E_x\left[\frac{\tau_n}{1+\omega_n^2\tau_n^2}\right]_{av}-\omega_n E_y\left[\frac{\tau_n^2}{1+\omega_n^2\tau_n^2}\right]_{av}\right\}\\ J_{yn}&=\frac{ne^2}{M_n}\left\{E_y\left[\frac{\tau_n}{1+\omega_n^2\tau_n^2}\right]_{av}+\omega_n E_x\left[\frac{\tau_n^2}{1+\omega_n^2\tau_n^2}\right]_{av}\right\}\end{aligned}\right\}. \qquad \ldots(7)$$

It may be shown that J_{xp}, J_{xq}, J_{yp} and J_{yq} are equivalent to the above with n replaced by p or q and the sign of ω changed.

For sufficiently low magnetic fields $\omega_p\tau_p$, $\omega_q\tau_q$ and $\omega_n\tau_n$ are small compared with unity. Alternatively, for sufficiently high magnetic fields $\omega_p\tau_p$, $\omega_q\tau_q$ and $\omega_n\tau_n$ are large compared with unity.

2.2. *Cases of Small Magnetic Field*

Expanding equation (7) and neglecting terms in powers of ω higher than the third we obtain:

$$\left.\begin{aligned} J_{x\mathrm{n}} &= \frac{ne^2}{M_\mathrm{n}}\{E_x[\tau_\mathrm{n}-\omega_\mathrm{n}^2\tau_\mathrm{n}^3]_\mathrm{av}-\omega_\mathrm{n}E_y[\tau_\mathrm{n}^2-\omega_\mathrm{n}^2\tau_\mathrm{n}^4]_\mathrm{av}\} \\ J_{y\mathrm{n}} &= \frac{ne^2}{M_\mathrm{n}}\{E_y[\tau_\mathrm{n}-\omega_\mathrm{n}^2\tau_\mathrm{n}^3]_\mathrm{av}+\omega_\mathrm{n}E_x[\tau_\mathrm{n}^2-\omega_\mathrm{n}^2\tau_\mathrm{n}^4]_\mathrm{av}\} \end{aligned}\right\} \quad \ldots\ldots(8)$$

with similar expressions for $J_{x\mathrm{p}}$, $J_{x\mathrm{q}}$ and $J_{y\mathrm{p}}$, $J_{y\mathrm{q}}$.

2.2.1. *Energy independent free time.*

For energy independent free time the averages may be dropped and we obtain from (8), by putting $H=0$, the classical expressions for mobility, namely

$$\mu_\mathrm{p}=e\tau_\mathrm{p}/M_\mathrm{p}, \quad \mu_\mathrm{q}=e\tau_\mathrm{q}/M_\mathrm{q}, \quad \mu_\mathrm{n}=e\tau_\mathrm{n}/M_\mathrm{n}. \quad \ldots\ldots(9)$$

Substituting (9) in (8), and using (1*a*) to obtain E_y in terms of E_x, it follows, when terms in H higher than the third order are neglected and the ratios $\mu_\mathrm{q}/\mu_\mathrm{p}$ and $\mu_\mathrm{n}/\mu_\mathrm{p}$ are written as a and b respectively, that the magnetoresistance is

$$\frac{\Delta\rho}{\rho}=\left[\frac{(a^3q+p+b^3n)}{(aq+bn+p)}-\frac{(a^2q+p-b^2n)^2}{(aq+bn+p)^2}\right]\mu_\mathrm{p}^2H^2, \quad \ldots\ldots(10)$$

and the Hall coefficient $A_\mathrm{H}=\dfrac{E_y}{J_xH}$ is

$$\begin{aligned} A_\mathrm{H}=\frac{a^2q+p-b^2n}{(aq+bn+p)^2e}\bigg[1+\bigg\{&\frac{2(b^3n+a^3q+p)}{(bn+aq+p)} \\ &-\left[\frac{p+a^2q-b^2n}{bn+aq+p}\right]^2-\left[\frac{a^4q+p-b^4n}{p+a^2q-b^2n}\right]\bigg\}\mu_\mathrm{p}^2H^2\bigg]. \end{aligned} \quad \ldots\ldots(11)$$

Thus in a highly p-type semiconductor if 1% of the holes have a mobility ten times that of the normal holes, the low-field Hall coefficient is almost doubled and a considerable magnetic variation is introduced.

2.2.2. *Lattice scattering.*

For lattice scattering $\tau=\tau_0/(\epsilon/\boldsymbol{k}\theta)^{1/2}$ where τ_0 is a relaxation time. Putting $H=0$ in equation (8) and averaging τ with respect to the distribution (5), the mobilities are found to be given by

$$\mu_\mathrm{p}=\frac{4\tau_0e}{3M_\mathrm{p}\sqrt{\pi}}\ ;\ \mu_\mathrm{q}=\frac{4\tau_0e}{3M_\mathrm{q}\sqrt{\pi}}\ ;\ \mu_\mathrm{n}=\frac{4\tau_0e}{3M_\mathrm{n}\sqrt{\pi}}. \quad \ldots\ldots(12)$$

Averaging over τ in equation (8) and using equations (1*a*) and (12) we obtain when terms above H^3 are neglected

$$\frac{\Delta\rho}{\rho}=\left[\left(\frac{b^3n+p+a^3q}{bn+p+aq}\right)-\frac{\pi}{4}\left(\frac{a^2q+p-b^2n}{bn+p+aq}\right)^2\right]\frac{9\pi}{16}\mu_\mathrm{p}^2H^2 \quad \ldots\ldots(13)$$

and

$$\begin{aligned} A_\mathrm{H}=\frac{3\pi}{8}\frac{(a^2q+p-b^2n)}{(aq+bn+p)^2e}\bigg\{1+\bigg[&\left(\frac{b^3n+a^3q+p}{bn+aq+p}\right) \\ &-\left(\frac{a^4q+p-b^4n}{a^2q+p-b^2n}\right)-\frac{\pi}{8}\left(\frac{a^2q+p-b^2n}{bn+aq+p}\right)^2\bigg]\frac{9\pi}{8}\mu_\mathrm{p}^2H^2\bigg\}. \end{aligned} \quad \ldots\ldots(14$$

In a strongly p-type semiconductor where for example $a=10$ and $q=0{\cdot}01p$, the magnetoresistance is increased about 30 times, the Hall coefficient almost doubled and the magnetic variation of the Hall coefficient increased a hundredfold.

2.3. *Cases of High Magnetic Field*

From equation (7) expanding and neglecting terms with negative powers of H beyond the second order we obtain

$$J_{x\mathrm{n}}=\frac{ne^2}{M_\mathrm{n}}\left\{\frac{E_x}{\omega_\mathrm{n}^2}\left[\frac{1}{\tau_\mathrm{n}}\right]_{\mathrm{av}}-\frac{E_y}{\omega_\mathrm{n}}\right\},\quad J_{y\mathrm{n}}=\frac{ne^2}{M_\mathrm{n}}\left\{\frac{E_y}{\omega_\mathrm{n}^2}\left[\frac{1}{\tau_\mathrm{n}}\right]_{\mathrm{av}}+\frac{E_x}{\omega_\mathrm{n}}\right\},\quad \ldots\ldots(15)$$

with similar expressions for $J_{x\mathrm{p}}$, $J_{x\mathrm{q}}$, $J_{y\mathrm{p}}$, and $J_{y\mathrm{q}}$.

2.3.1. *Energy independent free time.*

Dropping the averages in (15) and using equations (1*a*) and (9) it readily follows that the magnetoresistance effect at very high magnetic fields is

$$\frac{\rho_\mathrm{H}}{\rho}=\frac{(n/b+p+q/a)(bn+p+aq)}{(p+q-n)^2},\quad \ldots\ldots(16)$$

and the Hall coefficient is

$$A_\mathrm{H}=\frac{1}{(p+q-n)e}.\quad \ldots\ldots(17)$$

2.3.2. *Lattice scattering.*

Averaging (15) over τ and using (1*a*) and (12) it now follows that

$$\frac{\rho_\mathrm{H}}{\rho}=\frac{32(n/b+p+q/a)(bn+p+aq)}{9\pi(p+q-n)^2}\quad \ldots\ldots(18)$$

$$\mathrm{A}_\mathrm{H}=\frac{1}{(p+q-n)e}.\quad \ldots\ldots(19)$$

Equations (16), (17), (18) and (19) show a small percentage of fast holes have very little effect on the high field magnetoresistance and Hall coefficient. It is worth noting that equations (17) and (19) are identical since the high field Hall coefficient is independent of the scattering mechanism and thus measures carrier density directly.

2.4. *Discussion*

2.4.1. *Low magnetic fields.*

Equations (10), (11), (13) and (14) show that for semiconductors in low magnetic fields a few fast holes have a marked quantitative effect on magnetoresistance and the magnetic variation of the Hall coefficient and considerable effect on the low magnetic field limit of the Hall coefficient. This is in agreement with the expectation that the higher the power of mobility involved in an effect, the greater will be the influence of a few high mobility holes. The low-field limit of the Hall coefficient involves (mobility)^2, magnetoresistance involves (mobility)^3, while the magnetic variation of the Hall coefficient involves (mobility)^4.

When there is one type of electron and one type of hole, and energy independent scattering, the magnetoresistance becomes

$$\frac{\Delta\rho}{\rho}=\frac{(b+1)^2 n_i^2}{(bn+p)^2}\mu_n\mu_p H^2$$

where $n_i=(np)^{1/2}$ is the intrinsic carrier concentration. Thus in a highly extrinsic semiconductor the magnetoresistance would be very small. However, in practice energy independent scattering does not occur and with lattice scattering we have :

$$\left.\begin{aligned}\frac{\Delta\rho}{\rho}&=\left[\left(\frac{b^3n+p}{bn+p}\right)-\frac{\pi}{4}\left(\frac{b^2n-p}{bn+p}\right)^2\right]\frac{9\pi}{16}\mu_p{}^2H^2\\ A_H&=\frac{3\pi}{8}\frac{p-b^2n}{(bn+p)^2e}\left[1+\left\{\left(\frac{b^3n+p}{bn+p}\right)-\frac{\pi}{8}\left(\frac{b^2n-p}{bn+p}\right)^2\right.\right.\\ &\qquad\left.\left.-\left(\frac{b^4n-p}{b^2n-p}\right)\right\}\frac{9\pi}{8}\mu_p{}^2H^2\right].\end{aligned}\right\}\quad\ldots\ldots(20)$$

Thus the magnetoresistance in highly extrinsic semiconductors should be independent of carrier concentration for types of scattering other than energy independent since terms in n^2 (or p^2) on the numerator no longer cancel.

Equations (13) and (14) give the complete expressions for the low field Hall coefficient and magnetoresistance in the case of lattice scattering. In a strongly p-type semiconductor these expressions may be reduced to

$$\frac{\Delta\rho}{\rho}=\left[\left(\frac{p+a^3q}{p+aq}\right)-\frac{\pi}{4}\left(\frac{p+a^2q}{p+aq}\right)^2\right]\frac{9\pi}{16}\mu_p{}^2H^2$$

which agrees with the relation given by Willardson *et al.* (1954) and

$$\left.\begin{aligned}A_H&=\frac{3\pi}{8}\frac{a^2q+p}{(aq+p)^2e}\left\{1+\left[\left(\frac{p+a^3q}{p+aq}\right)-\left(\frac{p+a^4q}{p+a^2q}\right)\right.\right.\\ &\qquad\left.\left.-\frac{\pi}{8}\left(\frac{p+a^2q}{p+aq}\right)^2\right]\frac{9\pi}{8}\mu_p{}^2H^2\right\}.\end{aligned}\right\}\quad\ldots\ldots(21)$$

In p-type germanium at room temperature there is lattice scattering and putting $a=\mu_q/\mu_p=8$ and $q/p=2\%$ we obtain

$$\frac{\Delta\rho}{\rho}\simeq 12\mu_p{}^2H^2\,;\quad A_H\simeq\frac{2\cdot 0}{pe}[1-100\mu_p{}^2H^2].$$

Thus, in p-type germanium, if accuracy to the order of 4% is required, the expression for the low-field limit of the Hall coefficient must only be used when $H<1000$ gauss.

It is interesting to contrast the above relations with those obtained if the high mobility holes are ignored, i.e. where $q=0$,

$$\frac{\Delta\rho}{\rho}\simeq 0\cdot 39\mu_p{}^2H^2\,;\quad A_H\simeq\frac{1\cdot 2}{pe}[1-1\cdot 4\mu_p{}^2H^2].$$

The zero magnetic field limit of the Hall coefficient for lattice scattering is from equation (14)

$$\lim_{H\to 0}A_H=\frac{3\pi}{8}\frac{a^2q+p-b^2n}{(aq+bn+p)^2e}\quad\ldots\ldots(22)$$

which for $q=0$ reduces to the well-known two-carrier expression, and for $n=0$ reduces to that given by Willardson *et al.* (1954).

2.4.2. *High magnetic fields.*

In §2.3 the magnetoresistance and Hall coefficient are shown to saturate at sufficiently high fields and equations (18) and (19) give the relevant three-carrier expressions for lattice scattering. In germanium the presence of the third carrier hardly affects the saturation magnetoresistance and Hall coefficient.

From equations (26) and (27) the two-carrier expressions are

$$\left.\begin{aligned}\lim_{H\to\infty}\frac{\rho_{\mathrm{H}}}{\rho} &= \frac{32}{9\pi}\frac{(bp+n)(bn+p)}{b(p-n)^2}\\ \lim_{H\to\infty} A_{\mathrm{H}} &= \frac{1}{(p-n)e}.\end{aligned}\right\} \qquad \ldots\ldots(23)$$

The latter equation of this pair is given by Swanson (1955) and by Harman *et al.* (1954). It should be noted that in practice the geometry of the specimen will usually limit ρ_{H}/ρ and A_{H} at sufficiently high magnetic fields.

At intermediate magnetic fields the averaging of lifetime over thermal energy is difficult in general. However, in InSb, for example, the mobility ratio is so high that it is possible to use the high field approximation for electrons and the low field approximation for holes simultaneously over quite a range of magnetic field strengths.

§ 3. THE PHOTOELECTROMAGNETIC AND DEMBER EFFECTS

3.1. *General Theory*

In these effects uniform light falls on the upper surface of the specimen as shown in figure 1. A magnetic field is applied as before, but the ends of the specimen are shorted in the cases that we shall consider. The light releases carriers at the upper surface of the specimen producing concentration gradients of the three carriers in the y direction. Because the diffusion constants of the three kinds of carrier are different, the holes and electrons flow towards the lower surface at different rates thus charging the lower surface until the resulting electric field has adjusted the carrier velocities for no net current flow. This field acting across the specimen thickness gives rise to the Dember voltage.

Now the resulting equilibrium is dynamic and downward carrier flow is still taking place. The magnetic field deflects the carriers sideways and the currents due to each deflected flow are additive producing the photoelectromagnetic current in the x direction.

In addition to the assumptions (a) to (g) of 2.1 we assume

(h) Unit quantum efficiency.

(i) All the carriers are released at $y=0$.

(j) The surface recombination is linearly dependent on carrier concentration, with velocities s_1 and s_2 at the upper and lower surfaces respectively.

Now equation (7) showed that the relations between the current densities and electric fields were of the form:

$$\left.\begin{aligned}J_x &= (\mu_{xx}E_x+\mu_{xy}E_y)Ne\\ J_y &= (\mu_{yx}E_x+\mu_{yy}E_y)Ne\end{aligned}\right\} \qquad \ldots\ldots(24)$$

where μ_{xx}, μ_{xy}, μ_{yx} and μ_{yy} have the dimensions of mobility and N is the appropriate carrier concentration.

In general in a magnetic field the current densities due to concentration gradients $\partial N/\partial x$ and $\partial N/\partial y$ are given by expressions of the form

$$\left.\begin{aligned} J_x' &= \left(D_{xx}\frac{\partial N}{\partial x} + D_{xy}\frac{\partial N}{\partial y}\right)e \\ J_y' &= \left(D_{yx}\frac{\partial N}{\partial x} + D_{yy}\frac{\partial N}{\partial y}\right)e \end{aligned}\right\} \qquad \ldots\ldots(25)$$

where D_{xx}, D_{xy}, D_{yx} and D_{yy} have the dimensions of a diffusion constant.

Assuming that the Boltzmann distribution is still valid in a magnetic field, and by using it in conjunction with the continuity equation it readily follows that

$$D_{xx} = \frac{\boldsymbol{k}\theta}{e}\mu_{xx},\; D_{xy} = \frac{\boldsymbol{k}\theta}{e}\mu_{xy},\; D_{yx} = \frac{\boldsymbol{k}\theta}{e}\mu_{yx} \text{ and } D_{yy} = \frac{\boldsymbol{k}\theta}{e}\mu_{yy},$$

which are particular forms of the general Einstein relation.

Hence for the short-circuit photoelectromagnetic and Dember effects, the current densities are obtained by adding equations (24) and (25) with $\partial N/\partial x = 0$, since there are only concentration gradients in the y direction, and with $E_x = 0$ since $\partial E_x/\partial x = 0$ and $\partial E_x/\partial y = 0$ so that $E_x = 0$ everywhere. The resulting equations are

$$\left.\begin{aligned} J_{xn} &= \frac{-ne^2\omega_n}{M_n}\left(E_y + \frac{\boldsymbol{k}\theta}{ne}\frac{d(\Delta n)}{dy}\right)\left[\frac{\tau_n^2}{1+\omega_n^2\tau_n^2}\right]_{av} \\ J_{yn} &= \frac{ne^2}{M_n}\left(E_y + \frac{\boldsymbol{k}\theta}{ne}\frac{d(\Delta n)}{dy}\right)\left[\frac{\tau_n}{1+\omega_n^2\tau_n^2}\right]_{av} \end{aligned}\right\} \qquad \ldots\ldots(26)$$

with similar expressions for J_{xp}, J_{xq}, J_{yp} and J_{yq}. The continuity equations are taken as

$$\frac{dJ_{yn}}{dy} = \frac{e\Delta n}{\mathscr{T}}; \quad \frac{dJ_{yp}}{dy} = -e\frac{\Delta p}{\mathscr{T}}; \quad \frac{dJ_{yq}}{dy} = -e\frac{\Delta q}{\mathscr{T}} \qquad \ldots\ldots(27)$$

where $\mathscr{T}$ is the lifetime against recombination of electrons with holes, and it is assumed that transitions between slow and fast hole states occur very rapidly compared with interband transitions so that the ratio between slow and fast hole concentrations has its equilibrium value. Thus denoting q/p by α and n/p by β, we have

$$\frac{\Delta q}{\Delta p} = \frac{q}{p} = \alpha \quad\text{and}\quad \frac{n}{p} = \beta. \qquad \ldots\ldots(28)$$

It should be noted that $\mathscr{T}$ depends on the ratio n/p and that its appropriate value must be used in the expressions that are derived. From equations (27) and (28),

$$\Delta n = \frac{\mathscr{T}}{e}\frac{dJ_{yn}}{dy}; \quad \Delta p = \left(\frac{\mathscr{T}}{(1+\alpha)e}\right)\frac{dJ_{yn}}{dy}; \quad \Delta q = \left(\frac{\alpha\mathscr{T}}{(1+\alpha)e}\right)\frac{dJ_{yn}}{dy}. \qquad \ldots\ldots(29)$$

Substituting for Δn, Δp, and Δq in equation (26) the current densities become

$$\left.\begin{aligned} J_{xn} &= -\frac{ne^2\omega_n}{M_n}\left(E_y + \frac{\boldsymbol{k}\theta\mathscr{T}}{ne^2}\frac{d^2J_{yn}}{dy^2}\right)\left[\frac{\tau_n^2}{1+\omega_n^2\tau_n^2}\right]_{av} \\ J_{yn} &= \frac{ne^2}{M_n}\left(E_y + \frac{\boldsymbol{k}\theta\mathscr{T}}{ne^2}\frac{d^2J_{yn}}{dy^2}\right)\left[\frac{\tau_n}{1+\omega_n^2\tau_n^2}\right]_{av} \end{aligned}\right\} \qquad \ldots\ldots(30)$$

with similar equations for J_{xp}, J_{xq}, J_{yp}, and J_{yq}.

3.2. *Cases of Small Magnetic Field*

Expanding equation (30) and neglecting terms in powers of ω higher than the third, we obtain

$$\left.\begin{aligned} J_{x\mathrm{n}} &= -\frac{ne^2\omega_\mathrm{n}}{M_\mathrm{n}}\left(E_y + \frac{\boldsymbol{k}\theta\mathcal{T}}{ne^2}\frac{d^2J_{y\mathrm{n}}}{dy^2}\right)[\tau_\mathrm{n}^2 - \omega_\mathrm{n}^2\tau_\mathrm{n}^4]_\mathrm{av} \\ J_{y\mathrm{n}} &= \frac{ne^2}{M_\mathrm{n}}\left(E_y + \frac{\boldsymbol{k}\theta\mathcal{T}}{ne^2}\frac{d^2J_{y\mathrm{n}}}{dy^2}\right)[\tau_\mathrm{n} - \omega_\mathrm{n}^2\tau_\mathrm{n}^3]_\mathrm{av} \end{aligned}\right\} \quad \ldots\ldots(31)$$

with similar equations for $J_{x\mathrm{p}}$, $J_{x\mathrm{q}}$, $J_{y\mathrm{p}}$ and $J_{y\mathrm{q}}$.

3.2.1. *Energy independent free time.*

Equation (31) becomes on dropping the averages, using (9), and putting $J_{x\mathrm{n}}$ in terms of $J_{y\mathrm{n}}$

$$J_{x\mathrm{n}} = -\mu_\mathrm{n}HJ_{y\mathrm{n}}; \quad J_{y\mathrm{n}} = (1-\mu_\mathrm{n}^2H^2)\left(\sigma_\mathrm{n}E_y + D_\mathrm{n}\mathcal{T}\frac{d^2J_{y\mathrm{n}}}{dy^2}\right) \quad \ldots\ldots(32)$$

with similar expressions for $J_{x\mathrm{p}}$, $J_{x\mathrm{q}}$, $J_{y\mathrm{p}}$ and $J_{y\mathrm{q}}$.

Using equation (1 *a*) to eliminate E_y from (32) we obtain

$$\frac{(1+\alpha+\beta)}{(1+\alpha)\beta}L_\mathrm{p}^2\frac{d^2J_{y\mathrm{n}}}{dy^2} - \left\{\frac{1}{(1-\mu_\mathrm{q}^2H^2)\alpha a + (1-\mu_\mathrm{p}^2H^2)} + \frac{1}{\beta b(1-\mu_\mathrm{n}^2H^2)}\right\}J_{y\mathrm{n}} = 0$$

where L_p is the diffusion length for slow holes.

The solution of this equation is

$$J_{y\mathrm{n}} = A\cosh y/f + B\sinh y/f \quad \ldots\ldots(33)$$

where A and B are arbitrary constants, and to the third order in H

$$\left.\begin{aligned} f^2 &= L^2\left[1 + \left(\frac{b^2(1+\alpha a)^2 + \beta b(1+\alpha a^3)}{(1+\alpha a)(1+\alpha a+\beta b)}\right)\mu_\mathrm{p}^2H^2\right]^{-1} \\ L^2 &= \frac{(1+\alpha+\beta)(1+\alpha a)}{(1+\alpha)(1+\alpha a+\beta b)}L_\mathrm{n}^2. \end{aligned}\right\} \quad \ldots\ldots(34)$$

L being the three-carrier diffusion length in zero magnetic field and f the effective diffusion length in the magnetic field.

The boundary conditions for equation (33) are obtained by considering the current due to electron flow at the surfaces. Thus, using (29),

$$\text{At } y=0,\ J_{y\mathrm{n}} = -eQ + es_1\Delta n = -eQ + \mathcal{T}s_1\frac{dJ_{y\mathrm{n}}}{dy}$$

$$\text{At } y=r,\ J_{y\mathrm{n}} = -es_2\Delta n = -\mathcal{T}s_2\frac{dJ_{y\mathrm{n}}}{dy}$$

where Q is the absorbed photon flux and s_1 and s_2 are the surface recombination velocities at the illuminated and dark surfaces respectively. Hence

$$J_{y\mathrm{n}} = \frac{-eQ[(\gamma_2\cosh r/f + \sinh r/f)\cosh y/f - (\cosh r/f + \gamma_2\sinh r/f)\sinh y/f]}{(\gamma_1+\gamma_2)\cosh r/f + (1+\gamma_1\gamma_2)\sinh r/f} \quad \ldots\ldots(35)$$

where $\gamma_1 = \mathcal{T}s_1/f$, $\gamma_2 = \mathcal{T}s_2/f$.

The Dember voltage is given by

$$V^{\sim} = -\int_0^r E_y dy = \left[\frac{L_\mathrm{n}^2}{f^2} - (1-\mu_\mathrm{n}^2H^2)^{-1}\right]\int_0^r \frac{J_{y\mathrm{n}}}{\sigma_\mathrm{n}}dy.$$

But from equation (35)

$$\int_0^r J_{y\mathrm{n}}dy = eQSf \text{ where } S = \left[\frac{1-\cosh r/f - \gamma_2 \sinh r/f}{(\gamma_1+\gamma_2)\cosh r/f + (1+\gamma_1\gamma_2)\sinh r/f}\right] \qquad \ldots\ldots(36)$$

so that to the third order in H, on substituting for f from equation (34):

$$V_{\mathrm{D}} = \frac{[(b-a)q+(b-1)p]QSL}{(p+q+n)(aq+p)\mu_{\mathrm{n}}}\left\{1+\left[\frac{(p+q)(a^3q+p)-b(aq+p)^2}{(aq+p)[(b-a)q+(b-1)p]} - \frac{1}{2}\,\frac{b(aq+p)^2+n(a^3q+p)}{(aq+p)(aq+bn+p)}\right]\mu_{\mathrm{n}}\mu_{\mathrm{p}}H^2\right\}. \qquad \ldots\ldots(37)$$

This equation shows that in the absence of a magnetic field a small percentage of fast holes have little effect on the Dember voltage. For the magnetic variation however, 1% of holes having a mobility 10 times normal will reverse the sign of the variation and increase it in magnitude by a factor of about 5.

The photoelectromagnetic current per unit width of sample is

$$I_{\mathrm{sc}} = \int_0^r J_x dy = \int_0^r (J_{x\mathrm{n}} + J_{x\mathrm{p}} + J_{x\mathrm{q}})dy$$

$$= -\int_0^r [(a+b)J_{y\mathrm{n}} + (a-1)J_{y\mathrm{p}}]\mu_{\mathrm{p}}H dy.$$

Expressing $J_{y\mathrm{p}}$ in terms of $J_{y\mathrm{n}}$ from (32), substituting for f from equation (34), expanding and neglecting terms in powers of H higher than the third this reduces to:

$$I_{\mathrm{sc}} = -\frac{(b+1)p+aq(a+b)}{(aq+p)}\left[1-\left\{\frac{(a-1)^2aqp}{(aq+p)[(b+1)p+(a+b)aq]} + \frac{b^2(aq+p)^2+bn(a^3q+p)}{2(aq+p)(aq+bn+p)}\right\}\mu_{\mathrm{p}}^2H^2\right]eQSL\mu_{\mathrm{p}}H. \qquad \ldots\ldots(38)$$

If $q=0{\cdot}01$ and $a=10$ then the low field limit of I_{sc} will be increased by about 25% from that when $q=0$, while the magnetic variation will be increased by factors of about 2 and 14 for strongly p- and strongly n-type semiconductors respectively.

It should be noted that S is negative in equations (37) and (38), is given by equation (36), and in general depends on the magnetic field through f.

3.2.2. *Lattice scattering.*

Averaging over τ in (31), using (1*a*) and (12), and proceeding as for energy independent scattering, equations (35) and (36) are again obtained but with

$$f^2 = L^2\left[1+\left(\frac{b^2(1+\alpha a)^2+\beta b(1+\alpha a)^3}{(1+\alpha a)(1+\alpha a+\beta b)}\right)\frac{9\pi}{16}\mu_{\mathrm{p}}^2H^2\right]^{-1},$$

$$L^2 = \frac{(1+\alpha+\beta)(1+\alpha a)}{(1+\alpha)(1+\alpha a+\beta b)}L_{\mathrm{n}}^2, \qquad \ldots\ldots(39)$$

so that to the third order in H

$$V_{\mathrm{D}} = \frac{[(b-a)q+(b-1)p]QSL}{(p+q+n)(aq+p)\mu_{\mathrm{n}}}\left\{1+\left[\frac{(p+q)(a^3q+p)-b(aq+p)^2}{(aq+p)[(b-a)q+(b-1)p]} - \frac{1}{2}\,\frac{b(aq+p)^2+n(a^3q+p)}{(aq+p)(aq+bn+p)}\right]\frac{9\pi}{16}\mu_{\mathrm{n}}\mu_{\mathrm{p}}H^2\right\}. \qquad \ldots\ldots(40)$$

Thus the influence of the fast holes is the same as for energy independent scattering.

Also

$$I_{\mathrm{sc}} = -\left(\frac{(b+1)p+(a+b)aq}{(aq+p)}\right)\frac{3\pi}{8}\mu_{\mathrm{p}}HeQSL$$

$$\times\left\{1-\left(\frac{(b^3+1)p^2+(2a^3+2b^3-a^2-a+2)aqp+(b^3+a^3)a^2q^2}{(aq+p)[(b+1)p+(a+b)aq]}\right.\right.$$

$$\left.\left.+\frac{b^2(aq+p)^2+bn(a^3q+p)}{2(aq+p)(bn+aq+p)}\right)\frac{9\pi}{16}\mu_{\mathrm{p}}^2H^2\right\}. \qquad \ldots\ldots(41)$$

With $q=0{\cdot}01$ and $a=10$ the low field limit of I_{sc} is again increased by about 25% from that when $q=0$, while the magnetic variation is increased by factors of 10 to 15 according to the doping.

3.3. *Cases of High Magnetic Field*

From equation (30), expanding and neglecting terms with negative powers of H beyond the second, we obtain, when $J_{x\mathrm{n}}$ is expressed in terms of $J_{y\mathrm{n}}$,

$$J_{x\mathrm{n}} = \frac{-\omega_{\mathrm{n}}J_{y\mathrm{n}}}{[1/\tau_{\mathrm{n}}]_{\mathrm{av}}};\; J_{y\mathrm{n}} = \frac{ne^2}{M_{\mathrm{n}}\omega_{\mathrm{n}}^2}\left(E_y+\frac{\boldsymbol{k}\theta\mathscr{T}}{ne^2}\frac{d^2J_{y\mathrm{n}}}{dy^2}\right)\left[\frac{1}{\tau_{\mathrm{n}}}\right]_{\mathrm{av}} \qquad \ldots\ldots(42)$$

with similar expressions for $J_{x\mathrm{p}}$, $J_{x\mathrm{q}}$, $J_{y\mathrm{p}}$ and $J_{y\mathrm{q}}$.

3.3.1. *Energy independent free time.*

Dropping the averages in (42), introducing mobility from (9) and using (1*a*) to eliminate E_y, one again obtains (35) and (36) but where f is now given by

$$f^2 = \frac{L_{\mathrm{n}}^2(1+\alpha+\beta)/(1+\alpha)}{[b+\beta a/(a+\alpha)]\mu_{\mathrm{p}}\mu_{\mathrm{n}}H^2}.$$

Proceeding as before but putting

$$L_\infty^2 = \frac{(1+\alpha+\beta)}{(1+\alpha)[b+\beta a/(a+\alpha)]}L_{\mathrm{p}}^2 \text{ so that } f=\frac{L_\infty}{\mu_{\mathrm{p}}H}, \text{ we have}$$

$$V_{\mathrm{D}} = -\frac{QSL_\infty[b-ap/(ap+q)]}{(p+q+n)}H. \qquad \ldots\ldots(43)$$

$$\lim_{H\to\infty} I_{\mathrm{sc}} = -\left\{(a+b)-\frac{a(a-1)}{a+\alpha}\right\}eQSL_\infty. \qquad \ldots\ldots(44)$$

3.3.2. *Lattice scattering.*

Averaging over τ in equation (42) and using (1*a*) and (12), once more equations (35) and (36) are obtained but with f now given by

$$f^2 = \frac{32(1+\alpha+\beta)L_{\mathrm{n}}^2}{(1+\alpha)[b+\beta a/(a+\alpha)]9\pi\mu_{\mathrm{p}}\mu_{\mathrm{n}}H^2}$$

so that with the same notation as for energy independent scattering

$$V_{\mathrm{D}} = -\frac{[b-ap/(ap+q)]}{(p+q+n)}QSL_\infty\left(\frac{9\pi}{32}\right)^{1/2}H \qquad \ldots\ldots(45)$$

$$\lim_{H\to\infty} I_{\mathrm{sc}} = -\left(\frac{9\pi}{32}\right)^{1/2}\left\{(a+b)-\frac{a(a-1)}{a+\alpha}\right\}eQSL_\infty. \qquad \ldots\ldots(46)$$

Equations (43) to (46) show that a few high mobility holes scarcely influence the high field Dember voltage and photoelectromagnetic current.

3.4. *Discussion*

The quantity S which appears in the equations of §3 can in many experimental arrangements be given by a simple expression. For thick specimens where $r \gg f$, $\cosh r/f = \sinh r/f \gg 1$ so that $S = -1/(1+\gamma_1)$ and if also $\gamma_1 \ll 1$, or $\gamma_1 \gg 1$, i.e. low or high surface recombination velocities at the illuminated surface, we have respectively $S=-1$; $S=-1/\gamma_1$. Alternatively if $\gamma_1=\gamma_2=\gamma$, $S=-(\gamma+\coth r/2f)^{-1}$. It should be noted that both γ and S are magnetic field dependent through f.

3.4.1. *Low magnetic fields.*

Equations (37), (38), (40) and (41) show that in germanium where $a \simeq 8$, $b \simeq 2$ and $q \simeq p/50$, the third carrier has little effect on the Dember voltage in zero magnetic field, but a marked effect on the short-circuit photoelectromagnetic current and the magnetic variation of the Dember voltage. Thus in the latter two cases the third carrier should be taken into account when comparing theory with experiment.

In strongly p-type semiconductors when lattice scattering predominates, the low magnetic field expressions are obtained from equations (40) and (41) by putting $n=0$, i.e.

$$V_{\mathrm{D}}=\frac{[(b-a)q+(b-1)p]QSL_{\mathrm{n}}}{(p+q)(p+aq)\mu_{\mathrm{n}}}\left\{1+\left[\frac{(p+q)(p+a^3q)-b(aq+p)^2}{(aq+p)[(b-a)q+(b-1)p]}-\frac{b}{2}\right]\times\frac{9\pi}{16}\mu_{\mathrm{n}}\mu_{\mathrm{p}}H^2\right\}$$

$$I_{\mathrm{sc}}=-\left(\frac{(b+1)p+(a+b)aq}{(aq+p)}\right)\frac{3\pi}{8}\mu_{\mathrm{p}}HeQSL_{\mathrm{n}}\times\left\{1-\left[\frac{(b^3+1)p^2+(2a^3+2b^3-a^2-a+2)aqp+(b^3+a^3)a^2q^2}{(aq+p)[(b+1)p+(a+b)aq]}+\frac{b^2}{2}\right]\frac{9\pi}{16}\mu_{\mathrm{p}}{}^2H^2\right\}$$

where S is given by putting $n=0$ in equation (36). When $r \gg f$, for $\gamma_1 \ll 1, S=1$ but for $\gamma_1 \gg 1$

$$S=\frac{L_{\mathrm{n}}}{\mathscr{T}s_1}\left\{1+\frac{9\pi}{16}\mu_{\mathrm{n}}{}^2H^2\right\}^{-1/2}$$

which changes the field dependence slightly.

In p-type germanium at room temperature lattice scattering predominates and putting $a=8$, $q/p=0{\cdot}02$ and $b=2$ we obtain

$$V_{\mathrm{D}}=\frac{0{\cdot}74QSL_{\mathrm{n}}}{p\mu_{\mathrm{n}}}\{1+27\mu_{\mathrm{p}}{}^2H^2\}; \quad I_{\mathrm{sc}}=-4{\cdot}7\mu_{\mathrm{p}}HeQSL_{\mathrm{n}}\{1-62\mu_{\mathrm{p}}{}^2H^2\}.$$

It is interesting to contrast these with the relations obtained if the high mobility holes are ignored, i.e. when $q=0$:

$$V_{\mathrm{D}}=\frac{QSL_{\mathrm{n}}}{p\mu_{\mathrm{n}}}\{1-7\mu_{\mathrm{p}}{}^2H^2\}; \quad I_{\mathrm{sc}}=-3{\cdot}5\mu_{\mathrm{p}}HeQSL_{\mathrm{n}}\{1-9\mu_{\mathrm{p}}{}^2H^2\}.$$

For semiconductors with only one electron and one hole we see that for lattice scattering which is the most usual case in practice

$$\left.\begin{aligned}V_{\mathrm{D}}&=\frac{(b-1)QSL}{(p+n)\mu_{\mathrm{n}}}\left\{1-\left[1+\frac{1}{2}\frac{bp+n}{bn+p}\right]\frac{9\pi}{16}\mu_{\mathrm{n}}\mu_{\mathrm{p}}H^2\right\}\\ I_{\mathrm{sc}}&=-(b+1)eQSL\left\{1-\left[(b^2-b+1)+\frac{b}{2}\frac{bp+n}{bn+p}\right]\frac{9\pi}{16}\mu_{\mathrm{p}}{}^2H^2\right\}\frac{3\pi}{8}\mu_{\mathrm{p}}H\end{aligned}\right\} \quad \ldots\ldots(47)$$

where $L^2 = L_{\mathrm{n}}^2(n+p)/(bn+p)$ and S is given by putting $q=0$ in equation (36). If $r \gg f$ when $\gamma_1 \ll 1$, then $S=1$; but when $\gamma_1 \gg 1$,

$$S = \frac{L}{\mathscr{T} s_1}\left\{1 - \frac{1}{2}\left(\frac{bp+n}{bn+p}\right)\frac{9\pi}{16}\mu_{\mathrm{n}}\mu_{\mathrm{p}}H^2\right\}$$

which has the effect of removing the factor of $\frac{1}{2}$ from the field dependence terms in equation (47). Simpler expressions are obtained for the intrinsic case.

The zero magnetic field limit of the Dember voltage is for lattice scattering

$$\lim_{H\to 0} V_{\mathrm{D}} = \frac{[(b-a)q+(b-1)p]QS_0L}{(p+q+n)(aq+p)\mu_{\mathrm{n}}} \qquad \ldots\ldots (48)$$

where

$$S_0 = \left[\frac{1-\cosh r/L - (\mathscr{T} s_2/L)\sinh r/L}{[\mathscr{T}(s_1+s_2)/L]\cosh r/L + (1+\mathscr{T}^2 s_1 s_2/L^2)\sinh r/L}\right].$$

For sufficiently low magnetic fields, and for lattice scattering, the photoelectromagnetic short circuit current is

$$\underset{H\to 0}{I_{\mathrm{sc}}} = -\left(\frac{(b+1)p+(a+b)aq}{(aq+p)}\right)\frac{3\pi}{8}\mu_{\mathrm{p}}HeQS_0L. \qquad \ldots\ldots (49)$$

Both equations (48) and (49) reduce to relations given by Moss (1956) when $q=0$.

On dividing equation (49) by (48), S_0, Q and L cancel yielding the useful expression

$$\lim_{H\to 0}\left(\frac{I_{\mathrm{sc}}}{V_{\mathrm{D}}}\right) = \frac{[(a+b)aq+(b+1)p](p+q+n)e\mu_{\mathrm{n}}}{[(a-b)q-(b-1)p]}\frac{3\pi}{8}\mu_{\mathrm{p}}H$$

$$= \frac{3\pi}{8}\left(\frac{1+b}{1-b}\right)e(p+n)\mu_{\mathrm{p}}\mu_{n}H \quad \text{for } q=0.$$

3.4.2. *High magnetic fields.*

From equations (43), (44) (45) and (46) we see that at high magnetic fields when $r \gg f$, which will usually be the case since $f \propto H^{-1}$, I_{sc} saturates or becomes inversely proportional to H, while V_{D} increases linearly with H or saturates for low and high surface recombination velocities respectively. Kurnick and Zitter (1956) have observed both kinds of variation of I_{sc} with magnetic field in InSb where there is one type of electron and one type of hole only. These equations show that in germanium the presence of the third carrier should hardly affect I_{sc} and V_{D} at very high magnetic fields.

From equations (45) and (46), the two carrier expressions in the case of lattice scattering at very high magnetic fields are

$$\left.\begin{aligned} \lim_{H\to\infty} I_{\mathrm{sc}} &= -(b+1)eQSL_{\infty}\left(\frac{9\pi}{32}\right)^{1/2} \\ V_{\mathrm{D}} &= \frac{(1-b)}{p+n}QSL_{\infty}\left(\frac{9\pi}{32}\right)^{1/2}H \end{aligned}\right\} \qquad \ldots\ldots (50)$$

where

$$L_{\infty} = \left(\frac{n+p}{bp+n}\right)L_{\mathrm{p}}^2.$$

Again when $\gamma_1 \ll 1$, $S=-1$

$$\gamma_1 \gg 1, \quad S = \left[\frac{n+p}{(bp+n)9\pi\mu_{\mathrm{p}}\mu_{\mathrm{n}}/32}\right]^{1/2}\frac{L_{\mathrm{n}}}{\mathscr{T} s_1 H}.$$

It should be remembered that in practice the geometry of the specimen will affect I_{sc} and V_D at sufficiently high fields.

The remarks concerning intermediate magnetic fields which were made in §2.4 are again applicable. It is interesting that for InSb, Kurnick and Zitter (1956) obtained a better fit of two-carrier theory with experiment over a wide range of magnetic fields for energy independent scattering than for lattice or ionic scattering.

ACKNOWLEDGMENT.

This paper is published by permission of the Controller, H.M. Stationery Office.

REFERENCES

BROOKS, H., 1955, *Advances in Electronics* VII (New York: Academic Press).

DRESSELHAUS, G., KIP, A. F., and KITTEL, C., 1955, *Phys. Rev.*, **98,** 368.

HARMAN, T. C., WILLARDSON, R. W., and BEER, A. C., 1954, *Phys. Rev.*, **94,** 1065.

HARRICK, N. J., 1955, *Phys. Rev.*, **98,** 1131.

KURNICK, S. W., and ZITTER, R. N., 1956, *J. Appl. Phys.*, **27,** 278.

LANDAUER, R., and SWANSON, J., 1953, *Phys. Rev.*, **91,** 555.

MOSS, T. S., 1956, *Garmisch Semiconductor Conference, Halbleiter und Phosphore* (Braunschweig: Vieweg).

RITTNER, E. S., 1956, *Phys. Rev.*, **101,** 1291.

SWANSON, J., 1955, *Phys. Rev.*, **99,** 1799.

VAN ROOSBROECK, W., 1956, *Phys. Rev.*, **101,** 1713.

WILLARDSON, R. W., HARMAN, T. C., and BEER, A. C., 1954, *Phys. Rev.*, **96,** 1512.

On Disordered One-dimensional Crystals

By P. DEAN

Mathematics Division, National Physical Laboratory, Teddington, Middlesex

MS. received 10*th November* 1958

Abstract. A mathematical method is presented which leads in a direct manner both to an explicit expression for the frequency distribution of a disordered chain of atoms and to a powerful technique for the numerical evaluation of the spectrum. The application of the method to a model of a binary alloy is then considered.

§ 1. Introduction

In recent years considerable attention has been focused on a number of problems associated with the vibrations of disordered atomic lattices. The most central of these is, perhaps, that of the development of a general mathematical or computational technique for the evaluation of frequency spectra, for this would at once enable a number of, as yet, unknown thermodynamic quantities to be found. For example, in the theory of order–disorder transformations in binary alloys little is known of the effect of lattice vibrations on the specific heats of alloys having various degrees of order; consequently, the existing theories compute specific heats (and other thermodynamic quantities) only on the basis of configurational changes of energy. The neglect of possible vibrational contributions may well account, at least in part, for the limited success of these theories.

An adequate theory of the vibrations of disordered systems would not be restricted in use, though, to just the theory of alloys. There are direct applications to several fields including the physics of isotropic mixtures, the glass state, the electronic levels of liquids and alloys and the spin wave theory of magnetism; more particularly, the problems of impurity electronic states and the effect of structural defects on lattice vibrations would emerge as special cases of the general theory. The underlying problem, then, is one of some importance and it is this, coupled with the inherent mathematical interest of the subject, that has been the stimulus for the recent activity†.

Unfortunately, the difficulties of the general three-dimensional problem appear, at present, to be insurmountable. While some attempts at solution have been made, these are either of restricted validity or of an excessively formal nature, not easily adaptable for computational purposes (Prigogine, Bingen and Jeener 1954, Lifschitz and Stephanova 1956). It is, therefore, to the one-dimensional problem that interest has, in the main, turned, as indeed was the case in the early days of work on periodic lattices. Now, as then, it is hoped that the study of the simpler model will be of considerable value in future attempts to compute the spectra of more realistic lattices. There is also, of course, the possibility of direct application of the linear problem to the physics of polymers and allied systems.

---

† Examples of the work on the electronic levels of disordered systems are provided by the following papers: James 1949, James and Ginzbarg 1953, Landauer and Helland 1954.

In the first paper on the subject of disordered elastic chains, Dyson (1953) evolved a formal method for the determination of the spectrum of frequencies. His method of derivation was, however, needlessly complex and was later much simplified and somewhat extended (Bellman 1956, Dean 1956). The basic technique, though, is of no computational value for it demands the solution of an extremely complex numerical problem. Its use lies rather in its applicability to a number of special models (Dean 1957).

That the frequency spectrum of the elastic chain could be found *very simply* in terms of the solution to a functional (or in some cases homogeneous integral) equation was shown some three years later by Schmidt (1957). The mathematical argument, though ingenious, is somewhat involved; this, however, is no real disadvantage. The main difficulty is as before—that the method does not suggest a practical means for extensive computations. The underlying connection between Schmidt's formalism and that of Dyson is, to some extent, made clear by the work of des Cloizeaux (1957).

The greatest volume of work on disordered lattices, to date, has been based on purely approximate techniques for the evaluation of spectra (in one, two and three dimensions) and is very adequately described in the review articles by Muto and Takagi (1955) and Maradudin *et al.* (1958). Although several important facts have emerged—such as the acute sensitivity of the vibrational spectrum of binary alloys to the existing degree of order—the calculations referred to in these papers must be regarded as being only of qualitative accuracy, this being clearly seen by the application of the methods to periodic lattices having known frequency distributions.

In the present paper we introduce a method of treating the one-dimensional problem which is at once mathematically simple and very direct; in addition, it can be used as the basis of an extremely powerful computing technique. Some calculations on binary systems are, indeed, now in progress, and will be the subject of a further paper.

§ 2. DESCRIPTION OF THE MODEL

We consider a linear chain of N particles each of which is coupled to its nearest neighbours by elastic springs obeying Hooke's law. The equations of motion of the system are

$$m_i\ddot{x}_i = k_i(x_{i+1}-x_i)+k_{i-1}(x_{i-1}-x_i) \quad (i=1,2,\ldots N), \qquad \ldots\ldots(1)$$

where m_i is the mass of the ith particle (situated at x_i relative to its mean position), and k_i is the elastic modulus of the spring joining the i and $i+1$th particles.

By introducing new variables $y_i = m_i^{1/2}x_i$ and using the harmonic relation $\ddot{x}_i = -\omega^2 x_i$, it is easy to show that the equations (1) reduce to

$$\left.\begin{aligned} \beta_i y_{i-1}+(\alpha_i-\omega^2)y_i+\beta_{i+1}y_{i+1}=0, \\ \beta_1=\beta_{N+1}=0, \quad (i=1,2,\ldots N), \end{aligned}\right\} \qquad \ldots\ldots(2)$$

where

$$\left.\begin{aligned} \alpha_i &= (k_i+k_{i-1})/m_i, \\ \beta_i &= -k_{i-1}/(m_{i-1}{}^{1/2}m_i{}^{1/2}). \end{aligned}\right\} \qquad \ldots\ldots(3)$$

The squares of the characteristic frequencies of the chain are, therefore, the eigenvalues of the $N \times N$ Jacobian matrix **A**, the elements of which are defined by

$$\left.\begin{array}{l} A_{ii}=\alpha_i \\ A_{i,i+1}=A_{i+1,i}=\beta_{i+1} \\ \text{all other } A_{ij}=0. \end{array}\right\} \quad \ldots\ldots(4)$$

The matrix **A** has N discrete eigenvalues. It is generally assumed that as N becomes large the number of eigenvalues less than any given argument is given by an analytic function $M(\nu)$ where $\nu=\omega^2$, from which the density of eigenvalues $D(\nu)$, may be simply derived: $D(\nu)=dM(\nu)/d\nu$. The object of the theory of this paper is to determine this *spectral density* or *spectral distribution function* given statistical information on the masses and elastic moduli of the chain.

In order to fix ideas let us suppose our model is that of an alloy composed of t kinds of atoms having masses $m^1, m^2, \ldots\ldots m^t$. It follows, from the simple nearest neighbour interactions, that each (α_i, β_i) pair can assume one of t^3 possible values, depending upon the particular sequence of three atoms starting at $i-1$. Let $P^{p,q,r}(\alpha,\beta)$ denote the probability of (α_i,β_i) taking on the value determined by the sequence of a p-, q- and r-atom. In the limit $N\to\infty$, we may regard the $P^{p,q,r}(\alpha,\beta)$ as being derived from a probability distribution function $P(\alpha,\beta)$ which, for the case of an alloy, is the sum of t^3 δ-functions, and for a continuously disordered (liquid) structure is an analytic function of α and β. In an alloy, the existing degree of order will uniquely determine the function $P(\alpha,\beta)$; we touch upon this point again later in the application to a binary system.

There are two general points that should be mentioned in connection with our presentation of the problem. First, we neglect end-effects; that this is justified in the case of large N is now firmly established on the basis of a theorem by Ledermann (1944), though a simple method of proof for the co-diagonal matrix is indicated at the end of the next section. Secondly, our method of § 3.1 for the exact determination of the spectral distribution function gives, strictly, the mean over a statistical ensemble of chains. It is, however, a well-known result of statistical mechanics that this is the correct spectrum of any individual chain as $N\to\infty$. In the limit, then, we may take the results of this theory as being applicable to any single disordered chain.

§ 3. DETERMINATION OF THE FREQUENCY SPECTRUM

The algebraic basis to our treatment of the disordered elastic chain is, briefly, as follows. Consider the polynomials of the sequence $g_0(\nu)\equiv 1, g_1(\nu), g_2(\nu), \ldots g_N(\nu)$, where

$$g_i(\nu)=\begin{vmatrix} \alpha_1-\nu & \beta_2 & & & & 0 \\ \beta_2 & \alpha_2-\nu & \beta_3 & & & \\ & \beta_3 & \alpha_3-\nu & \beta_4 & & \\ & & \cdot & \cdot & \cdot & \\ & & & \cdot & \cdot & \cdot \\ 0 & & & & \beta_i & \alpha_i-\nu \end{vmatrix} \quad \ldots\ldots(5)$$

$(i=1,2,\ldots N)$.

An expansion of the determinant as a function of the elements of the last row (or column) leads to the recurrence relation

$$g_i(\nu)=(\alpha_i-\nu)g_{i-1}(\nu)-\beta_i^2 g_{i-2}(\nu) \qquad \ldots\ldots(6)$$

for $i=2, 3, \ldots N$. From this it is easy to see that the functions

$$g_0(\nu), g_1(\nu), \ldots . g_N(\nu)$$

satisfy the conditions for the validity of Sturm's theorem†, which may be stated as follows.

Theorem: *If a and b are any real numbers such that $b>a$, then the number of roots of the equation $g_N(\nu)=0$ which lie in the interval $a\leqslant\nu<b$ is equal to $v(b)-v(a)$ where $v(\xi)$ is the number of variations of sign between consecutive members of the sequence g_0, $g_1(\xi)$, $g_2(\xi)$, ... $g_N(\xi)$.* We overcome any possible ambiguities by defining the sign of a zero $g_i(\xi)$ to be that of $g_{i-1}(\xi)$, extending this process if necessary (i.e. if $g_{i-1}(\xi)=0$).

Now, the eigenvalues of the matrix $\mathbf{A}_N$ defined by (4) are given as the roots of its characteristic equation $|\mathbf{A}_N-\nu I|=0$, or $g_N(\nu)=0$. It follows, therefore, that the function $M(\nu)$ of the preceding section is equal to $v(\nu)-v(-\infty)$; we are thus led to the equation

$$M(\nu)=v(\nu) \qquad \ldots\ldots(7)$$

which is the relationship fundamental to the work of this paper.

3.1. *The Exact Solution*

We consider the model of §2 for large N and study, initially, that section of the chain near to the ith particle. Let us first choose a value of $\nu(=\nu')$ such that $g_{i-1}(\nu')\neq 0$. Subject to this condition equation (6) may be written as

$$h_i(\nu')=(\alpha_i-\nu')-\beta_i^2/h_{i-1}(\nu') \quad (i=2,3,\ldots . N) \qquad \ldots\ldots(8)$$

where, for values of ν at which it is permissible,

$$h_i(\nu)=g_i(\nu)/g_{i-1}(\nu) \quad (i=1,2,\ldots . N). \qquad \ldots\ldots(9)$$

Let the probability distribution function of $h_i(\nu')$ be $H(h_i)$ (—and it is at this point that we tacitly introduce the concept of a statistical ensemble of chains). Then, neglecting the influence of the ends of the chain, the *a priori* probability distribution of any other $h(\nu')$, in particular $h_{i-1}(\nu')$, is given by the same function $H(h)$.

Now, it can be seen from equations (6) and (9) that the quantities h_{i-1} and (α_i,β_i) are uncorrelated, h_{i-1} depending only upon $(\alpha_{i-1},\beta_{i-1})$, $(\alpha_{i-2},\beta_{i-2})$, etc. If, then, we equate the probabilities of the two sides of equation (8) we find, by a standard procedure, the following functional equation for $H(h)$:

$$H(h)=\sum_i P(\alpha_i,\beta_i)\frac{\beta_i^2}{(\alpha_i-\nu'-h)^2}H\left(\frac{\beta_i^2}{\alpha_i-\nu'-h}\right) \qquad \ldots\ldots(10)$$

where the summation extends over all possible pairs of values of (α_i,β_i). For a liquid model, in which $P(\alpha,\beta)$ is a continuous function of α(or β), equation (10) reduces to an integral equation one form of which is

$$H(h)=\int_0^\infty P[\alpha,\beta(\alpha)]H\left[\frac{\beta(\alpha)}{\alpha-\nu'-h}\right]\frac{\beta(\alpha)^2 d\alpha}{(\alpha-\nu'-h)^2} \qquad \ldots\ldots(11)$$

---

† A good exposition of this theorem is given by Burnside and Panton (1918).

the other being expressed in terms of an integration over the variable β. In order that the solutions to equations (10) and (11) be unique, the usual conditions of normalization and sign for a probability distribution function, viz.

$$\int_{-\infty}^{\infty} H(h)dh=1 \qquad \ldots\ldots(12)$$

and

$$H(h)\geqslant 0$$

should be imposed.

We now invoke the use of Sturm's theorem for our typical (i.e. average over the ensemble) chain. From this theorem and equation (9) it is easy to see that the fraction of negative terms of the sequence $h_1(\nu')$, $h_2(\nu')$, ... $h_N(\nu')$ is equal to the proportion of the total number of eigenfrequencies less than ν'; and, further, since (for large N) we take all the $h_1(\nu')$ to be described by the same probability function, this proportion must be equal to the probability of $h_i(\nu')$ being negative. We have, therefore,

$$M(\nu')=\int_{-\infty}^{0} H(h)dh \qquad \ldots\ldots(13)$$

thus enabling the frequency spectrum to be found directly from the solution to equation (10) (or (11)).

Unfortunately, the above derivation of the $M(\nu')$ is not complete, for we have defined only those $h_i(\nu')$ for which $g_{i-1}(\nu')\neq 0$. To overcome this restriction we make use of the following artifice. If, for the value $\nu=\nu'$, one or more of the functions $g_{i-1}(\nu)$ $(i=2, 3, \ldots N)$ (for any of the m chains of the ensemble) is zero, we define, instead of (9), the ratios

$$h_i(\nu')=\frac{g_i(\nu'-\epsilon)}{g_{i-1}(\nu'-\epsilon)} \quad (i=1,2,\ldots.N). \qquad \ldots\ldots(14)$$

ϵ is a small positive quantity such that

$$\epsilon<\nu'-\nu'' \qquad \ldots\ldots(15)$$

ν'' being the greatest (single or multiple) root, less than ν', of all the mN equations $g_j(\nu)=0$. On this basis we can derive equations which become identical to (10), (11) and (12) if ϵ is sufficiently small.

The derivation of these equations implies that the limit $m,N\to\infty$ may be taken without invalidating the argument based upon ϵ. This is, indeed, the case, for we can take ϵ to tend very rapidly to zero (say as e^{-mN}) with increasing m and N, thus ensuring the preservation of the property (15).

Let us consider, now, the sequence of functions $h_1(\nu')$, $h_2(\nu')$, ... $h_N(\nu')$ generated by (14). The fraction of negative terms is equal to the number of variations in the sequence $g_i(\nu'-\epsilon)$, $i=0, 1, \ldots. N$ which, in turn, is equal to the number of variations in $g_i(\nu')$, $i=0, 1, 2, \ldots. N$. It follows, therefore, that

$$M(\nu')=\int_{-\infty}^{0} H(h)dh,$$

as before. Thus, to an error which can be made arbitrarily small the equations (10) or (11), (12) and (13) may be taken as valid for the case where the functions $g_i(\nu')$ are not all necessarily non-zero. Hence they constitute a general solution for the frequency spectrum of the disordered linear chain.

3.2. *A Numerical Technique*†

This method is that of the direct calculation of successive functions $g_i(\nu')$ $(i=1, 2, \ldots. N)$ and the corresponding recording of the number of variations in sign $v(\nu')$ between adjacent members of the sequence. The proportion of eigenfrequencies smaller in value than ν' is then, simply, $v(\nu')/N$.

The technique is particularly well suited to high speed machine computation for, as can be seen from equation (6), there need be only a very simple (and correspondingly fast) basic cycle of instructions. The results of a calculation will, of course, apply only to the particular model defined by the sequence of elements α_i, β_i $(i=1, 2, \ldots. N)$ which are used by the machine (—these having previously been computed by a pseudo-random process). However, since it seems that chains having as many as 10^5 or 10^6 particles can easily be treated we may, with some justification, expect the results for any typical chain to correspond closely to that for the idealized infinite model.

A considerable advantage of the method is that, in building up a sequence of $g_i(\nu')$, results corresponding to models of smaller 'lengths' than N are incidentally obtained. Information on the convergence of the frequency spectrum with increasing length of chain is thus available, thereby enabling the accuracy of calculated results to be determined.

That the effects due to the ends of the chain are not serious, if N is large, may be seen in the following way. Consider the matrix $\mathbf{A}$, defined by equation (4). If we change the positions of both the first row and first column to form a new final row and final column, the eigenvalues of the matrix $\mathbf{B}$ thus formed will remain identical to those of $\mathbf{A}$. The finiteness of the chain, influencing the elements of the first and last rows of $\mathbf{A}$ will, in $\mathbf{B}$, affect only the elements of the $N-1$ and Nth rows. Now, from the definition (5), it can be seen that of all the functions $g_i(\nu)$ $(i=0, 1, 2, \ldots. N)$—referred now to the matrix $\mathbf{B}$—only two, namely g_{N-1} and g_N, depend upon the elements of these rows. It follows, therefore, that a calculation of $M(\nu)$ based upon the count of variations will be in error (due to the end conditions of the chain) by $2/N$ at most, a quantity which is not serious.

These, then, are the advantages of the technique we have outlined: a fast, direct and accurate method of computation and a means of estimating the accuracy of the results obtained. It promises to be a powerful tool in the study of many one-dimensional systems.

§ 4. APPLICATION TO A BINARY ALLOY

We now apply the general theory of §§ 2 and 3 to a one-dimensional model of a binary alloy, i.e. to a chain composed of (here, equal numbers of) atoms of two distinct kinds, randomly situated. Let the masses of the atoms be m^A and m^B and the interactions between nearest neighbours be described by the elastic constants k^{AA}, k^{AB} and k^{BB}. There are now eight distinct pairs of values for the matrix elements α_i, β_i, each corresponding to one of the possible combinations of the three atoms at the lattice sites $i-1$, i and $i+1$. If, for example, these atoms are respectively A, B and B we shall have, from the definitions of § 2,

---

† This is a modification of the Givens' process for the determination of the eigenvalues of symmetric matrices (Givens 1954, Wilkinson 1958). The author is indebted to a colleague, Dr. H. H. Robertson, who first pointed out the possibilities of the method described here and from which all the work of this paper is derived.

$k_{i-1}=k^{\mathrm{AB}}$, $k_i=k^{\mathrm{BB}}$ and therefore

$$\left.\begin{aligned}\alpha_i &= (k^{\mathrm{AB}}+k^{\mathrm{BB}})/m^{\mathrm{B}},\\ \beta_i^2 &= (k^{\mathrm{AB}})^2/m^{\mathrm{A}}m^{\mathrm{B}}.\end{aligned}\right\} \qquad \ldots\ldots(16)$$

In the table, below, all the possible values of α_i and β_i^2 are given as functions of the various values of k and m.

For a chain of specified statistical properties the eight values of the matrix elements α_i, β_i will, in general, occur with differing frequencies—frequencies which are calculable in terms of the order parameters of the chain. As an example, we consider an infinite chain described in terms of (i) the short range order parameter σ of Bethe (1935) and (ii) the long range order S of Bragg and Williams (1934, 1935). In each case we compute the probabilities of α_i and β_i having the values as in equation (16).

Let q_σ be the fraction of unlike linkages (i.e. unlike nearest neighbours) in a chain of short range order σ. Then q_σ and σ are related by the equation $\sigma=2q_\sigma-1$, σ being unity for perfect order and zero for complete randomness. Now, the probability $P^{\mathrm{ABB}}(\alpha_i,\beta_i)$ (of α_i and β_i being given by equation (16)) is in fact, the probability of an A-atom occurring at the $(i-1)$th position on the chain and B-atoms occurring at the i and $(i+1)$th places. Accordingly, we have

$$P^{\mathrm{ABB}}(\alpha_i,\beta_i)=\tfrac{1}{2}q_\sigma(1-q_\sigma)=\tfrac{1}{8}(1-\sigma^2)$$

since the probability of the A-atom is $\frac{1}{2}$, and this then influences the selection of the next atom, and this, in turn, the last.

If we describe the arrangement of atoms on the chain by the parameter S the calculation of $P^{\mathrm{ABB}}(\alpha_i,\beta_i)$ is only slightly more complicated than that above. Let p_S be the fraction of A-atoms on even numbered lattice sites. Then we have $S=2p_S-1$ and if, first, we take i to be an even number, we find

$$P_{\mathrm{even}}{}^{\mathrm{ABB}}(\alpha_i,\beta_i)=P_S\cdot P_S\cdot(1-P_S)=\tfrac{1}{8}(1+S)^2(1-S);$$

if i is odd

$$P_{\mathrm{odd}}{}^{\mathrm{ABB}}(\alpha_i,\beta_i)=(1-P_S)\cdot(1-P_S)\cdot P_S=\tfrac{1}{8}(1-S)^2(1+S).$$

It follows that

$$P^{\mathrm{ABB}}(\alpha_i,\beta_i)=\tfrac{1}{2}[P_{\mathrm{even}}+P_{\mathrm{odd}}]=\tfrac{1}{8}(1-S^2).$$

In the table we tabulate the probabilities of occurrence of all the values of α_i, β_i as functions of σ and of S. The letter j in the first column refers to the sequence of atoms starting at the chain site $i-1$.

Values and Probabilities of α_i, β_i^2 for the Binary Chain

j	Sequence of atoms starting at $i-1$	α_i	β_i^2	$8P^j(\alpha_i,\beta_i)$ as a function of	
				σ	S
1	AAA	$2k^{\mathrm{AA}}/m^{\mathrm{A}}$	$(k^{\mathrm{AA}}/m^{\mathrm{A}})^2$	$(1-\sigma)^2$	$1-S^2$
2	AAB	$(k^{\mathrm{AA}}+k^{\mathrm{AB}})/m^{\mathrm{A}}$	$(k^{\mathrm{AA}}/m^{\mathrm{A}})^2$	$1-\sigma^2$	$1-S^2$
3	ABA	$2k^{\mathrm{AB}}/m^{\mathrm{B}}$	$(k^{\mathrm{AB}})^2/m^{\mathrm{A}}m^{\mathrm{B}}$	$(1+\sigma)^2$	$1+3S^2$
4	ABB	$(k^{\mathrm{AB}}+k^{\mathrm{BB}})/m^{\mathrm{B}}$	$(k^{\mathrm{AB}})^2/m^{\mathrm{A}}m^{\mathrm{B}}$	$1-\sigma^2$	$1-S^2$
5	BAA	$(k^{\mathrm{AB}}+k^{\mathrm{AA}})/m^{\mathrm{A}}$	$(k^{\mathrm{AB}})^2/m^{\mathrm{A}}m^{\mathrm{B}}$	$1-\sigma^2$	$1-S^2$
6	BAB	$2k^{\mathrm{AB}}/m^{\mathrm{A}}$	$(k^{\mathrm{AB}})^2/m^{\mathrm{A}}m^{\mathrm{B}}$	$(1+\sigma)^2$	$1+3S^2$
7	BBA	$(k^{\mathrm{BB}}+k^{\mathrm{BA}})/m^{\mathrm{B}}$	$(k^{\mathrm{BB}}/m^{\mathrm{B}})^2$	$1-\sigma^2$	$1-S^2$
8	BBB	$2k^{\mathrm{BB}}/m^{\mathrm{B}}$	$(k^{\mathrm{BB}}/m^{\mathrm{B}})^2$	$(1-\sigma)^2$	$1-S^2$

The frequency spectrum of the binary model may be found from the solution to the functional equation

$$H(h) = \sum_{j=1}^{8} P^j H \frac{\beta^2}{\alpha - \nu' - h} \frac{\beta^2}{(\alpha - \nu' - h)^2} \qquad \ldots\ldots(17)$$

on using the conditions (12) and the equation (13), the $P^j \equiv P^j(\alpha, \beta)$ being given in the table.

The technique of § 3.1 lends itself very well to computations on binary systems. A predetermined value of the parameter σ (or S) may be used to generate a pseudo-random sequence of A's and B's having the requisite degree of order. This sequence (or chain) then determines consecutive values of the α_i, β_i with the estimated frequencies of occurrence as in the above table. There are no difficulties of machine storage for the selection of an α, β pair may be left until the stage of computation is reached at which the values are required.

A programme of the above nature has been prepared for use on the DEUCE of the National Physical Laboratory and calculations are, at present, in progress and will be fully reported in a second paper. Preliminary results (though these are by no means extensive) suggest that the high frequency end of the vibrational spectrum is very sensitive to changes in the order parameters, the low frequency end being appreciably less so. For the case $k^{AA} = k^{AB} = k^{BB}$; $m^A = 2m^B$ the spectral distribution function differs somewhat from that published previously (Maradudin *et al.* 1958) and obtained by more approximate methods.

§ 5. SUMMARY

The relationships (10) (or (11)), (12) and (13), together with $D(\nu) = dM(\nu)/d\nu$ constitute a formal method for the determination of the frequency spectrum of the disordered elastic chain. The equations are analogous to those of Schmidt (1957) (in section II(d) of his paper) although he considers only the case in which $k^{AA} = k^{AB} = k^{BB}$. Unfortunately, the difficulty of solution of the functional equation is such that the exact treatment promises to be of little use in the numerical evaluation of spectra except, perhaps, in a minority of special cases. The computing technique of § 3.2, which is based upon the same principle as that used in the derivation of the equations referred to above, appears, though, to be a very adequate answer to the numerical problem.

ACKNOWLEDGMENT

The work described above has been carried out as part of the research programme of the National Physical Laboratory and this paper is published by permission of the Director of the Laboratory.

REFERENCES

BELLMAN, R., 1956, *Phys. Rev.*, **101**, 19.

BETHE, H. A., 1935, *Proc. Roy. Soc.* A, **150**, 552.

BRAGG, W. L., and WILLIAMS, E. J., 1934, *Proc. Roy. Soc.* A, **145**, 699.

—— 1935, *Proc. Roy. Soc.* A, **151**, 540.

BURNSIDE, W. S., and PANTON, A. W., 1918, *Theory of Equations* (London: Longmans, Green and Co.), p. 198.

DE CLOIXEAUX, J., 1957, *J. Phys. Rad.*, **18**, 131.

DEAN, P., 1956, *Proc. Camb. Phil. Soc.*, **52**, 752.

—— 1957, *Ph.D. Thesis*, University of London.

Dyson, F. J., 1953, *Phys. Rev.*, **92,** 1331.
Givens, W., 1954, *Oak Ridge National Laboratory Report*, No. 1574.
James, H. H., 1949, *Phys. Rev.*, **76,** 1611.
James, H. H., and Ginzbarg, A. S., 1953, *J. Phys. Chem.*, **57,** 840.
Landauer, R., and Helland, J. C., 1954, *J. Chem. Phys.*, **22,** 1655.
Ledermann, W., 1944, *Proc. Roy. Soc.* A, **182,** 362.
Lifschitz, I. M., and Stephanova, G. I., 1956, *J. Exp. Theor. Phys.*, **3,** 656.
Maradudin, A. A., Mazur, P., Montroll, E. W., and Weiss, G. H., 1958, *Rev. Mod. Phys.*, **30,** 175.
Muto, T., and Takagi, Y., 1955, *Solid State Physics*, Vol. **1** (New York: Academic Press), p. 193.
Prigogine, I., Bingen, R., and Jeener, J., 1954, *Physica,* **20,** 383, 516.
Schmidt, H., 1957, *Phys. Rev.*, **105,** 425.
Wilkinson, J. H., 1958, *Computer J.*, **1,** 90.

The Magnetic Susceptibility of Silver–Manganese Solid Solutions between 100°K and 500°K

By D. P. MORRIS and I. WILLIAMS
Physics Department, University College of North Wales, Bangor

MS. received 27th October 1958

Abstract. The magnetic susceptibility of Ag–Mn solid solutions containing between 4·44 and 38·1 at. % Mn has been measured between 100 and 500°K. Alloys containing less than 20 at. % Mn obey a Curie–Weiss law and the p_{eff} values derived for the Mn atoms are discussed and compared with other published values for this system. Over the range 7–20 at. % the (p_{eff}, Mn concentration) curve is linear, indicating a $3d^5 4s^2$ configuration for the Mn atoms at infinite dilution. Our own and some other published values for more dilute alloys are however not in good agreement with a linear extrapolation. Examination of published data shows that a similar discrepancy between dilute and more concentrated alloys exists in Cu–Mn solid solutions. No explanation of such an effect can yet be advanced, but the sensitivity of the p_{eff} values to the diamagnetic correction in very dilute alloys is pointed out, as well as a difference between electronic configurations deduced from susceptibility and from electron spin resonance measurements. Beyond 20 at. % Mn the Ag–Mn alloys no longer obey a Curie–Weiss law and the possibility of short-range magnetic order in them is discussed. Some comparisons are drawn between the solid solutions of Mn in Cu, Ag and Au.

---

§ 1. INTRODUCTION

It is well known that valuable information about the electronic configuration of transition metal atoms can be obtained from the magnetic susceptibility of alloys containing these atoms in solid solution. If the susceptibility obeys a Curie–Weiss law, effective magneton numbers p_{eff} may be derived, and assuming the orbital momenta to be quenched, p_{eff} may be equated to $[4S(S+1)]^{1/2}$, where S is the total spin quantum number of the solute atom.

Dilute solutions of Mn in the noble metals have been much studied in this connection, particularly at elevated temperatures, and we have now carried out susceptibility measurements between 100°K and 500°K on Ag–Mn solid solutions containing from 4·44 to 38·1 at. % Mn, thus covering practically the whole of the solid solubility range given by Raub and Engel (1946). When our work started, no low temperature susceptibility measurements had been reported on this system, but Otter *et al.* (1955) have since examined one Ag–Mn alloy containing 14·58 at. % Mn, and Owen *et al.* (1957) one Ag–Mn alloy containing 4·2 at. % Mn. On the high temperature side the only references are Néel (1932) (2·5–12·25 at. % Mn, 0–650°C), Gustafsson (1936) (0·19–7·4 at. % Mn, 20–468°C), and Kronqvist and Giansoldati (1953) (7·52–19·8 at. % Mn, 20–700°C). Our work thus overlaps with and extends both towards low temperatures and in range of composition that of these latter workers. Facilities were unfortunately not available to study these alloys at very low temperatures at which interesting magnetic and electrical anomalies are known to occur.

§ 2. EXPERIMENTAL

2.1. *Preparation of the Alloys*

Alloys were prepared from spectroscopically standardized silver and manganese, the latter being first degassed by heating in a Pyrex tube for 1 hour at 300°c under continuous evacuation. The constituents were accurately weighed, placed in an alumina crucible with lid, and sealed into an evacuated silica tube. The alloys were kept molten for a period of about 1 hour and were vigorously shaken to ensure thorough mixing. They were then homogenized by heating for 24 hours at 900°c and quenched into water. For the higher concentrations of Mn, the quenched solid solution phase is supersaturated at room temperature but, as for the similar case of Au–Ni alloys investigated by Kaufmann, Pan and Clark (1945), it has definite properties, and unless heated to a relatively high temperature a stability which does not allow the Mn atoms to precipitate out and change the magnetic behaviour.

The silica tubes were then opened and the alloys in the form of small cylinders weighed and checked against the mass of the original ingredients. A small loss in weight, amounting to about 1 part in 500 of the total weight, was usually found. Although a slight taper occasionally necessitated breaking open a crucible, the alloys were clean and sound in appearance, with no sign of contamination, but there was usually a slight darkening of the top of the crucible. On the basis of previous extensive experience in this laboratory of preparing noble metal alloys (Owen and Roberts 1945) we have felt justified in attributing the weight loss to slight volatilization of Mn, and the nominal compositions have been adjusted accordingly. To minimize any errors due to possible segregation the whole ingot of each alloy, weighing approximately 0·5 g, was used for the magnetic measurements.

2.2. *Magnetic Measurements*

The magnetic susceptibility of the alloys was determined using a Sucksmith ring balance, the specimens being contained in a high-purity aluminium specimen holder. Corrections were applied at each temperature for the deflection due to the empty specimen holder and the thermocouple assembly, the latter consisting of a calibrated copper–constantan thermocouple whose junction lay inside the specimen holder and very close to the actual specimen. For elevated temperatures the specimen holder was surrounded by a long cylindrical heater contained in a Pyrex tube attached by means of an O-ring to the base of the balance. For low temperature work a conduction system similar to that of van Oort (1951) was employed, a Dewar sleeve providing the necessary insulation from the pole pieces of the electromagnet. The lowest specimen temperature attainable with liquid air was about − 175°c. The ring balance could be evacuated or filled with argon at a low pressure, and its sensitivity determined at each temperature by means of a rider operated by a small electromagnet.

The values of $H\,dH/dx$ were initially determined using Analar $MnSO_4 . 4H_2O$ (Bates 1951). Small discrepancies were however found between our measured susceptibilities of $FeSO_4 . (NH_4)_2SO_4 . 6H_2O$, $FeSO_4 . 7H_2O$, and $NiSO_4 . 7H_2O$

and published data for these salts, presumably on account of uncertainty in the exact number of molecules of water of crystallization. The values of $H\,dH/dx$ were then redetermined using pure tantalum (Hoare and Walling 1951). This removed some of the discrepancies previously found, and $FeSO_4(NH_4)_2SO_4 . 6H_2O$ was then used to investigate the variation of $H\,dH/dx$ with volume of specimen. This effect was allowed for in our measurements on the alloys. This salt was also used to check the performance of the balance at low temperatures and good agreement was obtained with the results of Jackson (1924). Tests showed that the insertion of the auxiliary equipment into the gap of the electromagnet did not affect the calibration.

The electromagnet had truncated and stepped pole-pieces of the type described by Sucksmith (1939) and was supplied from a large capacity storage battery, the current being measured with an accurate Weston ammeter. A calibrated search-coil and fluxmeter were used to determine the average field over the volume of the search-coil. As our specimens were of slightly different volumes this did not represent exactly the field in which the susceptibility measurements were made, but the fact that they were independent of field over the range 2000–10 000 Oe was established by comparing the ratio of their corrected deflections for different magnet currents with the corresponding values for the field-independent calibration material. It is estimated that the absolute values of the susceptibility are accurate to about 2 % at room temperature.

§ 3. RESULTS

It is first necessary to correct the measured susceptibilities for temperature-independent diamagnetism. This has been done in the conventional way by assuming that the main diamagnetic contribution comes from the silver. The measured susceptibilities were thus first converted into gramme-atomic susceptibilities χ_A and the corrected susceptibilities χ_C determined from the formula $\chi_A = \chi_C + a$, where $a = (1-x)\chi_{Ag}$, x = atomic concentration of Mn, $\chi_{Ag} = -19{\cdot}56 \times 10^{-6}$ e.m.u. (g atom)$^{-1}$ (Henry and Rogers 1956).† Strictly a correction is also necessary for the diamagnetism of the Mn atom cores, but there is uncertainty in the precise value to be taken. Néel (1936) has suggested a value of -43×10^{-6} e.m.u. (g atom)$^{-1}$ for the $3d^5 4s^2$ configuration, but the inclusion of this term makes only a few tenths per cent difference to any of the final corrected susceptibilities and it has therefore been omitted. It may also be noted that the measured susceptibilities of our alloys over the temperature range investigated are large enough to be little influenced by small error in the value of χ_{Ag}, but this and any omission or intrinsic error in the method of diamagnetic correction have increasingly greater effects as the temperature is raised and the concentration of Mn reduced.

The results are shown in figures 1 and 2 as graphs of $1/\chi_C$ plotted against T. For the alloys containing 4·44, 7·97, 12·90, 16·7 and 17·6 at. % Mn these graphs are linear, showing that the magnetic behaviour is well represented over the temperature range 100–500°K by a Curie–Weiss law $\chi = C/(T-\theta)$. We have also included in figure 1 the data of Owen *et al.* for 4·2 at. % Mn, and of Gustafsson for 7·4 at. % Mn. Reference to these will be made later. The values of θ, C and p_{eff} deduced from our results are given in table 1. C and θ were calculated for each alloy by dividing the observations into two groups and solving the simultaneous equations obtained by pairing an observation from the first group with one from the second. In this way a probable error based on between 8 and 13 values of C and θ could be given for each alloy. This represented how closely the observations obeyed an equation of the Curie–Weiss type. The values of these probable errors were about $\pm 1 \times 10^{-3}$ for C, and $\pm 1\,^{\circ}\mathrm{C}$ for θ for each alloy. In addition the absolute values of θ and C are affected by error of temperature measurement and by systematic error arising from the calibration of the ring balance. It is estimated that C is accurate to about 4% and θ to about 3–4 °K.

---

† This most recent value differs appreciably from the previously accepted value of $-21{\cdot}5 \times 10^{-6}$ e.m.u. (g atom)$^{-1}$.

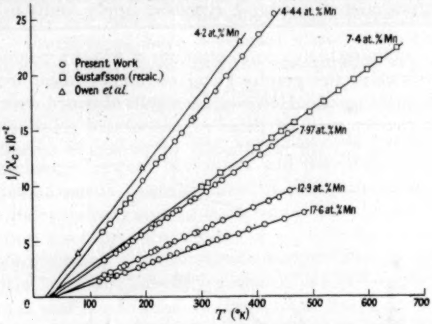

Figure 1. $(1/\chi_{\mathrm{C}}, T)$ graphs for Ag–Mn solid solutions containing up to 17·6 at. % Mn. χ_{C} is expressed in e.m.u. (g atom)$^{-1}$ of alloy.

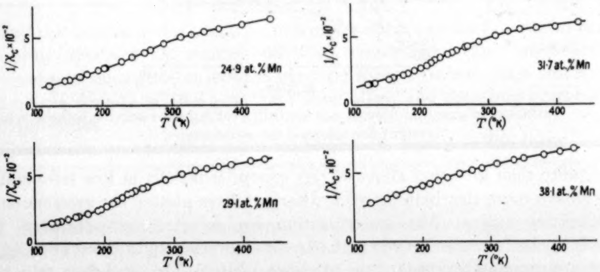

Figure 2. $(1/\chi_{\mathrm{C}}, T)$ graphs for Ag–Mn solid solutions containing between 24·9 and 38·1 at. % Mn. χ_{C} is expressed in e.m.u. (g atom)$^{-1}$ of alloy.

Table 1. θ, C and p_{eff} for Ag–Mn Alloys (present work)

At. % Mn	θ °K	$C \times 10^3$	p_{eff}
4·44	27	161	5·39
7·97	27	298	5·47
12·9	35	448	5·27
16·7	36	549	5·14
17·6	30	576	5·12

p_{eff} was calculated assuming $\mu_B = 9{\cdot}27 \times 10^{-21}$ e.m.u., $k = 1{\cdot}381 \times 10^{-16}$ erg deg^{-1}, $N = 6{\cdot}022 \times 10^{23}$. In addition to any uncertainty due to error in C, p_{eff} is also affected by error in composition. In view of the way the composition has been established the values quoted in table 1 represent upper limits to p_{eff} for each alloy.

For the alloys containing higher concentrations of Mn the magnetic behaviour is not so straightforward, the graphs being no longer linear over the whole temperature range investigated. However the results obtained were reproducible and appear to be characteristic of these supersaturated solid solutions. The alloy containing 38·1 at. % Mn was found to possess a considerably lower susceptibility than the other alloys of this group, especially at low temperatures. This is shown more clearly in figure 3, where we have plotted the gramme-atomic susceptibilities against Mn concentration for selected temperatures. The susceptibility increases uniformly with Mn concentration up to about 18 at. % Mn, remains approximately constant up to about 32 at. % Mn, and then falls as the Mn content increases still further. It is conceivable that this effect is due to precipitation of Mn from the supersaturated solid solution through inadequate quenching. Calculation, using published data for the susceptibility of α-Mn (Kriessman and Callen 1954), shows however that for the 38·1 at. % Mn alloy for example the solid solution would have to contain less than 10 at. % Mn to account for the effect. This hardly seems possible in view of the form of the equilibrium diagram. In addition, an X-ray photograph of a powder sample of this alloy quenched from 900°C showed only the lines of the face-centred cubic solid solution with a lattice spacing agreeing well with the results of Raub and Engel, so that the quenching procedure was here adequate to retain the supersaturated solid solution. The face-centred cubic structure was also observed when the sample was photographed at liquid-air temperature, and there was no indication of a distortion to lower symmetry. The direct determination of the susceptibility of these alloys in the stable solid solution range has not been attempted by us, since the temperature range involved is small for the more concentrated alloys and the work of Néel has shown that there is considerable difficulty in preventing volatilization of Mn at these high temperatures.

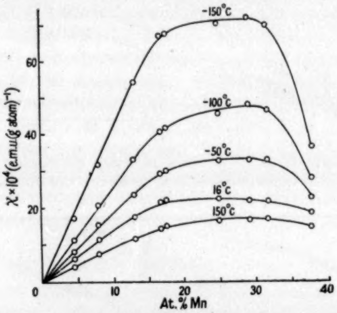

Figure 3. Variation of gramme-atomic susceptibility of Ag–Mn solid solutions with Mn content for selected temperatures.

§ 4. Discussion

It is now known that dilute solid solutions of Cu–Mn and Ag–Mn show a gradual transition from paramagnetism to antiferromagnetism as the temperature is reduced to very low values. This effect occurs below our lowest attainable temperature. Owen *et al.* have developed a two sub-lattice molecular field model of this effect which shows that the susceptibility is given by

$$\chi=\frac{C(1+\lambda\chi_e)^2}{T-\theta}+\chi_e$$

where C is the Curie constant, λ the molecular field parameter corresponding to indirect exchange between Mn atoms and the conduction electrons, and χ_e the Pauli paramagnetic susceptibility of the conduction electrons. The temperature independent term χ_e is of course allowed for in the diamagnetic correction, since the experimental value of χ_{Ag} includes the contribution due to the conduction electrons. The corrected susceptibilities thus obey a Curie–Weiss law but with a 'modified' Curie constant $C'=C(1+\lambda\chi_e)^2$. Owen *et al.* have shown however that λ is so small in these alloys that C', calculated in the usual way from the experimental results, can be taken as equal to C with negligible error.

As already remarked we have included in figure 1 the data of Owen *et al.* for 4·2 at. % Mn, and of Gustafsson for 7·4 at. % Mn. The former workers applied the normal diamagnetic correction for silver and the line drawn in figure 1 has been obtained by reading off $1/\chi_V$ values from their published graph (χ_V = volume susceptibility) and converting these first into mass susceptibilities assuming a density of 10·4 g cm^{-3} for their alloy, and then into gramme-atomic susceptibilities.

Gustafsson on the other hand expressed his results in the form

$$\chi=\chi_0+\frac{C}{T}$$

and deduced C and the temperature-independent part χ_0 from graphs of χ against $1/T$. This assumes that the susceptibilities obey a Curie rather than a Curie–Weiss law, an assumption which, for a finite θ, will be more nearly correct the higher the temperature. Gustafsson himself noted that there was a slight departure from linearity in his graphs at the lowest temperature (~ 290 °K) and highest Mn content (7·4 at. % Mn), and this curvature was very marked at the lower temperatures when our results and those of Owen *et al.* were represented as (χ, $1/T$) curves. A Curie law does not therefore correctly represent the behaviour of these alloys over the whole temperature range, and we have recalculated Gustafsson's data employing the conventional diamagnetic correction. As will be seen from figure 1, Gustafsson's results for the 7·4 at. % Mn alloy can be well represented by a Curie–Weiss law, and this also applies for his 0·19, 1·10, 2·105 and 3·16 at. % Mn alloys, although the graphs are not shown in figure 1 owing to the unsuitable scale. The two interpretations of Gustafsson's results however lead to somewhat different values of C and p_{eff} as may be seen from table 2. To show the sensitivity of θ, C and p_{eff} to the diamagnetic correction in these alloys we have also included in table 2 the values obtained taking $\chi_{Ag}=-21{\cdot}5\times10^{-6}$ e.m.u. (g atom)$^{-1}$.

In figure 4 we have plotted p_{eff} against Mn concentration, including our own results and those of Owen *et al.*, Gustafsson, and Kronqvist and Giansoldati

Table 2. Gustafsson's Results for Ag–Mn interpreted according to (*a*) Curie law, (*b*) Curie–Weiss law

At. % Mn	Curie law		Curie–Weiss law					
	$C \times 10^3$	p_{eff}	θ°K		$C \times 10^3$		p_{eff}	
			†	‡	†	‡	†	‡
0·19	7·15	5·50	− 7	−66	7·40	9·47	5·65	6·32
1·10	41·7	5·51	−20	−31	47·1	49·3	5·87	5·99
2·105	83·9	5·65	− 1	− 4	84·8	86·0	5·68	5·72
3·16	124·5	5·62	0	− 3	126·5	128·2	5·66	5·70
7·4	313	5·82	24	21	283·5	287·0	5·54	5·57

† $\chi_{\mathrm{Ag}} = -19{\cdot}56 \times 10^{-6}$e.m.u. (g atom)$^{-1}$. ‡ $\chi_{\mathrm{Ag}} = -21{\cdot}5 \times 10^{-6}$e.m.u. (g atom)$^{-1}$.

(over the range 290–570°K). With the exception of our value for 4·44 at. % Mn and that of Owen *et al.* for 4·2 at. % Mn the points lie on a straight line which can be extrapolated to give a p_{eff} value of about 5·8 at infinite dilution. This corresponds approximately to a $3d^54s^2$ state for the Mn atoms. However the two exceptions noted throw some doubt on the validity of this extrapolation since the estimated limits of accuracy place them both below this extrapolated line. As indicated above the values of Gustafsson could probably be reconciled with a departure from linearity below 5 at. % Mn in view of their sensitivity to the diamagnetic correction and error in composition.

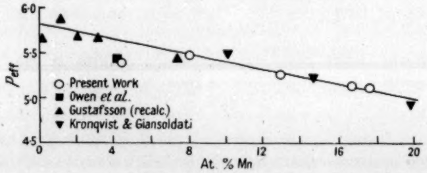

Figure 4. (p_{eff}, Mn concentration) graph for Ag–Mn solid solutions.

It is interesting to compare this situation with that for solid solutions of Mn in Cu and Au. We have assembled the available data in figure 5, all the p_{eff} values being based on the assumption of a Curie–Weiss law. For Au–Mn the number of available points is limited, but they lie reasonably well on a line which extrapolates linearly to about 5·8, corresponding fairly closely to a $3d^54s^2$ state for the Mn atoms. For Cu–Mn the work of Myers (1956) and of Valentiner and Becker (1933) shows the (p_{eff}, Mn concentration) curve is linear between 5 and 25 at. % Mn, and this extrapolates back to about 4·9, corresponding to a $3d^64s^1$ state. (Friedel (1956) has concluded from Myers' work that p_{eff} remains constant at about 5·0 up to large concentrations of Mn, but this seems unjustified, as Friedel's values were based on a Curie law interpretation. Friedel has also interpreted this p_{eff} value to correspond to a $3d^5$ state, which as pointed out by Schmitt and Jacobs (1957) is due to confusion between effective magneton numbers and saturation moments.) The results of Owen *et al.* and of Gustafsson, however, are not in agreement with this linear curve between 0 and 5 at. % Mn, but suggest that a maximum exists in this region.

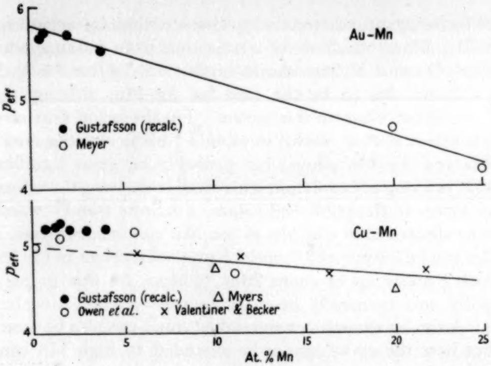

Figure 5. (p_{eff}, Mn concentration) graphs for Au–Mn and Cu–Mn solid solutions.

Whilst it cannot be entirely ruled out that these anomalous effects in Cu–Mn and Ag–Mn are attributable to the sensitivity of p_{eff} to the magnitude of the diamagnetic correction and to error in composition there is reasonable evidence that the p_{eff} values of the dilute alloys do not conform well with a linear extrapolation based on data on more concentrated alloys. The explanation of such an effect however is not clear. There is first of all an appreciable difference at high dilutions between the p_{eff} values for Cu–Mn on the one hand and Ag–Mn and Au–Mn on the other. For the former the electronic configuration of the Mn atoms approximates most closely to $3d^6 4s^1$, and for the latter to $3d^5 4s^2$. This is presumably due to the considerably smaller lattice spacing of the Cu alloys, the closer contact between solvent and solute atoms tending to make the Cu–Mn bonds more covalent in nature, the 3d-holes of the Mn atoms being no longer strictly localized near the Mn nucleus and therefore differing from the free atom configuration. The covalent bond leads not only to spin transfer between the two atoms but to the possibility of superexchange through Cu atoms as pointed out by Owen *et al.* These workers have suggested that this is responsible for the ferromagnetic coupling in these alloys, and direct exchange between nearest neighbour atoms for the antiferromagnetic coupling. The exchange effects are smaller in the Ag–Mn alloys presumably on account of their larger lattice spacing. If now the (p_{eff}, Mn concentration) curve for these systems was entirely linear, the gradual reduction in the magnetic moment per Mn atom could be regarded as similar to the reduced moment in ferromagnetics, where the conduction electrons can be pictured as partially filling up the d-holes. A curvature, and particularly a maximum, in the (p_{eff}, Mn concentration) curve is less easy to understand, for it implies that this filling-up process does not proceed uniformly with increasing Mn concentration and there is no obvious reason why this should be so. The situation is further complicated since in Cu–Mn there is also a discrepancy between the electronic configuration deduced from susceptibility measurements and that from electron spin resonance measurements, the former indicating a $3d^6 4s^1$ state and the latter a $3d^5 4s^2$ state (Owen *et al.*). These effects are not yet clearly understood.

Most antiferromagnetic materials are characterized by negative values of θ. For the Cu–Mn alloys which show a transition from paramagnetism to antiferromagnetism, Owen *et al.* have shown experimentally that θ is always positive, and we have found this to be the case for Ag–Mn, although we have not investigated very dilute alloys of this system. For the latter, Gustafsson's results yield negative values of θ, as shown in table 2 (this is also the case for his very dilute Cu–Mn and Au–Mn alloys) but probably no great significance can be attached to this, as a long extrapolation is involved in deriving the values. However, despite some scatter in the published values, a definite trend towards increasing θ values can be discerned in Cu–Mn as the Mn content increases, as shown in figure 6. This can be interpreted to mean a gradual increase in the ferromagnetic coupling which persists up to about 20 at. % Mn. At this point, θ begins to decrease rapidly and eventually becomes increasingly negative beyond about 45 at. % Mn. A similar though not so marked trend can also be seen for Ag–Mn (figure 6), but here the curve cannot be extended to high Mn concentrations, as a Curie–Weiss law no longer holds beyond about 18 at. % and in any case the solid solution only extends to about 40 at. % Mn. The decrease in θ suggests that the resultant ferromagnetic coupling is beginning to diminish, and it is interesting to observe that this diminution coincides well in both systems with the point at which the low temperature susceptibility of the alloys no longer increases uniformly with addition of Mn (see figures 3 and 7). For Cu–Mn the neutron diffraction experiments of Meneghetti and Sidhu (1957) indicate the onset of short range magnetic order at about 13 at. % Mn and this reaches a maximum at 50 at. % Mn. Beyond 69 at. % Mn an antiferromagnetic structure is observed, believed to be due to an antiferromagnetic coupling between Mn atoms as the Mn concentration becomes predominant. It seems reasonable to conclude that the decrease in θ and the change in the low temperature variation of the mass susceptibility with Mn concentration can be attributed to a gradual increase in the antiferromagnetic coupling as the Mn concentration increases and that an antiferromagnetic structure would also exist at high concentrations in Ag–Mn, although this cannot be tested as the solid solution does not extend

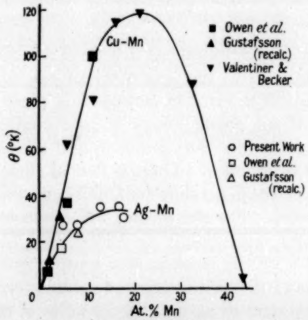

Figure 6. Variation of paramagnetic Curie temperature θ with Mn content for Cu–Mn and Ag–Mn solid solutions.

sufficiently far. It would be interesting however to see whether short range magnetic order could be detected by neutron diffraction in Ag–Mn. Our liquid-air x-ray photograph of the 38·1 at. % Mn alloy gave no indication of atomic ordering in the alloy.

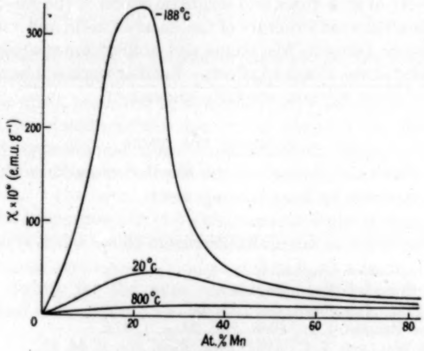

Figure 7. Variation of magnetic susceptibility of Cu–Mn solid solutions with Mn content at different temperatures.
– 188°c and 20°c Valentiner and Becker; 800°c Myers.

The variation of susceptibility with Mn concentration at the elevated temperatures must of course have a different explanation because as pointed out by Myers the effect in Cu–Mn is observed well above any temperature at which magnetic ordering is important. In fact there seems to be a definite difference in the nature of this variation for both Cu–Mn and Ag–Mn, as may be seen from figures 3 and 7, the high temperature results indicating that the susceptibility is independent of Mn concentration beyond a certain value, in contrast to the rapid fall which ultimately occurs at low temperatures. The high temperature effect is attributed by Myers for Cu–Mn to a transition at about 25 at. % Mn from localized states for the 3d electrons of the Mn atoms to a collective electron treatment of these electrons for the atoms of the alloy.

It will be noticed that θ is always numerically smaller at comparable compositions in Ag–Mn than in Cu–Mn, and this could well be due to an overall reduction in all the coupling parameters due to the increased separation of the atoms in this system. It may also be worth observing that the coupling parameters themselves may be temperature-dependent, in virtue of the thermal expansion of the lattice, and that their relative values may change with temperature. If so, the expression for θ derived by Owen *et al.* on their two sub-lattice model shows that θ itself will vary with temperature, and this may provide an explanation for the departure from a Curie–Weiss behaviour found for the more concentrated alloys.

Finally we note that the only one of the three solid solution systems exhibiting pronounced ferromagnetism is Au–Mn (Meyer 1956, 1957). This alloy system is considerably more complex both structurally and magnetically than either Cu–Mn or Ag–Mn, and ferromagnetism, antiferromagnetism, and metamagnetism (Meyer and Taglang 1956) are displayed at the appropriate compositions. In view of the nearly equal lattice dimensions of Ag and Au one would expect a greater similarity between Ag–Mn and Au–Mn than between either and Cu–Mn, but as regards magnetic properties this appears to be borne out mainly only with the p_{eff} values, and Cu–Mn and Ag–Mn seem more analogous. The greater variety of structures and magnetic effects of the Au–Mn system may well be due to the electronic structure of the Au atom itself, and it is not impossible that direct exchange between Mn atoms and unfilled inner shells in Au may be partly responsible for the observed effects. Further work will be necessary before the properties of these systems are fully understood.

ACKNOWLEDGMENTS

We wish to thank the Council of the Royal Society for a Grant-in-Aid and Professor E. R. Andrew for his encouragement.

REFERENCES

BATES, L. F., 1951, *Modern Magnetism*, 3rd Edn (Cambridge: University Press).
FRIEDEL, J., 1956, *Canad. J. Phys.*, **34**, 1190.
GUSTAFSSON, G., 1936, *Ann. Phys., Lpz.*, **25**, 545.
HENRY, W. G., and ROGERS, J. L., 1956, *Phil. Mag.*, **1**, 223.
HOARE, F. E., and WALLING, J. C., 1951, *Proc. Phys. Soc.* B, **64**, 337.
JACKSON, L. C., 1924, *Phil. Trans.* A, **224**, 1.
KAUFMANN, A., PAN, S., and CLARK, J., 1945, *Rev. Mod. Phys.*, **17**, 87.
KRIESSMAN, C. J., and CALLEN, H. B., 1954, *Phys. Rev.*, **94**, 837.
KRONQVIST, E., and GIANSOLDATI, A., 1953, *Ark. Fys.*, **7**, 343.
MENEGHETTI, D., and SIDHU, S. S., 1957, *Phys. Rev.*, **105**, 130.
MEYER, A. J. P., 1956, *C. R. Acad. Sci., Paris*, **242**, 2315.
—— 1957, *Ibid.*, **244**, 2028.
MEYER, A. J. P., and TAGLANG, P., 1956, *J. Phys. Radium*, **17**, 30.
MYERS, H. P., 1956, *Canad. J. Phys.*, **34**, 527.
NÉEL, L., 1932, *J. Phys. Radium*, **3**, 160.
—— 1936, *Ann. Phys., Paris*, **5**, 232.
VAN OORT, W. P., 1951, *J. Sci. Instrum.*, **28**, 279.
OTTER, F. A., FLANDERS, P. J., and KLOKHOLM, E., 1955, *Phys. Rev.*, **99**, 599.
OWEN, E. A., and ROBERTS, E. A. O'D., 1945, *J. Inst. Met.*, **71**, 213.
OWEN, J., BROWNE, M. E., ARP, V., and KIP, A. F., 1957, *J. Phys. Chem. Solids*, **2**, 85.
RAUB, E., and ENGEL, A., 1946, *Metallforschung*, **1**, (1/2), 62.
SCHMITT, R. W., and JACOBS, I. S., 1957, *J. Phys. Chem. Solids*, **3**, 324.
SUCKSMITH, W., 1939, *Proc. Roy. Soc.* A, **170**, 551.
VALENTINER, S., and BECKER, G., 1933, *Z. Phys.*, **80**, 735.

Spin–Orbit Coupling and the Extraordinary Hall Effect

By C. STRACHAN and A. M. MURRAY
Department of Natural Philosophy, The University, Aberdeen

MS. received 28th July 1958, in revised form 22nd October 1958

Abstract. In general terms a qualitative account of the extraordinary Hall effect in ferromagnetic media may be based on spin–orbit coupling. The magnitude of the effect produced is, classically, very sensitive to the actual path of the electron, or, quantum-mechanically, to some of the detail of its wave function. Here conventional quantum-mechanical transport theory is used in some quantitative detail to evaluate the actual magnitude of the extraordinary Hall coefficient R_s. The initial states of electrons after collisions with the lattice are assumed to be a superposition of Bloch functions with random phases. Bloch functions for the s- and d-bands of nickel are chosen in sufficient detail to make possible a numerical calculation. It is found that R_s/ρ^2, where ρ is the resistivity, increases very slightly for the pure metal with increasing temperature. At 290°K, R_s is found to be slightly less than -2×10^{-12} ohm cm gauss^{-1}.

§ 1. Introduction

The extraordinary Hall effect in ferromagnetics, i.e. the production of an electromotive force in a direction transverse to that of current flow and related to the magnetization, seems to call for the kind of force which arises from spin–orbit coupling. Many authors have investigated this, for example, Karplus and Luttinger (1954), Smit (1956). For anything more than qualitative results, the quantitative evaluation of matrix elements makes demands on theory which can at present be met only rather inadequately. In addition the status of the semi-classical Boltzmann equation of transport theory and indeed transport theory itself is the subject of increasingly searching analysis.

A preliminary estimate (Strachan and Murray 1958) shows that spin–orbit coupling can provide a transverse force on a conduction electron which is quite sufficient to account for the magnitude of the phenomenon, and which is much larger than that caused by any actual internal magnetic fields in the ferromagnetic material. This force is however very sensitive to the actual 'path' of the electron, i.e. to some of the detail of its wave function. It therefore seemed desirable to apply conventional quantum-mechanical transport theory to this problem and to evaluate the result in as much quantitative detail as is reasonably justified. Thus we have used the conventional Boltzman equation and have assumed that a relaxation time exists. The effect of an applied electric field and of the spin–orbit coupling on electrons described by an antisymmetrical wave function has been formulated in the equivalent one-electron problem. The initial states of the electrons after each collision we have chosen to be a superposition, with random phases, of states given by Bloch functions perturbed by spin–orbit interaction.

The effect of any actual internal magnetic fields is ignored in comparison with spin–orbit coupling. The equivalent field due to exchange is allowed for by assigning different energies to states which differ only in spin direction.

It has, of course, been recognized that the occurrence of the square of the resistivity in Karplus and Luttinger's result for the coefficient of the extraordinary Hall effect is not a consequence of detailed theory but rather of immediate definition as may be seen from equations (4) and (5) below. We have intentionally made more specific assumptions about the nature of Bloch wave functions than these authors have. While these assumptions are incomplete in detail they are reasonable and make possible a numerical estimate. In addition we have included in our evaluation of the velocity of an electron the occurrence of non-diagonal interference terms arising from pairs of bands. The spin of the electron occurs as a dynamical variable and not simply as a multiple of the magnetization. Our model is thus that of a number of electrons each of which, after a collision with the lattice and at the beginning of its next free path, is described by a wave function with random phase. The motion of each of these electrons, under the influence of electric field components and spin–orbit coupling, is calculated allowing for all possible intra- and inter-band transitions. The occurrence of collisions is described by allowing a distribution of probable times of flight in accordance with a mean collision time which occurs as a parameter. For simplicity we have taken the s electrons to be unpolarized although the analysis can be extended to include such polarization. Indeed the greater mobility of these electrons might partly compensate for small polarization in comparison with the larger polarization of the much less mobile d electrons. The distribution of electrons throughout the bands is affected by the electric field but not, to the first order, by the spin–orbit coupling. Karplus and Luttinger, somewhat tentatively, made the assumption that transitions between d bands were the important ones. We find that transitions beween s and d bands are the most significant ones.

At least part of this work was intended, in being applied to a more definite model, to be complementary to the interesting work of these authors.

§ 2. THE TRANSVERSE CONDUCTIVITY

The Hamiltonian for a single electron in a usual notation has the form

$$H=\frac{1}{2m_e}\mathbf{p}^2+V'+\lambda(\boldsymbol{\sigma}\times\operatorname{grad}V')\,.\,\mathbf{p}\,;\quad \lambda=\frac{\hbar}{4m_e{}^2c^2},$$

m_e being the electronic mass, and $\boldsymbol{\sigma}$ the unit spin operator. There are of course other terms which contain c^2 in the denominator but they cause small alterations in quantities which can only be related in general terms to effective masses etc., in the band picture of a metal and which also do not have the directional properties of the above term in λ. Hence, if $\boldsymbol{\mathfrak{E}}$ is the applied electric field and e the numerical magnitude of the electronic charge, $V'=V+e\boldsymbol{\mathfrak{E}}\,.\,\mathbf{r}$, where V is the potential energy of the electron in the lattice fields. Thus the equation for the one electron two component wave-function is

$$-\frac{\hbar}{i}\frac{\partial\Psi}{\partial t}=\left\{-\frac{\hbar^2}{2m_e}\nabla^2+V'+\lambda(\boldsymbol{\sigma}\times\operatorname{grad}V')\,.\,\mathbf{p}\right\}\Psi. \quad\ldots\ldots(1)$$

It follows that if $\Psi^\dagger$ be the Hermitian conjugate of Ψ the mean value of the velocity corresponding to the wave function Ψ is

$$\mathbf{v}=\int d\tau\left[\frac{1}{m_e}\Psi^\dagger\mathbf{p}\Psi+\lambda\Psi^\dagger(\boldsymbol{\sigma}\times\operatorname{grad}V)\Psi-\lambda e\boldsymbol{\mathfrak{E}}\times(\Psi^\dagger\boldsymbol{\sigma}\Psi)\right]. \quad\ldots\ldots(2)$$

The current density $\mathbf{J}$ is given by

$$\mathbf{J} = -e\int \mathbf{v} f n(\mathbf{k})\, d\mathbf{k} \qquad \ldots\ldots(3)$$

where $\mathbf{v}$ now means the velocity for a wave-packet Ψ whose propagation vector is $\mathbf{k}$, f if the relevant statistical distribution function, and $n(\mathbf{k})\delta\mathbf{k}$ is the number of states in the interval $(\mathbf{k}, \mathbf{k}+\delta\mathbf{k})$. To the first order in $\mathfrak{E}$ we have

$$\left.\begin{aligned} J_x &= \sigma_{xx}\mathscr{E}_x + \sigma_{xy}\mathscr{E}_y \\ J_y &= \sigma_{yx}\mathscr{E}_x + \sigma_{yy}\mathscr{E}_y \end{aligned}\right\} \qquad \ldots\ldots(4)$$

where we suppose that the x axis is in the direction of the current while the Hall electromotive force is measured in the y direction. The experimental conditions are such that $J_y = 0$. Since σ_{xy}, σ_{yx} will each be of order λ we may therefore write

$$\frac{\mathscr{E}_y}{J_x} = -\frac{\sigma_{yx}}{\sigma_{xx}\sigma_{yy} - \sigma_{xy}\sigma_{yx}} = -\frac{\sigma_{yx}}{\sigma^2} \qquad \ldots\ldots(5)$$

approximately where $\sigma_{xx} = \sigma_{yy} = \sigma$.

Karplus and Luttinger (1954) took $\mathscr{E}_y$ to be zero and evaluated $\sigma^{-1}J_y/J_x$. Strictly speaking their σ refers to conditions different from the above but can only differ from ours by terms of order λ which are unimportant when multiplied by σ_{yx}; σ_{yx} differs from zero in our formulation only because of spin–orbit coupling and is hence of order λ. We must therefore evaluate the coefficient of $\mathscr{E}_x$ in J_y by means of (2), (3) and (4). From (2) σ_{yx} is the sum of three parts $\sigma_{yx}^{(1)}$, $\sigma_{yx}^{(2)}$, $\sigma_{yx}^{(3)}$ arising in order from the three terms on the right-hand side of (2). The last part may be evaluated immediately. Since the last term in (2) already contains λ and $\mathscr{E}_x$ we need not consider any alteration in the distribution function f. Thus

$$\sigma_{yx}^{(3)} = -\lambda e^2 \int f n(\mathbf{k})\, d\mathbf{k} \int d\tau \Psi^\dagger \sigma_z \Psi = -eM_z/2m_e c \qquad \ldots\ldots(6)$$

where M_z is the z component of the mean magnetic moment per electron. We shall see later that this term is negligible in comparison with $\sigma_{yx}^{(1)}$.

§ 3. ONE-ELECTRON WAVE FUNCTIONS

In order to obtain $\sigma_{yx}^{(1)}$ and $\sigma_{yx}^{(2)}$ we expand Ψ in terms of Bloch functions for an electron in the lattice unperturbed by external fields. Thus

$$\Psi = \sum_m \int d\mathbf{k}\, \zeta_m(\mathbf{k}, t)\psi_m(\mathbf{k}, \mathbf{r}) \qquad \ldots\ldots(7)$$

where

$$\psi_m(\mathbf{k}, \mathbf{r}) = e^{i\mathbf{k}.\mathbf{r}}\, u_m(\mathbf{k}, \mathbf{r}) \qquad \ldots\ldots(8)$$

u_m having the lattice periodicity and being normalized over unit cell of the lattice. The index m labels both the band and the direction of spin, i.e. ψ_m is the product of a function of $\mathbf{r}$ and either of the two spin eigenfunctions. The direction of spin quantization is taken to be that of the Z axis in a triad X, Y, Z which is in general not coincident with the x, y, z axes. The Z axis has the direction of magnetization in the domain in which the electron is moving. We shall suppose that any given band will consist of two parts whose energies, for a given value of $\mathbf{k}$, but corresponding to the two spin eigenstates, differ by a band constant $2\eta_m$. This constant, in general, will be taken to be much larger than any splitting of levels due to spin–orbit interaction.

If Δ is the volume of the unit cell, and if Ψ is normalized over all space, the normalization of u_m over unit cell means that

$$\sum_m \int d\mathbf{k}\,\zeta_m{}^*(\mathbf{k},t)\zeta_m(\mathbf{k},t)=\frac{\Delta}{8\pi^3}. \qquad \ldots\ldots(9)$$

From (1) and (7)

$$-\frac{\hbar}{i}\frac{\partial}{\partial t}\zeta_m(\mathbf{k},t)=E_m\zeta_m(\mathbf{k},t)+ie\mathfrak{E}\,.\,\frac{\partial}{\partial\mathbf{k}}\zeta_m(\mathbf{k},t)$$
$$+\sum_{m'}\{e\mathfrak{E}\,.\,\mathbf{U}_{mm'}+\lambda W_{mm'}+\lambda e\mathfrak{E}\,.\,\mathbf{S}_{mm'}\}\zeta_{m'}(\mathbf{k},t) \qquad \ldots\ldots(10)$$

where

$$\left.\begin{aligned}\mathbf{U}_{mm'}&=i\int d\tau_0 u_m{}^*\frac{\partial}{\partial\mathbf{k}}u_{m'}=\mathbf{U}_{m'm}{}^*\\ W_{mm'}&=\int d\tau_0\,\psi_m{}^*\boldsymbol{\sigma}\,.\,(\text{grad}\,V\times\mathbf{p})\psi_{m'}=W_{m'm}{}^*\\ \mathbf{S}_{mm'}&=-\int d\tau_0\psi_m{}^*(\boldsymbol{\sigma}\times\mathbf{p})\psi_{m'}=\mathbf{S}_{m'm}{}^*\end{aligned}\right\} \qquad \ldots\ldots(10')$$

the integration being over unit cell.

We shall neglect the $\mathbf{U}_{mm'}$ in what follows†. Then, from (10)

$$-\frac{\hbar}{i}\frac{\partial\zeta_m}{\partial t}=E_m\zeta_m+ie\mathfrak{E}\,.\,\frac{\partial\zeta_m}{\partial\mathbf{k}}+\lambda\sum_{m''}W_{mm''}\zeta_{m''}+\lambda e\mathfrak{E}\,.\,\sum_{m''}\mathbf{S}_{mm''}\zeta_{m''}. \qquad \ldots\ldots(11)$$

In any band, for a given direction of spin and for a given value of $\mathbf{k}$, there will in general, when $\mathfrak{E}=0$, and in the absence of spin–orbit coupling, be degeneracies in energy. Spin–orbit coupling will remove part or all of this degeneracy and we shall choose our wave functions such that $W_{mm'}=0$ for $m'\neq m$, where $E_{m'}$ and E_m are equal in the absence of spin–orbit coupling. Thus we have stationary states given by

$$\left.\begin{aligned}\zeta_{m'}{}^0&=\alpha_{m'}\exp(-iE_{m'}t/\hbar)\\ \zeta_m{}^0&=(\lambda W_{mm'}\alpha_{m'}/\hbar\Delta_{m'm})\exp(-iE_{m'}t/\hbar)\quad\text{for } m\neq m',\end{aligned}\right\} \qquad \ldots\ldots(12)$$

where $\hbar\Delta_{m'm}=E_{m'}-E_m$. Here for convenience E_m is taken to include λW_{mm} although, for consistency, $\Delta_{m'm}$ should not contain terms in λ. The expressions for current and distribution function involve bilinear combinations of the ζ_m so that it is convenient to derive from (11) the equation

$$\frac{\partial}{\partial t}\zeta_{m'm}=i\Delta_{m'm}\zeta_{m'm}+\frac{e\mathfrak{E}}{\hbar}\,.\,\frac{\partial}{\partial\mathbf{k}}\zeta_{m'm}+\frac{i\lambda}{\hbar}\sum_{m''}{}'\{(W_{m''m'}+e\mathfrak{E}\,.\,\mathbf{S}_{m''m'})\zeta_{m''m}$$
$$-(W_{mm''}+e\mathfrak{E}\,.\,\mathbf{S}_{mm''})\zeta_{m'm''}\} \qquad \ldots\ldots(13)$$

with $\zeta_{m'm}=\zeta_{m'}{}^*\zeta_m$, and the prime on Σ denotes that $m''=m'$ is omitted from the first sum and $m''=m$ from the second.

---

† This does not contradict Karplus and Luttinger's emphasis of the importance of their $J_b{}^{nn'}$. Their Bloch functions refer to a periodic field including spin–orbit coupling while ours are for a field excluding spin–orbit coupling. Thus our perturbation calculation includes the important part of the $J_b{}^{nn'}$. We neglect a quantity which has no connection with spin–orbit coupling. It does modify conductance properties but these are described semi-empirically anyhow.

We have to solve (13) by adding to $\zeta_{m'm}{}^{0}$, which is the product arising from solutions of the type (12), a part linearly dependent on $\mathfrak{E}$ to our approximation, and vanishing at $t=0$. That is, we are assuming that after each collision the state of the electron is not determined by its detailed behaviour just before the collision. Also we shall assume that just after the collision the electron is in a superposition of states of the type (12) with random initial phases, and we shall average over phases. Hence in (13) our initial approximation is a superposition of $\zeta_{m'm}{}^{0}=\zeta_{m'}{}^{0*}\zeta_{m}{}^{0}$ derived from (12).

When $m=m'$ the terms in the summation in (13) are already of order λ so that

$$\frac{\partial\zeta_{m'm'}}{\partial t}=\frac{e\mathfrak{E}}{\hbar}\cdot\frac{\partial\zeta_{m'm'}}{\partial\mathbf{k}}. \qquad \ldots\ldots(14)$$

When $m\neq m'$, (13) becomes, to order λ,

$$\frac{\partial\zeta_{m'm}}{\partial t}=i\Delta_{m'm}\zeta_{m'm}+\frac{e\mathfrak{E}}{\hbar}\cdot\frac{\partial\zeta_{m'm}}{\partial\mathbf{k}}-\frac{i\lambda}{\hbar}(W_{mm'}+e\mathfrak{E}\,.\,\mathbf{S}_{mm'})\zeta_{m'm'}. \qquad \ldots\ldots(15)$$

The solution of (14) is

$$\zeta_{m'm'}=\zeta_{m'm'}{}^{0}(\mathbf{k}+e\mathfrak{E}t/\hbar). \qquad \ldots\ldots(16)$$

The function $(\lambda W_{mm'}/\hbar\Delta_{m'm})\zeta_{m'm'}{}^{0}(\mathbf{k}+e\mathfrak{E}t/\hbar)$, which is suggested by the first approximation and by the general effect of an electric field, is found to satisfy (15) except for terms in $\lambda\mathfrak{E}$. It is then easily possible, by including in the solution a term of order $\lambda\mathfrak{E}$ to deduce the complete solution, viz.

$$\zeta_{m'm}=\left[\frac{\lambda W_{mm'}}{\hbar\Delta_{m'm}}+\frac{\lambda e\mathfrak{E}.}{\hbar\Delta_{m'm}}\left\{\frac{\partial}{\partial\mathbf{k}}\left(\frac{iW_{mm'}}{\hbar\Delta_{m'm}}\right)+\mathbf{S}_{mm'}\right\}\{1-\exp(i\Delta_{m'm}t)\}\right]$$

$$\times\,\zeta_{m'm'}{}^{0}\left(\mathbf{k}+\frac{e\mathfrak{E}t}{\hbar}\right). \qquad \ldots\ldots(17)$$

We write

$$\frac{W_{mm'}}{\hbar\Delta_{m'm}}=A_{mm'},\quad \left\{\frac{\partial}{\partial\mathbf{k}}\left(\frac{iW_{mm'}}{\hbar\Delta_{m'm}}\right)+\mathbf{S}_{mm'}\right\}\Big/\hbar\Delta_{m'm}=\mathbf{B}_{mm'},$$

$$\zeta_{m'm}=\lambda[A_{mm'}(\mathbf{k})+e\mathfrak{E}\,.\,\mathbf{B}_{mm'}(\mathbf{k})\{1-\exp(i\Delta_{m'm}t)\}]\,\zeta_{m'm'}{}^{0}\left(\mathbf{k}+\frac{e\mathfrak{E}t}{\hbar}\right). \qquad \ldots\ldots(18)$$

Substituting (7) into the first two terms in (2) we obtain

$$\mathbf{v}^{(1)}=\frac{1}{\mu}\frac{8\pi^3}{\Delta}\int d\mathbf{k}\sum_{m',m}\mathbf{P}_{m'm}\zeta_{m'm},\quad \mathbf{v}^{(2)}=\lambda\frac{8\pi^3}{\Delta}\int d\mathbf{k}\sum_{m',m}\mathfrak{W}_{m'm}\zeta_{m'm} \qquad \ldots\ldots(19)$$

where

$$\mathbf{P}_{m'm}=\int d\tau_0\psi_{m'}{}^{*}\mathbf{p}\psi_m=\mathbf{P}_{mm'}{}^{*}$$

$$\mathfrak{W}_{m'm}=\int d\tau_0\psi_{m'}{}^{*}(\boldsymbol{\sigma}\times\mathrm{grad}\,V)\psi_m=\mathfrak{W}_{mm'}{}^{*}. \qquad \ldots\ldots(20)$$

For an electron originating from a definite band m_0 (16) and (18) give, with $m'=m_0$,

$$\mathbf{v}_{m_0}{}^{(1)}=\frac{1}{\mu}\frac{8\pi^3}{\Delta}\int d\mathbf{k}\left\{\mathbf{P}_{m_0m_0}\zeta_{m_0m_0}+\sum_{m\neq m_0}(\mathbf{P}_{m_0m}\zeta_{m_0m}+\mathrm{c.c.})\right\}$$

$$\mathbf{v}_{m_0}{}^{(2)}=\lambda\frac{8\pi^3}{\Delta}\int d\mathbf{k}\,\mathfrak{W}_{m_0m_0}\zeta_{m_0m_0}. \qquad \ldots\ldots(21)$$

Kikuchi and Nordheim (1930) have shown how, under certain restrictions, the 'drift' terms in the Boltzmann equation may be calculated for a many-electron problem from the solution of a corresponding one-electron problem. Here their result gives, if $f_m(\mathbf{k})$ represents the distribution function for m, $\mathbf{k}$,

$$\left[\frac{\partial f_m}{\partial t}\right]_{\text{collisions}} + \frac{\partial}{\partial t}\zeta_{mm}(\mathbf{k}, t) = 0$$

that is, to the first order in $\mathfrak{E}$, from (14)

$$\left[\frac{\partial f_m}{\partial t}\right]_{\text{collisions}} + \frac{e\mathfrak{E}}{\hbar} \cdot \frac{\partial \zeta_{mm}{}^0}{\partial \mathbf{k}} = 0.$$

Assuming the existence of a relaxation time τ

$$-\frac{1}{\tau}(f_m - f_{m0}) + \frac{e\mathfrak{E}}{\hbar} \cdot \frac{\partial \zeta_{mm}{}^0}{\partial \mathbf{k}} = 0,$$

$$\therefore f_m = f_{m0} + \frac{e\mathfrak{E}\tau}{\hbar} \cdot \frac{\partial \zeta_{mm}{}^0}{\partial \mathbf{k}}.$$

Thus f_{m0} must be the value of f when $\mathfrak{E}$ is zero, viz. the Fermi function

$$f = \{\exp[(E - \zeta)/kT] + 1\}^{-1}.$$

Hence

$$f_m = f + \frac{e\mathfrak{E}\tau}{\hbar} \cdot \frac{\partial \zeta_{mm}{}^0}{\partial \mathbf{k}}$$

and, to the first order in $\mathfrak{E}$, $\partial \zeta_{mm}{}^0/\partial \mathbf{k}$ will simply be $\partial f/\partial \mathbf{k}$. Thus

$$f_m = f + \frac{e\mathfrak{E}\tau}{\hbar} \cdot \frac{\partial f}{\partial \mathbf{k}}. \qquad \ldots\ldots(22)$$

Since the coefficient of the second term in this is equal to τ multiplied by the time rate of change of $\mathbf{k}$ with an electric field we may interpret τ as a mean collision time.

We multiply the distribution function for, say m_0, $\mathbf{k}_0$ by the contribution to the current flow given by every electron which at the instant considered is in the state m_0, $\mathbf{k}_0$. Such an electron, if time t has elapsed since its last collision, originated at m_0, $k_0 + e\mathfrak{E}t/\hbar$. Hence for it $\zeta_{m_0 m_0}$ at $t = 0$ is

$$(\Delta/8\pi^3)\,\delta(\mathbf{k} - et\mathfrak{E}/\hbar - \mathbf{k}_0)$$

i.e. at time t $\zeta_{m_0 m_0}$ is $(\Delta/8\pi^3)\delta(\mathbf{k} - \mathbf{k}_0)$. Hence

$$\left.\begin{aligned} \mathbf{v}_{m_0}{}^{(2)}(\mathbf{k}_0) &= \lambda \frac{8\pi^3}{\Delta} \int d\mathbf{k}\,\mathfrak{W}_{m_0 m_0}(\mathbf{k})\zeta_{m_0 m_0}(\mathbf{k}, t) \\ &= \lambda \mathfrak{W}_{m_0 m_0}(\mathbf{k}_0) \end{aligned}\right\} \qquad \ldots\ldots(23)$$

and similarly

$$\begin{aligned} \mathbf{v}_{m_0}{}^{(1)}(\mathbf{k}_0) = \frac{1}{\mu}[\mathbf{P}_{m_0 m_0}(\mathbf{k}_0) + \lambda \sum_{m \neq m_0} \{\mathbf{P}_{m_0 m}(\mathbf{k}_0)[A_{m m_0}(\mathbf{k}_0) \\ + e\mathfrak{E} \cdot \mathbf{B}_{m m_0}(\mathbf{k}_0)\{1 - \exp(i\Delta_{m_0 m} t)\}] + \text{c.c.}\}]. \end{aligned} \qquad \ldots\ldots(24)$$

We now have to average this assigning a probability $\tau^{-1}\exp(-t/\tau)$ for a time t having elapsed since the last collision. This leaves $\mathbf{v}_{m_0}{}^{(2)}(\mathbf{k}_0)$ unaffected but from (24) we obtain

$$\begin{aligned} \text{av.}\,\mathbf{v}_{m_0}{}^{(1)}(\mathbf{k}_0) = \frac{1}{\mu}\Bigg\{\mathbf{P}_{m_0 m_0}(\mathbf{k}_0) + \lambda \sum_{m \neq m_0} \Bigg[\mathbf{P}_{m_0 m}(\mathbf{k}_0)\Bigg\{A_{m m_0}(\mathbf{k}_0) \\ + \frac{i\Delta_{m_0 m}\tau}{i\Delta_{m_0 m}\tau - 1} e\mathfrak{E} \cdot \mathbf{B}_{m m_0}(\mathbf{k}_0)\Bigg\} + \text{c.c.}\Bigg]\Bigg\}. \end{aligned} \qquad \ldots\ldots(25)$$

From (3)

$$\mathbf{J} = -\frac{e}{8\pi^3}\int d\mathbf{k}\sum_m \mathbf{v}_m(\mathbf{k})f_m. \qquad \ldots\ldots(26)$$

From (23) and (26)

$$\sigma_{yx}^{(2)} = -\frac{\lambda e^2\tau}{8\pi^3\hbar}\int d\mathbf{k}\sum_m \mathfrak{W}_{ymm}\frac{\partial f_m}{\partial k_x}$$

and this vanishes by symmetry. From (24) and (26)

$$\sigma_{yx}^{(1)} = -\frac{e^2\tau}{8\pi^3\hbar\mu}\int d\mathbf{k}\sum_m P_{ymm}\frac{\partial f_m}{\partial k_x} - \frac{\lambda e^2}{8\pi^3\hbar\mu}\int d\mathbf{k}\sum_{\substack{m,m'\\ m\neq m'}}\Bigg[P_{ymm'}\Bigg\{\tau A_{m'm}\frac{\partial f_m}{\partial k_x}$$
$$+\frac{1}{1+i(\Delta_{mm'}\tau)^{-1}}\hbar B_{xm'm}f_m\Bigg\}+\text{c.c.}\Bigg]. \qquad \ldots\ldots(27)$$

The first integral vanishes by symmetry. Interchanging m and m' in the complex conjugate we have from (27), since $A_{mm'}{}^* = -A_{m'm}$ and $\mathbf{B}_{mm'} = -\mathbf{B}_{m'm}$,

$$\sigma_{yx}^{(1)} = -\frac{\lambda e^2}{8\pi^3\hbar\mu}\int d\mathbf{k}\sum_{m,m'} P_{ymm'}\Bigg\{\tau A_{m'm}\frac{\partial}{\partial k_x}(f_m - f_{m'})$$
$$+\hbar B_{xm'm}\frac{1}{1+i(\Delta_{mm'}\tau)^{-1}}(f_m - f_{m'})\Bigg\}.$$

Since $P_{ymm'}(\mathbf{k})A_{m'm}(\mathbf{k}) = -P_{ym'm}(-\mathbf{k})A_{mm'}(-\mathbf{k})$ (see Appendix I) the integral containing $A_{m'm}$ vanishes. Hence

$$\sigma_{yx}^{(1)} = \frac{\lambda e^2}{8\pi^3\mu}\int d\mathbf{k}\sum_{m,m'}\frac{P_{ymm'}}{E_m - E_{m'}}\left\{\frac{\partial}{\partial k_x}\left(\frac{iW_{m'm}}{E_m - E_{m'}}\right) + S_{xm'm}\right\}(f_{m'} - f_m)\frac{1}{1+i(\Delta_{mm'}\tau)^{-1}} \qquad \ldots\ldots(28)$$

It can be shown that, because of the relations derived in Appendix I and because of (10′), the imaginary part of the last factor in the integrand of (28) gives no contribution to the integral. Thus

$$\sigma_{yx}^{(1)} = \frac{\lambda e^2}{8\pi^3\mu}\int d\mathbf{k}\sum_{m,m'}\frac{P_{ymm'}}{E_m - E_{m'}}\left\{\frac{\partial}{\partial k_x}\left(\frac{iW_{m'm}}{E_m - E_{m'}}\right) + S_{xm'm}\right\}(f_{m'} - f_m)\frac{1}{1+(\Delta_{mm'}\tau)^{-2}} \qquad \ldots\ldots(29)$$

$$= \frac{\lambda e^2}{4\pi^3\mu}\int d\mathbf{k}\sum_{\text{pairs}}\mathscr{R}\left[\frac{P_{ymm'}}{E_m - E_{m'}}\left\{\frac{\partial}{\partial k_x}\left(\frac{iW_{m'm}}{E_m - E_{m'}}\right) + S_{xm'm}\right\}\right]$$
$$\times (f_{m'} - f_m)\frac{1}{1+(\Delta_{mm'}\tau)^{-2}}. \qquad \ldots\ldots(30)$$

§ 4. APPLICATION TO NICKEL

For a given domain we quantize spins along OZ which is in general not perpendicular to Ox, Oy. We shall assume that electrons in the s band are not appreciably polarized and that the energy of these electrons is not dependent on their direction of spin. These restrictions are not essential but simplify the calculations. For the d band we use tight-binding wave functions and a modulated plane wave for the s band. In one unit cell of the Wigner–Seitz type we take these to be respectively $f(r)Y_{2m}$ and $g(r)\exp(i\mathbf{k}\,.\,\mathbf{r})$ where $g(r)$ might be a function of $\mathbf{k}$. The function $f(r)$ has a zero only at $r = 0$ while $g(r)$ inside the cell will resemble in general terms an atomic 4s function but will not die away exponentially near the boundary of the cell. Much of the evaluation can be done without specifying these functions more closely. The second of these functions is not and ought not to be an s function, but is intended to be a reasonable approximation for the important values of **k** near the Fermi level. In principle $g(r)$ can be adjusted to give the required orthogonality to functions for the d band. Because of $P_{ymm'}$ in (30) the states m and m' must belong to the same eigenvalue of the spin.

In the d band, for different representations of the space-group connected with particular **k** vectors, the energy can assume different dependences on **k** (see, for example, Slater 1956). However only states near the Fermi level contribute appreciably to our result. In addition, for microcrystalline media, the directions with which we are concerned will be related differently to the crystal axes for different small crystals. We are concerned therefore only with a directional average and it is a reasonable approximation to what is known of these d bands to regard the energy for states which are relevant here as a single-valued increasing function of **k**. Since however all d states do not contribute to our calculation we shall multiply our final result by a constant θ which is a proper fraction whose magnitude may be estimated roughly. Thus

$$\sigma_{yx}{}^{(1)} = \frac{\lambda e^2\theta}{4\pi^3\mu}\int d\mathbf{k}\,\mathscr{R}\sum_{\mathrm{d,s}}\frac{P_{y\mathrm{ds}}}{E_\mathrm{s}-E_\mathrm{d}}\left\{\frac{\partial}{\partial k_x}\left(\frac{iW_\mathrm{sd}}{E_\mathrm{s}-E_\mathrm{d}}\right)-S_{x\mathrm{sd}}\right\}(f_\mathrm{s}-f_\mathrm{d}) \quad \ldots\ldots(31)$$

where the summation is taken over each d state together with the s state of the same spin, and we have neglected $(\Delta_{\mathrm{sd}}\tau)^{-2}$, an error of say 6% at room temperatures.

In the integral (10′) for W_sd we shall, in the unit cell, take V to have spherical symmetry so that $(\operatorname{grad} V\times\mathbf{p})=\{V'(r)/r\}\mathbf{L}$ where $\mathbf{L}$ is the orbital angular momentum. The integral W_sd referring to states of the same spin, only σ_Z gives a non-zero contribution. If α, β are spherical angles specifying the direction OZ relative to $Oxyz$

$$L_Z = \sin\alpha\cos\beta\, L_x + \sin\alpha\sin\beta\, L_y + \cos\alpha\, L_z.$$

The resultant magnetization being in the direction Oz, all values of β are equally probable so that, in the average over microcrystals, we may replace L_Z by $\overline{\cos\alpha}\, L_z$, the bar denoting an average over direction. We shall replace $\overline{\cos\alpha}$ by $\mathscr{M}$, the ratio of the magnetization to saturation magnetization at the given temperature. We shall ignore contributions from neighbouring cells to the tight-binding function in the unit cell which is the region of integration. This is justified by both the nature of $f(r)$ and the value of grad V. Thus we may write

$$L_z f(r) Y_{2m} = m\hbar f(r) Y_{2m}.$$

It can be shown (see Appendix II) that the contribution of $S_{x\mathrm{sd}}$ is negligible and that, writing $\sigma_Z' = \pm 1$ as the eigenvalue of σ_Z,

$$\sigma_{yx}{}^{(1)} = \frac{5\lambda e^2\hbar^2\mathscr{M}\theta}{\pi^2\mu}\int dk\sum_{\mathrm{d,s}}\left\{\frac{\sigma_Z'}{(E_\mathrm{s}-E_\mathrm{d})}\frac{\partial}{\partial k}\left(\frac{kI_1I_2}{E_\mathrm{s}-E_\mathrm{d}}\right)(f_\mathrm{s}-f_\mathrm{d})\right\},$$

where

$$I_1 = \int_0^{r_0} r\,dr\,f(r)\,g'(r)\,\mathrm{j}_2(kr), \quad I_2 = \int_0^{r_0} r\,dr\,f(r)\,g(r)\frac{dV}{dr}\,\mathrm{j}_2(kr) \quad \ldots\ldots(32)$$

$\mathrm{j}_2(kr)$ is a spherical Bessel function and r_0 is the radius of a sphere of the same volume as a Wigner–Seitz cell.

We shall write (32) as

$$\sigma_{yx}^{(1)}=\frac{5\lambda e^2\hbar^2\mathcal{M}\theta}{\pi^2\mu}\int dk\,(F_{\mathrm{sd}+}f_{\mathrm{s}}-F_{\mathrm{sd}+}f_{\mathrm{d}+}-F_{\mathrm{sd}-}f_{\mathrm{s}}+F_{\mathrm{sd}-}f_{\mathrm{d}-}) \qquad \ldots\ldots(33)$$

with

$$f_{\mathrm{s}}=[\exp{(E_{\mathrm{s}}-\zeta)}/kT+1]^{-1}\text{ etc.} \qquad \ldots\ldots(34)$$

For the states which, as discussed above, contribute significantly to our result we shall assume that

$$E_{\mathrm{s}}=\hbar^2k^2/2\mu_{\mathrm{s}},\quad E_{\mathrm{s}}-E_{\mathrm{d}+}=a(k^2-b_{\pm}{}^2) \qquad \ldots\ldots(35)$$

where $a=\hbar^2(\mu_{\mathrm{d}}-\mu_{\mathrm{s}})/2\mu_{\mathrm{d}}\mu_{\mathrm{s}}$, and therefore

$$E_{\mathrm{d}\pm}=\hbar^2k^2/2\mu_{\mathrm{d}}+ab_{\pm}{}^2 \qquad \ldots\ldots(36)$$

μ_{d}, μ_{s} being effective electron masses.

Hence

$$2\eta\equiv E_{\mathrm{d}-}-E_{\mathrm{d}+}=a(b_-{}^2-b_+{}^2). \qquad \ldots\ldots(37)$$

From (32), (35), we have, for example,

$$F_{\mathrm{sd}+}(k)=\frac{1}{a^2(k^2-b_+{}^2)}\frac{\partial}{\partial k}\left(\frac{kI_1I_2}{k^2-b_+{}^2}\right). \qquad \ldots\ldots(38)$$

For each $F(k)$ we define a function G to satisfy $F=\partial G/\partial k$. Then

$$\int dk\,Ff=\int dk\,\frac{\partial G}{\partial k}f=\int dE\,\frac{\partial G}{\partial E}f=\Big[Gf\Big]_{E_{\min}}^{E_{\max}}-\int dEG\,\frac{\partial f}{\partial E}$$

which gives approximately

$$\int dk\,Ff=\Big[Gf\Big]_{E_{\min}}^{E_{\max}}+G(\zeta)+\frac{\pi^2}{6}(kT)^2\frac{\partial}{\partial E}\left\{F\frac{\partial k}{\partial E}\right\}$$

(k being the Boltzmann constant) which, by (35), (36) is equal to

$$\Big[Gf\Big]_{E_{\min}}^{E_{\max}}+G(\zeta)+\frac{\pi^2}{6}(kT)^2\frac{\mu^2}{\hbar^4}\frac{1}{k}\frac{\partial}{\partial k}\left(\frac{F}{k}\right) \qquad \ldots\ldots(39)$$

In applying (39) it must be remembered that F and G are originally functions of k. They become functions of E by the expression of k as a function of E which is convenient because of the particular distribution function f with which G is associated. The diagram shows schematically the relations (35), (36) and indicates that the d_+ band is full. Since the value $E_{\mathrm{d}+}=\zeta$ is not reached, the second term in the integrand of (33) contributes only through the first term on the right-hand side of (39). For the values of k which occur and for values of r in the unit cell, kr is considerably less than the value which gives the first maximum of $\mathrm{j}_2(kr)$. In the integrals I_1, I_2, we shall therefore replace the dependence of $\mathrm{j}_2(kr)$ on k by that of the first term in its series expansion. That is, we shall replace kI_1I_2 by k^5J and ignore the dependence of J on k. Then, for example,

$$F_{\mathrm{sd}}(k)=\frac{J}{a^2}\frac{k^4(3k^2-5\mathrm{b}_-{}^2)}{(k^2-\mathrm{b}_-{}^2)^3}. \qquad \ldots\ldots(40)$$

Then, for example,

$$G_{\mathrm{sd}-}(k) = \frac{J}{a^2}\left\{3k + \frac{15}{8}b_-\ln\frac{k-b_-}{k+b_-} - \frac{1}{4}\frac{kb^2_-}{k^2-b_-{}^2} + \frac{1}{2}\frac{kb^4_-}{(k^2-b_-{}^2)^2}\right\}. \qquad \ldots\ldots(41)$$

From (33) and (40) it might appear that certain integrals would diverge. This is not so since at such apparent singularities of the integrand as $k = b_-$, there occurs in the integrand the difference $f_s - f_{d-}$ which vanishes when $E_s = E_{d-}$.

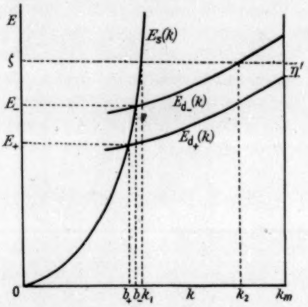

Schematic representation of energy E as a function of k.

From (33), (39), (40), (41), using the diagram,

$$\sigma_{yx}{}^{(1)} = \frac{5\lambda e^2\hbar^2\mathscr{M}\theta}{\pi^2\mu}\Big\{-(G_{\mathrm{sd}+})_{k_m} + (G_{\mathrm{sd}+})_{k_1} - (G_{\mathrm{sd}-})_{k_1} + (G_{\mathrm{sd}-})_{k_2}$$

$$-\frac{\pi^2(kT)^2J}{2a^2\hbar^4}\left[\mu_s{}^2\left(\frac{k_1{}^5-5k_1b_+{}^4}{(k_1{}^2-b_+{}^2)^4} - \frac{k_1{}^5-5k_1b_-{}^4}{(k_1{}^2-b_-{}^2)^4}\right)\right.$$

$$\left.+\mu_d{}^2\frac{k_2{}^5-5k_2b_-{}^4}{(k_2{}^2-b_-{}^2)^4}\right]\Big\}. \qquad \ldots\ldots(42)$$

Referring to the diagram we see that

$$\frac{\hbar^2b_\pm{}^2}{2\mu_s} = E_\pm, \qquad \frac{\hbar^2k_1{}^2}{2\mu_s} = \zeta,$$

and we write

$$\frac{\hbar^2k_2{}^2}{2\mu_d} = \zeta - \left(1-\frac{\mu_s}{\mu_d}\right)E_- = \frac{\mu_s}{\mu_d}\zeta', \qquad \ldots\ldots(43)$$

so that

$$\frac{\zeta'}{E_-} = \frac{\mu_d}{\mu_s}\left(\frac{\zeta}{E_-}-1\right)+1 \qquad \ldots\ldots(44)$$

and

$$\frac{\hbar^2k_m{}^2}{2\mu_s} = \zeta'', \qquad \ldots\ldots(45)$$

Then

$$\sigma_{yx}^{(1)}=\frac{5\sqrt{2\theta}\mathscr{M}Je^2}{\pi^2\hbar^2c^2}\frac{\mu_s^{5/2}\mu_d^2}{\mu^3(\mu_d-\mu_s)^2}\Bigg\{3(\sqrt{\zeta'}-\sqrt{\zeta''})$$

$$+\sqrt{E_-}\left[\frac{15}{8}\ln\frac{\left(\sqrt{\frac{\zeta'}{E_-}}-1\right)\left(\sqrt{\frac{\zeta}{E_-}}+1\right)}{\left(\sqrt{\frac{\zeta'}{E_-}}+1\right)\left(\sqrt{\frac{\zeta}{E_-}}-1\right)}-\frac{1}{4}\left[\frac{\sqrt{\frac{\zeta'}{E_-}}}{\frac{\zeta'}{E_-}-1}-\frac{\sqrt{\frac{\zeta}{E_-}}}{\frac{\zeta}{E_-}-1}\right]\right.$$

$$\left.+\frac{1}{2}\left[\frac{\sqrt{\frac{\zeta'}{E_-}}}{\left(\frac{\zeta'}{E_-}-1\right)^2}-\frac{\sqrt{\frac{\zeta}{E_-}}}{\left(\frac{\zeta}{E_-}-1\right)^2}\right]\right]$$

$$-\sqrt{E_+}\left[\frac{15}{8}\ln\frac{\left(\sqrt{\frac{\zeta''}{E_+}}-1\right)\left(\sqrt{\frac{\zeta}{E_+}}+1\right)}{\left(\sqrt{\frac{\zeta''}{E_+}}+1\right)\left(\sqrt{\frac{\zeta}{E_+}}-1\right)}-\frac{1}{4}\left[\frac{\sqrt{\frac{\zeta''}{E_+}}}{\frac{\zeta''}{E_+}-1}-\frac{\sqrt{\frac{\zeta}{E_+}}}{\frac{\zeta}{E_+}-1}\right]\right.$$

$$\left.+\frac{1}{2}\left[\frac{\sqrt{\frac{\zeta''}{E_+}}}{\left(\frac{\zeta''}{E_+}-1\right)^2}-\frac{\sqrt{\frac{\zeta}{E_+}}}{\left(\frac{\zeta}{E_+}-1\right)^2}\right]\right]$$

$$-\frac{1}{8}(\pi kT)^2\left[\frac{1}{\zeta^{3/2}}\left\{\frac{\left(\frac{\zeta}{E_+}\right)^4-5\left(\frac{\zeta}{E_+}\right)^2}{\left(\frac{\zeta}{E_+}-1\right)^4}-\frac{\left(\frac{\zeta}{E_-}\right)^4-5\left(\frac{\zeta}{E_-}\right)^2}{\left(\frac{\zeta}{E_-}-1\right)^4}\right\}\right.$$

$$\left.+\left(\frac{\mu_d}{\mu_s}\right)^2\frac{1}{\zeta'^{3/2}}\frac{\left(\frac{\zeta'}{E_-}\right)^4-5\left(\frac{\zeta'}{E_-}\right)^2}{\left(\frac{\zeta'}{E_-}-1\right)^4}\right]\Bigg\}\quad\ldots\ldots\ (46)$$

where, as explained before, a positive proper fraction θ has been introduced to represent the fraction of the d$_-$ band states which are energetically available.

§ 5. NUMERICAL RESULTS FOR NICKEL

We take the following numerical values in relation to the diagram

$\zeta=2{\cdot}72\times10^{-12}$ erg $\qquad\mu_d=30\mu$

$2\eta=3{\cdot}4\times10^{-13}$ erg $\qquad\mu_s=\mu$

$\eta'=0{\cdot}7\times10^{-13}$ erg

To find E_+ and ζ' we may obtain an estimate of $_-$ by calculating the number of empty states in the d$_-$ band. The energy in the band being given by (36) the number of states, per unit volume, for one direction of spin, between energies ζ and $\zeta+2\eta-\eta'$ is

$$[(2\mu_d^3)^{1/2}/3\pi^2\hbar^3][(\zeta+2\eta-\eta'-ab_-^2)^{3/2}-(\zeta-ab_-^2)^{3/2}].$$

Equating this to the number $0{\cdot}6 \div 10{\cdot}9 \times 10^{-24}$, corresponding to 0·6 per atom we find, approximately, that $ab_-{}^2 = 2{\cdot}47 \times 10^{-12}$ erg. Then, by (37),

$$ab_+{}^2 = 2{\cdot}13 \times 10^{-12}\,\text{erg}.$$

These give $E_- = 2{\cdot}56 \times 10^{-12}$ erg, $E_+ = 2{\cdot}20 \times 10^{-12}$ erg, $\zeta' = 7{\cdot}4 \times 10^{-12}$ erg.

Taking k_m as the radius of a sphere of volume equal to that of the first Brillouin zone we find $\zeta'' = 9{\cdot}66 \times 10^{-12}$ erg. The numerical result is that

$$\sigma_{yx}{}^{(1)} = -\frac{J\theta\mathcal{M}}{Ze^2} \times 2{\cdot}69 \times 10^5 Z \left\{1 + 0{\cdot}089\left(\frac{T}{100}\right)^2\right\} \qquad \ldots\ldots(47)$$

where, by (32),

$$\frac{J}{Ze^2} = \frac{1}{k^4}\int dr\, r f(r) g'(r)\, \mathrm{j}_2(kr) \int dr f(r) g(r) \frac{1}{r}\, \mathrm{j}_2(kr).$$

It may be verified that $\sigma_{yx}{}^{(3)} \ll \sigma_{yx}{}^{(1)}$. In order to estimate the magnitude of the effect of spin–orbit coupling we must form some estimate of J/Ze^2. First of all we may, for reasons already given, replace $\mathrm{j}_2(kr)$ by $k^2r^2/225$. We then replace $f(r), g(r)$ by hydrogenic 3d and 4s functions. (Normalization within unit cell does not make any appreciable alteration.) The extra factor $e^{i\mathbf{k}\cdot\mathbf{r}}$ multiplying $g(r)$ does not have an important effect on the integrals which we evaluate. We find thus the value

$$(-1{\cdot}37 \times 10^6)Z \text{ for } J/Ze^2. \qquad \ldots\ldots(48)$$

For comparison with experimental result we change now from gaussian units to practical ones and use the definition of the coefficient R_S of the extraordinary Hall effect, viz.

$$\frac{(E_y)\,\text{volt cm}}{(J_x)\,\text{ampere cm}^{-2}} = 4\pi R_\mathrm{S}\, M(T)\,\text{gauss} \qquad \ldots\ldots(49)$$

where $M(T)$ is the intensity of magnetization at temperature T.

Remembering that we have taken the lower energy to correspond to the positive spin-eigenvalue, to which belongs a negative magnetic moment, we have that, approximately,

$$\mathcal{M} = -M(T)/M_\mathrm{S}(T)$$

where $M_\mathrm{S}(T)$ is the spontaneous magnetization for a single domain. Hence by (47), (48), (49)

$$R_\mathrm{S} = -3{\cdot}25 \times 10^{-14}\,\frac{(\rho \times 10^6)^2}{M_\mathrm{S}(T)}\left\{1 + 0{\cdot}089\left(\frac{T}{100}\right)^2\right\} Z^2\theta \qquad \ldots\ldots(50)$$

where ρ is the resistivity in ohm cm. The estimation of Z is difficult. It may be made by the use of screening constants (Hartree 1957, Froese 1957, 1958), but a screening constant needs to be defined for each physical property. In addition the 3d wave functions for the electron in a Wigner–Seitz cell will extend to smaller distances from the nucleus than in the free atom. The same will be true for the parts of the 4s wave functions which lie in the region where the 3d wave functions are appreciable. For example, a reduction in scale of the important parts of the wave functions by any factor would imply the inverse increase in the effective nuclear charge. In addition the value of J/Ze^2 is determined to a considerable extent by the wave functions fairly near the nucleus, where dV/dr is large, and where screening is small. Thus a suitable Z may be considerably larger than suggested by the work of Froese (1958). Here we shall take the effective Z to be 20 and evaluate (50) at 0°c taking $\rho\times10^6=6{\cdot}68$, $M(273)=485$. Then by (50) $R_s(290)=2\times10^{-12}\theta$ ohm cm gauss^{-1}.

An estimate of θ might be made roughly from the kind of knowledge exemplified in figure 22 of the article by Slater (1956). It would appear that θ is not much less than unity. The value given by Smit (1956) is $2{\cdot}4\times10^{-12}$. This agreement is partly fortuitous on account of the many approximations which must be used, but it is of interest to see that spin–orbit coupling can account adequately for the magnitude of the extraordinary Hall effect at this temperature.

More generally the variation of R_s with T is caused mainly by the variation of ρ^2 with T. Indeed in our formula R_s appears to increase slightly faster than ρ^2 does. Our calculations, however, are sensitive to the value of $\zeta/E_- - 1$, and this in turn is sensitive to the value of μ_d which is chosen.

Fundamentally, many of the assumptions of transport theory and our assumption of random initial phases after collision need to be examined more fully.

It is hoped to extend this computation and also to apply the theory to substances whose unit cell has not the high degree of symmetry shown by nickel, in particular to a ferrite.

APPENDIX I

The periodic part $u_{\mathbf{k}m}$ of the Bloch function $\phi_{\mathbf{k}m}$ is a solution of

$$\nabla^2 u_{\mathbf{k}m} + 2i\mathbf{k}\,.\,\mathrm{grad}\,u_{\mathbf{k}m} + \left(E_{\mathbf{k}m} - \frac{\hbar^2k^2}{2\mu} - V\right)u_{\mathbf{k}m} = 0.$$

Then $u_{-\mathbf{k},m}{}^* = u_{\mathbf{k}m}$ and, since $\phi_{\mathbf{k}m} = e^{i\mathbf{k}\cdot\mathbf{r}}\,.\,u_{\mathbf{k}m}$, $\phi_{-\mathbf{k},m}{}^* = \phi_{\mathbf{k}m}$.

Consider $$I_{\mathbf{k}mm'} \equiv \int \phi_{\mathbf{k}m}{}^*\,O_1\,\phi_{\mathbf{k}m'}\,d\tau \int \phi_{\mathbf{k}m'}{}^*\,O_2\,\phi_{\mathbf{k}m}\,d\tau$$

where O_1, O_2 are, in general, operators.

Then $$I_{-\mathbf{k},mm'} = \int \phi_{\mathbf{k}m}\,O_1\,\phi_{\mathbf{k}m'}{}^*\,d\tau \int \phi_{\mathbf{k}m'}\,O_2\,\phi_{\mathbf{k}m}{}^*\,d\tau$$
and

$$I_{-\mathbf{k}mm'}{}^* = \int \phi_{\mathbf{k}m}{}^*\,O_1{}^*\,\phi_{\mathbf{k}m'}\,d\tau \int \phi_{\mathbf{k}m'}{}^*\,O_2{}^*\,\phi_{\mathbf{k}m}\,d\tau.$$

Hence if O_1, O_2 are, formally, both real or both imaginary,

$$I_{-\mathbf{k}mm'}{}^* = I_{\mathbf{k}mm'}. \qquad \ldots\ldots(\mathrm{I.1})$$

Hence

$$P_{ymm'}(\mathbf{k})\,W_{m'm}(\mathbf{k}) = P_{ymm'}(-\mathbf{k})\,W_{m'm}(-\mathbf{k}) \qquad \ldots\ldots(\mathrm{I.2})$$

and

$$\left\{\frac{\partial}{\partial k_x}P_{ymm'}(\mathbf{k})\right\}W_{m'm}(\mathbf{k}) = -\left\{\frac{\partial}{\partial k_x}P_{ymm'}(-\mathbf{k})\right\}W_{m'm}(-\mathbf{k}). \qquad \ldots\ldots(\mathrm{I.3})$$

APPENDIX II

We use the result

$$e^{i\mathbf{k}\cdot\mathbf{r}} = 4\pi\sum_{nm} i^n\,\mathrm{j}_n(kr)\,\mathrm{Y}_{nm}{}^*(\hat{\mathbf{r}})\,\mathrm{Y}_{nm}(\hat{\mathbf{k}}) \qquad \ldots\ldots(\mathrm{II.1})$$

where $\hat{\mathbf{r}}$ and $\hat{\mathbf{k}}$ stand for angle variables specifying the directions of these unit vectors. We shall, in the regions of the s band which are of importance, ignore the dependence of $g(r)$ on $\mathbf{k}$ and may thus write

$$P_{yds} = \int d\tau_0 \, \mathrm{Y}_{2m}{}^{*} f(r) \, \mathrm{e}^{i\mathbf{k}\cdot\mathbf{r}} \frac{\hbar}{i} \frac{\partial g}{\partial y} = -\hbar \frac{\partial}{\partial k_y} \int d\tau_0 \, \mathrm{Y}_{2m}{}^{*} f(r) \, \mathrm{e}^{i\mathbf{k}\cdot\mathbf{r}} \frac{1}{r} g'(r).$$

We shall integrate throughout a sphere of radius r_0 which has the same volume as a Wigner–Seitz cell and which is an approximation to it. Then, by (II.1),

$$P_{yds} = 4\pi\hbar \frac{\partial}{\partial k_y} \left\{ \mathrm{Y}_{2m}{}^{*}(\hat{\mathbf{k}}) \int r\,dr\,f g' \, \mathrm{j}_2(kr) \right\}$$

$$\mathcal{M}^{-1} W_{\mathrm{sd}} = m\hbar \int d\tau_0 \, \mathrm{e}^{-i\mathbf{k}\cdot\mathbf{r}} g(r) \frac{1}{r} \frac{dV}{dr} \mathrm{Y}_{2m} f(r) = -4\pi m\hbar \, \mathrm{Y}_{2m}(\hat{\mathbf{k}}) \int r\,dr\,f g \frac{dV}{dr} \mathrm{j}_2(kr).$$

Thus

$$\mathcal{M}^{-1} P_{yds} \frac{\partial}{\partial k_x} W_{\mathrm{sd}} = -16 m\pi^2\hbar^2 \int r\,dr\,f g' \frac{\partial}{\partial k_y} \left\{ \mathrm{Y}_{2m}{}^{*}(\hat{\mathbf{k}}) \mathrm{j}_2 \right\} \int r\,dr\,f g \frac{dV}{dr} \frac{\partial}{\partial k_x} \times \{ \mathrm{Y}_{2m}(\hat{\mathbf{k}}) \mathrm{j}_2 \}. \qquad \ldots\ldots \text{(II.2)}$$

If, for the moment, we take the direction cosines of $\hat{\mathbf{k}}$ to be $(\sin\theta\cos\phi, \sin\theta\sin\phi, \cos\theta)$, we may write, for example,

$$\frac{\partial}{\partial k_x} = \sin\theta\cos\phi \frac{\partial}{\partial k} + \frac{\cos\theta\cos\phi}{k} \frac{\partial}{\partial\theta} - \frac{\sin\phi}{k\sin\theta} \frac{\partial}{\partial\phi} \qquad \ldots\ldots \text{(II.3)}$$

with a similar expression for $\partial/\partial k_y$. Then using the identity

$$\sum_m \mathrm{Y}_{2m}{}^{*}(\theta, \phi) \, \mathrm{Y}_{2m}(\theta', \phi') = \frac{5}{4\pi} \mathrm{P}_2(\cos\omega) = \frac{5}{8\pi}(3\cos^2\omega - 1)$$

where $\qquad \ldots\ldots$ (II.4)

$$\cos\omega = \cos\theta\cos\theta' + \sin\theta\sin\theta'\cos(\phi - \phi')$$

we may, by differentiating (II.4) with respect to ϕ', θ, θ' etc., and then putting $\theta' = \theta$, $\phi' = \phi$, $\omega = 0$, derive many results such as

$$\sum \mathrm{Y}_{2m}{}^{*} \frac{\partial \mathrm{Y}_{2m}}{\partial\theta} = 0, \quad \sum \frac{\partial \mathrm{Y}_{2m}{}^{*}}{\partial\phi} \frac{\partial \mathrm{Y}_{2m}}{\partial\phi} = \frac{15\sin^2\theta}{4\pi}$$

Noting that the factor m in (II.2) can be produced by differentiating $\mathrm{Y}_{2m}(\hat{\mathbf{k}})$ to ϕ, and using the above results, we can evaluate all the sums of products of differential coefficients which arise from applying (II.3) etc. to $\mathrm{Y}_{2m}(\hat{\mathbf{k}})\mathrm{j}_2(kr)$ and its complex conjugate in (II.2).

Hence

$$\mathcal{M}^{-1} \sum_{m=-2}^{2} P_{yds} \frac{\partial}{\partial k_x} W_{\mathrm{sd}} = 20\pi i\hbar^2 \frac{1}{k^2} \frac{\partial}{\partial k}(k I_1 I_2), \qquad \ldots\ldots \text{(II.5)}$$

where I_1, I_2 are given by (33). Similarly, assuming $E_{\mathrm{s}} - E_{\mathrm{d}}$ to be a function of the magnitude k only

$$\sum_{m=-2}^{2} P_{yds} W_{\mathrm{sd}} \frac{\partial}{\partial k_x} \frac{1}{E_{\mathrm{s}} - E_{\mathrm{d}}}$$

may be evaluated and the final result is as given in the integrand in (32).

The term $P_{yds} S_{x\mathrm{sd}}$ in (31) gives rise to a similar summation. By (10′), remembering that, because of P_{yds}, only states of equal spin give a non-zero contribution, we obtain $S_{x\text{sd}} = \pm P_{y\text{sd}}$. The resulting summation may be evaluated by similar methods. In comparison with the other term in the integrand of (31) it is smaller by a factor which has the order of magnitude of the ratio of $E_{\text{s}} - E_{\text{d}}$ to the increase in V between the interior of the atom and the boundary of the cell of which it is the centre. It is thus negligibly small.

REFERENCES

FROESE, C., 1957, *Proc. Roy. Soc.* A, **239,** 311.

—— 1958, *Ibid.*, **244,** 390.

HARTREE, D. R., 1957, *The Calculation of Atomic Structures* (New York: Wiley).

KIKUCHI, S., and NORDHEIM, L., 1930, *Z. Phys.* **60,** 652.

KARPLUS, R., and LUTTINGER, J. M., 1954, *Phys. Rev.*, **95,** 1154.

SLATER, J. C., 1956, *Handb. Phys.*, **19,** 1 (Berlin: Springer).

SMIT, J., 1956, *Galvanomagnetic Properties of Ferromagnetic Metals and Alloys* (*Thesis*, Leiden).

STRACHAN, C., and MURRAY, A. M., 1958, *Nature, Lond.*, **181,** 1260.

Anomalous Polarization in Ferroelectrics and other Oxides

By J. D. HURD‡, A. W. SIMPSON† and R. H. TREDGOLD‡

‡Department of Physics, University College of North Wales, Bangor, Caerns.

† The Plessey Company, Caswell, Towcester, Northants.

MS. received 10*th October* 1958, *in final form* 21*st November* 1958

Abstract. The presence of a large relaxation polarization in a number of metal oxides is reported. It is shown that this phenomenon cannot be explained in terms of ferroelectricity or in terms of the Maxwell–Wagner effect. A series of experiments are described from the results of which it is deduced that the materials behave as solid state secondary cells. It is suggested that oxygen vacancies act as charge carriers and interact with the metal electrodes deposited on the specimen.

---

§ 1. THERMAL DEPOLARIZATION

IF a piece of ferroelectric material is polarized by the application of a suitable electric field and the field is then removed and the specimen heated above its Curie point, charge is released. This quantity of charge is usually equal to the remanent polarization of the specimen involved and the phenomenon is a particular example of the pyro-electric effect. However, in studying this effect in certain ceramic materials based on barium titanate it was found that heating led to the evolution of far more charge than could be accounted for in terms of the remanent polarization. Part of this charge did correspond to the remanent polarization and was released at the Curie temperature but the remaining charge released was evolved gradually as the temperature of the specimen was increased. It is the polarization corresponding to this latter constituent of the released charge which is referred to in this paper as anomalous polarization.

A similar effect has been reported by Blood, Levine and Roberts (1956) but the polarization described by them is in the opposite direction to the original polarizing field. We have attempted to reproduce their result but without success.

The quantity of charge released in our experiments is of the order 100 μc cm^{-2} and is thus much too large to be accounted for in terms of the relaxation of polarization first discussed by Maxwell (1873) and subsequently discussed by Wagner (1913) and by Koops (1951). It was thus decided to carry out a systematic study of the phenomena.

§ 2. PREPARATION OF THE SPECIMENS

The substances investigated were all oxides either of single metals or of combinations of two or more metals. In the latter case the oxides were first ground together in a ball mill and pre-fired at 1100°c to obtain chemical combination. The material was then compressed in a suitable die at a pressure of 10 tons per square inch to form blanks about one centimetre in diameter and one millimetre thick. The blanks were then heated to a temperature adequate to bring about sintering in the particular material in question. The plane surfaces of the blanks then had metal electrodes deposited on them either by chemical means or by evaporation *in vacuo*. The metal usually employed was silver but other metals were also employed for particular purposes and will be discussed below. Single crystals of barium titanate were also studied and will be discussed in context.

§ 3. EXPERIMENTAL METHOD

The specimens were immersed in temperature controlled silicone oil baths in order to maintain them at the required temperatures. Before each cycle of operations described below the specimens were maintained for 12 hours at 180°c in order to eradicate the effects of previous thermal and electrical history. The polarization processes were carried out at some fixed temperature chosen to lie between room temperature and 130°c. It was found that for applied fields of the order 7 kv cm^{-1} or above, the final anomalous polarization was independent of polarizing field. A field of 7 kv cm^{-1} was thus used throughout these experiments. It was not found possible to obtain a polarizing time sufficiently long so that the final polarization was independent of time. However, the effect of prolonging the polarization time beyond 15 minutes was small so that this time was fixed upon as a suitable interval in which all polarizing processes were carried out.

The depolarization was brought about by removing the applied field and either leaving the specimen in the original oil bath or transferring it to one at a higher or lower temperature. At the same time the electrodes were connected to a device designed to integrate and record the released charge.

To begin with a one microfarad condenser was used to integrate the charge released but it was found that the voltage across a condenser of this value rapidly rose to a level which stopped the further release of charge. Eventually it was found necessary to use a bank of 80 one-microfarad paper–wax condensers. In order to record the charge released the grid circuit of an electrometer triode used as a cathode follower was connected across this bank of condensers. The cathode circuit of this valve was connected via a suitable backing off arrangement to a recording millivoltmeter. In the case of specimens which released exceptionally large charges the 80 μF condenser was periodically discharged during the recording period and the individual charges registered were added together in order to obtain the total charge released. Thus by keeping the potential across the specimen small it was possible to avoid the errors which would otherwise be introduced by the electrical conductivity of the specimen and by the finite capacity of the integrating condenser.

When carrying out experiments on ferroelectric materials below their Curie temperatures corrections were made for the charge which would in any case be released from the material under the particular circumstances of the experiment.

§ 4. RESULTS FOR TITANATES

Initially single crystals of barium titanate (grown from a solution of $BaTiO_3$ in molten KF) were studied and it was found that they did not show an anomalous polarization of more than 1 μc cm^{-2} which is of the order of the total experimental error. Secondly, ceramic barium titanate of very high purity was studied and it was found that an anomalous polarization of not more than 5 μc cm^{-2} was obtained.

Thirdly, a study was made of ceramic barium titanate containing small quantities (of the order of 1%) of the oxides of a variety of metals. In so far as their effect on the subject under discussion is concerned the additives studied fall into two classes: those metals which have a negligible influence on the anomalous polarization include strontium, calcium, magnesium, manganese, chromium, copper and nickel; those metals which lead to a large anomalous polarization include cobalt and iron. As the addition of cobalt leads to the largest values of anomalous polarization a detailed study was made of barium titanate containing this metal and this study will be described below. The results obtained for barium titanate containing iron were generally similar but involved rather smaller values of anomalous polarization.

§ 5. TITANATES CONTAINING COBALT OXIDE

Barium titanate containing a variety of percentages of cobalt oxide was studied. The ratio of TiO_2 to BaO was varied slightly from the stoichiometric composition. The results for two particular compositions are discussed. In all cases it was found that the total anomalous charge released depended only on the temperature at which the material was polarized. The rate at which the charge was released depended on the temperature during the release. A typical

Table 1

Identifying Letter	Atomic % BaO	%TiO_2	%CoO
A	48·5	50	1·5
B	48·0	50·5	1·5

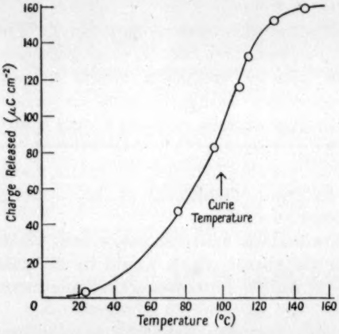

Figure 1. Total charge per cm^2 released as a function of polarizing temperature for material having composition A.

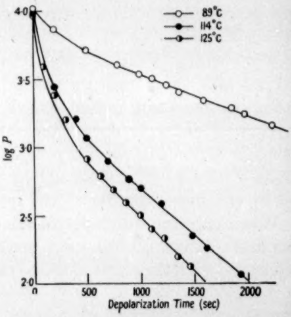

Figure 2. Logarithm of polarization versus time for composition A for various depolarizing temperatures.

half-life at 100°c was of the order 1000 seconds. Figure 1 shows the dependence of total anomalous charge on polarizing temperature for composition A. Figure 2 shows the time variation of anomalous polarization at three different temperatures for this composition. This result leads to an apparent activation energy associated with charge release of $0{\cdot}37 \pm 0{\cdot}02$ ev if the initial parts of the curves are neglected. Composition B is chiefly remarkable in that, using a polarizing temperature of 125°c, a total anomalous polarization in excess of $300\,\mu\mathrm{c\,cm^{-2}}$ was obtained.

Ceramic strontium titanate both pure and containing cobalt oxide was studied. The anomalous polarization found with this material was always less than $5\,\mu\mathrm{c\,cm^{-2}}$.

Single crystals of barium titanate containing cobalt were studied but did not show anomalous polarization.

§ 6. Magnetic Susceptibility Measurements

As the presence of cobalt or iron seems essential to the appearance of anomalous polarization in amounts greater than $5\,\mu\mathrm{c\,cm^{-2}}$ in ceramic barium titanate it is desirable to discover what valency these metals exhibit in this situation and how they are distributed in the material. The percentages of these materials which must be present before it would be possible to study their crystallographic locations by x-ray means are sufficient to change the whole structure of the material and thus other techniques must be employed.

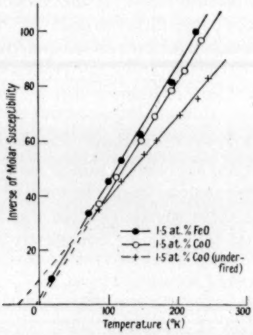

Figure 3. Inverse of molar magnetic susceptibility plotted against absolute temperature for transition metals in barium titanate.

The magnetic susceptibilities of composition A described above and also of a ceramic barium titanate containing iron were measured as a function of temperature. Similar measurements were also made on a specimen having composition A but which had been sintered at too low a temperature to obtain anomalous polarization. The inverse of these susceptibilities plotted against absolute temperature are shown in figure 3. (These results are corrected for diamagnetism.) Knowing the quantity of cobalt or iron present it is possible to deduce the effective Bohr magneton number, μ_{eff}, for these metals under these circumstances. For cobalt one finds $\mu_{\mathrm{eff}} = 4{\cdot}4 \pm 0{\cdot}1$ as compared with a range of from 4·4 to 5·2 for doubly ionized cobalt in other solids. For iron $\mu_{\mathrm{eff}} = 4{\cdot}75 \pm 0{\cdot}15$ as compared with a range of from 5·0 to 5·5 for doubly ionized iron in most other solids and a range of 5·4 to 6·0 for trebly ionized iron. From these figures one can deduce with reasonable certainty that both iron and cobalt occur in these crystals in the divalent form.

The inverse of susceptibility versus temperature plots for these materials follow a simple Curie law. In contrast to this result the plot for the under-fired composition A follows a Curie–Weiss law having a negative intercept on the absolute temperature axis (asymptotic Curie temperature) of 34°K. Now it is known that pure CoO is antiferromagnetic and that it has an asymptotic Curie temperature of −280°K (Henri le Blanchetais 1951). It seems probable that small islands of CoO in another crystal matrix should show a negative though numerically smaller asymptotic Curie temperature. Furthermore since antiferromagnetism is a cooperative phenomenon the CoO should, if randomly distributed through the material, lead to a pure paramagnetic behaviour. If one accepts these assumptions then one finds that the cobalt only gives rise to anomalous polarization if it is distributed through the lattice rather than being isolated in grain boundaries or other special regions. Furthermore the cobalt occurs as a divalent ion.

Now the ionic radius of Ti^{4+} is about 0·64 Å, that of Ba^{2+} about 1·40 Å and that of Co^{2+} about 0·77 Å and it thus seems likely that the cobalt would go into titanium sites rather than barium sites. If this is so and the cobalt behaves, as has been shown, as a divalent ion, then for each Co^{2+} ion present there must be an oxygen vacancy to preserve electrical neutrality. It is possible that the activation energy needed to detach a vacancy from a cobalt ion is small and the cobalt acts as a catalyst for the production of *free* oxygen vacancies.

§ 7. EFFECT OF HEAT TREATMENT

The following observations apply to barium titanate containing small quantities (of the order 1%) of either cobalt or iron. In view of the results of the previous section it is assumed that these metals exist in the solid in the divalent state.

Heating for 12 hours at 800°C in air completely destroys the ability of the

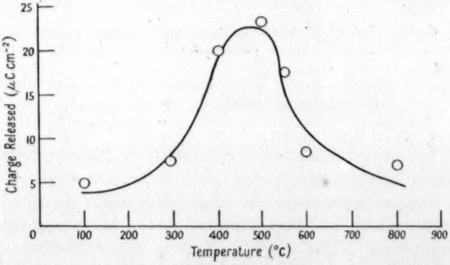

Figure 4. Total charge released as a function of the temperature of the vacuum furnace for composition A. Polarization and depolarization carried out at 90°C.

material to be polarized in the anomalous manner under discussion. This treatment appears to induce a reproducible state and this state is tentatively identified with one in which very few free oxygen vacancies exist. If the material which has been thus treated is now heated for two hours *in vacuo* at a temperature of about 500°c and then rapidly cooled to room temperature the ability to exhibit anomalous polarization is restored. Slow cooling was not effective. In order to study this effect quantitatively a number of specimens, having composition A described above and having fired on silver electrodes, were first heated for 12 hours in air at 800°c. Individual specimens were then heated at various temperatures *in vacuo* for two hours. They were then polarized at 90°c in the manner already described and finally the anomalous charge released at this temperature was measured. This charge is plotted as a function of the temperature of the vacuum furnace in figure 4. It will be seen that the phenomenon is critically dependent on temperature. Presumably the partially reduced state is stable in the region of 500°c and rapid cooling freezes this state in.

§ 8. INTERACTION WITH ORDINARY POLARIZATION

The very large charges released from some specimens led one to the belief that the anomalous polarization is not a real physical polarization but is rather due to a chemical effect analogous to the operation of a secondary electric cell. If this is the case then there will not be an internal electric field caused by the anomalous polarization. In order to investigate this question the hysteresis loops of a number of suitable specimens were examined both before and after the release of an induced anomalous polarization. Now the influence of a steady bias field on the form of the hysteresis loops could easily be determined. This effect was then compared with the influence of the presence of anomalous polarization. If this was a real physical polarization and led to an internal field of the order $4\pi P/3$ then the total anomalous polarization could only be of the order $2\,\mu\mathrm{c\,cm}^{-2}$. As the anomalous charges subsequently released were two orders of magnitude larger than this it is obvious that the effect must be of an essentially chemical nature.

§ 9. OTHER MATERIALS

As the anomalous polarization is capable of being both induced and released at temperatures above the Curie temperature of barium titanate it seemed likely that the effect was not particular connected with ferroelectricity as such. A study of oxides which are not ferroelectric was made in order to elucidate this point. Initial failure to obtain anomalous polarization with materials based on strontium titanate were disappointing, but not really surprising as it is known that $SrTiO_3$ is much harder to reduce than $BaTiO_3$. However molybdenum trioxide, which has a crystal structure related to that of barium titanate, does show a quite unambiguous anomalous polarization and is certainly not ferroelectric at temperatures down to 80°K.

Ceramic specimens of molybdenum trioxide prepared and polarized in the standard manner described above gave an anomalous charge release at room temperature of approximately $40\,\mu\mathrm{c\,cm}^{-2}$ with either silver or gold electrodes.

A specimen of an under-fired ceramic ferrite also showed considerable anomalous polarization. The composition of this material was NiO_3 49 atomic %, ZnO 1 atomic % and Fe_2O_3 50 atomic %. It was of a highly porous ceramic nature and had chemically deposited fired-on silver electrodes. At room temperature an anomalous polarization of approximately 100 $\mu c\,cm^{-2}$ was obtained with this specimen. Further attempts were made to obtain anomalous polarization with ceramic ferrites in which the sintering process was complete. These attempts were unsuccessful.

§ 10. Effect of Electrode Material

In order to test the hypothesis that the origin of anomalous polarization is in the chemical effects at the electrodes the following experiment was carried out. Two blanks of composition A had electrodes of silver deposited on one side and electrodes of palladium deposited on the other. These specimens were then heated at 500°c *in vacuo* for two hours and then polarized at 90°c in the standard manner and finally depolarized at this latter temperature.

The total charges expressed in $\mu c\,cm^{-2}$ released under these circumstances are given below. The rate of charge release for the first few minutes was approximately the same in all cases. However the subsequent rate of release depended on the polarity of the specimens. It thus seems likely that there is a battery mechanism associated with the electrodes which is fairly slow and a residual more rapid release of charge which is independent of electrode material.

Table 2

Specimen	1	2
Silver negative	49·6	53·6
Palladium negative	30·5	27·0

§ 11. Conclusions

The foregoing results indicate that a substantial part of the anomalous polarization can be explained by a model analogous to a secondary cell. Oxygen vacancies act as charge carriers and interact with the electrode material and surface layer of the crystal. The activation energy obtained from the straight portions of the curves in figure 2 is then the activation energy for the oyxgen vacancy diffusions in the material.

Acknowledgments

The authors wish to thank Professor W. Sucksmith and Professor E. R. Andrew for the facilities of their laboratories, the Plessey Company for provision of the majority of the specimens, the General Electric Company for the provision of some of the single crystals, Mr. J. M. Herbert for many valuable discussions and Dr. R. Street for assistance with the magnetic measurements.

References

Blood, H. L., Levine, S., and Roberts, N. H., 1956, *J. Appl. Phys.*, **27**, 660.
Henri le Blanchetais, C., 1951, *J. Phys. Radium*, **12**, 765.
Koops, C. G., 1951, *Phys. Rev.*, **83**, 121.
Maxwell, J. C., 1873, *Electricity and Magnetism* (Oxford : University Press), Vol. I, § 328.
Wagner, K. W., 1913, *Ann. Phys., Lpz.*, **40**, 817.

Van der Waals Forces

By A. DALGARNO and A. E. KINGSTON
Department of Applied Mathematics, The Queen's University of Belfast

MS. received 21*st October* 1958, *in final form* 26*th November* 1958

Abstract. Theoretical and experimental values of electric dipole oscillator strengths are used to calculate the coefficients of the leading terms in the series representations of the long range interactions between pairs of atoms. Values are obtained for pairs selected from the alkali metals, the inert gases, H, H^-, He^+ and Li^+ and are then employed to assess the accuracy of various approximate formulae. Where possible, comparison is made with experimental data and it is shown that the polarizabilities derived from molecular beam measurements are unreliable. A discussion is given of the measurements of elastic scattering of the alkali metals by the inert gases and it is concluded that the normal van der Waals interaction does not suffice to explain the observations at very low scattering angles.

---

§ 1. INTRODUCTION

A KNOWLEDGE of the magnitude of the long range interaction between a pair of atoms or between an ion and an atom is required in diverse fields of interest, but apart from single electron cases, accurate information is available only for the pairs H–H (Pauling and Beach 1935), He–He (Margenau 1939 a, Dalgarno and Lynn 1957) and He–He* and He*–He* (Dalgarno and Kingston 1958), the asterisk indicating the singlet or triplet metastable level. This scarcity may be partially remedied for there are available reliable values of electric dipole oscillator strengths in terms of which the leading term in the series representation may be expressed (cf. Margenau 1939 b); indeed the first accurate values for H–H were obtained by this method (Eisenschitz and London 1930, Lennard-Jones 1929).

§ 2. THE SERIES REPRESENTATION

Suppose the nucleus B of an atomic system, which has a nuclear charge Z_b and t_b electrons with position vectors $\mathbf{r}_b{}^j$ relative to B, is located at a position $\mathbf{R}$ relative to the nucleus A of a second atomic system, which has a nuclear charge Z_a and t_a electrons with position vectors $\mathbf{r}_a{}^i$ relative to A. Then for large internuclear separations R, the interaction potential may be expanded according to

$$\begin{aligned} V(\mathbf{r}_a, \mathbf{r}_b, \mathbf{R}) = \frac{\zeta_a\zeta_b}{R} &- \left(\zeta_a \sum_j z_b{}^j + \zeta_b \sum_i z_a{}^i \right) \frac{1}{R^2} \\ &+ \left\{ \tfrac{1}{2}\zeta_a \sum_j ({r_b{}^j}^2 - 3{z_b{}^j}^2) + \tfrac{1}{2}\zeta_b \sum_i ({r_a{}^i}^2 - 3{z_a{}^i}^2) \right. \\ &\left. + \sum_i \sum (2z_a{}^i z_b{}^j + x_a{}^i x_b{}^j + y_a{}^i y_b{}^j) \right\} \frac{1}{R^3} + \dots \qquad \dots\dots(1) \end{aligned}$$

where $\zeta_\mathrm{a} = Z_\mathrm{a} - t_\mathrm{a}$ and $\zeta_\mathrm{b} = Z_\mathrm{b} - t_\mathrm{b}$ are the excess charges on the atomic systems, (x, y, z) are Cartesian coordinates with the z_a axis parallel and the z_b axis antiparallel to $\mathbf{R}$, and all quantities are expressed in atomic units.

We are interested only in cases in which at least one of the interacting systems is neutral since otherwise the interaction energy is dominated by the Coulomb term $\zeta_\mathrm{a}\zeta_\mathrm{b}/R$. We take ζ_a equal to zero and let ϕ_0^a and ψ_0^b be the wave functions of systems A and B respectively when R is infinite. Then the first-order contribution to the energy of interaction for a finite separation R is given by

$$\mathscr{E}_1 = (\phi_0^\mathrm{a}\psi_0^\mathrm{b},\ V\phi_0^\mathrm{a}\psi_0^\mathrm{b}) \qquad \ldots\ldots(2)$$

and if both A and B are in S states, $\mathscr{E}_1$ vanishes from symmetry considerations. The second-order contribution is given by

$$\mathscr{E}_2 = \sum_{m,\,n\neq 0}{}'\sum{}' \frac{|(\phi_0^\mathrm{a}\psi_0^\mathrm{b},\ V\phi_m^\mathrm{a}\psi_{n\mathrm{b}})|^2}{(\epsilon_0^\mathrm{a} + \epsilon_0^\mathrm{b} - \epsilon_m^\mathrm{a} - \epsilon_n^\mathrm{b})} \qquad \ldots\ldots(3)$$

where ϕ_m^a is the mth excited state of system A with associated eigenvalue ϵ_m^a and ψ_n^b is the nth excited state of system B with associated eigenvalue ϵ_n^b. If ϕ_0^a and ψ_0^b refer to the ground states, then (3) is negative corresponding to an attractive force.

Substituting (1) into (3), we have to $\mathrm{O}(R^{-6})$

$$\begin{aligned}\mathscr{E}_2 = {} & \frac{\zeta_\mathrm{b}^2}{R^4}\sum_{m\neq 0}{}' \frac{|\phi_0^\mathrm{a},\ \sum_i z_\mathrm{a}^i\phi_m^\mathrm{a})|^2}{\epsilon_0^\mathrm{a} - \epsilon_{m\mathrm{a}}} \\ & + \frac{\zeta_\mathrm{b}^2}{R^6}\sum_{m\neq 0}{}' \frac{|(\phi_0^\mathrm{a},\ \frac{1}{2}\sum_i (r_\mathrm{a}^{i^2} - 3z_\mathrm{a}^{i^2})\phi_m^\mathrm{a})|^2}{\epsilon_0^\mathrm{a} - \epsilon_m^\mathrm{a}} \\ & + \frac{1}{R^6}\sum_{m,\,n\neq 0}{}'\sum{}' \frac{|(\phi_0^\mathrm{a}\psi_0^\mathrm{b},\ \sum_i\sum_j\ [2z_\mathrm{a}^i z_\mathrm{b}^j + x_\mathrm{a}^i x_\mathrm{b}^j + y_\mathrm{a}^i y_\mathrm{b}^j]\phi_m^\mathrm{a}\psi_n^\mathrm{b})|^2}{\epsilon_0^\mathrm{a} + \epsilon_0^\mathrm{b} - \epsilon_m^\mathrm{a} - \epsilon_n^\mathrm{b}} \qquad \ldots\ldots(4)\end{aligned}$$

which may be written

$$\begin{aligned}\mathscr{E}_2 = {} & -\frac{\zeta_\mathrm{b}^2}{2}\left(\frac{\alpha_\mathrm{d}^\mathrm{a}}{R^4} + \frac{\alpha_\mathrm{q}^\mathrm{a}}{R^6}\right) \\ & + \frac{3}{2R^6}\sum_{m,\,n\neq 0}{}'\sum{}' \frac{f_m^\mathrm{a} f_n^\mathrm{b}}{(\epsilon_0^\mathrm{a} - \epsilon_m^\mathrm{a})(\epsilon_0^\mathrm{b} - \epsilon_n^\mathrm{b})(\epsilon_0^\mathrm{a} + \epsilon_0^\mathrm{b} - \epsilon_m^\mathrm{a} - \epsilon_n^\mathrm{b})} \qquad \ldots\ldots(5)\end{aligned}$$

where $\alpha_\mathrm{d}^\mathrm{a}$ and $\alpha_\mathrm{q}^\mathrm{a}$ are respectively the dipole and quadrupole polarizabilities of A and f_m^a and f_n^b are electric dipole oscillator strengths defined according to

$$\begin{aligned} f_m^\mathrm{a} &= \tfrac{2}{3}(\epsilon_m^\mathrm{a} - \epsilon_0^\mathrm{a})|(\phi_0^\mathrm{a},\ \sum_i \mathbf{r}_\mathrm{a}^i\phi_m^\mathrm{a})|^2 \\ f_n^\mathrm{b} &= \tfrac{2}{3}(\epsilon_n^\mathrm{b} - \epsilon_0^\mathrm{b})|(\psi_0^\mathrm{b},\ \sum_j \mathbf{r}_\mathrm{b}^j\psi_n^\mathrm{b})|^2. \qquad \ldots\ldots(6)\end{aligned}$$

The last term of (5), which we shall write as $-C_\mathrm{ab}/R^6$ is the first non-vanishing term in the series representation of the interaction between neutral atoms.

§ 3. APPROXIMATE FORMULA

Of the several approximate formulae for C_ab that have been proposed (cf. Margenau 1939 b) we shall consider here only those which do not require a knowledge of the atomic wave functions. These are the London formula

$$C_\mathrm{ab} = \frac{3}{2}\frac{I_\mathrm{a}I_\mathrm{b}}{I_\mathrm{a} + I_\mathrm{b}}\,\alpha_\mathrm{d}^\mathrm{a}\alpha_\mathrm{d}^\mathrm{b} \qquad \ldots\ldots(7)$$

where I_a and I_b are the ionization potentials of A and B respectively, and the combination rules

$$C_{ab} = (C_{aa}C_{bb})^{1/2} \qquad \ldots\ldots(8)$$

and

$$C_{ab} = (C_{aa}C_{bb})^{1/2}\{2(I_aI_b)^{1/2}/(I_a+I_b)\}. \qquad \ldots\ldots(9)$$

There is a fourth formula useful for cases in which

$$\epsilon_0{}^a - \epsilon_m{}^a \ll \epsilon_0{}^b - \epsilon_n{}^b$$

for all m, n which contribute appreciably to (5). Then (5) simplifies to

$$C_{ab} = \tfrac{3}{4}\alpha_d{}^b \sum_n{}' f_n{}^a/(\epsilon_0{}^a - \epsilon_n{}^a). \qquad \ldots\ldots(10)$$

§ 4. OSCILLATOR STRENGTHS

In this section, we describe the oscillator strengths we have adopted for the evaluation of C_{ab}.

Atomic hydrogen H and the positive helium ion He⁺. For discrete transitions exact values have been tabulated by Green, Rush and Chandler (1957), but for continuum transitions no values of sufficient accuracy have been published and we have therefore computed them from the conventional formula (cf. Stobbe 1930).

Normal helium He. A set of values, consistent with various sum rules and which reproduce the measured polarizability (Essen 1953), has been obtained by Dalgarno and Lynn (1957). Their accuracy is such that the error in values of C_{ab} derived from them should not exceed 2%.

Singlet and triplet metastable helium $^{1,3}He^*$. A set of values, consistent with various sum rules, has been obtained by Dalgarno and Kingston (1958). The error in C_{ab} should not exceed 5%.

Negative hydrogen ion H^-. The most refined theoretical calculations are those by Chandrasekhar (1945) whose values are in harmony with the experimental data of Branscomb and Smith (1955) which refer to wavelengths between 4000 Å and 9000 Å. A further check on their accuracy is provided by the sum rules

$$\sum_n{}' f_n{}^b = t_b \qquad \ldots\ldots(11)$$

$$\sum_n{}' \frac{f_n{}^b}{(\epsilon_n{}^b - \epsilon_0{}^b)} = \tfrac{2}{3}(\psi_0{}^b, [\sum_j \mathbf{r}_b{}^j]^2\psi_0{}^b). \qquad \ldots\ldots(12)$$

For H^-, Henrich (1944) has obtained 22·97 for $(\psi_0{}^b, [r_b{}^{1\,2} + r_b{}^{2\,2}]\psi_0{}^b)$ and Dalgarno and Stewart (1958) have obtained $-0{\cdot}660$ for $(\psi_0{}^b, \mathbf{r}_b{}^1 . \mathbf{r}_b{}^2\psi_0{}^b)$ so that the right-hand side of (12) is 14·4. Since Chandrasekhar does not take account of transitions such as

$$\mathrm{H}^- + h\nu \rightarrow \mathrm{H}' + \mathrm{e}, \qquad \ldots\ldots(13)$$

H′ being an excited hydrogen atom, his values should satisfy the inequalities

$$\sum{}' f_n{}^b \leqslant 2 \qquad \ldots\ldots(14)$$

$$\sum{}' \frac{f_n{}^b}{(\epsilon_n{}^b - \epsilon_0{}^b)} \leqslant 14{\cdot}4 \qquad \ldots\ldots(15)$$

whereas, whilst we obtain 1·80 for $\Sigma' f_n{}^b$ in harmony with (14), we obtain 16·0 for $\Sigma' f_n{}^b/(\epsilon_n{}^b - \epsilon_0{}^b)$ in contradiction to (15). Unless the computed matrix elements are in error, it follows that some, at least, of Chandrasekhar's values are incorrect by more than 10%†, and the experimental data suggest that the erroneous values lie between 9000 Å and the spectral head 16434 Å. This is the region of importance for C_{ab} so that an overestimate of C_{ab} as large as perhaps 20% cannot be excluded. The error caused by neglect of contributions from (13) is negligible in comparison. It may be noted that a similar uncertainty attends the value $230a_0^3$‡ computed by Bates and Lewis (1955) for the polarizability of H^-.

Positive lithium ion Li^+. Apart from one value of uncertain accuracy computed by Veselov (1949) for the resonance transition, no values appear to be available for discrete transitions, but for continuum transitions we had access to unpublished calculations by A. L. Stewart and W. J. Wilkinson. To obtain discrete values, the following procedure was adopted: Initial estimates were obtained using the relationship

$$f_n(Z) = a(n) + b(n)/Z \qquad \ldots\ldots(16)$$

where Z is the nuclear charge, $a(n)$ is twice the oscillator strength of the nth transition in atomic hydrogen and $b(n)$ was determined so that the substitution of $Z=2$ in (16) reproduced the values for helium. The intitial estimates were modified so that the oscillator strengths satisfied the sum rules (11) and (12) and reproduced the polarizability of Li^+, calculated by Dalgarno and Stewart (1958). The consistency of the procedure was checked by the continuity rule for singly charged positive ions, which states that $n^3 f_n/4$ is continuous with the spectral head value. Despite the approximate nature of the derivation, the error in C_{ab} should not exceed 4%.

Lithium Li. For the resonance transition, an oscillator strength of about 0·75 appears to be well established, for it is insensitive to the wave functions employed (Trumpy 1930, Fock and Petrashen 1935, Veselov 1949, Bates and Damgaard 1949), but with the higher discrete transitions and the continuum transitions, the position is less clear (cf. Burgess and Seaton 1959). The experimental discrete values of Filipov (1931), when calibrated against the resonance value, merge smoothly with the experimental continuum values of Tunstead (1953, see also Ditchburn, Jutsum and Marr 1953), and a similar behaviour occurs with the theoretical values (Fock and Petrashen 1935, Bates and Damgaard 1949, Stewart 1954, Burgess and Seaton 1959). But there is a discrepancy of about two between the theoretical and experimental values.

We adopt the experimental values. The consequent uncertainty in C_{ab} is slight since the summation (10) is dominated by the resonance transition. A check on the accuracy of the adopted values is provided by the sum rule (12). Using Hartree–Fock wave functions (Fock and Petrashen 1935), we obtain 11·7 for the 2s electron compared to an oscillator strength sum of 11·8 of which the resonance transition contributes 11·0.

The inner shell contribution to (11) is 2, but to (12) is only 0·6 so that it is clear from the form of (5) that the error in C_{ab} arising from the neglect of transitions out of the inner shell is negligible. Consequently, the uncertainty in the derived

V. 19

---

† Using a more refined (20-parameter) discrete wave function, Chandrasekhar (1958) has recently computed some further values which differ little from earlier values calculated with a similar continuum function. However, it is his use of a plane wave or Hartree continuum function which is the probable source of the (apparent) inaccuracy.

‡ This value is so large that little weight can be attached to the calculations of the interaction between He^+ and H^- (Ross and Mason 1956) which ignore it.

values of C_{ab} depends primarily on the uncertainty of the oscillator strength of the resonance transition and is probably less than 5%.

Sodium Na. The oscillator strength of the resonance transition is 0·98 with a suggested possible error of 5% (cf. Korff and Breit 1932, Stephenson 1951). For higher discrete transitions we adopt the experimental values of Filipov and Prokofjew (1929), and for continuum transitions the experimental values of Ditchburn, Jutsum and Marr (1953). Using Hartree–Fock wave functions (Hartree and Hartree 1948), we obtain 13·8 for the contribution of the 3s electron to the right-hand side of (12) compared with an oscillator strength sum of 13·0 of which the resonance transition contributes 12·6. Since the Hartree–Fock functions probably over-estimate (12), we can be confident that the overall error is less than 6%.

An indication of the error arising in C_{ab} due to neglect of inner shell transitions is provided by observing that they contribute approximately 10 to sum rule (11), the total sum being 11, and approximately 0·8 (Buckingham, private communication) to sum rule (12), the total sum being 14·6. The relative contribution to (5) will be still smaller and we conclude that the possible error in C_{ab} is simply the possible error in the oscillator strength of the resonance transition.

Potassium K. The oscillator strength of the resonance transition has been measured by Stephenson (1951) to be about 0·99 in harmony with earlier measurements (cf. Korff and Breit 1932), and the ratio of it to that of the second line of the principal series by Prokofjew and Gamow (1927). Continuum values have been measured by Ditchburn, Tunstead and Yates (1943).

Examination of the tables of inner shell energies prepared by Slater (1955) shows that inner shell contributions are negligible so that only the resonance transition of the valence electron contributes significantly to C_{ab}, the possible error of which is therefore probably less than 5%.

Rubidium Rb. The oscillator strength of the resonance transition has been measured by Stephenson (1951) to be 1·00 and the ratio of it to that of the second line of the principal series by Roschdestventski (1921). Continuum values have been measured by Mohler and Boeckner (1929).

Just as for potassium, only the resonance transition is important and the possible error in C_{ab} is probably less than 5%.

Caesium Cs. The oscillator strengths of the principal series have been measured by Waibel (1929) and Minkowski and Muhlenbruck (1930), that for the resonance line being 0·98 with a possible error of 10%. Continuum values have been measured by Braddick and Ditchburn (1935).

Only the resonance transition is important and the possible error in C_{ab} is 10%.

§ 5. POLARIZABILITIES OF THE ALKALI METALS

As may be seen from table 1, there are serious discrepancies between the dipole polarizabilities of the alkali metals obtained from Stark effect measurements

Table 1. Dipole Polarizabilities α_d (a_0^3)

Atom	Li	Na	K	Rb	Cs
Stark effect	180	180	310	340	410
Molecular beam	80	—	230	—	280
Theoretical	165	166	281	296	363

(Fues 1933), and from molecular beam methods (Scheffers and Stark 1934). Now we may write

$$\alpha_d^{a} = \sum{}' f_n^{a}/(\epsilon_0^{a} - \epsilon_n^{a})^2 \qquad \ldots\ldots(17)$$

and the corresponding values are included in table 1, the possible error being 5% for all cases except caesium for which it is 10%. The Stark effect values are all about 10% higher than the theoretical values but the discrepancies are probably within the combined theoretical and experimental error and it is clear that the molecular beam values are incorrect.

§ 6. VALUES OF C_{ab}

The derived values for C_{ab} for pairs a–b selected from H^+, H, H^-, He, He*, He^+, Li^+ and the alkali metals are listed in table 2. The value for H–H is due to Pauling and Beech (1935), for He–He to Dalgarno and Lynn (1957) and for He–He* to Dalgarno and Kingston (1958). All other values are new, although Margenau (1939 b) has previously given values for Na–Na and K–K (apparently obtained by taking the oscillator strength of the resonance line to be unity and ignoring all others), which differ from ours by about 50%. The origin of the discrepancy is obscure.

Table 2 (*a*). Values of C_{ab} for H and He in atomic units†

b\a	H	H^-	He	$^1He^*$	$^3He^*$	He^+	Li^+	Li	Na	K	Rb	Cs
H	6·5	89	2·9	130	87	0·66	0·52	67	74	99	100	120
He	2·9	30	1·5	42	29	0·38	0·32	22	25	33	34	38

Table 2 (*b*). Values of C_{aa} for He* in atomic units†

b\a	H	He	He^+	$^1He^*$	$^3He^*$
$^1He^*$	130	42	8·6	$1{\cdot}1 \times 10^4$	$5{\cdot}7 \times 10^3$
$^3He^*$	87	29	6·1	$5{\cdot}7 \times 10^3$	$3{\cdot}3 \times 10^3$

Table 2 (*c*). Values of C_{ab} for the alkali metals in atomic units†

Li	Na	K	Rb	Cs
$1{\cdot}4 \times 10^3$	$1{\cdot}6 \times 10^3$	$3{\cdot}5 \times 10^3$	$3{\cdot}8 \times 10^3$	$5{\cdot}2 \times 10^3$

† The interaction energy is $(-C_{ab}/R^6)\, e^2/a_0$ if R is measured in units of a_0.

Attention is drawn to the considerable range of values that C_{ab} may take. The values for the alkali metals are so large that the use of perturbation methods to describe the interaction is a procedure of doubtful validity.

No detailed discussion of the accuracy of the approximate formulae (7), (8) and (9) will be given and it suffices to remark that none is uniformly superior to the others. They generally reproduce the correct order of magnitude but must be used with caution when the polarizability and ionization potential of atom A differ considerably from those of atom B.

For the interactions of He with Li, Na, K, Rb and Cs the approximate formula (10) yields values of C_{ab} equal to respectively 25, 27, 35, 36, 40 in good agreement with the more accurate values given in table 2 (*a*). We use it therefore to obtain C_{ab} for the alkali metals and all the inert gases, their polarizabilities being known to high accuracy (Essen 1951, 1953, Hector and Woernley 1946, Cuthbertson and Cuthbertson 1911, 1932). The results are given in table 3.

Table 3. Values of C_{ab} for the Alkali Metals and Inert Gases in atomic units

b\a	He		Ne		A		Kr	Xe
	exp.	theor.	exp.	theor.	exp.	theor.	theor.	theor.
Li	15	22	20	48	200	200	300	480
Na	19	25	42	52	200	210	330	530
K	33	33	53	68	370	280	420	680
Rb	27	34	51	69	260	280	430	700
Cs	31 390†	38	59	77	250	320	480	780

† This value is derived from the measurements of Esterman *et al.* (1947).

§ 7. Discussion

When one of the interacting species is an ion, the term arising from the quadrupole polarizability of the neutral atom must be included. For atomic hydrogen the contribution is $-7{\cdot}5/R^6$ for unit excess charge on the ion (cf. Dalgarno and Stewart 1956) so that for He$^+$–H

$$\mathscr{E}_2 \sim -\frac{2{\cdot}25}{R^4} - \frac{8{\cdot}2}{R^6},$$

and for Li$^+$–H

$$\mathscr{E}_2 \sim -\frac{2{\cdot}25}{R^4} - \frac{8{\cdot}0}{R^6},$$

the quadrupole term being dominant in each case. By contrast, for H$^-$–H

$$\mathscr{E}_2 \sim -\frac{2{\cdot}25}{R^4} - \frac{97}{R^6},$$

the normal van der Waals force being dominant.

The quadrupole contribution in the case of helium is not known exactly but is about $-1{\cdot}2/R^6$ (Das and Bersohn 1956, Sternheimer 1954), so that for He$^+$–He

$$\mathscr{E}_2 \sim -\frac{0{\cdot}69_5}{R^4} - \frac{1{\cdot}6}{R^6}$$

for Li$^+$–He

$$\mathscr{E}_2 \sim -\frac{0{\cdot}69_5}{R^4} - \frac{1{\cdot}5}{R^6}$$

and for H$^-$–He

$$\mathscr{E}_2 \sim -\frac{0{\cdot}69_5}{R^4} - \frac{31}{R^6}.$$

As for H, when a positive ion is involved, the quadrupole term is dominant, but when a negative ion is involved the normal van der Waals term is dominant.

The expression for the interaction of Li$^+$ with He may be compared with the expression

$$\mathscr{E}_2 \sim -\frac{0{\cdot}68_5}{R^4} - \frac{1{\cdot}9}{R^6}$$

proposed by Margenau (1941) and adopted by Mason, Schamp and Vanderslice

(1958) in their calculations of the mobility of Li^+ in He. The differences are unlikely to cause any significant modification of the results (cf. Dalgarno, McDowell and Williams 1958, Mason and Schamp 1958).

This may not be the case for the interpretation of the scattering experiments of H^- by He by Bailey, May and Muschlitz (1957), for which Mason and Vanderslice (1958) have assumed a second-order energy

$$\mathscr{E}_2 \sim -\frac{0\cdot68_5}{R^4} - \frac{1\cdot8}{R^6},$$

an expression in which the coefficient of the R^{-6} term is underestimated by a factor of about 15.

Large coefficients are to be expected for the interaction of negative ions with neutral atoms and the magnitude of $\mathscr{E}_2$ for H–H^- is such that the first-order calculations by Dalgarno and McDowell (1956) of the two lowest potential energy curves of H_2^- must considerably underestimate the depth of the minimum of the stable state.

The case of He^+–He is of special interest since there is a discrepancy between the experimental and theoretical values of the mobility of He^+ in He at low temperatures which may be due to the effect of the R^{-6} term (Biondi and Chanin 1957, Dalgarno 1958). However, this possibility can be rejected with confidence for the value we obtain for its coefficient is much too small.

We consider finally some data on the elastic scattering of neutral atoms by neutral atoms. The value of C_{ab} for H–He is of minor importance for the interpretation of the high energy data of Amdur and Mason (1956), our value of 2·9 being in harmony with that adopted by Mason, Ross and Schatz (1956), but the values of C_{ab} for the alkali metals and He, Ne and A are of major importance for the interpretation of the low energy data of Mais (1934), Rosin and Rabi (1935), Rosenberg (1939) and Esterman, Foner and Stern (1947).

Assuming that the effective interaction is $-C_{ab}/R^6$, Buckingham and Massey (1936) have used a cross-section formula due to Massey and Mohr (1934) to derive values of C_{ab} from the measured cross sections and their values are reproduced in table 3. The results obtained from the measurements of Mais, of Rosin and Rabi and of Rosenberg agree within the limits of experimental error but there is a serious discrepancy in the case of Cs in He with the value obtained from the measurements of Esterman, Foner and Stern whose angular resolution was much superior to that of earlier workers. Massey and Burhop (1952) concluded that the measurements of Mais, of Rosin and Rabi and of Rosenberg were in harmony with theoretical expectation but their conclusion was uncertain to the extent that they used an approximate formula to compute C_{ab} together with the molecular beam polarizabilities (which we have shown in § 5 to be incorrect). Our more accurate estimates of C_{ab} confirm their conclusions except possibly for Li in Ne where the discrepancy is rather large (cf. table 3).

Thus if the most recent measurements are accepted, it seems clear that an interaction must be occurring other than the normal van der Waals forces. A tentative explanation has been proposed by Dalgarno and McCarroll (1957).

ACKNOWLEDGMENTS

We are grateful to Dr. M. J. Seaton for his comments on the oscillator strengths of Li and to Dr. A. L. Stewart for his comments on the oscillator strengths of H^-.

V.
19

References

Amdur, I., and Mason, E. A., 1956, *J. Chem. Phys.*, **25**, 630.

Bailey, T. L., May, C. J., and Muschlitz, E. E., 1957, *J. Chem. Phys.*, **26**, 1446.

Bates, D. R. and Damgaard, A., 1949, *Phil. Trans. Roy. Soc.* A, **242**, 101.

Bates, D. R., and Lewis, J. T., 1955, *Proc. Phys. Soc.* A, **68**, 177.

Biondi, M. A., and Chanin, L. M., 1957, *Phys. Rev.*, **106**, 473.

Braddick, H. J. J., and Ditchburn, R. W., 1935, *Proc. Roy. Soc.* A, **188**, 350.

Branscomb, L. M., and Smith, S. J., 1955, *Bur. Stand. J. Res., Wash.*, **55**, 165.

Buckingham, R. A., and Massey, H. S. W., 1936, *Nature, Lond.*, **138**, 77.

Burgess, A., and Seaton, M. J., 1959, *Mon. Not. R. Astr. Soc.*, in the press.

Chandrasekhar, S., 1945, *Astrophys. J.*, **102**, 401.

—— 1958, *Ibid.*, **128**, 141.

Cuthbertson, C., and Cuthbertson, M., 1911, *Proc. Roy. Soc.* A, **84**, 13.

—— 1932, *Ibid.*, **135**, 44.

Dalgarno, A., 1958, *Phil. Trans. Roy. Soc.* A, **250**, 411.

Dalgarno, A., and Kingston, A. E., 1958, *Proc. Phys. Soc.*, **72**, 1053.

Dalgarno, A., and Lynn, N., 1957, *Proc. Phys. Soc.* A, **70**, 802.

Dalgarno, A., and McCarroll, R. A., 1957, *Proc. Roy. Soc.* A, **239**, 413.

Dalgarno, A., and McDowell, M. R. C., 1956, *Proc. Phys. Soc.* A, **69**, 615.

Dalgarno, A., McDowell, M. R. C., and Williams, A., 1958, *Phil. Trans. Roy. Soc.* A, **250**, 411.

Dalgarno, A., and Stewart, A. L., 1956, *Proc. Roy. Soc.* A, **238**, 276.

—— 1958, *Ibid.*, **247**, 245.

Das, T. P., and Bersohn, R., 1956, *Phys. Rev.*, **102**, 733.

Ditchburn, R. W., Jutsum, P. J., and Marr, G. V., 1953, *Proc. Roy. Soc.* A, **219**, 89.

Ditchburn, R. W., Tunstead, J., and Yates, J. W., 1943, *Proc. Roy. Soc.* A, **181**, 386.

Eisenschitz, R., and London, F., 1930, *Z. Phys.*, **60**, 491.

Essen, L., 1951, *Proc. Phys. Soc.* B, **64**, 862.

—— 1953, *Ibid.*, **66**, 189.

Esterman, I., Foner, S. N., and Stern, O., 1947, *Phys. Rev.*, **71**, 250.

Filipov, A., 1931, *Z. Phys.*, **69**, 526.

Filipov, A., and Prokofjew, W. K., 1929, *Z. Phys.*, **56**, 458.

Fock, V., and Petrashen, M. J., 1935, *Phys. Zeit. der Sowjet.*, **8**, 546.

Fues, E., 1933, *Z. Phys.*, **82**, 536.

Green, L. C., Rush, P. P., and Chandler, C. D., 1957, *Astrophys. J. Supplement*, **3**, 37.

Hartree, D. R., and Hartree, W., 1948, *Proc. Roy. Soc.* A, **193**, 304.

Hector, L. G., and Woernley, D. L., 1946, *Phys. Rev.*, **69**, 101.

Henrich, L. R., 1944, *Astrophys. J.*, **99**, 59.

Korff, S. A., and Breit, G., 1932, *Rev. Mod. Phys.*, **4**, 471.

Lennard-Jones, J. E., 1929, *Proc. Roy. Soc.* A, **129**, 598.

Mais, W. H., 1934, *Phys. Rev.*, **45**, 773.

Margenau, H., 1939 a, *Phys. Rev.*, **47**, 1000.

—— 1939 b, *Rev. Mod. Phys.*, **11**, 1.

—— 1941, *Philosophy of Science*, **8**, 603.

Mason, E. A., Ross, J., and Schatz, P. N., 1956, *J. Chem. Phys.*, **25**, 626.

Mason, E. A., and Schamp, H. W., 1958, *Annals of Physics*, **4**, 233.

Mason, E. A., Schamp, H. W., and Vanderslice, J. T., 1958, *Phys. Rev.*, **112**, 445.

Mason, E. A., and Vanderslice, J. T., 1958, *J. Chem. Phys.*, **28**, 253

Massey, H. S. W., and Burhop, E. H. S., 1952, *Electronic and Ionic Impact Phenomena* (Oxford: Clarendon Press).

Massey, H. S. W., and Mohr, C. B. O., 1934, *Proc. Roy. Soc.* A, **144**, 188.

Minkowski, R., and Muhlenbruck, W., 1930, *Z. Phys.*, **63**, 198.

Mohler, F. L., and Boeckner, C., 1929, *Bur. Stand. J. Res., Wash.*, **3**, 303.

Pauling, L., and Beach., J. Y., 1935, *Phys. Rev.*, **47**, 686.

Prokofjew, W., and Gamow, G., 1927, *Z. Phys.*, **44**, 887.

Roschdestventski, D. S., 1921, *Trans. Opt. Inst. Leningrad*, **2**, 13.

Rosenberg, P., 1939, *Phys. Rev.*, **55**, 1267.

ROSIN, S., and RABI, I. I., 1935, *Phys. Rev.*, **48,** 373.
ROSS, J., and MASON, E. A., 1956, *Astrophys. J.*, **124,** 485.
SCHEFFERS, H., and STARK, J., 1934, *Physik Z.*, **35,** 625.
SLATER, J. C., 1955, *Phys. Rev.*, **98,** 1039.
STEPHENSON, G., 1951, *Proc. Phys. Soc.* A, **64,** 458.
STERNHEIMER, R. M., 1954, *Phys. Rev.*, **96,** 951.
STEWART, A. L., 1954, *Proc. Phys. Soc.* A, **67,** 917.
STOBBE, M., 1930, *Ann. Phys., Lpz.*, **7,** 661.
TRUMPY, B., 1930, *Z. Phys.*, **66,** 720.
TUNSTEAD, J., 1953, *Proc. Phys. Soc.* A, **66,** 304.
VESELOV, M. G., 1949, *J. Exp. Theor. Phys. U.S.S.R.*, **19,** 959.
WAIBEL, F., 1929, *Z. Phys.*, **53,** 459.

Optical Frequency Response Characteristics in the presence of Spherical Aberration measured by an automatically recording Interferometric Instrument

By D. KELSALL

Department of Physics, Imperial College, London

Communicated by H. H. Hopkins; *MS. received* 25*th July* 1958, *in revised form* 29*th October* 1958

Abstract. An interferometric method is described which measures the frequency response characteristics of a lens, with automatic recording of the curves. The theory of the method is given, followed by a discussion of the problems arising in the design of the instrument. A new type of interferometer was devised, having very stable adjustment and permitting accurate control of the path length and relative lateral shear of the two interfering wave fronts. Using a double beam shearing interferometer, with corner cube reflectors, it was also possible to measure the spatial phase shift term of the complex frequency response and record this automatically.

The frequency response curves for a well-corrected lens in different focal planes have been compared with results obtained by Hopkins theoretically.

The influence of primary spherical aberration on the frequency response has been studied in certain cases and the results of theoretical calculations verified.

§ 1. Introduction

Since the introduction of the use of frequency response for specifying the performance of lens systems, a procedure which has largely followed on the work of Duffieux (1946), not only have several techniques for the measurement of frequency response been devised, but also both the theory and methods of computation have been developed. More recently the computation of the frequency response of optical systems having any given aberrations has also become a practical matter (Hopkins 1957 a, Goodbody 1958). In consequence, it has become both possible, and of increased importance, to confirm experimentally the validity of frequency response methods for the specification and calculation of image quality.

A technique employing a shearing interferometer was proposed by Hopkins (1955 a) for the measurement of response functions. Baker (1955 a) constructed an interferometer of this kind and used it to measure the influence of defect of focus on the response of an aberration-free lens in monochromatic light. The apparatus permitted simultaneously direct measurement of the wave front aberration from the interferogram of the sheared wave fronts. Baker succeeded in confirming a number of the theoretical results of Hopkins (1955 b).

The shearing interferometer has a higher photometric efficiency than the conventional scanning methods, affording the possibility of a more accurate measurement of the response function. This is of particular importance when results are required in monochromatic light, such as when the verification of theoretically computed values is in view. No precise direct verification of computed response curves appears yet to have been made, if we except the work of Baker on defect of focus. To give an adequate test of the theory for cases where the optical system has aberrations, a large number of measurements are called for. For example, spherical aberration normally requires two coefficients (of the primary and secondary terms respectively) for its specification. To study the influence of spherical aberration on the response, in different focal planes, therefore, requires the variation of three parameters. For this reason it seemed desirable to design an automatically recording instrument, which would permit the rapid and accurate study of a large number of cases. At the same time it was found possible with a radically re-designed system to obtain both improvement in photometric efficiency, and simpler operation and adjustment, compared with that obtained by Baker.

§ 2. THEORY OF THE METHOD

The response factor $g(s,t)$ is simply the inverse Fourier transform of the intensity distribution in the image of a point source, and (s,t) are spatial frequency parameters defined by

$$s=(\lambda/n\sin\alpha)R_x, \quad t=(\lambda/n\sin\alpha)R_y \qquad \ldots\ldots(1)$$

Here R_x, R_y denote the corresponding wave numbers (numbers of 'lines' per unit length) in the object. There is no loss of generality in considering the more convenient case of unidimensional structures, provided they are examined in different orientations ψ in the object plane. The normalized frequency response is generally complex and may conveniently be written in terms of a modulus and a phase

$$g(s,\psi)/g(0,\psi)=D(s,\psi)=T(s,\psi)\,\mathrm{e}^{i\theta(s,\psi)} \qquad \ldots\ldots(2)$$

where $T(s,\psi)$ is the contrast transfer factor and $\theta(s,\psi)$ represents a spatial phase shift. These two quantities are measured separately in the present instrument.

The wave front aberration at the point (x, y) of the exit pupil of the lens is denoted by $W(x,y)$, and the pupil function of the optical system is then written

$$f(x,y)=\tau(x,y)\,\mathrm{e}^{ikW(x,y)}, \qquad \ldots\ldots(3)$$

where $\tau(x,y)$ describes the variation of amplitude over the image-forming wave front and is zero outside the domain of the pupil. It may be shown that $D(s,\psi)$ can be expressed by means of the double integral

$$D(s,\psi)=(1/A)\iint_S f(x+\tfrac{1}{2}s,y)f^*(x-\tfrac{1}{2}s,y)\,dx\,dy \qquad \ldots\ldots(4)$$

where S, the region of integration, is the area common to two pupils centred respectively on the points $(\pm\tfrac{1}{2}s,0)$. The constant A is defined by

$$A=\iint_A |f(x,y)|^2\,dxdy=\iint_A \{\tau(x,y)\}^2\,dxdy \qquad \ldots\ldots(5)$$

the region of integration A being here the whole region of a pupil centred on the origin. A is thus proportional to the total light flux through the pupil. When the emergent wave fronts are of uniform amplitude, $\tau(x,y)=$ constant, and A is then simply proportional to the area of the pupil.

To determine $T(s,\psi)$ and $\theta(s,\psi)$ it is easily shown that only the total light flux in the interference pattern formed by a two-beam shearing interferometer need be measured. A collimated light beam from the lens under test is directed into the interferometer, the beam splitter dividing the incident beam into two beams of nearly equal amplitude. The interferometer has the general form of the Michelson interferometer, but uses corner cubes in place of the two plane mirrors. It is so designed that two separate beams may be laterally sheared relative to one another, thus altering the region of overlap, and therefore the region in which interference occurs. This is illustrated in figure 1, where S denotes the region of overlap, and A_1, A_2 are the regions of the wave fronts from the two arms of the interferometer exterior to S, so that no interference takes place here. If the pupils are circular and taken to be of unit radius, the relative shear is numerically equal to the spatial frequency parameter.

In figure 1, the complex amplitude at a current point (x, y) of the fringe plane consists of a complex amplitude $p_1 f(x+\frac{1}{2}s, y)$, produced by the wave front coming from arm 1 of the interferometer, together with a complex amplitude $p_2 f(x-\frac{1}{2}s, y)$ produced by the wave front from arm 2. A further factor, namely $e^{ik\delta}$, must be included if the path difference between the two arms is δ. The two real factors p_1, p_2 denote the transmissivities of the two arms, measured as ratios of real amplitudes. The total light fluxes in the region A_1, A_2, S respectively are then given by

$$F_1 = \iint_{A_1} p_1^2 \,|f(x+\tfrac{1}{2}s, y)|^2 \,dx dy \qquad \ldots\ldots (6)$$

$$F_2 = \iint_{A_2} p_2^2 \,|f(x-\tfrac{1}{2}s, y)|^2 \,dx dy \qquad \ldots\ldots (7)$$

$$F_S = \iint_S |p_1 f(x+\tfrac{1}{2}s, y) + p_2 f(x-\tfrac{1}{2}s, y)\, e^{ik\delta}|^2 \,dx dy. \qquad \ldots\ldots (8)$$

F_S may be expanded to give

$$F_S = \iint_S p_1^2 \,|f(x+\tfrac{1}{2}s, y)|^2 \,dx dy + \iint_S p_2^2 \,|f(x-\tfrac{1}{2}s, y)|^2 \,dx dy$$
$$+ 2R\left\{ p_1 p_2 \iint_S f(x+\tfrac{1}{2}s, y) f^*(x-\tfrac{1}{2}s, y)\, e^{-ik\delta} \,dx dy \right\} \qquad \ldots\ldots (9)$$

where R denotes the real part of the integral. The total light flux

$$F(\delta) = F_1 + F_2 + F_S,$$

so that

$$F(\delta) = p_1^2 \iint_{A_1+S} |f(x+\tfrac{1}{2}s, y)|^2 \,dx dy + p_2^2 \iint_{A_2+S} |f(x-\tfrac{1}{2}s, y)|^2 \,dx dy$$
$$+ 2p_1 p_2 R\left\{ e^{-ik\delta} \iint_S f(x+\tfrac{1}{2}s, y) f^*(x-\tfrac{1}{2}s, y) \,dx dy \right\}$$

or, shifting the origin in each of the first two integrals,

$$F(\delta) = (p_1^2 + p_2^2) \iint_A |f(x, y)|^2 \,dx dy$$
$$+ 2p_1 p_2 R\left\{ e^{-ik\delta} \iint_S f(x+\tfrac{1}{2}s, y) f^*(x-\tfrac{1}{2}s, y) + dx dy \right\}$$

where A denotes here the region of a pupil centred on the origin. The first integral is now simply the constant defined in (5), so that

$$F(\delta) = (p_1^2 + p_2^2) A \{1 + [2p_1 p_2/(p_1^2 + p_2^2)]\, R\, [e^{-ik\delta} D(s, \psi)]\},$$

the second integral having been replaced by the left-hand side of (4). Using the form (2), for $D(s, \psi)$, one obtains

$$F(\delta)=(p_1^2+p_2^2)A\{1+[2p_1p_2/(p_1^2+p_2^2)]T(s,\psi)\cos[k\delta-\theta(s,\psi)]\}. \qquad \ldots\ldots(10)$$

This treatment has assumed perfect coherence between the interfering wave fronts. In fact, there will be only partial coherence, the effect of which will be to include a factor $\Gamma_{21}=V_{21}\exp(i\beta_{21})$ in the product term of (9) (Hopkins 1953, 1957 b). Equation (10) will then become

$$F(\delta)=(p_1^2+p_2^2)A\{1+[2p_1p_2/(p_1^2+p_2^2)]\,V_{21}\,T(s,\psi)\cos[k\delta-\theta(s,\psi)-\beta_{21}]\}. \qquad \ldots\ldots(11)$$

Provided a source of symmetrical shape is used the coherence factor Γ_{21} is wholly real. Moreover to obtain good contrast the modulus V_{21} must not differ appreciably from unity. Under these conditions the phase factor β_{21} will be zero.

It is now evident from (11) that by causing δ to vary linearly with time a cosinusoidal variation in the total light flux in the interferogram is produced, whose amplitude and phase give respectively the modulus $T(s, \psi)$ and argument $\theta(s, \psi)$ of the frequency response for the lens system producing the initially incident wave front.

Inequality of the transmission of the two paths in the interferometer will materially affect only the ratio of the amplitude of the variable part relative to the zero-frequency component. This is expressed in the factor $2p_1p_2/(p_1^2+p_2^2)$ which is a function of the ratio p_2/p_1. It is equal to unity when the two arms of the interferometer have equal transmissions. Even if the ratio of intensity is $(p_2/p_1)^2=0{\cdot}64$ this factor is only reduced to 0·98. The effect of this factor on the a.c. signal-to-noise ratio will therefore be negligible in practical cases. Its effect on the measured values of the response is merely that of a scaling factor.

In practice an incoherently illuminated slit is used as the source, and the modulus V_{21} of the appropriate coherence factor may be used to determine the maximum permissible width. For this case, the spatial coherence factor has the form

$$V_{21}=|\Gamma_{21}|=|\sin\{(2\pi/\lambda)n'\sin\alpha_0(P_1P_2)\}/\{(2\pi/\lambda)n'\sin\alpha_0(P_1P_2)\}| \qquad \ldots\ldots(12)$$

where α_0 is the angular half width of the slit when viewed from the point P_1, which is situated in the pupil of the lens under test. In the final interference pattern the two wave fronts are sheared by a varying amount. For any given setting, let the shear, referred to the plane of the lens pupil, be denoted by $(P_1P_2)=sh$, where s is the reduced spatial frequency and h is the radius of the pupil. The visibility of the fringes formed by interference of light from P_1 with that from P_2 is then given by (12). Imposing a tolerance $|\Gamma_{21}|\geqslant 0{\cdot}99$, this expression gives for the permissible source size,

$$\alpha_0 \leqslant 0{\cdot}04\,\lambda/sh$$

where s is the maximum spatial frequency that will come in question. For the measurements reported later a slit width of approximately $10\,\mu$ was employed.

The spectral line width of the light source also influences the visibility of the fringes, and consequently a chromatic coherence factor must be included in expression (11). In the present case the total coherence factor is simply the product of the spatial coherence factor (depending upon slit width) and the chromatic coherence factor (depending upon the spectral line width). In equation (10) we can thus write (Hopkins 1957 b):

$$V_{21}=(V_{21})s\times(V_{21})c.$$

For an idealized rectangular line profile the form of $(V_{21})c$ may be shown to be (Michelson 1927, Hopkins 1957 b):

$$(V_{21})c = |\Gamma_{21}(l_1 - l_2)| = \left|\left(\sin \pi (l_1 - l_2) \frac{\delta\lambda}{\lambda^2}\right) \Big/ \left(\pi (l_1 - l_2) \frac{\delta\lambda}{\lambda^2}\right)\right|$$

where $\Gamma(l_1 - l_2)$ is the chromatic coherence factor (Wolf 1954, 1955, Hopkins 1957 b), $(l_1 - l_2)$ the path difference in the interferometer and $\delta\lambda$ the half width of the line of mean wavelength λ. Imposing the condition $(V_{21})c \geqslant 0{\cdot}99$ the maximum permissible path difference between the two arms of the interferometer is given by

$$|l_1 - l_2| \leqslant 0{\cdot}08 \frac{\lambda}{\delta\lambda/\lambda}.$$

The profile of the line used ($\lambda = 5461$ Å, produced by a medium pressure mercury lamp) was measured with a recording spectrograph and found to be of symmetrical form and of half width $\delta\lambda = 2{\cdot}2$ Å. Inserting these values the permissible maximum path difference obtained is

$$|l_1 - l_2| \simeq 200\lambda.$$

Provided the mean path lengths in the two arms of the interferometer are equalized initially, therefore, the change of path length that may be introduced during measurement must be kept less than 200 λ.

§ 3. THE INTERFEROMETER UNIT

To achieve stability of adjustment, a Michelson interferometer employing corner cube reflectors in place of plane mirrors (Peck 1948) was used, in which the moving parts employed for wave front shearing and path changing were mounted independently of the interferometer bed. The interferometer, itself mounted on a rigid base plate supported on a vibration free mounting, formed in effect a separate unit. In this way it was found possible to shear the wave fronts and alter the path difference without any detectable effect on the adjustment of the system. The two operations were entirely independent of one another and neither relative tilt or shearing of the wave front occurs. Having outlined the general principle of the operation of the instrument, it will be useful to record some of the design details.

3.1. *Corner Cube Reflectors*

It is essential to the working of the interferometer that the two interfering wave fronts have no detectable relative tilt. This would be easily achieved if perfect corner cubes were available. In practice the angles may easily have errors as great as thirty seconds of arc. To correct these errors two pairs of small nominally identical wedge prisms T (figure 2), each of about one degree angle, were employed. Each pair of prisms is arranged to form initially an effectively plane-parallel plate, producing no deviation of a light beam passing through the unit. One prism in each pair is rotatable about an axis perpendicular to its median plane and a small rotation of this prism relative to the second member of the pair produced a small deviation of the light beam. A deviation of the light beam by thirty seconds of arc required a rotation of the movable prism through an angle of half a degree. One pair of prisms was used to correct errors of tilt in the horizontal plane and the other pair for tilt in the vertical plane. It will be appreciated that a combination of corner cube reflectors, with corrector prisms of the kind described, remains stable against small rotations of the corner cubes caused, for example, by vibration.

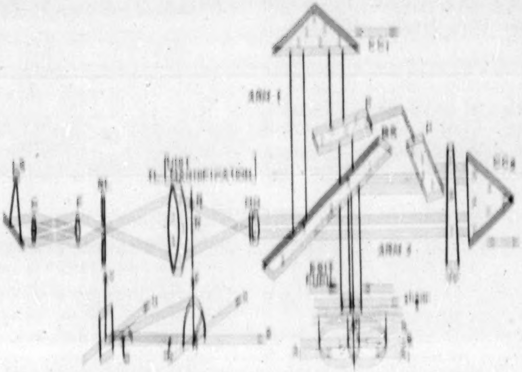

Figure 1. The interferometer with shear plates and path changing prism.

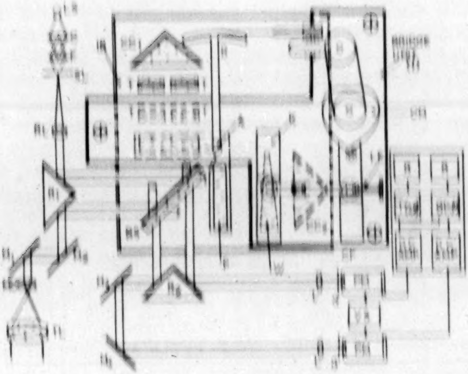

Figure 2. Plan of complete apparatus.

Key to figures 1 and 2.

CC₁, CC₂	Corner cubes	B	Bridge assembly (over interferometer)
P, P'	Shear plates	D	Shearing mechanism
W	Path changing prism	A	Axis for rotatable shear plate mounting
BS	Beam splitter	AM	Archimedean cam
MO	Microscope collimating objective	VL	Variable-area lever
L	Lens under test	K	Kinematic slide carrying path prism
S	Line source	LS	Lens holder slide
F	Field lens	RL	Reference lens
C	Condenser lens	IS	Integrating screen
LS	Light source	PM	Photomultipliers
TC	Tilt compensators	HV	Stabilised high voltage d.c. supply
CB	Cast iron base plate of interferometer	R	Pen recorder

3.2. *Path-changing Prism*

To produce the cosine signal, implied in expression (10), it is necessary to change δ linearly with time. To ensure good chromatic coherence between the interfering beams, on the other hand, this path difference is limited to a variation of about $\pm 50\lambda$. This was achieved by using a small angle prism whose angle was equal to 4·5 minutes of arc. This prism was reciprocated in the beam, with a length of stroke equal to 18 mm and a period of oscillation of 4 seconds, using an Archimedean cam. In this way a saw-toothed variation of δ with time was produced giving a frequency of 25 c/s for the varying component of the light flux.

3.3. *Pupil-shearing Mechanism*

The relative shear of the two interfering wave fronts must be capable of being varied over the complete range from $s=0$ to $s=2$. In the latter case the pupils no longer ovelap, but just touch. If only because of vibration, lateral movement of the corner cubes could not be used for producing the shear. A simple solution was found in the use of two plane-parallel optical flats, mounted rigidly on a triangular plate, with one positioned in each arm of the interferometer. On rotation of this assembly about the vertical axis A (figure 2), the two wave fronts are laterally sheared with no relative tilt between them and the path difference in the two arms is also unaffected. Two sets of shear plates, 0·15 inch thick and 0·4 inch thick respectively, allowed two different ranges of shear to be obtained with a convenient amount of rotation of the shearing assembly.

3.4. *Optical–mechanical Mountings*

The complete optical and mechanical system is shown in the figure 2. An achromatic dielectric beam splitter BS and two solid glass corner cube reflectors CC_1, CC_2 are carried on a heavy cast iron base plate of size 30 centimetres square. Each of these components has a conventional kinematic mounting and fine screw adjustment. The reflector CC_1 can be moved perpendicular to the optical axis on a kinematic slide thereby permitting an initial adjustment of the relative lateral shear of the interfering beams. Initial adjustment of the optical path difference in the two arms of the interferometer is made by displacing CC_2 along a similar slide arranged parallel to the optical axis.

A cast iron bridge shown as I in figure 2 is supported independently of the main interferometer unit by three steel rods of adjustable length. This bridge carries both the pivot for the axis A of the shearing mechanism and a kinematic slide K carrying the path-changing prism W. Both the shear plates and wedge prism are mounted in light duralumin holders, fitted with fine screw adjustments. Mounted in this way these components could be rotated and oscillated respectively without communicating detectable vibrations to the interferometer proper.

3.5. *Light Paths in the Interferometer*

When used at full aperture any small errors in the angles of the corner cube give rise to a doubling, or even tripling, of the reflected image. Even a perfect cube can exhibit these effects, because of polarization and diffraction effects at the edges (Mahan 1954, Zernike 1957). The dihedral edges of a corner cube will also usually cause narrow strips of the aperture to be lost unless great care is exercised in production. These disadvantages may be avoided if a collimated beam of small diameter is incident on, say, the upper left-hand part of the hypotenusal face of the corner cube, for this beam then emerges after three reflections at a diametrically opposite position in the lower right hand field, without encountering the dihedral edges. Apart from small deviations arising from errors in the angles of the corner cubes, the reflected beam returns parallel to the incident beam, but completely separated from it, as shown in figure 1. This permits the use of three separate channels of which two only are utilized in the present instrument. The incident beam, from the lens under test, enters the upper left-hand field of the instrument, so that the resultant interferogram is formed in the lower right-hand quadrant of the field. A reference beam, which serves as a standard for measurement of spatial phase shift, enters the upper right-hand quadrant of the field and gives an interference pattern in the lower left-hand corner of the field. For this reason two tilt compensators, one for each channel, are employed, which cover only the lower half of the field. Each shear plate, covering both channels, also occupies only the lower half of the field. The prism W on the other hand covers both halves of the field.

The diameters of the collimated light beams, that enter the interferometer from the lens under test, and the reference beam were restricted to about 5 mm. For most lenses under test, it was consequently necessary to reduce the beam diameter and this was arranged by using, as a collimating lens beyond the image, a good microscope objective of appropriate focal length. The image of the exit pupil of the lens under test formed by the collimating lens was then easily arranged to coincide with one entrance pupil of the interferometric unit, conveniently chosen to be positioned a few centimetres before the beam splitter. The other entrance pupil admitted light from the reference beam. A lens placed in the exit pupil of the interferometer was used to image these two entrance pupils of the interferometer in a convenient plane in the exit space. The interference patterns could then be visually examined in this plane. For the measurement of the total flux in the interferograms the beams from each channel were directed to photomultipliers, the photocathodes of which were made to coincide with the images of the exit pupils. To avoid errors arising from variations of sensitivity over the photocathodes, each light beam passed through a small diffusing element placed approximately 1 cm in front of the cathode surface. These elements were scalloped gratings used in the manner described by Baker (1955 b). A medium pressure mercury discharge lamp, operating at about 1 ampere from a stable 125 volt d.c. battery supply, free from any ripple, was used with a Wratten No. 77 A green filter to isolate the 5461 Å line. To obtain uniform illumination of the slit it was necessary to image the source at the entrance pupil of the lens and include a field lens to image the condenser lens in the plane of the slit as indicated in figure 1.

Because of the large number of air–glass interfaces, all the optical surfaces were 'bloomed' with anti-reflecting films; the reflecting faces of the corner cubes were aluminized to improve the overall photometric efficiency of the instrument.

§ 4. ADJUSTMENT AND AUTOMATIC OPERATION

To obtain a complete response curve, the wedge prism W must be oscillated with constant speed and the shear plates S simultaneously rotated at a constant rate through an angle of about 12° from the normal position, with the plates perpendicular to the optical axis. The former motion was derived from a reversible 1500 rev/min synchronous motor run from the 50 c/s mains supply.

Adjustment of the length of stroke was made by varying the length of the operating lever L. The rotation of the shear plates was effected by means of the lever, steel tape and drum D also shown in figure 2. Rotation of the shear plates from one side of their zero-shear position to the other side allowed a symmetrical response curve to be plotted, the two curves on either side of the zero frequency position being mirror images, with the instrument in correct adjustment. The symmetry of this curve served both as a check on the adjustment and also for accurate location of the zero frequency point. The time to plot a response curve was variable over a range from one to twelve minutes.

The mechanical systems were mounted on the bridge over the interferometer, the moving parts having only slow motions. The motor and a gear box (100 : 1) were mounted independently of the heavy frame carrying the main apparatus, the drives being made through flexible couplings. With this arrangement there was a good isolation of the interferometer and the bridge assembly from vibration. The complete interferometer and bridge assembly were enclosed in a light-tight enclosure which provided also some insulation from local thermal fluctuations and stray air currents.

When operated in the manner described above, the total light flux in the interferogram varies in accordance with expression (10) but with s changing slowly with time. The signal from the photomultipliers is amplified, passed through a simple low pass filter, transformed to a voltage signal of convenient amplitude, and fed to a pen recorder. The chart paper was driven by a synchronous motor, synchronizing with the shearing of the wave fronts. The filter serves to reduce noise, arising partly from vibrations in the interferometric unit and also in the photomultipliers. This circuit thus measures the sine-wave signal amplitude and therefore gives the modulus $T(s, \psi)$ of the frequency response, apart from a constant scale factor.

The signal from a second photomultiplier, detecting the flux in the reference channel, is amplified and fed to the phase measuring circuit, together with a tapped part of the signal from the lens under test, this latter being further amplified to equalize, approximately, the two signals. The spatial phase shift $\theta(s, \psi)$ is given by the phase difference between these two signals. The circuit used for this measurement consists of a pulsing circuit, the pulses from which trigger a flip-flop circuit. Pulses from each of the two signals generate a square wave signal of constant amplitude and frequency, the mark-to-space ratio being a measure of the time between two corresponding pulses. Consequently the phase between the two sine-wave signals is obtained by integration of this square wave, the final signal being fed directly to a pen recorder. With suitable calibration this circuit gives directly the argument of the frequency response.

With a diaphragm of 5 mm diameter placed in the entrance pupil plane, the collimated beam entering the interferometer was confined to one channel. With the shear mechanism decoupled, fine adjustments for path equilization and zero horizontal and vertical shear could be accurately and easily made using the maximum output signal on the pen recorder as the criterion. Under these conditions a 3% to 4% ripple of twice the cam period was observed, which was reduced to below 1% by adjustment to the length of stroke of the wedge prism W by the use of the variable lever L. This ripple appeared to arise from discontinuities in the a.c. signal at the turning points of the prism.

After completion of the adjustment of the interferometer in this manner, the shear mechanism was connected to the motor and a response curve plotted.

Calibration of the frequency axis was made in the first place by calculation from the measured constants of the shear plates and their mechanical drive.

§ 5. EXPERIMENTAL RESULTS FOR AXIAL IMAGES

One of the main purposes of constructing the instrument described above was the experimental study of the frequency response of lenses having known aberrations. Since it is now possible to calculate the frequency response associated with given monochromatic aberrations, such measurements afford a test of the validity of frequency response methods applied to image formation and can serve to verify the results of computations of frequency response.

An extensive series of measurements have been made on (1) an aberration-free lens in different planes of focus and (2) lenses having different amounts of primary spherical aberration viewed in different planes of focus. The first set of measurements were undertaken largely to test the experimental technique. The second set were used to make a comparison of the measured and calculated frequency response in the presence of aberrations. It will be seen that good agreement between these values was found.

5.1. *Frequency Reponse of an Aberration-free Lens*

A doublet lens of 50 cm focal length was placed near the entrance pupil plane of the interferometer and centrally with respect to a 5 mm diameter aperture, which served as entrance pupil for the interferometer and as exit pupil for the lens. For different positions of the slit object along the axis, the defect of focus w_{20} may be found from the formula

$$w_{20} = \frac{n\lambda}{\pi} = \tfrac{1}{2} n' \sin^2\alpha \{1/[1-(\delta z/F^2)(F-l')]\}\, \delta z$$

where $\sin\alpha$ is the angular aperture of the lens in the object space, δz is the axial displacement of the slit from the in focus position, and l' is the distance of the aperture from the second principal plane of the lens, which latter is of focal length F. The correction factor $(\delta z/F^2)(F-l')$ is necessary because the optical path difference used to specify the defect of focus has to be measured at the aperture stop, which implies a small change in angular aperture of the lens on defocusing. The parameter n was used by Hopkins in calculating, for integral values of n, the number of wavelengths of defocusing. The curves obtained with the particular values of n are shown in the figures 3 and 4, the points being values obtained by interpolation, with the required accuracy to $\pm 0{\cdot}01$, from Hopkins' (1955 b) calculated values.

For regions where the response $T(s) \geqslant 0{\cdot}1$, the agreement between calculated and measured values is within $\pm 0{\cdot}01$. Below this level a slightly larger discrepancy occurs, the experimental curves not falling exactly to zero. This appears to be due to the slow response of the recorder at the lower end of the scale, where it is largely determined by friction between the pen and paper.

To check the measurement of spatial phase shift, the reference beam was brought into play, and the variation of phase shift studied for a case of a defocused lens whose amplitude response had already been obtained. The phase jump of π on passing through the first zero of $D(s)$ was clearly demonstrated. A gradual drift of the curve was found, arising probably from a lack of exact parallelism between the test and reference beams. The measurement of phase shifts is not essential for the study of axial images, so that this was not pursued further. This will become important, of course, when curves for lenses having asymmetrical aberrations are investigated.

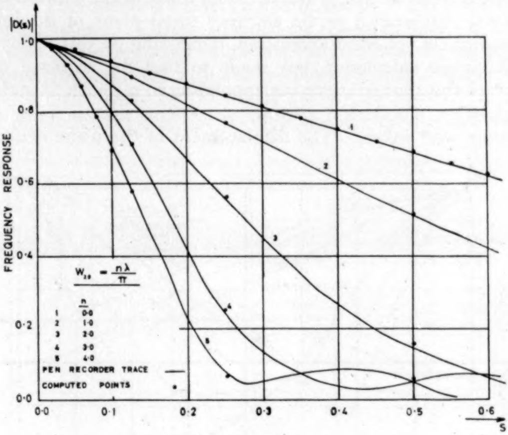

Figure 3.

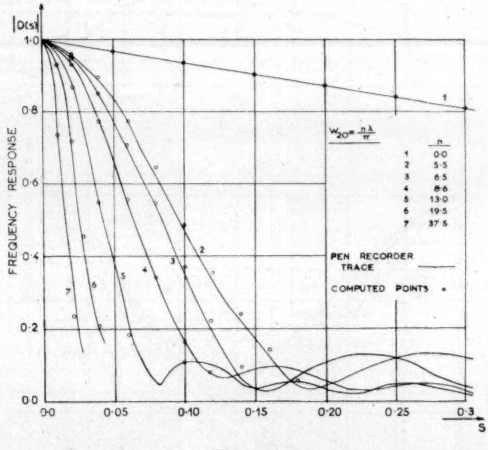

Figure 4.

Figures 3, 4. Response curves for a defocused lens with no aberration.

5.2. *Lens with Primary Spherical Aberration*

Numerical values of frequency response were available for lenses in the presence of primary spherical aberration and a direct confirmation of these results provided the next set of measurements. For this purpose a plano-convex lens, of approximately 28 mm focal length, was mounted on a focusing slide in the object space of the interferometer. A collimated light beam from an incoherently illuminated slit, of width equal to $10\,\mu$ and height 2 mm, was sent through one channel of the interferometer. The convex surface of the lens faced the slit and, by introducing diaphragms at the entrance pupil plane of the interferometer, different amounts of spherical aberration, depending on this diameter, could be studied. A simple calculation was made to find the required diameters for spherical (wave front) aberrations corresponding to $w_{40} = 2\lambda$, 3λ and 4λ.

For each value of spherical aberration, response curves for several different planes of focus were taken. The displacement of the plane of focus from the

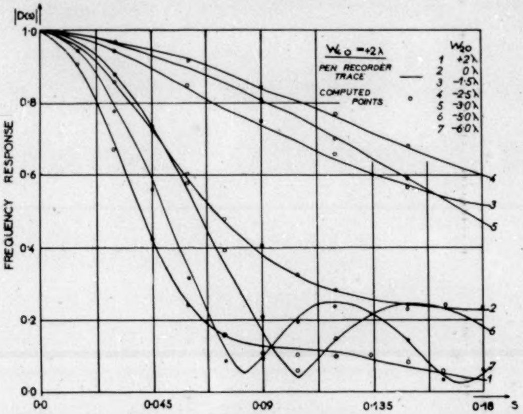

Figure 5 (*a*).

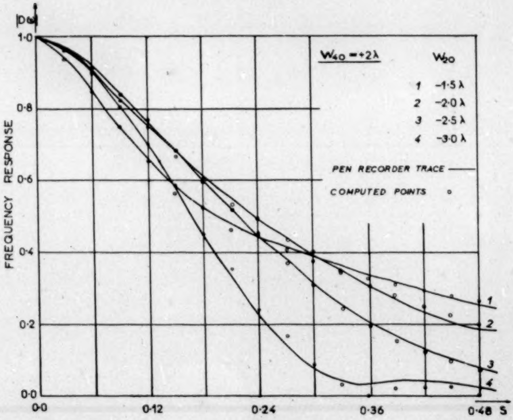

Figure 5 (*b*).

Gaussian focus was measured by means of a scale fitted to the focusing slide; values of defocusing corresponding to wavefront aberrations between $w_{20} = +2\lambda$ and -6λ were used. At different focal settings the sheared interferogram was photographed. Analysis of the fringe pattern served to calculate w_{20} and w_{40} for any given case. This afforded a direct check of the wave front aberrations for a particular response curve. Curves obtained are shown in figures 5, 6 and 7. In each case the scale of the frequency axis was calculated from the measurements on the sheared interferogram made with a micrometer eyepiece. Comparisons with points calculated numerically by Goodbody (1958) are shown. In a very few cases a small difference between the theoretical and experimental results of the

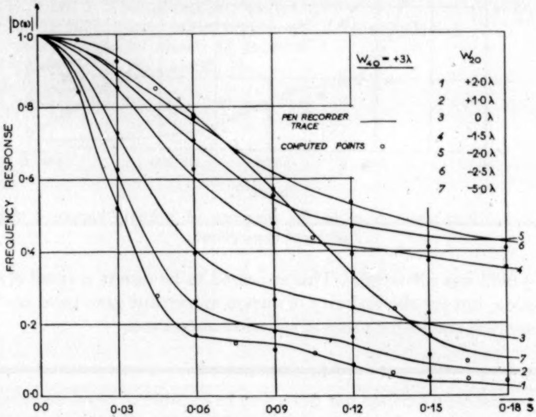

Figure 6 (*a*).

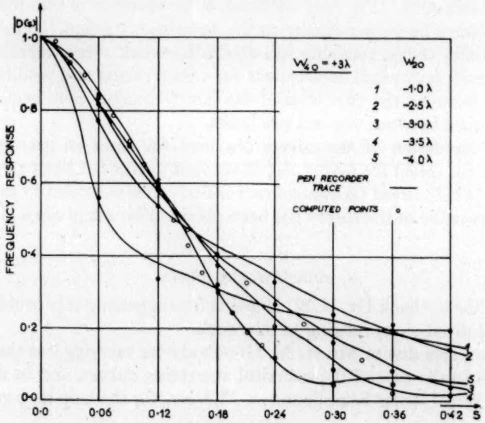

Figure 6 (*b*).

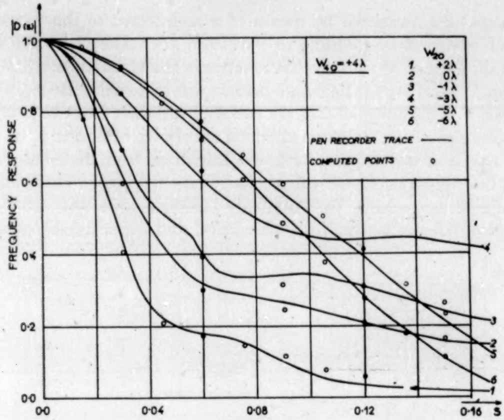

Figure 7.

Figures 5, 6, 7. Response curves in the presence of primary spherical aberration in different focal planes.

order of ±0·02 was observed. This appeared to be due to a small error in the focusing slide, but for the majority of curves agreement gave good confirmation of the theoretical results for primary spherical aberration.

§ 6. Conclusion

The instrument described has proved to be capable of rapid determination of series of response curves for a lens when monochromatic light has to be used. No additional difficulty would be presented in testing lenses at different field angles and different azimuths. The only condition to be observed is that the line source itself must always be perpendicular to the shearing direction. The instrument proved to be very stable, retaining its initial adjustment over several days. Even after a few weeks only small adjustments for vertical shear and equilization of the path lengths between the two arms of the interferometer were required. This resetting requires between one and two hours.

Detailed discussion of the curves obtained for cases of primary spherical aberration is not called for here. A full account of this has been given by Black and Linfoot (1957) based on theoretical results. It is sufficient to say that satisfactory confirmation of the theory has been obtained for many cases of axial image formation.

Acknowledgments

I should like to thank Dr. H. H. Hopkins for suggesting this problem, and for many helpful discussions relating to this work.

Thanks are also due to Mr. A. M. Goodbody for carrying out the theoretical computations in the case of the spherical aberration curves, and to the Ministry of Supply at Royal Radar Establishment, Malvern, for the help they gave with the electronics.

REFERENCES

BAKER, L. R., 1955 a, *Proc. Phys. Soc.* B, **68,** 871.

—— 1955 b, *J. Sci. Instrum.*, **32,** 418.

BLACK, G., and LINFOOT, E. H., 1957, *Proc. Roy. Soc.* A, **239,** 522.

DUFFIEUX, P. M., 1946, *L'Intégrale de Fourier et ses Applications à l'Optique* (Besançon: Published privately).

GOODBODY, A. M., 1958, *Proc. Phys. Soc.*, **72,** 411.

HOPKINS, H. H., 1953, *Proc. Roy. Soc.* A, **217,** 408.

—— 1955 a, *Optica Acta*, **2,** 23.

—— 1955 b, *Proc. Roy. Soc.* A, **231,** 91.

—— 1957 a, *Proc. Phys. Soc.* B, **70,** 1002.

—— 1957 b, *J. Opt. Soc. Amer.*, **47,** 508.

MAHAN, A. H., 1954, *J. Wash. Acad. Sci.*, **44,** 165.

MICHELSON, A. A., 1927, *Studies in Optics* (Chicago: University Press).

PECK, E. R., 1948, *J. Opt. Soc. Amer.*, **38,** 66, 1015.

WOLF, E., 1954, *Proc. Roy. Soc.* A, **225,** 96.

—— 1955, *Ibid.*, **230,** 246.

ZERNIKE, F., 1957, *J. Opt. Soc. Amer.*, **47,** 466.

On the Limiting Band Width of Interference Filters

By P. GIACOMO†‡, P. W. BAUMEISTER§ AND F. A. JENKINS§||
† Laboratoires du C.N.R.S., Bellevue (S. et O.), France
§ Department of Physics, University of California, Berkeley, California, U.S.A.

MS. received 16*th October* 1958, *in final form* 21*st November* 1958

Abstract. The effects of variations of the thickness of the individual layers of an interference filter made with dielectric multilayers are examined, with respect both to the displacement of the pass band and to its width as affected by random fluctuations in these thicknesses. It is shown that the use of special multilayer stacks having a large dispersion of the phase change on reflection can yield a much greater resolution only in the case of perfectly uniform films. The insensitivity of the pass band to variations of the spacer layer is compensated by a correspondingly large sensitivity to variations of the layers constituting the 'mirrors'. It is also shown that the effect of random thickness variations is a minimum when the sensitivities of all layers are proportional to their thicknesses. Sample calculations and experimental illustrations are given.

§ 1. INTRODUCTION

THE use of dielectric multilayers for the reflecting elements of interference filters, as described by Heavens (1955), would appear to open up the possibility of realizing band widths of a very few ångströms, or even fractions of an ångström. By merely increasing the number of layers in the quarter-wave stacks constituting the mirrors, one may obtain reflectances that would in principle yield resolutions well in excess of 1000, corresponding to a band width of 5 Å at 5000 Å. In practice, however, it is common experience that a resolution above about 500 cannot be obtained in this way. The extremely close tolerances that are required for the thicknesses of the individual layers afford one obvious reason for this limitation. Thus a variation of only 0·5% in the thickness of the half-wave spacer (9·3 Å change in the geometrical thickness of a cryolite spacer) shifts the peak of the band by 25 Å. Such a variation being of the order of atomic dimensions, it is also clear that the structure of the films may play an important part.

As was shown by Baumeister and Jenkins (1957), a promising way of overcoming this difficulty is the use of multilayers of a type that show a very rapid variation with wavelength of the phase change on reflection. Theoretically, and at first sight practically, this high phase dispersion has a marked influence in narrowing the pass band. It has also been shown (Jenkins 1958) that the wavelength of the maximum of the band (or bands) is at the same time rendered relatively insensitive to variations of the spacer thickness. Interference filters thus 'stabilized' by the phase dispersion do indeed yield narrower bands, as was shown by Baumeister, Jenkins and Jeppesen (1958). In their work, however,

---

‡ Now at Faculté des Sciences, Caen, France.

|| Fellow of the John Simon Guggenheim Foundation, now at the Clarendon Laboratory, Oxford.

no account was taken of the possible effects of variations of the thicknesses of the layers constituting the mirrors themselves. The position of the pass band depends on the thicknesses of all the layers. Any variation of these thicknesses across the surface of the filter will, if the light traverses the entire filter, have the effect of widening the band. Furthermore, even for a small area of the surface, the band width will be greater if there are deviations of the thicknesses from their prescribed values.

It will be necessary first to derive the relations between position of the pass band and the thicknesses of the various layers. These will lead to a consideration of the phase stabilization mentioned above. Afterwards, the effect of random variations of the thicknesses on the band width will be investigated and some examples and experimental verifications will be presented.

§ 2. DISPLACEMENTS OF THE PASS BAND AS A FUNCTION OF THE THICKNESSES

It will be assumed that the absorption, and the dispersion of the refractive indices, of the layers are negligible. One could take account of the latter by taking as variables the optical paths *nt* instead of the thicknesses *t*, but this would make the formulae unnecessarily cumbersome. It is also supposed, in order to simplify the expressions, that one is concerned with a symmetrical filter, such that the layers on either side of the spacer are mirror images. If the filter were unsymmetrical, it would suffice to substitute for the phase change on reflection ψ its average value for the two mirrors.

The wavelengths of the pass bands are fixed by the condition

$$\phi + 2\psi = 2k\pi, \qquad \ldots\ldots(1)$$

where k is any whole number and $\phi = -4\pi nt/\lambda = -4\pi nt\sigma$, the phase difference between two successive transmitted rays that is introduced by the spacer. If one postulates that the thicknesses of the different layers (t for the spacer, t_i for the ith layer of one of the mirrors) vary by δt and δt_i, the pass band shifts in wavenumber by $\delta\sigma$ such that

$$\frac{\partial\phi}{\partial t}\,\delta t + 2\sum_i \frac{\partial\psi}{\partial t_i}\,\delta t_i + \left(\frac{\partial\phi}{\partial\sigma} + 2\,\frac{\partial\psi}{\partial\sigma}\right)\delta\sigma \simeq 0, \qquad \ldots\ldots(2)$$

with

$$\frac{\partial\phi}{\partial t} = \frac{\phi}{t} = -\frac{2\pi p}{t}, \quad \text{and} \quad \frac{\partial\phi}{\partial\sigma} = \frac{\phi}{\sigma} = 2\pi p\lambda. \qquad \ldots\ldots(3)$$

Here p is the 'order of interference' in the spacer layer; $p = 2nt\sigma$.

The term in parentheses in equation (2) may be expressed in another form by noting that if one makes special variations δ_0 such that

$$\frac{\delta_0 t}{t} = \frac{\delta_0 t_i}{t_i},$$

one has

$$\frac{\delta_0\lambda}{\lambda} = \frac{\delta_0 t_i}{t_i} \simeq -\frac{\delta_0\sigma}{\sigma}.$$

Then $\phi = -4\pi nt/\lambda$ does not vary and relation (1) shows that ψ also remains constant. Hence

$$\frac{\partial\psi}{\partial\sigma}\,\delta_0\sigma + \sum_i \frac{\partial\psi}{\partial t_i}\,\delta_0 t_i = 0.$$

Since $\delta_0 t_i \simeq -(t_i/\sigma)\delta_0\sigma$, one finds

$$\frac{\partial\psi}{\partial\sigma} \simeq \sum_i \frac{\partial\psi}{\partial t_i}\frac{t_i}{\sigma}, \qquad \text{......} (4)$$

a result that is evidently independent of the assumption that the variations are restricted to δ_0. Equations (3) and (4) now allow equation (2) to be written in the form

$$\phi\frac{\delta t}{t} + 2\sum_i \frac{\partial\psi}{\partial t_i}\delta t_i + \left(\phi + 2\sum_i \frac{\partial\psi}{\partial t_i}t_i\right)\frac{\delta\sigma}{\sigma} \simeq 0. \qquad \text{......} (2')$$

Then, by setting $\delta t/t = \alpha$ and $\delta t_i/t_i = \alpha_i$, one obtains

$$\frac{\delta\sigma}{\sigma} \simeq -\frac{\phi\alpha + 2\sum_i \alpha_i \partial\psi/\partial\alpha_i}{\phi + 2\sum_i \partial\psi/\partial\alpha_i}. \qquad \text{......} (5)$$

From this general expression, the following conclusions may be drawn for special cases:

(*a*) If all layers vary proportionately ($\alpha = \alpha_i = \alpha_j = \alpha_0$), one has $\delta\sigma/\sigma \simeq -\alpha_0$.

(*b*) If only the spacer varies ($\alpha_i = \alpha_j = 0$, $\alpha \neq 0$), and if, in addition, the phase dispersion is large, so that

$$\left|2\frac{\partial\psi}{\partial\sigma}\right| \gg 2\pi p\lambda, \text{ or, by equation (4), } \left|2\sum_i \frac{\partial\psi}{\partial\alpha_i}\right| \gg |\phi|,$$

one has

$$\left|\frac{\delta\sigma}{\sigma}\right| \simeq \left|\frac{\phi\alpha}{2\sum_i \partial\psi/\partial\alpha_i}\right| = \left|\frac{\phi\alpha}{2\sigma\partial\psi/\partial\sigma}\right| = \left|\frac{2\pi p\lambda}{2\partial\psi/\partial\sigma}\right|\alpha \ll \alpha.$$

The insensitivity of the wavenumber to variations $\delta t = \alpha t$ of the spacer thickness is thereby verified.

(*c*) If only the layers forming the mirrors vary ($\alpha = 0$, $\alpha_i = \alpha_j = \alpha_0'$), and if the phase dispersion is still large, one finds

$$\frac{\delta\sigma}{\sigma} \simeq -\alpha_0'.$$

This is essentially the same result as was obtained in case (*a*), namely the filter retains a sensitivity with respect to the thicknesses t_i compensating for that which it lost with respect to the spacer thickness t.

(*d*) If, on the contrary, the phase dispersion is small, so that

$$\left|2\frac{\partial\psi}{\partial\sigma}\right| \ll 2\pi p\lambda,$$

one finds that the pass band is insensitive to the thickness of the component layers of the mirrors, but remains sensitive to that of the spacer.

These results may be summarized by characterizing the sensitivity to variations of the various thicknesses (t_i and t) by the quantities

$$\frac{\partial}{\partial\alpha_i}\left(\frac{\delta\sigma}{\sigma}\right) = \frac{t_i}{\sigma}\frac{\partial\sigma}{\partial t_i} = -\frac{\partial\psi/\partial\alpha_i}{\phi + 2\sum_i \partial\psi/\partial\alpha_i},$$

and

$$\frac{\partial}{\partial\alpha}\left(\frac{\delta\sigma}{\sigma}\right) = \frac{t}{\sigma}\frac{\partial\sigma}{\partial t} = -\frac{\phi}{\phi + 2\sum_i \partial\psi/\partial\alpha_i}.$$

Then *the sum of the sensitivities to the different variations of thickness is constant* and equals unity, no matter what the thickness of the spacer and the phase dispersion may be. What one gains in stabilization with respect to t one loses with respect to the thicknesses t_i of the layers forming the mirrors, and vice versa.

The necessity for this conclusion can be shown by the following dimensional considerations. Two filters are compared, one prepared for the wavelength λ and the other for the wavelength $\lambda'=\lambda+\delta\lambda$. The latter can obviously be obtained by multiplying all thicknesses of the first filter by λ'/λ. If one assumes that the two filters have a low sensitivity to the variation $\delta t=t\delta\lambda/\lambda$ in the spacer thickness, it follows that the passage from λ to λ' must be primarily due to the variations $\delta t_i=t_i\delta\lambda/\lambda$ in the thicknesses of the layers constituting the mirrors. Conversely, when the mirrors consist of 'classical' quarter-wave stacks, it is mostly due to δt, and very little to the δt_i. In any other case, there is some combination of the two effects adding up to the same total. Phase stabilization with respect to the spacer will, therefore, not improve the resolution since, given a certain lack of uniformity inherent in the method of depositing the layers, suppression of its effect through the spacer layer will merely enhance its effect through the layers comprising the mirrors. One loses in the one respect exactly what one gains in the other.

§ 3. INFLUENCE OF RANDOM VARIATIONS OF THE THICKNESSES ON THE BAND WIDTH

It has been assumed in the above examples that the relative variations α_i of the thicknesses t_i were equal. This case often occurs in practice when one is concerned with thicknesses on different parts of the surface of the filter, and an illustration of its effect will be given below. But even over a restricted area of the surface, the inaccuracies of control during the preparation of the filter will cause variations α and α_i from the desired thicknesses. If the number of operations is large, these variations may be taken as random and independent of each other. Similarly, any very localized variations of thickness within the specified area, arising from fortuitous fluctuations in the directional emission from the crucibles during evaporation, or from the structure of the films themselves, may also be considered as random and independent.

With this type of distribution of the departures α and α_i, one can only obtain statistical results based on the mean square deviations. They involve the quantities

$$\beta^2=\overline{\left(\frac{\delta\sigma}{\sigma}\right)^2},\quad a_i^2=\overline{\alpha_i^2},\quad \text{and}\quad a^2=\overline{\alpha^2}.$$

Since $\delta\sigma/\sigma$ is a sum of terms proportional to the α_i, one obtains β^2 by adding the mean squares of these terms:

$$\beta^2=\frac{\phi^2a^2+\sum_i(2\,\partial\psi/\partial\alpha_i)^2a_i^2}{(\phi+\sum_i 2\,\partial\psi/\partial\alpha_i)^2}\,. \qquad \ldots\ldots(6)$$

In order to study this expression one could set the root-mean-square relative deviations of thickness equal to each other for all layers: $a_i=a_j=a_0$. It is more correct, and hardly more complicated, to take the r.m.s. thickness variation as proportional to the thickness itself, as it would be if each layer were equivalent to a stack of elementary layers having independent fluctuations. Then one can represent the r.m.s. deviation of the thickness of the layer by

$$\epsilon_i = k\sqrt{t_i},$$

from which

$$a_i = \epsilon_i / t_i = k/\sqrt{t_i},$$

k being independent of the ordinal number i of the layer. β^2 then takes the form

$$\beta^2 = \frac{\dfrac{\phi^2}{t^2} + \sum\limits_i (2\,\partial\psi/\partial\alpha_i)^2 \dfrac{1}{t_i}}{(\phi + \sum\limits_i 2\partial\psi/\partial\alpha_i)^2}\, k^2.$$

Recalling that the factor 2 inside the summation derives from the presence of two mirrors, one can rewrite this equation as

$$\beta^2 = k^2 \sum_1^q \frac{1}{t_i} A_i^2 \Big/ \left(\sum_i^q A_i\right)^2, \qquad \ldots\ldots(7)$$

where q is now the *total* number of layers in the filter, and

$$A_i = \frac{\partial\psi}{\partial\alpha_i} \quad (\text{or } \phi).$$

From equation (7) it is seen that β^2 is a minimum when

$$\frac{1}{t_i} A_i = \frac{1}{t_j} A_j,$$

which can also be written

$$\frac{\phi}{t} = -\frac{4\pi n}{\lambda} = \frac{\partial\psi}{\partial t_i} = \frac{\partial\psi}{\partial t_j}. \qquad \ldots\ldots(8)$$

This condition, closely related to the 'sensitivities' defined above, can be simply expressed as follows: The different sensitivities should be proportional to the thicknesses of the corresponding layers. It is surprising that the condition thus obtained is independent of the order p of the spacer layer of the filter, since $\phi/t = -4\pi n\sigma$. Mirrors satisfying condition (8) will therefore be adaptable to a filter of any order whatever. This conclusion presupposes that the spacer layer is prepared by the same process as the constituent layers of the mirrors. The problem would present itself differently for a Fabry–Perot with an air layer (Giacomo 1958) or with a 'prefabricated' spacer layer of split mica (Ring, Beer and Hewison 1958).

The minimum value of β^2 is

$$\beta^2 = \frac{k^2}{\Sigma t_i} = \frac{k^2}{T} = \frac{k^2}{q t_0} = \frac{{a_0}^2}{q},$$

T being the total thickness of the filter and t_0 the mean thickness of one layer. The latter has the r.m.s. thickness variation a_0. Finally, one has the condition

$$\beta \geqslant \frac{k}{\sqrt{T}} = \frac{a_0}{\sqrt{q}}. \qquad \ldots\ldots(9)$$

The r.m.s. deviation β of the pass-band displacement $\delta\sigma/\sigma$ therefore has a lower limit, inversely proportional to $\sqrt{T}$, but independent of all other parameters.

This lower limit is achieved when the different terms ϕ/t, $\partial\psi/\partial t_i$, are equal among themselves, as required by equation (8). β can be very much larger than this lower limit, particularly when these terms have a sum near zero and at the same time rather high absolute values (with signs sometimes positive, sometimes negative).

The random variations of the pass band of an interference filter, measured by $\delta\sigma/\sigma$, have a considerable practical importance. If one permits the fluctuations of thickness, even over a localized area of the filter, to spread the band over a range $\delta\sigma$, the band can obviously not be narrower than the $\delta\sigma$ imposed by these fluctuations. One could hope to attain, for a given type of filter, a limiting resolution amounting to

$$R_0 = \frac{1}{\beta} \leqslant \frac{\sqrt{T}}{k}.$$

It is therefore of primary importance, if high resolutions are desired, on the one hand to decrease this limit β, and on the other to try to approach it as closely as possible by using mirrors that satisfy condition (8).

The lower limit of β depends only on T and k. One could consider increasing T, but the gain in $\sqrt{T}$ would be compensated by the increasing difficulties of preparation. To decrease k is the other possibility, generally considered as evident since one always strives to obtain layers of as accurate thickness as possible, and $k = \overline{\delta t_i}/\sqrt{t_i}$.

The problem of satisfying equation (8) is one of choosing the design of the mirrors in such a way that the various $\partial\psi/\partial t_i$ shall be as nearly as possible equal among themselves and equal to $4\pi n\sigma$. In filters of the classical type ($\lambda/4$ layers of alternately high and low indices) this condition is far from being realized, since the layers furthest from the spacer have practically no influence on the phase shift (Giacomo 1956). The behaviour, as far as relation (9) is concerned, is just as though these layers did not exist. This circumstance probably furnishes the explanation of the fact already mentioned that attempts to augment the resolution of this type of filter by increasing the number of layers in the mirrors have proved fruitless. One merely loses rapidly in transmittance with no appreciable gain in resolution. The reason will be apparent from the numerical example given in the following section.

The filters based on high phase dispersion come somewhat closer to the requirement of equation (8) but still fall far short of the ideal, as will be seen from the numerical results. The fact that the resolutions actually obtained are appreciably better than for classical filters cannot, as was shown above, be a direct consequence of the large value of $\partial\psi/\partial\sigma$. Indirectly, however, this has an influence, since if equation (8) is fulfilled it is necessary, in order to achieve high resolutions, not only to use a large number q of layers (thus increasing T) but also to have values of $\partial\psi/\partial\sigma$ which increase with the thickness of the filter. Applying condition (8) to equation (4) one finds

$$\left|\sigma\frac{\partial\psi}{\partial\sigma}\right| = \left|\sum_i t_i\frac{\partial\psi}{\partial t_i}\right| = \frac{4\pi n T_{\mathrm{m}}}{\lambda},$$

where T_{m} is the thickness of one of the mirrors. Hence the desired condition is

$$\left|\frac{\partial\psi}{\partial\sigma}\right| = 4\pi n T_{\mathrm{m}}.$$

The 'broad-band' multilayer mirror calculated by Baumeister and Stone (1956) comes close to fulfilling this relation. It has a total geometrical thickness of $1{\cdot}20\,\mu$. When two of these are incorporated in a filter with a cryolite spacer of index 1·35, one should therefore have $|\partial\psi/\partial\sigma| = 20{\cdot}4\,\mu$. The computed phase dispersions for the actual multilayer, in regions of the spectrum where they are large, vary between 10 and $23\,\mu$. For a classical multilayer of comparable reflectance, the phase dispersion is only $1{\cdot}7\,\mu$. This necessary condition is, therefore, approximately fulfilled for the broad-band multilayer, but it is not a sufficient one since equation (8) must also be obeyed. The extent to which this is true will be shown below.

§ 4. EXPERIMENTAL EXAMPLES

The measured width at half-maximum of the pass band of a 19-layer classical filter prepared by Dr. J. M. Stone at Berkeley was 15·4 Å. Since the peak wavelength was 5100 Å, this figure yields a resolution of 330.† Several filters consisting of two 15-layer broad-band films separated by cryolite spacers of various thicknesses have subsequently been prepared by similar techniques and the widths of some of the narrowest bands measured. In the earlier measurements (Baumeister and Jenkins 1957) the filter was placed before the slit of a 21-foot concave grating in the Paschen mounting, and the band widths determined by photographic photometry. The results indicated minimum widths of 12 Å corresponding to a resolution of 490 at 5900 Å. Although showing some improvement over the classical filter, this result is still below the theoretical value of 770 calculated from the measured reflectance of 0·978 of one of the films and the computed phase dispersion of $10{\cdot}1\,\mu$.

The origin of this discrepancy appeared when, in order to observe the transmission of localized portions of the phase-dispersion filter, it was placed in the spectrum directly in front of the plate-holder, instead of in front of the spectrograph slit. Under these conditions, the transmission took the form of a ring, a photograph of which is shown in figure 1. The circle expanded and became narrower as the filter was moved towards shorter wavelengths. Furthermore, its centre was displaced 4·9 mm (6·7 Å) toward shorter wavelengths from the geometrical centre of the filter. The width of the ring, when it was of the size shown in the illustration, was measured as 3·0 Å, and its peak transmission, 71% (Baumeister, Jenkins and Jeppeson 1958). With the classical filters, also, a ring showing the same general characteristics, but considerably more diffuse, was observed in this manner.

The cause of this circular symmetry lies in the fact that the filters, which were placed 20 inches above the crucibles, were continuously rotated during deposition of the films. The variation in film thickness from centre to edge clearly has a greater influence on the pass-band than does the variation of wavelength. To evaluate the former, it was observed that a displacement of the filter by 31 mm caused the ring to expand from the condition where it was a spot of maximum intensity near the centre of the filter to that where it was a narrow circle tangent to the upper and lower edges of the filter. Assuming that the thickness of all layers varies in the same proportion, this displacement corresponds to $\delta\sigma/\sigma = \delta t/t = 0{\cdot}0073$ from centre to edge of the filter.

---

† Although classical filters with a resolution higher than this have undoubtedly been produced, this filter will be best for purposes of comparison with other filters of different types that were prepared by the same technique.

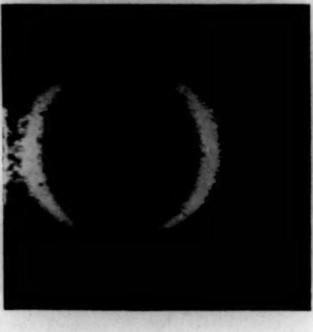

Figure 1. Transmission of filter when placed in the spectrum. The black square represents the entire area of the filter, of side 46 mm.

In order to verify quantitatively this interpretation of the ring, data on the $\partial\psi/\partial t_i$ and the sensitivities were needed. These were computed by the standard methods, using an IBM model 650 calculator. To illustrate the results, the table shows those obtained at $\sigma = 17\,000$ K for a 15-layer broad-band film, and at $\sigma = 20\,000$ K for a 15-layer classical film tuned at the latter frequency. The substrate, the medium from which the light is incident on the stack, and the refractive indices of corresponding layers, are the same in the two cases.

	Broad-band film				Classical film		
(1)	(2)	(3)	(4)	(5)	(2)	(4)	(5)
Substrate	—	1·52	—	—	—	—	—
1	0·0751	2·30	0·32	0·024	0·0543	0·01	0·001
2	0·1279	1·35	0·60	0·076	0·0926	0·02	0·002
3	0·0751	2·30	1·97	0·148	0·0543	0·05	0·003
4	0·1235	1·35	1·85	0·229	0·0926	0·06	0·005
5	0·0626	2·30	4·75	0·298	0·0543	0·16	0·009
6	0·1299	1·35	4·60	0·597	0·0926	0·16	0·015
7	0·0681	2·30	11·68	0·795	0·0543	0·48	0·026
8	0·0957	1·35	10·63	1·018	0·0926	0·48	0·044
9	0·0566	2·30	30·85	1·746	0·0543	1·39	0·075
10	0·0859	1·35	30·37	2·608	0·0926	1·39	0·128
11	0·0504	2·30	78·33	3·948	0·0543	4·03	0·219
12	0·0805	1·35	62·33	5·019	0·0926	4·03	0·373
13	0·0450	2·30	121·58	5·471	0·0543	11·69	0·635
14	0·0767	1·35	65·41	5·015	0·0926	11·69	1·082
15	0·0450	2·30	81·59	3·672	0·0543	33·92	1·843
Medium of incidence	—	1·35	—	—	—	—	—
$\sum$	1·1978	—	506·8	30·662	1·0829	69·53	4·460

(1) Layer number; (2) thickness $t_i(\mu)$; (3) index n; (4) $\delta\psi/\delta t_i$ (μ^{-1}); (5) $\delta\psi/\delta\alpha_i$.

Using the figures of the table, calculation yielded a displacement of the centre of the ring, which depends on the ratio of $\partial\psi/\partial\sigma$ to $\sum A_i$, of 4·7 mm, in good agreement with the observed value. The narrowing of the ring with increasing size could also be explained. In order to measure the band width for uniform layers, measurements were made with the filter before the slit of the spectrograph, but with a diaphragm exposing a circular area 3 mm in diameter at the centre of the filter. The measured width was then 9·5 Å, corresponding to a resolution of 620 as compared to the computed value of 770.

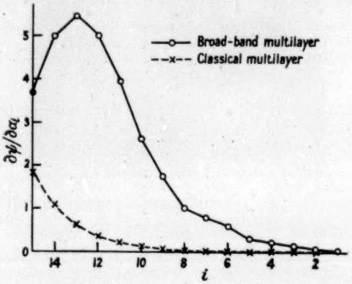

Figure 2. Sensitivities of the layers in two types of multilayer.

The remaining discrepancy must be attributed to the random errors of thickness and these may also be treated with the aid of the data of the table. The quantities $A_i = t_i\partial\psi/\partial t_i = \partial\psi/\partial\alpha_i$ given in the last column of each half of the table were used to compute the ratio between β and k by equation (7). The classical 31-layer filter gave $\beta = 1{\cdot}289k$, whereas the phase-dispersion filter gave $\beta = 1{\cdot}023\,k$. Here k has units $\mu^{1/2}$. These two figures are to be compared with the value $0{\cdot}652\,k$ given by equation (9) for a filter of total thickness $2{\cdot}35\,\mu$ which satisfies the condition (8) for minimum β. Two conclusions may be drawn from these results. The first is that while the phase-dispersion filter has some advantage over the classical one (since the limiting resolution equals $1/\beta$ and k measures the accuracy of the layer thicknesses) the gain is relatively slight. Figure 2, which shows plots of the sensitivities against layer number for the two types of multilayer, indicates that while values of A_i/t_i may be somewhat more nearly equal for the broad-band type, there is a rapid fall-off in both types for the deeper layers.

The second conclusion is that if a value of $\beta = 1/500$ is regarded as the practical limit for a classical filter, the errors involved in the preparation of the films must be about $1/1{\cdot}29\sqrt{t_i}$ of this figure, or 0·57%. It may well be that irregularities in the structure of the films may cause local variations of thickness of this magnitude, and there is evidence for such variations in the granulations visible in figure 1.

Whether any conceivable design of filter might come close to fulfilling condition (8) for the minimum β has not yet been determined. It seems certain that no arrangement of the refractive indices in a $\lambda/4$ stack will accomplish it, since one can show that regardless of the indices of the layers, the value of $\partial\psi/\partial t_i$ of the layer nearest the incident light asymptotically approaches $4\pi n_0/\lambda$, where

n_0 is the index of the medium from which the light is incident. The sensitivity of the last layer approaches zero, also irrespective of the indices of the layers. Variations of the thicknesses, on the other hand, can effect at least some improvement, as is shown by the results on the broad-band multilayer presented here.

ACKNOWLEDGMENT

The authors are indebted to the National Science Foundation for the award of a grant-in-aid in partial support of these investigations.

REFERENCES

BAUMEISTER, P. W., and JENKINS, F. A., 1957, *J. Opt. Soc. Amer.*, **47**, 57.

BAUMEISTER, P. W., JENKINS, F. A., and JEPPESEN, M. A., 1958, *Abstract* TA12, *Opt. Soc. Amer.*, Meeting of March, 1958.

BAUMEISTER, P. W., and STONE, J. M., 1956, *J. Opt. Soc. Amer.*, **46**, 228.

GIACOMO, P., 1956, *Rev. Opt.* (*theor. instrum.*), **35**, 317, 442.

—— 1958, *J. Phys. Radium*, **19**, 307.

HEAVENS, O. S., 1955, *Optical Properties of Thin Solid Films* (New York: Academic Press).

JENKINS, F. A., 1958, *J. Phys. Radium*, **19**, 301.

RING, J., BEER, R., and HEWISON, V., 1958, *J. Phys. Radium*, **19**, 321.

Properties of Solid and Liquid Solutions of Argon and Krypton

By R. HEASTIE

Department of Physics, Queen Mary College, London

Communicated by G. O. Jones ; MS. received 15th August 1958, in final form 4th November 1958

Abstract. The vapour pressure P of solid and liquid mixtures of argon and krypton of a number of different compositions has been measured over a temperature (T) range which includes the 'melting' and 'freezing' points of the mixtures. The solid–liquid phase-equilibrium diagram has been deduced by observation of discontinuities in slope of ($\log P$, $1/T$) graphs. The measurements show that argon and krypton are completely soluble in the liquid and solid states and that the solid solutions exhibit a positive deviation from ideality.

The solid solution data are compared with theory. Although the experimental results are not in complete agreement with any of the theories considered, the cell theory predicts approximately the observed magnitude of the deviations from ideality of the vapour pressure.

---

§ 1. INTRODUCTION

IN the last forty years, extensive experimental investigations of the properties of many types of solution have been made. The development of a theory of solutions is difficult but the problem is simplified by limiting consideration to solutions of components whose molecules (*a*) exhibit non-directional interaction forces, (*b*) have internal motions which are independent of the nature of their neighbours, (*c*) are of equal 'size'.

The first two requirements are satisfied by the molecules of the rare gases. While (*c*) cannot be exactly satisfied in this case, the difference between the molecular diameters may be as small as 7% (as in the case of A–Kr). It appears, therefore, that measurements of the properties of a binary solution of rare gases would serve as a useful test of the various solution theories. The choice of the particular rare gases used in the investigation described here was made because of the small difference in the molecular sizes and for experimental reasons.

§ 2. THE USE OF VAPOUR PRESSURE MEASUREMENTS

At the beginning of this investigation only one set of measurements of the properties of solid and liquid solutions of argon and krypton had been reported—the determination of the solid–liquid phase-equilibrium diagram (Veith and Schröder 1937). It was thought desirable, as a preliminary step, to redetermine this diagram. Because of the simplicity of the thermal analysis method employed by Veith and Schröder, it was decided to use this same method. An apparatus similar to that described in § 3 was constructed and heating curves were plotted for condensed mixtures of eight different compositions. These experiments were not satisfactory because of the lack of 'sharpness' of the freezing and melting points as shown by the temperature–time graphs and for the reasons given below an alternative method was adopted.

Thermal analysis, while being a convenient method of determining phase-equilibrium diagrams, yields no additional information concerning the solutions, as may other methods. The measurement of total vapour pressure P is one of the common methods of investigating the properties of a solution. In principle, if P is known as a function of the composition of the solution and the temperature, the chemical potentials of both components may be evaluated. If the measurements of the vapour pressure of a solid solution extend into the heterogeneous region and are continued until the mixture is entirely liquid, the phase transition points may be determined from observations of discontinuities in the slope of the (vapour pressure, temperature) curve. This method, which has been adopted in this investigation, has certain advantages (Heastie 1956) over others.

The vapour pressure measurements have been extended over a wider pressure range than is necessary solely to determine the phase–equilibrium diagram in order to obtain additional information about the solid solutions.

§ 3. EXPERIMENTAL APPARATUS AND METHOD

3.1. *General Description of the Apparatus and Method*

The apparatus used is shown diagrammatically in figure 1. The argon and krypton were obtained commercially in glass cylinders and attached to the apparatus with cone and socket junctions C. The two gases were mixed in the glass vessels (V_1, V_2 and V_3) of known volume. The Bourdon gauge, B (range 0–1 atm and accuracy to 1 mm of mercury) was used in the measurement of the composition of the gas mixtures (§ 3.3).

At the beginning of an experiment the cryostat D was evacuated by means of a diffusion pump and surrounded by liquid oxygen. The container F was filled with liquid oxygen through the tube E, which was then closed. This liquid oxygen was pumped off, cooling F and the attached calorimeter G to a temperature of about 60 °K. The valve S was opened and the gas mixture, passing through the heated tube K, condensed as solid into the calorimeter. The amount of gas mixture left uncondensed was in no case greater than $\frac{1}{3}\%$ of the total amount. S was closed and F was heated to boil away any remaining liquid oxygen.

When F was empty, the calorimeter was allowed to warm at a rate controlled by electrical heaters on the tube K and the radiation shield H. The maximum rate of heating was 4° per hour. The temperature of the calorimeter was measured at intervals of about $\frac{1}{2}$ °K with a thermocouple. At the instant of recording the temperature, the vapour pressure of the mixture was measured with the mercury manometer M_2, the bellows manometer M_1 being used as a null indicator. At the conclusion of the experiment, the valve S was opened, allowing the mixture to re-enter the vessel V_3.

3.2. *The Cryostat*

The low temperature apparatus was contained in the outer brass case D which was sealed to the brass plate forming the top with Woods metal. Figure 2 shows the radiation shield H and copper calorimeter G and cooling pot F. In order to present a large cooling surface to the condensing gas, the double helix of copper wire was placed inside the calorimeter. To prevent condensation of the gas mixture at the point of entry into the calorimeter, the special construction shown in figure 2 was used. The German silver tube K′ was joined to a thick-walled copper tube L which passed through the German silver tube N. While the gas was being condensed, the top of L was heated. Because of the difference in the thermal conductivities of N and L it was possible to raise the temperature of the top of L 50° above that of the calorimeter.

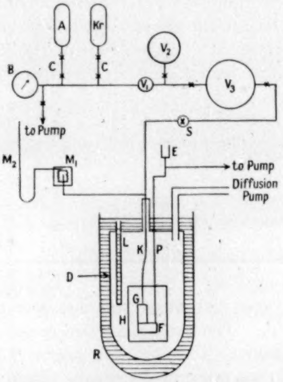

Figure 1. The apparatus. B Bourdon gauge, C ground glass joints, F cooling pot, G calorimeter, H radiation shield, M_2 mercury manometer, M_1 pressure nullpoint indicator, N radiation shield, R Dewar flask containing liquid oxygen.

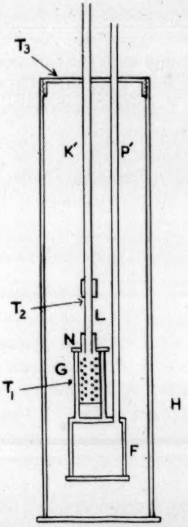

Figure 2. The radiation shield and calorimeter.

3.3. *The Determination of Gas Composition*

The method employed for the determination of the composition of the gas mixtures was devised to use the minimum amounts of argon and krypton. Because the krypton obtained for the first experiments contained 1% xenon, it was decided that an accuracy to ½–1% in the mole fractions of krypton in the mixtures would suffice.

The volumes of the vessels V_2 ($V_2 = 314\,\mathrm{cm}^3$) and V_3 ($V_3 = 1151\,\mathrm{cm}^3$) were determined, previous to attachment to the apparatus, by weighing them, first empty and then filled with water. V_1 ($80\,\mathrm{cm}^3$) represents the volume contained by the Bourdon gauge B and the tubes joining the various taps. The volume V_1 was determined by a method involving the repeated sharing of dry air between it and the known volumes V_2 and V_3, the pressures being measured by means of B.

In preparing the gas mixtures an amount (n moles) of argon (approximately $300\,\mathrm{cm}^3$ of gas at S.T.P.) was diluted successively with increasing amounts of krypton. From the amounts of the gases mixed, determined from the known volumes, V_1, V_2 and V_3 and the pressures recorded by the Bourdon gauge, the mole fraction X of krypton of each mixture was calculated. When X was slightly greater than 0·5, the mixture was discarded and a second series of experiments was started. In this case n moles of krypton was diluted successively with argon in stages until X was just less than 0·5. The overlap of the two sets of experiments provided a useful check on the experimental error in the *gas* composition measurements, which is estimated to be not greater than 1% in either X or $1-X$.

3.4. *Measurement of Temperature*

The temperature of the calorimeter was measured with a copper–constantan thermocouple. This was calibrated at the sublimation point of carbon dioxide and the boiling point of oxygen, the method of Scott (1947) and the data of Southard and Andrews (1929) being used for interpolation. Below 90°K the thermocouple was calibrated by measurement of the vapour pressure of argon and use of the vapour pressure equation (Clarke *et al.* 1951).

The measured triple point temperatures of argon and krypton are compared in table 1 with the latest determinations of other workers.

Table 1. Triple Point Data

Argon	T(°K)	83·8	83·78†
	P(cm Hg)	$51{\cdot}5_8$	51·57†
Krypton	T(°K)	115·8	115·94 ± 0·03‡
	P(cm Hg)	$54{\cdot}5_0$	54·9 ± 0·15‡

† Clarke *et al.* (1951). ‡ Keesom, Mazur and Meihuizen (1935).

3.5. *Measurement of Vapour Pressure*

The vapour pressure of the condensed mixtures was measured with the mercury manometer M_2 and the bellows manometer M_1. The essential requirement was that the amount of the gas mixture in the manometer should be small (see § 5.2). It was for this reason that M_1 was used. M_1 contained a standard Hydroflex bellows, made of brass of thickness 0·004 in. To reduce the volume available to the gas mixture, a brass cylinder was fixed inside the bellows. M_1 was used as a null indicator to balance the pressure (measured with M_2) of dry air outside the bellows against that of the gas mixture inside. Movements of the bellows were detected by an optical lever.

Vapour pressure measurements were normally made while the temperature of the calorimeter was increasing. The pressure difference between M_1 and the calorimeter due to the flow of gas through the tube K (figure 1) was estimated to be less than 0·1 mm of mercury. The absolute accuracy of the vapour pressure measurements is estimated to be to $\frac{1}{2}$ mm of mercury. The triple point pressures of argon and krypton measured independently of the thermocouple calibration are compared with previously reported values in table 1. The disagreement in both transition temperature and pressure in the case of krypton could be accounted for by the presence of $\frac{1}{2}$% xenon in the krypton finally used.

§ 4. RESULTS

The vapour pressure of mixtures of 20 different values of mole fraction of krypton was measured over a range of temperature. In figure 3 a typical (log P,

$1/T$) graph, BCDE, is shown for a mixture of composition X, where $X = 0·75$. M and N are the triple points of argon and krypton respectively. The phases present in the mixture are: along BC, solid and vapour; along CD, solid, liquid and vapour and along DE, liquid and vapour.

The three-phase portions, DC for all mixtures were plotted and a smooth curve, MCDN was drawn through the points. In the temperature range 86·6°–109·4° K this curve was particularly well defined because of the overlap of points recorded for mixtures of different values of X. Within this range the data were smoothed by the method of using an auxiliary function. The data for the three-phase curve are given in table 2.

Table 2. Three-phase Pressure Data

T(°K)	P(cm Hg)	T(°K)	P(cm Hg)
83·80	51·58	94·11	89·90
83·86	50·40	94·91	93·88
83·92	50·06	95·71	97·92
83·98	49·99	96·51	101·87
84·04	49·92	97·30	105·68
84·10	49·88	98·08	109·24
84·16	49·86	98·86	112·40
84·21	49·86	99·63	115·23
84·27	49·88	100·41	117·96
84·33	49·91	101·18	120·61
84·39	49·96	101·95	123·09
84·45	50·01	102·71	125·13
84·50	50·08	103·47	126·68
84·56	50·17	104·23	127·78
84·62	50·25	104·98	128·52
84·74	50·47	105·73	128·80
84·85	50·71	106·47	128·24
84·97	51·01	107·22	127·08
85·08	51·31	107·95	125·66
85·20	51·62	108·69	123·71
85·49	52·50	109·42	120·84
85·78	53·38	110·14	117·18
86·64	56·32	110·87	112·35
87·49	59·67	111·59	106·95
88·34	63·11	112·31	100·28
89·18	66·64	113·02	93·28
90·01	70·35	113·73	85·10
90·84	74·20	114·44	75·80
91·66	78·12	115·15	65·15
92·48	82·04	115·80	54·50
93·30	85·96		

Of the 20 experiments performed, only one (for $X = 0·053$) yielded any points near the minimum of the curve MCDN in figure 3. Because of the obvious interest of this minimum a separate set of experiments was carried out. The vapour pressure of dilute solutions of krypton in argon of four different values of X was measured. The results of these experiments are incorporated in table 2.

The (log P, $1/T$) graphs for solid solutions (BC on figure 3) were approximately straight lines while those for the liquid solutions, DE, had a slight curvature, as do those for the two components. The phase transition points C and D were determined (Heastie 1956) by extrapolation of BC and DE to meet MCDN. The phase transition temperatures are recorded in table 3.

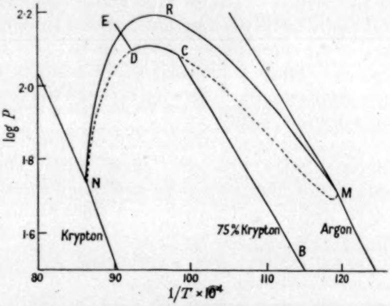

Figure 3. (log P, $1/T$) graphs for argon, krypton and a mixture containing 75% krypton in molar proportions. M and N are the triple points of argon and krypton. MCDN is the measured three-phase curve; MREN is the three-phase curve calculated on the assumption that both solid and liquid solutions are ideal.

Table 3. Phase-equilibrium Diagram Data

X	T_1(°K)	T_2(°K)	X	T_1(°K)	T_2(°K)
0·0	83·8	83·8	0·523	98·0	90·2
0·053	84·0	83·9	0·546	99·0	90·3
0·106	84·5	84·2	0·598	101·5	92·7
0·148	85·0	84·5	0·646	103·8	95·0
0·183	85·8	84·8	0·698	106·0	97·9
0·252	87·8	85·6	0·748	108·2	100·8
0·299	89·1	86·0	0·800	110·2	104·8
0·351	90·9	86·8	0·853	112·0	108·7
0·407	93·1	87·6	0·896	113·3	111·7
0·456	95·1	87·9	0·950	114·8	—
0·502	—	89·2	1·000	115·8	115·8

X = mole fraction of krypton, T_1 = 'freezing point' temperature, T_2 = 'melting point' temperature.

§ 5. DISCUSSION OF RESULTS

5.1. *The Three-phase Equilibrium Data*

The solid–liquid phase equilibrium diagram of argon and krypton may be drawn using the data in table 3. This diagram will differ from the usual (T, x) phase equilibrium diagram. In a 'normal' (T, x) diagram the solidus and liquidus are the loci of the melting and freezing points of the mixtures, of different compositions, measured at a common pressure (very often 1 atm). Table 3 contains the 'melting' and 'freezing' points of the mixtures, each one having been measured at the equilibrium pressure of the solution corresponding to that temperature. (The value of the pressure at any one of these phase transition points may be obtained directly from the curve MCDN in figure 3 or by interpolation of table 2.) The difference between the two types of phase equilibrium diagram may be seen by considering their derivations from the three-dimensional (P, T, x) figure of the system. The normal phase equilibrium diagram is an isobaric *section* of this figure while the diagram deduced from the present results is the *projection* of part of the three-phase surface in the (P, T, x) figure on to a constant pressure plane. Since condensed phase-transition temperatures are insensitive to pressure variations, the difference between the two-phase equilibrium diagrams for any one system is slight.

The condensed phase equilibrium diagram drawn from the data in table 3 has been compared (Heastie 1955) with the 'ideal' phase equilibrium diagram, calculated on the assumption that both solid and liquid solutions are ideal (Seltz 1934). The measured solidus and liquidus are continuous and show no discontinuities in slope, showing that argon and krypton are soluble in the solid and liquid states in all concentrations. For krypton-rich mixtures, the solidus and liquidus approximate to those of the ideal solutions. For other values of composition the mole fraction of krypton in both the solid and liquid solutions in equilibrium exceed those in the ideal solutions at the same temperature. The shape of the phase equilibrium diagram suggests that argon and krypton will be insoluble in the solid state at low temperatures. The vapour pressure measurements have extended down to about 65 °K and no discontinuities in the slopes of the $(\log P, 1/T)$ graphs at a temperature lower than that of the solidus have been observed.

In figure 3 is shown the three-phase $(\log P, 1/T)$ curve MRN that would result if both solid and liquid solutions were ideal. Comparison of this curve with the measured curve MCDN indicates, as in the case of the phase equilibrium diagram, deviations from ideality with the two curves approaching one another at high concentrations of krypton.

5.2. *Experimental Accuracy*

An estimate of the experimental error in the mole fractions of krypton X and argon $1-X$ in the gas mixtures has been made in § 3.3. In the determination of the phase equilibrium diagram and in the calculations described in § 5.3, it has been assumed that in two-phase mixtures the mole fractions of krypton in the liquid $(x_2^{(2)})$ or solid $(x_2^{(3)})$ phases were equal to X. Owing to the presence in the calorimeter and manometer of a small amount of vapour of composition $x_2^{(1)}$, this assumption cannot be true.

The 'system' composition X of a phase mixture may be defined by the equation

$$X = \frac{1}{N} \sum_i N_2^i \qquad \ldots\ldots (1)$$

where the system of N moles contains N_2^i moles of krypton in the ith phase. If N moles of a gas mixture of system composition X are completely transferred to a vessel to form a phase mixture of solid solution of composition $x_2^{(3)}$ and vapour (assumed to behave as an ideal gas) of composition $x_2^{(1)}$ at a pressure P and temperature T, it may be shown that

$$(x_2^{(3)} - x_2^{(1)})/(x_2^{(3)} - X) = N\boldsymbol{R}T/PV \qquad \ldots\ldots (2)$$

where V is the volume of the vapour and $\boldsymbol{R}$ is the universal gas constant per mole. In making the assumption that the composition of the solid solution is X (and not $x_2^{(3)}$) an error $\delta x_2^{(3)}$ is introduced where

$$\delta x_2^{(3)} = (x_2^{(3)} - X) = \frac{1}{1 - (N\boldsymbol{RT}/PV)}(x_2^{(1)} - X). \qquad \ldots\ldots(3)$$

From a consideration of the shape of the phase boundary surfaces on the (P, T, x) phase equilibrium figure it may be shown that $\delta x_2^{(3)}$ is always positive. Similar considerations apply to the corresponding error in composition ($\delta x_2^{(2)}$) in the case of a liquid–vapour phase mixture.

In order to obtain an estimate of the magnitude of $\delta x_2^{(2)}$ and $\delta x_2^{(3)}$ at the phase transition points, it has been assumed that $x_2^{(1)}$ is the equilibrium value of the vapour composition and that $(x_2^{(1)} - x_2^{(2)}) = (x_2^{(2)} - x_2^{(3)})$, i.e. that the two 'loops' of the complete three-phase equilibrium diagram are of equal width. Making allowance for the fact that part of the vapour is contained in the manometer at room temperature, the values of the errors in composition at the phase transition points have been calculated using equation (3). The greatest value of the correction to the composition of the condensed solutions has a magnitude of about 1% and occurs for solid solutions of composition of $X \simeq 0{\cdot}75$.

In the above calculation it has been assumed that the values of the vapour compositions in the calorimeter G and manometer M_1 are equal. Since G and M_1 were connected by a narrow tube, inhibiting the free mixing of the gas, this would in fact not be the case. Without a knowledge of the dependence of $x_2^{(1)}$ on pressure and temperature the required correction, which would have the effect of increasing $\delta x_2^{(2)}$ and $\delta x_2^{(3)}$, cannot be made. Since, however, the amount of gas evaporating from the condensed solution is small at low temperatures, the effect of the virtual isolation of the manometer from the calorimeter may reasonably be expected to be small.

5.3. *The Solid Solutions*

From the vapour pressure data obtained in this investigation, the chemical potentials of both components in the solid solutions may, in principle, be evaluated. It is considered that the accuracy of measurement is not sufficient to make this calculation (involving the interpolation of experimental results and the numerical integration of the Gibbs–Duhem equation) worth while. For this reason an alternative method of comparing the results with theory has been adopted. The comparison has been made for the solid solutions only, because (*a*) the temperature range over which the measurements of the vapour pressure of the liquid solutions extend is small and (*b*) the systematic error in the determination of composition discussed in § 5.2 is greater than in the case of the solid solutions.

The theories with which the solid solution vapour pressure measurements may be compared are (1) the strictly regular solution theory (Guggenheim 1952) (2) the cell theory (Prigogine 1957) and (3) the conformal solution theory (Longuet-Higgins 1951). Restricting consideration, in cases (1) and (2) to 'random mixing', i.e. the zeroth approximation† (Guggenheim 1952) and in case (2) to equal sized molecules whose interaction forces are dispersive, it may be shown that in all three cases the excess free energy (G^{E}) per mole of solution can be written:

---

† A calculation of σ (see equation (4)) has been made using the first order approximation. The values of σ obtained are sensibly the same as those given by equation (5).

$$G^{\mathrm{E}} = \sigma x_1^{(3)} x_2^{(3)} \qquad \ldots\ldots (4)$$

where $x_1^{(3)}$ and $x_2^{(3)}$ are the mole fractions of the components in the solution and σ is a parameter which is independent of $x_1^{(3)}$ and $x_2^{(3)}$. Allowance for the imperfection of the vapour in equilibrium with the solid solution may be made by writing the equation of state (Guggenheim 1952) of a mole of gaseous mixture occupying a volume V_{m} at a pressure P in the form

$$PV_{\mathrm{m}} = \boldsymbol{R}T + \frac{\boldsymbol{R}T}{V_{\mathrm{m}}}\left[(x_1^{(1)})^2 B_{11} + 2x_1^{(1)} x_2^{(1)} B_{12} + (x_2^{(1)})^2 B_{22}\right].$$

$x_1^{(1)}$ and $x_2^{(1)}$ are the mole fractions of the two components and B_{11} and B_{22} are the second virial coefficients of components 1 and 2 respectively. It may be shown that the vapour pressure P of a solid solution with excess Gibbs free energy given by equation (4) is

$$P = x_1^{(3)} p_1^0 \exp\left[\frac{(P-p_1^0)(V_1^{(3)} - B_{11}) + \sigma(x_2^{(3)})^2 - \delta(x_2^{(1)})^2 P}{\boldsymbol{R}T}\right] + x_2^{(3)} p_2^0 \exp\left[\frac{(P-p_2^0)(V_2^{(3)} - B_{22}) + \sigma(x_1^{(3)})^2 - \delta(x_1^{(1)})^2 P}{\boldsymbol{R}T}\right] \qquad \ldots\ldots (5)$$

where p_1^0 and p_2^0 are the vapour pressures and $V_1^{(3)}$ and $V_2^{(3)}$ are the molar volumes in the solid state of the components 1 and 2 at temperature T and

$$\delta = (2B_{12} - B_{11} - B_{22}).$$

Using the measured values of the vapour pressure of the solid solutions and data for argon (Clarke *et al.* 1951) and krypton (Keesom *et al.* 1935), equation (5) has been solved for σ. Because the values of $x_1^{(1)}$ and $x_2^{(1)}$ are unknown it has been assumed, as is common, that $\delta = 0$. The results show that, as is usual with liquid solutions, σ decreases with increasing temperature. Of greater theoretical interest is the variation of σ with composition at constant temperature. In figure 4 the values of σ calculated at 82·9°K are plotted against the mole fraction of krypton. In this figure (and in figure 5) the experimental uncertainty in the calculated quantity is represented by the length of the vertical line. This uncertainty has been calculated assuming random errors of the following magnitudes: vapour pressure, ±0·05 cm of mercury; temperature, ±0·03° (corresponding

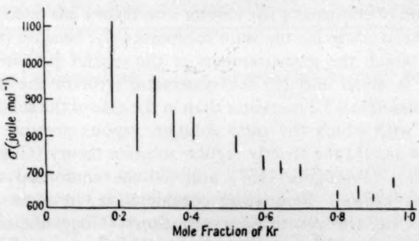

Figure 4. The variation of the parameter σ (eqn (5)) with the mole fraction of krypton at constant temperature (82·9°K).

to $\pm\frac{1}{2}\,\mu$v in the thermocouple e.m.f.); composition, $\pm 0{\cdot}01 x_2^{(3)}$ in $x_2^{(3)}$ in the first series of experiments (see § 3.3) and $\pm 0{\cdot}01 x_1^{(3)}$ in $x_1^{(3)}$ in the second series. Figure 4 shows that the theoretical prediction of a composition independent value of σ is not consistent with the experimental results.

The cell theory† of solutions allows a value of the free energy of the solid solution to be determined from values of certain properties of the components. Using the expression for G^E (Prigogine 1957, eqn 10.4.17), which takes account of the difference in size of the molecules of the two components, the chemical potential μ_1 of argon in the solid solution at 82·9°K has been calculated. Using reasonable values for the configuration properties of argon it is found that μ_1 (in joules per mole) is given by

$$\mu_1=\mu_1^0+\boldsymbol{R}T\ln x_1^{(3)}+716(x_2^{(3)})^2-0{\cdot}84(x_2^{(3)})^3+1{\cdot}9(x_2^{(3)})^4 \quad \ldots\ldots(6)$$

where μ_1^0 is the chemical potential of solid argon at 82·9°K. If the terms in $(x_2^{(3)})^3$ and $(x_2^{(3)})^4$ are neglected, equation (6) is consistent with equation (4), the value of σ being 716 joules per mole.

The result of this calculation is compared with experiment in figure 5. In this figure the difference between the measured vapour pressure and that (P^i) of the ideal solution at the same temperature ($T=82{\cdot}9$°K) is plotted against $x_2^{(3)}$, the experimental errors being indicated as described above. Also on this diagram is shown the variation of $P-P^i$ with $x_2^{(3)}$ where P has been calculated from equation (5) using the value of σ calculated above and two other values (675 and 750 joules per mole). As figure 4 shows, the experimental results are inconsistent with equation (5). However, it may be seen from figure 5 that the curve drawn for $\sigma=716$ joules per mole fits the experimental points closely.

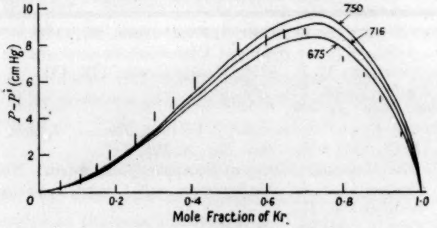

Figure 5. The variation of P–P^i with mole fraction of krypton at 82·9°K. The figures give the value of σ in joule mol^{-1}.

The vapour pressure measurements may be compared with those of solid solutions of (1) argon and krypton (Singleton and Halsey 1954, Halsey and Freeman 1956) and (2) krypton and xenon (Freeman and Halsey 1956). Both of these latter investigations show, in common with the present one, positive deviations of the solutions from ideality and an indication that σ, as calculated from equation (5), is dependent on composition. For solutions of argon and krypton Singleton and Halsey report a mean value (calculated from measurements in the range $x_2^{(3)}=0{\cdot}4$ to $x_2^{(3)}=1$) of $\sigma/\boldsymbol{R}T$ of about 1·3 at 77°K. The value of $\sigma/\boldsymbol{R}T$ at this temperature and at $x_2^{(3)}=\frac{1}{2}$ from the present results is $1{\cdot}2_8$.

---

† The conformal solution theory is not considered here because of the large difference (about 40%) in the critical temperature of the two components.

In the case of solutions of krypton and xenon, the value of σ increases from 1100 joules per mole at small concentrations of the heavier gas (xenon) to 1300 joules per mole at equimolar proportions. (Freeman and Halsey point out that the higher values of σ are subject to a large experimental error and consider that σ is effectively independent of composition.) If this variation of σ with composition is real, it is in the opposite sense to that determined in the present investigation for solutions of argon and krypton. Figure 4 shows that σ *decreases* as the mole fraction of the heavier gas (krypton) increases.

§ 6. CONCLUSION

In the previous section it is shown that the prediction of the solution theories that the excess free energy G^E of solid solutions of argon and krypton is proportional to the product of the mole fractions of the components is inconsistent with the experimental results. The precision of the present data is insufficient to allow the dependence of G^E on composition to be determined and further measurements are being made.

ACKNOWLEDGMENTS

I wish to thank Professor G. O. Jones, who suggested the investigation, for advice and encouragement and Dr. R. O. Davies for very many helpful discussions.

The construction of apparatus by Mr. W. Doy and Mr. W. A. G. Baldock of the College and Departmental workshops is gratefully acknowledged.

REFERENCES

CLARKE, A. M., DIN, F., ROBB, J., MICHELS, A., WASSENAAR, T., and ZWIETERING, TH., 1951, *Physica*, **17,** 876.
FREEMAN, M. P., and HALSEY, G. D., 1956, *J. Phys. Chem.*, **60,** 1119.
GUGGENHEIM, E. A., 1952, *Mixtures* (Oxford: Clarendon Press).
HALSEY, G. D., and FREEMAN, M. P., 1956, *Nature, Lond.*, **178,** 431.
HEASTIE, R., 1955, *Nature, Lond.*, **176,** 747.
—— 1956, *J. Chem. Phys.*, **24,** 490.
KEESOM, W. H., MAZUR, J., and MEIHUIZEN, J. J., 1935, *Physica*, **2,** 669.
LONGUET-HIGGINS, H. C., 1951, *Proc. Roy. Soc.* A, **205,** 247.
PRIGOGINE, I., 1957, *The Molecular Theory of Solutions* (Amsterdam: North-Holland).
SCOTT, R. B., 1947, *Temperature: Its Measurement and Control in Science and Industry* (New York: Reinhold) p. 217.
SELTZ, H., 1934, *J. Amer. Chem. Soc.*, **56,** 307.
SINGLETON, J. H., and HALSEY, G. D., 1954, *J. Phys. Chem.*, **58,** 1011.
SOUTHARD, J. C., and ANDREWS, D. H., 1929, *J. Franklin Inst.*, **207,** 323.
VEITH, H., and SCHRÖDER, E., 1937, *Z. Phys. Chem.* A, **179,** 16.

An Investigation of the Energy Levels of ^{26}Al

By S. HINDS and R. MIDDLETON
Atomic Weapons Research Establishment, Aldermaston, Berks.

Communicated by K. W. Allen; MS. received 4th November 1958

Abstract. The energy levels of ^{26}Al have been investigated by magnetic analysis using the reactions ^{27}Al(^{3}He, α)^{26}Al and ^{24}Mg(^{3}He, p)^{26}Al at an incident energy of 5·8 MeV. The positions of 70 excited states of ^{26}Al are reported below an excitation energy of 6·865 MeV. No evidence was found for a doublet at 2·08 MeV.

---

§ 1. Introduction

The recent successful application of the collective model to the nuclei of mass 25 (Litherland *et al.* 1958) has stimulated interest in other nuclei in this region such as ^{26}Al. The properties of the states of the latter can best be studied from the reaction ^{25}Mg(p, γ)^{26}Al, but the investigation of this reaction has been considerably impeded by a lack of information concerning the precise positions of the energy states. In this communication are reported the positions of 70 excited states of ^{26}Al determined from the reactions ^{24}Mg(^{3}He, p)^{26}Al and ^{27}Al(^{3}He, α)^{26}Al.

Previous to this work, Browne (1954, 1956) has determined the positions of the first six excited states by magnetic analysis of the α-particles from the reaction ^{28}Si(d, α)^{26}Al. Measurements have also been made on the lower excited states by several groups of workers (see Endt and Braams 1957), using the reaction ^{25}Mg(p, γ)^{26}Al. The positions of some highly excited states have been reported from observations of the ^{25}Mg + p resonances (Endt and Braams).

§ 2. Experimental Procedure

Singly ionized ^{3}He ions were accelerated in the Aldermaston Van de Graaff generator to energies in the neighbourhood of 5·8 MeV. After magnetic analysis the beam was allowed to strike thin targets of magnesium and aluminium and the charged reaction products were analysed in a high precision broad-range magnetic spectrograph. Several exposures were made with various thickness magnesium targets at angles of observation of 15°, 30° and 60°. In spite of the large angular acceptance of the spectrograph exposures were long, an average value being about 3000 microcoulombs. It may be noted that this figure refers to the incident singly ionized ^{3}He and not to the ions entering the Faraday cup which are doubly charged. The latter are formed in the target which acts as an electron stripper of almost 100% efficiency. At least fourteen exposures of similar strength were made with aluminium targets at angles ranging from 7½° to 95°.

The magnesium targets were prepared from separated ^{24}Mg isotope supplied by Atomic Energy Research Establishment, Harwell, in the form of magnesium oxide. The oxide was reduced during evaporation by the tantalum boat and the magnesium metal was collected on thin carbon films which had previously been mounted on the target holders. The films prepared in this way varied in thickness between 15 and 30 $\mu g\,cm^{-2}$ and an average thickness of the carbon backing was 8 $\mu g\,cm^{-2}$. The aluminium targets, which were self-supporting, were also prepared by evaporation. Thicknesses ranged from 15 to 30 $\mu g\,cm^{-2}$.

§ 3. RESULTS

A typical α-particle spectrum from the reaction $^{27}Al(^3He, \alpha)^{26}Al$, obtained at 30°, is shown in figure 1. For this exposure the spectrograph field setting was 9395 gauss, which permitted α-particles of 5·24 MeV to 13·5 MeV to be simultaneously recorded on one plate; the exposure strength was 3000 microcoulombs. Additional exposures were made at thirteen other angles ranging from $7\frac{1}{2}$° to 95°.

Groups corresponding to states in ^{26}Al were identified by their rate of energy change with angle. These are labelled in the figure numerically, 0 referring to the ground state. Two strong impurity groups were observed, from the reactions $^{12}C(^3He, \alpha)^{11}C$ and $^{16}O(^3He, \alpha)^{15}O$, both corresponding to ground state transitions, and are labelled in figure 1 by the symbol for the residual nucleus.

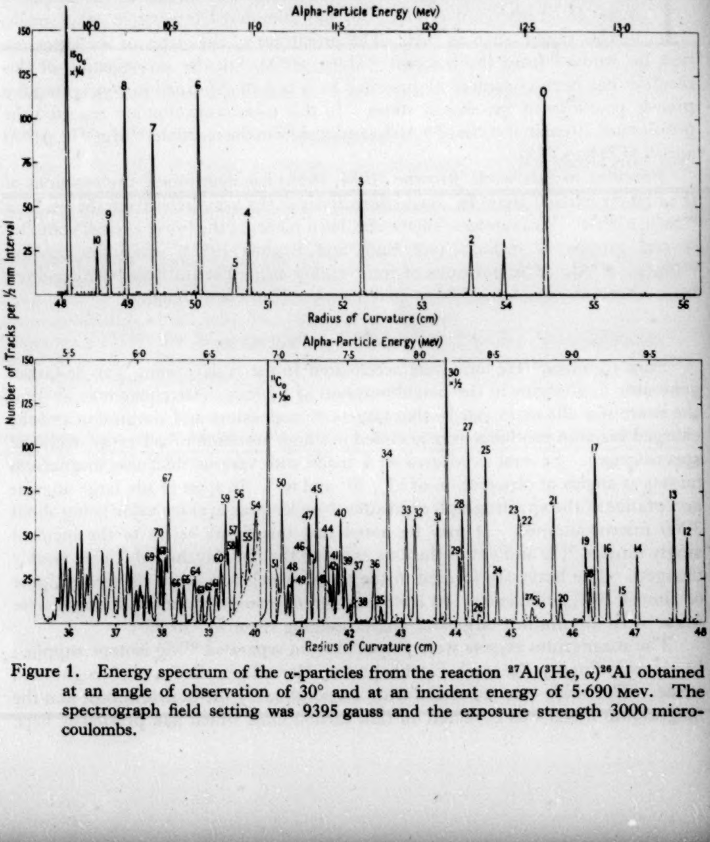

Figure 1. Energy spectrum of the α-particles from the reaction $^{27}Al(^3He, \alpha)^{26}Al$ obtained at an angle of observation of 30° and at an incident energy of 5·690 MeV. The spectrograph field setting was 9395 gauss and the exposure strength 3000 microcoulombs.

Group Number	(1)	(2)	(3)	(4)	(5)	(6) and (7)
1	0·228	0·230	0·229	0·228	0·23	0·219 (6)
2	0·416	0·416	0·416	0·418	0·42	
3	1·050	1·053	1·052	1·052	1·07	
4	1·755	1·755	1·755	1·750	1·76	
5	1·846	1·845	1·846	1·846	1·86	
6	2·065	2·069	2·067	2·064	2·08	
					2·09	2·074 (6)
7	2·360	2·363	2·362		2·32	
8	2·543	2·541	2·542		2·54	
9	2·659	2·659	2·659		—	
10	2·738	2·737	2·738		—	
11	2·909	2·910	2·910		—	
12	3·072	3·072	3·072		—	
13	3·155	3·156	3·155		3·16	
14	3·399	3·398	3·398		—	
15	3·504	3·503	3·504		—	
16	3·594	3·592	3·593		—	
17	3·674	3·677	3·675		3·67	
18	3·722	3·716	3·719		—	
19	3·747	3·746	3·746		3·76	
20	(3·918)	—	(3·918)			
21	3·960	3·965	3·962			
22	4·189	4·193	4·191			
23	4·203	4·201	4·202			
24	4·342	4·342	4·342			
25	4·424	4·424	4·424			
26	(4·470)	4·477	4·477			
27	4·540	4·542	4·541			
28	4·593	4·596	4·595			
29	4·611	4·615	4·613			
30	4·698	4·700	4·699			
31	4·766	4·766	4·766			
32	4·932	4·938	4·935			
33	5·002	5·003	5·002			
34	5·126	5·127	5·126			
35	5·193	(5·203)	5·193			
36	5·237	5·238	5·238			
37	5·388	5·391	5·390			
38	5·422	5·426	5·424			
39	5·447	5·453	5·450			
40	5·481	5·488	5·485			
41	5·505	5·507	5·506			
42	5·536	5·537	5·536			
43	5·558	5·559	5·558			
44	5·584	5·577	5·580			
45	5·665	5·665	5·665			
46	5·685	5·696	5·690			
47	5·715	(5·710)	5·715			
48	5·842	(5·835)	5·842			
49	5·874	5·875	5·875			
50	5·911	5·908	5·910			
51	(5·956)	5·942	5·942			
52	6·019	6·013	6·020			
53	6·078	6·083	6·080			
54	6·112	—	6·112			
55	6·190	6·187	6·188			

Group Number	(1)	(2)	(3)	(4)	(5)	(6) and (7)
56	6·236	(6·227)	6·236			
57	6·260	6·261	6·260			
58	6·336	6·334	6·335			
59	6·351	—	6·351			
60	6·386	6·391	6·388			
61	6·424	—	6·424			
62	6·487	—	6·487			
63	6·544	(6·543)	6·544			
64	6·593	(6·590)	6·593			6·608 (7)
65	6·668	6·673	6·670			6·680 (7)
66	6·715	6·716	6·715			6·723 (7)
67	6·776	6·776	6·776			6·780 (7)
	—	—	—			6·797 (7)
68	6·806	6·805	6·805			6·813 (7)
69	6·840	6·845	6·842			6·856 (7)
70	6·865	6·864	6·865			6·877 (7)

(1) Present investigation from the $^{27}\mathrm{Al}(^{3}\mathrm{He}, \alpha)^{26}\mathrm{Al}$ reaction; the experimental error is ±10 kev except for the values in parenthesis for which ±15 kev is possible.

(2) Present investigation from the $^{24}\mathrm{Mg}(^{3}\mathrm{He}, \mathrm{p})^{26}\mathrm{Al}$ reaction; errors as for (1).

(3) Mean values for the present investigation; errors as for (1).

(4) Browne (1954, 1956), from the $^{28}\mathrm{Si}(\mathrm{d}, \alpha)^{26}\mathrm{Al}$ reaction.

(5) Green, Singh and Willmott (1956), from the $^{25}\mathrm{Mg}(\mathrm{p}, \gamma)^{26}\mathrm{Al}$ reaction.

(6) Kavanagh, Mills and Sherr (1955), from the $^{25}\mathrm{Mg}(\mathrm{p}, \gamma)^{26}\mathrm{Al}$ reaction.

(7) From the $^{25}\mathrm{Mg} + \mathrm{p}$ resonances (see Endt and Braams 1957).

At 30° the group from the former reaction is particularly intense and completely masks groups 52 and 53, and the low energy tail partially obscures groups 54 and 55. The impurity group from the latter reaction completely obscures group 11. A weak group of α-particles was observed at a radius of 45·3 cm from the $^{28}\mathrm{Si}(^{3}\mathrm{He}, \alpha)^{27}\mathrm{Si}$ reaction leading to the ground state of ^{27}Si. Groups corresponding to other states of ^{27}Si were not observed, since from a previous investigation (to be published) these are known to be considerably less intense than the ground state group.

The energy of the ^{3}He ion beam was determined from measurements made on the elastically scattered groups from aluminium and carbon. A mean value of 5·690 ± 0·015 Mev was obtained which leads to a Q-value for the $^{27}\mathrm{Al}(^{3}\mathrm{He}, \alpha)^{26}\mathrm{Al}$ reactions of 7·523 ± 0·015 Mev. The latter is a mean of determinations made at four angles and agrees with the value of 7·528 Mev expected from the mass defects reported by Endt and Braams.

Listed in column (1) of the table are the excitation energies of 70 states of ^{26}Al determined from this reaction. The values quoted for groups 1 to 34 inclusive are the means of determinations made at angles of 15°, 30°, 45° and 60°. In almost all cases, the values obtained at different angles differed by less than 4 kev from the listed mean values. For groups 35 to 70 inclusive, determinations were made at fourteen angles. It may be noted that groups 56, 64 and 67 consistently appeared to be broad and may well be doublets. The experimental error is ±10 kev, except for the values in parentheses for which an error of ±15 kev is possible.

In figure 1 there are several unlabelled groups, beyond group 70, which almost certainly correspond to states in ^{26}Al. Unfortunately, the excitation energies calculated at various angles did not agree well and consequently these values are not listed in the table. This is thought due to many of the groups being unresolved multiplets, the components of which vary in intensity with angle thus making it difficult to locate the mean position.

Proton energy spectra from the magnesium target were measured at angles of 15°, 30° and 60°. The spectrum observed at 15°, with a field of 8925 gauss and an exposure of 2500 microcoulombs, is illustrated in figure 2. As for the previous reaction, groups were identified by their rate of change of energy with angle and those corresponding to states in ^{26}Al are labelled numerically.

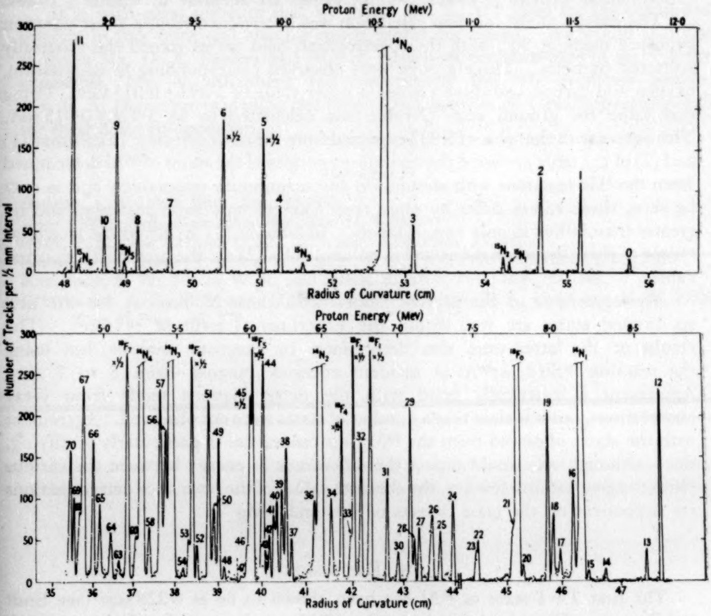

Figure 2. Energy spectrum of the protons from the reaction ^{24}Mg(^{3}He, p)^{26}Al obtained at an angle of 15° and at an incident energy of 5·893 MEV. The spectrograph field strength was 8925 gauss and the exposure strength 2500 microcoulombs.

As is evident from figure 2, there are considerably more impurity groups present than in the α-particle spectrum. Also these groups are relatively more intense and in some cases were uncountable. However, most of these arise from the same impurities, namely carbon and oxygen, except for a number of weak groups which were identified as due to the 1·1% of ^{13}C present in natural carbon. All impurity groups are labelled with the symbols for the residual nuclei, the subscript referring to the corresponding state. The large number of impurity groups complicated the analysis of the ^{24}Mg(^{3}He, p)^{26}Al reaction, and inevitably several groups were masked at each angle investigated. In the spectrum shown in figure 2 proton groups 35, 59, 61 and 62 are obscured by impurity groups.

Groups 20, 54 and 59 were observed to be weak at all angles and for these no reliable excitation energies could be determined. Apart from group 62, which was masked at all angles, and group 61 which was masked at all but one, all the other groups observed in the ^{27}Al(^{3}He, α)^{26}Al reaction were identified in the ^{24}Mg(^{3}He, p)^{26}Al reaction. In column (2) of the table are listed the calculated excitation energies. Most of the values are the means of three determinations. When one group was masked at a particular angle or was too weak to be accurately located the values are printed in parentheses and are subject to an experimental error of ± 15 kev. Other values are accurate to within ± 10 kev.

The energy of the incident ^{3}He beam was determined from a short duration exposure made at 90°, with the spectrograph field set to record the elastically scattered particles. Three groups were observed corresponding to magnesium, oxygen and carbon and these yielded a mean value of $5{\cdot}893 \pm 0{\cdot}015$ Mev. Using this value the ground state Q-value was calculated to be $5{\cdot}928 \pm 0{\cdot}015$ Mev. This agrees with the value of 5·933 expected from the mass defects. In columns (1) and (2) of the table are listed the excitation energies of the states of ^{26}Al determined from the ^{3}He reactions with aluminium and magnesium respectively and as may be seen, these values differ by more than 5 kev in only eight instances and by greater than 10 kev in only two instances. In column (3) are listed the weighted means of these determinations and in columns (4)–(7) are the previously reported values.

The agreement of the present values with those of Browne for the first six excited states are well within the experimental error of ± 10 kev. The results of the latter were also determined by magnetic analysis, but using the reaction ^{28}Si(d, α)^{26}Al at incident energies ranging from 5 to 7 Mev. Agreement is essentially good with the determinations made from γ-ray observations, but it is clear that a number of states were not observed. Agreement with the states observed from the ^{25}Mg + p resonances is particularly gratifying, since, although one would expect the differences in energy between the various states to agree within a few kev, the absolute values of the resonance determinations are dependent on the mass defects of ^{26}Al and ^{25}Mg.

§ 4. DISCUSSION

The first $T=1$ state of ^{26}Al has been shown to be at 0·228 Mev (see Endt and Braams). If on this basis the levels of ^{26}Mg are compared with those of ^{26}Al, the second $T=1$ state should be at about 2·1 Mev. Browne has investigated the reaction ^{28}Si(d, α)^{26}Al and although he observed a weak α-particle group corresponding to the 0·228 Mev state and thus violating the isotopic spin selection rule, he observed a strong group corresponding to a state at 2·064 Mev. Since the latter transition is strong this state is assumed to have $T=0$ and consequently there should be a second nearby state having $T=1$. Additional evidence favouring two nearby states comes from the γ-ray results of Kavanagh, Mills and Sherr (1955) and Green, Singh and Willmott (1956). They conclude that the $T=1$ state is at 2·09 Mev and the $T=0$ state at 2·08 Mev.

In (^{3}He, p) and (^{3}He, α) reactions, transitions to both $T=0$ and $T=1$ states are allowed and therefore if there is a doublet in ^{26}Al of approximately 10 kev spacing it should have been observed in the present investigation. No such doublet was observed. However, it is possible that it may have passed undetected if one member was very weakly excited, but this seems improbable since two different reactions have been investigated. An alternative and more likely explanation is that the doublet spacing is less than 10 kev. The group observed at 2·080 MEV like other nearby groups has a half-width of 9 kev and if the members of the doublet are equally excited the spacing would have to be less than 4 kev for it not to have been observed.

ACKNOWLEDGMENTS

It is with great pleasure that we thank Dr. K. W. Allen for his continued interest in this work and also for much useful discussion. We would also like to thank Mr. D. A. Procter and Mr. H. Marchant for assistance in making the exposures, Mr. V. Shepherd for constructing the ^{3}He recovery system, Mr. F. A. Howe for providing the targets and the Van de Graaff operating staff for their close co-operation.

REFERENCES

BROWNE, C. P., 1954, *Phys. Rev.*, **95**, 860.
—— 1956, *Bull. Amer. Phys. Soc.*, Ser. II, **1**, 212.
ENDT, P. M., and BRAAMS, C. M., 1957, *Rev. Mod. Phys.*, **29**, 683.
GREEN, L. L., SINGH, J. J., and WILLMOTT, J. C., 1956, *Proc. Phys. Soc.* A, **69**, 335.
KAVANAGH, R. W., MILLS, W. R., and SHERR, R., 1955, *Phys. Rev.*, **97**, 248.
LITHERLAND, A. E., MCMANUS, H., PAUL, E. B., BROMLEY, D. A., and GOVE, H. E., 1958, *Can. J. Phys.*, **36**, 378.

An Arc maintained on an Isolated Metal Plate exposed to a Plasma

By A. E. ROBSON and P. C. THONEMANN
Atomic Energy Research Establishment, Harwell

MS. received 14*th November* 1958

Abstract. It is shown theoretically that a cathode spot may be maintained on an isolated metal surface immersed in the plasma of a gas discharge. Two experiments are described in which arcs of this kind were produced on a mercury surface.

---

§ 1. Theory

A metal plate exposed to the plasma of a gas discharge will be bombarded by both electrons and positive ions. If the plate were at the potential of the plasma, the current of electrons would greatly exceed the current of ions, due to the greater random velocities of the electrons in the plasma. An electrically isolated metal plate will therefore take up a negative potential with respect to the plasma, so that it attracts ions and repels all but the fastest electrons, and in equilibrium the net current vanishes. The equilibrium negative potential is usually known as the floating potential, and can readily be derived by the analysis of Langmuir and Mott-Smith (1924) and Bohm (1949).

The negatively charged plate will receive a current density of ions given by

$$j_2 = n_2 e_2 \bar{v}_2 \qquad \ldots\ldots(1)$$

where n_2 is the density of ions, e_2 the charge on an ion, and $\bar{v}_2$ the mean velocity with which ions reach the boundary of the sheath which separates the plate from the plasma. This velocity is given by

$$\bar{v}_2 = \alpha (kT_1/m_2)^{1/2} \qquad \ldots\ldots(2)$$

where m_2 is the ionic mass, T_1 the electron temperature, and α is a factor of the order unity (Allen and Thonemann 1954).

If the plate is at a potential V with respect to the plasma, the current density of electrons reaching it is

$$j_1 = \tfrac{1}{4} n_1 e_1 \bar{v}_1 \exp(-e_1 V/kT_1) \qquad \ldots\ldots(3)$$

where n_1 is the electron density, e_1 the charge on the electron and $\bar{v}_1$ the mean random velocity of plasma electrons, given by

$$\bar{v}_1 = (8kT_1/\pi m_1)^{1/2}. \qquad \ldots\ldots(4)$$

When the plate is at the floating potential V_f, the total current $j_1 + j_2 = 0$. With $\alpha = 1$, and $e_2 = -e_1$ for singly charged ions, the foregoing equations give

$$V_f = \frac{kT_1}{2e_1} \ln\left(\frac{m_2}{2\pi m_1}\right). \qquad \ldots\ldots(5)$$

If the electron temperature is sufficiently high, V_f will exceed the potential difference required to sustain an arc. If under these circumstances a cathode spot is initiated on the plate, the strong local emission of electrons from it will reduce the potential difference between the plate and plasma from V_f to V_c, where V_c is the cathode fall in potential of the arc. More electrons can now reach the plate against the retarding potential and, except in the immediate vicinity of the cathode spot, a net electron current flows from the plasma to the plate. This current returns to the plasma through the arc spot, thereby satisfying the condition that the total current to the plate shall be zero.

Two equilibrium potentials are therefore possible. In the first case the plate is at V_f with respect to the plasma ($V_f < 0$) and receives a uniform and equal current density of particles of each sign, and in the second case the plate is at V_c ($V_c < 0$) and there is a circulating current through a cathode spot (figure 1).

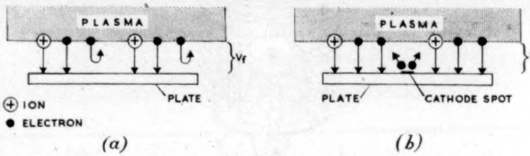

Figure 1. Alternative equilibrium potentials of isolated plate (*a*) without cathode spot, (*b*) with cathode spot.

The circulating current is given by

$$I_c = Ane_1\left(\frac{kT_1}{2\pi m_1}\right)^{1/2}\left\{\exp\left(-\frac{e_1V_c}{kT_1}\right)-\exp\left(-\frac{e_1V_f}{kT_1}\right)\right\} \qquad \ldots\ldots(6)$$

where A is the area of the plate exposed to the plasma. To maintain a stable cathode spot, a minimum current I_a is necessary, the value of which depends on the material of the plate. Provided that I_c is greater than I_a, the cathode spot, once initiated, will be maintained.

Whereas the usual form of arc requires two electrodes and an external source of e.m.f., this arc requires only one electrode and is maintained by the thermal energy of the plasma electrons. For this reason we call it a ' unipolar ' arc.

§ 2. EXPERIMENTS

Two experiments will be described in which a unipolar arc was maintained on a mercury electrode in the presence of a strong plasma generated by an electrodeless high-frequency discharge. For a cathode spot which is ' anchored ' at the meniscus of mercury and another metal, I_a is about one ampere and V_c about 8 volts. In mercury vapour, $m_2/m_1 = 3{\cdot}6 \times 10^5$, and therefore V_f exceeds V_c when kT_1 is greater than 1·5 electron volts.

The first experimental tube is shown in figure 2. This resembled a conventional mercury arc tube with anode A and mercury pool cathode C, in which there was a cylindrical nickel spot-anchor F surrounding a dielectric starter S (a glass-coated tungsten rod). A sheet of nickel forming an almost closed cylinder fitted closely inside the tube and dipped into the mercury pool at its lower edge. The combined surface area of mercury and nickel was 350 cm². The tube was evacuated to a residual gas pressure of less than 10^{-6} mm Hg.

The tube fitted closely inside a coil of 12 turns of 10 s.w.g. copper wire. This formed part of a tuned circuit which was coupled by a short transmission line to a high-frequency generator with a maximum power output of 3 kilowatts at a frequency of 12 Mc/s.

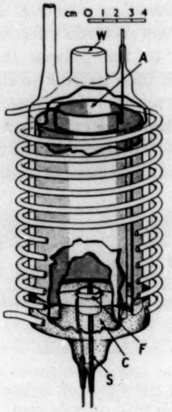

Figure 2. First unipolar arc tube: A, anode; C, cathode; F, spot-anchor; S, starter; W, viewing window.

A conventional direct current arc of a few amperes was first struck between the cathode and the anode A, by applying a high-voltage pulse to the starter S. After a short period necessary for the mercury to 'wet' the nickel, the cathode spot anchored at the meniscus of the mercury at the inner surface of the cylindrical anchor. The spot could be observed through the window W and appeared as a bright line, whose length was approximately proportional to the current.

The high-frequency generator was then used to generate an intense plasma in the tube. The arc spot could still be observed through the plasma if viewed through a deep red filter, and as the high-frequency power was raised, the length of the cathode line increased. This indicated that the cathode was carrying an increased current, although the current to the anode remained nearly constant. With the generator at full power, the d.c. supply to the anode was turned off and all external connections removed from the tube. The cathode spot however remained clearly visible, and from its length it was estimated that it was carrying about four amperes in the unipolar mode. As the intensity of the high-frequency excitation was reduced, the cathode line shortened, and vanished abruptly when its length corresponded to about one ampere.

A second experiment was carried out in the tube shown in figure 3. This tube contained a nickel anode of area 85 cm^2, and a small mercury pool cathode with a nickel spot-anchor. The circuit is shown in figure 4. When an arc of one ampere direct current was struck in this tube the voltage across the electrodes was 15 v. A strong plasma was then generated in the tube by means of the coil wound round it; as the high-frequency excitation was increased the voltage across the electrodes fell, and at the full power of the generator became zero, or a fraction of a volt negative. At this point the switch S_1 was closed and the switch S_2 opened. The ammeter connecting the electrodes continued to record one ampere d.c. and the cathode spot was clearly visible. The tube was then operating in the unipolar mode. Since the area of the anode was about twenty times the area of the cathode, the electrons collected by the cathode surface made only a small contribution to the current in the cathode spot. The ammeter registered the circulating current.

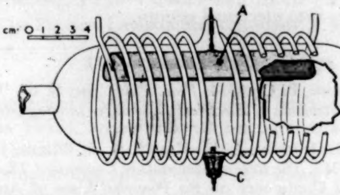

Figure 3. Second unipolar arc tube: A, anode; C, cathode.

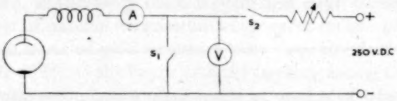

Figure 4. Circuit of second discharge tube (high-frequency circuit not shown).

On account of the considerable power dissipation in these experiments, the tubes became very hot after a short period of operation. The unipolar arcs would then vanish and could not be reproduced until the tubes had cooled down. This was presumably because a rise in mercury vapour pressure was accompanied by a fall in the electron temperature, and as can be seen from equations (5) and (6), the conditions for the existence of the unipolar arc are very sensitive to T_1.

§ 3. CONCLUSIONS

The unipolar arc may be expected whenever a plasma of sufficient density and electron temperature is in contact with a metal surface of sufficient area. However, even though the conditions for the maintenance of the arc may exist, additional conditions are in general necessary for its formation. In the experiments described here the arc was always initiated by means of an external circuit, but it is to be expected that under other conditions the bombardment of the metal surface by positive ions which have been accelerated through the sheath potential difference might initiate a unipolar arc.

In addition to the steady-state experiments just described, unipolar arcs have been observed on the metal walls of high-current pulsed-discharge tubes, such as ZETA, where they are responsible for contaminating the plasma with material from the walls (Craston *et al.* 1958) and introducing 'cold' electrons into the plasma. It seems likely that the scintillations frequently seen on metal surfaces exposed to plasma are transient unipolar arcs.

The experiment illustrated in figure 3 demonstrates that, by extracting 'hot' electrons from the plasma and substituting 'cold' electrons from the cathode spot, the unipolar arc provides a mechanism for the direct conversion of plasma thermal energy into electrical energy.

REFERENCES

ALLEN, J. E., and THONEMANN, P. C., 1954, *Proc. Phys. Soc.* B, **67**, 768.

BOHM, D., 1949, *The Characteristics of Electrical Discharges in Magnetic Fields* (New York: McGraw-Hill), ch. 3.

CRASTON, J. L., HANCOX, R., ROBSON, A. E., KAUFMAN, S., MILES, H. T., WARE, A. A., and WESSON, J. A., 1958, *The Role of Materials in Controlled Thermonuclear Research.* Second International Conference on the Peaceful Uses of Atomic Energy, Paper No. 34, Geneva, 1958.

LANGMUIR, I., and MOTT-SMITH, H., 1924, *Gen. Elect. Rev.*, **27**, 538.

RESEARCH NOTES

The ^{24}Mg(^{3}He, α)^{23}Mg Reaction

By F. de S. BARROS†, P. D. FORSYTH, A. A. JAFFE and I. J. TAYLOR
The Physical Laboratories, University of Manchester

MS. received 5*th December* 1958

The excited states of ^{23}Mg, which have not been studied previously (cf. Endt and Braams 1957), are of interest for comparison with the levels of the mirror nucleus ^{23}Na. The reaction ^{24}Mg(^{3}He, α)^{23}Mg was therefore investigated at a bombarding energy of 5·23 MeV using the Van de Graaff generator at Manchester University and the reaction products were analysed by means of a 90° broad range magnetic spectrograph (Barros *et al.* 1959).

Preliminary experiments indicated that in order to obtain reasonable yields from this reaction, moderately thick targets and large exposures would have to be used. A target of natural magnesium evaporated on to a plastic foil, previously coated with a thin layer of gold to ensure even deposition of the magnesium, was placed at an angle of 45° to the beam with the backing facing the beam. Exposures of up to 4500 micro-coulombs were made at angles of observation of 10°, 40° and 90° with respect to the ^{3}He beam. The spectrum of alpha particles at 40° is shown in figure 1.

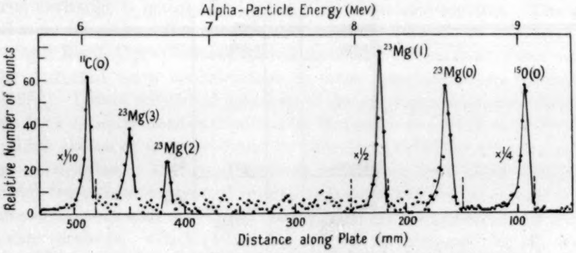

Figure 1. The 40° α-particle spectrum with a ^{3}He beam of 5·23 MeV.

The variation of energy with angle of the observed alpha particle groups showed that four of the groups came from the reaction ^{24}Mg(^{3}He, α)^{23}Mg. The group of highest energy gave good agreement with the known ground state Q-value for this reaction (4·048 MeV). The remaining three groups were assumed to result from the formation of the first three excited states of ^{23}Mg and the excitations of these levels were found to be 0·449 ± 5, 2·038 ± 8 and 2·350 ± 8 MeV.

The certain identification of higher excited states of ^{23}Mg proved difficult because the large yield from the reaction ^{12}C(^{3}He, α)^{11}C, $Q = 1{\cdot}863$ MeV, tended to obscure this region of the spectrum. The alpha particle groups from the second and third excited states of ^{23}Mg could not be observed at 10° because they were obscured by a very large proton peak from the reaction $^{16}O(^{3}He, p)^{18}F$, $Q = 2{\cdot}039$ MEV, and the alpha peak from the reaction $^{12}C(^{3}He, \alpha)^{11}C$, respectively. No groups originating from the reactions $^{25}Mg(^{3}He, \alpha)^{24}Mg$ and $^{26}Mg(^{3}He, \alpha)^{25}Mg$ were identified, but although these reactions have very high Q-values the proportions of ^{25}Mg and ^{26}Mg in the target are small. It is probable that alpha particles from these reactions contribute to the background.

---

† On leave of absence from the Centre for Physical Research, Rio de Janeiro.

Reaction $^{24}Mg(^{3}He, \alpha)^{23}Mg$

Group	Excitation of ^{23}Mg (MEV)	Differential cross section (mbn sterad^{-1}) at lab. angles of : 10°	40°	90°
α_0	0	0·55	0·48	0·10
α_1	0·449	0·50	1·00	0·08
α_2	2·038	—	0·15	0·16
α_3	2·350	—	0·35	0·14

The thickness of natural magnesium on the target was measured using an alpha particle thickness gauge and found to be 40 μg cm^{-2}. The absolute differential cross sections were calculated and are given in the table, with an estimated error of about 15%.

A comparison of the observed levels of ^{23}Mg with the known levels of its mirror ^{23}Na (Endt and Braams 1957) are shown in figure 2. The correspondence between the excitations of successive levels in the two nuclei is good and is particularly striking in the case of the first excited state.

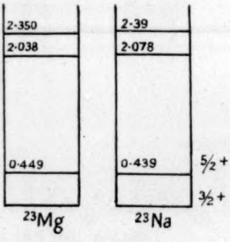

Figure 2. A comparison of the low-lying excited states of the mirror nuclei ^{23}Na and ^{23}Mg.

Although the differential cross sections of the ground and first excited state groups were found for only three angles, an attempt has been made to compare the angular distributions with those expected on the assumption that the reaction proceeds by a pick-up or direct surface interaction process (Butler 1957, Butler and Hittmair 1957). A peak at approximately 40° in the angular distribution of the α_1 group is consistent with an orbital angular momentum transfer of two units which would be allowed by a spin and parity of the first excited state of ^{23}Mg of 5/2+, corresponding to the known values for the mirror level in ^{23}Na (Endt and Braams 1957). However, the results from the three observed angles are sufficient to show that the angular distribution of the ground state group is unlikely to be explained on such a simple assumption. This is not surprising in view of the complicated configuration of the ^{23}Na ground state (and therefore that of ^{23}Mg) in which it is assumed that three $d_{5/2}$ particles couple to give the known spin of 3/2 (Elliott and Lane 1957).

REFERENCES

Barros, F. de S., Forsyth, P. D., Jaffe, A. A., and Taylor, I. J., 1959, *Proc. Phys. Soc.* (in the press).

Butler, S. T., 1957, *Phys. Rev.*, **106**, 272.

Butler, S. T., and Hittmair, O. H., 1957, *Nuclear Stripping Reactions* (London : Pitman).

Endt, P. M., and Braams, C. M., 1957, *Rev. Mod. Phys.*, **29**, 683.

Elliott, J. P., and Lane, A. M., 1957, *Handbuch der Physik*, **39**, 241 (Berlin : Springer).

Variational Calculations of the 1s–2s Electron Excitation Cross Section of Hydrogen

By N. LYNN

Department of Applied Mathematics, The Queen's University of Belfast

Communicated by D. R. Bates; MS. received 15*th December* 1958

A variational procedure suitable for the investigation of inelastic scattering of electrons by atoms has been given by Moiseiwitsch (1951). This procedure, which is a generalization of the variational methods of Hulthén (1944) and Kohn (1948) for elastic scattering problems, was applied by Massey and Moiseiwitsch (1953) to the calculation of the cross section for the 1s–2s excitation of hydrogen atoms by electron impact, both when the possibility of electron exchange is ignored and when it is taken into account. The results obtained were found to differ considerably not only from those calculated using the Born and Born–Oppenheimer approximations but also from those obtained using the distorted wave modifications of these approximations (Erskine and Massey 1952). Direct numerical solutions of the appropriate coupled differential equations have recently been carried out by Bransden and McKee (1956) for the case in which exchange is ignored and by Marriott (1958) for the case in which exchange is included. The cross sections of Massey and Moiseiwitsch differ considerably from these numerical results, although they are in general in better qualitative agreement with them than are the cross sections obtained by the other approximate methods. Huck (1957) has recently investigated the effectiveness of different variational methods for inelastic collision problems by applying them to the solution of certain model equations which are so designed as to simulate the actual differential equations which occur, but yet permit of exact solution. In view of the results of Huck's calculations, the difference between the cross sections obtained by numerical solution and those found by Massey and Moiseiwitsch is surprisingly large and this has led Huck to suggest that the work of these authors should be re-examined. Following this suggestion, the complete calculations for the case in which exchange is neglected have been repeated using the same trial function as was used originally. The results obtained are exactly the same as those which were obtained by Massey and Moiseiwitsch. Since the suspicion which attaches to the Massey–Moiseiwitsch results because of Huck's work applies as much to the case in which exchange is neglected as to the case in which it is included, it was considered unnecessary to recalculate the cross sections for the latter case, it being evident that the variational method as applied does in fact yield unsatisfactory results.

While it is to be expected that more accurate results would be obtained by employing more refined trial wave functions than those used by Massey and Moiseiwitsch, it is desirable, in view of the extensive analytical and numerical work involved, to have, before starting out on such a project, some idea of the order of the improvement in accuracy likely to be achieved. Huck, in his investigation, has tested the effectiveness of a trial wave function containing six parameters which includes, besides the terms contained in the Massey–Moiseiwitsch trial function, other terms to allow for mixing of the elastically and inelastically scattered waves. As applied to Huck's model equations the variational method using this trial wave function leads to values for the cross section which are within 5% of the exact values. However, some uncertainty attaches to the effectiveness of these model equations in describing the actual equations which arise in the problem and in view of the marked difference in the degree of accuracy obtained by Massey and Moiseiwitsch in solving the actual equations, and by Huck in solving the model equations using the same variational method with the original three-parameter trial function, it is clear that conclusions drawn using the model equations must be treated with some caution. As a consequence, it was decided to investigate directly the effectiveness of the addition of one extra term to the Massey–Moiseiwitsch trial function. The term chosen was one of those used by Huck to allow for mixing of elastically and inelastically scattered waves. In the notation of the paper of Massey and Moiseiwitsch the trial wave function adopted, which contains four variational parameters, is

$$\Psi(r_1, r_2) = r_2^{-1}\{f_0(r_2)\psi_0(r_1) + f_1(r_2)\psi_1(r_1)\}, \qquad \ldots\ldots(1)$$

where

$$f_0(r) = \sin kr + (a + b\,\mathrm{e}^{-r})(1 - \mathrm{e}^{-r}) \cos kr \qquad \ldots\ldots(2)$$

and

$$f_1(r) = (1 - \mathrm{e}^{-r}) d \exp(ik_1 r) + c\,\mathrm{e}^{-r} \sin kr. \qquad \ldots\ldots(3)$$

The cross sections obtained by applying the variational methods of Hulthén and Kohn as generalized by Moiseiwitsch using this trial wave function are given in the table[†] for two values of the energy of the incident electron. Included

Variational Calculations of the Cross Section for the 2s Excitation of Hydrogen (exchange neglected)

		Cross section (units of πa_0^2)			
		Three-parameter trial function		Four-parameter trial function	
E	N	HM	KM	HM	KM
13·5	0·204	0·076	0·075	0·139	0·142
54	0·0155	0·0081	0·0085	0·0166	0·0187

E = energy of incident electron (ev); N = numerical method (Bransden and McKee 1956); HM = Hulthén–Moiseiwitsch variational method; KM = Kohn–Moiseiwitsch variational method.

[†] The cross sections given are those calculated using corrected values for the variational parameter a which are obtained by following the proposal of Moiseiwitsch (1951). Huck (1957) has suggested a method whereby the parameter d might also be corrected but unfortunately this method was found to be inapplicable in the present case although it proved useful in Huck's own calculations.

for comparison are the corresponding cross sections found by the same methods using the original three-parameter trial function. The accuracy attained by the various calculations can be assessed by comparing with the cross sections of Bransden and McKee which are the exact results for the differential equations adopted. It is evident from the table that the cross sections obtained by both of the variational methods are considerably improved by the inclusion of the extra term in the trial wave function. Similar results are to be expected for the exchange case. It would seem reasonable to infer that use of the elaborate six-parameter wave function suggested by Huck would provide cross sections very close to the correct values.

ACKNOWLEDGMENTS

The author is indebted to Dr. B. L. Moiseiwitsch for his interest in the problem and for making available his original calculations. It is a pleasure to acknowledge also the proficient computational assistance of Mrs. N. Scott.

The research reported has been sponsored in part by the Air Force Cambridge Research Centre, Geophysics Research Directorate, of the Air Research and Development Command, U.S. Air Force, through its European Office, under contract No. AE61(052)-131.

REFERENCES

BRANSDEN, B. H., and MCKEE, J. S. C., 1956, *Proc. Phys. Soc.* A, **69,** 422.
ERSKINE, G. A., and MASSEY, H. S. W., 1952, *Proc. Roy. Soc.* A, **212,** 521.
HUCK, R. J., 1957, *Proc. Phys. Soc.* A, **70,** 369.
HULTHÉN, L., 1944, *K. Fysiogr. Sällsk. Lund Förh.*, **14,** No. 21.
KOHN, W., 1948, *Phys. Rev.*, **74,** 1763.
MARRIOTT, R., 1958, *Proc. Phys. Soc.*, **72,** 121.
MASSEY, H. S. W., and MOISEIWITSCH, B. L., 1953, *Proc. Phys. Soc.* A, **66,** 406.
MOISEIWITSCH, B. L., 1951, *Phys. Rev.*, **82,** 753.

An Objection to the Single-Domain Inclusion Theory of Magnetic Hysteresis in Dispersion-Hardened Alloys

BY F. D. STACEY
Department of Geophysics, Australian National University, Canberra, Australia

MS. received 17*th November* 1958

THE phenomenon of magnetic viscosity demonstrates the influence of thermal agitation in disturbing ferromagnetic domains, and its occurrence in Alnico has been examined by Street and Woolley (1949, 1950). They concluded that their experimental results were consistent with the theoretical description of magnetic hysteresis in heterogeneous alloys, given by Stoner and Wohlfarth (1948), in which the principal magnetic constituent of the alloys is considered to occur as a precipitate of fine grains which behave as essentially independent single domains. Here a quantitative consideration is given to the influence of thermal agitation on the magnetic moments of such domains to show that the relaxation time for decay of remanent magnetism according to this picture would be of the order 5×10^{-8} sec. While several modifications to the theory may be considered, an abandonment of the concept of single domain inclusions is indicated.

The probability that in a time dt a domain will derive from thermal agitation sufficient magnetic energy to change its moment by overcoming a potential barrier of height E is

$$dP = C\exp(-E/kT)\,dt, \qquad \ldots\ldots(1)$$

where k is Boltzmann's constant, T the absolute temperature and C is a frequency factor whose magnitude has been estimated by Stacey (1959). In considering single domain grains there are three contributions to E, which are due to magnetocrystalline, strain and shape anisotropies of the grains, and the total E can be expressed in terms of coercive force. In this respect thermal activation theory does not differ significantly from that of Stoner and Wohlfarth (1948).

In the presence of a field $\mathbf{H}$, E is decreased for changes in one direction and increased for opposite changes; considering only changes whose probability is increased by the application of $\mathbf{H}$ we may write

$$E = E_0 - \tfrac{1}{2}v\,\mathbf{H}\cdot\Delta\mathbf{I} \qquad \ldots\ldots(2)$$

for a grain of volume v undergoing a vectorial change in moment $\Delta\mathbf{I}$ per unit volume. E_0 is the height of a barrier in zero field. The factor $\frac{1}{2}$ may be only approximate in the general case and arises from the fact that the second term on the right-hand side of equation (2) is the energy released by the domain in 'climbing up' the potential barrier, which in the case of a symmetrical barrier is half the total energy released in the change. Then if H_c is the coercive force as observed in an experiment which takes a time τ (of the order $1/2\pi f$ in an a.c. measurement at frequency f) the integral of equation (1) over τ becomes of the order unity:

$$1 = C\tau\exp\{-(E_0 - \tfrac{1}{2}v\,\mathbf{H}_c\cdot\Delta\mathbf{I})/kT\}.$$

Assuming that H_c is measured in the same direction as the $\Delta\mathbf{I}$ which may occur in a grain,

$$E_0 = \tfrac{1}{2}v\,H_c\,\Delta I + kT\ln(C\tau). \qquad \ldots\ldots(3)$$

That H_c is very little dependent upon τ is evident partly from the fact that $E_0 \gg kT\ln(C\tau)$, except at high temperatures when E_0 becomes small, and in any case the large numerical value of C tends to mask the dependence upon τ.

Apart from the addition of the second term on the right-hand side, equation (3) differs by a numerical factor from the theory of Stoner and Wohlfarth (1948), who calculated the coercive force of a randomly oriented assembly of prolate ellipsoids. Their result will be assumed, being in this respect more general. The same authors considered the forms of the contributions to E_0 of the three anisotropies. For the present purpose it is sufficient to note that if either the magnetocrystalline or strain anisotropies or both together are predominant then an almost spherical form must be assumed for the single-domain inclusions and their maximum diameter is approximately 10^{-6} cm (Stoner and Wohlfarth 1948, Kittel 1946, 1949).

If shape anisotropy is predominant then the departure from spherical form allows a somewhat greater volume for the inclusions, which it is important to calculate. Assuming that each inclusion is a prolate ellipsoid of major and minor axes a and b then the ratio a/b and the maximum volume of one inclusion are readily estimated by using equations of Stoner and Wohlfarth (1948). From their equation (4.1) the difference between the demagnetizing factors in the directions of the minor and major axes is

$$N_b - N_a = 2{\cdot}09\, H_c/I_s \qquad \ldots\ldots (4)$$

where H_c is the observed coercive force of an assembly of randomly oriented prolate ellipsoids each of spontaneous magnetization I_s per unit volume. Taking $H_c \sim 500$ oersteds as representative and $I_s \sim 1700$ e.m.u., which would apply if the precipitated phase is nearly pure iron, as Stoner and Wohlfarth (1948) suggest, we find that the observed coercive forces are explained by shape anisotropy if

$$N_b - N_a \sim 0{\cdot}6, \qquad \ldots\ldots (5)$$

requiring $a/b \sim 1{\cdot}1$, which must be taken as the maximum value. The maximum possible volume of an inclusion which remains as a single domain is therefore

$$v = \frac{\pi}{6}\, ab^2 = \frac{1{\cdot}1\pi}{6}\, b^3, \qquad \ldots\ldots (6)$$

where b is given by equation (6.12) of Stoner and Wohlfarth (1948) for an iron ellipsoid as

$$\text{maximum } b = 4{\cdot}35 \times 10^{-7}\, Da^{-1/2}. \qquad \ldots\ldots (7)$$

To estimate the factor $D_a^{-1/2}$ we may note that $D_a = N_a/4\pi$ and that

$$N_a + 2N_b = 4\pi. \qquad \ldots\ldots (8)$$

Combining equations (5) and (8) we find $N_a = (\frac{4}{3}\pi - 0{\cdot}4)$ and $D_a = 0{\cdot}30_{15}$ so that equations (6) and (7) give

$$\text{maximum } v \sim 3 \times 10^{-19}\,\text{cm}^3. \qquad \ldots\ldots (9)$$

In the case where hysteresis is principally due to shape anisotropy of prolate ellipsoids, the factor ΔI in equations (2) and (3) is equal to $2I_s$, so that substituting equation (9) into equation (3), using the previously assumed values of I_s and H_c and neglecting the term $kT \ln (C\tau)$, we obtain

$$\text{maximum } E_0 = 2{\cdot}09\, v\, H_c\, I_s = 5 \times 10^{-13}\,\text{erg}. \qquad \ldots\ldots (10)$$

The numerical factor 2·09 is included to account for the fact that the observed H_c must be assumed to apply to an assembly of randomly oriented ellipsoids. Equation (10) gives the maximum value of E_0 which can be allowed on the single-domain inclusion theory.

At room temperature kT is 4×10^{-14} erg so that E_0/kT is 12·5. Using this value in equation (1) and assuming Stacey's (1959) value of C the probability of the moment of an inclusion undergoing a spontaneous reversal under the influence of thermal agitation during an interval dt second becomes $2{\cdot}2 \times 10^7\, dt$. Thus the remanence of an alloy of the dispersion-hardened type would decay spontaneously in a time of the order 5×10^{-8} sec if it depended upon single-domain inclusions, or in other words it would have no observable remanence. This problem is not avoided by choosing another value of C; if the single domain inclusion theory is to survive this criticism the following alternatives must be considered: (i) that the maximum size of single domains has been grossly underestimated, (ii) interactions between the inclusions are important.

It appears unlikely that sufficient revision of the estimated maximum size of single domains can be made; if the second alternative is selected then the interactions must be so strong that the concept of independent domains loses its meaning. Therefore it appears that the precipitated phase must be considered merely to break up the domain structure into a finer pattern rather than to form new independent domains. If the inclusions are the important magnetic constituent, as seems probable, and if they are essentially independent, it may be necessary to consider them as multidomains, similar to those occurring in rocks, in some of which high coercive forces are also observed.

References

Kittel, C., 1946, *Phys. Rev.*, **70**, 965.
—— 1949, *Rev. Mod. Phys.*, **21**, 541.
Stacey, F. D., 1959, *Proc. Phys. Soc.*, **73**, 136.
Stoner, E. C., and Wohlfarth, E. P., 1948, *Phil. Trans. Roy. Soc.*, **240**, 599.
Street, R., and Woolley, J. C., 1949, *Proc. Phys. Soc.* A, **62**, 562.
—— 1950, *Ibid.* B, **63**, 509.

Search for New Heusler Alloys

By D. P. MORRIS, R. R. PRESTON†, and I. WILLIAMS‡
Physics Department, University College of North Wales, Bangor

MS. received 4th November 1958

The Heusler alloys form a well-known group of ferromagnetic alloys composed of non-ferromagnetic elements. The general composition is Cu_2MnX, where X may be Al, In, Sn, and possibly Ga, and ferromagnetism is exhibited when the structure is highly ordered, being body-centred cubic with a face-centred cubic superlattice (figure 1 (*a*)). The properties of these alloys have been summarized by Bozorth (1953). The early work of Heusler (1904) also indicated that As, Sb or Bi may replace the Al or Sn of the original alloys but it has not been established whether the ferromagnetism is here associated with a Heusler-type structure or to the presence of the ferromagnetic binary phases MnAs, MnSb, or MnBi.

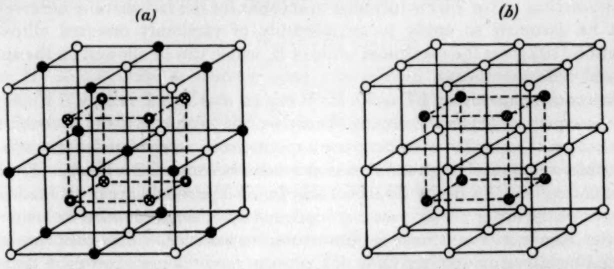

Figure 1. (*a*) Structure of Heusler alloy Cu_2MnAl. (*b*) Structure of alloy Au_2MnAl.

No completely satisfactory explanation of the ferromagnetism of the Heusler alloys is yet available. In general the necessary requirements for ferromagnetism are incomplete groups of electrons and positive exchange interaction. The latter is dependent on the ratio R/r of the atomic diameter (i.e. the internuclear distance between interacting atoms) to the diameter of the incomplete electron shell. Slater (1930) has shown that in general positive interaction occurs when $R/r > 1{\cdot}5$. For the Heusler alloys the R/r values for the Mn atoms lie between 2·84 and 2·98 and are considerably larger than those for the normal ferromagnetics. It has been suggested (Coles, Hume-Rothery and Myers 1949) that direct Mn–Mn interaction is the predominant factor in the ferromagnetism of these alloys but with R/r approaching the critical value at which ferromagnetism will disappear. The alternative explanation of Slater is that interaction could occur between Mn and Cu atoms existing in a divalent state in the alloys. Finally Zener (1951) has suggested that the ferromagnetism is due to coupling between the unfilled d-shells of the Mn atoms and the conduction electrons.

---

† Now at United Kingdom Atomic Energy Authority, Dounreay Experimental Reactor Establishment, Caithness.

‡ Now at De Havilland Aircraft Co., London.

In an attempt to throw further light on this problem we have begun a search for new Heusler alloys by replacing Cu by Ag or Au, the similarity of the binary phase diagrams of many elements with these noble metals suggesting that similar structures may exist in the corresponding ternary systems. No reference to any of the Au ternary alloys could be traced but Potter (1931) has investigated some Ag–Mn–Sn and Ag–Mn–Al alloys. For Ag–Mn–Sn he found that the observed ferromagnetism is due to the presence of the ferromagnetic phases of the binary Mn–Sn system. For Ag–Mn–Al the most magnetic alloy corresponded to the composition Ag_5MnAl which was believed by Potter to be a homogeneous face-centred cubic solid solution similar to Ag. This alloy is now available commercially as a permanent magnet alloy under the name Silmanal. The only subsequent investigation of this system we have traced is that of Geisler (1950), who showed that Silmanal is a precipitation-hardening rather than an ordering alloy but the identity of the precipitate could not be established. Some evidence was obtained for the existence of a Heusler-type structure in the Ag–Mn–Al system, but Ag_2MnAl was always found to contain a large proportion of Ag-rich solid solution, and the Silmanal problem remains unsolved.

It is the purpose of this note to report our findings to date on alloys of nominal composition Ag_2MnAl, Ag_2MnIn, Au_2MnAl, and Au_2MnIn. All the alloys could be machined but the two Au alloys were hard and fairly brittle. In none of these have we observed a Heusler structure but in contrast to the two silver alloys the gold alloys exhibit strong ferromagnetism at low temperatures. More detailed results are given below.

Ag Ternary Alloys

(*a*) *Ag_2MnAl.*

At room temperature powders quenched from 700°c and 530°c consisted almost entirely of face-centred cubic α-solid solution. One or two very faint extra lines were observable but they could not be identified as belonging to a Heusler-type structure. Similar results were found when the samples were photographed in a high-temperature camera. After heat-treatment at 250°c quenched powders consisted of α-solid solution and a β-Mn structure similar to Ag_3Al.

These results establish that no single-phase Heusler structure exists at the composition Ag_2MnAl, and after all heat-treatments the alloy was practically unaffected by a bar magnet even when cooled in liquid air.

(*b*) *Ag_2MnIn.*

This alloy was always found to be single phase with a hexagonal structure similar to Ag_3In, and was paramagnetic down to liquid air temperature.

The Ag alloys thus bear little if any resemblance either structurally or magnetically to the corresponding Cu series.

Au Ternary Alloys

(*a*) *Au_2MnAl.*

Powder samples quenched after three hours at 800°c, 40 hours at 580°c, and 88 hours at 160°c respectively all showed similar single-phase structures of CsCl type, with a lattice parameter of 3·179 Å at 23°c. The CsCl structure may be regarded as two interpenetrating simple cubic lattices 1 and 2, and the observed intensities of the diffraction lines in our alloys indicate that Au atoms lie on lattice 1, with Mn and Al on lattice 2 (figure 1 (*b*)). It is clear that if the Mn and Al atoms could be induced to order on lattice 2 in such a way as to form two interpenetrating face-centred cubic lattices the Heusler structure would be attained, the unit cell having an edge of length 6·358 Å. No superlattice lines corresponding to regions of long-range order of this kind were however detectable on our photographs. The postulated unit cell is in fact considerably larger than that of Cu_2MnAl (5·95 Å), Cu_2MnSn (6·161 Å) and Cu_2MnIn (6·186 Å), and the greater space available for the Mn and Al atoms in the body-centred sites of the Au alloy may make it energetically less favourable for ordering of these atoms to occur here. We are however subjecting our specimens to a prolonged low-temperature anneal in an attempt to develop a higher state of order.

The room-temperature magnetic susceptibility of the alloy is very high (416×10^{-6} e.m.u. g^{-1}), and the $(1/\chi, T)$ curve below 100°c shows a convexity to the T axis similar to that exhibited by most ferromagnetics just above their Curie points. The alloy was very strongly attracted by a bar magnet when cooled in liquid air, but as this is at present the lowest temperature attainable by us we are not able to study the ferromagnetic properties in detail. The $(1/\chi, T)$ curve gives an approximate value of -40°c for the Curie temperature. X-ray photographs taken at liquid-air temperature showed the structure to be still of CsCl type so that the onset of ferromagnetism cannot be attributed to a gross structural change. Ferromagnetism is thus exhibited although the Mn atoms are not apparently highly ordered on the simple cubic lattice 2.

(*b*) *Au_2MnIn.*

This alloy also possessed at room temperature a CsCl structure similar to Au_2MnAl, except that it was not entirely single phase, possibly due to slight departure from stoichiometry. This second phase has not been identified. Again the alloy was ferromagnetic at low temperatures but an additional feature was now found viz. that the CsCl structure had suffered a slight tetragonal deformation on cooling to liquid air temperature. This cubic–tetragonal transformation sets in at about -37°c, the estimated Curie temperature of the tetragonal structure being -130°c.

Our preliminary results clearly call for more detailed investigation. We are unable at present to study the ferromagnetic behaviour exhibited by these alloys at low temperature, but are investigating the possible development of a state of higher order in the CsCl structures, and the cubic–tetragonal transformation in the Au–Mn–In system. We have already established that this transformation occurs at a higher temperature (about 40°C) in $Au_2Mn_{1.5}In_{0.5}$, and this suggests that it may have some relation to the similar transformation in AuMn (Raub, Zwicker and Baur 1953, Giansoldati and Linde 1955, Morris and Preston 1956, Bacon and Street 1958), which is believed to be of antiferromagnetic origin. In $Au_2Mn_{1.5}In_{0.5}$, however, the (χ, T) curve showed no marked anomaly at 40°C, but a small peak occurred near 190°C. Finally we have found that Au_2MnZn, whilst having a structure similar to Au_2MnAl and Au_2MnIn, shows neither a cubic–tetragonal transformation nor ferromagnetism at least down to liquid-air temperature, which indicates that the magnitude if not the nature of the interactions is influenced by the third element in the alloys.

We wish to thank the Council of the Royal Society for a Grant-in-Aid and Professor E. R. Andrew for his encouragement.

REFERENCES

BACON, G. E., and STREET, R., 1958, *Proc. Phys. Soc.*, **72**, 3, 470.
BOZORTH, R. M., 1953, *Ferromagnetism* (New York: Van Nostrand).
COLES, B. R., HUME-ROTHERY, W., and MYERS, H. P., 1949, *Proc. Roy. Soc.* A, **196**, 125.
GEISLER, A. H., 1950, *Amer. Soc. Metals Preprint* No. 9.
GIANSOLDATI, A., and LINDE, J. O., 1955, *J. Phys. Radium*, **16**, 341.
HEUSLER, F., 1904, *Z. angew. Chem.*, **17**, 260.
MORRIS, D. P., and PRESTON, R. R., 1956, *Proc. Phys. Soc.* B, **69**, 849.
POTTER, H. H., 1931, *Phil. Mag.*, **2**, 255.
RAUB, E., ZWICKER, U., and BAUR, H., 1953, *Z. Metallk.*, **44**, 312.
SLATER, J. C., 1930, *Phys. Rev.*, **36**, 57.
ZENER, C., 1951, *Phys. Rev.*, **81**, 440.

Particle Selection in Crystals of CsI(Tl)

BY J. C. ROBERTSON AND A. WARD
Department of Natural Philosophy, The University, Glasgow

MS. received 23rd October 1958

THE decay time τ of the fluorescence produced in crystals of CsI(Tl) by ionizing particles has been shown (Storey, Jack and Ward 1958) to vary with density of ionization. The apparently limiting values of τ for electrons and alpha particles in the energy range of a few MEV are $0{\cdot}70\,\mu$sec and $0{\cdot}42\,\mu$sec respectively, in standard crystals (molar concentration of thallium, $0{\cdot}1\%$) at room temperature.

The technique described here has been developed to make use of this phenomenon to eliminate effects due to backgrounds of electrons in measurements of energy spectra of heavily ionizing particles. A block diagram of the apparatus is shown in figure 1. Integrated current pulses from the photomultiplier are recorded in the usual way by the pulse height analyser when a gate pulse is supplied by a circuit which effectively inspects the decay time of the current pulse from the photomultiplier. The circuit is arranged to produce no gate pulse when the original current pulse was due to an electron in the CsI(Tl) crystal. This is done by clipping the current pulse at the peak height to obtain a narrow pulse of the opposite polarity which is used to charge up a condenser through two crystal diodes. The value of a leakage resistor in parallel with the condenser can be varied (or 'tuned') to make the decay time of the pulse across the condenser coincide with the value of τ for electrons. When this pulse is mixed with the original current pulse the sum of the two is very small for electrons and sufficiently large for alpha particles to overcome the bias in a discriminator on the input of a pulse shaper which supplies a suitable gating pulse to the pulse height analyser. The circuits for the 'tuner' and 'mixer' in figure 1 are very simple but are given for convenience in figure 2. The amplifiers used are I.D.L. type No. 652.

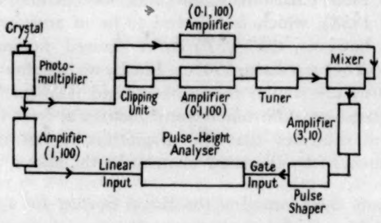
Crystal
Photo-multiplier
(0·1, 100) Amplifier
Mixer
Clipping Unit
Amplifier (0·1,100)
Tuner
Amplifier (3,10)
Amplifier (1,100)
Pulse-Height Analyser
Linear Input
Gate Input
Pulse Shaper

Figure 1. Block diagram of the apparatus. The numbers shown in brackets are the integration and differentiation time constants in the amplifiers. The integration time constant is given first.

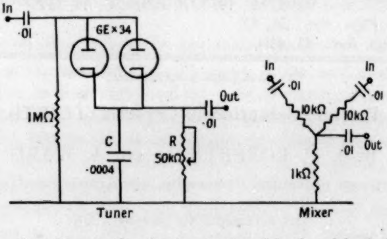
In
·01
GE×34
Out
·01
1MΩ
C
·0004
R
50kΩ
Tuner
In
In
·01
·01
10kΩ
10kΩ
·01
Out
1kΩ
Mixer

Figure 2. Circuits for the 'tuner' and 'mixer' in figure 1.

The operation of the circuits is illustrated by the pulse height distributions in figures 3 and 4, which were obtained using alpha particles from polonium and gamma rays from Th.C″ ($E_\gamma = 2{\cdot}6$ and 0·5 MeV). Figure 3 is the pulse height distribution of pulses from the 'mixer' when the CsI(Tl) was exposed to 2·5 MeV alpha particles and gamma rays. It can be seen that the bias on the discriminator following the mixer can be set above the height of pulses due to electrons. Statistical fluctuations in the peak heights of the original current pulses are the main cause of the relatively large width of the peak due to alpha particles and the finite size of pulses due to electrons. The latter sets an upper limit to the electron energy if pulses due to electrons are to be avoided completely.

The pulse height distributions shown in figure 4 are for the integrated current pulses from the photomultiplier. Figure 4 (*a*) shows the usual distribution obtained by allowing the pulse height analyser to record all pulses. Figure 4 (*b*) shows the effect of the gating pulse in selecting only pulses due to alpha particles.

The positions of the gamma-ray source and the polonium source were kept fixed in obtaining the distributions in figures 3, 4 (*a*) and 4 (*b*), and the counting time in each case was two minutes. The gamma-ray source was removed to obtain the distribution in figure 4 (*c*) which was measured by allowing the pulse analyser to record all pulses, again for two minutes. The points in figures 4 (*b*) and 4 (*c*) above the peak for 2·5 MeV alpha particles are due to alpha particles from polonium on the thin reflector foil above the CsI (Tl) crystal.

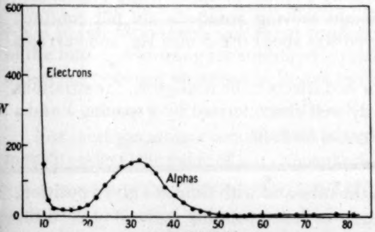

Figure 3.

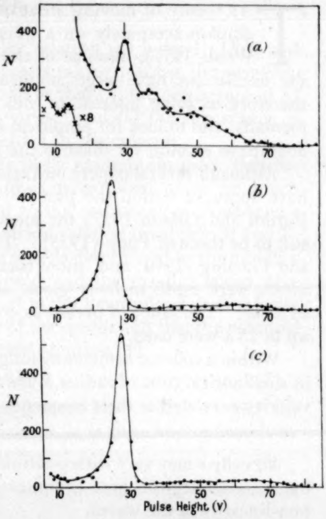

Figure 4.

Figure 3. Pulse height distribution of pulses from the 'mixer' due to 2·5 MeV alpha particles and 0·58 and 2·6 MeV gamma rays.

Figure 4. Pulse height distributions of integrated current pulses from the photomultiplier. In (*a*) and (*b*) the CsI (Tl) was exposed to alpha particles and gamma rays for the same time and under the same conditions in which the distribution shown in figure 3 was obtained. In (*a*) all pulses were recorded by the pulse height analyser. In (*b*) the gating pulse was used to select only pulses due to alpha particles. In (*c*) the gamma-ray source was removed and all pulses recorded by the pulse height analyser for the same time as in (*a*) and (*b*). The peak due to 2·5 MeV alpha particles is indicated by an arrow, pulses above this peak in (*b*) and (*c*) are due to higher energy alpha particles.

In the use of CsI crystals for measuring the energy specrtum of high-energy heavily ionizing particles, the size of the crystal is determined by the range of the highest energy particle to be detected. This lower limit on the thickness of the crystal usually results in unduly large electron backgrounds especially in the lower energy region of the spectrum. A comparison of figures 4 (*a*), 4 (*b*) and 4 (*c*) shows clearly that such large backgrounds of electron pulses can be eliminated.

REFERENCE

STOREY, R. S., JACK, W., and WARD, A., 1958, *Proc. Phys. Soc.*, **72**, 1.

Empirical Relations for Moving Striations

By K. G. EMELEUS† and N. L. OLESON‡

† Queen's University, Belfast.
‡ U.S. Naval Postgraduate School, Monterey, California, U.S.A.

MS. received 26*th November* 1958

The theory of moving striations in positive columns is proving difficult to develop accurately on a quantitative basis (Watanabe and Oleson 1955, Walsh 1957), because of the complexity of the phenomena and because the oscillations have large amplitude and require a non-linear theory. It is therefore of some interest to seek further guidance from data found experimentally, and to look for empirical relations between the quantities involved and attempt to account for these in the first instance on rather general grounds.

Although several papers on various experimental aspects of moving striations have appeared within the past few years (cf. Donahue and Dieke 1951, Pigg, Burton and Oleson 1957) the most extensive and useful data available appear still to be those of Pupp (1935). These have been summarized by Druyvesteyn and Penning (1940) and, more recently, by Francis (1956). Pupp's measurements were made in inert gases, although moving striations are not confined to these. The range of pressures covered was about 0·2–5 mm Hg, and currents up to 15 A were used.

Within a column sufficiently long for end effects to be negligible, the striations in a cylindrical tube of radius R are fairly well characterized by a spacing λ and a velocity v, related to their frequency f by the formula

$$f = v/\lambda. \qquad \ldots\ldots (1)$$

Actually v may vary with position in the tube and with time at a given position, but we shall neglect these complications, which are possibly connected with the non-linearity of the waves.

If p is the gas pressure (reduced to 0°C, to allow for temperature changes, as it is largely the density which matters) and i is the current, Pupp found that

(*a*) $$\lambda/R = F(pR, i/R), \qquad \ldots\ldots (2)$$

(*b*) $$fR = \phi(pR), \qquad \ldots\ldots (3)$$

(*c*) f varied only slightly with i,

(*d*) if fRM is plotted against pR/V_i, where M is the atomic weight and V_i is the ionization potential, the points for krypton, argon and neon lie nearly on one line, and those for helium a little above it. Using c.g.s. and volt-ampere units, F lies between about 9 and 3, and fR between 2×10^2 and 4×10^4, corresponding to striation velocities—towards the cathode—between 10^3 and 10^5 cm sec^{-1}.

We will now make an attempt to see whether equations (1), (2) and (3), and the results of (*d*), can be used to obtain further information, recognizing that this is likely to be at best only semi-quantitative.

Taking first equation (3), we notice that it would be similar to equation (1), if the striation spacing were a constant multiple of the tube radius or

$$\lambda = AR \qquad \ldots\ldots (4)$$

where A is a constant. In this case equations (1) and (3) give

$$v = A\phi(pR). \qquad \ldots\ldots (5)$$

Since p is inversely proportional to the atomic free path, equation (5) indicates that the velocity of the striations considered in equation (1) would depend on the ratio of tube radius to free path. Alternately, with the relation (4) assumed between R and λ, it would show that the velocity depends only on the number of free paths between neighbouring striations.

Equations (1), (2) and (3) can also be combined to give

$$v=\psi(pR, i/R) \qquad \ldots\ldots(6)$$

where ψ is a new function.

In order to explain at all the more complex relation (d) between fRM and pR/V_i, more detailed consideration of the processes taking place in the striations is necessary. The simplest assumptions seem to be that (a) the occurrence of M indicates that the mobility μ of the ions is involved; and (b) the appearance of V_i is connected with the mean longitudinal field X in the column.

If the relation (4) is valid, and the further likely assumption made that the potential difference between striations is V_i, or is proportional to or not much different from it, pR/V_i becomes proportional to the reciprocal of Townsend's parameter X/p. A simplified form of the empirical relation involving M and V_i can now be found if the striae were to have their speeds determined by the mobility motion of the ions in the mean longitudinal field, and the striation speed were equal to (cf. Druyvesteyn 1934) or proportional to the longitudinal drift velocity of the ions. Assuming for simplicity equality of the speeds and that the potential difference between striations is V_i, we have from equation (4)

$$v=X\mu=V_i\mu/(AR). \qquad \ldots\ldots(7)$$

For inert gas atomic ions in their parent gas (except He^+ in He for which the mobility is less) the value of μ at atmospheric pressure, μ_0 is given approximately by

$$\mu_0=4M_{Ne}/M \qquad \ldots\ldots(8)$$

where M_{Ne} is the atomic mass of neon, and the units the conventional v cm sec ones. At pressure p mm

$$\mu=760\mu_0/p=3040M_{Ne}/(Mp). \qquad \ldots\ldots(9)$$

The velocity (equation (7)) becomes

$$v=3040V_iM_{Ne}/(ARMp). \qquad \ldots\ldots(10)$$

Eliminating v between equations (1) and (10), using equation (4) to eliminate λ, and rearranging, with $M_{Ne}=20{\cdot}2$,

$$fRM=6{\cdot}14\ 10^4A^{-2}/(pR/V_i). \qquad \ldots\ldots(11)$$

According to this, the relation between fRM and pR/V_i should be hyperbolic. The graph connecting them is roughly of this form (Druyvesteyn and Penning 1940). The product is not however accurately constant, being for example for the Ne–A–Kr line about 8×10^3 and 6×10^3 for pR/V_i equal to 0·2 and 0·02 respectively; this could be due to changes in A, which are known to occur for smaller currents than those in most of Pupp's discharges. For He the products are also about 30% larger; this might be due to the ratio of molecular ions to atomic ions tending to be greater than for the other gases, resulting in a larger value of effective mobility (Hornbeck and Molnar 1951). For Ne–A–Kr, the constant of proportionality in equation (11) would have the mean experimental value of 7×10^3, if the value of A were approximately 3. A value of 8 can be deduced from data given by Pupp (1935, figure 8). Close agreement cannot be looked for in view of the approximations and assumptions made, but the grouping of p, R, M, p and V_1 in equation (11) is definitely in agreement with Pupp's empirical relation and the form of the latter reproduced rather closely. The use of what is essentially uniform column theory for a longitudinally periodic column may be tentatively justified by the fact that the flux of ions at any point is maintained jointly by the local concentration and potential gradients, and that the mobility is proportional to the diffusion coefficient.

For smaller currents where equation (4) is not satisfactory and the relation (c) not valid, similar, but less simple, relations are also likely to exist. It must however be remembered that the purity of the gases may have been different in high current and low current experiments done hitherto; if, therefore, the properties of the striations depend to any considerable extent, for example, on cumulative ionization via metastable or other excited states, the behaviour of the high current and low current discharges may not be strictly comparable.

ACKNOWLEDGMENT

The authors wish to thank Professor A. B. Stewart for reading this paper and for his comments.

REFERENCES

DONAHUE, T., and DIEKE, G. H., 1951, *Phys. Rev.*, **81,** 248.
DRUYVESTEYN, M. J., 1934, *Physica*, **1,** 1003.
DRUYVESTEYN, M. J., and PENNING, F. M., 1940, *Rev. Mod. Phys.*, **12,** 87.
FRANCIS, G., 1956, *Handb. d. Physik*, **XII,** II (Berlin: Springer), p. 140.
HORNBECK, J. H., and MOLNAR, J. P., 1951, *Phys. Rev.*, **84,** 621.
PIGG, M. K., BURTON, J. B., and OLESON, N. L., 1957, *Proc. Third International Conference on Ionization Phenomena in Gases* (Italian Physical Society, Venice), p. 833.
PUPP, W., 1935, *Phys. Z.*, **36,** 61, and a series of earlier papers.
WALSH, P. J., 1957, *Tenth Annual Gaseous Electronic Conference*, Cambridge, Mass.
WATANABE, S., and OLESON, N. L., 1955, *Phys. Rev.*, **99,** 1701.

Unitary Phase Shift Scattering Approximation

BY L. M. GARRIDO AND P. PASCUAL
Junta de Energia Nuclear, Madrid

MS. received 29*th October* 1958, *in revised form* 17*th December* 1958

§ 1. INTRODUCTION

PARK showed in a recent paper (Park 1957) how to improve the first Born approximation using, essentially, the unitarity relation of the S-matrix. He applies his theory to S-wave square-well potential scattering and finds that his method was better for angles less than 20°.

It is the purpose of this work to generalize such an approach to all orders in the interaction potential. We start from the well-known S-matrix theory (Lippmann and Schwinger 1950, Klein 1956, Garrido 1959) and introduce the unitarity relation in the expression for the phase shifts. By expanding in powers of the interaction we obtain an approximation that, with certain

V. 19

restrictions, is better than the Born approximation of the same order. And this happens to be so for all shift angles that are not close to 45° or 135°. Finally we study the S-wave square well.

§ 2. FORMULATION

We define the $T(E)$ matrix by the relation

$$T(E)=H_1+H_1\frac{1}{E+i\eta-H_0}T(E) \qquad \ldots\ldots(1)$$

$$\eta\to 0^+$$

which may be approximated by iteration in powers of H_1.

The phase-shift angles can be obtained from

$$\tan\delta_l=-\pi\frac{R^2+I^2}{R} \qquad \ldots\ldots(2)$$

where R and I are the real and imaginary parts of the matrix elements of $T(E)$ which are given by

$$\langle\Gamma|T(E)|\Gamma\rangle=\frac{mk(2l+1)}{2\pi^2\hbar^2}\int d^3r\,d^3r'j_{\mathrm{e}}(kr)\langle\mathbf{r}|T(E)|\mathbf{r}'\rangle j_{\mathrm{e}}(kr'). \qquad \ldots\ldots(3)$$

The S-matrix unitarity relation is expressed as

$$I^2+\frac{1}{\pi}I+R^2=0. \qquad \ldots\ldots(4)$$

§ 3. APPROXIMATIONS

Born's n-order approximation consists mainly in the simultaneous evaluation of the real and imaginary parts, R, I, of (3) utilizing the n first terms of (1) and substituting the results into (2).

It is evident that this way the unitarity relation (4) does not hold for the successive approximations.

However unitarity is preserved if we evaluate the imaginary part from

$$I=-\frac{1}{2\pi}\pm\left(\frac{1}{4\pi^2}-R^2\right)^{1/2}, \qquad \ldots\ldots(5)$$

Both solutions are valid. In this case the phase shifts are given by

$$\tan\delta_l=-\frac{1}{2\pi R}\left\{1\mp(1-4\pi^2R^2)^{1/2}\right\}. \qquad \ldots\ldots(6)$$

Here R must be approximated by means of (3) and (1) as above. The minus sign of (5) yields the phase angles between $0°<\delta_l<45°$ and $135°<\delta_l<180°$ while the plus sign yields the angles between $45°<\delta_l<135°$.

According to what has been said above, Born's $(n+1)$-order phase-shift approximation is given by

$$\tan\delta_{\mathrm{B}n+1}=-\pi R_{n+1}-\pi\frac{I_{n+1}{}^2}{R_{n+1}}$$

and the unitary n-order phase shift is

$$\tan\delta_{\mathrm{U}_n}=-\frac{1}{2\pi R_n}\{1\mp(1-4\pi^2R_n{}^2)^{1/2}\}.$$

When we are far away from the critical angles 45° and 135° the expression

$$I_{n+1} = -\frac{1}{2\pi} \pm \left(\frac{1}{4\pi^2} - R_{n+1}^2\right)^{1/2}$$

is valid up to $(n+2)$-order if $I_{n+2} - I_{n+1} \ll I_{n+1}$.

Now if $R_n \gg R_{n+1} - R_n$ then $\tan\delta_{\mathrm{B}_{n+1}} \simeq \tan\delta_{\mathrm{U}_n}$.

Therefore this unitary method gives a better and more rapid approximation when we are far from the critical angles 45° and 135°.

This result can be checked for the S-wave square-well first-order scattering because then the exact phase shift is

$$\tan\delta = \frac{\tan\,[ka(1+V_0/k^2)^{1/2}] - (1+V_0/k^2)^{1/2}\tan ka}{(1+V_0/k^2)^{1/2} + \tan ka \tan\,[ka(1+V_0/k^2)^{1/2}]}.$$

The first Born approximation is

$$\tan\delta_{\mathrm{B}} = \frac{1}{2}\frac{V_0}{k^2}\,[ka - \tfrac{1}{2}\sin 2ka]$$

and this unitary method gives

$$\tan\delta_{\mathrm{N}} = \left[\frac{V_0}{k^2}(ka - \tfrac{1}{2}\sin 2ka)\right]^{-1}\left[1 \mp \left\{1 - \left(\frac{V_0}{k^2}\right)^2 (ka - \tfrac{1}{2}\sin 2ka)^2\right\}^{1/2}\right]$$

when the square well is defined by

$$V(r) = -\frac{V_0\hbar^2}{2m} \qquad r \leqslant a,$$

$$V(r) = 0 \qquad r > a.$$

The results of the calculations when $ka = \pi/4$ are given in the table in agreement with what was said before.

V_0/k^2	$\tan\delta$	$\tan\delta_{\mathrm{U}}$	$\tan\delta_{\mathrm{B}}$	δ	$\epsilon_{\mathrm{U}}(\%)$	ϵ_{B} (%)
0·1	0·01456	0·01435	0·01427	0° 50′	1·43	2·0
0·5	0·07879	0·07246	0·07134	4° 30′	8·03	9·45
1·0	0·17589	0·14566	0·14269	9° 55′	11·0	13·2
1·5	0·29890	0·22485	0·21405	16° 38′	24·8	28·8
2·0	0·45980	0·31344	0·28540	24° 41′	32·6	37·9
2·5	0·68005	0·41841	0·35675	34° 13′	38·4	47·5
3·0	1·00000	0·56454 1·77142	0·42807	45° 0′	43·5 77·1	57·2
3·1	1·0823	1·6571	0·44237	47° 16′	53	59
3·2	1·1728	1·5410	0·4566	49° 33′	31·5	61·2
3·3	1·2730	1·4186	0·47091	51° 51′	11·5	63·5
3·4	1·3900	1·2795	0·4852	54° 17′	7·95	65
3·5	1·5125	1·0485	0·4995	56° 32′	30·6	67

REFERENCES

GARRIDO, L., 1959, *An. Soc. Esp. Fis. Quim.*, in the press.

KLEIN, A., 1956, *Lectures on π-meson Physics*, University of Pennsylvania.

LIPPMANN, B., and SCHWINGER, J., 1950, *Phys. Rev.*, **79**, 469.

PARK, D., 1957, *Proc. Phys. Soc.* A, **70**, 905.

Paramagnetic Resonance of Fe^{3+} in Sapphire at Low Temperatures

By G. S. BOGLE and H. F. SYMMONS†

Commonwealth Scientific and Industrial Research Organization, Division of Physics,
University Grounds, Sydney

MS. received 25th November 1958

The behaviour of paramagnetic ions in corundum (Al_2O_3) is of some importance for the theory of paramagnetism in crystals because of the simplicity of the lattice. We have studied the paramagnetic resonance spectrum of Fe^{3+} in corundum at a frequency of 9 Gc/s and temperatures of 299, 77 and 4·2°K, using a synthetic sapphire containing 0·005 ionic percentage of Fe^{3+} and a natural sapphire with 0·13%. The spectrum of a 0·1% sapphire has also been studied, at room temperatures and frequencies of 25 and 40 Gc/s, by Kornienko and Prokhorov (1957) (hereinafter referred to as KP), but neither the relative nor the absolute signs of the coefficients were determined.

In accordance with KP we find two spectra which coincide when the magnetic field is parallel or perpendicular to the trigonal axis of the crystal. For other directions the spectra are distinct, each exhibiting trigonal symmetry about the axis with the variation of one spectrum displaced 60° in azimuth from the other. Thus there are two types of ion with Hamiltonians identical except for a 60° axial rotation. We were unable to detect the further splitting into four spectra reported by KP; if it exists it must correspond to an azimuthal separation of less than 5°. We do not consider it to be expected from the space group ($R\bar{3}c$) since the four metallic ions in unit cell are related in pairs by inversion.

Our results confirm the spin-Hamiltonian of KP, which is of the same form as that found by Bleaney and Trenam (1954) in the dilute ferric alums:

$$H = g\beta B\,.\,S + D\left(S_z^2 - \tfrac{35}{12}\right) + \tfrac{1}{6}a\left(S_\xi^4 + S_\eta^4 + S_\zeta^4 - \tfrac{707}{16}\right)$$
$$+ \tfrac{7}{36}F\left(S_z^4 - \tfrac{95}{14}S_z^2 + \tfrac{81}{16}\right)$$

where g, β and S have their usual meanings, $S = 5/2$, B is the magnetic induction, and ξ, η and ζ are a set of orthogonal axes with respect to which z (the trigonal axis of the crystal) is the (111) direction. The $\xi\eta\zeta$ axes of both spectra lie in *ac* planes, one set being related to the other by reflection in the *rc* planes. This reflection produces the 60° displacement between the two spectra, and is associated with the *c* glide plane of the lattice.

Values of the Spin-Hamiltonian Coefficients, with D, a, and F in units of $10^{-4}\ cm^{-1}$. The results in the last column are taken from Kornienko and Prokhorov (1957)

T(°K)	4·2	77	299	~290 (KP)
g	2·003 ± 0·001	2·003 ± 0·001	2·003 ± 0·001	2·003 ± 0·001
D	+1719 ± 1	+1716 ± 1	+1679 ± 1	1684 ± 3
$\lvert a \rvert$	224 ± 4	236 ± 4	241 ± 4	262 ± 20
$a - F$	+339 ± 2	+337 ± 2	+329 ± 2	334 ± 2

All the lines of the parallel spectrum, ranging from 1000 to 10 000 gauss, are fitted within the experimental error of ± 5 gauss by the values of the coefficients given in the table.

---

† On leave from the Department of Physics, University of Otago, New Zealand.

The relative signs of $a - F$ and D were determined by the line positions, and the absolute sign of D by the change of relative intensities observed between 77 and 4°K. The sign of a cannot be determined because, owing to the transformation of the Hamiltonian under the 60° azimuthal rotation by which the two types of lattice site are related, a given spectrum may be attributed either to one type of site with one sign of a or to the other with the opposite sign. The determination of a from the parallel spectrum is unusually precise because at 9 Gc/s two transitions occur in a region of crossing energy levels where the normally second-order effect of a becomes almost of first order.

The narrowest observed half-widths at half-height of the resonance lines were 6 and 35 gauss in the 0·005 and 0·13% specimens respectively. The line-widths attributable to paramagnetic neighbours, calculated by an adaptation of the formula of Kittel and Abrahams (1953) are 1 and 20 gauss respectively. Since Pound (1950) has found a width of only 1·5 gauss in the nuclear resonance of ^{27}Al in corundum, it appears that the line-width in the more dilute specimen is mainly due to crystal imperfections. In neither specimen was hyperfine structure from ^{57}Fe observed.

A study of the recovery from saturation at 4·2°K in the 0·005% specimen yielded a spin–lattice relaxation time of 7 ± 2 milliseconds.

The zero-field eigenstates and energies calculated from the spin-Hamiltonian for 4·2°K are

$$|\pm\tfrac{1}{2}\rangle + 0{\cdot}032\,|\mp\tfrac{5}{2}\rangle \text{ at zero frequency}$$

$$|\pm\tfrac{3}{2}\rangle \text{ at } 12{\cdot}03 \pm 0{\cdot}02 \text{ Gc/s}$$

$$\text{and} \quad |\pm\tfrac{5}{2}\rangle - 0{\cdot}032\,|\mp\tfrac{1}{2}\rangle \text{ at } 31{\cdot}30 \pm 0{\cdot}04 \text{ Gc/s.}$$

Owing to the state-mixing of the highest and lowest levels a transition probability of 0·02 free-spin units exists between them. Sapphire is thus suitable for a zero-field maser (Bogle and Symmons 1959) with pumping and amplifying frequencies of 31·3 and 12·0 Gc/s. For magnetic field masers sapphire offers a wide range of frequencies with high transition probabilities, and the fact that the splitting of the $|\pm\tfrac{1}{2}\rangle$ states in a small field B perpendicular to the axis is nearly $6\beta B$ will permit the use of unusually low fields. A concentration of not less than 0·05% would be desirable.

The specific heat may be expected to show a Schottky anomaly at temperatures of a few tenths of a degree absolute. This property, coupled with the robustness and high thermal conductivity of sapphire, should make it useful for demagnetization experiments in that temperature region.

REFERENCES

BLEANEY, B., and TRENAM, R. S., 1954, *Proc. Roy. Soc.* A, **223**, 1.

BOGLE, G. S., and SYMMONS, H. F., 1959, *Aust. J. Phys.*, **12**, in the press.

KITTEL, C., and ABRAHAMS, E., 1953, *Phys. Rev.*, **90**, 238.

KORNIENKO, L. S., and PROKHOROV, A. M., 1957, *J. Exp. Theor. Phys.*, **33**, 805. (Translation: *Soviet Physics JETP*, 1958, **6**, 620.)

POUND, R. V., 1950, *Phys. Rev.*, **79**, 685.

The Variability of the Recombination of Hydrogen Atoms on Metal Surfaces

By J. W. FOX, A. C. H. SMITH and E. J. SMITH
Department of Physics, University College London

Communicated by H. S. W. Massey; MS. received 22nd December 1958

§ 1. Introduction

The measurement of the heat of recombination of H atoms on certain metallic surfaces has frequently been used to determine atomic concentrations in mixtures of atoms and molecules (Poole 1937). The probability of recombination γ has usually been assumed constant for a particular metal (Bonhoeffer 1924, Katz, Kistiakowsky and Steiner 1949). The purpose of this note is to emphasize the variability of γ that may occur, particularly in relation to calorimetric methods of determining atomic concentrations.

§ 2. Calorimetry

We have had considerable experience with two distinct types of calorimeter. The first, a continuous-flow calorimeter, consists essentially of a rhodium-plated, baffled tube around which a steady flow of water is maintained and through which the mixture of atoms and molecules is pumped. In the second, a micro-calorimeter, atoms and molecules effuse through an orifice system into a small platinum box and the steady temperature of the box is measured by a thermocouple, the elements of which provide the predominant path for loss of heat from the box. An electrical heating coil fixed to the box is used for calibration. Latterly the box has been replaced by a baffled tube. Our experiments with micro-calorimeters have been characterized by a decrease of reading with time, even after baking out the whole instrument. This phenomenon has been consistently observed using atoms produced from dry or damp hydrogen in d.c. or r.f. discharges, both in phosphoric acid-coated, and clean glass systems. The surface of the calorimeter evidently becomes progressively poisoned, probably by substances formed in the discharge or by chemical reactions involving H atoms in other parts of the system. The poisoning may become so severe that atoms can survive multiple collisions in, and emerge from baffled tubes. The poisoned surface can be reactivated by baking out, by bombardment with an intense flux of H atoms and by exposure to a discharge plasma.

§ 3. The Effect of Temperature on Poisoning

The poisoning and reactivation process is well illustrated by some experiments in which a thermocouple probe (Pt–Pt-Rh) was moved axially along a clean glass tube down which a mixture of atoms and molecules was pumped. One junction of the thermocouple, a sphere of diameter very small compared with the mean free path, was exposed to the atoms, the leads being sheathed in fine silica tubing. Some typical results are shown in figures 1 and 2. In figure 1 AB represents the variation of e.m.f. generated by the thermocouple as the hot junction is moved downstream, the atomic concentration decreasing owing to recombination of atoms on the glass tube and to pumping. The junction is left at B for a few minutes and is then returned upstream. Instead of the original curve being retraced, the lower curve BC is generated, indicating a poisoned probe surface with consequent decrease in γ. At C a clean-up by atom bombardment takes place. This clean-up process is illustrated in figure 2. The curve AB (figure 1) is quite reproducible provided that the surface of the thermojunction is activated when starting at A and provided other conditions, e.g. discharge, wall surface, are constant. The irreversibility is only observed if the temperature of the junction at B is less than a critical value in the neighbourhood of 150°c; the poisoning is more pronounced the longer the probe is maintained at B.

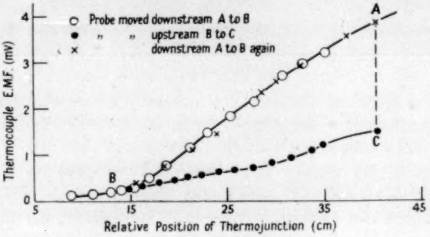

Figure 1.

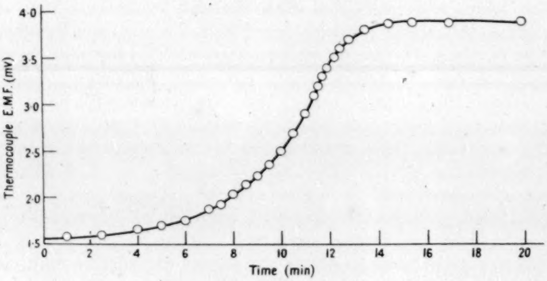

Figure 2. Clean up by H atom bombardment. This curve refers to portion CA of figure 1.

The thermocouple probe suffers from the disadvantage that no independent control of the temperature of the recombining surface is possible. This is overcome by using a fine wire heated by a variable electric current. The resistance of the wire and the electrical power dissipated in it are measured with the wire in molecular hydrogen and then in a mixture of small atomic concentration at sensibly the same pressure. At a given temperature, as determined by the wire resistance, the difference in electric power dissipated in the two cases is equal to the power generated at the wire surface by recombination of atoms. In this way it is possible to study the variation of γ as a function of wire temperature. We have carried out experiments with wires of platinum, tungsten and palladium and have observed a similar irreversible behaviour to that of the thermocouple probe. It appears that γ increases with temperature up to about 150°c for all three metals and then shows little variation up to 800°c, the limit of our experiments. Tungsten appears to poison more rapidly than platinum; the case of palladium is complicated by the change of resistance produced by occluded hydrogen, but it behaves otherwise in a similar manner to platinum.

Previous experiments on these lines (Roginsky and Schechter 1934) showed a variation of γ with temperature which was interpreted as indicating an activation energy for the reaction of gas atoms with those in a surface monolayer to produce molecules. It is clear from our experiments that such interpretation must bear in mind the complication of surface poisoning. We are now repeating the measurements with atomic hydrogen produced on a hot tungsten filament in order to eliminate the discharge as a source of poisoning agents, with the aim of studying further the temperature variation of γ.

A detailed account of our work will be published later.

REFERENCES

BONHOEFFER, K. F., 1924, *Z. Phys. Chem.*, **113,** 199.
KATZ, S., KISTIAKOWSKY, G. B., and STEINER, F., 1949, *J. Amer. Chem. Soc.*, **71,** 2258.
POOLE, H. G., 1937, *Proc. Roy. Soc.* A, **163,** 404.
ROGINSKY, S., and SCHECHTER, A., 1934, *Acta Phys.-Chim., U.R.S.S.*, **1,** 318.

LETTERS TO THE EDITOR

Radio Observations of the Lunar Surface

Recent lunar observations by radar methods found that the surface is surprisingly smooth to centimetre and metre length waves, and that, in contrast with the behaviour at optical wavelengths, the reflection is almost specular. Evans (1957) gives a power scattering law $P(\theta) = \cos^{30}\theta$ at a wavelength of $2\frac{1}{2}$ metres; Trexler (1958) finds that at $1\frac{1}{2}$ metres 50% of the returned echo power is received within $50\mu\mu$sec of the front edge of the pulse, equivalent to a similar law; Yaplee, Bruton, Craig and Roman (1958) observe that at 10 cm short pulses are reflected mainly from a similar region. The purpose of this note is to show from a statistical consideration of reflection and diffraction at the surface that the above results are explicable by a quite reasonable terrain, and to indicate that further experiments could reveal some characteristics of the surface.

Reflection by an irregular surface.

An electromagnetic signal originating from the earth reaches the moon with a wave front which is almost plane. If the surface features which intercept it are smooth over areas greater than several Fresnel zones, specular reflection will occur, and the power leaving the whole surface will be distributed over angles equal to twice the surface gradients. If the r.m.s. surface gradient of undulations on a plane is ψ_0 the reflected power is distributed with r.m.s. angle from the normal $\theta_0 = 2\psi_0$.

Diffraction by an irregular surface.

If the surface irregularities are much smaller than the Fresnel zones a diffraction treatment is necessary. Suitable theory, summarized by Ratcliffe (1956), has been developed for the study of irregularities in the terrestrial ionosphere. Let the height of a plane surface fluctuate about the mean with standard deviation h, and suppose the spatial correlation coefficient of the height variations as a function of distance along the surface, $\rho(d)$, follows a Gaussian law, $\rho(d) = \exp(-d^2/2d_0^2)$. d_0 is known as the structure size, being that value of d for which $\rho(d) = 0{\cdot}61$. If plane waves of length λ are incident on the surface, the phase corrugations imposed on the reflected wave front will have standard deviation $\phi = 4\pi h/\lambda$ radians and structure size d_0. The modulation is said to be shallow if $\phi < 1$; then the structure size l_0 in the receding wave equals d_0. But if the modulation is deep, $\phi > 1$, a smaller structure $l_0 = d_0/\phi$ will appear in the receding wave, and at great distance will dominate. Bowhill (1957) showed that at a great distance from the surface the random power of the initial phase variation becomes equally shared between fluctuations in the phase and amplitude of the signal, both having r.m.s. value $\phi/\sqrt{2}$. Moreover, the linear structure size in the wave front will be the same whether measured from the phase or amplitude variations. The apparent power spectrum is the Fourier transform of the spatial correlation coefficient, and can be represented by $P(\theta) = \exp(-\theta^2/2\theta_0^2)$ where $\theta_0 = \lambda/2\pi l_0$ for small θ_0. Hence, shallow modulation on a distant surface gives a power spectrum width $\theta_0 = \lambda/2\pi d_0$, and deep modulation gives $\theta_0 = \phi\lambda/2\pi d_0 = 2h/d_0$. At metre and centimetre wavelengths the lunar surface will impose deep modulation. These formulae are rigorously true for irregularities which extend in one dimension only, but have been found numerically close to computations for the two-dimensional case which concerns us.

Lunar scattering.

The scattering properties of the lunar surface can be determined by radar from the earth because signals scattered through an angle θ, by whatever mechanism, are received only from an annulus on the moon at which the earth's zenith angle is $\frac{1}{2}\theta$. A specular moon only returns signals from an area in the centre of the lunar disc and at the point nearest the earth, whereas a diffusing moon returns signals from the whole hemisphere facing the earth. It has been shown that areas greater than the Fresnel zones distribute the radiation over an angle $\theta_0 = 2\psi_0$, and irregularities less than the Fresnel zones over an angle $\theta_0 = 2h/d_0$. The radius of the first Fresnel zone is 1·4 km at $\lambda = 2\frac{1}{2}$ m, 300 m at $\lambda = 10$ cm, and about 1·5 m for visible light. Clearly, both mechanisms are relevant, and it is of interest that each gives a numerically similar result, since $\psi_0 \sim h/d_0$ (Longuet-Higgins 1957). Thus the observed spectrum is determined, first, by the average gradient of the surface, sampled in areas a few Fresnel zones in magnitude, and, second, by the diffraction within those areas, which depends on the average gradient within them. The result of Evans, $P(\theta) = \cos^{30}\theta$, is closely represented by a Gaussian with $\theta_0 = 0{\cdot}18$ radian. Therefore $h/d_0 \leqslant 0{\cdot}09$ and $\psi_0 \leqslant 5°$, implying average gradients not greater than about 1 in 10, which is likely to be the case in natural terrain sampled in areas several kilometres across. Reduction of the wavelength reduces the Fresnel zones and the size of the samples; the resolution of observation to smaller surface objects is thereby increased. If the shape of the irregularities is independent of their size, so that the average values of ψ_0 over the larger irregularities and h/d_0 over the smaller ones remains constant, θ_0 should not vary with the observing wavelength. The uniform brightness observed visually is evidence that the average gradient increases if the samples are sufficiently reduced. This would be expected of an undulating surface covered with smaller, rounder, objects such as rocks and stones. Radar observations at shorter wavelength should be able to determine where the spectrum broadens, so giving some interesting statistical information about the features of the moon's surface.

This approach may also find application to some terrestrial problems, such as the back-scattering of radio waves from the ground.

I am indebted to Dr. J. V. Evans and Dr. F. G. Smith for helpful discussions.

9 Red Lane,
Frodsham,
Nr. Warrington, Lancs.
27th November 1958.

J. K. Hargreaves.

Bowhill, S. A., 1957, *J. Atmos. Terr. Phys.*, **11**, 91.
Evans, J. V., 1957, *Proc. Phys. Soc.* B, **70**, 1105.
Longuet-Higgins, M. S., 1957, *Phil. Trans. Roy. Soc.* A, **250**, 20.
Ratcliffe, J. A., 1956, *Rep. Progr. Phys.*, **19**, 188 (London: Physical Society).
Trexler, J. H., 1958, *Proc. Inst. Radio Engrs*, **46**, 286.
Yaplee, B. S., Bruton, R. H., Craig, K. J., and Roman, N. G., 1958, *Proc. Inst. Radio Engrs*, **46**, 293.

The Transition $\mathrm{v}^1\Sigma^+ - \mathrm{x}^1\Sigma^+$ in Hydrogen Chloride

As is well known, the ground electronic state of hydrogen chloride correlates, at infinite internuclear separation with the ground state atoms, H + Cl. The existence of a stable, highly ionic, excited state, $\mathrm{v}^1\Sigma^+$, was predicted many years ago (Pauling 1932), and some of the properties of this state were discussed by Mulliken (1936, 1937). In particular, Mulliken considered that the state v would probably dissociate into $\mathrm{H} + \mathrm{Cl}(3s^2\,3p^4\,4s)$, lying about 0·5 ev below $\mathrm{H}^+ + \mathrm{Cl}^-$, and that the energy separation $\mathrm{V}(\sigma\pi^4\sigma^*) - \mathrm{Q}(\sigma^2\pi^3\sigma^*)$, where Q represents the upper states of the continuous ultra-violet absorption spectrum (Romand 1949), should be about the same as the separation $\mathrm{A}^2\Sigma^+(\sigma\pi^4)$–$\mathrm{X}^2\Pi_i(\sigma^2\pi^3)$ in HCl^+.

Electrodeless discharges through hydrogen chloride vapour give rise to the emission of a many-line spectrum in the ultra-violet region. Photographs taken on a 1-m grazing incidence vacuum spectrograph show that it extends at least to 1800 Å: at the long wavelength end the spectrum cuts off sharply at about 2375 Å. We have photographed the spectrum in the range 1980 to 2375 Å on a Hilger E.478 large quartz spectrograph, using ordinary HCl, $\mathrm{H}^{35}\mathrm{Cl}$ and DCl. Of the 2000 lines measured in the HCl spectrum about 1000, including most of the strong lines, have been assigned to 15 bands involving $v' = 0$, 1 and 2 in $\mathrm{v}^1\Sigma^+$ and $v'' = 10$ to 16 in $\mathrm{x}^1\Sigma^+$. The agreement between the infra-red and ultra-violet constants for the ground state of $\mathrm{H}^{35}\mathrm{Cl}$ is illustrated in figure 1. Constants for $\mathrm{v}^1\Sigma^+$ are as follows: $T_0 = 76\,210$, $\omega_e = 880\ \mathrm{cm}^{-1}$, $r_e = 2{\cdot}43$ Å.

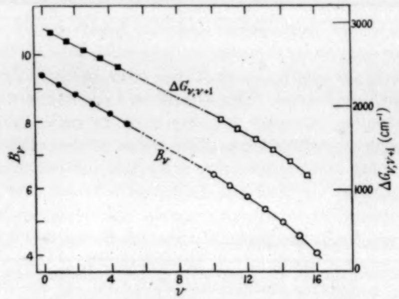

Figure 1. Values of $\Delta G_{v,\,v+1}$ and of B_v plotted against v for the ground state of $\mathrm{H}^{35}\mathrm{Cl}$. Black circles and squares represent points from the vibration–rotation spectrum (Herzberg 1950). Open circles and squares represent points from the present analysis of the ultra-violet bands.

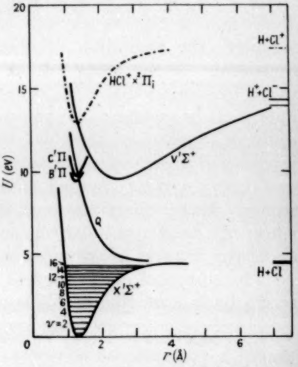

Figure 2. Potential energy–distance curves for the known states of HCl. The state $\mathrm{v}^1\Sigma^+$ is shown as dissociating to $\mathrm{H}^+ + \mathrm{Cl}^-$: in fact it is more probable (Mulliken 1937) that the dissociation products are $\mathrm{H} + \mathrm{Cl}\ (3p^4\ 4s\ {}^2p)$.

Potential curves for the known states of HCl are given in figure 2. The separation V–Q in HCl (at $r = r_e''$) is 3·6 ev, in good agreement with the separation $\mathrm{A}^2\Sigma^+$–$\mathrm{X}^2\Pi$ (at $r = r_e''$) of $3{\cdot}8_5$ ev.

A continuum with $\lambda_{\max}=2570$ Å observed in the same sources may arise from the transition V–Q.

This result has led us to consider an alternative interpretation of the spectra analysed and ascribed to HF^+ and DF^+ by Johns and Barrow (1957). By an unexpected arithmetical accident, it proves possible to assign new vibrational quantum numbers to the lower state, which both fit the HF–DF isotope shifts, and which show that the transition is not in fact $B^2\Sigma^+–A^2\Sigma^+$ in HF^+, but $V^1\Sigma^+–X^1\Sigma^+$ in HF. Thus there is now no spectroscopic information about HF^+, and the previous agreement between the spectroscopic and electron-impact values (Frost and McDowell 1958) of the ionization potential was quite fortuitous.

The corresponding spectrum $V–X^1\Sigma^+$ in HBr has been photographed in this laboratory by Mr. J. G. Stamper, and the analysis of this work will be published in due course.

Our best thanks are due to Dr. A. E. Douglas, who sent us an excellent plate of the long wavelength end of the HCl spectrum, to Professor K. Clusius, who gave us a generous sample of $H^{35}Cl$, which enabled us to evaluate the chlorine isotope effect, and to the Department of Scientific and Industrial Research for a Studentship (J. K. J.).

Physical Chemistry Laboratory,
Oxford University.
26th November 1958.

J. K. JACQUES.
R. F. BARROW.

FROST, D. C., and MCDOWELL, C. A., 1958, *Canad. J. Chem.*, **36**, 39.
HERZBERG, G., 1950, *Molecular Spectra and Molecular Structure I. Spectra of Diatomic Molecules* (New York: Van Nostrand).
JOHNS, J. W. C., and BARROW, R. F., 1957, *Nature, Lond.*, **179**, 374, 1186.
MULLIKEN, R. S., 1936, *Phys. Rev.*, **50**, 1017.
—— 1937, *Ibid.*, **51**, 310.
PAULING, L., 1932, *J. Amer. Chem. Soc.*, **54**, 988.
ROMAND, J., 1949, *Ann. Phys., Paris*, **4**, 528.

REVIEWS OF BOOKS

A Handbook of Lattice Spacings and Structures of Metals and Alloys, by W. B. Pearson. Pp. x + 1044. (London, New York, Paris, Los Angeles : Pergamon Press, 1958.) 12½ guineas.

This Handbook is Volume 4 of the International Series of Monographs on Metal Physics and Physical Metallurgy, under the general editorship of G. V. Raynor. It contains information on all binary and ternary alloys examined up to 1956, presented in tabular form and followed by detailed and critical summaries of the relevant publications. A rapid scrutiny revealed full coverage of the literature, and no errors, in the sections selected for test.

It seems doubtful whether the elementary general introduction in Part I is really needed for those who will use Part II, but as Part I occupies less than 8% of the whole volume its deletion would not have reduced the deplorably high price from the level where only libraries can buy, to one within the reach of the individual scientist. W. H. TAYLOR.

Les Ondes Centimétriques, by G. Raoult. Pp. viii + 401. (Paris : Masson, 1958.) 6.500 *fr.* (linen cardboard, 7.300 *fr.*).

The author, who is Professeur à la Faculté des Sciences de Clermont-Ferrand, bases the book on a course given to the students there. The aim is successfully achieved of providing, in the French language, an introduction to the study of microwave techniques, which can be appreciated with the minimum of mathematics, thus linking conventional physics textbooks with the more advanced and specialized literature on the subject. Thus the book, comprising some 400 pages, is a worthwhile addition to those available to the French student, who, unlike his English counterpart, has had to read much of the work on microwaves in a foreign language.

The first five chapters, dealing with the transmission of microwaves, are well illustrated, a good feature being the inclusion of worked examples, such as the use of the Smith chart to evaluate impedances. Waveguide components and various high frequency measurements are described in the next four chapters. Klystrons and magnetrons are then treated in fair detail and brief mention is made of travelling-wave-tube amplifiers and backward wave oscillators. The chapter on microwave detection extends from a consideration of energy levels in a semiconductor to the physical form of point contact diodes as video detectors or as microwave mixers. Aerial theory necessarily involves rather more mathematics, but the balance of the chapter is maintained by clear diagrams of horns, guide-fed dipoles, linear arrays, dielectric radiators, etc., together with the polar diagrams obtained in practice. The use of quasi-optical devices in microwave instrumentation is discussed as an illustration of optical theory. The two short final chapters deal with two uses of microwave techniques in branches of pure science, i.e. radio-astronomy and paramagnetic resonance. The appendices are devoted to units and some of the underlying electromagnetic theory.

Taken as a whole, the book is logically planned and the task of selecting the topics which can be covered in one volume of this size has been accomplished well. An especially attractive feature is the large number of clear diagrams, which should be of great assistance to a physics student in enabling him to appreciate, for example, the electric and magnetic field patterns of various modes of propagation in a waveguide and their use to explain coupling into other structures, and also dissected perspective views of valves such as cavity magnetrons. There are a few small points about which the expert may quibble, but these do not detract significantly from a textbook which succeeds in giving a general background to the subject, against which the student may more profitably read the specialized literature. The book is well bound and clearly printed on good paper, the clear diagrams and photographs completing an attractive appearance. C. R. DITCHFIELD.

Integral Equations, by F. SMITHIES. Pp. vii + 172. Cambridge Tracts in Mathematics and Mathematical Physics No. 49. (Cambridge : University Press, 1958.) 27*s*. 6*d*.

It would not be proper for this reviewer to attempt to pass judgment on the mathematical worth, or even content, of a volume such as this which appears to set forth in beautiful clarity the theory of linear integral equations of the second kind. It is entirely proper, however, if he indicates whether a mathematical text is likely to be useful to physicists, and comments upon it from this point of view. Integral equations of the second kind are now the most fashionable tool of theoretical physicists, particularly of those engaged in the quantum theory of scattering processes. Furthermore, there is a regrettable shortage of textbooks which deal appropriately with the techniques involved in solving these integral equations. The physicist is therefore only too glad to welcome a new text if it shows him how to solve equations similar to those with which he is faced. Unfortunately, this book is not of this kind; for it restricts itself to non-singular equations and thereby rules out many of the more interesting applications to scattering theory from the beginning. Moreover, the fact that few examples are given explicitly and those merely to illustrate more pathological features, is more likely to irritate than to educate the average physicist. Finally, our dispirited physicist may well wonder why, out of 25 presently available *Tracts in Mathematics and Mathematical Physics*, so called, only two seem to have any bearing on mathematical physics. If it were merely that the *Tracts* were misleadingly named, this would not matter : but there is a real need for books of just this size, price and scope, which do genuinely deal with the more specialized methods of mathematical physics. B. H. FLOWERS.

Applied Analysis, by CORNELIUS LANCZOS. Pp. xx + 539. (London : Pitman, 1957.) 55*s*.

The titles of the seven chapters are : Algebraic Equations, Matrices and Eigenvalue Problems, Large-scale Linear Systems, Harmonic Analysis, Data Analysis, Quadrature Methods, and Power Expansions. There are also Appendices containing formal and numerical information relevant to the processes which are described in the text.

The kernel of Lanczos' thinking in this book is that, in numerical analysis, the problem is not the absolute accuracy of the ' pure ' mathematician to obtain a desired accuracy with a minimum of means, but to obtain the maximum accuracy which can be obtained by limited means, and for this kind of process the author has coined the word ' parexic '. These portmanteau chapter headings, however, give only the vaguest indication of the variety of topic and the fertility of suggestion which each chapter contains.

Lanczos' contributions to various branches of Numerical Analysis are well known to those who work in the subject. They have an imaginative originality and this is characteristically evident in the book under review.

This is not a treatise, but a collection of longish, loosely connected chapters, dealing with those topics upon which Lanczos has thought and worked, and his freshness of outlook permeates the book.

The first chapter, one of the shorter ones, is one of the least convincing, but in the chapters on matrix processes and on harmonic analysis and its applications the author is on surer ground.

The author has not been well served by his proof-readers, and printing errors are too common. There are also some numerical mistakes—not mere printers' errors—and, here and there, quite unintelligible sentences. These defects, however, cannot hide the merits of the book, and, although the tyro must read it with care, none who has more than a cursory interest in numerical analysis can afford to ignore this stimulating and suggestive book. W. G. B.

Classical Mechanics, by J. W. LEECH. Methuen Monographs on Physical Subjects. Pp. ix + 149. (London : Methuen ; New York : John Wiley, 1958.) 12*s.* 6*d.*

This is a very useful little book. No one can understand physics who is not familiar with the elements of classical mechanics : and for the understanding of quantum mechanics, more than a superficial acquaintance with classical mechanics is required. There is therefore a real need for a concise treatment of classical mechanics, which is admirably fulfilled here.

The exposition is always clear and crisp. The premisses of any argument are clearly stated and when their analysis would lead beyond the scope of the book, as in the critical discussion on the basis of Newton's laws of motion, this is frankly said without any attempt to gloss over the omission. Starting from Newton's laws, their application to mechanical systems, along the lines of d'Alembert's principle, is developed. Lagrange's equations, Hamilton's canonical equations, Hamilton's variational principle and the Hamilton–Jacobi transformation are discussed in separate chapters. The analogies between geometrical and wave optics, and between geometrical optics and particle mechanics are succinctly brought out.

There is a separate chapter on Poisson brackets, whose importance in classical mechanics is enhanced by the simplicity of their quantum-mechanical definition. The chapter on relativistic mechanics gives the relativistic generalizations of the previous classical mechanics of particles, first with the time, and then with the proper-time, as the development parameter. There are chapters on continuous systems, and fields, whose relevance to quantum field theory has no need to be stressed.

This is a book which deserves high praise. It contains all that it should, and nothing that it should not. M. H. L. PRYCE.

Concepts of Classical Optics, by JOHN STRONG. Pp. xxii + 692. (San Francisco: W. H. Freeman; London: Bailey Bros. and Swinfen, 1958.) $9.50.

This book contains an introduction to optics (370 pp. on wave-theory and 100 pp. on geometrical optics) followed by 16 appendices whose total length is about 300 pages. Each of the first 15 appendices is an article on some modern development by a specialist in the appropriate field. In the text the standard propositions of classical optics are developed " with mathematics of modest rigour " and the sixteenth appendix introduces the reader to this mathematics. The main topics of wave theory are treated at a level between that of a general degree and a special honours physics course in a British University. In regard to technical optics and practical applications, the book goes beyond the standard of most of our special honours courses.† The author has omitted or treated very briefly (*a*) the interaction of radiation and matter, (*b*) quantum theory, (*c*) spectroscopy and (*d*) crystal optics. The section on geometrical optics is divided into four chapters on (i) Images of Points by Single Surfaces (this includes something on aberrations and on aspherical surfaces), (ii) Images of Points by Systems of surfaces, (iii) Aperture and Field and (iv) Aberrations.

In the main text the author quotes *in extenso* from original papers and from other books. Most of the appendix material has been written by other writers. This plan has both advantages and disadvantages. With regard to the main text the author might fairly retort to a critic that he quotes with acknowledgments (and with permission when the author is living), whereas others paraphrase without permission. The choice of a different writer for each appendix gives the reader immediate contact with several very distinguished workers in optics. Zernike's account of microscope image formation in relation to phase-contrast is just what is needed in this book and only Zernike could have written it so well. The article by Jacquinot on Apodization is also very good but some of the other material is not suitable for separation into short articles. Five of the appendices are on Applications of Interferometry (a reprinted chapter of W. E. Williams' book), Interferometers (Dyson), Köster's Prism (Saunders), Savart's Plate (van Heel) and Interferometric Spectroscopy (Vanasse and Strong). Each of these is good in itself and a teacher of optics who can fill in the gaps may like to have the material presented this way. For the student it would be better to have the subject treated as an integrated whole in the main text.

Even though the feast is rich something must be omitted. The author has probably omitted the application of information theory and spatial frequency analysis because he considers them too difficult for his readers. I wish that Bergstrand's method for the velocity of light had been described (instead of Anderson's) and the Benoït, Fabry and Pérot determination of the metre (instead of Michelson's). However, these are small grumbles. I wish to recommend this highly individual and interesting book especially to university lecturers and young research workers. R. W. DITCHBURN.

---

† I refrain, with some difficulty, from discussing whether this pinpoints a fault in our courses.

Solid State Physical Electronics, by A. van der Ziel. Pp. xii + 604. (London: Macmillan, 1958.) 37*s*. 6*d*.

This book sets out to give a comprehensive discussion of the physical mechanisms which are called into play in the operation of a large number of devices which now make use of the electronic properties of solids. In such a ' comprehensive ' treatment there is a grave danger that in attempting to instil a little knowledge of everything one ends up with an adequate knowledge of nothing. The present text does not altogether avoid this danger, and while a number of topics are dealt with fairly fully, many are treated in a very sketchy fashion. Nevertheless the author succeeds in giving a panoramic view of the vast field which he has attempted to cover. The book is intended as a course for students of electrical engineering, and while it should serve as an introduction to the subject, a good deal of wider reading will be needed to provide the student with an adequate knowledge of any one of the many types of device discussed.

The book is divided into four main sections. The first deals with the basic atomic and solid-state physics used in the discussion of devices in the later sections. It seems a great pity that the first two chapters have been included in a book already over-crowded: they deal with very elementary quantum theory and simple atomic spectra. A large number of excellent *elementary* accounts of these topics is already available and it seems stretching the word ' comprehensive ' a long way to include them in the present book. There is perhaps a little more justification for the inclusion of the next two chapters on elementary quantum statistics, crystal structure and the electronic structure of solids, though the treatment is so sketchy that it might have been better to be content with reference to existing literature.

The next main section of the book deals with thermionic emission, the photoelectric effect and devices such as vacuum tubes, photocells, photomultipliers etc. Then follows a section on semiconductor devices such as transistors, junction diodes, solar batteries etc., and the book ends with a discussion of the properties of dielectrics and magnetic materials and of their uses. The treatment varies greatly, some devices being discussed clearly and concisely while in other instances the treatment is very sketchy.

The printing and general presentation are good and the price, for a book containing such a wealth of information, is very modest. The treatment is generally clear and concise as should be expected from a well-tried course of lectures from which the book originated. It should serve its intended purpose as an introduction to this rapidly growing and important subject. R. A. SMITH.

The Capture of Negative Pions in Hydrogen and Deuterium—I : Hydrogen

By J. A. KUEHNER†, A. W. MERRISON‡ and S. TORNABENE§
Nuclear Physics Research Laboratory, University of Liverpool

MS. received 26*th June* 1958

Abstract. A high-energy pair spectrometer has been used to determine the ratio of the radiative to mesonic capture of pions stopped in liquid hydrogen. This measurement agrees well with the value expected from the charge-exchange scattering and photoproduction of pions.

§ 1. Introduction

The experiments carried out by Panofsky, Aamodt and Hadley (1951) on the capture of negative pions in hydrogen and deuterium gave a number of results which were vital to pion physics. They showed that the charged pion has odd parity and gave values for the masses of the neutral and negative pions. Shortly after, Anderson and Fermi (1952) showed, by a simple theoretical argument, that the hydrogen experiment provided a link between meson photoproduction experiments and the charge-exchange scattering of negative pions by protons.

Panofsky's experiments with hydrogen studied the radiative and mesonic capture of negative pions in mesonic hydrogen atoms, the reactions being

$$\pi^- + p \rightarrow n + \gamma, \qquad \ldots\ldots(1)$$

$$\pi^- + p \rightarrow n + \pi^0. \qquad \ldots\ldots(2)$$

The gamma rays from these processes were studied with a high energy pair spectrometer and their energies and relative intensities studied. It has been shown by Wightman (1950) and by Brueckner, Serber and Watson (1951) that by far the most probable fate of a negative pion slowed down in liquid hydrogen is that it should form a mesonic atom and then be captured by the proton from a K-orbit.

Anderson and Fermi pointed out that if one measured the relative rates of reactions (1) and (2) and deduced the absolute rate for radiative capture from meson photoproduction data, then one could deduce the absolute rate of the mesonic capture, which corresponds to charge-exchange pion–proton scattering. This gives a value for $(\alpha_3 - \alpha_1)/\eta = 0{\cdot}19 \pm 0{\cdot}04$ radian (Bethe and de Hoffmann 1955) where α_3 and α_1 are the S-wave phase shifts for pion–nucleon scattering in the $T = 3/2$ and $T = 1/2$ states. The value deduced by Orear (1954) from the best fit to the scattering data is $(\alpha_3 - \alpha_1)/\eta = 0{\cdot}27 \pm 0{\cdot}03$ radian.

Because of this discrepancy it was clearly important to check the original measurement of Panofsky. We have used a pair spectrometer with focusing properties rather different to those of Panofsky's instrument to do this. We have also taken advantage of the large external pion beam now available from the Liverpool synchrocyclotron and have stopped the mesons in this beam in a liquid hydrogen target.

---

† Now at Atomic Energy of Canada Ltd., Chalk River.

‡ Now at CERN, Geneva.

§ Now at Atomic Energy Research Establishment, Harwell, Berks.

§ 2. Experimental Arrangement

The general arrangement of apparatus is shown in figure 1. Negative pions of mean energy 100 Mev were produced by bombardment of an internal target in the synchrocyclotron, spiralled out through the fringe field of the cyclotron magnet, and were focused by a strong-focusing octupole magnet and a small wedge magnet. The wedge magnet served also to clear the beam of unwanted particles, and the final intensity of the beam was 8×10^4 pions per second with a contamination of 4% μ mesons and 15% electrons. The beam was monitored by a small scintillation counter and then slowed down in a block of polythene.

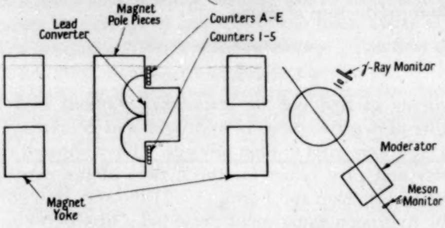

Figure 1. Layout of experiment.

A proportion of the pions finally stopped in a spherical liquid hydrogen target of diameter 16 in. As a check on the monitoring, a scintillation telescope with a lead converter detected the gamma rays from mesons stopped in the liquid hydrogen target. Figure 2 shows the counting-rate in this telescope as a function of polythene absorber thickness.

The pair spectrometer is '180° focusing' (Walker 1948), and has two banks of five scintillation counters each. This type of focusing has two main advantages: firstly, the gamma-ray energy is proportional to the detector separation and is independent of the horizontal position of pair creation in the converter; and secondly, the angular effects in the resolution are minimized. The phosphors are blocks of plastic scintillator 1 in. × $\frac{3}{4}$ in. × $3\frac{3}{4}$ in., the $3\frac{3}{4}$ in. × 1 in. face being presented to the electrons. Adjacent phosphors are separated only by a thin aluminium foil which acts as a light-seal. The light is transmitted to photomultipliers outside the magnetic field of the spectrometer by Perspex light guides. The distance between the central phosphors of each bank is 22 in., which gives an energy resolution of $4\frac{1}{2}$% (see § 5).

The magnet has a maximum field of 15 000 gauss across a $3\frac{1}{2}$ in. gap. The pole pieces are shaped so that there is a clearing field 9 in. long before the gamma rays reach the converter. The field was electronically stabilized to better than 0·1%, and the field for all magnet settings was measured during experimental runs to better than 0·1% by a nuclear resonance magnetometer. The general field shapes were plotted using the magnetoresistance of a bismuth spiral. The deviation of the electron tracks from perfectly circular arcs amounted to 1·4% at the highest field settings. A correction was made for this effect.

A simplified block diagram of the electronics of the pair spectrometer is shown in figure 3. Each detector provides a 'fast' and a 'slow' pulse. The fast pulses from each bank are paralleled to a fast coincidence unit. If a fast coincidence between the two banks of detectors is recorded, a 'gate' is opened and the slow pulses are allowed to pass through to amplitude discriminators and an analysing matrix of coincidence circuits which records the pair of counters that have detected the electron pair.

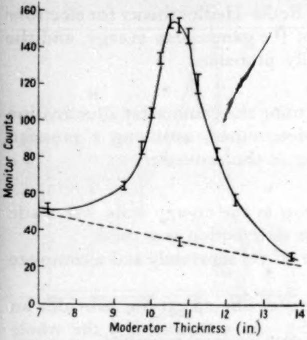

Figure 2.

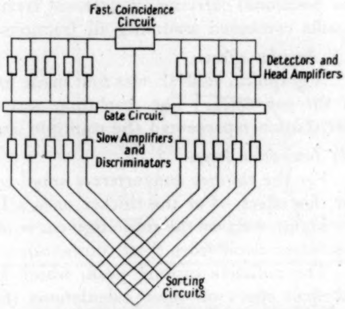
Fast Coincidence Circuit
Detectors and Head Amplifiers
Gate Circuit
Slow Amplifiers and Discriminators
Sorting Circuits

Figure 3. Block diagram of electronics.

Before all experimental runs, the spectrometer was set up and its performance checked by observing the gamma rays from an internal target bombarded by protons.

§ 3. Experimental Procedure

Because of the limited energy range of the spectrometer $(1 \pm \frac{1}{4})E$ for a mean energy E, each run was broken up into four different magnetic field settings. At each of these field settings the converter thickness was chosen so that the Coulomb scattering of the electrons into the pole pieces remained the same. In this way no corrections need be made for this effect throughout the energy spectrum. The thickest converter used in a normal run was 0·017 in. A thicker set of converters was used to check resolution and efficiency and this will be discussed below.

The background due to unwanted gamma rays was measured by removing the hydrogen from the target, and was found to be negligible. The background from other effects was measured by removing the converter. It was found that this background was nearly independent of the magnetic field setting. However, as thinner and so less efficient converters were used at the lower energies the background was most troublesome here, and for the lowest energy channels was equal to the effect.

§ 4. Resolution and Treatment of the Experimental Data

Although the radiative and mesonic gamma rays were resolved, it was still essential to know the resolving power of the instrument so that the experimental points could be fitted by the correct resolution curve. The main components of the resolution are (*a*) finite detector width, (*b*) energy loss of the electrons in the converter due to bremsstrahlung production, (*c*) angular effect, which includes geometrical effects and horizontal scattering of the electrons, and (*d*) ionization losses of the electrons in the converter. These will be discussed briefly.

(*a*) *Finite detector width.*

The finite widths of a pair of detectors lead to a triangular resolving curve with a full width at half height of 4%.

(*b*) *Bremsstrahlung losses.*

These were calculated numerically from the Bethe–Heitler theory for electrons (or positrons) carrying off different fractions of the gamma-ray energy, and the results combined assuming all fractions equally probable.

(*c*) *Angular effects.*

A graphical analysis was first made to determine the gamma-ray illumination of the converter. The resolution was then determined, assuming a gaussian distribution represented the multiple scattering in the converter.

(*d*) *Ionization losses.*

For the thinner converters a small correction to the energy scale was made for this effect. For the thicker ones a Landau distribution was used.

Figure 4 shows the resolution curve of these effects separately and a complete resolution curve from their combination.

The radiative capture peak, which is a natural line spectrum, provides an excellent check on these calculations (figure 5). As a further test the whole experiment was repeated using a set of converters which was four times as thick as the set used in a normal run. To make this test more sensitive the two sets of results were subtracted and an analysis carried out on the difference. The results fitted by the calculated resolution curve are shown in figure 6.

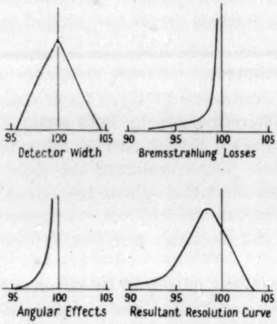

Figure 4. Major causes of resolution width. Resultant resolution curve.

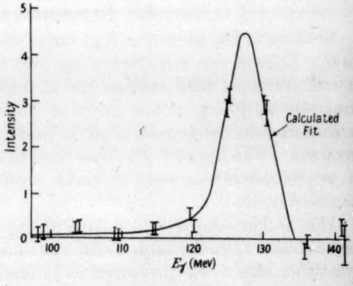

Figure 5. High energy spectrum with thin converter.

Resolution curves for the mesonic capture spectrum were obtained by folding the instrumental resolution curve with the natural spectrum shape, which is rectangular. The experimental results obtained for the mesonic capture peak are shown in figure 7. Several corrections have to be applied to these curves before one can deduce the relative intensity of the two processes. The major correction is for the variation of the pair production cross section with energy, for which we used the results of Davies, Bethe and Maximon (1954). Smaller corrections had to be made for gamma-ray absorption in the hydrogen target (3%), dependence of the efficiency on the fractional energy given to the electron (4%), and corrections for electrons or positrons detected in more than one channel (5%). The correction for the overlap of the spectra of the two reactions was less than 1%.

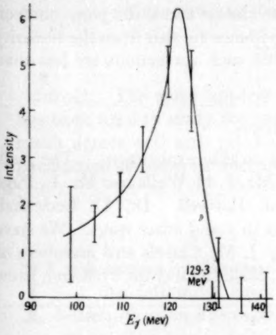

Figure 6. Difference spectrum between thick and thin converters.

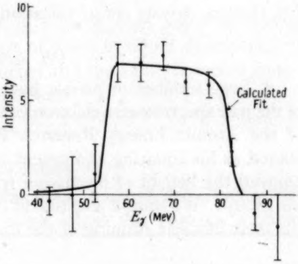

Figure 7. Low energy spectrum.

§ 5. Discussion

Cassels *et al.* (1957) have measured the Panofsky ratio with a total energy Cerenkov counter. Their result, together with ours and Panofsky's, is given in the table and the weighted mean calculated. The errors quoted are standard deviations.

Panofsky *et al.*	Cassels *et al.*	This paper	Weighted mean
$0{\cdot}94 \pm 0{\cdot}30$	$1{\cdot}50 \pm 0{\cdot}15$	$1{\cdot}60 \pm 0{\cdot}17$	$1{\cdot}52 \pm 0{\cdot}11$

One can deduce the absolute rate of the mesonic capture reaction at zero energy and hence $(\alpha_3 - \alpha_1)/\eta$, if one knows the Panofsky ratio and the absolute value of the radiative capture reaction. A value for the latter may be deduced from the photoproduction experiments $\gamma + \mathrm{p} \rightarrow \pi^+ + \mathrm{n}$ and the ratio at threshold

$$r_0 = \frac{\sigma(\gamma + \mathrm{d} \rightarrow \pi^- + \mathrm{p} + \mathrm{p})}{\sigma(\gamma + \mathrm{d} \rightarrow \pi^+ + \mathrm{n} + \mathrm{n})}.$$

If one assumes that

$$r_0 = \frac{\sigma(\gamma + \mathrm{n} \rightarrow \pi^- + \mathrm{p})}{\sigma(\gamma + \mathrm{p} \rightarrow \pi^+ + \mathrm{n})}$$

then one can deduce a value for $\sigma(\gamma + \mathrm{n} \rightarrow \pi^- + \mathrm{p})$ and hence of its inverse. Beneventano *et al.* (1956) give a value for the S-wave part of the reaction

$\gamma + p \to \pi^+ + n$ as $(1{\cdot}43 \pm 0{\cdot}02)\eta \times 10^{-28}$ cm^2 where η is the pion momentum in units of *c*. They give also a value for $r_0 = 1{\cdot}87 \pm 0{\cdot}13$. These results give the S-wave part of the reaction $\pi^- + p \to n + \gamma$ as $(4{\cdot}69 \pm 0{\cdot}33)\eta \times 10^{-28}$ cm^2 and hence $(\alpha_3 - \alpha_1)/\eta = 0{\cdot}25 \pm 0{\cdot}03$ radian. This agrees very well with the recent Orear value of $0{\cdot}27 \pm 0{\cdot}015$ radian.

The above arguments ignore the charge-dependent corrections which were introduced by Noyes (1956). However, it can be shown that if the pion–nucleon interaction has a short range, and there is good evidence for this from the linearity of the S-wave phase shifts and other sources, then such corrections are less than 1% (Dalitz, private communication).

§ 6. ACKNOWLEDGMENTS

A large number of people have contributed to this experiment. The bulk of the pair spectrometer electronics was built by Mr. F. H. Wells and Mr. L. Page of the Atomic Energy Research Establishment, Harwell. Dr. D. Eccleshall loaned us his counting equipment and helped us in many other ways. We have enjoyed the benefit of discussion with Professor J. M. Cassels and members of his group. We should also like to thank Mr. B. Halliday and the cyclotron crew for their efficient running of the machine.

REFERENCES

ANDERSON, H. L., and FERMI, E., 1952, *Phys. Rev.*, **86**, 794.
BENEVENTANO, M., BERNARDINI, G., CARLSON-LEE, D., STOPPINI, G., and TAU, L., 1956, *Nuovo Cim.*, **4**, 323.
BETHE, H. A., and DE HOFFMANN, F., 1955, *Mesons and Fields*, Vol. 2 (New York : Row, Peterson), p. 99.
BRUECKNER, K., SERBER, R., and WATSON, K., 1951, *Phys. Rev.*, **81**, 575.
CASSELS, J. M., FIDECARO, G., WETHERELL, A. M., and WORMALD, J., 1957, *Proc. Phys. Soc.* A, **70**, 405.
DAVIES, H., BETHE, H. A., and MAXIMON, L. C., 1954, *Phys. Rev.*, **93**, 788.
NOYES, H. P., 1956, *Phys. Rev.*, **101**, 320.
OREAR, J., 1954, *Phys. Rev.*, **96**, 176.
PANOFSKY, W. K. H., AAMODT, R. L., and HADLEY, J., 1951, *Phys. Rev.*, **81**, 565.
WALKER, R. L., and MCDANIEL, B. D., 1948, *Phys. Rev.*, **74**, 315.
WIGHTMAN, A. S., 1950, *Phys. Rev.*, **77**, 521.

The Capture of Negative Pions in Hydrogen and Deuterium—II : Deuterium

By J. A. KUEHNER,† A. W. MERRISON‡ and S. TORNABENE§
Nuclear Physics Research Laboratory, University of Liverpool

MS. received 26th June 1958

Abstract. The same apparatus described in a companion paper on hydrogen has been used to study the radiative capture of pions in liquid deuterium. The result agrees well with previous measurements and the value expected from the production of pions in nucleon–nucleon collisions.

§ 1. Introduction

It was shown by the experiments of Panofsky, Aamodt and Hadley (1951) that the following reactions could occur when the pion in a mesonic deuterium atom was captured:

$$\pi^- + d \rightarrow n + n + \gamma, \qquad \ldots\ldots(1)$$

$$\pi^- + d \rightarrow n + n. \qquad \ldots\ldots(2)$$

The reaction $\pi^- + d \rightarrow n + n + \pi^0$ was not observed. As gamma rays only were detected in these experiments, the existence of the non-radiative capture was inferred by observing the relative rate of gamma-ray production in mesonic hydrogen and deuterium atoms. In hydrogen the reactions $\pi^- + p \rightarrow n + \gamma$ and $\pi^- + p \rightarrow n + \pi^0$ are the only reactions which can occur and if the relative rates of these are known, then the non-radiative part of the deuterium capture can be deduced. That this reaction occurs at all was perhaps the most important result of Panofsky's experiments, for Ferretti (1946) had shown earlier that if the capture takes place in an S-state, as it does in this case (Wightman 1950), then the pion must have odd intrinsic parity. Panofsky obtained for the relative rate of non-radiative capture to radiative capture in deuterium, the value $2{\cdot}37 \pm 0{\cdot}75$.

Brueckner, Serber and Watson (1951) have shown too that this ratio can be used to link the photo-production of positive pions to their production in proton–proton collisions. Because the values of the Panofsky ratio of mesonic to radiative capture in the mesonic hydrogen atom which have been determined recently (Kuehner, Merrison and Tornabene 1959, Cassels *et al.* 1957) are considerably different from Panofsky's original value, it was clearly imperative to repeat the deuterium experiment to see whether there is now any serious discrepancy between the photoproduction and proton–proton production data. We have used the external pion beam of the Liverpool synchrocyclotron and a large pair spectrometer to do this, as we did in our similar experiment with hydrogen (Kuehner, Merrison and Tornabene 1959). Essentially the experiment compared the number of gamma rays from pions stopped in identical volumes of liquid hydrogen and liquid deuterium. As in Panofsky's experiment, the ratio of non-radiative to radiative capture in deuterium can then be inferred.

---

† Now at Atomic Energy of Canada Ltd., Chalk River.
‡ Now at CERN, Geneva.
§ Now at Atomic Energy Research Establishment, Harwell, Berks.

§ 2. APPARATUS AND EXPERIMENTAL ARRANGEMENT

The experimental arrangement differed principally from that used for the hydrogen experiment only in the target. In the present experiment a target vessel was used which could be filled either with liquid hydrogen or liquid deuterium. This target was designed by Dr. S. G. F. Frank of this laboratory. The hydrogen (or deuterium) is condensed from the gas phase into the target in a condenser surrounded by liquid hydrogen. The target also has the very important facility that it may be emptied and then refilled quickly, so that background runs may be made.

The pair-spectrometer was visually positioned so that its collimator channel was in line with the target. The useful height of the target was defined by this collimator while the width was defined by the diameter of the target. It was assumed in the calculations of the energy resolution of the spectrometer that this area acted as a uniform source of gamma rays.

The meson beam was monitored independently by a small scintillation counter and an ionization chamber in the beam. These monitors agreed to within 2%. To reduce background counts to a minimum a large amount of shielding, in the form of lead bricks and iron-loaded concrete blocks, was placed between the pair-spectrometer detectors and the meson beam.

The experiment was first run with hydrogen and was broken up into runs of one to two hours duration. The total running-time on this part of the experiment was 18 hours, of which about one-third was spent in measuring the background. The change-over to deuterium took three days, and then 25 hours total running-time were spent with the deuterium target, of which 6½ hours were spent measuring the background. The counting rates were approximately 0·7 count per minute with either hydrogen or deuterium in the target and 0·1 count per minute with the target empty.

§ 3. RESULTS

The pair-spectrometer was set to cover an energy range from 100–140 MeV. The 'tails' on both the hydrogen and deuterium spectra extend below this. The tail in the hydrogan case is, of course, due solely to the experimental resolution of the instrument and had been investigated thoroughly in the previous hydrogen experiment. In the deuterium spectrum there is a natural broadening as it represents a three-body decay, and we have used the theory of Watson and Stuart (1951) and the experimental results of Phillips and Crowe (1954) to estimate this effect. Watson and Stuart's calculations extend down to 120 MeV only. Fortunately, however, most of the gamma rays are emitted with energies above this. In fitting the results above 120 MeV we used a value of $\hbar c\alpha = -12$ MeV, where α is the inverse of the scattering length for the singlet neutron–neutron force. The spectrometer was also set in one run to observe the gamma rays between 40 and 80 MeV but no significant number of gamma rays was detected here.

The procedure used to determine approximately the shape of the energy spectrum between 80 and 120 MeV was to draw in a set of smooth curves and, after folding the known resolution with this set of curves, to fit the resultant curves to the experimental points. A least-squares fit on each curve then gives the curve which best fits the experimental points, and the standard deviation to be assigned to the total area under the spectrum. This error was $\pm 6{\cdot}7\%$.

Figure 1 shows the calculated curves for hydrogen and deuterium fitted to the experimental points. The curves have been normalized to the same number of incoming mesons. The ratio of the areas under these curves multiplied by the ratio of the atomic densities of liquid deuterium and liquid hydrogen gives the ratio of radiative capture in hydrogen to that in deuterium. The result is

$$\frac{\text{Radiative capture in hydrogen}}{\text{Radiative capture in deuterium}} = \frac{(\mathrm{H})_{\gamma+\mathrm{n}}}{(\mathrm{D})_{\gamma+2\mathrm{n}}} = 1{\cdot}34 \pm 0{\cdot}13.$$

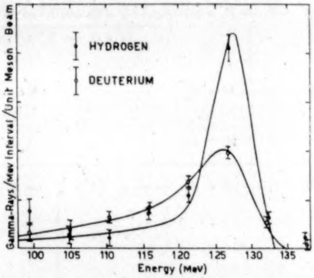

Figure 1. Gamma-ray spectra for hydrogen and deuterium.

If we now assume that *only* radiative and non-radiative capture takes place in deuterium, and only radiative and mesonic capture takes place in hydrogen then we can write:

$$\frac{(\mathrm{D})_{2\mathrm{n}}}{(\mathrm{D})_{2\mathrm{n}+\gamma}} = \frac{(\mathrm{H})_{\mathrm{n}+\gamma}}{(\mathrm{D})_{2\mathrm{n}+\gamma}} \left[\frac{(\mathrm{H})_{\mathrm{n}+\pi^0}}{(\mathrm{H})_{\mathrm{n}+\gamma}} + 1 \right] - 1.$$

The ratio $(\mathrm{H})_{n+\pi^0}/(\mathrm{H})_{n+\gamma}$ is given in the previous paper (Kuehner, Merrison and Tornabene 1959) as $1{\cdot}50 \pm 0{\cdot}15$. Using this value we obtain the ratio

$$\frac{\text{Non-radiative capture in deuterium}}{\text{Radiative capture in deuterium}} = 2{\cdot}35 \pm 0{\cdot}35.$$

This values agrees very well with the $2{\cdot}37 \pm 0{\cdot}75$ found by Panofsky, Aamodt and Hadley (1951).

§ 4. Discussion

The argument connecting the pion photoproduction from hydrogen to the production in nucleon–nucleon collisions (see figure 2) depends on first separating out the S-wave part of the photoproduction. This may be done from the results of Beneventano *et al.* (1956) to give a value for

$$\sigma_{\mathrm{S}}(\gamma + \mathrm{p} \rightarrow \pi^+ + \mathrm{n}) = (1{\cdot}43 \pm 0{\cdot}02)\eta \times 10^{-28}\ \mathrm{cm}^2$$

where η is the pion momentum in units of μc. Beneventano *et al.* also give a value for the ratio of the photoproduction of negative pions to positive pions from deuterium at threshold,

$$r_0 = \frac{\gamma + \mathrm{d} \to \pi^- + \mathrm{p} + \mathrm{p}}{\gamma + \mathrm{d} \to \pi^+ + \mathrm{n} + \mathrm{n}} = 1{\cdot}87 \pm 0{\cdot}13.$$

If one assumes that

$$r_0 = \frac{\gamma + \mathrm{n} \to \pi^- + \mathrm{p}}{\gamma + \mathrm{p} \to \pi^+ + \mathrm{p}},$$

then one can deduce a value for $\sigma_{\mathrm{S}}(\gamma + \mathrm{n} \to \pi^- + \mathrm{p})$ or, by detailed balancing, its inverse. The above results give $\sigma_{\mathrm{S}}(\pi^- + \mathrm{p} \to \mathrm{n} + \gamma) = (4{\cdot}69 \pm 0{\cdot}33)\ \eta \times 10^{-28}\ \mathrm{cm}^2$. To obtain from this a value for the radiative capture cross section in deuterium, one can use the argument of Brueckner, Serber and Watson which essentially

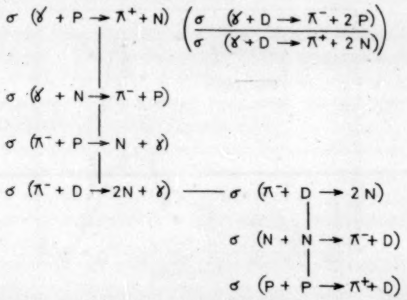

Figure 2. Connection between photoproduction and nucleon–nucleon production of mesons.

is based on the impulse approximation and calculates the different phase space available for the one neutron in the hydrogen case and the two neutrons in the deuterium case, to arrive at

$$\frac{\sigma_{\mathrm{S}}(\pi^- + \mathrm{d} \to \mathrm{n} + \mathrm{n} + \gamma)}{\sigma_{\mathrm{S}}(\pi^- + \mathrm{p} \to \mathrm{n} + \gamma)} = \frac{2}{3}.$$

And so we can deduce a value for $\sigma_{\mathrm{S}}(\pi^- + \mathrm{d} \to \mathrm{n} + \mathrm{n} + \gamma)$, and hence from the present experiment a value for $\sigma_{\mathrm{S}}(\pi^- + \mathrm{d} \to \mathrm{n} + \mathrm{n})$. Again by detailed balancing one arrives at $\sigma_{\mathrm{S}}(\mathrm{n} + \mathrm{n} \to \pi^- + \mathrm{d}) = (0{\cdot}17 \pm 0{\cdot}03)\eta \times 10^{-27}\ \mathrm{cm}^2$. This agrees very well for the directly measured value for the charge symmetric reaction (Crawford and Stevenson 1955) of $\sigma_{\mathrm{S}}(\mathrm{p} + \mathrm{p} \to \pi^+ + \mathrm{d}) = (0{\cdot}14 \pm 0{\cdot}01)\eta \times 10^{-27}\ \mathrm{cm}^2$, and shows that any deviations from charge symmetry near threshold in these reactions is small.

ACKNOWLEDGMENTS

We owe a great deal to Dr. S. G. F. Frank for the loan of his target and the help he gave us during the experimental runs. Dr. R. H. Dalitz gave us very generously a great deal of theoretical advice, particularly in the ratio of radiative capture in deuterium and hydrogen. As in our experiment on hydrogen, we have enjoyed and greatly benefited from discussion with Professor J. M. Cassels.

REFERENCES

BENEVENTANO, M., BERNARDINI, G., CARLSON-LEE, D., STOPPINI, G., and TAU, L., 1956, *Nuovo Cim.*, **4,** 323.

BRUECKNER, K., SERBER, R., and WATSON, K., 1951, *Phys. Rev.*, **81,** 575.

CASSELS, J. M., FIDECARO, G., WETHERALL, A., and WORMALD, J., 1957, *Proc. Phys. Soc.* A, **70,** 405.

CRAWFORD, F. S., and STEVENSON, M. L., 1955, *Phys. Rev.*, **97,** 1305.

FERRETTI, B., 1946, *International Conference on Fundamental Particles and Low Temperatures, Cambridge* (London: Physical Society).

KUEHNER, J. A., MERRISON, A. W., and TORNABENE, S., 1959, *Proc. Phys. Soc.*, **73,** 545.

PANOFSKY, W. K. H., AAMODT, R. L., and HADLEY, J., 1951, *Phys. Rev.*, **81,** 565.

PHILLIPS, R. H., and CROWE, K. M., 1954, *Phys. Rev.*, **96,** 484.

WATSON, K., and STUART, R., 1951, *Phys. Rev.*, **82,** 738.

WIGHTMAN, A. S., 1950, *Phys. Rev.*, **77,** 521.

Internal Pair Emission at Small Angles

By G. GOLDRING
Weizmann Institute of Science, Rehovot

Communicated by S. Devons; MS. received 10*th December* 1958

Abstract. The process of electron positron pair emission in nuclear electromagnetic transitions is investigated in the special case where the angle between the directions of emission of the electron and positron is small. It is shown that experimentally this process can be of value in determining the absolute emission rates of high energy γ-rays.

---

§ 1. Introduction

The emission of pairs from nuclei has been studied so far mainly as a tool for determining the multipolarity of electromagnetic transitions (Horton 1948, Rose 1949, Goldring 1953). It has already been noted (Devons and Goldring 1954) that this information is most appropriately obtained in measurements on pairs in which the angle between positron and electron is large, where the ' large ' angles Θ are defined by $1-\cos\Theta > 1/k$, and k is the transition energy in units of mc^2. In this region of large angle pairs both the angular distribution and the spectrum at any given angle depend strongly on the multipolarity of the transition. Other features of this region are weak dependence of the pair emission intensity on the transition energy, and a rather complicated dependence on the orientation of the momenta in space in cases where the γ-ray emission is not isotropic. A different region with quite distinct characteristics is the ' small angle ' region $1-\cos\Theta < 1/k$. Here the emission intensity is almost independent of multipolarity but strongly dependent on k, and the spatial distribution of the momenta is very simple: it will be shown in the following paragraph that it is essentially the same as the angular distribution of the γ-rays emitted in the same transition.

The difference between the two regions can be understood qualitatively in the following way: the small angle pairs are produced at a large distance from the nucleus, in the radiation zone of the multipole field where the electromagnetic field approximates the field pattern at infinity, whereas the large angle pairs are produced close to the nucleus, in the ' near zone ', where the field depends mainly on the structure of the radiating multipole.

§ 2. General Considerations

The number of electron positron pairs emitted per quantum into solid angles $d\Omega_+, d\Omega_-$ and positron energy interval dW_+ in any given transition, may be computed from the transition matrix elements given by Goldring (1953). We shall deal specifically with integrated distribution functions which are obtained from the original functions by integrating over the energy W_+ and by averaging over the azimuthal angles of the momenta $\mathbf{p}_+$, $\mathbf{p}_-$ about the total momentum $\mathbf{q}$, $(\mathbf{q}=\mathbf{p}_+ + \mathbf{p}_-)$. These distribution functions can be written for M*l* transitions:

$$F_{\mathrm{M}l}(k,\Theta,\hat{\mathbf{q}})d\Omega_+ d\Omega_- = \frac{\alpha k^2}{60\pi^2}\Phi_1{}^l(k_1\Theta)f_1{}^l(\hat{\mathbf{q}})d\Omega_+ d\Omega_- \qquad \ldots\ldots (1)$$

for E*l* transitions:

$$F_{\mathrm{E}l}(k,\Theta,\hat{\mathbf{q}})d\Omega_+ d\Omega_- = \frac{\alpha k^2}{60\pi^2}\left\{\Phi_1{}^{l-1}(k,\Theta)f_1{}^l(\hat{\mathbf{q}}) - \frac{l^2}{l(l+1)}\Phi_0{}^{l-1}(k,\Theta)f_0{}^l(\hat{\mathbf{q}})\right\} d\Omega_+ d\Omega_-$$

where

$$\Phi_1{}^l(k,\Theta) = 15\int_1^{k-1}\frac{p_+p_-}{k^3}\left(\frac{q}{k}\right)^{2l}\left\{\frac{4}{(k^2-q^2)^2} - \frac{2}{k^2-q^2}\frac{(\mathbf{p}_+\times\mathbf{p}_-)^2}{q^2}\right\}dW_+$$

$$\Phi_0{}^l(k,\Theta) = 30\int_1^{k-1}\frac{p_+p_-}{k^3}\left(\frac{q}{k}\right)^{2l}\frac{4}{(k^1-q^2)^2}\left\{W_+W_-\left(\frac{q}{k}\right)^2 + \frac{(\mathbf{p}_+\mathbf{q})(\mathbf{p}_-\mathbf{q})}{q^2} - \frac{W_+}{k}(\mathbf{p}_-\mathbf{q}) - \frac{W_-}{k}(\mathbf{p}_+\mathbf{q})\right\}dW_+.$$

$f_1{}^l(\hat{\mathbf{q}}), f_0{}^l(\hat{\mathbf{q}})$ are angular distribution functions; $f_1{}^l$ is the distribution function for the γ-rays emitted in the given transition (as determined by the degree of polarization of the nucleus before emission), and $f_0{}^l$ is the distribution function of a spinless particle emitted in the same transition with angular momentum l.α is the fine structure constant, and natural units $(\hbar = m = c = 1)$ have been used.

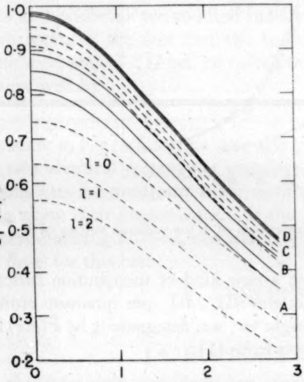

Figure 1. $\Phi_1{}^l(k,\epsilon)$ as a function of ϵ for various values of k, l. A, $k=6$; B, $k=10$; C, $k=15$; D, $k=32$. Values of l as in A.

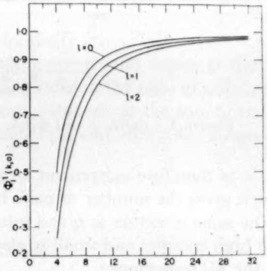

Figure 2. $\Phi_1{}^l(k,0)$ as a function of k for various values of l.

The integration over W_+ has in this case been carried out for a fixed position of the vector $\mathbf{q}$. This does not correspond to the situation usually encountered in experimental arrangements where the integration over W_+ is carried out for fixed positions of the vectors $\mathbf{p}_+$, $\mathbf{p}_-$. However, if $\mathbf{p}_+$, $\mathbf{p}_-$ are nearly parallel, the distinction becomes unimportant, and this is in fact one of the reasons for the relative simplicity and ease of interpretation of the small angle emission.

In the region of small angles, the most convenient parameter for the description of the angle Θ between the momenta of the electron and the positron is ϵ, defined by $1-\cos\Theta=\epsilon^2/k^2$.

In figures 1, 2 and 3 $\Phi_1{}'(k, \epsilon)$ and $\Phi_0{}^l(k, \epsilon)$ are given for various values of k, l and ϵ. $\Phi_0{}^l(k, \epsilon)$ is rather insensitive to ϵ and is drawn for just two values of this parameter. It is apparent from the figures that if $k \gg 1$ and $\epsilon < 3$ then $\Phi_0{}^l(k, \epsilon)$ is very much smaller than $\Phi_1{}^l(k,\epsilon)$. Bearing in mind that for small angles $\mathbf{p}_+$, $\mathbf{p}_-$ and $\mathbf{q}$ are all nearly parallel, one gets from (1) the important result that at high energies and small angles the angular distribution of the pairs is the same as the angular distribution of the γ-rays emitted in the same transition.

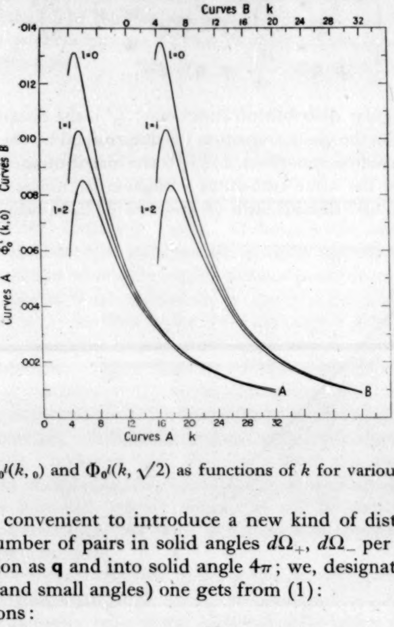

Figure 3. $\Phi_0{}^l(k, {}_0)$ and $\Phi_0{}^l(k, \sqrt{2})$ as functions of k for various values of l.

It is therefore convenient to introduce a new kind of distribution function which gives the number of pairs in solid angles $d\Omega_+$, $d\Omega_-$ per quantum emitted in the same direction as $\mathbf{q}$ and into solid angle 4π; we, designate it by $\tilde{F}(k,\epsilon)$ and (for high energies and small angles) one gets from (1):

for Ml transitions:

$$\tilde{F}_{\mathrm{M}l}(k,\epsilon)d\Omega_+d\Omega_- = \frac{\alpha k^2}{240\pi^3}\Phi_1{}^l(k,\epsilon)d\Omega_+d\Omega_- \qquad \ldots\ldots (2)$$

for El transitions:

$$\tilde{F}_{\mathrm{E}l}(k,\epsilon)d\Omega_+d\Omega_- = \frac{\alpha k^2}{240\pi^3}\Phi_1{}^{l-1}(k,\epsilon)d\Omega_+d\Omega_-.$$

The ratio of small angle pairs to quanta emitted in any direction is therefore determined uniquely by the function $\Phi_1{}^l(k, \epsilon)$. If more than one multipolarity occurs in a given transition, the appropriate Φ's are simply added with the proper weights, since it can be shown that under the conditions considered here no interference terms will appear.

§ 3. APPLICATION TO γ-YIELD DETERMINATION

The main difficulty in the absolute counting of γ-rays lies in the fact that all 'γ-counters' are actually electron counters and the γ-rays can only be detected through some intermediary process (photo effect, Compton effect, or external pair creation). In counting internal pairs one gains the advantage that the electrons are produced in the primary electromagnetic transition, and their number (and hence the transition intensity) can be determined directly.

Small angle pairs afford particular advantages for this application: (i) the rather weak dependence on multipolarity allows one to determine the total transition probability from pair measurements even in cases where the multipolarity is not known; (ii) because of the similarity in spatial distribution of γ-rays and small angle pairs, one can determine the angular distribution with a γ-counter and the pair measurement can be carried out at one fixed position.

We consider a counter system which counts electrons (of both signs) in coincidence in sold angles Ω_1, Ω_2 close to zero angle, for all energies but with the sum of the energies in both counters always being $k-2$. The number of coincidence counts per quantum (in the same direction as the pair) is given by

$$N_c = 2\int \bar{F}_{Ml}(k,\epsilon)\,d\Omega_1 d\Omega_2 = 2\int \bar{F}_{El+1}(k,\epsilon)\,d\Omega_1 d\Omega_2 = \frac{\alpha k^2}{120\pi^3}\Phi_1{}^l(k,0)G\Omega_1\Omega_2. \qquad \ldots\ldots(3)$$

The factor 2 has been introduced because it is assumed that in both Ω_1 and Ω_2 electrons and positrons are counted indiscriminately. G is a geometrical factor which corrects for the fact that the counters have a finite angular separation and finite solid angles. G can be calculated quite easily since Φ can be approximated very well by

$$\Phi = a + b\Theta^2 + c\Theta^4$$

with constant a, b, c; where one may also put for simplicity $\Theta = \sqrt{2\epsilon}/k$.

For two identical rectangular counters, subtending given solid angles at the source, one gets the maximum G for rectangles having sides in the ratio of $\sqrt{7}:1$, touching along their longer sides. If the longer side subtends at the source an angle corresponding to $\epsilon = 2$, one has $G = 0{\cdot}88$ for all $l \leqslant 2$ and all $k > 4$. From (3) one finds for this case:

$$N_c = 1{\cdot}58\ 10^{-5}\,\frac{\Phi_1{}^l(k,0)}{k^2}.$$

§ 4. PRACTICAL CONSIDERATIONS

All the foregoing considerations were based on the assumption that the azimuthal angle of $\mathbf{p}_+$, $\mathbf{p}_-$ about $\mathbf{q}$ has been averaged over. This condition may be realized by averaging the azimuthal distribution over two positions which differ in 90°. (The azimuthal angle δ enters into the expression only as $\cos^2\delta$ and $\sin^2\delta$.) In practice this averaging procedure will hardly ever be necessary, as the difference in the distribution function for the two positions will always be small. This difference will of course be zero for isotropic emission; for the anisotropies normally encountered in γ-distributions, and for the range of ϵ here considered the relative difference will be 0·01 or less.

The solid angles Ω_1, Ω_2 are limited by the requirement that the various approximations made in the calculation should be justified, namely: the constancy of the direction of **q** for all energies W_+, the relation $\Phi_0 \ll \Phi_1$, and also the ease of calculating G.

These are all rather mild requirements. If one also requires that the distribution functions for different multipolarities be similar, so that an absolute measurement could be carried out even if the multipolarity were unknown, a much more severe limitation is placed on the solid angles.

ACKNOWLEDGMENTS

The author wishes to express his gratitude to Mrs. H. Lifson and to Mr. M. Loewenstein for their help in carrying out the computations on the Weizmann Institute electronic computer.

REFERENCES

DEVONS, S., and GOLDRING, G., 1954, *Proc. Phys. Soc.* A, **67,** 413.
GOLDRING, G., 1953, *Proc. Phys. Soc.* A, **66,** 341.
HORTON, G. K., 1948, *Proc. Phys. Soc.*, **60,** 457.
ROSE, M. E., 1949, *Phys. Rev.*, **76,** 678.

Resonance Capture of Neutrons in Infinite Homogeneous Media†

By R. SCHERMER‡§ and N. CORNGOLD||
‡ Massachusetts Institute of Technology, Cambridge, Mass.
|| Brookhaven National Laboratory, Upton, New York

MS. received 10*th November* 1958

Abstract. In a previous paper, a variational principle was introduced for $1-p$, the capture probability for neutrons slowing down in a homogeneous medium of infinite extent. In the present paper, the variational principle is used together with simple but accurate trial functions to obtain expressions for (i) corrections to the commonly used 'narrow resonance' formula for capture and (ii) interference effects in the capture of neutrons by closely spaced resonances.

§ 1. Introduction

In studying the slowing down of neutrons in, say, homogeneous media of infinite extent one is quite interested in the probability that a neutron will be captured by a nucleus of the moderating material during the slowing down process. A typical slowing-down medium might consist of a mixture of light moderator (hydrogen, carbon, ...) and heavy fertile or fissile material (thorium, uranium, ...). The capture probability will be related to the neutron absorption cross section of the heavy nucleus. This cross section shows in general a characteristic resonance structure, and the existing analytical approximations for the capture probability take the effect of this violent variation into account only poorly (see for example Sampson and Chernick 1957).

The most popular analytical expression is based on the narrow resonance approximation, in which it is assumed that a given resonance covers such a narrow energy range that a single scattering collision with any nucleus in the medium will degrade the neutron energy below the resonance. This approximation leads to a neutron collision density through the resonance that is identical with the unperturbed, asymptotic density. It does not take into account the finite width of the resonance or the possibility of interference between resonances. A second approximation, called 'infinite absorber' denies the heavy nucleus the power to moderate neutrons (heavy nuclear mass tending to ∞), so that only collisions with the light nuclei can knock nucleons out of the resonance. This last approximation is useful for the broad resonances which occur at the lowest energies. It is not difficult to see that most resonances encountered satisfy neither the narrow resonance nor the infinite absorber conditions.

In this paper we use a quite accurate variational technique, introduced by one of us (Corngold 1957) in an earlier paper. We obtain analytical results for corrections to the narrow resonance formula in single resonances and for the interference effects in capture by closely spaced resonances.

---

† Work performed under the auspices of the U.S. Atomic Energy Commission.

§ Research Assistant, Brookhaven National Laboratory, Summer, 1958.

§ 2. Mathematical Development

The variational expression for the resonance capture $1-p$, is expressed in terms of the functional $J[\phi,\phi^+]$, where

$$J[\phi,\phi^+]=\frac{\int_0^\infty du\sum_s g_s(u)\phi^+(u)\phi(u)+\int_0^\infty du\sum_l g_l(u)\phi^+(u)\int_0^u du'\sum_s \bar{\psi}_s(u-u')g_s(u')}{\int_0^\infty du\sum_l g_l(u)\phi(u)\int_0^\infty du'\sum_s g_s(u')\phi^+(u')} \qquad \ldots\ldots(1)$$

and the symbols have the meaning: the lethargy $u=\ln(E_0/E)$ where E_0 is the source energy and E the energy variable; $g_s(u)=h_s(0)-h_s(u)$, where $h_s(u)$ is the probability that a collision at lethargy u is a scattering collision with an s-type nucleus,

$$h_s(u)=\overset{\text{scat}}{\underset{s}{\Sigma}}(u)/\Sigma(u),$$

and Σ^{scat}, Σ are respectively macroscopic scattering and total cross sections. $\bar{\psi}_s$ is the collision density solution to an idealized slowing-down problem in the mixture under consideration; it obtains when all the $g_s(u)\equiv 0$ and neutrons produced by a source at $u=0$ make their first collision with a nucleus of type s. ξ_{av} has its customary meaning. The functional $J[\phi,\phi^+]$ is equal to $1/[\xi_{\text{av}}(1-p)]$ when $\phi(u)$ is the collision density solution to the full slowing-down problem and $\phi^+(u)$ is stationary with regard to small changes $\delta\phi$, $\delta\phi^+$ in these solutions.

From the form of the equations defining ϕ, ϕ^+ (Corngold 1957), it appears that $\phi_0=\phi_0{}^+=1/\xi_{\text{av}}$ is a good first guess at trial functions. Insertion of this value into (1) leads to what we shall call $(1-p)_{\text{var}}$. That this value is a considerable improvement over the narrow resonance value—which we obtain by discarding the double integral in (1) and again choosing $\phi_0=\phi_0{}^+=1/\xi_{\text{av}}$—is apparent from the structure of the double integral and is borne out by actual numerical computation. The last statement holds also for the broad, low energy resonances where the variational result lies close to the infinite absorber results. For convenience we rewrite (1), with the choice discussed above for ϕ and ϕ^+, as

$$\frac{(1-p)_{\text{var}}}{(1-p)_{\text{NR}}}=\rho_0=\frac{1}{1+\chi}\qquad \chi=I\Big/\int_0^\infty\sum_s g_s(u)\,du \qquad \ldots\ldots(2a)$$

$$I=\int_0^\infty\sum_l g_l(u)\,du\int_0^u du'\sum_s\bar{\psi}_s(u-u')g_s(u'), \qquad \ldots\ldots(2b)$$

$$(1-p)_{\text{NR}}=\frac{1}{\xi_{\text{av}}}\int_0^\infty\sum_s g_s(u)\,du. \qquad \ldots\ldots(2c)$$

The error in the narrow resonance formula ($2c$) is due to the replacement of $\phi(u)$ by its asymptotic form $1/\xi_{\text{av}}$ in regions where it may deviate considerably from this value. By its stationary nature, the variational principle is much less sensitive to such variations in $\phi(u)$.

An analytical treatment of equations (2) is made difficult by the discontinuous nature of the functions $\bar{\psi}_s$ and the fact that the investigation involves integration over domains containing several singularities of $\bar{\psi}_s$. Thus direct substitution of $\bar{\psi}_s$ into the double integral ($2b$) leads to exceedingly complicated algebra. We have found the double integral to be much more tractable if handled by

Laplace transform methods. Indeed, for the resonance shapes we consider the variational expression may be put into a form such that effects occurring in successive collision intervals may be clearly identified.

Absorption in a single, isolated resonance in a system of hydrogen moderator and some heavier resonance absorber will now be discussed in detail. The result will then be generalized to heavier moderators and to the question of interference between two resonances lying close together. In all cases we will assume a simple, yet physically representative, shape for $g_s(u)$. The results will be expressible in terms of a double series. The important parameters of this series are λ, a quantity to be defined later and related to ξ_{av}; the width of the resonance; the spacing in the interference problem; and $\Sigma_s g_s/(1-\alpha_s)$, which characterizes the strength of the resonance.

Numerical results will be presented for the correction to the narrow resonance result, as predicted by the variational principle, for resonances of the chosen shape. These may be shown to be upper bounds to the corrections for real resonances.

§ 3. SINGLE RESONANCE ABSORPTION

We now seek to evaluate (2*b*) for the case of absorption by one isolated resonance. To this end we write the

$$\int_0^u \sum_s g_s(u')\tilde{\psi}_s(u-u')\,du'$$

appearing in (2*b*) as the Laplace inverse of its Laplace transform

$$\int_0^u \sum_s g_s(u')\tilde{\psi}_s(u-u')\,du' = \frac{1}{2\pi i}\int_{\Gamma-i\infty}^{\Gamma+i\infty} \mathrm{e}^{u\eta}\mathrm{L}\left\{\int_0^u \sum_s g_s(u')\tilde{\psi}_s(u-u')\,du'\right\}d\eta. \qquad \ldots\ldots(3)$$

where the Laplace transform is defined by

$$\mathrm{L}\{b(u)\} = \int_0^\infty \mathrm{e}^{-u\eta}b(u)\,du = \tilde{b}(\eta). \qquad \ldots\ldots(4)$$

The contour is any line lying to the right of all singularities of the integrand in the η plane. We insert (3) in (2*b*) and interchange the order of integration whence

$$I = \frac{1}{2\pi i}\int_{\Gamma-i\infty}^{\Gamma+i\infty} \sum_l \tilde{g}_l(-\eta)\sum_s \tilde{g}_s(\eta)\tilde{\psi}_s(\eta)\,d\eta \qquad \ldots\ldots(5\,a)$$

where

$$\tilde{g}_s(-\eta) = \int_0^\infty g_s(u)\mathrm{e}^{u\eta}\,du \qquad \ldots\ldots(5\,b)$$

and $\tilde{\psi}_s(\eta)$ may be written in terms of the scattering kernel $K_s(\eta)$ which characterizes the scattering by an *s*-type nucleus.

$$K_s(u) = \frac{\mathrm{e}^{-u}}{1-\alpha_s} \quad q_s \geqslant u \geqslant 0, \qquad q_s = \ln\left[\frac{(m_s+1)}{(m_s-1)}\right]^2 = -\ln\alpha_s$$

$$= 0 \qquad \text{elsewhere}, \qquad \ldots\ldots(6\,a)$$

$$\tilde{\psi}_s(\eta) = \frac{\tilde{K}_s(\eta)}{1-\sum_s h_s(0)\tilde{K}_s(\eta)}. \qquad \ldots\ldots(6\,b)$$

It is easily shown that $\lim\limits_{u\to\infty} \tilde{\psi}_s(u) = 1/\xi_{\mathrm{av}}$.

The functions $g_s(u)$ describe the resonance and are different from zero only within the resonance. We shall describe our resonances by the simple shape:

$$g_s(u)=\begin{cases} 0 & u<0 \\ g_s & 0\leqslant u\leqslant a \\ 0 & u>a. \end{cases} \qquad \ldots\ldots(7)$$

We may take the resonance at $u=0$, without loss of generality, since the results are invariant under a translation of the origin of u.

The reader should note that in the realistic case of cross sections described by Doppler-broadened, Breit–Wigner resonance shapes $g_s(u)$ is indeed nearly constant over the energy range in which the cross sections have appreciable size. In a typical case a numerical calculation showed only a 10% drop in magnitude of g_s in an energy interval in which the total cross section fell by a factor of twenty. Moreover, by stating the problem in terms of the g_s we obtain results which are close to universal in that they are almost independent of the height of the cross section peak. As long as we choose and compare profiles for $g_s(u)$ whose widths are cut off at a certain number of practical widths, $\tilde{g}_s(\eta)$ will have no poles in the finite plane and the form of $g_s(u)$ modifies only the residues in our integral (5 *a*). We have examined the consequences of using triangular and parabolic profiles and we obtain results that have functional form similar to those obtained with the rectangular profile, but with magnitudes that are somewhat smaller.

The terms 'resonance height' and/or 'resonance width' will henceforth refer to the characteristics of g_s. Using (4), (5 *b*), (6) and (7) in (2 *b*) we find that

$$I=\frac{1}{2\pi i}\int_{\Gamma-i\infty}^{\Gamma+i\infty} d\eta\left(\frac{e^{a\eta}-1}{\eta}\right)\left(\frac{1-e^{-a\eta}}{\eta}\right)\sum_{l,s}\frac{g_l\,g_s}{1-\alpha_s}\,\frac{1-\alpha_s\exp(-q_s\eta)}{1+\eta-\sum\limits_p\dfrac{h_p(0)}{1-\alpha_p}\left\{1-\alpha_p\exp(-q_p\eta)\right\}}. \qquad \ldots\ldots(8)$$

The simplest non-trivial case is that of hydrogen ($s=1$) mixed with some heavier resonance absorber ($s=2$). In this case (8) may be expressed via the substitutions

$$\lambda=\sum\nolimits_p\frac{h_p(0)}{1-\alpha_p}-1, \qquad y_2=\frac{h_2(0)\alpha_2 q_2}{(1-\alpha_2)}, \; \nu=q_2\eta$$

as integrals of the form

$$I'=\frac{1}{2\pi i}\frac{q_2}{\lambda}\int_{\Gamma-i\infty}^{\Gamma+i\infty}\frac{e^{p\nu}\,d\nu}{\nu^2(\nu/y_2+e^{-\nu}-1)}, \qquad \ldots\ldots(9)$$

where p takes the values a/q_2, $-a/q_2$, 0, $(a-q_2)/q_2$, $-(a+q_2)/q_2$, $-q_2/q_2$. Note that the identity $-\lambda+y_2/q_2=0$ holds.

The integrals (9) are inconvenient to evaluate directly by the method of residues, since $(\nu/y_2+e^{-\nu}-1)^{-1}$ has a simple pole at the origin and an infinite set of complex-conjugate pole pairs in the left half-plane extending out to infinity. This portion of the denominator, it should be emphasized, is due to $\tilde{\psi}_s(\eta)$. The chosen functions $\tilde{g}_s(\eta)$, $\tilde{g}_s(-\eta)$ have no singularities in the finite part of the plane.

Consider the expansion

$$\left(\frac{\nu}{y_2}+e^{-\nu}-1\right)^{-1}=\frac{y_2}{\nu}\sum_{k=0}^{\infty}(-y_2)^k\left(\frac{e^{-\nu}-1}{\nu}\right)^k. \qquad \ldots\ldots(10)$$

This is readily shown to converge for $\mathscr{R}\nu > 0$, since in this region $|(e^{-\nu}-1)/\nu|^2 < 1$ and $0 < y_2 < 1$. This expansion has an interesting physical significance. It is essentially an expansion of (6*b*) in the form

$$\tilde{\psi}_s(\eta) = \tilde{K}_s(\eta)\left[1 + \sum_s h_s(0)\tilde{K}_s(\eta) - \left(\sum_s h_s(0)\tilde{K}_s(\eta)\right)^2 + \ldots\right] \quad \ldots\ldots (11)$$

which represents source neutrons making successively 1, 2, ... collisions. On summing the successive integrands which result when (10) is inserted into (9) we will get the contribution to the resonance capture due to neutrons making 1, 2, 3, ... collisions in the resonance.

Next we expand $(e^{-\nu}-1)^k$ by the binomial theorem and interchange sums and integrals to obtain

$$I' = \frac{1}{2\pi i}\frac{q_2 y_2}{\lambda}\sum_{j=0}^{\infty}\sum_{k=j}^{\infty}\int_{\Gamma-i\infty}^{\Gamma+i\infty}(-1)^j (y_2)^k \frac{\binom{k}{j}e^{(p-j)\nu}}{\nu^{3+k}}\,d\nu. \quad \ldots\ldots (12)$$

The sum over j is also physically interesting. Each term represents, as will become more apparent when the integration is performed, the full contribution to the capture due to a region of width q_2 at distance jq_2 from the source.

The integral (12) will now be evaluated in the customary manner by closing the straight line path with a curved contour whose radius is made to approach infinity, and upon which the integral approaches zero. When $p-j<0$ the closed contour extends to the right of the original path, when $p-j>0$ it extends to the left. In the case $p-j \leqslant 0$ the contour encloses no singularities of the integrand and $I'=0$. For $p-j>0$ we have the residue of a pole of order $3+k$ at the origin. This means that j takes on a maximum value equal to the largest integer less than p, symbolized as $[N]<p$. Performing the integration for y_2 and expanding $\binom{k}{j}$ we get as a result:

$$I' = \frac{1}{\lambda^2}\sum_{j=0}^{[N]<p}\sum_{k=j}^{\infty}\frac{(-1)^j[\lambda q_2(p-j)]^{k+2}}{j!\,(k-j)!\,(k+2)(k+1)} \quad \ldots\ldots (13)$$

From the values that p takes on and the above discussion regarding choice of contours, we see that only two values of p gives non-zero contributions. $p=a/q_2$, $a>0$; $p=a/q_2-1$, $a>q_2$. (8) then may be rewritten as

$$I = \left(\sum_l g_l\right)\left[I'(a)\sum_s \frac{g_s}{1-\alpha_s} - \frac{y_2\alpha_2}{1-\alpha_s}I'(a-q_2)\right] \quad \ldots\ldots (14)$$

where it is understood that the second term vanishes if $a<q_2$. It may readily be verified that (13) may also be written as the single sum:

$$\lambda^2 I' = \sum_{j=0}^{[N]<p}\left\{\frac{(-T^j)}{j!}\frac{d^j}{dT^j}\left[\frac{e^T-1-T}{T^2}\right]\right\}_{T=y_2[p-j]}. \quad \ldots\ldots (15)$$

The sums converge very rapidly with j. Four terms ($j \leqslant 3$) give accuracy to approximately 0·1% for the largest argument $y_2 p$ we have calculated ($y_2 p = 0{\cdot}94$, corresponding to a resonance $20q_2$ wide in a 10:1, H–^{238}U mixture). This is equivalent to the usual statement in the literature that $\psi_s(u)$ reaches its asymptotic value within $3q_2$ of sources or sinks.

With these results, we may write (2*a*) in a particularly instructive form:

$$\rho_0 = \left[1 + a\sum_s \frac{g_s}{1-\alpha_s}\left(\frac{I'(a)}{a^2}\right) - \alpha_2 a\frac{g_2}{1-\alpha_2}\left(\frac{I'(a-q_2)}{a^2}\right)\right]^{-1}. \quad \ldots\ldots (16)$$

Here

$$\frac{I'(a)}{a^2} = F(\lambda a) \quad \text{for} \quad a \geqslant 0,$$
$$= 0 \quad \text{for} \quad a < 0.$$

For example,

$$F(\lambda a) = \frac{1}{2!} + \frac{\lambda a}{3!} + \frac{(\lambda a)^2}{4!} + \ldots \text{ when } a \leqslant q_2.$$

The important quantities in (16) are: $g_s a/(1-\alpha_s)$, $s = 1, 2$, whose magnitudes are less than 1 in all practical cases, and are parameters describing the effective strength of the perturbing resonance, and the function $F(\lambda a)$, which depends upon the nature of the mixture and whose value is a measure of the average number of collisions required to carry a neutron through the resonance. As we shall see later, a similar equation results in the case of moderation by uranium and arbitrary moderator, so long as $a < q_1$. The strength parameters are isolated neatly in these calculations and since they are often small an expansion of (16) in terms of them yields a rapidly converging sequence of corrections to the narrow resonance result.

3.1 *Non-Hydrogenous Systems*

The case of systems in which the heavy absorber is mixed with moderator other than hydrogen is more complicated algebraically than the previous case but follows the same lines. The last term in the denominator of $\bar{\psi}_s(\eta)$ becomes

$$\sum_s \frac{h_s(0)\alpha_s}{1-\alpha_s} e^{-q_s\eta} \quad \text{instead of} \quad \frac{h_2(0)\alpha_2}{1-\alpha_2} e^{-q_2\eta}.$$

The denominator is first expanded as in (10). Two binomial expansions are now necessary; one in j, measuring distances in units of q_2, and one in i, measuring distances in units of q_1. The only non-zero terms contributing to the integral (8) are for $p = a/q_2$, $a > 0$; $p = (a-q_2)/q_2$, $a > q_2$; and $p = (a-q_1)/q_2$, $a > q_1$. For practical moderators (carbon or lighter), the last case would represent an unrealistically wide resonance and may be ignored. With this proviso (13) becomes

$$I'(p) = \frac{1}{\lambda^2} \sum_{j=0}^{\infty} \sum_{k=j}^{\infty} (-1)^j \frac{[\lambda q_2(p-j)]^{k+2}}{j!\,(k-j)!\,(k+1)(k+2)} \left(\frac{y_2}{\lambda q_2}\right)^j, \qquad p < \frac{q_1}{q_2}. \qquad \ldots\ldots(17)$$

y_2 and λ are as defined previously, but they now obey the relation

$$\lambda - \frac{y_2}{q_2} - \frac{y_1}{q_1} = 0, \quad \text{where} \quad y_1 = \frac{h_1(0)\alpha_1 q_1}{1-\alpha_1}.$$

For mixtures containing hydrogen $y_1 = 0$, and these expressions reduce to ones quoted earlier. I' is still related to I by (14) and the discussion following (16) applies here as well.

In order to consider the expression for ρ_0 in some detail, we must examine the quantities h_s and g_s. In all cases $0 \leqslant h_s(u) \leqslant 1$, $\Sigma_s h_s(0) = 1$ and $-1 \leqslant g_s(u) \leqslant 1$. If we assume that the light material does not capture neutrons we can deduce further that $g_1(u) > 0$, while g_2 can have either sign. Since $1/(1-\alpha_2) \gg 1/(1-\alpha_1)$ the sign of $\Sigma_s g_s/(1-\alpha_s)$ and of the correction depends largely upon the sign of g_2. From its definition it will be seen that if $g_2 > 0$, $0 < g_2 < h_2(0)$, and is generally quite small. However, when g_2 is negative its magnitude may be of the order of unity. Therefore the corrections for resonances characterized by $g_2 > 0$, which will henceforth be called absorption resonances, will be less than those of the second type (scattering resonances). One should note that the definition of scattering resonance given here encompasses resonances characterized approximately by $\Gamma_n/\Gamma > h_2(0)$, which may include resonances with $\Gamma_\gamma > \Gamma_n$.

Figure 1 shows the corrections ρ_0 to the narrow resonance as a function of resonance width for three systems, two hydrogen-moderated and one carbon-moderated.

We have taken nominal potential scattering cross sections as $\sigma_{\mathrm{C}}(0) = 5b$; $\sigma_{\mathrm{H}}(0) = 20b$; $\sigma_{\mathrm{U}}(0) = 10b$. The scattering resonance chosen has peak resonance cross section $\sigma_2^{\mathrm{scat}}(\mathrm{res}) = 600b$, $\sigma_2^a(\mathrm{res}) = 1000b$, while the absorption resonance has $\sigma_2^{\mathrm{scat}}(\mathrm{res}) = 0$, $\sigma_2^a(\mathrm{res}) = 1000b$. Moderators are compared at equal values of $h_s(0)$ (potential scattering per heavy atom). Thus 40:1, C–U is to be compared with 10:1, H–U.

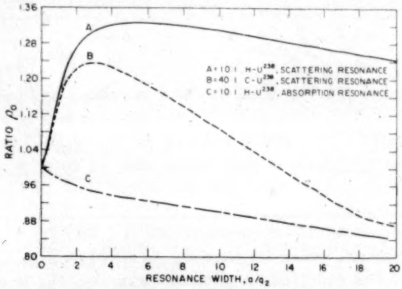

Figure 1. Ratio of variational to narrow resonance calculations of capture in single resonance in variety of systems. Resonance width is measured in lethargy units of size q_2.

Note that for scattering resonances $\rho_0 > 1$ since the narrow resonance result ignores the build-up of the collision density in the resonance, which would lead to greater capture. For absorption resonances $\rho_0 < 1$ since the narrow resonance result ignores the depletion due to absorption, which would lead to lower capture.

§ 4. INTERFERENCE BETWEEN RESONANCES

We now consider two resonances, of width a and b, each with $g_s(u)$ of the rectangular shape discussed above, with edges located at $u = 0$, a, $a + l$, $a + b + l$.

If the transform of such a function is inserted into (5 a) we may separate the integrand into four groups of terms with the following physical significance. Two are equivalent to (8) and represent the effect of the two resonances acting independently. Two are interaction terms, one of which represents the effect of the second resonance on the first, which we expect should be zero. Indeed it is found that the normal form (9) of this integral contains only integrands with $p \leqslant 0$, all of which integrate to zero, following an earlier discussion. The fourth group we call the interference integral J. It has the form

$$J = \frac{1}{2\pi i} \sum_r g_{rb} \sum_s \frac{g_{sa}}{1-\alpha_s} \times \int_{\Gamma - i\infty}^{\Gamma + i\infty} d\eta \frac{(1-\alpha_s e^{-q_s\eta})(e^{(a+b+l)\eta} + e^{l\eta} - e^{(a+l)\eta} - e^{(b+l)\eta})}{\eta^2 \left[1 + \eta - \sum_s \frac{h_s(0)}{1-\alpha_s} + \sum_s \frac{h_s(0)\alpha_s}{1-\alpha_s} e^{-q_s\eta} \right]}. \qquad \ldots\ldots(18)$$

Note that if a or b equals zero, the integral vanishes, as it should. If $l=0$, the numerator becomes $e^{(a+b)\eta}-e^{a\eta}-e^{b\eta}+1$. The last term does not contribute, the second and third terms cancel the contributions from the integrals which represent a and b acting alone, and we are left with the contribution of a resonance of width $a+b$.

The integration is exactly that which we have performed previously. For the case of a general mixture

$$J'=\frac{1}{\lambda^2}\sum_{m=1}^{4}(-1)^m\sum_{j=0}^{[N_m]<p_m}\sum_{k=j}^{\infty}\frac{(-1)^j[(p_m-j)\lambda q_2]^{k+2}}{j!\,(k-j)!\,(k+2)(k+1)}\left(\frac{y_2}{\lambda q_2}\right)^j p_m<\frac{q_1}{q_2}, \qquad \text{......(19 a)}$$

$$p_1=\frac{a+l}{q_2},\quad p_2=\frac{a+b+l}{q_2},\quad p_3=\frac{b+l}{q_2},\quad p_4=\frac{l}{q_2} \qquad \text{......(19 b)}$$

where J' is related to J in the same way as I' is related to I (14). Note the J' is a sum of four series of the form (17). The sum over m is an artifice to take care of the four terms in (18). (19 a) holds if all $p_m<q_1/q_2$, certainly the case in hydrogen-moderated systems. New terms start to enter when any of the p_m become greater than q_1/q_2. Note that the upper limit of the sum over j may be different for the different p_m.

It may be shown that the series converges as l, and hence all the p_m become very large. The result, which we term J_∞, is equal to $\Sigma_r g_{ra}\Sigma_s g_{sb}(ab/\xi_{\text{av}})$ which is independent of l as expected on physical grounds. J_∞ is easily shown to be the portion of (18) due to the $\eta=0$ pole of $\psi_s(\eta)$, i.e. the asymptotic value $\psi(u)=1/\xi_{\text{av}}$ in the u-plane. It is related to the 'bite' taken out of the flux by the first resonance. We will subtract this portion from J in the numerical work.

Finally, we exhibit the form of the correction in analogy with equations (2),

$$\frac{(1-p)_{\text{var}}}{(1-p)_{\text{NR}}}=\rho=\frac{1}{1+X+Y}, \qquad \text{......(20 a)}$$

$$X=\frac{I_a+I_b+J_\infty}{(1-p)_{\text{NR}}}, \qquad Y=\frac{J-J_\infty}{(1-p)_{\text{NR}}}. \qquad \text{......(20 b)}$$

I_a and I_b refer to (17) applied to resonances a and b respectively. For the interference studies we define $\rho_1=1/(1+X)$ and use the parameter $\rho_2=(\rho-\rho_1)/\rho_1=-\rho_1 Y/(1+\rho_1 Y)$ to indicate the magnitude of the interference effect. ρ_2 is the ratio of captures due to interference to non-interference captures.

§ 5. Numerical Results

The basic series (17) is very rapidly convergent. Convergence in j has been previously discussed, and the series in k converges like the exponential, as indicated by (15). Thus for any given system specified by λq_2 and y_2 with resonance width or spacing specified by the p_m, it is a simple matter to generate the series by hand computation, or, as we have done, with a small computing machine.

Specific results are presented below in the form of figures. These are based, of course, on the rectangular profile chosen for $g_s(u)$. Examination of the consequences of refining the profile has convinced us that the results here presented are a slight overestimate of the values to be obtained for real systems.

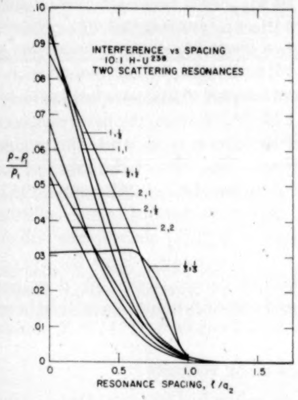

Figure 2. Ratio of captures ascribed to interference to captures obtained when the resonance spacing is made infinite. Resonance spacing is measured in lethargy units of size q_2.

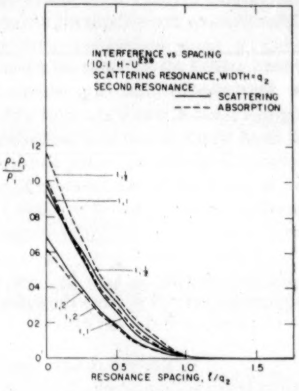

Figure 3. As figure 2. Here a scattering resonance of fixed width scatters into a variety of second resonances.

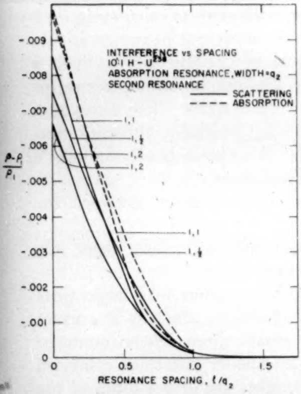

Figure 4. As figure 2. Here an absorption resonance of fixed width scatters into a variety of second resonances.

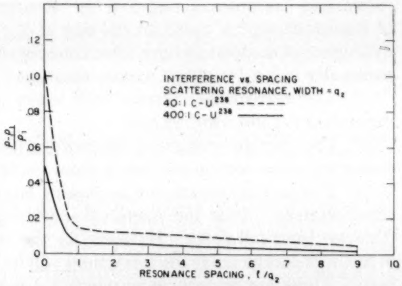

Figure 5. As figure 2. We consider two different mixtures of $C{-}^{238}U$ and interference between two identical scattering resonances.

Figure 1 deals with capture by a single resonance in typical C–^{238}U, H–^{238}U mixtures and displays the ratio $(1-p)_{\text{var}}/(1-p)_{\text{NR}}$ as a function of resonance width. Figures 2 to 4 display the interference effect ρ_2 as a function of resonance spacing l/q_2 for several systems. In figure 2, two scattering resonances of varying width in a 10 : 1 H–^{238}U system are studied. The notation (a, b) for each curve tells the width in units of q_2 of the first and second resonances respectively. In figures 3 and 4, which also deal with a 10 : 1 H–^{238}U system, the first resonance is of fixed width q_2 and is of scattering, then absorption type, while the second resonance is of varying width and varying type. The sign of the interference effect is governed by the function $\Sigma_s g_s \bar{\psi}_s$ and it is not difficult (Corngold 1957) to predict the result found in these figures, that perturbations in the collision density caused by a $\left[\begin{smallmatrix}\text{scattering}\\ \text{absorption}\end{smallmatrix}\right]$ resonance cause a $\left[\begin{smallmatrix}\text{positive}\\ \text{negative}\end{smallmatrix}\right]$ interference effect. Figure 5 shows interference effects in two C–^{238}U systems. Here the curves do not fall rapidly to zero because the effect of carbon scattering does not disappear for several q_1 from the resonance, and the calculations have only been done to points slightly less than q_1.

§ 6. SUMMARY AND DISCUSSION OF RESULTS

We believe that the following conclusions regarding real systems of moderator and resonance absorber may be drawn from our work.

1. The narrow resonance approximation may be very bad in any given resonance, especially one in which the resonance is of the order of or larger than q_2 and/or $\Sigma_s g_s/(1-\alpha_s)$ is significantly different from zero. Similar conclusions may be found in the studies of Spinney (1957) and Schermer (unpublished), the latter quoted partially by Corngold (1957). They deal with 1 : 1 H–^{238}U mixtures, and thus it is not surprising that the corrections are even larger than those calculated above for a 10 : 1 mixture. The overall error in calculating $1-p$ using the narrow resonance approximation for all resonances may be comparatively small however due to cancellation of large errors of opposite sign. Such a calculation has been shown by Spinney (1957). The correction is positive for ‘scattering’ resonances, negative for ‘absorption’ resonances. The distinction of resonance type is based on the sign of $\Sigma_s g_s/(1-\alpha_s)$ generally, although non-hydrogenous moderators have other considerations. This is essentially Spinney’s parameter in his ‘modified narrow resonance’ calculations.

2. The corrections increase with heavy atom concentration, although the dependence is not a strong one.

3. The (single resonance) correction decreases with moderator mass, the scattering cross section per heavy atom being held constant.

4. The corrections are not necessarily larger for resonances with larger peak cross sections. It is the fractional scattering probability which is important (this we have called h_s). However for the very small resonances encountered in the high energy range the corrections will be much smaller than those exhibited here. These are resonances in which the peak heights are of the order of the potential cross sections.

5. The interference portion of the correction term is quite small even at its largest values.

6. The interference at essentially zero spacing is a maximum for two resonances both on the order of $\frac{1}{2}q_2$ to q_2 wide. It is smaller for both narrower and wider resonances.

7. The interference drops off with spacing more slowly for narrow resonances ($a < q_2$) than for wide ones. For hydrogen moderator the interference is essentially zero for spacings $l > q_2$. The drop is less sharp with heavier moderators, but the interference is still small at spacings $l > q_2$.

8. The interference is greatest for a scattering resonance at the higher energy. It is completely negligible for an absorption resonance at the higher energy.

ACKNOWLEDGMENT

The authors acknowledge with thanks the computational assistance given them by Mr. William Bornstein.

REFERENCES

CORNGOLD, N., 1957, *Proc. Phys. Soc.* A, **70,** 793.

SAMPSON, J., and CHERNICK, J., 1957, *Progress in Nuclear Energy, Series I—Physics and Mathematics,* **2,** 223 (London: Pergamon Press).

SPINNEY, K. T., 1957, *J. Nuclear Energy,* **6,** 53.

Theoretical Transport Coefficients for Polar Semiconductors

By R. T. DELVES
Communication from the Staff of the Research Laboratories of The General Electric Company Limited, Wembley, England

MS. received 8th December 1958

Abstract. The mobility, thermoelectric power and weak field Hall coefficient have been calculated when the charge carriers of a polar semiconductor are scattered by an optical mode of vibration of the lattice. The collision operator derived by Fröhlich, and Howarth and Sondheimer was used, and the Boltzmann transport equation was integrated directly on an electronic computer. Results are given for $2\theta \geqslant T \geqslant \theta/2$ and $5 \geqslant \eta \geqslant -2$. ($\eta$ is the reduced Fermi level, $\theta = \nu_l \boldsymbol{h}/\boldsymbol{k}$, and ν_l is the frequency of the longitudinal optical mode.) These results are compared where possible with those obtained from a different method of calculation by Howarth, Lewis and Sondheimer. Rough values are also given for the Lorenz number and weak field Ettingshausen coefficient.

§ 1. Introduction

In this paper numerical values are given for the conductivity, thermoelectric power, Lorenz number and the weak field Hall and Ettingshausen coefficients when the charge carriers in a polar semiconductor are scattered by an optical mode of the lattice vibrations. The collision operator which was derived by Fröhlich (1937) and by Howarth and Sondheimer (1953) was used. These authors assumed that the interaction between the lattice and a charge carrier was weak, that the energy band was spherical and the density of states parabolic, that the phonons of the optical mode had a single frequency ν_l and that they lay in a sphere in wave vector space. The collision operator is such that a relaxation time can only be defined at very high temperatures when $\boldsymbol{k}T \gg \boldsymbol{h}\nu_l$ or at very low temperatures for non-degenerate material, and consequently the usual methods of determining the transport coefficients are not applicable. Numeral values for the thermoelectric power, conductivity and Hall coefficient have been calculated by Howarth and Sondheimer (1953), and Lewis and Sondheimer (1955). These authors used Kohler's variational principle. In the present paper a different method of calculation was used, and the results of the two methods are compared in §4.

Optical mode scattering has been considered for sintered CdO by Wright and Bastin (1958), for PbS by Finlayson and Greig (1956) and also by Petritz and Scanlon (1955), and for Mg_2Si and Mg_2Ge by Morris, Redin and Danielson (1958). Ehrenreich (1957) has given a detailed discussion of the electron mobility in intrinsic InSb. He extended the theory to cover the non-parabolic density of states in n-type InSb, and used Howarth and Sondheimer's method to calculate the conductivity and thermoelectric power.

§ 2. METHOD OF SOLUTION

It is convenient to define a temperature θ associated with the longitudinal optical mode of frequency ν_l by $\boldsymbol{k}\theta = \boldsymbol{h}\nu_l$. The Boltzmann equation in weak magnetic fields can be reduced to a second-order finite difference equation, relating the values of a certain distribution function f at energies E, $E-\boldsymbol{k}\theta$, and $E+\boldsymbol{k}\theta$. The details are given in Howarth and Sondheimer's paper. These authors used Kohler's variational principle to solve the equation. The unknown distribution function was represented as a power series in energy, and the coefficients were determined by making a certain integral a maximum. The transport coefficients were then expressed as the ratios of infinite determinants. Howarth and Sondheimer broke off the determinants after two or three rows and columns in order to obtain numerical values for the transport coefficients. This is equivalent to taking two or three terms in the power series for the distribution function, and the conductivity calculated in this way is always less than the exact value. The difficulty in this method is to estimate the importance of the omitted terms in the determinants.

The results given in the present paper were obtained by integrating the Boltzmann equation numerically on an electronic computer. The method used was roughly as follows.

The number of charge carriers must be finite and so f must tend to infinity less rapidly than $\exp(E/\boldsymbol{R}T)$ as E tends to infinity. If $E/\boldsymbol{k}\theta$ is written as $r+a$, with r an integer and $0 \leqslant a < 1$, the Boltzmann equation can be written as

$$A_r = B_r f_{r+1} + C_r f_r + D_r f_{r-1}. \qquad \ldots\ldots(1)$$

f_r is the distribution function at $E = \boldsymbol{k}\theta(r+a)$, and A_r, B_r, C_r and D_r are known functions of θ/T, η, a and r. In a particular calculation the first three of these are fixed. It is assumed that f_r is known from f_0 to f_{n-1} and it is shown how f_n was calculated. Equation (1) was used to calculate f_r (for $r > n$) in the form

$$f_r = G_r f_n + H_r \qquad \ldots\ldots(2)$$

with G_r and H_r known functions of A, B, C and D.

It was found that as r tends to infinity G_r and H_r both become proportional to $\exp(mr)$, and that m is a positive constant. So if f_r is to satisfy the boundary condition, f_n must be determined by

$$f_n = -\lim_{r\to\infty} \frac{H_r}{G_r}. \qquad \ldots\ldots(3)$$

This process was used to calculate f_n from f_0 to the point where f made a negligible contribution to the transport integrals. This established f from $E = \boldsymbol{k}\theta a$ at intervals of $\boldsymbol{k}\theta$. The calculation is repeated for different values of a until f is known at sufficiently close values of E. Generally this must be at intervals of $\frac{1}{2}\boldsymbol{k}T$ or less.

§ 3. NUMERICAL RESULTS

Results were obtained for $2\theta \geqslant T \geqslant \frac{1}{2}\theta$ and $5 \geqslant \eta \geqslant -2$. The conductivity was expressed as

$$\sigma = \frac{16VM}{3(e^*)^2}(\nu_l)^3 C(z,\eta). \qquad \ldots\ldots(4)$$

V is the volume of the unit cell, M the reduced mass of the ions, ν_l the frequency of the longitudinal optical mode, $z = \theta/T$, η the reduced Fermi level and e^* is the effective ionic charge. The latter can be found from the relations (Born and Huang 1954)

$$(e^*)^2 = \frac{(\epsilon_0 - \epsilon_\infty)}{\epsilon_\infty^2} VM2\pi\nu_t^2, \qquad \ldots\ldots(5)$$

$$\nu_l^2 = \nu_t^2(\epsilon_0/\epsilon_\infty). \qquad \ldots\ldots(6)$$

ϵ_0 is the static dielectric constant, ϵ_∞ the high-frequency one and ν_t is the transverse optical mode frequency, or the reststrahlen frequency which is measured experimentally. The $C(z, \eta)$ are shown in table 1. This C is $(e^z - 1)/z^2$ times the G of Howarth and Sondheimer.

Table 1. The Conductivity Function $C(z, \eta)$ defined in equation (6)

z \ η	−2	−1	0	1	3	5
†0·25	0·521	1·35	3·27	7·19	24·3	56·5
0·5	0·259	0·668	1·63	3·60	—	—
1	0·147	0·374	—	1·91	6·41	15·2
1·5	—	—	—	1·49	4·82	11·3
2·0	0·167	0·405	—	1·44	4·34	9·94

† Calculated assuming a relaxation time $\tau \propto E^{+1/2}$.

Table 2. The Thermoelectric Power × ***e*/*k***

z \ η	−2	−1	0	1	3	5
†0	5·00	4·12	3·29	2·59	1·67	1·17
0·5	4·89	3·98	3·16	2·43	—	—
1	4·40	3·47	—	2·22	1·44	0·98
1·5	—	—	—	1·90	1·25	0·86
2·0	3·70	2·81	—	1·56	1·12	0·79

† Calculated assuming a relaxation time $\tau \propto E^{+1/2}$.

Table 3. ***Rnec***

z \ η	−2	−1	0	1	3	5
†0	1·105	1·094	—	1·068	1·04	1·02
0·5	1·05	1·04	1·02	—	—	—
1	1·10	1·09	—	1·01(5)	1·01	1·00
1·5	—	—	—	1·05	1·01	1·00
2·0	1·34	1·33	—	1·13	1·02	1·01

† Calculated assuming a relaxation time $\tau \propto E^{+1/2}$.

The thermoelectric power Q, is given as Q***e*/*k*** in table 2. ***k*/*e*** is 86·17 μv deg^{-1}. ***Rnec*** is given in table 3. R is the Hall coefficient and n is the number of charge carriers. These results should be accurate to at least 5%.

Results for non-degenerate material were not calculated specifically, but those for $\eta = -2$ can be used to estimate what they will be. It was not though worth while to extend the results to lower temperatures, as for most semiconductors other scattering mechanisms must be included below $T = \frac{1}{2}\theta$. Strong field effects can be calculated in a similar way to the method used for weak field effects, but no numerical results are reported here.

It is known that if $T \gg \theta$, a relaxation time exists, proportional to $E^{1/2}$. The results of tables 1 and 2 show that if $T = 2\theta$ such a relaxation time gives the thermoelectric power and conductivity correct to 5%, but not the Hall coefficient.

Table 4. The Dimensionless Ettingshausen Coefficient E_D defined in equation (7)

z \ η	-2	-1	0	1	3	5
†0	+0·50	+0·48	—	+0·42	+0·33	—
0·5	+0·35	+0·25	(+0·3)	—	—	—
1	−0·10	−0·08	—	+0·06	+0·06	+0·04
1·5	—	—	—	−0·15	−0·05	−0·03
2·0	−0·20	−0·20	—	−0·25	−0·1	−0·08

† Calculated assuming a relaxation time $\tau \propto E^{+1/2}$.

Table 5. The Dimensionless Lorenz Number L_D defined in equation (8)

z \ η	-2	-1	0	1	3	5
†0	3·0	—	3·0	—	3·06	3·1
0·5	2·2	2·2	2·1	—	—	—
1	2·5	—	—	2·5	2·4	2·2
1·5	—	—	—	2·1	1·9	1·7
2·0	1·1	1·1	—	1·6	1·5	1·4

† Calculated assuming a relaxation time $\tau \propto E^{+1/2}$.

The distribution functions that were used to obtain the results of tables 1, 2 and 3 can also be used to calculate the Lorenz number and weak field Ettingshausen coefficient. These two effects depend on the difference of two similar numbers and the results of tables 4 and 5 are of low accuracy. In particular, the Ettingshausen coefficient could be wrong by 100%, but the results reported should be qualitatively correct. It is convenient to define dimensionless quantities E_D, L_D as follows.

For the Ettingshausen effect one has

$$\frac{dT}{dy} = \frac{J_x(RH\sigma)}{\kappa_t}\frac{\boldsymbol{k}T}{\boldsymbol{e}}E_D. \qquad \ldots\ldots(7)$$

E_D is given in table 4: κ_t is the total thermal conductivity. The Lorenz number is written as

$$\frac{\kappa_e}{\sigma T} = \frac{\boldsymbol{k}^2}{\boldsymbol{e}^2}L_D. \qquad \ldots\ldots(8)$$

L_D is given in table 5.

§ 4. DISCUSSION

The method used by Howarth and Sondheimer to solve the difference equation works best if the distribution function is a slowly varying function of energy. Some of the distribution functions calculated by the method of this paper for T less than θ have maxima and are clearly not slowly varying functions. Even so the results of Howarth and Sondheimer for the thermoelectric power and conductivity agree to within 15% with those of this paper. This illustrates the power of the variational procedure to give useful results with a trial distribution function which is only a poor approximation for the exact one.

The greatest difference between the Hall coefficients of this work and that given by Lewis and Sondheimer is less than 25%. Ziman (1956) has shown how the intuitive method used by Lewis and Sondheimer can be rigorously based on a variational principle. However, though certain integrals which are obtained by the variational method are rigorous lower bounds to the exact values, the magnetoresistance effects are functions of these integrals and can be greater or less than the exact values.

REFERENCES

BORN, M., and HUANG, K., 1954, *Dynamical Theory of Crystal Lattices* (Oxford: Clarendon Press), Chap. II.

EHRENREICH, H., 1957, *J. Phys. Chem. Solids*, **2,** 131.

FINLAYSON, D. M., and GREIG, D., 1956, *Proc. Phys. Soc.* B, **69,** 796.

FRÖHLICH, H., 1937, *Proc. Roy. Soc.* A, **160,** 280.

HOWARTH, D. J., and SONDHEIMER, E. H., 1953, *Proc. Roy. Soc.* A, **219,** 53.

LEWIS, B. F., and SONDHEIMER, E. H., 1955, *Proc. Roy. Soc.* A, **227,** 241.

MORRIS, R. G., REDIN, R. D., and DANIELSON, G. C., 1958, *Phys. Rev.*, **109,** 1909, 1916.

PETRITZ, R. L., and SCANLON, W. W., 1955, *Phys. Rev.*, **97,** 1620.

WRIGHT, R. W., and BASTIN, J. A., 1958, *Proc. Phys. Soc.*, **71,** 109.

ZIMAN, J. M., 1956, *Canad. J. Phys.*, **34,** 1256.

Diffusion of Phosphorus into Silicon under Conditions of Controlled Vapour Pressure

By M. J. COUPLAND†
Services Electronics Research Laboratory, Baldock, Herts.

MS. received 15*th April* 1958, *in final form* 30*th December* 1958

Abstract. The diffusion of phosphorus into silicon has been studied and a relationship between the surface concentration of phosphorus and the vapour pressure of the phosphorus ambient is presented. It is shown that control of the surface concentration over the range 3×10^{15} atoms/cm^3 to 5×10^{18} atoms/cm^3 has been achieved. Factors setting the limits to the range are discussed and a method of raising the upper limit to 10^{20} atoms/cm^3 is indicated. The results are discussed in relation to the theory presented by Smits and Miller.

§ 1. INTRODUCTION

DIFFUSION of phosphorus into silicon from an infinite source, that is, one which is large compared with the total quantity diffused, gives a surface concentration of about 10^{20} atoms/cm^3, a value which apparently only depends on the solubility of phosphorus in silicon at the diffusion temperature. Measurements made in this laboratory suggest, in agreement with the theoretical considerations of Thurmond and Struthers (1953), that the solubility is practically constant over a range of diffusion temperatures from about 900–1300°c.

For some applications it is desirable that the value of surface concentration be controllable and this paper describes a method using a controlled vapour pressure of phosphorus, which has given values of the surface concentration in the range 10^{16} to 5×10^{18} atoms/cm^3, and a technique for extending the upper limit to 10^{20} atoms/cm^3 is indicated. The experiments are described in some detail as it is believed that consistent results depend markedly on the correct procedure. A preliminary report on the results has been published (Coupland 1958).

§ 2. EXPERIMENTAL DETAIL

A diagram of the apparatus is shown in figure 1. Boron-doped p-type silicon slices from vacuum-pulled crystals are lapped on Unirundum 85 powder, thoroughly cleaned in an ultrasonic wash and finally polished to a mirror finish in an etch of $4HNO_3:HF$, about $100\,\mu$ being etched off each face to ensure freedom from working layers at the surface. Slices with visible imperfections are rejected. The slices are mounted vertically in a 'toast rack' of vacuum pulled silicon of better than 200 ohm cm resistivity, and placed in a quartz tube.

Pure distilled yellow phosphorus is dropped into a thin-walled glass phial, previously partly filled with solid CO_2 to displace oxygen, pumped to a vacuum of about 10^{-5} mb and sealed off. The phial is placed in an extension of the quartz tube, in a constant temperature bath, together with a steel ball used later to break it open. The whole system with the end containing the silicon slices held in a vacuum furnace is sealed to a pumping system and care taken to arrange that the phosphorus is in the coldest part of the system, heating tapes being used where necessary.

---

† Now at British Joint Services Mission (Navy Staff), Washington, D.C.

The furnace is raised to 700°c over a period of about 2·5 hours, the system being pumped to a hard vacuum to ensure thorough outgassing of the quartz and some measure of vacuum clean-up of the silicon. At 700°c the tube is sealed off from the pump, the phosphorus phial broken and the temperature slowly raised to 1000°c over two hours to allow the phosphorus vapour to come to equilibrium throughout the system. The furnace is then rapidly raised to the desired diffusion temperature and controlled to within ±2°c.

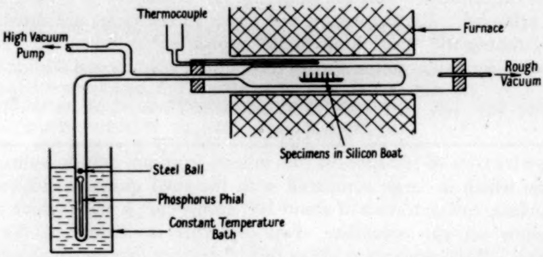

Figure 1.

It is believed that consistency of the results depends largely on the cleanliness of the silicon surfaces and the lowest possible level of residual gas in the system.

After diffusion and cooling, at a rate of 10 deg min^{-1} at the maximum temperature, the slices are clean in appearance but have a matt surface.

The junction depths for each batch are measured by lapping a 5° bevel and staining, to show up the p-region. The impurity concentration through the surface layer is then determined by successive etching and four probe conductance measurements, both techniques being described by Fuller and Ditzenberger (1956), the variation of mobility with impurity concentration needed in this determination being taken from Morin and Maita (1954). This technique gives close agreement with values found by radio-activation analysis.

§ 3. RESULTS

Table 1, columns (1)–(6), gives details of the experimental results. It will be noted that several experiments were tried at −43°c and only one was successful. The value of surface concentration given for that experiment is probably only reliable to ±100%. The negative results do show, however, that the junctions are not produced by heat treatment effects, presumably due to the fact that crystals are vacuum pulled.

Figure 2 is a plot of surface concentration and phosphorus vapour pressure against temperature. The phosphorus vapour pressure has been reported by McRae and Van Voorhis (Tennessee Valley Authority 1950) for the range +20° to +40°c and these results fitted to an equation which has thermodynamic

Table 1

(1)	(2)	(3)	(4)	(5)	(6)	(7)	(8)
7	0·8	1200	12	78	10^{18}	—	—
10	0·8	1200	12	34	5×10^{18}	$9{\cdot}4 \times 10^{3}$	0·4
1	1·0	1200	24	20	10^{18}	$5{\cdot}2 \times 10^{3}$	0·2
2	1·0	1200	24	20	$1{\cdot}5 \times 10^{18}$	$7{\cdot}8 \times 10^{3}$	0·3
5	0·7	1200	17	20	2×10^{18}	$1{\cdot}05 \times 10^{4}$	0·4
6	0·6	1200	12	20	$1{\cdot}5 \times 10^{18}$	$7{\cdot}8 \times 10^{3}$	0·3
8	0·8	1200	12	0	5×10^{17}	$1{\cdot}6 \times 10^{4}$	0·6
9	0·8	1200	8	−20·05	$1{\cdot}5 \times 10^{17}$	$3{\cdot}3 \times 10^{4}$	1·4
14	0·7	1200	12	−26·5	6×10^{16}	$2{\cdot}4 \times 10^{4}$	1·0
20	80·0	1200	18	−29·0	$2{\cdot}5 \times 10^{16}$	$1{\cdot}5 \times 10^{4}$	0·6
21	80·0	1200	18	−39·7	$1{\cdot}5 \times 10^{16}$	$3{\cdot}5 \times 10^{4}$	1·4
22	80·0	1200	18	−45·0	3×10^{15}	$1{\cdot}3 \times 10^{4}$	0·6
15	99·8	1200	12	−43·0	No n-type region		
13	0·7	1200	10	−43·0	No n-type region		
11	0·8	1100	44	20·0	4×10^{18}	2×10^{4}	0·8
27	0·7	1100	36	0	$1{\cdot}3 \times 10^{18}$	$3{\cdot}8 \times 10^{4}$	1·6
30	0·7	1150	18	0	$7{\cdot}5 \times 10^{17}$	$2{\cdot}2 \times 10^{4}$	0·9
29	0·7	1250	12	0	$3{\cdot}3 \times 10^{17}$	$1{\cdot}1 \times 10^{4}$	0·4

(1) Experiment No. ; (2) slice resistivity (ohm cm) ; (3) diffusion temperature (°c) ; (4) diffusion time (hours) ; (5) phosphorus temperature (°c) ; (6) surface concentration (atoms/cm³) ; (7) k_g ; (8) S/K (sec⁻¹).

validity. The curve given here is an extrapolation of this equation but as a check the vapour pressure at 0°c has been determined. This value is shown to be in good agreement with the extrapolated value.

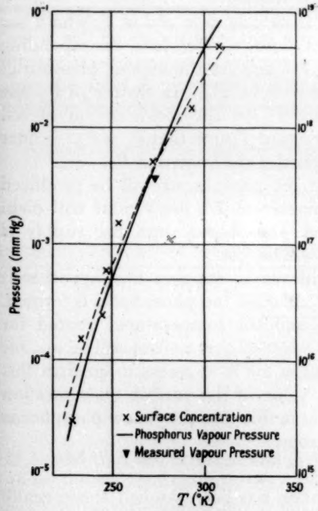

Figure 2.

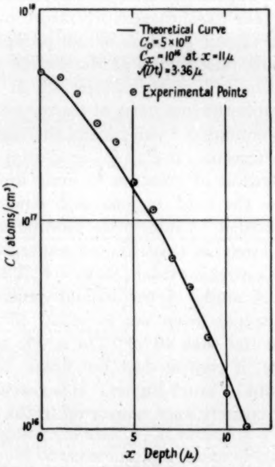

Figure 3.

Figure 3 is a typical curve for impurity concentration against diffusion depth. The solution of Fick's law for an infinite source of diffusant at the surface $x=0$, which is of the form

$$C(x, t)=C_0 \operatorname{erfc} x/2(Dt)^{1/2} \quad \ldots (1)$$

(D = diffusion constant), has been fitted both to the measured value of C_0 at $x=0$ and to the measured value of x for which $C(x, t)=10^{16}$ atoms/cm^3. This is plotted as a full curve in figure 3, the reasonable agreement with the individual experimental points showing that equation (1) is obeyed under the conditions of the experiment. From the fitted curve a value of D can be deduced, and when averaged from over all the measurements at 1200°c this gives $D=2{\cdot}7\pm0{\cdot}5\times10^{-12}$ cm^2 sec^{-1} for phosphorus in silicon at 1200°c. This value agrees closely with that given by Fuller and Ditzenberger (1956), but the individual scatter amounts to ±50%, due to uncertainties on the temperature and concentration measurements.

§ 4. Discussion

4.1. *Use of Yellow Phosphorus*

Red phosphorus would be easier to handle than yellow, but there is considerable uncertainty as to its composition and to whether, under the usual methods of preparation, it has a unique vapour pressure (Tennessee Valley Authority 1950). Early experiments with red phosphorus at temperatures of 200°c gave inconsistent results. Yellow phosphorus which is readily available in a highly purified form is therefore used. However, at some temperature, which seems to be uncertain, the vapour will condense in the form of red phosphorus, a deposit of which is found on the tube in all these experiments. It may be argued as follows that under certain conditions this will not affect the results.

Suppose the temperature of conversion from yellow to red is T, which lies between the furnace temperature and the cool source temperature, corresponding to a vapour pressure of red phosphorus of P_T, and let the vapour pressure of yellow phosphorus at the source temperature θ be P_θ. If then $P_\theta < P_T$ the system will reach equilibrium at a pressure P_θ by the condensation of red phosphorus into parts of the tube at a temperature T such that $P_T = P_\theta$. Under this condition θ will control the vapour pressure in the system at P_θ.

However, if $P_\theta > P_{T'}$ it is supposed that red phosphorus will be produced regardless of pressure at some limiting temperature T', the vapour will distil from the cold regions and convert to red phosphorus until the supply is exhausted. Under these conditions control will be lost.

There is only limited experimental evidence to support this hypothesis: (i) Control is evident from −45°c to +34°c although red phosphorus is formed. (ii) A study of the vapour pressure data and the temperatures quoted for conversion from red to yellow phosphorus suggests that control will be lost for θ greater than 40°c. The single experiment at $\theta=78$°c seems to confirm this since, if control does not break down, the value of the surface concentration should be much higher. It is noteworthy that in this case the yellow phosphorus had entirely been converted to the red allotrope.

4.2. *Theory*

Diffusion of antimony out from germanium has been studied theoretically and practically by Smits and Miller (1956, 1957), and also by Lehovic *et al.*

(1957). Experiments of the diffusion of antimony into germanium have also been reported by Kosenko (1956).

A parameter k_g is defined by Smits and Miller,

$$k_g = \frac{\text{Surface density of diffusant atoms in solid}}{\text{Density of diffusant atoms in vapour}} = \frac{N_e}{N_g}$$

which is constant for a particular experiment provided a state of 'quasi-equilibrium' is achieved.

It is supposed that at the surface of the solid a potential barrier of magnitude E ev exists, which must be overcome by a molecule that is to attach itself to the surface, from whence it will either diffuse into the bulk material or re-evaporate.

By kinetic theory the number N of molecules striking unit area of a surface in unit time is given by $N = \frac{1}{4} N_g \bar{V}$ where $\bar{V}$ is the mean molecular velocity.

Of these only a fraction S will have sufficient energy to overcome the barrier potential and hence the number attaching to the surface will be $\frac{1}{4} S N_g \bar{V}$ where S represents the fraction of molecules such that $\frac{1}{2} mu^2 \geqslant E$, where u is the molecular velocity. The number re-evaporating will be proportional to the surface density, that is, KN_e where K = a rate constant. At equilibrium, then,

$$KN_e = \tfrac{1}{4} N_g \bar{V} S$$

i.e.

$$N_e = \frac{S}{K} \frac{p}{2\pi m \boldsymbol{k} T^{1/2}} \qquad \ldots\ldots (2)$$

where p = diffusant gas pressure determined by the temperature θ, m = mass of impurity molecule, T = temperature of the solid, $\boldsymbol{k}$ = Boltzmann's constant.

Since S and K are independent of the phosphorus pressure, N_e should be proportional to p for constant T. This is verified by the results in figure 2.

Equation (1) is only strictly true when diffusion into the solid has ceased, but it will be shown later that a state of 'quasi-equilibrium' exists where the surface concentration is effectively constant and the rate of flow of impurities into the solid is very much less than the number re-evaporating; here this equation becomes a good approximation. From the experimental results values of k_g and S/K are deduced and given in columns (7) and (8) of table 1. For a given diffusion temperature the ratio S/K should be constant; the values obtained show some variation, which is not correlated with the phosphorus temperature and is probably due to the different states of the surfaces in different experiments.

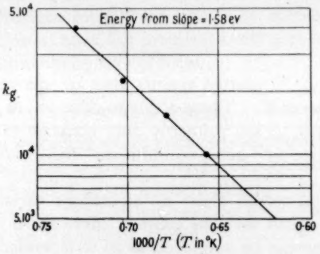

Figure 4.

Smits and Miller have shown that the value of the barrier potential E may be estimated from the slope of the curve of k_g plotted against I/T shown in figure 4. Then, assuming a Maxwellian velocity distribution in the gas, and applying the condition $\frac{1}{2}mu^2 \geqslant E$, the value of S may be estimated, and a value for K follows from the experimentally determined ratio S/K. Application of this analysis to the results in figure 4 gives $E = 1{\cdot}4$ ev and hence

$$S = 10^{-4}, \quad K = 10^{-4}\ \text{sec}^{-1} \text{ at } 1200°\text{c}.$$

The solution to the diffusion equation under the particular boundary conditions of constant diffusant density (in the gaseous phase) and zero concentration in the solid at $t = 0$ is given as

$$N(y, z)/N_e = \exp y^2\ [\exp(y^2) \operatorname{erfc} y - \exp\{(y+z)^2\} \operatorname{erfc}(y+z)] = f(y, z) \qquad \ldots\ldots (3)$$

where $N(y, z)$ is the density at (y, z), D is the diffusion constant, x is distance measured from $x = 0$ at the surface, $y = x/2(Dt)^{1/2}$ and $z = (Dt)^{1/2}K/d$. As t, $z \to \infty$, $f(y, z)$ reduces to the asymptotic form (equation (1)) $f(y, z) = \operatorname{erfc} y$ which is the equation for diffusion from a constant supply and represents the 'quasi-equilibrium' state.

At the surface $x = 0$ and equation (3) reduces to

$$N(0, z)/N_e = 1 - \exp(z^2) \operatorname{erfc} z.$$

Hence the state of 'quasi-equilibrium' exists when $\exp(z^2) \operatorname{erfc} z$ is less than the experimental error of the measurements.

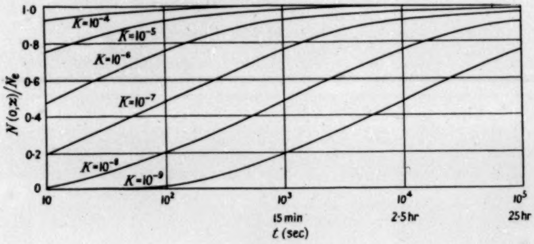

Figure 5.

Curves of $N(0, z)/N_e$ plotted against time are shown in figure 5 for various values of the parameter K. These apply to diffusion at 1200°c. Since experimental values of $N(0, z)$ are probably only accurate to about 50% a value of $K > 10^{-7}$ gives a state of 'quasi-equilibrium' for diffusion times greater than 1 hour or so.

The experimental values show no significant variation with the diffusion period; this fact, coupled with the estimate given above for K, shows that under these conditions time can be employed as an independent parameter to produce varying junction depths.

4.3. *Limitations of Application*

The simple theory outlined above takes no account of the evaporation of silicon during diffusion. This could be expected to affect the theory in two ways: (i) by causing sufficient loss of material during the diffusion so that the boundary conditions leading to equation (2) no longer apply, (ii) by collision of the phosphorus molecules with the mass flow of silicon atoms, evaporated from the surface, moving to cooler parts of the system.

To the first order, the former will only affect the diffusion constant, since the rate of displacement of the surface will be a slowly varying function of time. This effect is believed to be negligible within the experimental accuracy.

The latter will only assume importance when the vapour pressure of silicon becomes comparable with that of the phosphorus. This will vary with diffusion temperature and reference to figure 2 indicates the approximate lower limit of surface concentration set by this effect.

These values are given in table 2 with values of silicon vapour pressure reported by Honig (1957).

Table 2

Temperature (°c)	1100	1200	1300	1350
Surface concentration (atoms/cm^3)	3×10^{14}	2×10^{15}	2×10^{16}	10^{17}
Silicon vapour pressure (mm Hg)	3×10^{-6}	2×10^{-5}	2×10^{-4}	10^{-3}

Reference to table 1 shows that difficulty has been found in producing junctions with surface values of 3×10^{15} atoms /cm^3 at 1200°c which supports the above conclusions. It should, however, be possible to lower the surface concentration below 3×10^{15} atoms/cm^3 by diffusion at a lower temperature, at the expense of very much longer diffusion times for a given junction depth. The upper limit in these experiments is about 5×10^{18} atoms/cm^3; however there appears to be no reason why a similar process could not be used for red phosphorus, provided this could be obtained in a pure unique state. Values in the range 10^{18}–10^{20} can readily be obtained by the two stage diffusion process. Phosphorus is diffused from an infinite source to produce a thin layer with the saturated surface concentration value, the total amount of diffused phosphorus then being calculable as a function of diffusion time. A second stage of diffusion with no external source, then causes the phosphorus to diffuse further into the solid to the required depth. Since the total number of phosphorus atoms is now constant, the concentration at the surface must decrease. The surface concentration is a function of the first diffusion time, but practical limits gives about 10^{18} atoms/cm^3 as the lowest value attainable by this process.

§ 5. CONCLUSION

A method has been described which enables phosphorus diffused junctions in silicon to be prepared with a given surface concentration within the range 10^{16}–5×10^{18} atoms/cm^3 and a given junction depth. A method of extending the upper limit is indicated. The limitations have been discussed and the results agree with the theory by Smits and Miller.

ACKNOWLEDGMENTS

The author would like to acknowledge the help of Miss B. Hart and Mr. T. James for assistance in preparing the apparatus and Miss J. Goodson for the conductivity measurements. Acknowledgment is made to the Admiralty for permission to publish this paper.

REFERENCES

COUPLAND, M. J., 1958, *Nature, Lond.*, **181**, 1331.
FULLER, C. S., and DITZENBERGER, J. A., 1956, *J. Appl. Phys.*, **27**, 544.
HONIG, R. E., 1957, *R.C.A. Review*, **18**, 195.
KOSENKO, V. E., 1956, *Isv. Akad. Nauk. S.S.S.R, Ser. Fiz.*, **20**, 1526.
LEHOVIC, K., SCHOENI, K., and ZULEEG, R., 1957, *J. Appl. Phys.*, **28**, 420.
MORIN, F. J., and MAITA, J. P., 1954, *Phys. Rev.*, **96**, 28.
SMITS, F. M., and MILLER, R. C., 1956, *Phys. Rev.*, **104**, 1242.
—— 1957, *Ibid.*, **107**, 65.
TENNESSEE VALLEY AUTHORITY, 1950, *Chem. Eng. Report* No. 8.
THURMOND, C. D., and STRUTHERS, J. D., 1953, *J. Phys. Chem.*, **57**, 831.

Competitive Processes in the Photodisintegration of Nickel

By J. H. CARVER and W. TURCHINETZ
Research School of Physical Sciences, Australian National University, Canberra

MS. received 22nd September 1958, in final form 9th December 1958

Abstract. Excitation functions have been measured for the (γ, n), (γ, p) and (γ, pn+γ, 2n) reactions in ^{58}Ni and the (γ, p) reaction in ^{62}Ni, from threshold to 32 MeV. A preponderance of protons is found from ^{58}Ni with the ratio

$$\int_0^{32} \sigma(\gamma,\ \mathrm{p})dE \Big/ \int_0^{32} \sigma(\gamma,\ \mathrm{n})dE = 2{\cdot}35 \pm 0{\cdot}20.$$

The shapes of the (γ, n) and (γ, p) cross sections are found to be very similar, peaking near 19 MeV with widths of about 4·3 MeV. The ^{58}Ni (γ, pn+γ, 2n) cross section increases monotonically from threshold to 32 MeV, and the integrated cross section is about 12% of the total which is

$$\int_0^{32} [\sigma(\gamma,\mathrm{n}) + \sigma(\gamma,\mathrm{p}) + \sigma(\gamma,\mathrm{pn}+\gamma,2\mathrm{n})]\, dE = (0{\cdot}84 \pm 0{\cdot}10)\ \text{MeV barns}.$$

The ^{62}Ni (γ, p) reaction is found to have an integrated cross section of (0·13 ± 0·02) MeV barns and to peak at 22 MeV, with a width of about 5·2 MeV.

§ 1. Introduction

Experiments on the competitive modes of decay of medium-weight nuclei bombarded by charged particles with energies of about 20 MeV have shown a preponderance of protons among the reaction products (Cohen and Newman 1955, Cohen, Newman and Handley 1955, Cohen 1957, Ghoshal 1950). It is therefore of interest to see whether a similar preponderance of protons occurs among the photodisintegration products of medium-weight nuclei.

^{58}Ni is a suitable nucleus for this work since the (γ, p), (γ, n), (γ, 2n) and (γ, pn) reactions all lead to radioactive products so that a comparison of, in particular, the (γ, p) and (γ, n) yields can be made very simply. This method should lead to a better estimate of the relative proton and neutron yields than can, for example, be obtained by combining the ^{58}Ni (γ, n) activation data of Katz *et al.* (1951) with the data of Halpern and Mann (1951), who counted the photo-protons emitted from foils of natural nickel. The photo-proton and photo-neutron yields for ^{58}Ni estimated from these two experiments are approximately equal, whereas Cohen, Newman and Handley (1955) find that for ^{58}Ni

$$\sigma(\mathrm{p}, 2\mathrm{p})/\{\sigma(\mathrm{p}, \mathrm{pn}) + \sigma(\mathrm{p}, 2\mathrm{n})\} = 2{\cdot}8.$$

The reactions which have been studied in the present experiment are listed in table 1, together with their thresholds and some properties of the residual radioactive nuclei. Further details of the decay schemes are given in the next section.

The four listed reactions in ^{58}Ni, taken together with ^{58}Ni (γ, α) (Spicer *et al.* 1957), should virtually exhaust the total absorption cross section thus permitting a meaningful comparison with sum rule calculations. The ^{60}Ni (γ, pn) reaction

Table 1

(1)	(2)	(3)	(4)	(5)
^{58}Ni(γ, n)	67·8	11·7	36 hr ^{57}Ni	γ^+, 123, 1360
^{58}Ni(γ, p)	67·8	7·7	270 day ^{57}Co	127
^{58}Ni(γ, 2n)	67·8	22·8	6·4 day ^{56}Ni	Many
^{58}Ni(γ, pn)	67·8	19·3	77 day ^{56}Co	γ^+, 845, 1200 etc.
^{60}Ni(γ, pn)	26·2	19·8	72 day ^{58}Co	γ^+, 805
^{62}Ni(γ, p)	3·66	11·3	99 min ^{61}Co	70

(1) Reaction; (2) target % abundance; (3) threshold (MEV); (4) product activity; (5) prominent γ-rays (kev). γ^+ indicates positron annihilation radiation.

gives rise to a complication that will be discussed below, while the ^{62}Ni(γ, p) reaction provides an interesting comparison with the (γ, p) reaction in ^{58}Ni. The approximate symmetry of ^{58}Ni ($Z=28$, $N=30$) makes a careful measurement of the (γ, p) and (γ, n) cross section shapes of some interest from the viewpoint of the single-particle theory of photon absorption (Wilkinson 1956) insofar as the giant resonance behaviour is expected to reflect the properties of the nuclear potential seen by neutrons and protons.

§ 2. EXPERIMENTAL PROCEDURE

Samples of nickel metal ($<0{\cdot}1$% cobalt impurity) were irradiated in the bremsstrahlung from the Canberra electron-synchrotron in 1-MEV steps from 12 to 32 MEV. The lower limit of 12 MEV was that at which no yield from the ^{58}Ni (γ, n) reaction was observed after a six-hour irradiation. Although the ^{58}Ni (γ, p) threshold is some 4 MEV lower in energy, owing to the very long half-life of the product nucleus ^{57}Co (270 days) and the shape of the cross section (figure 2), prohibitively long irradiation and counting times would have been required to extend the measurements below 12 MEV. Irradiations were of duration from six hours to one hour as the bremsstrahlung energy was increased. Target samples were cylinders of $\frac{1}{2}$-inch in diameter and of two different thicknesses: 390 mg cm^{-2} (thin) and 5 g cm^{-2} (thick). Two cylinders were irradiated simultaneously with two thin foils of tantalum metal on each side of the thick sample and with the thin sample on the side of the target facing the synchrotron. This procedure was necessary owing to the long half-lives of some of the reaction products of interest. The tantalum foils were used to monitor the dose per irradiation through the yield of the ^{181}Ta (γ, n) reactions. The radioactive product yields† were measured with the aid of a scintillation spectrometer, a detailed description of which has been published (Carver and Turchinetz 1958). The procedures adopted for each particular reaction are outlined below.

^{58}Ni (γ, n). Relative yields were determined from the intensity of the annihilation radiation and the 1·36 MEV gamma radiation. The absolute yield was obtained by comparing the yield of the annihilation radiation with the annihilation radiation from ^{62}Cu produced by simultaneous irradiation of similar nickel and copper discs and counting in the same geometry. The ^{57}Ni decay scheme adopted was that of Konijn, Hagedoorn and Van Nooijen (1958), and the ^{62}Cu decay scheme was taken from the compilation of Way *et al.* (1955). The contribution of the uncertainties in the decay scheme of ^{57}Ni to the probable error in the absolute yield is about 10%.

---

† All radioactive yields have been corrected for decay during irradiation.

The absolute yield of the ^{63}Cu (γ, n) reaction was taken from the work of Berman and Brown (1953) which is the adopted standard in this laboratory. Berman and Brown estimate their uncertainty in the ^{63}Cu (γ, n) integrated cross section as 5%. In this work it is estimated that the integrated cross section for the ^{58}Ni (γ, n) reaction is known to within 15%, while the ordinate of the excitation function (figure 2) may be in error by as much as 20%.

^{58}Ni (γ, p). Because ^{57}Ni decays to form ^{57}Co, the total ^{57}Co activity some weeks after an irradiation is an index of the combined (γ, p + γ, n) yield. Owing to the presence of a line at 123 kev in the spectrum of ^{57}Ni, it was necessary to allow the ^{57}Ni to decay and to determine this combined yield by measuring the intensity of the 127 kev line in the ^{57}Co spectrum. To separate the contributions of the (γ, p) and (γ, n) reactions to the total ^{57}Co activity a chemical procedure was used.† Ten grams of finely divided nickel powder ($<$ 0·01% cobalt impurity) were irradiated at 30 Mev for three hours, at the end of which a modified cobalti-nitrite separation of the cobalt fraction allowed a measure of the (γ, p) yield. After two weeks a second cobalt separation gave a measure of the (γ, n) yield through the same activity. This procedure has the obvious advantage of eliminating all uncertainties from the ratio of (γ, p) and (γ, n) yields, except those due to counting statistics and chemical extraction efficiency. In both separations, 5 mg of Co carrier was used and better than 99% recovery could be achieved in 45 minutes. From the ratio (γ, p)/(γ, n) obtained in this way and the (γ, n + γ, p) activation curve derived from the ^{57}Co yield, the (γ, p) activation curve was extracted.

The half-life of ^{57}Co is 270 days; hence to measure the (γ, n + γ, p) activation curve with adequate statistical accuracy (within 3%) in reasonable irradiation and counting times, it was necessary to use the thick samples. To check on the possible effect the use of the thick sample might have on the shape of the activation curve through differential absorption of the bremsstrahlung spectrum, measurements were made of the ratio of the yields (γ, n)/(γ, n + γ, p) at three different energies (14, 24 and 30 Mev) in both the thin and the thick samples. From the agreement of these ratios, within 3%, for the two thicknesses of target it was concluded that this expedient introduced no appreciable systematic error in the (γ, n + γ, p) yield curve.

^{58}Ni (γ, pn + γ, 2n). The half-life (6·4 days) and the characteristic radiation of ^{56}Ni are such that it was not possible to extract from the counting data a reliable activation curve for the reaction ^{58}Ni (γ, 2n). Fortunately, however, ^{56}Ni decays to form ^{56}Co which is also the product of the reaction ^{58}Ni (γ, pn). Thus by measuring the ^{56}Co yield about 40 days ($\sim$ 6 ^{56}Ni half-lives) after the irradiation, it was possible to determine the combined (γ, pn + γ, 2n) activation curve. The most prominent features in the ^{56}Co γ-ray spectrum are the positron annihilation line and a line at 845 kev. Owing to the presence of ^{58}Co, which is produced through the (γ, pn) reaction in the 26·2% isotope ^{60}Ni, and whose γ-ray spectrum comprises two lines at 511 and 850 kev, the ^{56}Co yield was determined by counting the γ-rays in a broad group centring at about 1·25 Mev. To estimate the absolute yield the decay scheme proposed by Diddens *et al.* (1958) was adopted.

^{62}Ni (γ, p). A separate series of 1-hour runs, using the thin targets, was performed to measure the activation curve for this reaction, via the 99-min ^{61}Co activity.

---

† We are indebted to Dr. R. Mills and Mr. M. J. Vernon for performing the chemical separations.

Sufficient ^{57}Ni activity was generated so that an independent determination of the ^{58}Ni (γ, n) activation curve was made. The absolute yield of the reaction ^{62}Ni (γ, p) was determined adopting the decay scheme proposed by Way *et al.* (1955).

§ 3. Results and Discussion

The activation curves for the reactions studied are shown in figure 1. Also plotted in this figure is the yield ratio ^{58}Ni (γ, p)/^{58}Ni (γ, n) which shows clearly the predominance of protons, at all energies, in the photodisintegration of ^{58}Ni, and suggests a small but real difference in the shape of the giant resonance for the (γ, n) and (γ, p) reactions. The excitation functions derived from the activation curves by an iterative method (Carver and Lokan 1957) are shown in figure 2. In table 2 are collected the parameters relevant to the discussion that follows.

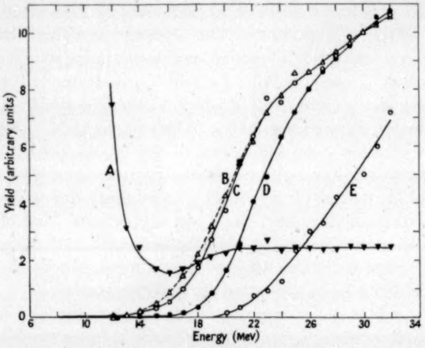

Figure 1. Activation curves for the photodisintegration of nickel: A, ^{58}Ni(γ, p)/^{58}Ni(γ, n); B, ^{58}Ni(γ, n); C, ^{58}Ni(γ, p); D, ^{62}Ni(γ, p); E, ^{58}Ni$(\gamma, np+\gamma, 2n)$. The ordinates for curves B, C, D, E are in arbitrary units, while those for curve A give the ratio absolutely.

Table 2

(1)	(2)	(3)	(4)	(5)
^{58}Ni(γ, n)	0·032	4·4	19·0	0·22 ± 0·03
^{58}Ni(γ, p)	0·093	4·2	19·5	0·52 ± 0·09
^{58}Ni$(\gamma, pn+\gamma, 2n)$	0·013	—	> 32	> 0·10 ± 0·02
^{58}Ni$[(\gamma, n)+(\gamma, p)+(\gamma, pn)+(\gamma, 2n)]$	0·125	4·8	19·5	0·84 ± 0·10
^{62}Ni(γ, p)	0·019	5·2	22	0·13 ± 0·02

(1) Reaction; (2) $\sigma_{\max}$ (barns); (3) $\Gamma(\frac{1}{2}\sigma_{\max})$ (Mev); (4) $E\sigma_{\max}$ (Mev); (5) $\int_0^{32} \sigma dE$ (Mev barns).

The ^{58}Ni (γ, n) cross section has been measured previously by Katz *et al.* (1951), who obtained the value 0·33 Mev barns for the cross section integrated to 22 Mev. Part of the difference between this and the present value of 0·22 ± 0·03 Mev barns is due to the fact that present data are normalized to the value 0·55 ± 0·03 MeV barns for the ^{63}Cu (γ, n) cross section integrated to 30 MeV (Berman and Brown 1953), whereas the Saskatchewan data relate to a value of 0·66 MeV barns for this cross section integrated to 22 MeV.

The value obtained for the ^{58}Ni (γ, p) integrated cross section, 0·52 ± 0·09 MeV barns, is considerably larger than that which can be inferred from the data of Halpern and Mann (1951). These authors measured the proton yield from foils of natural nickel and if, on account of its low (γ, p) threshold, all the protons are assumed to come from ^{58}Ni, their cross section integrated to 22 MeV is 0·32 MeV barns. The absolute proton yields of Halpern and Mann may have been underestimated, however, since the low counting rates required the use of thick (~5 MeV) targets and involved substantial corrections for self-absorption, which corrections are difficult to make owing to uncertainties in the initial proton energy spectrum. It is noteworthy that the (γ, p) yields of this group, and those of Johansson (1955) who normalized his data to those of Halpern and Mann (1951), when combined with (γ, n) yields in the same elements, fall below the integrated absorption cross section predicted for electric dipole radiation, whereas the present results show that, for ^{58}Ni,

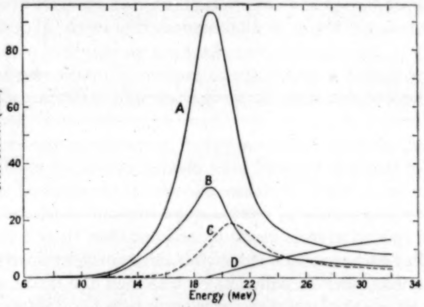

Figure 2. Excitation functions for the photodisintegration of nickel: A, ^{58}Ni(γ, p); B, ^{58}Ni(γ, n); C, ^{62}Ni(γ, p); D, ^{58}Ni(γ, np + γ, 2n).

$$\int_0^{32} [\sigma(\gamma, \mathrm{n}) + \sigma(\gamma, \mathrm{p}) + \sigma(\gamma, \mathrm{pn} + \gamma, 2\mathrm{n})]\,dE = (0{\cdot}84 \pm 0{\cdot}10) \text{ MeV barns,}$$

which may be compared with the value 0·87 MeV barns required by the sum rule with zero exchange parameter (Levinger and Bethe 1950). That the present estimate is a lower limit to the total integrated cross section is evident from the presence of high-energy 'tails' on both the (γ, p) and (γ, n) excitation functions and from the fact that up to 32 MeV the cross section for the (γ, pn + γ, 2n) reaction has not reached its maximum but has already contributed about 12% of the total integrated cross section. In addition, Spicer *et al.* (1957) have reported that the yield of α-particles from nickel is about 3% of the proton yield for 17·5 MeV bremsstrahlung.

The ratio $\int\sigma(\gamma, \mathrm{p})\,dE / \int\sigma(\gamma, \mathrm{n})\,dE$ is independent of the absolute scales and, in the present work, is 2·35 compared with about 1 as determined from the combined results of Katz *et al.* (1951) and Halpern and Mann (1951). In the present experiment the yield ratio depends only on the counting statistics and the chemical extraction efficiency and is known to within 5% as judged from the self-consistency of four separate determinations at 30 Mev. An additional uncertainty of about 10% exists in the ratio of the integrated cross sections owing to the necessity of unfolding the bremsstrahlung distribution from the yield curves to get the excitation functions. This uncertainty is always least when the activation curves are similar, as is approximately the case for ^{58}Ni (γ, p) and ^{58}Ni (γ, n).

The present experiment clearly shows the predominance of protons among the photodisintegration products of ^{58}Ni. It is interesting to compare this result with those of Cohen and Newman (1955). Cohen, Newman and Handley (1955) and Cohen (1957) who bombarded ^{58}Ni with 21·5 Mev protons and found that the (p, 2p) reaction was the most probable process with the cross section ratio $\sigma(p, 2p)/\{\sigma(p, pn) + \sigma(p, 2n)\} = 2{\cdot}8$. These and other data obtained by Cohen and his collaborators for medium-weight nuclei are difficult to explain in terms of the statistical theory, and Cohen suggests that direct interactions play an important role in these reactions. The incoming proton is assumed to have a large chance of being re-emitted after making one or, at most, a few collisions within the nucleus. This explains the observed preponderance of (p, pn) reactions over (p, 2n) reactions but does not explain those cases, such as ^{58}Ni, in which the (p, 2p) reaction is much more important than the (p, pn) reaction. A similar result has been obtained in this laboratory by Purser and Titterton (1959), who bombarded ^{58}Ni with 14 Mev neutrons and find

$$\sigma(n, np)/\sigma(n, 2n) = 4{\cdot}5 \pm 0{\cdot}9.$$

Thus for proton and neutron bombardment and for photon-induced reactions, proton emission from excited ^{58}Ni appears to be favoured over neutron emission by about the same factor.†

These results are difficult to understand in terms of the usual statistical theory (Blatt and Weisskopf 1952). However, the recent measurements of Butler and Gossett (1957) on the radiative capture of protons by ^{58}Ni and ^{60}Ni show that large fluctuations in level density occur near the closed shells $N, Z = 28$. Butler and Gossett find that ^{61}Cu with five particles outside the doubly closed $f_{7/2}$ shell has five times the level density of ^{59}Cu with three particles beyond the closed shells. Thus one would expect ^{57}Co, with one hole in the $f_{7/2}$ proton shell and two neutrons outside the $f_{7/2}$ neutron shell, to have a much higher level density than ^{57}Ni which has one neutron beyond a doubly closed shell. A difference of about a factor of 15 between the level densities of ^{57}Co and ^{57}Ni could account for the observed predominance of proton emission. Within the framework of the statistical theory an enhancement of proton emission can also be obtained by rounding off the Coulomb barrier (Scott 1954).

However, the energy and angular distribution measurements of Cohen (1957) on the (p, 2p) reaction and of Lijkin *et al.* (1956) on the (γ, p) reaction indicate that a substantial number of protons are emitted in direct processes and that this direct proton emission probably exceeds the total neutron yield. This latter observation is difficult to reconcile with the direct interaction theory of photodisintegration discussed by Wilkinson (1956). According to this theory, in ^{58}Ni with $N=30$ and $Z=28$, the total E1 photon absorption must proceed through the same transitions[†] in both the proton and neutron shells. The effect of the two 'valence' neutrons is expected to be small. Whether an excited nucleon is captured into a compound nucleus state or escapes in a 'resonance direct' process depends essentially on its mean free path in the nucleus, and to ask that this be larger for protons than for neutrons, when both are in the same state, would be to conspire against the charge independence of nuclear forces.

---

† In both the particle-induced reactions it seems proper to regard one of the emitted particles as being identical with the incident particle so that these experiments are measuring relative proton and neutron emission from excited ^{58}Ni.

The other nickel isotopes for which photodisintegration data are available are ^{60}Ni and ^{62}Ni. For ^{60}Ni Goldemberg and Katz (1954) report that the integrated (γ, n) cross section is 0·42 MEV barn, while the present experiment has yielded for ^{62}Ni an integrated (γ, p) cross section of $0{\cdot}13 \pm 0{\cdot}02$ MEV barn. Assuming that the (γ, n) and (γ, p) yields add up to the same value for each isotope (0·74 MEV barn for ^{58}Ni), a steady decline in the proton yield is evident as A increases. That this trend is due in part to the increasing proton threshold with A is suggested by figure 2, curve C, where the peak in the ^{62}Ni (γ, p) cross section (threshold 11·3 MEV) is about 2·5 MEV higher in energy than that for ^{58}Ni (γ, p) (threshold 7·7 MEV).

Similar trends are apparent in other elements, Fe and Cu, for example, where the neutron yields of the lightest isotopes, ^{54}Fe (Carver and Lokan 1957) and ^{63}Cu (Berman and Brown 1953), appear to be anomalously low, and Mo where the photoproton yield of ^{92}Mo is again very high (Butler and Almy 1953). These observations have led D. C. Peaslee (private communication) to suggest that in those isotopes for which the charge-to-mass ratio is too large, as revealed by a low proton binding energy, the proton distribution could project far enough beyond the nuclear mass distribution to result in an abnormally high associated electric dipole matrix element for proton emission. Electron scattering experiments (Hofstadter 1957), however, indicate that the mean square charge radius for ^{60}Ni is not much different from that of ^{58}Ni.

[†] The fact that $\sigma(\gamma, \mathrm{n})$ and $\sigma(\gamma, \mathrm{p})$ have peaks at about the same energy and are of approximately equal width (see figure 2) implies no great differences in the potential wells seen by protons and neutrons.

REFERENCES

BERMAN, A. I., and BROWN, K. L., 1953, *Phys. Rev.*, **96**, 83.

BLATT, J. M., and WEISSKOPF, V. F., 1952, *Theoretical Nuclear Physics* (New York: John Wiley & Sons).

BUTLER, J. W., and GOSSETT, C. R., 1957, *Phys. Rev.*, **108**, 1473.

BUTLER, W. A., and ALMY, G. M., 1953, *Phys. Rev.*, **91**, 58.

CARVER, J. H., and LOKAN, K. H., 1957, *Aust. J. Phys.*, **10**, 312.

CARVER, J. H., and TURCHINETZ, W., 1958, *Proc. Phys. Soc.*, **71**, 618.

COHEN, B. L., 1957, *Phys. Rev.*, **108**, 768.

COHEN, B. L., and NEWMAN, E., 1955, *Phys. Rev.*, **99**, 718.

COHEN, B. L., NEWMAN, E., and HANDLEY, T. H., 1955, *Phys. Rev.*, **99**, 723.

DIDDENS, A. N., HUISKAMP, W. J., SEVERIENS, J. C., MIEDEMA, A. R., and STEENLAND, M. J., 1958, *Nuclear Physics*, **5**, 58.

GHOSHAL, S. N., 1950, *Phys. Rev.*, **80**, 939.

GOLDEMBERG, J., and KATZ, L., 1954, *Can. J. Phys.*, **32**, 49.

HALPERN, J., and MANN, A. K., 1951, *Phys. Rev.*, **83**, 370.

HOFSTADTER, R., 1957, *Ann. Rev. Nucl. Sci.*, **7**, 231 (Palo Alto, Calif.: Ann. Rev. Inc.).

JOHANSSON, S. A. E., 1955, *Phys. Rev.*, **97**, 1186.

Katz, L., Baker, R. G., Haslam, R. N. H., and Douglas, R. A., 1951, *Phys. Rev.*, **82,** 271.
Konijn, J., Hagedoorn, H. L., and van Nooijen, B., 1958, *Physica*, **24,** 129.
Levinger, J. S., and Bethe, H. A., 1950, *Phys. Rev.*, **78,** 115.
Lijkin, E., Osokina, R., and Ratner, B., 1956, *Nuovo Cim.*, 10, **3,** Suppl. **1,** 105.
Purser, K., and Titterton, E. W., 1959, *Aust. J. Phys*, in the press.
Scott, J. M. C., 1954, *Phil. Mag.*, **45,** 441.
Spicer, B. M., Muirhead, E. G., and Shute, G. G., 1957, *Aust. J. Phys.*, **10,** 217.
Way, K., King, R. W., McGinnis, C. L., and van Lieshout, R., 1955, *Nuclear Level Schemes*, U.S.A.E.C. Report TID-5300.
Weinstock, E. V., and Halpern, J., 1954, *Phys. Rev.*, **94,** 1651.
Wilkinson, D. H., 1956, *Physica*, **22,** 1039.

Internal Ferromagnetic Resonance in Nickel

By J. C. ANDERSON† and B. DONOVAN‡

† Department of Physics, University of the Witwatersrand, Johannesburg
‡ Department of Physics, Bedford College, London

MS. received 3rd November 1958

Abstract. The internal resonance, revealed by measurements of the complex permeability, has been investigated in nickel over the temperature range 5°–100°c. The resonant frequency is found to be a decreasing function of temperature and, over the range studied, the variation is roughly from 450 to 300 Mc/s in the case of a polycrystalline disc, and from 270 to 40 Mc/s in the case of a colloidal suspension of nickel particles. This behaviour is consistent with the view that the resonance is due to the internal magnetic field associated with the anisotropy energy and a quantitative interpretation is attempted using the available experimental values for the anisotropy constants.

---

§ 1. Introduction

In an earlier paper (Anderson and Donovan 1957, to be referred to as I) an investigation of the complex permeability of iron–nickel alloys was described, with particular reference to the resonance phenomenon observable in the frequency range 300–400 Mc/s. This resonance may be interpreted in terms of the internal magnetic field in the crystal, arising from the anisotropy energy. In I the resonant frequency was measured for a series of compositions and the resulting variation was shown to be similar to that which would be expected on the basis of the known behaviour of the principal anisotropy coefficient upon which the internal field depends.

The measurements described in I were carried out on polycrystalline specimens at room temperature and the information obtained was essentially of a qualitative nature. In order to extend these experiments various other techniques have since been devised, primarily with the object of making measurements over a range of temperature, and the present paper deals with the results which have been obtained in the case of nickel. In this work, in addition to the study of polycrystalline samples, an attempt has been made to discover a specimen for which quantitative information can be deduced, i.e. for which a reliable value for the internal field can be calculated from the anisotropy coefficients. In view of the difficulty of producing a nickel single crystal suitable for apparatus covering a wide frequency range, it was decided to investigate the resonance in a dilute suspension of colloidal nickel particles.

The resonant frequency exhibited by the colloidal suspension is considerably lower than that for the polycrystalline specimen, as might be expected, and in both cases the frequency decreases with temperature over the range 5°–100°c. This behaviour is in accordance with the interpretation discussed in I and, in fact, the results for the small particles may be correlated to a reasonable extent with the available experimental data on the anisotropy coefficients.

§ 2. EXPERIMENTAL DETAILS: DISC SPECIMEN

The fundamental quantities to be measured are the real and imaginary parts of the complex permeability and in the earlier experiments, described in I, the method of Wieberdink (1950) was used, involving a coaxial transmission line with the test specimen forming the inner conductor. In view of the manifest unsuitability of this method for measurements over a range of temperature, a modification was introduced for polycrystalline nickel in the present work and the specimen took the form of a disc terminating the coaxial line. This technique proved eminently suitable for covering the frequency range 250–450 Mc/s in which the resonance was observed.

The outer conductor of the coaxial system was a silver plated copper tube of internal diameter 3·82 cm and the inner conductor was a solid silver rod of diameter 0·33 cm. The terminating disc (thickness 0·26 cm) was produced to special order from pure electrolytic nickel by the Mond Nickel Company. The final anneal was at 1000°c in an atmosphere of dry hydrogen and the subsequent rate of cooling was about 100°c per hour. The disc was electrolytically polished before being fitted to the apparatus. Heating was provided by a current of hot air, guided by a brass tube; the temperature was measured by two thermistors attached to the inside of the disc and it was found relatively simple to maintain the temperature constant to within 1°c.

The relevant transmission line theory (see, for example, Jackson 1945) may be put into a form whereby the surface impedance of the termination may be derived from measurements of the position of a short-circuiting piston on the line. The positions actually determined are those corresponding to the maxima of the first and second peaks of current in the terminating disc, and also those at which the magnitude of the first peak is equal to the maximum of the second. The current in the disc was measured (apart from a constant factor, which need not be known) by means of a galvanometer reading the direct current from a crystal rectifier connected to a pick-up loop close to the disc.

Having obtained the surface resistance and reactance the appropriate skin effect equation may be solved, bearing in mind that the thickness of the disc is much greater than the skin depth, and explicit expressions may be derived for the real and imaginary parts of the complex permeability, $\mu=\mu_1-i\mu_2$. The only other parameters required (apart from the operating frequency and the radii of the coaxial system) are the d.c. resistivity of the disc and its external self-inductance, which may be evaluated using a disc of identical form made of non-ferromagnetic metal.

§ 3. EXPERIMENTAL DETAILS: COLLOIDAL SUSPENSION

3.1. *Preparation of Specimen*

The magnetic properties of small ferromagnetic particles have been studied extensively and it is well known that particles of sufficiently small size behave as single domains. This property was demonstrated in the case of nickel particles by a significant experiment, described by Kittel, Galt and Campbell (1950), relating to very dilute suspensions in which the magnetic interactions between the particles could be neglected.

The method of preparing the colloidal suspension in the present work was similar to that used by Kittel *et al.* and involved the decomposition of nickel formate in diethyl phthalate. The latter was first distilled under partial vacuum and the middle fraction taken to ensure freedom from phthalic acid. The mixture was heated to 250°c under a reflux condenser until the reaction was complete. After filtering to remove the larger particles of nickel, the solution was boiled until the volume was halved and finally stabilized by the addition of a few drops of 1% soap solution.

A quantitative analysis of the solution was undertaken, using the nickel dimethyl glyoxime complex, and from comparative measurements with a Zeiss spectrophotometer the concentration of nickel was found to be 0·05% by weight. The particles were shown by electron micrographs to be approximately spherical in shape, with diameters in the range 25–50Å. This is considerably less than the critical diameter for single domain behaviour, estimated by Kittel *et al.* to be in the region of 600 Å.

3.2. *Measurement of Permeability*

The resonance phenomenon was observed to occur in the colloidal specimen at a considerably lower frequency than in the case of polycrystalline nickel. Accordingly an entirely different technique was developed for the measurement of permeability, in which the specimen could be placed inside a coil carrying an induced current of the desired frequency. When the specimen is inserted in the coil the magnitude of the induced current changes by an amount proportional to $|\mu| = (\mu_1{}^2 + \mu_2{}^2)^{1/2}$, and there is also a phase shift of $\tan^{-1}(\mu_2/\mu_1)$. The measurements of amplitude and phase were carried out by means of a modification of the Foster–Seeley discriminator circuit which, in the form developed, proved suitable for covering the frequency range 10–300 Mc/s.

A detailed description of the apparatus, together with the theory of the method, will be published elsewhere (Anderson 1959) and a brief outline only will be given here. L_1, L_2 and L_3 (figure 1) are three coils wound on a common former, into which a small test-tube containing the colloidal sample can be inserted. The primary coil L_1 is situated between the other two, which are wound in opposite directions and form the two identical halves of the secondary. A signal generator with high internal impedance is connected across L_1 and the primary e.m.f. is measured by means of the valve voltmeter V. The capacitance C_1 is used to

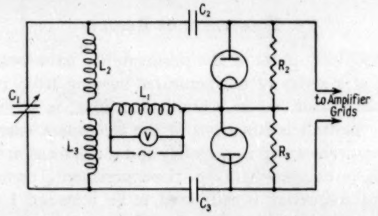

Figure 1. Phase discriminator used for measurements of complex permeability of colloidal suspension.

adjust the phase difference between the e.m.f. induced in the secondary coil and the primary e.m.f. The r.f. voltages across $L_2 + L_1$ and $L_3 + L_1$ are rectified and the d.c. voltages developed respectively across R_2 and R_3 are applied, after filtering, to the grids of a cathode-coupled amplifier. The time constants C_2R_2 and C_3R_3 must be smaller than the period of the r.f. signal at the highest operating frequency.

The method is essentially comparative, a 'blank' specimen of pure diethyl phthalate being used as a reference. With this 'blank' specimen in position C_1 is adjusted until the e.m.f. in the secondary is 90 degrees out of phase with the primary voltage. Under this condition the voltages across R_2 and R_3 are equal in magnitude and opposite in sense and the output observed at the amplifier is zero. When the 'blank' specimen is replaced by the colloidal sample the phase difference between the primary and secondary voltages departs from 90° by a small amount, and the net output produced may be measured in terms of the reading on a micro-ammeter connected between the anodes of the amplifier. In addition, the amplitude of the e.m.f. induced in the secondary coil may also be obtained from measurements at the amplifier, which is calibrated beforehand.

The variation of the temperature of the colloid raised practical difficulties, since no heating coil could be introduced into the test-tube owing to its effect on the electrical characteristics. The method finally adopted was to maintain the specimen at a constant temperature, insert it rapidly into the apparatus and take readings immediately. Separate measurements with a thermistor thermometer enabled the fall in temperature to be evaluated for the time interval of the operation. A similar procedure was adopted for the 'blank' specimen, but no change in the readings was detected for a temperature variation of ± 5°c.

The values of permeability for the colloidal suspension are, of course, very different from those obtained for polycrystalline specimens by the method described in § 2. In fact, as can be seen in figure 3, μ_2 is very small and μ_1 is very nearly unity; nevertheless, the resonance phenomenon, as discussed in I, is clearly exhibited. The error in the permeability measurements is estimated to be about 0·0005, i.e. of the order of 1% in μ_2 and 0·05% in μ_1.

§ 4. Discussion of Results

The real and imaginary parts of the permeability have been derived for the polycrystalline disc at a series of temperatures varying from room temperature to 100°c. A typical pair of curves, obtained at 20°c, is shown in figure 2, in which μ_1 and μ_2 are plotted as functions of the free-space wavelength λ_0. The dispersion phenomenon shows up very clearly and it will be seen that the resonance peak, exhibited by μ_2, is remarkably sharp; the experimental error in the determination of the resonant frequency is estimated to lie between 1 and 2%. When the resonant frequency is plotted as a function of temperature a reasonably smooth curve is obtained, as shown in figure 4, the downward trend of which indicates that the internal field diminishes with increasing temperature. It may be noted in passing that the frequency of 416 Mc/s obtained here at 20°c is slightly higher than the value of 378 Mc/s quoted in I for a long nickel wire.

In the case of the colloidal specimen the measurements were extended to 5°c and typical results, obtained at 55°c, are shown in figure 3, in which μ_1 and μ_2 are plotted directly against frequency. In this case a small subsidiary peak appears

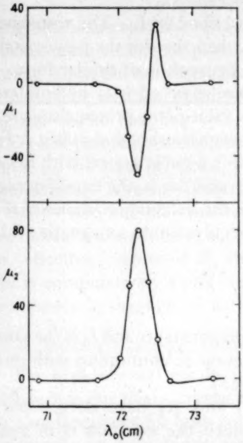

Figure 2. Variation of real and imaginary parts of complex permeability with free-space wavelength for nickel disc at 20°c.

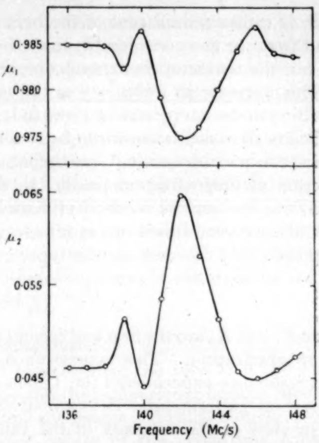

Figure 3. Variation of real and imaginary parts of complex permeability with frequency for suspension of nickel particles at 55°c.

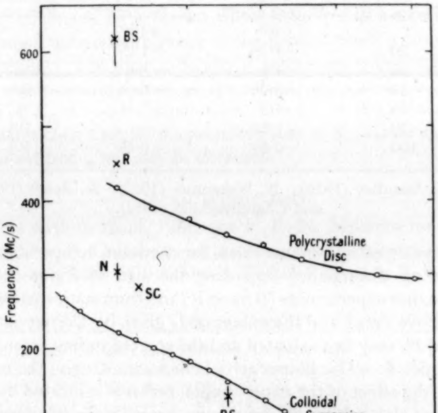

Figure 4. Variation of resonant frequency with temperature for polycrystalline disc and colloidal suspension. The crosses show the values obtained from the anisotropy constants listed in the table; experimental errors are indicated by vertical lines. For abbreviations see footnote to table.

which is rather reminiscent of the behaviour described in I. The resonance is found to occur at a considerably lower frequency than that for the polycrystalline disc but the temperature dependence, shown in figure 4, is of similar form.

This decrease in frequency as the temperature is raised is to be anticipated according to the interpretation given in I, since the value of the principal anisotropy coefficient in nickel is known to be small in the neighbourhood of 100°C. For a precise comparison one requires the internal field in a cubic crystal with the easy direction of magnetization parallel to the (111) axis, as is the case for nickel. Following the general method of Kittel (1948), the calculation shows that the effect of the crystal anisotropy may be regarded as equivalent to a magnetic field H_i, along the (111) direction, given by

$$H_i = \frac{4}{3I_s}\left(K_1 + \frac{K_2}{3}\right),$$

where K_1 and K_2 are the first and second anisotropy constants and I_s is the saturation magnetization. This expression is also relevant in connection with microwave resonance experiments (cf. Dillon *et al.* 1955).

Several experimental determinations of K_1 and K_2 have been reported, but in view of the diversity of the values obtained the situation is in general rather unsatisfactory. Some of the more recent results are summarized in the accompanying table.

Anisotropy Constants for Nickel

Temp. (°C)	K_1 (erg cm^{-3}) $\times 10^4$	K_2 (erg cm^{-3}) $\times 10^4$	Reference
20	−4·26	+1·09	N
20	−4·6	−3·6	R
20	−6·06	−6·06	BS
26	−4·5	+2·34	SC
50	−1·83	—	BS
100	−0·49	+0·49	BS

BS, Barlow and Standley (1958); N, Nakamura (1955); R, Reich (1956); SC, Sato and Chandrasekhar (1957).

While some measure of agreement exists for the room temperature values of K_1, there is a puzzling discrepancy regarding the sign of K_2 as determined from microwave resonance experiments (BS and R) and from static methods (SC and N).

Using the above data† and the values of I_s given by Corner and Hunt (1955), the internal field H_i may be evaluated and the corresponding resonant frequencies are shown in figure 4. The points are labelled according to the references given in the table and the effect of the experimental errors is indicated by a vertical line.

It will be seen that, although the results for the polycrystalline specimen are not of quantitative significance, those for the suspension of small particles do, in fact, suggest the possibility of an explanation in terms of the calculated internal field and good agreement is obtained at 50° and 100°C. At lower temperatures the situation is obscure on account of the conflicting experimental values for K_2. The magnitude of the internal field in this region, derived from the present work, is smaller than any of the values given by the 'theoretical' expression, even though these are spread over a range of 2:1. The main conclusion to be drawn is that a more consistent picture may be obtained with the present results if the value of K_2 in the neighbourhood of room temperature is positive.

---

† K_2 has been taken as zero at 50°C.

A further relevant point which may be mentioned is the correction due to magneto-elastic coupling and its effect on the anisotropy constants. Baltzer (1957) has pointed out that the ' intrinsic ' magnitudes of K_1 and K_2 are slightly larger, in the case of nickel, than the ' effective ' values obtained from static experiments. It seems likely that at the high frequency ($3{\cdot}5 \times 10^{10}$ c/s) employed by Barlow and Standley mechanical relaxation effects are insignificant and therefore Baltzer's correction is not relevant. In the present work, on the other hand, the ' effective ' values of K_1 and K_2 are required, but the effect on the internal field is comparatively small and a genuine comparison is not possible until the discrepancy in the sign of K_2 is resolved.

§ 5. CONCLUSION

The experimental results presented here confirm the view that the internal resonance is due to the crystal anisotropy and the temperature dependence of the resonant frequency for both polycrystalline specimens and single domain particles is generally in accordance with observed values of the anisotropy constants. In the case of small particles the results may be quantitatively explained in terms of the internal field calculated for a single crystal, though the agreement is least satisfactory in the neighbourhood of room temperature.

Several attempts have been made to explain the temperature dependence of the anisotropy constants by a formal theoretical treatment (cf. Carr 1958) but over the restricted temperature range of the present work a comparison does not prove enlightening. The main difficulty is associated with the lack of agreement between the experimental values of the anisotropy constants, and particularly with the sign of K_2 at room temperature. So far as the present measurements are concerned it is clear that, with a positive value of K_2, closer agreement with the observed resonant frequency may be obtained.

ACKNOWLEDGMENTS

The authors wish to thank Professor F. R. N. Nabarro for many invaluable discussions, and Mr. P. C. Roberts for assistance in the construction of apparatus. The helpful co-operation of the Mond Nickel Company is also acknowledged with gratitude.

REFERENCES

ANDERSON, J. C., 1959, *Rev. Sci. Instrum.*, in the press.
ANDERSON, J. C., and DONOVAN, B., 1957, *Proc. Phys. Soc.* B, **70,** 186.
BALTZER, P. K., 1957, *Phys. Rev.*, **108,** 580.
BARLOW, G. S., and STANDLEY, K. J., 1958, *Proc. Phys. Soc.*, **71,** 45.
CARR, W. J., 1958, *Phys. Rev.*, **109,** 1971.
CORNER, W. D., and HUNT, G. H., 1955, *Proc. Phys. Soc.* A, **68,** 133.
DILLON, J. F., GESCHWIND, S., and JACCARINO, V., 1955, *Phys. Rev.*, **100,** 750.
JACKSON, W., 1945, *High Frequency Transmission Lines* (London: Methuen).
KITTEL, C., 1948, *Phys. Rev.*, **73,** 155.
KITTEL, C., GALT, J. K., and CAMPBELL, W. E., 1950, *Phys. Rev.*, **77,** 725.
NAKAMURA, Y., 1955, *J. Phys. Soc., Japan*, **10,** 937.
REICH, K. H., 1956, *Phys. Rev.*, **101,** 1647.
SATO, H., and CHANDRASEKHAR, R. S., 1957, *J. Phys. Chem. Solids*, **1,** 228.
WIEBERDINK, A., 1950, *Appl. Sci. Res.* B, **1,** 439.

The Beta Rays of Praseodymium-144 and the Axial Vector Beta Interaction

By N. J. FREEMAN†
Physics Department, Bedford College, London

Communicated by H. O. W. Richardson; MS. received 30th October 1958

Abstract. The shapes, intensities and end-points of the three strong components of the ^{144}Pr beta spectrum have been measured with a prolate spheroidal field spectrometer and coincidence techniques. A spin of 0^- has been assigned to the ground state of ^{144}Pr on the basis of these measurements. It is shown that the pure axial vector correction factor for a $\Delta I = 0$ (yes) transition provides a good fit to the ground state spectrum. The spectrum of the β-transition to the 695 kev level in ^{144}Nd has a unique first forbidden shape.

§ 1. Introduction

Laubitz (1956) found evidence for a large value of the coupling constant g_P for the pseudoscalar (P) interaction in β-decay by studying the shape of the β-spectrum between the ground states of ^{144}Pr and ^{144}Nd. It was assumed that these states had zero spin but differing parity so that the scalar S and vector V interactions could not contribute. At that time there was strong evidence from the decay of ^{6}He (Rustad and Ruby 1955) that the axial vector A coupling constant was very weak in comparison with the tensor T coupling. Laubitz showed that the T or P interactions acting alone could not explain the shape of his spectrum, but he found a good fit with the combined T + P correction factor of Rose and Osborne (1954). It was, however, necessary to adopt a very large value greater than 100 for the ratio g_P/g_T. Alaga, Kofoed-Hansen and Winther (1953) have shown that such a large pseudoscalar coupling would influence the shape of allowed spectra with $\Delta I = \pm 1$. An attempt to explain the shape using the P + T combination has also been made by Alaga, Sips and Tadic (1957), using a correction factor which contained additional terms taking into account the influence of nuclear forces.

It seemed desirable to remeasure the spectrum with special attention to the avoidance of distortions due to source thickness and instrumental resolving power and to the contributions of partial β-spectra. In addition it was important to test the fit provided by the A interaction in view of new measurements which support the V + A combination and indicate that the S + T combination is weak or absent. These measurements include recoil experiments on positron emission in ^{35}A (Herrmannsfeldt *et al.* 1957) on electron emission in ^{6}He (Herrmannsfeldt *et al.* 1958), on K-capture in ^{152}Eu (Goldhaber, Grodzins and Sunyar 1958) and on the decay of polarized neutrons (Burgy *et al.* 1958).

It is shown in § 6 that the shape found in the present work differs somewhat from that found by Laubitz and can, in fact, be fitted satisfactorily by the axial vector interaction. This confirms a similar result recently announced by Graham, Geiger and Eastwood (1958), whose spectrum shape differs slightly from our own.

---

† Now at Atomic Weapons Research Establishment, Aldermaston, Berks.

§ 2. EVIDENCE FOR A $0^- \rightarrow 0^+$ TRANSITION IN ^{144}PR

^{144}Pr is known to decay with a half-life of 17·5 minutes (Alburger and Kraushaar 1952) by the emission of beta rays of maximum energy 3 MEV. The main features of the decay scheme are given in figure 1 in which the intensities and end-point energies are the author's values.

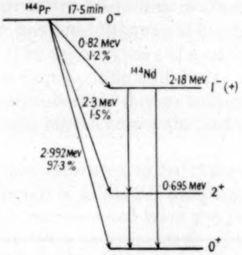

Figure 1. The decay scheme of ^{144}Pr.

Recently, Firsov and Bashilov (1957) have shown that three other gamma rays of energy 1·1, 1·7 and 2·8 MEV are present in the decay scheme. The intensity of these γ-rays ($<2\%$ of the 2·18 MEV gamma ray) is too low to affect our conclusions.

Previous reports listed in the table reveal some discrepancies in the intensity of the beta-ray components. In particular the measurements of Emmerich, Auth and Kurbatov (1954) from allowed Fermi–Kurie plots were a factor two greater than corresponding estimates from the gamma-ray intensities. This suggests that some or all of the spectra have non-allowed shapes.

Summary of Previous Results

	β-ray energy (MEV)			γ-ray energy (MEV)			β-ray int. (%)				log *ft*		
A	β_0	β_1	β_2	γ_1	γ_2	γ_3	β_0	β_1	β_2	B	β_0	β_1	β_2
1	2·965	2·3	0·86	2·185	1·48	0·695	~90	~5	~5	a	6·6		
2	2·97	2·27	0·78	2·185	1·497	0·696	>98	<1	<1	a	6·53		
3	2·98	2·28	0·80				95·5	1·7	2·8	a	6·5	8·1	6·0
4				2·185	1·49	0·695	97·3	1·44	1·26	b			
5	3·12		0·92	2·18	1·49	0·688	98·5		1·5	a			
6	3·15	2·45	0·90				95	3	2	a	6·7	7·8	6·0†
7	2·984	2·293	0·803	2·181	1·49	0·691	97·7	1·3	1·0	b			
8	2·992	2·3	0·82	2·18	1·49	0·695	97·3	1·5	1·2	c	6·55	7·9	6·3

Column A. References: 1. Alburger & Kraushaar 1952, 2. Porter & Cook 1952, 3. Emmerich *et al.* 1954; 4. Kreger & Cook 1954; 5. Cork *et al.* 1954; 6. Hickok *et al.* 1958; 7. Graham *et al.* 1958; 8. present work.

Column B. Method: a, from Fermi–Kurie plot; b, from γ-intensity; c, from coincidence spectra.

† A higher value of 6·2 for log *ft* seems to be compatible with the energy and intensity given by Hickok *et al.*

The angular correlations of the ^{144}Nd γ-rays have been determined by Alburger and Kraushaar (1952) and Steffen (1954). Assuming the ground state spin of this even–even nucleus to be 0^+, they obtained a $1^- \rightarrow 2^+ \rightarrow 0^+$ cascade. An odd parity for the upper level at 2·18 Mev was deduced by Steffen from unpublished polarization measurements of Brazos and Roberts. The log *ft* values of the partial β-spectra to these levels are consistent with either 0^- or 1^- for the spin of the ground state of the parent nucleus ^{144}Pr.

The shell model predicts an $f_{7/2}$ state for the 85th neutron, while the 59th proton can be in a $g_{7/2}$ or $d_{5/2}$ state. Applying the rules of Nordheim (1951) we would expect a ground state spin of 0^- in the first case, and in the second case a spin greater than 1^-. This supplies indirect evidence for a ground state spin of 0^-.

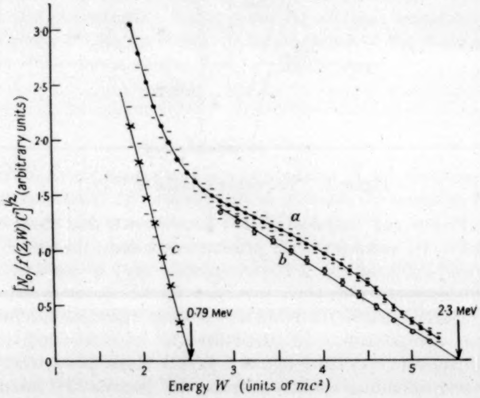

Figure 2. Fermi–Kurie plots of spectrum in coincidence with the 695 kev γ-ray; *a*, allowed plot; *b*, corrected by unique first forbidden correction factor; *c*, allowed plot of low energy component.

More direct evidence is provided by the unique first forbidden shape found in figure 2 for the β-transition to the 2^+ level in ^{144}Nd. This shape demands a spin change of 2 units with a change of parity. Graham, Geiger and Eastwood (1958) have reported measurements of β–γ coincidence spectra and β–γ correlations, with results consistent with the spin assignments in figure 1. In agreement with the present work an allowed shape for the 820 kev and a unique first forbidden shape for the 2·3 Mev transition were determined. Their measurement of the β(2·293 Mev)–γ(0·691 Mev) directional correlation did not exclude the possibility of a 1^- assignment to the spin of the ground state of ^{144}Pr but they point out that no other $\Delta I = 1$(yes) transitions are known with a shape resembling that of the unique first forbidden spectra. Grace, Johnson, Scurlock and Taylor (unpublished) using a nuclear alignment method have found $I = 0$ or 1 for ^{144}Pr. The latter value is possible if the nuclear moment is very small.

§ 3. SOURCE PREPARATION

The beta rays were measured with a source of ^{144}Pr in equilibrium with the parent nucleus ^{144}Ce ($T_{1/2} = 285$ days). The maximum energy of the ^{144}Ce beta rays is 320 kev (author's measurement), which is below the energy range plotted in figures 2–6.

High specific activity ^{144}Ce was supplied as a solution of $Ce(NO_3)_2$ in 1 N HNO_3 by Atomic Energy of Canada Ltd. The 5 mm diameter disc-shaped sources were prepared by vacuum distillation of the cerium nitrate from a tungsten filament on to a 250 μg cm^{-2} aluminium leaf strengthened by a nylon backing of thickness 50 μg cm^{-2}. According to Owen, Cook and Owen (1950) no back-scattering distortion above 50 kev is apparent with a backing thickness of less than 1·6 mg cm^{-2}. The deposits were of a uniform blue colour, suggesting that the chemical form was Ce_4O_7. The uniformity and centricity of the activity was verified by counting scintillations due to collimated β-rays emerging from a 0·5 mm aperture which was moved across the source in two directions at right angles.

The source thickness was estimated to be 15 μg cm^{-2} from the figure given by the suppliers for the amount of solids per millicurie of the solution. Evidence of the quality of the source was obtained from the linearity of the Fermi plot of the 196 kev β-spectrum of ^{144}Ce in coincidence with the 134 kev γ-ray. No detectable difference was recorded between the line shape of the 92 kev conversion line and the F-line of ThB with sources of the same size.

§ 4. BETA AND GAMMA SPECTROMETERS

β–γ coincidence measurements necessitate a high transmission in both β- and γ-counters to attain the required statistical accuracy in a reasonable counting time. However, to avoid distortions in the shape of the beta spectrum, a good resolving power is also desirable. A prolate spheroidal field spectrometer (Evans *et al.* 1958) combining the two requirements was used with the baffle system adjusted to give a resolving power of 1·3% and a transmission of 2·6% of 4π with a 5 mm source. The mode of focusing in this instrument reduces the likelihood of recording scattered electrons.

The beta particles were detected by a ring-shaped N.E. 102 plastic phosphor. Light from the phosphor was piped through the iron polepiece to a 13-stage E.M.I. type 9514B photomultiplier by means of a $\frac{3}{4}$ in. diameter 10 in. long Perspex rod. Tests indicated a detection efficiency of 100% above 40 kev. The $B\rho$ values of Siegbahn and Gerholm, Siegbahn (1955), for the A, B, F, I, L and X lines of Th(B+C+C″) were used as a momentum calibration. The gamma detector was a $1\frac{1}{2}$ in. diameter 1 in. long Harshaw NaI(Tl) crystal, optically coupled with silicone fluid to a 9514B photomultiplier. The instrument was capable of a 9% resolution for the 661 kev γ-ray of ^{137}Cs.

The photopeak efficiency was determined from measurements on single γ-ray sources (e.g. ^{141}Ce, ^{203}Hg, ^{137}Cs, ^{65}Zn) with the aid of tables giving total efficiencies computed by the Mathematics Panel at the Oak Ridge National Laboratories (private communication from P. R. Bell). The efficiency thus found was checked at 661 kev by a measurement with a ^{137}Cs source of known strength. The tables of Davisson (in Siegbahn 1955, p. 857) were used to correct for the absorption in the aluminium window, MgO reflector and the $\frac{1}{2}$ in. thick

Perspex needed to absorb the 3 Mev β-rays. Variations in pulse height due to the magnetic field of the spectrometer were precluded by surrounding the photomultiplier with an iron cylinder. To achieve stability of operation at high pulse rates the photomultiplier circuits were modelled on a design by L. R. Jenkin (private communication) which incorporated neon stabilizers between the later dynode stages. An overall stability of at least $\pm 3\%$ was maintained.

Pulses from the photomultiplier anodes operated a modified Bell, Graham and Petch (1952) coincidence unit with a resolving time of $2\tau = 2{\cdot}5 \times 10^{-8}$ sec. Gamma-ray energy discrimination was achieved by feeding the output of the fast coincidence unit to a slow coincidence unit ($2\tau = 5\,\mu$sec) gated by a pulse height analyser fed from the 8th dynode of the gamma photomultiplier. The coincidence efficiency was found to exceed 99% by measurements of the pulse distribution at the output of the fast coincidence unit.

§ 5. EXPERIMENTAL PROCEDURE

The total β-spectrum was measured in 30 kev steps with the statistical standard deviation of each point varying from 0·4% at the centre of the spectrum to 0·6% at the edges.

To obtain the ground state spectrum it was necessary to subtract the partial spectra to the 695 kev and 2·185 Mev levels in ^{144}Nd. The β-spectrum in coincidence with the 695 kev γ-ray was recorded in 60 kev steps from 450 kev to the end-point. From the Fermi plot in figure 2 it was possible to resolve the spectrum into two components of maximum energy 2·3 Mev and approximately 800 kev (see § 6). The spectrum in curve *c* is due to those β-transitions to the 2·185 Mev level which are followed by the 1·49 and 0·695 Mev γ-transitions in cascade. Assuming the intensities of the competing 1·49 and 2·185 Mev γ-rays to be in the ratio of 3 : 10 (Kreger and Cook 1954, Firsov and Bashilov 1957) the intensity of all β-rays to the 2·185 Mev level was calculated. From these results the ground state spectrum from 450 kev to the end-point was computed.

Since the intensity of the β-rays to the 695 kev level is approximately 1·5% of the total, a statistical accuracy of 10% in the coincidence spectrum is sufficient to limit the errors introduced into the ground state spectrum to less than 0·2%. Errors in the 820 kev β-spectrum will be rather larger owing to the uncertainty in the relative intensities of the 1·49 Mev and 2·185 Mev γ-rays. This, however, only affects the results from 450 kev to 820 kev.

The coincidence spectrum was recorded with a standard deviation of 8% at the centre and 10% at the edge.

§ 6. THE COINCIDENCE SPECTRA

All Fermi plots were made using Fermi functions and screening corrections published by the National Bureau of Standards (*Applied Mathematics Series No.* 13).

Figure 2, curve *a*, represents the allowed Fermi plot of the β-rays in coincidence with the 695 kev γ-ray. Above an energy of $3mc^2$ the graph is distinctly concave to the energy axis. Application of the correction factor corresponding to the B_{ij} matrix element (Konopinski and Uhlenbeck 1941) yielded a linear plot with an end-point of 2·3 Mev (figure 2, curve *b*). In this analysis no correction was

V. 19

made for the variation with energy of the anisotropy of the β–γ directional correlation. Addition of the γ-ray energy of 695 kev, measured with the scintillation spectrometer, gives a value of 2·995 Mev in good agreement with the end-point energy of 2·992 Mev found for the ground state spectrum.

After correcting for the efficiency of the γ-counter the intensity of the 2·3 Mev spectrum was determined to be $1{\cdot}5 \pm 0{\cdot}2\%$. Using the curves of Feenberg and Trigg (1950) a $\log f_0t$ value of 7·90 was calculated. Davidson (1951) showed that comparative half-lives of unique first forbidden spectra are more precisely represented by $\log f_1t$ where:

$$f_1 = [a(W_0^2 - 1) + b(W_0 - 1)]f_0, \qquad \ldots\ldots (1)$$

W_0 = maximum energy in units of mc^2, and a, b are computed functions of Z. The calculated value of $\log f_1t = 7{\cdot}98$ lies well within the range 7·3 to 9·1 reported by Davidson.

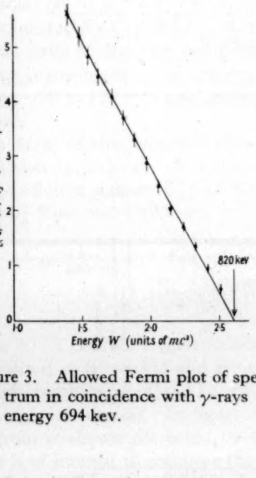

Figure 3. Allowed Fermi plot of spectrum in coincidence with γ-rays of energy 694 kev.

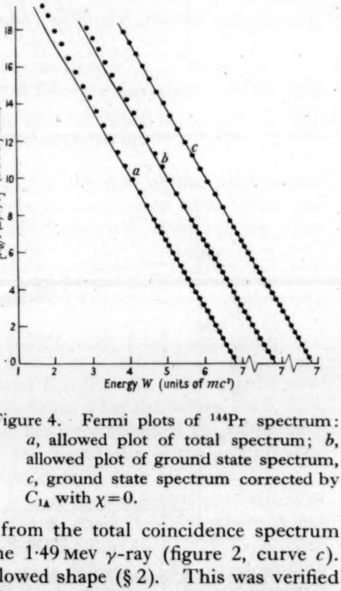

Figure 4. Fermi plots of ^{144}Pr spectrum: a, allowed plot of total spectrum; b, allowed plot of ground state spectrum, c, ground state spectrum corrected by C_{1A} with $\chi = 0$.

Subtraction of the unique spectrum from the total coincidence spectrum yielded the β-rays in coincidence with the 1·49 Mev γ-ray (figure 2, curve c). The Fermi plot is expected to have an allowed shape (§ 2). This was verified by measuring the β-rays in coincidence with γ-rays of energy greater than 695 kev. The result of this experiment gave an end-point of 820 ± 20 kev as indicated in figure 3. The intensity of the 820 kev component was calculated to be $1{\cdot}2 \pm 0{\cdot}3\%$. This corresponds to a value of $\log f_0t = 6{\cdot}3$, suggesting that the transition is first forbidden. The spin of the 2·185 Mev level in ^{144}Nd would then be 1^+ in disagreement with the angular correlation results of Steffen.

§ 7. The Ground State Spectrum

Figure 4, curve a, represents the allowed Fermi plot of the total β-spectrum. A straight line fitted to the points above 2·4 Mev by the method of least squares, each point being weighted inversely as its squared statistical error, yielded an end-point of 2·992 (± 0·005) MeV. Taking into account a possible calibration error would probably double the quoted error.

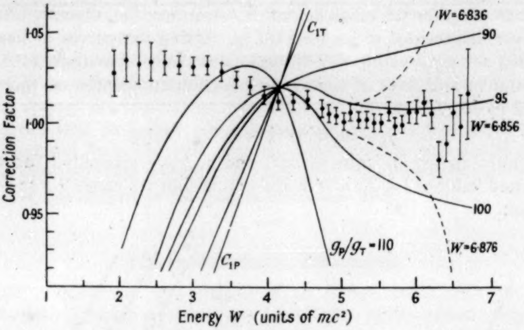

Figure 5. Correction factors for pure tensor T, pure pseudoscalar P and T–P mixtures in the region of destructive interference.

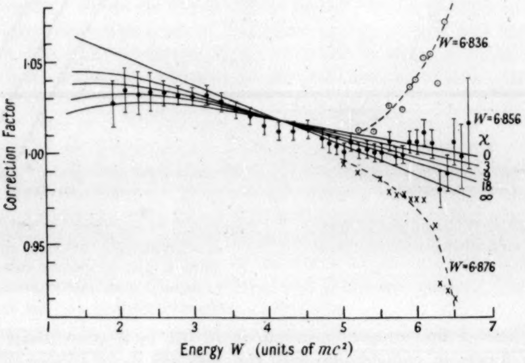

Figure 6. Correction factors for pure axial vector A with various values of $\chi = i\int\gamma_5/\int\boldsymbol{\sigma}.\mathbf{r}$

The Fermi plot of the ground state spectrum showed a slight curvature as indicated in figure 4, curve *b*. The shape of the spectrum is given by

$$N(p)(dp) = (\text{const.})F(Z, W)p^2(W_0 - W)^2C(W)\,dp. \qquad \ldots\ldots(2)$$

The deviation from linearity is shown more clearly in figures 5 and 6 where W is plotted against the shape factor:

$$C = \frac{N_0}{f(W_0 - W)^2} \qquad \ldots\ldots(3)$$

where $f=p^2F(Z, W)$ and $N_0=N(p)/B\rho$. The experimental points are plotted for three values of maximum energy W_0. The figure shows that a value of $W_0=6{\cdot}856$ (2·992 MeV) is the most reasonable choice. The errors indicated are due only to the counting statistics.

An attempt was made to fit the points to the theoretical correction factors given by Rose and Osborne (1954), and more recently by Morita and Morita (1958). The functions L_0, M_0, N_0, etc. were taken from the tables of Rose, Perry and Dismuke (in Siegbahn 1955), and a nuclear radius of $R=1{\cdot}41\times10^{-13}A^{1/3}$ cm was chosen.

The correction factors for pure tensor and pure pseudoscalar interactions are given in figure 5. Application of either to the Fermi plot would merely increase the deviation from linearity.

The T–P correction factor was next tried. The shape is given by

$$C_1=g_T{}^2C_{1T}+g_Tg_PC_{1TP}+g_P{}^2C_{1P} \qquad \ldots\ldots(4)$$

where g_T and g_P are the coupling constants for the T and P interactions. Equations 60, 61 and 62 of Rose and Osborne were used to evaluate the T and P correction factors C_{1T} and C_{1P} and the interference term C_{1TP}. These formulae are still valid in the two component neutrino theory if invariance under time reversal is assumed. It is apparent from the curves given in figure 5 for values of $g_P/g_T=90$ to 110 that a fit to the experimental data cannot be achieved by this method.

In view of the recent evidence (see § 1) for the size of the axial vector interaction in β-decay, the experimental curve was compared with theoretical shapes calculated from C_{1A} of Konopinski and Uhlenbeck (1941) in the form given by Rose and Osborne:

$$C_{1A}=k\left\{\left|\int \boldsymbol{\sigma}\,.\,\mathbf{r}\right|^2\left[\frac{1}{9}K^2L_0-\frac{2}{3}KN_0+M_0\right] +2i\left(\int\gamma_5\right)\left(\int\boldsymbol{\sigma}\,.\,\mathbf{r}\right)^*\left[\frac{1}{3}KL_0-N_0\right]+\left|\int\gamma_5\right|^2L_0\right\}$$

where k is a convenient normalizing factor and $K=W_0-W$. The graphs were normalized at $W=4{\cdot}123$ and are presented in figure 6 for the values $\chi=0$, 3, 9, 18 and ∞ where $\chi=i\int\gamma_5/(\int\boldsymbol{\sigma}\,.\,\mathbf{r})$. The best fits were obtained for values of χ ranging from 0 to 10. In figure 4, curve *c*, the Fermi plot of the ground state spectrum is shown corrected by C_{1A} corresponding to $|\int\boldsymbol{\sigma}\,.\,\mathbf{r}|^2$ alone.

It is of interest to compare the values of χ with the theoretical predictions of Ahrens and Feenberg (1952) who estimated it to equal $\Lambda\alpha Z/2R$ where Λ has a value between 1 and 2 and α is the fine structure constant ($=137{\cdot}0$), $Z=$ nuclear charge and $R=$ nuclear radius ($=\frac{1}{2}\alpha A^{1/3}$) in units $h/2\pi mc$. The corresponding range of values for χ is from 11·5 to 23. If the sensitivity of the experimental shape above $W=4{\cdot}5mc^2$ to small variations of maximum energy W_0 is taken into account, it is possible to fit the curve for all positive values of χ. The curvature between $W=2$ and 3·5, however, is better fitted by values of χ below 20, in accord with the theoretical estimate.

§ 8. CONCLUSION

Since this experimental work was completed Graham, Geiger and Eastwood (1958) have reported similar results for the shape of the ^{144}Pr spectrum. They conclude that a pure axial vector correction factor fits the experimental points, and that a combination of A with T is only possible with the A interaction predominating.

Hamilton and Langer (1958) have measured the spectrum and found a Fermi plot which was linear to within ± 1% between 2·4 and 3 MEV.

Both of these reports are consistent with the present experimental results. We conclude that previous estimates of the deviations from linearity were incorrect, and that the pure axial vector correction factor is sufficient to fit the experimentally observed spectrum. This conclusion provides independent evidence for the inclusion of the axial vector interaction in the theory of β-decay.

ACKNOWLEDGMENTS

I wish to express my thanks to Professor H. O. W. Richardson for his interest in this work, to Dr. P. R. Evans for his help while taking the coincidence measurements and to Exeter University and Bedford College for the award of Research Scholarships.

REFERENCES

Ahrens, T., and Feenberg, E., 1952, *Phys. Rev.*, **86**, 64.

Alaga, G., Kofoed-Hansen, O., and Winther, A., 1953, *K. Danske Vidensk. Selsk., Mat.-fys. Medd.*, **28**, No. 3.

Alaga, G., Sips, L., and Tadic, D., 1957, *Period. Mat.-Phys. Astr., Zagreb*, **12**, 207.

Alburger, D. E., and Kraushaar, J. J., 1952, *Phys. Rev.*, **87**, **448**.

Bell, R. E., Graham, R. L., and Petch, H. E., 1952, *Canad. J. Phys.*, **30**, 35.

Burgy, M. T., Krohn, V. E., Novey, T. B., Ringo, G. R., and Telegdi, V. L., 1958, *Phys. Rev.*, **110**, 1214.

Cork, J. M., Brice, M. K., and Schmid, L. C., 1954, *Phys. Rev.*, **96**, 1295.

Davidson, J. P., 1951, *Phys. Rev.*, **82**, 48.

Emmerich, W. S., Auth, W. J., and Kurbatov, J. D., 1954, *Phys. Rev.*, **94**, 110.

Evans, P. R., Freeman, N. J., McGinty, G. K., Armitage, B. H., and Richardson, H. O. W., 1958, *Proc. Phys. Soc.*, **72**, 949.

Feenberg, E., and Trigg, G., 1950, *Rev. Mod. Phys.*, **22**, 406.

Firsov, E. I., and Bashilov, A. A., 1957, *Izv. Akad. Nauk, SSR, Ser. Fiz.*, **21**, 1633.

Goldhaber, M., Grodzins, L., and Sunyar, A. W., 1958, *Phys. Rev.*, **109**, 1015.

Graham, R. L., Geiger, J. S., and Eastwood, T. A., 1958, *Canad. J. Phys.*, **36**, 1084.

Hamilton, J. H., and Langer, L. M., 1958, *Bull. Amer. Phys. Soc.*, Series II, **3**, 208.

Herrmannsfeldt, W. B., Burman, R. L., Stähelin, P., Allen, J. S., and Braid, T. H., 1958, *Phys. Rev. letters*, **1**, 61.

Herrmannsfeldt, W. B., Maxson, D. R., Stähelin, P., and Allen, J. S., 1957, *Phys. Rev.*, **107**, 641.

Hickok, R. L., McKinley, W. A., and Fultz, S. C., 1958, *Phys. Rev.*, **109**, 113.

Konopinski, E. J., and Uhlenbeck, G. E., 1941, *Phys. Rev.*, **60**, 308.

Kreger, W. E., and Cook, C. S., 1954, *Phys. Rev.*, **96**, 1276.

Laubitz, M. J., 1956, *Proc. Phys. Soc.* A, **69**, 789.

Morita, M., and Morita, R. S., 1958, *Phys. Rev.*, **109**, 2048.

Nordheim, L. W., 1951, *Rev. Mod. Phys.* 23, 322.

Owen, G. E., Cook, C. S., and Owen, P. H., 1950, *Phys. Rev.*, **78**, 686.

Porter, F. T., and Cook, C. S., 1952, *Phys. Rev.*, **87**, 464.

Rose, M. E., and Osborne, R. K., 1954, *Phys. Rev.*, **93**, 1315.

Rustad, B. M., and Ruby, S. L., 1955, *Phys. Rev.*, **97**, 991.

Siegbahn, K., 1955, *Beta- and Gamma-Ray Spectroscopy* (Amsterdam: North Holland Publishing Co.).

Steffen, R. M., 1954, *Phys. Rev.*, **95**, 614.

Electron–Phonon Interaction in Metals
I: The Harmonic Approximation

By G. V. CHESTER and A. HOUGHTON
Department of Mathematical Physics, University of Birmingham

Communicated by R. E. Peierls; MS. received 3rd November 1958

Abstract. The problem of electron–phonon coupling is investigated using the Born–Oppenheimer expansion. The expansion is carried out in this paper to second order in the expansion parameter $(m/M)^{1/4}$. It is shown that to this order the expansion can be conveniently generated by a canonical transformation. The advantage of the canonical transformation is that a direct comparison can be made with the usual theories of the electron–phonon interaction. The frequency spectrum, and matrix elements of the electron–phonon interaction, of a monovalent metal are calculated and shown to be essentially identical with those derived by Nakajima and Bardeen and Pines. To second order in $(m/M)^{1/4}$ the effects on the specific heat and spin susceptibility are calculated and found to be negligible at all temperatures.

§ 1. INTRODUCTION

ONE of the outstanding problems in the theory of metals is to give an adequate description of the coupling of the electronic and ionic motions. This problem, which is usually referred to as the electron–phonon interaction problem, has received considerable attention recently. A review of this work has been given in detail by Bardeen (1956). The purpose of this and a subsequent paper is to discuss to what extent it is possible to obtain a satisfactory treatment of this problem by a straightforward application of the Born–Oppenheimer expansion. At this point it will be helpful if we outline the methods that have been used in this problem and then compare them with the Born–Oppenheimer expansion.

Firstly, it is always assumed that in some sense the displacements of the ions from their equilibrium positions are small. This assumption is used to justify the replacement of the exact Hamiltonian by one which contains only linear and quadratic terms in the displacements. A set of normal coordinates are then introduced to describe the motion of the ions and the problem is then easily reduced to the standard electron–phonon interaction problem. To simplify the problem further it is assumed that the electrons only interact with the longitudinal vibrations. The Hamiltonian H can then be written in the form

$$H = H_{\mathrm{el}} + H_{\mathrm{tr}} + H_{\mathrm{ph}} + H_{\mathrm{int}}$$

where H_{el} is the Hamiltonian of the electrons moving in the static field of the ions, H_{tr} is the Hamiltonian of the transverse vibrations, H_{ph} that of the longitudinal vibrations and H_{int} is the interaction term, linear in the normal coordinates, between the electrons and the longitudinal vibrations. It is clear that since H_{int} couples the electronic motion to the longitudinal vibrations we must expect that the frequency spectrum of these vibrations will in some way be influenced by the electronic motion, and equally one must expect that the electronic motion will in some way be influenced by the longitudinal vibrations.

The first attempt to deal with this problem was due to Bardeen (1937). He essentially showed, by a simple extension of the usual Hartree method, that the effect of the Coulomb interactions between the electrons on the electron–phonon interaction could be taken into account by introducing a screened Coulomb interaction for H_{int}.

Fröhlich (1952) approached the problem in a more general way. However, the Hamiltonian he started from was not the same as that described above. He assumed that H_{int} is given by a screened Coulomb interaction and that the vibrational frequencies vanish in the limit of small wave numbers. These assumptions actually make it difficult to calculate the effect of the Coulomb interaction between the electrons. This is because a large part of their effect is already included in the assumptions and care must be taken not to count these effects twice over. Fröhlich avoided this difficulty by simply ignoring the Coulomb interaction. He found a canonical transformation that would eliminate H_{int} from the Hamiltonian and replace it by a modified H_{ph} and an interaction term between the electrons. The transformation was carried to second order in the electron–phonon coupling constant. A more fundamental treatment of the problem was given by Nakajima (1953). He found a canonical transformation that would remove H_{int} from the basic Hamiltonian, with the Coulomb terms included.

The results of this transformation are, to second order in the electron–phonon coupling constant,

(*a*) that the frequencies are renormalized so that they vanish in the limit of small wave numbers, whereas the frequencies in the basic Hamiltonian do not (Bardeen 1956),

(*b*) the electron–phonon interaction is screened out at large distances and can effectively be replaced by a screened Coulomb interaction, and

(*c*) a new interaction term between the electrons is introduced into the Hamiltonian.

Results (*a*) and (*b*) were, as we have mentioned, assumed by Fröhlich.

The new interaction term, which is of second order in the effective electron–phonon coupling constant turns out to be identical with the one obtained by Fröhlich (1950) using second-order perturbation theory. The derivation by Nakajima is, however, more satisfactory for it shows clearly how the renormalization effects due to H_{int} arise ; it also shows how the Coulomb interactions between the electrons reduce the strength of the electron–phonon matrix elements. Very similar results have been obtained by Bardeen and Pines (1955) who extended the work of Bohm and Pines (1952) to give a collective description of the electron–phonon interactions. This method has been discussed in detail by Bardeen (1956) and we shall not describe it here. It is hardly necessary to remark that the additional electron interaction term introduced into the Hamiltonian by the canonical transformation is assumed to be the interaction responsible for superconductivity (Bardeen 1956, Bardeen, Cooper and Schrieffer 1957). It seems to us that two important approximations are inherent in all of these methods. Firstly, the displacements of the ions are assumed to be small so that all cubic and higher order terms in them can be neglected. Secondly, the effective electron–phonon coupling constant is assumed to be sufficiently small so that the canonical transformation need only be carried out to second order in it.

In this paper we shall abandon the assumption that the effective electron–phonon coupling constant is small and we shall show how a *systematic* application of the small displacement approximation leads, in second order, to essentially the same renormalization of the phonon frequencies and to the same effective electron–phonon interaction as were found by Nakajima. In a subsequent paper we shall discuss the higher order terms in the expansion in powers of the displacements. The systematic application of the approximation that the displacements of the ions from their equilibrium positions are small, is of course identical with the Born–Oppenheimer expansion (Born and Oppenheimer 1927). It is appropriate at this point to make some general remarks on the validity of this expansion when applied to this particular problem. The expansion provides a method of calculating the energy levels and wave functions of a system of interacting electrons and ions in powers of $(m/M)^{1/4}$. It is of course just because this expansion parameter is always very small ($<10^{-1}$) that it seems well worthwhile to explore the application of the expansion to metals. The criterion for the convergence of the expansion is usually stated to be that $\hbar U/l \ll \Delta E$ (Peierls 1955, Section 1.2). Here U is the average velocity of the ions, l is a length characteristic of the rate of variation of an electronic wave function due to the motion of the ions and ΔE is the separation between the electronic energy levels. This criterion is clearly violated in a metal where the electronic levels form a continuum.

Now the question whether or not the Born–Oppenheimer expansion converges in this case seems to be closely analogous to the question whether ordinary perturbation theory can be applied to a system whose unperturbed energy levels form a continuum. The conventional criterion for the convergence of a perturbation expansion is that $\bar{V} \ll \Delta E$ where $\bar{V}$ is some measure of the strength of the perturbing potential and ΔE is the separation of the unperturbed levels. This criterion is quite meaningless for a system whose unperturbed levels form a continuum. However, for the ground state of such a system, it is likely that ordinary perturbation theory can in fact be applied, and a perfectly reasonable criterion for convergence can be given. For example, it follows from the work of Euler (1937)† that we may expect the perturbation expansion to converge for a Fermi–Dirac system if the two conditions $\bar{V}/\epsilon_a \ll 1$ and $a\rho^{1/3} \ll 1$ are satisfied. Here $\bar{V}$ is the strength of the perturbing potential, a is the range of the potential, ϵ_a is the kinetic energy of a particle with wave number equal to $2\pi/a$ and ρ is the number of particles per unit volume in the system. These criteria were obtained by comparing the size of the first and second order terms in the perturbation expansion. Now the Born–Oppenheimer expansion may be regarded as a kind of perturbation expansion in which the perturbing term is the kinetic energy of the ions. Consequently this example suggests that, at least under some conditions, it may be quite legitimate to apply the expansion to a metal. We shall in fact show that the expansion leads to what are qualitatively perfectly reasonable results for both the frequency spectrum and the electron phonon matrix elements of a monovalent metal. It is not profitable to discuss the question of convergence in any more detail until we have examined some of the higher order terms in the expansion. We shall do this in a subsequent paper where we shall show that the expansion can be expected to give a good approximation to the ground state of a non-superconducting metal. The expansion does not, however, converge at all well if we attempt to use it to calculate the thermodynamic properties of a metal at very low temperatures. On the other hand for temperatures considerably greater than the Debye temperature, the expansion again appears to converge very rapidly.

---

† We are indebted to Professor J. Levinger for drawing our attention to Euler's work.

In the next section we outline the Born–Oppenheimer expansion. This method of deriving the expansion from equation (10), though quite straightforward, does not appear to have been given before. We then remark that identical results can be obtained using a canonical transformation. This canonical transformation has the advantage that it allows a very direct comparison to be made with the usual theories of electron–phonon interaction.

In §3 we use the Born–Oppenheimer expansion to calculate the frequency spectrum and electron–phonon matrix elements of a monovalent metal, and show that our results are essentially the same as those due to Nakajima and Bardeen and Pines.

In §4 we calculate the effects on the specific heat and the spin susceptibility of the second order terms in the expansion. We find that the effects are small at all temperatures.

§ 2. THE BORN–OPPENHEIMER EXPANSION

In this section we first outline one of the conventional methods of deriving the Born–Oppenheimer expansion; afterwards we show how the same results can be obtained by applying a canonical transformation to the Hamiltonian.

We start from the Hamiltonian H given by the equation

$$H = T_{\mathrm{el}} + V_{\mathrm{el}} + T_{\mathrm{ion}} + V_{\mathrm{ion}} + H_{\mathrm{int}} \qquad \ldots\ldots(1)$$

where T_{ion} and T_{el} are the kinetic energies of the ions and electrons respectively, V_{el} and V_{ion} are the Coulomb interaction energies of the electrons and ions, and H_{int} is the Coulomb interaction energy between the electrons and ions. It should be emphasized that we have assumed that both V_{ion} and H_{int} are given by sums of two body Coulomb interactions. This is likely to be a good approximation as long as the separation between any two ions or between an electron and an ion is large compared with the ionic radius. For separations smaller than this the Coulomb potential will be considerably modified; we shall see that for the purposes of this paper the details of this modification are not important. We next define an electronic Hamiltonian H_{el} by the equation

$$H_{\mathrm{el}} = T_{\mathrm{el}} + V_{\mathrm{el}} + H_{\mathrm{int}}. \qquad \ldots\ldots(2)$$

H_{el} is the Hamiltonian for N electrons moving under the influence of their mutual Coulomb repulsions and the static field provided by H_{int}. This interaction term depends parametrically on the positions of the N ions. To emphasize this dependence we shall sometimes write $H_{\mathrm{el}}(\mathbf{R})$ for H_{el}, $\mathbf{R}$ standing for the set of all the position vectors $\mathbf{R}_j$. Since H_{el} is an Hermitian operator it, together with suitable boundary conditions, defines a complete set of eigenfunctions given by the equation

$$H_{\mathrm{el}}(\mathbf{R})\psi_n = E_n\psi_n \qquad \ldots\ldots(3)$$

where E_n is the nth eigenvalue of H_{el} and ψ_n the corresponding wave function.

Since H_{el} depends parametrically on $\mathbf{R}$, E_n and ψ_n will also. It is legitimate to assume that the ψ_n form a complete orthonormal set for every value of $\mathbf{R}$.

The exact eigenvalue equation of the problem is

$$H\Phi_m = \mathscr{E}_m \Phi_m \qquad \ldots\ldots(4)$$

where $\mathscr{E}_m$ is the exact eigenvalue and Φ_m the exact wave function. Using our assumption about the completeness of the ψ_n we may expand Φ_m in the following way

$$\Phi_m = \sum_n \chi_{mn}(\mathbf{R})\psi_n. \qquad \ldots\ldots(5)$$

The expansion coefficients can be determined by substituting this expansion in equation (4), multiplying by $\psi_n{}^*$ and integrating over all the electronic degrees of freedom. We find that χ_{mn} must satisfy the following equation

$$(T_{\mathrm{ion}} + V_{\mathrm{ion}} + E_n)\chi_{mn} + \sum_{n'} C_{nn'}\chi_{mn'} = \mathscr{E}_m \chi_{mn} \qquad \ldots\ldots(6)$$

where

$$C_{nn'} = A_{nn'} + B_{nn'} \qquad \ldots\ldots(7)$$

with

$$A_{nn'} = -\frac{\hbar^2}{M}\sum_j \int \psi_n{}^* \nabla_{\mathbf{R}j}\psi_{n'}\,d\tau \,.\, \nabla_{\mathbf{R}j} \qquad \ldots\ldots(8)$$

and

$$B_{nn'} = -\frac{\hbar^2}{2M}\sum_j \int \psi_n{}^* \nabla_{\mathbf{R}j}{}^2\psi_{n'}\,d\tau. \qquad \ldots\ldots(9)$$

In equations (8) and (9) M is the ionic mass and the integrations are over all the coordinates of the electrons. We shall assume that there is no magnetic field present and we can therefore take the ψ_n to be real. In this case, we see at once that $A_{nn} = 0$; it is also convenient to separate B_{nn} from the sum over all n' in equation (6), which can then be written in the form

$$(T_{\mathrm{ion}} + V_{\mathrm{ion}} + E_n + B_{nn})\chi_{mn} + \sum_{n \neq n'} C_{nn'}\chi_{mn'} = \mathscr{E}_m \chi_{mn}. \qquad \ldots\ldots(10)$$

This equation is due to Born (1953). We may remark here that if the $C_{nn'}$ are in some sense small and can be neglected in equation (10) then the system can be accurately described by an adiabatic wave function $\chi_{mn}\psi_n$ where χ_{mn} satisfies the equation

$$(T_{\mathrm{ion}} + V_{\mathrm{ion}} + E_n + B_{nn})\chi_{mn} = \mathscr{E}_m \chi_{mn}. \qquad \ldots\ldots(11)$$

It is now a straightforward matter to derive the Born–Oppenheimer expansion from equations (3) and (10). The spirit of the expansion is to treat the displacements of the ions from their equilibrium positions as small quantities. We therefore set $\mathbf{R}_j = \mathbf{R}_j{}^{(0)} + \kappa\mathbf{u}_j$ where κ is some dimensionless expansion parameter, $\mathbf{R}_j{}^{(0)}$ is the value of $\mathbf{R}_j$ when the ion is at its equilibrium position, and $\kappa\mathbf{u}_j$ is the displacement of the ion from that position.

Since the displacements of the ions must vanish identically in the limit of infinite ionic mass κ must also vanish in this limit; since κ must be dimensionless, this suggests that it is equal to $(m/M)^\alpha$ where m is the mass of an electron and α is a positive number. Finally, if the kinetic energy of the ions is to be of the same order in κ as the quadratic terms in the expansion of the Hamiltonian then α must be equal to $\frac{1}{4}$. We now proceed as follows: in equation (3) H_{el} depends on the $\mathbf{u}_j$'s through H_{int}. We expand H_{int} in a power series in the displacements $\mathbf{u}_j$,

$$H_{\text{int}} = H_{\text{int}}^{(0)} + \kappa H_{\text{int}}^{(1)} + \kappa^2 H_{\text{int}}^{(2)} + \dots \qquad \dots\dots(12)$$

where $H_{\text{int}}^{(n)}$ is the nth term in the Taylor expansion of H_{int}. Equation (3) is then solved by standard perturbation methods to obtain ψ_n and E_n as power series in κ; the perturbing potentials being $\kappa H_{\text{int}}^{(1)}$, $\kappa^2 H_{\text{int}}^{(2)}$ etc. Next both sides of equation (10) are expanded in powers of κ; the expansion of ψ_n is used to calculate the expansion of $B_{nn'}$ and $C_{nn'}$. It follows from equations (8) and (9) that the expansions of $B_{nn'}$ and $A_{nn'}$ start with terms of order κ^4 and κ^3 respectively. Equating equal powers of κ on both sides of equation (10) we obtain the following system of equations

$$(V_{\text{ion}}^{(0)} + E_n^{(0)})\chi_{mn}^{(0)} = \mathscr{E}_m^{(0)}\chi_{mn}^{(0)}, \qquad \dots\dots(13\,a)$$

$$(V_{\text{ion}}^{(0)} + E_n^{(0)} - \mathscr{E}_m^{(0)})\chi_{mn}^{(1)} = (\mathscr{E}_m^{(1)} - V_{\text{ion}}^{(1)} - E_n^{(1)})\chi_{mn}^{(0)}, \qquad \dots\dots(13\,b)$$

$$(V_{\text{ion}}^{(0)} + E_n^{(0)} - \mathscr{E}_m^{(0)})\chi_{mn}^{(2)} = (\mathscr{E}_m^{(1)} - V_{\text{ion}}^{(1)} - E_n^{(1)})\chi_{mn}^{(1)} + (\mathscr{E}_m^{(2)} - V_{\text{ion}}^{(2)} - E_n^{(2)} - T_{\text{ion}})\chi_{mn}^{(0)}. \qquad \dots\dots(13\,c)$$

Since $V_{\text{ion}}^{(0)}$ and $E_n^{(0)}$ are constants we see from equation (13 a) that $\mathscr{E}_m^{(0)} = V_{\text{ion}}^{(0)} + E_n^{(0)}$ and consequently this equation does not determine $\chi_{mn}^{(0)}$. From equation (13 b) we see that $\mathscr{E}_m^{(1)} = V_{\text{ion}}^{(1)} + E_n^{(1)}$; since $V_{\text{ion}}^{(1)}$ and $E_n^{(1)}$ are linear in the displacements $\mathbf{u}_j$ we must have $\mathscr{E}_m^{(1)} = 0$. This is of course just the condition that the ions be in equilibrium under the forces acting on them. Equation (13 c) therefore becomes

$$(T_{\text{ion}} + V_{\text{ion}}^{(2)} + E_n^{(2)})\chi_{mn}^{(0)} = \mathscr{E}_m^{(2)}\chi_{mn}^{(0)}. \qquad \dots\dots(14)$$

This equation determines the motion of the ions to the lowest order in κ. It is important to notice that the frequency spectrum of the ions, as given by this equation, is not determined solely by $V_{\text{ion}}^{(2)}$, but by $V_{\text{ion}}^{(2)} + E_n^{(2)}$. It is just this extra term that is responsible for the renormalization of the frequencies. The quantity $E_n^{(2)}$ is easily shown to be given by the equation

$$E_n^{(2)} = \langle n|H_{\text{int}}^{(2)}|n\rangle + \sum_{n' \neq n} \frac{|\langle n|H_{\text{int}}^{(1)}|n'\rangle|^2}{E_n^{(0)} - E_{n'}^{(0)}}. \qquad \dots\dots(15)$$

Thus to the second order in κ the energy levels of the system are given by the equation

$$\mathscr{E}_m = \mathscr{E}_{nl} = E_n^{(0)} + \kappa^2 \mathscr{E}_l^{(2)} \qquad \dots\dots(16)$$

while the wave functions are given by

$$\Phi_m = \chi_{mn}^{(0)}(\psi_n^{(0)} + \kappa\psi_n^{(1)} + \kappa^2\psi_n^{(2)}) \qquad \dots\dots(17)$$

where $\psi_n^{(0)}$ is the solution of

$$H^{(0)}\psi_n^{(0)} = E_n^{(0)}\psi_n^{(0)} \qquad \dots\dots(18)$$

and $\psi_n^{(1)}$ and $\psi_n^{(2)}$ are given by the standard first and second order formulae of perturbation theory. The wave functions given by equation (17) are of course adiabatic wave functions. We shall not calculate any higher order corrections to the energy levels or wave functions in this paper.

We now remark that it is a straightforward matter to show that these results can be obtained by a canonical transformation that eliminates the term linear in κ from the Hamiltonian. If S is this transformation then it must satisfy

$$\frac{i}{\hbar}[H^{(0)}, S] + \kappa H^{(1)} = 0. \qquad \dots\dots(19)$$

This equation in fact uniquely determines S. With S defined in this way the transformed Hamiltonian H' is to second order in S,

$$H' = T_{\mathrm{el}} + V_{\mathrm{el}} + V_{\mathrm{ion}}^{(0)} + \kappa^2(T_{\mathrm{ion}} + V_{\mathrm{ion}}^{(2)} + E_n^{(2)}), \qquad \ldots\ldots(20)$$

where $E_n^{(2)}$ is given in terms of S by the equation

$$E_n^{(2)} = \langle n|H^{(2)}|n\rangle + \frac{i}{2\hbar}\langle n|[H^{(1)}, S]|n\rangle. \qquad \ldots\ldots(21)$$

This Hamiltonian obviously leads to the same set of energy levels and wave functions as those given by equations (16) and (17).

The advantage of using a canonical transformation to generate the Born–Oppenheimer expansion is that it will allow us to make a very direct comparison with the other theories of electron–phonon interaction.

§ 3. APPLICATION OF THE BORN–OPPENHEIMER EXPANSION TO METALS

To apply the Born–Oppenheimer method as we have outlined it we must solve equation (19) for the canonical transformation S. It turns out that it is not possible to do this exactly and we have to content ourselves with an approximate solution. This solution does, however, give a very reasonable description of the longitudinal vibration spectrum in the limit of small wave numbers. We shall discuss the approximation that is necessary to solve equation (19) in more detail later.

The Hamiltonian, correct to second order in the displacements, is given by

$$H = H^{(0)} + \kappa H_{\mathrm{int}}^{(1)} + \kappa^2 H^{(2)} + \ldots \qquad \ldots\ldots(22)$$

where the symbols have the same meaning as before, and we have dropped $V_{\mathrm{ion}}^{(1)}$ since it can be assumed to vanish identically. It is convenient to work in a second quantization scheme for the electrons and to introduce a set of normal coordinates for the ionic degrees of freedom. Two simplifying assumptions will now be made: (*a*) we assume that the lattice vibrations are either longitudinal or transverse, and (*b*) we assume that only the longitudinal vibrations are coupled to the electronic motion. These assumptions are merely introduced to simplify the calculations and are not essential to the method we use. Bardeen (1956) has shown that with these assumptions the Hamiltonian can be reduced to the form

$$H = H_{\mathrm{el}} + H_{\mathrm{tr}} + H_{\mathrm{ph}} + H_{\mathrm{int}}^{(1)} \qquad \ldots\ldots(23)$$

where we have absorbed the κ and κ^2 factors for convenience. The symbols in equation (23) have the following meanings

$$H_{\mathrm{el}} = \sum_{\mathbf{k}} C_{\mathbf{k}}^* C_{\mathbf{k}} \epsilon_{\mathbf{k}} + \tfrac{1}{2}\sum_{\mathbf{f}} M_{\mathbf{f}}^2 \rho_{\mathbf{f}} \rho_{-\mathbf{f}}, \qquad \ldots\ldots(24)$$

$$H_{\mathrm{tr}} = \tfrac{1}{2}\sum_{\mathbf{f},\sigma} (p_{\mathbf{f},\sigma} p_{\mathbf{f},\sigma}^* + \Omega^2_{\mathbf{f},\sigma} q_{\mathbf{f},\sigma} q^*_{\mathbf{f},\sigma}), \qquad \ldots\ldots(25)$$

$$H_{\mathrm{ph}} = \tfrac{1}{2}\sum_{\mathbf{f}} (p_{\mathbf{f}} p_{\mathbf{f}}^* + \Omega_{\mathbf{f}}^2 q_{\mathbf{f}} q^*_{\mathbf{f},\sigma}), \qquad \ldots\ldots(26)$$

$$H_{\mathrm{int}}^{(1)} = \sum_{\mathbf{f}} V_{\mathbf{f}}^i \rho_{-\mathbf{f}} q_{\mathbf{f}} \qquad \ldots\ldots(27)$$

where

$$\rho_{\mathbf{f}} = \sum_{\mathbf{k}} C^*_{\mathbf{k}-\mathbf{f}} C_{\mathbf{k}}, \qquad \rho_{-\mathbf{f}} = \sum_{\mathbf{k}} C^*_{\mathbf{k}+\mathbf{f}} C_{\mathbf{k}}, \qquad \ldots\ldots(28\,a,\,b)$$

$$V_{\mathbf{f}}^i = -(NM)^{-1/2}\int \psi^*_{\mathbf{k}+\mathbf{f}}\left[\sum_j \epsilon_{\mathbf{f}} \cdot \nabla_{\mathbf{r}} v(\mathbf{r} - \mathbf{R}_j^{(0)}) \exp(-i\mathbf{f} \cdot \mathbf{R}_j^{(0)})\right]\psi_{\mathbf{k}}\, d\tau \qquad \ldots\ldots(29)$$

and

$$M_{\mathbf{f}}^2 = 4\pi e^2 \mathbf{f}^{-2}. \qquad \ldots\ldots(30)$$

The operators $C_{\mathbf{k}}{}^*$ and $C_{\mathbf{k}}$ are the usual creation and annihilation operators for the electrons, $\epsilon_{\mathbf{k}}$ is the energy of an electron with wave vector $\mathbf{k}$ and $\psi_{\mathbf{k}}$ is the corresponding wave function. In these last two definitions we assume that the effect of the periodic lattice is included. The $q_{\mathbf{f}}$ are the normal coordinates of the lattice degrees of freedom and $p_{\mathbf{f}}$ are the conjugate momenta. M is the mass of an ion and N is the number of ions and electrons. The term $\frac{1}{2}\sum M_{\mathbf{f}}{}^2\rho_{\mathbf{f}}\rho_{-\mathbf{f}}$ represents the Coulomb interaction of the electrons, $M_{\mathbf{f}}{}^2$ is the Fourier transform of the Coulomb interaction. Finally, $v(\mathbf{r}-\mathbf{R}_j{}^{(0)})$ is the Coulomb interaction energy of an electron with the ion at $\mathbf{R}_j{}^{(0)}$. As we have remarked earlier, $v(\mathbf{r}-\mathbf{R}_j{}^{(0)})$ is not strictly a Coulomb interaction for all values of $(\mathbf{r}-\mathbf{R}_j{}^{(0)})$; it certainly deviates considerably from Coulomb form for values of $(\mathbf{r}-\mathbf{R}_j{}^{(0)})\sim a$ where a is the radius of an ion. However, it is easily shown that the matrix element $V_{\mathbf{f}}{}^i$ will be essentially independent of the behaviour of the potential for small values of $|\mathbf{r}-\mathbf{R}_j{}^{(0)}|$ provided $fa \ll 1$. Since a is certainly less than an interatomic distance, we merely have to limit our consideration to frequencies corresponding to wavelengths greater than one or two atomic distances.

The frequencies $\Omega_{\mathbf{f}}$ that appear in equations (24) and (25) are the frequencies defined by the Hamiltonian $T_{\text{ion}}+V_{\text{ion}}{}^{(2)}$ and will be referred to as the 'bare' frequencies. Similarly, the matrix element $V_{\mathbf{f}}{}^i$ will be referred to as the 'bare' matrix element. Our main task is to show how both $\Omega_{\mathbf{f}}$ and $V_{\mathbf{f}}{}^i$ can be replaced in the Hamiltonian by 'renormalized' values $\omega_{\mathbf{f}}$ and $V_{\mathbf{f}}$. Since $H_{\text{int}}{}^{(1)}$ only affects the longitudinal frequencies, the transverse frequencies will retain their original values.

The equation for S is, in the notation of this section,

$$\frac{i}{\hbar}[H_{\text{el}}, S]+H_{\text{int}}{}^{(1)}=0. \qquad \ldots\ldots(31)$$

At this point, we have essentially to guess a suitable form for S. Since S and $H_{\text{int}}{}^{(1)}$ appear linearly in equation (31), S must be linear in the normal coordinates $q_{\mathbf{f}}$; for the same reason it must depend linearly on $V_{\mathbf{f}}{}^i$. Finally, since $\mathrm{H}_{\text{int}}{}^{(1)}$ contains a sum of operators $C_{\mathbf{k}}{}^*C_{\mathbf{k}-\mathbf{f}}$ it is reasonable to assume that S will also. These considerations lead one to suggest the following form for S

$$S=i\hbar\sum_{\mathbf{k}}\sum_{\mathbf{f}} C_{\mathbf{k}}{}^*C_{\mathbf{k}-\mathbf{f}}V_{\mathbf{f}}{}^i q_{\mathbf{f}}\phi(\mathbf{k},\mathbf{f})$$

where $\phi(\mathbf{k},\mathbf{f})$ is an unknown function of $\mathbf{k}$ and $\mathbf{f}$ to be determined from equation (31). If we set $iS/\hbar=-S'$ then

$$S'=\sum_{\mathbf{k}}\sum_{\mathbf{f}} C_{\mathbf{k}}{}^*C_{\mathbf{k}-\mathbf{f}}V_{\mathbf{f}}{}^i q_{\mathbf{f}}\phi(\mathbf{k},\mathbf{f}) \qquad \ldots\ldots(32)$$

and we easily find that

$$\left[\sum_{\mathbf{k}} C_{\mathbf{k}}{}^*C_{\mathbf{k}}\epsilon_{\mathbf{k}}, S'\right]=\sum_{\mathbf{k}}\sum_{\mathbf{f}}(\epsilon_{\mathbf{k}}-\epsilon_{\mathbf{k}-\mathbf{f}})V_{\mathbf{f}}{}^i q_{\mathbf{f}}\phi(\mathbf{k},\mathbf{f})C_{\mathbf{k}}{}^*C_{\mathbf{k}-\mathbf{f}}, \qquad \ldots\ldots(33)$$

$$\left[\tfrac{1}{2}\sum_{\mathbf{f}} M_{\mathbf{f}}{}^2\rho_{\mathbf{f}}\rho_{-\mathbf{f}}, S'\right]=\sum_{\mathbf{f}} M_{\mathbf{f}}{}^2[\rho_{\mathbf{f}}[\rho_{-\mathbf{f}}, S']+[\rho_{\mathbf{f}}, S']\rho_{-\mathbf{f}}] \qquad \ldots\ldots(34a)$$

where

$$[\rho_{\mathbf{f}}, S']=\sum_{\mathbf{k}'}\sum_{\mathbf{f}'} V_{\mathbf{f}}{}^i q_{\mathbf{f}}\phi(\mathbf{k}'\mathbf{f}')[C^*{}_{\mathbf{k}-\mathbf{f}}C_{\mathbf{k}'-\mathbf{f}'}-C_{\mathbf{k}'}{}^*C_{\mathbf{k}'-\mathbf{f}'+\mathbf{f}}] \qquad \ldots\ldots(34b)$$

and a similar equation holds for $[\rho_{-\mathbf{f}}, S']$. It is at this stage that we introduce an essential approximation. In the expression given by equation (34*b*) for $[\rho_{\mathbf{f}}, S']$ we shall keep only the terms in the sum for which $\mathbf{f}'=\mathbf{f}$, This is, as

Bardeen and Pines (1955) have pointed out, a Hartree type of approximation. For in doing this we are neglecting diagonal exchange terms in the commutator. The same approximation is made by both Nakajima and Bardeen and Pines. However, the latter authors make it plausible that this simplification is correct at least at long wavelengths. This conclusion is confirmed by the fact that the approximation leads to essentially reasonable results for the renormalized frequencies and matrix elements. A more detailed justification of this approximation would, however, be desirable. With this approximation we find that

$$\left[\tfrac{1}{2}\sum_{\mathbf{f}} M_{\mathbf{f}}^2\rho_{\mathbf{f}}\rho_{-\mathbf{f}}, S\right] = \sum_{\mathbf{k}}\sum_{\mathbf{f}} M_{\mathbf{f}}^2 V_{\mathbf{f}}^i q_{\mathbf{f}} C_{\mathbf{k}}^* C_{\mathbf{k}-\mathbf{f}} \sum_{\mathbf{k}'} \phi(\mathbf{k}',\mathbf{f})[n(\mathbf{k}'-\mathbf{f})-n(\mathbf{k}')]. \qquad \ldots\ldots(35)$$

If we now substitute the expressions given by equations (33), (34) and (35) into equation (31), we find that $\phi(\mathbf{k},\mathbf{f})$ must satisfy the following equation

$$M_{\mathbf{f}}^2\sum_{\mathbf{k}'}\phi(\mathbf{k}',\mathbf{f})[n(\mathbf{k}'-\mathbf{f})-n(\mathbf{k}')]+\phi(\mathbf{k},\mathbf{f})(\epsilon_{\mathbf{k}}-\epsilon_{\mathbf{k}-\mathbf{f}})=1. \qquad \ldots\ldots(36)$$

Since

$$\sum_{\mathbf{k}'}\phi(\mathbf{k}',\mathbf{f})[n(\mathbf{k}'-\mathbf{f})-n(\mathbf{k}')]$$

is independent of $\mathbf{k}$ we must have $\phi(\mathbf{k},\mathbf{f})(\epsilon_{\mathbf{k}}-\epsilon_{\mathbf{k}-\mathbf{f}})$ independent of $\mathbf{k}$ as well. So we may set $\phi(\mathbf{k},\mathbf{f})(\epsilon_{\mathbf{k}}-\epsilon_{\mathbf{k}-\mathbf{f}})=\chi(\mathbf{f})$ and then we find that $\chi(\mathbf{f})$ is given by

$$\chi(\mathbf{f})=\left[1+M_{\mathbf{f}}^2\sum_{\mathbf{k}'}\frac{n(\mathbf{k}'-\mathbf{f})-n(\mathbf{k}')}{\epsilon_{\mathbf{k}'}-\epsilon_{\mathbf{k}'-\mathbf{f}}}\right]^{-1}. \qquad \ldots\ldots(37)$$

Finally setting $V_{\mathbf{f}}=\chi(\mathbf{f})V_{\mathbf{f}}^i$ we have

$$S'=\sum_{\mathbf{k},\mathbf{f}} C_{\mathbf{k}}^* C_{\mathbf{k}-\mathbf{f}} V_{\mathbf{f}} q_{\mathbf{f}}(\epsilon_{\mathbf{k}}-\epsilon_{\mathbf{k}-\mathbf{f}})^{-1}. \qquad \ldots\ldots(38)$$

Thus S' depends only on the renormalized matrix element $V_{\mathbf{f}}$. From equation (19) we see that the renormalized frequencies which we shall call $\omega_{\mathbf{f}}$ are defined by a Hamiltonian which contains the two terms $\langle n|[H_{\text{int}}^{(1)}, S]|n\rangle$ and $\langle n|H^{(2)}|n\rangle$. The term $H^{(2)}$ is easily shown to have no diagonal part and consequently can be neglected. We therefore have to calculate the diagonal part of $[H_{\text{int}}^{(1)}, S]$ in order to determine the $\omega_{\mathbf{f}}$. Now,

$$\frac{i}{2\hbar}[H_{\text{int}}^{(1)}, S]=-\tfrac{1}{2}[H_{\text{int}}^{(1)}, S']$$

and using the above definition for S' we find that

$$-\tfrac{1}{2}[H_{\text{int}}^{(1)}, S']=\tfrac{1}{2}\sum_{\mathbf{k}}\sum_{\mathbf{f}}\sum_{\mathbf{f}'} V_{\mathbf{f}}^i V_{\mathbf{f}'}^i q_{\mathbf{f}} q_{\mathbf{f}'}\phi(\mathbf{k},\mathbf{f})[C_{\mathbf{k}}^* C_{\mathbf{k}-\mathbf{f}-\mathbf{f}'}-C_{\mathbf{k}+\mathbf{f}'}^* C_{\mathbf{k}-\mathbf{f}}].$$

Therefore the diagonal part of $[H_{\text{int}}^{(1)}, S]$ is given by the equation

$$-\tfrac{1}{2}[H_{\text{int}}^{(1)}, S']=\tfrac{1}{2}\sum_{\mathbf{k}}\sum_{\mathbf{f}} V_{\mathbf{f}}^i V_{-\mathbf{f}}^i q_{\mathbf{f}} q_{\mathbf{f}}^*\phi(\mathbf{k},\mathbf{f})[n(\mathbf{k})-n(\mathbf{k}-\mathbf{f})]. \qquad \ldots\ldots(39)$$

This last expression enables us to write down the following equation for $\omega_{\mathbf{f}}$

$$\Omega_{\mathbf{f}}^2-\omega_{\mathbf{f}}^2=-V_{\mathbf{f}}^i V_{-\mathbf{f}}^i\sum_{\mathbf{k}}\phi(\mathbf{k},\mathbf{f})[\bar{n}(\mathbf{k})-\bar{n}(\mathbf{k}-\mathbf{f})] \qquad \ldots\ldots(40)$$

where $\bar{n}(\mathbf{k})$ is the expectation value of the operator $n(\mathbf{k})$ in state $|n\rangle$. If we now substitute for $\phi(\mathbf{k},\mathbf{f})$ we find that

$$\Omega_{\mathbf{f}}^2-\omega_{\mathbf{f}}^2=-V_{-\mathbf{f}}^i V_{\mathbf{f}}\sum_{\mathbf{k}}[\bar{n}(\mathbf{k})-\bar{n}(\mathbf{k}-\mathbf{f})]/(\epsilon_{\mathbf{k}}-\epsilon_{\mathbf{k}-\mathbf{f}}). \qquad \ldots\ldots(41)$$

Equations (31) and (41) are our final expressions for the renormalized matrix elements and frequencies, and we now compare these expressions with those given by Nakajima and Bardeen and Pines. These authors define the matrix elements by the equation

$$V_{\mathbf{f}} = \chi'(\mathbf{f}) V_{\mathbf{f}}^{i}$$

where

$$\chi'(\mathbf{f}) = \left[1 + M_{\mathbf{f}}^{2} \sum_{\mathbf{k}} \frac{\bar{n}(\mathbf{k}) - \bar{n}(\mathbf{k}-\mathbf{f})}{\epsilon_{\mathbf{k}} - \epsilon_{\mathbf{k}-\mathbf{f}} + \hbar\omega_{\mathbf{f}}} \right]^{-1}, \qquad \ldots\ldots(42)$$

while their equation for $\omega_{\mathbf{f}}$ is

$$\Omega_{\mathbf{f}}^{2} - \omega_{\mathbf{f}}^{2} = - V_{\mathbf{f}} V_{-\mathbf{f}}^{i} \sum_{\mathbf{k}} \frac{\bar{n}(\mathbf{k}) - \bar{n}(\mathbf{k}-\mathbf{f})}{\epsilon_{\mathbf{k}} - \epsilon_{\mathbf{k}-\mathbf{f}} + \hbar\omega_{\mathbf{f}}}. \qquad \ldots\ldots(43)$$

The only difference therefore between our definitions and theirs is that all the energy denominators in their expressions have an extra term $\hbar\omega_{\mathbf{f}}$ in them. Now it is easily shown that

$$\sum_{\mathbf{k}} \frac{\bar{n}(\mathbf{k}) - \bar{n}(\mathbf{k}-\mathbf{f})}{\epsilon_{\mathbf{k}} - \epsilon_{\mathbf{k}-\mathbf{f}}} \Big/ \sum_{\mathbf{k}} \frac{\bar{n}(\mathbf{k}) - \bar{n}(\mathbf{k}-\mathbf{f})}{\epsilon_{\mathbf{k}} - \epsilon_{\mathbf{k}-\mathbf{f}} + \hbar\omega_{\mathbf{f}}} = 1 + \mathrm{O}\left(\frac{k\theta}{\zeta}\right), \qquad \ldots\ldots(44)$$

where k is Boltzmann's constant, θ is the Debye temperature and ζ is the Fermi energy. In evaluating the sums in equation (44) we have assumed that the $\bar{n}(\mathbf{k})$ correspond to the Fermi distribution. Since $k\theta/\zeta$ is always less than a few per cent for the alkali metals, we see that there is no essential difference between our results and those due to Nakajima and Bardeen and Pines.

We end this section by making a few qualitative remarks about the significance of our results. Firstly, it is easily seen that $V_{\mathbf{f}}$ and $\omega_{\mathbf{f}}$ differ qualitatively, not merely quantitatively, from the bare matrix elements and frequencies. For example, $V_{\mathbf{f}} \sim \mathbf{f}$ for small $\mathbf{f}$, whereas $V_{\mathbf{f}}^{i} \sim \mathbf{f}^{-1}$ for small $\mathbf{f}$. Again $\omega_{\mathbf{f}} = C|\mathbf{f}|\hbar$ for small $\mathbf{f}$ while $\Omega_{\mathbf{f}}$ is essentially the plasma frequency of the ions and is a constant for small $\mathbf{f}$. From the quantitative point of view, both $V_{\mathbf{f}}$ and $\omega_{\mathbf{f}}$ are in reasonable agreement with the value determined experimentally. For example, the longitudinal velocity of sound calculated from equation (41) agrees within 20% with the experimental values for the alkali metals (Bardeen and Pines 1955), while the electron–phonon interaction constant which is contained in $V_{\mathbf{f}}$ is always with a factor of 2 for the monovalent metals, and often considerably closer. This degree of agreement between theory and experiment seems to be quite striking when one considers the simplicity of the model.

Finally, we remark that if the lattice degrees of freedom are treated classically, as presumably they may be when $T \gg \theta$, then the difference between our expressions and those given by Nakajima and Bardeen and Pines vanishes. This is simply because the $\hbar\omega_{\mathbf{f}}$ that appears in their denominators arises from commutators of the form $[p_{\mathbf{f}}, q_{\mathbf{f}}]$: these commutators are obviously zero if the lattice degrees of freedom are treated in a classical approximation. In a subsequent paper we shall discuss the higher order terms in the Born–Oppenheimer expansion and their effects on the thermodynamic functions of a metal, and we show that while they give a good approximation at high temperatures ($T \gg \theta$) they do not give a good approximation at low temperatures ($T \ll \theta$).

§ 4. THE THERMODYNAMIC FUNCTION

In the last section, we have shown that the longitudinal frequencies of a monovalent metal depend on the electronic configuration. This fact is explicitly expressed in equation (43) where $\omega_{\mathbf{f}}^{2}$ is given as a function of the occupation numbers $\bar{n}(\mathbf{k})$. In other words for an electronic configuration defined by a set of occupation numbers $\bar{n}(\mathbf{k})$ there will be a different set of longitudinal frequencies

$\omega_{\mathfrak{f}}$. This at once implies that the free energy of the metal will no longer be the sum of an electronic free energy and a lattice free energy. We shall show, however, in this section that in practice the free energy is given very accurately by the sum of an electronic term and a lattice term, the corrections to this sum being less than a few per cent for the alkali metals. Consequently, both the specific heat and the spin susceptibility of the system are given to within a few per cent by their usual free electron values. It is in fact easy to see why the corrections to the free energy are so small. The important point is that even though the frequencies do depend on the electronic configuration, the electronic configurations we have to consider in a metal, at least at the usual temperatures, are all very close to the ground state configuration. For example, on a simple free electron model the number of electrons above the Fermi surface at a temperature T is of order kT/ζ. Since kT/ζ is only about 1% in the alkali metals, even at their melting point, we see that for all practical purposes the frequencies will be the same for all electronic configurations. We now outline an explicit calculation of the thermodynamic functions for the system which will confirm this qualitative argument.

The free energy F is given as usual by

$$F = -kT\log Z \qquad \text{......(45)}$$

where

$$Z = \mathrm{Tr}\,[\exp(-\beta H')] \qquad \text{......(46)}$$

and the eigenvalues E_{nl} of H' are given by the equation

$$E_{nl} = E_n^{(0)} + \kappa^2 E_{nl}^{(2)}. \qquad \text{......(47)}$$

Here $E_n^{(0)}$ is an eigenvalue of the equation

$$H^{(0)}\psi_n^{(0)} = E_n^{(0)}\psi_n^{(0)} \qquad \text{......(48)}$$

and $E_{nl}^{(2)}$ an eigenvalue of the equation

$$(T_{\text{ion}} + V_{\text{ion}}^{(2)} + E_n^{(2)})\chi_{nl}^{(0)} = E_{nl}^{(2)}\chi_{nl}^{(2)}. \qquad \text{......(49)}$$

The argument we have just given leads us to expect that the wave functions $\chi_{nl}^{(0)}$ and energy levels $E_{nl}^{(2)}$ will be essentially the same for all electronic states ψ_n. Consequently, in equation (49) we replace $E_n^{(2)}$ by $E_0^{(2)}$ and treat the difference $E_n^{(2)} - E_0^{(2)}$ as a small perturbation in the equation. Then to first order in this difference we find that

$$E_{nl}^{(2)} = E_{0l}^{(2)} + \langle l|E_n^{(2)} - E_0^{(2)}|l\rangle \qquad \text{......(50)}$$

where $|l\rangle$ is an eigenstate of the Hamiltonian $T_{\text{ion}} + V_{\text{ion}}^{(2)} + E_n^{(2)}$. If we now substitute this expression for $E_{nl}^{(2)}$ in equation (47) we obtain the following approximate expression for the free energy,

$$F = F_{\text{el}} + F_l + F_{\text{c}} \qquad \text{......(51)}$$

where

$$F_{\text{el}} = -kT\log\left[\sum_n \exp(-\beta E_n^{(0)})\right], \qquad \text{......(52)}$$

$$F_l = -kT\log\left[\sum_l \exp(-\beta E_{0l}^{(2)})\right] \qquad \text{......(53a)}$$

and

$$F_{\text{c}} = \sum_n\sum_l \langle l|E_n^{(2)} - E_0^{(2)}|l\rangle \exp[-\beta(E_n^{(0)} + E_{0l}^{(2)})] \times \sum_n\sum_l \exp[-\beta(E_n^{(0)} + E_{0l}^{(2)})]^{-1}. \qquad \text{......(53b)}$$

Thus F is the sum of the usual two terms F_{el} and F_l together with a correction term F_c. It should be noticed that F_c vanishes identically at absolute zero. If $\bar{\nu}(\mathbf{k})$ is the set of occupation numbers defining the usual Fermi distribution at absolute zero we have, using equation (47),

$$E_0^{(2)} = \tfrac{1}{2} \sum_{\mathbf{f}} V_{\mathbf{f}}^{i} V_{\mathbf{f}} q_{\mathbf{f}} q_{\mathbf{f}}^{*} \sum_{\mathbf{k}} [\bar{\nu}(\mathbf{k}-\mathbf{f}) - \bar{\nu}(\mathbf{k})]/(\epsilon_{\mathbf{k}} - \epsilon_{\mathbf{k}-\mathbf{f}}) \qquad \ldots\ldots (54)$$

and if $\bar{n}(\mathbf{k})$ are the occupation numbers for any other state,

$$E_n^{(2)} = \tfrac{1}{2} \sum_{\mathbf{f}} V_{-\mathbf{f}}^{i} V_{\mathbf{f}} q_{\mathbf{f}} q_{\mathbf{f}}^{*} \sum_{\mathbf{k}} [\bar{n}(\mathbf{k}-\mathbf{f}) - \bar{n}(\mathbf{k})]/(\epsilon_{\mathbf{k}} - \epsilon_{\mathbf{k}-\mathbf{f}}). \qquad \ldots\ldots (55)$$

Remembering that $|l\rangle$ is an eigenstate of $T_{\text{ion}} + V_{\text{ion}}^{(1)} + E_0^{(2)}$ we find that

$$\langle l | E_n^{(2)} - E_0^{(2)} | l \rangle = \tfrac{1}{2} \sum_{\mathbf{f}} V_{-\mathbf{f}}^{i} V_{\mathbf{f}} \frac{[N(\omega_{\mathbf{f}}) + \frac{1}{2}]}{\hbar\omega_{\mathbf{f}}} \sum_{\mathbf{k}} \frac{\bar{n}(\mathbf{k}) - \bar{\nu}(\mathbf{k})}{\epsilon_{\mathbf{k}} - \epsilon_{\mathbf{k}-\mathbf{f}}} \qquad \ldots\ldots (56)$$

where we have used the fact in a free electron model $\epsilon_{\mathbf{k}} = \epsilon_{-\mathbf{k}}$. Finally, we have the following expression for F_c

$$F_c = \sum_{\mathbf{f}} V_{-\mathbf{f}}^{i} V_{\mathbf{f}} \frac{[N(\omega_{\mathbf{f}}) + \frac{1}{2}]}{\hbar\omega_{\mathbf{f}}} \sum_{\mathbf{k}} [f_{\mathbf{k}} - \bar{\nu}(\mathbf{k})]/(\epsilon_{\mathbf{k}} - \epsilon_{\mathbf{k}-\mathbf{f}}). \qquad \ldots\ldots (57)$$

In this equation $f_{\mathbf{k}}$ is the usual Fermi distribution function and $\bar{N}(\omega_{\mathbf{f}})$ the mean number of phonons with energy $\hbar\omega_{\mathbf{f}}$. Since we are only interested in the order of magnitude of F_c we shall make a number of simplifying assumptions in order to evaluate it explicitly. Firstly, we set $V_{-\mathbf{f}}^{i} V_{\mathbf{f}} = \chi(\mathbf{f}) V_{\mathbf{f}}^{2}$ where $\chi(\mathbf{f})$ is given by equation (37), we next approximate $V_{\mathbf{f}}^{2}/\hbar\omega_{\mathbf{f}}$ by $C|\mathbf{f}|$ where C is related to the usual interaction constant g by the equation (Fröhlich 1952)

$$C = \frac{1}{G} \frac{4}{3} g \frac{\hbar s}{n} \zeta, \qquad \ldots\ldots (58)$$

where G the volume of the system. Finally $\chi(\mathbf{f})$ is replaced by the expression $1 + \alpha_0 k_0^2/f^2$ where $\alpha_0 = e^2 |\mathbf{k}|_0 / 2\pi\zeta$ and k_0 is the wave number of an electron at the Fermi surface. This last approximation was obtained by replacing the function

$$\sum_{k} \frac{\bar{\nu}(\mathbf{k}) - \bar{\nu}(\mathbf{k}-\mathbf{f})}{\epsilon_{\mathbf{k}} - \epsilon_{\mathbf{k}-\mathbf{f}}}$$

by its mean value over all allowed values of $\mathbf{f}$. Since the function varies slowly for almost all values of $\mathbf{f}$ this should be a good approximation. With these approximations it is a simple matter to evaluate F. We find that

$$\left.\begin{aligned} &(a)\ T \ll \theta, \qquad F_c^{\mathrm{L}} = \frac{\pi^2}{4} \frac{(kT)^2}{\zeta} \frac{k\theta}{\zeta} \,.\, g N_1 2 r(\nu) \\ &(b)\ T \gg \theta, \qquad F_c^{\mathrm{H}} = \frac{\pi^2}{4} \frac{(kT)^2}{\zeta} \frac{k\theta}{\zeta} \frac{T}{\theta} g N_2 \,.\, 2 \end{aligned}\right\} \qquad \ldots\ldots (59)$$

Here N_1 and N_2 are two numerical factors which depend only on the density of the metal and $r(\nu) = (2)^{-1/3}$ for a monatomic metal. In the table below

Metal	$r(\nu)g$	$\frac{k\theta}{\zeta} \times 10^{-3}$	N_1	N_2	F_c^{L}	F_c^{H}
Li	1·1	6·93	−0·514	−2·33	$-7{\cdot}84 \times 10^{-3} F_0$	$-44{\cdot}6 \times 10^{-3} \left(\frac{T}{\theta}\right) F_0$
Na	0·3	4·40	−0·567	−2·56	$-1{\cdot}50 \times 10^{-3} F_0$	$-8{\cdot}50 \times 10^{-3} \left(\frac{T}{\theta}\right) F_0$
K	0·23	4·01	−0·629	−2·80	$-1{\cdot}16 \times 10^{-3} F_0$	$-6{\cdot}51 \times 10^{-3} \left(\frac{T}{\theta}\right) F_0$

$$F_0 = -\frac{\pi^2}{4} \frac{(kT)^2}{\zeta}$$

we have tabulated the various quantities for the three alkali metals, Li, Na and K. We see that in no case does the correction to the free energy exceed a few per cent of the thermal energy F_0 of the free electrons. Consequently, the correction to the specific heat will be quite negligible in all these substances. We have also calculated the corrections to the spin susceptibility χ and find that

$$\left.\begin{aligned} &(a)\ T \ll \theta, && \chi_c = \chi_0 \frac{k\theta}{\zeta} g N_1 \\ &(b)\ T \gg \theta, && \chi_c = \chi_0 \frac{k\theta}{\zeta} \frac{T}{\theta} g N_2. \end{aligned}\right\} \qquad \ldots\ldots(60)$$

where χ_c is the correction to χ. The corrections to the susceptibility are therefore exactly the same in form as those to the specific heat and are hence quite negligible.

In conclusion we should like to mention the connection between our calculations of the correction to the specific heat and the calculation carried out by Jones (1957). Jones is concerned with exactly the same corrections but with a different model; namely one in which the Fermi surface is extremely close to a zone boundary. In such circumstances he showed that one can expect to find a very large correction to the free electron specific heat. Although his method of calculation is quite different from ours the result can be interpreted quite simply in our language.† The large effect that he finds arises because in the sum over electron wave numbers in equation (57) very large contributions come from terms which correspond to Umklapp transitions; such transitions take place with great frequency when the Fermi surface is very close to a zone boundary, leading to a very large correction to the specific heat. It will be of considerable interest to see if this effect is observed experimentally.

ACKNOWLEDGMENTS

It is a pleasure to thank Professor R. E. Peierls, T. D. Schultz and J. S. Levinger for stimulating discussions with them during the course of this work. One of us (A. H.) wishes to acknowledge the receipt of a grant from the Department of Scientific and Industrial Research.

REFERENCES

BARDEEN, J., 1937, *Phys. Rev.*, **52**, 689.
—— 1956, *Handbuch der Physik*, **15**, 274.
BARDEEN, J., COOPER, L. N., and SCHRIEFFER, J. R., 1957, *Phys. Rev.*, **108**, 1175.
BARDEEN, J., and PINES, D., 1955, *Phys. Rev.*, **99**, 1140.
BOHM, D., and PINES, D., 1952, *Phys. Rev.*, **85**, 338.
BORN, M., 1953, *Nach. Akad. Wiss. Göttingen*, **1**.
BORN, M., and OPPENHEIMER, J. R., 1927, *Ann. Phys., Paris*, **84**, 457.
EULER, H., 1937, *Z. Phys.*, **105**, 553.
FRÖHLICH, H., 1950, *Phys. Rev.*, **79**, 845.
—— 1952, *Proc. Roy. Soc.* A, **215**, 291.
JONES, H., 1957, *Proc. Roy. Soc.* A, **240**, 321.
NAKAJIMA, S., 1953, *Buss. Kenkyu*, **65**, 116.
PEIERLS, R. E., 1955, *Quantum Theory of Solids* (Oxford: Clarendon Press).

---

† We are indebted to Professor H. Jones for the following remarks.

The Behaviour of Some Impurities in III–V Compounds

By J. T. EDMOND
Services Electronics Research Laboratory, Baldock, Herts.

MS. received 22*nd October* 1958, *in revised form* 10*th December* 1958

Abstract. Some aspects of the behaviour of group II, IV and VI elements as impurities in InSb, InAs, GaSb and GaAs have been studied. It is of particular interest to know whether these behave as donors or acceptors. In some cases, which are discussed, e.g. magnesium in GaAs, abnormal behaviour is observed.

---

§ 1. Introduction

The study of impurities in germanium and silicon has proved of considerable interest and technological value. The III–V compounds, although not yet developed or understood to the same degree, are increasingly important and it was considered that investigation of the behaviour of impurities in the latter semiconductors would be valuable.

With germanium and silicon a natural starting point was to study the behaviour of group III and group V impurities which occupy substitutional sites. The principal effects were those of strain on the lattice affecting the covalent bond energy etc. and the production, at room temperature in the case of germanium and at higher temperatures in the case of silicon, of a free carrier and a localized charge centre. This situation, compared with the case of interstitial impurities is easier to understand and the more susceptible to calculation. The case of III–V compounds is more complicated since the impurity may substitute for either element singly or in a pair for an adjacent group III and group V atom; the question may be complicated by the stoichiometry of the compound. Similarly, there are positions in the lattice in which an interstitial atom could have four nearest neighbours of the group III element or four of the group V element. Consequently, it was decided to investigate first those elements which were most likely to occupy substitutional sites and to determine whether they acted as donor or acceptor centres. Magnesium, zinc, cadmium of group II, silicon, germanium, tin and lead of group IV and sulphur, selenium, tellurium of group VI were chosen as impurities in InSb, InAs, GaSb and GaAs. Work along partly similar lines has been reported by Smirous (1955, 1956) Schillman (1956), Folberth and Schillman (1957), Kolm, Kulin and Averbach (1957) and Jenny and Braunstein (1958). The results of the present work are not completely in agreement with those of some of the authors mentioned above.

§ 2. Experimental Procedure

The method employed to prepare the material was to take about 5 grammes of the compound, as pure as possible, and to melt this in a small evacuated quartz tube with a few milligrammes of impurity. To GaAs a little arsenic was also added, sufficient to create a vapour pressure of one atmosphere at the melting point. The material was heated and kept in a liquid state for an hour or more at approximately 200°C above the melting point in the case of InSb, InAs and GaSb and 40°C above the melting point in the case of GaAs, which is close to the softening point of quartz. The cooling procedure was not completely standard but in each case between one and two hours was taken to reach a temperature of approximately half the melting point. Thereafter, the cooling procedure was usually more rapid. Single crystal sections of GaAs and GaSb were formed usually of sufficient size to provide rectangular specimens for measurements of Hall constant R and resistivity. The InSb and InAs were more often polycrystalline. Since the measurements on these materials are scarcely affected by grain boundaries, the use of single crystals was not essential. In a few cases the ingots, though small, were given one zone pass after initial freezing (see table 1).

§ 3. RESULTS

Values of R were obtained in most cases at room temperature and, if necessary, also at 90°K. Table 1 indicates which impurities were donors and which acceptors. When more than one ingot was doped with a particular impurity or when several specimens were measured, the lowest value of R was taken; that is, the figures quoted are the maximum concentration of carriers in the extrinsic range. It follows that unless an impurity produces more than one carrier per atom, the solubility of the impurity is at least that represented by column (3).

Table 1

(1)	(2)	(3)	(4)	(5)
InSb	Mg	2·4	5·7	A
	Zn	0·7	0·9	A
	Si†	~0·002	2·5	A
	Ge†	0·053	0·96	A
	Sn†	0·034	0·52	D
	Pb†	0·012	0·30	D
	Te	0·78	0·92	D
InAs	Mg	0·52	6·2	A
	Zn	0·022	0·085	A
	Cd	1·6	—	A
	Te	0·9	0·7	D
GaSb	Mg	2·9	5·7	A
	Zn	1·1	5·7	A
	Si	2·1	2·1	A
	Ge	1·2	1·1	A
	Sn	0·029	0·7	D
	Te	0·28	26·0	D
GaAs	Mg	0·27	5·7	D
	Zn	0·57	1·6	A
	Si	0·42	3·9	D
	Sn	0·048	1·0	D
	S	0·45	2·6	D
	Te	0·35	14·0	D

(1) Compound ; (2) impurity ; (3) no. of carriers (10^{19} cm^{-3}) ; (4) average impurity added to compound (10^{19}cm^{-3}); (5) impurity type : A = acceptor, D = donor.

† These ingots had one zone pass.

§ 4. Discussion

4.1. *General*

The interpretation of the results is complicated for the following reasons:

(*a*) It is not certain that one hour was sufficient in all cases for complete diffusion of the impurity through the molten ingot. For a diffusion coefficient D of $5 \times 10^{-5}\,\mathrm{cm^2\,sec^{-1}}$, which is about that observed in molten metals, and for a time t of one hour the diffusion depth $2(Dt)^{1/2}$ is equal to 8·5 mm. Convection and agitation probably improved the mixing but it is not certain that this was sufficient.

(*b*) Some ingots showed a non-uniform concentration of impurity, presumably due to segregation.

(*c*) Some of the impurity may have frozen out at grain boundaries.

(*d*) Some of the impurity may have vaporized and, on cooling, condensed on the walls, or diffused into the quartz.

Despite these uncertainties some conclusions, which are believed to be reliable, may be drawn from the results. Table 2 contains the results from the present work and other sources showing which impurities are donors or acceptors in the four compounds mentioned above. The results in each left-hand column are those of the present work, in the right-hand column from the references indicated. The results in brackets are those in which there is some uncertainty either because the solubility was small (e.g. tin in GaSb) or because there was some evidence that the impurity might behave in more than one way (e.g. magnesium and zinc in InAs).

Table 2

Group	Element	InSb		InAs		GaSb		GaAs	
II	Mg	A		(A)	A[4]	A	A[7, 5]	D	
	Zn	A		(A)	A[4]		A[5]	A	
	Cd			A	A[4]		A[5]	A	
IV	Si	(A)	A[3]		D[4]	A		D	
	Ge	A	A[1]		D[1, 4]	A	A[1]		D[6]
	Sn	(D)	D[1]		D[1, 4]	(A)	A[1]	(D)	
	Pb	(D)	O[1]		O[1]		O[1]		
VI	S		D[2]		D[4]				
	Se		D[2]		D[4]		D[5]		
	Te	D	D[2]		D[4]	D	D[5]	D	

O = insoluble

[1] Folberth and Schillman (1957); [2] Harman (1956); [3] Hulme and Mullin (private communication); [4] Schillman (1956); [5] Smirous (1956); [6] Jenny and Braunstein (1958); [7] Welker (1954).

To obtain some insight into the behaviour of the above impurities, we record their tetrahedral radii, given by Pauling, and compare them (see figure) with those of the relevant group III and V elements. Of course for an ionized impurity atom some modification in its radius should be considered due to the charge: for example a group IV element replacing a group III element would be positively charged and the radius smaller; on the other hand a group IV element replacing a group V element would be negatively charged and the radius larger. Pauling (1940) has given a rule for estimating the change in radius; according to this for example we have estimated the radius 1·13 Å for silicon as a donor and 1·21 Å as an acceptor. However, the significance of these factors has not emerged clearly in the present work and for simplicity the tetrahedral radii will be considered henceforth unmodified.

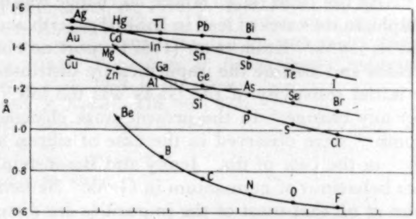

Values of tetrahedral radii (*after* Pauling).

4.2. *Group IV Impurities*

It is thought that the impurities silicon, germanium, tin and lead enter the lattice of any of the four compounds by substitution and at most will be singly charged, either positively or negatively. Three possibilities may be borne in mind, that the group IV element replaces only one of the two lattice atoms, as suggested by Welker (1952), that the group IV element can occupy either a group III or a group V site but one with a greater probability than the other, and thirdly that it enters the lattice partly or wholly in pairs of atoms (Kolm *et al.* 1957), since this may be energetically favourable.

Initially we shall neglect the question of solubility and consider only whether the impurity acts as a donor or as an acceptor. Two criteria are examined: that the impurity replaces the larger of the two parent atoms (Welker 1952) and that the impurity replaces the parent atom to which it is nearest in size, thus causing least distortion of the lattice. The evidence is in favour of the first hypothesis. Firstly, with the exception of germanium and probably silicon in InSb, all the group IV elements silicon, germanium, tin and lead are donors where the group III element is the larger; and acceptors where the group V element is the larger. With the exceptions noted these results are consistent with the first hypothesis but not with the second. For example, silicon and germanium are much nearer in radius to arsenic than to indium; yet they both replace indium in InAs. Folberth and Schillman (1957) have suggested there is a tendency for preferential substitution in the group V site to explain the p-type role of germanium in InSb. Our results with silicon in InSb have not been quite consistent, presumably due to the smallness of the changes observed and the presence of some other impurities in small (but significant) amounts. Using very pure InSb, however, silicon was found by Hulme and Mullin and by the author to be an acceptor impurity like germanium.

A feature of table 1 is that in most cases the value of the apparent impurity concentration in the ingot, derived from the Hall constant, does not correspond to the relative amounts of impurity and compound. This may be due to one of the reasons mentioned earlier such as segregation, or it may be due to the pairing of impurities in adjacent sites or the possibility of the impurity occupying either site; otherwise it means that the impurity is not sufficiently soluble. The best agreement occurs with silicon and germanium in GaSb, and tellurium in InSb and InAs; it may be significant that in these cases it is the group V element which is replaced.

On the other hand some solubility of impurity, indicated by changes in Hall constant and resistivity has been found where no change was observed by other, workers; for example, in the cases of lead in InSb (Folberth and Schillman 1957) and silicon and tin in GaAs. Kolm *et al.* (1957) report no change in resistivity in the latter two cases and assume the impurities are distributed in pairs. It is believed that the initial resistivity of the GaAs was too low ($\sim 0{\cdot}003$ ohm cm) for them to detect any change. In the present work changes in R from -88 to $-1{\cdot}5\,\mathrm{cm^3\,coulomb^{-1}}$ were observed in the case of silicon and from -35 to $-13\,\mathrm{cm^3\,coulomb^{-1}}$ in the case of tin. Jenny and Braunstein (1958) have also observed the donor behaviour of germanium in GaAs. Nevertheless the general conclusion of Kolm *et al.* that most of the impurities are distributed in pairs is likely to be correct. Rhoderick (1959) has also obtained measurements on nuclear magnetic resonance which confirm that Si atoms enter the GaAs lattice in two forms, one of which acts as a donor while the other is electrically neutral.

4.3. *Group II and Group VI Impurities*

The second factor which governs the ‘choice’ of sites is that impurities tend to displace the group III or group V atom in such a way as to avoid local centres of excessive charge. For example, zinc replaces gallium in GaSb, sulphur replaces arsenic in InAs although from consideration of the tetrahedral radii alone this behaviour could appear unlikely. However, there is at least one exceptional case; magnesium, contrary to expectation, acts as a donor impurity in GaAs. It is probable that a negatively charged magnesium atom would have a large radius, too big to allow it to substitute for gallium (see figure). On the other hand, if it lost one or both of its two outer electrons (i.e. acted as a donor) its size would be much reduced and the atom might occupy an interstitial position. While this behaviour would be in accordance with the present observations it is still rather surprising that cadmium, which is also a large atom, acts in the normal way as an acceptor.

There are also indications of abnormal behaviour from magnesium and zinc in InAs. That of zinc in InAs has been described by Folberth and Weiss (1956). Some magnesium doped specimens of InAs have been found to be n-type, others p-type. These elements may possibly act as donors (interstitially) at low concentration and acceptors (substitutionally) at high concentrations. Another important factor may be the heat treatment of the ingot after solidification as in the case of zinc in InAs (Dixon 1958) and the possible diffusion of impurity from the surface.

ACKNOWLEDGMENTS

The author is very grateful to Miss V. Muckleston and Mrs. I. S. Pinnock for assistance in preparing the ingots and making the measurements, to Dr. J. B. Mullin for samples of very pure InSb, to Dr. O. Simpson for assistance in the preparation of the manuscript and to the Admiralty for permission to publish.

REFERENCES

DIXON, J. R., 1958, *Bull. Amer. Phys. Soc.*, II, **3**, 120.
FOLBERTH, O. G., and SCHILLMAN, E., 1957, *Z. Naturf.*, **12a**, 943.
FOLBERTH, O. G., and WEISS, H., 1956, *Z. Naturf.*, **11a**, 510.
HARMAN, T. C., 1956, *J. Electro chem. Soc.*, **103**, 128.
JENNY, D. A., and BRAUNSTEIN, R., 1958, *J. Appl. Phys.*, **29**, 596.
KOLM, C., KULIN, S. A., and AVERBACH, B. A., 1957, *Phys. Rev.*, **108**, 965.
PAULING, L., 1940, *The Nature of the Chemical Bond* (Oxford : University Press).
RHODERICK, E. H., 1959, *Proceedings of International Conference on Semiconductors, Rochester, New York*, 1958, in the press.
SCHILLMAN, E., 1956, *Z. Naturf.*, **11a**, 463, 472.
SMIROUS, K., 1955, *Czech. J. Phys.*, **5**, 537.
—— 1956, *Ibid.*, **6**, 39.
WELKER, H., 1952, *Z. Naturf.*, **11**, 744.
—— 1954, *Physica*, **20**, 893.

Measurements of Sonoluminescence from Pure Liquids and some Aqueous Solutions

By P. JARMAN
Department of Physics, Imperial College, London

Communicated by R. W. B. Stephens; MS. received 30th October 1958, in final form 18th December 1958

Abstract. An exhaustive study of sonoluminescence has been made at a frequency of 16·5 kc/s. The temperature dependence of the luminescence from 15 pure liquids and some aqueous solutions has been determined in the range 4°c to 80°c. The intensity of luminescence was correlated with various parameters; the best correlation was found with (surface tension)^2/(vapour pressure). Photographs have been taken showing that sonoluminescence generally occurred as a single discrete flash once every sound cycle. This flash appeared to occur within a tenth of a period from the sound pressure minimum with non-volatile liquids like water; with volatile liquids, the flash apparently occurred shortly before or at the sound pressure maximum. Sometimes a secondary flash occurred shortly before or after the main flash. No sonoluminescence was detected from any liquid when the cavitation bubbles collapsed, i.e. shortly after the sound pressure was a maximum.

The results would appear to substantiate the theories that sonoluminescence is caused by electrical microdischarges occurring within the cavitation bubbles and by the photochemical recombination of dissociated molecules at the nascent surfaces of these bubbles.

---

§ 1. Introduction

Sonoluminescence is a weak luminescence that occurs in liquids when they are cavitated by sound fields of a few watts per square centimetre. Cavitation is the process whereby a gas bubble expands and collapses as the net pressure within the liquid becomes negative and then increases to above atmospheric. These conditions occur, for example, around ships' propeller blades, in flow through a narrow orifice and in sonically irradiated liquids. The initial diameter of the gas bubbles in the case of sonically induced cavitation using ultrasonic frequencies in the megacycle region is thought to be a few microns; with magnetostrictive oscillators at frequencies of 10 to 100 kc/s, the bubbles may be larger. Sonoluminescence is most intense in the nodes or antinodes of a stationary wave system and can be seen, by a dark-adapted eye, in water and other non-volatile liquids. The addition of certain non-polar organic solutes like carbon disulphide enhances the luminescence; the addition of highly volatile liquids like ether inhibits it. Restrictions on parameters like frequency, bubble size, sound and hydrostatic pressure, which control the onset of cavitation, will also control the onset of sonoluminescence.

Since a review of existing knowledge about sonoluminescence has just been published (Jarman 1958) only a brief mention of previous work will be given in this paper. Chambers (1937) has published the only available results of a comprehensive visual examination of sonoluminescence from some thirty liquids, which were cavitated using a magnetostrictive transducer at a frequency of 8·9 kc/s. He advanced an empirical law that the intensity of luminescence was proportional to the product of the dipole moment and the viscosity of the liquid. Recent quantitative work (Griffing and Sette 1955, Srinivasan 1955) has concentrated on the chemical effects associated with cavitation and on the influence of the gas dissolved in cavitating water on the intensity and spectral distribution of the luminescence. (See also Guenther *et al.* 1957).

There are four existing theories of sonoluminescence: the electrical micro-discharge theory (Frenkel 1940, Bresler 1940, Natanson 1948, Harvey 1939), which supposes that lens-shaped cavities are produced in the liquid by the sound field and that the electrical double layers surrounding these cavities are torn apart and discharges occur; the mechano-chemical theory (Weyl and Marboe 1949, 1951), which assumes that free ions are formed when molecules are mechanically dissociated at nascent surfaces created by the sound field, and that light is emitted when these ions recombine; the hot spot theory (Neppiras and Noltingk 1951), which shows that sonoluminescence is merely black body radiation from incandescent gas inside the cavitation bubbles when they collapse; finally, the chemiluminescence theory (Weissler 1951, Griffing and Sette 1952, Rust 1953), which, like the mechano-chemical theory, attributes the luminescence to the photochemical recombination of dissociated molecules but, in contradiction, presumes that the molecules are thermally dissociated when the cavitation bubbles collapse.

No quantitative work has so far been published on the different intensities of sonoluminescence from a series of pure liquids and solutions, but Wagner (1958) has recently published some work concerning the phase of the luminescence with respect to the sound cycle. He worked with krypton saturated water at 200 kc/s and obtained some excellent photographs showing a series of plane fronts of luminescence at the antinodes of a stationary wave system. He proved that the luminescence occurred as a single discrete flash once every sound cycle and within a tenth of a period of the sound pressure minimum. The effect of reducing the temperature of the water to about 5°c and the occurrence of secondary flashes is discussed by Wagner. The present work was designed to give quantitative information on these aspects of sonoluminescence. A magnetostrictive transducer was used as cavitation effects are enhanced at the lower frequencies and it was desirable to compare the results with those of Chambers (1937).

§ 2. EXPERIMENTAL WORK

2.1. *Preliminary Work*

A preliminary qualitative study of visible sonoluminescence was made using a 25 kc/s window-type transducer coupled by a double exponential velocity transformer to a small glass tank containing about a litre of liquid. Cavitation and sonoluminescence occurred but they were localized exclusively in a small region adjacent to the transducer stub. The luminescence could just be seen in tap-water by the dark-adapted eye; it was enhanced by the addition of a few drops of carbon disulphide or carbon tetrachloride whereas it was suppressed on the addition of a few drops of ether. A bright luminescence was seen in glycerine provided it contained a small quantity of water. A rough examination of cavitation noise was made with a noise analyser and considerable sub-harmonic content was found (Esche 1952). This form of transducer was thought to be unsuitable as the cavitation occurred only at the transducer stub and it is known that solid surfaces enhance cavitation. A toroidally wound cylindrical nickel transducer, resonant in its radial mode at 16·5 kc/s, was used instead. This gave a focused region of cavitation along its axis and, by using polythene beakers as liquid containers and as coupling media, a whole series of liquids could be cavitated well away from any solid surface. This solved the problems of spurious cavitation and of contamination by chemical action at the metal–liquid interface. It is believed that this is one of the first experiments to use a radial magnetostrictive transducer to provide a convenient focus of cavitation in a range of liquids. A theoretical account of this type of transducer has been given by Butterworth and Smith (1931), and some account of its use is given by Richardson (1957) and Crawford (1955).

Attempts were made to measure sonoluminescence quantitatively with moderately sensitive nine stage photomultipliers using d.c. and chopper techniques. Rough observations were obtained from those liquids giving large (visible) intensities of luminescence. Some attempts were made to detect r.f. radiation, which may originate from electrical microdischarges near to the surfaces of the cavitation bubbles or from some other mechanism associated with cavitation, but these attempts were unsuccessful: the experiments did not however conclusively exclude the possibility of any such radiation.

2.2. *Apparatus*

Figure 1 shows the light-tight assembly, which was designed to include a highly sensitive photomultiplier and a continuously cooled cylindrical transducer. The photomultiplier, an E.M.I. type 6256, has thirteen dynodes together with a photocathode and an anode collector, which give an overall gain of 10^8 when connected to a high tension supply supplying 150 volts per stage. The dark current limits its sensitivity to about 2×10^{-13} phot at the photocathode. A quartz window is sealed on to the tube so that ultra-violet light can be detected. The transducer has an internal diameter of 6 cm and a height of 4·5 cm; it is fed by an oscillator-rectifier circuit giving a d.c. polarizing current of 5 amperes and an a.c. supply at 16·5 kc/s, which can be adjusted up to a maximum of 250 watts electrical power input to the transducer. A thin aluminium cylinder, closed by a $\frac{1}{16}$ in. quartz window, shields the photomultiplier with its leads from the vapour of the liquid underneath; another horizontal shield protects the cavitated liquids from the vapour of the cooling water. The photomultiplier can be moved up and down along its own axis; usually it was clamped so that the quartz window of its shield was just above a cleaned polythene beaker, which contained about 150 cm^3 of liquid. Cavitation occurred along the axis of the transducer when the sound pressure amplitude in the liquid exceeded a threshold of one to two atmospheres. Sonoluminescence was detected just above this threshold.

The signal from the photomultiplier was measured by a simple Miller integrating circuit in which charge was stored up in a 250 μF electrolytic condenser in a grid-earth circuit of a pentode. The object of this integrator was to average the luminous flux over an interval of about half a minute as the instantaneous reading of a microammeter in the anode-earth circuit of the photomultiplier was unsteady due to the rapid changes of the cavitation pattern within the various liquids. The cavitation region increased in size as more power was fed to the transducer: when the electrical power input was about 150 watts, the acoustical power output was about 35 watts and cavitation extended over a cylindrical region about 2 cm in diameter and 4 cm in depth along the axis of the transducer. The photocathode, which was 1 cm in diameter, was placed about 7 cm above this region so that about a hundredth to a thousandth of the available luminescence was detected assuming that the luminous flux was isotropic. At higher power inputs to the transducer, the cavitation broke up from the axis into a ring near to the walls of the beaker.

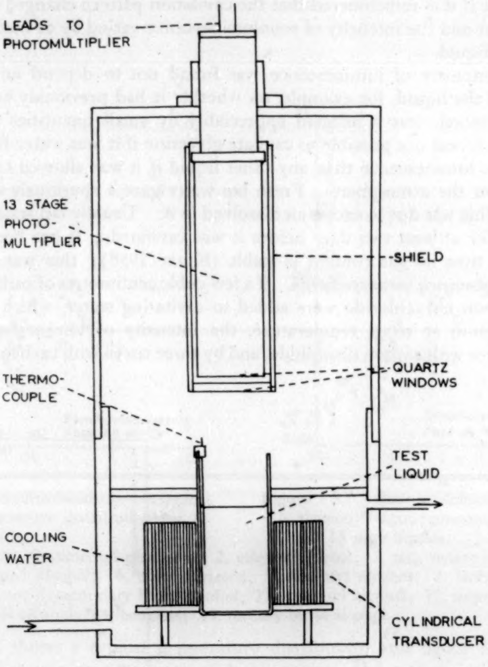
LEADS TO PHOTOMULTIPLIER
13 STAGE PHOTO-MULTIPLIER
SHIELD
THERMO-COUPLE
QUARTZ WINDOWS
TEST LIQUID
COOLING WATER
CYLINDRICAL TRANSDUCER

Figure 1. Apparatus.

2.3. *Quantitative Work with a series of Liquids*

The object of this work was to determine the dependence of sonoluminescence on the temperature, vapour pressure, viscosity, surface tension and dipole moment of the liquid. Some twenty pure liquids with widely different properties were chosen (see table). The flux from the non-volatile liquids contained a larger proportion of ultra-violet than did the flux from the volatile liquids.

In practice, the rate of flow of the cooling water was adjusted to give a suitable temperature rise in the liquid when the transducer was energized and readings of the intensity of luminescence taken every minute for about twenty minutes. Nearly a dozen of these runs was made with each liquid and the observations were found to agree within a factor of two. This is quite a remarkable order of agreement if it is remembered that the cavitation pattern changed from moment to moment and the intensity of sonoluminescence varied by as much as 10^4 from liquid to liquid.

The intensity of luminescence was found not to depend on the previous history of the liquid, for example, on whether it had previously been cavitated; nor, in general, was it affected appreciably by small quantities of impurities. However, it was not possible to cavitate glycerine if it was water-free; glycerine gave more luminescence than any other liquid if it was allowed to absorb some water from the atmosphere. Fresh tap water gave a spuriously strong luminescence; this was due to excess air dissolved in it. Usually tap water was allowed to stand for at least two days before it was cavitated. It has been shown that after this time its gas content is stable (Kurze 1958); this was confirmed by sonoluminescence measurements. If a few cubic centimetres of carbon disulphide or of carbon tetrachloride were added to cavitating water, which are sufficient for saturation at room temperature, the intensity of luminescence increased by ten times with carbon disulphide, and by three times with carbon tetrachloride.

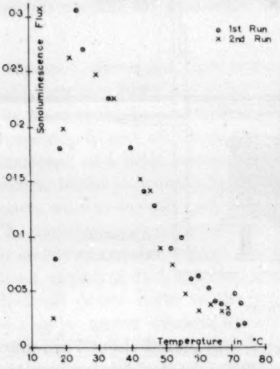

Figure 2. Sonoluminescence–temperature distribution for secondary butyl alcohol.

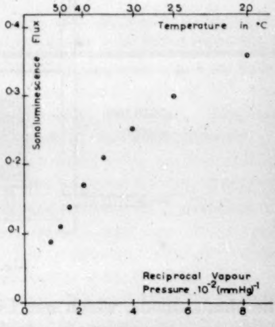

Figure 3. Sonoluminescence–reciprocal vapour pressure graph at a series of temperatures for secondary butyl alcohol.

Sonoluminescence was measured over a temperature range from 15°c to 80°c for all the liquids except chlorobenzene and the aromatic hydrocarbons, which attack polythene when they are hot. In each case, the luminescence took a minute or two to develop (see Levsin and Rzevkin 1937). This time lag before the luminescence reached its maximum intensity was independent of the initial temperature of the liquid. It was probably due to the time taken

V. 19

for the cavitation nuclei to become effective. Methyl alcohol, chloroform, carbon tetrachloride and carbon disulphide gave insufficient luminescence to be detected; trichlorobenzene and amyl acetate gave a small intensity of luminescence, and aniline, nitrobenzene and oleic acid all gave large intensities of luminescence but were unsuitable for quantitative measurements.

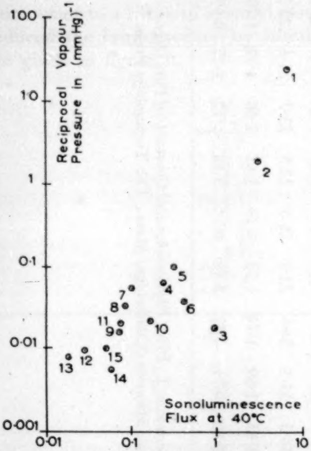

Figure 4. Sonoluminescence–reciprocal vapour pressure distribution for 15 pure liquids.

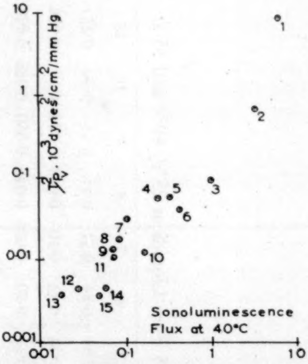

Figure 5. Sonoluminescence–(surface tension)^2/vapour pressure distribution for 15 pure liquids.

Key to liquids: 1, dimethyl phthalate; 2, ethylene glycol; 3, tap water; 4, O-xylene; 5, isoamyl alcohol; 6, chlorobenzene; 7, n butyl alcohol; 8, isobutyl alcohol; 9, toluene; 1, secondary butyl alcohol; 11, n propyl alcohol; 12, isopropyl alcohol; 13, ethyl alcohol; 14, benzene; 15, tertiary butyl alcohol.

Figure 2 shows a typical temperature distribution and figure 3 shows the correlation between the intensity of luminescence and the reciprocal vapour pressure of the liquid. There was a similar correlation when viscosity was plotted instead of the reciprocal vapour pressure.

(The units of sonoluminescence flux refer to the intensity of illumination at the photocathode in 3×10^{-11} phot. These units are somewhat arbitrary as they take into account only visible light. The photomultiplier was calibrated with a tungsten lamp at a colour temperature of 2850°K; the above units are corrected for an equivalent colour temperature of 9000°K (Srinivasan 1955). For most purposes, it is best to regard these units as relative.)

The intensity of sonoluminescence for 15 pure liquids at three temperatures is given in the table and in figure 4 the intensity of luminescence at 40°C for these liquids is plotted against their reciprocal vapour pressure. Liquids like water and chlorobenzene appear to have an unusually large intensity of luminescence but if their surface tensions are taken into account, as in figure 5, the correlation is better. Other parameters have been considered for correlation with the

Sonoluminescence Flux for 15 Pure Liquids at 25°c, 40°c and 55°c

Liquid	1	2	3	4	5	6	7	8	9	10	11	12	13	14	15
Flux at 25°c	16	12	3·6	0·36	0·54	0·84	0·21	0·17	0·15	0·30	0·21	0·054	0·04	0·23	—
Flux at 40°c	6·6	3·4	1·0	0·24	0·28	0·43	0·10	0·088	0·074	0·17	0·076	0·028	0·018	0·060	0·050
Flux at 55°c	2·4	0·5	—	0·14	0·18	0·20	0·030	0·046	0·050	0·086	0·038	0·012	—	0·010	0·025
S.V.P. at 25°c (mm Hg)	0·02	0·2	24	6·6	4·6	12	7·0	12	28	19	20	44	44	94	42
S.V.P. at 40°c (mm Hg)	0·04	0·5	55	16	10	26	19	30	60	45	50	106	130	180	102
S.V.P. at 55°c (mm Hg)	0·07	1·0	115	32	25	53	45	68	130	110	115	—	280	310	224
Surface tension at 20°c (dyn cm^{-1})	60	60	73	30·2	24·3	33·3	24·6	23·0	28·5	23·5	23·7	21·4	22·3	28·9	19·6
Dipole moment at about 20°c	2·2	2·28	1·87	0·51	1·85	1·69	1·74	1·72	0·34	1·65	1·66	1·78	1·70	0·00	1·66
Viscosity at 30°c (10^{-3}P)	Large	Large	0·80	0·69	2·96	0·71	2·27	2·88	0·53	3·18	1·72	1·77	0·99	0·57	3·32

The physical properties of the liquids are taken largely from Timmermann, J., 1950, *Physico-chemical Constants of Pure Organic Liquids* (London: Elsevier Publishing Co.) and Wesson, L. E., *Tables of Electrical Dipole Moments* (Cambridge, Mass., The Technology Press M.I.T.).

intensity of luminescence: for example, viscosity, which gives a poor correlation, or the product of the dipole moment and the viscosity (Chambers 1937), which gives a very poor correlation.

A number of sonoluminescence–temperature runs were made with 2% aqueous solutions of primary alcohols. The effect of the alcohols was to inhibit the luminescence to varying extents. Methyl alcohol reduced the luminescence from water to a half and isoamyl alcohol reduced it to a sixth; the other alcohols reduced the luminescence by intermediate extents. The results of this work are given in figure 6.

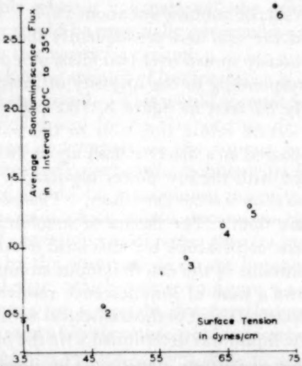

Figure 6. Graph showing the inhibitory effects of primary alcohols on the intensity of sonoluminescence from tap water. 2% vol/vol solutions of the following alcohols were used: 1, isoamyl; 2, n butyl; 3, isopropyl; 4, ethyl; 5, methyl; 6, none (tap water only).

A further series of sonoluminescence–temperature runs were made with colourless inorganic solutions. The effect of each solute was determined where possible at three different concentrations. The solutions were prepared by adding normal solutions of the salts to tap water, which had been standing for at least two days. The salts used were potassium iodide, thorium nitrate, mercurous nitrate, mercuric chloride, sodium carbonate and sodium bicarbonate. In general the intensity of luminescence was not significantly different from that of tap water. However, the luminescence from some N/10 to N/100 solutions was inhibited by a factor of ten if they were cavitated immediately after they had been prepared. This inhibition disappeared after two or three days.

2.4. *Determination of the Phase of Sonoluminescence Flashes with respect to the minimum of the Sound Cycle*

The photographs (figures 7–10, Plate) show clearly that sonoluminescence generally occurred as a single discrete flash once every sound cycle. Sometimes there was a secondary flash shortly before or after the main flash.

The potential difference developed across a 5000 ohm resistance in the anode–earth lead from the photomultiplier was displayed on the upper trace of a double-beam oscilloscope. The other plates were connected across the transducer so that its a.c. input was displayed on the lower trace; this signal was also used to synchronize the oscilloscope. Many photographs were taken of the two traces when sonoluminescence took place in liquids giving sufficient light. The flashes of luminescence were not always discrete as figure 8 shows. This was due to cavitation breaking away from the axis of the transducer towards the walls of the beaker as the power input was increased. The bubbles cavitating near to the walls were out of phase with those cavitating along the axis since the phase of the sound pressure was different in these two regions. Along the axis there was a pressure antinode of the stationary wave system and at 16·5 kc/s, and in water there was a nodal ring about 2 cm in diameter. Therefore the difference in phase between the two sets of bubbles was about $3\pi/4$. There was also cavitation between the walls and the axis and consequently the luminescence sometimes appeared to be continuously spread over two fifths of a period of the sound cycle with a maximum corresponding to the majority of cavitating bubbles along the axis. This can clearly be seen in figure 8. At higher inputs, the cavitation broke away from the centre into a ring near to the walls of the beaker. The luminescence then appeared as a discrete flash about $3\pi/4$ ahead in phase of the discrete flash associated with the low power inputs.

Figures 7 and 8 also show a secondary flash. This occurred rather arbitrarily before or after the main flash. The flashes of sonoluminescence were received by suitably adjusting the oscilloscope but this kind of resolution was necessarily limited by the time constants of the external input circuit and of the oscilloscope itself. Figure 10 shows a flash of luminescence resolved as much as possible.

The phase of the electrical input to the transducer with respect to the minimum of the sound cycle in the liquid was determined with the help of a small cylindrical probe hydrophone made of barium titanate. The phase characteristics of this hydrophone were determined by impulse methods. The signal from the hydrophone was fed through a filter to the oscilloscope and a number of phase correlations were made with the hydrophone immersed at various positions within different liquids.

The main flash of luminescence, for non-volatile liquids like water, appeared to occur within a tenth of a period of the sound pressure minimum. The flashes of luminescence for volatile liquids appeared to occur nearly half a period later, shortly before or at the sound pressure maximum. Often secondary flashes were seen from volatile liquids; for example, with isoamyl alcohol, the main flash of luminescence occurred just before the sound pressure maximum and a secondary flash occurred shortly afterwards. With chlorobenzene the secondary flash occurred before the main flash which was at the sound pressure maximum. In general the phase of the main flash of luminescence tended to move towards that for water as the liquid became less volatile.

No liquid gave any luminescence when its cavitation bubbles collapsed, i.e. shortly after the sound pressure was a maximum.

§ 3. DISCUSSION

The sonoluminescence–temperature studies with pure liquids showed that the best correlation of the intensity of luminescence with other parameters of the liquids was with (surface tension)^2/vapour pressure. The effect of reducing the surface tension was further demonstrated in the studies of aqueous solutions of alcohols. Chambers' visual observations were found to be substantially correct, but he should have been able to see sonoluminescence from chlorobenzene and the aromatic hydrocarbons; his glycerine could not have been free of water. There was little correlation between the intensity of luminescence and the product of the dipole moment and the viscosity of the liquid as Chambers suggested.

The present observations are in sympathy with the generally held view of cavitation that the initial formation of the cavitation bubbles depends on the gas content of the liquid, but their growth and collapse depends on vaporization (Beeching 1942). Sufficient vapour might evaporate into the bubble as it expands so that the occurrence of any electrical microdischarges, the temperature increase inside the bubble when it collapses and the erosion pressure exerted by the collapsing bubble, would be essentially governed by the amount of vapour within the bubble. It is this vaporous cavitation which gives rise to sonoluminescence since it is found that the amount of luminescence is inversely proportional to the vapour pressure of the liquid. This would account for the large difference in flux from liquid to liquid and for its temperature dependence. However, the flux does not increase indefinitely as the vapour pressure of the liquid diminishes, for there comes a stage when the bubble will contain more dissolved gas than vapour. There should be a maximum intensity of luminescence for any liquid at any temperature which would depend on the gas content of the liquid and the number of cavitation nuclei rather than its vapour pressure. This upper limit is suggested by the observations on the luminescence from ethylene glycol and dimethyl phthalate, which appear in figure 4 and 5. These liquids gave too little luminescence for a straight line correlation. The cavitation in these two liquids was presumably therefore predominately gaseous.

The effect of reducing the surface tension of a liquid, i.e. of reducing the surface energy of the gas–liquid interface, is to diminish the surface electrification of the bubble that results from a tearing apart of the Helmholtz double layer around it (see Lenard 1915, Frenkel 1940). A change in surface tension would also affect the size, growth and collapse of the cavitation bubble which, in turn, would modify the temperature increase and the erosion pressure (Neppiras and Noltingk 1950). Both these effects, electrical and physical, would influence considerably the intensity of sonoluminescence obtained on cavitation. The observations on aqueous solutions of primary alcohols as in figure 6 agree well with some work on the fixation of nitrogen in an ultrasonic field (Virtanen and Ellfolk 1952). This fixation was also inhibited by the addition of primary alcohols in proportion to their effect on the surface tension.

The work with inorganic solutions has shown that sonoluminescence was not affected by the presence of an electrolyte. The intensity of luminescence did not appear to depend appreciably on either the dipole moment or the conductivity of the liquid. The temporary inhibition, which was noticed in some dilute solutions, can be attributed to some kind of adjustment of the cavitation nuclei or of the dissolved gas.

There are two possible explanations as to why small quantites of carbon disulphide or of carbon tetrachloride considerably enhance the sonoluminescence from water. These non-polar organic molecules may act as 'holes' in the tetrahedral lattice of water molecules; these holes could act as cavitation nuclei and they are known to decrease the tensile strength of water (Weyl 1951).

Alternatively, the organic molecules might easily dissociate in an ultrasonic field and recombine with the dissociated water molecules; this action could be photochemical (Weissler 1951, Rust 1953). The reason why carbon disulphide enhances the luminescence from water more than carbon tetrachloride may be that carbon disulphide molecules are more effective 'holes' in the water lattice than carbon tetrachloride molecules, or that the energetics of the photochemical reactions may favour the dissociated carbon disulphide molecules rather than the dissociated molecules of carbon tetrachloride.

The results should be considered together with the other quantitative work of Srinivasan and Griffing and Sette. Their work showed the effect of dissolved gas on luminescence and Srinivasan found that the intensity of luminescence was proportional to the solubility of the gas. His spectrophotometric studies showed that the luminescence from the monatomic gases argon and helium corresponded to black-body radiation at 11 000°K (a maximum intensity at 2700 Å), and that from the diatomic gases oxygen and nitrogen corresponded to black-body radiation at 8800°K (maximum intensity at 3300 Å). Srinivasan's results do not necessarily implicate the hot spot theory of sonoluminescence as the spectra of electrical discharges or of chemiluminescence, particularly bioluminescence, are also closely similar to that of a black body radiating at about 10 000°K. It would require instruments with very high resolution to discriminate between the different spectra and it is doubtful whether this could be done with the very small intensities of sonoluminescence. Duca *et al.* (1958) have shown that the physical conditions realized by cavitation in water are sufficient to dissociate the water molecules into free radicals which ultimately recombine to produce hydrogen peroxide, but they are insufficient to dissociate the oxygen molecules in the dissolved gas. A puzzling feature of Srinivasan's work is that, in spite of using sensitive absorption spectrophotometrical and microanalytical methods, he could not detect any chemical products from water saturated with argon or helium although these liquids gave large intensities of luminescence.

All these results taken together slightly favour the electrical microdischarge and mechanochemical theories rather than the chemiluminescence and hot spot theories of sonoluminescence, but the work on the phase of sonoluminescence flashes does decide for the first two theories. The other theories, which depend on the adiabatic compression of the contents of the cavitation bubbles, are invalid if the flashes of luminescence do not occur at the stage of the sound cycle when the bubbles collapse. This observation is in agreement with that of Wagner (1958).

The apparatus was not particularly well suited to this kind of work as there was only one pair of nodes and antinodes in the stationary wave system. This meant that the cavitation often occurred simultaneously in regions where the phase of the sound cycle was different. An account has already been given of how this difficulty was overcome but it would have been better to have used a plane wave system at a higher frequency with a whole series of nodes and antinodes. The motion of the cavitation bubbles would then have been more coherent and it would have been worthwhile to have increased the resolution of the oscilloscope signals. Fortunately such a system was used by Wagner.

If Srinivasan's results with argon and helium saturated water are valid, then only an electrical microdischarge theory could account for the sonoluminescence from water. This theory has not received any serious attention in the last twenty years although more is now known about static electrification (Loeb 1957). At the stage of the sound cycle when sonoluminescence flashes occurred, the bubble surface is expanding rapidly, by a factor of a million times in a microsecond according to Neppiras and Noltingk (1950), so there could be considerably more surface electrification than that which occurs in waterfall or cataphoresis experiments. With the exception of these few results of Srinivasan, the mechanochemical theory is just as promising for it is now established that free radicals are formed in cavitated liquids (see Weissler 1958, who assumes that the molecules are dissociated by electrical microdischarges). Some recent work on cavitation erosion has shown that it is due, partly at least, to chemical action initiated by free radicals created by the sound field (Wheeler, unpublished).

It is significant that the flashes of luminescence occurred at a later stage of the sound cycle with the volatile liquids. This may be because the cavitation bubbles have to be much larger before the combined pressure of the gas and vapour within the bubbles is sufficiently low for a discharge to take place. The frequent occurrence of a secondary flash would suggest that an electrical microdischarge takes place shortly before or after a photochemical reaction.

There is a unique report on the observation of luminescence in cavitation induced by hydrodynamic flow around a cylindrical profile; this was thought to be due to electrical microdischarges (Konstantinov 1947). If this work is considered together with some work on the cavitation cycle and erosion by Rasmussen (1949) and Shalnev (1956), it would appear that these discharges occurred where the cavitation bubbles were forming and breaking away downstream and not where they collapsed, although the author takes a contrary view which is also substantiated by the work of Knapp (1955) and others. Konstantinov's observations, therefore, may be in agreement with Wagner's and with those presented in this paper. Some experiments to study luminescence from hydrodynamically induced cavitation are in progress.

§ 4. ACKNOWLEDGMENTS

The author wishes to thank Dr. R. W. B. Stephens and Dr. G. G. Parfitt for their valuable advice; he is also grateful to Mr. E. A. Neppiras of Mullards Research Laboratories for some helpful suggestions and for the loan of equipment and to Mr. R. I. Clayton for electrical apparatus.

REFERENCES

BEECHING, R., 1942, *Trans. Inst. Engrs, Shipb. Scot.*, **85**, 273.

BRESLER, S. E., 1940, *Acta Phys.-chim. URSS*, **12**, 323.

BUTTERWORTH, S., and SMITH, F. D., 1931, *Proc. Phys. Soc.*, **43**, 166.

CHAMBERS, L. A., 1937, *J. Chem. Phys.*, **5**, 290.

CRAWFORD, A. E., 1955, *Ultrasonic Engineering* (London: Butterworths Scientific Publications), Chap. 4.

DUCA, M. D., YEAGER, E., DAVIES, M. O., HOVORKA, F., 1958, *J. Acoust. Soc. Amer.*, **30**, 301.

ESCHE, R., 1952, *Akust. Beih.*, **2**, 208.

FRENKEL, J., 1940, *Acta Phys.-chim. URSS*, **12**, 317.

GRIFFING, V., and SETTE, D., 1952, *Phys. Rev.*, **87**, 234.

—— 1955, *J. Chem. Phys.*, **23**, 503.

GUENTHER, P., ZEIL, W., GRISAR, U., and HEIM, E., 1957, *Z. Electrochem.*, **61**, 188.

HARVEY, E. N., 1939, *J. Amer. Chem. Soc.*, **61**, 2392.

JARMAN, P., 1958, *Science Progress*, **46**, 632.

KNAPP, R. T., 1955, *Trans. Amer. Soc. Mech. Engrs*, **77**, 1045.

KONSTANTINOV, V. A., 1947, *Dokl. Acad. Nauk SSSR*, **56**(3), 259.
KURZE, G., 1958, *Nachr. Akad. Wiss. Göttingen, Klasse Nr.* 1.
LENARD, P., 1915, *Ann. Phys., Lpz.*, **47**, 463.
LEVSIN, V. L., and RZEVKIN, S. N., 1937, *C. R. Acad. Sci., URSS*, **16**, 399.
LOEB, L. B., 1957, *Static Electrification* (Berlin: Springer-Verlag).
NATANSON, G. L., 1948, *Dokl. Acad. Nauk SSSR*, **59**, 83.
NEPPIRAS, E. A., and NOLTINGK, B. E., 1950, *Proc. Phys. Soc.* B, **63**, 674.
—— 1951, *Ibid.*, B, **64**, 1032.
RASMUSSEN, R. E. H., 1949, *Trans. Danish Acad. Tech. Sci.*, No. 1, 1.
RICHARDSON, E. G., (ed.), 1957, *Technical Aspects of Sound* (London: Elsevier), **2**, 103.
RUST, H. H., 1952, *Angew. Chem.*, **64**, 162.
—— 1953, *Ibid*, **65**, 249.
SHALNEV, K. K., 1954, *Izvestiya Akad. Nauk. SSSR, Otdelene. Tech. Nauk.* No. 5, 119.
—— 1956, *Cavitation in Hydrodynamics* (London: H.M. Stationery Office) Section 22.
SRINIVASAN, D., 1955, *Ph.D. Thesis*, University of Missouri.
SRINIVASAN, D., and HOLROYD, L. V., 1955, *Phys. Rev.*, **99**, 633.
VIRTANEN, A. I., and ELLFOLK, N., 1950, *Acta. Chem. Scand.*, **4**, 93.
—— 1952, *Ibid*, **6**, 660.
WAGNER, W. U., 1958, *Z. angew. Phys.*, **10**, 445.
WEISSLER, A., 1951, *Chem. Eng. Prog. Symp.*, No. 1, 22.
—— 1958, *J. Acoust. Soc. Amer.*, **30**, 678.
WEYL, W. A., 1951, *J. Colloid Sci.*, **6**, 389.
WEYL, W. A., and MARBOE, E. C., 1949, *Research, Lond.*, **2**, 19.

A Possible Model for the Switching of Barium Titanate Crystals

By J. C. BURFOOT

Queen Mary College, University of London

MS. received 9th October 1958, *in revised form* 18*th December* 1958

Abstract. It is suggested that an adequate explanation of the switching current in barium titanate single crystals can be given by a domain model which includes an effective wall mass and a 'viscous' opposition, but no depolarizing field and no specific representation of impurities or lattice imperfections. The form of the switching current and also its variations with the magnitude of the switching field can be derived, if the domain growth is controlled by the nucleation process, and if the nucleation rate lies within certain limits.

---

§ 1. Introduction

Thin plate-like crystals of ferroelectric barium titanate can be produced in which the only direction of polarization is the normal to the plate (the *c* axis). The sense of this polarization may be reversed ('switched') by applying an electric field between electrodes on the two opposite crystal faces, and this switching is of possible interest for computer applications. Ferroelectricity is more common than was once supposed, so that it may also be of more general interest to understand the switching in this material, which has a relatively simple crystal structure.

The reversal process is apparently accomplished by the passage of long thin domains of reversed polarization (Merz 1954) growing lengthwise through the crystal from face to face when the field is applied. It is convenient at times to call these 'microdomains' to distinguish them from the much larger twinning domains excluded from this discussion. The resultant current in an external circuit ('the switching current') may be partly due to the formation of 'nuclei' of these antiparallel domains and partly due to their growth. It is not known with any certainty to what extent such nuclei may be present before the application of the field, nor how they change in size, shape and number during growth. One of the reasons for this uncertainty is the small size of these 'microdomains' (of the order of a micron thick) and another is the rapidity of the motion, which may be completed in a few microseconds. One of the most direct representations of the process is the switching current, which has been observed, for example, by Merz (1954) and Wieder (1956), and in this laboratory. Its variations with the time and with the magnitude of the applied field are shown in figure 1, and the problem is to explain these variations in terms of domain motions, and to explain the domain motions in terms of the properties of the material.

Too many factors are involved to retain them all in a manageable description; this paper suggests one particular simplification, which appears to be capable of explaining the observations. The possibilities of explaining the switching currents are discussed, and the relative significances of the nucleation and growth processes. It is shown that simple models of the growth process, which may appear to explain at least part of the observed variations with time, will not readily explain the variations with field; but these can be derived if we suppose the growth process to be controlled by the nucleation process, *provided that* the growth time of a single domain falls within certain limits, with respect to the mean nucleation rate; the form of the variation with time also follows.

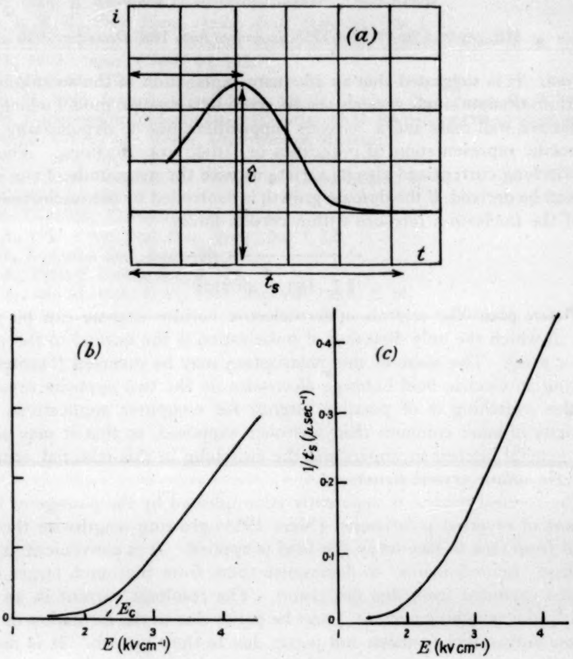

Figure 1. The switching current.

§ 2. Nucleation

When studying the variations with field E, the variations with time are usually put aside, following Merz, by extracting two parameters to describe them, viz. $\hat{\imath}$, and t_s, using the notation of figure 1 (*a*). Merz supposed that the low-field portions of the $\hat{\imath}(E)$ and $1/t_s(E)$ curves were largely due to nucleation rather than growth, and he found they could be described in terms of a nucleation rate proportional to $\exp(-\alpha/E)$ (α is a function of the temperature T, but this paper is wholly concerned with room-temperature observations). He did not discuss the variation of nucleation rate with time.

Nothing is known about the size and shape of the nuclei, and little about them during subsequent growth. To make predictions from known properties of the material, such as the polarization P and the domain wall energy σ, we must severely limit the allowed shapes (e.g. to cones or to ellipsoids) in order to describe the domains in terms of a few parameters; success of the predictions is entirely dependent upon this arbitrary selection of a model. Merz's 'daggers' use three parameters per domain; so would an ellipsoid. If the microdomains are symmetric about the c axis, as electron micrographs taken in this laboratory suggest, a thickness parameter r and a length parameter l may suffice. The free energy F of a domain as a function of these two parameters exhibits what is sometimes called a 'saddle field', in topological or contour terms (e.g. Landauer 1957). The position (r, l) of the saddle defines critical dimensions for the domain; a smaller domain will shrink, a larger one will grow. The height of the saddle defines an activation energy; this is the minimum energy a domain must obtain in order to reach the critical dimensions. We shall define a smaller domain as a 'nucleus', a larger one as a 'growing domain'.

Let us make the usual assumption that all nucleation occurs at the face. Merz found for the nucleation current i_{nu}, $i_{\mathrm{nu}} \sim dn/dt \sim \exp(-\alpha/E)$. We shall suppose that the mean nucleation rate is also proportional at any instant to the amount of face not yet nucleated, $dn/dt = b(n_0 - n)$ where $b \equiv k' \exp(-\alpha/E)$ so that

$$\frac{n}{n_0} = 1 - \exp(-bt) \qquad \ldots\ldots(1)$$

or

$$\frac{dn}{dt} = n_0 b \exp(-bt). \qquad \ldots\ldots(2)$$

Here n is the total number of microdomains under the electrodes, and n_0 the maximum possible number. Our observations show that 'coagulation' of microdomains occurs during growth, but the attempt in this paper is to set up a very simple picture, and for this purpose coagulation is ignored. One might suppose that the amount of charge released for each nucleus formed is $2Pa$, where a is the area of face occupied by the nucleus, so that

$$i_{\mathrm{nu}} = 2Pa\,\frac{dn}{dt}. \qquad \ldots\ldots(3)$$

Some considerations of Landauer's however (Landauer 1957, especially figure 5), show that this view is incorrect, and my next section confirms this experimentally.

§ 3. GROWTH

It is possible to set up models which predict the domain parameters (such as the length l) as functions of t for a single domain (see Appendix). The current due to charge u, moving across the crystal thickness d with velocity v, is uv/d, so that contributions to the growth current i_g from the various parts of the various domains can now be calculated. For a single domain the solutions initially have the forms shown in figure 5 (b) and we might identify these curves with the rising part of figure 1 (a) by supposing separate domains to grow similarly and simultaneously. But the variations of these curves with field are not correct, i.e. they do not show the experimental form of figure 1 (b) (see Appendix).

However, if the growth process is controlled by nucleation according to equation (1), and if the growth-time is suitable, the rise of $i(t)$ is largely controlled, not by figure 5 (b), but by the successive appearances of the nuclei from the time $t = 0$ when E is switched on, according to equation (1). What is required is an expression for the addition of large numbers of curves figure 5 (*b*), when their individual time origins occur successively in a random manner, but with their mean numbers in accord with equation (1). This would be difficult, and I shall content myself with an approximate picture, in which the statistical variations are smoothed out and in which the current 'micropulses' due to growth of individual domains are represented by the rectangular pulse of figure 2 (*a*). This figure defines the amplitude h of the micropulse, and its growth-time τ_c.

Detailed knowledge of the form of the micropulse is not needed, and its variations with E are irrelevant ($f(E)$ in figure 2 (*a*) is an unspecified function of the field E); it is sufficient to know the growth-time τ_c and the area under the curve, which is chosen (see h in figure 2 (*a*)) to represent the charge Pa' passed during the growth of a microdomain†. Successive nuclei make their appearance under the electrodes at intervals τ_n given by $1/\tau_n = dn/dt$; τ_n may be millimicroseconds or less.

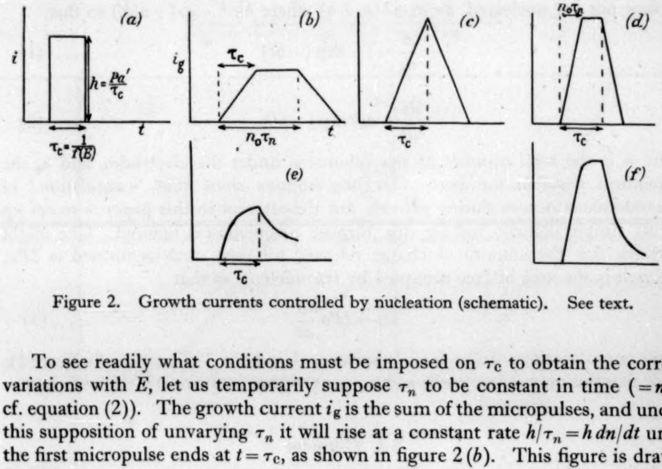

Figure 2. Growth currents controlled by nucleation (schematic). See text.

To see readily what conditions must be imposed on τ_c to obtain the correct variations with E, let us temporarily suppose τ_n to be constant in time ($= n_0 b$, cf. equation (2)). The growth current i_g is the sum of the micropulses, and under this supposition of unvarying τ_n it will rise at a constant rate $h/\tau_n = h\,dn/dt$ until the first micropulse ends at $t = \tau_c$, as shown in figure 2 (*b*). This figure is drawn for the case

$$\tau_n < \tau_c < n_0\tau_n. \qquad \ldots\ldots (4)$$

(If $\tau_n > \tau_c$ successive micropulses do not overlap at all.) The flat top results from the dynamic equilibrium when successive micropulses are appearing and disappearing at an equal rate. We may define a 'critical' amount of overlap by $\tau_n = \tau_c/n_0$, when i_g takes the form of figure 2 (*c*); for 'overcritical overlap' $\tau_n < \tau_c/n_0$ we have figure 2 (*d*), where the time parameters τ_c and $n_0\tau_n$ are now interchanged. Here the flat top represents the schematic flat top of figure 2 (*a*), and would not occur with a less idealized form for the micropulse.

---

† Variations of E simply change the i and $1/t$ scales by the same factor. This is true for micropulses from the form of the model equations in the Appendix, and also for i_g in equations (5) following. The similarity of figures 1(*b*) and 1(*c*) is a consequence.

The areas under figures 2 (*b*)–(*d*) must be $n_0 Pa'$, since they represent the switching of n_0 microdomains. Therefore the maximum values are $\hat{\imath}_g = Pa'/\tau_n$ for subcritical overlap (figure 2 (*b*)), but $\hat{\imath}_g = n_0 Pa'/\tau_c$ for overcritical overlap (figure 2 (*d*)). But in the latter expression, the factor $1/\tau_c$ carries the incorrect variation with E, say $1/\tau_c = f(E)$ (see figure 2 (*a*) and Appendix), while in the former, $1/\tau_n$ is proportional to b, and figure 3 (*a*) shows that this has the required form for $\hat{\imath}(E)$; by comparison with the coercive field E_c shown in figure 1 (*b*), this curve is satisfactory up to several times E_c. Therefore subcritical overlap, equation (4), is the required condition.

Abandoning the assumption of constant τ_n, the definition of critical overlap becomes imprecise, but clearly the same qualitative conclusions can be drawn.

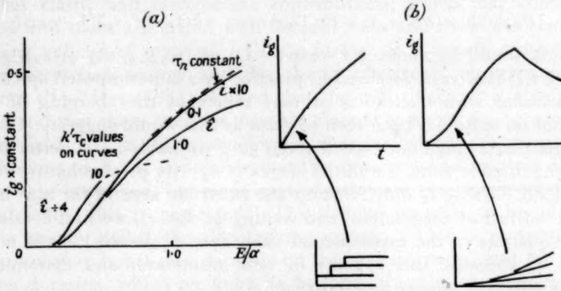

Figure 3. (*a*) Variations of $\hat{\imath}_g$ with E (equation 6). Broken lines: τ_n constant; (*b*) initial rise of $\hat{\imath}_g$.

i_g still rises at a rate $di_g/dt = h\,dn/dt$ until $t = \tau_c$ so that $i_g = hn$, but this is now not a uniform rise but

$$i_g = \frac{Pa'n_0}{\tau_c}\{1 - \exp(-bt)\} \qquad \ldots\ldots (5a)$$

using equation (1) and h from figure 2 (*a*). When the first micropulse ends there is a discontinuity (figure 2 (*e*)) and thereafter the slope is negative, $di_g/dt = (Pa'/\tau_c)\{dn/dt - (dn/dt)_{t-\tau_c}\}$ so that

$$i_g = \frac{Pa'n_0}{\tau_c}\{\exp(b\tau_c) - 1\}\exp(-bt). \qquad \ldots\ldots (5b)$$

The maximum value is

$$\hat{\imath}_g = \frac{Pa'n_0}{\tau_c}\{1 - \exp(-b\tau_c)\} \qquad \ldots\ldots (6)$$

and figure 3 (*a*) shows the form of this $\hat{\imath}_g(E)$ for various values of $k'\tau_c$ where $k'\tau_c$ is the field-independent factor in the exponential index $b\tau_c$ in equation (6) (see definition of b above equation (1)). Figure 2 (*f*) shows overcritical overlap, which gives the incorrect variation with E; the discontinuities in figures 2 (*e*)–(*f*) are due to the abrupt termination assumed in figure 2 (*a*). Figure 3 (*b*) shows a more realistic version of the initial rise.

Figure 2 (*e*) falls exponentially from the peak value $\hat{\imath}_g$ at τ_c with a time-constant $1/b$, so if we define t_s (see figure 1 (*a*)) by a suitable choice of a small integer p such that t_s is that time at which the curve has fallen to $\hat{\imath}_g/\exp p$, then $t_s - \tau_c = p/b$, from equation (5b) and figure 2 (e). Then from equation (2), $1/(n_0\tau_n)$ at $t=0$ is $p/(t_s-\tau_c)$ and falls off as $\exp(-bt)$ after $t=0$. So the condition for the correct E variation for i_g is $\tau_c<(t_s-\tau_c)/p$, that is, the peak must occur before half the time t' at which $i=\hat{i}/e$.

Figure 1 (a) shows that in fact it occurs close before that time, though the simplified form of figure 2 (d) does not allow a more precise statement; that is, the extent of the overlap must be not far short of critical, and the initial nucleation interval $(\tau_n)_{t=0}$ must be rather more than half of t'/n_0.

3.1. *Numerical Comparison*

If we include the expression for i_{nu} from equation (3), we have

$$i=i_{nu}+i_g=2Pa\,dn/dt+(Pa'/\tau_c)n=Pn_0[2ab\exp(-bt)+(a'/\tau_c)\{1-\exp(-bt)\}].$$

With $a'\sim a$, i_g would be about $\frac{1}{2}\{1-\exp(-1)\}$ of $(i_{nu})_{t=0}$, say $\frac{1}{3}(i_{nu})_{t=0}$. The initial part of $i(t)$ is always obscured in practice by a superimposed spike which may be associated with nucleation or may represent the charging of circuit capacities, but no spike has been seen so great as this would suggest. Observed spikes suggest that a could not exceed about $\frac{1}{3}a'$; probably i_{nu} is better thought of as indistinguishable from the initial stages of i_g; its precise nature remains to be explained. Using i_g only, writing the electrode area A for n_0a' in spite of the observed fact of coagulation, and writing $\frac{1}{2}t'$ for τ_c, we find a value for $\hat{i}$ about three-quarters of the experimental value (see Appendix); it is not very sensitive to τ_c (because this appears in both numerator and denominator); $\tau_c=\frac{1}{3}t'$ gives only 8% greater peak current.

3.2. *Viscous Opposition*

In drawing our conclusions we have not needed to know the form of the micropulse. More detailed examination would depend upon the arbitrary selection of a domain model. Models considered in the Appendix are very simple, but probably order-of-magnitude conclusions could be drawn from them. In particular, it has been pointed out that figure 1 (a) shows that the overlap is not far short of critical, and it is interesting to note that reasonable choices of the adjustable parameters in the models indicate velocities several orders too high to agree with this, unless a viscous opposition is inserted (see Appendix). It is possible that impurities or imperfections may provide such an effect.

ACKNOWLEDGMENTS

We are indebted to Dr. D. R. Young of I.B.M., Poughkeepsie, and to Dr. E. White of G.E.C., Wembley, for crystals. R. V. Peacock, who has undertaken measurements and electronmicrographs, was in receipt of a grant from the Ministry of Education.

APPENDIX

If the choice of model is suitable, a domain in any state will have a representative point on the energy contours of § 2. Growth is described by the motion of this point on the contours; the path of steepest descent describes growth in which all inertial and viscous effects associated with a domain are neglected, so that it is not possible to predict growth as a function of time. Consider whether the inclusion of an inertial term allows an adequate description of the switching current. The behaviour of one domain may be thought of as the motion of the representative point, no longer following a path of steepest descent, because it now has an effective mass (which may be variable). Since 'non-conservative forces' have been excluded the growth is given by a suitable solution of the equation

$$\tfrac{1}{2}Mv^2 + F = \text{constant}. \qquad \ldots\ldots(7)$$

When E changes the contours change, and the new set of solutions will describe the way growth varies with field.

F has elastic and electrostatic contributions, which may conveniently be grouped into those associated with domain walls and those associated with the remaining volume of material. Of the former, it is usually supposed that the dipolar interaction energy and the elastic anisotropic energy are significant, and from this Merz (1954) showed that the wall thickness is about one lattice spacing and that these energies together amount to about $\sigma = 7\,\text{ergs}\,\text{cm}^{-2}$ in zero applied field. It is these *equilibrium* energies which are required for the contributions to F. It is possible that the anisotropic energy will differ slightly when a field is applied, but since applied fields are very much smaller than the internal fields, this is neglected. The volume energies to be added include what is usually called the depolarizing energy. This is proportional to the domain volume, but it also depends on the domain shape, and for use only for growing domains, which we know to be long and thin, the term will be small, and is neglected; this may lead to unreliable results near the start of growth, if the critical dimensions are not also slender. Finally there is the electrostatic energy due to the presence of a polarized material in an external field. This may be regarded as providing the prime driving force, and with respect to the ideal virgin state when no antiparallel material exists, it may be written as a negative contribution to F of magnitude $2EP$ per unit volume of antiparallel material. So we have $F = -(2EP \times \text{domain volume}) + (\sigma \times \text{domain wall area})$, and it can be seen that the driving force tends to increase the microdomain volume, but is opposed by an effect in some ways analogous to a surface tension, tending to decrease the domain wall area.

If the driving field is suddenly removed, only the opposing effect remains, and the growing domains will collapse. However, if growth and coagulation of neighbouring domains had at that time occurred in such a manner that some *original* (rather than reversed) material was enclosed in a domain wall (see figure 4, Plate), this wall would also collapse, so that the switching process is furthered rather than undone. Both these predictions are contrary to observations made in this laboratory (to be published), and this probably reflects the fact that no term has been included in F to represent the effects on the elastic energy of impurity inclusions or lattice imperfections. This omission, which concerns largely the zero-field condition, is not further discussed in this paper.

Little is known about the domain shapes so that the following models are chosen for simplicity rather than realism.

Model 1: Suppose a microdomain to be a cone of fixed angle 2θ. Then

$$F(l) = -2EP(\pi l^3 \tan^2\theta)/3 + \sigma\pi l^2 \tan\theta \sec\theta.$$

If the tip travels at velocity V along the c axis, the normal velocity of the curved surface is $V\sin\theta$, so that equation (7) becomes

$$F(l)+\tfrac{1}{2}m\pi l^2\tan\theta\sec\theta\,(V\sin\theta)^2=F(l_0)$$

where m is the effective wall mass per cm^2 and l_0 is the initial value of l. Writing for $(2l_0EP\sin\theta)/3\sigma$ and K^2 for $(l_0{}^2m\sin^2\theta\cos\theta)/2\sigma$, this is

$$K^2(x\dot{x})^2=q(x^3-1)-(x^2-1)$$

where $x\equiv l/l_0$. This model exhibits a critical length $\sigma/(EP\sin\theta)$, corresponding to $q=\frac{2}{3}$. To allow easy solution, approximate the right-hand side as follows (the function used has the same slope-dependence near the starting point $x=1$): $Kx\dot{x}=q^{1/2}(x-2/3q)^{3/2}$. The solution is

$$\frac{tq^{1/2}}{K}=\frac{6qx-8}{3q(x-2/3q)^{1/2}}-\frac{6q-8}{3q(1-2/3q)^{1/2}}$$

and is shown in figure 5 (*a*) for values of q corresponding to l_0 up to about twice the critical length. uv/d integrated over the surface is proportional to $x^2\dot{x}$; for large enough x, this is proportional to t^5.

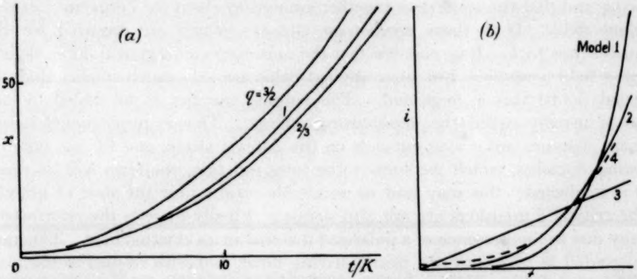

Figure 5. Domain length and microcurrents, according to models ($l_0\sim d/50$ in model 4).

Model 2: a wedge of fixed angle 2θ, and of indefinite sideways extent. A similar procedure leads to the equation $K^2x\dot{x}^2=q(x-1/2q)^2$ where

$$q\equiv(l_0EP\sin\theta)/\sigma,\qquad K^2\equiv(l_0{}^2m\sin^2\theta)/2\sigma$$

with the solution

$$\frac{tq^{1/2}}{K}=2(x^{1/2}-1)-\left(\frac{2}{q}\right)^{1/2}\{\coth^{-1}(2qx)^{1/2}-\coth^{-1}(2q)^{1/2}\}.$$

Integrated, uv/d is proportional to $x\dot{x}$; for large x this is proportional to t^3.

Model 3: a cylinder of fixed circular base, radius r. This model does not exhibit a critical length, but r must exceed σ/EP.

$$F=-2EP\pi r^2l+\sigma 2\pi rl.$$

So equation (7) is $F(l)+\frac{1}{2}m\pi r^2V^2=F(l_0)$. The solution is $l-l_0=t^2(EP-\sigma)/m$. Integrated, uv/d is $P\pi r^2V/d$, which is proportional to t.

Model 4: a cone of fixed base, and consequently with θ decreasing. A somewhat awkward integration over the cone shows that equation (7) is here

$$-2EP\pi r^2(l-l_0)/3+\sigma\pi r(l'-l_0')+r^3m\pi\dot{l}^2/12l'=0$$

where $l'^2\equiv l^2+r^2$. For $l\gg r$ and $l\gg l_0$, this becomes $V=Bl$ where

$$B^2\equiv 4(2EPr-3\sigma)/mr^2.$$

The solution is $l = l_0 \exp(Bt)$. Integrated, uv/d is one-third of that of model 3, and here is proportional to $\exp(Bt)$.

Figure 5 (*b*) shows these microcurrents normalized to represent the same quantity of reversed polarization for each, in an equal time.

After making 'impact' with the far side of the crystal, a large part of the moving charge no longer contributes to i_g and it is plausible that the remaining *uv* product should first become constant and then decrease, to account for the fall of i_g. But from the footnote of § 3 it follows that the form of $f(E)$ can be seen from the leading portion only, figure 5 (*b*). In each model E occurs together with a term in σ, which can be neglected if $\sigma \ll EPr$ in each case. Writing 75 000 e.s.u. for P, and with r of the order of a micron, this is $E \gg 1$ e.s.u. cm^{-1}. Thus for fields significantly above the coercive field (which is about 3 e.s.u. cm^{-1}), the leading term remaining in each model is of form approximately $t\sqrt{E} \propto l$ ($\log l$ in model 4) so that the time to reach impact at $l = d$ is inversely proportional to $\sqrt{E}$. It follows that $f(E) \sim \sqrt{E}$.

Viscous opposition. In these models the impact times are three orders too small (and, incidentally, an order less than the time for passage of a sound wave). For in the rather crude model 3, which has no adjustable parameters, writing say $E = 13$ e.s.u. cm^{-1} (4 kv cm^{-1}) and $m \sim 10^{-10}$ g cm^{-2} (Kittel 1951), we find for $l = d = 9 \times 10^{-3}$ cm, the impact time $0{\cdot}95 \times 10^{-9}$ sec. Models 1 and 2 give respectively $1{\cdot}2\sqrt{\sin 2\theta} \times 10^{-9}$ and $0{\cdot}43\sqrt{\sin\theta} \times 10^{-9}$; if θ is taken as large as 5°, these values are $0{\cdot}48 \times 10^{-9}$ and $0{\cdot}38 \times 10^{-9}$ sec respectively. τ_c must be of the same order, but compare the experimental value $t_s = 2{\cdot}5 \times 10^{-6}$ sec at that field. If we suppose the domains travel so much more slowly because of some sort of 'viscous' opposition, model 3 becomes approximately $dV/dt = 2EP/m - kV$, with solution

$$l = 2EP\{kt - 1 + \exp(-kt)\}/mk^2 \simeq 2EPt/mk.$$

$k = \frac{2}{3} \times 10^{12}$ sec^{-1} will give an impact time $0{\cdot}3 \times 10^{-6}$ sec. Notice that in the viscous model $f(E) \sim E$.

Values of $\hat{\imath}_g$. If we define t_s by $p = 3$ (see text), which corresponds to a fall of current to $\hat{\imath}_g/20$, we have $t_s - \tau_c = 3/b$, $t' - \tau_c = 1/b$. Taking $\tau_c \simeq \frac{1}{2}t'$ we find $\tau_c = \frac{1}{4}t_s$, $b\tau_c = 1$, so that equation (6) becomes $\hat{\imath}_g = (4PA/t_s)(1 - e^{-1})$. With the figures quoted, this is $2{\cdot}5 \times 10^4$ mA cm^{-2} compared with an experimental value of $3{\cdot}3 \times 10^4$ mA cm^{-2}.

REFERENCES

KITTEL, C., 1951, *Phys. Rev.*, **83**, 458.
LANDAUER, R., 1957, *J. Appl. Phys.*, **28**, 227.
MERZ, W. J., 1954, *Phys. Rev.*, **95**, 690.
WIEDER, H. H., 1956, *J. Appl. Phys.*, **27**, 413.

Fermi–Thomas Angular-dependent Potential for Iron

By D. M. HUM
Department of Mathematics, University College of the West Indies

Communicated by H. Jones; *MS. received* 30*th October* 1958, *in final form* 19*th December* 1958

Abstract. A method is developed for determining the angular-dependent solution of the Fermi–Thomas equation for the potential within a body-centred or face-centred cubic lattice, calculations being performed for iron. By comparison with the spherically symmetric solution of the form obtained by Slater and Krutter it is possible to obtain estimates of the errors involved in the use of a spherically symmetric potential field. For iron the correction to the potential causes an increase of 0·67 ev in energy of the Fermi level, a decrease of 1·32 ev in the potential energy barrier between atoms and an increase of 3·0 ev in the total energy per atom. The total energy per atom of any metal, in the angular-dependent case, is reduced to a sum of integrals over the surface of the atomic polyhedron.

---

§ 1. Introduction

Various methods are available for the calculation of energy band structures of solids based on the one-electron approximation. In such calculations it has generally been necessary to make the additional approximation of assuming the potential field within the unit polyhedron to be spherically symmetric. This assumption is essential in the Wigner–Seitz cellular method but, in calculations using, for example, the augmented plane wave or orthogonalized plane wave methods, its necessity has arisen from the great increase in labour which would be involved were an angular-dependent potential to be used. In monatomic body-centred and face-centred cubic lattices the approximation will incur an error which is small but in crystals whose unit polyhedra depart more widely from a spherical form, the error is expected to be greater. In calculations on PbS (Bell *et al.* 1953) the assumption of spherical symmetry was found to be poor and an attempt was made to include an angular-dependent term in the potential field. Leigh (1958) has made estimates of the effect on eigenvalues of including the angular-dependent part of a potential of the type used in augmented plane wave calculations.

Pincherle (1954) suggested that a first approximation to an angular-dependent potential might be obtained by solution of the Fermi–Thomas (FT) equation and such a potential could then be used in his variational-cellular or some other suitable method for the calculation of electronic band structures. Such an attempt to solve the FT equation was made by March (1954, 1957) but apparently it was not taken successfully beyond the inclusion of a single angular term. The method developed here for obtaining an angular-dependent solution of the FT equation for a body-centred or face-centred cubic lattice is similar to the method used by March but avoids the very rapid increase in numerical work which he found with the inclusion of each extra term in the series expansion for the potential field. Another method of obtaining the potential field in a crystal has recently been developed by Payne (1958). In this, the crystalline field is first approximated by a lattice sum of atomic FT fields and the field in the crystal is then corrected, preserving its lattice symmetry, until it satisfies the FT equation.

§ 2. THE FERMI–THOMAS FIELD FOR A METAL

The non-dimensional form of the FT equation is

$$\nabla_{\boldsymbol{\rho}}^2\chi(\boldsymbol{\rho})=\chi^{3/2}(\boldsymbol{\rho}). \qquad \ldots\ldots(1)$$

$\mathbf{V}(\mathbf{r})$, the electrostatic potential field due to the atomic nuclei and all electrons and $-eE$, the maximum total energy of an electron i.e. the energy of the Fermi level, are such that

$$V(\mathbf{r})-E=\frac{Ze}{\mu}\,\chi(\boldsymbol{\rho})$$

where,

$$\mathbf{r}=\mu\boldsymbol{\rho} \quad \text{and} \quad \mu=\left(\frac{9\pi^2}{128Z}\right)^{1/3}\frac{h^2}{4\pi^2me^2}.$$

For a monatomic lattice the exact boundary conditions are

$$\rho\chi(\rho)=1 \quad \text{at} \quad \rho=0 \qquad \ldots\ldots(2)$$

and

$$\frac{\partial\chi}{\partial n}=0 \qquad \ldots\ldots(3)$$

at all points on the surface of the polyhedron. We shall select the metal for which the solution is to be obtained and make use of the experimental value of the lattice constant so that $\chi(\boldsymbol{\rho})$ is uniquely determined for that metal, by equations (1) to (3).

The potential $V(\mathbf{r})$ possesses the full symmetry of the lattice. For the body-centred and face-centred cubic lattices, taking the origin of coordinates at the nucleus, the potential within the atomic polyhedron may be written

$$\chi(\boldsymbol{\rho})=\chi_s(\rho)+A\chi_0(\rho)+Bg\chi_4(\rho)+Ci\chi_6(\rho)+Dk\chi_8(\rho)+ \qquad \ldots\ldots(4)$$

Here the functions χ_s, χ_0, χ_4, … depend only on the radial distance,

$$\rho=(\xi^2+\eta^2+\zeta^2)^{1/2}$$

while 1, g, i, k, … are Kubic Harmonics (KH) possessing the symmetries of the full cubic group and are of order $l=0, 4, 6, 8, \ldots$:

$$g=\frac{\xi^4+\eta^4+\zeta^4}{\rho^4}-\tfrac{3}{5}$$

$$i=\frac{\xi^6+\eta^6+\zeta^6}{\rho^6}-\tfrac{15}{11}g-\tfrac{3}{7}$$

$$k=\frac{\xi^8+\eta^8+\zeta^8}{\rho^8}-\tfrac{28}{15}i-\tfrac{210}{143}g-\tfrac{1}{3}.$$

The KH g and i have been used previously and are listed by Bell (1954). The author has not seen mention of the KH k. This and further KH may be determined without the construction of group character tables, etc. by a direct application of the operators, under which the atomic polyhedron is invariant, to the full series expansion of the potential in terms of spherical harmonics. This is the method used by Howarth and Jones (1952).

§ 3. THE SLATER–KRUTTER APPROXIMATION

Slater and Krutter (1935, to be referred to as SK) made the approximation of replacing the polyhedron by a sphere of equal volume having radius ρ when a spherically symmetric potential $\chi_S(\rho)=\phi_S(\rho)/\rho$ may be determined from

$$\frac{d^2\phi_S}{d\rho^2}=(\phi_S{}^3/\rho)^{1/2} \qquad \ldots\ldots(5)$$

$$\phi_S(0)=1 \qquad \ldots\ldots(6)$$

$$\frac{d}{d\rho}(\phi_S/\rho)=0 \quad \text{at} \quad \rho=\rho_0. \qquad \ldots\ldots(7)$$

For ρ small, the well-known power series solution of (5) which satisfies (6) is given in table 1, and is†

$$\phi_S(\rho)=1+b\rho+\tfrac{4}{3}\rho^{3/2}+\frac{2b}{5}\rho^{5/2}+\ldots. \qquad \ldots\ldots(8)$$

A slight variation of the parameter b causes an appreciable variation in the value of ρ_0 for which the boundary condition (7) will be satisfied. Latter (1956) has published a set of solutions of the SK problem corresponding to various values of the atomic radius ρ_0. By interpolation between these tables it is possible to obtain a good approximation to the value of the parameter b for which (7) is satisfied for a radius close to the radius ρ_0 of the chosen metal. The solution of (5) for this value of b may then be found by the usual integration procedures, the initial values being calculated from (8). A second approximation to the solution of the SK problem which satisfies (7) at the required value ρ_0 may be found by replacing $\phi_S(\rho)$ by $\phi_S(\rho)+A_S\phi_0(\rho)$ in equations (5) to (8) and assuming that $|A_S\phi_0/\phi_S|\ll 1$ for $\rho\leqslant\rho_0$. The resulting differential equation for $\phi_0(\rho)=\rho\chi_0(\rho)$ and the series expansion when ρ is small are given by equation (14) and table 1. The constant A_S is determined by the boundary condition corresponding to (7), viz.

$$\frac{d}{d\rho}\left(\frac{\phi_S+A_S\phi_0}{\rho}\right)=0 \quad \text{at} \quad \rho=\rho_0. \qquad \ldots\ldots(9)$$

In calculations for iron, $\phi_S(\rho)$ was determined for $b=-1{\cdot}587\,780\,00$ and the condition (7) was satisfied at $\rho=8{\cdot}72$ whereas for iron $\rho_0=8{\cdot}9063$. The value of A_S given by (9) was $-0{\cdot}000\,028\,3(1)$. The SK potential for iron has therefore an initial slope $b+A_S=-1{\cdot}587\,808\,3(1)$ and $|A_S\phi_0/\phi_S|=0{\cdot}0598$ when $\rho=\rho_0$.

§ 4. THE ANGULAR-DEPENDENT POTENTIAL

Write (1) in the form

$$\nabla^2\chi_S(\rho)+\nabla^2\{\chi(\boldsymbol{\rho})-\chi_S(\rho)\}$$
$$=\chi_S{}^{3/2}+\tfrac{3}{2}\chi_S{}^{1/2}(\chi-\chi_S)+\tfrac{3}{8}\chi_S{}^{-1/2}(\chi-\chi_S)^2+\ldots. \qquad \ldots\ldots(10)$$

The SK potential $\chi_S(\rho)=\phi_S(\rho)/\rho$ is defined by equations (5) to (7). Hence

$$\nabla^2(\chi-\chi_S)=\tfrac{3}{2}\chi_S{}^{1/2}(\chi-\chi_S)+\tfrac{3}{8}\chi_S{}^{-1/2}(\chi-\chi_S)^2+\ldots. \qquad \ldots\ldots(11)$$

We will now assume that the expression

$$(\chi-\chi_S)/4\chi_S \qquad \ldots\ldots(12)$$

---

† The initial slope b has been denoted variously as B by SK, $-a_2$ by March and others, while in the formulation of Latter (1956) it is equal to $(\phi_0 r_0/\mu)^{-1}(d\phi/dx^2)_{x=0}$. It should be noted that the value quoted by Latter is in error and differs from this value by the omission of a factor $-1/\phi_0$ where ϕ_0 is the value of Latter's function ϕ at $x=0$.

is so small at all points within the atomic polyhedron that the second and subsequent terms on the right hand side of (11) may be neglected. This will be justified when numerical calculations have been completed but seems reasonable in the case of the body-centred and face-centred cubic lattices. In terms of the expansion (4) we now obtain

$$A\nabla^2\chi_0+Bg\nabla^2\chi_4+Ci\nabla^2\chi_6+\ldots-B(20/\rho^2)g\chi_4-C(42/\rho^2)i\chi_6-\ldots$$
$$=G(\rho)[A\chi_0+Bg\chi_4+Ci\chi_6+\ldots] \qquad \ldots\ldots(13)$$

where $G(\rho)=\frac{3}{2}\chi_S{}^{1/2}(\rho)=\frac{3}{2}(\phi_S(\rho)/\rho)$. Multiplying (13) by one of the KH 1, g, i, …, integrating over the surface of a sphere and dividing by $4\pi\rho^2$ we are led in turn to each of the equations

$$\phi_0''=G(\rho)\phi_0, \qquad \ldots\ldots(14)$$
$$\phi_4''=[G(\rho)+(20/\rho^2)]\phi_4, \qquad \ldots\ldots(15)$$
$$\phi_6''=[G(\rho)+(42/\rho^2)]\phi_6, \qquad \ldots\ldots(16)$$

and so on, where $\phi_0(\rho)=\rho\chi_0(\rho)$, $\phi_4(\rho)=\rho\chi_4(\rho)$, etc. For small values of ρ, the first few terms in the series expansions of $G(\rho)$, ϕ_0, ϕ_4 and ϕ_6 are given by the coefficients listed in table 1. It may be noted that each of the series expansions involves the parameter b, for which a suitable value, for any chosen metal, has previously been found in the SK approximation. Equations (14) to (16), and others if needed, may now be integrated independently.

Table 1. Coefficients in Series Expansions for ρ small

Power of ρ	0	1	3/2	2	5/2	3	7/2
$\phi_S(\rho)$	1	b	4/3	0	$2b/5$	1/3	$3b^2/70$
$\rho^{1/2}G(\rho)$	3/2	$3b/4$	1	$-3b^2/16$	$-b/5$	$(-8+9b^3)/96$	$9b^2/35$
$\rho^{-1}\phi_0(\rho)$	1	0	2/5	0	$3b/35$	2/15	$-b^2/84$
$\rho^{-5}\phi_4(\rho)$	1	0	2/21	0	$3b/115$	2/63	$-3b^2/700$
$\rho^{-7}\phi_6(\rho)$	1	0	2/29	0	$3b/155$	2/87	$-b^2/308$

Power of ρ	4	9/2	5	11/2
$\phi_S(\rho)$	$2b/15$	$(56-3b^3)/756$	$b^2/175$	$\dfrac{992b+45b^4}{47520}$
$\rho^{1/2}G(\rho)$	$(352b-75b^4)/1280$			
$\rho^{-1}\phi_0(\rho)$	$2b/175$	$(248+45b^3)/11880$	$4b^2/525$	
$\rho^{-5}\phi_4(\rho)$	$-18b/10465$	$(40+63b^3)/40824$	$508b^2/140875$	
$\rho^{-7}\phi_6(\rho)$	$-13b/76415$	$(56+261b^3)/219240$	$2092b^2/741675$	

This procedure may be contrasted with the method of March (1954, 1957). Whereas the above method depends on expansion (4) which involves two spherically symmetric terms χ_S and $A\chi_0$, March included only one spherical term ψ_S, say (different from the SK solution). Again, whereas we here neglect the third term on the right hand side of (10), March chose his function ψ_S so as to retain the spherically symmetric part of this term. This however has the grave disadvantage that the differential equation for the term ψ_S now involves a term which is quadratic in $B\chi_4$, $C\chi_6$, …. Since the equations for χ_4, χ_6, … involve ψ_S, March had to use an iterative procedure for solving the set of equations for ψ_S, $B\chi_4$, $C\chi_6$ … until a consistent set of solutions was obtained. It is apparent that this method greatly increases in complexity with the addition of each angular-dependent term to the potential.

In contrast, when using the method developed above, the labour of computation is not greatly increased by the addition of a further term to the potential, for the previously included radial functions $\chi_8, \chi_0, \chi_4 \ldots$ do not need recalculation. It remains to evaluate the constants A, B, C, ...

§ 5. BOUNDARY CONDITIONS ON THE POLYHEDRON

It will not be possible to retain more than a few terms of the expansion (4), and (3) may only be satisfied at a finite number of points. The selection of sets of points at which (3) is to be satisfied is at best somewhat arbitrary, though a systemetic procedure has been developed by Howarth and Jones (1952). An alternative method, is that used by March (1957), viz. the minimization of

$$\mathscr{I} = \int_S \left(\frac{\partial\chi}{\partial n}\right)^2 dS, \qquad \ldots\ldots(17)$$

the integration extending over the surface of the polyhedron, S. Neither this nor the previous procedure of point-matching will lead to an electrically neutral atom. The condition for charge neutrality is that

$$\mathscr{J} = \int_S \frac{\partial\chi}{\partial n}\, dS = 0. \qquad \ldots\ldots(18)$$

A potential field for which the atomic polyhedron is electrically neutral may be obtained by the use of an 'undetermined multiplier' to minimize (17) subject to the condition (18). Retaining the first four terms only of (4), four equations are derived from which A, B, C, and the 'undetermined multiplier' may be obtained.

Each of the above three methods for estimating the constants A, B, C, was tried but, in the subsequent numerical calculations, the values adopted were those obtained by minimization of $\mathscr{I}$ subject to $\mathscr{J} = 0$.

§ 6. TOTAL ENERGY PER ATOM OF THE METAL

SK showed that, provided the atomic polyhedron is electrically neutral, the total electronic kinetic and potential energy per atom is

$$T = \frac{1}{8\pi}\,\frac{Z^2e^2}{\mu}\left[4\pi(b+A) + \frac{1}{5}\int_V \chi^{5/2}(\boldsymbol{\rho})\,dV\right]$$

where $b+A$ is the initial slope of $\chi(\boldsymbol{\rho})$ in the expansion (4) and the integration is over the volume V of the polyhedron. The volume integral was evaluated, for the spherically symmetric approximation, by Milne (1927) who found that it could be expressed simply in terms of the value of the potential $\chi_8(\rho)$ on the surface of the sphere. For the angular-dependent potential $\chi(\boldsymbol{\rho})$ the volume integral may again be reduced to a surface integration.

Using (1) and Green's theorem

$$\int_V \chi^{5/2}\, dV = \int_{S+S_1} \chi\nabla\chi\cdot\mathbf{dS} - \int_V (\nabla\chi)^2\, dV. \qquad \ldots\ldots(19)$$

The surface integral is to be evaluated over the atomic polyhedron S and over a small sphere S_1 surrounding the origin. The last integral in (19) may be transformed:

$$3\int_V (\nabla\chi)^2\, dV = \int_{S+S_1} (\nabla\chi)^2\boldsymbol{\rho}\cdot\mathbf{dS} - \int_V (\boldsymbol{\rho}\cdot\nabla)(\nabla\chi)^2\, dV. \qquad \ldots\ldots(20)$$

Now $(\boldsymbol{\rho}\cdot\nabla)(\nabla\chi)^2 = 2\nabla\cdot\{(\boldsymbol{\rho}\cdot\nabla\chi)\nabla\chi\} - 2(\boldsymbol{\rho}\cdot\nabla\chi)\nabla^2\chi - 2(\nabla\chi)^2$. Substituting in (20), if we again use (1) and the divergence theorem, we may write

$$\int_V (\nabla\chi)^2\,dV = \int_{S+S_1}(\nabla\chi)^2\boldsymbol{\rho}\cdot d\mathbf{S} - 2\int_{S+S_1}(\boldsymbol{\rho}\cdot\nabla\chi)\nabla\chi\cdot d\mathbf{S} + 2\int_V(\boldsymbol{\rho}\cdot\nabla\chi)\chi^{3/2}\,dV.$$

Using the identity

$$\tfrac{5}{2}(\boldsymbol{\rho}\cdot\nabla\chi)\chi^{3/2} = \nabla\cdot(\boldsymbol{\rho}\chi^{5/2}) - 3\chi^{5/2}$$

we obtain

$$\frac{7}{5}\int_V \chi^{5/2}\,dV = \int_{S+S_1}\left\{\frac{4}{5}\chi^{5/2} + (\nabla\chi)^2\right\}\boldsymbol{\rho}\cdot d\mathbf{S} - \int_{S+S_1}\{\chi + 2\boldsymbol{\rho}\cdot\nabla\chi\}\nabla\chi\cdot d\mathbf{S}.$$

Now for ρ small $\chi(\rho) \simeq [1 + (b+A)\rho + \ldots]/\rho$ so that evaluation of the integrals over S_1 gives

$$\frac{7\mu}{3Z^2e^2}T = b + A + \frac{1}{24\pi}\int_S\left\{\frac{4}{5}\chi^{5/2} + (\nabla\chi)^2\right\}\boldsymbol{\rho}\cdot d\mathbf{S} - \frac{1}{24\pi}\int_S\{\chi + 2\boldsymbol{\rho}\cdot\nabla\chi\}\nabla\chi\cdot d\mathbf{S}.$$

For the body-centred cubic lattice the integrals over the whole surface S will be equal to 48 times the sum of the integrals over the triangle LPC (region a) and the quadrilateral CQMP (region b) shown in figure 1. Writing

$$I_1 = \frac{8}{5\pi}\int_{\mathrm{a+b}}\chi^{5/2}\boldsymbol{\rho}\cdot d\mathbf{S} \qquad \ldots\ldots(21)$$

$$I_2 = \frac{2}{\pi}\int_{\mathrm{a+b}}(\nabla\chi)^2\boldsymbol{\rho}\cdot d\mathbf{S} \qquad \ldots\ldots(22)$$

$$I_3 = \frac{2}{\pi}\int_{\mathrm{a+b}}\{\chi + 2\boldsymbol{\rho}\cdot\nabla\chi\}\nabla\chi\cdot d\mathbf{S} \qquad \ldots\ldots(23)$$

then

$$\frac{7\mu}{3Z^2e^2}T = b + A + I_1 + I_2 - I_3. \qquad \ldots\ldots(24)$$

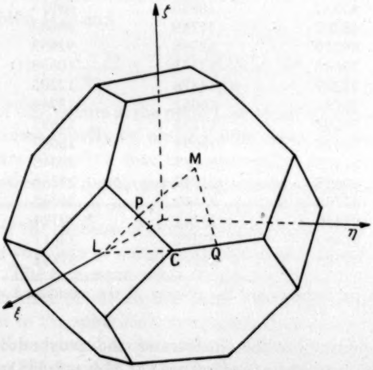

Figure 1. Atomic polyhedron of the body-centred cubic lattice.

It may be noted that for the exact potential $\chi(\boldsymbol{\rho})$, when all the terms in (4) are retained, the condition (3) is satisfied at all points on the polyhedron, in which case $I_3 = 0$.

In the spherically symmetric approximation $\nabla\chi=0$ on the equi-volume sphere $\rho=\rho_0$ and the total energy T_s is given by

$$\frac{7\mu}{3Z^2e^2}T_s=b+A_s+\frac{2}{15}\rho_0^{1/2}\{\chi_s(\rho_0)+A_s\chi_0(\rho_0)\}^{5/2} \qquad \ldots\ldots(25)$$

and for the isolated atom, since $\chi(\boldsymbol{\rho})$ vanishes at large distances the corresponding energy T_∞ is given by

$$\frac{7\mu}{3Z^2e^2}T_\infty=b_\infty=-1{\cdot}588\,071\,02$$

the value obtained by Latter (1956).

§ 7. NUMERICAL CALCULATIONS FOR IRON

Calculations of the potential field were made for iron (lattice constant $=2{\cdot}86\times10^{-8}$ cm, $\mu=1{\cdot}5831\times10^{-9}$ cm, $\rho_0=8{\cdot}9063$). The function $\phi_s(\rho)$ has the usual form and its initial slope was taken to be $b=-1{\cdot}587\,780\,00$. In table 2, the radial functions ϕ_s, ϕ_0, ϕ_4, ϕ_6 are tabulated for ρ having the values 6·0(0·2)10·6.

Table 2. Values of the Radial Functions ϕ_s, ϕ_0, ϕ_4, ϕ_6

ρ	$\phi_s(\rho)$	$\phi_0(\rho)$	$\phi_4(\rho)$	$\phi_6(\rho)$
6·0	72882(−6)†	46788(−3)†	13711(0)†	42207(1)†
6·2	71084	51228	16461	53832
6·4	69590	55996	19659	68162
6·6	68387	61116	23365	85721
6·8	67462	66608	27643	10712(2)
7·0	66807	72499	32566	13306
7·2	66412	78816	38212	16435
7·4	66273	85586	44668	20192
7·6	66385	92843	52031	24685
7·8	66745	10062(−2)	60408	30036
8·0	67352	10896	69915	36384
8·2	68207	11789	80682	43890
8·4	69310	12748	92852	52734
8·6	70665	13775	10658(1)	63124
8·8	72277	14878	12205	75293
9·0	74151	16062	13944	89509
9·2	76294	17333	15897	10607(3)
9·4	78716	18699	18087	12532
9·6	81425	20167	20540	14765
9·8	84435	21747	23286	17349
10·0	87758	23449	26355	20333
10·2	91410	25282	29784	23774
10·4	95409	27259	33611	27735
10·6	99773	29393	37881	32286

† The numbers in parentheses are the powers of ten associated with the entries, e.g. $\phi_s(6{\cdot}0)=0{\cdot}072\,882$.

At prominent points on the surface of the polyhedron, the boundary condition (3) reduces to conditions as follows: at M ($\rho=7{\cdot}833$): a radial condition (M_ρ); at L ($\rho=9{\cdot}044$): a radial condition (L_ρ); at Q ($\rho=9{\cdot}593$): a radial condition (Q_ρ); at P ($\rho=9{\cdot}593$): a radial condition ($P_\rho=Q_\rho$) and one transverse condition (P_τ); at C ($\rho=10{\cdot}112$): a radial condition (C_ρ) and one transverse condition (C_τ). By selecting suitable combinations of three of these conditions, sets of values of A, B, C were determined and their values are listed in table 3. For reasons similar to those listed by Bell *et al.* (1953), the combinations ($L_\rho M_\rho Q_\rho$) and ($L_\rho M_\rho C_\rho$) are likely to give the most reliable estimates of the constants A, B, C but the values given by these two combinations do not agree sufficiently well for any reliance to be placed on the values of the physial parameters which will subsequently be calculated with their aid.

Table 3. Values of A, B, C obtained from various Boundary Conditions and net number of Electrons in Polyhedron

Type of boundary condition	$A\times 10^5$	$B\times 10^7$	$C\times 10^9$	Net no. of electrons
SK approximation $\phi_s + A_s\phi_0$	$-28{\cdot}31$	—	—	$+0{\cdot}0163$
Point conditions $L_\rho M_\rho Q_\rho$	$+2{\cdot}960$	$-2{\cdot}369$	$+22{\cdot}62$	$-0{\cdot}0561$
Point conditions $L_\rho M_\rho P_\rho$	$-7{\cdot}267$	$-2{\cdot}307$	$+46{\cdot}78$	$-0{\cdot}2736$
Point conditions $L_\rho M_\rho C_\rho$	$+0{\cdot}887$	$-2{\cdot}357$	$+27{\cdot}51$	$-0{\cdot}1001$
Minimization of $\mathcal{J}$	$-0{\cdot}0990$	$-2{\cdot}395$	$+4{\cdot}702$	$-0{\cdot}0317$
Minimization of $\mathcal{J}$ when $\mathcal{J}=0$	$+0{\cdot}2285$	$-2{\cdot}406$	$+4{\cdot}710$	zero

The second procedure mentioned in § 5, the minimization of (17), gave the values listed in table 3. This method is more cumbersome than the method of point matching but it avoids the arbitrary character of the latter. However, the polyhedron has a net charge as was also a defect of the method of point matching. This defect does not arise with the third method—the minimization of (17) subject to the condition (18). This method is but slightly longer than the minimization of (17) alone. The corresponding values of A, B, C are again listed in table 3. It is these values which have been used in subsequent calculations, particularly because the derivation of (24) assumes the charge neutrality of the atomic polyhedron.

In equation (11) the ratio of the second to the first term on the right-hand side is given by expression (12) and

$$\frac{\chi-\chi_s}{4\chi_s} \simeq \frac{A\chi_0+Bg\chi_4+Ci\chi_6}{4\chi_s}. \qquad \ldots\ldots(26)$$

The largest value of (26) occurs at the point L at which its value is $-0{\cdot}0412$. The value of (26) decreases rapidly on moving away from the surface into the polyhedron. It appears therefore that the assumption that (12) is very small is justified for calculations on metals possessing a body-centred cubic lattice though the neglect of the second term on the right hand side of (11) may not be adequate for calculations near the surfaces of atomic polyhedra of other lattices.

Figure 2 shows contours of constant charge density on the faces of the polyhedron, for iron. The minimum value of $\chi(\boldsymbol{\rho})$ on the surface of the polyhedron occurs at L, the centres of the square faces. At these points χ has the value $6{\cdot}8878\times 10^{-3}$ while in the spherically symmetric approximation the least value is $7{\cdot}7307\times 10^{-3}$. SK suggested various ways in which the arbitrary constant in the potential might be determined. The method which is the more reasonable physically is to choose the constant so that the x-ray levels shall be independent of the lattice spacing. In a wave-mechanical calculation, these levels are determined by the potential near the nucleus. We therefore determined the constant terms in the potentials for the metal, in both the spherically symmetric and angular-

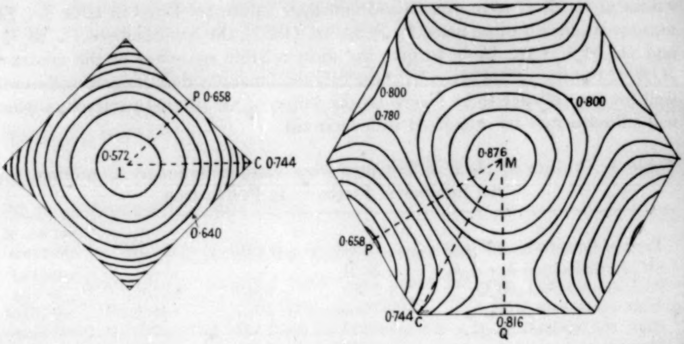

Figure 2. Charge density : contours of $\chi^{3/2} \times 10^3$ on the faces of the polyhedron for iron.

dependent approximations, to be equal to the constant term for the potential of the isolated atom. Then

$$-e(E-E_S) = (Ze^2/\mu)(A-A_S)$$

is the change in the energy of the Fermi level due to the inclusion of the angular-dependent terms in the potential. The resulting decrease in the potential energy barrier between atoms is

$$(Ze^2/\mu)[(A-A_S) + \chi(\min) - \chi_s(\min)]$$

where $\chi(\min)$, $\chi_s(\min)$ are the least values of χ in the respective approximations referred to above. In the calculations for iron, the energy of the Fermi level increased by 0·67 ev while the potential barrier between atoms decreased by 1·32 ev. Figure 3 shows the calculated form of the potential $\chi(\boldsymbol{\rho})$ between neighbouring atoms along the (1, 0, 0) and (1, 1, 1) direction passing through L and M respectively.

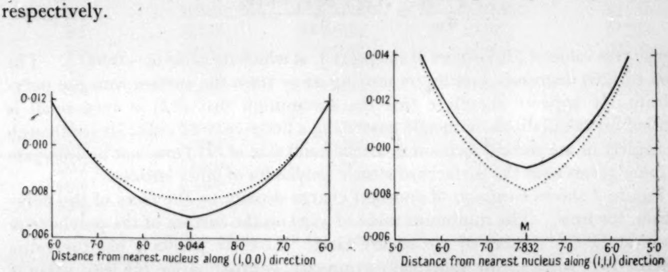

Figure 3. Graphs of the SK approximation, $\chi_s + A\,\chi_0$ (dotted curves) and of the angular-dependent approximation, $\chi_s + A\chi_0 + Bg\chi_4 + Ci\chi_6$ (full curves) for iron, plotted between nuclei along the (1, 0, 0) and (1, 1, 1) directions through L and M respectively.

The total energy per atom in the angular-dependent field is found using (24). For iron the integrals (21) to (23) took values $I_1 = 0{\cdot}5683 \times 10^{-3}$; $I_2 = 0{\cdot}0222 \times 10^{-3}$;

$I_3 = 0{\cdot}0132 \times 10^{-3}$, hence $(7\mu/3Z^2e^2)T = -1{\cdot}587\,200$ while for the spherically symmetric field, from (26) $(7\mu/3Z^2e^2)T_s = -1{\cdot}587\,315$. The total energy per atom is increased by 3·0 ev. For the isolated atom, the corresponding value, $b_\infty = -1{\cdot}588\,071\,02$ (Latter 1956). The angular dependent terms introduce a correction of about 15% in the value of $T_s - T_\infty$. It may be further noted that I_3, which would be zero for the exact potential, corresponds to about 15% of $T - T_s$. It may be that the estimate of $T - T_s$ is in error by as much as 15%.

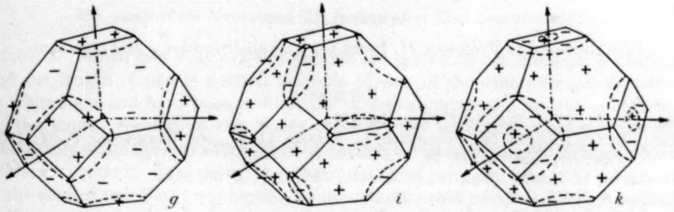

Figure 4. Diagrams show the regions on the surface of the unit polyhedron in which the Kubic Harmonics *g, i, k* are positive or negative.

Figure 4 shows the variations in sign of the KH *g, i, k* on the surface of the polyhedron. From these, we can see the type of contribution made by each of the terms of expansion (4). In the calculations for iron, it has been found that the terms $Bg\chi_4$ and $Ci\chi_6$ have considerably reduced the integral $\mathscr{I}$ but $\partial\chi/\partial n$ is still appreciable close to L and M and along the edges. $\mathscr{I}$ would apparently be considerably reduced and the accuracy of the field increased by the inclusion of the next term of (4) beyond those used in the present calculations.

§ 8. CONCLUSIONS

A method has been developed for calculating angular-dependent potential fields which, at least, is suitable for body-centred and face-centred cubic structures. The method is similar to that used by March (1957) but has the advantage that whereas March's procedure required the use of a self-consistent procedure which rapidly increased in complexity with the retention of a second angular-dependent term in the potential, here the radial functions χ_0, χ_4, $\chi_6 \ldots$ are evaluated independently.

The total energy per atom T for the angular-dependent field has been reduced to an integration over the surface of the atomic polyhedron. The reduction assumes the charge neutrality of the atom. By means of a Lagrange 'undetermined multiplier', a suitable boundary condition yielding an electrically neutral atom may be used without greatly increasing the labour of computation for such calculations are again needed in the computation of the total energy. Calculations of the potential field of iron have led to estimates of the changes in T and in the height of the potential barrier between atoms, resulting from the angular-dependent terms in the potential. In the present calculations it appears that the accuracy of the field and of the parameters obtained from it would be appreciably increased by the retention of one or perhaps two more terms in the series expansion of the potential.

In wave-mechanical calculations it has been found that the results of self-consistent field calculations are approximated rather well by the corresponding FT field. It may therefore be expected that the changes found here due to the inclusion of angular terms in the FT field will be good estimates of the values which would be obtained were the excessively long wave-mechanical calculations to be performed. Finally, it is noted that the present method may also be used to form angular-dependent solutions of the Fermi–Thomas–Dirac equation.

ACKNOWLEDGMENT

I am indebted to Professor H. Jones for his valuable advice and criticism.

REFERENCES

BELL, D. G., 1954, *Rev. Mod. Phys.*, **26**, 311.
BELL, D. G., HUM, D. M., PINCHERLE, L., SCIAMA, D. W., and WOODWARD, P. M., 1953, *Proc. Roy. Soc.* A, **217**, 71.
HOWARTH, D. J., and JONES, H., 1952, *Proc. Phys. Soc.* A, **65**, 355.
LATTER, R., 1956, *J. Chem. Phys.*, **24**, 280.
LEIGH, R. S., 1958, *Proc. Phys. Soc.*, **71**, 33.
MARCH, N. H., 1954, *Symposium on Band Structures*, R.R.E., Malvern, p. 24.
—— 1957, *Advanc. Phys.*, **6**, 1.
MILNE, E. A., 1927, *Proc. Camb. Phil. Soc.*, **23**, 794.
PAYNE, H., 1958, *Phys. Rev.*, **111**, 418.
PINCHERLE, L., 1954, *Physica*, **20**, 965
SLATER, J. C., and KRUTTER, H. M., 1935, *Phys. Rev.*, **47**, 559.

Developments in the Comparison of Lengths using Fringes of Superposition in White Light

A. H. COOK AND H. M. RICHARDSON
National Physical Laboratory, Teddington, Middlesex

MS. received 6th November 1958, in final form 22nd December 1958

Abstract. When two Fabry–Perot etalons are placed one in front of the other, and the length of one is a small multiple of that of the other, fringes are seen in white light and have been used in the past to compare the lengths of etalons. In the study reported in this paper these fringes have been observed photoelectrically while the optical length of one etalon is varied by changing the pressure of the air inside it. It is shown that the variation of intensity with path difference is the sum of two Fourier integrals involving an intensity function and the phase shifts at the reflecting surfaces. By forming cosine and sine Fourier transforms these quantities can be obtained separately and a correction applied for the error introduced into the comparison of lengths by the change of the phase shifts with wavelengths. It is shown that phase shifts can be measured more accurately by this method than by other interferometric means. It is possible to compare a metre length with a 20 cm length to about 1 in 10^8.

§ 1. INTRODUCTION

SUPPOSE that two pairs of plates with semi-reflecting surfaces are set up parallel to each other as shown in figure 1, so that the separation D of one pair of plates, 1, is a small multiple n of the separation d of the other pair, 2. If a collimated beam of light is incident on the plates, light which is reflected once between the pair 1 will be retarded by the same amount as light which is reflected n times between the pair 2. In these circumstances interference fringes may be seen between the two reflected beams and since the path difference is nominally zero, the fringes will be seen in white light. Such fringes known as Brewster's fringes, or fringes of superposition, have often been used to compare one length with another and in this way a length which is too great to measure directly in terms of a standard wavelength by optical interference may be compared with a shorter one which can be so measured directly. By this means the metre has been evaluated in terms of standard wavelengths of light despite the fact that with visual radiations interference cannot be obtained over so great a path difference.

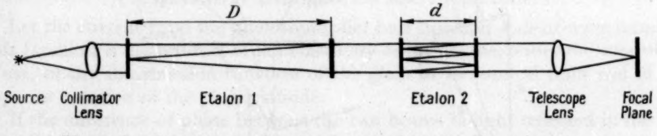

Figure 1. Arrangement for observation of fringes of superposition.

These white light fringes have in the past been observed visually but they are not usually very easy to see especially if the greater length is more than three times the lesser. The principal reason for this is that the two interfering beams have often quite different intensities and the fringes have to be observed over the background of all the light which is transmitted directly or undergoes other numbers of reflections. It therefore seemed worth while to try to observe the fringes photoelectrically and at the same time to bring the retardations between the two pairs of plates to the correct ratio by altering the pressure, and therefore the refractive index, of the air between the closer pair.

A pair of parallel semi-reflecting plates with a fixed separation will be called, as is usual, an etalon.

§ 2. PRINCIPLE OF THE METHOD

If light incident normally on an etalon is reflected between the plates, the retardation it suffers may be represented by a vector $\mathbf{R}$ normal to the plates and of magnitude proportional to the separation of the plates multiplied by the number of reflections. If the incident light makes an angle α with $\mathbf{R}$, the retardation is $R\cos\alpha$, that is $\mathbf{R}.\mathbf{n}$ where $\mathbf{n}$ is a unit vector parallel to the incident light. When two etalons, not necessarily parallel, are placed one in front of the other, the difference between the retardations is $(\mathbf{R}_1-\mathbf{R}_2).\mathbf{n}$. We denote the difference vector $\mathbf{R}_1-\mathbf{R}_2$ by $\boldsymbol{\delta}$ (figure 2). In general the scalar product $\boldsymbol{\delta}.\mathbf{n}$ will be zero only if $\boldsymbol{\delta}$ and $\mathbf{n}$ are perpendicular, and a bright white fringe will be seen if the etalons are observed in a direction perpendicular to $\boldsymbol{\delta}$. As the angle between $\boldsymbol{\delta}$ and $\mathbf{n}$ is altered, there are ranges on either side of the central white fringe in which $\boldsymbol{\delta}.\mathbf{n}$ is equal to $\frac{1}{2}\lambda$ for some visible radiations. These correspond to 'dark' fringes on either side of the central fringe. At greater deviations coloured fringes are seen, the contrast being reduced as the magnitude of $\boldsymbol{\delta}.\mathbf{n}$ increases. Directions $\mathbf{n}$ for which $\boldsymbol{\delta}.\mathbf{n}$ has a specified value form a cone about $\boldsymbol{\delta}$ as axis and the fringes therefore appear as the intersections of these cones with the focal plane of the telescope used to view the fringe system. A general discussion has been given by Cabrera and Terrien (1941).

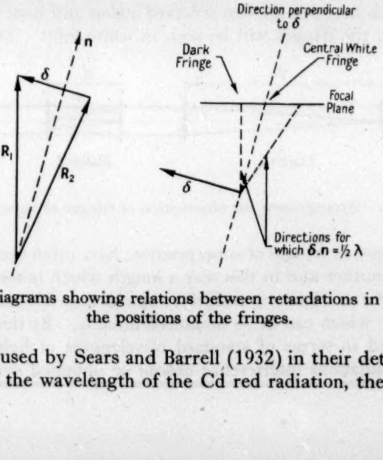

Figure 2. Vector diagrams showing relations between retardations in the two etalons and the positions of the fringes.

In the system used by Sears and Barrell (1932) in their determination of the metre in terms of the wavelength of the Cd red radiation, the etalon for which the retardation was greatest was tilted until the angle between the vectors $\mathbf{R}_1$ and $\mathbf{R}_2$ was such that $\boldsymbol{\delta}$ was perpendicular to the fixed one, $\mathbf{R}_1$ say, (figure 3 (*a*)) when the central white fringe appeared on the axis of this etalon. The movable etalon was then tilted in the opposite direction until $\boldsymbol{\delta}$ was again perpendicular to $\mathbf{R}_1$. Then if θ is the angle between the two directions of $\mathbf{R}_2$, $R_1 = R_2 \cos \frac{1}{2}\theta$.

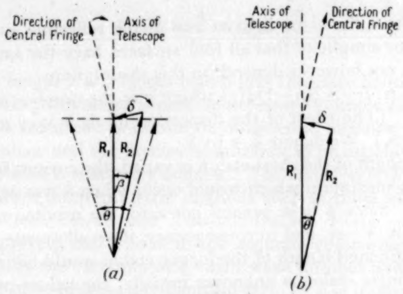

Figure 3. Use of white light fringes for comparison of lengths. (*a*) System of Sears and Barrell: vectors $\mathbf{R}_1$ and $\mathbf{R}_2$ of constant magnitude, angle β varied; (*b*) present system: $\mathbf{R}_2$ and θ fixed, magnitude of $\mathbf{R}_1$ varied.

If however, the magnitude of $\mathbf{R}_1$ can be varied by changing the pressure of the air in the etalon, the angle between the etalons can be fixed at a very small value and $\boldsymbol{\delta}$ can be made perpendicular to $\mathbf{R}_1$ by altering the magnitude of $\mathbf{R}_1$ (figure 3 (*b*)). It is this method which is used in the apparatus described here. A telescope is set up with its axis, as defined by a pinhole in the focal plane, parallel to the axis of one of the etalons, the axis of the other making a small angle with the telescope axis. The pressure of the air in the first etalon is varied and as the fringes move across the pinhole the current from a photomultiplier behind the pinhole varies correspondingly.

§ 3. INTENSITY DISTRIBUTION AND PHASE SHIFTS

Let the current from the photomultiplier be a function $I_\nu \, d\nu$ of wave number. This function is the product of the emissivity of the source, under the conditions of use, of the transmission function of the glass in the optical train and of the response function of the photocathode.

If the difference of phase between the two beams of light reflected in the two etalons is $\Phi(\nu)$ then the current from the photomultiplier due to a component of wave number ν may be taken to be

$$I_\nu \{1 + \cos \Phi(\nu)\} \, d\nu.$$

The intensity distribution of monochromatic light transmitted by two etalons in line has been given by various authors (see, for instance, Schuster 1924) and is the product of two Airy distributions. This may be expanded in a series of terms proportional to $\cos \Phi(\nu)$, $\cos 2\Phi(\nu)$, ..., but the method of analysis developed below takes account only of the fundamental term and ignores the higher harmonics, provided the range of wave number considered is less than two to one. A more detailed analysis of the validity of this argument, and of the effect of the size and position of the pinhole, is being prepared for publication.

The total current from the photomultiplier is thus effectively given by:

$$\int_0^\infty I_\nu\{1+\cos\Phi(\nu)\}\,d\nu.$$

Let the phase shifts suffered by light at any of the reflecting surfaces be $\phi(\nu)$, it being assumed for simplicity that all four surfaces have the same properties; the argument does not however depend on this assumption.

Then $\Phi(\nu)=\boldsymbol{\delta}\,.\,\mathbf{n}\,.\,2\pi\nu+2(n-1)\phi(\nu)$ where n is the number of reflections in the shorter etalon. (The effect of the dispersion of air is very small compared with the other terms.) We denote $\boldsymbol{\delta}\,.\,\mathbf{n}$ by δ.

As the optical length of the short etalon is varied, the current from the photomultiplier attains a maximum which would occur when δ was zero if the phase shift ϕ were zero. Since ϕ is in general not zero, the maximum may occur at some non-zero value, δ' say, and in consequence, if no allowance were made for phase shifts, the estimated length of the longer etalon would be in error. Since the length of the longer etalon is unknown initially, the values of δ determined from pressure changes in the short etalon can only be expressed as differences from the value δ' at which the photomultiplier current attains its greatest maximum.

We therefore write

$$\Phi(\nu)=2\pi\nu(\delta+\delta')+2(n-1)\phi(\nu)$$

and

$$I-I_{\mathrm{m}}=\int_0^\infty I_\nu\cos\{2\pi\nu(\delta+\delta')+2(n-1)\phi\}\,d\nu,$$

where

$$I_{\mathrm{m}}=\int_0^\infty I_\nu\,d\nu.$$

Then

$$I-I_{\mathrm{m}}=\int_0^\infty I_\nu\cos\{2\pi\nu\delta'+2(n-1)\phi\}\cos2\pi\nu\delta\,d\nu-\int_0^\infty I_\nu\sin\{2\pi\nu\delta'+2(n-1)\phi\}\sin2\pi\nu\delta\,d\nu$$

showing that $I-I_{\mathrm{m}}$, the measured variation of current, may be expressed as the sum of cosine and sine Fourier integrals.

Taking the Fourier transforms of the current fluctuation, we have

$$I_\nu\cos\{2\pi\nu\delta'+2(n-1)\phi\}=\pi^{-1}\int_{-\infty}^{+\infty}(I-I_{\mathrm{m}})\cos2\pi\nu\delta\,d\delta;$$

$$I_\nu\sin\{2\pi\nu\delta'+2(n-1)\phi\}=\pi^{-1}\int_{-\infty}^{+\infty}(I-I_{\mathrm{m}})\sin2\pi\nu\delta\,d\delta.$$

From these two expressions, I_ν and $2\pi\delta'\nu+2(n-1)\phi$, to be denoted by θ_ν, may be found separately.

In using these white light fringes to determine the mechanical length L of the longer etalon in terms of the mechanical length l of the shorter, we have $\delta'=2(nl-L)$.

By measurements of the order of interference in the shorter etalon at wave number ν we obtain the optical length l_ν say, equal to $(l+\phi/\pi\nu)$. Hence

$$L=n\left(l_\nu-\frac{\phi}{\pi\nu}\right)-\frac{\delta'}{2}$$

or

$$L_\nu=L+\frac{\phi}{\pi\nu}=nl_\nu-\frac{\theta_\nu}{2\pi\nu}.$$

The optical length of the longer etalon may therefore be found if θ_ν is known. For mechanical measurements it may be necessary to know L for which purpose the value of ϕ is required. ϕ cannot be obtained in absolute terms from optical measurements alone and the precise significance to be attached to it will depend on the way in which L is actually defined. The variation of ϕ with wave number can be found from interferometric methods such as those using multiple beam Fizeau fringes (see Barrell and Teasdale-Buckell 1951) and is the quantity required for applying corrections in the accurate comparisons of wavelengths. It is also given by the variation of θ_ν with wave number and is in fact the only significant part of θ_ν because any constant term in ϕ is inseparable from δ'.

The precision with which θ_ν may be determined is discussed at the end of § 5.

§ 4. APPARATUS

The experimental work was done on the wavelength comparator of Sears and Barrell (1932) using the 1 m etalon and a 20 cm etalon. The reflecting plates of each etalon were coated with aluminium films of about 80% reflectivity. The axis of the 20 cm etalon was parallel to that of the telescope as defined by a pinhole (of diameter about 0·8 mm) in the focal plane. The angle between the etalons was adjusted so that the width of the fringes was large compared with the diameter of the pinhole. The pressure of the air in the 20 cm etalon could be varied by a piston which was either adjusted by hand or else was driven by a constant speed motor.

The incident light was interrupted at 200 c/s by a rotating sector disc shutter. The light passing through the pinhole fell on a photomultiplier behind it and the output from the photomultiplier was amplified and rectified to give a direct current proportional to the intensity of light falling on the pinhole; this current was either measured with a galvanometer or recorded on a potentiometric recorder with constant paper speed.

If this system is to be used to measure the longer etalon in terms of a standard wavelength the optical length of the shorter must be known in terms of this standard at the pressure for which the central white light fringe falls on the pinhole; to preserve the precision of the electronic setting the pressure should be known to a few thousandths of a millibar for a 20 cm etalon. The difficulty of measuring the pressure so accurately is avoided if the length of the shorter etalon is measured in terms of the standard wavelength simultaneously with the white light comparison, for then the pressure needs to be known only with the accuracy, to about 1 mb, needed to obtain the integral part of the order of interference in the short etalon; it is supposed that the optical length as a function of air pressure has been found in preliminary measurements.

The apparatus for such a simultaneous comparison is shown schematically in figure 4. It is very similar to a spectrometer for the simultaneous comparison of wavelengths that we are developing (Cook 1959).

A white light source illuminates both etalons while a source of a standard monochromatic radiation (from ^{198}Hg) illuminates the shorter etalon by means of a semi-reflecting mirror. The rotating shutter referred to above obscures the sources alternately. When the axis of the telescope is parallel to that of the short etalon, the centre of the monochromatic Haidinger ring system formed by that etalon coincides with the pinhole and as the air pressure is changed the photomultiplier current varies with the intensity at the centre of the pattern, so enabling the order of interference at a given pressure in the short etalon to be determined.

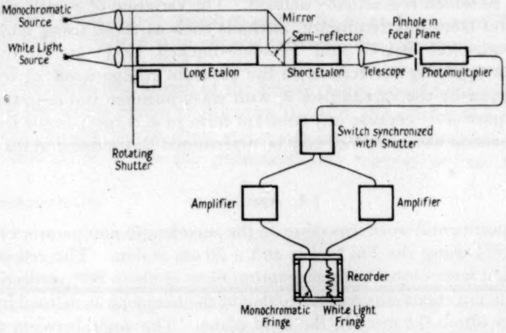
Monochromatic Source
Mirror
Pinhole in Focal Plane
Semi-reflector
White Light Source
Long Etalon
Short Etalon
Telescope
Photomultiplier
Switch synchronized with Shutter
Rotating Shutter
Amplifier
Amplifier
Recorder
Monochromatic Fringe
White Light Fringe

Figure 4. Block diagram of apparatus for simultaneous observation of white light and monochromatic fringes.

The output of the photomultiplier is connected alternately to two amplifiers by a switch synchronized with the shutter obscuring the sources so that the output of one amplifier is proportional to the intensity of the white light and that of the other to the intensity of the monochromatic light. The two outputs are recorded simultaneously with a potentiometric recorder and then, if the air pressure changes at a steady rate, a record such as that shown in figure 5 (Plate) is obtained. From it the order of interference in monochromatic light corresponding to the central white light fringe may be measured without needing to know the air pressure very precisely.

Because of the characteristics of the recorder, the record shown in figure 5 took about three-quarters of an hour to obtain and as there appeared to be a slow leak in the pressure system, the horizontal scale is not strictly proportional to pressure. A complete record is not necessary for a measurement of the long etalon and in practice the air pressure would be adjusted by hand to obtain in quick succession the setting for the central white fringe and the monochromatic fringes on either side of it, the changes in pressure being read from a scale on the piston.

§ 5. STUDY OF FOURIER TRANSFORMS

With the preliminary apparatus just described there were three difficulties in obtaining reliable records of intensity as a function of path difference. There was a small leak in the pressure system leading to a non-uniform change of path differencewith time and therefore to an artificially asymmetrical record as obtained on a recorder with a constant paper speed. This is an instance of what could be a very serious error since any such artificial asymmetry would give rise to spurious calculated phase shifts. To attempt to eliminate this error, records were taken in pairs, one with pressure increasing and the other with pressure decreasing. The second difficulty was that random fluctuations were quite appreciable (see figure 5) and to reduce their effect a mean record was derived from three pairs of records with increasing and decreasing pressure—that is, from six records in all. The third difficulty was that appreciable drifts in the lamp output and the amplifiers sometimes occurred, for which allowance had to be made. It was assumed that such drifts were linear and were defined by the recorded values at great path differences where the systematic fluctuations in intensity were less than the noise level. In the spectrometer we are constructing, drifts of this sort are avoided by recording the ratio of the light transmitted by the interferometer to that incident on it.

The mean of six records corrected for drift is analysed in figure 6 into two parts, the mean curve for corresponding positive and negative path differences (measured from the central maximum) and the curve of the difference between values for corresponding positive and negative path differences. The difference curve would be zero for a symmetrical variation of intensity with respect to path difference. The cosine and sine Fourier transforms were computed from the mean and difference curves for a few wave numbers and the derived values of I_ν and of the displacements corresponding to θ_ν are shown in figure 7. The integrations were extended over the range of measurable variation of I, about eight to ten periods.

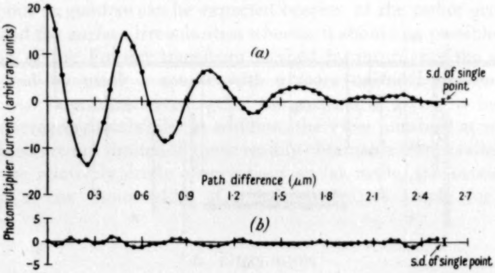

Figure 6. Mean of six records corrected for drift. (*a*) Mean of values for positive and negative path differences; (*b*) difference between values for positive and negative path differences.

The maximum of the intensity curve is displaced towards the red as compared with the stated response of the photocathode to tungsten light; this is because the lamp was under-run so that the photomultiplier current should be comparable with that from the monochromatic source.

Before discussing the values of the phase shifts we estimate the uncertainties of the Fourier transforms. Let the variance of a value of $I - I_m$ be σ^2. Then the variance of the cosine transform is

$$\frac{\sigma^2}{\pi^2} \int \cos^2 2\pi\nu\delta \, d\delta = \frac{N\sigma^2}{2\pi^2}$$

where N is the number of periods of $2\pi\nu\delta$ over which the integration extends. The variance of the sine transform is the same. In practice the variances will be slightly greater because I is measured only at discrete points.

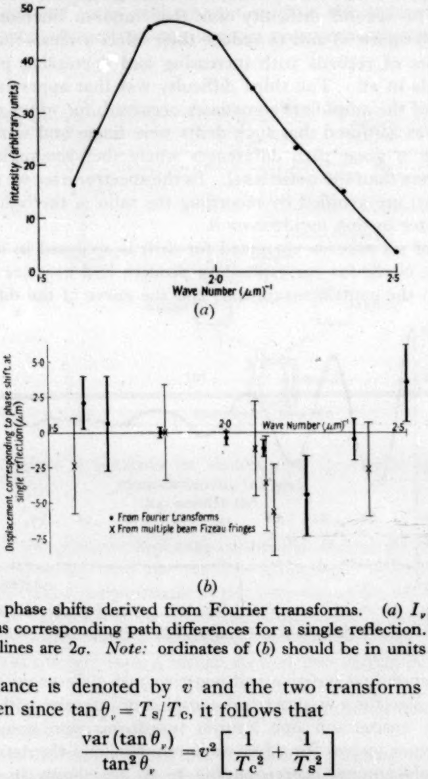

Figure 7. I_ν and phase shifts derived from Fourier transforms. (*a*) I_ν; (*b*) phase shifts expressed as corresponding path differences for a single reflection. Overall lengths of vertical lines are 2σ. *Note:* ordinates of (*b*) should be in units of mµm not µm.

If each variance is denoted by v and the two transforms by T_c and T_s respectively, then since $\tan\theta_\nu = T_s/T_c$, it follows that

$$\frac{\operatorname{var}(\tan\theta_\nu)}{\tan^2\theta_\nu} = v^2\left[\frac{1}{T_c{}^2} + \frac{1}{T_s{}^2}\right]$$

(the covariance of the two transforms is zero) and hence that

$$\operatorname{var}\theta_\nu = \frac{v^2}{4}\sin^2 2\theta_\nu\left[\frac{1}{T_c{}^2} + \frac{1}{T_s{}^2}\right]$$

From the scatter of the means of the three pairs of records used σ^2 is estimated to be 0·30 in the arbitrary units employed. The corresponding standard deviations are indicated in figure 6. This estimate may be inflated by systematic differences between the records taken with increasing and decreasing pressure. The standard deviations of θ_ν calculated from the formula above are indicated in figure 7 (*b*).

Values of the relative phase shifts for the plates of the 20 cm etalon have also been obtained from measurements on the multiple-beam Fizeau fringes produced when the plates are separated by about 20 μm. The zero value was taken to be that for the ^{198}Hg-green line ($\lambda = 5461$ Å). The results are shown in figure 7 (*b*). The computation of the results is complicated by the fact that the departures of the surfaces of the plates from true planes are greater than the displacements corresponding to the phase shifts and the estimates of the latter and of their uncertainties are therefore affected to some extent by the form assumed for the separation of the surfaces. The values shown in figure 7 (*b*) were calculated on the assumption that the separation of the plates as a function of distance measured perpendicular to the fringes is represented by two straight lines. The variation of phase shift with wave number does not however seem to depend critically on the assumption made and may be rather better established than the calculated standard deviations indicated. The uncertainties of the observations are determined largely by the errors of the form of the surfaces and by the fact that the widths of the fringes exceed one-twentieth of an order on account of the relatively low reflectivities of the surfaces—80 to 85%.

The variations of phase shift with wave number as given by the two methods agree better than would be expected from the uncertainties of either. It is clear, nonetheless, that the Fourier transform method is capable of much greater precision than the multiple beam Fizeau fringe method. The results with the latter are about as good as can be expected because of the rather great width of the fringes and the surface irregularities whereas it should be possible to increase the precision of the Fourier transform method by improving the air pressure equipment and by using a source with a more uniform emission over the waveband. An important advantage of the method is that it is insensitive to local surface irregularities while, in addition, the wave numbers at which values can be obtained are not limited to those readily obtainable from available sources. Even with the relatively crude observations so far made, the precision, corresponding to a few thousandths of a micrometre, is ample for almost all applications.

§ 6. DISCUSSION

It has been emphasized more than once that the air pressure and electronic equipment used in these experiments was relatively crude and it was in no sense designed for continuous reliable operation. The comparison of white light and monochromatic fringes will be much easier if the differential of the monochromatic fringes is recorded so that the positions of the maxima of the latter are obtained from the zeros of the differential; these can be determined much more accurately than the maxima of intensity. We have tried out the equipment for this; the principle is that the air pressure is driven into oscillations with a very small amplitude at a frequency of about 40 c/s. Then the mean photomultiplier current is proportional as before to the intensity of the light transmitted by the etalon whereas the oscillating part of the photomultiplier current is proportional to rate of change of intensity with respect to air pressure, that is, with respect to path difference. With this system the positions of maximum intensity can be obtained to a few thousandths of an order.

The accuracy with which the monochromatic order corresponding to the central white fringe can be estimated depends on the accuracy of setting on the monochromatic fringes since the white light fringes are so much sharper. There should usually be no difficulty in setting to a few thousandths of an order in about 400 000 orders, corresponding to 1 in 10^8 or better of the lengths of the etalons. It has already been shown that corrections for phase shifts can be made with uncertainties of a few thousandths of a micrometre, say to 1 in 10^8 on 20 cm, and that relative phase shifts for semi-reflecting surfaces can be measured more accurately than by other interferometric methods.

ACKNOWLEDGMENT

This work forms part of the research programme of the National Physical Laboratory and this paper is published by permission of the Director of the Laboratory.

REFERENCES

BARRELL, H., and TEASDALE-BUCKELL, P., 1951, *Proc. Phys. Soc.* B, **64**, 413.
CABRERA, N., and TERRIEN, J., 1941, *Rev. Opt. (théor. instrum.)*, **20**, 35.
COOK, A. H., 1959, *Proc. Int. Symposium on Optics in Metrology* (London: Pergamon Press) in the press.
SEARS, J. E., and BARRELL, H., 1932, *Phil. Trans. Roy. Soc.* A, **231**, 75.
SCHUSTER, A., 1924, *Phil. Mag.*, **48**, 609.

RESEARCH NOTES

The Optical Properties of Noble Metals

By M. SUFFCZYNSKI†
Department of Mathematics, Imperial College, London

Communicated by H. Jones; MS. received 22nd December 1958

In recent years numerous results of the experiments on the optical properties of metals have been published (see for instance the review articles by Givens 1958, Schulz 1957, Ginsburg and Motulevich 1955). These new data justify a further analysis of the theory of the optical properties of these metals.

In the region between wavelengths $10\,\mu$ to $1\,\mu$ the Drude theory predicts the optical constants with some success. In this region the real part of the dielectric constant agrees reasonably well with the values deduced from experimental data, but the absorption coefficient is always too small. For wavelengths between $1\,\mu$ and $0{\cdot}1\,\mu$ photoelectric absorption sets in, and it is in this region that the optical constants may be expected to depend most strongly on the band structure of the metal. The highest occupied valence band and the next higher unoccupied bands play the predominant role in this connection.

The theory of photoelectric interband absorption, as related to the band structure of a solid, was first put forward by Kronig (1929, 1931), and later by Wilson (1935) and others. It has been developed by Sergeiev and Tchernikovsky (1934), by Fan (1945), and by Butcher (1951) and has been applied with success to the alkali metals. The necessary assumptions about the band structures were made on the basis of the nearly free electron approximation. It is the intention here to propose the corresponding theory for the optical constants of the noble metals. Again the nearly free electron approximation was found helpful but emphasis has been laid on the bending of energy surfaces near the boundary of the Brillouin zone, since in the noble metals, because of their face-centred cubic structure, the Fermi surface may well touch the boundary or approach it closely. As is well known the bending of energy surfaces near the Brillouin zone boundary results in a pronounced modification of the dielectric constant and the absorption coefficient (Wilson 1935), and also of other properties depending on the density of states such as the thermoelectric power (Jones 1955) and the magnetic susceptibility (Blatt 1958, preprint). The simple model proposed here is intended to enable a study to be made of details of the optical properties in a more quantitative way. The need for such a study emerges in connection with several recent papers (see Pippard 1957, Cohen 1958).

A two-band model has been considered; the energy surfaces for the two energy bands, lower (−) and upper (+) have been taken in the form

$$E_{\pm}(k_x, k_y, k_z) = \frac{\hbar^2}{2m}\,[k_x^2 + k_y^2 + (k_0 - k_z)^2 + k_0^2 \pm 2k_0\{(k_0 - k_z)^2 + V^2\}^{1/2}].$$

Here k_x, k_y, k_z are the components of the wave vector with the z axis taken along ΓL line which is the line from the origin to the centre of a hexagonal face of the Brillouin zone. The distance ΓL in the reciprocal space is denoted by k_0. The constant V is proportional to the energy gap at the point L.

---

† On leave of absence from the Institute of Theoretical Physics of Warsaw University.

The surface containing the occupied states is given by the equation $E_- = E_F$, where the constant E_F is the Fermi energy. The matrix elements for the transitions between occupied and unoccupied states have been assumed constant. With these assumptions the necessary summations, as indicated for example by Wilson (1935), can be carried out analytically. The resulting dielectric constant and electrical conductivity have been added to the respective Drude coefficients, and the extinction coefficient $k(\lambda)$ has been calculated. The curves for copper

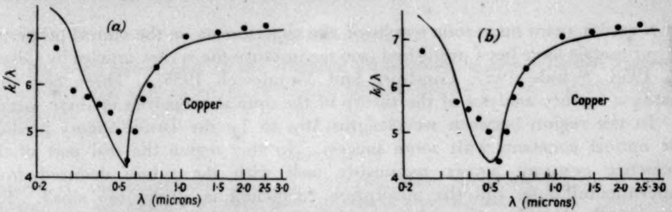

Figure 1. Graph showing k/λ values for copper as a function of wavelength λ. The circles are the experimental points of Schulz. The curve is computed with the Fermi surface having distance from the L point : (*a*) $h=0$, (*b*) $h=0{\cdot}05k_0$.

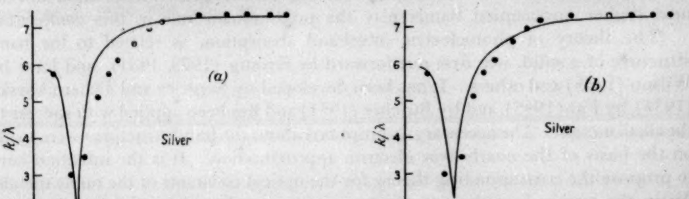

Figure 2. Graph showing k/λ values for silver as a function of wavelength λ. The circles are the experimental points of Schulz. The curve is computed with the Fermi surface having distance from the L point : (*a*) $h=0$, (*b*) $h=0{\cdot}05k_0$.

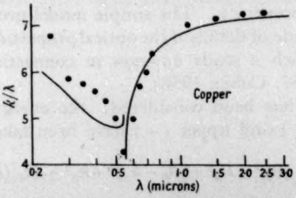

Figure 3. Graph showing k/λ values for copper as a function of wavelengh λ. The circles are the experimental points of Schulz. The curve is computed with the Fermi surface having an area of contact with the hexagonal face of the Brillouin zone boundary $A=0{\cdot}0036\pi k_0^2$.

and silver have been compared with the recent experimental data of Schulz (1957), see figures 1 and 2, where the quantity k/λ is plotted against the wavelength λ.

The calculated dielectric constant and the absorption coefficient are finite for the Fermi surfaces inside the Brillouin zone. They exhibit infinities in the present model if the Fermi surface has a finite area of contact with the Brillouin zone boundary. An example of such a situation as calculated with an area of contact $A=0{\cdot}0036\pi k_0^2$ is presented in figure 3.

The infinity of the dielectric constant and the absorption coefficient is removed, when the transverse effective masses in the lower and upper bands, m_- and m_+, are unequal. The curve of k/λ against λ, however, still shows a sharp peak but this is now of finite magnitude. The magnitude of the peak in the absorption coefficient at the absorption edge is proportional to $(1/m_+ - 1/m_-)^{-1/2}$, when $m_- > m_+ > 0$. The respective expressions for the optical constants are very lengthy. They may be of importance if the optical absorption in the noble metals is related to some excitation of the filled d-band (see Friedel 1952).

When the Fermi surface lies further away inwards from the zone boundary, the peak in the curve of the dielectric constant becomes smaller in absolute value and so it becomes difficult to account for the whole dip observed in the curve of the extinction coefficient. Also to produce the dip at the wavelength given by experiment it is necessary to assume a correspondingly smaller value for V, since the frequency at which the extinction coefficient curve is a minimum is determined by the energy gap between the lower and upper energy band at the highest filled state. This frequency is given exactly by the energy gap at the point L, when the Fermi surface just touches the Brillouin zone boundary, and is larger than this gap, when the Fermi surface is inside the Brillouin zone. Only 'vertical' optical transitions are considered here.

The width of the minimum in the dispersion curve is determined mainly by the spread of the energy bands involved. For copper, where the ratio of the energy gap (taken as 2·25 ev) to the free electron energy at the point L (8·67 ev) is small, the dip in the computed curve is broad, too broad in fact. For silver, where this ratio has been taken as 3·81/6·76 it is too narrow.

If in the present model the constant matrix element for the transitions between occupied and unoccupied states is replaced by one which varies in k-space, the width of the dip in the k/λ curve changes. If the absolute value of the matrix element is diminishing away from the Brillouin zone boundary toward the centre of the zone, the resulting minimum in the k/λ curve becomes narrower.

Starting from an analysis of experimentally determined optical constants it seems rather difficult to make a definite statement about the touching of the Brillouin zone boundary. One conclusion which can certainly be drawn from the present investigation is that it is exceedingly important to take the energy gap and the consequent bending of energy surfaces into account. The dip in the k/λ curve can be simple related to the increasing density of states near the Brillouin zone boundary. The situation is somewhat similar to one in the superconductor where the energy gap exists in the microwave region of frequencies (see in connection with this problem Mattis and Bardeen 1958 and Biondi *et al.* 1958). The effectively observed extinction coefficient depends very sensitively on the dielectric constant for wavelengths in the vicinity of the threshold for interband absorption.

Acknowledgments

The author wishes to thank Professor H. Jones for suggesting this investigation and for many valuable discussions, and also for his kind hospitality extended to the author at Imperial College. The grant from the Polish Academy of Science was held when this work was being made.

References

Biondi, M. A., Forrester, A. T., Garfunkel, M. P., and Satterthwaite, C. B., 1958, *Rev. Mod. Phys.*, **30**, 1109.
Butcher, P. N., 1951, *Proc. Phys. Soc.* A, **64**, 765.
Cohen, M. H., 1958, *Phil. Mag.*, **3**, 762
Fan, H. Y., 1945, *Phys. Rev.*, **68**, 43.
Friedel, J., 1952, *Proc. Phys. Soc.* B, **65**, 769.
Ginsburg, V. L., and Motulevich, G. P., 1955, *Adv. Phys. Sci., Moscow*, **55**, 469.
Givens, M. P., 1958, *Solid State Physics*, **6**, 313.
Jones, H., 1955, *Proc. Phys. Soc.* A, **68**, 1191.
Kronig, L., 1929, *Proc. Roy. Soc.* A, **124**, 409.
—— 1931, *Ibid.*, **133**, 255.
Mattis, D. C., and Bardeen, J., 1958, *Phys. Rev.*, **111**, 412.
Pippard, A. B., 1957, *Phil. Trans. Roy. Soc.* A, **250**, 325.
Schulz, L. G., 1957, *Advanc. Phys.*, **6**, 102.
Sergeiev, M. I., and Tchernikovsky, M. G., **1934**, *Phys. Z. Sowjet*, **5**, **106**.
Wilson, A. H., 1935, *Proc. Roy. Soc.* A, **151**, 274.

The Influence of Arsenic Content in Copper Crystals on Easy Glide at −183° C

By K. SCHRÖDER†

Division of Tribophysics, Commonwealth Scientific and Industrial Research Organization, University of Melbourne, Australia

MS. received 16*th December* 1958

Recent investigations (Rosi 1954, Garstone, Honeycombe and Greetham 1956) have shown that the addition to a pure metal of a soluble impurity increases the range of easy glide observed in tensile tests of single crystals. The purpose of this note is to report some experiments which confirm and extend these results and to advance further suggestions with respect to their interpretation.

Crystals approximately 2 mm in diameter and 30–40 mm long were prepared in graphite moulds by induction heating *in vacuo*. The materials used were as follows:

Batch	Material
A	Spectroscopically pure copper
B	O.F.H.C. Copper
C	O.F.H.C. Copper + 0·032% As
D	,, ,, 0·084% As
E	,, ,, 0·76 % As
F	,, ,, 1·72 % As

---

† Now at Department of Mining and Metallurgical Engineering, University of Illinois, Urbana, Ill., U.S.A.

The arsenic contents were calculated from measurements of electrical resistivity. Loops were silver soldered to the ends of the crystals which were then etched with concentrated nitric acid before straining in a Polanyi type testing machine described elsewhere (Schröder 1958). All specimens were immersed in liquid oxygen during testing and the strain rate was chosen to give an initial rate of shear strain of 4×10^{-5} sec^{-1}.

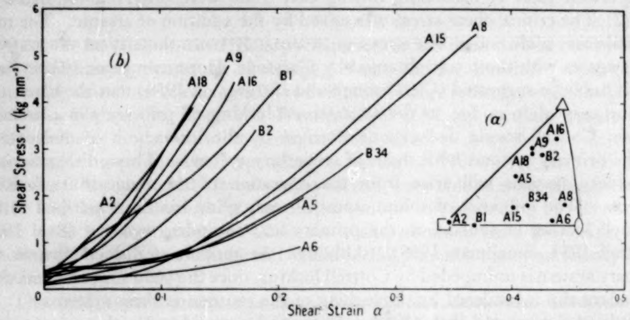

Figure 1. (*a*) Orientations of crystals of batches A and B. (*b*) (Shear stress, shear strain) curves for crystals of batches A and B.

The (shear stress, shear strain) curves for crystals of batches A and B are shown in figure 1, together with the orientation of the crystals. There is no marked difference in the behaviour of these two batches and the variation with orientation is as is usually observed, namely, easy glide is greatest for orientations near, but not at, [110] and decreases as [100], [111] or the [100]–[111] boundary is approached. For batches C, D and E, the variation with orientation was also of this nature.

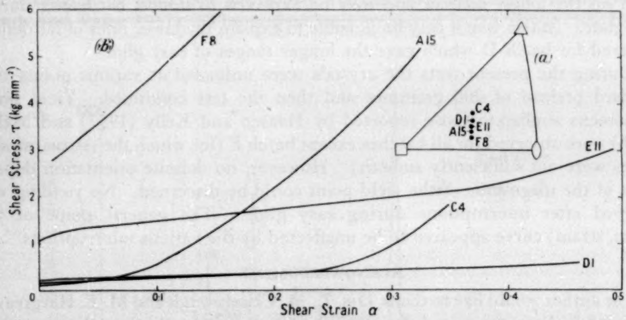

Figure 2. (*a*) Orientations of crystals of various batches. The letter preceding the number indicates the batch to which each crystal belongs. (*b*) (Shear stress, shear strain) curves for these crystals of various compositions but similar orientations.

However, the following new features appeared in the curves for the batches of crystals with arsenic added.

(1) The extent of easy glide was greater for batch C (compared with batches A and B), still greater for batch D, and diminished only slightly for batch E, compared with batch D. For batch F the rate of hardening was so great that only a small strain could be given and it was not possible to decide whether easy glide was present. A comparison of the (shear stress, shear strain) curves for crystals of similar orientation but different compositions is given in figure 2. The lowest rates of hardening during easy glide were observed for batch D.

(2) The critical shear stress was raised by the addition of arsenic. For most crystals easy glide ended at a stress approximately twice the critical shear stress. This agrees with the result obtained by Garstone, Honeycombe and Greetham.

It has been suggested (Clarebrough and Hargreaves 1959) that the hardening during easy glide is due to the successive blocking of primary slip planes by Lomer–Cottrell sessile dislocations, formed by the interaction of dislocations of the primary systems with those of secondary systems. These dislocations of secondary systems will arise from the operation of the longest Frank–Read sources. The influence of solute atoms on easy glide has been ascribed to the Cottrell locking of sources on the primary and secondary systems (Rosi 1954, Cottrell 1954, Smallman 1955). Although the motion of dislocations on the primary system is unimpeded by Cottrell locking, once the yield stress is exceeded, secondary slip is hindered by the locking of the sources on these systems.

It is now suggested that a further factor to be considered with respect to the locking of these secondary sources is the relation of the locking force to the length of the source. Since the stress to operate a source is inversely proportional to its length and the stress to move a dislocation from an atmosphere is independent of its length, the presence of an atmosphere has relatively greater effect on the longer sources and may be expected to inhibit hardening during easy glide. In this way it may be possible to explain the lower rates of hardening observed for batch D which gave the longer ranges of easy glide.

During the present tests the crystals were unloaded at various points to a standard preload of 200 grammes and then the test continued. Yield point phenomena similar to those reported by Haasen and Kelly (1957) and Makin (1958) were observed for all batches except batch F (for which the (stress, strain) curves were not sufficiently smooth). However, no definite orientation dependence of the magnitude of the yield point could be discerned. No yielding was observed after interruptions during easy glide. The general shape of the (stress, strain) curve appeared to be unaffected by the various interruptions.

ACKNOWLEDGMENT

The author would like to thank Drs. L. M. Clarebrough and M. E. Hargreaves for helpful discussions and for their assistance in preparing this note for publication.

REFERENCES

CLAREBROUGH, L. M., and HARGREAVES, M. E., 1959, *Progress in Metal Physics*, **8**, in the press.

COTTRELL, A. H., 1954, *Relation of Properties to Microstructure* (American Society for Metals), p. 131.

GARSTONE, J., HONEYCOMBE, R. W. K., and GREETHAM, G., 1956, *Acta Met.*, **4**, 485.

HAASEN, P., and KELLY, A., 1957, *Acta Met.*, **5**, 192.

MAKIN, M. J., 1958, *Phil. Mag.*, **3**, 281.

ROSI, F. D., 1954, *Trans. Amer. Inst. Min. (Metall.) Engrs*, **200**, 1009.

SCHRÖDER, K., 1958, *Proc. Phys. Soc.*, **72**, 33.

SMALLMAN, R. E., 1955, *J. Inst. Met.*, **84**, 10.

The ^{39}K(d, p)^{40}K Reaction

By A. W. DALTON, G. PARRY AND H. D. SCOTT
Nuclear Physics Research Laboratory, University of Liverpool

Communicated by H. W. B. Skinner; *MS. received 9th December* 1958

§ 1. INTRODUCTION

PREVIOUS work on the ^{39}K(d, p)^{40}K reaction has been carried out by Sailor (1950) using deuterons of energy 3·9 MeV and by Buechner *et al.* (1953) using deuterons of energy 4·76 to 5·65 MeV. More recently, while the present work was in progress, Enge and Weaner (1957 a, b) reported the results of a comprehensive high resolution study of this reaction using 6·0 MeV deuterons and measuring protons corresponding to levels of ^{40}K with excitations up to 4·9 MeV. They identified fifty-seven levels and were able to make measurements of the angular distributions of the proton groups corresponding to forty-two of these levels. Information on ^{40}K levels is also obtained from the ^{39}K(n, γ)^{40}K reaction (Kinsey, Bartholomew and Walker 1952, Bartholomew and Kinsey 1953, Adyasevich *et al.* 1956).

The work reported here was done using 8·9 MeV deuterons. Protons were investigated from levels up to an excitation of 5·34 MeV and angular distribution measurements were made on a number of groups.

§ 2. PROCEDURE AND RESULTS

The protons from the potassium target were magnetically analysed using the arrangement described previously (Green and Middleton 1956, Dalton, Hinds and Parry 1957). The targets were prepared in the target chamber by

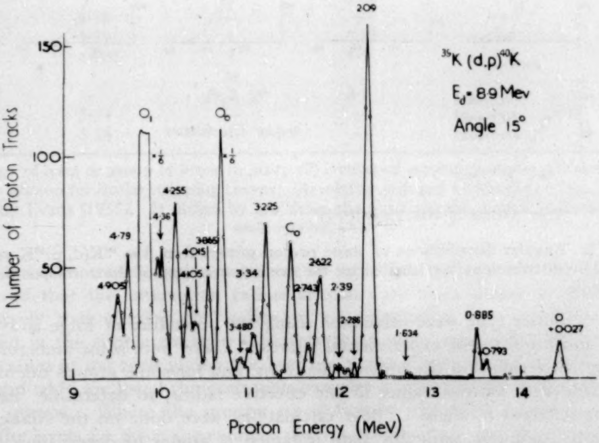

Figure 1. Energy spectrum of protons emitted at 15° from a target of potassium bombarded by 8·9 MeV deuterons.

evaporation of potassium metal on to a thin gold foil. For small angles of observation the nuclear plates were covered with aluminium foil to cut out deuterons coming from the target.

A typical proton energy spectrum obtained at an angle of 15° is shown in figure 1. The groups labelled O_0, O_1 and C_0 are due to oxygen and carbon impurities in the target. Identification of the groups from potassium was made using the known energy calibration of the spectrograph, and by comparison with the results of Enge and Weaner. These groups are labelled with the excitation energy in MeV of the final state. Angular distributions were obtained for a number of the groups and these are shown in figure 2. Theoretical stripping curves of Butler type were calculated using the procedure of Enge and Graue (1955) and fitted to the experimental curves. There were some ambiguities in deciding the *l*-values of the ingoing neutrons, and for some groups calculations were made with various values of the effective radius, to determine 'best-fit' radii for different *l*-values. These calculations were done on the Manchester University computer using the data obtained at angles of observation within about 20° of the experimental peak. The use of a computer permitted a thorough search for the best radius. The significance of varying the radius to improve

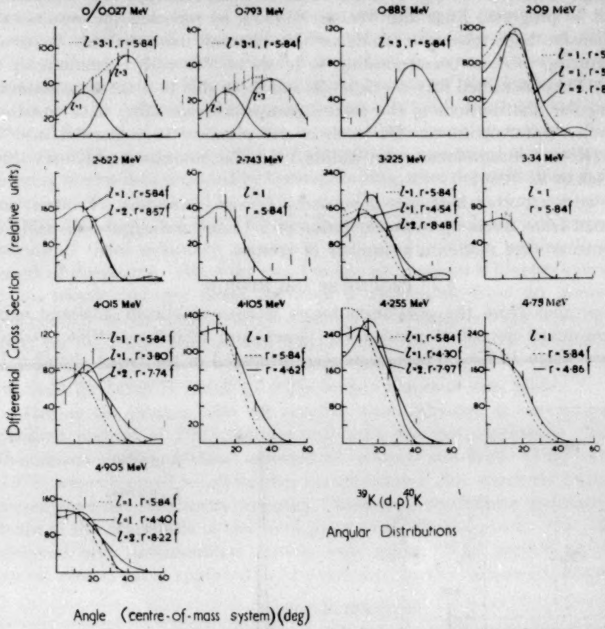

Figure 2. Angular distributions of some proton groups from the ^{39}K(d, p)^{40}K reaction. The distributions are labelled by the excitation energy of the corresponding final state.

(1)	(2)	(3)	(4)
0/0·027	3	5·84	22
	+		
	1	5·84	1·7
0·793	3	5·84	7·0
	+		
	1	5·84	0·9
0·885	3	5·84	17
1·634	—	—	—
2·09	1	5·00	22
	or		
	2	8·80	22
2·286	—	—	—
2·39	—	—	—
2·569	—	—	—
2·622	1	5·84	3·8
	or		
	2	8·57	2·7
2·664	—	—	—
2·743	1	5·84	0·9
3·225	1	4·54	6·7
	or		
	2	8·50	3·4
3·34	1	5·84	1·3
3·626	—	—	—
3·865	—	—	—
4·015	1	3·80	4·5
	or		
	2	7·74	1·8
4·105	1	4·62	4·1
4·255	1	4·30	10
	or		
	2	8·00	4·9
4·36	—	—	—
4·79	1	4·85	4·4
4·905	1	4·4	4·0
	or		
	2	8·2	1·9
5·14	—	—	—
5·34	—	—	—

(1) Energy of level or group of levels in MEV; (2) l-value of ingoing neutron; (3) radius, R, in fermis chosen for Butler stripping curves; (4) relative reduced widths $(2J_f+1)\gamma$. γ is as defined by Evans (1955). It differs by $1/R$ from the more usually quoted reduced width with symbol γ^2.

the fit between theory and experiment is not obvious however. It may be considered that the interaction radius should vary from group to group, or alternatively that altering the radius in a computation can simulate effects neglected in the simple theory. Certainly there were appreciable fluctuations in the values of the radii giving the best fits to the experimental curves.

In the table are listed the excitation energies corresponding to the observed proton groups. Where the groups are definitely identified as due to single levels, the levels are given the energies determined by Enge and Weaner to three decimal places. Where the groups are composite they are given the energy deduced from our spectrograph calibration with an accuracy to 40 kev. A number of the groups were weak and angular distributions could not be obtained. Some of the weak groups were identified using spectra obtained at angles other than 15°.

The ground state of ^{40}K has $J=4$ (Ramsey 1953) and together with the states at 27, 793 and 885 kev is considered to form a quadruplet with spins and parities 4^-, 3^-, 2^- and 5^- (Endt and Kluyver 1954). The quadruplet results from the coupling of a $f_{7/2}$ neutron with a $d_{3/2}$ proton hole, so that the angular distributions for groups corresponding to these levels should have $l=3$. We cannot resolve the groups to the ground and 27 kev states and their combined distribution appears to be a distorted $l=3$ distribution in which the yields at forward angles are considerably bigger than theory predicts. A similar effect occurs for the group corresponding to the 793 kev level. These distorted experimental distributions are in agreement with the results of Enge and Weaner for a sum of their distributions corresponding to the 0 and 27 kev levels, and for that corresponding to the 793 kev level. The distortion at forward angles can be accounted for by a small $l=1$ contribution as shown in figure 2. The selection rules for the transitions to the 27 kev and 793 kev levels would allow $l=1$ transitions, but for these transitions to be possible on the shell model it is necessary for these states to contain some 2p configuration. In this connection it is interesting to see that in the work on the ^{39}K(n, γ)^{40}K reaction, strong gamma rays are observed to the levels at 0·027 and 0·793 Mev. The capturing state has spin and parity 2^+ or 1^+ and these gamma rays are probably E1 radiation.

The angular distributions corresponding to subsequent levels or groups of levels are rather ambiguous in their interpretation with a possible choice between $l=1$ and $l=2$. Enge and Weaner in their work with $E_d=6{\cdot}0$ Mev, reported that the majority of their angular distributions corresponded to $l=1$ transitions. In the work here with 8·9 Mev deuterons, if calculations are made using the Gamow–Critchfield (1949) radius of 5·84 fermis, the experimental peak often lies between the peaks of the theoretical $l=1$ and $l=2$ curves. By reducing the radius the $l=1$ curve can be made to fit at the peak and higher angles, but then there is a pronounced dip at forward angles of the experimental points below the theoretical curve. If the radius is increased, sometimes by as much as 3 fermis, then the $l=2$ curve gives a reasonable fit to most of the experimental points. The assignment of $l=1$ or $l=2$ would seem to depend on what is thought to be the more reasonable value for the radius. For the groups in question bias possibly exists towards a choice of $l=1$, since the radii for these curves are closer to the Gamow–Critchfield radius, which has already been used in obtaining reasonable fits for angular distributions of protons corresponding to the lower levels. If the transitions do correspond to $l=1$ for the ingoing neutron, there are considerably more than the six expected to the $p_{3/2}$ and $p_{1/2}$ states.

A group in our spectrum marked 3·34 Mev probably corresponds to a combination of groups found by Enge and Weaner from transitions to levels at 3·365 ($l=1$) and 3·412 ($l=0$). In the angular distribution of the composite group we observe no strong signs of an $l=0$ transition.

There are no signs of strong $l=3$ transitions which could correspond to the ingoing neutron entering $f_{5/2}$ states.

ACKNOWLEDGMENTS

We wish to thank Mr. A. Kirk for programming the Mk. 1 computer of Manchester University and Dr. H. C. Newns for helpful discussions.

References

Adyasevich, B. P., Groshev, L. V., Demidov, A. M., and Lutsenko, V. N., 1956, *Atomnaja Energ.*, **2,** 28.
Bartholomew, G. A., and Kinsey, B. B., 1953, *Canad. J. Phys.*, **31,** 927.
Buechner, W. W., Sperduto, A., Browne, C. P., and Bockelman, C. K., 1953, *Phys. Rev.*, **91,** 1502.
Dalton, A. W., Hinds, S., and Parry, G., 1957, *Proc. Phys. Soc.* A, **70,** 586.
Endt, P. M., and Kluyver, J. C., 1954, *Rev. Mod. Phys.*, **26,** 95.
Enge, H. A., and Graue, A., 1955, *Univ. Bergen Årb. Naturv. R.*, Nr. 13.
Enge, H. A., and Weaner, D. H., 1957 a, *Bull. Amer. Phys. Soc.*, **2,** 179.
—— 1957 b, Massachusetts Institute of Technology, Annual Progress Report of Laboratory for Nuclear Science, May, 1957.
Evans, R. D., 1955, *The Atomic Nucleus* (New York: McGraw-Hill), p. 401.
Gamow, G., and Critchfield, C. L., 1949, *Theory of the Atomic Nucleus* (Oxford: University Press), p. 11.
Green, T. S., and Middleton, R., 1956, *Proc. Phys. Soc.* A, **69,** 16.
Kinsey, B. B., Bartholomew, G. A., and Walker, W. H., 1952, *Phys. Rev.*, **85,** 1012.
Ramsey, N. F., 1953, *Nuclear Moments* (New York: John Wiley).
Sailor, V. L., 1950, *Phys. Rev.*, **77,** 794.

The Description of the Ejected Electron in K-shell Ionization

By A. M. ARTHURS

Department of Applied Mathematics, The Queen's University of Belfast

Communicated by D. R. Bates; MS. received 22nd November 1958

§ 1. Introduction

Recently Merzbacher and Lewis (1958) reviewed the treatment of K-shell ionization of atoms on the basis of the Born approximation. They emphasized the importance of the screening effect of the outer electrons which causes the actual K-shell ionization potential to be somewhat less than the approximate value corresponding to the hydrogenic model adopted in the theoretical work. The actual, rather than the approximate, ionization potential has been taken in all calculations, but there are two quite different methods of describing the ejected electron. One, due to Bethe (cf. Henneberg 1933), has been used in the treatment of nuclear impacts (Walske 1952), while the other, due to Stobbe (1930) and to Massey and Mohr (1933) has been used in the treatment of photon and electron impacts. This division of the fields of application has no special significance but seems rather to have arisen by chance. The principal aim in both methods is simply to ensure that the threshold of the calculated cross section–energy curve coincides with the threshold of the corresponding observed curve. A quantitative comparison of the two methods has not been made.

§ 2. Theory

2.1. *Total Cross Section*

The cross section for K-shell ionization by particles of mass M, charge Z_1, energy E and momentum $\hbar\mathbf{k}_1{}^0$ is given in the non-relativistic Born approximation by†

$$Q_1 = \frac{Z_1{}^2 M^2}{Z_e{}^2 k_1{}^{02}} \mathcal{S} \pi a_0{}^2, \qquad \ldots\ldots(1)$$

---

† All quantities are in atomic units.

where
$$\mathscr{S}=8Z_e^2\int_{k^2_{\min}}^{k^2_{\max}}\int_{q_{\min}}^{q_{\max}}|\epsilon_{\mathbf{k}}(\mathbf{q})|^2q^{-3}k\,dq\,dk^2, \qquad \ldots\ldots(2)$$

$$\epsilon_{\mathbf{k}}=\frac{1}{k}\int\exp(i\mathbf{q}.\mathbf{r})\bar{\psi}_{\mathbf{k}}(\mathbf{r})\psi_0(\mathbf{r})\,d\mathbf{r}, \qquad \ldots\ldots(3)$$

$$\mathbf{q}=\mathbf{k}_1{}^0-\mathbf{k}_1{}', \qquad \ldots\ldots(4)$$

in which $\hbar\mathbf{k}_1{}'$ is the momentum of the scattered particle, $\hbar\mathbf{k}$ is the momentum of the ejected electron, ψ_0 and $\psi_{\mathbf{k}}$ are the initial and final state wave functions of the atomic electron and $Z_e=Z-0{\cdot}3$ is the effective nuclear charge. Introducing the parameter

$$\eta=E/MZ_e^2\,Ryd \qquad \ldots\ldots(5)$$

we have

$$Q_1=\frac{Z_1{}^2}{Z_e{}^4}\frac{1}{\eta}\mathscr{S}(\eta,\vartheta), \qquad \ldots\ldots(6)$$

ϑ denoting the ratio of the actual K-shell ionization energy E_0 to the fictitious ionization energy $Z_e^2/2$ which would arise in the absence of outer screening.

A low energy approximation to the Born formula for the K-shell ionization cross section has been derived by Henneberg (1933) using hydrogenic wave functions. This may be written

$$Q_2=\frac{2^{11}Z_1{}^2M^2Z_e{}^6}{k_1{}^{02}}\int_{k^2_{\min}}^{k^2_{\max}}\int_{q_{\min}}^{q_{\max}}\frac{Z_e{}^2+3q^2}{3q(Z_e{}^2+q^2)^6}\exp\left[-\frac{4Z_e{}^2}{Z_e{}^2+q^2}\right]dq\,dk^2\,\pi a_0{}^2. \qquad \ldots\ldots(7)$$

2.2. *Outer Screening*

The limits of integration in equation (2) are found from the conservation of energy equation

$$\frac{1}{2M}k_1{}^{02}-\frac{1}{2}\vartheta Z_e{}^2=\frac{1}{2M}k_1{}'^2+T, \qquad \ldots\ldots(8)$$

where T is the actual kinetic energy of the ejected electron. Thus

$$\left.\begin{aligned}q_{\min}&=k_1{}^0-[k_1{}^{02}-M(\vartheta Z_e{}^2+2T)]^{1/2},\\ q_{\max}&=k_1{}^0+[k_1{}^{02}-M(\vartheta Z_e{}^2+2T)]^{1/2},\end{aligned}\right\} \qquad \ldots\ldots(9)$$

and

$$\left.\begin{aligned}T_{\min}&=0,\\ T_{\max}&=[k_1{}^{02}-M\vartheta Z_e{}^2]/2M.\end{aligned}\right\} \qquad \ldots\ldots(10)$$

In the Bethe method one takes

$$T=\tfrac{1}{2}k^2+\tfrac{1}{2}Z_e{}^2(1-\vartheta), \qquad \ldots\ldots(11)$$

whence using (10) it is seen that

$$k_{\min}{}^2=-Z_e{}^2(1-\vartheta)\leqslant 0. \qquad \ldots\ldots(12)$$

The integration thus includes that part of the *discrete* spectrum which lies between an energy of $-\frac{1}{2}Z_e{}^2(1-\vartheta)$ and zero.

The method adopted by Stobbe and by Massey and Mohr is to take

$$T=\tfrac{1}{2}k^2, \qquad \ldots\ldots(13)$$

where k is the wave number of the continuum wave function. Thus, from (10) we have

$$k_{\min}{}^2=0. \qquad \ldots\ldots(14)$$

The region of integration in the first method has been shifted relative to that in the second by an amount $Z_e^2(1-\vartheta)$ in the $-k^2$ direction. Thus, for $\vartheta \neq 1$ the corresponding cross sections will not be identical.

The two methods, however, give cross sections which tend to the same limit in the region of low impact energies, since the integrand of Henneberg's formula (7), which may be used in this region, is independent of T and consequently the derived cross section does not depend on which choice of T is made.

§ 3. RESULTS AND DISCUSSION

Merzbacher and Lewis (1958) have presented results of calculations for nuclear impact with the Born formula (1) and the Bethe limits for values of ϑ between 0·75 and 1 and for values of η up to 2. The case with $\vartheta = 1$ had been treated before by Bates and Griffing (1953). However, no results were available of calculations for $\vartheta < 1$ and the Stobbe–Massey–Mohr limits. Such calculations were therefore carried out for $\vartheta = 0{\cdot}65$ and $\vartheta = 0{\cdot}8$ with the aid of a DEUCE computer. The figure contains the results together with the corresponding ones for the Bethe limits obtained directly, or by extrapolation, from those of Merzbacher and Lewis.

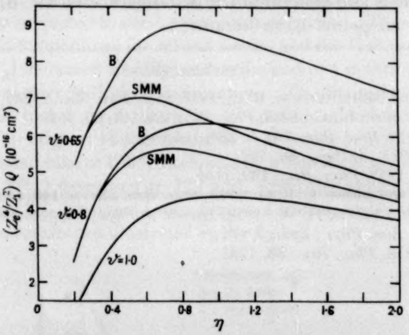

Plot of $(Z_e^4/Z_1^2)\,Q$ against η for nuclear impact. B: Bethe method; SMM: Stobbe–Massey–Mohr method.

It is seen that at moderate values of η the discrepancy between the results of the two methods for a given value of $\vartheta(<1)$ is appreciable, while at small values of η the curves come together, as expected from Henneberg's formula.

The Bethe method is the more consistent one in that the wave functions adopted actually correspond to the energies for the theoretical model. However, an integration over the discrete spectrum down to where the principal quantum number is only about 2 is involved. Quite apart from the doubt as to whether integration at such low principal quantum numbers is justified, it is clearly unsatisfactory to represent the ejected electron by a bound wave function. There is no reason to suppose that the use of this incorrect wave function compensates for the fact that the ground state wave function adopted is too compact—indeed the contrary is the case.

As mentioned earlier, the Bethe method has been used only in the study of nuclear impacts and comparison with experiment is limited to the low incident energy region near $\eta = 0{\cdot}25$, where the alternative method yields almost the same cross section.

Although no quantitative comparison of the two methods has been made for photon and electron impacts, the behaviour of the corresponding cross sections is similar to that for nuclear impact in so far as for low incident energies the cross sections are approximately equal, by Henneberg's formula, while at higher energies those obtained by the Bethe method are greater than those obtained by the Stobbe–Massey–Mohr method. Now at these higher energies, calculations using the Stobbe–Massey–Mohr method yield cross sections in close agreement with the observed cross sections for photoelectric K-shell absorption (Stobbe 1930), for the ionization of helium by electrons (Erskine 1954, Mapleton 1958), and for K-shell ionization of heavier atoms by electrons (Arthurs and Moiseiwitsch 1958). The agreement with experiment would be less good if the Bethe method were employed, suggesting that the Stobbe–Massey–Mohr method is the better one.

ACKNOWLEDGMENTS

The writer wishes to thank Professor D. R. Bates for his guidance and interest in this work. He is also grateful to Dr. A. Dalgarno and Dr. B. L. Moiseiwitsch for clarifying certain points in the literature.

REFERENCES

ARTHURS, A. M., and MOISEIWITSCH, B. L., 1958, *Proc. Roy. Soc.* A, **247,** 550.
BATES, D. R., and GRIFFING, G., 1953, *Proc. Phys. Soc.*, A, **66,** 961.
ERSKINE, G. A., 1954, *Proc. Roy. Soc.* A, **224,** 362.
HENNEBERG, W., 1933, *Z. Phys.*, **86,** 592.
MAPLETON, R. A., 1958, *Phys. Rev.*, **109,** 1166.
MASSEY, H. S. W., and MOHR, C. B. O., 1933, *Proc. Roy. Soc.* A, **140,** 613.
MERZBACHER, E., and LEWIS, H. W., 1958, *Handb. d. Phys.*, **34,** 166 (Berlin: Springer).
STOBBE, M., 1930, *Ann. Phys., Lpz.*, **7,** 661.
WALSKE, M. C., 1952, *Phys. Rev.*, **88,** 1283.

LETTERS TO THE EDITOR

Some Effects of Copper as an Impurity in Indium Arsenide

Heat treatment of InAs at temperatures above 300°c makes the material more n-type. Measurements here and at other laboratories (Dixon 1958, Dixon and Enright (Naval Ordnance Laboratory), Lee and Roberts (Plessey Research Laboratory), private communications) show that the changes can be annealed out by heating at temperatures below 200°c, and even at room temperature appreciable annealing is observed. We have obtained similar results by doping with copper.

The copper was introduced either into the melt or by diffusion from a plated surface. The final carrier concentration was dependent both on the amount of copper added and the cooling cycle which followed, but in all cases specimens with added copper showed considerably higher electron concentrations than control specimens subjected to similar temperature cycles. The doped specimens were held at room temperature for several weeks, and the Hall constant measured frequently. $|R_H|$ increased steadily, and at the end of a month only a quarter of the added carriers were still electrically active. To obtain a comparison, some undoped material had a similar number of carriers added by heat treatment. Specimens with an original Hall constant of -250 were heat treated by a 6 hour bake in a small sealed tube at 850°c, followed by a slow-cool to room temperature over 48 hours. $|R_H|$ decreased to 120 and, when the specimens were held at room temperature, $|R_H|$ increased with time in a similar way to the copper-doped specimens. The results are illustrated in the figure.

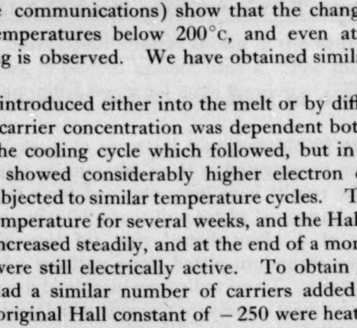

Room-temperature annealing of copper-doped and heat-treated InAs.

Dixon and Enright have suggested that the heat treatment effects are due to impurities collecting around dislocations; at temperatures above 300°c the impurities escape and may be frozen in their new position. Annealing allows them to migrate back to the dislocations. Copper diffuses rapidly through

InAs and it therefore seems possible that some of the heat treatment effects which have been observed are due to a residual copper impurity, which acts as a donor.

The author is grateful to Ann Rayner for her help in these experiments, and to the Admiralty for permission to publish.

Services Electronics Research Laboratory, C. HILSUM.
Baldock, Herts.
6th January 1959.

DIXON, J., 1958, *Bull. Amer. Phys. Soc.*, **3**, 120.

Thermal Diffusion in Methanol–Carbon Tetrachloride Mixtures

Thermal diffusion in binary liquid mixtures of methyl alcohol and carbon tetrachloride has been investigated in these laboratories using a simple parallel-plate apparatus. The results have been obtained for a temperature difference of 35°C between two horizontal plates a distance 9·0 mm apart. The apparatus consisted essentially of a 'Pentathene' ring (of internal diameter 4·1 cm) clamped between two chromium-plated brass surfaces which formed the hot and cold walls respectively. These walls were machined to a perfectly flat surface and formed part of two heat reservoirs through which water was circulated at thermostatically controlled temperatures. These temperatures were controlled to within ±0·05°C. To avoid convection effects the upper wall was maintained at the higher temperature. For the filling of the cell and withdrawal of samples for analysis, a small hole was drilled in the side of the Pentathene ring. During an experiment this hole was sealed with rubber. Small amounts of solution (about two or three drops) were withdrawn by means of a hypodermic syringe, the needle of which was inserted through the rubber seal. Samples were withdrawn, at the completion of each determination, from both hot and cold walls. The analysis of these samples was carried out using an Abbe refractometer. The disturbance of the system by sampling means that only one experimental reading can be made for each experiment.

The Soret coefficient σ is usually defined (Grew and Ibbs 1952, Denbigh 1952) as

$$\sigma = \frac{1}{T' - T} \log \left\{ \frac{x_a/x_b}{x_a'/x_b'} \right\},$$

where T', T are the temperatures of the two walls ($T' > T$), x_a, x_b are the mole fractions of the two components a and b of the binary mixture at the cold wall, and x_a', x_b' are the corresponding mole fractions at the hot wall. It follows that σ may be written in terms of molalities, ν_a (moles per 1000 g of solvent):

$$\sigma = \frac{1}{T' - T} \log \left(\frac{\nu_a}{\nu_a'} \right).$$

This equation was used in the calculation of the results shown in the table. In this table, all mole fractions x and molalities ν refer to CH_3OH. We have chosen the definition of the Soret coefficient so that it is a positive quantity in the table.

V.
19

This table also shows the change in mole fraction Δx for methanol at Soret equilibrium. Maximum separation is seen to occur at an initial methanol mole fraction of about 0·46.

x	Δx	ν'	ν	$10^2\sigma$
0·193	0·043	1·79	1·31	0·890
0·373	0·093	5·05	2·91	1·574
0·455	0·153	7·46	4·00	1·780
0·544	0·137	10·46	6·00	1·588
0·656	0·111	15·82	9·68	1·404
0·703	0·094	19·73	12·56	1·290
0·750	0·078	25·57	16·46	1·257

The approach to Soret equilibrium is shown in the figure, where the change in refractive index Δn_D is plotted against time t. The mixture considered in the figure possessed an initial methanol mole fraction of 0·703.

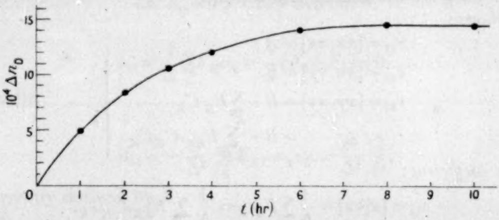

One of us (P. C.) is indebted to the South African Council for Scientific and Industrial Research for a research bursary, and we acknowledge financial assistance from Messrs. African Explosives and Chemical Industries Ltd.

Department of Chemistry, P. CROWTHER.
University of Natal, C. J. G. RAW.
Pietermaritzburg, South Africa.
16th December 1958.

DENBIGH, K. G., 1952, *Trans. Faraday Soc.*, **48,** 1.
GREW, K. E., and IBBS, T. L., 1952, *Thermal Diffusion in Gases* (Cambridge: University Press), Ch. VIII.

Correction to the Theory of the Calcium Fluoride Lattice

Recently a calculation of the elastic constants of calcium fluoride has been made by Dr. R. Srinivasan (1958) in these proceedings using Born's atomic theory of crystal lattices. Unfortunately, there is an error in the expressions for the elastic constants given by Born in his book *Atomtheorie des festen Zustandes* (1923). Because of this error Born obtained a non-zero value for the piezoelectric coefficient e_{14} of CaF_2. Since CaF_2 belongs to the O_h class, it should not possess any piezoelectric moment. Also Born gave the expression for c_{44} as

$$c_{44} = c_{12} - \frac{2C^2}{D}$$

in his notation. This expression is wrong and hence the value of c_{44} calculated by Srinivasan (1958) is incorrect. The value of c_{44} is recalculated and an estimate of the difference in dielectric constants at high and low frequencies is also made.

In Born's notation,

$$\left.\begin{aligned} \left[{}^{KK'}_{xx}\right] &= D_{KK'} & \left[{}^{K}_{xyz}\right] &= C_K \\ \left[{}^{KK'}_{xx}\right] &= E_{KK'} & \left[{}^{K}_{x|yz}\right] &= F_K = \sum_{K'} E_{KK'} C_{K'} \end{aligned}\right\} \qquad \ldots\ldots (1)$$

ϵ_K is the change on the Kth atom.

$$\left.\begin{aligned} &\sum_{K'} D_{KK'} = 0 \qquad \sum_{K'} E_{KK'} = 0 \\ &\sum_{K} C_K = 0 \qquad\ \ \sum_{K} F_K = 0 \\ \text{and} \qquad &\sum_{K} \epsilon_K = 0 \end{aligned}\right\} \qquad \ldots\ldots (2)$$

The following are the general expressions.

Elastic constants:

$$\left.\begin{aligned} c_{11} &= [xx, xx] = A \\ c_{12} &= [xx, yy] = B \\ c_{44} &= [xy, xy] = B + \sum_{K} F_K C_K \\ &= B + \sum_{KK'} E_{KK'} C_K C_{K'}. \end{aligned}\right\} \qquad \ldots\ldots (3)$$

Piezoelectric coefficient:

$$e_{14} = [x|yz] = \frac{1}{\Delta} \sum_{K} F_K \epsilon_K = \frac{1}{\Delta} \sum_{KK'} E_{KK'} C_{K'} \epsilon_K. \qquad \ldots\ldots (4)$$

Dielectric constant: The difference in dielectric constants is given by

$$\left.\begin{aligned} b_{11} &= \frac{K - K_0}{4\pi} = a_{11} + \frac{e_{14}{}^2}{C_{44}} \\ \text{where} \qquad a_{11} &= [xx] = -\frac{1}{\Delta^2} \sum_{KK'} E_{KK'} \epsilon_K \epsilon_{K'}. \end{aligned}\right\} \qquad \ldots\ldots (5)$$

In CaF_2, the unit cell contains three atoms, two of which are identical (fluorine). So, K and K' take the values 1, 2, 3.

$$\left.\begin{aligned} \text{And} \qquad & \epsilon_1 = 2\epsilon; \quad \epsilon_2 = \epsilon_3 = -\epsilon. \\ \text{Also} \qquad & C_1 + C_2 + C_3 = 0. \end{aligned}\right\} \qquad \ldots\ldots (6)$$

That the coefficient C_1 is zero follows from the expression for C_K given by Born

$$C_K = \frac{1}{\Delta} \sum_{K'} \sum_{l} S Q^l{}_{KK'} x^l{}_{KK'} y^l{}_{KK'} z^l{}_{KK'}.$$

Because Ca ($K = 1$) is at a position of centre of symmetry, $C_1 = 0$. This can also be seen from the coupling coefficients given by Srinivasan (1958).

$$\left.\begin{aligned} \text{So,} \qquad & C_1 = 0, \quad C_2 = -C_2 = -C \text{ (say)} \\ \text{Born assumed} \qquad & C_1 = 2C; \quad C_2 = C_3 = -C. \end{aligned}\right\} \qquad \ldots\ldots (7)$$

The other results derived by Born for the D's and E's are correct. They are

$$\left.\begin{aligned} D_{11} &= -2D & D_{22} &= D_{33} = -(D + D') \\ D_{12} &= D_{13} = D & D_{23} &= D' \end{aligned}\right\} \qquad \ldots\ldots (8)$$

$$\left.\begin{aligned} E_{11} &= -\frac{2}{9D} \qquad & E_{22} &= E_{33} = -\frac{1}{9D}\,\frac{5D+D'}{D+2D'} \\ E_{12} &= E_{13} = \frac{1}{9D} \qquad & E_{23} &= \frac{1}{9D}\,\frac{4D-D'}{D+2D'} \end{aligned}\right\} \quad \ldots\ldots(9)$$

In the light of (7) and (9) the F's are evaluated and they are

$$F_1 = 0,\ F_2 = -F_3 = -\frac{C}{(D+2D')}. \qquad \ldots\ldots(10)$$

Hence from (3)

$$\left.\begin{aligned} c_{11} &= A, \qquad c_{12} = B, \\ c_{44} &= B - \frac{2C^2}{(D+2D')}. \end{aligned}\right\} \qquad \ldots\ldots(11)$$

This expression for $c_{12}-c_{44}$ changes the value quoted by Srinivasan from $0{\cdot}74\times10^{11}$ to $0{\cdot}26\times10^{11}$.

$$\text{i.e. } c_{44} = 4{\cdot}5\times10^{11}\ \text{dyn cm}^{-2}. \qquad \ldots\ldots(12)$$

Now

$$e_{14} = \frac{1}{\Delta}\sum_K F_K \epsilon_K = \frac{\epsilon}{\Delta}(F_2+F_3) = 0 \qquad \ldots\ldots(13)$$

as it should be.

And

$$a_{11} = -\frac{1}{\Delta^2}\sum_{KK'} E_{KK'}\epsilon_K\epsilon_{K'} = \frac{\epsilon^2}{\Delta^2}\,\frac{2}{D},$$

a result correctly derived by Born.

Hence

$$K - K_0 = 4\pi\left(\frac{\epsilon^2}{\Delta^2}\,\frac{2}{D}\right). \qquad \ldots\ldots(14)$$

This comes out to be $K-K_0 = 3{\cdot}47$. Mott and Gurney (1940) give the experimental value $K-K_0 = 6{\cdot}44$ which is nearly double that calculated theoretically. This and the discrepancy in $c_{12}-c_{44}$ may be because of the assumption of central forces of interaction between the ions.

It should be pointed out that this correction does not invalidate the conclusion reached by Dr. Srinivasan namely that Born's theory is able to give the sign but not the magnitude of $c_{12}-c_{44}$ correctly. Also his expressions for the coupling coefficients are correct and any further lattice dynamical calculation can be based upon them.

The author thanks Professor R. S. Krishnan for his discussions and encouragement, and Dr. R. Srinivasan for his guidance and help. His thanks are also due to the referee for his helpful suggestions.

Department of Physics,
Indian Institute of Science,
Bangalore 3 (India).
A. K. Rajagopal.

9th December 1958.

Born, M., 1923, *Atomtheorie des festen Zustandes*, *Math. Wiss.* Bd V, p. 572.
Mott, N. F., and Gurney, R. W., 1940, *Electronic Processes in Ionic Crystals* (Oxford: University Press), p. 12.
Srinivasan, R., 1958, *Proc. Phys. Soc.*, **72**, 566.

Ultrasonic Vibration Potentials in Non-Ionic Liquids†

When ultrasonic waves are transmitted through an electrolytic solution, alternating potentials are developed within the solution. This effect was predicted first by Debye (1933) and has been studied subsequently in electrolytes with both standing waves (Yeager *et al.* 1949, Dérouet and Denizot 1951, Rutgers and Rigole 1958) and pulse-modulated waves (Yeager *et al.* 1953, Hunter 1958). Quantitative studies (Yeager *et al.* 1959) in KCl solutions at concentrations from 0·001 to 0·05 normal indicate a value of 3 to 4 μv per unit velocity amplitude (1 cm $\sec^{-1}$) at frequencies from 200 to 1000 kc/s.

Hunter (1958) has called attention to the existence of alternating potentials with glass mounted platinum probes in conductivity water. With pulse-modulated waves at a frequency of 465 kc/s, Hunter has found an effect for pure water of approximately 50 μv per unit velocity amplitude, a value one order of magnitude greater than for alkali halide solutions such as 0·01 N KCl. Rutgers and Rigole (1958), using standing waves at 1000 kc/s, have observed an apparent effect not only in distilled water but also in such pure liquids as methanol, ethanol, isopropanol, nitrobenzene, and even n-heptane. No appreciable effect was found in benzene. A satisfactory explanation for these potentials in non-ionic systems has not yet been advanced by either Hunter or Rutgers and Rigole but both suggest that such an effect may cause serious complications in the quantitative interpretation of ultrasonic vibration potentials in electrolytic solutions.

Further experimental work has been undertaken at Western Reserve University in an attempt to clarify this situation. Measurements have been made with pulse-modulated ultrasonic waves at 1000 kc/s with apparatus and techniques similar to those involved in earlier work (Yeager *et al.* 1953). A single platinum probe has been used in a thin-walled glass spherical vessel, the outside of which was covered with conducting silver paint, maintained at ground potential. The spherical vessel was only half-filled with liquid. The platinum probe consisted of a wire of 0·025 cm diameter, sealed in soft glass tubing of 0·6 cm o.d. with a 1·0 cm length of the platinum wire exposed. Capacitive loading effects associated with the probe mounting have been reduced to less than 10 pF through the use of a double concentric shield arrangement, described elsewhere (Dietrick *et al.* 1953). The axis of the platinum probe was oriented mutually perpendicular to the surface of the liquid and the direction of propagation of the ultrasonic waves.

The data in column (1) of the table were obtained with the platinum probe submerged to such a depth that approximately 1 cm of the glass mounting was within the liquid. The data in column (2) were obtained with 0·5 to 0·7 cm of the platinum wire submerged but none of the glass tubing in the liquid. The velocity amplitude has been estimated to have been 5 cm $\sec^{-1}$ on the basis of a comparison of the observed value for the KCl solution with that obtained under conditions more suited to a reliable evaluation of the velocity amplitude at 1000 kc/s. No significant difference was observed for the KCl solution with the glass tubing either in or completely out of the solution. Likewise, shunting the probe with a 40 pF condenser to ground had no effect on the observed signal

---

† This research has been partially supported by the U.S. Office of Naval Research under Contract No. Nonr 1439(04), Project No. NR 384–305.

in the case of 0·01 N KCl but greatly reduced the observed signal for the other cases in the table. In all instances where the effect has been designated as zero in the table, no effect was found above the noise level, which was 1 to 2 μv, depending on the liquid. The introduction of a second long grounded wire into the liquids within the vessel had no appreciable effect on the observed signals. Similar results to those in the table have been found also at 200 kc/s.

Observed Potentials (μv) in Various Liquids at 1000 kc/s with a Velocity Amplitude of approximately 5 cm sec^{-1}

Liquid	(1) Glass in liquid	(2) Glass out of liquid
Distilled water	54	0
0·01N KCl, aqueous	21	18
Methanol	11	0
Benzene	0	0
Iso-octane	0	0
n-heptane	0	0
Nitrobenzene	15	0

On the basis of these results, the effect in non-ionic systems appears to be associated with the glass tubing in which the platinum is sealed. To examine this hypothesis further, the glass tubing was replaced by polyethylene. The observed effect for distilled water was approximately ½ of that listed in column (1) of the table.

One explanation for these observations is that the section of the tubing immediately adjacent to the platinum-glass seal is acting as a condenser microphone with the platinum wire within the tubing as one surface of the condenser and the glass-liquid interface as the other. The response of such a condenser microphone should depend on the charge and this in turn should be a function of the liquid. The absence of an effect with the glass tubing submerged in benzene, *iso*-octane, and *n*-heptane probably can be explained in terms of such charging effects as well as the high electrical impedances of these liquids at radio frequencies. No immediate explanation is available as to why Rutgers and Rigole found a small effect in *n*-heptane.

If the condenser-microphone concept is correct, an a.c. response should be found with a probe in which the wire is completely enclosed in the glass tube and does not contact the liquid. This has been demonstrated experimentally with the observed response in distilled water of the same order of magnitude as listed in column (1) of the table.

The a.c. response associated with the glass tubing is characterized by a high internal impedance. At reasonable ionic concentrations (e.g. > 0·001 N) in aqueous solution, the internal impedance associated with the ionic vibration potentials is much lower. As a consequence, the observed response in ionic solutions should be characteristic of the ionic vibration potentials and not false effects associated with the glass tubing.

Ultrasonics Research Laboratory,
Western Reserve University,
Cleveland, Ohio, U.S.A.
14th January 1959.

E. Yeager.
J. Booker.
F. Hovorka.

DEBYE, P., 1933, *J. Chem. Phys.*, **1**, 13.
DÉROUET, B., and DENIZOT, F., 1951, *C.R. Acad. Sci., Paris*, **233**, 368.
DIETRICK, H., YEAGER, E., BUGOSH, J., and HOVORKA, F., 1953, *J. Acoust. Soc. Amer.*, **25**, 461.
HUNTER, A., 1958, *Proc. Phys. Soc.*, **71**, 847.
RUTGERS, A., and RIGOLE, W., 1958, *Trans. Faraday Soc.*, **54**, 139.
YEAGER, E., BOOKER, J., and HOVORKA, F., 1959, *Electrolytes*, Ed. W. Hamer (New York: Wiley), Chap. 6, in the press.
YEAGER, E., BUGOSH, J., HOVORKA, F., and MCCARTHY, J., 1949, *J. Chem. Phys.*, **17**, 411.
YEAGER, E., DIETRICK, H., and HOVORKA, F., 1953, *J. Acoust. Soc. Amer.*, **25**, 456.

The Influence of Fast Holes on the Photoelectromagnetic Effect in Germanium

The presence of two types of hole carrier in germanium has been indicated by cyclotron resonance experiments (Dresselhaus, Kip and Kittel 1953) and substantiated by conductivity, Hall effect and magnetoresistance measurements (Willardson, Harman and Beer 1954) on p-type germanium. The latter measurements suggest that about 2% of the holes have a mobility eight times that of the normal holes. Attempts to detect these high mobility holes by drift techniques (Harrick 1955) have failed for reasons given by Rittner (1956). A magnetic field is necessary to reveal the presence of the fast holes, and the higher the order of the magnetic field dependence of an effect, the greater will be the influence of a small number of fast holes on its magnitude. It was therefore of interest to investigate the magnetic variation of the photoelectromagnetic current (Moss 1959) since this has a higher order field dependence than magnetoresistance.

Assuming that (*a*) the (E, k) curve is parabolic, (*b*) the energy surfaces in k-space are spherical, (*c*) changes in carrier concentrations are small compared with equilibrium values, (*d*) end effects are negligible, (*e*) negligible space charge exists, (*f*) classical statistics may be used, (*g*) all the photo-carriers are produced at the illuminated surface, then for lattice scattering it can be shown that for the experimental conditions used the magnetic variation of the photoelectromagnetic short circuit current I is given by

$$\frac{16}{9\pi\mu_{\mathrm{p}}^2 H^2}\left\{\frac{(I/H)_{H\to 0} - I/H}{(I/H)_{H\to 0}}\right\} = \frac{b^2(aq+p)^2 + bn(a^3q+p)}{2(aq+p)(bn+aq+p)} + \frac{(b^3+1)p^2 + (2a^3+2b^3-a^2-a+2)aqp + (b^3+a^3)a^2q^2}{(aq+p)[(b+1)p+(a+b)aq]}$$

where p, q, and n are the densities of slow and fast holes and electrons, and μ_{p}, $a\mu_{\mathrm{p}}$ and $b\mu_{\mathrm{p}}$ are their mobilities (Walton and Moss 1959).

Measurements of the short-circuit photoelectromagnetic current were made on specimens cut from a slice of a large single crystal ingot. The material was p-type having a resistivity of 16 ohm cm. The orientation of the crystallographic axes with respect to the slice were determined by x-rays and three long rectangular bars cut with their edges parallel to various principal axes in the crystal. Platinum electrodes were soldered to the end faces and the specimens etched with superoxal to minimize surface recombination. The length to width ratios of all the finished specimens were greater than 7 to minimize end effects.

The specimens were illuminated by a tungsten lamp source through a Perspex filter ½ in. thick. Spectral measurements of the transmission of the filter in conjunction with absorption data for germanium showed that 97% of the photons entering the specimens were absorbed within 100 microns of the surface so that assumption (*g*) was met to a good approximation.

The radiant power incident on the specimens was determined using a thermopile and from the measured source temperature and carrier lifetime the change in carrier concentration at the surface was calculated. This change was then made sufficiently small to satisfy assumption (*c*).

A potentiometric circuit was used to measure the short-circuit photoelectromagnetic current, the magnetic field being reversed to eliminate thermoelectric and photovoltaic currents. The variation of the current from a linear dependence on magnetic field was found to be accurately quadratic up to 3140 oersteds. The magnitude of this variation from linearity at 3140 oersteds for various specimens is given in the table. The direction of illumination and magnetic field were in each case mutually perpendicular to the length of the specimen. The variation is seen to be virtually isotropic.

Specimen	1	2	3	4
Direction of Illumination	$0\bar{1}1$	100	100	$0\bar{1}1$
Direction of Magnetic Field H	100	$0\bar{1}1$	010	011
Variation (%)	7	8	7	8

Accuracy to ± 1%.

In view of the experimental evidence it is reasonable to interpret the results in terms of the theoretical expression quoted which does not include anisotropy terms. It may be seen, on inserting numerical values for germanium in this expression, that the dependence on *b* and hence electron mobility is rather slight, in spite of the fact that photoelectrons and photoholes are produced in equal numbers. Thus the anisotropy due to the ellipsoidal conduction band energy surfaces would be expected to be small. In general the magnetic variation of the photoelectromagnetic current will be dominated by the fastest carrier present, and if the energy surfaces for *this* carrier are spherical the variation must be approximately isotropic.

The carrier concentrations p and n were calculated from Hall coefficient and resistivity measurements using three carrier formulae. Values of the fast hole parameters used were $a = 8$, $q = p/50$ as suggested by Willardson, Harman and Beer (1954) and drift values (Prince 1953) corrected for the presence of fast holes (Rittner 1956) were taken for μ_p and b. Taking the above values for p, n, q, a, b and μ_p the theoretical magnitude of the magnetic variation of the short-circuit photoelectromagnetic current is 17%. If fast holes are neglected, i.e. q put equal to zero, the theoretical variation becomes 3·2%. The experimental variation is seen to be between these theoretical values. Retaining 2% fast holes, our results are fitted well with $a = 6$.

Thanks are due to Mr. S. E. Bradshaw of the General Electric Company, Wembley for providing the germanium and to Dr. Mitchell of Reading University

for providing the x-ray facilities. Published by permission of the Controller, Her Majesty's Stationery Office.

Royal Aircraft Establishment,
Farnborough,
Hants.
15th December 1958.

A. K. Walton.
T. S. Moss.

Dresselhaus, G., Kip, A. F., and Kittel, C., 1953, *Phys. Rev.*, **92**, 827.
Harrick, N. J., 1955, *Phys. Rev.*, **98**, 1131.
Moss, T. S., 1959, *Optical Properties of Semiconductors* (London: Butterworths).
Prince, M. B., 1953, *Phys. Rev.*, **92**, 681.
Rittner, E. S., 1956, *Phys. Rev.*, **101**, 1291.
Walton, A. K., and Moss, T. S., 1959, *Proc. Phys. Soc.*, **73**, 399.
Willardson, R. W., Harman, T. C., and Beer, A. C., 1954, *Phys. Rev.*, **96**, 1512.

Ferromagnetic Domain Sizes in Polycrystalline Silicon–Iron

We have measured the sizes of domains in polycrystalline silicon–iron over the range of grain diameters from about 0·01 to 0·10 cm. The results are in reasonable accord with calculations of optimum sizes reported previously by one of us (Martin 1957).

Sample strips of 2·79% silicon–iron (Mn 0·1%, others <0·05%), 0·03 cm thick, were well annealed and carefully demagnetized, and examined by the powder pattern technique. Those grains which produced patterns in which the domain walls carried small 'tree-patterns' were selected for study since it is known that, in these cases, the visible grain surfaces are within a degree or two of the (100) crystallographic orientation. The patterns then reveal the main domains of the grain and not merely surface structures. The photograph in figure 1 (Plate) shows one example. Most of the grains of this type had domains separated by 180° walls only, 90° walls being rare. The mean width of the domains in each grain was determined and is plotted, on a logarithmic scale, in figure 2, against the mean length of the grain measured in the direction of domain magnetization, i.e. [100]. The marked spread of the results was to be expected for two main reasons. Firstly, the effective length of a grain is not necessarily that revealed in the sample surface since the grain might become larger or smaller beneath the surface. Most grains were observed to pass right through the strips without large changes in size, however. Secondly, it is not to be expected that each grain will attain exactly its optimum (equilibrium) domain size since domain nucleation and growth are not entirely reversible processes.

In the calculations previously reported (Martin 1957) the optimum width D of domains separated by 180° walls in a single crystal plate, whose main faces are separated by a distance L and have (111) orientation, is given by

$$L = 0{\cdot}352\left(\frac{K}{\gamma}\right)^{1/3} D^{4/3} + 0{\cdot}144\left(\frac{C_{11}\lambda^2}{\gamma}\right) D^2.$$

Here K is the first anisotropy constant, γ is the domain wall energy density, λ is the magnetostriction constant and C_{11} an elastic constant. Whereas for large single crystals, with $L \sim 1$ cm, the second term is dominant and was found to give roughly the correct domain sizes, no previous test has been made of the calculations for small crystals with L smaller than 0·1 cm, when the first term is dominant. In order to compare the calculations with our measurements on roughly spherical grains we have used the relation above to obtain an expression for the mean domain width $\bar{D}$ in a crystal bounded by four (100) faces (two in the surfaces of the sample) and four (111) faces, as illustrated in figure 2. Then

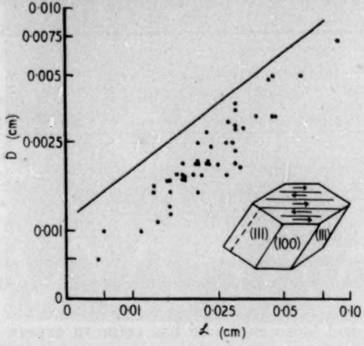

Figure 2. Variation of mean domain width $\bar{D}$ with mean grain length $\mathscr{L}$. The points record the experimental results and the line is the theoretical relation for crystals of the type illustrated in the diagram.

$$\bar{D} = 1{\cdot}32\left(\frac{\gamma}{K}\right)^{1/4}\mathscr{L}^{3/4}$$

where $\mathscr{L}$ is the mean length of the crystal *in the* [100] *direction*. We have neglected the second term above since it is never greater than 0·2 of the first term over our present range of $\mathscr{L}$. This dependence of $\bar{D}$ on $\mathscr{L}$ is drawn in figure 2. We have used $K = 3{\cdot}59 \times 10^5\,\mathrm{erg\,cm^{-3}}$ and $\gamma = 1{\cdot}4\,\mathrm{erg\,cm^{-2}}$ as appropriate for 2·79% Si–Fe. It can be seen that in absolute magnitude and slope there is agreement with the experimental results to a degree which is satisfactory in a problem of this kind. The theoretical relations apply, strictly, only to crystals whose end-faces are (111) planes, whereas the grains in the polycrystalline samples were bounded by faces of all orientations. Except for the special cases of near (100) or (110) orientations, however, the surface energies will not differ very greatly from that of the (111) case and domain widths would not be expected to be much larger than the calculated values. In fact the observed tendency is for them to be somewhat smaller. The agreement between the calculated and observed domain widths strongly suggests that the surface structures at the faces of polycrystalline grains closely resemble those found in isolated single crystals. It would have been desirable to make measurements on grains in the intermediate range between 0·1 and 1·0 cm, but with crystals of this size too many specimens would have to be prepared in order to find a sufficient number of grains with a suitable orientation.

Department of Physics,
Queen Mary College,
London.
13th January 1959.

D. Bloor.
D. H. Martin.

Martin, D. H., 1957, *Proc. Phys. Soc.* B, **70**, 77.

REVIEWS OF BOOKS

Nuclear Scattering, by K. B. MATHER and P. SWAN. Pp. viii + 469. (Cambridge Monographs on Physics.) (Cambridge: University Press, 1958.) 80*s*.

The subject of nuclear scattering is a large one covering many experimental and theoretical techniques the choice of which is strongly energy dependent. At the one end there is the scattering of slow neutrons by molecules, at the other the interaction of GeV protons with complex nuclei, and a great deal lies between. In the present volume the authors have attempted to give a complete account of the whole field. It is an ill-conceived work, for the task is too wide to be treated in this manner and they have indubitably failed. One simply cannot discuss the peculiarities of charged particle detectors and the contamination of targets by pump-oil in the same pages as one reveals the limitations of the impulse approximation and the intricacies of the confluent hypergeometric function. Such a mixture may be welcome enough in the privacy of the laboratory tea-room, but it certainly does not make for a good book. Much of it reads like an assortment of lecture notes—a somewhat odd assortment—with all the inaccuracies and loose ends one has come to expect in such material; inconsistencies of statement and of notation abound, sometimes within the space of a few lines. In several places the authors appear only too glad to forsake a physical discussion that could have been interesting only to plunge into a maze of impenetrable mathematical detail. One wonders who would understand the discussion of low-energy proton–proton scattering had he not known it all before: the ' theory ' is little more than a catalogue of Coulomb functions. It is difficult to see whom this book was intended to enlighten: it certainly cannot be recommended to the student, and as a reference book it is too capriciously selective and incomplete to be of much value. B. H. FLOWERS.

Nuclear Structure, by L. EISENBUD and EUGENE P. WIGNER. Pp. viii + 121. (Oxford: University Press, 1958.) 25*s*.

With the rapid progress in theoretical nuclear physics that we witness to-day, there is an increasing need of up-to-date books for the benefit of students and others not actively engaged in research in the subject. If the textbooks are to be of manageable size, the writing should be restricted to essential parts, and if they are to stand the test of time, one must guard against the tendency to weight recent developments too heavily. These matters, particularly the second, the authors seem to have borne in mind in the writing of this book. That they managed to confine their treatment, in spite of its broad scope, to a book of so small a size is noteworthy. They achieve this by using a very terse style which is limited to bare descriptions with little, if any, mathematical development.

The main part deals with the different nuclear models. Here, the accent is on the shell model while recent developments such as those associated with the collective model and the many-body problem are given a more succinct treatment. The chapter on nuclear reactions is excellent as would be expected of the authors who have played a prominent role here. This is followed by a brief sketch of topics related to nuclear structure including deuteron stripping, electric excitation, beta and gamma decay.

A novelty is the bibliography which is supplemented by a running commentary on the significance of the papers to the subject as a whole. This should be of particular value to those readers who will wish to carry on further reading and is a practice which other authors might copy. L. J. B. GOLDFARB.

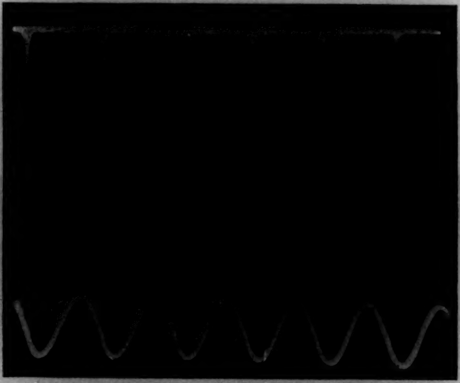

Figure 7. Discrete sonoluminescence flashes from water saturated with carbon disulphide. Acoustic power about 20 watts.

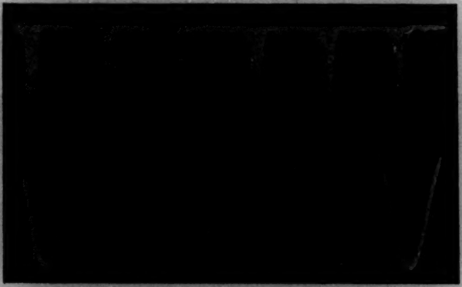

Figure 8. Sonoluminescence flashes from water. Acoustic power about 45 watts.

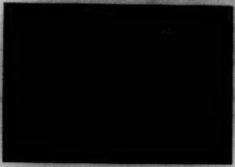

Figure 9. Strong sonoluminescence flashes from ethylene glycol. Acoustic power about 30 watts.

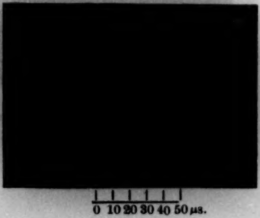

Figure 10. A single flash of sonoluminescence from water saturated with carbon disulphide. Acoustic power, about 20 watts. The flash is resolved as far as is possible.

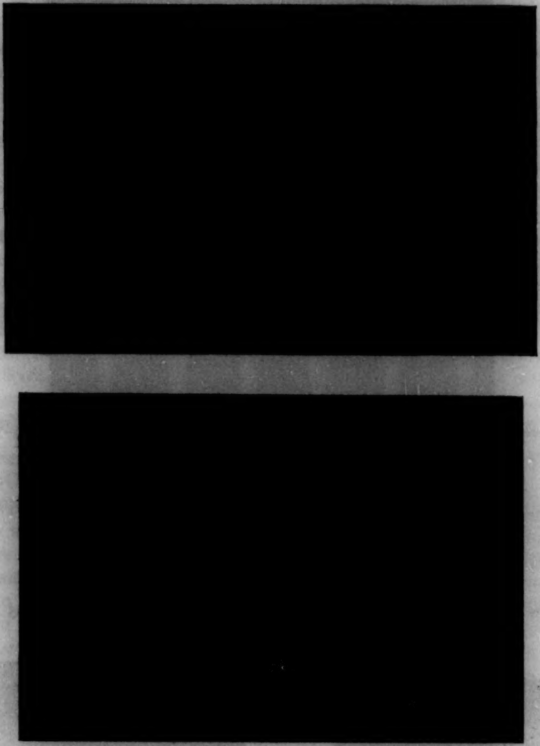

Figure 4. Opposite faces part-way through the switching process (one print reversed). Magnification about × 1000.

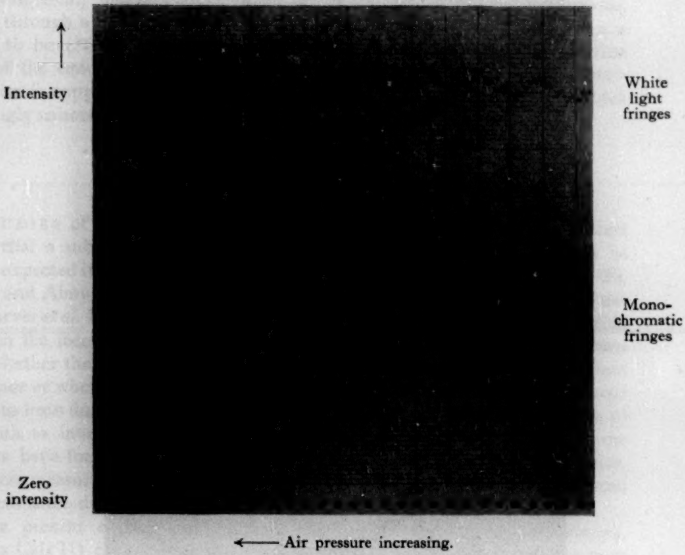

Figure 5. Record obtained with apparatus shown in figure 4.

PROC. PHYS. SOC. VOL. 73, PT. 4 (D. BLOOR AND D. H. MARTIN)

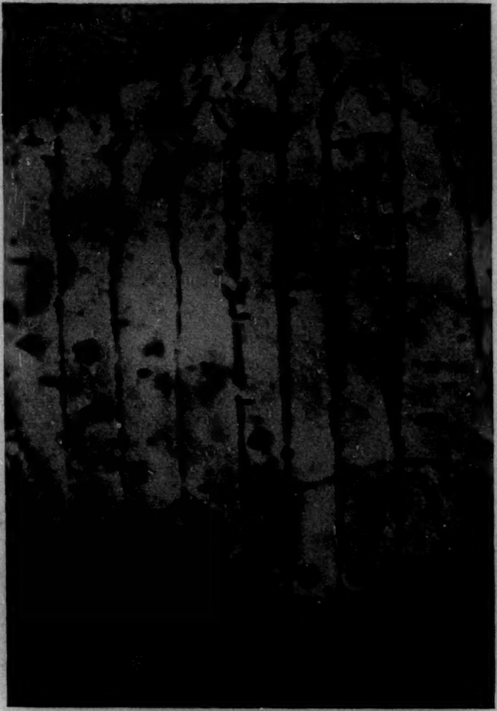

Figure 1. Powder pattern on a grain of Si–Fe about 0·02 cm across.

High-Energy Photoprotons from Silver

By K. H. LOKAN

Research School of Physical Sciences, Australian National University, Canberra

MS. received 18*th November* 1958, *in final form* 19*th January* 1959

Abstract. The energy distributions and absolute yields of photoprotons of energy greater than 10 MeV from silver have been measured for maximum bremsstrahlung energies between 16 and 32 MeV. The derived cross section for this component, which may be identified as arising from direct interactions, passes through a maximum at about 22 MeV, and the integrated cross section is found to be (36 ± 9) MeV mbn. This result is consistent with the idea that most of the emission arises from a 2p–2d transition at 22 MeV, and this interpretation is supported by the angular distribution measured at 30 MeV, which is strongly anisotropic.

---

§ 1. INTRODUCTION

STUDIES of the energy distributions of photonucleons have established that a substantial number is emitted with more energy than would be expected if a compound nucleus were invariably formed (Curtis *et al.* 1950, Diven and Almy 1950, Byerly and Stephens 1951, Price 1954, and others; see also Carver *et al.* 1957). This high energy excess is attributed to direct interaction between the incoming photon and the emergent nucleon. The question arises as to whether the cross section for this direct component displays the usual giant resonance or whether it arises from some separate interaction mechanism. Some work has been done on the problem by Ferrero *et al.* (1956) using threshold (n, p) detectors to investigate the cross section for direct neutron emission; these workers have found that the cross section closely follows the giant resonance, and their measured yields agree reasonably well with the yields predicted from the 'resonance-direct' mechanism proposed by Wilkinson (1956).

The present experiment examines the same feature for direct protons. Using a CsI(Tl) crystal as a proton detector and selecting the direct component by pulse height analysis of the scintillator output, the yield of fast photoprotons from silver has been measured as a function of maximum bremsstrahlung energy and a cross section curve for direct proton emission has been obtained. In addition, the angular distribution of this component has been measured at a maximum bremsstrahlung of 30 MeV, in order to identify the angular momentum states from which the protons emerge.

§ 2. EXPERIMENTAL ARRANGEMENT

2.1. *Yield and Energy Distribution*

The experimental arrangement is shown in figure 1. A collimated beam from the Canberra 33-MeV electron synchrotron entered the evacuated target tube through a thin aluminium window and irradiated a target of thin silver foil (40 mg cm^{-2}). The crystal, of dimensions 1 in. × 1 in. × 0·1 in. (sufficiently thick to stop protons of up to 24 MeV), was mounted parallel to and directly opposite the target so as to intercept protons emerging at 90°. The crystal was contained within a spherical reflecting shell having a thin (4 mg cm^{-2}) aluminium window and similar in design to an assembly described by Weinstock and Halpern (1955). With this arrangement, the energy resolution attained for the 8·8 and 6·9 MeV alpha particles from ThC + ThC′ was approximately 6%; a typical alpha-particle spectrum is shown in figure 2 (*a*). In addition to the permanent lead, concrete and steel shielding between the bremsstrahlung source and the research room, the crystal itself was shielded by at least 3 in. of lead except for the incoming proton port.

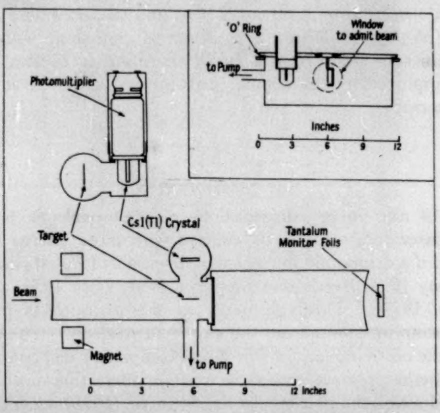

Figure 1. The proton counter. Inset : Angular distribution chamber.

The energy calibration, or light output, for protons relative to that for 8·8 MeV alpha particles was obtained by comparing the pulse heights of the alpha-particle group and known proton groups from the reaction ^{10}B(d, p)^{11}B on a separate CsI crystal. Using this calibration, the maximum proton energy measured for an irradiation at 30 MeV was 24 ± 1 MeV, in good agreement with the value expected for protons leaving the nucleus in its ground state. (The proton binding energy for both silver isotopes is close to 6 MeV (Diven and Almy 1950).)

To help discrimination against electrons, pulses from the photomultiplier were clipped to a total length of one microsecond and biased immediately to remove pulses corresponding to proton energies below 5 MeV; this eliminated electron pulses before stray capacities increased their length and allowed them to 'pile up'. Thereafter, the pulses were amplified in the usual way and analysed with a Hutchinson–Scarrott 80-channel pulse height analyser. The duration of the bremsstrahlung output pulse from the synchrotron was increased to about 200 microseconds by switching off the radio-frequency accelerating voltage less sharply, and the pulse height analyser was gated to accept pulses only during this interval; this helped further to minimize 'pile-up'.

To differentiate between proton and electron pulses, 150 mg cm^{-2} aluminium absorber was placed between the target and the detector, and the spectrum obtained from an irradiation at 30 MeV compared with that of an identical irradiation without absorber. This thickness of aluminium was chosen as the best compromise between an absorber which would stop all protons and one which would not alter the electron background too seriously. The result of these irradiations is shown in figure 2 (*b*). The end-point of the spectrum is reduced by the absorber from 24 MeV to about 22 MeV, and the yield of protons with a net energy greater than 8 MeV is the same as the yield above 13 MeV from the run with no absorber. Since 150 mg cm^{-2} reduces the energy of a 13-MeV proton to 8 MeV (Aron *et al.* 1949), this indicates that all pulses beyond 13 MeV were due to protons, and if the absorber did not distort the electron edge too severely, then most pulses above 8 MeV also arose from protons. It was considered, therefore, that the counter could be used to detect and measure the energies of protons above 8 MeV.

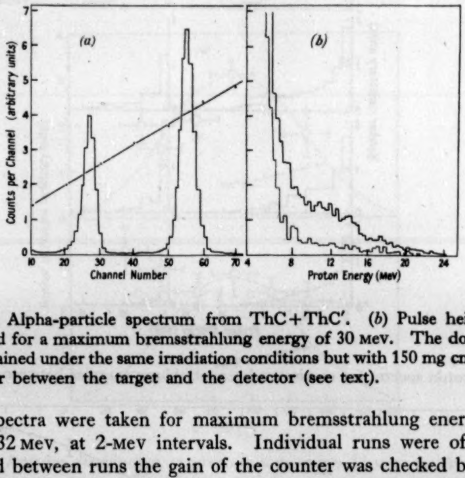

Figure 2. (*a*) Alpha-particle spectrum from ThC + ThC′. (*b*) Pulse height spectrum observed for a maximum bremsstrahlung energy of 30 MeV. The dotted spectrum was obtained under the same irradiation conditions but with 150 mg cm^{-2} aluminium absorber between the target and the detector (see text).

Proton spectra were taken for maximum bremsstrahlung energies ranging from 16 to 32 MeV, at 2-MeV intervals. Individual runs were of two hours' duration, and between runs the gain of the counter was checked by measuring the thorium alpha-particle spectrum. The total bremsstrahlung dose was monitored by the activity induced in tantalum foils, the yield curve for the reaction ^{181}Ta(γ, n)^{180}Ta having been measured previously in this laboratory (Carver *et al.* 1957). Counting rates were low, at best not more than 2 or 3 per minute, and sufficient statistics to determine the yield curve adequately could only be accumulated over a number of runs, which were added together. The 30-MeV spectrum, for example, is the sum of five 2-hour runs, and contains approximately 1200 pulses corresponding to protons above 8 MeV. The set of spectra shown in figure 3, for which channels have been added together in groups of three, represents a total running time of about 100 hours.

The absolute proton yield was determined relative to the known ^{63}Cu(γ, n) cross section (Berman and Brown 1954). A square foil of copper, of the same dimensions as the silver target, and known mass, was placed in the target position and irradiated with 30-MeV bremsstrahlung for 20 minutes, the same tantalum monitoring procedure being used. Annihilation radiation from the 9·4 min ^{62}Cu activity was detected in a known geometry with a scintillation detector and the absolute neutron yield per mole of ^{63}Cu per unit tantalum activity calculated. This was related to the photoproton yield through the monitor activity and gave the ratio

$$\frac{\text{Yield of photoprotons above 8 MeV per mole of Ag}}{\text{Yield of neutrons per mole of }^{63}\text{Cu}} = 0{\cdot}066 \pm 0{\cdot}02.$$

The method is not entirely free of objection, because the detection efficiency of both the proton counter and the scintillation counter had to be calculated from

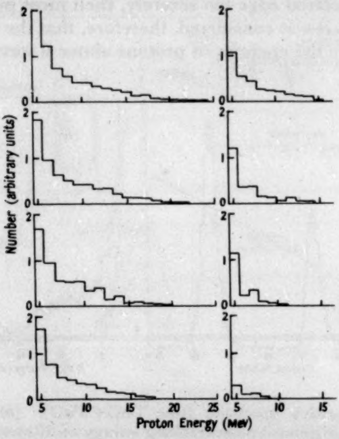

Figure 3. Proton spectra for maximum bremsstrahlung energies between 16 and 30 MeV.

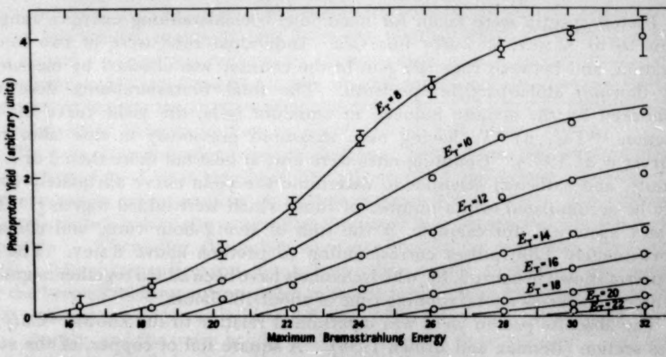

Figure 4. Photoproton yield curves for increasing values of counter threshold.

the respective geometries; the rather generous errors quoted include such uncertainties. Furthermore, the photoproton yield may have been overestimated, since it was assumed that protons were emitted isotropically, and the angular distribution measurement described later does not help since only protons above 13 MeV were detected in that case.

2.2. *Angular Distribution*

The chamber used to measure the angular distribution at 30 MeV is shown in the inset to figure 1. The crystal was mounted on a Perspex light pipe through the lid of the circular chamber, the lid resting on an ' O ' ring and able to be rotated so as to set the angle of the detector with respect to the axis of the beam. The beam entered and left the chamber through extended tubes with thin aluminium ends, and was monitored with tantalum foils. The chamber could not be as effectively shielded as the previous counter, and the background edge was moved upwards in energy so that only protons of energy greater than 13 MeV could be identified reliably.

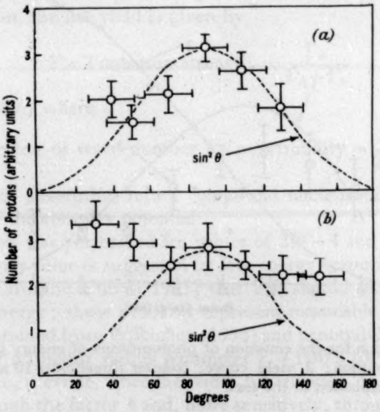

Figure 5. Angular distribution of photoprotons above 13 MeV, (*a*) from silver, (*b*) from nickel.

The proton yield at 30 MeV, normalized to unit monitor activity, was measured as a function of angle at intervals of 20°. The measured angular distribution was markedly anisotropic, as shown in figure 5 (*a*). The errors indicated are root mean square deviations, determined from the statistics, and the horizontal bars represent the angular resolution of the detector (22°); no correction has been applied for variations in energy loss within the target as a function of angle. To check that the angular distribution was not affected by a systematic error in the method, the angular distribution from nickel was also measured, since this has been determined previously (Leiken *et al.* 1956) and found to be almost isotropic. The distribution obtained, which is fairly flat and certainly different from the distribution for silver, is shown in figure 5 (*b*).

§ 3. Discussion

The results obtained in the yield measurements are summarized by the family of yield curves shown in figure 4. These have been drawn for counter thresholds increasing in steps of 2 MeV from 8 MeV to 22 MeV. The curves drawn for thresholds of 8, 10 and 12 MeV indicate a peak in the cross section for emission of protons of more than these energies in the region of 22 MeV. Beyond these counter thresholds, the uncertainties of the points preclude any definite conclusions being drawn, though the typical inflected shape of the curves would be destroyed, as it appears to be, as the yield curve approached and moved beyond 22 MeV.

The curve drawn for a counter threshold of 10 MeV has been analysed by an iterative method (Carver and Lokan 1957) to give the cross section curve shown in figure 6. The integrated cross section for the emission of protons of energy greater than 10 MeV is $\int_{16}^{32} \sigma dE = 36 \pm 9$ MeV mbn, assuming isotropy.

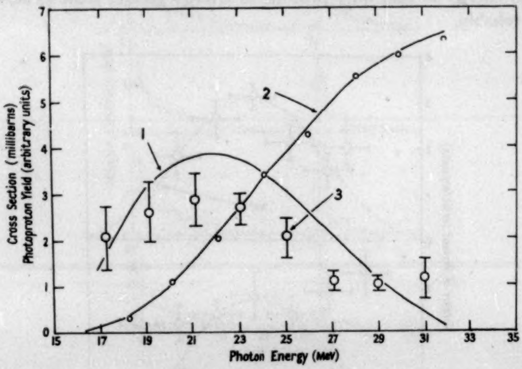

Figure 6. Cross section for the emission of photoprotons of energy greater than 10 MeV. 1, interative solution; 2, yield curve: counter threshold = 10 MeV; 3, 'successive differences', explained in the text.

An estimate of the cross section for protons leaving the nucleus in its ground state has also been obtained from the proton spectra themselves. It is noticeable that as the end-point of the bremsstrahlung distribution is increased in steps of 2 MeV, the end-point of the proton spectrum moves out accordingly. The protons emitted into the added 2 MeV must have come from interactions with photons contained in the last 2 MeV of the bremsstrahlung distribution. Thus an 'average' cross section over each 2-MeV interval has been obtained, by taking the number of protons in the last 2 MeV of each spectrum, and normalizing against the number of photons in the last 2 MeV of the bremsstrahlung distribution. These are the points labelled 'successive differences'. It is seen that the same general shape is preserved, and the integrated cross section measured in this way is 30 ± 10 MeV mbn.

Calculations by Diven and Almy of the 'evaporation' spectrum for silver indicate that few protons are emitted with more energy than 10 MeV in the decay of a compound nucleus so that, in this connection, the criterion which is taken to define a 'direct' proton is that it emerges with greater than this energy. This does not necessarily provide a complete measure of the direct cross section, since direct protons of lower energy can presumably be emitted following the absorption of lower-energy photons in the bremsstrahlung spectrum or, alternatively, by the ejection of protons from deeper lying shells.

The integrated cross section for the (γ, n) reaction in silver is approximately 1650 MeV mbn (Diven and Almy 1950), so that the component measured in this experiment accounts for about 2% of the total absorption. Moreover, the agreement between the cross section for the emission of all protons above 10 MeV and for the emission of protons leaving the nucleus close to its ground state suggests that most of the increase in yield is accounted for by the extra protons added at the tip as the maximum bremsstrahlung energy is increased. This would imply that at the peak of the cross section at 22 MeV, the energy of the ejected protons is approximately 16 MeV.

Assuming this value for the proton energy, the 'resonance-direct' yield has been calculated for the important E1 transitions from closed shells in silver. For each transition, the net yield is given by

$$Y = \text{Transition strength} \times \frac{\Gamma_d}{\Gamma_d + \Gamma_a}$$

(cf. Wilkinson 1956) where

$$\Gamma_d = \text{width for proton of wave number } k \times \text{penetrability} = \frac{3\hbar^2 k}{2mR^2} P_l$$

and Γ_a = width for absorption into a compound nucleus $= 2W$ where W is the imaginary part of the complex potential.

The calculation was performed for values of $2W = 4$ and $2W = 10$ MeV since, although the former value is suggested by low-energy scattering data, it has been suggested (e.g. Cini and Fubini 1955) that $2W$ should increase quite rapidly with excitation energy; these probably represent reasonable limits. Transition strengths were obtained from Wilkinson (1956) and penetrabilities from Morrison (1953), assuming a nuclear radius parameter $r_0 = 1{\cdot}30 \times 10^{-13}$ cm. The result, shown in the table, is crude, since the width for emission depends on the proton energy both through the factor k and, more sensitively, through the penetrability term P_l. However, the experiment indicates that at the maximum of the cross section, the majority of protons is emitted with about 16 MeV; and this energy was therefore taken for the calculation.

Under these assumptions, direct proton emission accounts for 24–32% of the proton transitions, or roughly 12–16% of the total absorption, and is about

Proton Yields for Transitions from Closed Shells

			Net yield	
Transitions	Strength (%)	Penetrability	$2W=4$	$2W=10$
1f–1g	78	0·41	22%	18%
2p–2d	14	0·8	8%	5%
2p–3s	3	1·0	2%	1%
Totals	95		32%	24%

an order of magnitude larger than the measured integrated cross section. This is because of the large contribution from the 1f–1g transitions, if the proton energy is taken as 16 MeV, and suggests that these transitions are probably not associated with the observed peak at 22 MeV. In fact, it is reasonable to identify the 1f–1g transitions (which are the strongest, and account for about 40% of the total absorption) with the giant resonance at 17 MeV. Then the net yield from them is reduced by at least a factor of twenty because of the smaller penetrability, and the calculated direct emission becomes 3–6% of the total absorption, depending on the choice of $2W$, in closer agreement with experiment. Actually, the calculated yield from the 2p–2d transitions is about sufficient in itself to account for the measured yield.

This later interpretation is further reinforced by the angular distribution measurement. The angular distribution of protons from a 2p–2d transition is proportional to $1+1\cdot5\sin^2\theta$ (Courant 1951), while that from a 1f–1g transition is proportional to $1+0\cdot83\sin^2\theta$ and contains a much larger isotropic component. In fact, the anisotropy appears to be stronger than would be expected from the 2p–2d transitions, though the errors are comparatively large and such a distribution is not definitely excluded. However, the distribution is not consistent with that expected for protons from the 1f shell, and supports the suggestion that the observed protons are emitted in transitions from shells of lower angular momentum.

REFERENCES

ARON, W. A., HOFFMAN, B. G., and WILLIAMS, F. C., 1949, U.S. Atomic Energy Commission *Report* No. AECU.663.

BERMAN, A. I., and BROWN, K. L., 1954, *Phys. Rev.*, **96**, 83.

BYERLY, P. R. (Jnr.), and STEPHENS, W. E., 1951, *Phys. Rev.*, **83**, 54.

CARVER, J. H., EDGE, R. D., and LOKAN, K. H., 1957, *Proc. Phys. Soc.* A, **70**, 415.

CARVER, J. H., and LOKAN, K. H., 1957, *Aust. J. Phys.*, **10**, 312.

CINI, M., and FUBINI, S., 1955, *Nuovo Cim.*, **2**, 75.

COURANT, E. D., 1951, *Phys. Rev.*, **82**, 703.

CURTIS, N. W., HORNBOSTEL, J., LEE, D. W., and SALANT, E. O., 1950, *Phys. Rev.*, **77**, 290 L.

DIVEN, B. C., and ALMY, G. M., 1950, *Phys. Rev.*, **80**, 407.

FERRERO, F., HANSON, A. O., MALVANO, R., and TRIBUNO, C., 1956, *Nuovo Cim.*, **4**, 418.

LEIKEN, S., OSOKINA, R. M., and RATNER, B. S., 1956, *Nuovo Cim. Suppl.*, **3**, 105.

MORRISON, P., 1953, *Experimental Nuclear Physics*, Vol. 2, edited by E. Segrè (New York : John Wiley & Sons Inc.), p. 193.

PRICE, G. A., 1954, *Phys. Rev.*, **93**, 1279.

WEINSTOCK, E. V., and HALPERN, J., 1955, *Phys. Rev.*, **100**, 1293.

WILKINSON, D. H., 1956, *Physica*, **22**, 1039.

The Stripping Reaction of ^{3}He and Alpha Particles

By M. EL NADI and M. EL KHISHIN
Faculty of Science, Cairo University, Cairo, Egypt

MS. received 19*th August* 1958, *in revised form* 12*th January* 1959

Abstract. The recent experimental data on the (^{3}He, p) differential cross section showing forward and backward peaks are interpreted as due to the ^{3}He particle stripping and heavy particle stripping respectively. Reasonable agreement is obtained between the derived theoretical formulae and the experimental data. Some (*d*, α) reactions are interpreted in a similar way.

---

§ 1. Introduction

Recent studies (Bromley *et al.* 1957) of the angular distributions of (^{3}He, p) reactions showed clearly that in many cases the reaction does not proceed by the compound nucleus model. Forward peaks were observed (Johnston *et al.* 1958) in the angular distributions which suggest a direct action mechanism. A formula for the differential cross section of (α, d) (^{3}He, p) reactions of the stripping type was given lately (El Nadi 1957) which could explain the existence of the forward peak found in these reactions.

Another characteristic feature, observed in the recently published data on the differential cross section of the (^{3}He, p) and (d, α) reactions is the appearance of another peak in the backward direction. This peak seems relatively stronger than the corresponding ones observed in the differential cross section for the (d, p) reactions. This can be seen clearly in the recent data of Johnston *et al.* (1958) on the differential cross section for the ^{12}C(^{3}He, p)^{14}N reaction. The existence of a backward peak in some deuteron reactions was well explained by Owen and Madansky (1957). It is assumed that the target nucleus could itself be stripped by the incoming deuteron. Thus in a (d, p) reaction, the outgoing proton could come out either from the deuteron or from the target nucleus. This latter effect, called heavy particle stripping, forms a component in the differential cross section and gives rise to a backward peak in the angular distribution. Thus it may be expected that the backward peak in the (^{3}He, p) and similar reactions is also due to heavy particle stripping.

In this note the reaction ^{12}C(^{3}He, p)^{14}N is considered in a manner similar to that used by Owen and Madansky for deuteron stripping. We shall assume that the ^{12}C-nucleus is composed of a core C + a proton 1, see figure 1. The ^{3}He nucleus will be assumed to consist of two protons 2 and 3, and a neutron n.

The differential cross section for the considered reaction can be written as (in the centre-of-mass system)

$$d\sigma = \frac{M_{\mathrm{p}}^* M_{\mathrm{n}}^*}{(2\pi\hbar^2)^2}\frac{k_{\mathrm{p}}}{k_{\mathrm{n}}}\Sigma\,|\langle\Psi_{\mathrm{f}}|V|\Psi_{\mathrm{i}}\rangle|^2 d\Omega \qquad \ldots\ldots(1)$$

M^* and k refer to the reduced mass and wave number, V is the interaction potential, Ψ_{i} and Ψ are the initial and final total state wave functions of the system. The sum is extended over all the final states and averaged over all the initial states.

Now the outgoing proton may have come either from the two protons in the projectile or from the target nucleus. This can be taken account of by the complete antisymmetrization (Owen and Madansky 1957) of the final wave function with respect to each of these protons. Effecting this antisymmetrization we get for the differential cross section for the (^{3}He, p) reaction†:

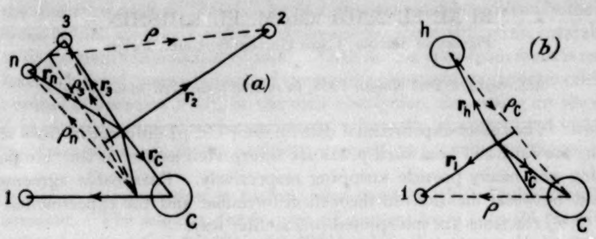

Figure 1.

$$d\sigma \propto \Sigma\,|C_1\mathscr{F} - C_2\mathscr{B}|^2 d\Omega, \qquad \ldots\ldots (2)$$

where C_1 and C_2 are normalized constants,

$$\mathscr{F} = \int \exp(-i\mathbf{k}_2 . \mathbf{r}_2)\psi^*_{\mathrm{R}}(\mathbf{r}_1\mathbf{r}_3\mathbf{r}_n\mathbf{r}_c) \exp(-i\mathbf{k}_{\mathrm{R}}.\mathbf{r}_{\mathrm{R}})[V]\psi_{\mathrm{h}}(\mathbf{r}_2\mathbf{r}_3\mathbf{r}_n)\exp(i\mathbf{k}_{\mathrm{h}}.\mathbf{r}_{\mathrm{h}})$$
$$\times\,\psi_{\mathrm{t}}(\mathbf{r}_1\mathbf{r}_c)\exp(i\mathbf{k}_{\mathrm{t}} . \mathbf{r}_{\mathrm{t}})d\mathbf{r}_1 d\mathbf{r}_2 d\mathbf{r}_3 d\mathbf{r}_n d\mathbf{r}_c \qquad \ldots\ldots (3)$$

and

$$\mathscr{B} = \int \exp(-i\mathbf{k}_1 . \mathbf{r}_1)\psi^*_{\mathrm{R}}(\mathbf{r}_2\mathbf{r}_3\mathbf{r}_n\mathbf{r}_c) \exp(-i\mathbf{k}_{\mathrm{R}}.\mathbf{r}_{\mathrm{R}})\,[V]\psi_{\mathrm{h}}(\mathbf{r}_2\mathbf{r}_3\mathbf{r}_n)\exp(i\mathbf{k}_{\mathrm{h}}\ \ \mathbf{r}_{\mathrm{h}})$$
$$\times\,\psi_{\mathrm{t}}(\mathbf{r}_1\mathbf{r}_c)\exp(i\mathbf{k}_{\mathrm{t}} . \mathbf{r}_{\mathrm{t}})d\mathbf{r}_1 d\mathbf{r}_2 d\mathbf{r}_3 d\mathbf{r}_n d\mathbf{r}_c, \qquad \ldots\ldots (4)$$

ψ_{R}, ψ_{h}, ψ_{t} are the wave functions of the residual, ^{3}He and target nuclei respectively, and $\mathbf{k}_{\mathrm{R}}$, $\mathbf{k}_{\mathrm{h}}$ and $\mathbf{k}_{\mathrm{t}}$ refer to the respective wave vectors of the residual, ^{3}He and target nuclei, $\mathbf{k}_1$, $\mathbf{k}_2$ are wave vectors of the outgoing proton, $\mathbf{r}_n$, $\mathbf{r}_1$, $\mathbf{r}_2$, $\mathbf{r}_3$, $\mathbf{r}_c$, $\mathbf{r}_{\mathrm{R}}$, and $\mathbf{r}_{\mathrm{h}}$ are the position vectors of the particles as shown in figure 1, all with respect to the centre-of-mass system.

§ 2. EVALUATION OF $\mathscr{F}$

In this part the outgoing proton comes out from the projectile (^{3}He). Therefore the potential V will involve the positions of the particles 3 and n, relative to the target nucleus. Therefore we shall take the centre of mass of the target nucleus t as origin and denote by ρ the new coordinates. We shall take for the internal wave function of the ^{3}He particle the Gaussian form $\exp(-\gamma^2\Sigma_{i\neq j}\rho_{ij}^2)$. Assuming the potential to be such as to cause capture of the particles n and 3 to occur at the surface of the nucleus, let us consider the following quantity:

$$Z = i\{-\mathbf{k}_2 . \mathbf{r}_2 - \mathbf{k}_{\mathrm{R}} . \mathbf{r}_{\mathrm{R}} + \mathbf{k}_{\mathrm{h}} . \mathbf{r}_{\mathrm{h}} + \mathbf{k}_{\mathrm{t}} . \mathbf{r}_{\mathrm{t}}\} = i\{-\mathbf{k}_2[\boldsymbol{\rho} + \tfrac{1}{2}(\mathbf{r}_3 + \mathbf{r}_n)]$$
$$-\mathbf{k}_{\mathrm{R}}[\mathbf{r}_{\mathrm{t}} + \frac{M_{\mathrm{D}}}{M_{\mathrm{R}}}\tfrac{1}{2}(\boldsymbol{\rho}_3 + \boldsymbol{\rho}_n)] + \mathbf{k}_{\mathrm{t}} . \mathbf{r}_{\mathrm{t}} + \mathbf{k}_{\mathrm{h}}[\boldsymbol{\rho}/3 + \tfrac{1}{2}(\mathbf{r}_3 + \mathbf{r}_n)]\} \qquad \ldots\ldots (5)$$

---

† This can be done in a way similar to that given by Schiff (1955) for the elastic scattering of an electron from a helium atom, and as given by Owen and Madansky (1957) in their analysis of the ^{11}B (d, n)^{12}C reaction.

where

$$\boldsymbol{\rho}=\mathbf{r}_2-\tfrac{1}{2}(\mathbf{r}_\mathrm{n}+\mathbf{r}_3), \qquad \boldsymbol{\rho}_j=\mathbf{r}_j-\mathbf{r}_\mathrm{t}, \qquad j=1,\ 3,\ \mathrm{n\ and\ c}.$$

Since $\mathbf{k}_\mathrm{t}=-\mathbf{k}_\mathrm{h}$ and $\mathbf{k}_\mathrm{R}=-\mathbf{k}_2$ (5) becomes

$$Z=i\boldsymbol{\rho}\,.\,\mathbf{F}+\tfrac{1}{2}i(\boldsymbol{\rho}_3+\boldsymbol{\rho}_\mathrm{n})\,.\,\mathbf{f} \qquad \ldots\ldots(6)$$

where

$$\mathbf{F}=\tfrac{1}{3}\mathbf{k}_\mathrm{h}-\mathbf{k}_2, \qquad \mathbf{f}=\mathbf{k}_\mathrm{h}-\frac{M_\mathrm{t}}{M_\mathrm{R}}\mathbf{k}_2. \qquad \ldots\ldots(7)$$

we get:

$$\mathscr{F}\propto\int\psi^*{}_{l_3}(\boldsymbol{\rho}_3)\psi^*{}_{l_\mathrm{n}}(\boldsymbol{\rho}_\mathrm{n})\exp\{-\gamma^2(3R^2+2\rho^2-3R^2\cos\omega)\}\exp i\mathbf{F}\,.\,\boldsymbol{\rho}$$

$$\exp[\tfrac{1}{2}i\mathbf{f}(\boldsymbol{\rho}_3+\boldsymbol{\rho}_\mathrm{n})]d\boldsymbol{\rho}_3 d\boldsymbol{\rho}_\mathrm{n} d\boldsymbol{\rho} \qquad \ldots\ldots(8)$$

where the integration has been carried out over $\boldsymbol{\rho}_1$ and $\boldsymbol{\rho}_\mathrm{c}$, giving a constant factor, and where ω is the angle between $\boldsymbol{\rho}_3$ and $\boldsymbol{\rho}_\mathrm{n}$. The integral (8) is of the type evaluated before (El Nadi 1957), from which we find

$$|\mathscr{F}|^2\propto\exp\left(\frac{-\mathrm{F}^2}{4\gamma^2}\right)|[(2l_\mathrm{n}+1)(2l_3+1)]^{1/2}\sum_{n=0}^{\infty}I_{n+\frac{1}{2}}(3\gamma^2R^2)(n+\tfrac{1}{2})$$

$$\times\sum_{m=-\mathrm{n}}^{\mathrm{n}}(-1)^{m_\mathrm{n}+m_3+m}\sum_{LML'M'}C_{l_\mathrm{n}n}(L0,\,00)C_{l_\mathrm{n}n}(L0,\,-m_\mathrm{n}m) \qquad \ldots\ldots(9)$$

$$C_{l_3n}(L'0,\,00)C_{l_3n}(L'0,\,-m_3m)\quad \mathscr{I}_L(\tfrac{1}{2}fR)\quad \mathscr{I}_{L'}(\tfrac{1}{2}fR)|^2$$

where

$$F^2=(k_2-\tfrac{1}{3}k_\mathrm{h})^2+\tfrac{4}{3}k_2k_\mathrm{h}\sin^2\tfrac{1}{2}\theta$$

$$f^2=\left(k_\mathrm{h}-\frac{M_\mathrm{t}}{M_\mathrm{R}}k_2\right)^2+4\frac{M_\mathrm{t}}{M_\mathrm{R}}k_2k_\mathrm{h}\sin^2\tfrac{1}{2}\theta \qquad \ldots\ldots(10)$$

and θ is the angle between $\mathbf{k}_2$ and $\mathbf{k}_\mathrm{h}$.

The following selection rule then applies:

$$\mathbf{J}_\mathrm{R}=\mathbf{J}_\mathrm{t}+\mathbf{l}_\mathrm{n}+\mathbf{l}_3+\tfrac{1}{2}+\tfrac{1}{2}. \qquad \ldots\ldots(11)$$

The agreement between the present and the previous derivation shows that the assumption that the target nucleus consists of a core C and a proton 1, is not essential in the final result.

§ 3. EVALUATION OF $\mathscr{B}$

In this case the proton comes out of the target nucleus, and hence the interaction potential can be expressed as

$$[V]=-V_\mathrm{c}\delta(|\mathbf{r}_\mathrm{c}-\mathbf{r}_\mathrm{h}|-R) \qquad \ldots\ldots(12)$$

the centre of coordinates will therefore be shifted to the centre of mass of ³He, so that $\boldsymbol{\rho}_j=\mathbf{r}_j-\mathbf{r}_\mathrm{h}$ ($j=2$, 3, n and c); similarly $\boldsymbol{\rho}=\mathbf{r}_1-\mathbf{r}_\mathrm{c}$. Therefore

$$i\{-\mathbf{k}_1\,.\,\mathbf{r}_1-\mathbf{k}_\mathrm{R}\,.\,\mathbf{r}_\mathrm{R}+\mathbf{k}_\mathrm{h}\,.\,\mathbf{r}_\mathrm{h}+\mathbf{k}_\mathrm{t}.\,\mathbf{r}_\mathrm{t}\}=i\left\{-\mathbf{k}_1(\mathbf{r}_\mathrm{c}+\boldsymbol{\rho})-\mathbf{k}_\mathrm{R}\left(\mathbf{r}_\mathrm{c}-\frac{M_\mathrm{h}}{M_\mathrm{R}}\boldsymbol{\rho}_\mathrm{c}\right)\right.$$

$$\left.+\mathbf{k}_\mathrm{h}\,.\,\mathbf{r}_\mathrm{h}+\mathbf{k}_\mathrm{t}\left(\mathbf{r}_\mathrm{c}+\frac{M_\mathrm{p}}{M_\mathrm{t}}\boldsymbol{\rho}\right)\right\}=i\mathbf{b}\,.\,\boldsymbol{\rho}+i\mathbf{B}\,.\,\boldsymbol{\rho}_\mathrm{c} \qquad \ldots\ldots(13)$$

where

$$\mathbf{b}=-\left\{\mathbf{k}_1+\frac{M_\mathrm{p}}{M_\mathrm{t}}\mathbf{k}_\mathrm{h}\right\}, \qquad \mathbf{B}=-\left\{\frac{M_\mathrm{n}}{M_\mathrm{R}}\mathbf{k}_1+\mathbf{k}_\mathrm{h}\right\} \qquad \ldots\ldots(14)$$

where M_h, M_p, M_t, M_r are the masses of ³He, proton, target and residual nuclei. $\mathbf{k}_1$ and $\mathbf{k}_\mathrm{h}$ are the wave vector of the emitted proton and ³He.

The expression for $\mathscr{B}$ may now be written as:

$$\mathscr{B}=\int\psi^*{}_{l_c}(\boldsymbol{\rho}_c)\psi^*{}_{l_h}(\boldsymbol{\rho}_2\boldsymbol{\rho}_3\boldsymbol{\rho}_n)[-V_c\delta(\rho_c-R)]\psi_t(\boldsymbol{\rho})$$
$$\psi_h(\boldsymbol{\rho}_2\boldsymbol{\rho}_3\boldsymbol{\rho}_n)\,e^{i\mathbf{b}\rho}\exp(i\mathbf{B}.\boldsymbol{\rho}_c)\,d\boldsymbol{\rho}d\boldsymbol{\rho}_2d\boldsymbol{\rho}_3d\boldsymbol{\rho}_c. \qquad \ldots\ldots(15)$$

The integral (15) can be separated into:

$$X=\int\psi^*{}_{l_h}(\boldsymbol{\rho}_2\boldsymbol{\rho}_3\boldsymbol{\rho}_n)\psi_h(\boldsymbol{\rho}_2\boldsymbol{\rho}_3\boldsymbol{\rho}_n)d\boldsymbol{\rho}_2d\boldsymbol{\rho}_3$$

which is constant,

$$Y(b)=\int\psi_t(\boldsymbol{\rho})\,e^{i\mathbf{b}\cdot\rho}\,d\boldsymbol{\rho} \qquad \ldots\ldots(16)$$

where $\psi_t(\boldsymbol{\rho})$ is the wave function of the proton 1 with respect to the core C, and:

$$Z(B)=\int\psi^*{}_{l_c}(\boldsymbol{\rho}_c)[-V_c\delta(\rho_c-R)]\exp(i\mathbf{B}\,.\,\boldsymbol{\rho}_c)d\boldsymbol{\rho}_c. \qquad \ldots\ldots(17)$$

If the principal axis for quantization is taken in the direction of $\mathbf{B}$, then:

$$\exp(i\mathbf{B}\,.\,\boldsymbol{\rho}_c)=\sum_{l_c}[4\pi(2l_c+1)]^{1/2}i^{l_c}\mathscr{J}_{l_c}(B\rho_c)Y_{l_c}{}^{0}(\Omega_c) \qquad \ldots\ldots(18)$$
$$e^{i\mathbf{b}\cdot\rho}=\sum_{lm}4\pi i^l\mathscr{J}_l(b\rho)Y_l{}^m(\Omega)Y^*{}_l{}^m(\mathbf{b}\,.\,\mathbf{B}). \qquad \ldots\ldots(19)$$

Using (18) in (17) we get

$$Z(B)\propto i^{l_c}[4\pi(2l_c+1)]^{1/2}f^*{}_{l_c}(R)[-V_c]\mathscr{J}_{l_c}(BR). \qquad \ldots\ldots(20)$$

Substituting (19) in (16) we get for the factor $Y(b)$

$$Y(b)=\sum_{lm}4\pi i^lY^*{}_l{}^m(\mathbf{b}\,.\,\mathbf{B})\int f_{l_1}(\rho)Y_{l_1}{}^{m_1}(\Omega)Y_l{}^m(\Omega)J_l(b\rho)d\boldsymbol{\rho} \qquad \ldots\ldots(21)$$

where we have put $\psi_t(\boldsymbol{\rho})=f_{l_1}(\rho)Y_{l_1}{}^{m_1}(\Omega)$.

Evaluating (21) we get:

$$Y(b)=4\pi i^{l_1}Y^*{}_{l_1}{}^{m_1}(\mathbf{b}\,.\,\mathbf{B})\int_R^\infty f_{l_1}(\rho)\mathscr{J}_{l_1}(b\rho)\rho^2d\boldsymbol{\rho}.$$

Since the variation of the Bessel function is slow it can be taken outside the integral (Austern *et al.* 1953) at the value R, giving:

$$Y(b)=4\pi i^{l_1}Y^*{}_{l_1}{}^{m_1}(\mathbf{b}\,.\,\mathbf{B})\mathscr{J}_{l_1}(bR)\,.\,\epsilon(R). \qquad \ldots\ldots(22)$$

Thus we get finally for $\mathscr{B}$:

$$\mathscr{B}\propto i^{l_c+l_1}Y^*{}_{l_1}{}^{m_1}(\mathbf{b}\,.\,\mathbf{B})\mathscr{J}_{l_1}(bR)\mathscr{J}_{l_c}(BR). \qquad \ldots\ldots(23)$$

Now l_c can be determined from the parities of the projectile h, the nucleus formed from the core C, and the final residual nucleus R.

To compare these formulae with the experimental results of Johnston *et al.* (1958) on the ^{12}C(^{3}He, p)^{14}N reaction we observe that the ground state of ^{14}N is 1^+, of ^{3}He is $\frac{1}{2}^+$ and of ^{11}B is $\frac{3}{2}^-$, therefore the capture angular momentum l_c must be odd. This could be 1 or 3.

To determine l_1, which is the orbital angular momentum of p_1 in the nucleus ^{12}C, relative to the core C, which is ^{11}B, we notice that ^{12}C has even parity and ^{11}B has odd parity, so that l_1 must be odd i.e. l_1 must be 1 or 3.

The theoretical curves are shown together with the experimental points in figures 2 and 3.

In fitting the forward part, the values of l_n and l_p were chosen in accordance with the selection rule (11).

A similar type of reaction to the (^{3}He, p) is the (α, d) reaction. Recent measurement (Marion and Weber 1956) on ^{13}C(d, α)^{11}B shows clearly the existence of both a forward and a backward maximum. This suggests also the existence of the light as well as the heavy particle stripping. Symmetry considerations will give for the differential cross section:

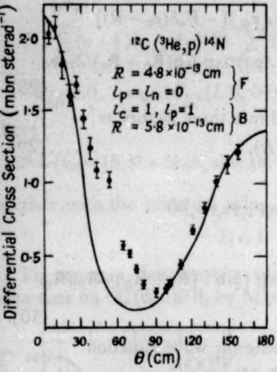

Figure 2. The differential cross section as a function of angle in the centre-of-mass system for the first excited state proton groups at 4·5 MeV incident ^{3}He energy.

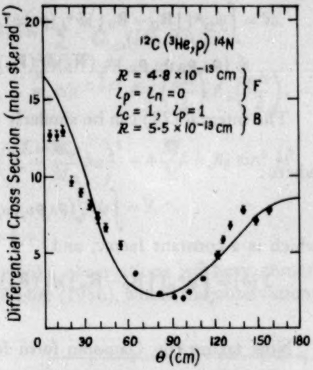

Figure 3. The differential cross section as a function of angle in the centre-of-mass system for the second excited state proton groups at 4·5 MeV incident ^{3}He energy.

$$d\sigma \propto \Sigma\,|\,C_1\mathscr{F} + C_2\mathscr{B}\,|^2 \qquad \ldots\ldots(24)$$

where C_1 and C_2 are normalization constants.

The forward term $\mathscr{F}$ will be almost identical with (9) (El Nadi 1957). Proceeding in a similar manner to the (^{3}He, p) reaction we get for $\mathscr{B}$ the following form:

$$\mathscr{B} = \int \exp\,(-i\mathbf{k}_{\mathrm{D}}\,.\,\mathbf{r}_{\mathrm{D}})\psi^*{}_{\mathrm{D}}(|\,\mathbf{r}_{\mathrm{p}} - \mathbf{r}_{\mathrm{n}}\,|)\exp\,(-i\mathbf{k}_{\mathrm{R}}\,.\,\mathbf{r}_{\mathrm{R}})\psi^*{}_{\mathrm{R}}(\mathbf{r}_{\mathrm{c}}, \mathbf{r}_{\mathrm{p}_1}\mathbf{r}_{\mathrm{n}_1}, \mathbf{r}_{\mathrm{p}_2}\mathbf{r}_{\mathrm{n}_2})[V]$$
$$\times \exp\,(i\mathbf{k}_{\alpha}\,.\,\mathbf{r}_{\alpha})\psi_{\alpha}(\mathbf{r}_{\mathrm{p}_1}\mathbf{r}_{\mathrm{n}_1}, \mathbf{r}_{\mathrm{p}_2}\mathbf{r}_{\mathrm{n}_2})\exp\,(i\mathbf{k}_{\mathrm{t}}\,.\,\mathbf{r}_{\mathrm{t}})\psi_{\mathrm{t}}(\mathbf{r}_{\mathrm{c}}\mathbf{r}_{\mathrm{p}}\mathbf{r}_{\mathrm{n}})d\tau. \qquad \ldots\ldots(25)$$

The perturbing potential is taken of the form:

$$V = -V_{\mathrm{c}}\delta(|\,\mathbf{r}_{\mathrm{c}} - \mathbf{r}_{\alpha}\,| - R).$$

Transforming the origin to the centre-of-mass of the incident alpha particles and putting $\boldsymbol{\rho}_j = \mathbf{r}_j - \mathbf{r}_\alpha$ where j refers to $\mathrm{p_1n_1p_2n_2c}$, and

$$\mathbf{R}_{\mathrm{p}} = \mathbf{r}_{\mathrm{p}} - \mathbf{r}_{\mathrm{c}}, \qquad \mathbf{R}_{\mathrm{n}} = \mathbf{r}_{\mathrm{n}} - \mathbf{r}_{\mathrm{c}}. \qquad \ldots\ldots(26)$$

Therefore

$$i\{-\mathbf{k}_{\mathrm{p}}\,.\,\mathbf{r}_{\mathrm{p}} - \mathbf{k}_{\mathrm{R}}\,.\,\mathbf{r}_{\mathrm{R}} + \mathbf{k}_{\alpha}\,.\,\mathbf{r}_{\alpha} + \mathbf{k}_{\mathrm{t}}\,.\,\mathbf{r}_{\mathrm{t}}\} = i\mathbf{B}\,.\,\boldsymbol{\rho}_{\mathrm{c}} + i\mathbf{b}(\mathbf{R}_{\mathrm{p}} + \mathbf{R}_{\mathrm{n}})/2$$

where

$$\mathbf{b} = -\left\{\frac{M_{\mathrm{D}}}{M_{\mathrm{t}}}\mathbf{k}_{\alpha} + \mathbf{k}_{\mathrm{D}}\right\}, \qquad \mathbf{B} = -\left\{\mathbf{k}_{\alpha} + \mathbf{k}_{\mathrm{D}}\frac{M_{\alpha}}{M_{\mathrm{R}}}\right\} \qquad \ldots\ldots(27)$$

and M_α, M_D, M_t, M_R are the masses of alpha, deuterons, target and residual nucleus, $\mathbf{k}_D$ and $\mathbf{k}_\alpha$ are the wave vectors of the emitted deuteron and the incident alpha particle.

The matrix element $\mathscr{B}$ referred to the new origin may be expressed by

$$\mathscr{B}=\int \psi_D^*(|\mathbf{R}_p-\mathbf{R}_n|)\psi^*_{l_c}(\boldsymbol{\rho}_c)\psi^*_{l_\alpha}(\boldsymbol{\rho}_{n_1}\boldsymbol{\rho}_{p_1}\boldsymbol{\rho}_{n_2}\boldsymbol{\rho}_{p_2})[-V_c\delta(\rho_c-R)]$$
$$\psi_\alpha(\boldsymbol{\rho}_{n_1}\boldsymbol{\rho}_{p_1}\boldsymbol{\rho}_{n_2}\boldsymbol{\rho}_{p_2})\psi_{l_p}(\mathbf{R}_p)\psi_{l_n}(\mathbf{R}_n)\exp(i\mathbf{B}\,.\,\boldsymbol{\rho}_c)\exp\{i\mathbf{b}(\mathbf{R}_p+\mathbf{R}_n)/2\}d\tau. \qquad \ldots\ldots(28)$$

The integral (28) can be similarly separated into three factors as:

$$\mathscr{B}=X\,.\,Y(b)\,.\,Z(B), \qquad \ldots\ldots(29)$$

where:

$$X=\int \psi^*_{l_\alpha}(\boldsymbol{\rho}_{n_1}\boldsymbol{\rho}_{p_1}\boldsymbol{\rho}_{n_2}\boldsymbol{\rho}_{p_2})\psi_\alpha(\boldsymbol{\rho}_{n_1}\boldsymbol{\rho}_{p_1}\boldsymbol{\rho}_{n_2}\boldsymbol{\rho}_{p_2})d\tau,$$

which is a constant factor, and

$$Y(b)=\int \psi^*_D(|\mathbf{R}_p-\mathbf{R}_n|)\psi_{l_p}(\mathbf{R}_p)\psi_{l_n}(\mathbf{R}_n)\exp\{\tfrac{1}{2}i\mathbf{b}\,.\,(\mathbf{R}_p+\mathbf{R}_n)\}d\mathbf{R}_p d\mathbf{R}_n. \qquad \ldots\ldots(30)$$

Now taking the Gaussian form for the deuteron wave function

$$\exp(-\gamma^2|\mathbf{R}_p-\mathbf{R}_n|^2),$$

and assumimg that ω is the angle between $\mathbf{R}_p$ and $\mathbf{R}_n$ we get:

$$\psi_D|\mathbf{R}_p-\mathbf{R}_n|=\exp\{-\gamma^2(R_p^2+R_n^2)\}\exp(2\gamma^2R_pR_n\cos\omega).$$

Expanding the second exponential in terms of the modified Bessel function and putting $|\mathbf{R}_p|=|\mathbf{R}_n|=R$, we get:

$$\exp(2\gamma^2R_pR_n\cos\omega)=\left(\frac{2\pi}{2\gamma^2R^2}\right)^{1/2}\sum_{n=0}^{\infty}\sum_{m=-n}^{n}2\pi I_{n+1/2}(2\gamma^2R^2)$$
$$\times Y^{*m}_{n}(\theta_p\phi_p)Y_n^m(\theta_n\phi_n). \qquad \ldots\ldots(31)$$

Substituting in (30) for the wave functions:

$$\psi_{l_p}(\mathbf{R}_p)\psi_{l_n}(\mathbf{R}_n)=f_{l_p}(R)Y_{l_p}^{m_p}(\theta_p\phi_p)f_{l_n}(R)Y_{l_n}^{m_n}(\theta_n\phi_n), \qquad \ldots\ldots(32)$$

using (31), and expressing the product of two spherical harmonics of the same angle in terms of a single spherical harmonic and the vector addition coefficients, we get:

$$Y(b)\simeq\sum_{n=0}^{\infty}\sum_{L,L'}(-1)^m i^{L+L'}[(2l_p+1)(2l_n+1)]^{1/2}(n+\tfrac{1}{2})\mathrm{I}_{n+1/2}(2\gamma^2\mathbf{R}^2)$$
$$\times C_{nl_p}(L000)C_{nl_n}(L'000)C_{nl_p}(L0,-m,m_p)C_{nl_n}(L'0,mm_n)$$
$$\times\mathscr{I}_L(\tfrac{1}{2}bR)\quad\mathscr{I}_{L'}(\tfrac{1}{2}bR), \qquad \ldots\ldots(33)$$

where the summation over L and L' extend from $|n-l_p|$ to $|n+l_p|$ and from $|n-l_n|$ to $|n+l_n|$respectively.

The third factor in (29) is given by

$$Z(B)\simeq\int\psi^*_{l_c}(\boldsymbol{\rho}_c)[-V_c\delta(\rho_c-R)]\exp(i\mathbf{B}\boldsymbol{\rho}_c)d\boldsymbol{\rho}_c$$
$$\simeq 4\pi i^{l_c}Y^{*m_c}_{l_c}(\mathbf{b}\,.\,\mathbf{B})(-V_c)f^*_{l_c}(R)\mathscr{I}_{l_c}(BR).$$

Now the value of $\mathscr{B}$ as given by (29) is to be substituted in equation (24). For the factor $\mathscr{F}$, we have the expression (El Nadi 1957)

$$\mathscr{F} \sum_{\substack{l_n m_n \\ l_p m_p}} \left\langle f \,|V_n + V_p|\, i, l_n m_n, l_p m_p \right\rangle \{(2l_n+1)(2l_p+1)\}^{1/2} \exp(-G^2/16\gamma^2)$$

$$\sum_{n=0}^{\infty} (n+\tfrac{1}{2}) \mathrm{I}_{n+\frac{1}{2}}(4\gamma^2 R^2) \sum_{m=-n} (-1)^{m_n+m_p+m} \sum_{LM,\, L'M'} \boldsymbol{C}_{l_n n}(L0, 00)$$

$$C_{l_n n}(L0, -m_n m) C_{l_p n}(L'0, 00) C_{l_p n}(L'0, -m_p m) i^{L+L'} \mathscr{I}_L\left(\frac{gR}{2}\right) \mathscr{I}_L\left(\frac{gR}{2}\right),$$

where:

$$G^2 = (k_d - \tfrac{1}{2}k_\alpha)^2 + 2k_d k_\alpha \sin^2 \tfrac{1}{2}\theta, \text{ and } g^2 = \left(k_\alpha - \frac{M_\tau}{M_R} k_d\right)^2 + 4\frac{M_\tau}{M_R} k_\alpha k_d \sin^2 \tfrac{1}{2}\theta$$

together with the selection rule

$$\mathbf{J}_f = \mathbf{J}_i + \mathbf{l}_p + \mathbf{l}_n + \tfrac{1}{2} + \tfrac{1}{2}.$$

To compare those results with experimental observations we have chosen some data on ^{13}C(d, α)^{11}B, by Marion and Weber (1956), where the observations extend up to about 150°. To determine the value of the capture angular momentum quantum number l_c, we notice that the parity of ^{13}C is odd, that of ^{9}Be is odd, and that of the α-particle is even. Therefore l_c must be even. The value $l_c = 0$ was found to give the best fit with the experimental observations, together with the values $l_p = l_n = 0$. In the forward factor $\mathscr{F}$, the values

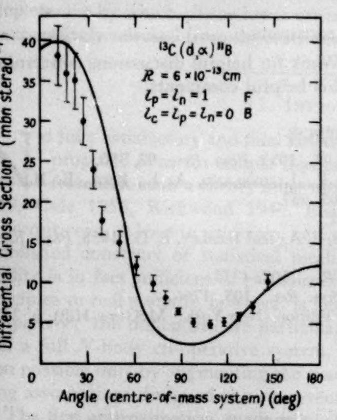

Figure 4. Differential cross section for the ^{13}C (d, α)^{11}B ground state) reaction at a bombarding energy of 2·28 MEV. The heavy line is the theoretical curve defined by $R = 6 \times 10^{-13}$ cm, $l_p = l_n = 1$ for the forward part and $l_c = l_p = l_n = 0$ for the backward contribution. The experimental curve is that of Marion and Weber.

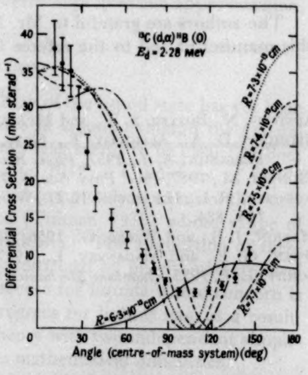

Figure 5. Differential cross section for the ^{13}C(d, α)^{11}B (ground state) reaction at a bombarding energy of 2·28 MEV. The lines drawn refer to the theoretical curves given only by the heavy particle stripping term with $l_c = 0$, $l_p = l_n = 1$, for different values of the nuclear radius.

$l_p = l_n = 1$ were chosen. The value chosen for γ in the calculations is given by $1/\gamma = 6{\cdot}1 \times 10^{-13}$ cm (El Nadi 1957). Figure 4 shows the theoretical curve together with the experimental observations. General agreement is observed. In figure 5 are plotted curves showing the bahaviour of the heavy particle stripping term $\mathscr{B}$, for different radii.

In comparing the theoretical formula with the experimental observations on the ^{13}C(d, α)^{11}B reaction, it was found that, for the amplitude $\mathscr{B}$, the values of the orbital angular momenta of the neutron and proton, ejected from ^{11}B, which gave best fitting, were $l_p = l_n = 0$.

This is not in accord with the expectations of the shell model, as these would be p nucleons, i.e. $l_p = l_n = 1$.

A similar situation was found with the amplitude $\mathscr{F}$ for the ^{12}C(^{3}He, p)^{14}N reaction, where the captured neutron and proton would be expected, according to the shell model, to go into p orbits, i.e. to have $l_p = l_n = 1$. Best fitting was obtained, however, with $l_p = l_n = 0$.

In the above treatment, the spins of the various particles were not completely taken into account, as it is presumed that the modifications which might occur in the final results by doing so would be negligible.

ACKNOWLEDGMENTS

The authors are grateful to Mr. M. Wafik for helpful discussions concerning this manuscript and to the referee for his helpful comments.

REFERENCES

AUSTERN, N., BUTLER, S. T., and MCMANUS, H., 1953, *Phys. Rev.*, **92**, 350.
BROMLEY, D. A., ALMQVIST, E., GOVE, H. E., LITHERLAND, A. E., PAUL, E. B., and FERGUSON, A. J., 1957, *Phys. Rev.*, **105**, 957.
EL NADI, M., 1957, *Proc. Phys. Soc.* A, **70**, 62.
JOHNSTON, R. L., HOLMGREN, H. D., WOLICKI, E. A., and ILLSLEY, E. G., 1958, *Phys. Rev.*, **109**, 884.
MARION, J. B., and WEBER, G., 1956, *Phys. Rev.*, **102**, 1355.
OWEN, G. E., and MADANSKY, L., 1957, *Phys. Rev.*, **105**, 1766.
SCHIFF, L. I., 1955, *Quantum Mechanics*, 2nd Edition (New York: McGraw-Hill), p. 243.

On Reducing the Effect of the Liquid Superposition Approximation

By G. H. A. COLE

Physics Division, Clarke, Chapman & Co. Ltd., Gateshead, 8, Co. Durham

Communicated by H. S. W. Massey; *MS. received* 30*th October* 1958,
in final form 21*st January* 1959

Abstract. A procedure involving a coupling parameter is described by which the pair distribution for a classical condensed system of particles can be calculated without the need for applying the superposition approximation to the triplet distribution itself, although it is still needed for the higher order distributions. For the special case of spherical particles interacting with central forces the approach takes on its simplest form and should provide a feasable means of deriving highly accurate information about the structure of a simple classical liquid under uniform conditions. An extension of the method is suggested for completeness by which all the lower order distribution functions can in principle be successively released from the restrictions of the superposition approximation.

---

§ 1. INTRODUCTION

No fully satisfactory and final kinetic theory of the liquid state has yet been proposed even for simple liquids (such as argon) although the general form that such a theory must ultimately take seems to be clear (de Boer 1949, Cole 1956, Kirkwood 1946, Eisenschitz 1952). Conditions of liquid uniformity can, at least in principle, be discussed completely in terms of the well-established construct of statistical mechanics (Tolman 1938) whose range of validity is in fact sufficient to embrace all equilibria. The application of these principles to real systems, however, is heavily restricted by purely mathematical complexity: the difficulties are particularly severe for liquids where concern is with a full N-body co-operative system. Progress for liquids has, as a result, been possible only by augmenting the exact theory with two independent simplifying assumptions designed to circumvent the mathematical difficulties.

The first approximation, made in conformity with the experimental data for the diffraction of electromagnetic radiation or of neutrons, asserts that the short-range molecular spatial ordering characteristic of simple liquids can be adequately represented in terms of the distribution of molecular pairs in the liquid, described mathematically by the pair distribution function (Gingrich 1943). A knowledge of functions of order higher than the second would seem unnecessary for this purpose, except possibly for very special circumstances (Green 1952, p. 213). To calculate the pair distribution it has always been necessary so far to invoke a second assumption of a purely mathematical character relating explicitly the correlation which exists between the constituents of a group of many particles to the correlation which exists between a representative component particle pair. This relation is generally called the superposition approximation and was first applied to the study of liquids by Kirkwood (1935).

This whole method of approach must clearly be subjected to the most careful scrutiny, and this is all the more necessary in view of the definite and at present unavoidable imprecision of the experimental data. The use of the superposition approximation is suspect and the need to introduce this approximation into the theory more carefully is generally recognised.

A first step in this direction was recently made by Cole (1958), following the earlier work of Born and Green (1949), Yvon (1935), and Kirkwood and Boggs (1942). In the present paper the introduction of the superposition approximation into the theory of the pair distribution for a classical condensed system of particles is considered again, and a procedure is proposed which, although numerically lengthy to apply, does not require the use of the approximation for the triplet distribution. An extension of the method would allow theoretically for all the lower order distribution functions to be successively freed from the approximation, but its actual application is likely to be heavily curtailed by the extreme complexity of the associated numerical work. Nevertheless even the first step, which avoids the application of the superposition approximation to the triplet distribution but which still involves its use in the quadruplet and higher order functions, should be capable of evaluation for the case of central forces, and should provide highly accurate information about the structure of a simple uniform liquid.

§ 2. DISTRIBUTION FUNCTIONS

The classical liquid is represented by N identical particles contained in a volume V, the average particle density being denoted by $n(=N/V)$. The system is at temperature T, and k as usual denotes the Boltzmann constant. Each particle is in interaction with its neighbours, and if $\mathbf{r}_i$ is the configuration vector of the i-th particle then the total interaction potential for the system will be written $\Psi(\mathbf{r}_1, \mathbf{r}_2, \ldots \mathbf{r}_N)$. It will be convenient later to use a reduced potential $X(\mathbf{r}_1, \mathbf{r}_2, \ldots \mathbf{r}_N)$, defined according to the expression $kTX = \Psi$.

The normalized probability for the instantaneous occurrence of $h(<N)$ chosen particles in the configuration $(\mathbf{r}_1, \mathbf{r}_2, \ldots \mathbf{r}_h)$ is written $n^{(h)}(\mathbf{r}_1, \mathbf{r}_2, \ldots \mathbf{r}_h)$, and according to statistical mechanics is defined by:

$$n^h n^{(h)}(\mathbf{r}_1, \mathbf{r}_2, \ldots \mathbf{r}_h) = \frac{1}{(N-h)!}\frac{1}{Z_N}\int \ldots \int \exp(-X)\, d\mathbf{r}_{h+1} \ldots d\mathbf{r}_N. \qquad \ldots\ldots (1)$$

Z_N is here the configurational partition function chosen to normalize the dimensionless distribution $n^{(h)}$ to unity:

$$Z_N = \frac{1}{N!}\int \ldots \int \exp(-X)\, d\mathbf{r}_1\, d\mathbf{r}_2 \ldots d\mathbf{r}_N. \qquad \ldots\ldots (2)$$

A relation between the consecutive functions $n^{(h)}$ and $n^{(h+1)}$ follows immediately from (1):

$$n^{(h)}(\mathbf{r}_1, \mathbf{r}_2, \ldots \mathbf{r}_h) = \frac{1}{V}\int n^{(h+1)}(\mathbf{r}_1, \mathbf{r}_2, \ldots \mathbf{r}_h, \mathbf{r}_{h+1})\, d\mathbf{r}_{h+1}. \qquad \ldots\ldots (3)$$

If $n^{(h+1)}$ is known, then $n^{(h)}$ follows by integration over the configuration volume of the unwanted particle.

The change of $n^{(h)}$ consequent upon an elementary change of the position of any constituent particle of the group h, say particle 1, is obtained from (1) by direct differentiation. The first derivative gives the partial gradient of $n^{(h)}$ at the point, while the second derivative provides a measure of the deviation of $n^{(h)}$ from the local mean value in the region.

The potential function Ψ is temperature independent to very good approximation so that the reduced function X is temperature dependent only through the factor $1/T$. Consequently $n^{(h)}$ is temperature dependent in a way that can be determined by the direct differentiation of equations (1) and (2) with respect to the temperature. For small temperature increments only the first derivative is of interest.

For simple liquids such as will be considered in the present paper these various formulae apply with h set equal to 2, equation (1) then defining the pair distribution, $n^{(2)}$. For these liquids the total potential is to be equated to the sum of the separate pair potentials, each member being concerned with the mutual interaction between a single particle pair. If $\psi(\mathbf{r}_i, \mathbf{r}_j)$ is the mutual force potential for the particles i and j and if we define a corresponding reduced potential function $\chi(\mathbf{r}_i, \mathbf{r}_j)$ according to the relation $kT\chi = \psi$, then

$$\mathrm{X}(\mathbf{r}_1, \mathbf{r}_2, \ldots \mathbf{r}_N) = \sum_{i=1}^{N} \sum_{j>i}^{N} \chi(\mathbf{r}_i, \mathbf{r}_j). \qquad \ldots\ldots(4)$$

In what follows it will always be assumed that (4) is inserted into equations (1) and (2).

Three expressions involving $n^{(2)}$ will be of interest later. The first is the primitive recurrence relation (3) which now becomes:

$$n^{(2)}(\mathbf{r}_1, \mathbf{r}_2) = \frac{1}{V} \int n^{(3)}(\mathbf{r}_1, \mathbf{r}_2, \mathbf{r}_3)\, d\mathbf{r}_3. \qquad \ldots\ldots(5)$$

The second is the non-linear gradient equation relating the effect of small movements of particle 1 of the pair on the pair distribution, and obtained by differentiating (1) once with respect to $\mathbf{r}_1$, with $h = 2$. Using (4) the resulting expression can be arranged into the form given by Born and Green (1949):

$$\frac{\partial n^{(2)}(\mathbf{r}_1, \mathbf{r}_2)}{\partial \mathbf{r}_1} + \frac{\partial \chi(\mathbf{r}_1, \mathbf{r}_2)}{\partial \mathbf{r}_1} n^{(2)}(\mathbf{r}_1, \mathbf{r}_2) = -n \int \frac{\partial \chi(\mathbf{r}_1, \mathbf{r}_3)}{\partial \mathbf{r}_1} n^{(3)}(\mathbf{r}_1, \mathbf{r}_2, \mathbf{r}_3)\, d\mathbf{r}_3. \qquad \ldots\ldots(6)$$

For the general particle interaction this is a vector equation having three component equations, but for the special case of the central force field (spherical particles) it reduces to a scalar equation showing symmetry about the axis of the particle pair.

The third expression for $n^{(2)}$ relates the dependence on small temperature increments. From equations (1), (2), and (4) it follows that:

$$\frac{\partial n^{(2)}(\mathbf{r}_1, \mathbf{r}_2)}{\partial T} = n^{(2)}(\mathbf{r}_1, \mathbf{r}_2)\{\chi(\mathbf{r}_1, \mathbf{r}_2) + \mathscr{A}\} + 2n \int \chi(\mathbf{r}_1, \mathbf{r}_3) n^{(3)}(\mathbf{r}_1, \mathbf{r}_2, \mathbf{r}_3)\, d\mathbf{r}_3$$
$$+ n^2 \iint \chi(\mathbf{r}_3, \mathbf{r}_4) n^{(4)}(\mathbf{r}_1, \mathbf{r}_2, \mathbf{r}_3, \mathbf{r}_4)\, d\mathbf{r}_3\, d\mathbf{r}_4 \qquad \ldots\ldots(7)$$

where

$$\mathscr{A} = \frac{1}{T} \iint \chi(\mathbf{r}_1, \mathbf{r}_2) n^{(2)}(\mathbf{r}_1, \mathbf{r}_2)\, d\mathbf{r}_1\, d\mathbf{r}_2. \qquad \ldots\ldots(7a)$$

Each term appearing on the right hand side of (7) refers to the temperature T.

The equations for the pair distribution are to be solved subject to the boundary conditions:

$$n^{(2)}(\mathbf{r}_1,\mathbf{r}_2)\to 0 \quad (|\mathbf{r}_1-\mathbf{r}_2|\to 0): \quad n^{(2)}(\mathbf{r}_1,\mathbf{r}_2)\to 1 \quad (|\mathbf{r}_1-\mathbf{r}_2|\to\infty) \qquad \ldots\ldots(8a)$$

$$n^{(2)}(T)\to 1 \quad (T\to\infty). \qquad \ldots\ldots(8b)$$

In conclusion it is noted that the physical interpretation of $n^{(2)}$ is made in terms of molecular dynamics by equating the factor $(-kT\log n^{(2)})$ to the potential of the average force which determines the liquid particle motion.

§ 3. SUPERPOSITION AND THE INTERPARTICLE FORCE

The total impracticability of the direct determination of $n^{(2)}$ by evaluating the integral in (1) is well known: alternatively equations (5), (6), and (7) can be employed only if the distributions $n^{(3)}$ and $n^{(4)}$ are known either completely or explicitly in terms of $n^{(2)}$. Theory cannot directly provide this information at the present time although ultimately it might be inferred numerically from mathematical models involving electronic computational techniques (Alder and Wainright 1957, Wood and Jackobson 1957). It has, therefore, become customary to augment the exact theory with the superposition approximation in order that $n^{(2)}$ may be calculated. Applied to the triplet, quadruplet, and quintuplet functions the approximation asserts the validity of the expressions:

$$n^{(3)}(\mathbf{r}_1,\mathbf{r}_2,\mathbf{r}_3)=n^{(2)}(\mathbf{r}_1,\mathbf{r}_2)n^{(2)}(\mathbf{r}_1,\mathbf{r}_3)n^{(2)}(\mathbf{r}_2,\mathbf{r}_3) \qquad \ldots\ldots(9a)$$

$$n^{(4)}(\mathbf{r}_1,\mathbf{r}_2,\mathbf{r}_3,\mathbf{r}_4)=n^{(3)}(\mathbf{r}_1,\mathbf{r}_2,\mathbf{r}_3)n^{(2)}(\mathbf{r}_1,\mathbf{r}_4)n^{(2)}(\mathbf{r}_2,\mathbf{r}_4)n^{(2)}(\mathbf{r}_3,\mathbf{r}_4) \qquad \ldots\ldots(9b)$$

$$n^{(5)}(\mathbf{r}_1,\mathbf{r}_2,\mathbf{r}_3,\mathbf{r}_4,\mathbf{r}_5)=n^{(4)}(\mathbf{r}_1,\mathbf{r}_2,\mathbf{r}_3,\mathbf{r}_4)\left(\prod_{i=1}^{4}n^{(2)}(\mathbf{r}_i,\mathbf{r}_5)\right). \qquad \ldots\ldots(9c)$$

The superposition approximation is not exact because it neglects the particle interaction. This is seen immediately by inserting (9a) into (5): the resulting integral equation is satisfied only by a quantity which is independent of the particle separation distance. The interparticle force plays a less critical rôle in equation (6) and Kirkwood, Lewinson, and Alder (1952) have shown the solution to have physical interest for data adapted (though rather crudely) to argon. Cole (1958) has suggested instead the use of a second order equation in place of (6).

In what follows we shall consider an alternative mathematical procedure involving a coupling parameter which allows the effect of the interparticle force to be gradually accounted for, starting from the case with no mutual interaction ($\chi=0$; $\psi=0$ or $T=\infty$) where the relations (9) are exact.

§ 4. COUPLING PARAMETER

Suppose the temperature of the actual condensed system is T_{R}: then the corresponding reduced potential function is $\chi_{\mathrm{R}}=\psi/kT_{\mathrm{R}}$. If the particle interaction for all the particles of the system is (hypothetically) reduced, the situation can be described by the introduction of a coupling parameter γ, which is a continuous function in the range 0 to 1. The reduced potential for any value of γ is then $\chi=\gamma\chi_{\mathrm{R}}$, so that $0\leqslant\chi\leqslant\chi_{\mathrm{R}}$. Any particular value of χ obtained using the coupling parameter can be obtained without its use by a suitable choice of the temperature. A formal correspondence, then, can be made between values of the coupling parameter in the range $0 \leqslant \gamma \leqslant 1$, and values of the temperature in the range $T_R \leqslant T \leqslant \infty$. When $\gamma = 0$ the particles of all move independently with no mutul interaction; when $\gamma = 1$ the coupling is complete as in the actual system. This procedure is an extension of that used earlier by Kirkwood and Boggs (1942) (see also Kirkwood, Lewinson, and Alder (1952)): but whereas these authors considered variable coupling between just one particle and the remainder, we now extend the technique to apply to all particles simultaneously.

The variation of the distribution functions due to changes of γ can be inferred directly from (1) by inserting $\chi = \gamma\chi_R$ and differentiating the resulting expression with respect to γ. Alternatively the effect of one differentiation can be written down directly by reference to the temperature variation equations, viz. (7) for $n^{(2)}$, if the equivalence $T(\partial/\partial T) \sim -\gamma(\partial/\partial\gamma)$ is used. For the pair and triplet distributions (i.e. h successively equated to 2 and 3 in equation (1)), the changes due to an elementary increment $\Delta\gamma$ of the coupling parameter are given respectively by:

$$\frac{\partial n^{(2)}(\mathbf{r}_1, \mathbf{r}_2; \gamma)}{\partial\gamma} = -n^{(2)}(\mathbf{r}_1, \mathbf{r}_2)\{\chi_R(\mathbf{r}_1, \mathbf{r}_2) + \mathscr{A}_R\} + n\int\left(\sum_{i=1}^{2} \chi_R(\mathbf{r}_i, \mathbf{r}_3)\right) n^{(3)}(\mathbf{r}_1, \mathbf{r}_2, \mathbf{r}_3)\, d\mathbf{r}_3$$

$$+ n^2 \iint \chi_R(\mathbf{r}_3, \mathbf{r}_4) n^{(4)}(\mathbf{r}_1, \mathbf{r}_2, \mathbf{r}_3, \mathbf{r}_4)\, d\mathbf{r}_3\, d\mathbf{r}_4 \qquad \ldots\ldots(10a)$$

and

$$\frac{\partial n^{(3)}(\mathbf{r}_1, \mathbf{r}_2, \mathbf{r}_3; \gamma)}{\partial\gamma} = -n^{(3)}(\mathbf{r}_1, \mathbf{r}_2, \mathbf{r}_3)\left\{\sum_{i=j}^{3}\sum_{j>i}^{3} \chi_R(\mathbf{r}_i, \mathbf{r}_j) + \mathscr{A}_R\right\}$$

$$+ n\int\left(\sum_{i=1}^{3} \chi_R(\mathbf{r}_i, \mathbf{r}_4)\right) n^{(4)}(\mathbf{r}_1, \mathbf{r}_2, \mathbf{r}_3, \mathbf{r}_4)\, d\mathbf{r}_4$$

$$+ n^2 \iint \chi_R(\mathbf{r}_4, \mathbf{r}_5) n^{(5)}(\mathbf{r}_1, \mathbf{r}_2, \mathbf{r}_3, \mathbf{r}_4, \mathbf{r}_5)\, d\mathbf{r}_4\, d\mathbf{r}_5. \qquad \ldots\ldots(10b)$$

$\mathscr{A}_R$ is obtained from (7*a*) by replacing χ by χ_R. In each expression (10) the right hand side of the equation refers to the value γ of the coupling parameter.

Macroscopic effects such as phase change which would be expected to result from any actual reduction of coupling such as we theoretically postulate are as difficult to assess in the present connection as with any particle-in-box idealization of matter. However, the equations of § 2 can be expected to apply also in the interphase region. Because of the correspondence noted above between coupling parameter and the inverse of temperature, it is plausible to expect that the equations themselves will account, at least crudely, for any effects which might be difficult to reconcile with liquid structure during the progress of the mathematical procedure of variable coupling.

§ 5. SOLUTION PROCEDURE

It will now be explained how the pair distribution can be calculated without the use of the superposition approximation in the form (9*a*).

5.1. *Negligible Coupling*

If X appearing in (1) is sufficiently small (i.e. $X \gg X^2$, and γ is virtually zero) the integrations necessary for the evaluation of $n^{(2)}$, $n^{(3)}$, . . . can proceed with little difficulty, since the associated exponential term need be expanded only as far as the first power in X. In these circumstances we find for $n^{(2)}$ the expression:

$$n^{(2)}(\mathbf{r}_1, \mathbf{r}_2) = \frac{\left[1 - \chi(\mathbf{r}_1, \mathbf{r}_2) - n\int\left(\sum_{i=1}^{2} \chi(\mathbf{r}_i, \mathbf{r}_3)\right) d\mathbf{r}_3 - n^2 \iint \chi(\mathbf{r}_3, \mathbf{r}_4)\, d\mathbf{r}_3\, d\mathbf{r}_4\right]}{\left[1 - \frac{n^2}{2}\iint \chi(\mathbf{r}_1, \mathbf{r}_2)\, d\mathbf{r}_1\, d\mathbf{r}_2\right]} \qquad \ldots\ldots(11a)$$

and for $n^{(3)}$ the expression:

$$n^{(3)}(\mathbf{r}_1, \mathbf{r}_2, \mathbf{r}_3) = \frac{\left[1 - \sum_{i=1}^{3} \sum_{j>i}^{3} \chi(\mathbf{r}_i, \mathbf{r}_j) - n\int\left(\sum_{i=1}^{3} \chi(\mathbf{r}_i, \mathbf{r}_4)\right) d\mathbf{r}_4 - \frac{n^2}{2} \iint \chi(\mathbf{r}_4, \mathbf{r}_5)\, d\mathbf{r}_4\, d\mathbf{r}_5\right]}{\left[1 - \frac{n^2}{2}\iint \chi(\mathbf{r}_1, \mathbf{r}_2)\, d\mathbf{r}_1\, d\mathbf{r}_2\right]} \qquad \ldots\ldots(11b)$$

The remaining lower order functions can be similarly found, but will not be written down since they become successively more complex. A sensitive test of the range of γ for which the relations (11) are valid is provided by the recurrence integral (5).

5.2. *Appreciable Coupling*

The expressions (11) do not apply if γ is greater than some very small value, say γ_1, and the procedure of including more terms in the exponential expansion has only limited value. Instead for $\gamma > \gamma_1$ it is more profitable to make appeal to the equations (10) together with the first order differential equation (6). If the triplet distribution is known for some value of the coupling parameter, such as $\gamma = \gamma_1$, then (10*b*) allows this distribution to be inferred at the neighbouring value $\gamma_1 + \Delta\gamma_1$, and written $n^{(3)}(\gamma_1 + \Delta\gamma_1)$, if the functions $n^{(4)}$ and $n^{(5)}$ are also known at $\gamma = \gamma_1$. By writing $\chi = (\gamma_1 + \Delta\gamma_1)\chi_R$ in (6), and using the already inferred triplet function $n^{(3)}(\gamma_1 + \Delta\gamma_1)$, this equation involves the unknown pair function $n^{(2)}(\gamma_1 + \Delta\gamma_1)$. The pair distribution corresponding to the coupling parameter $(\gamma_1 + \Delta\gamma_1)$ can therefore be calculated by solving the resulting first order differential equation subject to the boundary conditions (8*a*).

With $n^{(2)}(\gamma_1 + \Delta\gamma_1)$ and $n^{(3)}(\gamma_1 + \Delta\gamma_1)$ both known the procedure can be repeated for a further coupling increment $\Delta\gamma_2$, say, provided the quadruplet and quintuplet distributions at $(\gamma_1 + \Delta\gamma_1)$ are determined using the superposition approximation in the form (9*b*) and (9*c*).

Starting from the value $\gamma = \gamma_1$, where conditions of inappreciable coupling still apply, the procedure can be repeated for successive increments $\Delta\gamma$ until the final interval is used which gives γ its maximum value unity. The accuracy of the calculation at each point can be tested by making appeal to (5).

The simplest case is that for central forces, when (6) reduces to a scalar equation. Although involving only elementary mathematical operations the numerical work associated with the procedure is certain to be very lengthy. However, it will be realized that the superposition approximation has not now been involved explicitly in the triplet distribution and this should lead to greatly improved accuracy in the calculation of $n^{(2)}$.

§ 6. Extension in Principle

In principle the method outlined in the last section can be extended to take on a form allowing all the lower order distribution functions to be freed from the superposition approximation. This would involve making an appeal to the further members of the sequence (10), such as $\partial n^{(4)}/\partial \gamma$ and $\partial n^{(5)}/\partial \gamma$, together with further members of the sequence (11), such as $n^{(4)}$ and $n^{(5)}$, applying for very small $\gamma(\leqslant \gamma_1)$. What has been said in the last section about the determination of $n^{(3)}$ using (10*b*) can be repeated essentially for $n^{(4)}$, and then for $n^{(5)}$ with the difference that, for $n^{(4)}$ the superposition approximation must be used for the functions $n^{(5)}$ and $n^{(6)}$ while for $n^{(5)}$ it must instead be applied to $n^{(6)}$ and $n^{(7)}$. In this way the superposition approximation need not, in principle, appear explicitly at all in either of the equations (10).

One small simplification is now likely to arise, viz. that because the superposition approximation is not invoked for $n^{(4)}$ it may be sufficient in each of the successive evaluations of $n^{(2)}$ throughout the range $\gamma_1 \leqslant \gamma \leqslant 1$ to use (10*a*) directly, without resorting to the differential equation (6). Although this modified procedure involves only the evaluation of integrals, they are multiple integrals and the associated numerical work must be severe.

These arguments of extension are related to the notorious problem of the evaluation of the partition function. They have the important advantage that approximations are introduced (superposition approximation) in a controlled way, and may be steadily eliminated as the techniques of numerical evaluation and the stamina of the operator both improve.

§ 7. Conclusions

A procedure has been proposed by which the need to invoke the superposition approximation in connection with the triplet distribution is avoided in the calculation of the pair distribution for a condensed classical system of particles. The method involves the use of a coupling parameter which allows the total interaction between all the particles of the system to be varied continuously between the value zero (no coupling) and that value which corresponds to the coupling which describes the actual system.

The approach involves the evaluation of three single and one double integral, and the solution of a linear first order inhomogeneous differential equation at each successive step of a sequence of increasing partial interparticle couplings. Although involving only elementary mathematics any numerical evaluation will prove lengthy, even for spherical particles.

The procedure has a natural extension to include distributions of higher order than the triplet but any practical interest is damped by extreme numerical complexity. Nevertheless the first step of the procedure, outlined in § 5, should, for spherical particles, prove practicable to carry through with the aid of standard computer techniques, and can be expected to result in highly accurate data for the structure of a simple uniform liquid.

REFERENCES

ALDER, B., and WAINWRIGHT, T., 1957, *J. Chem. Phys.*, **27**, 1208.
DE BOER, J., 1949, *Rep. Progr. Phys.*, **12**, 305 (London: Physical Society).
BORN, M., and GREEN, H. S., 1949, *A General Kinetic Theory of Liquids* (Cambridge: University Press).
COLE, G. H. A., 1956, *Rep. Progr. Phys.*, **19**, 1 (London: Physical Society).
—— 1958, *J. Chem. Phys.*, **28**, 912.
EISENSCHITZ, R., 1952, *Proc. Roy. Soc.* A, **215**, 29.
GINGRICH, N. S., 1943, *Rev. Mod. Phys.*, **15**, 90.
GREEN, H. S., 1952, *Molecular Theory of Fluids* (Amsterdam: North-Holland Pub. Co.).
KIRKWOOD, J. G., 1935, *J. Chem. Phys.*, **3**, 300.
—— 1946, *Ibid.*, **14**, 180.
KIRKWOOD, J. G., and BOGGS, M. B., 1942, *J. Chem. Phys.*, **10**, 394.
KIRKWOOD, J. G., LEWINSON, V. A., and ALDER, B. J., 1952, *J. Chem. Phys.*, **20**, 929.
TOLMAN, R. C., 1938, *Principles of Statistical Mechanics* (Oxford : University Press).
WOOD, W. W., and JACKOBSON, J. D., 1957, *J. Chem. Phys.*, **27**, 1207.
YVON, J., 1935, *Actualités Scientifiques et Industrielles* (Paris: Hermann & Cie).

The Energy Levels of ^{18}F

By S. HINDS and R. MIDDLETON
Atomic Weapons Research Establishment, Aldermaston, Berks.

Communicated by K. W. Allen; MS. received 13th October 1958

Abstract. The energy levels of ^{18}F have been investigated using the reactions ^{16}O(^{3}He, p)^{18}F and ^{19}F(^{3}He, α)^{18}F. In both cases magnetic analysis was employed and the incident ^{3}He energy was 5·9 Mev. The excitation energies of 40 levels have been determined below 7·493 Mev.

---

§ 1. Introduction

The positions and properties of the low lying even parity states of ^{18}F have been predicted by Elliott and Flowers (1955) in the course of their detailed shell model calculations of the structure of nuclei of mass 18 and 19. Until quite recently, however, few experimental investigations of the level structure of ^{18}F have been undertaken. Using conventional projectiles such as protons and deuterons it is difficult to excite ^{18}F, but if ^{3}He is used the reactions ^{16}O(^{3}He, p)^{18}F and ^{19}F(^{3}He, α)^{18}F are very convenient, particularly if magnetic analysis is employed. These reactions excite both $T=0$ and $T=1$ states and differ in this respect from the ^{20}Ne(d, α)^{18}F reaction and some resonance reactions such as ^{14}N + α, which have previously been used to investigate ^{18}F.

Energy levels have been observed in ^{18}F previously by Middleton and Tai (1951) using the ^{20}Ne(d, α)^{18}F reaction, by El-Bedewi and Hussein (1957) and also by Almqvist, Bromley and Kuehner (1958) from an investigation of the γ-rays from the ^{16}O(^{3}He, p)^{18}F and ^{14}N + α reactions. A number of states above 5·6 Mev have been reported by Herring (1957), Phillips (1958) and Ahnlund (1957) from observations of resonances in the reactions ^{14}N + α and ^{17}O + p.

The excitation energies of 40 levels of ^{18}F are reported in this communication. These have been determined from an investigation by magnetic analysis of the ^{3}He reactions with ^{16}O and ^{19}F.

§ 2. Experimental Procedure

Singly ionized ^{3}He ions were accelerated in the Aldermaston Van de Graaff generator to about 5·9 Mev and after deflection through 90° by a 60 cm radius magnet, were allowed to strike thin targets containing oxygen and fluorine. Immediately prior to the target the beam was defined by a slit to 2 mm wide by ½ mm high and reduced in intensity to about 0·5 μa. The charged reaction products were analysed by a broad-range magnetic spectrograph capable of an energy resolution in excess of 1 part in 1000, a description of which will be published later. By rotating the spectrograph about the target chamber, it was possible to make exposures at various angles. At least four exposures were made at different angles using both the oxygen and the fluorine targets. Average exposure strengths were 1000 microcoulombs for oxygen and 2000 microcoulombs for fluorine.

The oxygen targets were prepared by evaporation and consisted of thin (about $20\,\mathrm{g\,cm^{-2}}$) self-supporting films of pure silica and silica containing separated ^{28}Si isotope. To prevent the accumulation of electrostatic charge on the target during bombardment, a $20\,\mu\mathrm{g\,cm^{-2}}$ layer of gold was evaporated on to its surface. The fluorine target was prepared by evaporating about $30\,\mu\mathrm{g\,cm^{-2}}$ of calcium fluoride on to a $8\,\mu\mathrm{g\,cm^{-2}}$ film of carbon. As for the oxygen target, a small quantity of gold was also evaporated on to the surface.

§ 3. RESULTS

The energy levels of ^{18}F have been determined up to 4·350 MeV from an investigation of the ^{16}O(^{3}He, p)^{18}F reaction and up to 7·493 MeV from the ^{19}F(^{3}He, α)^{18}F reaction. In both cases spectra have been measured at four angles at least.

A typical proton spectrum obtained at 30° using a separated ^{28}Si silica target is shown in figure 1. The groups labelled 0 to 16 were identified by their rate of change of energy with angle as arising from the reaction ^{16}O(^{3}He, p)^{18}F. In a similar manner the majority of the remaining weak groups were identified as due to ^{28}Si, but these have not been labelled. It may be noticed that group 10 is missing from the figure. This is because at this particular angle of observation it was completely masked by very intense groups of elastically scattered ^{3}He particles. The strong and rather broad group labelled 'elastic protons' is the recoil proton group arising from the elastic scattering of ^{3}He by hydrogen occluded in the target.

Group 3, which is extremely weak, was initially confused with the large number of weak groups due to ^{28}Si and was only identified after observation of the 1·08 MeV level in the ^{19}F(^{3}He, α)^{18}F reaction. However, this assignment was confirmed after extensive measurements had been made on groups 1, 2, 3 and 4 at twelve or more angles using both silica targets and targets prepared from molybdenum dioxide. At an angle of 40°, group 3 shows more clearly, and a portion of the spectrum obtained at this angle is shown in figure 2.

The energy of the ^{3}He beam was determined by making a short duration exposure at 90° to record the elastically scattered particles. The mean of four determinations corresponding to the elastically scattered groups from gold, silicon, oxygen and carbon gave a value of $5{\cdot}896 \pm 0{\cdot}015$ MeV. Using this value the ground state Q-value of the ^{16}O(^{3}He, p)^{18}F reaction was calculated to be $2{\cdot}044 \pm 0{\cdot}015$ MeV. This is in agreement with the value of 2·040 MeV expected from the mass defects. The excitation energies of the 17 groups observed from this reaction are listed in column (2) of the table. It may be noted that the quoted experimental error of ± 10 keV is less than that of the ground state Q-value. This is because the major uncertainty in the latter lies in the determination of the beam energy and this has little effect on excitation energies which are obtained from differences between Q-values.

A spectrum of the α-particles from the reaction ^{19}F(^{3}He, α)^{18}F, obtained at 15°, is shown in figure 3. As in the case of the ^{16}O(^{3}He, p)^{18}F reaction, groups were identified by their energy variation with angle and those assigned to ^{18}F are labelled numerically. The strong group of α-particles at a radius of

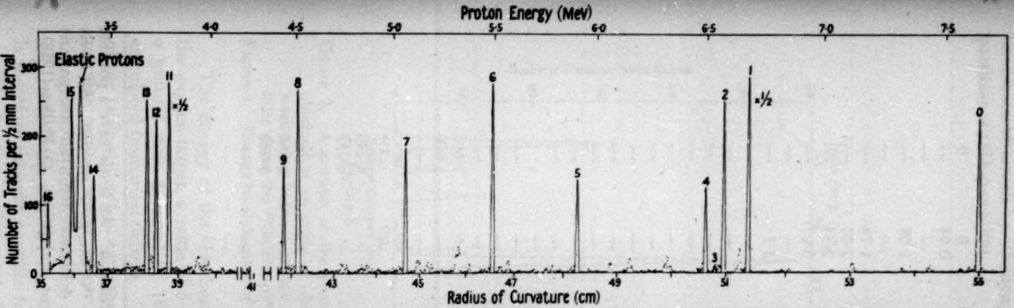

Figure 1. A proton energy spectrum from the reaction $^{16}O(^3He, p)^{18}F$ obtained at an angle of 30° with a field setting of 7281 gauss. The target consisted of a thin film of silica containing separated ^{28}Si and the incident ^3He energy was 5·896 MEV. The groups labelled numerically correspond to states of ^{18}F and the large number of weak unlabelled groups arise from the reaction $^{28}Si(^3He, p)^{30}P$.

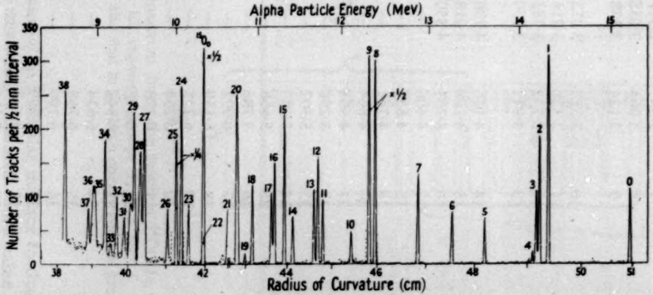

Figure 3. An α-particle spectrum from the reaction $^{19}F(^3He, \alpha)^{18}F$ obtained at an angle of observation of 15°. The target consisted of a thin film of CaF_2 deposited on a carbon backing, the spectrograph field setting was 11 039 gauss and the incident ^3He energy 5·870 MEV.

Energy Levels of ^{18}F

Group No.	(1)	(2)	(3)	(4)	(5)
0	0	0	0	0	0
1	0·942	0·934	—	0·94	—
2	1·043	1·038	1·05	—	—
3	1·086	1·076	—	1·08	—
4	1·130	1·119	—	—	—
5	1·692	1·698	1·83	1·74	—
6	2·107	2·096	2·20	2·09	—
7	2·531	2·517	2·61	2·54	—
8	3·064	3·055	—	3·07	—
9	3·134	3·128	—	—	—
			3·23	3·3	—
10	3·357	3·352	—	—	—
11	3·726	3·715	—	—	—
12	3·792	3·783	—	—	—
13	3·841	3·830	—	—	—
			3·92	—	—
14	4·116	4·108	—	—	—
15	4·229	4·218	—	—	—
16	4·361	4·350	—	—	—
17	4·400	—	4·42	—	—
18	4·651	—	—	—	—
19	4·741	—	—	—	—
20	4·844	—	—	—	—
21	4·964	—	5·01	—	—
22	5·295	—	—	—	—
23	5·502	—	—	—	—
24	5·603	—	5·61	5·6	5·602
25	5·668	—	—	—	5·670
26	5·786	—	—	—	—
27	6·092	—	—	—	—
28	6·139	—	—	—	—
29	6·235	—	—	—	6·240
30	6·264	—	—	—	6·255
31	6·376	—	—	—	—
32	6·472	—	—	—	—
33	6·548	—	—	—	6·564
34	6·634	—	—	—	6·650
35	6·765	—	—	—	—
36	6·790	—	—	—	—
37	6·859	—	—	—	—
38	7·184	—	—	—	—
39	7·315	—	—	—	—
40	7·493	—	—	—	—

(1) Present investigation, from the ^{19}F(^{3}He, α)^{18}F reaction. All levels have a possible error of ± 15 kev ; (2) Present investigation, from the ^{16}O(^{3}He, p)^{18}F reaction. All levels have a possible error of ± 10 kev except for that at 4·350 Mev for which the error is ± 15 kev. (3) Middleton and Tai (1951). (4) Almqvist *et al.* (1958). (5) Phillips (1958): only the sharp levels are tabulated.

curvature of about 42 cm is due to an oxygen impurity in the target and arises from the reaction ^{16}O(^{3}He, α)^{15}O leading to the ground state of ^{15}O. At this particular angle of observation, this group completely obscures group 22. The background of α-particles extending from a radius of about 41 cm to the low-energy end of the plate is probably due to very broad virtual states which have been observed by Phillips, and to the confusion of spuriously scattered ^{3}He particles with α-particles.

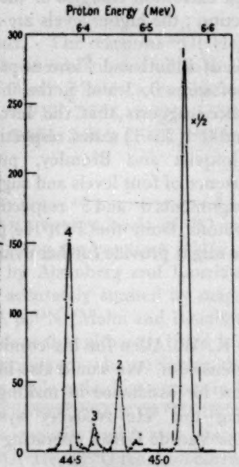

Figure 2.

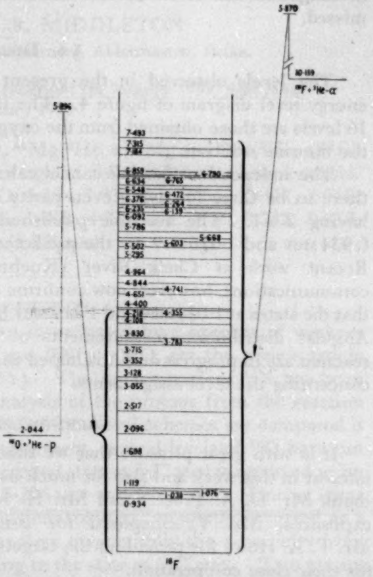
5·870
10·159
^{19}F + ^{3}He – α
5·896
2·044
^{16}O + ^{3}He – p
7·493
7·315
7·184
6·859
6·790
6·765
6·634
6·548
6·472
6·376
6·264
6·235
6·139
6·092
5·786
5·668
5·603
5·502
5·295
4·964
4·844
4·741
4·651
4·400
4·355
4·218
4·108
3·830
3·783
3·715
3·352
3·128
3·055
2·517
2·096
1·698
1·119
1·038
1·076
0·934
^{18}F

Figure 4.

Figure 2. A portion of the proton energy spectrum from the reaction ^{16}O(^{3}He, p)^{18}F obtained at an angle of observation of 40° showing groups 1, 2, 3 and 4. The weak group between groups 1 and 2, and also that in the high energy edge of group 1, arise from the ^{28}Si(^{3}He, p)^{30}P reaction.

Figure 4. Energy level diagram of ^{18}F.

The energy of the ^{3}He beam was measured in a similar manner to that for the oxygen target, a value of $5{\cdot}870 \pm 0{\cdot}015$ Mev being obtained. This value gave a ground state *Q*-value of $10{\cdot}159 \pm 0{\cdot}015$ Mev which agrees with 10·164 Mev calculated from mass defects. The energy levels obtained are listed in column (1) of the table and are in agreement with those measured from the ^{16}O(^{3}He, p)^{18}F reaction within about 10 kev. This difference is larger than usual and is thought to be due to the high spectograph field strength required to analyse the α-particles from the ^{19}F(^{3}He, α)^{18}F reaction. An experimental error of ± 15 kev is therefore thought possible for the levels obtained from the latter reaction.

The energy levels reported by other workers are listed in columns (3), (4) and (5) of the table and as can be seen, are not inconsistent with the present results. The larger number of levels observed in the present investigation is probably due to improved resolution. It may be noted that the 1·05 Mev level reported by Middleton and Tai cannot be identified with the 1·076 Mev level since the latter has been given a $T=1$ assignment by Almqvist *et al.* and consequently should not be excited in the ^{20}Ne(d, α)^{18}F reaction. It should be stressed that only the narrow virtual levels have been seen in the present investigation and levels several hundred kilovolts wide may easily have been missed.

§ 4. Discussion

The levels observed in the present investigation are summarized in the energy level diagram of figure 4. The indicated excitation energies of the first 16 levels are those obtained from the oxygen reaction ; the higher levels are from the fluorine reaction.

The independent particle model calculations of Elliott and Flowers predict there to be three low-lying even parity states of spins 0, 3 and 5, the 0 state having $T=1$. The available published evidence suggests that the levels at 0·934 Mev and 1·076 Mev are the predicted 3^+ and 0^+ ($T=1$) states respectively. Recent work at Chalk River (Kuehner, Almqvist and Bromley, private communication), however, now confirms the existence of four levels and suggests that the states at 1·038 Mev and 1·119 Mev have assignments 0^- and 5^+ respectively. Angular distribution measurements of the protons from the ^{16}O(^{3}He, p)^{18}F reaction are in progress and it is hoped that these might provide further evidence concerning the level assignments.

Acknowledgments

It is with great pleasure that we thank Dr. K. W. Allen for his continued interest in this work and also for much useful discussion. We would also like to thank Mr. D. A. Procter and Mr. H. Marchant for assistance in making the exposures, Mr. V. Shepherd for constructing the ^{3}He recovery system, Mr. F. A. Howe for providing the targets and the Van de Graaff operating staff for their close co-operation.

References

Ahnlund, K., 1957, *Phys. Rev.*, **106**, 124.

Almqvist, E., Bromley, D. A., and Kuehner, J. A., 1958, *Bull. Amer. Phys. Soc.*, Series II, **3**, 27.

El-Bedewi, F. A., and Hussein, I., 1957, *Proc. Phys. Soc.* A, **70**, 233.

Elliott, J. P., and Flowers, B. H., 1955, *Proc. Roy. Soc.* A, **229**, 536.

Herring, D. F., 1957, *Bull. Amer. Phys. Soc.*, Series II, **2**, 303.

Middleton, R., and Tai, C. T., 1951, *Proc. Phys. Soc.* A, **64**, 801.

Phillips, W. R., 1958, *Phys. Rev.*, **110**, 1408.

The Energy Levels of ^{15}O, ^{23}Mg and ^{27}Si

By S. HINDS and R. MIDDLETON
Atomic Weapons Research Establishment, Aldermaston, Berks.

Communicated by K. W. Allen; *MS. received* 13*th January* 1959, *final form* 5*th February* 1959

Abstract. The reactions ^{16}O(^{3}He, α)^{15}O, ^{24}Mg(^{3}He, α)^{23}Mg and ^{28}Si(^{3}He, α)^{27}Si have been investigated at an incident energy of 5·8 Mev by magnetic analysis. The following levels were observed: ^{15}O, 5·174, 5·233 Mev; ^{23}Mg, 0·451, 2·048, 2·356, 2·712, 2·768, 2·904, 3·792, 3·856, 3·968, 4·353 Mev; ^{27}Si, 0·782, 0·958, 2·165, 2·651, 2·866, 2·908, 3·540, 3·800, (4·13) Mev.

§ 1. Introduction

The energy levels of ^{15}O have been investigated by a number of workers using the reactions ^{14}N(d, n)^{15}O and ^{14}N(p, γ)^{15}O, see the review article by Ajzenberg and Lauritsen (1955). The mirror nucleus ^{15}N has been more accurately studied by magnetic analysis of the protons from the reaction ^{14}N(d, p)^{15}N (Malm and Beuchner 1950). If the level schemes are compared it is evident that although there is some agreement, several levels of ^{15}O have not been observed. In particular, the first excited state at 5·27 Mev is reported to be single while a doublet occurs in ^{15}N at 5·276 Mev and 5·305 Mev. During some recent investigations of ^{3}He induced reactions, oxygen frequently occurred as a target impurity and it was possible to analyse magnetically the α-particles from the ^{16}O(^{3}He, α)^{15}O reaction corresponding to the state at 5·27 Mev. Two groups of α-particles were observed corresponding to states at 5·174 Mev and 5·233 Mev.

The nuclei ^{23}Mg and ^{27}Si have not previously been investigated, probably because they are difficult to excite with conventional projectiles such as protons and deuterons. However, with ^{3}He, they can conveniently be studied from the reactions ^{24}Mg(^{3}He,α)^{23}Mg and ^{28}Si(^{3}He, α)^{27}Si. The level schemes of the corresponding mirror nuclei, ^{23}Na and ^{27}Al, are accurately known and it has therefore been possible to make two new mirror nuclei comparisons.

§ 2. Experimental Procedure

Singly charged ^{3}He ions accelerated to energies of about 5·8 Mev in the Aldermaston Van de Graaff generator, were used to bombard thin targets containing ^{16}O, ^{24}Mg and ^{28}Si. The ^{28}Si targets consisted of evaporated films of pure silica or silica containing separated ^{28}Si isotope. To prevent the accumulation of electrostatic charge on the target during bombardment, a very thin layer of gold was evaporated on one surface. Due to the high oxygen content of these targets, they were also used for the ^{16}O(^{3}He, α)^{15}O investigation. The magnesium targets were also prepared by evaporation (Hinds and Middleton 1959) and consisted of about 20 μg cm^{-2} of separated ^{24}Mg isotope deposited on thin carbon backings. Again, they proved to be useful oxygen targets due to the high impurity content of oxygen caused by oxidation.

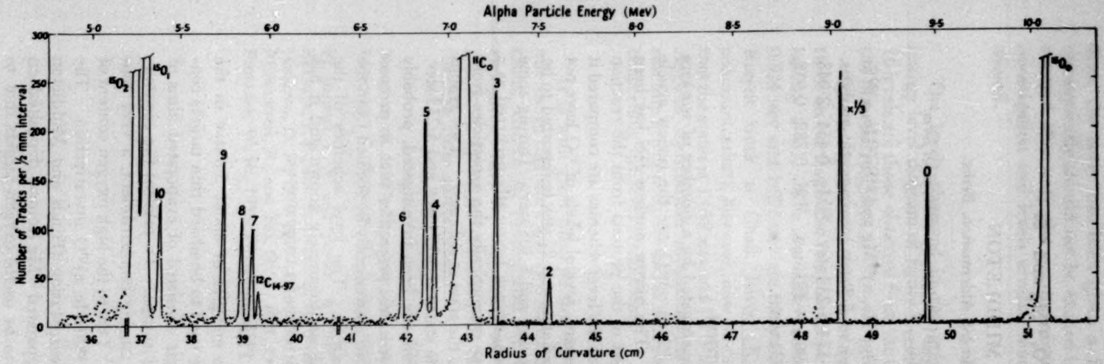

Figure 1. An α-particle energy spectrum from the reaction ^{24}Mg(^{3}He, α)^{23}Mg obtained at 30°, with a bombarding energy of 5·905 Mev and a field strength of 8925 gauss.

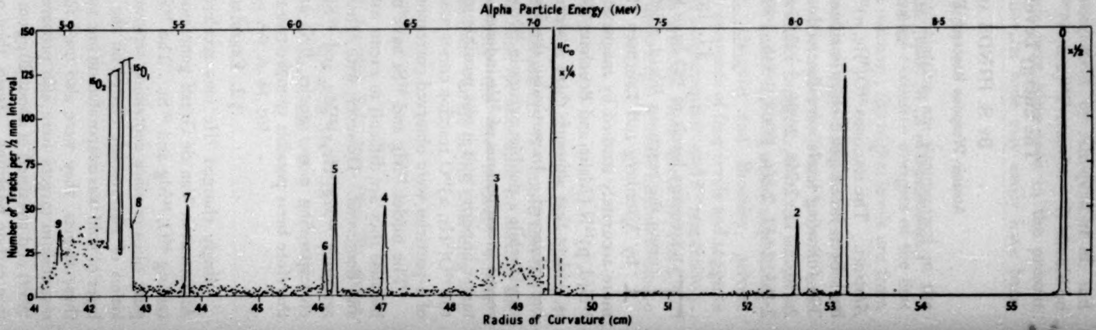

Figure 3. An α-particle energy spectrum from the reaction ^{28}Si(^{3}He, α)^{27}Si obtained at 30°, with a bombarding energy of 5·89[illegible] Mev

The energies of the charged reaction products were measured with a high precision broad-range magnetic spectrograph. Two exposure series were made with silica targets at energies of 5·700 MeV and 5·891 MeV. At the lower energy, exposures were made at ten angles ranging from $7\frac{1}{2}°$ to 60° and at the higher energy, at angles 15°, 30° and 60°. Three exposures were also made at 5·905 MeV energy at angles of 15°, 30° and 60° with the magnesium targets. Exposures varied between 500 and 3000 microcoulombs.

§ 3. THE $^{24}Mg(^3He, \alpha)^{23}Mg$ REACTION

An α-particle spectrum, obtained from the $^{24}Mg(^3He, \alpha)^{23}Mg$ reaction at an angle of 30°, is shown in figure 1. Eleven groups were identified as corresponding to states of ^{23}Mg by their rate of energy variation with angle. These are labelled numerically in the figure, 0 referring to the ground state. The intense group at a radius of 43 cm arises from ^{12}C and corresponds to the formation of ^{11}C in its ground state. A number of weak groups were also observed which are thought to be due to the $^{13}C(^3He, \alpha)^{12}C$ reaction. However, since they were weak, it was only possible to assign the group at 39·2 cm to a level at 14·97 MeV in ^{12}C. This value was reported by Moak *et al.* (1958). The intense groups labelled $^{15}O_0$, $^{15}O_1$ and $^{15}O_2$, are due to oxygen and correspond to the ground, first and second excited states of ^{15}O, respectively. These will be discussed in § 5.

The bombarding energy was determined by measuring the energies of the elastically scattered ^3He particles from ^{12}C, ^{16}O and ^{24}Mg. For this purpose a short exposure was made at 90° with a reduced magnetic field. These measurements yielded a mean value of $5·905 \pm 0·010$ MeV which leads to a ground state Q-value of $4·048 \pm 0·015$ MeV. This agrees with the value of 4·048 MeV calculated from the mass defects reported by Endt and Braams (1957).

In table 1 are listed the excitation energies of the first ten excited states of ^{23}Mg. With the exception of groups 3 and 10, which were observed only at two angles, the values are the means of three determinations and are subject to an experimental error of ±10 keV. For groups 3 and 10 an error of ±15 keV is possible.

Table 1. Energy levels of ^{23}Mg from $^{24}Mg(^3He, \alpha)^{23}Mg$

Group Number	Excitation Energy (MeV)	Error (keV)
0	0	0
1	0·451	±10
2	2·048	±10
3	2·356	±15
4	2·712	±10
5	2·768	±10
6	2·904	±10
7	3·792	±10
8	3·856	±10
9	3·968	±10
10	4·353	±15

In figure 2 the energy level diagram for ^{23}Mg is compared with that for its mirror nucleus ^{23}Na. The excitation energies quoted for the latter nucleus were determined by Buechner and Sperduto (1957) from the magnetic analysis of the inelastically scattered protons from sodium.

§ 4. THE ^{28}Si(^{3}He, α)^{27}Si REACTION

In figure 3 is shown an α-particle energy spectrum obtained from this reaction at an angle of 30°. The target contained separated ^{28}Si isotope, the field strength was 7751 gauss and the beam energy 5·891 Mev. Groups arising from ^{28}Si are labelled numerically; impurity groups are labelled in the same manner as in figure 1.

Table 2. Energy levels of ^{27}Si from ^{28}Si(^{3}He, α)^{27}Si. Series I values obtained with a beam energy of 5·700 Mev and Series II with 5·891 Mev

Group Number	Excitation Energy (Mev) I	Excitation Energy (Mev) II	Mean Excitation Energy (Mev)	Error (kev)
0				
1	0·787	0·776	0·782	±10
2	0·963	0·953	0·958	±10
3	2·167	2·162	2·165	±10
4	2·650	2·651	2·651	±10
5	2·868	2·864	2·866	±10
6	2·912	2·904	2·908	±10
7	3·543	3·537	3·540	±10
8	—	3·800	3·800	±15
9	—	(4·13)	(4·13)	±20

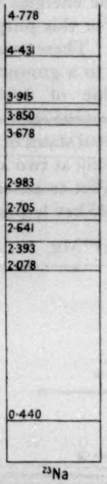
4·778
4·431
3·915
3·850
3·678
2·983
2·705
2·641
2·393
2·078
0·440
^{23}Na
4·353
3·968
3·856
3·792
2·904
2·768
2·712
2·356
2·048
0·451
^{23}Mg

Figure 2. A comparison of the energy levels of the mirror nuclei ^{23}Na and ^{23}Mg.

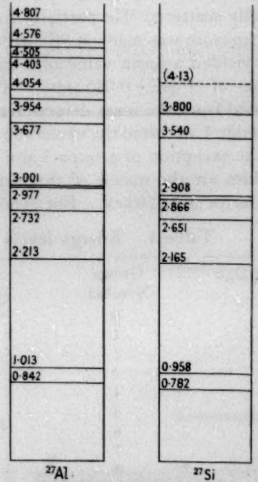
4·807
4·576
4·505
4·403
4·054
3·954
3·677
3·001
2·977
2·732
2·213
1·013
0·842
^{27}Al
(4·13)
3·800
3·540
2·908
2·866
2·651
2·165
0·958
0·782
^{27}Si

Figure 4. A comparison of the energy levels of the mirror nuclei ^{27}Al and ^{27}Si.

In columns I and II of table 2 are listed the energy levels of ^{27}Si determined from the first series of exposures at a beam energy of 5·700 Mev and also those from the second series with a beam energy of 5·891 Mev. In both cases, the values listed represent the means of three separate determinations at different angles.

Groups 8 and 9 were not observed in the first series because a stronger field was used to record the protons from the $^{16}O(^{3}He, p)^{18}F$ reaction. All values are subject to an experimental error of ± 10 kev except for groups 8 and 9 for which errors of 15 ± kev and ± 20 kev respectively may be possible. Group 9 is doubtful and was only observed clearly at 60°. At other angles it was either completely or partially obscured by spuriously scattered α-particles and ^{3}He particles.

The bombarding energies were determined for both series of exposures in a similar manner to that employed for magnesium. From these a mean *Q*-value for the $^{28}Si(^{3}He, \alpha)^{27}Si$ reaction was calculated to be 3·405 ± 0·015 Mev. This value is in good agreement with 3·401 Mev expected from the mass defects.

The energy levels of ^{27}Si are shown compared with those of the mirror nucleus ^{27}Al in figure 4. The energy levels of the latter nucleus were obtained by Browne, Zimmerman and Buechner (1954) from magnetic analysis of the inelastically scattered protons from ^{27}Al.

§ 5. THE $^{16}O(^{3}He, \alpha)^{15}O$ REACTION

During the investigation of the two previous reactions, three strong groups from the $^{16}O(^{3}He, \alpha)^{15}O$ reaction were consistently observed at all angles and bombarding energies. These were identified as corresponding to the ground and excited states of ^{15}O at 5·174 ± 0·010 Mev and 5·233 ± 0·010 Mev respectively. It is evident that these two excited states correspond to the levels at 5·276 Mev and 5·305 Mev in the mirror nucleus ^{15}N but it is interesting to note that the spacing has increased from 29 kev to 59 kev.

Table 3. *Q*-values for the reaction $^{16}O(^{3}He, \alpha)^{15}O$. Weighted mean *Q*-value 4·916 ± 0·010 Mev

Angle	*Q*-value (1)	Angle	*Q*-value (2)
7½°	4·918	15°	4·918
10°	4·918	30°	4·914
15°	4·919	60°	4·910
20°	4·919		
25°	4·918		
30°	4·913		
35°	4·917		
40°	4·917		
50°	4·913		

(1) *Q*-value determined from exposures using a silica target.
(2) *Q*-value determined from oxygen impurity occurring in magnesium target.

Many determinations were made of the ground state *Q*-value for this reaction and these are listed in table 3. The value determined at angles 7½° to 50° were obtained with a silicon target and the values at 15°, 30° and 60° with a magnesium target. The respective beam energies being 5·700 ± 0·010 Mev and 5·905 ± 0·010 Mev. The weighted mean *Q*-value is 4·916 ± 0·010 Mev. This differs from the value of 4·977 Mev calculated from the mass defects reported by Wapstra (1955). However, if the mass of ^{15}O is calculated using the present *Q*-value, a value of 15·007834 ± 0·000010 is obtained which is in good agreement with 15·007832 ± 0·000010 calculated from the very precisely determined *Q*-value of the $^{15}N(p, n)^{15}O$ reaction reported by Lidofsky, Weil and Jones (1957).

ACKNOWLEDGMENTS

It is with great pleasure that we thank Dr. K. W. Allen for his continued interest in this work and also for much useful discussion. We would also like to thank Mr. D. A. Procter and Mr. H. Marchant for assistance in making the exposures and the Van de Graaff operating staff for their close co-operation.

REFERENCES

AJZENBERG, F., and LAURITSEN, T., 1955, *Rev. Mod. Phys.*, **27**, 77.
BROWNE, C. P., ZIMMERMAN, J. R., and BUECHNER, W. W., 1954, *Phys. Rev.*, **96**, 725.
BUECHNER, W. W., and SPERDUTO, A., 1957, *Phys. Rev.*, **106**, 1008.
ENDT, P. M., and BRAAMS, C. H., 1957, *Rev. Mod. Phys.*, **29**, 683.
HINDS, S. and MIDDLETON, R., 1959, *Proc. Phys. Soc.*, **73**, 501.
LIDOFSKY, L. J., WEIL, J. L., and JONES, K. W., 1957, *Bull. Amer. Phys. Soc.*, II, **2**, 182.
MALM, R., and BUECHNER, W. W., 1950, *Phys. Rev.*, **80**, 771.
MOAK, C. D., GALONSKY, A., TRAUGHBER, R. L., and JONES, C. M., 1958, *Phys. Rev.*, **110**, 1369.
WAPSTRA, A. H., 1955, *Physica*, **21**, 367.

Work Function of Sodium Chloride

By L. J. VASEK† and J. M. ANDERSON
Department of Physics, University of Toronto

MS. received 11th November 1958

Abstract. The work function ϕ of evaporated films of sodium chloride and the energy gap δ from the filled levels to the Fermi level have been determined by photoelectric measurements using the complete electrode substitution method. The values found are

$$\phi = 5{\cdot}12(3) \pm 0{\cdot}018\,\text{ev} \quad \text{and} \quad \delta = 1{\cdot}55(0) \pm 0{\cdot}034\,\text{ev}.$$

§ 1. Introduction

In spite of many papers regarding energy levels of alkali halides there seems, as noted by Turner (1956), to be no measurement of the position of the Fermi level. The photoemission threshold of sodium chloride has been measured for powdered specimens by Lukirsky, Gudris and Kulikowa (1926) and the results are discussed by Tartakowsky (1934) in trying to establish the energy level scheme for sodium chloride. Thus information fixing the energy levels of this substance relative to either the vacuum level or the energy levels of materials in contact with it is either scanty or non-existent.

§ 2. Method

The method of electrode substitution as first used by Apker, Taft and Dickey (1948) and extended by West (1953) involves a photocell in which the emitter in the former case and both emitter or collector in the latter may be changed from a metallic material to an insulator or a semiconductor.

Table 1. Combinations of Emitter and Collector

Combination	Emitter	Collector
No. 1	metal	metal
No. 2	metal	insulator
No. 3	insulator	metal
No. 4	insulator	insulator

Accepting the facts that the Fermi levels of materials in contact coincide when they are in charge equilibrium, that the photocurrent to the collector ceases at a voltage V_c (on the collector re-emitter) such that the retarding field between the surfaces just stops the most energetic electrons emitted due to the photoelectric effect and that a saturation voltage V_s exists when the field between emitter and collector surfaces just reaches zero, we can easily set up equations for the four possible combinations shown in table 1,

$$V_c = \phi_c + \delta_e - h\nu; \quad V_s = \phi_c - \phi_e.$$

---

† Now at University of St. Thomas.

Thus we have eight possible experimental measurements of which V_{s_1} and V_{s_4} must be zero and may be used to test the uniformity and similarity of the surfaces. Using the fact that δ for metals is zero, we have six equations to solve for three unknowns, ϕ_l, ϕ_m and δ, where ϕ_l and ϕ_m are the work functions of the metal and insulator respectively and δ is the separation of the Fermi level from the filled levels of the insulator. Three conditional equations which must be identically satisfied exist between these quantities. In the work of West (1953) and in this work all four combinations were realized.

§ 3. APPARATUS

A photocell shown in figure 1 was designed for the measurements. Platinum was used as the metal electrode since experience confirmed the results of West and also those of Hinteregger and Watanabe (1953) that surfaces of this metal were very reproducible under repeated cycles of condensing vapour on it and evaporating it off. The alignment and separation of the electrode plates are maintained constant since the glass rods R and S mounting the plates are prevented from turning by being joined to the auxiliary glass rods E and F (figure 1(*b*)). These rods can be slid forward to the right by using a magnet attracting the iron slugs sealed in the glass (H). Sliding contacts are avoided by the coiled chromel wire inside the moving electrode supports which remains connected to the outlet leads X and Y at all times. The four movable glass rods are mounted inside a glass carriage which can be rotated by magnetic attraction on the iron slugs K and N. This allows the angle of incidence of the light entering at right angles to this axis to be fixed at any desired value on either plate.

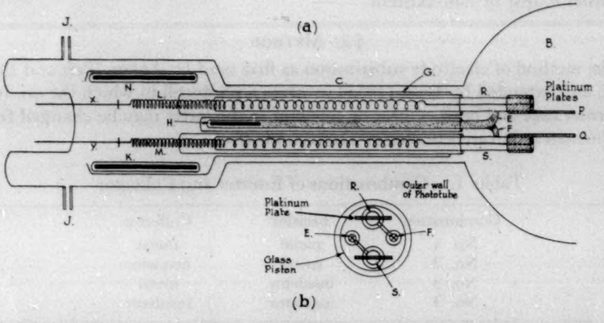

Figure 1. (*a*) Section of photocell showing movable piston and electrodes. (*b*) End view of piston.

The light source was a Pyrex discharge tube with ring electrodes viewed end-on, from the photocell plates, through a long capillary collimating the light and directing it on the middle of the upper of the two plates. This capillary was closed at the discharge end by a lithium fluoride window cemented across the end by araldite resin. Initially an air discharge was used since it had been used successfully by West and also by Ferguson (1944). Photographic study of the spectrum transmitted showed that the lowest wavelength group was at 1542 Å, with a possible trace of a group at 1527 Å. Though it was almost certain that this latter group at 1527 Å was not strong enough to be noticed in photoemission, later work was done as a check with a xenon discharge in which only the 1469 Å line was appreciably transmitted in the far ultra-violet region.

The discharge tube was attached to the cell by a ground-glass taper joint and the electrometer terminal leads were led out through a cap mounted on a ground butt joint. Both of these were lightly greased with high vacuum silicone grease. Permanently attached to the cell system were a charcoal trap, a VG-1A ionization gauge and a steel oven containing the salt. This oven was enclosed in a Pyrex bulb and presented an opening toward a Pyrex tube fixed at right angles to the main axis of figure 1 and so placed that the platinum plates of the cell could be placed one at a time in a beam of evaporated salt atoms from the oven and then retracted into measuring position.

§ 4. DIRECT CURRENT MEASUREMENTS

Voltages of the collector electrode were set using a voltmeter which had been standardized. Readings of photocurrent between the electrodes were taken at 0·05 volt intervals in the neighbourhood of the critical voltages and at 0·10 volt intervals for the remainder of the curves. Current was measured using a Lindemann electrometer as a null detector in a current balance. Balancing the current through a 10^{12} ohm resistor to zero, allowed a wide range of current values to be measured without changing the resistor and permitted currents down to 10^{-15} ampere to be detected. The balancing current flowed through an auxiliary resistance of known value and was changed by changing the voltage applied from a potentiometer calibrated against a cadmium standard cell. Because of the non-spherical geometry V_S was indicated by a change in slope of the curve and not by complete saturation. Regularity and repeatability of the curves were excellent.

§ 5. PROCEDURE

The entire system was evacuated using the usual mercury diffusion pump system. The steel oven was heated to bright red heat using an induction heater and thoroughly outgassed with no salt present. An opening was made and fine NaCl was dropped into the oven after which the oven and salt were outgassed for many hours at the highest temperature which could be used without evaporation of the salt. The charcoal trap was then maintained at red heat for 24 to 36 hours with the final pressure reading being 10^{-5} mm Hg. The system was then closed off from the pumps and liquid air put on the charcoal trap and kept there for a series of several complete runs, after which the outgassing procedure was repeated. Pressure in the cell remained below 10^{-6} mm (lowest detectable pressure) during all runs and no traces of changes due to contamination were ever found. Each plate of the cell was moved forward and outgassed at red heat by the induction heater and measurements of combination No. 1 made. If V_{S_1} ever differed from zero the plates were treated until this condition was satisfied. One plate was then moved forward and coated with salt by evaporation from the oven. Pressure registered by the ionization gauge never exceeded 10^{-5} mm during this process. The plate was moved back and combination No. 2 and, by rotating the plates, combination No. 3 were studied. The other plate was then coated and combination No. 4 studied. V_{S_4} provided a check that the coatings were similar and uniform. One plate was then moved forward and the induction heater so placed as to drive off the salt starting first at one end, so that interference colours showed in the wedge shaped film. This allowed a measure of the thickness which was usually about five microns. This plate was moved back and combination Nos. 2 and 3 repeated. The other plate was then heated and combination No. 1 repeated as a check that both plates were restored to the original condition. A complete run required about two hours, and several runs were usually taken before outgassing the charcoal tube again. Several different fillings of salt were used in the oven. The light source intensity was adjusted by changing the d.c. current in the discharge tube. The d.c. voltage came from a filtered rectified supply for which the a.c. input could be set by a Variac. Once set it was held constant by a Sorensen regulator.

Photocurrents were usually of the order of 10^{-13} ampere and could be varied by change of light intensity. The critical voltages were found to be independent of current so that the potential drop across the insulating salt films was negligibly small. Currents emitted from the insulator were of the same order but somewhat smaller than those from the platinum metal. Measurements with combination No. 3 were difficult since large amounts of light reached the collector surface and gave rise to large reverse currents unless the angle of incidence was adjusted with extreme care. For this reason this combination was not used with the xenon illumination.

§ 6. RESULTS

All measurements of each critical voltage, made in series satisfying the required saturation voltage conditions for identical surfaces, were averaged. This average was assigned a weight in proportion to the number of readings. Because of the greater experimental uncertainty of V_s values, weights of V_c measurements were doubled. Using the method of correlatives outlined by Merriman (1934) the most probable values of the six voltages satisfying the conditional equations exactly were found. Probable errors of these voltages were found by the usual least square procedures. With these values of voltages and values of $h\nu$ for the sources, the equations were solved for the three unknown quantities and probable errors of the results for each of the sources. The results are shown in table 2. Since the results are consistent, they are averaged to give the final results :

Table 2. Values of the Quantities ϕ_m, ϕ_i, and δ_i

Quantity	Air Discharge		Xenon Discharge	
	Value (ev)	Probable Error	Value (ev)	Probable Error
ϕ_m	5·69	0·02	5·68	0·02
ϕ_i	5·12	0·02	5·13	0·03
δ	1·55	0·03	1·55	0·05

$$\phi_m = 5{\cdot}68(5) \pm 0{\cdot}014 \text{ ev} \qquad \delta = 1{\cdot}55(0) \pm 0{\cdot}029 \text{ ev}$$

$$\phi_i = 5{\cdot}12(3) \pm 0{\cdot}018 \text{ ev} \qquad \phi_i + \delta = 6{\cdot}67(3) \pm 0{\cdot}034 \text{ ev}$$

§ 7. DISCUSSION

These results may be considered in agreement with the early threshold value $\phi_i + \delta$ quoted by Lukirsky for powdered salt. They are also in agreement with the negative results of Turner who found no photoemission from silver into salt up to 2500 Å. Taking into account the contact potential between them as predicted from

ϕ_1 above, no results should be expected below 5·12 ev. The results are in disagreement with the present interpretation of results from the absorption spectra of similar sublimed films by Schneider and O'Bryan (1937) and those of Hartman, Siegfried and Nelson (1957). The first of these reports an absorption peak at 1280 Å which is not present in the results of the more recent work. Both report the peak at 1580 Å (7·8 ev) which has been thought to represent transitions from the filled levels to exciton levels below the conduction band. This is said to explain why no photoconductivity accompanies irradiation of the crystal in the region of the 1580 Å peak. The results of this paper place the filled band only 6·67 ev below vacuum level in rough agreement with the results of Lukirsky. Because the photocurrents from the sodium chloride films were of the same order as those obtained from the platinum, it does not seem possible that the photoemission levels could be those of defects or impurities.

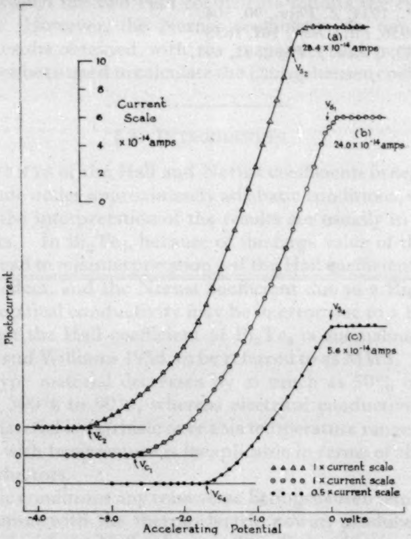

Figure 2. Typical curves illustrating the regularity of the experimental points.

It seems possible that the conduction band does not exist in the crystal. Thus absorption could take place only by photoemission resulting in a charged double layer at the surface. This would perturb the filled levels downward relative to vacuum level and cause the structure of the absorption to be dependent on the insulating properties of the absorption specimen and mount as well as on the spectral constitution of the source. A rough estimate shows that assigning a resistivity to the salt which would still leave the shift of critical voltages with photocurrent in our experiment negligible by a factor of 500 is sufficient to account roughly for the results of the absorption measurements.

ACKNOWLEDGMENTS

The authors wish to acknowledge a grant of funds to one of us (J.M.A.) (DRB 9512–23) from the Defence Research Board, Ottawa, Canada, which allowed purchase of some necessary equipment. The leave of absence granted to one of us (L.J.V.) by the University of St. Thomas, is gratefully acknowledged.

REFERENCES

APKER, L., TAFT, E., and DICKEY, J., 1948, *Phys. Rev.*, **73**, 46.
FERGUSON, J. N., 1940, *Phys. Rev.*, **57**, 1089 (A).
—— 1944, *Ibid.*, **66**, 220.
HARTMAN, P. L., NELSON, J. R., and SIEGFRIED, J. G., 1957, *Phys. Rev.*, **105**, 123.
HINTEREGGER, H. E., and WATANABE, K., 1953, *J. Opt. Soc. Amer.*, **43**, 604.
LUKIRSKY, P., GUDRIS, N., and KULIKOWA, L., 1926, *Z. Phys.*, **37**, 308.
MERRIMAN, M., 1934, *Method of Least Squares* (New York : John Wiley and Sons).
SCHNEIDER, E. G., and O'BRYAN, M. H., 1937, *Phys. Rev.*, **51**, 293.
TARTAKOWSKY, P., 1934, *Z. Phys.*, **90**, 504.
TURNER, W. J., 1956, *Phys. Rev.*, **101**, 1653.
WEST, D. C., 1953, *Canad. J. Phys.*, **31**, 691.

Some Adiabatic and Isothermal Effects in Bismuth Telluride

By W. WILLIAMS
Physics Department, Bedford College, London

MS. received 1*st January* 1959

Abstract. Isothermal and quasi-adiabatic Hall and Nernst coefficients were measured on n- and p-type Bi_2Te_3 over a temperature range 100°K to about 450°K. The current flow was parallel to the cleavage planes, and measurements were made with the magnetic field either parallel or perpendicular to the cleavage planes. The difference between the two Hall coefficients follows the expected variation with temperature. However, the Nernst coefficients do not, and the reason is not known. Results obtained with the magnetic field perpendicular to the cleavage planes have been used to calculate the Ettingshausen coefficient.

---

§ 1. INTRODUCTION

MEASUREMENTS of the Hall and Nernst coefficients in semiconductors are often made under approximately adiabatic conditions, whereas formulae used in the interpretation of the results are usually in terms of the isothermal coefficients. In Bi_2Te_3, because of the large value of the thermoelectric power, this could lead to misinterpretation—if the Hall coefficient is in error due to an Ettingshausen effect, and the Nernst coefficient due to a Righi–Leduc effect. In addition, the electrical conductivity may be in error due to a Peltier effect.

It is known that the Hall coefficient of Bi_2Te_3 is anomalous in the extrinsic region (Mansfield and Williams 1958, to be referred to as MW). The value of the coefficient for p-type material decreases by as much as 50% on decreasing the temperature from 300°K to 90°K, whereas electrical conductivity measurements indicate that the material is extrinsic over this temperature range. This variation of Hall coefficient with temperature is inexplicable in terms of the usual theory of impurity semiconductors.

Under adiabatic conditions any transverse Ettingshausen temperature gradient would, in conjunction with the thermoelectric power, produce a voltage which would be combined with the Hall voltage. This Ettingshausen voltage cannot be separated from the Hall voltage by the normal direct current method of making Hall coefficient measurements. Measurements have therefore been made simultaneously of both adiabatic (or near adiabatic) and isothermal Hall coefficients from 100°K to approximately 450°K for both n- and p-type material.

§ 2. EXPERIMENTAL PROCEDURE AND RESULTS

Previous workers have used various methods, including alternating current methods, to obtain the isothermal Hall coefficient of metals and semiconductors. However, in MW it was suggested that the method of measuring isothermal effects by using probes of the same material as the specimen (Jan 1957) is particularly suited to Bi_2Te_3. Hence the isothermal Hall coefficient R_I was measured

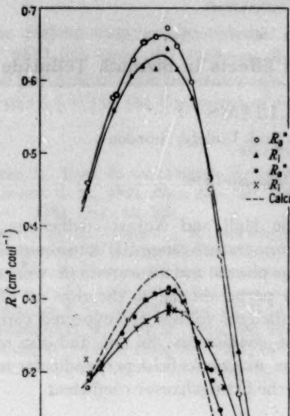

Figure 1. Hall coefficient of specimen R5 (p-type).

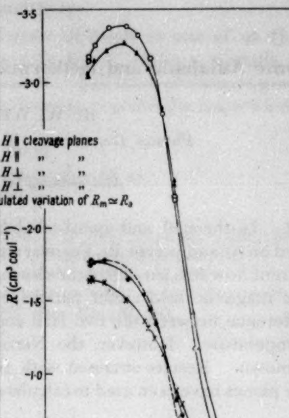

Figure 2. Hall coefficient of specimen R9 (n-type).

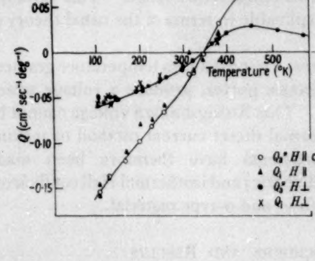

Figure 3. Nernst coefficient of specimen R5.

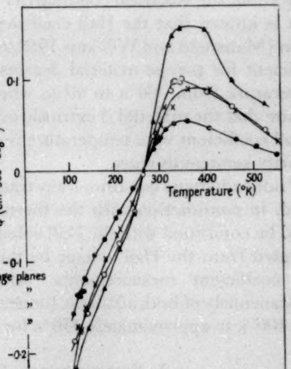

Figure 4. Nernst coefficient of specimen R9.

using probes of Bi_2Te_3 cut from material originally adjacent to the specimen used. A quasi-adiabatic coefficient, $R_a{}^*$, was measured using probes of T_1 alloy. Measurements were made with the magnetic field both parallel and perpendicular to the cleavage planes. The results obtained are shown in figures 1 and 2. The p-type specimen is the one labelled R5 in MW. Specimen R9 is n-type.

The corresponding values of the isothermal and quasi-adiabatic Nernst coefficients (Q_i and $Q_a{}^*$ respectively) are shown in figures 3 and 4.

Measurements were also made of the electrical conductivity and thermoelectric power of both specimens over the temperature range 100°K to 600°K.

§ 3. Discussion of Results

The sign convention used is that stated by Gerlach (1928) together with a convention for the thermoelectric power which gives this quantity the same sign in the extrinsic region as the charge carriers. Thermoelectric power is positive when conventional current flows from metal to semiconductor at the hot junction.

Using a right-handed system of coordinates in which the primary electric current J or primary thermal current ω is in the x direction and the magnetic field H is applied in the z direction, the transverse galvanomagnetic and thermomagnetic effects respectively are measured in the y direction. The qualification of 'isothermal' and 'adiabatic' then refers to conditions in the y direction. For isothermal conditions $\partial T/\partial y=0$, and for adiabatic conditions $\omega_y=0$. Thus :

$$\text{Isothermal Hall coefficient } R_i=\frac{E_y}{H_zJ_x}\ ;\ \left[J_y=0,\ \frac{\partial T}{\partial x}=\frac{\partial T}{\partial y}=0\right]$$

$$\text{Adiabatic Hall coefficient } R_a=\frac{E_y}{H_zJ_x}\ ;\ \left[J_y=0,\ \frac{\partial T}{\partial x}=0,\ \omega_y=0\right].$$

The relations between isothermal and adiabatic coefficients (Heurlinger relations) follow directly from the definitions of the various coefficients. With the sign convention used in the present paper, the relation between R_i and R_a is (cf. Chambers 1952):

$$R_a=R_i-\frac{dE}{dT}P \qquad \ldots\ldots(1)$$

where dE/dT is the absolute thermoelectric power of Bi_2Te_3 relevant to heat flow in the y direction and P is the Ettingshausen coefficient. The conditions under which P is defined are necessarily adiabatic and are the same as for R_a.

Taking into account the lattice thermal conductivity when deriving the Bridgman relation,

$$P=\frac{Q_iT}{K_y} \qquad \ldots\ldots(2)$$

where Q_i is the isothermal Nernst coefficient, and K_y is the isothermal thermal conductivity relevant to heat flow in the y direction and in a transverse magnetic field†.

This relation should hold for an isotropic medium over the whole temperature range investigated. Bi_2Te_3 is anisotropic. However, when the magnetic field is perpendicular to the cleavage planes, the cleavage planes are in the xy plane and thus the x and y directions in the crystal are equivalent. With primary currents in the x direction and the transverse effects measured in the y direction, the Bridgman relation should apply.

---

† For a comprehensive account of the definitions of all the possible effects and the relations between them, see Jan (1957).

The sign of P is thus always the same as that for Q_l, and R_a should equal R_l at the temperature where $Q_l = 0$. Then from equation (1) $|R_a| > |R_l|$ below, and $|R_a| < |R_l|$ above this temperature for both n- and p-type specimens. It is seen that the general behaviour is as predicted, not only for the case considered, with the magnetic field perpendicular to the cleavage planes, but also when the magnetic field is applied parallel to the cleavage planes.

Under adiabatic conditions, with $\omega_y = 0$, the adiabatic Hall coefficient R_a is not directly measurable. The measured Hall coefficient R_m is given by the relation

$$R_m = R_l - \left(\frac{dE}{dT}\right)_{T_1} P \qquad \ldots\ldots (3)$$

where $(dE/dT)_{T_1}$ is the thermoelectric power of Bi_2Te_3 relative to T_1 alloy, the material of the measuring probes (Jan 1957). However, the thermoelectric power of Bi_2Te_3 is large compared with that of the metal of the measuring probes, so that the value of R_m is approximately equal to R_a.

The measurements of thermoelectric power were made with the heat flow parallel to the cleavage planes. The variation of K_y with temperature was calculated for each specimen from the measured electrical conductivity and data given by Goldsmid (1958) from measurements made on Bi_2Te_3 with the heat flow parallel to the cleavage planes. Thus, for the case when the magnetic field is perpendicular to the cleavage planes, values of P have been calculated from the measured values of Q_l using equation (2). These have been used to calculate $|R_m - R_l|$ from equation (3). Then, using the measured values of R_l, the variation of R_m with temperature has been calculated. This is plotted for both specimens on figures 1 and 2. It is seen that this theory always predicts a larger value for $|R_m - R_l|$ than is, in fact, found experimentally.

In equations (2) and (3), K_y and $(dE/dT)_{T_1}$ are respectively the thermal conductivity and thermoelectric power in a transverse magnetic field. In the calculations values of these quantities were used which had been obtained for zero magnetic field. However, it is known that these quantities are almost independent of magnetic field (Goldsmid 1958, Bowley *et al.* 1958), and this factor would not lead to the observed differences between the measured and calculated values of R_m. There are also other second order effects which can contribute to the measured voltage in the adiabatic case (Fieschi 1955, Jan 1957). Probably the main factor contributing to this difference is the fact that ω_y is not zero and true adiabatic conditions are not obtained. It is, in fact, difficult to know the exact experimental conditions in the y direction. In preliminary experiments no effort was made to reduce the transverse heat flow, and an even smaller value of $|R_m - R_l|$ was observed. While taking the readings shown in figures 1 and 2, an effort was made to reduce this heat flow to a minimum. However, if $\omega_y \neq 0$, the quantity measured would be a quasi-adiabatic Hall coefficient R_a^*, where

$$|R_a^* - R_l| < |R_m - R_l|.$$

Thus, assuming equation (2) to be obeyed in Bi_2Te_3 for this direction of the magnetic field with respect to the cleavage planes, the variation of the Ettingshausen coefficient with temperature, obtained using this relation, is plotted in figure 5. Sufficient data are not available for interpreting the corresponding results obtained with the magnetic field parallel to the cleavage planes.

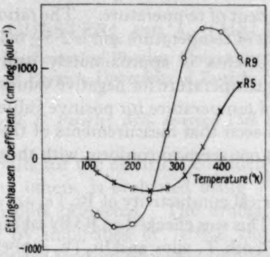

Figure 5. Ettingshausen coefficient of Bi_2Te_3.

An interpretation of the adiabatic and isothermal Nernst coefficients is more complicated. The relation between the two quantities is (cf. Chambers 1952)

$$Q_a = Q_i - \frac{dE}{dT} \cdot S \qquad \ldots\ldots(4)$$

where S is the Righi–Leduc coefficient.

Now there is no simple relation giving the sign of S from some experimentally determined quantity over the whole temperature range. However, according to simple semiconductor theory, S is positive for p-type specimens and negative for n-type specimens in the extrinsic range, only changing sign in p-type specimens ($b > 1$) after Hall and thermoelectric power readings have indicated that the specimens have become intrinsic (Putley 1955). Thus, over the complete temperature range studied, S should be negative for R9 and positive for R5, and from equation (4) below the temperature where $Q_i = 0$, it is predicted that $|Q_a| > |Q_i|$, while above this temperature $|Q_a| < |Q_i|$. As with the adiabatic Hall coefficient, the quantity Q_a is not directly measurable. However, following the same reasoning as for the Hall coefficient, a quasi-adiabatic Nernst coefficient Q_a^* should be obtained such that $|Q_a^* - Q_i|$ is smaller than predicted. No definite results could be obtained for R5 (figure 3). For R9, the results are not as predicted, and S does not appear to behave according to the simple theory.

R9 is a zone-refined specimen of n-type material which was tested for uniformity along its length. A plot of log σ_0 against log T, where σ_0 is the electrical conductivity corrected for degeneracy, gives a temperature dependence of mobility of $T^{-1\cdot 91}$ compared with the previous value for electrons of $T^{-1\cdot 63}$. A plot of log (np/T^3), obtained from electrical conductivity data as in MW, against $1/T$ gives a value for the energy gap at 0°K of 0·19 ev compared with the previous value of 0·21 ev.

In MW it was shown that, except in the intrinsic region, Be_2Te_3 obeys the Moreau relation

$$Q = -T \frac{d^2E}{dT^2} R\sigma$$

where σ is the electrical conductivity. Use of the isothermal quantities in this relation did not give better agreement in the intrinsic region. The ratio of the coefficients for the two orientations of the magnetic field is of interest. The ratio of the isothermal Hall coefficients is $2{\cdot}2 \pm 0{\cdot}1$ for R5 and $2{\cdot}3 \pm 0{\cdot}2$ for R9, both quantities being independent of temperature. The ratio of the Nernst coefficients for R5 is also independent of temperature and is $2{\cdot}3 \pm 0{\cdot}1$. For R9 the ratio of the isothermal Nernst coefficients is approximately unity at 100°K. The ratio increases with increasing temperature for negative values of the Nernst coefficient, becoming independent of temperature for positive values of the coefficient with a value of $1{\cdot}7 \pm 0{\cdot}1$. It is seen that measurements of the Nernst coefficient of R9 in the extrinsic range do not seem to conform with those on the other specimens studied here and in MW.

Readings of the electrical conductivity of Bi_2Te_3 are subject to a possible error due to Peltier heating. This was checked on R5 by taking readings simultaneously of the conductivity using both T_1 alloy and Bi_2Te_3 probes. R5 is a long specimen (7 cm) so that for small currents both quantities should be the same. Readings were taken for different values of the current J_x at room temperature and at 110°K. Over the range of currents normally used, no evidence could be found of an error in σ due to the Peltier effect. However, such an error would depend on the size of the specimen and is much more likely to be appreciable for small specimens.

§ 4. CONCLUSIONS

A simple method has been used to obtain the isothermal Hall and Nernst coefficients in Bi_2Te_3 and it is found that the value of these coefficients can differ appreciably from the quasi-adiabatic coefficients often measured. Measurement of the isothermal Nernst coefficient provides a simple method of obtaining the Ettingshausen coefficient. The extrinsic Hall coefficient in p-type material is known to be anomalous, but although this anomaly is decreased by measuring the isothermal coefficient, it is not removed.

ACKNOWLEDGMENTS

The author wishes to thank Dr. R. Mansfield for helpful discussions and advice, and the General Electric Company for supplying the specimens of Bi_2Te_3.

This work was aided by a grant from the research fund of the University of London.

REFERENCES

BOWLEY, A. E., DELVES, R., and GOLDSMID, H. J., 1958, *Proc. Phys. Soc.*, **72**, 401.
CHAMBERS, R. G., 1952, *Proc. Phys. Soc.* A, **65**, 903.
FIESCHI, R., 1955, *Nuovo Cim. Suppl. Ser.* 10, **1**, 1.
GERLACH, W., 1928, *Handb. d. Phys.*, **13**, 228 (Berlin: Springer).
GOLDSMID, H. J., 1958, *Proc. Phys. Soc.*, **72**, 17.
JAN, J. P., 1957, *Solid State Physics*, Vol. 5 (New York: Academic Press), p. 1.
MANSFIELD, R., and WILLIAMS, W., 1958, *Proc. Phys. Soc.*, **72**, 733.
PUTLEY, E. H., 1955, *Proc. Phys. Soc.* B, **68**, 35.

On the Electrical Conductivity of Metals

By G. V. CHESTER† AND A. THELLUNG‡

† Department of Mathematical Physics, University of Birmingham
‡ Department of Physics, University of Zurich, Switzerland

Communicated by R. E. Peierls; *MS. received* 15*th December* 1958

Abstract. The exact formula for the electrical conductivity of a metal, derived by Kubo, Greenwood, and others, is evaluated using Van Hove's methods for quantum mechanical transport problems. The evaluation is restricted to the case of elastic scattering by impurities or lattice vibrations, but completely avoids the use of the customary random phase assumption. In the limit of weak coupling our method yields formulae for the conductivity that are identical with those derived from the Boltzmann equation. The accuracy of the weak coupling approximation is investigated and it is found to be accurate as long as $\hbar/\tau \ll \eta$, where τ is the collision time and η is the Fermi energy. A general treatment of the conductivity in an anisotropic metal is given and an explicit expression for the conductivity is written down in terms of the eigenvalues and eigenvectors of an integral equation. A general and rigorous derivation of the conventional Boltzmann equation is given using Van Hove's results on the quantum mechanical master equation.

§ INTRODUCTION

THE conventional theory of the electrical conductivity of metals is based on the quantum mechanical Boltzmann equation. The usual derivation of this equation contains twoi mportant assumptions (Peierls 1934 a, 1955). Firstly, the derivation requires the use of the so-called 'repeated random phase' assumption (Peierls 1955, Pauli 1928). This assumption states that if an exact eigenfunction of the system is expanded in eigenstates of the unperturbed Hamiltonian then the coefficients in this expansion have at *all times* randomly distributed phases. The unperturbed Hamiltonian is, of course, the complete Hamiltonian apart from the scattering potential that leads to the electrical resistance. The unsatisfactory nature of this assumption is quite obvious and we shall not comment on it further. Secondly, if τ is the collision time (or if a collision time does not exist then we take some other suitable measure of the strength of the scattering potential), then it is assumed that $\hbar/\tau \ll kT$ (Peierls 1934 a, 1955). Here k is Boltzmann's constant and T is the absolute temperature. This assumption is quite unjustified in many metals and is never true at very low temperatures where τ becomes independent of the temperature. We shall refer to the first of these assumptions as the repeated random phase assumption and to the second as the collision time assumption.

The purpose of this paper is two-fold. First, we shall show that by using techniques recently developed by Van Hove (1955) it is possible to derive the results of the conventional theory without any use of the repeated random phase assumption. Secondly, we shall show by an extension of Van Hove's methods that these results are accurate as long as $\hbar/\tau \ll \eta$, where η is an energy equal in order of magnitude to the Fermi energy. The only really restrictive assumption we shall make in our work is that the electrons are scattered elastically either by static impurities or by lattice vibrations. We hope to discuss the more general case of inelastic scattering in a future publication. The main conclusion to be drawn from this paper is that, at least in the case of elastic scattering, neither of the two traditional assumptions that are inherent in the Boltzmann equation are necessary in the theory of the electrical conductivity of metals. As there has been considerable interest in this problem recently it will be useful if we briefly survey some of the literature before discussing our own method in more detail.

The repeated random phase assumption has been discussed in connection with the Boltzmann equation of Kohn and Luttinger (1957) and by Greenwood (1958). These authors derived the usual Boltzmann equation from the equation of motion of the density matrix and showed that for elastic scattering by impurities, the repeated random phase assumption can be replaced by the assumption that the scattering centres are randomly distributed. Kohn and Luttinger did not discuss the conditions under which the usual formula for the conductivity is valid. Greenwood showed that even though the repeated random phase assumption can be avoided in the derivation of the Boltzmann equation it is still necessary to use the collision time assumption. Landau (Peierls 1934 b) has however given a rather general, though somewhat abstract, argument which strongly suggests that in the calculation of the conductivity the collision time assumption is really quite spurious and should be replaced by the much weaker condition that $\hbar/\tau \ll \eta$. The crux of Landau's argument rests on an exact formula for the conductivity which he proposed. Greenwood (1958) has in fact shown that this formula can be derived rigorously from first principles. Landau's argument has also received support from the explicit calculations of some of the correction terms to the conductivity that were carried out by van Wieringen (1954). He found that the corrections he calculated (which are not as we shall see *all* the correction terms) were small as long as $\hbar/\tau \ll \eta$. We conclude that for elastic scattering by impurities the Boltzmann equation can be derived without the use of the repeated random phase assumption; but that no satisfactory derivation of it had been given which definitely avoids using the collision time assumption.

Our method of calculating the conductivity is based on a new approach that has been proposed by several authors. These authors (Kubo 1956, Nakano 1956, Nakajima 1956, Greenwood 1958, Lax 1958) have shown that *exact* formal expressions for the conductivity can be obtained by solving the equation of motion for the density matrix of the system to first order in the electric field. For example, Kubo has derived the following expression for the conductivity tensor

$$\sigma_{\mu\nu}(\omega) = \mathrm{Tr}\left\{\int_0^{t-t_0} du \int_0^{\beta} d\lambda\, \rho_0\, \mathrm{J}_\nu(0)\, \mathrm{J}_\mu(u+i\lambda)\, \mathrm{e}^{-i\omega u}\right\}. \quad \ldots\ldots(1.1)$$

In this equation $\mathrm{J}_\nu(0)$ is the νth component total current operator for the system, ρ_0 is the equilibrium density matrix $\exp(-\beta\mathscr{H})/\mathrm{Tr}\exp(-\beta\mathscr{H})$, where $\mathscr{H}$ is the total Hamiltonian and $\beta = 1/kT$. The operator $\mathrm{J}_\mu(u+i\lambda)$ is given by

$$\mathrm{J}_\mu(u+i\lambda) = \exp\{i(u+i\lambda)\mathscr{H}\}\, \mathrm{J}_\mu(0) \exp\{-i(u+i\lambda)\mathscr{H}\}.\dagger \quad \ldots\ldots(1.2)$$

---

† We choose our units in this paper so that $\hbar = 1$.

The symbol 'Tr' stands for a trace over any complete set of wave functions that obey periodic boundary conditions, and $t-t_0$ is the time that has elapsed since the field was switched on. It should be emphasized that this formula is exact and that no important assumption is required to derive it. It is, however, very formal in structure and apparently bears no simple relation to the usual formula for the conductivity. It is particularly interesting to note that this expression, although exact, does not yield a well-defined conductivity except in the limit N, $V \rightarrow \infty$ so that N/V remains finite. Here N is the number of degrees of freedom of the system and V is the volume. For a fixed finite N and V it is a straightforward matter (Bocchieri and Loinger 1958) to show that the conductivity as defined by (1.1) is an almost periodic function of the time $t-t_0$. The limiting process N, $V \rightarrow \infty$ so that N/V remains finite removes the quantum mechanical equivalent of the Poincaré cycles from the system, and when this is done the conductivity becomes a well-defined quantity.

The only attempts to relate these exact formulae to the conventional ones are due to Lax (1958) and Edwards (1958). Lax has shown in principle that Van Hove's work on the quantum mechanical master equation implies that the two approaches are in fact equivalent. He did not, however, evaluate the conductivity explicitly or discuss the validity of the result one obtains by using Van Hove's methods. Edwards showed by quite independent methods, which are in fact closely related to Van Hove's, that for weak elastic scattering by impurities the exact expression given by Greenwood reduces to the standard form. Again no discussion was given of the range of validity of this result.

In this paper we shall show how Van Hove's techniques can be used to carry out an explicit and rigorous calculation of the conductivity. As we have mentioned before the only really restrictive assumption that we make is that the electrons are scattered elastically either by impurities or by lattice vibrations. While in this paper we mainly re-derive 'old' results (apart from those of § 5) in a much more rigorous fashion we hope in the future to apply the same methods to some of the more difficult problems in the theory of transport phenomena in metals.

In § 2 we write down the exact expressions for the conductivity that we shall work with in this paper. We have written down three different, though equivalent, expressions because each of these will be required in different portions of our work.

We begin § 3 by giving an outline of Van Hove's (1955) methods and results. This outline is given firstly because the actual methods of Van Hove do not appear to be widely known and secondly because we shall require this summary in order to make intelligible the extension of Van Hove's work that we give in § 4. We next apply these results to calculate the conductivity of a simple model in which free electrons are scattered by static isotropic scattering centres. In the weak scattering limit, we re-derive the usual formula for the conductivity without any use of the repeated random phase assumption.

The validity of this result is investigated in detail in § 4. We show that the usual formula for the conductivity is a good approximation as long as $\hbar/\tau \ll \eta$, where η is the Fermi energy of the electrons. We believe that this is the first time that a detailed investigation of the validity of the standard formula for the conductivity has been made.

In § 5 we deal with the more general model in which electrons moving in an arbitrary periodic lattice are scattered by anisotropic scattering centres. We show that even in this case an effective collision time may be defined explicitly and we express the conductivity in terms of it. We conclude this section by giving a rigorous derivation, using Van Hove's results, of the usual Boltzmann equation for this general model. This derivation entirely avoids any use of the collision time assumption.

Finally in § 6 we treat by the same methods the model in which the electrons are scattered elastically by lattice vibrations. We again derive the usual results and conclude that they are valid as long as $\hbar/\tau \ll \eta$ and $T \gg \theta$, where θ is the Debye temperature of the metal.

§ 2. EXACT FORMAL EXPRESSIONS FOR THE CONDUCTIVITY

In this section we shall write down the exact formal expressions for the conductivity that we shall use in the rest of this paper.

The many-particle formula for the conductivity is given by (1.1). This formula is due to Kubo; alternative expressions have been given by Nakajima and Lax. A much simpler single-particle formula can be derived from (1.1) if (*a*) the total Hamiltonian $\mathscr{H}$ for the system is a sum of single particle Hamiltonians H_α, where the subscript α refers to the αth particle, and (*b*) the applied electric field is static. Under these conditions it is a straightforward matter to show that (1.1) can be written in the form

$$\sigma_{\mu\nu} = -\operatorname{tr}\left\{\frac{\partial f}{\partial H}\int_0^{t-t_0} dt'\, j_\mu(t')j_\nu(0)\right\}. \qquad \ldots\ldots (2.1)$$

Here $j_\nu(0)$ is the single particle current operator, H is the single particle Hamiltonian and

$$j_\mu(t') = \exp(it'H)j_\mu(0)\exp(-it'H). \qquad \ldots\ldots (2.2)$$

The function $f(H)$ is the statistical distribution function for the electrons when they are in thermal equilibrium. We shall assume that the electrons obey Fermi Dirac statistics and then

$$f(H) = [\exp \beta(H-\mu)+1]^{-1}, \qquad \ldots\ldots (2.3)$$

where μ is the chemical potential. The symbol 'tr' in (2.1) implies that the trace is to be taken with any complete set of one particle wave functions that obey periodic boundary conditions. This formula is equivalent to that given by Greenwood (1958) and that proposed by Landau (Peierls 1934b).

We shall sometimes find it convenient to work with a more symmetrical form of (2.1), namely,

$$\sigma_{\mu\nu} = -\operatorname{tr}\left\{\frac{\partial f}{\partial H}\int_0^{t-t_0} dt'\, \tfrac{1}{2}[j_\mu(t')j_\nu(0)+j_\mu(0)j_\nu(t')]\right\}. \qquad \ldots\ldots (2.4)$$

We conclude this section with two remarks. Firstly, the usual derivations of these formulae use a scalar electric potential to represent the applied electric field. This potential is not in general a periodic operator and should not be used if we wish to apply periodic boundary conditions to the system. The derivation of the single-particle formula (2.1) given by Greenwood avoids this difficulty by representing the electric field by a vector potential, which can easily be chosen to be periodic. We believe that this method can be used to give a much more satisfactory derivation of the many-particle formula (1.1)[†]. Secondly, we should like to point out that perhaps the main advantage of these formulae is that their form is such that the statistical factors such as $\partial f/\partial H$, which depend on kT, are clearly separated from the dynamical factors such as $j_\mu(t')$. It seems to us that it is just because these factors are not clearly separated in the usual derivations of the Boltzmann equation that the spurious condition that $\hbar/\tau \ll kT$ arises.

[†] In his derivation Greenwood obtained an extra contribution to the current. This so called 'ripple current' is however easily shown to be proportional to exp $(-\alpha V^{2/3})$, $\alpha > 0$, and hence vanishes in the limit $V \to \infty$.

§ 3. THE EXPLICIT CALCULATION OF THE CONDUCTIVITY

The single particle Hamiltonian H that occurs in the conductivity formula is given by

$$H = H_0 + \lambda V. \qquad \ldots\ldots(3.1)$$

Here H_0 is the Hamiltonian of the conduction electrons moving in the periodic potential of the lattice and λV is the scattering potential for one electron due to the static impurities. It is assumed that the number of scattering centres is of the same order of magnitude as the total number of electrons. The parameter λ is a dimensionless quantity giving a measure of the strength of the scattering potential. The trace in the conductivity formula is most conveniently evaluated in the representation in which H_0 is diagonal; we label the states of this representation by a wave vector $\mathbf{k}$ and denote the eigenvalues by $E_{\mathbf{k}}$. If V has diagonal elements in this representation we include them in H_0. The conductivity tensor $\sigma_{\mu\nu}$ can now be written as

$$\sigma_{\mu\nu} = -\sum_{\mathbf{k},\mathbf{k}'} \left(-\frac{\partial f}{\partial H}\right)_{\mathbf{k},\mathbf{k}'} \int_0^T dt' \langle \mathbf{k}' | j_\mu(t') | \mathbf{k} \rangle \langle \mathbf{k} | j_\nu(0) | \mathbf{k} \rangle. \qquad \ldots\ldots(3.2)$$

For simplicity we have limited ourselves to a single band and have used the fact that the current operators $j_\nu(0)$ then have only diagonal elements; T is equal to $t - t_0$. We now wish to evaluate this expression for $\sigma_{\mu\nu}$ in the limit $\lambda \to 0$. The factor $(\partial f/\partial H)_{\mathbf{k},\mathbf{k}'}$ is a well-behaved function of λ, and can be expanded in a power series in λ by well-known techniques. However, if one makes a naïve attempt to expand the integral

$$\int_0^T dt' \langle \mathbf{k}' | j_\mu(t') | \mathbf{k} \rangle \qquad \ldots\ldots(3.3)$$

in a power series in λ it is obvious that the zero order term is proportional to T. This term would lead to a 'conductivity' that increases without limit as $T \to \infty$. In fact for large T every term in the expansion of (3.3) in powers of λ is equally important. What we must do therefore is to select, in some way, the 'biggest' part of each term in the power series and then sum up all these parts. When this is done it is found that in the limit of large T and small λ the integral becomes independent of T and is proportional to λ^{-2}. The sense in which there is a 'biggest' part to each term will be made precise when we outline Van Hove's work. We therefore proceed as follows. The factor $(\partial f/\partial H)_{\mathbf{k},\mathbf{k}'}$ is expanded in powers of λ and the leading term $(\partial f/\partial H_0)_{\mathbf{k},\mathbf{k}}\,\delta_{\mathbf{k},\mathbf{k}'}$ in the series is taken together with the leading term in the integral (3.3). Since the latter is of order λ^{-2} the conductivity will also be of this order. The correction to $\sigma_{\mu\nu}$ arising from higher order terms in λ will be considered in detail in the next section where we shall also make some remarks about the general validity of the expansion method. We can therefore write

$$\sigma_{\mu\nu} = -\sum \left(\frac{\partial f}{\partial H_0}\right)_{\mathbf{k},\mathbf{k}} \int_0^T dt \langle \mathbf{k} | U(-t) j_\mu(0) U(t) | \mathbf{k} \rangle \langle \mathbf{k} | j_\nu(0) | \mathbf{k} \rangle \qquad \ldots\ldots(3.4)$$

where

$$U(t) = \exp\{-it(H_0 + \lambda V)\}, \qquad \ldots\ldots(3.5)$$

and it is understood that the time integral is to be evaluated to order λ^{-2}. Van Hove's work on the quantum mechanical master equation is concerned with the behaviour, as functions of λ and t, of expressions of precisely the form $\langle \mathbf{k} | U(-t) j_\mu(0) U(t) | \mathbf{k} \rangle$. We shall now give an outline of his work to show how one can evaluate the time integral in (3.4) to order λ^{-2}.

3.1. *An Outline of Van Hove's Work*

Van Hove first shows that $U(t)$ can be written in the form

$$U(t) = U_\mathrm{D}(t) + \sum_{n=1}^{\infty} (-i\lambda)^n \int_0^t dt_n \ldots\ldots\ldots \int_0^{t_2} dt_1$$
$$\times \{U_\mathrm{D}(t-t_n) V U_\mathrm{D}(t_n - t_{n-1}) V \ldots . \; V U_\mathrm{D}(t_1)\}_\mathrm{nd} . \qquad \ldots\ldots (3.6)$$

Here U_D stands for the diagonal part of U, and the subscript 'nd' means that when we evaluate any of the terms in the curly brackets the intermediate states must be kept pair by pair different. The first approximation that Van Hove introduces is to replace the operators $U_\mathrm{D}(t)$ in (3.6) by operators $U^W(t)$ defined as follows :

$$U^W(t) = \exp(-iH_0 t) + \sum_{n=1}^{\infty} U_{2n}{}^W(t) \qquad \ldots\ldots (3.7)$$

where

$$\langle \mathbf{k} | U_{2n}{}^W(t) | \mathbf{k}' \rangle = (-\lambda^2)^n \delta_{\mathbf{k},\mathbf{k}'} \exp(-iE_\mathbf{k} t) \int_0^t dt_{2n} \ldots\ldots \int_0^{t_2} dt_1$$
$$\times \sum_{\mathbf{k}_n} W_{\mathbf{k},\mathbf{k}_n} \exp\{-i(E_{\mathbf{k}_n} - E_\mathbf{k})(t_{2n} - t_{2n-1})\} \qquad \ldots\ldots (3.8)$$
$$\times \sum_{\mathbf{k}_{n-1}} W_{\mathbf{k},\mathbf{k}_{n-1}} \exp\{-i(E_{\mathbf{k}_{n-1}} - E_\mathbf{k})(t_{2n-2} - t_{2n-3})\} \ldots\ldots$$
$$\ldots\ldots \times \sum_{\mathbf{k}_1} W_{\mathbf{k},\mathbf{k}_1} \exp\{-i(E_{\mathbf{k}_1} - E_\mathbf{k})(t_2 - t_1)\},$$

and

$$W_{\mathbf{k},\mathbf{k}'} = | V_{\mathbf{k},\mathbf{k}'} |^2 . \qquad \ldots\ldots (3.9)$$

Because we prefer to work with a large but finite system we have defined these matrix elements with a Kronecker delta symbol rather than with a Dirac delta function. However, whenever it is mathematically convenient we shall replace summation by integrations. Physically U^W is that part of U_D in which every second intermediate state is identical with the initial and final states. Such a sequence of intermediate states can be conveniently represented by the following diagram :

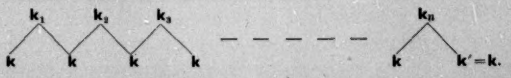

For obvious reasons we shall call such a transition scheme a saw-tooth scheme. The time integrals in (3.8) can readily be performed if we notice that the $W_{\mathbf{k},\mathbf{k}'}$ are slowly varying functions of their arguments and it is therefore legitimate to use the following approximate formula :

$$\int d\epsilon f(\epsilon) \int_0^{t_3} dt_2 \int_0^{t_2} dt_1 \frac{\exp\{-i\epsilon(t_2 - t_1)\} t_1{}^{p-1}}{(p-1)!} = \frac{t_3{}^p}{p!} \left[\pi f(0) - i \int d\epsilon P \frac{f(\epsilon)}{\epsilon} \right] . \qquad \ldots\ldots (3.10)$$

We shall investigate the corrections to this formula in § 4 where we shall show that they are small as long as $\hbar/\tau \ll \eta$. The repeated application of (3.10) yields

$$\langle \mathbf{k} \,|\, U_{2n}{}^{W} \,|\, \mathbf{k}' \rangle = (-\lambda^2 t)^n / n!\, \delta_{\mathbf{k},\mathbf{k}'} \exp(-iE_{\mathbf{k}} t) \{\Gamma(\mathbf{k}) + i\Delta(\mathbf{k})\}^n \quad \ldots\ldots (3.11)$$

where

$$\Gamma(\mathbf{k}) = \pi \int d^3\mathbf{k}_1\, W_{\mathbf{k},\mathbf{k}_1} \delta(E_{\mathbf{k}} - E_{\mathbf{k}_1}), \quad \ldots\ldots (3.12)$$

and

$$\Delta(\mathbf{k}) = \int d^3\mathbf{k}_1\, W_{\mathbf{k},\mathbf{k}_1} P\left(\frac{1}{E_{\mathbf{k}} - E_{\mathbf{k}_1}}\right). \quad \ldots\ldots (3.13)$$

For convenience we have chosen units so that the volume of the system equals $(2\pi)^3$; therefore no extra factors occur when the sums are replaced by integrals. The summation in (3.7) can now be performed to give

$$\langle \mathbf{k} \,|\, U^{W}(t) \,|\, \mathbf{k}' \rangle = \delta_{\mathbf{k},\mathbf{k}'} \exp\{-iE_{\mathbf{k}} t - i\lambda^2 t \Delta(\mathbf{k}) - \lambda^2 t\, \Gamma(\mathbf{k})\}. \quad \ldots\ldots (3.14)$$

Apart from terms of relative order N^{-1}, which we can obviously neglect, U^W is the only part of U_{D} that does not vanish in the limit $\lambda \to 0$, $t \to \infty$ so that $\lambda^2 t$ remains finite. In other words, apart from transition schemes that yield statistically negligible contributions, all other transition schemes, other than the saw-tooth scheme, yield contributions of relative order $\lambda^p (\lambda^2 t)^s$ and can therefore be said to vanish as λ^p for $\lambda \to 0$. We should emphasize that Van Hove's proof that certain transition schemes yield contributions of relative order N^{-1} depends on an important property λV, namely that for any diagonal operator A,

$$\langle \mathbf{k} \,|\, VAV \ldots AV \,|\, \mathbf{k}' \rangle = X_A(\mathbf{k}) \delta_{\mathbf{k},\mathbf{k}'} + Y_A(\mathbf{k}, \mathbf{k}'), \quad \ldots\ldots (3.15)$$

where Y_A is of relative order N^{-1} compared with X_A. It is easily shown that the potential for a set of *random* scatterers has just this property. It is this property of the potential that replaces the repeated random phase approximation that is usually used in the derivation of the Boltzmann equation. Both Kohn and Luttinger (1957) and Greenwood (1958) used the fact that the scatterers can be assumed to be distributed randomly to avoid the random phase assumption in their derivation of the Boltzmann equation. Now

$$\langle \mathbf{k}' \,|\, U(-t) j_\mu(0)\, U(t) \,|\, \mathbf{k} \rangle = \int d^3\mathbf{k}'' \langle \mathbf{k}' \,|\, U(-t) \,|\, \mathbf{k}'' \rangle \langle \mathbf{k}'' | j_\mu(0) | \mathbf{k}'' \rangle \langle \mathbf{k}'' \,|\, U(t) \,|\, \mathbf{k} \rangle, \quad \ldots\ldots (3.16)$$

and if we define

$$U_n(t) = (-i\lambda)^n \int_0^t dt_n \ldots\ldots \int^{t_2} dt_1 \{U^W(t - t_n) V U^W(t_n - t_{n-1}) \ldots U^W(t_1)\}_{\mathrm{nd}} \qquad n \neq 0, \quad \ldots\ldots (3.17)$$

and

$$U_0(t) = U^W(t) \quad \ldots\ldots (3.18)$$

then (3.16) can be written

$$\langle \mathbf{k}' \,|\, U(-t) j_\mu\, U(t) \,|\, \mathbf{k} \rangle$$

$$= \sum_{nn'} \int d^3\mathbf{k}'' \langle \mathbf{k}' \,|\, U_n(-t) \,|\, \mathbf{k}'' \rangle \langle \mathbf{k}'' \,| j_\mu(0) \,|\, \mathbf{k}'' \rangle \langle \mathbf{k}'' \,|\, U_{n'}(t) \,|\, \mathbf{k} \rangle. \quad \ldots\ldots (3.19)$$

Van Hove has shown that the expression on the right-hand side of this equation can be easily evaluated if one considers only the following contributions.

(i) Only the terms for which $n=n'$ are taken.

(ii) If the factors $\langle \mathbf{k}' \,|\, U_n \,|\, \mathbf{k}'' \rangle$ and $\langle \mathbf{k}'' \,|\, U_n \,|\, \mathbf{k} \rangle$ are written out in terms of the matrix elements of V and U^W then to the right of the factor $\langle \mathbf{k}'' \,|j_\mu \,|\, \mathbf{k}'' \rangle$in (3.19) we shall have a sequence (read from left to right) of intermediate states $\mathbf{k}_1 \ldots\ldots \mathbf{k}_n = \mathbf{k}$; to the left of $\langle \mathbf{k}'' \,|j_\mu \,|\, \mathbf{k}'' \rangle$ we shall have another sequence (read from right to left) $\mathbf{k}_1' \ldots\ldots \mathbf{k}_n' = \mathbf{k}'$. We now take only those transition schemes for which $\mathbf{k}_j \equiv \mathbf{k}_j'$; we shall call such a scheme a symmetrical transition scheme.

(iii) As before the time integrals are approximated by their asymptotic values for long times and therefore lead to δ functions.

All other contributions to (3.19) are either of relative order N^{-1} or λ^p, and can therefore be consistently neglected. We can now give a precise definition of the word 'biggest' that we used previously. The biggest contributions to (3.19) are those which do not vanish in either of the limits $N \to \infty$ or $\lambda \to 0$ and $t \to \infty$, so that $\lambda^2 t$ remains finite. At this stage it is convenient to introduce a change of notation. Instead of labelling the states by a wave vector $\mathbf{k}$ we label them by their energy E and a symbol α which stands for any other two independent variables that complete the specification of the state. The volume element in $\mathbf{k}$ space $d^3\mathbf{k}$ will be replaced by $dE\lambda\alpha$, where $d\alpha$ is not only the product of the differentials of the two new variables but in general will contain a density function $\rho(E, \alpha)$. With this notation it is simple to write down Van Hove's final expression for $\langle \mathbf{k}' \,|j_\mu(t) \,|\, \mathbf{k} \rangle$; it is

$$\begin{aligned}\langle \mathbf{k}' \,|j_\mu(t) \,|\, \mathbf{k} \rangle &= \langle E'\alpha' \,|j_\mu(t) \,|\, E\alpha \rangle \\ &= \delta_{E,E'}\, \delta_{\alpha,\alpha'} \int d\alpha''\, P_t(E\alpha'', E\alpha)\, j_\mu(E\alpha'') \qquad \ldots\ldots(3.20)\end{aligned}$$

where $j_\mu(E\alpha'')$ stands for the diagonal element $\langle E\alpha'' \,|j_\mu(0) \,|\, E\alpha'' \rangle$ and $P_t(E\alpha'', E\alpha)$ is defined by the infinite series

$$\begin{aligned}P_t(E\alpha'', E\alpha) = \delta_{\alpha'',\alpha} \exp\{-2\lambda^2 t \Gamma(E\alpha)\} + \sum_{n=1}^{\infty} (2\pi\lambda^2)^n \int_0^t dt_n \ldots\ldots \int_0^{t_2} dt_1 \\ \times \int d\alpha_{n-1} \ldots\ldots \int d\alpha_1 \exp\{-2\lambda^2 (t-t_n)\, \Gamma(E\alpha'')\}\, W(E\alpha'', E\alpha_{n-1}) \\ \times \exp\{-2\lambda^2 (t_n - t_{n-1})\, \Gamma(E\alpha_{n-1})\}\, W(E\alpha_{n-1}, E\alpha_{n-2}) \\ \times \ldots\ldots W(E\alpha_1, E\alpha) \exp\{-2\lambda^2 t_1\, \Gamma(E\alpha)\}. \qquad \ldots\ldots(3.21)\end{aligned}$$

If we differentiate both sides of (3.21) with respect to time we find that $P_t(E\alpha'', E\alpha)$ obeys the 'master' equation

$$\begin{aligned}\frac{dP_t}{dt}(E\alpha'', E\alpha) &= 2\pi\lambda^2 \int d\alpha'\, W(E\alpha'', E\alpha')\, P_t(E\alpha', E\alpha) \\ &\quad - 2\pi\lambda^2 \left\{ \int d\alpha'\, W(E\alpha', E\alpha'') \right\} P_t(E\alpha'', E\alpha). \qquad \ldots\ldots(3.22)\end{aligned}$$

We refer to this equation as the 'master' equation for a single electron; it is not of course the master equation for the entire system. The solution of this equation must obey the initial condition,

$$P_0(E\alpha'', E\alpha) = \delta_{\alpha'',\alpha}. \qquad \ldots\ldots(3.23)$$

Equations (3.20) and (3.21) are the results of Van Hove's work that we require to evaluate the formula for the conductivity.

3.2. *The Calculation of the Conductivity*

We now turn to the evaluation of the conductivity tensor given by (3.4). For simplicity we specialize to the case of free electrons and spherically symmetrical scattering centres, though it is easily shown that our results are in fact valid as long as $E_{\mathbf{k}}$ is a function of $|\mathbf{k}|$ alone. The more general case of electrons in a periodic lattice and asymmetrical scatterers will be treated in § 5. It is convenient to work with spherical polar coordinates in (E, α) space, taking for α the two polar angles θ and ϕ of the wave vector $\mathbf{k}$. There are two important consequences of our simplifying assumptions. Firstly, it is a simple matter to show that $\Gamma(E\alpha)$ is only a function of E. Equation (3.21) can therefore be written as

$$P_t(E\alpha'', E\alpha) = \exp\{-2\lambda^2 t\,\Gamma(E)\}\Bigg[\delta_{\alpha'',\alpha} + \sum_{n=1}^{\infty}\frac{(2\pi\lambda^2 t)^n}{n!} \times \int d\alpha_{n-1}\dots\int d\alpha_1\,W(E\alpha'', E\alpha_{n-1})\dots\dots W(E\alpha_1, E\alpha)\Bigg]. \quad \dots\dots(3.24)$$

Secondly, $W(E\alpha_1, E\alpha_2)$ is a function only of the energy E and the angle Θ between the two directions defined by α_1 and α_2. This enables us to show that

$$\int d\alpha_1 j_\mu(E\alpha_1)\,W(E\alpha_1, E\alpha_2) = j_\mu(E\alpha_2)\,\Gamma_1(E) \qquad \dots\dots(3.25)$$

where $\Gamma_1(E)$ is only a function of the energy. To prove this one chooses the coordinate system to perform the integration in such a way that the angular dependence of $j_\mu(E\alpha_1)$ is given by $\cos\theta_1$. Next W is expanded in spherical harmonics of argument $\cos\Theta$ and these in turn are expanded, by the addition theorem, in terms of $Y_l^m(\theta_1, \phi_1)\,Y_l^{m*}(\theta_2, \phi_2)$. Integration over the variables θ_1, ϕ_1 yields (3.25) with

$$\Gamma_1(E) = 2\pi\int_{-1}^{+1}\rho(E)\cos\theta\,W(E, \cos\theta)\,d(\cos\theta) \qquad \dots\dots(3.26)$$

where $\rho(E)$ is defined by $d^3\mathbf{k} = \rho(E)\,d(\cos\theta)\,d\phi$. Combining (3.20), (3.24) and (3.25) we find that

$$\langle\mathbf{k}\,|j_\mu(t)|\,\mathbf{k}'\rangle = \delta_{\mathbf{k},\mathbf{k}'}\langle\mathbf{k}\,|j_\mu(0)|\,\mathbf{k}\rangle\exp\{-2\lambda^2 t(\Gamma - \Gamma_1)\}, \qquad \dots\dots(3.27)$$

from which it follows that,

$$\int_0^T dt\langle\mathbf{k}\,|j_\mu(t)|\,\mathbf{k}\rangle = \frac{\langle\mathbf{k}|j\mu(0)|\mathbf{k}\rangle}{2\lambda^2(\Gamma - \Gamma_1)}[1 - \exp\{-2\lambda^2 T(\Gamma - \Gamma_1)\}] \qquad \dots\dots(3.28)$$

Since $\Gamma - \Gamma_1$ is always positive and T may be taken as large as we please the exponential can be neglected. The standard definition of the collision time $\tau(E)$ is

$$\frac{1}{\tau(E)} = 4\pi\lambda^2\rho(E)\int_{-1}^{+1}(1 - \cos\theta)\,W(E, \cos\theta)\,d(\cos\theta) \qquad \dots\dots(3.29)$$

or, in our notation,

$$\frac{1}{\tau(E)} = 2\lambda^2\{\Gamma(E) - \Gamma_1(E)\}. \qquad \dots\dots(3.30)$$

If we substitute (3.28) and (3.30) into (3.4) we obtain the standard formula for the conductivity,

$$\sigma_{\mu\nu} = -\sum_{\mathbf{k}}\frac{\partial f}{\partial E_{\mathbf{k}}}\langle\mathbf{k}\,|j_\mu|\,\mathbf{k}\rangle\langle\mathbf{k}\,|j_\nu|\,\mathbf{k}\rangle\,\tau(E_{\mathbf{k}}). \qquad \dots\dots(3.31)$$

We have therefore shown that Van Hove's results can be used to derive the standard formula for the conductivity without any use of the repeated random phase approximation. In the next section we shall show that the higher order corrections to $\sigma_{\mu\nu}$ are small as long as the condition $1/\tau \ll \eta$ is fulfilled.

§ 4. CORRECTIONS TO THE CONDUCTIVITY

In § 3 we calculated the conductivity to order λ^{-2}; we shall now estimate the magnitude of the next highest order term in the expansion of $\sigma_{\mu\nu}$ in powers of λ. We begin by writing the basic formula (3.2) in the form

$$\sigma_{\mu\nu} = -\sum_{\mathbf{k},\mathbf{k}'} S_{\mathbf{k},\mathbf{k}'} D_{\mathbf{k}',\mathbf{k}} \langle \mathbf{k} | j_\nu | \mathbf{k} \rangle \qquad \ldots\ldots (4.1)$$

where

$$S_{\mathbf{k},\mathbf{k}'} = (\partial f/\partial H)_{\mathbf{k}\,\mathbf{k}} \qquad \ldots\ldots (4.2)$$

and

$$D_{\mathbf{k}',\mathbf{k}} = \int_0^T dt\, \langle \mathbf{k}' | U(-t) j_\mu(0)\, U(t) | \mathbf{k} \rangle. \qquad \ldots\ldots (4.3)$$

We now expand $S_{\mathbf{k},\mathbf{k}'}$ and $D_{\mathbf{k}',\mathbf{k}}$ in powers of λ and write,

$$S_{\mathbf{k},\mathbf{k}'} = S_{\mathbf{k},\mathbf{k}'}{}^{(0)} + S_{\mathbf{k},\mathbf{k}'}{}^{(1)} + S_{\mathbf{k},\mathbf{k}'}{}^{(2)} + \ldots\ldots \qquad \ldots\ldots (4.4)$$

and

$$D_{\mathbf{k},\mathbf{k}'} = D_{\mathbf{k},\mathbf{k}'}{}^{(-2)} + D_{\mathbf{k},\mathbf{k}'}{}^{(-1)} + D_{\mathbf{k},\mathbf{k}'}{}^{(0)} + \ldots\ldots \qquad \ldots\ldots (4.5)$$

In these expansions the superscript (n) implies that the term in question is of order λ^n. If we substitute (4.4) and (4.5) into (4.1), and remember that V has no diagonal elements, we obtain the following expansion for $\sigma_{\mu\nu}$:

$$\sigma_{\mu\nu} = \sigma_{\mu\nu}{}^{(-2)} + \sigma_{\mu\nu}{}^{(0)} + \ldots\ldots \qquad \ldots\ldots (4.6)$$

where

$$\sigma_{\mu\nu}{}^{(-2)} = -\sum_{\mathbf{k},\mathbf{k}} S_{\mathbf{k},\mathbf{k}'}{}^{(0)} D_{\mathbf{k}'\mathbf{k}}{}^{(-2)} \langle \mathbf{k} | j_\nu | \mathbf{k} \rangle \qquad \ldots\ldots (4.7)$$

and

$$\sigma_{\mu\nu}{}^{(0)} = C_{2,-2} + C_{1,-1} + C_{0,0} \qquad \ldots\ldots (4.8)$$

with

$$C_{2,-2} = -\sum_{\mathbf{k},\mathbf{k}'} S_{\mathbf{k},\mathbf{k}'}{}^{(2)} D_{\mathbf{k}',\mathbf{k}}{}^{(-2)} \langle \mathbf{k} | j_\nu | \mathbf{k} \rangle \qquad \ldots\ldots (4.9\,a)$$

$$C_{1,-1} = -\sum_{\mathbf{k},\mathbf{k}'} S_{\mathbf{k},\mathbf{k}'}{}^{(1)} D_{\mathbf{k}',\mathbf{k}}{}^{(-1)} \langle \mathbf{k} | j_\nu | \mathbf{k} \rangle \qquad \ldots\ldots (4.9\,b)$$

$$C_{0,0} = -\sum_{\mathbf{k},\mathbf{k}'} S_{\mathbf{k},\mathbf{k}'}{}^{(0)} D_{\mathbf{k}',\mathbf{k}}{}^{(0)} \langle \mathbf{k} | j_\nu | \mathbf{k} \rangle. \qquad \ldots\ldots (4.9\,c)$$

$\sigma_{\mu\nu}{}^{(-2)}$ is of course the contribution to $\sigma_{\mu\nu}$ that we calculated in § 3. Our task in this section will be to make a careful estimate of the magnitude of $\sigma_{\mu\nu}{}^{(0)}$ compared with $\sigma_{\mu\nu}{}^{(-2)}$. Before proceeding we make two remarks. First, since we wish to estimate the magnitude of $\sigma_{\mu\nu}{}^{(0)}$ for a wide class of scattering potentials it is necessary to use dimensional arguments. We believe that these arguments are in fact quite rigorous. For the sake of those readers who are sceptical about their validity we remark that we have always verified that our conclusions are correct by carrying out explicit calculations with simple models.

Secondly, we wish to point out that the use of this expansion does involve the assumption that the conductivity can be approximated, at least under some conditions, by a power series in λ. The reason we make this remark is that there are some problems for which it is known that one cannot approach the correct solution at all by a perturbation expansion. For example in the de Haas–van Alphen effect the magnetic susceptibility as a function of the magnetic field H contains terms of the form $\exp(-\pi^2 kT/\mu H)$. Clearly a function such as this cannot be approximated at all by a power series in H. We shall not enter into any further discussion of this problem and we shall assume that the conductivity can be approximated by the power series (4.6).

We estimate the size of each of the three contributions to $\sigma_{\mu\nu}^{(0)}$ separately.

4.1. *The Contribution* $C_{2,-2}$

The factor $S_{\mathbf{k},\mathbf{k}'}^{(2)}$ can be calculated by standard methods (Schafroth 1951); it is given by the equation,

$$S_{\mathbf{k},\mathbf{k}'}^{(2)} = \lambda^2 \sum_{\mathbf{k}''} V_{\mathbf{k},\mathbf{k}''} V_{\mathbf{k}'',\mathbf{k}'} \left\{ \frac{f'(E)}{(E-E'')(E-E')} + \frac{f'(E'')}{(E''-E)(E''-E')} + \frac{f'(E')}{(E'-E)(E'-E'')} \right\}, \qquad \ldots\ldots (4.10)$$

where for shortness we have written E for $E_{\mathbf{k}}$ etc. and $f'(E) = \partial f(E)/\partial E$. It follows from (3.20) that

$$D_{\mathbf{k}',\mathbf{k}}^{(-2)} = D_{\mathbf{k},\mathbf{k}}^{(-2)} \delta_{\mathbf{k},\mathbf{k}'}, \qquad \ldots\ldots (4.11)$$

while from (3.28) and (3.30)

$$D_{\mathbf{k},\mathbf{k}}^{(-2)} = \langle \mathbf{k} | j_\mu | \mathbf{k} \rangle \tau(E). \qquad \ldots\ldots (4.12)$$

The diagonal part of $S_{\mathbf{k},\mathbf{k}}^{(2)}$ is given by the equation

$$S_{\mathbf{k},\mathbf{k}}^{(2)} = \lambda^2 \sum_{\mathbf{k}''} | V_{\mathbf{k},\mathbf{k}''} |^2 \left\{ \frac{f''(E)}{E-E''} - \frac{f'(E)-f'(E'')}{(E-E'')^2} \right\}. \qquad \ldots\ldots (4.13)$$

Substituting (4.12) and (4.13) in (4.9 *a*) we find that

$$C_{2,-2} = -\lambda^2 \sum_{\mathbf{k},\mathbf{k}''} | V_{\mathbf{k},\mathbf{k}''} |^2 \langle \mathbf{k} | j_\mu | \mathbf{k} \rangle \langle \mathbf{k} | j_\nu | \mathbf{k} \rangle \tau(E) g(E,E''), \qquad \ldots\ldots (4.14)$$

where

$$g(E,E'') = \frac{f''(E)}{E-E''} - \frac{f'(E)-f'(E')}{(E-E'')^2}. \qquad \ldots\ldots (4.15)$$

If we assume, as is reasonable, that $| V_{\mathbf{k},\mathbf{k}''} |^2$ has no singularities for real $\mathbf{k}, \mathbf{k}''$, then we can show that the sum over $\mathbf{k}$ and $\mathbf{k}''$ in (4.14) converges. First, a simple calculation shows that $g(E,E) = \frac{1}{2} f'''(E)$, and hence the point $E = E''$ is not a singular point in the summation. Secondly, although the sum might appear to diverge for large values of the energies E and E'' it is easily shown that the summand goes to zero rapidly enough as $E, E'' \to \infty$ for the sum to converge†. We now estimate the size of $C_{2,-2}$ compared with $\sigma_{\mu\nu}^{(-2)}$ by introducing dimensionless variables in the summation in (4.14). We first note that all the factors in (4.14) except $g(E,E'')$ are slowly varying functions (over intervals of order η) of the energies E and E''. This allows us to replace the Fermi functions in $g(E,E'')$ by their values at absolute zero, the corrections due to the fact that the system is at a finite temperature are of relative order $(kT/\eta)^2$ and are hence negligible. Since we measure the strength of the scattering potential by λ the only parameters in $C_{2,-2}$ are the range a of the potential and the Fermi energy η. Now if we measure all energies in units of η and all lengths in units of k_F^{-1}, where k_F is the Fermi wave number, then $C_{2,-2}$ can be written as

---

† While this statement is generally true there are certain potentials (namely those with r^{-1} singularities at the origin) for which the sum does not converge at large energies. However, it is found that the singular terms in $C_{2,-2}$ are exactly cancelled by singular terms in $C_{1,-1}$. The arguments we use should in this case be applied to $C_{2,-2} + C_{1,-1}$ rather than to $C_{2,-2}$ and $C_{1,-1}$ individually.

$$C_{2,-2}=\frac{\lambda^2\gamma}{\eta}\int_0^\infty\int_0^\infty \phi(z,z'',s)\,dz\,dz''=\frac{\lambda^2\gamma}{\eta}I_1(s) \qquad \ldots\ldots(4.16)$$

where $z=E/\eta, z''=E''/\eta$; ϕ is a dimensionless function obtained by carrying out the angular integrations in the right-hand side of (4.14), and γ has the dimensions of $j_\mu j_\nu\,\tau$. The constant s on which ϕ depends is equal to $k_F a$ and is of order unity for all potentials of interest. It follows at once from our discussion about the rate of variation of the factors in $C_{2,-2}$ that the integral I_1 exists and is of order unity. By introducing the same set of units we can write,

$$\sigma_{\mu\nu}^{(-2)}=\frac{\gamma}{\eta}I_2(s), \qquad \ldots\ldots(4.17)$$

and

$$1/\tau(\eta)=\lambda^2\eta\,I_3(s), \qquad \ldots\ldots(4.18)$$

where I_2 and I_3 are two integrals of order unity. Then

$$C_{2,-2}/\sigma_{\mu\nu}^{(-2)}=\frac{\lambda^2\eta}{\eta}\,\frac{I_1}{I_2}, \qquad \ldots\ldots(4.19)$$

or using (4.18)

$$C_{2,-2}/\sigma_{\mu\nu}^{(-2)}=\frac{1}{\tau(\eta)\eta}\,\frac{I_1}{I_3 I_2}. \qquad \ldots\ldots(4.20)$$

Consequently $C_{2,-2}$ will be small compared with $\sigma_{\mu\nu}^{(-2)}$ as long as

$$\frac{1}{\tau(\eta)\eta}\ll 1. \qquad \ldots\ldots(4.21)$$

4.2. *The Contribution* $C_{1,-1}$

If we use the more symmetrical form for $\sigma_{\mu\nu}$, given by (2.5), $C_{1,-1}$ can be written as

$$C_{1,-1}=-\tfrac{1}{2}\sum_{\mathbf{k},\mathbf{k}'}S_{\mathbf{k},\mathbf{k}'}^{(1)}\left[\langle\mathbf{k}|j_\nu|\mathbf{k}\rangle+\langle\mathbf{k}'|j_\nu|\mathbf{k}'\rangle\right]D_{\mathbf{k}',\mathbf{k}}^{(-1)}. \qquad \ldots\ldots(4.22)$$

The factor $S_{\mathbf{k},\mathbf{k}'}^{(1)}$ is given by

$$S_{\mathbf{k},\mathbf{k}'}^{(1)}=\lambda V_{\mathbf{k},\mathbf{k}'}\frac{f'(E)-f'(E')}{E-E'}. \qquad \ldots\ldots(4.23)$$

The factor $D_{\mathbf{k}',\mathbf{k}}^{(-1)}$ can be calculated using equation (3.19), taking those terms in the double sum over n and n' for which $|n-n'|=1$. The other approximations that were used in calculations of $D_{\mathbf{k},\mathbf{k}'}^{(-2)}$ are of course retained. We find that

$$D_{\mathbf{k}',\mathbf{k}}^{(-1)}=\lambda V_{\mathbf{k}',\mathbf{k}}\left[-i\pi\delta(E'-E)+P\frac{1}{E'-E}\right]\times\left[D_{\mathbf{k}',\mathbf{k}'}^{(-2)}-D_{\mathbf{k},\mathbf{k}}^{(-2)}\right]. \qquad \ldots\ldots(4.24)$$

Equations (4.23) and (4.24) lead at once to the following expression for $C_{1,-1}$:

$$C_{1,-1} = \tfrac{1}{2}\lambda^2 \sum_{\mathbf{k},\mathbf{k}'} |V_{\mathbf{k},\mathbf{k}'}|^2 [\langle \mathbf{k}|j_\nu|\mathbf{k}\rangle + \langle \mathbf{k}'|j_\nu|\mathbf{k}'\rangle]$$
$$\times [\langle \mathbf{k}|j_\mu|\mathbf{k}\rangle \tau(E) - \langle \mathbf{k}'|j_\mu|\mathbf{k}'\rangle \tau(E')]\, P\frac{1}{E'-E} h(E,E'). \quad \ldots\ldots (4.25)$$

The imaginary terms in $C_{1,-1}$ cancel identically; $h(E, E')$ is given by

$$h(E,E') = \frac{f'(E)-f'(E')}{E-E'} \quad \ldots\ldots (4.26)$$

and is a function of E and E' without singularities. By similar arguments to those we have just used, we can easily show that $C_{1,-1}$ is small compared with $\sigma_{\mu\nu}^{(-2)}$ as long as (4.21) is fulfilled.

4.3. *The Contribution* $C_{0,0}$

Since

$$S_{\mathbf{k},\mathbf{k}'}^{(0)} = \frac{\partial f}{\partial E}\delta_{\mathbf{k},\mathbf{k}'}. \quad \ldots\ldots (4.27)$$

we need only consider $D_{\mathbf{k},\mathbf{k}}^{(0)}$. As there are several different contributions to $D_{\mathbf{k},\mathbf{k}}^{(0)}$ we shall not write down explicit expressions for all of them. What we shall do is to point out exactly how the various contributions arise and show how their magnitude may be estimated. To calculate $D_{\mathbf{k},\mathbf{k}}^{(0)}$ we essentially have to improve the approximations that we made in calculating $D_{\mathbf{k},\mathbf{k}}^{(-2)}$. These approximations were of two different kinds. Firstly, we took into account certain very simple transition schemes, namely the saw-tooth and symmetrical schemes. Secondly, all the time integrals were approximated by their asymptotic values for long times; for example in calculating U^W we used (3.10) repeatedly. It is therefore convenient to list the contributions to $D_{\mathbf{k},\mathbf{k}}^{(0)}$ under these two headings.

Transition scheme corrections.

(i) Corrections to U^D from transition schemes other than the saw-tooth schemes.

(ii) Corrections to (3.20), (3.21) from terms in the sum over n and n' in (3.19) for which $|n-n'| \neq 2$.

(iii) Corrections to (3.20), (3.21) from non symmetrical transition schemes.

Time integral corrections.

(iv) Correction to U^W arising from a more accurate treatment of the time integrals in (3.8).

(v) Corrections to (3.20), (3.21) arising from a more accurate treatment of the time integrals in (3.19).

Corrections in which one takes into account simultaneously transition scheme and time integral corrections are of higher order in λ and do not contribute to $D_{\mathbf{k},\mathbf{k}}^{(0)}$.

The transition scheme corrections can be estimated quite simply by means of the following argument. We notice that no matter what transition schemes we consider only terms of order $\lambda^{p-2}(\lambda^2 T)^s (p, s \geqslant 0)$ can occur in the expansion of $D_{\mathbf{k},\mathbf{k}}$ in powers of λ. This result is easily obtained if one uses the asymptotic formula for the time integrals involved. As we have just pointed out this is perfectly justified. The sum of all terms in the expansion for which $p=0$ is $D_{\mathbf{k},\mathbf{k}}^{(-2)}$, while the sum of all terms for which $p=2$ contributes to $D_{\mathbf{k},\mathbf{k}}^{(0)}$. This argument strongly suggests that these contributions to $D_{\mathbf{k},\mathbf{k}}^{(0)}$ are of relative magnitude λ^2 compared with $D_{\mathbf{k},\mathbf{k}}^{(-2)}$. The reason that the argument does not prove that this is so is that we have not shown that the sum of all terms for which $p=2$ converges to a limit that is independent of T. For the simple model with constant matrix elements it is easy to verify that this sum does in fact converge to a limit independent of T. We see no reason to doubt that it converges for more general potentials. We can therefore say that the contributions to $D_{\mathbf{k},\mathbf{k}}^{(0)}$ from the transition scheme corrections are of relative magnitude λ^2 compared with $D_{\mathbf{k},\mathbf{k}}^{(-2)}$. From this it follows that they will be small as long as (4.21) is fulfilled.

We now turn to the time integral corrections (iv) and (v). As these corrections are very similar we shall deal with (iv) in some detail and we merely remark that the treatment of (v) proceeds along very similar lines.

Equation (3.14) for the matrix elements of U^W was obtained by using the asymptotic formula (3.10) for the time integrals in the saw-tooth transition scheme. Our task is to estimate the error thereby introduced into the conductivity. We do this by simply writing down a more accurate formula for the basic double integral $I_p(t)$;

$$I_p(t)=\frac{1}{p!}\int_0^t dt_2\int_0^{t_2} dt_1 t_1^p\int_{-E}^{\infty} f(\epsilon)\,d\epsilon\exp\{-i\epsilon(t_2-t_1)\}. \qquad \ldots\ldots(4.28)$$

Here we have written ϵ for a typical energy difference and the integral over ϵ runs from $-E$ to ∞ because the density of states vanishes for negative energies. A convenient formula for I_p can be obtained by the theory of residues. To apply this theory we assume (*a*) that $f(z)$ has no poles on the real axis and (*b*) that $|f(z)|\to 0$ as $|z|\to\infty$. These assumptions do not appear to us to be at all restrictive. It is then a straightforward matter to show that

$$\pi f(0)-i\int_{-E}^{\infty} P\frac{f(\epsilon)}{\epsilon}\,d\epsilon=-2\pi\sum_n\frac{f_n}{a_n}+i\int_{-i\infty-E}^{-E}\frac{f(z)}{z}\,dz. \qquad \ldots\ldots(4.29)$$

Here a_n is the position of the nth pole of $f(z)$ in the lower half of the complex plane to the right of the line $z=-E$, and f_n is the residue of $f(z)$ there. It is equally easy to show that

$$\int_{-E}^{\infty} f(\epsilon)\exp\{-i\epsilon(t_2-t_1)\}\,d\epsilon=-2\pi i\sum_n f_n\exp\{-ia_n(t_2-t_1)\}$$
$$-\int_{-i\infty-E}^{-E} f(z)\exp\{-iz(t_2-t_1)\}. \qquad \ldots\ldots(4.30)$$

If we substitute this expression into (4.28) we obtain the following approximate expression for I_p

$$I_p(t)=\frac{t^{p+1}}{(p+1)!}\left(\pi f(0)-i\int_{-E}^{\infty} P\frac{f(\epsilon)}{\epsilon}\,d\epsilon\right)$$
$$+\frac{t^p}{p!}\left(-2\pi i\sum_n\frac{f_n}{a_n^2}-i\int_{-i\infty-E}^{E}\frac{f(z)}{z^2}\,dz\right). \qquad \ldots\ldots(4.31)$$

This expression, although not exact, is in general accurate enough to allow us to estimate the corrections to the matrix elements of $U^W(t)$. The other terms in

I_p are either of order t^{p-1} or are exponentially damped in time. Now in our notation,

$$\Gamma + i\Delta = \pi f(0) - i\int_{-E}^{\infty} P\frac{f(\epsilon)}{\epsilon}\,d\epsilon, \qquad \ldots\ldots(4.32)$$

and we define Γ' and Δ' by the equation

$$\frac{\Gamma' + i\Delta'}{E} = -2\pi i\sum_n \frac{f_n}{a_n^2} - \int_{-i\infty-E}^{-E} \frac{f(z)}{z^2}\,dz. \qquad \ldots\ldots(4.33)$$

We now assert that Γ' and Δ' are of the same order of magnitude as Γ and Δ. This follows from a comparison of (4.33) with the definition of $\Gamma + i\Delta$ given by combining (4.32) and (4.29). We see that the sum over residues in (4.33) has an extra factor a_n in the denominator as compared with that in (4.29) while the integral in (4.32) has an extra factor z^{-1} in the integrand as compared with that in (4.29). If we now use our familiar dimensional arguments and note that $|V_{\mathbf{k},\mathbf{k}'}|^2$ is a function of E and E' that only changes appreciably when E or E' changes by an amount of order η then it is easily seen that Γ' and Δ' are of the same order of magnitude as Γ and Δ. The general term $U_{2n}{}^{W}$ that occurs in the expansion of U^W contains n pairs of time integrations; since we are interested in only the highest order corrections to U^W we need only correct one pair of time integrations at a time. If we correct the pth pair of integrations and sum over all p we find that

$$\langle \mathbf{k}|\, U_{2n}{}^{W} |\mathbf{k}'\rangle = \frac{(-\lambda^2 t)^W}{n!}\exp(-iE_{\mathbf{k}}t)\,\delta_{\mathbf{k},\mathbf{k}'}(\Gamma + i\Delta)^n - \delta_{\mathbf{k},\mathbf{k}'}\exp(-iE_{\mathbf{k}}t)\,\lambda^2$$
$$\times\frac{(\Gamma' + i\Delta')}{E}\,\delta_{n,1} + \frac{-(\lambda^2 t)^{n-1}}{(n-1)!}\exp(-iE_{\mathbf{k}}t)\,(\Gamma + i\Delta)^{n-1}\frac{\lambda^2(\Gamma' + i\Delta')}{E}. \qquad \ldots\ldots(4.34)$$

The extra term for $n = 1$ arises because equation (4.31) is not quite accurate enough for this particular term. A more accurate treatment leads to the extra term we have written down. From (4.34) we have at once that

$$\langle \mathbf{k}|\, U^W |\mathbf{k}'\rangle = \delta_{\mathbf{k},\mathbf{k}'}\exp(-iE_{\mathbf{k}}t)\exp\{-\lambda^2(\Gamma + i\Delta)t\}\Big[1 + \lambda^2\frac{(\Gamma' + i\Delta')}{E}$$
$$-\lambda^4 t(\Gamma + i\Delta)\frac{(\Gamma' + i\Delta')}{E}\Big] - \delta_{\mathbf{k},\mathbf{k}'}\exp(-iE_{\mathbf{k}}t)\frac{\lambda^2(\Gamma' + i\Delta')}{E}. \qquad \ldots\ldots(4.35)$$

We notice that at $t = 0$, $\langle \mathbf{k}|\, U^W |\mathbf{k}'\rangle = \delta_{\mathbf{k},\mathbf{k}'}$ as it should. Since $\lambda^2 t(\Gamma + i\Delta)$ is essentially of order unity all the correction terms in (4.35) are of the same order of magnitude. For simplicity we only estimate the contribution to U^W from the terms

$$\delta_{\mathbf{k},\mathbf{k}'}\exp(-iE_{\mathbf{k}}t)\exp\{-\lambda^2(\Gamma + i\Delta)t\}\left[1 - \lambda^4 t(\Gamma + i\Delta)\frac{(\Gamma' + i\Delta')}{E}\right]. \qquad \ldots\ldots(4.36)$$

Then to our degree of accuracy (4.35) can be written as

$$\langle \mathbf{k}|\, U^W |\mathbf{k}'\rangle = \delta_{\mathbf{k},\mathbf{k}'}\exp(-iE_{\mathbf{k}}t)\exp\{-\lambda^2(\bar{\Gamma} + i\bar{\Delta})t\} \qquad \ldots\ldots(4.37)$$

where

$$\bar{\Gamma} + i\bar{\Delta} = (\Gamma + i\Delta)\{1 + \lambda^2(\Gamma' + i\Delta')/E\}. \qquad \ldots\ldots(4.38)$$

If we compare (4.37) with (3.14) we see that they are identical except that Γ and Δ have been replaced by $\bar{\Gamma}$ and $\bar{\Delta}$. Consequently the contributions of these terms to $\sigma_{\mu\nu}$ can be written down at once:

$$\sigma_{\mu\nu} = -\sum_{\mathbf{k}} \frac{\partial f}{\partial E_{\mathbf{k}}} \langle \mathbf{k}|j_\mu|\mathbf{k}\rangle \langle \mathbf{k}|j_\nu|_{\mathbf{k}}\rangle \bar{\tau}(E). \qquad \ldots\ldots(4.39)$$

where $1/\bar{\tau}(E) = 2\lambda^2(\bar{\Gamma} - \bar{\Gamma}_1)$. Now $\bar{\Gamma}$ and $\bar{\Gamma}_1$ only differ from Γ and Γ_1 by terms of relative order Γ'/E or Δ'/E. That is, of relative order Γ/η or Δ/η, since $\Gamma' \sim \Gamma$, $\Delta' \sim \Delta$ and $E \sim \eta$. From this it follows that the time integral corrections to U^W will be small as long as $\Gamma/\eta \ll 1$, which is equivalent to (4.21).

In a very similar way the time integrals in (3.19) can be treated in a more accurate manner and it can again be shown that these corrections are small as long as (4.21) is fulfilled.

We have therefore shown in this section that the next highest order term $\sigma_{\mu\nu}^{(0)}$ in the expansion of $\sigma_{\mu\nu}$ is small compared with $\sigma_{\mu\nu}^{(-2)}$ as long as (4.21) is fulfilled. As far as we are aware the only other attempt to estimate the range of validity of the usual formula for the conductivity is due to van Wieringen (1954). He made an explicit calculation of what we have called the transition scheme corrections and came to the same conclusion as we have, namely that they are small as long as (4.21) is fulfilled. He did not however investigate any of the other correction terms we have just discussed.

§ 5. THE CONDUCTIVITY IN THE ANISOTROPIC CASE

In this section we deal with the most general case of elastic scattering of Bloch electrons by static obstacles. H_0 is now the Hamiltonian of the electrons in an arbitrary periodic potential and the scattering potential λV may now be anisotropic. We discuss (3.20) and (3.21) under these assumptions. The corrections to (3.20) and (3.21) will not be considered; it is obvious that they can be dealt with in a similar manner to that of § 4.

We find it convenient to assume that the variables characterized by α in § 3 take only discrete values (which they actually do for a large but finite system). Since the *same* value E of the energy occurs in all quantities in (3.20) and (3.21) we use the simplified notations

$$\left.\begin{array}{ll} \langle E\alpha|j_\mu|E\alpha\rangle = j_{\mu\alpha}; & P_t(E\alpha', E\alpha) = P_{t\alpha'\alpha} \\ \Gamma(E\alpha) = \Gamma_\alpha; & W(E\alpha', E\alpha) = W_{\alpha'\alpha} \end{array}\right\} \qquad \ldots\ldots(5.1)$$

always remembering that all quantities depend on E as a parameter. Then (3.20) and (3.21) may be written

$$\langle E'\alpha'|U(-t)j_\mu U(t)|E\alpha\rangle = \delta_{E,E'}\delta_{\alpha,\alpha'} \sum_{\alpha''} j_{\mu\alpha''} P_{t\alpha'',\alpha}, \qquad \ldots\ldots(5.2)$$

$$\begin{aligned} P_{t\alpha''\alpha} = {} & \delta_{\alpha'',\alpha} \exp(-2\lambda^2 t\Gamma_\alpha) + \sum_{n=1}^{\infty} (2\pi\lambda^2)^n \int_0^t dt_n \ldots \int_0^{t_2} dt_1 \\ & \times \sum_{\alpha_{n-1}} \ldots \sum_{\alpha_1} \exp\{-2\lambda^2(t-t_n)\Gamma_{\alpha''}\} W_{\alpha'',\alpha_{n-1}} \exp\{-2\lambda^2(t_n - t_{n-1})\Gamma_{\alpha_{n-1}}\} \\ & \times W_{\alpha_{n-1},\alpha_{n-2}} \ldots W_{\alpha_1,\alpha} \exp(-2\lambda^2 t_1 \Gamma_\alpha). \end{aligned} \qquad \ldots\ldots(5.3)$$

The quantities $W_{\alpha\alpha'}$ may be considered as the matrix elements of an operator W. W is completely determined by the elements $W_{\alpha\alpha'}$. Similarly we may define an operator Γ with matrix elements

$$\Gamma_{\alpha,\alpha'}=\delta_{\alpha,\alpha'}\Gamma_{\alpha}. \qquad \ldots\ldots(5.4)$$

Schwinger's (1951) formula for e^{A+B} then shows that the expression (5.3) is simply

$$P_{t\alpha''\alpha}=[\exp\{-2\lambda^2 t(\Gamma-\pi_1 W)\}]_{\alpha''\alpha}. \qquad \ldots\ldots(5.5)$$

Substituting (5.2) and (5.5) into (3.4) we can formally carry out the time integration and obtain

$$\sigma_{\mu\nu}=-\sum_{E,\alpha,\alpha''}\frac{\partial f}{\partial E}j_{\mu\alpha''}\left(\frac{1-\exp\{-2\lambda^2 T(\Gamma-\pi W)\}}{2\lambda^2(\Gamma-\pi W)}\right)_{\alpha''\alpha}j_{\nu\alpha}. \qquad \ldots\ldots(5.6)$$

In order to discuss this expression we first have to establish some of the properties of the eigenvalues of the operator

$$\Omega=\Gamma-\pi W. \qquad \ldots\ldots(5.7)$$

From the definition (3.9) of $W_{\mathbf{k},\mathbf{k}'}$ it follows that $W_{\mathbf{k},\mathbf{k}'}$ is real and equal to $W_{\mathbf{k}',\mathbf{k}}$ and therefore Ω is a real symmetric matrix:

$$\Omega_{\alpha\alpha'}=\Omega_{\alpha'\alpha}. \qquad \ldots\ldots(5.8)$$

Hence Ω can be brought into diagonal form and has real eigenvalues $\omega^{(s)}$. We call the corresponding (real) eigenvectors $x^{(s)}$ with components $x_\alpha^{(s)}$. They fulfil the equations

$$\sum_{\alpha}\Omega_{\alpha,\alpha'}x_{\alpha'}^{(s)}=\omega^{(s)}x_\alpha^{(s)} \qquad \ldots\ldots(5.9)$$

and we assume them to be a complete set of orthonormal vectors, i.e.

$$\sum_{\alpha}x_\alpha^{(s)}x_\alpha^{(s')}=\delta_{s,s'}. \qquad \ldots\ldots(5.10)$$

Equation (3.12) reads in our new notation

$$\Gamma_\alpha=\pi\sum_{\alpha'}W_{\alpha',\alpha} \qquad \ldots\ldots(5.11)$$

and therefore Ω has the property

$$\sum_{\alpha'}\Omega_{\alpha',\alpha}=\sum_{\alpha'}\Omega_{\alpha,\alpha'}=0. \qquad \ldots\ldots(5.12)$$

From this we can immediately find a solution of (5.9), namely

$$x_\alpha^{(1)}=\text{const.}=1/\sqrt{N},\quad \omega^{(1)}=0 \qquad \ldots\ldots(5.13)$$

where N is the number of values of α. All the eigenvalues $\omega^{(s)}\geqslant 0$, for from (5.9) and 5.10) it follows that

$$\sum_{\alpha,\alpha'}x_\alpha^{(s)}\Omega_{\alpha,\alpha'}x_{\alpha'}^{(s)}=\omega^{(s)} \qquad \ldots\ldots(5.14)$$

and from (5.7), (5.4), (5.11) and (5.8) it follows that

$$\begin{aligned}\sum_{\alpha,\alpha'}x_\alpha^{(s)}\Omega_{\alpha,\alpha'}x_{\alpha'}^{(s)}&=\pi\sum_{\alpha\alpha'}W_{\alpha,\alpha'}(x_{\alpha'}^{(s)2}-x_\alpha^{(s)}x_{\alpha'}^{(s)})\\&=\tfrac{1}{2}\pi\sum_{\alpha\alpha'}W_{\alpha,\alpha'}(x_{\alpha'}^{(s)}-x_\alpha^{(s)})^2\geqslant 0. \qquad \ldots\ldots(5.15)\end{aligned}$$

since $W_{\alpha,\alpha'}\geqslant 0$. We now make the physically reasonable assumption that the matrix $W_{\alpha,\alpha'}$ is not reducible, i.e. one cannot divide the α's into two classes such that all $W_{\alpha,\alpha'}=0$ if α and α' belong to different classes. Then it follows that

(5.13) is the only solution of (5.9) with the eigenvalue $\omega^{(s)}=0$. All other eigenvalues are different from zero:

$$\omega^{(s)}>0; \qquad s\neq 1. \qquad \ldots\ldots (5.16)$$

We now transform (5.6) from the α-representation into the s-representation. To do this, we expand $j_{\mu\alpha}$ in terms of the eigenvectors $x^{(s)}$ of Ω

$$j_{\mu\alpha}=\sum_s A_{\mu s}x_\alpha^{(s)}, \qquad \ldots\ldots (5.17)$$

where, according to (5.10),

$$A_{\mu s}=\sum_\alpha x_\alpha^{(s)}j_{\mu\alpha}. \qquad \ldots\ldots (5.18)$$

From (5.13) we deduce the important result that

$$A_{\mu 1}=0, \qquad \ldots\ldots (5.19)$$

since $\langle \mathbf{k}|j_\mu|\mathbf{k}\rangle=-\langle -\mathbf{k}|j_\mu|-\mathbf{k}\rangle$ and therefore $\Sigma_\alpha j_{\mu\alpha}=0$. Representing the two currents in (5.6) by means of (5.17) and using (5.9) and (5.10) we obtain

$$\sigma_{\mu\nu}=-\sum_{E,s}\frac{\partial f}{\partial E}A_{\mu s}\frac{1-\exp(-2\lambda^2 T\omega^{(s)})}{2\lambda^2\omega^{(s)}}A_{\nu s}. \qquad \ldots\ldots (5.20)$$

Since $A_{\mu 1}=0$ the term $s=1$ will not occur in the sum and only the positive eigenvalues of Ω will contribute. For sufficiently large T the exponential tends to zero and (5.20) becomes independent of T. Going back to the α-representation we can now write

$$\sigma_{\mu\nu}=-\sum_{E,\alpha,\alpha''}\frac{\partial f}{\partial E}j_{\mu\alpha''}\left(\frac{1}{2\lambda^2\Omega}\right)_{\alpha'',\alpha}j_{\nu\alpha} \qquad \ldots\ldots (5.21)$$

knowing now that this sum converges. The peculiarity of the isotropic case is that j_μ is an eigenvector of Ω and hence the double sum over α and α'' reduces to a single sum and only one eigenvalue of Ω occurs. But even in the anisotropic case one can, by a suitable definition of a 'mean collision time', write the expression for the conductivity in the usual form. Choosing our coordinate system in such a way that the conductivity tensor is diagonal (this is possible since $\sigma_{\mu\nu}=\sigma_{\nu\mu}$) we consider (5.21) for $\mu=\nu=1$, say. Defining a quantity $\tau_1(E)$ by

$$\sum_{\alpha,\alpha''}j_{1\alpha''}\left(\frac{1}{2\lambda^2\Omega}\right)_{\alpha''\alpha}j_{1\alpha}=\tau_1(E)\sum_\alpha(j_{1\alpha})^2 \qquad \ldots\ldots (5.22)$$

or in the s-representation

$$\tau_1(E)=\sum_s A_{1s}^{\;2}\frac{1}{2\lambda^2\omega^{(s)}}\Big/\sum_s A_{1s}^{\;2}, \qquad \ldots\ldots (5.23)$$

we obtain

$$\sigma_{11}=-\sum_{E,\alpha}\frac{\partial f}{\partial E}\tau_1(E)(j_{1\alpha})^2. \qquad \ldots\ldots (5.24)$$

This is exactly what we have in the isotopic case. The fact that in this general case an effective collision time $\tau_1(E)$ can be defined explicitly has been noted by Peierls (1955).

We conclude this section by using Van Hove's results to derive the standard Boltzmann equation for this general anisotropic model.

We write (3.4) with the help of (3.20) as

$$\begin{aligned}\sigma_{\mu\nu}&=\int dE\int d\alpha\int d\alpha''\int_0^\infty dt\left(\frac{\partial f}{\partial H_0}\right)_{E,\alpha}j_\nu(E\alpha)j_\mu(E\alpha'')P_t(E\alpha'',E\alpha)\\ &=\int dE\int d\alpha'' R_\nu(E\alpha'')j_\mu(E\alpha'').\end{aligned}$$

Our task is to show that the function $R_\nu(E\alpha'')$ satisfies the usual Boltzmann equation.

We have

$$R_\nu(E\alpha'') = \int d\alpha \int_0^\infty dt \left(\frac{\partial f}{\partial H_0}\right)_{E\alpha} j_\nu(E\alpha) P_t(E\alpha'', E\alpha). \qquad \ldots\ldots (5.25)$$

Now the 'master' equation (3.22) can be written in the form

$$\frac{dP_t}{dt}(E\alpha'', E\alpha) = \bar{\Omega} P_t(E\alpha'', E\alpha) \qquad \ldots\ldots (5.26)$$

where $\bar{\Omega}$ is essentially the integral operator related to the Ω we have introduced earlier in this section; its precise definition follows at once from a comparison of (3.22) and (5.26). Applying this operator to both sides of (5.25) we find that

$$\begin{aligned} \bar{\Omega} R_\nu(E\alpha'') &= \int d\alpha \int dt \left(\frac{\partial f}{\partial H_0}\right)_{E\alpha} j_\nu(E\alpha) \frac{dP_t}{dt}, \\ &= -\int d\alpha P_0(E\alpha'', E\alpha) \left(\frac{\partial f}{\partial H_0}\right)_{E\alpha} j_\nu(E\alpha) \qquad \ldots\ldots (5.27) \end{aligned}$$

and remembering that $P_0(E\alpha'', E\alpha) = \delta_{\alpha'', \alpha}$ we find

$$\bar{\Omega} R_\nu(E\alpha'') = -\left(\frac{\partial f}{\partial H_0}\right)_{E\alpha''} j_\nu(E\alpha'') \qquad \ldots\ldots (5.28)$$

which is the standard form of the Boltzmann equation for this model. This derivation makes no use whatsoever of either the collision time assumption or the repeated random phase assumption.

§ 6. Elastic Scattering by Phonons

In this section we shall calculate the conductivity when the electrons are scattered elastically by lattice vibrations, that is, by phonons. We again take the simple model of free electrons and calculate the conductivity to order λ^{-2}, λ is now a measure of the strength of the electron–phonon interaction. The extension to the case in which the electrons move in a periodic lattice can be made using the techniques of § 5. The higher order terms in λ in the coductivity can be calculated by the methods of § 4; it can again be shown that these terms are small as long as $1/\tau(\eta) \ll \eta$ and $T \gg \theta$.

If the electrons are scattered elastically by the phonons then the energy of each electron is conserved throughout the motion of the system. If $\mathscr{H}$ is the total Hamiltonian of the system and H_α that for the electron α then H_α will be a constant of the motion provided that

$$[H_\alpha, \mathscr{H}] = 0. \qquad \ldots\ldots (6.1)$$

Now $\mathscr{H}$ is of the form

$$\mathscr{H} = \mathscr{H}_{\rm ph} + \mathscr{H}_{\rm el} \qquad \ldots\ldots (6.2\,a)$$

where

$$\mathscr{H}_{\rm ph} = \tfrac{1}{2} \sum_f (p_f^2 + \omega_f^2 q_f^2) \qquad \ldots\ldots (6.2\,b)$$

and

$$\mathscr{H}_{\rm el} = \sum_\alpha H_\alpha. \qquad \ldots\ldots (6.2\,c)$$

Here p_f and q_f are the normal coordinates and momenta of the lattice and the ω_f are the frequencies of vibration. We can therefore write (6.1) as

$$[H_\alpha, \mathscr{H}_{\rm ph}] = 0. \qquad \ldots\ldots (6.3)$$

Since H_α contains a linear function of the normal coordinates q_f this equation can only be satisfied if

$$[p_{\mathbf{f}}, q_{\mathbf{f}}] = 0 \qquad (\text{all } \mathbf{f}), \qquad \ldots\ldots(6.4)$$

in other words the electrons will be scattered elastically if the lattice degrees of freedom are treated classically. In a metal this requirement can be met as long as $T \gg \theta$, where θ is the Debye temperature of the lattice. If (6.3) is fulfilled then it follows at once that the lattice degrees of freedom remain in statistical equilibrium at all times and are quite unaffected by the presence of the electric current in the system. It now follows from equations (6.2 *a*), (6.2 *c*) and (6.3) that the equilibrium density matrix ρ_0 for the system is of the form,

$$\rho_0 = \rho_{\mathrm{ph}}{}^{(c)}\rho_{\mathrm{el}} \qquad \ldots\ldots(6.5)$$

where $\rho_{\mathrm{ph}}{}^{(c)}$ is the classical equilibrium distribution function for the normal coordinates and momenta of the lattice. Likewise it follows that

$$\begin{aligned} J_\mu(u+i\lambda) &= \exp\{i(u+i\lambda)\mathscr{H}\}J_\mu(0)\exp\{-i(u+i\lambda)\mathscr{H}\} \\ &= \exp\{i(u+i\lambda)\mathscr{H}_{\mathrm{el}}\}J_\mu(0)\exp\{-i(u+i\lambda)\mathscr{H}_{\mathrm{el}}\} \\ &= \mathcal{J}_\mu(u+i\lambda). \qquad \ldots\ldots(6.6) \end{aligned}$$

If we substitute these results in (1.1) then we find that $\sigma_{\mu\nu}$ can be written in the form

$$\sigma_{\mu\nu} = \mathrm{Tr}^{(\mathrm{ph})}\rho_{\mathrm{ph}}{}^{(c)}\left[\mathrm{Tr}^{(e)}\left\{\int_0^T du\int_0^\beta d\lambda\rho_{\mathrm{el}}J_\nu(0)\mathcal{J}_\mu(u+i\lambda)\right\}\right]. \qquad \ldots\ldots(6.7)$$

In this equation $\mathrm{Tr}^{(\mathrm{ph})}$ stands for an integration over the normal coordinates and momenta; $\mathrm{Tr}^{(e)}$ stands for a trace over any complete set of wave functions (that obey periodic boundary conditions) for the electronic degrees of freedom. Now since $\mathscr{H}_{\mathrm{el}}$ is a sum of single-particle Hamiltonians H_α it is possible to reduce the expression

$$\mathrm{Tr}^{(e)}\left\{\int_0^T du\int_0^\beta d\lambda\rho_{\mathrm{el}}J_\nu(0)\mathcal{J}_\mu(u+i\lambda)\right\}$$

to the single particle form

$$-\,\mathrm{tr}^{(e)}\left\{\frac{\partial f}{\partial H}\int_0^T du j_\mu(u)j_\nu(0)\right\}.$$

Substituting this expression into (6.7) we find that the conductivity becomes

$$\sigma_{\mu\nu} = -\,\mathrm{Tr}^{(\mathrm{ph})}\rho_{\mathrm{ph}}{}^{(c)}\mathrm{tr}^{(e)}\left\{\int_0^T du j_\mu(u)j_\nu(0)\frac{\partial f}{\partial H}\right\}. \qquad \ldots\ldots(6.8)$$

The evaluation of this formula can be carried out in the following way. First we remark that the electron phonon interaction potential V_{ep} has the essential diagonal property (3.15). This statement is of course true quite generally and does not depend in any way on the assumption that the electrons are scattered elastically by the phonons. Van Hove (1957) has in fact given a detailed discussion of this property for the electron–phonon interaction. When the lattice degrees of freedom are treated classically it is simple matter to show that this the diagonal property must hold. One merely has to remark that the normal coordinates q_f, which appear linearly in V_{ep} are statistically independent and each one has a Gaussian distribution $\exp(-\alpha q_f{}^2)$. In other words the normal coordinates are independent random variables; this property is sufficient to establish the diagonal property of V_{ep}. Since V_{ep} has the necessary properties we can evaluate (6.8) in essentially the same way as we evaluated the conductivity in § 3. The only change that is required is to replace the $V_{\mathbf{k},\mathbf{k}'}$ that occur in § 3 by the appropriate matrix elements of V_{ep}. If we use the conventional Bloch interaction, Peierls (1955), for V_{ep} then

$$|(V_{\text{ep}})_{\mathbf{k},\mathbf{k}'}|^2 = |v_{\mathbf{k}-\mathbf{k}'}|^2 q_{\mathbf{k}-\mathbf{k}'}{}^2 \qquad \ldots\ldots(6.9)$$

where $v_{\mathbf{f}}$ is the matrix element for electron–phonon scattering with momentum transfer $\hbar\,\mathbf{f}$, and $q_{\mathbf{k}-\mathbf{k}'}$ is the normal coordinate corresponding to the wave vector $\mathbf{k}-\mathbf{k}$. Because the normal coordinates are distributed independently $q_{\mathbf{k}-\mathbf{k}'}{}^2$ can be replaced by its average value,

$$\langle q_{\mathbf{k}-\mathbf{k}'}{}^2\rangle = kT/|\omega_{\mathbf{k}-\mathbf{k}'}|^2 \qquad \ldots\ldots(6.10)$$

and hence $|(V_{\text{ep}})_{\mathbf{k},\mathbf{k}'}|^2$ can also be replaced by its average value

$$\langle|(V_{\text{ep}})_{\mathbf{k},\mathbf{k}'}|^2\rangle = \tilde{W}_{\mathbf{k},\mathbf{k}'} = |v_{\mathbf{k}-\mathbf{k}'}|^2 kT/|\omega_{\mathbf{k}-\mathbf{k}'}|^2. \qquad \ldots\ldots(6.11)$$

We can now replace the $W_{\mathbf{k},\mathbf{k}'}$ of § 3 by the $\tilde{W}_{\mathbf{k},\mathbf{k}'}$ defined by (6.11), and the conductivity tensor is therefore given by the equation

$$\sigma_{\mu\nu} = -\sum_{\mathbf{k}} \frac{\partial f}{\partial E}\langle\mathbf{k}|j_\mu|\mathbf{k}\rangle\langle\mathbf{k}|j_\nu|\mathbf{k}\rangle\tau(E) \qquad \ldots\ldots(6.12)$$

where

$$\frac{1}{\tau(E)} = 4\pi\lambda^2\rho(E)\int_{-1}^{+1}\tilde{W}(E,\cos\theta)(1-\cos\theta)\,d(\cos\theta) \qquad \ldots\ldots(6.13)$$

with

$$\tilde{W}(E,\cos\theta) = \int \tilde{W}_{\mathbf{k},\mathbf{k}'}\delta(E-E')\,dE'. \qquad \ldots\ldots(6.14)$$

θ in (6.13) is the angle between $\mathbf{k}$ and $\mathbf{k}'$ and $\rho(E)$ is the density of states. If we make the customary approximation (Peierls 1955) that

$$|v_{\mathbf{k}-\mathbf{k}'}|^2/|\omega_{\mathbf{k}-\mathbf{k}'}|^2 = \text{const.} = c^2 \qquad \ldots\ldots(6.15)$$

then

$$1/\tau(E) = 8\pi kT\lambda^2\rho(E)c^2 \qquad \ldots\ldots(6.16)$$

and the conductivity reduces at once to the standard form.

ACKNOWLEDGMENTS

It is a pleasure to thank Professor R. E. Peierls for his interest and encouragement throughout the course of this work. We are also indebted to Professor R. Jost for an illuminating conversation. One of us (A. T.) wishes to thank Professor R. E. Peierls for the hospitality extended to him during his stay at Birmingham University. The other (G. V. C.) wishes to thank Professor W. Heitler for the hospitality extended to him during his stay at Zurich University.

REFERENCES

BOCCHIERI, P., and LOINGER, A., 1958, *Phys. Rev.*, **107**, 337.
EDWARDS, S. F., 1958, *Phil. Mag.*, **3**, 33, 1020.
GREENWOOD, D. A., 1958, *Proc. Phys. Soc.*, **71**, 585.
KOHN, W., and LUTTINGER, J. M., 1957, *Phys. Rev.*, **108**, 590.
KUBO, R., 1956, *Canad. J. Phys.*, **34**, 1274.
LAX, M., 1958, *Phys. Rev.*, **109**, 1921.

NAKAJIMA, S., 1956, *Proc. Phys. Soc.* A, **69**, 441.
NAKANO, H., 1956, *Progr. Theor. Phys.*, **15**, 77.
PAULI, W., 1928, *Festschrift zum 60 Geburtstage A. Sommerfelds* (Leipzig: Hirzel), p. 30.
PEIERLS, R. E., 1934 a, *Z. Phys.*, **88**, 786.
—— 1934 b, *Helv. Phys. Acta*, **7**, Suppl., 24.
——1955, *The Quantum Theory of Solids* (Oxford: Clarendon Press).
SCHAFROTH, M. R., 1951, *Helv. Phys. Acta*, **24**, 645.
SCHWINGER, J., 1951, *Phys. Rev.*, **82**, 664.
VAN HOVE, L., 1955, *Physica*, **21**, 517.
—— 1957, *Ibid.*, **23**, 441.
VAN WIERINGEN, J. S., 1954, *Proc. Phys. Soc.* A, **67**, 206.

On the Derivation of Reaction Parameters from Observations of Ultrasonic Relaxation

By R. O. DAVIES† and J. LAMB‡

† Physics Department, Queen Mary College, London

‡ Electrical Engineering Department, Imperial College, London

MS. received 24th September 1958

Abstract. Measurements of ultrasonic relaxation in liquids and gases provide experimental data from which it is desired to obtain theoretically useful parameters such as heats of reaction and transition probabilities. It is shown here that even if full experimental results are available concerning the variation of the ultrasonic relaxation strength r with pressure and temperature it is still necessary to make at least three assumptions before thermodynamic reaction parameters can be evaluated.

The main purpose of the paper is to set out a logical theory which makes the nature of these assumptions explicit. It is first shown how the experimental results can best be analysed to yield the relaxation strength. The formula connecting the relaxation strength with the reaction parameters leads to a partial differential equation which is integrated in a form convenient for practical application.

The general implications of the theoretical work are discussed in relation to experimental observations and the need for further experimental work at high pressures is emphasized.

§ 1. INTRODUCTION

THERE has been a growing realization that the measurement of ultrasonic absorption and dispersion in liquids and gases provides an excellent tool for the investigation of certain ‘fast’ molecular processes. Unfortunately the translation of experimental results into theoretically useful parameters such as heats of reaction and transition probabilities is not straightforward. Part of the difficulty arises because the experiments yield direct information concerning adiabatic parameters whereas the physical chemist normally prefers to discuss isothermal quantities. In other words one is confronted with the general problem of converting from a formulation with S and p as independent variables to one with T and p as independent variables. However, if the experimental data can be fitted to ‘single relaxation time’ formulae and one is then prepared to assume (*a*) a single effective mechanism of reaction and (*b*) the stoichiometric nature of the reaction, then it is possible to obtain a relationship between a ‘relaxation strength’ r—determined from experiments—and the chemical parameters which govern the reaction. The relaxation strength is essentially the relaxing component of the adiabatic compressibility. For present purposes we shall be concerned with the particular case of an isomeric reaction of the type $A_1 \rightleftharpoons A_2$ in ideal solution. This example is taken partly for reasons of simplicity and partly because it is the most important case in practice; other types of reaction can, in principle, be dealt with in a similar fashion.

It will appear in §2, and is indeed well known, that acoustic measurements at a given temperature and pressure yield only a value for r which, according to the theory, can be expressed in terms of three independent reaction parameters, namely, ΔG_0, ΔV_0 and ΔH_0. It is clear that we cannot evaluate the three unknown parameters from a single piece of information. In order to surmount this difficulty four main courses of action suggest themselves.

(i) We can envisage measuring relaxing parameters other than the adiabatic compressibility. In fact, to our knowledge, this has not been accomplished.

(ii) The acoustic measurements can be made at different temperatures. This procedure has been relatively common (see for example Davies and Lamb 1957).

(iii) The pressure can be varied in the acoustic experiments. This is experimentally more troublesome but preliminary experimental results are encouraging (Litovitz and Carnevale 1958).

(iv) Partial information about the reaction can sometimes be deduced from other types of physical measurement. Thus ΔH_0 can be obtained in some cases from infra-red studies: for example, Kagarise (1952, 1955, 1956) has found values of ΔH_0 for some substituted ethanes, and for one of these a correlation has been obtained with acoustic measurements (Krebs and Lamb 1958).

Although variation of the chemical composition in the ultrasonic experiments can lead to identification of the molecular mechanism responsible for the relaxation (Young and Petrauskas 1956, de Groot and Lamb 1957) it cannot by itself help towards numerical determination of the thermodynamic parameters of the reaction.

If we neglect the possibilities suggested by (i) and (iv) above and consider only the interpretation of ultrasonic experiments, it still remains that even if these are carried out over wide ranges of temperature and pressure the reaction parameters cannot be evaluated without further assumptions.

It is the main purpose of this paper to set out a logical theory which makes the nature of these assumptions explicit. It is necessary first to show how the experimental data can best be analysed to yield the relaxation strength r and to state the formula which connects r with the reaction parameters; this is done in §2. The theory presented in §3 shows how the formula for r leads to a partial differential equation for the reaction parameters which is integrated in a form convenient for practical application. The implications of this analysis are discussed with reference to selected experimental data in §§4 to 7. Conclusions are drawn in §8 which have an important bearing on the investigation of chemical reactions by ultrasonic techniques.

§ 2. THE INTERPRETATION OF ACOUSTIC MEASUREMENTS

It is known that the propagation number k for a sound wave in a relaxing medium is given by

$$\frac{k^2}{\omega^2}=\rho\bar{\kappa}_S\left\{1-\sum_j\frac{ir_j\omega\tau_j}{1+i\omega\tau_j}\right\} \qquad \ldots\ldots(1)$$

where $r_j=\delta_j\kappa_S/\bar{\kappa}_S$ is the jth relaxation strength, τ_j is the jth adiabatic–isobaric relaxation time, $\bar{\kappa}_S$ is the equilibrium adiabatic compressibility of the fluid, ρ is its density and $\delta_j\kappa_S$ is the jth incremental component of the compressibility. From this we may calculate

$$\alpha/\omega(\rho\bar{\kappa}_S)^{1/2} = \tfrac{1}{2}\sum_i r_i\omega\tau_i/[1+(\omega\tau_i)^2] + \tfrac{1}{4}\sum_i\sum_j r_i r_j(\omega\tau_i)^2\omega\tau_j/[1+(\omega\tau_i)^2][1+(\omega\tau_j)^2], \qquad \ldots\ldots(2)$$

$$c(\rho\bar{\kappa}_S)^{1/2} = 1 + \tfrac{1}{2}\sum_i r_i(\omega\tau_i)^2/[1+(\omega\tau_i)^2] + \tfrac{1}{8}\sum_i\sum_j r_i r_j(\omega\tau_i)(\omega\tau_j)[3(\omega\tau_i)(\omega\tau_j)-1]/[1+(\omega\tau_i)^2][1+(\omega\tau_j)^2], \qquad \ldots\ldots(3)$$

$$\mu/2\pi = \alpha c/\omega = \tfrac{1}{2}\sum_i r_i(\omega\tau_i)/[1+(\omega\tau_i)^2] + \tfrac{1}{2}\sum_i\sum_j r_i r_j(\omega\tau_i)^2(\omega\tau_j)/[1+(\omega\tau_i)^2][1+(\omega\tau_j)^2]. \qquad \ldots\ldots(4)$$

α is the amplitude absorption coefficient per unit distance, c is the phase velocity, μ $(=\alpha\lambda)$ is the absorption per wavelength and the working is carried to the second powers of the relaxation strength. The velocity at low frequencies is $\bar{c} = (\rho\bar{\kappa}_S)^{-1/2}$. It is customary experimentally to measure α as a function of frequency. In order to interpret such results it is convenient to re-express equation (2) in a form which is appropriate to the case in which the experimental range of frequencies extends over the relaxation range of the first relaxation ($i=1$, say). Other remaining relaxations are assumed to occur at much higher frequencies so that $\omega\tau_j \ll 1$ for $j>1$. Then to the second order in the variables r_j and $\omega\tau_j$ $(j>1)$ we have

$$\frac{\alpha\bar{c}}{\omega} = \frac{1}{2}\,\frac{r_1\omega\tau_1}{1+\omega^2[\tau_1(1-r_1)^{1/4}]^2} + \frac{1}{2}\sum_{j>1} r_j\omega\tau_j \qquad \ldots\ldots(5)$$

or

$$\frac{\alpha}{f^2} = \frac{A}{1+(f/f_c)^2} + B, \qquad \ldots\ldots(6)$$

where

$$A = \frac{2\pi^2}{\bar{c}}\,r_1\tau_1, \qquad B = \frac{2\pi^2}{\bar{c}}\sum_{j>1} r_j\tau_j$$

and

$$f_c = [2\pi\tau_1(1-r_1)^{1/4}]^{-1}. \qquad \ldots\ldots(7)$$

It can be shown that the viscous absorption contributes in effect to the term 'B' by means of the expression

$$(r\tau)_{\text{visc}} = 4\eta/3\rho\bar{c}^2$$

where η is the shear viscosity of the fluid. It should be noted that the above relation between f_c and τ_1 involves r_1: it is precisely this fact that makes equation (5) correct to the second order (Bass and Lamb 1957, 1958).

Methods of obtaining the parameters A, B and f_c from measured values of α/f^2 have been adequately described elsewhere; the above formulae can then be used to derive the relaxing parameters r_1 and τ_1 from any set of measurements at a given temperature and pressure.

We shall be concerned with the problem of how to work from the knowledge of r_1 as a function of pressure and temperature to information concerning the thermodynamic parameters of the associated reactions. As we have emphasized elsewhere (Davies and Lamb 1957) it is necessary to assume *a priori* the nature of the mechanism responsible for the relaxation. Consider the isomeric reaction $A_1 \rightleftharpoons A_2$ in ideal solution. It can then be shown (Davies and Lamb 1957) that the relaxation strength, r_1 $(=\delta_1\kappa_S/\bar{\kappa}_S)$, is related to the chemical reaction parameters by the formula (correct to the lowest power of r_1):

$$F(p,T)=\left[\frac{\Delta H_0}{RT}-\frac{\bar{C}_p}{\bar{\alpha}V}\frac{\Delta V_0}{RT}\right]\frac{\exp(\Delta G_0/2RT)}{1+\exp(\Delta G_0/RT)} \qquad \ldots\ldots(8)$$

where

$$F(p,T)\equiv\left[\frac{\bar{C}_p}{R}\frac{r_1}{\bar{\gamma}-1}\right]^{1/2}$$

ΔH_0, ΔV_0 and ΔG_0 are, respectively, the enthalpy, volume and Gibbs free energy changes of the reaction, $\bar{C}_p$ is the equilibrium molar heat capacity of the fluid, $\bar{\gamma}=\bar{C}_p/\bar{C}_v$, and $\bar{\alpha}$ is the expansivity of the fluid. F is an experimentally accessible function of pressure and temperature. Our problem is to recover ΔH_0, ΔV_0 and ΔG_0 from measured values of F.

§ 3. SOME RELATIONSHIPS BETWEEN THE STRENGTH AND THERMODYNAMIC REACTION PARAMETERS

It is convenient to introduce the following dimensionless variables:

$$\left.\begin{array}{lll}\theta\equiv\ln(T/T_0), & & P\equiv\dfrac{\bar{\alpha}V}{\bar{C}_p}p \\ \mathbf{G}\equiv\dfrac{\Delta G_0}{RT}, & \mathbf{H}\equiv\dfrac{\Delta H_0}{RT}, & \mathbf{V}\equiv\dfrac{\bar{C}_p}{\bar{\alpha}V}\dfrac{\Delta V_0}{RT}, \\ \mathbf{C}\equiv\dfrac{\Delta C_{p0}}{R}, & \mathbf{A}\equiv\dfrac{\bar{C}_p}{R}\dfrac{\Delta\alpha_0}{\bar{\alpha}}, & \mathbf{K}\equiv\dfrac{\bar{C}_p}{R}\dfrac{\bar{\gamma}}{(\bar{\gamma}-1)}\dfrac{\Delta\kappa_0}{\kappa_0}\end{array}\right\} \qquad \ldots\ldots(9)$$

in which T_0 is a reference temperature and κ is the isothermal compressibility. We make the major assumption that: $\bar{\alpha}V/\bar{C}_p$ *is independent of pressure and temperature over the range of interest*[†].

$\mathbf{G}$ is of course a thermodynamic potential function which can be differentiated to give the other reaction parameters. In fact we have

$$\left.\begin{array}{lll}\mathbf{H}=-\dfrac{\partial\mathbf{G}}{\partial\theta}, & \mathbf{V}=\dfrac{\partial\mathbf{G}}{\partial P}, & \mathbf{C}=-\dfrac{\partial\mathbf{G}}{\partial\theta}-\dfrac{\partial^2\mathbf{G}}{\partial\theta^2}, \\ \mathbf{A}=\dfrac{\partial\mathbf{G}}{\partial P}+\dfrac{\partial^2\mathbf{G}}{\partial P\partial\theta}, & \mathbf{K}=-\dfrac{\partial^2\mathbf{G}}{\partial P^2}. & \end{array}\right\} \qquad \ldots\ldots(10)$$

If the dimensionless variables and the first two members of (10) are used in equation (8) we find that this basic equation can be written

$$(\mathbf{H}-\mathbf{V})\operatorname{sech}\tfrac{1}{2}\mathbf{G}-2F=0,$$

or

$$\left(\frac{\partial\mathbf{G}}{\partial\theta}+\frac{\partial\mathbf{G}}{\partial P}\right)\operatorname{sech}\tfrac{1}{2}\mathbf{G}+2F=0. \qquad \ldots\ldots(11)$$

For the integration of (11) it is convenient to introduce an auxiliary function $\mathscr{G}$ defined by means of

$$\tanh\tfrac{1}{4}\mathbf{G}=\tan\tfrac{1}{2}\mathscr{G}. \qquad \ldots\ldots(12)$$

[†] This would be appropriate if the Helmholtz free energy were a function of $T/\Theta(V)$. It is essentially a 'linearization' of the problem. Alternative assumptions would affect the terms involving $\mathbf{K}$ and $\mathbf{A}$ in what follows.

Then equation (11) may be written as the inhomogeneous linear equation

$$\frac{\partial \mathscr{G}}{\partial \theta} + \frac{\partial \mathscr{G}}{\partial P} + F = 0. \qquad \ldots\ldots(13)$$

Let it now be assumed that the observations of F provide a linear representation around the reference point:

$$F = F_0(1 + \tau\theta + \Pi P) \qquad \ldots\ldots(14)$$

where $\tau \equiv \partial \ln F/\partial \ln T$ and $\Pi \equiv \partial \ln F/\partial P$ are taken as constants. Equation (13) then becomes

$$\frac{\partial \mathscr{G}}{\partial \theta} + \frac{\partial \mathscr{G}}{\partial P} + F_0(1 + \tau\theta + \Pi P) = 0 \qquad \ldots\ldots(15)$$

of which the general solution is

$$\mathscr{G} = \phi(P - \theta) - F_0\{\tfrac{1}{2}(\theta + P) + \tfrac{1}{2}\tau\theta^2 + \tfrac{1}{2}\Pi P^2\} \qquad \ldots\ldots(16)$$

where ϕ is an arbitrary function of its argument. Let this function be taken as a polynomial expansion up to the second power in $P - \theta$. Then, correct to this order in P and θ, we have

$$\mathscr{G} = \gamma + F_0\{(k_1 - \tfrac{1}{2})\theta - (\tfrac{1}{2} + k_1)P - \tfrac{1}{2}(\tau + k_2)\theta^2 + k_2\theta P - \tfrac{1}{2}(\Pi + k_2)P^2\} \qquad \ldots\ldots(17)$$

where γ, k_1 and k_2 are constants.

With the help of equation (12) we may now form

$$\begin{aligned}\mathbf{G} = {} & 4\tanh^{-1}\tan\tfrac{1}{2}\gamma + F_0\sec\gamma \\ & \times\{-2(\tfrac{1}{2} - k_1)\theta - 2(\tfrac{1}{2} + k_1)P + [-(\tau + k_2) + F_0(k_1 - \tfrac{1}{2})^2\tan\gamma]\theta^2 \\ & + [2k_2 + 2F_0(\tfrac{1}{4} - k_1{}^2)\tan\gamma]P\theta + [-(\Pi + k_2) + F_0(k_1 + \tfrac{1}{2})^2\tan\gamma]P^2\}\end{aligned} \qquad \ldots\ldots(18)$$

and hence by (10) we can calculate the complete set of reaction parameters:

$$\left.\begin{aligned}\mathbf{G} &= 4\tanh^{-1}\tan\tfrac{1}{2}\gamma, \\ \mathbf{H} &= 2(\tfrac{1}{2} - k_1)F_0\sec\gamma, \\ \mathbf{V} &= -2(\tfrac{1}{2} + k_1)F_0\sec\gamma, \\ \mathbf{C} &= 2[(\tfrac{1}{2} - k_1) + \tau + k_2 - F_0(k_1 - \tfrac{1}{2})^2\tan\gamma]\,F_0\sec\gamma, \\ \mathbf{A} &= 2[-(\tfrac{1}{2} + k_1) + k_2 + F_0(\tfrac{1}{4} - k_1{}^2)\tan\gamma]F_0\sec\gamma, \\ \mathbf{K} &= 2[\Pi + k_2 - F_0(\tfrac{1}{2} + k_1)^2\tan\gamma]F_0\sec\gamma.\end{aligned}\right\} \qquad \ldots\ldots(19)$$

The set (19) expresses the six thermodynamic parameters on the left in terms of three 'experimental' constants (τ, Π, F_0) and three constants of integration (γ, k_1, k_2). It is clear that at least three additional assumptions or supplementary pieces of information must be introduced before the collection (19) becomes useful.

It is desirable to make (19) more surveyable by eliminating two of the constants, namely k_1 and k_2. We may also drop the subscripts on F. This yields the set:

$$\left.\begin{aligned}\mathbf{G} &= 4\tanh^{-1}\tan\tfrac{1}{2}\gamma, \\ \mathbf{H} - \mathbf{V} &= 2F\sec\gamma, \\ \mathbf{C} - \mathbf{A} &= 2(1 + \tau)F\sec\gamma - \mathbf{H}F\tan\gamma, \\ \mathbf{K} - \mathbf{A} &= 2\Pi F\sec\gamma - \mathbf{V} + F\tan\gamma.\end{aligned}\right\} \qquad \ldots\ldots(20)$$

Before further analysis we shall give two independent proofs of the set (20).

(i) Let it be supposed that we have an expansion of $\mathbf{G}(\theta, P)$ taken to the second order in P and θ. Let it be written as

$$\mathbf{G} = D - \mathbf{H}\theta + \mathbf{V}P + \tfrac{1}{2}(\mathbf{H} - \mathbf{C})\theta^2 + (\mathbf{A} - \mathbf{V})\theta P - \tfrac{1}{2}\mathbf{K}P^2. \quad \ldots\ldots(21)$$

The form of these coefficients is chosen because (as can easily be verified from (10)) the symbols have—at the reference point—precisely the meaning assigned earlier in equations (9).

Now let us substitute (21) into (11) and expand to the first power in θ and P:

$$\begin{aligned}(-\mathbf{H}+\mathbf{V})\operatorname{sech}\tfrac{1}{2}D + \theta\{\tfrac{1}{2}\mathbf{H}(-\mathbf{H}+\mathbf{V})\operatorname{sech}\tfrac{1}{2}D\tanh\tfrac{1}{2}D + (\mathbf{H}-\mathbf{C}+\mathbf{A}-\mathbf{V})\operatorname{sech}\tfrac{1}{2}D\}\\ + P\{-\tfrac{1}{2}\mathbf{V}(-\mathbf{H}+\mathbf{V})\operatorname{sech}\tfrac{1}{2}D\tanh\tfrac{1}{2}D + (\mathbf{A}-\mathbf{V}-\mathbf{K})\operatorname{sech}\tfrac{1}{2}D\} + 2F = 0.\end{aligned} \quad \ldots\ldots(22)$$

Remembering that $\tau = (1/F)(\partial F/\partial\theta)$ and $\Pi = (1/F)(\partial F/\partial P)$, it follows by differentiating (22) that $\mathbf{G} = D$ and hence

$$\left.\begin{aligned}\mathbf{H} - \mathbf{V} &= 2F\cosh(\tfrac{1}{2}\mathbf{G}),\\ \mathbf{C} - \mathbf{A} &= 2(1+\tau)F\cosh\tfrac{1}{2}\mathbf{G} - \mathbf{H}F\sinh\tfrac{1}{2}\mathbf{G},\\ \mathbf{K} - \mathbf{A} &= 2\Pi F\cosh\tfrac{1}{2}\mathbf{G} - \mathbf{V} + \mathbf{V}F\sinh\tfrac{1}{2}\mathbf{G}.\end{aligned}\right\} \quad \ldots\ldots(23)$$

Comparing now the set (20) with the set (23), we see that under the substitution $\tanh\tfrac{1}{4}\mathbf{G} = \tan\tfrac{1}{2}\gamma$ (which implies $\cosh\tfrac{1}{2}\mathbf{G} = \sec\gamma$, $\sinh\tfrac{1}{2}\mathbf{G} = \tan\gamma$) they are completely equivalent.

(ii) Finally, a very simple proof of the set (23) comes by differentiating equation (11) with respect to θ and P in turn. Thus we have

$$\left.\begin{aligned}\frac{\partial^2\mathbf{G}}{\partial\theta^2} + \frac{\partial^2\mathbf{G}}{\partial\theta\partial P} + F\sinh(\tfrac{1}{2}\mathbf{G})\frac{\partial\mathbf{G}}{\partial\theta} + 2\cosh(\tfrac{1}{2}\mathbf{G})\frac{\partial F}{\partial\theta} &= 0,\\ \frac{\partial^2\mathbf{G}}{\partial P} + \frac{\partial^2\mathbf{G}}{\partial\theta\partial P} + F\sinh(\tfrac{1}{2}\mathbf{G})\frac{\partial\mathbf{G}}{\partial P} + 2\cosh(\tfrac{1}{2}\mathbf{G})\frac{\partial F}{\partial P} &= 0.\end{aligned}\right\} \quad \ldots\ldots(24)$$

Substitute from (10) for the derivatives of $\mathbf{G}$ and we recover, with the help of (11) again, the set (23).

We conclude that the equivalent sets of equations (20) and (23) are concise representations of the relationships between the thermodynamic parameters of an isomeric reaction in ideal solution and the results obtainable from ultrasonic measurements.

§ 4. GENERAL REMARKS ABOUT THE MAGNITUDES OF ΔV_0, $\Delta\alpha_0$ and $\Delta\kappa_0$

The quantities $\mathbf{G}$, $\mathbf{H}$ and $\mathbf{C}$ are direct and obvious dimensionless measures of ΔG_0, ΔH_0 and ΔC_p and require no further discussion here.

In existing work it has always been assumed that $\Delta V_0 = 0$. At first sight this seems a reasonable assumption for isomeric changes, since one naturally expects $\Delta V_0/V$ to be small and (say) $\lesssim 10\%$. However, the theory shows (equations (8) and (11)) that the important quantity is not $\Delta V_0/V$ but rather $\mathbf{V} \equiv (\bar{C}_p/\bar{\alpha}RT)(\Delta V_0/V)$ which must be compared with $\mathbf{H} = \Delta H_0/RT$. To illustrate this point consider the following typical values: $\bar{C}_p = 50$ cal mol^{-1} deg^{-1}, $RT = 600$ cal mol^{-1} deg^{-1}, $\bar{\alpha} = 10^{-3}$ deg^{-1}, $\Delta V_0/V = 10\%$, $\Delta H_0 = 3$ kcal mol^{-1}. We find $\mathbf{V} = 8$ and $\mathbf{H} = 5$. Clearly in such a case one cannot neglect the volume change of the reaction.

A specific case for which ΔV_0 and ΔH_0 are known is that of the chemically separable *cis* and *trans* isomers of 1 : 2 dichloroethylene. Using the most recent figures quoted by Timmermans (1950) together with some thermal data given by Pitzer and Hollenberg (1954), we estimate that at 300°K $\Delta V_0 = 1{\cdot}63\ \mathrm{cm}^3\ \mathrm{mol}$, $\Delta H_0 = 445\ \mathrm{cal\ mol}^{-1}$, $\bar{C}_\mathrm{p} = 15{\cdot}8\ \mathrm{cal\ mol}^{-1}\ \mathrm{deg}^{-1}$, $\bar{\alpha} = 1{\cdot}37 \times 10^{-3}\ \mathrm{deg}^{-1}$, $V = 76{\cdot}4\ \mathrm{cm}^3\ \mathrm{mol}^{-1}$. Hence $\mathbf{V} = 0{\cdot}41$ and $\mathbf{H} = 0{\cdot}74$. It is clear that the assumption that $\mathbf{V}$ is small compared with $\mathbf{H}$ is a very dangerous one unless supported by quite specific arguments.

Turning now to $\mathbf{A}$ and $\mathbf{K}$, concerning which even less is known than about $\mathbf{V}$, we find, taking $\bar{C}_\mathrm{p}/R = 25$ and $\bar{\gamma} = 1{\cdot}25$, that $\mathbf{A} \simeq 25\,\Delta\alpha_0/\bar{\alpha}$ and $\mathbf{K} \simeq 100\,\Delta\kappa_0/\bar{\kappa}$. Thus a 4% change in expansivity and a 1% change in compressibility are sufficient to make $\mathbf{A}$ and $\mathbf{K}$ comparable with unity.

§ 5. THE RESULT OF MAKING THE TWO ASSUMPTIONS $\Delta\alpha_0 = \Delta\kappa_0 = 0$.

We have just seen that there is no obvious assumption to be made concerning the thermodynamic parameters. But in order to use the theory further assumptions have to be made and since we are wholly ignorant about $\Delta\alpha_0$ and $\Delta\kappa_0$ let us make:

Assumption 1: $\Delta\alpha_0 = 0$, i.e. $\mathbf{A} = 0$,

and

Assumption 2: $\Delta\kappa_0 = 0$, i.e. $\mathbf{K} = 0$.

With the substitution $x = F \sinh \tfrac{1}{2}\mathbf{G}$, the set (23) now becomes

$$\left.\begin{aligned} \mathbf{H} &= 2(F^2+x^2)^{1/2}(1+\Pi-x)/(1-x), \\ \mathbf{V} &= 2(F^2+x^2)^{1/2}\Pi/(1-x), \\ \mathbf{C} &= 2(F^2+x^2)^{1/2}\{1+\tau-x(2+\tau+\Pi)+x^2\}/(1-x) \\ \mathbf{G} &= 2\log\{[x+(F^2+x^2)^{1/2}]/F\} \qquad (\mathbf{A}=\mathbf{K}=0). \end{aligned}\right\} \quad \ldots\ldots(25)$$

These equations may be used by making a third assumption which enables x to be found, and hence the other unknowns.

Before proceeding, there is an immediate conclusion to be drawn from the second member of the set (25): since x is real, the quadratic equation

$$\mathbf{V}^2(1-x)^2 = 4\Pi^2(F^2+x^2)$$

must have real roots. Hence

$$|\mathbf{V}| > 2F|\Pi|/(1+F^2)^{1/2}. \qquad \ldots\ldots(26)$$

This sets a lower limit on the value of $|\mathbf{V}|$ and hence of ΔV_0. Similar (although more complicated) reality conditions could be found from the 1st and 3rd members of (25).

§ 6. ALTERNATIVE THIRD ASSUMPTIONS

If it happens that the equilibrium constant of the reaction be known then, since this is equivalent to knowing $\mathbf{G}$, x could be found from the last member of (25) and hence $\mathbf{H}$, $\mathbf{V}$ and $\mathbf{C}$. If it should happen that $\mathbf{G}$ be such that $e^{\mathbf{G}/2}$ is large, then we should have the more specialized results under:

Assumption 3a.

$\mathbf{G}$ *is known and* $e^{\mathbf{G}/2}$ *is large.*

Then (25) becomes

$$\left.\begin{array}{ll} x=\tfrac{1}{2}F\mathrm{e}^{\mathbf{G}/2}, & \mathbf{H}=F\mathrm{e}^{\mathbf{G}/2}, \\ \mathbf{V}=-2\Pi, & \mathbf{C}=-\tfrac{1}{2}F^2\mathrm{e}^{\mathbf{G}}, \\ (\mathbf{A}=\mathbf{K}=0, & \mathrm{e}^{\mathbf{G}/2}\gg 1). \end{array}\right\} \qquad \ldots\ldots(27)$$

Another assumption which might be thought the simplest and most plausible of all is:

Assumption 3b.

$$\Delta C_{\mathrm{p}0}=0, \quad \text{i.e.} \quad \mathbf{C}=0.$$

From the third member of (25) we see that x must then satisfy the quadratic equation

$$x^2-x(2+\tau+\Pi)+(1+\tau)=0 \qquad (\mathbf{A}=\mathbf{K}=\mathbf{C}=0). \qquad \ldots\ldots(28)$$

It is of course necessary that x be real so that we must have

$$(\tau+\Pi)^2+4\Pi>0 \qquad (\mathbf{C}=0). \qquad \ldots\ldots(29)$$

This inequality being satisfied, a root of (28) can be substituted into the first two members of (25) to give $\mathbf{V}$ and $\mathbf{H}$.

As an additional specialization on (28), one may care to consider the case where, in addition to $\mathbf{C}=0$, $\mathbf{V}\ll 1$. Then Π must also be small and $x\simeq 1+\tau$. Hence:

$$\left.\begin{array}{l} \mathbf{H}=2\{F^2+(1+\tau)^2\}^{1/2}, \\ \mathbf{V}=-2\{F^2+(1+\tau)^2\}^{1/2}\Pi/\tau, \\ \mathbf{G}=2\ln\left[\{1+\tau+[F^2+(1+\tau)^2]^{1/2}\}/F\right], \\ \qquad (\mathbf{A}=\mathbf{K}=\mathbf{C}=0, \quad \mathbf{V}\ll 1). \end{array}\right\} \qquad \ldots\ldots(30)$$

As a limiting case of (30) we have that $\mathbf{V}=0$ implies and is implied by $\Pi=0$. This ultimate limit is the case which has always been treated in the literature. For example, a rigorous detailed derivation of it has been given previously by us (Davies and Lamb 1957).

It is obvious that the set of assumptions that we have built up (1 and 2 followed by 3*a* or 3*b* with or without further restrictions on the size of $\mathbf{V}$) by no means exhaust the possibilities. Other quite different assumptions may in particular cases be convenient and/or necessary.

§ 7. A NUMERICAL ILLUSTRATION OF THE THEORY USING DATA FOR TRIETHYLAMINE

The only substance known to us to which the above two-state theory might be applicable and for which the ultrasonic relaxation parameters have been determined as functions of pressure and temperature is triethylamine. Heasell and Lamb (1956) measured these parameters at atmospheric pressure over the temperature range 25–70°C; Litovitz and Carnevale (1958) have obtained corresponding data at a temperature of 0°C and pressures up to 3500 atm. It is apparent that the temperature ranges of these independent measurements do not overlap. As will be seen presently, this important fact makes it impossible to test the theory. Nevertheless since this is the only relevant information available we shall proceed by way of illustration to use figures drawn from the work cited above.

(i) In the first place consider only the temperature variation investigated by Heasell and Lamb. Assume in the usual way that the volume change is small and that in accordance with the theory of §§4–6 equations (30) can be applied ($\mathbf{A}=\mathbf{K}=\mathbf{C}=0$, $\mathbf{V}\ll 1$). Take a reference temperature of 300°K. Then $F=1{\cdot}16$, $\tau=\partial\ln F/\partial\ln T=1{\cdot}82$. Substituting these values in the first and third members of (30),

$$\Delta H_0=RT\mathbf{H} \quad =3{\cdot}7\,\text{kcal mol}^{-1},$$

$$\Delta G_0=RT\mathbf{G} \quad =1{\cdot}9\,\text{kcal mol}^{-1},$$

$$\Delta S_0=R(\mathbf{H}-\mathbf{G})=5{\cdot}7\,\text{cal mol}^{-1}\,\text{deg}^{-1}.$$

These values may be compared with those obtained by Heasell and Lamb using a different graphical approach in which certain approximations were made:

$$\Delta H_0=3{\cdot}4\,\text{kcal mol}^{-1},$$

$$\Delta G_0=2{\cdot}0\,\text{kcal mol}^{-1},$$

$$\Delta S_0=4{\cdot}7\,\text{cal mol}^{-1}\,\text{deg}^{-1}.$$

The agreement may be considered satisfactory but it should be noticed that the method used here is much easier to handle than the original one.

(ii) Consider now the data taken by Litovitz and Carnevale at 0°C and at high pressures. Using for this purpose the heat capacity given by Heasell and Lamb ($\bar{C}_p=51$ cal deg^{-1} mol^{-1}) and an expansivity estimated from density values quoted by Timmermans (1950) ($\bar{\alpha}=1{\cdot}25\times 10^{-3}$ deg^{-1}) we find

$$\Pi=(\bar{C}_p/\bar{\alpha}V)\,.\,\partial\ln F/\partial p=-1{\cdot}60.$$

Let us assume uncritically that the values of F and τ cited under (i) above at a temperature of 300°K can be used in conjunction with the present value of Π obtained at 273°K. We wish to proceed under assumption 3*b* of §6. The first step is to test the inequality (29). It is immediately apparent that this is *not* satisfied. Hence with this data all we obtain from the theory is the inequality (26) which yields $|\mathbf{V}|>2{\cdot}5$ and $\Delta V_0/V>3{\cdot}0\%$. (It may be observed that this value of $\mathbf{V}$ is comparable with the value of $\mathbf{H}$ obtainable from (i) above, namely $\mathbf{H}=6{\cdot}1$.)

We wish to emphasize that this *impasse* should not be regarded as a test of the theory but merely an illustration of how the theory might be applied. This is because we have good reason to believe that at a temperature between 0°C (at which Litovitz and Carnevale worked) and 25°C (the lowest temperature at which Heasell and Lamb worked) F passes through a minimum and hence τ changes sign. It is possible under these circumstances that the inequality (29) will in fact be satisfied at 0°C, thus permitting an application of the theory.

§ 8. CONCLUSIONS

We conclude that, even given full information concerning the variation of the ultrasonic relaxation strength with pressure and temperature, it is necessary to make at least three assumptions before thermodynamic reaction parameters can be evaluated. If, as is usually the case, the pressure data are not available values of the reaction parameters which have been obtained by assuming that $\Delta V_0=0$ should be treated with caution. It seems important to us that the questions raised here should be settled and in particular that further experimental work should be aimed at a systematic study under conditions of variable pressure and temperature.

ACKNOWLEDGMENTS

We wish to thank Dr. T. A. Litovitz for making his data available to us before publication and for stimulating discussions on the subject of this paper. We are also grateful to Dr. J. H. Andreae for helpful discussion and suggestions.

REFERENCES

BASS, R., and LAMB, J., 1957, *Proc. Roy. Soc.* A, **243**, 94.
—— 1958, *Ibid.*, **247**, 168.
DAVIES, R. O., and LAMB, J., 1957, *Quart. Rev. Chem. Soc., Lond.*, **11**, 134.
DE GROOT, M. S., and LAMB, J., 1957, *Proc. Roy. Soc.* A, **242**, 36.
HEASELL, E. L., and LAMB, J., 1956, *Proc. Roy. Soc.* A, **237**, 233.
KAGARISE, R. E., 1952, *Trans. Faraday Soc.*, **48**, 394.
—— 1955, *J. Chem. Phys.*, **23**, 207.
—— 1956, *Ibid.*, **24**, 300.
KREBS, K., and LAMB, J., 1958, *Proc. Roy. Soc.* A, **244**, 558.
LITOVITZ, T. A., and CARNEVALE, E. H., 1958, *J. Acoust. Soc. Amer.*, **30**, 134.
PITZER, K. S., and HOLLENBERG, J. L., 1954, *J. Amer. Chem. Soc.*, **76**, 1493.
TIMMERMANS, J., 1950, *Physico-chemical Constants of Pure Organic Compounds* (Amsterdam: Elsevier).
YOUNG, J. M., and PETRAUSKAS, A. A., 1956, *J. Chem. Phys.*, **25**, 943.

Lens Designing by Electronic Digital Computer: I

By C. G. WYNNE
Wray (Optical Works) Ltd., Bromley, Kent

MS. received 24*th October* 1958, *in revised form* 5*th January* 1959

Abstract. The problem of automatic lens designing by an electronic digital computer is considered in the light of existing aberration theory. Methods previously suggested are discussed, and a new iterative method of linear approximation is described.

---

§ 1. Introduction

THE problem of designing an optical imaging system whose aberrations are below some specified limit of size for a given magnification, numerical aperture and field angle is not at present amenable to a fully analytic solution except for some simple system of limited practical interest. The use of electronic digital computers to obtain numerical solutions for particular cases has been suggested by a number of authors, but most of these attempts have approached the problem more or less *ab ovo*, without much reference to the considerable body of knowledge of the basic properties of optical systems which have emerged from the study of aberration theory over the past century. An attempt has been made, therefore, to consider the problem of programming a computer for lens designing in the light of this existing knowledge.

§ 2. General Aberration Theory

Since the general aberration function A of a centred optical system is not evaluable analytically, traditional methods of lens designing depend on a dual approach to the problem of aberration correction. The seven primary aberrations are first considered (the five Seidel aberrations for monochromatic imagery and the two primary chromatic aberrations) which are the lowest terms in the series expansion of A in powers of ρ and σ, the ray aperture and distance of an object point from the lens axis.

These seven primary aberrations again cannot be treated analytically save for the simplest systems, but for a given set of design parameters they can be calculated fairly readily and the general form of their dependence on the design parameters is known, so that the designer can make changes to these parameters to give a first-order design for which these seven primary aberrations are reduced to zero, or suitable small values. Since these primary aberrations describe accurately the performance of the optical system for small apertures and object sizes (small ρ and σ) they must be reduced to small values for any well corrected system. For most practically interesting cases a number of higher order terms in A are significant. The second stage of design is to trace numerically the paths of a number of rays through the system whose primary aberrations have been reduced to zero or small values; these rays are chosen to pass through suitable 'sampling points' of the object and the aperture, and these give the actual value of A at these points of the aperture and field. The primary design may then be modified so as to introduce small amounts of primary aberration to give the best compromise balance with the higher order aberrations revealed by the ray-tracing over the aperture and field required.

This stage of the design process is reached by the experienced lens designer fairly quickly, and for some simple systems no further free parameters exist and no further basic improvement is possible. For more complicated systems, first-order correction will generally be possible for an infinite variety of forms with different values of the design parameters. The exploration of these, to determine the form having the lowest values of the higher order aberrations over the aperture and field required, together with finding the most effective way of increasing the complexity of the system to give smaller total higher order aberrations, constitutes the main part of optical designing, and is the least systematic. It is at this stage that electronic digital computers appear most likely to be useful.

For any complete lens system for which the primary aberrations are reduced to small values, these aberrations will in general have relatively large values for individual components of the system, the correction of the whole system being achieved by the balancing of large terms of opposite sign arising on the different components. Now for any single lens for which the primary aberrations are uncorrected, for example a single component of a complex optical system, the higher order aberrations are generally small compared with the primary ones arising at that component, though they may be large for the complete system for which the primary aberrations have been corrected. Accordingly, as individual design parameters of a complete system are changed, the changes in the aberrations of the system are predominantly changes to the first-order, the higher order changes being small relative to these. This fact, which is fundamental to the design process, means that the introduction into a first-order corrected system of small amounts of primary aberrations to balance higher order ones, referred to above, will generally effect only small changes to the higher order aberrations; and it also means that if the higher order aberrations revealed by ray-tracing in a first-order corrected system are to be reduced, a series of changes to the design parameters will be required, each of which considered alone will introduce large changes to the primary aberrations and so upset the first-order balance of the system, and make the state of correction of the whole system worse. The relevance of this to lens design on electronic digital computers is discussed below.

§ 3. THE USE OF ELECTRONIC DIGITAL COMPUTERS

The tracing of rays through an optical system, which is a fundamental part of any optical designing and is a relatively simple iterative process which has to be repeated a great number of times, is obviously suitable for programming on an electronic digital computer, and it was to this that these machines were first applied. For a relatively simple lens of six or seven surfaces, some twelve rays in a meridian section are generally enough to give reasonably full information about the performance. For more complicated lenses, which will generally be more highly corrected, 20 or more rays, including some skew rays, may be necessary, all of which may have to be traced through up to sixteen or eighteen surfaces. A ray in a meridian plane takes from five to ten minutes per surface to trace on a desk machine (depending on the extent of the checks and the amount of subsiduary information calculated) and a skew ray about twice as long. On the Ferranti Mark 1* machine which we have been using, the time is of the order of a fifth of a second per surface for a meridian ray trace.

Such rapid ray-tracing makes possible different approaches to the design problem. Primary aberrations are not generally calculated explicitly, since this would introduce a separate programme and occupy additional storage space in the machine which, in any automatic design process, is likely to be required for other purposes; instead, an approximation to the primary aberrations of any system is obtained by tracing rays at small values of ρ and σ. With rapid ray-tracing it becomes possible to calculate the change of the aberration of each of the chosen rays for changes of the various design parameters, as has been done by a number of workers. Various differential formulae have been given, the first by M'Aulay and Cruikshank (1945) for calculating these from quantities obtained by ray-tracing, but this again would require a separate programme occupying additional storage space, and the process of ray-tracing is so rapid that it is reasonable simply to repeat the tracing of the set of rays through the system whose design parameters have been changed, and so to find the change of the aberration of each ray for small finite differences. Small changes to the design parameters are necessary, since the aberration changes are highly non-linear with respect to design parameter changes for large variations. The radii, separations, etc. may be changed singly, but this will produce changes in the focal length of the complete systems. We have chosen a method of composite variables consisting of altering each radius, separation, or glass, one at a time, by a small amount, altering the next following air–glass or glass–air surface to restore the convergence of a paraxial ray emerging from that surface to what it was before the change, and scaling the radii of the remainder of the system so that the paraxial angles of incidence on each surface are unchanged. This is simply programmed, and it eliminates any drift of focal length as changes are made. Aspheric surfaces are rarely used in optical systems, and our work has accordingly been restricted to surfaces of constant curvature. Similar considerations of method to those given in this paper would however apply to the more general problem of lens design with non-spherical surfaces.

Repeating the ray-tracing programme for a series of systems in each of which a different alteration Δ_j of the design parameters has been made from the initial system yields a matrix of numbers, a_{ij} giving the change to the aberration A_i of each of the rays traced for a given small change of the jth design parameter, where j goes from 1 to n, the number of available design variables, and i from 1 to m, the number of aberrations calculated. The procedure this far, with various minor modifications, has been followed by a number of authors. Beyond this point serious difficulties arise, and different methods of working have been suggested.

3.1. *Linear Methods*

The obvious course, if the aberration variations could be considered as linear, mutually independent functions of the design parameters, would be to choose the number of aberrations calculated, m to be equal to the number n of design parameters, and to solve the simultaneous equations showing what proportion x_j of each of the n parameter changes Δ_j is required to reduce each of the aberrations A_i to zero. In matrix notation, the equations may be written

$$[a_{ij}]x_{(j} + A_{(i} = 0 \qquad \ldots\ldots(1)$$

where $x_{(j}$ and $A_{(i}$ are the column vectors $\{x_1x_2 \ldots x_j \ldots x_n\}$ and $\{A_1A_2 \ldots A_i \ldots A_m\}$ and the x_j values can be obtained by inversion of the matrix $[a_{ij}]$, though in fact in numerical work the solution of the equations by successive elimination, using pivotal condensation, would be used rather than actual matrix inversion. In fact, the aberration differentials are not linear or independent, and can only be reasonably so considered for small values of each x_j, while equations (1) are in general essentially ill-conditioned, having a solution at large values of x_j. This follows from the discussion of aberration theory above. Consider two aberrations A_i, A_{i+1}, which relate to an aberration of the same type for two values of one of the variables ρ, σ defining the ray positions, for example the longitudinal spherical aberration of the imagery of an axial object point for the full aperture $\rho_{\max}$ and an intermediate one, which will commonly be taken as that having $\rho = \rho_{\max}/\sqrt{2}$. Then any change in the design parameters which produces a change of primary spherical aberration alone will give $a_{ij}/a_{i+1,\,j} = (\rho_{\max}/\rho)^2$, since primary longitudinal spherical aberration varies as the square of the aperture; if all parameter changes give purely first order aberration changes, the ratio $a_{ij} : a_{i+1,\,j}$ will be constant for all values of j, the matrix $[a_{ij}]$ will be singular since two rows in its determinant are in a constant ratio, and no solution of the equations will be possible unless $A_i : A_{i+1} :: a_{ij} : a_{i+1,j}$, i.e. the whole system is free from higher order aberration. In actual optical systems the ratio $a_{ij} : a_{i+1,\,j}$ will not be exactly constant, but since most parameter changes give higher order aberration changes which are small compared with the first order changes, the ratio will be almost the same for all j values, and large values of x_j will result from equations (1). This state of affairs will generally arise for each set of aberrations A_i relating to an aberration of the same type for different values of the ray aperture or field, for example the sagittal or tangential field curvature at different field sizes σ, the coma either at a given aperture and different field sizes or at different apertures for a given field size, and so on.

An alternative procedure, which allows the number m of aberrations calculated to be larger than the number n of available design parameters, is to solve the normalized equations giving a least squares solution to equations (1), which may be written

$$[a_{ji}]\,[a_{ij}]x_{(j} + [a_{ji}]A_{(i} = 0 \qquad \ldots\ldots(2)$$

where $[a_{ji}]$ is the transpose of $[a_{ij}]$. Equations (2) have the same solutions as equations (1) when $m = n$. This method has been suggested by Rosen and Eldert (1954); there seems to be no reason why this method, in common with others that have been suggested which are discussed below, should not lead to a first-order solution, which is a stage normally reached quite quickly by traditional methods. But for the main and most difficult part of optical design which follows this, which consists of reducing the higher order aberrations of the whole system while maintaining a first-order correction, the fundamental difficulty which is inherent in the physical problem remains, namely that to produce significant changes to the higher order aberrations, using variables each of which produces changes in these higher order aberrations which are small compared with the first-order changes, such large changes of a number of the variables simultaneously will generally be required as to lie outside the range of linearity assumed in equations (1).

3.2. *Method of Steepest Descent*

A third method, suggested by Black (1955), some aspects of which have been discussed in detail by Feder (1957), is to form an optical merit function ψ from the calculated aberrations A_i, for example by forming the sum of their squares and to use a steepest descent method to reduce this function, using the differentials a_{ij}. A series of iterations can be made, using changes in the design parameters small enough for the aberration changes to be approximately linear, the differentials a_{ij} being recomputed after each change to the system, if necessary. This method again seems to lead fairly satisfactorily to a system whose primary aberrations are balanced against its higher order ones. Thus Feder took a corrected triplet design of lens whose aberrations had been calculated, changed its design parameters in a random fashion, and subjected this deranged lens to automatic correction using a steepest descent method, reaching a design with approximately the state of correction of the initial lens, after a 'large number' of iterations. As explained above, the random changes to the design parameters may be expected to produce changes to the aberrations which are predominantly first-order ones. However, the nature of the physical problem is such that the method is inherently inefficient for the later stages of design. The inefficiency of the method arises firstly from the fact that in operating only on the function ψ formed from the separate aberrations A_i, information is discarded about the distribution of the aberration between the various A_i, this information being essential to an efficient process of correction, and secondly that in addition to the inherent non-linearities of the aberrations with respect to the design parameters, a second and often much more serious non-linearity is introduced by the necessarily non-linear form of ψ.

The steepest descent method consists in making simultaneous changes to each of the design parameters of amounts x_j proportional to $-\partial\psi/\partial x_j$ which, when $\psi = \Sigma A_i^2$ means that

$$x_j = -K \sum_{i=1}^{i=m} A_i a_{ij} \qquad \ldots\ldots (3)$$

where the constant of proportionality K may be chosen in various ways. The simplest plausible choice would be to choose K so that ψ would be reduced to zero if the higher derivatives of ψ were zero; this is not generally satisfactory and, at the expense of some extra computing, the value of K may be found which leads to a minimum value of ψ with the design parameters taken in the ratio defined by equation (2), the minimum arising from the quadratic form of ψ (Feder described this as the optimum gradient method) or if these criteria lead to values of x_j outside the range of approximate linearity of the aberrations, K may be reduced appropriately. This is not generally necessary, since the effects from the non-linearity of ψ are normally the more significant. The steepest descent method is well known to be unsatisfactory for dealing with systems of ill-conditioned equations, requiring a great number of iterations, and the degree of ill-conditioning occurring in the equations arising in the later stages of lens designing is sufficient to show this effect very markedly. The effect can be considered descriptively as arising from two characteristics of equation (3). Firstly, each variable in this method is taken in the direction in which it, considered alone, decreases ψ; as has been shown above, for a first-order design any of the variables singly is likely to increase ψ except for quite small changes, for which the reduction in ψ will be small, and these small changes are almost as likely as not to be in the 'wrong' direction, i.e. changes of opposite sign to the corresponding root of equations (1). This effect becomes more serious as the number of aberrations A_i being corrected increases but it can be illustrated by simple examples. Consider first a system in which two aberrations only, A_1, A_2, are calculated, the initial values for these and their differentials with respect to two variables Δ_1 and Δ_2 being given by

$$\begin{array}{cc} & A_1=1 \qquad\qquad A_2=1 \\ \left[\begin{array}{ll} \Delta_1 & a_{11}=3 \\ \Delta_2 & a_{12}=2 \end{array}\right. & \left.\begin{array}{l} a_{21}=0 \\ a_{22}=-1 \end{array}\right]. \end{array}$$

The values of x_1 and x_2 for complete correction are given by the equations, by no means obviously ill-conditioned,

$$\left.\begin{array}{r} 3x_1+2x_2+1=0 \\ -x_2\ \ +1=0 \end{array}\right\}$$

with the solution $x_1=-1$, $x_2=+1$. However, since the second change Δ_2, considered alone, decreases $\psi=A_1^2+A_2^2$ when x_2 is taken as negative, the steepest descent method takes a first step of x_2 in this 'wrong' direction. The results of a series of iterations using the optimum gradient method are

$$\begin{array}{ll} A_1=1{\cdot}0 & A_2=1{\cdot}0 \\ {}_1A_1=0{\cdot}0983 & {}_1A_2=1{\cdot}0820 \\ {}_2A_1=0{\cdot}0619 & {}_2A_2=0{\cdot}7310 \end{array}$$

where ${}_pA_i$ is the value of A_i after p iterations. The process is obviously not highly efficient.

For more obviously ill-conditioned equations the rate of convergence is lower. Take a typical case of the kind discussed above where A_1, A_2 denote an aberration of the same type for two values of one of the ray-parameters ρ, σ, for example longitudinal spherical aberration at full aperture $\rho_{\max}$ and at an intermediate one $\rho_{\max}/\sqrt{2}$, and start from an initial first-order balance where A_1 and A_2 are equal and opposite, with two variables, the first showing only primary aberration ($a_{21}=2a_{11}$) and the second considerable higher order in addition to the primary term; then the values

$$\begin{array}{ccc} & A_1=-1 & A_2=+1 \\ \Delta_1 & \left[\begin{array}{l} a_{11}=1 \\ a_{12}=1 \end{array}\right. & \left.\begin{array}{l} a_{21}=2 \\ a_{22}=3 \end{array}\right] \\ \Delta_2 & & \end{array}$$

give complete correction $A_1=A_2=0$ for $x_1=4$, $x_2=-3$. In an actual system, departures from linearity of the aberrations might appear for these values of x_1, x_2 but the A's would be likely to be at any rate greatly reduced. The optimum gradient method is illustrated in the figure where the ellipses are contours of constant ψ on the x_1x_2 plane, and the solution follows the zigzag line. The successive values of A_1 and A_2 are

$$\begin{array}{ll} A_1=-1{\cdot}0 & A_2=1{\cdot}0 \\ {}_1A_1=-1{\cdot}2055 & {}_1A_2=0{\cdot}4520 \\ {}_2A_1=-0{\cdot}8288 & {}_2A_2=0{\cdot}8288 \end{array}$$

after which, A_1 and A_2 being again equal and opposite, the process repeats, reducing each A by a factor of 0·8288 after each pair of iterations, alternate changes of x_3 being away from the solution $\psi = 0$.

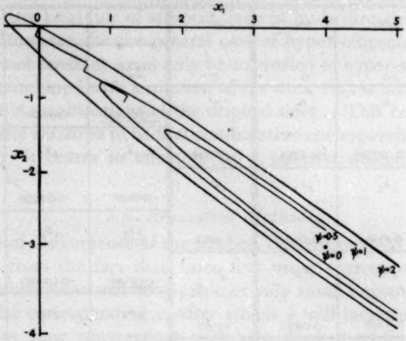

A second characteristic of descent methods which makes the rate of convergence slow with the typical optical problem is that since, due to the quadratic form of ψ, $\partial\psi/\partial x_j = 2\Sigma A_i a_{ij}$, if any aberration A_i is initially zero or very small, the contribution to the gradient of ψ of all the corresponding elements a_{ij} is zero or small, although these elements may themselves be relatively large. In a first-order corrected system a number of aberrations will generally be zero or small, and the effect is that the direction of steepest descent is very local, large values of a_{ij} turning a descent into an ascent for quite small values of the x's, thereby severely restricting the value of K in the optimum gradient method, and allowing only very small steps and slow convergence. A third example in which a third aberration A_3, initially zero, has been added to the second example, together with a third variable which makes correction of the three aberrations possible, will illustrate this.

$$\begin{array}{cc} & \begin{matrix} A_1 = -1{\cdot}0 & A_2 = 1{\cdot}0 & A_3 = 0 \end{matrix} \\ \begin{matrix} \Delta_1 \\ \Delta_2 \\ \Delta_3 \end{matrix} & \begin{bmatrix} a_{11} = 1 & a_{21} = 2 & a_{31} = 2 \\ a_{12} = 1 & a_{22} = 3 & a_{32} = 2 \\ a_{13} = 0 & a_{23} = 0 & a_{33} = -2 \end{bmatrix} . \end{array}$$

This has a solution $A_1 = A_2 = A_3 = 0$ at, as before $x_1 = 4$, $x_2 = -3$ and $x_3 = 1$. The values of the aberrations A_i and of ψ after successive iterations, and the x_j at each iteration, again distinguished by prefixes, and the total change of each variable after 6 iterations, are given in the table.

One third of all the parameter changes, those values of ${}_px_i$ underlined, have been taken in the 'wrong' direction, the total change of x_3 is in the 'wrong' direction, and after six iterations A_1 and A_3 have been increased from their initial values. This example also illustrates how the rate of convergence decreases as the number of equations increase, even when no obvious increase in the ill-condition of the equations is involved. A measure of the degree of ill-condition is the ratio of the principal axes of the hyper-ellipsoids defined by $\psi = \text{constant}$, which for the general case are in the ratio of the square roots of the eigenvalues of the matrix $[a_{ji}]\,[a_{ij}]$. For the second example above, these are as 1 : 14·9 and for the third as 1 : 6·4 : 19·6.

${}_0A_1$ -1·0	${}_0A_2$ 1·0	${}_0A_3$ 0	${}_0\Psi$ 2			
${}_1A_1$ -1·1376	${}_1A_2$ 0·60330	${}_1A_3$ -0·2752	${}_1\Psi$ 1·7706	$\underline{{}_1X_1}$ $\underline{-0{\cdot}04587}$	${}_1X_2$ -0·09174	${}_1X_3$ 0
${}_2A_1$ -1·0916	${}_2A_2$ 0·6791	${}_2A_3$ 0·0572	${}_2\Psi$ 1·6559	${}_2X_1$ +0·09211	${}_2X_2$ -0·04606	$\underline{{}_2X_3}$ $\underline{-0{\cdot}12014}$
${}_3A_1$ -1·1592	${}_3A_2$ 0·4939	${}_3A_3$ -0·0890	${}_3\Psi$ 1·5957	$\underline{{}_3X_1}$ $\underline{-0{\cdot}01789}$	${}_3X_2$ -0·04980	${}_3X_3$ 0·00537
${}_4A_1$ -1·1080	${}_4A_2$ 0·5602	${}_4A_3$ 0·1024	${}_4\Psi$ 1·5520	${}_4X_1$ 0·08732	${}_4X_2$ -0·03611	$\underline{{}_4X_3}$ $\underline{-0{\cdot}04447}$
${}_5A_1$ -1·1559	${}_5A_2$ 0·4270	${}_5A_3$ -0·0131	${}_5\Psi$ 1·5189	$\underline{{}_5X_1}$ $\underline{-0{\cdot}01046}$	${}_5X_2$ -0·03744	${}_5X_3$ 0·00986
${}_6A_1$ -1·0949	${}_6A_2$ 0·5228	${}_6A_3$ 0·1229	${}_6\Psi$ 1·4872	${}_6X_1$ 0·08728	${}_6X_2$ -0·02624	$\underline{{}_6X_3}$ $\underline{-0{\cdot}00698}$
				TOTAL CHANGE X_1 0·19249	X_2 -0·28739	X_3 -0·15636

The inherent slow convergence of the steepest descent method for the type of equation encountered in the optical design problem, illustrated in the three simple examples above, will generally be considerably worse in actual optical problems, both because the size of the matrix will be much greater and because the equations will be more highly ill-conditioned; Feder (1957) states that ratios of the smallest to the largest eigenvalue in excess of 10^6 occur in practical systems. The examples given have been ones where the minimum of ψ occurred at values of each x_j small enough for the linear approximation (equation (1)) to be reasonably close, so that the matrix a_{ij} need only be computed once, and used for a series of steps; the calculation of this matrix, for an optical system of any complexity, is a fairly lengthy process even on a fast computer, and to recompute it at each step, with a rate of convergence like that of the third example or worse, would make the process intolerably slow. For the typical optical problem, however, large total changes of the design parameters are necessary to achieve an optimum correction, and repeated recalculations of the a_{ij} matrix would be necessary at intervals, for which some criterion would have to be provided to the machine.

Feder (1957) has discussed various expedients which accelerate the convergence in some cases. In an example in two variables that he gives, where the ψ = constant ellipses lie parallel to the one of the x axes, a simple numerical scaling of one of the Δ's i.e. one column of the matrix a_{ij}, converts the ellipses into circles, and any local line of steepest descent leads directly to the minimum at the centre. However, for the general case of hyper-ellipsoids inclined to the axes, the surfaces of constant ψ can only be converted to hyper-spheres by scaling of the variables combined with a rotation of the axes, that is taking new variables formed by suitable combinations of the original ones. This can be achieved by choosing one of the variables to be that combination corresponding to the solution of equations (2); it ceases in effect to be a steepest descent method and is discussed in § 3.4.

3.3. *Relaxation Methods*

The low rate of convergence of the steepest descent method applied to optical problems arises from the fact that, once first-order correction is reached, any single variable taken alone will be capable of only small improvement to ψ, for a small value of the corresponding x, after which ψ will increase. This fact will clearly also cause slow convergence with any descent method, including the simple relaxation method used by Black (1955) in which ψ was reduced by successive use of each variable. In addition to the relaxation method taking one variable at a time, Black also used group and block relaxations, in which a number of variables were changed simultaneously, either by arbitrary groupings, or in groups constituted by extrapolating from an earlier system to a later, better corrected, one obtained by application of the simpler methods. These procedures are clearly unlikely greatly to increase the convergence rate for first-order corrected systems.

3.4. *Successive Linear Approximation with Maximum Steps*

In terms of the discussion hitherto, the optical design problem is that of minimizing ψ, starting from an initial lens design for which $\psi = \Sigma A_i^2$, the hypersurfaces of constant ψ in n-dimensional x_j space conforming to hyper-ellipses within the region of the origin for which the variations of the A_i's with respect to the design parameters can be approximated by the first terms in the Taylor expansion, corresponding to the values a_{ij}, both the minimum of ψ and the centre of the hyper-ellipsoids often lying at considerable distances from the origin. So long as only the variation of ψ with the design parameters is considered (as in descent methods), and not the separate variations of its components A_i, the available methods of treating the problem all appear inefficient, since with ill-conditioned equations these methods require very many iterations at very small step-sizes, far smaller than the range of approximate linearity of the aberrations with the design parameters would allow. On the other hand a simple least-squares solution (equation (2)), again due to the ill-condition of the basic equations, generally leads to steps in the variables x_j far greater than the range of linearity. A smaller step-size, chosen to be as large as is compatible with linearity, might be taken in the direction of the centre of hyper-ellipsoids defined by the least-squares solution of equations (2), but this is liable to give a relatively small reduction of ψ, where the roots of (2) are large, since the direction of the centre may lie almost parallel to the constant ψ surfaces in the region of the origin. This corresponds to the fact that, when equations (2) are set up and solved for actual optical systems, the solution generally gives very large values of one or a few of the x_j, the remainder being relatively small. Simple scaling down of all x_j so that the largest is within the range of reasonable linearity will then make most of the x_j values much smaller than is necessary for linearity, and the variables corresponding to these smaller x_j's, suitably combined, would generally be capable of effecting further reductions of the aberrations; that is to say the improvement of the optical system in each step using this method is not likely to be the maximum that is attainable within the range of linearity of the equations. What is required is a method which, instead of limiting the size of the largest x_j's to maintain linearity, limits the size of Σx_j^2. This is achieved by a method we have evolved†, which might be called Successive Linear Approximation with Maximum Steps (SLAMS).

Let equations (1) be set up together with the equations specifying that each x_j multiplied by some weighting factor P shall be zero, i.e.

$$\left.\begin{aligned}[a_{ij}]x_{(j}+A_{(i}&=0\\ Px_{(j}&=0\end{aligned}\right\} \quad \ldots\ldots (4)$$

and let these two sets of equations be normalized to give the n simultaneous equations corresponding to a least-squares solution for the complete set. Then if the values ${}_1x_j$ obtained by solving these equations be substituted into the left-hand side of the first of equations (4), the residuals will be the aberration ${}_1A_i$, forecast assuming linearity, of the optical system whose design parameters have been modified in accordance with these values ${}_1x_j$; the residuals from the second of equations (4) will be the values P_1x_j; and the least squares solution of the combined equations (4) is the one which minimizes the squares of all these residuals, i.e. which minimizes $({}_1\psi+P^2\Sigma_1x_j^2)$, where ${}_1\psi$ is the value of ψ for the modified system. It follows immediately that for a step-size $\Sigma_1x_j^2$ that lies within the range of linearity of the aberrations with the design parameters, this must give a system with a lower value of ψ than the original for all finite values of P, for if $x_{(j}=0$ be substituted into equations (4) the sum of the squared residuals is simply ψ; if the least squares solution gives any other values than $x_{(j}=0$, the sum of the squared residuals must be less than this, i.e.

$${}_1\psi+P^2\sum{}_1x_j^2<\psi$$

and hence ${}_1\psi<\psi$. Now the size of step $\Sigma\,{}_1x_j^2$ can be controlled by the choice of P, and in fact the two earlier methods, that of solving equations (2) and of steepest descent, are special limiting cases of this SLAMS method. At one extreme, when $P=0$, the second set of equations (4) are identically satisfied for all values of ${}_1x_j$ and the least squares roots of (4) are therefore identical with the roots of (2), $\Sigma\,{}_1x_j^2$ becoming the square of the distance from the origin to the centre of the hyper-ellipsoids $\psi=$constant; at the other extreme as P approaches infinity, the values of ${}_1x_j$ become infinitesimal in the ratio of the values of $\partial\psi/\partial x_j$, corresponding to the direction of steepest descent. For any intermediate value of P,

---

† I am indebted to a referee for bringing to my attention two papers by Girard (1958) in which a similar numerical method is described and applied to the design of a separated triplet lens system. Since a relatively small electronic digital computer was used for this work, it was not practicable to use the method for simultaneous variation of all the design parameters; a series of applications of the method was therefore made, using different sets of a few of the design parameters in successive cycles.

$\Sigma_1 x_j^2 = R^2$, say, will take some value such that R is intermediate between zero and the distance of the centre of the hyper-ellipsoids, R becoming less as P is increased, and the least squares solution of equations (4) will give the values of ${}_1x_j$ corresponding to the smallest value of ψ within a hyper-sphere of radius R about the origin. The SLAMS method is then to use the least squares solution of equations (4) at each step of the linear approximation, with P chosen to make R as large as the range of approximate linearity of the aberrations with the design parameters allows. This may be found by trial of different values of P in equations (4), setting up of the optical system corresponding to the values of ${}_1x_j$ found, calculating its A_i and ψ, and comparing this with the ψ predicted by the linear approximation. The choice of P is obviously not critical; if P is taken rather small, the linearly predicted reduction of ψ, which will be larger since R is larger, will depart more from the actual calculated ψ due to increased non-linearity, and vice versa if P is too large. In practise it is found satisfactory to choose P from a few trials at the first cycle so that the lens design given by the x_j with this choice of P has values of A_i found by ray-tracing which are reasonably near to those forecast by the linear approximation, and this value of P is then generally found suitable for subsequent iterations, which may give a reduction of ψ at each stage equivalent to some hundreds of steepest descent cycles.

This method of Successive Linear Approximation with Maximum Steps has been successfully applied to a variety of optical design problems. An account of the machine programming and the results achieved will be given in a subsequent paper.

REFERENCES

BLACK, G., 1955, *Proc. Phys. Soc.* B, **68,** 729.

FEDER, D. P., 1957, *J. Opt. Soc. Amer.*, **47,** 902.

GIRARD, A., 1958, *Rev. Opt.* (*Théor. Instrum.*), **37,** 225, 397.

M'AULAY, A. L., and CRUIKSHANK, F. D., 1945, *Proc. Phys. Soc.*, **57**, 302.

ROSEN, S., and ELDERT, C., 1954, *J. Opt. Soc. Amer.*, **44,** 250.

On the Determination of the Principal *g*-values in Electron Spin Resonance

By D. S. SCHONLAND
Department of Applied Mathematics, University of Southampton

MS. received 12*th November* 1958, *in final form* 28*th December* 1958

Abstract. A method of inferring the principal values and the directions of the principal axes of the *g*-tensor for a paramagnetic complex in a single crystal from measurements of the *g*-value variation in three different planes is described, and an ambiguity in the determination of the principal values that will often arise in practice is pointed out and discussed. An estimate of the root mean square error in the determination is given.

---

§ 1. Introduction

When a paramagnetic complex in a single crystal possesses no obvious axis or plane of symmetry its principal *g*-values and the directions of the corresponding principal axes have to be inferred from measurements of the *g*-value variation in planes which are defined in relation to a convenient set of axes O123 fixed in the crystal. If the magnetic field has direction cosines l_1, l_2, l_3 with respect to these axes, the square of the corresponding *g*-value is given by an expression of the form (Pryce 1950, Weil and Anderson 1958)

$$g^2 = \sum_{i,j=1}^{3} A_{ij} l_i l_j, \quad (A_{ij} = A_{ji}), \qquad \ldots\ldots (1)$$

where the coefficients A_{ij} depend on the choice of reference axes. When these coefficients are known for a particular set of axes, the principal *g*-values and principal axes are found by diagonalizing the matrix A. The three roots λ_1, λ_2, λ_3 of the secular equation

$$\det(A - \lambda I) = 0, \qquad \ldots\ldots (2)$$

where I is the unit matrix, are the squares of the principal *g*-values; the direction cosines of the principal axes satisfy

$$\sum_{j=1}^{3} A_{ij} l_{kj} = \lambda_k l_{ki}, \quad i = 1, 2, 3, \qquad \ldots\ldots (3)$$

where the l_{kj} $(j = 1, 2, 3)$ are the direction cosines corresponding to the root λ_k of (2).

The practical problem then is to determine the six independent coefficients A_{ij} relative to a definite set of axes fixed in the crystal. Some ways of doing this have been described by Weil and Anderson; their methods, however, demand measurements which may be rather difficult to carry out on certain crystal types. A method which should be generally applicable to orthorhombic or monoclinic crystals is described below, and an ambiguity in the determination of the principal *g*-values which will arise in many practical cases is pointed out and discussed. Finally, the probable errors in the determination are discussed.

§ 2. DETERMINATION OF THE A_{ij}

2.1. *The Fundamental Type of Measurement*

The kind of g-value measurement that is normally made is to rotate the magnetic field about an axis fixed in the crystal and to measure the g-value variation in the plane perpendicular to this axis. If θ is an angular coordinate specifying the direction of the magnetic field in the plane of measurement it can be shown from (1) that in this plane the g-value is given as a function of θ by an expression of the general form

$$g^2 = \alpha + \beta \cos 2\theta + \gamma \sin 2\theta, \qquad \ldots\ldots (4)$$

where α, β and γ are functions of the A_{ij}, of the parameters specifying the orientation of the plane of measurement relative to the reference axes, and of the origin chosen for θ. The quantities α, β, γ will be most accurately determined by obtaining the best fit of (4) to a large number of g-value measurements at different angles θ, but should this procedure prove impracticable they can alternatively be expressed in terms of three directly measurable quantities. These are the maximum and minimum g-values in the plane, denoted by g_+ and g_- respectively, and the angle θ_+ at which the maximum g-value occurs. One has

$$\left.\begin{aligned} 2\alpha &= g_+{}^2 + g_-{}^2, \\ 2\beta &= (g_+{}^2 - g_-{}^2)\cos 2\theta_+, \\ 2\gamma &= (g_+{}^2 - g_-{}^2)\sin 2\theta_+. \end{aligned}\right\} \qquad \ldots\ldots (5)$$

It should be noted that the sign of γ depends on that of the angle θ_+, i.e. a complete determination of α, β, γ requires a specification of the positive sense of rotation of the magnetic field about the axis fixed in the crystal. This point will be returned to below; we remark here that a positive value of γ implies that g increases as the magnetic field is rotated in the positive sense through the position $\theta = 0$.

Since α, β, γ depend on the A_{ij}, their measurement in a single plane gives rise to three equations satisfied by the A_{ij}. In order to obtain in this way sufficient equations to determine all the A_{ij} it is necessary to measure the g-value variation in three different planes. This will give nine equations to determine the six independent A_{ij}; this redundancy is unavoidable and gives a useful check on the internal consistency of the measurements.

2.2. *Method of Determining the A_{ij}*

The simplest choice for the reference axes O123 with respect to which the coefficients A_{ij} are to be determined will be the crystallographic *a*, *b* and *c* axes in the case of an orthorhombic crystal. If the crystal is monoclinic one can take the *a*, *b* and *c*′ axes, where *c*′ is perpendicular to *a* and *b*. It will generally be possible to mount the crystal so that g-value measurements can be made in planes containing one or more of these axes without too much difficulty.

We suppose now that measurements are made in the 12 and 31 planes and in a third plane which contains the axis 2 and which meets the 31 plane in a line making an angle ϵ with the axis 3, measured in the positive sense from O3 to O1. Thus in a monoclinic crystal we can identify O1, O2 and O3 with the *a*, *b* and *c*′ axes respectively and suppose that measurements are made in the *ab*, *ac*′, and *bc* planes, the *c* axis making an angle ϵ with *c*′ and lying in the *ac*′ plane.

We distinguish the quantities α, β, γ of (4) and (5) when measured in the 12 plane by the suffix 3, when in the 31 plane by the suffix 2, and when in the third plane by the suffix 1. The angle θ appearing in (4) is to be measured in these three planes respectively from O1, from O3 and from O2 in the positive right-handed sense.

Then one can deduce from (1) and (4) that for the measurements in the 12 plane

$$A_{11}=\alpha_3+\beta_3,\quad A_{22}=\alpha_3-\beta_3,\quad A_{12}=\gamma_3; \qquad \ldots\ldots(6)$$

for those in the 31 plane

$$A_{33}=\alpha_2+\beta_2,\quad A_{11}=\alpha_2-\beta_2,\quad A_{31}=\gamma_2; \qquad \ldots\ldots(7)$$

and for those in the third plane

$$A_{22}=\alpha_1+\beta_1, \qquad \ldots\ldots(8)$$

$$A_{33}\cos^2\epsilon+A_{11}\sin^2\epsilon+2A_{31}\sin\epsilon\cos\epsilon=\alpha_1-\beta_1, \qquad \ldots\ldots(9)$$

$$A_{23}\cos\epsilon+A_{12}\sin\epsilon=\gamma_1. \qquad \ldots\ldots(10)$$

It will be seen that (6) and (7) serve to determine all the A_{ij} except A_{23} and give two independent determinations of A_{11} to act as a consistency check. Two further checks are provided by (8) and (9) and the remaining coefficient A_{23} is determined from (10).

The last three equations reduce to equations of the form of (6) and (7) if it is possible to mount the crystal in three mutually perpendicular planes and so choose $\epsilon=0$. In this special case it is unnecessary to measure β and γ separately, and the results can be expressed in terms of α and the quantity

$$\delta=(\beta^2+\gamma^2)^{1/2}=\tfrac{1}{2}(g_+{}^2-g_-{}^2), \qquad \ldots\ldots(11)$$

measured in each of the three planes, by means of the equations

$$\left.\begin{aligned} A_{11}&=(\alpha_2+\alpha_3-\alpha_1),\\ A_{12}&=\pm\,[(\delta_3+\alpha_1-\alpha_2)(\delta_3-\alpha_1+\alpha_2)]^{1/2}.\end{aligned}\right\} \qquad \ldots\ldots(12)$$

The remaining A_{ij} satisfy similar equations obtained from (12) by cyclic permutation of the sufficies 1, 2, 3. The sign of A_{12} is that of γ_3 and cyclically. This special case has been treated in a different way by Weil and Anderson and also by Geusic and Brown (1958).

§ 3. AMBIGUITY IN THE DETERMINATION

In order to determine the signs of the γ_k appearing in equations (6) to (10) it is essential to be able to distinguish between the positive and negative senses of rotation about the reference axes. In principle this could be done by marking the positive ends of these axes on the surface of the crystal but, since more than one crystal is normally required in order to obtain a complete set of measurements, this procedure may not be possible in practice. Furthermore, it often happens that the crystals contain two or more paramagnetic complexes in the unit cell which are symmetrically, but differently, oriented with respect to the crystal axes. Each of these will produce a g-value variation and one cannot decide *a priori* which of the plots of g-value against angle obtained in the different planes of measurement should be taken together. This means that in general it will only be possible to measure the magnitudes but not the absolute values of the γ_k.

This ambiguity in the sign of the γ_k gives rise in fact to only two distinct possibilities, for one can always choose two of the γ_k, say γ_2 and γ_3, to be positive. From the remarks following after (5) above it will been that choosing γ_3 positive defines the positive sense of rotation in the 12 plane and so the positive direction of the third axis. Then making γ_2 positive will define the octant formed by the positive 1, 2 and 3 axes, but will leave the sign of the angle ϵ unknown. With this assumption for the sign of γ_2 and γ_3 (6) and (7) determine all the A_{ij} except A_{23}, the correct sign to take for ϵ will be determined by (9), and finally (10) with the two possible signs for γ_1 will determine two possible values of A_{23}. In the special case where $\epsilon=0$ and equations (12) are used, one may choose say A_{12} and A_{31} positive; then both possible signs for A_{23} need to be considered.

The situation may be visualized by imagining the construction of a three-dimensional model of the g-value variation from polar diagrams of the variations in each of the planes of measurement. Two of these can be fitted together along their line of intersection; there are then two ways of fitting the third polar diagram into the model.

Thus from the type of measurement we have discussed it will in general be possible to deduce two sets of principal g-values and principal axes, and some further information will be required to enable a decision between these to be made. This information may be obtained by making further g-value measurements in a direction or in a plane not included in the previous measurements and by comparing these with the results predicted by the two possible sets of principal values. If we denote the principal axes by x, y, z with corresponding g-values g_x, g_y, g_z, then the g-value in a direction whose direction cosines with respect to x, y and z are l, m, n respectively is given by

$$g^2=g_x{}^2l^2+g_y{}^2m^2+g_z{}^2n^2.$$

On the other hand if the g-value variation is measured in a plane whose normal has direction cosines l, m, n with respect to the principal axes, the maximum and minimum g-values in this plane will satisfy the relations

$$g_+{}^2+g_-{}^2=g_x{}^2(1-l^2)+g_y{}^2(1-m^2)+g_z{}^2(1-n^2),$$

and

$$g_+{}^2\cdot g_-{}^2=g_x{}^2g_y{}^2n^2+g_y{}^2g_z{}^2l^2+g_z{}^2g_x{}^2m^2.$$

§ 4. PROBABLE ERROR OF THE DETERMINATION

Denote the principal g-values by g_x, g_y, g_z and the direction cosines of the corresponding principal axes with respect to the reference axes O123 by l_{xk}, l_{yk}, l_{zk} $(k=1, 2, 3)$. Then the solution of (2) and (3) can be expressed in the form

$$G=P'AP, \qquad \ldots\ldots(13)$$

where G is a diagonal matrix whose diagonal elements are $g_x{}^2$, $g_y{}^2$, $g_z{}^2$, and P is an orthogonal matrix whose columns are the vectors l_{xk}, l_{yk}, l_{zk}.

If the error in estimating the matrix element A_{ij} from the measurements is ϵ_{ij}, one can show on the basis of (13) that the error in the determination of g_x is

$$dg_x=\left\{\sum_{i,j=1}^{3}\epsilon_{ij}l_{xi}l_{xj}\right\}\Big/2g_x, \qquad \ldots\ldots(14)$$

and that the errors in the direction cosines l_{xk} of the corresponding principal axis are

$$dl_{xk} = \alpha_{xy} l_{yk} + \alpha_{xz} l_{zk}, \quad (k = 1, 2, 3), \qquad \ldots\ldots(15)$$

where

$$\alpha_{xy}(g_x{}^2 - g_y{}^2) = \sum_{i,j=1}^{3} \epsilon_{ij} l_{xi} l_{yj} ;$$

$$\alpha_{xz}(g_x{}^2 - g_z{}^2) = \sum_{i,j=1}^{3} \epsilon_{ij} l_{xi} l_{zk} .$$

Similar expressions obtained by cyclic permutation of the suffices x, y, z hold for the other principal axes.

The root mean square errors in the determination of g_x and the l_{xk} are obtained by squaring (14) and (15) and taking their mean values. This involves the evaluation of the mean values of products of the form $\epsilon_{ij}\epsilon_{pq}$. These can be obtained by using equations (6) to (10) to express the ϵ_{ij} in terms of the errors in the α, β, γ obtained for each plane of measurement. These errors can in turn be expressed in terms of the independent errors of measurement of g_+, g_- and θ_+ in each plane by using (5). In order to obtain manageable expressions this process was carried through only for the special case in which measurements are made in three mutually perpendicular planes so that $\epsilon = 0$ in (9) and (10). Each diagonal element was taken as the mean of the two independent determinations of it afforded by (6) to (10), and it was assumed that all the g-value measurements were subject to the same r.m.s. error Δ, and that all the angular measurements were subject to the same r.m.s. error Θ.

The results of a rather lengthy calculation then give the following expressions for the r.m.s. error $\langle dg_x \rangle$ in the determination of g_x, and for the r.m.s. error $\langle dl_{xk} \rangle$ in the determination of l_{xk}.

$$4g_x{}^2 \langle dg_x \rangle^2 = F(1, 2, 3) + F(2, 3, 1) + F(3, 1, 2), \qquad \ldots\ldots(16)$$

$$\langle dl_{xk} \rangle^2 = M(1, 2, 3;\ k) + M(2, 3, 1;\ k) + M(3, 1, 2;\ k); \qquad \ldots\ldots(17)$$

with

$$\begin{aligned} F(1, 2, 3) = {} & \tfrac{1}{2}\Delta^2\{4A_{11} l_{x1}{}^4 + \alpha_1 \sin^2\phi_1 (18 l_{x2}{}^2 l_{x3}{}^2 - l_{x2}{}^4 - l_{x3}{}^4) \\ & + 8 l_{x2} l_{x3} [(\gamma_1 + \alpha_1 \sin\phi_1 \cos\phi_1) l_{x2}{}^2 + (\gamma_1 - \alpha_1 \sin\phi_1 \cos\phi_1) l_{x3}{}^2]\} \\ & + \Theta^2 [4\beta_1 l_{x2} l_{x3} - \gamma_1 (l_{x2}{}^2 - l_{x3}{}^2)]^2 ; \qquad \ldots\ldots(18) \end{aligned}$$

and

$$\begin{aligned} M(1, 2, 3;\ k) = {} & \tfrac{1}{2}\Delta^2\{4A_{11} l_{x1}{}^2 Q_{1k}{}^2 + \alpha_1 \sin^2\phi_1 [4(l_{x2} Q_{3k} + l_{x3} Q_{2k})^2 \\ & - (l_{x2} Q_{2k} - l_{x3} Q_{3k})^2] + 4(l_{x2} Q_{3k} + l_{x3} Q_{2k}) [(\gamma_1 + \alpha_1 \sin\phi_1 \cos\phi_1) \\ & \times l_{x2} Q_{2k} + (\gamma_1 - \alpha_1 \sin\phi_1 \cos\phi_1) l_{x3} Q_{3k}]\} \\ & + \Theta^2 [2\beta_1 (l_{x2} Q_{3k} + l_{x3} Q_{2k}) - \gamma_1 (l_{x2} Q_{2k} - l_{x3} Q_{3k})]^2 . \qquad \ldots\ldots(19) \end{aligned}$$

In these expressions

$$Q_{ik} = \frac{l_{yi} l_{yk}}{g_x{}^2 - g_y{}^2} + \frac{l_{zi} l_{zk}}{g_x{}^2 - g_z{}^2},$$

and $\phi = 2\theta_+$, with a suffix to denote the plane of measurement. The remaining F and M in (16) and (17) are obtained from (18) and (19) by cyclic permutation of the suffices 1, 2, 3.

REFERENCES

GEUSIC, J. E., and BROWN, L. C., 1958, *Phys. Rev.*, **112**, 64.
PRYCE, M. H. L., 1950, *Proc. Phys. Soc.* A, **63**, 25.
WEIL, J. A., and ANDERSON, J. H., 1958, *J. Chem. Phys.*, **28**, 864.

The Reactions ^{27}Al(p, p′)^{27}Al and ^{27}Al(α, p)^{30}Si

By F. de S. BARROS, P. D. FORSYTH, A. A. JAFFE and I. J. TAYLOR
The Physical Laboratories, University of Manchester

MS. received 29th September 1958, in final form 2nd December 1958

Abstract. The reactions ^{27}Al(p, p′)^{27}Al and ^{27}Al(α, p)^{30}Si have been studied at 5 MeV incident energy using a high resolution broad range magnetic spectrograph. Angular distributions of several of the proton groups from each of the reactions were determined and the results suggest that some of the final states are formed by direct processes. The excitations of the first four states of ^{30}Si were found to be $2{\cdot}258 \pm 0{\cdot}006$, $3{\cdot}518 \pm 0{\cdot}007$, $3{\cdot}798 \pm 0{\cdot}009$ and $4{\cdot}85 \pm 0{\cdot}01$ MeV.

---

§ 1. INTRODUCTION

THE spectra of protons from the reactions ^{27}Al(p, p′) and ^{27}Al(α, p)^{24}Mg, at approximately 5 MeV bombarding energy, have been investigated at high resolution using a broad range magnetic spectrograph in conjunction with the Manchester University 6 MeV Van de Graaff accelerator. Angular distributions and absolute cross sections of several proton groups were found for both reactions.

Large anisotropies were observed in the angular distributions of some of the proton groups and most of these are asymmetric about the 90° direction in the centre of mass system. This asymmetry may originate from overlapping levels in the compound nucleus but it is also possible that the reactions may proceed, at least in part, by some direct interaction process.

In one such process the incident particle interacts directly with a single particle or small group of particles at the nuclear surface. A detailed discussion of such reactions has been given by Butler (1957) and it is expected that the angular distributions of the reaction products should be characteristic of the net orbital angular momentum $l\hbar$ which is transferred to the nucleus.

For strongly deformed nuclei, excitation of rotational levels by direct excitation inelastic scattering may be predicted by the collective model and is particularly likely for quadrupole deformations (Brink 1955, Hayakawa and Yoshida 1955 a, b). The Born approximation method yields angular distributions which are similar to those predicted by the Butler process. Direct excitation inelastic scattering has been reviewed by Devons and Goldfarb (1957). More recently, Sawicki (1958) has applied the unified model to include both rotational and individual particle direct excitations by inelastic scattering.

Investigations of reactions leading to discrete final levels with incident energies of from 10 to 30 MeV have been found to support the direct interaction theory and good agreement has been obtained with the predicted angular distributions (Butler 1957, Silver 1957, Von Herrmann and Pieper 1957). If a nuclear reaction is found to proceed predominantly by a direct surface interaction, measurement of the angular distribution of the resolved groups of outgoing particles can yield information about the spins and parities of the final levels.

At lower bombarding energies than those referred to above, Coulomb effects and interaction of the incident and final particles with the core cannot be neglected but these effects are more important in determining the cross section than the angular distribution, as is also the case for deuteron stripping (Yoccoz 1954). For lower incident energy there should be greater separation of the peaks of the angular distributions corresponding to different l values.

§ 2. EXPERIMENTAL TECHNIQUE

The magnetic spectrograph is of the 90° broad range type, having circular pole edges giving second order spherical aberration correction for symmetrical object and image positions. This instrument is similar to the 20 in. radius, $\frac{1}{2}$ in. field gap, spectrograph described by Browne and Buechner (1956) although the construction of the yoke is simpler. The main differences are that the pole radius is 18 in. but the gap is $1\frac{1}{2}$ in. Used as a broad range spectrograph the performance is approximately the same as that of the instrument of Browne and Buechner.

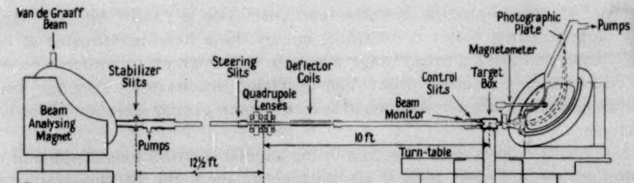

Figure 1. Diagram of the experimental arrangement with the magnetic spectrograph in the 0° position.

The spectrograph is mounted on a turntable (figure 1) which may be rotated to observe particles in the range −10° to 115°, though it would be possible to extend observations to 135° with only minor modifications. The beam from the Van de Graaff accelerator is analysed by a 90° magnet and is refocused by magnetic quadrupole lenses. Horizontal and vertical deflections are provided by two pairs of coils, whose currents are determined by signals from two sets of control slits placed close to the target chamber, so that the beam is automatically centred on the final slit. In this way more than 25% of the total analysed beam of the accelerator can be used to irradiate a target area of 0·020 in. high and 0·060 in. long. The system ensures that the beam may readily be regained even after rotation or other disturbance of the beam analyser magnet when the accelerator has been used for other experiments.

Calibration of the spectrograph was made using a thin polonium α-particle source, taking the value $Hr = 3{\cdot}31644 \times 10^4$ gauss cm, to find the values of r corresponding to different points on the focal surface. Energy resolutions of better than 1 in 1000 were obtained with the polonium source over the whole range.

The magnetic field is measured by the proton and (at the higher fields) lithium nuclear magnetic resonances, the resonant frequency being found on a Hewlett–Packard type 524B frequency meter, which gives a continuous check on the magnetometer oscillator frequency. The spectrograph is excited by a motor generator whose field winding is controlled by the output of a chopper type d.c. amplifier and the field stability is 1 part in 10 000. The spectra were recorded on 50 μ thick C2 nuclear emulsion plates.

Two targets were used: the first a self-supporting aluminium foil 170 μg cm^{-2} thick giving more than adequate resolution for the investigation of the first three excited states of ^{27}Al by the ^{27}Al(p, p′) reaction, and for the remaining experiments 70 μg cm^{-2} Al evaporated on to a VYNS plastic foil of about 10 μg cm^{-2}.

The plane of the target was set along the $-45°$ direction with respect to the incident beam, with the backing, if any, facing the beam. The beam current was integrated by collection in a Faraday cup fitted with a suppressing electrode and an additional check was provided by monitoring the more energetic protons emitted from the target in the $-135°$ direction with a 0·005 in. thick plastic scintillator.

The target thickness was measured with an α-particle gauge (Enge *et al.* 1957). The absolute cross sections were calculated directly and also, where possible, by comparison with Rutherford scattering. The absolute values of the cross sections are believed to be accurate to within approximately 15%.

§ 3. RESULTS

The ^{27}Al(p, p′) reaction was studied in two ranges and typical spectra are shown in figure 2. In each case the beam energy was held constant for all angles. The beam energy was computed from the elastic proton peak for the higher field setting and from the p_3 group for the lower settings. Six excited states of ^{27}Al

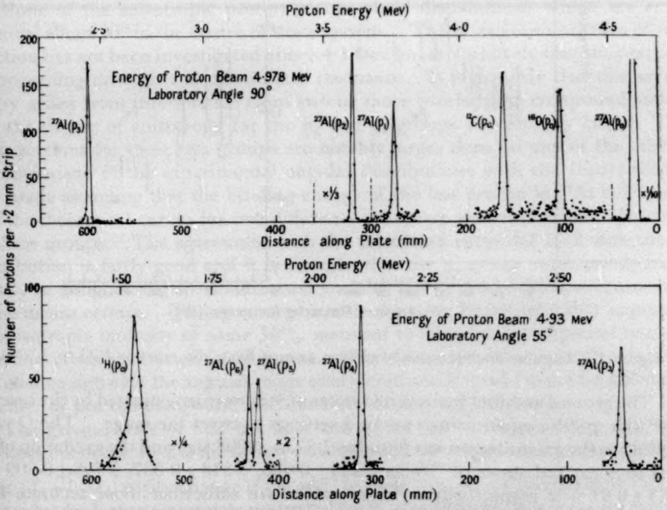

Figure 2. Proton spectra from proton bombardment of ^{27}Al.

were observed with the following excitations: 0·840 ± 0·004, 1·010 ± 0·004, 2·219 ± 0·004, 2·736 ± 0·006, 2·980 ± 0·006 and 3·002 ± 0·006 Mev. These values are in good agreement with recent data reviewed by Endt and Braams (1957), though the energy of the third excited state was found to be higher than their value of 2·208 Mev by about three times our estimated standard deviation.

The angular distributions of four of the proton groups are shown in figure 3. The groups p_1 and p_6 yielded distributions which were approximately isotropic with cross sections of 1·3 and 0·8 mbn sterad^{-1} respectively.

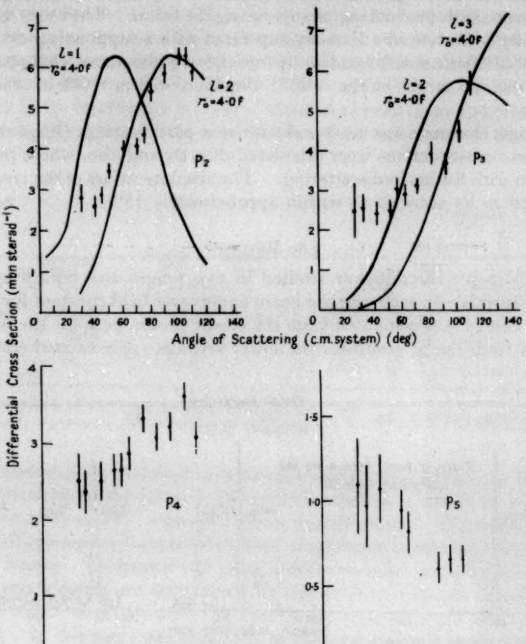

Figure 3. Angular distributions of proton groups from the reaction ^{27}Al (p, p′) ^{27}Al.

The ground and first four excited states of ^{30}Si were investigated by the reaction of ^{27}Al(α, p)^{30}Si, again using two field settings to cover the range. The *Q* value leading to the ground state was found as 2·373 ± 0·008 Mev and the excitation of the first four excited states of ^{30}Si as 2·258 ± 0·006, 3·518 ± 0·007, 3·798 ± 0·009 and 4·85 ± 0·01 Mev respectively. These values are somewhat more accurate than previous determinations e.g. Van Patter and Buechner (1952). The angular distributions of the ground and second excited state groups are shown in figure 4.

The proton group leading to the third excited state was found to be relatively weak with an approximately constant differential cross section of 180 μbn sterad^{-1}. Only incomplete information was obtained about the angular distribution of the p_1 group since at angles below 40° it was obscured by the peak of elastically scattered α-particles, but no large variation of cross section was found over the angular range of 40°–110°, and a cross section of 0·85 mbn sterad^{-1} was observed.

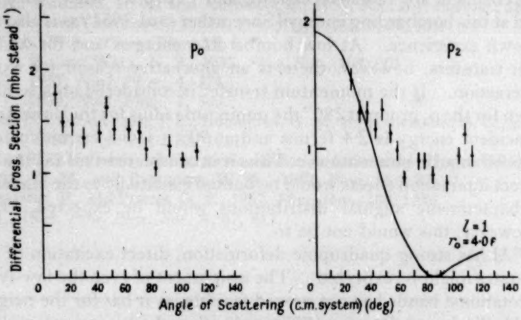

Figure 4. Angular distributions of proton groups from the reaction ^{27}Al(α, p)^{30}Si at 5·15 MeV incident energy.

§ 4. Discussion

(*a*) ^{27}Al(p, p′).

None of the anisotropic proton groups show distributions which are symmetrical about 90° in the centre of mass system. The resonance structure of this reaction has not been investigated above 4·1 MeV but it is unlikely that the reaction is proceeding through a single isolated resonance. It is possible that this asymmetry arises from interference from two or more overlapping compound states, but the degree of anisotropy for the p_2 and p_3 groups is strikingly large. The cross sections for these two groups are notably larger than for any of the others. A comparison of the experimental angular distributions with the Butler theory was made assuming that the binding energy of the last proton in ^{27}Al is 8·2 MeV and the theoretical curves for two different l values are shown in figure 3 for each of these groups. The agreement with the calculated curve for $l=2$ with the p_2 distribution is fairly good and it is thought that the p_3 group corresponds more closely to a higher angular momentum transfer ($l=3$) though this assignment is by no means certain. The agreement could, of course, be considerably improved if an isotropic intensity of some 30%, assumed to arise from compound nucleus formation, was subtracted in each case. The direct interaction amplitude does not change sign over the angular range considered and it would make no difference whether or not the compound nucleus contribution was coherent.

The ground state of ^{27}Al has spin and parity 5/2$^+$ and, assuming that spin flip does not occur, $l=2$ is the lowest value allowed by the spin and parity selection rules ($\vec{J}_i+\vec{l}=\vec{J}_f$, parity change if l is odd) to form the second excited state (3/2$^+$). The value $l=3$, very tentatively suggested for p_3, would mean that the third excited state has negative parity.

The observed angular distributions indicate that the second and third excited states may be formed predominantly by a direct surface interaction. One explanation for the limitation of a direct interaction to the surface would be that the mean free path for compound nucleus formation is small and that the compound nucleus decays into alternative channels. This is improbable for ^{27}Al(p, p′) at 5 MeV since the mean free path of the protons in the nucleus is large and the only competing channels are radiative capture and ^{27}Al(p, α)^{24}Mg. The former is unfavoured at this bombarding energy (Shoemaker *et al.* 1951) as is also the latter, from our own experience. At low bombarding energies and for high angular momentum transfers, however, there is an alternative reason for expecting a surface interaction. If the momentum transfer is considered on a semi-classical picture, then for the p_2 group at 180° the minimum radius for the direct interaction at 5 MeV incident energy is 2·4 fermis and at 90° it is 3·3 fermis for a transfer of two units of angular momentum. Thus it is considered that for the p_2 and p_3 groups, direct interaction effects would be limited essentially to the nuclear surface and the characteristic angular distributions would be expected. For lower l values, however, this would not be so.

Since ^{27}Al has strong quadrupole deformation, direct excitation of collective rotational states might be expected. The assignment of even the low-lying levels of ^{27}Al to rotational bands has not proved feasible, as it has for the neighbouring nucleus ^{25}Al (Endt and Braams 1957) and although the ground and first two excited states of ^{27}Al have the same spins and parities as the corresponding states in ^{25}Al their spacing is not consistent with a similar assignment (Rakavy 1957). If these are, in fact, rotational levels analogous to those of ^{25}Al the inelastic scattering process leading to the first or second excited states would involve a change of two units in K, the projection of the nuclear angular momentum on the symmetry axis. Such a case is covered by the general relation derived by Sawicki.

(*b*) ^{27}Al(α, p)^{30}Si.

The angular distributions of the ground and first excited states have been investigated by Von Herrmann and Pieper (1957) at 8·1 and 7·1 MeV who find that the angular distributions varied fairly rapidly with energy; Hunting and Wall (1957) have also investigated the ground state distribution at 30·5 MeV. The most markedly anisotropic group is p_2, but it is not clear whether or not it is symmetrical about 90°. A good fit with the Butler theory could only be obtained if a comparatively large isotropic contribution was deducted (figure 4).

§ 5. CONCLUSION

The results for the reaction ^{27}Al(p, p′), whilst strongly suggesting the possibility of interpretation in terms of direct interaction effects, may be capable of alternative explanation. In the absence of evidence at other bombarding energies the possibility that the asymmetries about 90° arise from overlapping compound states cannot be eliminated.

ACKNOWLEDGMENTS

The authors wish to thank Professor S. Devons, Professor L. Rosenfeld, Dr. L. Goldfarb and Dr. A. Herzenberg for their useful comments and discussions.

REFERENCES

Brink, D. H., 1955, *Proc. Phys. Soc.* A, **68**, 994.

Browne, C. P., and **Buechner**, W. W., 1956, *Rev. Sci. Instrum.*, **27**, 899.

Butler, S. T., 1957, *Phys. Rev.*, **106**, 272.

Devons, S., and **Goldfarb**, L. J. B., 1957, *Angular Correlations, Handbuch der Physik*, Vol. 42 (Berlin : Springer).

Endt, P. M., and **Braams**, C. M., 1957, *Rev. Mod. Phys.*, **29**, 683.

Enge, H. A., **Wahling**, H. A., and **Aanderaa**, I., 1957, *Rev. Sci. Instrum.*, **28**, 145.

Hayakawa, S., and **Yoshida**, S., 1955 a, *Proc. Phys. Soc.* A, **68**, 656.

—— 1955 b, *Progr. Theor. Phys.* **14**, 1.

Hunting, C. E., and **Wall**, N. S., 1957, *Phys. Rev.*, **108**, 901.

Rakavy, G., 1957, *Nucl. Phys.*, **4**, 375.

Sawicki, J., 1958, *Nucl. Phys.*, **7**, 503.

Shoemaker, F. C., **Faulkner**, J. E., **Bouricius**, G. M. B., **Kaufmann**, S. G., and **Mooring**, F. P., 1951, *Phys. Rev.*, **83**, 1011.

Silver, R., 1957, *University of California Radiation Laboratory Report*, URCL–3887.

Van Patter, D. M., and **Buechner**, W. W., 1952, *Phys. Rev.* **87**, 51.

Von Herrmann, P., and **Pieper**, G. F., 1957, *Phys. Rev.*, **105**, 1556.

Yoccoz, J., 1954, *Proc. Phys. Soc.* A, **67**, 813.

Collisional Relaxation in Gases

By N. J. PHILLIPS
Department of Mathematics, Imperial College, London

Communicated by R. Latham; MS. received 11*th December* 1958,
in final form 26*th January* 1959

Abstract. Solutions of the time-dependent Boltzmann equation for gases are considered. The Boltzmann equation is first linearized by considering only small deviations from equilibrium. From the solutions of the linearized equation, a variational principle is developed, which permits the estimation of the eigenvalues by a method of successive approximations. In this paper we calculate the lowest non-zero characteristic rate of relaxation for spherically symmetrical distributions. The distribution function is assumed to be uniform in the configuration space. Eigenvalues have been evaluated for gases whose particles interact with a law of force of the form $Q(a/r)^s$ where r is the distance between a pair of particles. The cases $s=2$, 5 and infinity have been considered in detail. In the cases $s=2$, the impact parameter is cut off at the Debye shielding distance. The calculations are extended to include the case of a two-component mixture of gases.

---

§ 1. Introduction

It was first shown by Boltzmann (1872) in his celebrated H theorem, that a gas in the absence of body forces would approach a state in which the distribution of particle velocities is Maxwellian.

In this paper we shall estimate, by a method based on the time-dependent Boltzmann equation, the lowest non-zero characteristic rate of relaxation of a gas in a non-steady state. The distribution function is assumed to differ by a small amount from the equilibrium Maxwellian form.

We have chosen to study the relaxation of spherically symmetrical distributions. In practice, the relaxing distribution is usually not spherically symmetrical. It is usual for there to be some drift motion of the particles which decays into random motion or for there to be more energy in one dimension than in the others. In these cases the distribution starts off asymmetric and decays into a spherically symmetrical state in the absence of any forces.

In general, the smallest characteristic rate of relaxation will be zero. This corresponds to a perturbation constructed entirely of collisional invariants, i.e. number density, momentum and energy. What we are interested in is the decay of perturbations which are not constructed of these invariants but give rise to a real non-equilibrium state. As is usually the case in linearized theories, it is possible to use a variational calculation of the lowest eigenvalues of the equation. The eigenvalues are calculated by means of a method of successive approximations.

The eigenvalues in the case $s=2$ are applicable to the theory of fully ionized gases. In this case great interest is centred around the variation of the high energy tail of the distribution. We make no attempt to analyse any particular perturbation of the equilibrium distribution, but the eigenvalues here throw some light on the rate of decay of the various terms in the expansion of the general perturbation in terms of the eigenfunctions of the equation.

§ 2. THE TIME-DEPENDENT BOLTZMANN EQUATION

For a gas which is uniform in the configuration space, in the presence of no body forces, taking into account only binary collisions, it may be shown (Chapman and Cowling 1953) that the distribution of particle velocities is given by the equation

$$\partial f(\mathbf{v},t)/\partial t=\int [f(\mathbf{v}_1,t)f(\mathbf{u}_1,t)-f(\mathbf{v},t)f(\mathbf{u},t)]\sigma g\, d\boldsymbol{\sigma}\, d\mathbf{u} \qquad \ldots\ldots(2.1)$$

where $\mathbf{u}$, $\mathbf{v}$ are the velocities of a pair of particles before collision and $\mathbf{u}_1$, $\mathbf{v}_1$ the corresponding velocities after collision. The quantities g and σ are respectively the relative speed before impact and the collision cross section.

We shall consider solutions of the equation near equilibrium, so that

$$f(\mathbf{v},t)=f_{\mathrm{e}}(\mathbf{v})[1+h(\mathbf{v},t)] \qquad \ldots\ldots(2.2)$$

where $f_{\mathrm{e}}(\mathbf{v})$ is the equilibrium solution, given by

$$f_{\mathrm{e}}(\mathbf{v})=n(m/2\pi kT)^{3/2}\exp(-m\mathbf{v}^2/2kT)$$

and h is such that $|h|\ll 1$. Here m is the particle mass, n the number density and T the temperature.

With this form of solution, equation (2.1) takes the form

$$f_{\mathrm{e}}(\mathbf{v})\partial h(\mathbf{v},t)/\partial t=\int f_{\mathrm{e}}(\mathbf{v})f_{\mathrm{e}}(\mathbf{u})[h]\sigma g\, d\boldsymbol{\sigma}\, d\mathbf{u}, \qquad \ldots\ldots(2.3)$$

since $f_{\mathrm{e}}(\mathbf{v})f_{\mathrm{e}}(\mathbf{u})=f_{\mathrm{e}}(\mathbf{v}_1)f_{\mathrm{e}}(\mathbf{u}_1)$ because energy is assumed to be conserved during collisions. The bracket $[h]$ is defined by the equation

$$[h]=h(\mathbf{u}_1,t)+h(\mathbf{v}_1,t)-h(\mathbf{u},t)-h(\mathbf{v},t) \qquad \ldots\ldots(2.4)$$

and we see that if h is a collisional invariant, then

$$[h]=0. \qquad \ldots\ldots(2.5)$$

We attempt a solution of equation (2.3) in the form $h(\mathbf{v},t)=\exp(-qt)\alpha(\mathbf{v})$ and it follows that

$$qf_{\mathrm{e}}(\mathbf{v})\alpha(\mathbf{v})=-\int f_{\mathrm{e}}(\mathbf{v})f_{\mathrm{e}}(\mathbf{u})[\alpha]\sigma g\, d\boldsymbol{\sigma}\, d\mathbf{u}. \qquad \ldots\ldots(2.6)$$

We denote by α_m the eigenfunctions of this equation and by q_m, the corresponding eigenvalues.

In what follows, we shall outline a method of evaluating the lowest eigenvalue of the equation. It would seem that this is the physically most interesting eigenvalue as it gives us a limit to the rate of relaxation of the characteristic solutions. We shall set up a theory of the eigenfunctions which is exactly analogous to the quantum mechanical problem of determining the ground state energy of a given system.

§ 3. A Variational Principle

By analogy to the scalar product in wave mechanics we define

$$(\alpha_m, \alpha_n) = \int \alpha_m(\mathbf{v})\alpha_n(\mathbf{v}) f_e(\mathbf{v})\, d\mathbf{v}, \qquad \ldots\ldots (3.1)$$

which clearly satisfies the relations

$$(\alpha_m, \alpha_n) = (\alpha_n, \alpha_m) \quad \text{and} \quad (\alpha_m, \alpha_m) > 0. \qquad \ldots\ldots (3.2)$$

We then define a 'matrix element'

$$[\alpha_m, \alpha_n] = -\int f_e(\mathbf{v}) f_e(\mathbf{u}) \alpha_m(\mathbf{v}) [\alpha_n] \sigma g\, d\boldsymbol{\sigma}\, d\mathbf{u}\, d\mathbf{v}, \qquad \ldots\ldots (3.3)$$

then it follows (Chapman and Cowling 1953) that

$$[\alpha_m, \alpha_n] = [\alpha_n, \alpha_m] \quad \text{and} \quad [\alpha_m, \alpha_m] > 0. \qquad \ldots\ldots (3.4)$$

Equation (2.6) is equivalent to

$$q_m(G, \alpha_m) = [G, \alpha_m], \qquad \ldots\ldots (3.5)$$

where G is an arbitrary function of $\mathbf{v}$.

Taking G to be α_m in equation (3.5), it follows that

$$q_m \geqslant 0, \text{ for all } m. \qquad \ldots\ldots (3.6)$$

Thus the solution of the equation must tend to the equilibrium solution $f_e(\mathbf{v})$ as time elapses.

Taking G to be α_n in equation (3.5) and then considering the same equation with m and n interchanged, it follows by subtraction that

$$(q_m - q_n)(\alpha_m, \alpha_n) = 0, \qquad \ldots\ldots (3.7)$$

and it is known that we may choose

$$(\alpha_m, \alpha_n) = 0, \quad (m \neq n), \qquad \ldots\ldots (3.8)$$

(see Courant and Hilbert 1953).

Now let us expand the arbitrary function G in the form

$$G = \sum_m c_m \alpha_m \qquad \ldots\ldots (3.9)$$

then

$$\begin{aligned} [G, G] &= \sum_m c_m [G, \alpha_m] && \text{by (3.9)} \\ &= \sum_m c_m q_m (G, \alpha_m) && \text{by (3.5)} \\ &= \sum_m c_m{}^2 q_m (\alpha_m, \alpha_m) && \text{by (3.8) and (3.9).} \end{aligned}$$

Let q_0 be the smallest eigenvalue, then we have

$$[G, G] \geqslant q_0 \sum_m c_m{}^2 (\alpha_m, \alpha_m) = q_0(G, G),$$

thus

$$q_0 \leqslant [G, G]/(G, G). \qquad \ldots\ldots (3.10)$$

This is the variational principle which forms the basis of our calculations.

§ 4. Estimation of q_0

To determine q_0, we choose a trial function with a number of arbitrary parameters and then minimize the calculated value of q_0 in (3.10) with respect to these parameters.

We restrict our attention to spherically symmetrical distributions, so that

$$h(\mathbf{v}, t) = h(v^2, t). \qquad \ldots\ldots (4.1)$$

In the case in which the particles interact with the inverse fifth power of the distance, the eigenfunctions are known. These eigenfunctions are the Sonine polynomials defined by the relation

$$\sum_{m=0}^{\infty} t^m S_m(X) = (1-t)^{-3/2} \exp\{-Xt/(1-t)\}. \qquad \ldots\ldots (4.2)$$

It may be shown that these polynomials satisfy the orthogonality conditions

$$\int_0^\infty x^{1/2} e^{-x} S_m(x) S_n(x)\, dx = [\Gamma(m+3/2)/m!]\delta_{mn}. \qquad \ldots\ldots (4.3)$$

This is equivalent to saying that

$$(S_m, S_n) = 0, \quad (m \neq n).$$

Since these polynomials are the eigensolutions for one particular type of particle interaction it seems likely that for a different type of interaction the eigensolutions may be strongly related to the above polynomials.

If we take as a trial function

$$G = \sum_{m=0}^{r} b_m S_m(V^2) \quad \text{where} \quad \mathbf{V} = (m/2kT)^{1/2}\mathbf{v}, \qquad \ldots\ldots (4.4)$$

in the equation (3.10), we have

$$q_0 \leqslant \sum_{m=0}^{r} b_m b_n [S_m, S_n] \Big/ \sum_{m=0}^{r} b_m{}^2 (S_m, S_m). \qquad \ldots\ldots (4.5)$$

We simply take an increasing number of coefficients in the expansion of G and continually minimize the calculated value of q_0 with respect to these coefficients.

The first two Sonine polynomials are

$$S_0 = 1 \quad \text{and} \quad S_1 = 3/2 - V^2$$

and since these are both collisional invariants, the brackets $[S_0]$ and $[S_1]$ vanish identically. From the definition of the brackets $[S_0, S_m]$ and $[S_1, S_m]$, we see that they are both zero.

We thus start off our trial function at $m=2$, i.e. $G = \overset{r}{\Sigma} b_m S_m(V^2)$, $(m \geqslant 2)$. As a first solution we take $G = b_2 S_2$ and the first aproximation to q_0 is

$$q_{01} = [S_2, S_2]/(S_2, S_2). \qquad \ldots\ldots (4.6)$$

As a second solution we take $G = b_2 S_2 + b_3 S_3$ and the second approximation to q_0 is

$$q_{02} = \frac{b_2{}^2[S_2, S_2] + 2b_2 b_3 [S_2, S_3] + b_3{}^2 [S_3, S_3]}{b_2{}^2 (S_2, S_2) + b_3{}^2 (S_3, S_3)}, \qquad \ldots\ldots (4.7)$$

which is then minimized with respect to the ratio b_3/b_2 and so on.

§ 5. CALCULATION OF q_0 FOR SPECIFIC PARTICLE INTERACTION

The evaluation of the matrix elements $[S_m, S_n]$ though tedious, is straightforward and we shall not describe the evaluation here.

For the first approximation to q_0, we require the values of $[S_2, S_2]$ and (S_2, S_2). In terms of the particle interaction $Q(a/r)^s$, these have been evaluated to give

$$m^{-1/2} n^2 \sqrt{(2\pi)}\, \Gamma[4 - 2/(s-1)] A_2(s) (Qa^s)^{2/(s-1)} (2kT)^{(s-5)/2(s-1)}$$

and $15n/8$ respectively, where, as before, n is the number density and m the particle mass. The quantity $A_2(s)$ is a numerical constant depending on the law of interaction and is defined on page 171 of Chapman and Cowling (1953). By equation (4.6), the first approximation to q_0 is given by

$$\frac{8}{15}\sqrt{(2\pi)}\Gamma\left[4-\frac{2}{s-1}\right]A_2(s)(Qa^s)^{2/(s-1)}nm^{-1/2}(2kT)^{(s-5)/2(s-1)}$$

and we now go on to consider specific values of s.

Rigid spheres.

When the particles behave like rigid spheres, the force Q is zero except when the particles are actually touching. This may be regarded as a limiting case of the general law of interaction when s tends to infinity. The force is zero if $r > a$ and tends to infinity as r tends to a. The integrals for this case were worked out separately to give

$$[S_2, S_2] = 4\sqrt{\pi}n^2a^2(kT/m)^{1/2}$$

where a is the particle diameter and the first approximation to q_0 is

$$q_{01} = \frac{32}{15}\sqrt{\pi}na^2\left(\frac{kT}{m}\right)^{1/2}.$$

Coulomb interaction ($s=2$).

The evaluation of the constants $A_2(s)$ is straightforward except in the case $s=2$. Mathematical difficulties arise because the integrals involved diverge. The physics of the problem reveals that it is the slow falling-off of the interaction potential which is responsible for the trouble.

In a real ionized gas, the Coulomb potential of a given charged particle is effectively screened by the effect of local space charge fluctuations and the usual Coulomb potential e/r, is modified to become

$$(e/r)\exp(-r/D), \qquad D = (kT/4\pi ne^2)^{1/2},$$

where e is the electronic charge and D is the Debye shielding distance. What we do here is to use the Coulomb potential for collisions in which the impact parameter is less than D and we ignore all collisions in which the distance between the colliding particles is greater than D. The screening effect is only present in a gas composed of particles of both sign and in our study of a gas of one type of charged particle we assume that such screening is still present.

For the case $s=2$, we write $Qa^2 = Z^2e^2$ where Z is the charge number of the particles. In terms of these constants, we find that

$$A_2(2) = 2[\ln(1+L^2) - L^2/(1+L^2)]$$

where $L^2 = (4/\pi)(kT)^3/ne^6$. Thus we may write the first approximation to q_0 in the form

$$q_{01} = \frac{8}{15}\sqrt{\pi}Z^4e^4nm^{-1/2}(kT)^{-3/2}[2\ln L - 1],$$

since in all cases of practical interest, $L \gg 1$.

Maxwellian particles.

The particles for which $s=5$ are commonly called Maxwellian. Putting $s=5$ in the general formula, we have the first approximation to q_0 in the form

$$q_{01} = \pi\sqrt{2}A_2(5)(Qa^5)^{1/2}nm^{-1/2}$$

and for this special case there is no dependence on temperature. As we have already mentioned, the Sonine polynomials are actually the eigenfunctions in this case and the above expression for the smallest non-zero eigenvalue is exact.

The first approximations to q_0 have been improved by the method of successive approximations and the results corrected to a few percent are:

Rigid spheres.

$$q_0 = 0{\cdot}97\,\frac{32}{15}\,\sqrt{\pi}\,na^2\left(\frac{kT}{m}\right)^{1/2}:$$

Coulomb interaction.

$$q_0 = 0{\cdot}56\,\frac{8}{15}\,\frac{\sqrt{\pi}\,nZ^4e^4(2\ln L-1)}{m^{1/2}(kT)^{3/2}}\,.$$

§ 6. GAS MIXTURES

When we have a mixture of gases, it is possbile to develop a similar more general theory of the relaxation process.

Using a similar method of solution to that used in the case of a simple gas, we can write the Boltzmann equations for the two component gas in the form

$$\begin{aligned} qf_{1e}(\mathbf{v}_1)\alpha_1(\mathbf{v}_1) = &-\int f_{1e}(\mathbf{v}_1)f_{1e}(\mathbf{v})[\alpha]_{11}\sigma_{11}g_1\,d\sigma\,d\mathbf{v} \\ &-\int f_{1e}(\mathbf{v}_1)f_{2e}(\mathbf{v}_2)[\alpha]_{12}\sigma_{12}g_{12}\,d\sigma\,d\mathbf{v}_2 \qquad \ldots\ldots(6.1) \end{aligned}$$

and

$$\begin{aligned} qf_{2e}(\mathbf{v}_2)\alpha_2(\mathbf{v}_2) = &-\int f_{1e}(\mathbf{v}_1)f_{2e}(\mathbf{v}_2)[\alpha]_{21}\sigma_{21}g_{21}\,d\sigma\,d\mathbf{v}_1 \\ &-\int f_{2e}(\mathbf{v}_2)f_{2e}(\mathbf{v})[\alpha]_{22}\sigma_{22}g_2\,d\sigma\,d\mathbf{v} \qquad \ldots\ldots(6.2) \end{aligned}$$

where the expressions $[\alpha]_{ij}$ are defined by the relations

$$[\alpha]_{ij} = \alpha_i(\mathbf{v}_i') + \alpha_j(\mathbf{v}_j') - \alpha_i(\mathbf{v}_i) - \alpha_j(\mathbf{v}_j)$$

and $\mathbf{v}_i'$, $\mathbf{v}_j'$ are the velocities of a pair of particles after collision. By considering the eigensolutions of these equations we may by a similar method obtain an inequality for the lowest eigenvalue q_0.

Let $\mathbf{F}$ be an arbitrary vector of the form $\mathbf{F} = [F_1(\mathbf{v}_1), F_2(\mathbf{v}_2)]$ where

$$F_1(\mathbf{v}_1) = \sum_m b_m\alpha_{1m} \quad\text{and}\quad F_2(\mathbf{v}_2) = \sum_m b_m\alpha_{2m}. \qquad \ldots\ldots(6.3)$$

We can then show that

$$\begin{aligned} &\tfrac{1}{4}\int f_{1e}(\mathbf{v}_1)f_{1e}(\mathbf{v})([F]_{11})^2\sigma_{11}g_1\,d\sigma\,d\mathbf{v}_1\,d\mathbf{v} \\ &+\tfrac{1}{4}\int f_{2e}(\mathbf{v}_2)f_{2e}(\mathbf{v})([F]_{22})^2\sigma_{22}g_2\,d\sigma\,d\mathbf{v}_2\,d\mathbf{v} \\ &+\tfrac{1}{2}\int f_{1e}(\mathbf{v}_1)f_{2e}(\mathbf{v}_2)([F]_{12})^2\sigma_{12}g_{12}\,d\sigma\,d\mathbf{v}_1\,d\mathbf{v}_2 \\ &\qquad \geqslant q_0\left[\int f_{1e}(\mathbf{v}_1)F_1^2\,d\mathbf{v}_1 + \int f_{2e}(\mathbf{v}_2)F_2^2\,d\mathbf{v}_2\right] \qquad \ldots\ldots(6.4) \end{aligned}$$

and we have the variational principle for the mixture of gases.

We have obtained the first approximation to q_0 for the case of Coulomb interaction by the use of a trial function of the form $F = [b_1 S_1(V_1^2), -b_1 S_1(V_2^2)]$. This corresponds to the case of a real fully-ionized gas in which the energy content of the electrons is not equal to the energy content of the ions. The result for the first approximation to q_0 is

$$q_{01} = \frac{8\sqrt{(2\pi)}Z^2 e^4 n(2\ln L)}{3(kT)^{3/2} m_e^{1/2}(m_i/m_e)},$$

where we assume that the number density of electrons is equal to the number density of ions, Z is the charge number of the ions and L has the same significance as before.

§ 7. CONCLUSION

What we have done here is to determine the lowest eigenvalues of the linearized Boltzmann equation. These eigenvalues are the smallest non-zero characteristic rates of relaxation of the spherically symmetrical distribution. These would appear to be the most interesting as their inverse gives a measure of the minimum characteristic time of relaxation.

It is clear from the analysis that if we wish to study the decay of asymmetric distributions then we need only take a more general expansion of the trial functions G, to include the angular variation.

We have not attempted to study the behaviour of any specific perturbation of the equilibrium distribution but should we wish to do this, it seems that the expansion of the perturbation h in the form

$$h(v^2, t) = \sum_m b_m S_m(V^2)\exp(-q_m t),$$

where the exponents q_m are obtained by the substitution of the above expansion in the equation, would be a reasonable method.

The results are similar to some obtained by Spitzer (1956) who used the method of Chandrasekhar to obtain relaxation times for various types of collision process involving the interaction of a particle with a background of particles in equilibrium.

ACKNOWLEDGMENTS

My thanks are due to Dr. O. Penrose for many helpful discussions and to the Department of Scientific and Industrial Research for a maintenance grant.

REFERENCES

BOLTZMANN, L., 1872, *Wien. Ber.*, **66**, 275.

CHAPMAN and COWLING, 1953, *The Mathematical Theory of Non-Uniform Gases* (Cambridge: University Press).

COURANT, R., and HILBERT, D., 1953, *Methods of Mathematical Physics* (New York : Interscience Publishers).

SPITZER, L., 1956, *Physics of Fully Ionized Gases* (New York : Interscience Publishers).

The Effect of Copper on the Work Function of Liquid Tin

BY T. C. TOYE
The Technical College, Swansea

MS. received 19*th November* 1958, *in final form* 19*th January* 1959

Abstract. The effect of small quantities of copper, up to 1%, covering the eutectic at 0·7% Cu, on the photoelectric work function of liquid tin has been determined by measurement of stopping potential when the surface is irradiated with light from a tin spark. It is found that the apparent value of the work function obtained changes with composition, the change being greatest near the eutectic. The results are briefly discussed with reference to other published work on structure effects in liquids.

§ 1. INTRODUCTION

PREVIOUS work (Toye and Jones 1958) has shown that a number of physical properties of liquid binary alloys have minimum values at compositions which can be associated with eutectics. It has been shown (Zadumkin 1953) that the electrons at the surface of a metal make a large contribution to the surface tensions, in fact Zadumkin claims that they account for the abnormally high surface tension of metals. If this assumption is correct then it may be that the electrons in metals have a greater influence on physical properties than is perhaps thought, and in order to examine this further it was decided to measure the influence of an alloying element on the work function of a liquid metal. No particular importance is claimed for the system chosen, the reason for its choice being that it is easily handled, has a low melting point and the eutectic is at low copper percentage, thus allowing the making of the alloys in the actual apparatus by adding the required small quantities of copper.

§ 2. APPARATUS AND METHOD

The liquid metal was contained in a sealed-off B34 standard Pyrex joint A (see figure 1), which was immersed to the metal level in a solder bath at 280°c. Contact to the liquid metal was made by means of a tungsten wire sealed into the glass below the metal level, and a carbon rod immersed into the solder bath. The necessary stopping potential was applied from the potentiometer system 'D', the actual value being measured by means of a Tinsley potentiometer. The platinum anode assembly was fitted using a second standard joint as shown, the platinum wire being sealed into the glass at B. To ensure a good joint, since Pt–Pyrex is often suspect, the tube above and below the seal was filled with picein wax. The anode was connected to the quadrant electrometer, the needle of which was charged to 120 v before the start of each measurement.

Ultra-violet illumination was obtained from the spark between pure tin electrodes E situated very close to the wall of the glass container. The spark was supplied by means of a Tesla coil, a condenser being connected across the gap to give the maximum amount of light. Approximately 8 foot candles total light actually reached the tin surface. The transmission of Pyrex (Morey 1954) to ultra-violet is about 30% at 3000 Å. Although the actual intensity of ultra-violet reaching the tin surface is small, this only affects the sensitivity and not the value of the stopping potential. Since the limit of transmission of Pyrex is at about 2800 Å and the strongest line in the tin spark nearest to this is 2919·82 Å (McCormick and Sawyer 1938) this latter value of frequency is chosen for the calculations since the photoelectrons produced by the highest frquency present will require the highest stopping potential and the transmission of Pyrex at this wavelength is over 25%. This would seem a reasonable assumption but since monochromatic light was not used it is not claimed that the values of work function are very accurate; at the same time a large number of repeat experiments have proved that the values obtained are consistent, which is sufficient for the purpose of this work.

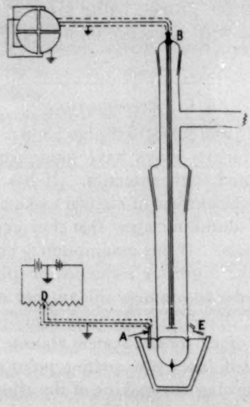

Figure 1.

The alloys were made under high vacuum by placing the necessary weighed quantity of Cu on to the surface of the tin or alloy when cold and heating to 300°c. The solution of the Cu could then be observed. On occasion it was found necessary to clean the surface by heating with a little NH_4Cl powder, under high vacuum, the anode assembly being replaced during this operation with a plain sealed off male joint at B. The alloys near the eutectic composition were analysed chemically as a check.

The vacuum system consisted of a rotary pump backing a two stage oil diffusion pump and it will be seen that practically all joints were standard cone type. The Pirani gauge was used down to one micron, beyond this reliance being placed on there being no discharge current between the anode and the tin when high d.c. voltages were applied between them (about $1000\,\mathrm{v\,cm^{-1}}$). Occasionally, as a check, 7000 v was applied but no current could be detected. The long path between the anode seal and the liquid metal surface ensured no leakage currents.

It was concluded that the vacuum obtained was of the order of the ultimate for the pump, i.e. about 10^{-6} mm Hg. It was necessary to ensure that the liquid metal surface was absolutely clean and bright, the finest haze of oxide being sufficient to ruin the experiment. It was not possible to degas at a very high temperature with the apparatus used, and in order therefore to minimize outgassing effects and to standardize measurement conditions the following procedure was adopted. The temperature of the bath, with glass vessel immersed to a level about ½ inch above the anode, was first held at 450°C for 2½ to 3 hours, sometimes longer, at the ultimate vacuum. The temperature was then allowed to fall to a steady 280°C and a few measurements made at this temperature; the apparatus was left for an hour and the measurements repeated.

After completion over the composition range, pure tin as well as the 0·69 and 0·70% Cu alloys were repeated with fresh tin and new alloys and no discrepancy found. This together with the precision of measurement indicated below was taken as sufficient to justify acceptance of the observations.

In making a measurement it was found best to obtain an approximate value of stopping potential and then proceed in steps until the actual value was found. With this value applied, switching on the spark produced no deflection.

§ 3. OBSERVATIONS

The values of stopping potential together with the calculated values of work function are given in the table and the work function composition graph is shown in figure 2. The values of work function are calculated from the equation

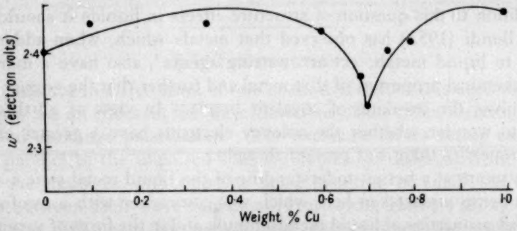

Figure 2.

Alloy					Stopping	
Weight %		Atomic %		M.P.	Potential	Work function
Sn	Cu	Sn	Cu	(°K)	(v)	(ev)
100	0	100	0	505·1	1·854	2·40
99·90	0·10	99·81	0·19	504·4	1·816	2·43
99·65	0·35	99·33	0·67	502·5	1·820	2·43
99·40	0·60	98·87	1·13	501·0	1·831	2·42
99.31	0·69	98·72	1·28	500·2	1·885	2·37
99·30	0·70	98·68	1·32	500·2	1·907	2·34
99·25	0·75	98·59	1·41	501·0	1·855	2·40
99·20	0·80	98·49	1·51	502·1	1·839	2·41
99·00	1·00	98·15	1·85	508·3	1·815	2·44

$$V_e = h\nu - w_0 \times 1{\cdot}602 \times 10^{-12}$$

whence

$$w_0 = \frac{h\nu - V_e}{1{\cdot}602 \times 10^{-12}} \text{ ev}$$

V being in e.s.u.

Accuracy of measurement was to 0·0001 volt with estimation to 0·00005 volt and the greatest scatter on any measurement was found to be 0·0004 volt, i.e. ± 0·0002 volt; the figures are therefore quoted to the nearest reliable place.

§ 4. CONCLUSIONS

The value of work function obtained for pure tin does not agree with the other published value 4·64 ev (Hischberg and Lange 1952). The present paper does not however claim new absolute values but rather indicates changes in work function with varying composition. The greatest change occurs near the eutectic and it is wondered whether some structure effect is responsible.

It is of interest that Zadumkin (1953) has derived a relation between surface tension and work function which gives very satisfactory agreement with experimental values. His calculations are based upon definite crystal structure in the solid state and are used to calculate values of surface tension. The published values of the latter with which he compares his results are, of course, for liquid surface tension, though admittedly at the melting point, and as he observes, "the good agreement with experimental values for molten metals indicates that the short range order does not seem to change upon melting for most metals studied".

In addition to this question of structure effects in liquids it should be noted here that Bondi (1953) has observed that metals which, when added in small quantities to liquid metals, act as 'wetting agents', also have a marked effect upon the chemical properties of that metal and further that the energy of vaporization involves the breaking of covalent bonds. In view of all this is seems pertinent to wonder whether the valency electrons have a greater effect upon physical properties than is at present thought.

In an attempt at a better understanding of the liquid metal state a scheme of research is being undertaken here which will commence with a careful study of the electrical properties of liquid metals in bulk and in the form of very thin films.

ACKNOWLEDGMENTS

The author is grateful to Mr. S. Jepson of the British Iron and Steel Research Association, Swansea, for performing the glass blowing and to Mr. L. S. Garley of the Swansea Technical College for his assistance in setting up the apparatus. He wishes to record his sincere thanks to Mr. W. J. Lewis, Vice-Principal, Swansea Technical College, for his active encouragment and guidance during the course of the work and in the preparation of the paper. Finally, he wishes to thank the Swansea Education Committee for permission to perform the work and to publish this paper.

REFERENCES

BONDI, A., 1953, *Chem. Rev.*, **52,** 417.
HISCHBERG, R., and LANGE, E., 1952, *Naturwissenschaften*, **39,** 131.
MCCORMICK, W. W., and SAWYER, R. A., 1938, *Phys. Rev.*, **54,** 71.
MOREY, G. W., 1954, *The Properties of Glass* (London: Chapman and Hall), p. 433.
TOYE, T. C., and JONES, E. R., 1958, *Proc. Phys. Soc.*, **71,** 88.
ZADUMKIN, S. R., 1953, *J. Phys. Chem., Moscow*, **27,** No. 5402 (H.B. 3172).

Contribution of Core Polarization to the Atomic Hyperfine Structure and Knight Shift of Li and Na

By M. H. COHEN†§, D. A. GOODINGS‡ and V. HEINE‡
† Cavendish Laboratory, Cambridge
‡ Royal Society Mond Laboratory, Cambridge

MS. received 3rd December 1958, *in final form 29th January* 1959

Abstract. The effect of exchange forces on the wave functions of an atom resulting from the unpaired spin of a single electron outside closed shells is considered. Calculations were carried out for lithium and sodium starting from the usual self-consistent field wave functions using a modified type of perturbation theory. These yield an increase of 31% for Li and 5½% for Na in the value of the hyperfine coupling constant. In addition, the effect of this core polarization on the theory of the Knight shift in metals is developed in detail.

§ 1. Introduction

The presence in a free atom of one or more electrons unpaired with respect to spin has an effect on the wave functions of the other electrons which is termed exchange polarization. The exchange forces acting on electrons with spin parallel to the unpaired spin are somewhat different from the forces acting on the electrons with opposite spin, resulting in small but significant differences between their wave functions (Pratt 1956, Heine 1957 a). One can evaluate these differences by perturbation theory since the exchange term appearing in the wave equation is small. An ordinary perturbation theory expansion in terms of the bound levels of the atom turned out to be completely useless because the continuum states were neglected, but no difficulty was experienced in finding a suitable set of rapidly converging expansion functions (Boys, Cook, Reeves and Shavitt 1956).

The effect of core polarization is particularly noticeable in the hyperfine structure. The contact term in the hyperfine interaction is given by (Fermi 1930)

$$a(\mathrm{s}) = \frac{16\pi}{3}\left(\frac{\mu_{\mathrm{I}}}{I}\right)\mu_{\mathrm{B}} \sum_i \pm |\psi_i(0)|^2, \qquad \ldots\ldots (1)$$

where μ_{I} is the nuclear magnetic moment in units of the nuclear magneton, I is the nuclear spin, μ_{B} is the Bohr magneton, and, in the summation, the sign is taken as positive for electrons of positive spin and negative for electrons having opposite spin. The coupling constant is written $a(\mathrm{s})$ to indicate that only s-electrons contribute non-zero values of $|\psi_i(0)|^2$. In the usual theory for a single s-electron outside closed shells, the contributions to $a(\mathrm{s})$ from the closed shells completely cancel, the valence electron alone giving a contribution which we shall denote by $a_0(\mathrm{s})$. In reality, however, there are also contributions to $\Sigma_i \pm |\psi_i(0)|^2$ from the core electrons due to exchange polarization by the valence electron. The magnitude of this contribution can be calculated by perturbation theory as mentioned above.

---

§ Guggenheim Fellow 1957–58 on leave from the Institute for the Study of Metals, University of Chicago.

We wish to report here preliminary results for lithium and sodium relating these results to the experimental values of $a(\mathrm{s})$ in the free atoms. We also give the theory of the effect of core polarization on the Knight shift in metals.

§ 2. ATOMIC LITHIUM

Let us assume that in atomic lithium in the ground state, the 2s-electron has up spin ↑. Then the radial wave equation for the 1s ↑ electron includes a term representing exchange with the 2s-electron, while the 1s ↓ equation does not include this term. In writing down these two equations we shall use Hartree's standard notation (Hartree 1957) in which the radial wave functions, $P_{nl}(r)$, are normalized by the condition

$$\int_0^\infty P_{nl}^2\, dr = 1,$$

and the functions $Y(nl, nl;\, r)/r$ represent the contributions of the electrons to the central field potential. Then the equations can be written,

$$\mathscr{H}_0 P_{1s\downarrow} = E_{1s\downarrow} P_{1s\downarrow}, \qquad \ldots\ldots(2)$$

$$\mathscr{H}_0 P_{1s\uparrow} + \zeta = E_{1s\uparrow} P_{1s\uparrow}, \qquad \ldots\ldots(3)$$

where

$$\mathscr{H}_0 = \left\{ -\frac{1}{2}\frac{d^2}{dr^2} - \frac{3}{r} + \frac{Y_0(1\mathrm{s}, 1\mathrm{s};\, r)}{r} \right\} \qquad \ldots\ldots(4)$$

and

$$\zeta = -\frac{Y_0(1\mathrm{s}\uparrow, 2\mathrm{s}\uparrow;\, r)}{r} P_{2s\uparrow}.$$

Here, $Y_0(1\mathrm{s}, 2\mathrm{s};\, r)$ is the exchange integral between the 1s and 2s wave functions. Two approximations have been made in writing the equations in this manner. First, the term $Y_0(2\mathrm{s}, 2\mathrm{s};\, r)/r$ has been omitted from $\mathscr{H}_0$. This will have a very small effect on $P_{1s\uparrow}$ and $P_{1s\downarrow}$ because $Y_0(2\mathrm{s}, 2\mathrm{s};\, r)/r$ is nearly constant over the range of P_{1s}. In any case, $P_{1s\uparrow}$ and $P_{1s\downarrow}$ are affected equally so that the effects cancel in the hyperfine structure, $|P_{1s\uparrow}(0)|^2 - |P_{1s\downarrow}(0)|^2$, to first order. The second approximation concerns neglecting the departures from self-consistency. In particular we neglect the difference between $Y_0(1\mathrm{s}\uparrow, 1\mathrm{s}\uparrow;\, r)$ and $Y_0(1\mathrm{s}\downarrow, 1\mathrm{s}\downarrow;\, r)$ and take both functions equal to $Y_0(1\mathrm{s}, 1\mathrm{s};\, r)$ as obtained for the ion Li^+. That the effect on the wave functions of such changes is small is known from experience of self-consistent field calculations in which successive cycles of iteration become rapidly insensitive to small changes in the Y functions.

Having made these approximations, equation (2) is exactly the equation which was solved numerically by Fock and Petrashen (1935). Hence, equation (3) can be solved by treating ζ as a perturbation, making use of the tabulated solutions of Fock and Petrashen. One might hope to use the eigenfunctions P_{2s}, P_{3s}, . . . as perturbation expansion functions. Unfortunately, these are unsatisfactory because, although they adequately describe $P_{1s\uparrow}$ at small r, they introduce spurious 'bumps' at large r where these functions have their main maxima. For the sake of interest, such an expansion in terms of the bound eigenfunctions was tried, and gave a 3% effect compared with the correct value of 31% (see below). Of course, in principle the inclusion of the continuum states would give a complete set of functions and remedy this, but such a procedure is not practicable. A much better type of expansion function for the present problem is,

$$(a+br+cr^2+\ldots+kr^n)re^{-\lambda r}, \qquad \ldots\ldots(5)$$

where the constants a, b, ... are chosen so that the functions, together with the unperturbed function, P_{1s}, are orthonormal, and the value of λ is chosen so that the exponential falls off in roughly the same way as P_{1s}, P_{2s}, or whatever function one is trying to correct (Boys *et al.* 1956).

Table 1. Results for Lithium

	$\Sigma_i \pm \|\psi_i(0)\|^2$ (atomic units)	a(s) (cm^{-1})
Experimental value (Kusch and Taub 1949)		0·0134
Contribution from 2s ↑ only	0·165	0·0095
Contributions from 1s ↑ , 1s ↓ and 2s ↑		
(i) using one expansion function	0·165 + 0·063 (38%)†	0·0132
(ii) using two expansion functions	0·165 + 0·058 (35%)†	0·0129
(iii) relaxation calculation	0·165 + 0·050 (30½%)†	0·0124
Calculations from empirical potentials		
Jones and Schiff (1954)	0·142	0·0082
Kohn (1954)	0·223	0·0129

† Additional contribution as percentage of the 2s-term.

The results of calculations of exchange polarization in lithium are given in table 1. Two perturbation calculations were performed: one using as expansion functions the unperturbed function P_{1s} of Fock and Petrashen together with *one* function of the type (5); the second using P_{1s} together with *two* functions of the type (5). As a check on the validity of this method, a solution of the original differential equation (3) was carried out by a relaxation process (Southwell 1940) and gave the value 30½% for the contribution to $\Sigma_i \pm |\psi_i(0)|^2$ or a(s) from the exchange polarization of the core. One further check was necessary in view of the fact that the perturbation partially destroys the orthogonality between $P_{1s\uparrow}$ and P_{2s}. It was found that re-orthogonalization of P_{2s} produced a change in $|\psi_{2s}(0)|^2$ of only ½%.

Agreement with experiment is fairly good, but might be considerably improved by including in some way the effect of correlation. In this respect, Kohn's value (Kohn 1954), which was calculated using the Seitz potential, is noteworthy. The empirical Seitz potential does in part include correlation, but is not very satisfactory with regard to exchange. However, it is strange that Kohn's value differs so much from that of Jones and Schiff (1954) which was calculated from a similar type of potential.

§ 3. ATOMIC SODIUM

The perturbation method described for the calculation in lithium was used for similar calculations in sodium, though with somewhat less accuracy. Although wave functions for sodium given by D. R. Hartree and W. Hartree (1948) are the best ones available, the Y functions necessary in our calculation are not tabulated by them. Consequently we used the wave functions of Fock and Petrashen (1934). In sodium there are contributions from both

$$|\psi_{1s\uparrow}(0)|^2-|\psi_{1s\downarrow}(0)|^2 \quad \text{and} \quad |\psi_{2s\uparrow}(0)|^2-|\psi_{2s\downarrow}(0)|^2.$$

The 2p-electrons are also polarized, but do not contribute to the hyperfine structure because of the requirement that the 2p-wave function have a node at the origin.

Table 2. Results for Sodium

	$\Sigma_i \pm \lvert\psi_i(0)\rvert^2$ (atomic units)	a(s) (cm^{-1})
Experimental value (Kusch and Taub 1949)		0·0296
Contribution from 3s ↑ only	0·671	0·0264
Contribution from 1s ↑ and 1s ↓	0·050 (7½%)†	
Contribution from 2s ↑ and 2s ↓	−0·013 (−2%)†	
Total	0·708 (5½%)†	0·0279
Calculation of D. R. and W. Hartree (1948) (3s ↑ contribution only)	0·497	0·0196
Calculation of Jones and Schiff (1954)	0·528	0·0208
Calculation of Kjeldaas and Kohn (1956)	0·685	0·0270

† Additional contribution as percentage of the 3s-term.

The results of calculations are given in table 2. It can be seen that the contributions to $\Sigma_i \pm |\psi_i(0)|^2$ from the 1s and 2s electrons tend to cancel. This cancellation shows up clearly in the perturbation expansion where the integrals

$$\int_0^\infty [Y_0(1s,3s;\ r)/r]P_{2s}\,P_{3s}\,dr \quad \text{and} \quad \int_0^\infty [Y_0(2s,3s;\ r)/r]P_{1s}\,P_{3s}\,dr,$$

which can be shown analytically to be equal, appear over energy denominators differing only in sign, and so cancel each other exactly. However, an explanation of this occurrence in physical terms is somewhat more difficult.

It is convenient for the following discussion of the results to introduce a quantity called the exchange potential, V_{exch}, (Slater 1951, Heine 1957b) by writing the exchange term in the form,

$$\zeta=\left\{-\frac{[Y_0(1s,2s;\ r)/r]}{P_{1s\uparrow}}\,P_{2s\uparrow}\right\}P_{1s\uparrow}=V_{\text{exch}}P_{1s\uparrow}. \qquad \ldots\ldots(6)$$

Returning briefly to lithium, V_{exch} is negative for small r, positive for larger r and approaches zero at roughly the same value of r as in the case of P_{1s}. Its effect on the unperturbed wave function, P_{1s}, is to pull it in towards the origin, so that we expect $|P_{1s\uparrow}(0)|^2>|P_{1s\downarrow}(0)|^2$, as was found to be the case.

In sodium the exchange potential appropriate to the 1s-electrons has roughly the same shape as that just discussed for lithium. It follows by the same argument that the contribution from the 1s-electrons is positive. In the 2s-case, the exchange potential $-[Y_0(2s,3s;\ r)/r]P_{3s}/P_{2s}$ likewise has a similar shape, apart from an unimportant singularity, but it operates over a greater range of r. The main effect on P_{2s} is now to raise its energy and increase the tail at large r. Then, as a result of altering the shape of $P_{2s\uparrow}$, it is necessary to normalize again to unity, which has the net effect of actually decreasing the probability distribution at the origin, so that $|\psi_{2s\uparrow}(0)|^2<|\psi_{2s\downarrow}(0)|^2$.

The net result of contributions from 1s and 2s electrons is an addition of about $5\frac{1}{2}\%$ to the value of $|\psi_{3s}(0)|^2$ or $a_0(\mathrm{s})$. That this value is so much less than for lithium can be mainly attributed to the two cancellation effects just described.

Since the value of $|\psi_{3s}(0)|^2$ calculated by D. R. Hartree and W. Hartree is considerably lower than that of Fock and Petrashen, it would be most interesting to find out whether the net contribution from the 1s and 2s electrons is correspondingly greater. The answer to this must await a recalculation of the necessary Y functions.

§ 4. THE KNIGHT SHIFT IN METALS

It was found by Knight (1949) that the frequencies at which nuclear magnetic resonance occurs in a metal are slightly displaced from the respective frequencies in non-metallic compounds of the metal in the same magnetic field. This is attributed (Townes, Herring and Knight 1950) to the magnetic field ΔH produced at the nucleus by the strong hyperfine interaction between the nuclear magnetic moments and the conduction electrons. It can be written,

$$\frac{\Delta H}{H}=\frac{8\pi}{3}\chi_{\mathrm{P}}\Omega\langle|\psi_{\mathrm{F}}(0)|^2\rangle_{\mathrm{av}}, \qquad \ldots\ldots(7)$$

where χ_{P} is the spin susceptibility per unit volume, Ω is the volume of the unit cell and $\langle|\psi_{\mathrm{F}}(0)|^2\rangle_{\mathrm{av}}$ is an average value of the probability density at the nucleus taken over the electrons having energies near the Fermi level. However, in view of the considerations above, it is clear that the excess of conduction electrons with, say, spin $\uparrow$, produced by the external magnetic field, polarizes the core electrons through the exchange forces. As a result, we expect a contribution to ΔH from the difference between the probability densities at the nucleus of spin $\uparrow$ and spin $\downarrow$ electrons in the core. This additional contribution is, of course, proportional to the number of spins which have been turned over by the magnetic field, i.e. to χ_{P}, just as in (7), the ordinary part of the Knight shift.

To calculate the magnitude of both the main contribution to the Knight shift and the contribution from core polarization, let us consider the following expansion for the wave function of a conduction electron at the Fermi surface in lithium:

$$\psi_{\mathbf{k}}(\mathbf{r})=\left(\frac{\Omega}{V}\right)^{1/2}(A_{\mathbf{k}}\phi_{2\mathrm{s}}+B_{\mathbf{k}x}\phi_{2\mathrm{p}x}+B_{\mathbf{k}y}\phi_{2\mathrm{p}y}+B_{\mathbf{k}z}\phi_{2\mathrm{p}z}). \qquad \ldots\ldots(8)$$

The functions $\phi_{2\mathrm{s}}$, $\phi_{2\mathrm{p}x}$, $\phi_{2\mathrm{p}y}$, $\phi_{2\mathrm{p}z}$ give a quite accurate representation of $\psi_{\mathbf{k}}(\mathbf{r})$ over the region of the core, as is confirmed by detailed band structure calculations, and are a convenient set of expansion functions for our purposes. On substituting in the exchange terms of the equations for the 1s $\uparrow$ and 1s $\downarrow$ core wave functions it is found that in each case the exchange term splits into two parts, recognizable as exchange with the 2s and 2p terms in $\psi_{\mathbf{k}}(\mathbf{r})$. Defining $\alpha=\overline{(|A_{\mathbf{k}}|^2)}^{\mathrm{F}}$ and $\beta=\overline{(|B_{\mathbf{k}x}|^2+|B_{\mathbf{k}y}|^2+|B_{\mathbf{k}z}|^2)}^{\mathrm{F}}$ where both quantities are averages taken over the Fermi surface, then the 1s $\uparrow$ wave equation can be written,

$$\mathscr{H}_0P_{1\mathrm{s}\uparrow}-\frac{\Omega\chi_{\mathrm{P}}H}{2\mu_{\mathrm{B}}}\alpha\zeta_{2\mathrm{s}}-\frac{\Omega\chi_{\mathrm{P}}H}{2\mu_{\mathrm{B}}}\beta\zeta_{2\mathrm{p}}=E_{1\mathrm{s}\uparrow}P_{1\mathrm{s}\uparrow}, \qquad \ldots\ldots(9)$$

where $\zeta_{2\mathrm{s}}=[Y_0(1\mathrm{s},2\mathrm{s};\,r)/r]P_{2\mathrm{s}}$ and $\zeta_{2\mathrm{p}}=[Y_1(1\mathrm{s},2\mathrm{p};\,r)/r]P_{2\mathrm{p}}$. The exchange terms involving $\zeta_{2\mathrm{s}}$, $\zeta_{2\mathrm{p}}$ can be treated as independent perturbations. If only the term in $\zeta_{2\mathrm{s}}$ is included, the equation is the same as (3) for the free atom, except for the coefficient of ζ_{2s}. It is therefore a simple matter to express the polarization of the core wave functions in the metal in terms of the results for the free atom.

The effect of exchange from a single 2s-electron was calculated for the free atom in § 2. We shall denote the fractional contribution to $\Sigma_i \pm |\psi_i(0)|^2$ from the core wave functions relative to $|\phi_{2s}(0)|^2$ by a, where a was found to be 0·31 for lithium. Similarly, one can calculate the polarization of the core wave functions for the configuration $1s^2 2p$, and denote the corresponding fractional contribution to $\Sigma_i \pm |\psi_i(0)|^2$ relative to $|\phi_{2s}(0)|^2$ by b. A calculation similar to that in § 2 gave $b = -0{\cdot}03$.

Finally, one arrives at the following expression for the Knight shift in lithium:

$$\frac{\Delta H}{H} = \frac{8\pi}{3}\chi_{\mathrm{P}}\Omega\alpha|\phi_{2s}(0)|^2 + \Omega\chi_{\mathrm{P}}a\alpha|\phi_{2s}(0)|^2 + \Omega\chi_{\mathrm{P}}b\beta|\phi_{2s}(0)|^2. \qquad \ldots\ldots(10)$$

The first term is the usual expression (7), whereas the second and third terms come from the core polarization effects. Substituting the calculated values of a and b for lithium,

$$\frac{\Delta H}{H} = \frac{8\pi}{3}\chi_{\mathrm{P}}\Omega\alpha\left(1{\cdot}31 - \frac{0{\cdot}03\beta}{\alpha}\right)|\phi_{2s}(0)|^2. \qquad \ldots\ldots(11)$$

It is convenient to write the Knight shift in lithium in the form

$$\frac{\Delta H}{H} = \frac{8\pi}{3}\chi_{\mathrm{P}}\Omega\xi|\phi_{2s}(0)|^2. \qquad \ldots\ldots(12)$$

In the usual treatment (7), $\xi = \alpha$ and ξ represents the ratio of the probability densities at the origin in the metal and in the free atom. On adding the effects of core polarization, ξ becomes,

$$\xi = (1 + a)\alpha + b\beta = 1{\cdot}31\alpha - 0{\cdot}03\beta.$$

In metallic lithium there is considerable evidence that the Fermi surface actually contacts the nearest faces of the Brillouin zone and that the states at the zone faces are p-like (Cohen and Heine 1958). Therefore β may well be larger than α. Let us guess 5α as an upper limit for β. For lithium the experimental value for ξ is 0·43 (Knight 1956), giving $0{\cdot}33 < \alpha_{\mathrm{Li}} < 0{\cdot}37$. This may be compared with Kohn's (1954) value of 0·49 for α_{Li}, calculated on the assumption of a spherical Fermi surface.

The treatment of the Knight shift just described can be extended to sodium without difficulty, noting, that the core polarization will contain contributions from both 1s and 2s core electrons. With this difference only, the quantities a and b can be defined as before. In § 3, it was found that $a = 0{\cdot}055$. A similar calculation gives $b = -0{\cdot}0145$. Hence,

$$\frac{\Delta H}{H} = \frac{8\pi}{3}\Omega\chi_{\mathrm{P}}\alpha\left(1{\cdot}055 - \frac{0{\cdot}0145\beta}{\alpha}\right)|\phi_{3s}(0)|^2. \qquad \ldots\ldots(13)$$

The value of ξ including core polarization is $\alpha(1{\cdot}055 - 0{\cdot}0145\beta/\alpha)$. In contrast to lithium, all evidence points to a nearly spherical Fermi surface for sodium, in which case it is reasonable that $\beta \simeq \alpha$. Using the experimentally determined value $\xi = 0{\cdot}72$ (Knight 1956), one can assert that $0{\cdot}68 < \alpha_{\mathrm{Na}} \simeq 0{\cdot}69$. This is to be compared with the value $\alpha_{\mathrm{Na}} = 0{\cdot}81$ calculated by Kjeldaas and Kohn (1956).

REFERENCES

BOYS, S. F., COOK, G. B., REEVES, C. M., and SHAVITT, I., 1956, *Nature, Lond.*, **178**, 1207.
COHEN, M. H., and HEINE, V., 1958, *Advanc. in Phys.*, **7**, 395.
FERMI, F., 1930, *Z. Phys.*, **60**, 320.
FOCK, V., and PETRASHEN, M. J., 1934, *Phys. Z. Sowjet*, **6**, 368.
—— 1935, *Ibid.*, **8**, 547.
HARTREE, D. R., 1957, *The Calculation of Atomic Structures* (New York: John Wiley).
HARTREE, D. R., and HARTREE, W., 1948, *Proc. Roy. Soc.* A, **193**, 299.
HEINE, V., 1957 a, *Phys. Rev.*, **107**, 1002.
—— 1957 b, *Proc. Roy. Soc.* A, **240**, 361.
JONES, H., and SCHIFF, B., 1954, *Proc. Phys. Soc.* A, **67**, 217.
KJELDAAS, T., and KOHN, W., 1956, *Phys. Rev.*, **101**, 66.
KNIGHT, W. D., 1949, *Phys. Rev.*, **76**, 1259.
—— 1956, *Solid State Phys.*, **2**, 97.
KOHN, W., 1954, *Phys. Rev.*, **96**, 590.
KUSCH, P., and TAUB, H., 1949, *Phys. Rev.*, **75**, 1477.
PRATT, G., 1956, *Phys. Rev.*, **102**, 1303.
SLATER, J. C., 1951, *Phys. Rev.*, **81**, 385.
SOUTHWELL, R. V., 1940, *Relaxation Methods in Engineering Science* (Oxford: University Press).
TOWNES, C. H., HERRING, C., and KNIGHT, W. D., 1950, *Phys. Rev.*, **77**, 852.

RESEARCH NOTES

Negative Ions in the Positive Column of the Oxygen Discharge

By J. B. THOMPSON
Physics Department, University College London

Communicated by H. S. W. Massey; MS. received 17th December 1958

§ 1. Introduction

When a low pressure electric discharge is run in an electro-negative gas, negative ions are formed by attachment of electrons to atoms or molecules. If the discharge is continuous the wall of the containing vessel is maintained at a negative potential with respect to the centre by a flux of energetic electrons and this tends to inhibit the escape of negative ions from the plasma. The concentration of these ions therefore builds up until they are destroyed at a sufficient rate by a gas phase process. In some circumstances they may be removed by a drift towards the anode or by relaxation oscillations which accelerate them to the walls of the vessel.

In a study of the oxygen discharge, these negative ions have been detected and their concentration and temperature measured by a refined probe technique. Figure 1 shows a typical energy distribution function for the negative particles in the striated positive column. The two groups at 15 ev and 4 ev are electrons corresponding to the groups described by Boyd and Twiddy (1959) in hydrogen. The low energy group is due to negative ions and when account is taken of the weighting factor $\sqrt{(M_-/m_e)}$ it appears that the ratio of negative ion concentration to that of electrons is of order 20/1.

§ 2. Ambipolar Diffusion

This large concentration of negative ions naturally affects the ambipolar diffusion conditions in the positive column and the problem may be dealt with in general terms as follows.

Under conditions of pressure where the flux of ions to the wall is governed by diffusion we have

$$\left.\begin{aligned}\Gamma_+ &= -D_+\nabla n_+ + \mu_+ n_+ E\\ \Gamma_- &= -D_-\nabla n_- - \mu_- n_- E\\ \Gamma_e &= -D_e\nabla n_e - \mu_e n_e E.\end{aligned}\right\} \qquad \ldots\ldots(1)$$

Γ is the particle flux out of the region at whose boundary $\Gamma_+ = \Gamma_- + \Gamma_e$ and within which $n_+ = n_- + n_e$ to a close approximation. Writing

$$\gamma = V_e/V_+ = V_e/V_-$$

for the ratio of electron to ion temperature and $\alpha = n_-/n_e$ for the ratio of negative ion to electron concentration we have on eliminating E from (1)

$$\left.\begin{aligned}\Gamma_+ &= -D_+^a\nabla n_+\\ \Gamma_- &= -D_-^a\nabla n_-\\ \Gamma_e &= -D_e^a\nabla n_e\end{aligned}\right\} \qquad \ldots\ldots(2)$$

where

$$\left.\begin{aligned} D_+^{\mathrm{a}} &= D_+\left[\frac{(1+\gamma+2\alpha\gamma)(1+\alpha\mu_-/\mu_{\mathrm{e}})}{(1+\alpha\gamma)\{1+\mu_+(1+\alpha)/\mu_{\mathrm{e}}+\alpha\mu_-/\mu_{\mathrm{e}}\}}\right]\\ D_-^{\mathrm{a}} &= \mathrm{D}_+\left[\frac{1}{\gamma}\,\frac{\mu_-}{\mu_{\mathrm{e}}}\;\frac{1+\gamma+2\alpha\gamma}{1+\mu_+(1+\alpha)/\mu_{\mathrm{e}}+\alpha\mu_-/\mu_{\mathrm{e}}}\right]\\ D_{\mathrm{e}}^{\mathrm{a}} &= D_+\left[\frac{1+\gamma+2\alpha\gamma}{1+\mu_+(1+\alpha)/\mu_{\mathrm{e}}+\alpha\mu_-/\mu_{\mathrm{e}}}\right]. \end{aligned}\right\}\quad\ldots\ldots(3)$$

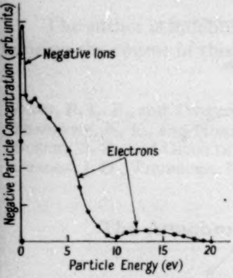

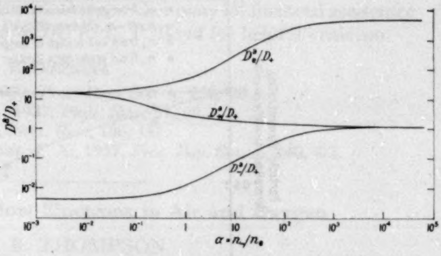

Figure 1. Negative particle energy distribution in the striated positive column of an oxygen discharge.

Figure 2. Ambipolar diffusion coefficients as a function of $\alpha = n_-/n_{\mathrm{e}}$. The curves refer to oxygen for which $\gamma = 16$, $\mu_-/\mu_{\mathrm{e}} = 0{\cdot}0043$ and $\mu_+/\mu_{\mathrm{e}} = 0{\cdot}0022$.

The ambipolar diffusion coefficients D^{a} are plotted in figure 2 as a function of the ratio α. A value of $\gamma = 16$ was used in this calculation corresponding to the distribution function of figure 1. The ion mobilities used are taken from Burch and Geballe (1957) and the electron mobilities from Bradbury and Nielson

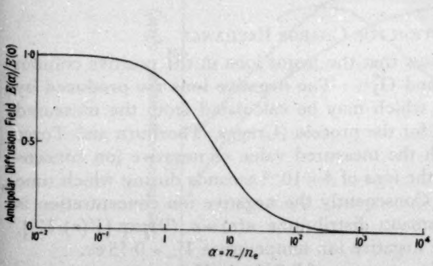

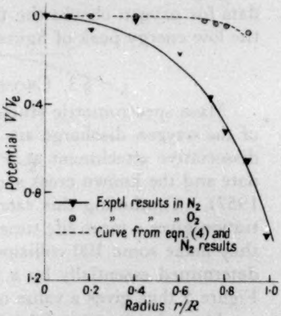

Figure 3. Variation of ambipolar diffusion field $E(\alpha)/E(0)$ with α for the case of oxygen.

Figure 4. Space potential as a function of radius in the positive column of oxygen and nitrogen discharges.

(1937). Using equations (1) and (2), the ambipolar diffusion field E may be expressed as a function of α

$$\frac{E(\alpha)}{E(0)} = \frac{1 - D_{+}/D^{a}_{+}}{1+\alpha}\left(\frac{1+\gamma}{\gamma}\right) \qquad \ldots\ldots (4)$$

where $E(0)$ is the normal ambipolar field for an electropositive gas ($\alpha = 0$). In figure 3 this function is plotted for the case $\gamma = 16$ and shows how the ambipolar field falls to very low values as the ratio of negative ions to electrons becomes greater than 10.

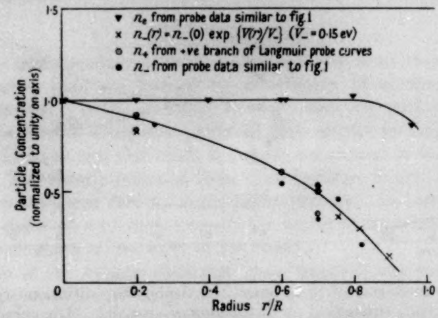

Figure 5. Radial variation of charged particle concentration.

For a direct current discharge in a cylindrical tube the appropriate field component is radial. Measurements of space potential made in oxygen and nitrogen under these discharge conditions are shown in figure 4. A curve is drawn through the experimental points for nitrogen from which a corresponding curve for oxygen may be calculated using equation (4) and the data of figure 5. The agreement obtained between the calculated curve and the experimental data for oxygen checks the theory and confirms the interpretation placed upon the low energy peak of figure 1.

§ 3. CROSS SECTION FOR CHARGE EXCHANGE

Mass spectrometric studies show that the major ions in the positive column of the oxygen discharge are O^- and O_2^+. The negative ions are produced by dissociative attachment at a rate which may be calculated from the measured data and the known cross section for the process (Craggs, Thorburn and Tozer 1957). Combining this rate with the measured value of negative ion concentration gives a mean life time for the ions of 4×10^{-4} seconds during which time they make some 100 collisions. Conseqently the negative ion concentration is determined essentially by a Boltzmann distribution $n(r) = n_-(0)\exp\{V(r)/V_-\}$. Figure 5 thus gives a value of the negative ion temperature $V_- = 0{\cdot}15$ ev.

At a tube current of 4 mA and a pressure of 0·040 mm Hg an average rate of production of O^- is 10^{12} ions cm^{-3} sec^{-1}, and a corresponding negative ion concentration $[O^-]$ is 4×10^8 ions cm^{-3}. Even if all the O^- ions were lost by charge exchange according to $O^- + O_2 \rightarrow O_2^- + O$, the cross section required would only be 2×10^{-17} cm^2 at an ion temperature of 0·15 ev.

This figure may therefore be regarded as an extreme upper limit since other evidence (to be published) indicates that the major destruction process for O$^-$ involves collisions with atoms.

§ 4. Conclusion

The concentration of negative ions in the positive column of an oxygen discharge has been measured by a Langmuir probe technique. It is shown how the negative ions affect the ambipolar diffusion and potential distribution in such a plasma.

Acknowledgments

The author is indebted to the British Oxygen Company for financial assistance during the course of this work and to Dr. R. L. F. Boyd for helpful criticism.

References

Boyd, R. L. F., and Twiddy, N. D., 1959, *Proc. Roy. Soc.* A, **250**, 53.
Bradbury, N. E., and Nielson, R. A., 1937, *Phys. Rev.*, **51**, 69.
Burch, D. S., and Geballe, R., 1957, *Phys. Rev.*, **106**, 183.
Craggs, J. D., Thorburn, R., and Tozer, B. A., 1957, *Proc. Roy. Soc.* A, **240**, 473.

The Attachment of Slow Electrons in Air and Oxygen

By J. B. THOMPSON
Department of Physics, University College London

Communicated by H. S. W. Massey; MS. received 2nd January 1959

The recent work on electron attachment in oxygen and air (Craggs, Thorburn and Tozer 1957, Tozer, Thorburn and Craggs 1958) appears open to criticism. The effective mean cross section for a particular mean energy *E*, should read

$$\sigma_E^- = \int \sigma_p n_p v_p dp \Big/ \int n_p v_p dp.$$

The inclusion of the velocity weighting factor has the effect of increasing σ_E^- at

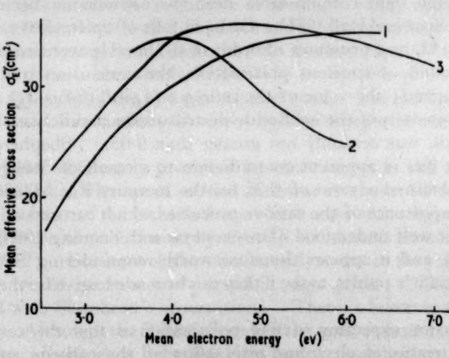

Mean attachment cross section as a function of mean electron energy: 1, Tozer *et al.*, 2, Harrison and Geballe; 3, recalculated curve.

low mean electron energies and decreasing it at high mean energies as compared with the values of σ_E^- calculated by Tozer, Thorburn and Craggs (1958). This effect is accentuated in the present case because the range of σ_p is limited to $4{\cdot}8 < p < 8{\cdot}5$ ev approximately.

In order to illustrate the order of magnitudes involved, the mean cross sections for attachment in oxygen when a Maxwellian energy distribution for the electrons is assumed, have been recalculated and are shown in the figure together with the data of Harrison and Geballe (1953) and the curves of figure 1 of Tozer, Thorburn and Craggs (1958). Similar corrections apply to the data for air.

REFERENCES

CRAGGS, J. D., THORBURN, R., and TOZER, B. A., 1957, *Proc. Roy. Soc.* A, **240,** 473.
HARRISON, M. A., and GEBALLE, R., 1953, *Phys. Rev.*, **91,** 1.
TOZER, B. A., THORBURN, R., and CRAGGS, J. D., 1958, *Proc. Phys. Soc.*, **72,** 1081.

Note on the Cathode Glow†

BY K. G. EMELEUS
Physics Department, Queen's University, Belfast

MS. received 19*th January* 1959

SHEPHERD (1955) has recently developed in this laboratory a photoelectric technique for studying the polarization of the light of isolated lines in the spectrum of the cathode glow of a cold cathode discharge. This has been used by him (Shepherd 1959) to investigate H_β, which, with other Balmer lines, is prominent in the light coming from near the cathode in discharges through hydrogen (Emeleus and Hall 1931). Cathode falls of up to 1500 v, with currents of order of 10^{-3} A, and pressures of order of 0·1 mm Hg were employed. After careful elimination of spurious polarization, the conclusion was reached that H_β was unpolarized; the value of the ratio $p=(J_1-J_2)/(J_1+J_2)$, where J_1 and J_2 denote the intensity of the light with electric vector parallel and perpendicular to the tube axis, was certainly not greater than 0·05. Shepherd pointed out that this result was in apparent contradiction to a result of Seeliger and Handt (1929), who obtained a ratio of 0·25 for the mercury line $\lambda 4347 (6^1P_1 - 7^1D_2)$. The relative importance of the various processes which can occur in the cathode glow is still not well understood (Druyvesteyn and Penning 1940, Stewart and Emeleus 1955), and it appears therefore worth reconsidering Shepherd's, and Seeliger and Handt's results, to see if they can be made to give further information on these points.

The reason for expecting to find polarization is that the cathode glow is traversed by streams of electrons, originating at the cathode surface, and of positive rays (positive ions together with some neutral particles) moving in the opposite direction: ionic retrograde rays (Thomson 1921, p. 96) can probably be ignored for the present purpose, as they are likely to be too slow near the cathode to excite an appreciable part of the light observed. It is well known that excitation by a beam of slow electrons can produce polarized light under certain conditions (Massey and Burhop 1952), and that the light emitted from hydrogen positive rays behind the cathode is polarized (Thomson 1921, p. 165). Conditions might therefore seem to be favourable for occurrence of polarization in the cathode glow light.

---

† *Erste Kathodenschicht.*

An analysis of all available data for polarization of the Balmer lines from hydrogen positive rays has been made by Ecker (1951), on the basis of a quantum mechanical theory of the principal processes involved (Ecker 1950). Ecker has shown that theory and experiment are in reasonable agreement. If we use typical results from his theory (Ecker 1951, figures 3 and 4), we should expect Shepherd's ratio p to be 0·1 or greater, since the maximum speed of the positive rays in Shepherd's tube was less than 7×10^7 cm sec^{-1}, from the maximum cathode fall used. This could have been readily observed.

Failure to find the polarization could arise from several causes. For example:

(*a*) There may have been sufficient random motion of the rays radially in the tube to reduce the value of p below the detectable limiting value. This is a definite possibility. Although many ions may reach the neighbourhood of the cathode without undergoing previous collisions under Shepherd's conditions (Emeleus 1951), little is known with certainty about their motion inside the cathode dark space; the fact that those emerging at the rear of the cathode through a perforation move predominantly parallel to the tube axis gives little useful information, since the type of perforation usually employed acts as a directional filter.

(*b*) The fraction of the light arising from the positive rays may have been small compared with the fraction due to electrons, and the latter (*infra*) have been unpolarized or with polarization too small to detect. Again, little is known definitely about the relative importance of the two processes. It has been suggested that the increase in brightness of the light which occurs on passing from normal to abnormal cathode falls in neon, with disappearance of the primary dark space, is due to onset of excitation by positive rays (Druyvesteyn and Penning 1940); there is also similarity between the spectra of the cathode glow and of positive rays behind the cathode in other gases. The last two observations imply that at least a substantial part of the light in Shepherd's tube was due to positive rays.

(*c*) If the light was largely produced by electrons, it is still uncertain if it should be polarized. The speed of the electrons is above 10^8 cm sec^{-1} at the equipotentials in front of the cathode from where most of the light comes. The theory of production of polarization by electron collisions is incomplete (Massey and Burhop 1952). For ions of the same speed, so far as they provide a valid comparison, p would be less, or reversed in sign (Ecker 1950). This is in general accord with Shepherd's observations. There is however another source of uncertainty. Although the Balmer lines are the most prominent feature of the spectrum of the cathode glow light, this does not necessarily show that the gas is mainly atomic in this neighbourhood. The relative proportions of molecules H_2 and atoms H present are unknown. It is therefore possible in principle for the excited atom to be produced direct from the molecule in its ground state via an unstable neutral or charged molecule, by one or other of the processes

$$\left.\begin{aligned} H_2(x^1\Sigma) + e(\text{fast}) &\rightarrow H_2' + e(\text{slow}) \\ H_2' &\rightarrow H + H' \end{aligned}\right\}$$

or

$$\left.\begin{aligned} H_2(x^1\Sigma) + e &\rightarrow H_2^{+\prime} + 2e \\ H_2^{+\prime} &\rightarrow H^+ + H' \end{aligned}\right\}$$

If either of these processes contributes much to the observed light, the latter is unlikely to be polarized when produced in such a relatively complex way. No basic difficulty arises in accounting for Seeliger and Handt's observation for λ4347 HgI, if this is excited by electron impact, since polarization parallel to a beam occurs for all beam voltages between the excitation potential and 70 v (Massey and Burhop 1952).

We may summarize the conclusions of this note by saying (*a*) there is no definite inconsistency between the results of Shepherd, and of Seeliger and Handt, (*b*) as emphasized previously, knowledge of the properties of the cathode glow is still very incomplete.

ACKNOWLEDGMENTS

The author wishes to thank Professor J. D. Craggs, Professor G. Ecker and Mr. R. S. Shepherd for their comments on this note.

REFERENCES

DRUYVESTEYN, M. J., and PENNING, F. M., 1940, *Rev. Mod. Phys.*, **12**, 87.
ECKER, G., 1950, *Z. Phys.*, **128**, 511.
—— 1951, *Ibid.*, **129**, 161.
EMELEUS, K. G., 1951, *Conduction of Electricity through Gases* (London : Methuen), p. 56.
EMELEUS, K. G., and HALL, O., 1931, *Proc. Roy. Irish Acad.*, **40**, 1.
MASSEY, H. S. W., and BURHOP, E. H. S., 1952 *Electronic and Ionic Impact Phenomena* (Oxford : University Press), pp. 82, 165.
SEELIGER, R., and HANDT, T., 1929, *Ann. Phys., Lpz.*, **3**, 575.
SHEPHERD, R. S., 1955, *Thesis*, Queen's University of Belfast.
—— 1959, *Proc. Phys. Soc.*, **73**, 126.
STEWART, D. T., and EMELEUS, K. G., 1955, *Trans. Faraday Soc.*, **51**, 491.
THOMSON, J. J., 1921, *Rays of Positive Electricity* (Cambridge : University Press).

Anomalous Behaviour in the Hall Coefficients of the Semiconducting Compounds SnSe and GeSe

BY S. ASANABE† AND A. OKAZAKI
Department of Physics, Kyusyu University, Japan

MS. received 1*st October* 1958, *in revised form* 22*nd January* 1959

IN the present experiment semiconducting specimens of SnSe (p-type, single crystals, melting point = 860°c) and GeSe (p-type, polycrystals, melting point = 780°c) were prepared, by melting the stoichiometric amounts of their component materials (Sn, J.M. 99·998% pure; Ge, about 10Ω cm; Se, 99·999% pure) in an evacuated quartz tube.

† Now at Research Laboratory, Nippon Electric Co., Kawasaki-shi, Japan.

The specimen container used for measurements was evacuated (10^{-5} mm Hg) at low temperatures and was evacuated or filled with nitrogen gas (15 cm Hg) at high temperatures. The measured resistivity ρ and Hall coefficient R of the SnSe crystal exhibited maxima at about 200°c as shown by the curve marked O in figures 1 and 2. When the temperature was decreased from the value corresponding to these maxima, ρ and R did not vary in accordance with the original curves but took higher values. These increased gradually, and approached saturation as the specimen was subjected to successive heat treatments for a series of temperature cycles between room temperature and 200°c. In this saturation state the behaviour of ρ and R with increasing temperature is represented by curves B in the figures. The anomalous hump of R is no longer seen on curve B in figure 2. After quenching to room temperature from the highest temperature (about 500°c) encountered during the determination of curves B, the behaviour of ρ and R with increasing temperature is shown by curves A in the figures, where the anomalous hump of R is found again and indeed, at the same temperature as on curve O. The value of R always varies along the curve A after quenching from about 500°c and always along the curve B after annealing below 200°c for a long time. The behaviour of ρ and R at high temperatures was independent of the presence of the nitrogen gas atmosphere. The Hall mobility R/ρ corresponding to curves O, B and A in figures 1 and 2

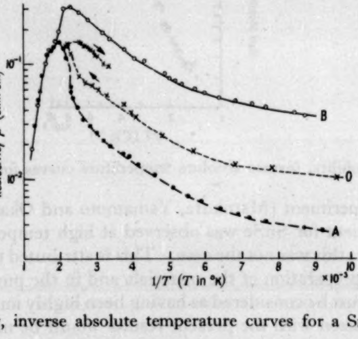

Figure 1. Resistivity, inverse absolute temperature curves for a SnSe single crystal.

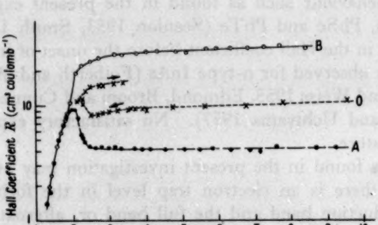

Figure 2. Hall coefficient, inverse absolute temperature curves for a SnSe single crystal.

is illustrated in figure 3, which shows that the Hall mobility is nearly independent of the above heat treatments. A similarly anomalous behaviour was observed in the Hall coefficient of GeSe above room temperature, though it could not be measured at low temperatures because of the high resistivity.

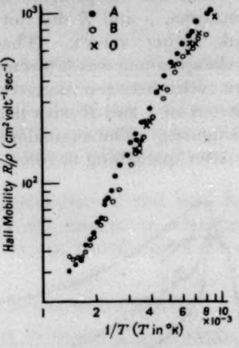

Figure 3. Hall mobility, inverse absolute temperature curves for SnSe single crystal.

In an early experiment (Matukura, Yamamoto and Okazaki 1953) a reversal of the Hall coefficient for SnSe was observed at high temperatures, while in the present experiment this was not the case. This is attributed to marked differences in the method of preparation of the materials and in the purity of the tin. The early specimens must be considered as having been highly impure and disordered. A detailed comparison with the present results would be meaningless.

Irreversible behaviour such as found in the present experiment has been reported for PbS, PbSe and PbTe (Scanlon 1953, Smith 1954). A similarly anomalous hump in the Hall coefficient before the onset of intrinsic conduction has recently been observed for n-type InAs (Folberth and Weiss 1956), n-type GaAs (Folberth and Weiss 1955, Edmond, Broom and Cunnell 1956) and p-type PbTe (Shogenji and Uchiyama 1957). No satisfactory explanation has been given in the literature.

The anomalies found in the present investigation may be explained by the assumption that there is an electron trap level in the forbidden energy gap between the conduction band and the full band or, alternatively, that at high temperatures some impurity atoms diffuse through the crystal to be trapped in vacancies where they may form new acceptors, different from the original ones existing at low temperatures. Further investigations are now being made to find whether either of the above assumptions is appropriate. A more comprehensive report will be published elsewhere in the near future.

ACKNOWLEDGMENTS

We wish to express our thanks to Dr. H. K. Henisch for assistance with the manuscript. The present experiment was partially supported by the Scientific Research Expenditure of the Ministry of Education.

REFERENCES

Edmond, J. T., Broom, R. F., and Cunnell, F. A., 1956, *Report of the Conference on Semiconductors* (London: Physical Society), p. 109.

Folberth, O. G., and Weiss, H., 1955, *Z. Naturf.*, **10a**, 615.

—— 1956, *Ibid.*, **11a**, 510.

Matukura, Y., Yamamoto, T., and Okazaki, A., 1953, *Mem. Fac. Sci. Kyusyu Univ.* B, **1**, 98.

Scanlon, W. W., 1953, *Phys. Rev.*, **92**, 1573.

Shogenji, K., and Uchiyama, S., 1957, *J. Phys. Soc. Japan*, **12**, 252.

Smith, R. A., 1954, *Physica*, **20**, 910.

REVIEWS OF BOOKS

The General Properties of Matter, by F. H. Newman and V. H. L. Searle. 5th Edition. Pp. xi + 428. (London: Edward Arnold, 1957.) 32*s*. 6*d*.

For nearly thirty years ' Newman and Searle ' has been a standard textbook on the properties of matter for university physics students. This new edition (revised by Dr. Searle) retains all the qualities that have made the book so popular in the past, and incorporates the changes needed to bring it thoroughly and refreshingly up-to-date.

Much of the material traditionally included in a properties of matter course is really applied mathematics, and one of the virtues of Newman and Searle is the clarity with which this essential mathematics is set out. Formulae can readily be traced, and the book is thus a useful vade mecum for the research worker as well as for the undergraduate. It gives immediate answers to such questions as the period of a pendulum on a yielding support, or the extension of a spiral spring; the relations between the elastic constants; the shapes of soap films; the flow of liquids and gases through tubes; molecular constants from kinetic theory; forced vibrations; and the propagation of waves on water. Only a modest mathematical equipment is assumed: thus calculus is used but not vector algebra. The more sophisticated student may possibly regret this when faced with the proliferation of symbols in the chapters on vibrations and wave motion, but there is, no doubt, some virtue for a beginner in seeing things done the long way.

The chapter on gyroscopic motion gives as clear an account of the subject as exists in an elementary book; but it would have spared the beginner several worries about signs if consistent use had been made of right-handed axes and of the axial vector convention (which the authors do not quote) that the positive direction of rotation about an axis is given by the corkscrew rule.

Throughout the book, references are given to original research papers, many of them being of recent date. This may help to combat the too-prevalent notion that ' properties of matter ' is a closed subject, in which there is little worth while left to be done. Accounts are given of gravity surveys carried out in the 1950's, and of submarine gravity measurements. Under elasticity there is a brief mention of the behaviour of single crystals, while viscosity is made the occasion for a reasonably full account of non-Newtonian liquids. Such additions add leavening to the treatment of more fundamental material, which constitutes the solid and enduring worth of this excellent textbook.

H. R. ALLAN.

Electromagnetic Isotope Separators and Applications of Electromagnetically Enriched Isotopes, by J. Koch, R. H. V. M. Dawton, M. L. Smith and W. Walcher. Pp. xi + 314. (Amsterdam: North Holland, 1958.) 53*s*.

This useful book describes the principles which are used in the electromagnetic separation of isotopes, the practical details for accomplishing this and some of the uses to which the separated isotopes are put. The book contains a wealth but not an overpowering wealth of detail about the construction of a large number of separators both large and small. It is also lavishly illustrated with photographs.

The first part of the book is by J. Koch and describes the history of electromagnetic isotope separation until the beginning of the war and the work done since the war with smaller separators, chiefly in the Scandinavian countries. The second section of the book is by R. H. V. M. Dawton and M. L. Smith and is devoted to discussions of isotope separation on the grand scale of gramme to kilogramme quantities. It is to be regretted that details of the very large Russian isotope separators which became available shortly before this book went to press could not be included in this section. A striking feature of the comparison between Russian and British methods in this field is the near identity of several elements of the systems—for example the construction of graphite ion sources and the techniques evolved for the production of machining of sufficiently flexible graphite.

The final section by W. Walcher considers certain general problems involved in isotope separation in more detail. Here we find a treatment of dispersion and resolving power, discussions of the effects of space charge and considerations behind the production of the very high currents which are needed to effect a rapid separation.

The book is well produced and printed and should form a valuable and effective starting point for anyone interested in these problems. Workers in many fields, as this book shows, are vitally dependent on the supply of separated stable isotopes which is effected chiefly through A.E.R.E., Harwell, and Oak Ridge. It is essential to the work of many laboratories that these supplies should be maintained and it is to be hoped that the authorities at these two great institutions appreciate the degree to which this service is valued.

D. H. WILKINSON.

Semiconductors and Phosphors.—Proceedings of the International Colloquium 1956 at Garmisch-Partenkirchen. Ed. M. SCHÖN and H. WELKER. Pp. viii + 684. (Braunschweig : Vieweg & Sohn, 1958.) DM. 68.

The first International Conference on Semiconductors took place at Reading in 1950. Its proceedings were published by Butterworths in 1951. The second Conference, in Amsterdam 1954, was reported in *Physica*, **20,** 1954. The present volume shares with the earlier reports its great value as a first-hand summary of the position of the subject, of the work in progress, and of the trend of ideas. It differs from the preceding reports by being twice the size, by including luminescence, and by a long delay in its publication. The volume contains 100 contributions in English, French, and German, varying in length from half a page to fifty pages, and relating to a wide variety of problems in the field of semiconductors and luminescence.

At least ever since Mott and Gurney's *Electronic Processes* . . . the connection between semiconductors and phosphors is well recognized, so that one Conference might reasonably deal with both subjects. The combination has not, however, been entirely successful because in only few of the contributions to this volume this connection is apparent : as the papers on luminescence take less than one-third of the space, the burden of the double scope falls more heavily on readers with a particular interest in luminescence.

The fourth Conference on Semiconductors (Rochester 1958) did in fact, wisely restrict the scope to semiconduction proper.

It is obvious that of the material presented in this book, a large portion is by now available elsewhere, or improved upon. In spite of this, the present volume must, as well as the earlier ones, be regarded as a basic book on semiconductors, and to a somewhat lesser extent on luminescence.

These volumes form, to my mind, the most readable and valuable progress reports on the subject. W. EHRENBERG.

Satellites and Space Flight, by E. BURGESS. Pp. vii + 159. (London: Chapman and Hall, 1957.) 21*s*.

The subject of this book is one which only a few years ago would have been regarded as decidedly futuristic. This may still be true as far as it is concerned with manned flight to the moon, but the use of space probes is already developing rapidly. The author was perhaps unfortunate in that his book first appeared just before the Russians launched the first satellite, but in other respects it is quite up to date. Thus the first chapter, which deals with Instrumented Earth Satellites, is concerned mainly with the ill-fated American Vanguard Project, but the third chapter on Probing into Space is now most appropriate and a useful source of information about the possibilities and difficulties of lunar probing. Chapters 2, 4 and 5 are concerned with manned space flight, the second dealing with Manned Satellite Stations, the fourth with Expeditions to the Moon, and the fifth with the Establishment of a Lunar Base. The concluding chapter deals with Interplanetary Flight.

Although the emphasis of the book is mainly on space travel, rather than the use of space probes, the scientific study of the earth's outer atmosphere, interplanetary space and the moon, it is technically quite sound, is well illustrated and clearly written. That the author is reasonably conservative may be gathered from his statement in the preface that " Experience gained . . . . . may be used to send an expedition to the Moon by the end of the present century ".

H. S. W. MASSEY.

Stellar Populations, edited by D. J. K. O'CONNELL. Pp. xiii + 544. (Amsterdam: North-Holland Publishing Company, 1958.) 76*s*.

This book is a report of the proceedings of a conference sponsored by the Pontifical Academy of Science and held in the Vatican in May 1957. The 24 invited to this restricted conference were all authorities in this field of work. There were 36 papers contributed and in each case the ensuing discussion was fully reported.

The report is not in any sense a review of the subject but is a collection of original contributions. It will be required by all astronomical or general scientific libraries that cater for astronomical or astrophysical readers. The subject headings are galaxies, clusters, young populations, variable stars, evolution and element abundance, our own galaxy, and galactic evolution and kinematic behaviour. Summaries from the physical and astronomical points of view were provided by F. Hoyle and J. H. Oort. C. W. ALLEN.

Expansion Machines for Low Temperature Processes, by S. C. Collins and R. L. Cannaday. Pp. vii + 115. (Oxford Library of the Physical Sciences.) (Oxford : University Press, 1958.) 12*s*. 6*d*.

In 1958 Professor Collins was awarded the Kamerlingh Onnes Medal for the development of the helium liquefier which bears his name and which is commercially produced by the A. D. Little Company. This important development in cryogenics has led to a very wide application of low temperature research and techniques since the war. His little book on low temperature expansion machines, written in collaboration with Lieutenant Cannaday, deals more generally with cryogenic devices doing external work. After a short chapter in which the principle of such cooling machines is set out in its barest form, an interesting account of early refrigerating machines is given. This is followed by a discussion of cooling systems such as cascades, Joule–Thomson cooling, expansion engines and combinations of these systems. The next section, again largely historical, deals with reciprocating expansion engines. It is here where the story of the successful helium engine is traced from Kapitza's original model over a diaphragm engine, developed by Collins but never fully tested, to the model which has gone into large scale production. Cooling turbines, another field in which Kapitza did pioneer work and which has assumed very great importance in the production of tonnage oxygen, are dealt with next. The final chapter is devoted to a short description of refrigeration cycles embodying expansion engines and among these is the Philips engine developed by Köhler and Jonkers.

In addition to the rather small number of low temperature physicists who are interested in refrigeration, this excellent little book will mainly appeal to students of refrigeration, mechanical and chemical engineering. It is therefore perhaps to be deplored that it should have come out as the fourth volume in a series in which it is preceded by three books on theoretical physics. K. MENDELSSOHN.

The Physics of Flow through Porous Media, by A. E. Scheidegger. Pp. xii + 236. (Toronto : University Press ; London : Oxford University Press, 1957.) £5 10*s*.

Flow through fine channels is a study which is gaining importance in various fields of pure and applied research and Dr. Scheidegger's monograph will be welcomed by all who are in one way or another connected with the subject. Very few books on the subject exist so far, and some of these are in Russian. Apart from providing a clear and readable account, the author gives an exhaustive list of references to original papers which is particularly useful in a borderline field where the relevant papers are scattered over a wide variety of journals.

The author begins by describing the nature of porous media and the investigation of their basic properties. Next, a short outline of fluid mechanics, insofar as it is necessary for the treatment of the whole problem, is given. After a third introductory chapter, on hydrostatics in porous media, the main problem is treated in five chapters. Two of these deal with Darcy's law and its solutions. The theoretical treatment of permeability is discussed in some detail and the author gives a critical appraisal of the hydraulic radius theory. The problems arising from the influence of molecular effects and at high flow velocities, both of which lie outside the limits within which Darcy's law is applicable, are dealt with in a chapter on general flow equations. Finally a short but very useful survey is made of the phenomena encountered in the flow of more than one component. Most of this is taken up with the study of immiscible fluids but the important case of seepage of fresh into salt water is also treated.

While it is clear that the book will be mainly of value to geologists and engineers, those physicists into whose work problems of capillary flow enter will find it informative and useful. K. MENDELSSOHN.

Progress in Crystal Physics, Vol. 1, edited by R. S. KRISHNAN. Pp. vi + 198. (Madras : S. Viswanathan, 1958.) 30*s*.

The volume under review is the first of a series giving an account of branches of solid state physics which are of particular interest to the group working in Bangalore under Dr. R. S. Krishnan. The subjects covered in this volume are : thermal expansion, thermal conductivity, elastic constants, photoelasticity, thermo-optical behaviour, the Faraday effect in diamagnetic crystals and the dielectric properties of ionic crystals.

Each of the articles is a survey by the editor or by one or more of his collaborators. These are written to a more or less uniform plan. The theoretical background and the main experimental techniques are considered in brief ; the more recent work in the subject is treated in a little more detail and the article closes with a comprehensive bibliography and with sets of tables containing numerical data.

The book will serve a useful purpose in drawing attention to the work carried out at Bangalore in fields which have not received much attention elsewhere ; though many of the subjects have been reviewed during the past few years, it is always desirable to have up-to-date surveys, particularly when the authors have themselves worked in the fields covered.

What is somewhat disappointing is the absence of any marked point of view, particularly on the theoretical side. In the section on thermal expansion one finds, for instance, that Raman's views on lattice vibrations are given the same consideration as the work of Born. One might have expected that a group which has been concerned with solid state physics for seventeen years (as pointed out by Dr. Krishnan in the preface) would have definite views on the relative merits of theories and of techniques. If such views exists, these have been remarkably well concealed.

In what is a particularly useful aspect of the surveys, the compilation of data, one misses the use of diagrams, which are also conspicuously absent throughout the book. This may well be due to the desire to limit the cost of the book, which is remarkably low considering the high quality of the printing and the presentation M. BLACKMAN.

Nuclear Magnetic Resonance Absorption in *Iso*-butyl Bromide as a Crystal and as a Supercooled Liquid

By J. G. POWLES AND J. A. E. KAIL
Physics Department, Queen Mary College, London

MS. received 23rd December 1958, *in final form 2nd February* 1959

Abstract. The proton magnetic resonance absorption in *iso*-butyl bromide ($(CH_3)_2CHCH_2Br$) in the temperature range $-196°$c to $-115°$c has been measured both in the crystalline form and as a supercooled liquid. (Measurements on the normal liquid will be reported elsewhere.) The measurements confirm a very considerable difference in freedom of molecular motion as between the two forms indicated by earlier dielectric loss measurements. The results indicate that in the *iso*-butyl bromide molecule *one* of the methyl groups is less able to rotate about its C_3 axis than the other and that therefore the stable isomer is in what may be called the *gauche* configuration. A severe line narrowing in the supercooled liquid centred at $-157°$c is interpreted as due to reorientation of the molecule as a whole at a rate which is in excellent agreement with dielectric loss measurements. Reorientation of the whole molecule in the crystal only occurs slowly, if at all, below the melting point. The line widths are 7·2 gauss and 4×10^{-4} gauss respectively just below the melting point.

---

§ 1. Introduction

The proton magnetic resonance absorption line width in the material and in the temperature range under discussion is due to direct dipole–dipole interaction between the nuclear magnets. The absorption therefore depends on the distances between the nuclei and the orientation of the lines joining any pair with respect to the main magnetic field. Since the lines have no structure we report only the line width δH which is the distance between maxima of $d\eta/dH$ where η is the nuclear resonance absorption coefficient, and the second moment of the line shape

$$\Delta H_2^2 = \int \eta(H)(H-H_0)^2\,dH \bigg/ \int \eta(H)\,dH$$

which has a particularly simple theoretical significance. The measurements were made at a resonant frequency of 15 Mc/s using apparatus of now well-known form (Gutowsky *et al.* 1953, Powles 1956). The absorption line width and the experimental second moment are reduced by motion above a particular frequency partly because the magnetic field at a nucleus due to another tends to be averaged out. This effect can be used to deduce rates of motion in the material, what is moving and how it is moving. For instance in the present example it is possible to distinguish motion of part of the molecule (a CH_3 group) and the molecule as a whole.

§ 2. Results

Figure 1 shows the variation in line width δH with temperature. Figure 2 shows the variation of ΔH_2^2. On cooling *iso*-butyl bromide normally forms a supercooled liquid and eventually a glass although the glass transition point has not been reported. The present results suggest the glass transition temperature is well below −160°c on the usual criteria (e.g. Kauzmann 1942). The supercooled liquid is stable over a period of days with the exception mentioned below. The lower curves in figures 1 and 2 are for this material.

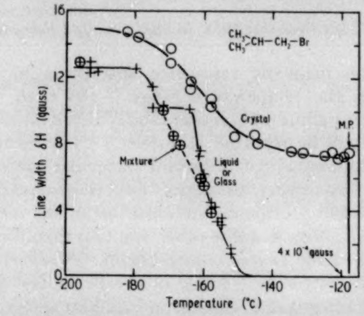

Figure 1. Variation in line width as a function of temperature for *iso*-butyl bromide, as a crystal and as a supercooled liquid. Some measurements are also shown for a mixture containing less than 20% crystal. Note the difference between the two curves at higher temperatures.

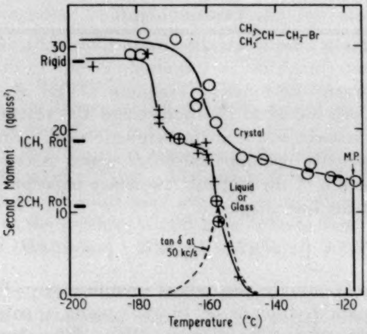

Figure 2. The second moment as a function of temperature for *iso*-butyl bromide, as a crystal and as a supercooled liquid. Calculated values of $\Delta H_2{}^2$ are indicated for the rigid lattice, for one methyl group per molecule in completely effective C_3 reorientation and for two methyl groups reorienting. Dielectric loss measurements on the supercooled liquid at 50 kc/s are also shown (Baker and Smyth 1939).

If the glass is held at −190°c over night and then brought up to about −135°c the crystal begins to form and the sample changes almost completely to the crystal in about two hours. Presumably crystal nuclei form at the lower temperature but cannot grow at an appreciable rate until the temperature is raised. Any desired proportion of crystal to glass can be obtained by allowing crystallization to proceed to the desired extent and then cooling by 20°c or more when no further crystallization occurs as far as we can tell over a period of several hours. The degree of crystallization can be measured from the nuclear resonance measurements themselves with an accuracy to about $\pm 200/k$ per cent where k is the percentage of crystal. Figure 3 shows derivative absorption curves at -122°c for various percentages of crystal. During the formation of the crystal the broad line grows at the expense of the narrow one. The narrow line does not show the true line width but reflects the inhomogeneity of the static magnetic field.

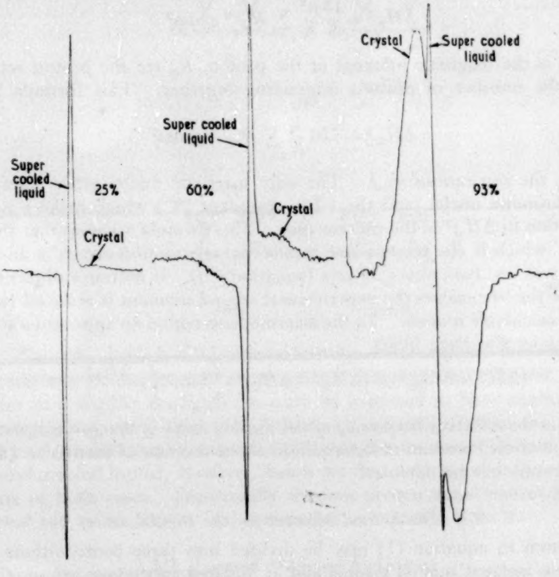

Figure 3. Derivative absorption curves for various crystal–supercooled liquid mixtures estimated as 25%, 60% and 93% crystal (broad line). The liquid (narrow) line is inhomogeneity broadened.

The true line width of the supercooled liquid in this temperature region (4×10^{-4} gauss) was measured by the spin echo technique (Hahn 1950) and these results are reported elsewhere (Luszczynski and Powles 1959). We have found no evidence that the line width of the supercooled liquid part of a mixture differs from that in 100% supercooled liquid except that a mixture with less than 20% crystal showed (figure 1) a *lower* value of δH in the region -160 to -175°c although this does not significantly affect the second moment (figure 2). This surprising result merits closer investigation since we have here very probably a rather intimate mixture of crystalline and amorphous materials. Crystalline polymers often give results which are difficult to interpret in terms of two distinct phases (e.g. Powles and Kail 1958).

§ 3. INTERPRETATION OF THE RESULTS

The line shapes showed no structure as indeed is to be expected from a substance so crowded with protons. Our interpretation is therefore based predominantly on the second moment values.

Van Vleck (1948) has shown that the second moment of an absorption line, adapted to the present situation, i.e. for interaction between protons and for a crystalline or amorphous mass, is

$$\Delta H_{2r}^2 = \frac{18}{5}\frac{\mu^2}{N}\sum_{i>j} R_{ij}^{-6} \text{ gauss}^2 \qquad \ldots\ldots(1)$$

where μ is the magnetic moment of the proton, R_{ij} are the proton separations and N the number of protons interacting together. This formula becomes

$$\Delta H_{2r}^2 = 720\,\frac{1}{N}\sum_{i>j} R'^{-6}_{ij} \text{ gauss}^2 \qquad \ldots\ldots(1')$$

with R'_{ij} the separations in Å. The only magnetic nuclei other than protons are the bromine nuclei (and the 1·1% abundant ^{13}C) which make a negligible contribution to ΔH_{2r}^2 in the present case. This formula assumes that the lattice is 'rigid' which in the present case means that any motion occurs at an effective frequency of less than about 50 kc/s (equation (2)). If motion sufficiently rapid to narrow the line occurs the experimental second moment is reduced (to ΔH_{2m}^2 say) in a calculable manner. In the intermediate region an approximate formula is (Gutowsky and Pake 1950)

$$(\Delta H_2^2 - \Delta H_{2m}^2) = (\Delta H_{2r}^2 - \Delta H_{2m}^2)\,\frac{2}{\pi}\tan^{-1}\left(\gamma\,\frac{\Delta H_2}{\pi\nu_c}\right) \qquad \ldots\ldots(2)$$

where ν_c is the effective frequency of the motion and γ is the gyromagnetic ratio. Hence a restricted amount of information about the rate of motion as a function of temperature can be obtained.

3.1. *The Second Moment for the Rigid Lattice*

The sum in equation (1) may be divided into three contributions (i) that due to two isolated methyl groups and an isolated methylene group, (ii) other interactions internal to the molecule, (iii) interactions with protons in neighbouring molecules. The contribution (i) is readily calculated assuming C–H = 1·09 Å, and the angle HCH = 109·6°. ΔH_2^2 for $CH_3 = 22{\cdot}5$ gauss² and ΔH_2^2 for $CH_2 = 11{\cdot}2$ gauss² so that ΔH_2^2 for (i) = 17·5 gauss². Contribution (ii) depends on the structure of the molecule which can exist in two isomeric forms. We have calculated the contribution to ΔH_2^2 for the configurations of figure 4 (*a*) which we shall call the *trans* and *gauche* forms and have assumed that the methyl group(s) near the bromine atom in each case are placed with two protons equidistant from the bromine, although the result does not depend much on this choice and find ΔH_2^2(i) + (ii) = 22·5 gauss² for both *gauche* and *trans* (the exact equality is a coincidence). Contribution (iii) cannot be estimated with any confidence in the absence of crystal structure data, and even less so for the supercooled liquid. However, in such a material with a high concentration of protons it is not unreasonable to assume that each proton has roughly three protons belonging to other molecules at the van der Waals distance from it (2·4 Å). The final theoretical values for the rigid lattice second moments are therefore $\Delta H_{2r}^2 = 28{\cdot}1$ gauss^2 for *gauche* and *trans*. ΔH_{2r}^2 by experiment (figure 2) is 29 gauss^2 for the liquid and 31 gauss^2 for the crystal. Thus in view of the difficulty in estimating contribution (iii) there is reasonable agreement between the theoretical and experimental values of ΔH_{2r}^2 and either isomer is possible.

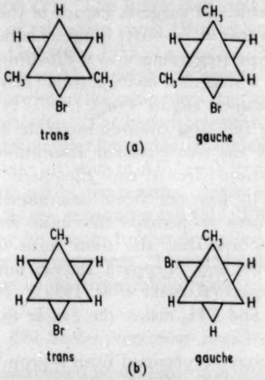

Figure 4. Isomers of (*a*) *iso*-butyl bromide, and (*b*) *n*-propyl bromide.

The crystal may be expected to show a rather larger second moment, since the molecules in a regular configuration may be expected to have slightly shorter inter-proton distances. Thus ΔH_{2r}^2 does not indicate whether the molecules in the crystal are different isomers or a different distribution of isomers from that in the supercooled liquid; however, below we find evidence that the isomers are the same in both cases. Incidentally the lone proton signal proves to be well broadened and so no narrow line component is expected from it.

3.2. *Limited Motional Narrowing*

The liquid line narrows to a new value of second moment of 18 gauss^2 at about −165°c with the transition (in ΔH_2^2) centred at −175°c. The crystal line narrows to a rather smaller value centred at about −160°c but continues to fall rather slowly towards the melting point at −118°c. It is well known (e.g. Powles and Gutowsky 1953) that in molecular crystals in which the molecules have methyl groups that the first line narrowing is frequently associated with reorientation of the methyl group about its own C_3 axis, indeed the narrowing often occurs at about −170°c. The second moment for C_3 reorientation of one or both methyl groups in the molecule is readily calculated. In the contribution (i) ΔH_2^2 for CH_3 is now $22{\cdot}5/4 = 5{\cdot}6$ gauss^2 and the effect on (ii) and (iii) may be estimated (Andrew 1950). We find

ΔH_2^2, for one CH_3 per molecule rotating, is 18·8 gauss^2,
for two CH_3 per molecule rotating, is 10·6 gauss^2.

Again the figures are only slightly dependent on the isomer and the ones given are for the *gauche* form. We conclude that at −165°c close to 50% of the methyl groups are in effective rotation. This could be due to (*a*) close to 50% all methyl group in the sample in effective rotation or (*b*) some molecules having both methyl groups rotating, others with one, others with none (possibly isomers) so proportioned that 50% of the total methyl groups are rotating or (*c*) each molecule has one of its two methyl groups rotating. In the liquid a regular environment is not present which tends against (*a*). (*b*) is in itself improbable. (*c*) seems most reasonable and suggests a study of the structure of the molecule.

The most stable isomer of *iso*-butyl bromide is not known. General results on molecules of this type (regarding it as a substituted ethane) make it almost certain that it exists in a staggered configuration (Mizushima 1954) so that there are only two distinct isomers (figure 4 (*a*)).

The corresponding *iso*-butyl chloride molecule exists in both forms in the liquid as evidenced by the two infra-red absorption lines associated with the C–Cl stretching vibration (Brown and Sheppard 1954 b) although which is the lower energy form has not been determined. In *n*-propyl bromide ($(CH_3)CH_2CH_2Br$) which is perhaps the most similar molecule for which definite information is available, the *trans* form is the most stable in the crystalline phase (Brown and Sheppard 1954 a) but the difference in energy is very small in the liquid (Komaki *et al.* 1955). It may be that electrostatic attraction between Br and CH_3 makes the *gauche* form less unfavourable than expected (Szasz 1955).

Iso-butyl bromide may be obtained from *n*-propyl bromide by replacement of one hydrogen by a methyl group but then *trans n*-propyl bromide becomes *gauche iso*-butyl bromide so that unless this substitution changes the intramolecular forces the *gauche* form of *iso*-butyl bromide is favoured. Again steric considerations (Szasz 1955) suggest that the *gauche* is more stable than the *trans* by analogy with the situation in isopentane ($(CH_3)_2CHCH_2CH_3$) and 1, 1, 2-trichloroethane (Cl_2CHCH_2Cl) (Scott *et al.* 1954, DiGiacomo and Smyth 1955). However, both forms are observed in infra-red (Szasz 1955) and Raman spectra (Kohlrausch 1943) at room temperature so that the energy difference cannot be greater than about 1 kcal mol^{-1} if 10% of one species is detectable. A contemporary interpretation of the Raman spectra would seem to indicate that the form we have called *gauche* is the lower energy one. If we assume that one isomer predominates (say 90%) at −165°c, as seems likely from the nuclear resonance results, the energy difference must be greater than about 0·3 kcal mol^{-1} if the supercooled liquid contains the equilibrium proportion of isomers and intermolecular forces are ignored. The equilibrium seems to be assured by the observation, in a later section, that the whole molecule reorients with a relaxation time of about 10^{-5} seconds even at −157°c and it may be assumed that this gives frequent opportunities for internal conversion.

Using the usual interatomic distances and the van der Waals radii (Pauling 1948) suggests that in the *trans* form of *iso*-butyl bromide the bromine atom may seriously hinder the rotation of both the methyl groups whereas in the *gauche* form only one is blocked. The closest approach between the Br nucleus and one of the protons of a methyl group as the latter rotates is 2·5 Å but the sum of the van der Waals radii of bromine and hydrogen is 3·15 Å. Alternatively one may postulate forces between the close bromine and methyl group which will increase the energy barriers to the rotation of both or one of the methyl groups according to the isomer.

The nuclear magnetic resonance results indicate clearly that one methyl group can reorient much more rapidly than the other. This is in favour of the *gauche* configuration and that this form may be stable with respect to the other isomer by a few hundred cal mol^{-1}.

The energy barrier to reorientation even of this freer methyl group may be greater than 12 ± 4 kcal mol^{-1} if the fall of ΔH_2^2 with temperature in the region of -175°c is used in equation (2). This figure may well be low in view of the possibility of a distribution of relaxation times (Powles and Luszczynski 1959) and tunnelling (Powles and Gutowsky 1955).

In the crystal a similar line width transition to about 16 gauss^2 occurs some 15° higher and may be interpreted in the same way. In this case the crystal may also contain only *gauche* molecules. The higher transition temperature may be due to the slightly larger intermolecular forces due to the closer packing. However this does not fit with the slower variation of ΔH_2^2 with temperature. This could be ascribed to a higher but partly temperature dependent barrier associated with intermolecular forces in the expanding crystal. The slow fall in second moment above -150°c may be due to further restricted motion which we are unable to identify from these measurements. It could be due to the reorientation of the second methyl groups as the temperature rises.

3.3. *The Severe Narrowing Region*

The narrowing in the supercooled liquid centred at about -157°c is so great as to require thermal reorientation of the molecule as a whole (which will narrow the signal even if one methyl group in the molecule is blocked) and even requires translational motion with correlation time of less than 10^{-5} second. This interpretation receives support from the measurements of dielectric loss which reflect the rate of reorientation of the C–Br bond. The measured dielectric $\tan \delta$ at 50 kc/s as a function of temperature is shown on figure 2 (Baker and Smyth 1939) and the correlation is excellent. The reorientation of the C–Br bond only necessarily causes reorientation of the inter-proton directions for the protons attached to the same carbon atom. However, the whole of the nuclear resonance line narrows so all the protons take part in the motion with substantially the same correlation time, in other words the whole molecule moves.

It is notable that this severe narrowing does not occur in the crystal below the melting point. This means that molecular reorientation, if any, is at a rate lower than about 50 kc/s. In concert with this the dielectric constant shows no dipolar contribution in the crystal at least for frequencies down to 500 c/s (Baker and Smyth 1939). Presumably the molecules in the regular arrangement in the crystal are prevented from reorienting by larger intermolecular forces. At the melting point freedom of reorientation is acquired and this narrow line region will be discussed elsewhere (Luszczynski and Powles 1959). The melting was not sharp in that over a range of some 5°c the proportion of narrow to broad line increased continuously. No intermediate line width was observed. The low frequency dielectric constant is reported to rise gradually to the liquid value in a similar range (Baker and Smyth 1939) and this is evidently the dielectric constant of a mixture rather than a premelting phenomenon in the solid.

The difference between the infra-red spectra for glass and crystal for some substituted ethanes has been studied but not for *iso*-butyl bromide (Brown and Sheppard 1950).

ACKNOWLEDGMENTS

One of us (J. A. E. K.) was supported during this work by a grant from the Imperial Chemical Industries Ltd. (Plastics Division).

We wish to thank Dr. K. Luszczynski for allowing us to use his results of spin echo measurements prior to publication.

REFERENCES

ANDREW, E. R., 1950, *J. Chem. Phys.*, **18**, 607, Appendix II.
BAKER, W. O., and SMYTH, C. P., 1939, *J. Amer. Chem. Soc.*, **61**, 2063.
BROWN, J. K., and SHEPPARD, N., 1950, *Disc. Faraday Soc.*, No. 9, p. 144.
—— 1954 a, *Trans. Faraday Soc.*, **50**, 535.
—— 1954 b, *Ibid.*, **50**, 1164.
DIGIACOMO, A., and SMYTH, C. P., 1955, *J. Amer. Chem. Soc.*, **77**, 1361.
GUTOWSKY, H. S., MAYER, L. H., and MCCLURE, R. E., 1953, *Rev. Sci. Instrum.*, **24**, 644.
GUTOWSKY, H. S., and PAKE, G. E., 1950, *J. Chem. Phys.* **18**, 669.
HAHN, E. L., 1950, *Phys. Rev.*, **80**, 580.
KAUZMANN, W., 1942, *Rev. Mod. Phys.*, **14**, 12.
KOHLRAUSCH, K. W. F., 1943, *Ramanspectren* (Leipzig: Akademische Verlagsgesellschaft), p. 241.
KOMAKI, C., ICHISHIMA, I., KURATANI, K., MIYAZAWA, T., SHIMANOUCHI, T., and MIZUSHIMA, S., 1955, *Bull. Chem. Soc. Japan*, **28**, 330.
LUSZCZYNSKI, K., and POWLES, J. G., 1959, *Proc. Phys. Soc.*, **74**, in the press.
MIZUSHIMA, S.-I., 1954, *Structure of Molecules and Internal Rotation* (New York: Academic Press).
PAULING, L., 1948, *Nature of the Chemical Bond* (Ithaca : Cornell University Press).
POWLES, J. G., 1956, *Proc. Phys. Soc.* B, **69**, 281.
POWLES, J. G., and GUTOWSKY, H. S., 1953, *J. Chem. Phys.*, **21**, 1695.
—— 1955, *Ibid.*, **23**, 1692.
POWLES, J. G., and KAIL, J. A. E., 1958, *J. Polym. Sci.*, **31**, 183.
POWLES, J. G., and LUSZCZYNSKI, K., 1959, *Physica*, in the press.
SCOTT, D. W., MCCULLOUGH, J. P., WILLIAMSON, K. A., and WADDINGTON, G., 1954, *J. Amer. Chem. Soc.*, **73**, 1707.
SZASZ, G. J., 1955, *J. Chem. Phys.*, **23**, 2449.
VAN VLECK, J. H., 1948, *Phys. Rev.*, **74**, 1168.

Self-Absorption in an Electrodeless Discharge in Hydrogen and Helium

By J. A. HARRISON
Department of Electrical Engineering, The University of Liverpool

Communicated by J. D. Craggs; MS. received 5th January 1959, *in final form 9th February* 1959

Abstract. The paper describes a simple and direct way of measuring self-absorption in a 24 Mc/s discharge. The results obtained with hydrogen and helium at pressures between 12 microns and 1·6 mm of Hg are used to determine absorption coefficients and excited level populations. Under the conditions described, self-absorption of H_α and H_β must be taken into account when measuring line intensities.

---

§ 1. Introduction

This paper describes self-absorption measurements which were made on the line spectra from low pressure electrodeless discharges in hydrogen, helium and helium–hydrogen mixtures. The work is part of a fuller study described elsewhere (Harrison 1957).

§ 2. Theory

Cowan and Dieke (1948) have made a theoretical study of self-absorption and they give many references to other work. Bartels (1950) describes a method of measuring discharge temperatures from self-absorption. Edels (1952) has discussed the problem of self-absorption in arcs in thermal equilibrium, and Minkowski (1930) has studied flames. Recently workers have studied the Balmer spectrum from electrodeless, and d.c. discharges, in hydrogen, but very few have considered the importance of self-absorption when measuring intensities. Some workers used the measured line intensity ratios, to deduce excitation temperatures. The results described here show that these temperatures may be incorrect if no allowance is made for self-absorption in H_α, H_β and H_γ.

The self-absorption was measured by placing a plane mirror behind the discharge tube so that light from the plasma was reflected back, through the plasma, and into the spectrograph. By comparing the intensity reaching the spectrograph, first with and then without, the mirror covered by black paper, the absorption coefficient was obtained as follows: The discharge plasma can be regarded as a uniform cylinder of diameter D and length d. The optical arrangement is represented by figure 1, provided $2\theta(t+2d+2a)<D$, which was the case for all measurements. Suppose F is the fraction of normally incident light which is reflected by the mirror and F_q is the fraction of normally incident

light transmitted through one quartz window. (Both these quantities were determined experimentally at all wavelengths.)

Consider an element dx of the plasma: the volume of this element which can radiate into the spectrograph is

$$(W+2t\theta+2x\theta)(h+2t\theta+2x\theta)\,dx; \qquad \ldots\ldots(1)$$

only a fraction $F_q hW/4\pi(t+x)^2$ of the radiation enters the spectrograph and since $W \ll h \ll 2\theta(t+x)$ the effective volume

$$dV = F_q \frac{hW\theta^2}{\pi}\,dx. \qquad \ldots\ldots(2)$$

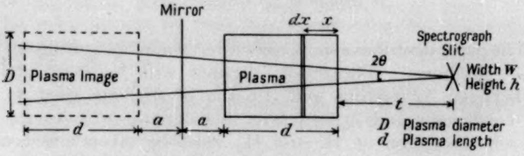

Figure 1. Diagram of the optical arrangement.

Suppose the intensity emitted in the frequency interval df is $E_f\,df$ per unit volume of the plasma, then the total intensity of the emitted line is $I = \int E_f\,df$, the integration being across the whole line.

Suppose also that light from the element dx is partly absorbed according to $E_{fx} = E_{f0}\exp(-k_f x)$ where k_f is the absorption coefficient for light of frequency f in cm^{-1}. The intensity reaching the spectrograph directly is

$$I_0 = \int^f \int_0^d F_q E_f \frac{hW\theta^2}{\pi}\exp(-k_f x)\,dx\,df \qquad \ldots\ldots(3)$$

and similarly the intensity reaching the spectrograph after reflection in the mirror is

$$I_R = \int^f \int_0^d F F_q{}^3 E_f \frac{hW\theta^2}{\pi}\exp\{-k_f(d-x)\}\exp(-k_f d)\,dx\,df. \qquad \ldots\ldots(4)$$

The ratio I_R/I_0 was measured experimentally. The variation of E_f and k_f with frequency depends on the line profile. If a rectangular shape is assumed $I_R/I_0 = F_q{}^2 F\exp(-k_0 d)$ where k_0 is the absorption coefficient at the line centre.

In practice the lines probably had a Doppler profile (Harrison 1957) so that $k_f = k_0\exp(-w^2)$ and $E_f = E_0\exp(-w^2)$

where
$$w = \frac{2(f-f_0)}{\Delta f_D}(\ln 2)^{1/2}$$
and
$$\Delta f_D = \frac{2(2R\ln 2)^{1/2}}{c} f_0 \left(\frac{T}{M}\right)^{1/2}$$

where Δf_D = the Doppler breadth (see, for example, Mitchell and Zemansky 1934); f_0 = frequency at line centre; R = gas constant; M = molecular weight;

T = absolute temperature, taken to be 400°K; c = velocity of light. Then the ratio $I_B/I_0 = FF_q^2G(k_0d)$ where

$$G(k_0d) = \frac{{}^{w}\!\int \{1-\exp[-k_0d\exp(-w^2)]\}\exp[-k_0d\exp(-w^2)]\,dw}{{}^{w}\!\int \{1-\exp[-k_0d\exp(-w^2)]\}\,dw} \quad \ldots\ldots(5)$$

Figure 2 shows some values of $G(k_0d)$ which the author has evaluated by graphical integration.

Multiple reflections between the mirror and the tube, and inside the tube, have been neglected because a more detailed calculation has shown that the value of $G(k_0d)$ is increased by only 0·5% if these reflections are taken into account. This error is very small compared with the experimental error and can therefore be ignored.

It is convenient to be able to calculate the intensity I_t, which would have been observed had there been no self-absorption from the measured intensity, I_m. It can be shown that $I_t = I_mG'(k_0d)$

where
$$G'(k_0d) = k_0d\,\frac{{}^{w}\!\int \exp(-w^2)\,dw}{{}^{w}\!\int \{1-\exp[-k_0d\exp(-w^2)]\}\,dw}\,. \quad \ldots\ldots(6)$$

The function $G'(k_0d)$ has also been evaluated and is shown in figure 2.

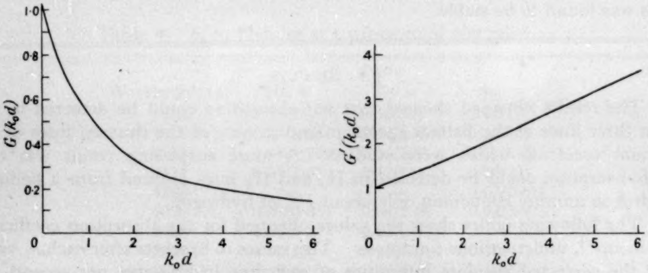

Figure 2. Graphs of the functions $G(k_0d)$ and $G'(k_0d)$.

The values of k_0 obtained assuming a Doppler profile are between 1·5 and 1·9 times greater than those obtained assuming a rectangular profile. It seems likely, therefore, that the values for k_0 are of the right order, even if the profile was not of true Doppler shape.

This mathematical treatment can be refined to allow for radial non-uniformity in the plasma: this was done for the results which follow by using as references, lines which had previously been shown to be free from self-absorption. The method showed that the hydrogen plasma was more intense at the centre, at pressures below 100 microns and tended to become a 'ring' discharge above this pressure. At 100 microns the plasma was radially uniform within the errors of the experiment. The helium plasma behaved in a similar way, being radially uniform at 400 microns.

§ 3. APPARATUS

The apparatus used was similar to Johnson's (1955) and is described in detail by Harrison (1957). It consists essentially of three parts:

(i) A glass vacuum system which could be evacuated and held at a pressure below 10^{-6} mm Hg and equipped with a means of maintaining a flow of spectrally pure hydrogen or helium. The gas did not flow directly through the quartz discharge tube (5 cm in diameter, 6 cm long, with a flat window at each end) but did allow impurities which diffused from the walls of the tube, to be pumped away.

(ii) A 24 Mc/s oscillator capable of running continuously with a variable input power of up to 500 watts (or 900 watts by exceeding the maximum rating), to the final stage. The power was coupled to the discharge tube by a three or four turn coil which was loosely wrapped round the tube. No attempt was made to measure the power going into the discharge, but every effort was made to ensure optimum coupling.

(iii) A quartz spectrograph fitted with a photomultiplier and a microammeter. The signal from the intense lines was attenuated as described by Harrison and Craggs (1958). Care was taken to calibrate the spectrograph slits and to check the linearity of the photomultiplier, the stability of its power supply, and the overall spectral response of the system.

The mirror finally chosen to reflect the light back through the discharge was not a front silvered or aluminized one, as these types were found to vary in reflectivity with time; instead an ordinary back silvered mirror was used and this was found to be stable.

§ 4. RESULTS

The results obtained showed that self-absorption could be detected in the first three lines of the Balmer spectrum and in nine of the thirteen lines of the helium spectrum which were studied. A more surprising result was that self-absorption could be detected in H_α and H_β lines emitted from a helium–hydrogen mixture containing only about 1% of hydrogen.

The following tables show the values obtained for the absorption coefficient k_0, in cm^{-1}, under various conditions. The values in brackets after each k_0 value are the corrected absolute intensities of each line in kilo-ergs per second per cubic centimetre of plasma, accurate to 10%. In each case the power quoted is the power fed into the last stage of the oscillator.

Table 1. k_0 (cm^{-1}) in Hydrogen at 500 watts

	Pressure of Hydrogen					
Line	12μ	25μ	50μ	100μ	200μ	400μ
H_α	0·05(160)	0·14(310)	0·19(630)	0·64(1000)	0·82(1200)	0·42(810)
H_β	0·04(30)	0·06(46)	0·07(83)	0·12(100)	0·29(110)	0·11(58)
H_γ	0·04(8·2)	0·03(11)	0·05(18)	0·06(21)	0·07(19)	0·06(8·7)
d (cm)	6	6	5·5	5	4·5	4

The quantity d is the observed length of the plasma.

Table 2. k_0 in Hydrogen at a pressure of 200 microns

	Power		
Line	200 w	400 w	900 w
H_α	0·18(160)	0·67(1000)	1·2(2800)
H_β	0·06(22)	0·13(95)	0·18(220)
H_γ	0·03(4·0)	0·06(16)	0·07(27)
d(cm)	4·5	4·5	4·5

Table 3. k_0 in Helium at 500 watts

	Pressure of Hydrogen					
Wavelength (Å)	50μ	100μ	200μ	400μ	800μ	1·6 mm
5876	0·25(170)	0·42(390)	0·47(730)	0·50(810)	0·40(800)	0·20(510)
5016	0·07(34)	0·12(44)	0·10(64)	0·10(65)	0·10(64)	0·04(39)
4922	—	0·03(15)	0·06(29)	0·06(25)	0·04(23)	0·03(13)
4472	0·07(25)	0·17(54)	0·17(100)	0·14(98)	0·12(85)	0·06(49)
4388	—	—	—	0·03(3·7)	0·03(3·1)	—
4026	0·03(8·1)	0·06(13)	0·06(21)	0·03(15)	0·04(13)	—
3965	—	0·03(5·7)	0·03(7·9)	0·03(6·7)	0·03(5·5)	—
3889	0·19(74)	0·25(140)	0·26(250)	0·19(220)	0·17(190)	0·12(100)
3820	—	0·03(3·2)	0·03(4·0)	—	—	—
d(cm)	6	5·5	5	4·5	4	3·5

No value is given for k_0 when the measured value was found to be less than 0·03 because the maximum experimental error is about 0·04 or 20% whichever is the larger.

Table 4. k_0 in Helium at a pressure of 400 microns

	Power		
Wavelength (Å)	100 w	200 w	400 w
5876	0·37(23)	0·44(84)	0·45(170)
5016	0·12(2·1)	0·12(6·6)	0·10(14)
4922	0·04(0·96)	0·06(2·9)	0·06(6·2)
4472	0·07(3·6)	0·13(11)	0·13(22)
4388	—	—	0·03(0·82)
4026	0·03(0·85)	0·04(2·0)	0·04(3·4)
3965	0·05(0·27)	0·05(0·76)	—
3889	0·26(10)	0·23(26)	0·19(47)
d(cm)	4·5	4·5	4·5

The values of k_0 in helium plus 1% hydrogen, at 500 watts are not being given in full. The k_0 values for H_α were found to be 0·07 at 400 microns, 0·04 at 800 microns and 0·04 at 1·6 mm while those for H_β were 0·05 at 400 microns and 0·03 at 800 microns. At 200 microns and below no self-absorption of the Balmer lines could be detected. The self-absorption and intensities of the helium lines were both reduced compared with table 3, the reductions being greater at the higher pressures.

The importance of self-absorption in the electrodeless discharge can be judged rather better by substituting values in equation (6) for k_0d, than from the k_0d values alone. With 200 microns of hydrogen excited at 500 watts, H_α appears as only 40% of its true intensity, H_β only 66% and H_γ 90%; the k_0d values were taken from table 1. Similar results can easily be obtained from the other tables.

As all the results, table 1 to table 4, were obtained using the same discharge tube, it was felt that it would be desirable to see if the results could be reproduced with a different tube. The second tube was made of quartz, 3 cm diameter by 5·5 cm long, again with a flat window at each end. Most of the previous experiments were repeated and are given in Harrison (1957) but only the helium results at constant pressure are given here as a comparison.

Table 5. k_0 in Helium at a pressure of 400 microns

	Power			
Wavelength (Å)	100 w	200 w	400 w	600 w
5876	0·42(490)	0·38(440)	0·53(1200)	0·51(1300)
5016	0·09(41)	0·10(44)	0·12(130)	0·12(140)
4922	0·05(17)	0·05(17)	0·08(48)	0·08(48)
4472	0·08(61)	0·09(58)	0·22(170)	0·20(180)
4388	—	—	0·03(5·8)	0·03(6·2)
4026	0·03(9·1)	0·03(9·6)	0·07(25)	0·08(24)
3965	—	0·03(4·3)	0·05(12)	0·04(12)
3889	0·20(130)	0·20(130)	0·21(380)	0·22(390)
3820	—	—	0·05(5·0)	0·05(5·0)
d(cm)	4·5	4·5	4·5	4·5

§ 5. DISCUSSION OF RESULTS

It will be noticed that the absolute intensities per cubic centimetre are very much higher in table 5. This is partly because the volume of the discharge tube is less (by a factor of 3), and partly because better matching of the oscillator could be obtained with the smaller tube. The k_0 values of table 5, however, compare well with table 4.

From the k_0 values for the hydrogen discharge, the number of excited atoms in level $n=2$ can be found as follows: It has been shown (Mitchell and Zemansky 1934) that

$$k_0 = \frac{2}{\Delta f_{\mathrm{D}}}\left(\frac{\ln 2}{\pi}\right)^{1/2}\frac{\lambda_0^2}{8\pi}\frac{g_n}{g_{n'}}N_{n'}A_{nn'} \quad \text{provided} \quad \frac{g_{n'}N_n}{g_nN_{n'}}$$

can be neglected compared with unity. In this case $g_{n'}N_n/g_nN_{n'}=0{\cdot}024$ so can be neglected. λ_0 is the wavelength of the absorbed line; g_n is the statistical weight of the upper level; $g_{n'}$ is the statistical weight of the lower (absorbing) level; $N_{n'}$ is the number of atoms/cm^3 in the lower level; $A_{nn'}$ is the Einstein transition probability for transitions from level n to level n'.

The formula for k_0 holds only if Doppler broadening is the process which determines the emitted line profile. For H_α, $\Delta f_{\mathrm{D}}=6{\cdot}55\times10^9\ \mathrm{sec}^{-1}$, and substituting the appropriate values in the equation for k_0 gives $N_2=4{\cdot}14\times10^{11}k_0$. For H_β, $\Delta f_{\mathrm{D}}=8{\cdot}84\times10^9\ \mathrm{sec}^{-1}$ so that $N_2=30\times10^{11}k_0$. By considering again table 2, the following N_2 level populations can be obtained.

	200 w	400 w	900 w
From H_α	$7{\cdot}5\times10^{10}$	28×10^{10}	50×10^{10}
From H_β	18×10^{10}	39×10^{10}	54×10^{10}

Although the agreement is not very good it is within the experimental error in the k_0 determination.

At higher intensities and power levels the values for N_2 calculated from H_β became increasingly larger than those calculated from H_α. This may be due to the electron density becoming high enough to modify the Doppler line profile. This effect can be seen in the $200\,\mu$ values in table 1, where N_2 from $H_\alpha = 34 \times 10^{10}$ while N_2 from $H_\beta = 87 \times 10^{10}$.

The populations of the other hydrogen levels can be obtained from the absolute intensities and this has been done in another paper by Harrison and Craggs (1958). The excited atom densities of all the $n=2$ levels of helium can be found in the same way. Considering table 3, the 400 microns results give the level populations in excited atoms per cubic centimetre which are shown in table 6. The Einstein probabilities were taken from Petrie (1948) and Tsui (1954).

It will be noticed that the lowest lying excited state, the 2^3S, contains many more atoms than the other three levels added together. The work of Phelps and Pack (1953) showed that helium singlet metastables (2^1S) were converted into triplet metastables (2^3S) as a result of collisions with slow electrons. This might explain why the observed 2^3S density is about six times greater than the 2^1S density. A rather surprising result is the fact that the 2^1S and 2^1P are almost equally favoured while the former is lower lying and metastable and the other is not.

Table 6

(1)	(2)	(3)	(4)	(5)	(6)
5016	2^1S	13·7	4·28	0·10	11
3965	2^1S	8·13	5·42	0·03	11
4922	2^1P	19·7	4·37	0·06	8·8
4388	2^1P	8·67	4·89	0·03	14
3889	2^3S	9·28	5·53	0·19	67
5876	2^3P	68·0	3·65	0·50	13
4472	2^3P	25·0	4·80	0·14	22
4026	2^3P	12·8	5·34	0·03	13

(1) Wavelength (Å); (2) absorbing level; (3) Einstein transition probability in units of 10^6 sec^{-1}; (4) Doppler width Δf_D at 400°K in units of 10^9 sec^{-1}; (5) k_0; (6) excited atom density in units of 10^{10} cm^{-3}.

The total excited atom density is in the region of 10^{12} cm^{-3} while the total atom density is $1{\cdot}4 \times 10^{16}$ cm^{-3}, thus only about one atom in every 14000 is excited at any instant.

The difference between the 2^3P level density as calculated from the 5876 Å line and the 4472 Å line is difficult to explain.

§ 6. CONCLUSIONS

Using a mirror to reflect the light emitted from an electrodeless discharge back through the plasma is a conveniently simple and direct way of measuring self-absorption. The method is only applicable if the emitted line profile is known. In the case of lines which are appreciably broadened it would be more satisfactory to measure the line shape, both with and without the mirror, with a high resolution spectrometer. In this way the absorption coefficient at any part of the line profile, not only the centre value k_0, can be found.

The helium work shows that excited atoms favour the triplet states more than the corresponding singlet levels which supports the work of Phelps and Pack (1953, 1955).

ACKNOWLEDGMENTS

The author is indebted to Professor J. D. Craggs for his help and encouragement, and also to the Atomic Energy Research Establishment, Harwell, for financial assistance.

REFERENCES

BARTELS, H., 1950, *Z. Phys.*, **127**, 243; **128**, 546.
COWAN, R. D., and DIEKE, G. H., 1948, *Rev. Mod. Phys.*, **20**, 418.
EDELS, H., 1952, *Proc. Phys. Soc.* B, **65**, 794.
HARRISON, J. A., 1957, *Ph.D. Thesis*, University of Liverpool.
HARRISON, J. A., and CRAGGS, J. D., 1958, *J. Electronics and Control*, **4**, 289.
JOHNSON, M., 1955, *Mon. Not. R. Astr. Soc.*, **115**, 15.
MINKOWSKI, R., 1930, *Z. Phys.*, **63**, 188.
MITCHELL, A. C. G., and ZEMANSKY, M. W., 1934, *Resonance Radiation and Excited Atoms* (Cambridge: University Press).
PETRIE, W., 1948, *Canad. J. Res.* A, **26**, 359.
PHELPS, A. V., and PACK, J. L., 1953, Paper D7, Conference on Gaseous Electronics, Washington, D.C.
—— 1955, *Rev. Sci. Instrum.*, **26**, 45.
TSUI, F., 1954, *Ph.D. Thesis*, University of Liverpool.

Lattice Screening in Polar Semiconductors†

By S. DONIACH

Department of Theoretical Physics, The University of Liverpool

Communicated by H. Fröhlich; *MS. received* 15*th January* 1959

Abstract. The influence of space charge screening on electron–phonon scattering in a polar semiconductor is discussed. Owing to the high optical mode frequency the polarization of conduction electron space charge, by the lattice, must be treated in a dynamic way.

In the limit of long lattice waves the classical Drude formula may be used, suggesting that the space charge polarization may lead to the enhancement of electron-optical mode phonon scattering probabilities, as opposed to the near static screening effect occurring for acoustic mode phonons.

A calculation is made of the detailed wave number and frequency dependence of the space charge polarization by the lattice, using a self-consistent field approximation. At low temperatures, and for fairly low conduction electron concentrations, the Drude type enhancement is confirmed.

§ 1. DISCUSSION

CALCULATIONS of electron–phonon scattering probabilities in semiconductors usually ignore the possibility of screening effects due to the conduction electron space charge. In the case of long wave acoustic mode phonons where the lattice frequency is low enough, an estimate of such screening effects can be made using the classical Debye–Hückel theory. This predicts a slight quenching of electron–phonon scattering probabilities for lattice waves with wavelengths longer than the Debye length, $(4\pi ne^2/\epsilon_0 KT)^{1/2}$ (n is the number concentration of conduction electrons, ϵ_0 the background dielectric constant).

In polar semiconductors, on the other hand, the important electron-scattering modes of the lattice may be the optical mode vibrations which have a high vibration frequency at long wavelengths. The purpose of this paper is to point out that at such high frequencies the static, Debye, treatment of screening must break down. This can be qualitatively understood by considering the screening of very long wave optical mode lattice vibrations. In this limit the electron response follows from the classical Drude formula for the response $\mathbf{E}$ to an oscillating applied electric field $\mathbf{D}=\mathbf{D}_0 e^{i\omega t}$:

$$\mathbf{E}=\frac{1}{1-\omega_p{}^2/\omega^2}\mathbf{D} \qquad \ldots\ldots(1)$$

(where ω_p is the plasma frequency, $(4\pi ne^2/m^*)^{1/2}$; m^* is the conduction electron effective mass). Since for a polar lattice ω may be larger than ω_p, the Drude dielectric constant can then be less than unity and the effect of space charge screening may therefore be, actually, to lead to increased electron–phonon scattering probabilities, as opposed to the quenching which would be expected (Ehrenreich 1957) from the Debye theory.

---

† Based on Electrical Research Association report LT/368.

In practice the dominant optical modes involved in electron scattering will be of relatively short wavelength, even at low temperatures T for which $KT \ll \hbar\Omega$ (where Ω is the optical mode frequency). This follows from the demand for energy conservation in individual scatterings:

$$\left(\mathbf{q}.\mathbf{v}+\frac{\hbar q^2}{2m^*}\right)=\Omega \qquad \ldots\ldots(2)$$

(where $\mathbf{v}$ is the electron velocity, with magnitude of order $(KT/m^*)^{1/2}$, $\mathbf{q}$ is a phonon wave number). Then for $KT \ll \hbar\Omega$, q may be of order $(m^*\Omega/\hbar)^{1/2}$. Use of the Drude formula for these short wavelengths is suspect, and in the calculations of this paper we use a more general theory of space charge response (Lindhard 1954) based on the self-consistent field theory of Vlasov (1945). This theory is applied, in a phenomenological way, to calculate the effect of the space charge polarization on electron–phonon scattering. The transition from the static, Debye screening, response to the high frequency Drude limit is now clearly defined.

These results are used to calculate the dependence of electron mobility on the conduction electron concentration. A low temperature approximation is used and the results are evaluated in the limit of weak plasma–lattice coupling, where the parameter $(\omega_p/\Omega)^2(\hbar\Omega/KT)^{1/2}$ is smaller than unity. Under these conditions the calculations confirm the high frequency effect of the space charge suggested by the Drude theory, leading to an electron mobility which decreases with increasing conduction electron concentration.

§ 2. PHENOMENOLOGICAL DESCRIPTION OF THE PLASMA–LATTICE SYSTEM

As a model for the description of electron-optical mode phonon scattering in a polar semiconductor we consider a system consisting of a non-degenerate gas of free electrons with effective mass m^*, effective charge e/ϵ_0 (where ϵ_0 is a background optical dielectric constant) in the field of a vibrating polar continuum, vibration frequency Ω independent of wavelength. The electrons' charge is assumed to be neutralized by a uniform positive background. In order to calculate the effect of space charge screening on electron–phonon scattering probabilities the assumption is made that one can separate out the motion of a particular electron which is undergoing a transition, on the energy shell, through interaction with the lattice, from the motion of the rest of the electrons which are reacting to the lattice in an average way. The effects of energy shell scattering are calculated using a Boltzmann equation argument, while the polarization of the remaining electrons is treated phenomenologically in terms of a dielectric response function for the electron gas. This separation is analogous to that made by Bardeen (1937) in his treatment of lattice screening in metals, though its justification presents certain difficulties in the non-degenerate case where the majority of the electrons can undergo scattering. A more detailed analysis of this point has been made elsewhere by the author (Doniach 1958), using a collective treatment of the space charge motion.

The Lagrangian for the lattice field in interaction with the electronic space charge, Fourier density components $\rho_{\mathbf{q}}(t)$, may be written

$$\mathscr{L}=\tfrac{1}{2}\sum_{\mathbf{q}}\{\dot{Q}_{\mathbf{q}}\dot{Q}_{-\mathbf{q}}+\Omega^2 Q_{\mathbf{q}}Q_{-\mathbf{q}}\}+\sum_{\mathbf{q}}\gamma_{\mathbf{q}}Q_{-\mathbf{q}}\rho_{\mathbf{q}} \qquad \ldots\ldots(3)$$

where $Q_{\mathbf{q}}(t)$ are the amplitudes of lattice waves with wave number $\mathbf{q}$. The interaction term in (3) can be rewritten in terms of an electric potential set up by the lattice waves, components $\phi_{\mathbf{q}}{}^0$, since one could then write

$$\mathscr{L}_{\text{int}} = \sum_{\mathbf{q}} \phi^0{}_{-\mathbf{q}}\rho_{\mathbf{q}}. \qquad \ldots\ldots (4)$$

Hence from (3) one has

$$\phi_{\mathbf{q}}{}^0(t) = \gamma_{\mathbf{q}} Q_{\mathbf{q}}(t). \qquad \ldots\ldots (5)$$

We now introduce a dielectric response function $\epsilon(\mathbf{q}, \omega)$ for the electrons, defined through their response to an applied travelling wave electric field of the form

$$\mathbf{D}(\mathbf{x}, t) = \mathbf{D}_{\mathbf{q},\omega} \exp\left[i(\mathbf{q}\,.\,\mathbf{x} - \omega t)\right]. \qquad \ldots\ldots (6)$$

The response field, $\mathbf{E}$, is then

$$\mathbf{E}_{\mathbf{q},\omega} = \frac{1}{\epsilon(\mathbf{q}, \omega)} \mathbf{D}_{\mathbf{q},\omega}. \qquad \ldots\ldots (7)$$

In terms of $\epsilon(\mathbf{q}, \omega)$ the passive response of the space charge to the lattice potential leads to a modified potential

$$\phi_{\mathbf{q}}(\omega) = \frac{1}{\epsilon(\mathbf{q}, \omega)} \phi^0(\mathbf{q}, \omega) \qquad \ldots\ldots (8)$$

where

$$\phi^0(\mathbf{q}, \omega) = \int_{-\infty}^{\infty} \mathrm{e}^{-i\omega t} \phi_{\mathbf{q}}{}^0(t)\, dt. \qquad \ldots\ldots (9)$$

This modified potential (8) will be used below to determine the screened electron–lattice scattering probabilities. For this purpose an effective equation of motion for the potential $\phi^0(t)$ set up by the lattice must be determined, through (5), (3).

The modified motion of the lattice due to its interaction with the space charge can be calculated, to within the dielectric approximation, by evaluating the lattice-induced polarization of the space charge density components, $\delta\rho_{\mathbf{q}}$. Inserting (8) in the Poisson equation one has

$$\frac{e}{\epsilon_0} 4\pi\delta\rho_{\mathbf{q}}(\omega) = q^2[\phi_{\mathbf{q}}(\omega) - \phi_{\mathbf{q}}{}^0(\omega)] = q^2\left(\frac{1}{\epsilon(\mathbf{q}, \omega)} - 1\right) \phi_{\mathbf{q}}{}^0(\omega) \qquad \ldots\ldots (10)$$

so that the effect of this part of the space charge polarization on the lattice motion is given, through equation (4), in terms of

$$\begin{aligned} \mathscr{L}^{\text{eff}}_{\text{int}} &= \sum \gamma_{-\mathbf{q}} Q_{-\mathbf{q}} \delta\rho_{\mathbf{q}}(t) \\ &= \sum \frac{\epsilon_0}{e} \frac{\mathbf{q}^2}{4\pi} Q_{-\mathbf{q}} \int_{-\infty}^{\infty} dt' [\epsilon_{\mathbf{q}}{}^{-1}(t - t') - 1] Q_{\mathbf{q}}(t') \qquad \ldots\ldots (11) \end{aligned}$$

where

$$\epsilon_{\mathbf{q}}{}^{-1}(t - t') = \int_{-\infty}^{\infty} d\omega \exp\left[i\omega(t - t')\right] \frac{1}{\epsilon(\mathbf{q}, \omega)}. \qquad \ldots\ldots (12)$$

Thus, on making the separation, as discussed above, of the average space charge motion, from the individual electron scatterings, the effective equations of motion for the modified lattice amplitudes become, through (3) and (11),

$$\ddot{Q}_{\mathbf{q}}(t) + \Omega^2 Q_{\mathbf{q}}(t) + q^2 \frac{\gamma_{\mathbf{q}}{}^2}{4\pi} \frac{\epsilon_0}{e} \int_{-\infty}^{\infty} dt' [\epsilon_{\mathbf{q}}{}^{-1}(t - t') - \delta(t - t')] Q_{\mathbf{q}}(t') = 0 \quad \ldots\ldots (13)$$

which have solutions of the form

$$Q_{\mathbf{q}}(t) = Q_{\mathbf{q}}{}' \exp\left(i\Omega_{\mathbf{q}} t\right) \qquad \ldots\ldots (14)$$

where the new lattice frequencies, $\Omega_{\mathbf{q}}$, are determined by

$$(-\Omega_{\mathbf{q}}^2+\Omega^2)+\frac{\epsilon_0}{4\pi e}q^2\gamma_{\mathbf{q}}^2\left[\frac{1}{\epsilon(\mathbf{q},\Omega_{\mathbf{q}})}-1\right]=0. \qquad \ldots\ldots(15)$$

The properties of the solutions, $\Omega_{\mathbf{q}}$ of (15) will be discussed below in terms of Lindhard's approximation to $\epsilon(\mathbf{q},\omega)$ for the electron gas.

In the particular case of a polar crystal with static dielectric constant ϵ_s one has (Fröhlich 1954)

$$\frac{\epsilon_0}{4\pi e}q^2\gamma_{\mathbf{q}}^2=\left[\Omega^2\left(1-\frac{\epsilon_0}{\epsilon_s}\right)\right] \qquad \ldots\ldots(16)$$

so that in this case (15) reads

$$[-\Omega_{\mathbf{q}}^2+\Omega^2]+\Omega^2\left(1-\frac{\epsilon_0}{\epsilon_s}\right)\left[\frac{1}{\epsilon(\mathbf{q},\Omega_{\mathbf{q}})}-1\right]=0. \qquad \ldots\ldots(17)$$

§3. SELF-CONSISTENT FIELD APPROXIMATION FOR THE SPACE CHARGE RESPONSE

In this section Lindhard's (1954) theory for the electron dielectric response function is summarized and the resulting expression for $\epsilon(\mathbf{q},\omega)$ evaluated approximately in the region of $\mathbf{q}$, ω, of interest for the mobility problem.

Following Lindhard, the polarization induced in a statistical distribution of electrons is simply derived using first-order perturbation theory for the electrons moving in a self-consistent potential of the form

$$\phi(\mathbf{x},t)=\phi_{\mathbf{q},\omega}\exp\,[i(\mathbf{q}\,.\,\mathbf{x}-\omega t)].$$

The displaced charge density is then given as

$$\delta\rho_{\mathbf{q},\omega}=\left[\frac{en}{\epsilon_0}\sum_{\mathbf{k}}\frac{f_{\mathbf{k}+\mathbf{q}}-f_{\mathbf{k}}}{(E_{\mathbf{k}+\mathbf{q}}-E_{\mathbf{k}})-\hbar\omega}\right]\phi_{\mathbf{q},\omega} \qquad \ldots\ldots(18)$$

where $E_{\mathbf{k}}=\hbar^2k^2/2m^*$, and the electron distribution function, $f_{\mathbf{k}}$, normalized to unity, is proportional to $\exp(-E_{\mathbf{k}}/KT)$ for a non-degenerate gas at temperature T.

This leads, using the Poisson equation, to

$$\epsilon(\mathbf{q},\omega)\simeq 1+\frac{4\pi ne^2}{\epsilon_0 q^2}\sum_{\mathbf{k}}\frac{f_{\mathbf{k}+\mathbf{q}}-f_{\mathbf{k}}}{(E_{\mathbf{k}+\mathbf{q}}-E_{\mathbf{k}})-\hbar\omega} \qquad \ldots\ldots(19)$$

In the limit of large volume where this sum becomes an integral, some prescription is needed at the pole, to give finite results. Physically, the pole arises through the possibility of energy shell transitions for the electrons, caused by interaction with the oscillating external field (in our case, the lattice). Since we have made the assumption that such transitions can be treated separately, through the Boltzmann equation, contributions from these processes will be omitted in the definition of $\epsilon(\mathbf{q},\omega)$ leading to a principal value prescription in the sum (18).

From the symmetry of $f_{\mathbf{k}}$ (19) can be rewritten as

$$\epsilon(\mathbf{q},\omega)\simeq 1+\frac{4\pi ne^2}{\epsilon_0 q^2}\sum_{|\mathbf{k}|>0}(f_{\mathbf{k}+\mathbf{q}/2}-f_{\mathbf{k}-\mathbf{q}/2})\frac{\hbar^2\mathbf{k}\,.\,\mathbf{q}/m^*}{(\hbar^2\mathbf{k}\,.\,\mathbf{q}/m^*)^2-(\hbar\omega)^2} \qquad \ldots\ldots(20)$$

and since, from equation (2), electron–phonon scattering at low temperatures mainly occurs for lattice waves of wave number $q\sim u=(m^*\Omega/\hbar)^{1/2}$, which is much larger than the thermal electron wave number, $\bar{k}=(m^*KT/\hbar^2)^{1/2}$, we will neglect contributions from the $f_{\mathbf{k}+\mathbf{q}/2}$ term in (20).

In this approximation (20) can be expressed, in polar coordinates with $\mathbf{k}.\mathbf{q}=xq$, as

$$\epsilon(\mathbf{q},\omega)\simeq 1-\frac{m^*\omega_{\mathrm{p}}{}^2}{q^2}\frac{\mathscr{P}}{\pi}\int_0^\infty\frac{dx}{\bar{k}}\exp\left(-\frac{(x-\frac{1}{2}q)^2}{2\bar{k}^2}\right)\frac{m^*qx/\hbar^2}{\frac{1}{4}u^4-q^2x^2} \quad \ldots\ldots(21)$$

A rough evaluation of (21) will now be made by replacing the Gaussian distribution with a square distribution and expanding the results to first order in $X(q)$; $(1/X(q))$ for $X<1$; $X>1$ where

$$X(q)=\frac{(2\bar{k}/q)}{(u^2/q^2-1)}. \quad \ldots\ldots(22)$$

Introducing a parameter

$$\eta=\frac{\omega_{\mathrm{p}}{}^2}{\omega^2}\left(\frac{u}{\bar{k}}\right) \quad \ldots\ldots(23)$$

this leads to

$$\epsilon(q,\omega)\simeq\begin{cases}1-\eta\dfrac{u^3}{q^3}X(q) & \text{for } |X|<1 \quad \ldots\ldots(24a)\\[2ex] 1-\eta\dfrac{u^3}{q^3}(1/X(q)) & \text{for } |X|>1 \quad \ldots\ldots(24b)\end{cases}$$

at $|X|=1$ the square distribution gives infinite results, but a slightly more elaborate approximation, using a triangulation for e^{-x^2} confirms (24) as giving a reasonable qualitative estimate of $\epsilon(q,\omega)$ over the whole range of q provided $q\gg\bar{k}$.

Inspection of the q-dependence of (24), for fixed ω, thus provides a semi-quantitative picture of the transition from the high frequency Drude-type polarizability ($\epsilon\leqslant 1$ for $q\leqslant u$) to the Debye-type screening effect ($\epsilon\geqslant 1$ for $q\geqslant u$). However, the above estimate is made under strictly non-classical conditions, $q\gg\bar{k}$, so that the details of the q, ω dependence of ϵ are different from those of the classical formulae.

§ 4. CALCULATION OF ELECTRON MOBILITY

The above approximate evaluation of $\epsilon(q,\omega)$ will now be applied to a calculation of electron–phonon scattering probabilities and hence of electron mobility, using the phenomenological formulation of § 2 for the space charge modification of the lattice field, through (8), and of the lattice frequency, through (17).

From (11), (14), the effective lattice Hamiltonian may be written

$$H_{\mathrm{eff}}=\tfrac{1}{2}\sum\{P_{\mathbf{q}}{}'P_{-\mathbf{q}}{}'+\Omega_{\mathbf{q}}{}^2Q_{\mathbf{q}}{}'Q_{-\mathbf{q}}{}'\} \quad \ldots\ldots(25)$$

where the $Q_{\mathbf{q}}{}'$ are modified lattice amplitudes, $P_{\mathbf{q}}{}'$ their canonical conjugates. Through (8), (9), (5), (14) the effective lattice potential leading to electron transitions becomes

$$\phi_{\mathrm{eff}}(\mathbf{x})=\sum_{\mathbf{q}}\mathrm{e}^{i\mathbf{q}.\mathbf{x}}\frac{\gamma_{\mathbf{q}}}{\epsilon(\mathbf{q},\Omega_{\mathbf{q}})}Q_{\mathbf{q}}{}'. \quad \ldots\ldots(26)$$

Electron transition probabilities will therefore be determined by the matrix elements of (26) between phonon eigenstates of (25). From the usual theory, the matrix element of $Q_{\mathbf{q}}{}'$ for a transition from a state with $n_{\mathbf{q}}$ phonons in the **q**th mode to one with $n_{\mathbf{q}}-1$ phonons is

$$\langle n_{\mathbf{q}}|Q_{\mathbf{q}}{}'|n_{\mathbf{q}}-1\rangle=\left(\frac{\hbar}{2\Omega}\,n_{\mathbf{q}}\right)^{1/2}. \quad \ldots\ldots(27)$$

So that the transition rate for absorption of a phonon by an electron of wave number **k** is

$$\frac{dW_{\mathbf{k},\mathbf{k}+\mathbf{q}}}{dt}=\frac{2\pi}{\hbar}\left|\frac{\gamma_{\mathbf{q}}}{\epsilon(\mathbf{q},\Omega_{\mathbf{q}})}\left(\frac{\hbar n_{\mathbf{q}}}{2\Omega_{\mathbf{q}}}\right)^{1/2}\right|^{2}\delta(E_{\mathbf{k}+\mathbf{q}}-E_{\mathbf{k}}-\hbar\Omega_{\mathbf{q}}). \qquad \ldots\ldots(28)$$

This differs from the transition rate obtained on neglecting space charge effects by a factor

$$\left(\frac{1}{\epsilon(\mathbf{q},\Omega_{\mathbf{q}})}\right)^{2}\left(\frac{\Omega}{\Omega_{\mathbf{q}}}\right). \qquad \ldots\ldots(29)$$

The approximate formula (24) for $\epsilon(\mathbf{q},\omega)$ will be used to compute this factor: the modified lattice frequency is a solution of equation (17). This reads

$$(\Omega^{2}-\Omega_{q}^{2})\epsilon(q,\Omega_{q})+\Omega^{2}(1-\epsilon_{0}/\epsilon_{s})\{1-\epsilon(q,\Omega_{q})\}=0. \qquad \ldots\ldots(30)$$

Under conditions of weak coupling of a single electron to the lattice, ϵ_0 will be near to ϵ_s, and one may attempt to solve (28) by iteration in powers of $1-\epsilon_0/\epsilon_s$. There result two solutions, one near to Ω, and one near to the zero of $\epsilon(q,\Omega_q)$, i.e. near to the plasma frequency for wave number q. However, such an iteration is only possible provided q is such that this plasma frequency is not too near to Ω; otherwise the modification of the lattice frequency, which goes as $1/\epsilon(q,\Omega_q)$, could become so large that iteration would not be possible. In order to avoid this difficulty, the calculation will be made under the condition that, for wave numbers of interest, $q \sim u$, the lattice frequency will not be too strongly modified. Inspection of the form of (24) shows that this is true provided (cf. (23))

$$\eta=\frac{\omega_{\mathrm{p}}^{2}}{\Omega^{2}}\left(\frac{\hbar\Omega}{KT}\right)^{1/2} \ll 1. \qquad \ldots\ldots(31)$$

From the definition of the plasma frequency (after equation (1)) this restriction therefore imposes an upper bound to the conduction electron densities for which our results can be applied.

Under these conditions, the change of lattice frequency will not affect the transition rate, (28), to lowest order in $(1-\epsilon_0/\epsilon_s)\eta$. It is further assumed that electron–plasma mode scattering will not lead to loss of momentum from the electron system, so will not directly affect the electron mobility.

Finally the mobility will be calculated, from (28) in the low temperature approximation (Fröhlich 1954), where the relaxation time is chiefly determined by the rate of absorption of phonons by the conduction electrons, proportional, from (28), to $n_q \sim \mathrm{e}^{-\hbar\Omega/KT}$. In this approximation the total relaxation time is then simply the sum over absorption rates, giving

$$\frac{1}{\tau(k)}=\sum_{\mathbf{q}}\left[\frac{2\pi}{\hbar}\,\frac{\hbar}{2\Omega}\left(\frac{\gamma_{\mathbf{q}}}{\epsilon(\mathbf{q},\Omega)}\right)^{2}\delta(E_{\mathbf{k}+\mathbf{q}}-E_{\mathbf{k}}-\hbar\Omega)\right]. \qquad \ldots\ldots(32)$$

For $k=\bar{k}$ the delta function restricts this sum to a range for which $|2\bar{k}q/(u^2-q^2)|<1$, so that (24*a*) can be used for $\epsilon(q,\Omega)$, giving (for $\eta \ll 1$ as stated above)

$$\frac{1}{\tau(\bar{k})}\simeq[\mathrm{e}^{-\hbar\Omega/KT}\Omega]\alpha\int_{q_0}^{q_1}dq\,\frac{u}{\bar{k}q}\left[\frac{1}{\epsilon(\mathbf{q},\Omega)}\right]^{2} \qquad \ldots\ldots(33)$$

where α is the usual electron-polar lattice coupling constant. In the limit of $KT \ll \hbar\Omega$ this evaluates to

$$\frac{1}{\tau(\bar{k})}=(\mathrm{e}^{-\hbar\Omega/KT}\Omega)2\alpha[1-4\eta^{2}]^{-1}. \qquad \ldots\ldots(34)$$

Where the condition $\eta \ll 1$ implies, from (23)

$$n \ll n_0 \left(\frac{KT}{\hbar\Omega}\right)^{1/2} \qquad \ldots\ldots(35)$$

where

$$n_0 = \Omega^2 \frac{m^* \epsilon_0}{4\pi e^2} \simeq \left(\frac{m^*}{10^{-1} m_e}\right) \epsilon_0 \left(\frac{\hbar\Omega}{K.400}\right)^2 10^{17}\ \mathrm{cm}^{-3}. \qquad \ldots\ldots(36)$$

Thus, the space charge polarization has the effect of decreasing the usual collision time for unscreened scattering by a factor

$$\{1 - 4(n/n_0)^2 (\hbar\Omega/KT)\} \qquad \ldots\ldots(37)$$

provided n satisfies (35). As this factor approaches zero the approximations made above start to break down, and a more detailed calculation would be required.

ACKNOWLEDGMENTS

The author wishes to thank Professor H. Fröhlich for suggesting this work and for his valuable advice. He is grateful to the Electrical Research Association for a grant.

REFERENCES

BARDEEN, J., 1937, *Phys. Rev.*, **52**, 688.
DONIACH, S., 1958, *Ph.D. Thesis*, University of Liverpool.
EHRENREICH, H., 1957, *J. Phys. Chem. Solids*, **2**, 131.
FRÖHLICH, H., 1954, *Phil. Mag. Suppl.*, **3**, 325.
LINDHARD, J., 1954, *K. Danske Vidensk. Selsk.*, **28**, No. 8.
VLASOV, A., 1945, *J. Phys., Moscow*, **9**, 25.

The Elastic Scattering of 98 MeV Negative Pions by Hydrogen

By D. N. EDWARDS, S. G. F. FRANK AND J. R. HOLT
Nuclear Physics Research Laboratory, University of Liverpool

Communicated by H. W. B. Skinner; MS. received 8*th December* 1958, *in final form* 6*th February* 1959

Abstract. The elastic scattering by hydrogen of negative pions with mean energy 98 MeV has been measured at 13 angles between 30° and 150° (lab.). The pion beam was monitored with a calibrated ionization chamber and its muon and electron contamination determined by means of a Čerenkov counter. This counter was also used in the scattering telescope to separate out the electrons produced by charge exchange γ-radiation. The results were corrected for Coulomb effects and a 3-parameter curve fitted to the nuclear parts. The curve is $d\sigma/d\Omega = (1 \pm 0{\cdot}027)\,[0{\cdot}385 \pm 0{\cdot}008 + (0{\cdot}276 \pm 0{\cdot}015)\cos\theta + (0{\cdot}282 \pm 0{\cdot}031)\cos^2\theta]$.

Thus the forward scattering intensity is $0{\cdot}942 \pm 0{\cdot}043$ mbn sterad^{-1}. In a separate transmission experiment the total nuclear cross section for scattering of 98 MeV negative pions by hydrogen was found to be $21{\cdot}9 \pm 0{\cdot}7$ mbn. These two figures yield a value for the real part of the forward scattering amplitude $D_- = 0{\cdot}195 \pm 0{\cdot}006$ in units $\hbar/m_\pi c$. The corresponding value of f^2 from the dispersion relation is 0·073.

---

§ 1. INTRODUCTION

DURING the past few years a considerable amount of experimental work has been done on the differential scattering by hydrogen of beams of positive and negative pions having energies up to about 500 MeV (see reviews by Gell-Mann and Watson 1954 and Lindenbaum 1957, also Barnes *et al.* 1958 and Zinov and Korenchenko 1958). These experimental results have usually been expressed in terms of the six phase shifts in the S- and P- states with isotopic spin 1/2 or 3/2 (see Bethe and de Hoffmann 1955). Whereas the large resonant phase shift α_{33} has been well determined over a wide energy range, the information on the smaller phase shifts is much less satisfactory and the primary aim of the present work was to improve the knowledge of these. Recently a suggested discrepancy in the application of dispersion relations to the scattering process has lent added point to the results.

Much more work has been done on the scattering of positive pions than of negative pions because of certain difficulties peculiar to the latter. In the energy region we are considering the differential cross section for elastic scattering of negative pions is smaller by a factor of 9 than for positive pions and is only about half that for charge exchange scattering. Fast electrons produced by the latter process through interactions of the neutral pion decay γ-radiation may comprise up to 50% of the particles detected at certain angles of scattering in experiments with negative pions.

Also, because negative pions are accepted in the forward direction from the target in the cyclotron, as opposed to the backward direction for positive pions beams of negative pions are usually contaminated with high energy electrons as well as muons, and a careful determination of the composition of the beam is an important part of the measurements.

In the present work a water Čerenkov counter was used to analyse the beam and also to determine the proportion of electrons amongst the scattered particles.

In order to take advantage of the high intensity of the negative pion beam of the Liverpool synchrocyclotron the beam was monitored with an ionization chamber rather than with a counter telescope as in previous work.

§ 2. APPARATUS

Negative pions produced in a beryllium target are focused by a double quadrupole magnet and then deflected through 30° and focused horizontally by a sector shaped field. The flux at the focus is about 100 000 pions per second through an area 10 cm high by 8 cm broad. The area of the beam was reduced by means of the copper collimator C (figure 1) 5·0 cm × 2·5 cm, the flux then being about 30 000 per second. The maximum instantaneous rate was about 10^6 per second, since the beam was modulated in bursts about 300 μsec in duration with a repetition rate of 110 per second. No reliable scaler was available for such a counting rate so the beam was measured, after passing through the target, by an air-filled ionization chamber I.

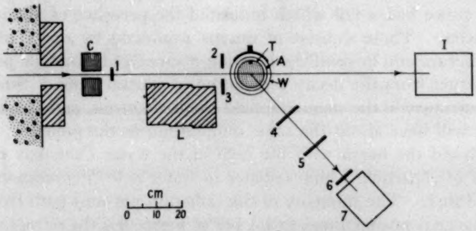

Figure 1. Plan of scattering experiment.

The target was liquid hydrogen contained in a cylindrical cup T of ' Vibrac ' steel 9·2 cm in diameter and of wall thickness 0·05 mm. This was joined to a spherical reservoir of capacity 30 litres, surrounded by a liquid nitrogen jacket. Suspended from the bottom of the latter was a cylindrical radiation shield of aluminium A, 0·05 mm thick, surrounding the target. The window W of the target box was 10 cm high and covered with Mylar 0·2 mm thick. The target could be emptied into the reservoir through a pipe which reached nearly to the bottom, by closing the gaseous hydrogen escape pipe from the top of the target and applying heat via a small electric element. The hydrogen level was indicated through the electrical capacity between pairs of plates at the top and bottom of the target.

Scattered particles were detected with a telescope of three plastic scintillation counters, 10 cm × 10 cm, 10 cm × 10 cm, and 7·5 cm diameter, all 6 mm thick. The last was the defining counter placed 50 cm from the centre of the target. Behind it was a Čerenkov counter 7 consisting of a cylindrical glass container 12·5 cm in diameter and 15 cm long filled with water and mounted on a 5 in.

EMI 6099 photomultiplier. All the other counters used EMI 6260 photomultipliers.

To reduce the background counts in the telescope to reasonable proportions it was necessary to place a coincidence counter 1 in the beam beyond the collimator, and anticoincidence counters 2 and 3 on either side of the beam near the target. These latter helped to eliminate particles scattered into the telescope from the heavy walls of the target container and from the collimator. The lead screen L served a similar purpose. When the telescope was set at angles greater than 90° this lead and the nearer anticoincidence counter were removed.

The coincidence circuit was of the Garwin type fed by single valve head amplifiers using EFP 60 tubes. The integrator for the ionization chamber used the sensitive and stable circuit described by Lewis and Collinge (1953), which records the total charge entering it as a number of 'clicks', each click corresponding to a definite quantity of charge.

§ 3. Experimental Procedure

3.1. *Determination of the Composition of the Beam*

By absorption in copper the mean energy of the pion beam at the centre of the hydrogen was determined to be 98 Mev, the spread in energy being about $\pm 4{\cdot}5$ Mev. In addition there is a loss in energy of 3 Mev as the pions traverse the target. The absorption curve had a tail which indicated the presence of about 10% of long range particles. These consist of muons produced by decay of the pions in flight both before and beyond the bending magnet and electrons produced in the beryllium target from the decay γ-radiation of neutral pions. Since they follow the same trajectory in the magnetic field these electrons, and also the majority of the muons, will have about the same momentum as the pions.

We analysed the beam with the help of the water Čerenkov counter. The minimum β of a particle which radiates in water is 0·75 corresponding to pions of energy 73 Mev. The intensity of the radiation per unit path from particles of the same charge is proportional to $1-1/\beta^2 n^2$ where n is the refractive index of the medium. Allowing for the slowing down of the particles after entering the counter we find for the ratio of intensities of the radiation from the pions, muons and electrons in the beam approximately 1 : 5 : 15.

A telescope consisting of two scintillators followed by the Čerenkov cell was placed in the beam at the position normally occupied by the target. The pulses from the Čerenkov cell, after linear amplification were gated by double coincidences from the scintillators and passed to a 50-channel pulse height analyser. A representative spectrum obtained in this way is displayed in figure 2. The separation into electron and muon groups is clear and by comparing the number of pulses within these groups with the corresponding number of double coincidences the composition of the beam was determined. This varied slightly on different occasions and was about 86% pions, 11% electrons and 3% muons.

3.2. *Alignment of Apparatus*

In order to fix the position of the target the beam was first scanned at the focus by a vertical strip of scintillator, 6 mm wide whose horizontal position could be varied remotely. In this way the profile of the beam was measured and the positions of the two anticoincidence counters adjusted so that they clipped off the tails of the beam. The total width of the beam was about 5 cm. The scintillator was then moved to the centre of this profile and used to enable a pointer to be rigidly fixed in the same vertical line and some distance below the plane of the beam. The counter having been removed, the turntable with the liquid hydrogen target mounted at the centre was wheeled into position. The centre of the hydrogen cup had been adjusted to be exactly over the centre of the turntable with the help of sighting holes cut in the aluminium radiation shield and the centre of the table was then moved to coincide with the fixed pointer. It was then known that the beam would pass centrally through the cup and the shape of the illuminated volume of hydrogen could be determined from the beam profile and the dimensions of the cup.

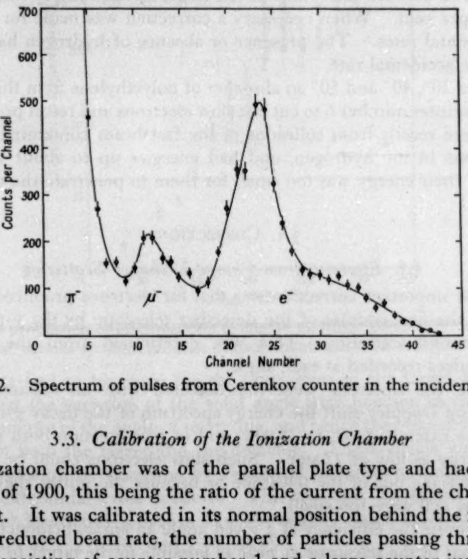

Figure 2. Spectrum of pulses from Čerenkov counter in the incident beam.

3.3. *Calibration of the Ionization Chamber*

The ionization chamber was of the parallel plate type and had a multiplication factor of 1900, this being the ratio of the current from the chamber to the beam current. It was calibrated in its normal position behind the full target by counting, at reduced beam rate, the number of particles passing through it with a telescope consisting of counter number 1 and a large counter just behind the target together with the two anticoincidence counters. Various values of beam intensity were used and an extrapolation made to zero intensity to eliminate the effect of counting losses in the fast scaler. This calibration was performed at the start and finish of every run on the cyclotron and frequent intermediate checks made with a 1 mc radium source placed in a standard position on the ionization chamber. The drift was less than 2% over a period of a week and the necessary corrections were made for this.

3.4. *Measurements*

Measurements of the number of scattered particles were made at intervals of 10° between 30° and 150°. The quadruple coincidences between counters 1, 4, 5 and 6 with 2 and 3 in anticoincidence were counted for a certain number of clicks of the ionization chamber integrator with the target alternately full and empty and the time also measured. The spectrum of pulses from the Čerenkov counter, gated by these coincidences, was also recorded on a pulse height analyser. From this the number of electrons in the scattered beam could be deduced.

The counting rate varied from about 40 per minute at 30° to 12 per minute at 150°. Over most of the angular range about 50% of this rate was background which persisted when the cup was emptied of hydrogen; at the extreme backward angles the proportion increased to 70%. By placing a cable having a delay of one r.f. period in the lead from counter number 1 it was found that about half this background consisted of accidental coincidences between this counter and the rest. The number of accidentals per click of the monitor is proportional to the beam intensity. However, the constancy of the beam was such that the time difference between the runs with the target full and empty was rarely greater than a few per cent. When necessary a correction was made for the difference in the accidental rates. The presence or absence of hydrogen had a negligible effect on the accidental rate.

At angles 30°, 40° and 50° an absorber of polyethylene 5 cm thick was placed in front of counter number 6 to cut out slow electrons and recoil protons. These electrons were recoils from collisions of the fast beam contamination electrons with electrons in the hydrogen, and had energies up to about 10 MeV at 30°. Beyond 50° their energy was too small for them to penetrate the counters.

§ 4. CORRECTIONS

4.1. *Electrons from Charge Exchange Scattering*

The most important correction was that for electrons produced in the target wall and in the first counter of the detecting telescope by the γ-radiation from charge exchange scattering. This was determined from the spectrum of Čerenkov pulses recorded at each angle.

However, the electrons were not detected with an efficiency of 100%. Because of the Doppler shift the energy spectrum of the decay γ-radiation from neutral pions extends down to 24 MeV, and in pair creation both members may have an energy as low as 12 MeV. Such slow electrons could be missed either through scattering out of the telescope or because the pulses they produced in the Čerenkov cell were too small.

To determine the efficiency at a given angle an anticoincidence counter was placed in front of the telescope as near as possible to the target to veto scattered charged particles. Immediately behind it was a 3 mm thick copper radiator in which the charge exchange γ-rays produced electrons. These were detected by the telescope and the gated Čerenkov spectrum recorded. The efficiency of the Čerenkov counter above a certain pulse level, which was fixed at the valley between the pion tail and muon peak in the spectrum of the direct beam, could then be obtained. This procedure was repeated at several angles and the efficiency found to be nearly constant at about 70%.

At angles greater than 70° the energy of the scattered pions is such that they come to rest within the Čerenkov counter. To make sure that the resulting nuclear stars were not effective in producing pulses a test was made in the direct pion beam, reduced in energy by various thicknesses of absorber. No such pulses were found. In figure 3 the electron correction is shown as a function of angle in terms of a percentage of the total number of scattered particles.

4.2. *Angular Corrections*

The solid angle for acceptance of scattered particles is defined primarily by the area of counter number 6 and the distance between the centre of this counter and the centre of the target.

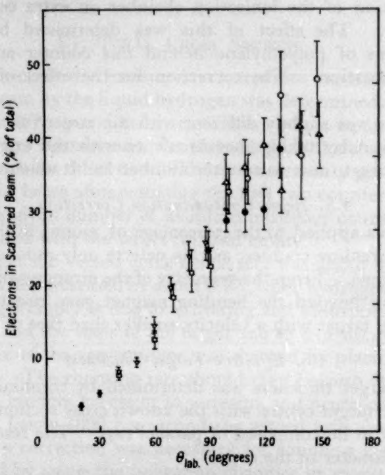

Figure 3. The proportion of electrons due to charge exchange γ-radiation in the scattered beam. The various symbols indicate measurements made on different occasions.

Corrections had to be made for the finite sizes of the target and detector. These involved the variation of the solid angle with position in the target and also the dependence of the angle of scattering, and hence the intensity of scattering on position in both the target and the detector. These effects were evaluated for several angles of the telescope by numerical integration, making use of the uncorrected differential cross sections. The resultant correction to the solid angle was much less than 1% over most of the angular range, increasing at smaller angles to values of 1% at 40° and 1·4% at 30°.

An uncertainty in the solid angle arises from the finite thickness of the defining counter. The effective plane of detection depends on the depth of penetration of a particle which produces a pulse of threshold size. The uncertainty was estimated to be 2 mm on either side of the median plane of the scintillator, giving an uncertainty of $\pm 0{\cdot}8\%$ in solid angle.

4.3. *Telescope Efficiency*

The first two counters of the telescope were made sufficiently larger than the third so that particles scattered out through small angles by multiple Coulomb scattering to miss the third counter were compensated by particles similarly scattered in. Decay of pions in flight between the target and detector leads to a loss much less than 1% since most of the decay muons are registered.

However, there is still some loss due to nuclear absorption and large angle scattering. The correction for this was determined in the direct pion beam by placing extra absorbers near counters number 4 and 5; it amounted to 3%. The correction for loss in the absorber used at small scattering angles in front of counter number 6 was determined in the same way and was 6%.

4.4. *Ionization Chamber Corrections*

In the calibration of the ionization chamber an extra counter was placed behind the target. The effect of this was determined by introducing an additional thickness of polyethylene behind this counter and measuring the change in the calibration. The correction for the effect of the counter was 1·3%.

The calibration was slightly different with the target full and empty. The difference was found by taking measurements with the extra counter on the other side of the target, near to counter number 1. It amounted to 1·3%.

4.5. *Beam Contamination Correction*

A correction was applied to the percentage of muons in the beam as determined with the Čerenkov counter, as this detects only muons having a greater velocity than the pions. From the geometry of the arrangement it was estimated that pions decaying beyond the bending magnet gave rise to about 1·2% of muons entering the target with a velocity smaller than that of the pions.

4.6. *Effective Target Thickness*

The effective target thickness was determined by combining the measured beam profile at the target centre with the known cross section of the steel cup, assuming the beam to be composed of parallel rays. The result was about 4% smaller than the diameter of the cup.

§ 5. ERRORS

The differential cross section is expressed in terms of the following measured quantities; (i) the number of counts in the telescope due to scattered pions for one click of the ionization chamber current integrator, (ii) the effective solid angle of the telescope for scattered pions, (iii) the number of pions passing through the target for one click and (iv) the effective number of hydrogen atoms in the target.

The first was based on several measurements at each angle during two or three runs with the cyclotron. Altogether there were six runs, each of about ten days duration, three for the forward angles and three for the backward angles. The error on this quantity is mainly a statistical one, with a small contribution from the uncertainty in the subtraction of the electrons from charge exchange scattering. The standard deviation ranged between 2½% and 11%.

The error in the effective solid angle is mainly due to the uncertainty in the plane of detection of the defining counter together with a smaller error in the correction for the integration over the target. The overall deviation was estimated to be ± 1%. In addition there is an uncertainty of ± 0·5% in the detection efficiency of the telescope.

The error in (iii) involves the uncertainty in the composition of the beam and in the ionization chamber calibration. The deviations were estimated to be ± 2% and ± 1% respectively.

The error in (iv) includes those in the effective target thickness and in the densities of hydrogen liquid and vapour (0·0709 g cm^{-3} and 0·0013 g cm^{-3}

respectively, Woolley, Scott and Brickwedde 1948). A deviation of ±1% was assigned.

The errors in the quantities (ii), (iii), and (iv) are practically independent of the angle of detection and it is convenient to combine them. The result is a standard deviation of 2·7%.

§ 7. Total Cross Section

The total cross section was measured in a separate experiment in which the attenuation of the beam by the liquid hydrogen was determined. The beam was defined and monitored by two circular scintillators 3·8 cm in diameter and 4 mm thick. A third counter 10 cm square was placed behind the target and connected in anticoincidence with the other two. Thus we count only particles which have disappeared from the beam after actuating the first two counters. The number of such counts for a given number of double coincidence counts in the defining counters was measured with the target full and empty.

With empty target the vetoed coincidence rate was about 4% of the double coincidence rate and this increased by about 0·7% when hydrogen was introduced. The effect with target empty is due to scattering and absorption of the beam in the second counter and the walls of the target and to π–μ decays.

The performance of the veto counter was checked by placing it between the other two counters. The counting rate should then be zero apart from double coincidences due to random events or to γ-quanta and neutrons. In fact, if the beam rate was kept below 1000 per second the vetoed rate was effectively zero.

With this beam a correction was necessary for counting loss in the scalers; this was determined by using the ionization chamber to monitor the beam and plotting a curve of counts per click of the monitor against counts per second. This was a straight line which could be extrapolated to zero counts per second to give the true number of counts per click. The correction for counting loss was 3% at 1000 per second.

Several series of measurements were made with the target alternately full and empty and with the centre of the veto counter at distances 12·60, 13·65, 18·90 and 23·85 cm from the target centre. The difference between the counting rates with full and empty target increased by about 8% over this range of distances.

The corrections for beam contamination and the determination of the mean target thickness were made according to the procedure already described. The rate in the beam counters was corrected for attenuation in the second counter and in half the target to give the beam rate at the centre of the target. This correction was 1·5 ± 0·5%. Recoil protons from backward scattered pions may enter the veto counter and cause a reduction in counting rate. The correction to the total cross section was estimated to be 0·55 mbn when the veto counter was closest to the target and 0·19 mbn for the farthest position.

In order to determine the total cross section for nuclear scattering over the whole angular range from 0° to 180° a correction which depends on the angles subtended at the target by the periphery of the veto counter has to be made. Nuclear scattering into small angles is not detected because the scattered pions enter the veto counter. On the other hand scattering due to Coulomb and Coulomb–nuclear interference effects which extends to angles beyond the veto counter is detected.

The correction for these two effects was made with the help of the results of the differential cross section measurements and the separation of the nuclear scattering from the rest which is described below. The procedure was a graphical one and the corrections to the total cross section for the four positions of the veto counter were (in mbn) $-0{\cdot}2\pm0{\cdot}1$, $-0{\cdot}4\pm0{\cdot}2$, $-0{\cdot}9\pm0{\cdot}2$ and $-1{\cdot}5\pm0{\cdot}5$ in order of increasing distance from the target. A correction of 1·4% for random coincidences was also applied.

The four corrected values of the total nuclear cross section were consistent. A final correction of 2% was applied for the known energy spread of the beam using an approximate form of variation of cross section with energy. The result was $21{\cdot}9\pm0{\cdot}7$ mbn where the error includes contributions from the various corrections as well as the statistical one.

§ 8. RESULTS

The measured values of the differential cross section are given in column 2 of the table and are plotted in figure 4. The quoted errors are the angle dependent

(1)	(2)	(3)	(1)	(2)	(3)
36·6	1·101 ± 0·054	0·748	112·3	0·321 ± 0·017	0·333
48·4	0·840 ± 0·042	0·680	121·5	0·327 ± 0·019	0·342
60·1	0·718 ± 0·019	0·637	130·6	0·336 ± 0·022	0·353
71·2	0·531 ± 0·017	0·490	139·2	0·319 ± 0·021	0·338
82·0	0·402 ± 0·020	0·385	147·8	0·296 ± 0·029	0·316
92·5	0·363 ± 0·019	0·360	156·0	0·302 ± 0·036	0·322
102·6	0·331 ± 0·016	0·337			

(1) Angle of scattering (c.m.) (in degrees); (2) measured differential cross section (c.m.) (in mbn sterad^{-1}), in addition to the standard deviations shown there is a contribution of ±2·7% common to all angles; (3) nuclear part of the differential cross section after subtracting Coulomb effects.

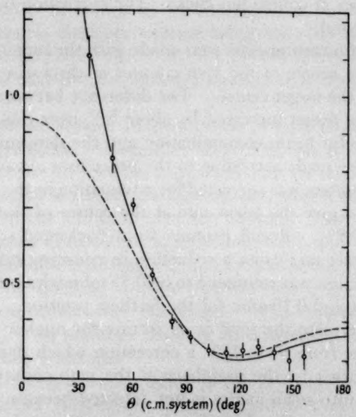

Figure 4. Differential cross section (c.m.) for elastic scattering of 98 MEV negative pions by hydrogen. The solid curve is a least squares fit to the data, the broken curve represents the nuclear part of the scattering after subtraction of Coulomb effects.

ones. In addition there is a common error of ±2·7%. At the energy of this experiment only S and P waves are expected to be scattered appreciably by the nucleon field so the differential cross section due to this scattering should follow the form

$$\frac{d\sigma}{d\Omega}=a+b\cos\theta+c\cos^2\theta. \qquad \ldots\ldots (1)$$

We have made a least squares fit to our data using this form with the addition of Coulomb terms. The differential cross section can then be written

$$\frac{d\sigma}{d\Omega}=|x+y\cos\theta+f'|^2+|z\sin\theta+f''|^2 \qquad \ldots\ldots (2)$$

where the first term represents scattering without spin flip and the second term scattering with spin flip. The quantities x, y, z, are scattering amplitudes related in the following way to a, b, c:—

$$a=|x|^2+|z|^2, \quad b=2\mathcal{R}x^*y, \quad c=|y|^2-|z|^2$$

while f' and f'' are the Born approximation Coulomb amplitudes, without and with spin flip, given by Solmitz (1954).

We aim to evaluate the scattering intensity due to coulomb effects at each of our angles of measurement and by subtraction get the pure nuclear intensity. Since the Born approximation Coulomb amplitude is real it interferes only with the real part of the nuclear amplitude. The imaginary parts of x, y, and z were estimated by expressing them in terms of phase shifts and using approximate values of the latter by interpolation of known data. These values of x, y, and z inserted into the expression for the differential cross section gave an angular distribution everywhere less than 10% of the measured one. This was subtracted and the following iterative procedure then used. Firstly the experimental data were fitted by a least squares method to the approximate form,

$$\frac{d\sigma}{d\Omega}=a+b\cos\theta+c\cos^2\theta+\frac{d}{1-\cos\theta}$$

to obtain rough values of a, b, and c. These were used to obtain values of x, y, and z taking them to be real quantities.

Equation (2) was then evaluated both with and without the Coulomb amplitude and the difference gave the first approximation to the Coulomb effects. These were subtracted from the experimental points and a least squares fit to the remaining nuclear scattering made to the form of equation (1). The values of a, b and c so found were used in turn to evaluate a better approximation for the Coulomb effects. After the first two iterations the results converged rapidly. The nuclear cross sections obtained by subtracting these Coulomb components from the measured cross sections are displayed in column (3) of the table. The least squares fit to the data and the nuclear cross section curve are shown in figure 4. The latter curve is

$$\frac{d\sigma}{d\Omega}=(1\pm0{\cdot}027)\;[0{\cdot}385\pm0{\cdot}008+(0{\cdot}276\pm0{\cdot}015)\cos\theta+(0{\cdot}282\pm0{\cdot}031)\cos^2\theta].$$

A test of the goodness of the fit to the data is provided by computing $M=\Sigma_i(\Delta_i/\epsilon_i)^2$ where Δ_i is the deviation of the ith experimental points from the curve and ϵ_i its standard deviation. The value found is 18·9 whereas the expected value is $M_0=10$ (the number of points minus the number of parameters).

Possible reasons for this large value might be that the errors assigned to the points are too small or that a three parameter fit is inadequate. In fact an M-value much closer to M_0 could be obtained using five parameters. On the other hand the large value may be just a statistical fluctuation, the probability being about 1 in 20, and we are inclined to favour this explanation.

The total nuclear cross section for elastic scattering is given by $4\pi(a+1/3c)$ which is $6{\cdot}15 \pm 0{\cdot}22$ mbn. The corresponding cross section for charge exchange scattering can be obtained by subtracting this figure from the total cross section measured by attenuation, making an allowance for the small contribution from the reaction $\pi^- + \mathrm{p} \rightarrow \mathrm{n} + \gamma$. The cross section for this process was estimated from known photo-production cross sections to be $0{\cdot}7 \pm 0{\cdot}2$ mbn. Thus we find for the total nuclear cross section for charge exchange scattering $15{\cdot}0 \pm 0{\cdot}8$ mbn.

Considerable interest has recently been centred on the application of dispersion relations to pion–proton scattering. The real part of the forward scattering amplitude D can be expressed in terms of an integral of the total cross section over all energies and a term involving the pion–nucleon coupling constant f^2.

The forward scattering intensity can be written in the form $|F|^2 = |D+iA|^2$. The nuclear part of our angular distribution yields

$$|F|^2 = 0{\cdot}942 \pm 0{\cdot}043 \text{ mbn sterad}^{-1}$$

where the error is derived from the error matrix of the least squares fit and the $2{\cdot}7\%$ angle independent error.

Additional uncertainty in the value of $|F|^2$ is introduced by our lack of knowledge concerning the scattering of D waves. Our extrapolation to the forward direction could be altered by a few per cent if the D phase shifts were a few tenths of a degree and such values cannot be excluded. However, in view of the uncertainty about the precise form of the curve we prefer to use a three-parameter fit and the value of $|F|^2$ and its error are based on this assumption.

The imaginary part A of the forward scattering amplitude can be derived from the total cross section by the optical theorem (Schiff 1955):

$$\sigma_{\text{tot}} = \frac{4\pi}{\eta} A = 21{\cdot}9 \pm 7 \text{ mbn}.$$

Using these results we obtain

$$D_- = 0{\cdot}195 \pm 0{\cdot}006 \text{ in units of } \hbar/m_\pi c.$$

Puppi and Stanghellini (1957) used a total cross section curve consistent with the data (figure 5) then available to compute the integral parts of the dispersion relations for D. The term involving f^2 could then be used to adjust the integral term to fit experimental values. Over the energy interval up to 400 MeV all the experimental results for the real part of the forward scattering amplitude for the scattering of positive pions by protons were consistent with a coupling constant $f_+^2 = 0{\cdot}09 \pm 0{\cdot}01$. For negative pions, however, the results below the resonance required $f_-^2 = 0{\cdot}04$. Fundamental symmetry requirements of local field theory require that $f_+^2 = f_-^2$ and several attempts have been made to reconcile the experimental results with the dispersion theory. The integral term is sensitive to the energy dependence of the total cross sections in the region approaching the resonance and Zaidi and Lomon (1957) showed that the large experimental errors in the known values of these cross sections about 100 MeV enabled the discrepancy to be considerably reduced by suitable choice of the energy dependence (figure 5).

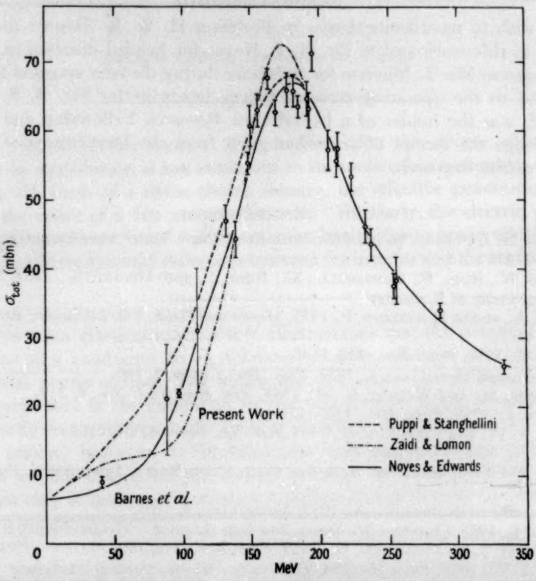

Figure 5. Total cross section for scattering of negative pions by hydrogen as a function of energy. The curves are those used in three investigations of the dispersion relations.

Our value for the total cross section and the recent value of Barnes *et al.* (1958) at 42 MeV are not consistent with the curves used either by Puppi and Stanghellini or by Zaidi and Lomon. Using these new values of total cross sections Noyes and Edwards (1958, private communication) fitted a curve to all the available experimental points, using a form corresponding to a P wave resonance below 350 MeV (figure 5) and a polynominal expression at higher energies. This curve agrees closely with those given by Anderson (1956) and by Piccioni (1956). Making use of this curve the Orear scattering lengths ($a_1 = 0{\cdot}165$ and $a_3 = -0{\cdot}105$) and the experimental value of D_- the dispersion relation was applied to determine f^2. The value found was 0·073. An error of ±0·003 should be attributed to this on account of the error in D_- and other errors of the same order come from the uncertainties in the scattering lengths and from that in the integral over the total cross sections. Thus we feel that our value for f^2 is not inconsistent with a figure of 0·08 which would also be compatible with the existing data on positive pion scattering.

Analyses of the discrepancies in the application of dispersion relations to pion–proton scattering have recently been made by Hamilton (1958), Chiu (1958), Schnitzer and Salzman (1958) and Chiu and Hamilton (1958). It remains difficult to fit the negative pion results above 100 Mev with $f^2 = 0{\cdot}08$ and there is an obvious need for more accurate experimental results.

ACKNOWLEDGMENTS

We wish to record our thanks to Professor H. W. B. Skinner for his close interest in this work and to Dr. H. P. Noyes for helpful discussions. Thanks are due also to Mr. T. Massam for assistance during the later stages of the experiment and to the operating crew of the cyclotron under Mr. B. S. Halliday. D. N. E. was the holder of a Leverhulme Research Fellowship and wishes to acknowledge the receipt of an earlier grant from the Department of Scientific and Industrial Research.

REFERENCES

ANDERSON, H. L., 1956, *Proc. 6th Rochester Conf.* (New York: Interscience Publications), p. I–23.

BARNES, S. W., ROSE, B., GIACOMELLI, G., RING, J., and MIYAKE, K., 1958, NYO-2170, University of Rochester.

BETHE, H. A., and DE HOFFMANN, F., 1955, *Mesons and Fields*, Vol. 2 (Illinois: Row, Peterson & Co.).

CHIU, H-Y., 1958, *Phys. Rev.*, **110,** 1140.

CHIU, H-Y., and HAMILTON, J., 1958, *Phys. Rev. Letters*, **1,** 146.

GELL-MANN, M., and WATSON, K. M., 1954, *Ann. Rev. Nucl. Sci.*, **4,** 219.

HAMILTON, J., 1958, *Phys. Rev.*, **110,** 1134.

LEWIS, I. A. D., and COLLINGE, B., 1953, *Rev. Sci. Instrum.*, **24,** 1113.

LINDENBAUM, S. J., 1957, *Ann. Rev. Nucl. Sci.*, **7,** 317.

PICCIONI, O., 1956, *Proc. 6th Rochester Conf.* (New York: Interscience Publications), p. IV–7.

PUPPI, G., and STANGHELLINI, A., 1957, *Nuovo Cim.*, **5,** 1305.

SCHIFF, L. I., 1955, *Quantum Mechanics*, 2nd Edn (London: McGraw-Hill), p. 105.

SCHNITZER, H. J., and SALZMAN, G., 1958, *Phys. Rev.*, **112,** 1802.

SOLMITZ, F. T., 1954, *Phys. Rev.*, **94,** 1799.

WOOLLEY, H. W., SCOTT, R. B., and BRICKWEDDE, F. G., 1948, *J. Res. Nat. Bur. Stands*, **41,** 379.

ZAIDI, M. H., and LOMON, E. L., 1957, *Phys. Rev.*, **108,** 1352.

ZINOV, V. G., and KORENCHENKO, S. M., 1958, *Soviet Phys. J.E.T.P.*, **6,** 260, 1006.

Charge Penetration into a Conductor in Equilibrium

By R. FÜRTH and E. MORRIS†
Birkbeck College, University of London

MS. received 22nd January 1959

Abstract. Statistical mechanics is used to show that the electric charge on a conductor in equilibrium is not restricted to its surface but penetrates into the interior in the form of a space charge density, the effective penetration depth being of the order of a few atomic distances. Similarly, the electric potential in a charged conductor is not strictly constant but varies in space which results in a small but finite potential difference between the interior and the surface layers.

It follows from classical macroscopic electrostatics that the potential v in the interior of a conductor in equilibrium must be constant and equal to the potential at the surface, and hence that the space charge density ρ must vanish everywhere in the conductor so that any charge on the conductor must reside strictly on its surface in the form of a surface charge density σ.

This cannot, however, be literally true because the charge carriers in a conductor are not at rest but perform an irregular movement. Thus in actual fact v must vary in space, and instead of a surface charge density there must be a varying space charge density.

The authors were unable to find a reference to this problem in the literature and they therefore present in this paper the solution, derived from statistical mechanics, although the final results are almost trivial from the physical point of view. Use is made of the Sommerfeld model of a metal in which the ionic potential is smoothed out, and the possible existence of quantum surface states is not taken into consideration. These alter only the detailed interpretation of the results and not their main import. More relevant to the method is that the energy states immediately available to the conduction electrons should range over a 'band'.

The total charge, fixed ions plus variable electron gas, at any point in the conductor, must be in statistical equilibrium with the charge at any other point, and must also give rise to an electrostatic potential obeying Poisson's equation. This combination of statistical mechanics and electrostatics seems to have been first used by von Laue (1918) in a discussion of space-charge distributions in electronic valves. It is also much used in the discussion of the charge distribution near the interface of two semiconductors (Shockley 1950).

At any given position in the condutor, the fraction of electrons $f(E)$ in an energy state E, is given by the Fermi–Dirac distribution function

$$f(E)=\frac{CE^{1/2}}{\exp(-B+E/\boldsymbol{k}T)+1} \qquad \ldots\ldots(1)$$

where C is a constant, and T is the uniform temperature of the conductor.

---

† Now at Dept. of Physics, University of Syracuse, Syracuse, N.Y., U.S.A.

The chemical potential B, is here to be calculated with respect to the local energy zero which, because of the possibly varying potential v, need not be the same at different points of the conductor.

However, the requirement for statistical equilibrium is that the chemical potential at each point of the conductor, measured with respect to a consistent zero, should be the same. Thus, if suffixes 1 and 2 refer to two different positions in the conductor, the condition for equilibrium is

$$B_1 - \boldsymbol{e}v_1 = B_2 - \boldsymbol{e}v_2 \quad \text{or} \quad B_1 - B_2 = \boldsymbol{e}(v_1 - v_2) \qquad \ldots\ldots(2)$$

where $\boldsymbol{e}$ is the magnitude of the electronic charge.

It is well known (e.g. Fowler and Guggenheim, 1939, eqns. 1102, 10 and 1104, 9) that

$$B = g\left(1 - \frac{\pi^2}{12}\frac{\boldsymbol{k}T^2}{g} + \ldots\right), \qquad \ldots\ldots(3)$$

where

$$g = \frac{\boldsymbol{h}^2}{8\boldsymbol{m}}\left(\frac{3n}{\pi}\right)^{2/3}. \qquad \ldots\ldots(4)$$

Here n is the density of electrons, about $10^{23}\,\mathrm{cm}^{-3}$, $\boldsymbol{m}$ the mass of the electron, and $\boldsymbol{h}$ Planck's constant.

It will be valid to neglect all but the first term of the right-hand side of equation (3) if $\boldsymbol{k}T/g \ll 1$, that is $\boldsymbol{k}T \ll 10^{-10}$, or $T \ll 6 \times 10^5$ deg K, and this approximation is seen to be valid for all temperatures at which the conductor remains solid.

We are now in a position to connect the variable electron number density n, and the potential v. From equations (2), (3) and (4) one obtains easily

$$n_1 = n_0(1 + \boldsymbol{e}v/g_0)^{3/2} \qquad \ldots\ldots(5)$$

where the zero of potential has been chosen at the position where $n = n_0$. If $|\boldsymbol{e}v/g_0| \ll 1$, then equation (5) can be expanded giving the approximate expression

$$n = n_0(1 + 3\boldsymbol{e}v/2g_0). \qquad \ldots\ldots(6)$$

The validity of this approximation will be investigated later.

It is convenient to choose the zero of potential to be also at a point where there is no net charge, that is we put $\boldsymbol{e}n_0 = \rho_0$ where ρ_0 is the constant positive charge density of the fixed ions. The charge density of the electron gas ρ_1, is given by $\rho_1 = -\boldsymbol{e}n_1$ and the total charge density, $\rho = \rho_1 + \rho_0$, by

$$\rho = \boldsymbol{e}(n_0 - n_1) = -3n_0\boldsymbol{e}^2v/2g_0. \qquad \ldots\ldots(7)$$

The charge density is also connected to the potential by Poisson's equation

$$\nabla^2 v = -4\pi\rho = 6\pi\boldsymbol{e}^2 n_0 v/g_0 = v/\zeta^2. \qquad \ldots\ldots(8)$$

where

$$\zeta = (6\pi n_0 \boldsymbol{e}^2/g_0)^{-1/2} \qquad \ldots\ldots(9)$$

has the dimension of a length. From equations (7) and (9) we have

$$\rho = -v/4\pi\zeta^2. \qquad \ldots\ldots(10)$$

The quantity ζ plays the part of a penetration depth of charge into the surface and its magnitude is of the order of an atomic radius. For from equations (9) and (4) one has

$$\zeta^2 = \frac{\pi}{12}\frac{\boldsymbol{h}^2}{4\pi^2\boldsymbol{m}\boldsymbol{e}^2}\left(\frac{g}{n_0\pi^2}\right)^{1/3}$$

or approximately

$$\zeta^2 \simeq \tfrac{1}{4} r_{\mathrm{B}}\, d. \qquad \ldots\ldots(11)$$

Here r_B is the Bohr radius of the hydrogen atom and, provided the ratio of free electrons to ions is not grossly different from unity, d is approximately the distance between adjacent atoms in the conductor lattice. Thus ζ is of atomic size.

The physical meaning of ζ will become more apparent when the solution of equation (8) for the particular case of a sphere of radius R is considered. The solution, finite at the centre of the sphere, for the potential at a distance r from the centre is

$$v(r) = v(0)\,\frac{\sinh(r/\zeta)}{r/\zeta}. \qquad \ldots\ldots(12)$$

The corresponding distribution of charge density is, from equation (10)

$$\rho(r) = \frac{-v(0)}{4\pi\zeta r}\sinh(r/\zeta). \qquad \ldots\ldots(13)$$

The potential at the centre $v(0)$ is determined if the total charge on the sphere is known to be $4\pi R^2\sigma$. By integrating (13) over the whole interior of the sphere one finds

$$\begin{aligned} v(0) &= \frac{-4\pi R^2\sigma}{R\cosh(R/\zeta) - \zeta\sinh(R/\zeta)} \\ &\simeq \frac{-8\pi R\sigma}{\exp(R/\zeta)}, \end{aligned} \qquad \ldots\ldots(14)$$

provided that $R \gg \zeta$, a condition that will be assumed to hold from now on.

From equation (12) the potential $v(R)$ at $r = R$ is

$$v(R) = -4\pi\sigma\zeta, \qquad \ldots\ldots(15)$$

and from equation (13) the charge density $\rho(R)$ at $r = R$ is

$$\rho(R) = \sigma/\zeta. \qquad \ldots\ldots(16)$$

Also the charge density at a small distance δ from the surface, i.e. at $r = R - \delta$ is

$$\rho(R-\delta) = \rho(R)\exp(-\delta/\zeta). \qquad \ldots\ldots(17)$$

All the equations (15), (16) and (17) lead to the conclusion that the charge is effectively confined to within a distance ζ from the surface. No detailed interpretation can of course be given to equation (17), as the ionic potential can certainly not be considered to be smooth over distances of atomic size.

As $v(0) \ll v(R)$ the latter quantity is essentially the difference in potential between the interior and surface of the conductor, and hence the 'surface potential', is also the maximum value of potential occurring in equation (5). The condition for the approximate equation (6) to be valid is thus

$$4\pi\sigma\zeta\boldsymbol{e}/g_0 \ll 1$$

or

$$\sigma \ll g_0/4\pi\boldsymbol{e}\zeta \simeq 3\times10^6\ \text{e.s.u. cm}^{-2}.$$

However, the permissible surface charge density is limited by the onset of corona discharge, which occurs with densities of about 100 e.s.u. cm^{-2}. The approximation is therefore valid for all practical applications.

The results derived here can also be obtained in a different manner. Suppose that all electrons in states below the Fermi level are immovable, and that the ratio of the electrons above that level at two positions is equated to the Boltzman factor $\exp[(v_1 - v_2)/\boldsymbol{k}T]$. Then equations (8) and (9) can be recovered exactly, though under a less stringent set of approximations. This is rather a justification for the use of such methods than an alternative derivation of the result.

The existence of specific surface states only strengthens the conclusion that the excess of charge on a conductor is confined to a very few layers of ions near to the, probably irregular, surface.

REFERENCES

FOWLER, R. H., and GUGGENHEIM, E. A., 1939. *Statistical Thermodynamics* (Cambridge: University Press).
VON LAUE, M., 1918, *Jahrb. Rad. Elektr.*, **15**, 205.
SHOCKLEY, W., 1950, *Electrons and Holes in Semiconductors* (New York : van Nostrand).

On the Measurement of π^+ Meson Photoproduction from Hydrogen near Threshold

By G. M. LEWIS and R. E. AZUMA
Department of Natural Philosophy, The University, Glasgow

MS. received 11*th December* 1958, *in final form* 11*th February* 1959

Abstract. A new counter method has been developed for measuring π^+ meson photoproduction near threshold. It has been employed, in particular, to examine the variation with energy of the differential cross section from hydrogen, at laboratory angles of 115° and 90° to the gamma-ray beam of the Glasgow synchrotron. Polythene and carbon targets were used. Results are compared with theory and an assessment can be made of the matrix element in the gamma-ray range 165–190 MEV. Values of absolute cross section at various energies were also obtained, e.g. for an angle of 90° and a gamma-ray energy of 170 MEV, the absolute differential cross section in centre-of-mass coordinates is $(0{\cdot}48 \pm 0{\cdot}11) \times 10^{-29}$ cm^2 per steradian. The measurements also confirm the generally accepted value of the π^+ meson lifetime.

---

§ 1. INTRODUCTION

An experimental examination of the variation with gamma-ray energy of the differential cross section of π^+ meson photoproduction close to threshold is of considerable importance, since there exist very few experimental data which can be compared with theoretical predictions of the variation in this region. The precise experimental form of this variation is not known, and even the general trend has, in the main, to be inferred by extrapolation from experimental points away from threshold.

The differential π^+ meson cross section near threshold, in centre-of-mass coordinates will be given by

$$\frac{d\sigma}{d\Omega} = \frac{2e^2f^2}{\mu^2}\left\{p\epsilon\left(1+\frac{\omega}{M}\right)^{-2}\right\}H^2 \qquad \ldots\ldots(1)$$

where p is the momentum and ϵ the energy (including the contribution from the rest mass μ) of the meson, and ω is the gamma-ray energy, all in centre-of-mass coordinates: M is the nucleon mass and c has been taken as unity. Here f is the coupling constant, the bracketed term relates to the density of final states in the theory and to the cross section kinematics, while H is proportional to the matrix element of the transition (cf. Beneventano *et al.* 1956). The value of H^2 can be expected to be of the form

$$H^2 = \frac{1}{\omega\epsilon}\left[1 - \frac{\mu^2}{2\omega^2}\frac{v^2\sin^2\theta}{(1-v\cos\theta)^2} + g_{\mathrm{M}}\right] \qquad \ldots\ldots(2)$$

where v is the meson velocity in units of c, and θ the angle of π^+ emission to the gamma-ray beam, all in centre-of-mass coordinates, and g_{M} is a function which includes recoil effects and higher order terms (cf. Chew 1954, Marshak 1952).

To a first approximation, near threshold, H^2 is then only slowly varying and $d\sigma/d\Omega$ can be expected to vary predominantly as p and to be isotropic. (This is associated with the dominant role of the negative energy nucleon intermediate states in pseudoscalar coupling theory.) Since there are few experimental results in this region to confirm the above predictions it seemed desirable to examine the variation of the cross section as a function of p, and from this to determine the feasibility of measuring any departure from constancy of H^2. The possible variation of H^2 has recently been discussed in the interpretation of π^-/π^+ ratios in photoproduction (cf. Cini *et al.* 1958).

Threshold measurements are, however, difficult since the low-energy mesons have very little penetrating power, and require the use of a thin target; also the differential cross section approaches zero near threshold. The π^+ mesons, which occur in a background of other particles and gamma rays, may be identified by their $2{\cdot}6 \times 10^{-8}$ sec decay into 4·15 MEV μ^+ mesons. A single counter 'decay-product' method has been used by Janes and Kraushaar (1954) to study π^+ meson photoproduction near threshold, at 90° in the laboratory frame, down to a meson energy of about 12 MEV in the centre-of-mass frame. The statistical uncertainties in these measurements at the lowest energies tend, however, to be rather large. Bernardini and Goldwasser (1954) (cf. also Beneventano *et al.* 1956) have examined the variation of the differential cross section at low energies, with photographic plates, and give results for mesons of 10 MEV in the centre-of-mass frame. A few isolated values at lower meson energies have been reported, with nuclear plates for gas targets (Osborne *et al.* 1954).

A comparatively new counter method has been developed by the authors capable of the detection of π^+ mesons down to an energy of less than 5 MEV. This method depends partly on the decay property, viz. $\pi^+ \to \mu^+$, to identify the π^+ meson. An accurate overall display can be obtained which shows directly the number of mesons incident on the counter as a function of meson energy, where the range of energies included extends from approximately 5 MEV up to a maximum determined by the thickness of the scintillator. It is important that the method should also be able to specify the π^+ meson counting unambiguously in the presence of intense electron and gamma-ray backgrounds which can simulate the $\pi^+ \to \mu^+$ decay property. These random effects, particularly for observations on π^+ mesons of energy less than 10 MEV must therefore be reduced to a minimum and a precise assessment of their magnitude must be possible. The technique which achieves these ends, and its mode of operation, are described in § 2 below.

Investigations of π^+ meson photoproduction from thin carbon and polythene targets have been made at angles of 115° and 90° to the gamma-ray beam of the Glasgow synchrotron. Apart from providing a comparison with theory, the capabilities of the method could be assessed.

§ 2. METHOD OF DETECTION

The system employs two counters. There is a main thick counter in which the π^+ meson must stop and decay into a μ^+ meson. This event is recorded as a π^+ meson only if the μ^+ meson, which always has an energy of 4·15 MEV, is totally absorbed in the thick counter and if it occurs within a short, specified, interval of time of the π^+ meson. This main counter is preceded by a 'thin' indicator counter, equipped with a 10/1000 in. plastic scintillator, which responds to the passage of a π^+ meson through it. A real $\pi^+(\rightarrow\mu^+)$ event in the thick counter is thus associated with the one, and only one, time-related event from the thin counter.

A block diagram of the two counters and the associated electronics is shown in figure 1. The details of operation and the time sequence of pulses for a $\pi^+\rightarrow\mu^+$ decay are as follows. On arrival of a π^+ meson the collector of the main counter produces a rectangular pulse of length 3×10^{-8} sec, which is delayed before being applied to the coincidence unit. The output pulses from dynode 10 of the main counter are kept as short as possible to keep the π^+ and μ^+ pulses distinct. These are amplified by a distributed amplifier, and fed directly to the coincidence unit. There is a small amount of delay line clipping using an 80 Ω termination on a short clipping length to reduce the length of the tails of these pulses. Figure 2 shows the time sequence of the pulses arriving at the coincidence unit and demonstrates the overlap between the collector pulse and the 4·15 Mev μ^+ pulse, which activates the coincidence unit. Hence the coincidence unit will give coincidences over a known portion of the $\pi^+\rightarrow\mu^+$ decay curve, and these coincidences are used to trigger the time base of the oscilloscope. The output from dynode 8 is displayed on the oscilloscope to show the two pulses from the

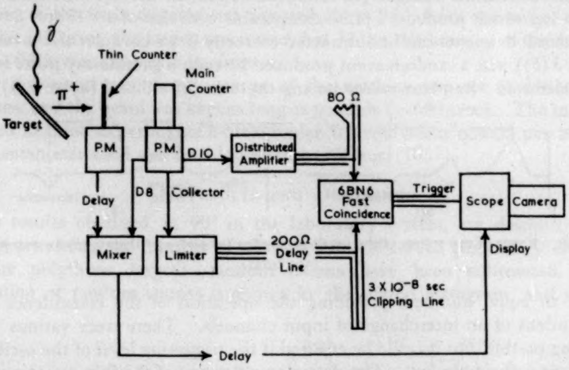
γ
Thin Counter
Main Counter
π⁺
Target
80 Ω
P.M.
P.M.
D10
Distributed Amplifier
6BN6 Fast Coincidence
Trigger
Scope
Camera
Delay
D8
Collector
Mixer
Limiter
200Ω Delay Line
Display
3 X 10⁻⁸ sec Clipping Line
Delay

Figure 1. Schematic diagram of γ-ray beam, target and counter system. The photomultipliers are type RCA 6342 and the plastic scintillators were supplied by Nuclear Enterprises (G.B.). Two Mullard E.180 F valves in parallel were used in the limiter, and the inputs to the fast coincidence unit went straight to the grids of the 6BN6 valve. The oscilloscope was a Tektronix 517A.

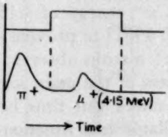
π⁺
μ⁺(4·15 Mev)
Time

Figure 2. Time sequence of pulses from the main counter arriving at the coincidence unit.

$\pi^+\!\rightarrow\mu^+$ decay. Now if the π^+ meson comes from the target it must pass through the thin counter, whereas the μ^+ meson cannot since it is produced and must stop in the main counter. The output from the thin counter is mixed, opposite in phase and with a fixed long delay T, with the dynode 8 output of the main counter and displayed on the oscilloscope; also the trace of the oscilloscope is photographed. A π^+ meson, then, will give rise to an oscilloscope trace as shown in figure 3 (*a*). This figure shows that the only random events which cannot be recognized immediately, and hence discarded, are those which are produced by an electron, or other charged particle, followed in the correct time interval by a gamma ray which produces a pulse comparable with that of a 4·15 MeV μ^+ meson. These random events can be subtracted correctly if we consider the inverse case (figure 3 (*b*)), viz. a random event produced by such a gamma-ray pulse followed by an electron. Random events having the form of either 3 (*a*) or 3 (*b*) should appear in equal numbers providing the operation of the coincidence unit is independent of an interchange of input channels. There were various ways of checking on this, but it could be ensured if the triggering level of the oscilloscope were kept sufficiently low. The detection efficiency of the thin counter was also shown to be adequate.

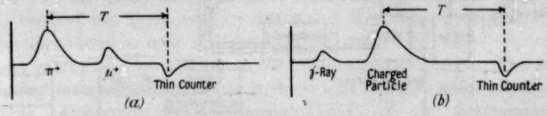

Figure 3. Form of the traces of the oscilloscope for (*a*) a $\pi^+\!\rightarrow\mu^+$ decay, (*b*) a random inverse (see text).

The operation of the main counter and coincidence unit could be adequately checked by appropriate measurements using the 2·6 MeV gamma ray of ThC″. The Compton edge of these gamma rays can be used as a subsidiary energy calibration. The method is, however, self-calibrating. The μ^+ meson pulse height can be correlated to a π^+ energy of 4·15(π^+ mass/μ^+ mass) MeV by the Seitz relation (cf. Taylor *et al.* 1951) to provide a low-energy calibration point. The maximum energy of the π^+ mesons observed is that associated with mesons whose range is just the thickness of the main scintillator; this provides a high-energy calibration point. A check can thus be made experimentally on the fluorescent yield of the scintillator as a function of the π^+ energy. Any non-linearity can be expected to be small (cf. Taylor *et al.* 1951). This was confirmed by the results obtained here, and no correction to the final data was made on this account.

Lastly, the observed time distribution of the μ^+ mesons with respect to the π^+ mesons serves as a check based on the lifetime of the π^+, and is used in assessing the absolute cross sections (cf. § 4).

§ 3. Experimental Procedure

From the kinematics of the process

$$\gamma + \mathrm{p} \rightarrow \pi^+ + \mathrm{n}$$

it is desirable to work at angles as forward as possible, and at low meson energies. The main work referred to below was carried out at 90° in the laboratory system with a 1 in. thick crystal preceded by the thin counter. Some early work with a $\frac{1}{2}$ in. thick crystal, alone, at 115° in the laboratory system is also described.

The gamma-ray beam from the synchrotron passed through an evacuated collimator, with its scrubber magnet, and the gamma-ray beam had a diameter of about $1\frac{1}{2}$ in. at the target. The target consisted either of a polythene sheet $0{\cdot}272\,\mathrm{g\,cm^{-2}}$ thick or of a carbon sheet $0{\cdot}284\,\mathrm{g\,cm^{-2}}$ thick. In the 90° run the target was inclined to the beam at 45°. The two counters were surrounded at the sides by lead 2–3 in. thick, with an inner lining of 1 in. iron, to reduce scattering; and the system was screened by considerable amounts of lead on the machine side. The front of the main counter was situated about 9 in. from the target centre.

In the 115° run, the target was inclined at 37° to the beam, and the front of the $\frac{1}{2}$ in. thick counter was 8 in. from it.

The maximum gamma-ray energy of the machine was set at 240 Mev for these runs, and the beam was kept as long as possible ($\sim 600\,\mu$sec). The machine produced in these experiments a little under 10^9 equivalent quanta per minute. The quantameter used was one described by Wilson (1957).

§ 4. Results and Discussion

The results obtained, at 90° in the laboratory system, are described first. Figure 4 (*a*) shows the number of π^+ mesons n_{p} observed per energy channel, with the polythene target; random counts have been subtracted. The distribution of random counts is shown by the dotted histogram, and is only

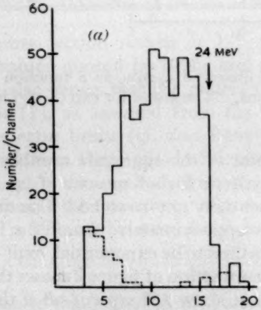

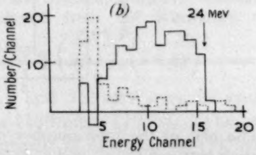

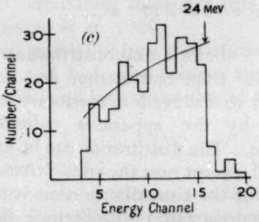

Figures 4 (*a*, *b*). The solid histogram shows the pulse height distribution of π^+ mesons, after subtraction of random events which are shown dotted, observed from a (*a*) polythene, (*b*) carbon target at 90° laboratory angle. Events whose energies lie in the three lowest channels are not recorded. This cut-off corresponds to 5 Mev mesons. The high energy cut-off is 24 Mev.

Figure 4 (*c*). Histogram of the number of π^+ mesons per energy channel observed at 90° to the beam from hydrogen, deduced from the data of figures 4 (*a*), 4 (*b*). Mesons shown in this figure arise from γ-rays in the range 162–190 Mev. The curve superimposed in this figure is that which would be obtained if the matrix element of equation (1) were constant.

important below about 10 MeV. Figure 4 (*b*) shows the number of π^+ mesons n_c observed per energy channel with the carbon target, with the random counts subtracted. The distribution of mesons from hydrogen can be deduced from those of figures 4 (*a*) and (*b*) by subtraction, when adjustments are made for the relative carbon content of the two targets and the integrated gamma-ray fluxes. The number of π^+ mesons per energy channel from hydrogen is then $n_p - 1{\cdot}16 n_c$, and this plot is shown in figure 4 (*c*). This difference figure corrects essentially, too, for mesons produced in the air, shown to be small in number by subsidiary experiments. Only π^+ mesons in the range 5–24 MeV will produce μ^+ mesons which wholly stop in the scintillator (cf. Rich and Madey 1954). Also shown in figure 4 (*c*) is the theoretical distribution which could be expected in this experiment in laboratory coordinates if the matrix element in equation (1) were assumed constant. It has been corrected for energy lost in the target, for solid angle variation with energy, for the synchrotron spectrum and for decay in flight. The curve and the histogram of figure 4 (*c*) certainly indicate that to a first approximation, the differential cross section varies as p. The correlation is discussed further below.

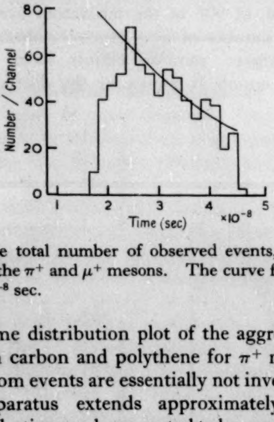

Figure 5. The plot of the total number of observed events, as a function of the time separation between the π^+ and μ^+ mesons. The curve for exp $(-t/\tau)$ is also shown where $\tau = 2{\cdot}60 \times 10^{-8}$ sec.

Figure 5 shows a time distribution plot of the aggregate number of $\pi^+ \to \mu^+$ events at 90° from both carbon and polythene for π^+ mesons of energy greater than 10 MeV so that random events are essentially not involved. The time interval examined by the apparatus extends approximately from 2×10^{-8} sec to 5×10^{-8} sec. The distribution can be expected to be exponential, $\exp(-t/\tau)$, over the interval, except near the ends. An examination of figure 2 shows that the left-hand edge of the time distribution will not show a sharp cut-off if the π^+ pulse possesses a long tail. The lifetime figure τ, deduced from these results, and from the work at 115°, was $(2{\cdot}60 \pm 0{\cdot}15) \times 10^{-8}$ sec and agrees with accepted values (cf. Crowe 1957). From figure 5 it is possible to assess the fraction of π^+ mesons which decay during the period of observation. It is 0·28. The absolute differential cross sections can then be deduced.

The values of the differential cross sections in centre-of-mass coordinates obtained from the 90° measurements are listed in the table for various gamma-ray energies, with corrections as before. The cross sections are calculated on the basis of a thin synchrotron target bremsstrahlung spectrum. The synchrotron target actually consists of a 60/1000 in. diameter tungsten wire. On the basis of photon angular distribution measurements (McFarlane and Hughes, unpublished) the bremsstrahlung spectrum appeared to be that of an equivalent 20/1000 in. target. According to Powell *et al.* (1951) a uniform target of this thickness would produce a change in the thin target cross sections of only 3%, since the dominant part of the radiation arises from the initial few thousandths of an inch of target.

The earlier work at 115° showed, likewise, a fall of meson photoproduction near threshold, of similar form, though the maximum meson energy was now only 15 Mev, as the scintillator thickness was here only ½ in. Time distributions were observed in this case and a curve analogous to that shown in figure 5 was obtained. Absolute cross sections for the 115° position were calculated, and these values are also quoted in the table, again on the basis of thin target bremsstrahlung.

Differential Cross Sections ($d\sigma/d\Omega$) for π^+ Photoproduction from Hydrogen in centre-of-mass coordinates, and values of $2e^2f^2H^2$ derived from the 90° results

(1)	(2)	(3)	(4)
170		$0{\cdot}48 \pm 0{\cdot}11$	$1{\cdot}36 \pm 0{\cdot}30$
175	$0{\cdot}60 \pm 0{\cdot}10$	$0{\cdot}58 \pm 0{\cdot}09$	$1{\cdot}41 \pm 0{\cdot}22$
180	$0{\cdot}68 \pm 0{\cdot}10$		
185		$0{\cdot}73 \pm 0{\cdot}11$	$1{\cdot}42 \pm 0{\cdot}22$

(1) Laboratory γ-ray energy (Mev); (2) $d\sigma/d\Omega$ deduced from 115° laboratory measurements (10^{-29} cm^2 sterad^{-1}); (3) $d\sigma/d\Omega$ deduced from 90° laboratory measurements (10^{-29} cm^2 sterad^{-1}); (4) $(2e^2f^2H^2)_{90} \times 10^{29}$; $2e^2f^2H^2 = \left(\frac{d\sigma}{d\Omega}\right)\frac{\mu^2}{p\epsilon}\left(1+\frac{\omega}{M}\right)^2$.

The cross section results at 175 Mev and 185 Mev may be compared with previous values quoted by Bethe and de Hoffmann (1955). The results agree. The table also shows that the matrix element H of equation (1), with the units of equation (1), as assessed from the 90° laboratory measurements is constant within the error limits (cf. also Beneventano *et al.* 1956).

In conclusion, the method of detection proved to be a powerful one and it is hoped to apply the method, with thin liquid hydrogen targets, to the further investigations of the low-energy region, at 90° and forward angles, so that possible variations in H^2 can be more fully assessed.

ACKNOWLEDGMENTS

We wish to thank Dr. W. McFarlane and the synchrotron technicians for the use of the synchrotron beam, Mr. H. C. Evans for suggestions leading to the introduction of the thin front counter and Professor P. I. Dee for the interest shown in the work. One of us (R. E. A.) expresses appreciation to I.C.I. Ltd., for a Fellowship held during the course of this work.

References

Beneventano, M., Bernardini, G., Carlson-Lee, D., Stoppini, G., and Tau, L., 1956, *Nuovo Cim.*, **4**, 323.

Bernardini, G., and Goldwasser, E. L., 1954, *Phys. Rev.*, **95**, 856.

Bethe, H. A., and de Hoffmann, F., 1955, *Mesons and Fields* (New York: Row, Peterson) Vol. II, p. 149.

Chew, G. F., 1954, *Phys. Rev.*, **95**, 1669.

Cini, M., Gatto, R., Goldwasser, E. L., and Ruderman, M., 1958 (cf. Puppi, G., C.E.R.N. Conference Proceedings, p. 49).

Crowe, K. M., 1957, *Nuovo Cim.*, **5**, 541.

Janes, G. S., and Kraushaar, W. L., 1954, *Phys. Rev.*, **93**, 900.

Marshak, R. E., 1952, *Meson Physics* (New York: McGraw-Hill), p. 10.

Osborne, L. S., Goldschmidt-Clermont, Y., and Parker, G., 1954, *Phys. Rev.*, **95**, 637 (A).

Powell, W., Hartsough, W., and Hill, M., 1951, *Phys. Rev.*, **81**, 213.

Rich, M., and Madey, R., 1954, *Range Energy Tables* (Berkeley).

Taylor, C. J., Jentschke, W. K., Romley, M. E., Ely, F. S., and Kruger, P. G., 1951, *Phys. Rev.*, **84**, 1034.

Wilson, R. R., 1957, *Nucl. Instrum.*, **1**, 101.

Angular Distributions of High Energy Protons inelastically scattered by Light Nuclei

By D. J. HOOTON†§ and G. R. ALLCOCK‡
† Department of Applied Mathematics, University of Liverpool
‡ Department of Theoretical Physics, University of Liverpool

MS. received 3rd December 1958

Abstract. The effect of the central optical potential in the quasi-elastic scattering of high energy nucleons is treated by the semi-classical approximation. For non-radial excitation of the nucleus the optical potential leads to a considerable *angle-independent* reduction in intensity. It also produces some forward scattering when two units of orbital angular momentum are communicated to the nucleus by the scattered particle. The angular distributions for radial nuclear excitation are more seriously distorted by the optical potential; the main effect here consists in a more or less angle-independent reduction in intensity of the diffraction peaks, and the appearance of a large extra peak in the forward direction.

§ 1. Introduction

The excitation of a level of a light nucleus by a fast proton (or neutron) is expected to result largely from a single energetic collision between the high energy particle and one of the constituent nucleons of the nucleus. The amplitude for such a collision is, however, considerably modified by the presence of the other nucleons. It seems reasonable to simulate their effect by that of the complex optical potential which is used to describe the elastic scattering. In this way one obtains the *distorted impulse approximation*, whose theoretical foundations have been discussed by Levinson and Banerjee (1958) and McCauley and Brown (1958). Levinson and Banerjee find that the distorted impulse approximation gives results in quantitative agreement with experimental data on the excitation of the 4·4 Mev level in ^{12}C within the energy range 14–186 Mev. Similar quantitative agreement has been obtained by Benoist, Marty and Meyer (1957), Mohr (1958) and Squires (1958) at energies within the range 96–185 Mev.

At energies in the region of 100 Mev or higher one may estimate the distortions produced by the optical potential with the help of the semi-classical approximation. This approximation was originally formulated for large angle elastic scattering in slowly varying potentials by Schiff (1956). It is essentially a B.W.K. approximation with straight line paths before and after the single energetic collision. Benoist, Marty and Meyer (1957) and Squires (1958) have carried over this simplified treatment to inelastic collisions, and much the same method has been formulated by McCauley and Brown (1958)‖. Even with the help of the semi-classical approximation very heavy numerical computation is required to obtain the detailed predictions of the theory for any particular choice of initial and final nuclear wave functions. However, an inspection of the main features of the angular distributions of the inelastically scattered protons often enables one to make reasonably certain inferences as to the spin and parity change in the nuclear transition (cf. Maris and Tyrén 1957 and Tyrén and Maris 1958). It is therefore of interest to study the effect which the optical distortion has upon the general character of the angular distributions.

---

§ Now at Department of Physics, Wellington University, New Zealand.

‖ These authors give a number of references to earlier work on the semi-classical treatment of elastic scattering.

In the present paper we study the effect of the central part of the optical potential, making a number of simplifying assumptions as to the angle dependence and spin dependence of the nucleon–nucleon scattering matrix and the radial dependence of the nuclear wave functions, and find certain salient features which will be reproduced in any more realistic treatment.

For *non-radial* nuclear transitions we find in the first place that the optical distortion of the ingoing and outgoing waves leads only to a very slight broadening of the peaks of the angular distribution curves, leaving their shape and position otherwise much the same as they would be without optical distortion (see figures 1–4). Thus the determination of an orbital angular momentum transfer from the angular distribution is not rendered unreliable by optical distortion. In the second place, the differential cross section around the peak is reduced considerably, by a factor which we designate as $|f_0|^2$. It will be seen from table 1.

Table 1. Analysis of the optical factor (10) for ^{40}Ca at various energies of the incident proton. The nuclear shape parameters are $R=4\cdot275$f, $t=2\cdot5$f. The optical potentials V assumed for the analysis are listed in the table.

Radius r		0	$R-\frac{1}{2}t$	R	$R+\frac{1}{2}t$
E (Mev)	$f_0(r)$	$-0\cdot111+0\cdot088i$	$-0\cdot067+0\cdot200i$	$0\cdot161+0\cdot304i$	$0\cdot560+0\cdot186i$
96	$f_2(r)$	0	$-0\cdot014-0\cdot026i$	$-0\cdot086-0\cdot041i$	$-0\cdot181+0\cdot026i$
V (Mev)	$f_4(r)$	0	$0\cdot003+0\cdot003i$	$0\cdot019-0\cdot006i$	$0\cdot008-0\cdot033i$
$24+19i$	$f_6(r)$	0	$-0\cdot003+0\cdot001i$	$-0\cdot003+0\cdot005i$	$0\cdot016+0\cdot000i$
E (Mev)	$f_0(r)$	$0\cdot100+0\cdot165i$	$0\cdot198+0\cdot193i$	$0\cdot386+0\cdot193i$	$0\cdot671+0\cdot111i$
185	$f_2(r)$	0	$-0\cdot022-0\cdot005i$	$-0\cdot074-0\cdot000i$	$-0\cdot136+0\cdot031i$
V (Mev)	$f_4(r)$	0	$0\cdot004+0\cdot001i$	$0\cdot010-0\cdot003i$	$0\cdot002-0\cdot010i$
$13+21i$	$f_6(r)$	0	$0\cdot001+0\cdot003i$	$0\cdot001+0\cdot004i$	$0\cdot011+0\cdot000i$
E (Mev)	$f_0(r)$	$0\cdot191+0\cdot076i$	$0\cdot279+0\cdot084i$	$0\cdot447+0\cdot079i$	$0\cdot703+0\cdot044i$
350	$f_2(r)$	0	$-0\cdot021-0\cdot001i$	$-0\cdot065+0\cdot002i$	$-0\cdot121+0\cdot013i$
V (Mev)	$f_4(r)$	0	$0\cdot004+0\cdot001i$	$0\cdot010+0\cdot001i$	$0\cdot002-0\cdot003i$
$6+25i$	$f_6(r)$	0	$0\cdot003+0\cdot001i$	$0\cdot003+0\cdot002i$	$0\cdot009+0\cdot000i$

that at 350 Mev f_0 is almost real. Here it represents simply a suitable average of the absorption arising from the imaginary part of the optical potential. At 96 and 185 Mev, however, f_0 has a large imaginary part, showing that the real part of the optical potential is important at these energies in determining the magnitude of the cross section. In the third place, a central optical potential, because it refracts the incoming and outgoing waves, can make possible a non-zero momentum transfer in the single nucleon–nucleon collision even when the *total* momentum transfer to the nucleus is zero. This effect leads to forward and small angle inelastic scattering for nuclear transitions involving an even orbital angular momentum transfer L. Forward scattering would otherwise be absent except for $L=0$ non-radial spin–flip transitions. The finite forward scattering produced by the optical distortions can be seen in the curves for $L=2$ in figures 1–4. In practice it will be subject to some modification from Coulomb effects. For $L=4$, 6 ... the terms giving forward scattering are negligible, and they have in fact been ignored in plotting the curves for $L=4$ in figures 1–4.

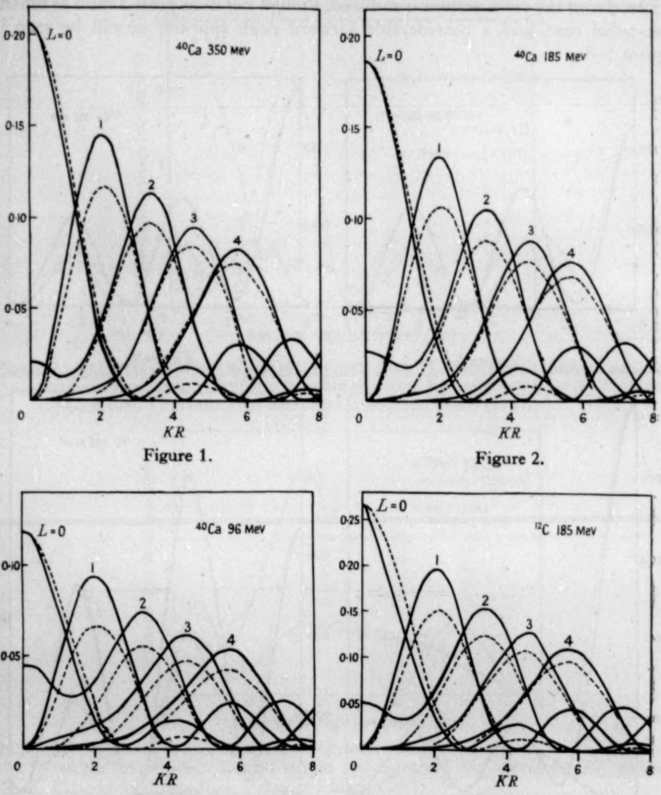

Figure 1. Figure 2.

Figure 3. Figure 4.

Figures 1–4. Effect of distortion on the angular distributions for non-radial excitation. The full lines represent the distorted angular distribution (19), with optical angular momenta $\lambda=0$ and 2 taken into account. The broken lines represent the undistorted but damped distribution, $|f_0(\overline{R})|^2(2L+1)j_L{}^2K\overline{R}$. Figures 1–3 are calculated using the distortion factors of table 1 and taking for $\overline{R}$ the halfway radius $R=4{\cdot}275$f. Figure 4 is calculated similarly using the distortion factors of table 2.

We have studied *radial* transitions only for the simplest case, where one additional node is induced in the radial part of the nuclear wave function without any accompanying transfer of orbital angular momentum. Without distortion such transitions give differential cross sections exhibiting a number of diffraction peaks at finite angles, but falling off to zero in the forward direction (in contrast to the non-radial $L=0$ spin–flip transitions mentioned above). When distortion is introduced the cross section is reduced, though not in as great a ratio as for the non-radial case, and a considerable forward peak appears, as will be seen in figures 5–8.

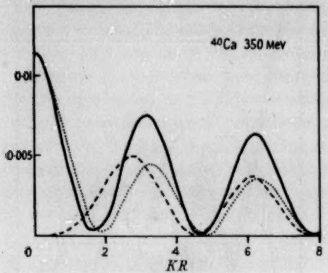

Figure 5.

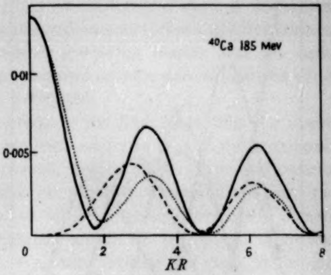

Figure 6.

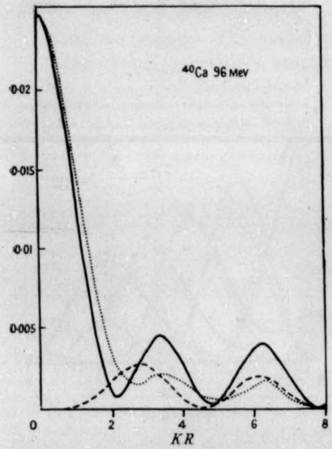

Figure 7.

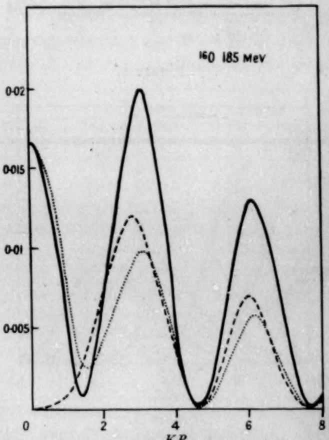

Figure 8.

Figures 5–8. Effect of distortion on the angular distributions for an excitation involving zero orbital angular momentum transfer and the creation of one extra radial node. The full lines represent the angular distribution (20), with optical angular momenta $\lambda=0$ and 2 taken into account. The dotted lines represent the same distribution with only $\lambda=0$ included. The broken lines show the undistorted distribution damped by a factor $|f_0(\frac{1}{2}\bar{R}_1+\frac{1}{2}\bar{R}_2)|^2$. Figures 5–7 are calculated using the distortion factors of table 1, taking $\bar{R}_1=R-\frac{1}{4}t$ and $\bar{R}_2=R+\frac{1}{4}t$, with $R=4{\cdot}275$f, $t=2{\cdot}5$f. Figure 8 is calculated using distortion factors obtained from those in table 2, again taking $\bar{R}_1=R-\frac{1}{4}t$ and $\bar{R}_2=R+\frac{1}{4}t$, with $R=3{\cdot}150$f, $t=2{\cdot}5$f.

We have compared the angular distributions obtained as above with experimental data on the inelastic scattering of 185 Mev protons from ^{12}C, ^{16}O and ^{40}Ca, as given by Tyrén and Maris (1957) (see figures 9–11).

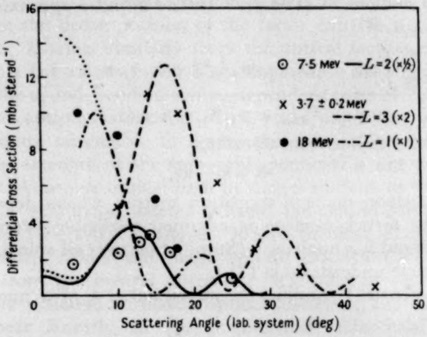

Figure 9. Inelastic scattering of 185 Mev protons from ^{40}Ca interpreted through non-radial nuclear transitions. Dotted curves are corrected for estimated E2 and E1 additions respectively. Experimental data from Tyrén and Maris (1957).

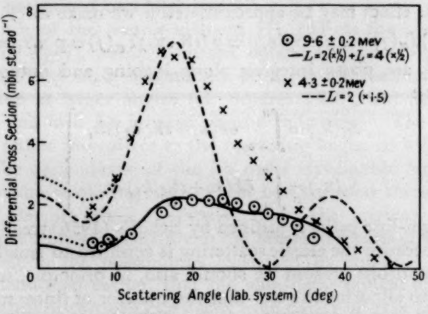

Figure 10. Inelastic scattering of 185 Mev protons from ^{12}C interpreted through non-radial nuclear transitions. Dotted curves are corrected for estimated E2 additions. Experimental data from Tyrén and Maris (1957).

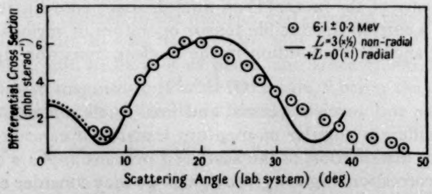

Figure 11. Inelastic scattering of 185 Mev protons from ^{16}O interpreted through a mixture of non-radial and radial nuclear transitions. Dotted curve is corrected for estimated E2 addition. Experimental data from Tyrén and Maris (1957).

§ 2. The Inelastic Scattering Amplitude

Neglecting nuclear recoil, we consider the matrix element for the inelastic scattering of a nucleon, with momentum $\mathbf{k}_i$ and spin and isotopic spin wave function u_i, on a nucleus in state ψ_i. In the impulse approximation, without optical distortions, it is

$$M_{fi} = \sum_{j=1}^{n} \int d\mathbf{x}_1 \ldots d\mathbf{x}_j \ldots d\mathbf{x}_n \psi_f^*(\ldots \sigma_j, \tau_j, \mathbf{x}_j, \ldots) \times u_f^* T_{\mathbf{K}}(j) \exp(i\mathbf{K} . \mathbf{x}_j) u_i \psi_i(\ldots \sigma_j, \tau_j, \mathbf{x}_j, \ldots), \quad \ldots\ldots(1)$$

where $\mathbf{K}$ denotes the momentum transfer,

$$\mathbf{K} = \mathbf{k}_i - \mathbf{k}_f, \quad \ldots\ldots(2)$$

and $T_{\mathbf{K}}$ is the nucleon–nucleon transition matrix, whose dependence on the momentum of the struck nucleon is assumed negligible within the range of momenta encountered in a nucleus. (Summation over all spin and isotopic spin variables is of course understood in (1).)

The optical potential V modifies the wavenumber k of a nucleon in nuclear matter:

$$k \to k + \delta k,$$
$$\delta k = -EV/k, \quad \ldots\ldots(3)$$

and so distorts the factor $\exp(i\mathbf{K} . \mathbf{x}_j)$ in (1). For energies $E - M$ greater than about 100 Mev its effect may be approximated if we make in (1) the substitution

$$\exp(i\mathbf{K} . \mathbf{x}_j) T_{\mathbf{K}}(j) \to \exp\{iS_2(\mathbf{x}_j)\} \exp(i\mathbf{K} . \mathbf{x}_j) T_{\mathbf{K}}(j) \exp\{iS_1(\mathbf{x}_j)\}. \quad \ldots\ldots(4)$$

Here S_1 and S_2 are phase integrals along ingoing and outgoing straight-line paths through $\mathbf{x}_j$:

$$\left.\begin{aligned} S_1(\mathbf{x}_j) &= \int_{-\infty}^{0} \delta k(\mathbf{x}_j + s\mathbf{k}_i/k_i)\, ds, \\ S_2(\mathbf{x}_j) &= \int_{0}^{\infty} \delta k(\mathbf{x}_j + s\mathbf{k}_f/k_f)\, ds. \end{aligned}\right\} \quad \ldots\ldots(5)$$

The use of straight-line paths is justified by Schiff's (1956) treatment; essentially it is legitimate because the elastic scattering is confined to small forward angles. With optical distortions present we should also, in principle, make a correction to $T_{\mathbf{K}}(j)$ in (1), to allow for the fact that the transfer of linear momentum in the energetic collision differs from $\mathbf{K}$†. In the following, however, we shall ignore the $\mathbf{K}$-dependence of $T_{\mathbf{K}}(j)$ altogether, so that we shall not be concerned with this correction.

The dependence of the factor (4) on nuclear space coordinates and spins may be expressed as a sum of irreducible tensor operators of various integer ranks J. Conservation of angular momentum in the nuclear transition then reads

$$\mathbf{J}_f = \mathbf{J}_i + \mathbf{J}. \quad \ldots\ldots(6)$$

When we average and sum over initial and final nuclear states, the interference terms between different angular momentum transfers J cancel in the usual way. Thus the angular distribution of the scattered protons appears as a sum of contributions, each corresponding to a given J, and we may consider each contribution separately. However, the *form* of each such contribution is not characterized by J so much as by the orbital part of J, as will be seen directly.

---

† The factors $\exp(iS)$ in (4) give a good account of the refraction, so that the wave vectors of the ingoing and outgoing distorted waves within the nucleus are not parallel to $\mathbf{k}_i$ and $\mathbf{k}_f$ respectively.

The angular momentum transfer J is built up of three contributions:

$$\mathbf{J}=\mathbf{l}+\boldsymbol{\lambda}+(\mathbf{0}\text{ or }\mathbf{1}). \qquad \ldots\ldots(7)$$

Here $\mathbf{l}$ arises from the decomposition of the factor $\exp(i\mathbf{K}.\mathbf{x}_j)$ and can assume any integer value; $\boldsymbol{\lambda}$ arises similarly from the optical factors $\exp(iS)$, and we shall find that only the values 0 and 2 are important; the angular momenta $\mathbf{0}$ and $\mathbf{1}$ arise from the $\boldsymbol{\sigma}_j$-independent and $\boldsymbol{\sigma}_j$-dependent parts of $T_{\mathbf{K}}(j)$ respectively.

In treating the optical factors $\exp\{iS_2(\mathbf{x}_j)\}$ and $\exp\{iS_1(\mathbf{x}_j)\}$ it is expedient and apparently quite reasonable to ignore the spin–orbit part of the optical potential V. The strength of the spin–orbit potential is not very well known, but for the most favourable optical path in such a nucleus as ^{40}Ca it is unlikely to contribute to S_1+S_2 more than 0·5 radians; the central part of V contributes here as much as $1{\cdot}7+1{\cdot}4i$ radians at 96 MeV incident energy, or $0{\cdot}3+1{\cdot}1i$ radians at 350 MeV. Thus the main optical distortion in the scattering amplitude arises from the central potential. It should, however, be noted that in contrast to the situation in elastic optical scattering, the optical spin–orbit terms may appear linearly in the unpolarized differential cross section, since the transition operator $T_{\mathbf{K}}(j)$ has large spin-dependent parts. Thus spin–orbit effects may be quite important even in obtaining a *detailed* fit to the unpolarized angular distribution for any particular transition. (The treatment of polarization is postponed to a later paper.)

The dependence of the matrix element (1), (4) on the scattering angle θ comes partly from $T_{\mathbf{K}}(j)$, partly from the optical factors $\exp(iS)$, and partly from $\exp(i\mathbf{K}.\mathbf{x}_j)$. The angle-dependence of $T_{\mathbf{K}}(j)$ will lead to some reduction of the cross section at larger angles (cf. Squires 1958), but this is not a very important effect and will be ignored in the following. The optical factors $\exp(iS)$ are also rather insensitive to the scattering angle, as will be seen in the next section. The dependence of the lth order irreducible tensor component of $\exp(i\mathbf{K}.\mathbf{x}_j)$ on the scattering angle θ can be expressed through the familiar factor $\mathrm{j}_l(Kr_j)\sim\mathrm{j}_l(2kr_j\sin\frac{1}{2}\theta)$. Evidently, then, the angular dependence of the differential cross section lies mainly in the Bessel functions $\mathrm{j}_l(Kr)$, but various l interfere according to the possibilities expressed by equation (7). With the approximation mentioned earlier, that the spin–orbit optical potential is to be neglected, the optical distortions carry only even parity, so that l is also restricted to have the parity of the nuclear transition.

§ 3. ANALYSIS OF THE OPTICAL FACTOR

We take axes x, y, z centred in the nucleus, and directed respectively along the three orthogonal vectors $\mathbf{k}_\mathrm{i}\times\mathbf{k}_\mathrm{f}$, $\mathbf{K}=\mathbf{k}_\mathrm{i}-\mathbf{k}_\mathrm{f}$, and $(\mathbf{k}_\mathrm{i}\times\mathbf{k}_\mathrm{f})\times\mathbf{K}$. The incident and scattered rays $\mathbf{k}_\mathrm{i}$ and $\mathbf{k}_\mathrm{f}$ lie in a yz plane, and since $k_\mathrm{i}\sim k_\mathrm{f}$, they both make angles of approximate magnitude $\frac{1}{2}\theta$ with the z-axis, θ being the scattering angle. For the phases appearing in (5) we have the expansion

$$S_1(\mathbf{x}_j)+S_2(\mathbf{x}_j)=\int_{-\infty}^{\infty}\delta k(x_j,y_j,z_j+s)\,ds$$
$$-\tfrac{1}{2}\theta\int_{-\infty}^{\infty}\{\partial\delta k(x_j,y_j,z_j+s)/\partial y_j\}|s|\,ds+\mathrm{O}(\theta^2). \qquad \ldots\ldots(8)$$

The term containing θ in (8) is clearly of order $\theta R\delta k$, where R is the nuclear radius: it will contribute to the matrix element (1), (4) a factor $\exp(i\theta R\delta k)$, which is equal to unity for forward scattering, and whose angular dependence is much less than that of the factor $\exp(i\mathbf{K}.\mathbf{x}_j)\sim\exp(i\theta y_j k)$, since (in the region above 100 Mev) $\delta k \lesssim \frac{1}{8}k$. Moreover, it can largely be absorbed into $\exp(i\mathbf{K}.\mathbf{x}_j)$ by a slight change in r_j. The terms in θ^2 are very small. For these reasons it is quite sufficient to approximate S_1+S_2 by the θ-independent terms in (8):

$$S_1(\mathbf{x}_j)+S_2(\mathbf{x}_j)\sim\int_{-\infty}^{\infty}\delta k(x_j,y_j,z_j-s)\,ds. \qquad \ldots\ldots(9)$$

This approximation was used by Squires (1958)†.

Having in mind the spherical symmetry of δk, we may now express the exponential of the optical phase (9) as a sum over even-parity spherical harmonics:

$$\exp[i\{S_1(\mathbf{x}_j)+S_2(\mathbf{x}_j)\}]=\sum_{\text{even }\lambda}(2\lambda+1)f_\lambda(r_j)\mathrm{P}_\lambda(z_j/r_j). \quad \ldots\ldots(10)$$

We have calculated the functions $f_\lambda(r)$ for calcium at 96, 185 and 350 Mev, taking for the optical potential $24+i19$, $13+i21$ and $6+i25$ Mev respectively. A trapezoidal form factor was used, with inner radius $R-\frac{1}{2}t$, outer radius $R+\frac{1}{2}t$, $R=1{\cdot}25A^{1/3}$f, $t=2{\cdot}5$f. The results are shown in table 1.

As well as using the trapezoidal potential we have determined the functions $f_\lambda(r)$ on the surface of a rectangular potential with appropriate 'equivalent' radius $R=1{\cdot}62A^{1/3}$f. A rectangular potential does not give a realistic account of the radial dependence of the $f_\lambda(r)$, but is useful in estimating these quantities at the nuclear radius, where analytic computation is possible. Using the optical parameters as given above, we have calculated f_0 and f_2 for ^{40}Ca in this way. The results are shown in the third column of table 2, and are in excellent agreement with the corresponding parts of table 1 ($r=R$). In view of this agreement we have repeated the rectangular-potential calculation for ^{12}C; the results are shown in the fourth column of table 2. From these figures it will be seen that the distortion factors are not at all sensitive to the (light) nucleus considered, apart from the obvious overall increase in absorption with larger radius.

Table 2. Analysis of the optical factor (10) for ^{40}Ca and ^{12}C using a square-well optical potential of radius $R=1{\cdot}62A^{1/3}$f. For ^{40}Ca, $R=5{\cdot}5$f; for ^{12}C, $R=3{\cdot}7$f.

E (Mev)		^{40}Ca	^{12}C
96	$f_0(R)$	$0{\cdot}163+0{\cdot}208i$	$0{\cdot}293+0{\cdot}280i$
	$f_2(R)$	$-0{\cdot}112-0{\cdot}047i$	$-0{\cdot}132-0{\cdot}008i$
185	$f_0(R)$	$0{\cdot}351+0{\cdot}164i$	$0{\cdot}486+0{\cdot}172i$
	$f_2(R)$	$-0{\cdot}108-0{\cdot}001i$	$-0{\cdot}100+0{\cdot}014i$
350	$f_0(R)$	$0{\cdot}416+0{\cdot}070i$	$0{\cdot}537+0{\cdot}069i$
	$f_2(R)$	$-0{\cdot}097+0{\cdot}002i$	$-0{\cdot}088+0{\cdot}007i$

§ 4. ANGULAR DISTRIBUTIONS

Within the approximations adopted, the angular momentum λ carried by the optical factors $\exp(iS)$ is entirely orbital, and is expressed by equation (10).

---

† Similar terms of order θ are omitted by M^cCauley and Brown (1958), where a straight path along $\mathbf{k}_1$ is used.

It is profitable to combine it with the angular momentum l carried by $\exp(iKy_j)$, to give a resultant orbital angular momentum L:

$$\mathbf{L} = \boldsymbol{\lambda} + \mathbf{l}, \qquad \ldots\ldots(11)$$

$$\mathbf{J} = \mathbf{L} + (\mathbf{0} \text{ or } \mathbf{1}). \qquad \ldots\ldots(12)$$

The addition of $\boldsymbol{\lambda}$ and $\mathbf{l}$ is most easily accomplished by taking the direction of the momentum transfer $\mathbf{K}$ (the y-axis) as pole for spherical harmonics, and the z-axis as having azimuthal angle zero. The right-hand side of equation (10) then transforms into

$$\sum_{\text{even } \lambda} f_\lambda(r_j) 4\pi \sum_{\mu} \mathrm{Y}_\lambda^{\mu}(\mathbf{x}_j) \mathrm{Y}_\lambda^{\mu *}\left(\frac{\pi}{2}, 0\right), \qquad \ldots\ldots(13)$$

while for $\exp(iKy_j)$ one has the familiar expansion

$$\exp(iKy_j) = \sum_{l=0}^{\infty} i^l \mathrm{j}_l(Kr_j)\{4\pi(2l+1)\}^{1/2} \mathrm{Y}_l^{0}(\mathbf{x}_j). \qquad \ldots\ldots(14)$$

Multiplying (13) and (14) gives

$$\exp(iKy_j)\exp[i\{S_1(\mathbf{x}_j) + S_2(\mathbf{x}_j)\}] = (4\pi)^{1/2} \sum_{L,\mu} a_L^{\mu}(r_j) \mathrm{Y}_L^{\mu}(\mathbf{x}_j), \qquad \ldots\ldots(15)$$

where

$$a_L^{\mu}(r) = (4\pi)^{1/2} \sum_{\text{even } \lambda} \sum_{l} i^l \mathrm{j}_l(Kr)(2l+1)$$
$$\times \{(2\lambda+1)/(2L+1)\}^{1/2} C(l\lambda L;\, 0\mu) C(l\lambda L;\, 00) f_\lambda(r) \mathrm{Y}_\lambda^{\mu *}\left(\frac{\pi}{2}, 0\right). \qquad \ldots\ldots(16)$$

Since λ is even, the summand in (16) vanishes unless $l - L$ and μ are both even. Reflection symmetry in the yz-plane is expressed through the relation

$$a_L^{\mu}(r) = (-)^{\mu} a_L^{-\mu}(r). \qquad \ldots\ldots(17)$$

Particular interest attaches to the cases $L = 0$ and 2, where the distortion brings in quite large admixtures. The expression (16) gives here

$$a_0^{0}(r) = f_0(r)\mathrm{j}_0(Kr) + \tfrac{5}{2} f_2(r)\mathrm{j}_2(Kr) + \ldots, \qquad \ldots\ldots(18\,a)$$

$$a_2^{2}(r) = a_2^{-2}(r) = \sqrt{\left(\frac{15}{2}\right)}\left\{\frac{1}{2} f_2(r)\mathrm{j}_0(Kr) + \frac{5}{7} f_2(r)\mathrm{j}_2(Kr) + \ldots\right\}, \qquad \ldots\ldots(18\,b)$$

$$a_2^{0}(r) = \sqrt{(5)}\left\{-f_0(r)\mathrm{j}_2(Kr) - \frac{1}{2} f_2(r)\mathrm{j}_0(Kr) + \frac{5}{7} f_2(r)\mathrm{j}_2(Kr) + \ldots\right\}. \qquad \ldots\ldots(18\,c)$$

The form of the angular distribution depends upon the radial integration in the scattering amplitude. In this connection it is necessary to distinguish between radial and non-radial excitation, corresponding to whether or not there is a change in the number of radial nodes of the nuclear wave function.

4.1. *Non-radial Transitions*

From table 1 it will be seen that contributions from near the centre of the nucleus are heavily damped. Taking this into account, and bearing in mind also the expected radial dependence of the nuclear transition density, we see that for non-radial excitation we may work as though the transition density be concentrated at an effective interaction radius $\bar{R}$ close to the nuclear radius. Such a simplified treatment of the radial integration suffices to indicate the extent to which the optical potential mixes the various angular factors $\mathrm{j}_l(Kr)$, although it leaves the absolute magnitude of the cross section a little uncertain because of the strong radial dependence of the absorption factor $f_0(r)$ (see table 1). Assuming now a spin-independent transition matrix $T_{\mathbf{K}}(j)$, one finds on this basis that the differential cross section for a non-radial excitation with orbital angular momentum transfer L is proportional to

$$\sum_{\mu} |a_L^{\mu}(\bar{R})|^2. \qquad \ldots\ldots(19)$$

4.2. *Radial Transitions*

The same type of approximation may be made for the treatment of radial excitation, although in this case more than one interaction radius is required. If the transition results in one extra radial node in the nuclear wave function we need two interaction radii $\bar{R}_1$ and $\bar{R}_2$. Taking account of orthogonality in the radial integration, and again assuming a spin-independent $T_{\mathbf{K}}(j)$, one obtains in this way an angular distribution proportional to

$$\tfrac{1}{4}\sum_{\mu} | a_L^{\mu}(\bar{R}_1) - a_L^{\mu}(\bar{R}_2)|^2. \qquad \ldots\ldots(20)$$

In the angular distributions of figures 5–8 we have taken $\bar{R}_2 = R + \frac{1}{2}t$ and $\bar{R}_1 = R - \frac{1}{2}t$. The form of the curves will not be changed very much by taking any other reasonable choice, however.

The angular distributions (19) and (20) still apply when the matrix $T_{\mathbf{K}}(j)$ contains besides a spin-independent term a spin-dependent term of the form $\boldsymbol{\sigma} . \boldsymbol{\sigma}_j$; in this case J can either be equal to L or to $L \pm 1$, according to the parity of the transition.

4.3. *Electromagnetic Excitation*

In none of the preceding have we considered the effect of electromagnetic interactions. In the first place the Coulomb contribution to the optical phase S for a proton passing into any light nucleus is much smaller than the nuclear contribution, and the Coulomb deflection of the classical path is very small, at the energies considered. Thus Coulomb distortions may be neglected. In the second place, a rough estimate of direct electromagnetic excitation, based on the relative strength of Yukawa and Coulomb forces, and on the absorption factors f_0 given in table 1, indicates that the scattering amplitude for electromagnetic excitation can exceed the f_0 part of that for Yukawa excitation only when the momentum transfer K is less than about half the pion mass. This corresponds to scattering angles less than $1{\cdot}3(kR)^{-1}$. For larger angles the electromagnetic contributions fall off very fast because of the factor K^{-2} in the electromagnetic amplitude. It is interesting to note that at the above angle much of the electromagnetic excitation amplitude arises from paths which do not pass into the nucleus, while at smaller angles it arises almost entirely in this way. Thus a treatment of electromagnetic excitation using plane waves should give reasonable results.

§ 5. NUMERICAL RESULTS

Taking various incident energies and various nuclei, and neglecting the very small contributions from $\lambda > 2$ in equation (10), we have plotted the distorted angular distributions (19) for non-radial excitation in figures 1–4. The broken curves show, for comparison, the undistorted distributions $(2L+1)\mathrm{j}_L{}^2 K\bar{R}$, reduced in intensity by the factor $|f_0(\bar{R})|^2$. They correspond to breaking off the series (10) at $\lambda = 0$. It will be seen that the effects of the optical potential are as stated in the introduction. In particular, it is quite sufficient around the peaks of these non-radial distributions to use the undistorted distributions with the reduction factor $|f_0|^2$. These calculations indicate therefore that the mixing of orbital angular momenta by the optical potential may be ignored around the peaks. Thus any dominant orbital angular momentum transfer L will produce an undistorted peak $\mathrm{j}_L{}^2(K\bar{R})$, and this will remain true irrespective of any complications which may arise from a better treatment of the spin-dependence of the matrix $T_{\mathbf{K}}(j)$. This gives one some measure of confidence in the interpretation of experimental distributions. The non-vanishing forward scattering predicted for $L=2$ non-radial transitions has been observed by Strauch and Titus (1956), and is apparent also in the calculations of Levinson and Banerjee (1958), Mohr (1958) and Benoist, Marty and Meyer (1957). The absence of subsidiary maxima and minima in experimental angular distributions may be accounted for by a proper treatment of the radial integration (cf. Levinson and Banerjee 1958, Mohr 1958). The spin–orbit potential and multiple inelastic scattering within the nucleus may also have a similar effect.

We have plotted the angular distributions (20) for radial excitation in figures 5–8, taking zero orbital angular momentum transfer L. The broken curves represent the undistorted distributions modified by a factor $|f_0(\frac{1}{2}\bar{R}_1+\frac{1}{2}\bar{R}_2)|^2$. These show no forward peak. The dotted curves were obtained taking account of the radial dependence of $f_0(r)$, but neglecting the terms containing $f_2(r)$. The difference between these and the full curves is quite large, showing that the optical mixing of angular momenta expressed in equation (18*a*) is important here.

§ 6. COMPARISON WITH EXPERIMENT

We have compared the preceding angular distributions with the experimental distributions obtained when certain levels in the nuclei ^{12}C, ^{16}O and ^{40}Ca are excited by 186 Mev protons, as investigated by Tyrén and Maris (1957). The matrix $T_{\mathbf{K}}(j)$ can be derived from a table given by Squires (1958). The central and spin-dependent parts of $T_{\mathbf{K}}(j)$ are equally important on the average over the range of angles required (about 0°–45° in the laboratory). Because of the various spin–orbit contributions to $T_{\mathbf{K}}(j)$, interference terms such as $a_L{}^{\mu}a_{L'}{}^{\mu'*}$ should appear in the angular distributions (19) and (20), but we do not anticipate that their inclusion would alter the features of the predicted angular distributions in any transitions where one L-value is dominant. Distributions due to two L-values mixing together through the spin–orbit parts of $T_{\mathbf{K}}(j)$, e.g. $L=J-1$ and $L=J+1$, should be distinguishable by the broadness of the resultant angular distribution peak.

Although individual terms in $T_{\mathbf{K}}(j)$ depend appreciably on the scattering angle, we expect that the resultant angle-dependence of the differential cross section is largely compensated as between one term and another. A direct comparison with the angular distributions (19) and (20) is therefore relevant. An average value for $T_{\mathbf{K}}(j)$ at 186 Mev, appropriate to the units used in equation (1), is given by $(2\pi)^{-2}|k^2T|^2 \sim 0{\cdot}5$. The scale of our theoretical angular distributions is set by multiplying (19) and (20) by the above number and by E^2/k^4. Reduced nuclear matrix elements of the operators $\mathrm{Y}_L{}^{\mu}(j)$ and $\mathrm{Y}_L{}^{\mu}(j)\boldsymbol{\sigma}_j$, and other nuclear angular momentum factors, will give a further factor of order unity, which however we do not attempt to predict theoretically in the present work.

The nuclei ^{12}C, ^{16}O and ^{40}Ca all have 0^+ ground states, so that the angular momentum transfer J is unique. This reduces the number of possibilities to be considered. In figures 9–11 we show experimental points and theoretical curves fitted to them. The vertical scale has been fixed in each case as just explained, with however additional overall factors to obtain the best fit. These extra factors, listed in the figures, range from 0·5 to 2, in reasonable agreement with what might be expected from the detailed nuclear matrix elements mentioned above, and other small corrections. The curves are in all cases taken from figures 1–8, but in setting the horizontal scale we have used $R=1{\cdot}5A^{1/3}$, as this gives a better fit to the positions of the peaks than would be obtained with the halfway radius $R=1{\cdot}25A^{1/3}$.

There are two cases of particular interest: the 9·6 MeV excitation in ^{12}C and the excitation at 6·1 MeV in ^{16}O, for both of which the observed peak is considerably broader than the characteristic diffraction maximum $j_L{}^2$. The peak for the carbon level is centred at an angle appropriate to (non-radial) $L=3$, but the distribution also shows some tendency to non-zero forward scattering, appropriate to distorted $L=2$. We should thus be led to a superposition of $L=2$ and $L=4$, which gives an excellent fit, as shown by the full line in figure 10. However, the interpretation $L=J\pm 1$, $J=3^+$ is not in agreement with the known low-lying levels of even–even nuclei. There remains the possible mixing of two distinct levels, $J=2^+$ and $J=4^+$, lying within the range of experimental energy, 9·6 ± 0·2 MeV. There are other grounds for believing in the presence of these two levels. Thus the cross section in the forward direction for excitation by electrons of a known level at 9·61 MeV can be explained on the basis of a 2^+ transition (Fregeau 1956). (An alternative explanation in terms of a 1^- transition (Ferrell and Visscher 1956) seems definitely to be ruled out by the present approach.) A 4^+ level in this energy region has been predicted by Kurath (1956), on the basis of the intermediate coupling model.

The excitation at 6·1 ± 0·2 MeV in ^{16}O is also roughly centred at $L=3$, with a tendency to non-zero forward scattering. However, the distribution falls off beyond the peak more rapidly than in the preceding case, which tends to rule out a contribution from $L=4$, and the objection to a 3^+ level is the same for this nucleus as for ^{12}C. A mixture of radial 0^+ transition with a normal 3^- transition is shown in figure 11, and is in very good agreement with the data. Both these levels are in fact believed to occur within the range of experimental energy, the 3^- at 6·13 MeV and the single particle 0^+ radial transition as the major contribution to a level at 6·06 MeV (Elliott and Lane 1957).

Little uncertainty arises in fitting the other experimental angular distributions in figures 9 and 10, and the resulting spins and parities are in agreement with those assigned from other data to levels with the same excitation energies.

We may conclude that the theory may be used with some confidence as one line of attack in predicting the spins and parities of unknown transitions.

ACKNOWLEDGMENTS

We wish to thank Professor J. M. Cassels for bringing this problem to our attention and for his stimulating remarks, and Dr. R. Huby and Dr. H. C. Newns for their good advice. We also wish to thank Miss M. Elmslie and Miss M. Stynes for their valuable assistance in calculating the angular distributions.

REFERENCES

BENOIST, P., MARTY, C., and MEYER, P., 1957, *C. R. Acad. Sci., Paris*, **245**, 1389.
ELLIOTT, J. P., and LANE, A. M., 1957, *Handbuch der Physik*, **34**, 368 (Berlin: Springer).
FERRELL, R. A., and VISSCHER, W. M., 1956, *Phys. Rev.*, **104**, 475.
FREGEAU, J. H., 1956, *Phys. Rev.*, **104**, 225.
KURATH, D., 1956, *Phys. Rev.*, **101**, 216.
LEVINSON, C. A., and BANERJEE, M. K., 1958, *Annals of Physics*, **3**, 67.
MARIS, TH. A. J., and TYRÉN, H., 1957, *Nucl. Phys.*, **3**, 35; **4**, 662.
McCAULEY, G. P., and BROWN, G. E., 1958, *Proc. Phys. Soc.*, **71**, 893.
MOHR, C. B. O., 1958, *Proc. Phys. Soc.*, **71**, 717.
SCHIFF, L. I., 1956, *Phys. Rev.*, **103**, 443.
SQUIRES, E. J., 1958, *Nucl. Phys.*, **6**, 504.
STRAUCH, K., and TITUS, F., 1956, *Phys. Rev.*, **103**, 200.
TYRÉN, H., and MARIS, TH. A. J., 1957, *Nucl. Phys.*, **3**, 52, **4**, 637.
—— 1958, *Ibid.*, **6**, 82.

Direct Interaction with Strong Coupling in Nuclear Collisions

By C. B. O. MOHR
Physics Department, University of Melbourne

Communicated by L. H. Martin; MS. received 8th December 1958

Abstract. For direct nuclear reactions in which there is a large probability of a particular inelastic collision, coupling between the waves in the two channels will modify the elastic and inelastic scattering as given by the distorted wave approximation. The extent of the modifications is investigated for the simplest case of E0 excitations, taking rectangular wells for the nuclear potential and the transition potential. The case of several open channels is briefly considered.

---

§ 1. INTRODUCTION

It has now become evident that, for most nuclear reactions above 10 MeV, direct interaction throughout the nucleus is the main mechanism, compound nucleus formation playing a comparatively small part.

The angular distribution of inelastic scattering often seems to be accounted for by the simplest approximation available, the Born approximation, in which the incident particles are represented by plane waves. Since the theory is a wave theory, it gives diffraction effects such as are observed at the lower energies, and a fit is often obtained with the position of the maxima and minima by arbitrary adjustment of the nuclear radius.

Such agreement must be somewhat fortuitous, since there are many cases in which there is no resemblance between theoretical and experimental curves, unless account is taken of the distortion of the incident waves by the nuclear potential. Even at 90 MeV it has been found necessary to use the distorted wave approximation to obtain satisfactory agreement with experiment (Mohr 1958).

The distorted wave approximation has, however, run into difficulties. Thus Levinson and Banerjee (1958), in a systematic investigation of inelastic proton scattering in carbon over a wide range of energies, were able to obtain satisfactory agreement with experiment only by using a nuclear potential two-thirds that required to fit the elastic scattering, although they tried varying other nuclear parameters.

The next improvement in the theory is to allow for the coupling between the elastically and inelastically scattered waves; and it may sometimes be necessary to take account of the coupling for the following reason. In the distorted wave approximation the intensity is proportional to the square of the transition potential and so increases without limit, whereas there is an upper bound to the total inelastic cross section—from considerations of conservation—which is implicit in the strong coupling theory. This upper bound is of the order of the geometrical cross section, and as inelastic scattering cross sections of comparable value are found, the coupling may appreciably modify results obtained in the distorted wave approximation. Furthermore, results obtained for the elastic scattering by the usual phase shift (distorted wave) method may be appreciably modified by the coupling to the inelastic scattering.

Strong coupling in the rotational excitation of a heavy nucleus by neutrons has been considered by Chase, Wilets and Edmonds (1958), using the collective model. The present paper considers strong coupling in single-particle excitation of a light nucleus, using the independent particle model.

§ 2. THEORY

Let the ingoing and elastically scattered particles have mass M, wave number $k/2\pi$, energy E, radial wave function F_0, and move in a potential $-V_{00}$; and when the particles go out through channel n let the corresponding quantities be $k_n/2\pi$, E_n, F_n, $-V_{nn}$. Denote the transition potentials by $-V_{nm}$ (the values of the V's are then all positive). Let the quantities E, E_n, $-V_{nm}$ have incorporated in them the factor $8\pi^2M/h^2$ associated with them in the wave equation, so that we may write

$$E=k^2, \qquad E_n=k_n^2. \qquad \qquad ......(1)$$

Then the coupled equations take the form

$$(\nabla^2+E_n)F_n=-\sum_m V_{nm}F_m; \quad m, n=0, 1, 2 .... \qquad ......(2)$$

In this paper we discuss only the case where all the potentials V_{nm} are spherically symmetrical, which implies consideration of E0 excitations only. Otherwise calculations are complicated and very lengthy. Putting

$$F_0=r^{-1}\sum_l F_0^l(r)\mathrm{P}_l(\cos\theta), \qquad ......(3)$$

F_n similarly, the coupled equations become

$$\frac{d^2F_n^l}{dr^2}+[E_n-l(l+1)r^{-2}]F_n^l=-\sum_m V_{nm}F_m^l. \qquad ......(4)$$

If there are only two channels the coupled equations may be written

$$\frac{d^2F_0^l}{dr^2}+[E+V_{00}-l(l+1)r^{-2}]F_0^l=-V_{01}F_1^l, \qquad ......(5a)$$

$$\frac{d^2F_1^l}{dr^2}+[E_1+V_{11}-l(l+1)r^{-2}]F_1^l=-V_{01}F_0^l. \qquad ......(5b)$$

The best form for V_{00} and V_{11} is a Saxon potential, with an imaginary component to allow for absorption of the waves in the nucleus. V_{01} is the potential energy of the direct interaction between the incident and the nuclear particle, averaged over the transition density $\psi_0\psi_1$ of the nuclear particle; and as the interaction is of short range, V_{01} has approximately the form of $\psi_0\psi_1$. The equations (5) then have to be solved by numerical integration from the origin outwards. There are two independent solutions for F_0^l and F_1^l which vanish at the origin, and they may be started off by taking V_{00} and V_{11} constant for small r, for then the exact solutions are known (see below). A linear combination of the two interior solutions must be joined smoothly at the nuclear boundary $r=R$ to the exterior solutions which have the form

$$F_0^l(r\geqslant R)=(2l+1)i^l[kr\mathrm{j}_l(kr)+\alpha_l kr\mathrm{h}_l^{(1)}(kr)], \qquad ......(6a)$$

$$F_1^l(r\geqslant R)=(2l+1)i^l\beta_l k_1 r\mathrm{h}_l^{(1)}(k_1 r). \qquad ......(6b)$$

The terms containing j_l and $\mathrm{h}_l^{(1)}$ are for the incident and outgoing wave respectively, the j_l and $\mathrm{h}_l^{(1)}$ being spherical Bessel and spherical Hankel functions respectively, with $\mathrm{h}_l^{(1)}$ given by $\mathrm{j}_l + i\mathrm{n}_l$.

The four continuity equations involving F_0, F_1 and their slopes at the boundary can be solved for the quantities α_l and β_l. These satisfy the conservation theorem

$$|\alpha_l|^2 \leqslant 1, \qquad (k_1/k)|\beta_l|^2 \leqslant \tfrac{1}{4}. \qquad \ldots\ldots(7)$$

The differential cross sections for elastic and inelastic scattering are given by

$$\sigma_{\mathrm{el}}(\theta) = k^{-2}|\sum_l (2l+1)\alpha_l \mathrm{P}_l(\cos\theta)|^2, \qquad \ldots\ldots(8\,a)$$

$$\sigma_{\mathrm{in}}(\theta) = k_1 k^{-3}|\sum_l (2l+1)\beta_l \mathrm{P}_l(\cos\theta)|^2, \qquad \ldots\ldots(8\,b)$$

and the corresponding integrated cross sections by

$$\sigma_{\mathrm{el}} = 4\pi k^{-2}\sum_l (2l+1)|\alpha_l|^2, \qquad \ldots\ldots(9\,a)$$

$$\sigma_{\mathrm{in}} = 4\pi k_1 k^{-3}\sum_l (2l+1)|\beta_l|^2. \qquad \ldots\ldots(9\,b)$$

When V_{01} is small, α_l and β_l tend to the values given by the distorted wave approximation:

$$\alpha_l = \tfrac{1}{2}[\exp(2i\eta_l^0) - 1], \qquad \ldots\ldots(10\,a)$$

$$\beta_l = k_1^{-1}\int V_{01}\,{}_0F_0^l\,{}_0F_1^l\,dr, \qquad \ldots\ldots(10\,b)$$

where the distorted waves ${}_0F_0^l$ and ${}_0F_1^l$ are the regular solutions of (5 *a*) and (5 *b*) with $V_{01} = 0$, normalized to the asymptotic values

$${}_0F_0^l \sim (2l+1)i^l \exp(i\eta_l^0)\sin(kr - \tfrac{1}{2}l\pi + \eta_l^0), \qquad \ldots\ldots(11\,a)$$

$${}_0F_1^l \sim (2l+1)i^l \exp(i\eta_l^1)\sin(k_1 r - \tfrac{1}{2}l\pi + \eta_l^1). \qquad \ldots\ldots(11\,b)$$

For larger V_{01} the asymptotic form of F_0^l in (6 *a*) is easily seen to be (11 *a*) with a complex phase $\eta_l = \eta_l^r + i\eta_l^i$ in place of the real phase η_l^0, where η_l is related to α_l and β_l by

$$\alpha_l = \tfrac{1}{2}[\exp(2i\eta_l) - 1], \qquad \ldots\ldots(12\,a)$$

$$|\beta_l|^2 = \tfrac{1}{4}[1 - \exp(-4\eta_l^i)]. \qquad \ldots\ldots(12\,b)$$

There appears to be some connection here with the optical model; but a complex potential which will produce the complex phases cannot be the same for different orders l and for different energies. In the optical model a complex V_{00} is chosen arbitrarily to give a 'consistent' set of η_l^i and hence of $|\beta_l|^2$, such that the resulting value of σ_{in} is of the observed magnitude; but the β_l themselves, and hence $\sigma_{\mathrm{in}}(\theta)$, cannot be determined. We shall use the optical model to represent the effect of channels additional to the two under investigation.

For V_{00}, V_{11} and V_{01} constant within the nuclear radius, the interior solutions of the coupled equations are of the form

$$F_0^l = L\lambda r\mathrm{j}_l(\lambda r) + M\mu r\mathrm{j}_l(\mu r), \qquad \ldots\ldots(13\,a)$$

$$F_1^l = \gamma_1 L\lambda r\mathrm{j}_l(\lambda r) + \delta_1 M\mu r\mathrm{j}_l(\mu r), \qquad \ldots\ldots(13\,b)$$

for the equations are satisfied on substitution, if λ and μ are the positive roots of χ in the equation

$$(\chi^2 - E - V_{00})(\chi^2 - E_1 - V_{11}) = V_{01}^2, \qquad \ldots\ldots(14\,a)$$

and if

$$\gamma_1 = (\lambda^2 - E - V_{00})/V_{01}, \qquad \delta_1 = (\mu^2 - E - V_{00})/V_{01}. \qquad \ldots\ldots(14\,b)$$

Fitting the interior solutions (13) smoothly to the exterior solutions (6) at the nuclear boundary gives four equations containing the four unknowns L, M, α_l and β_l. The values of α_l and β_l are then given in terms of 4×4 determinants containing spherical Bessel functions and their derivatives and a few zero terms. Substituting for the α_l and β_l in (8) and (9) gives the angular distributions and total cross sections.

If we neglect the energy loss of the incident particles in comparison with their incident energy, so that $E_1 = E$ and $V_{11} = V_{00}$, we have from (14) the following simplifications:

$$k_1 = k,$$

$$\lambda = (E + V_{00} + V_{01})^{1/2}, \qquad \mu = (E + V_{00} - V_{01})^{1/2}, \qquad \ldots\ldots (15\,a)$$

$$\gamma_1 = 1, \qquad \delta_1 = -1. \qquad \ldots\ldots (15\,b)$$

§ 3. CALCULATIONS

For simplicity a square well was taken for $V_{00} = V_{11}$ and V_{01}. The radius R was taken to be 2·9 fermi and the depth V_{00} to be 47 MeV, these values being about the average of those used in the most recent optical model calculations of the elastic scattering of protons in carbon (e.g. Glassgold and Kellogg 1957). The value of V_{01} was varied in the calculations. The case of carbon is of particular interest, as the angular distribution of inelastically scattered protons for the principal energy loss (4·4 MeV) has been studied over a wide range of energies. Furthermore the total cross section for this loss reaches two-thirds the geometrical cross section at 14 MeV (Peelle 1957), so that we have a clear case of strong coupling. Unfortunately the excited state does not have the same spin as the ground state, so that V_{01} is not spherically symmetrical. In such case the coupled equations have the same left-hand sides as (5), but right-hand sides with wave functions of order different from l, and the solution of the equations is a very lengthy process.

Although a case of single-particle E0 excitation of high probability might be hard to find, it was decided to study such a case first, since it provides a good deal of information comparatively quickly. Once the general features emerging from the study are understood, the more confidently can excitations of other multipolarities be tackled.

The excitation energy was taken to be negligible in comparison with the incident energy, so that $k_1 = k$, for this assumption nearly halves the labour of computing the α_l and β_l. This simplification will certainly not alter the general conclusions. The calculations will be valid for proton as well as neutron scattering, since the height of the Coulomb barrier for carbon is small compared with the incident energies studied here; and experiment shows that the angular distribution is practically the same for neutrons and protons at 14 MeV for both the elastic scattering (Peelle 1957, Nakada *et al.* 1958) and the inelastic scattering (Anderson *et al.* 1958).

For complex V_{00} the necessary spherical Bessel and Hankel functions of complex argument were readily calculated by expansion in a Taylor series of powers of the imaginary part of the argument, the required derivatives of the j_l and n_l of real argument being obtained in terms of finite differences, using closely tabulated values of j_l and n_l (National Bureau of Standards 1947).

§ 4. Results and Discussion

4.1. *Partial Cross Sections*

The variation of $|\alpha_l|^2$ and $|\beta_l|^2$ with V_{01} for real V_{00} at $E=18$ Mev is shown in figure 1. The values of $|\alpha_4|^2$ and $|\beta_4|^2$ and higher order terms are too small to show in the diagram or affect results. The $|\beta_l|^2$ start to deviate from the values given by the distorted wave method at about $V_{01}=5$ Mev, and each reaches its maximum value of 0·25 at a different value of V_{01}.

The fall in $|\beta_l|^2$ when V_{01} is increased still further is due to the splitting of the wave number $(E+V_{00})^{1/2}/2\pi$ of the interior wave for $V_{01}=0$ into two values $(E+V_{00}\pm V_{01})^{1/2}/2\pi$ by the coupling term V_{01}. The larger V_{01}, the more the two component waves in (13) are out of step near the nuclear boundary, and hence the smaller the amplitude of the outgoing waves. Thus $\lambda R-\mu R=\pi$ for $V_{01}/(E+V_{00})=0{\cdot}57$ at $E=18$ Mev. For this reason the best basis of comparison of curves for different energies is with $V_{01}/(E+V_{00})$ as abscissa rather than V_{01}/V_{00}.

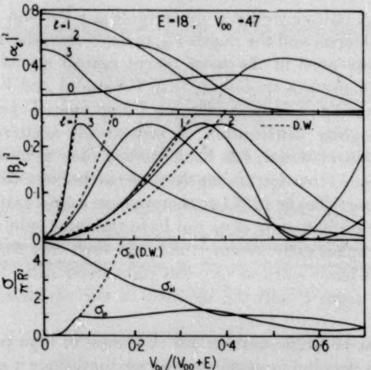

Figure 1. Scattering of neutrons of energy $E=18$ Mev by a square well of radius $R=2{\cdot}9$ fermi and depth $V_{00}=47$ Mev. $|\alpha_l|^2$ is the probability of elastic scattering, $|\beta_l|^2$ of inelastic scattering, for neutrons with angular momentum $l^{1/2}(l+1)^{1/2}\hbar$. σ_{el} and σ_{in} are the total cross sections for elastic and inelastic scattering respectively. These quantities are graphed as a function of the transition potential V_{01}, which is taken to be spherically symmetrical (E0 excitation). The broken curves (marked D.W.) are for the distorted wave approximation.

The maxima vary their positions with energy, generally being closer together as the energy increases. The more rapid the initial rise in a particular $|\beta_l|^2$, the more rapid is the deviation of the corresponding $|\alpha_l|^2$ from its initial value as V_{01} increases. The value of $|\alpha_l|^2$ for $V_{01}=0$ is, of course, that given by the phase shift method for elastic scattering, as may be seen from (10*a*) and (9*a*).

In the distorted wave approximation, the variation of the $|\beta_l|^2$ amongst themselves is seen to be much greater than that of the $|\alpha_l|^2$, and throughout this and related work it was found that the inelastic scattering was much more sensitive than the elastic scattering to changes in the nuclear potential V_{00}. With strong coupling the values of the different $|\beta_l|^2$ for a given V_{01} vary much less. Thus in figure 1 the contribution of the third order wave to the inelastic scattering is particularly large in the distorted wave approximation, but it is much reduced by strong coupling.

The α_l and β_l are complex, and their phases vary differently with V_{01} for different l. We have here an additional cause for $\sigma(\theta)$ to vary with V_{01} for strong coupling. In the distorted wave approximation $\sigma_{\text{in}}(\theta)$ does not vary in form with V_{01}, though it varies in magnitude as V_{01}^2.

A further improvement in this work—though it requires more labour—is to allow for absorption of the incident waves in exciting the nucleus, not only to the level under consideration, but to other levels also. This is done by taking a complex V_{00} in (14), and hence complex λ and μ in (13). Figure 2 shows cross sections obtained for $E = 18$ Mev with $V_{00} = 47 + 2{\cdot}5i$ Mev and $47 + 10i$ Mev. Increasing the absorption is seen to diminish the cross sections, in both the distorted wave and the strong coupling methods, as is to be expected; for when more channels are open, less particles emerge through a particular channel (see § 5). Increasing absorption also brings the positions of the maxima in the different $|\beta_l|^2$ closer together.

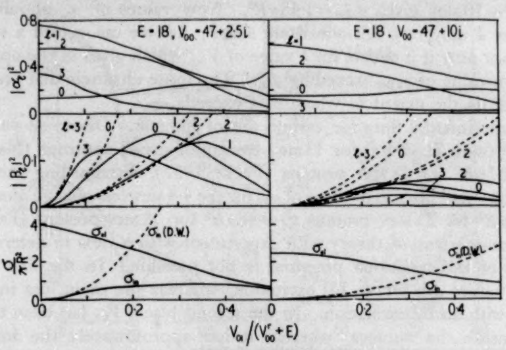

Figure 2. As for figure 1, but for complex wells of depths $V_{00} = 47 + 2{\cdot}5i$ Mev and $47 + 10i$ Mev. $V_{00}{}^{r}$ is the real part of V_{00}.

4.2. *Total Cross Sections*

The total cross sections σ_{el} and σ_{in}, expressed in units of the geometrical cross section πR^2, are shown in the bottom sections of figures 1 and 2. Increasing the coupling between the waves F_0 and F_1 tends to bring σ_{el} and σ_{in} to approximate equality and then diminish both.

For no absorption (figure 1) there is a resonance in the third order wave for $V_{01} = 0$ which causes most of the initial rapid rise in σ_{in} and initial rapid fall in σ_{el} with increasing V_{01}. For $E = 12{\cdot}6$ Mev the resonance was found to be less marked and to be shifted to larger V_{01}, $\sigma_{\text{in}}/\pi R^2$ reaching a maximum value of 1·9 at $V_{01}/(E + V_{00}) = 0{\cdot}3$ and $\sigma_{\text{el}}/\pi R^2$ rising from 3·3 to a maximum of 4·4 as $V_{01}/(E + V_{00})$ increases from 0 to 0·2. Resonance occurs in general for equality at the nuclear boundary of the logarithmic derivatives of one of the two terms in (13) comprising the interior wave function and the exterior wave function.

Allowing for absorption by putting $V_{00}=V_{00}^{r}+iV_{00}^{i}$ (figure 2) damps any resonance and causes σ_{in} to rise more slowly to reach a smaller maximum value, this value being $0{\cdot}88\pi R^2$ and $0{\cdot}34\pi R^2$ when V_{00}^{i} is 2·5 MeV and 10 MeV respectively. It was at first thought that such a large reduction in σ_{in} might arise partly from the use of a step function for V_{00} and V_{01}, but a similar result was obtained with a rounded-off potential of the Saxon type, the coupled equations being solved by numerical integration. Chase, Wilets and Edmonds (1958), using a complex potential in their collective model, have obtained similar reductions in their rotational excitation cross sections.

Using the complex potential in the usual optical model calculation, it is found that $V_{00}^{i}=2{\cdot}5$ MeV gives an absorption cross section σ_{abs} of $0{\cdot}81\pi R^2$, while $V_{00}^{i}=10$ MeV gives $\sigma_{\mathrm{abs}}=1{\cdot}48\pi R^2$. Now values of σ_{in} should be taken from figure 2 only in a self-consistent sense; i.e. we can accept a value of σ_{in} as significant only if it occurs for a value of V_{00}^{i} which gives in the optical model treatment a value of σ_{abs} exceeding σ_{in}. The more channels that are open, the greater will be the extent to which σ_{abs} exceeds σ_{in}.

The experimental data for carbon are of interest. Observed values of σ_{el} are $2{\cdot}0\pi R^2$ (with $R=2{\cdot}9$ f) for 13 MeV (centre-of-mass) neutrons (Nakada *et al.* 1958), and $3\pi R^2$ for 18 MeV protons (Peelle 1957), disregarding the Coulomb contribution; and observed values of σ_{in} for the 4·4 MeV loss change monotonically from $0{\cdot}85\pi R^2$ for 13 MeV protons to $0{\cdot}48\pi R^2$ for 18 MeV protons (Peelle 1957).

Exact comparison of theory with experiment with a view to determining the magnitude of the transition potential is not possible. In the first place, the calculated values are for an E0 excitation, whereas the main loss in carbon is associated with an E2 excitation. In the second place, V_{01} has been taken to be constant inside the nucleus, whereas it has approximately the form of the transition density of the excited nucleon, and so is strongly peaked. But one can safely predict that if the cross section for excitation to one or more levels is comparable with πR^2, σ_{el} will be reduced appreciably below the value calculated with neglect of coupling.

4.3. *Differential Cross Sections*

Differential cross sections for $E=18$ MeV are shown in figure 3. Curves for inelastic scattering obtained in the distorted wave approximation have the same form for all V_{01}, and magnitude proportional to V_{01}^2; and it is seen that they depart seriously from the curves obtained with strong coupling for $V_{01}/(E+V_{00})>0{\cdot}1$. It must be remembered that the logarithmic scale used tends to minimize differences except near a low minimum, where differences are over-emphasized. The strong coupling curves for both the elastic and inelastic scattering vary their form considerably with V_{01} for $V_{00}=47$ MeV, while the variation is much less for $V_{00}=47+10i$ MeV.

For $E=12{\cdot}6$ MeV (figure 4) corresponding pairs of curves for complex V_{00} and real V_{00} are most markedly different for $V_{01}=12$ MeV, whereas for $E=18$ MeV the most marked difference occurs for $V_{01}=0$. This is because the resonance in the f wave occurs for $V_{01}=12$ MeV at $E=12{\cdot}6$ MeV and for $V_{01}=0$ at $E=18$ MeV, as remarked in § 4.2.

Since $V_{01}/(E+V_{00})$ has to be at least 0·2 to obtain a value of σ_{in} comparable with πR^2, it is clear that angular distributions calculated with neglect of coupling may be seriously in error when σ_{in} for a particular excitation is comparable with πR^2.

At these energies the angular distributions are sensitive, not only to V_{01} but also to V_{00}. Thus at $E=18$ Mev, $\sigma_{\text{in}}(\theta)$ has three minima for $V_{00}=47$ Mev, but only two for $V_{00}=32$ Mev, the form of the curves being entirely changed. For $V_{00}=47$ Mev the f wave is predominant, $\sigma_{\text{in}}(\theta)$ having very approximately the form $[\text{P}_3(\cos\theta)]^2$ for small V_{01}, while for $V_{00}=32$ Mev the resonance in the f wave disappears. $\sigma_{\text{el}}(\theta)$ is much less affected than $\sigma_{\text{in}}(\theta)$ by the change in V_{00}.

For $E=90$ Mev (figure 5) the $\sigma(\theta)$ are relatively little affected in form by changes in V_{01}, though the magnitude of σ_{in} is altered. Introducing an imaginary component into V_{00} has previously been found to have relatively little effect on the form of $\sigma(\theta)$ at this energy (Mohr 1958), and changes in the magnitude of V_{00} will have less effect than at lower energies. But the curves are more sensitive than at lower energies to the form of V_{00} and V_{01}. The use of rectangular wells is seen to give marked diffraction maxima and minima, whereas the use of rounded-off potentials largely eliminates them (Mohr 1958), as shown by the dotted curve in figure 5 (magnitude arbitrarily adjusted for purposes of comparison). This smoothing-out of maxima and minima occurs much less at lower energies, where the diffraction effect often arises largely from a single predominant spherical harmonic.

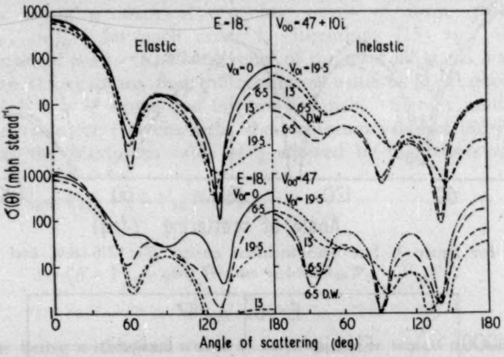

Figure 3. Differential cross sections for the elastic and inelastic scattering of neutrons of energy $E=18$ Mev by square wells of radius $R=2{\cdot}9$ fermi and depth $V_{00}=47+10i$ Mev and 47 Mev, for values of the transition potential V_{01} indicated on the curves (in Mev). The curves marked D.W. are for the distorted wave approximation, for $V_{01}=6{\cdot}5$ Mev. Distorted wave curves for other values of V_{01} will have the same form, but magnitude proportional to $V_{01}{}^2$, and will agree with the exact curves for sufficiently small V_{01}.

We have so far discussed E0 excitations. For E2 excitations the distorted wave approximation was found to give an inelastic angular distribution at 18 Mev with $V_{00}=47$ Mev considerably different from that observed in carbon (Peelle 1957), the discrepancy arising largely from the predominance of the f wave. A fit has been obtained with the distorted wave approximation with a Saxon well with depth 32 Mev and other parameters suitably chosen (Levinson and Banerjee 1958). With strong coupling a large contribution from a single harmonic should be much reduced for excitations of any multipolarity, so that a fit to the

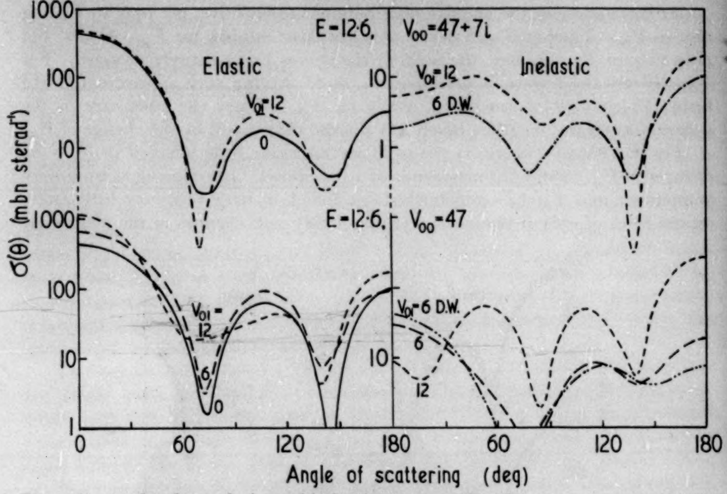

Figure 4. As for figure 3, but with incident energy $E = 12{\cdot}6$ MEV, and well depths $V_{00} = 47 + 7i$ and 47 MEV.

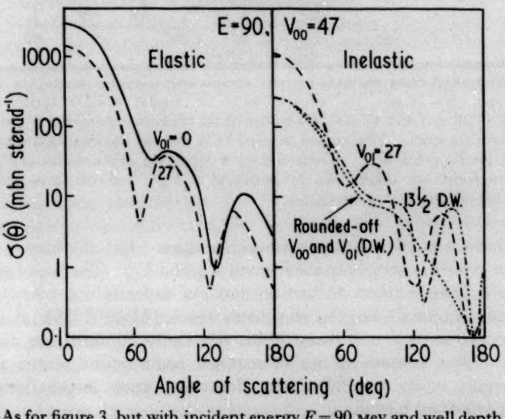

Figure 5. As for figure 3, but with incident energy $E = 90$ MEV and well depth $V_{00} = 47$ MEV. The dotted curve is for the distorted wave approximation with a Saxon potential for V_{00} and with V_{01} having the form of a p nucleon distribution within the nucleus.

inelastic scattering may be obtained with parameters more nearly the same as those required to fit the elastic scattering.

§ 5. MORE THAN TWO CHANNELS

At sufficiently high energies there will be several channels of comparable importance. Suppose there are $n+1$ channels with the same spin and parity.

We then have to solve $n+1$ coupled equations, one of them like (5 *a*) and n like (5 *b*). Take $E_s = E$ and $V_{ss} = V_{00}$ where $s = 1, 2, \ldots n$. In order to obtain insight into the most general features of the problem, we take V_{00} real and consider two cases which permit of easy solution.

Case (*i*). $V_{0s} = V_{01}$, $V_{st} = 0$ for $t \neq s$.

Then

$$\lambda = (E + V_{00} + n^{1/2} V_{01})^{1/2}, \quad \mu = (E + V_{00} - n^{1/2} V_{01})^{1/2}, \quad \ldots\ldots (16\,a)$$

$$\gamma_1 = \gamma_2 = \ldots = \gamma_n = n^{-1/2}, \quad \delta_1 = \delta_2 = \ldots = \delta_n = -n^{-1/2}, \quad \ldots\ldots (16\,b)$$

there now being n identical outgoing waves of form (6 *b*), for which $\beta_l^{(1)} = \beta_l^{(2)} = \ldots = \beta_l^{(n)}$ for each order l. Equations (15) are, of course, the particular case of $n = 1$. The occurrence of the term $n^{1/2} V_{01}$ in λ and μ in place of V_{01} as in (15 *a*) means that the maximum value of $|\beta_l^{(s)}|^2$ occurs at a value of V_{01} which is $n^{-1/2}$ times that for two channels. Since γ_s and δ_s have $n^{-1/2}$ times their value for two channels, the maximum value of $|\beta_l^{(s)}|^2$ is $\frac{1}{4} n^{-1}$, and $\Sigma_s |\beta_l^{(s)}|^2$ has the maximum value of $\frac{1}{4}$ allowed by the conservation theorem

Case (*ii*). $V_{0s} = V_{01}$, $V_{st} = V_{01}$ for $t \neq s$.

Then

$$\lambda = (E + V_{00} + n V_{01})^{1/2}, \quad \mu = (E + V_{00} - V_{01})^{1/2}, \quad \ldots\ldots (17\,a)$$

$$\gamma_1 = \gamma_2 = \ldots = \gamma_n = 1, \quad \delta_1 = \delta_2 = \ldots = \delta_n = -n^{-1}, \quad \ldots\ldots (17\,b)$$

there again being n identical waves of form (6 *b*) for which $\beta_l^{(1)} = \beta_l^{(2)} = \ldots = \beta_l^{(n)}$. The maximum of $|\beta_l^{(s)}|^2$ is found to occur at a value of V_{01} which is very approximately $2(n+1)^{-1}$ times that for two channels, while the maximum value of $\Sigma_s |\beta_l^{(s)}|^2$ falls further and further below the maximum permissible value of $\frac{1}{4}$ as n increases. The variation of the phase of $\beta_l^{(s)}$ with V_{01} is considerably different from that for case (i).

Cases (*i*) *and* (*ii*). Allowing for absorption will not reduce $\beta_l^{(s)}$ much, for the imaginary component which one includes in V_{ss} must correspond to an absorption coefficient for channel s only, not for all the channels as in § 4.1, as this would count the absorption in each channel a number of times. The maximum value of $\sigma_{\text{in}} = \Sigma_s |\beta_l^{(s)}|^2$ will therefore be close to πR^2. Remembering that we have not been considering nuclear reactions other than inelastic collisions, the calculated value of σ_{in} must be compared with experimental values of the non-elastic cross section. For neutrons with energies above 10 MeV and for a wide range of elements, the non-elastic cross section is found to be close to the geometrical cross section obtained after allowing for surface diffuseness (MacGregor *et al.* 1958).

The shift of the maximum in $|\beta_l^{(1)}|^2$ to smaller V_{01} when there are more channels open is not inconsistent with the shift of the maximum to larger V_{01} with increased $V_{00}{}^{\text{i}}$ shown in figure 2. For in the former case we have in effect an 'absorption' associated with channel 1 due to loss of particles to the other $n-1$ channels, and this varies as $|\beta_l^{(s)}|^2$ and so is small for small V_{01}. But in the latter case (figure 2) the absorption is taken to be constant for all V_{01}.

§ 6. EXTENSION OF THE WORK

It is not clear whether the use of more realistic forms for V_{00} and V_{01} will appreciably modify the general conclusions for the lower energies considered here. It is possible that much of the contribution to the inelastic scattering comes from the diffuse surface of the nucleus, because of partial suppression of volume effects by internal reflection, for energies below about 40 Mev; and a satisfactory representation of this effect may be achieved by taking a form for V_{00}^{i} and V_{01} which is peaked at the nuclear surface.

A more fundamental—but more difficult—question is how modifications due to coupling depend on the change of spin of the target nucleus in the collision.

Introduction of strong coupling certainly makes the problem of direct nuclear reactions much harder, but it seems that it may sometimes be unsafe to attach full significance to results obtained with the distorted wave approximation.

REFERENCES

Anderson, J. D., Gardner, C. C., McClure, J. W., Nakada, M. P., and Wong, C., 1958, *Phys. Rev.*, **111**, 572.

Chase, D. M., Wilets, L., and Edmonds, A. R., 1958, *Phys. Rev.*, **110**, 1080.

Glassgold, A. E., and Kellogg, P. J., 1957, *Phys. Rev.*, **107**, 1372.

Levinson, C. A., and Banerjee, M. K., 1958, *Annals of Physics*, **3**, 67.

MacGregor, M. H., Ball, W. P., and Booth, R., 1958, *Phys. Rev.*, **111**, 1155.

Mohr, C. B. O., 1958, *Proc. Phys. Soc.*, **71**, 717.

Nakada, M. P., Anderson, J. D., Gardner, C. C., and Wong, C., 1958, *Phys. Rev.*, **110**, 1439.

National Bureau of Standards, 1947, *Tables of Spherical Bessel Functions*, Volume 1 (Columbia University Press.)

Peelle, R. W., 1957, *Phys. Rev.*, **105**, 1311.

The Three-dimensional Intensity Distribution near the Focus of Waves Diffracted by Slit and Rectangular Apertures

BY B. J. THOMPSON
College of Science and Technology, Manchester 1

Communicated by H. Lipson; *MS. received* 11*th November* 1958, *in final form* 20*th February* 1959

Abstract. The intensity near the focus of a converging wave diffracted by a rectangular aperture is investigated both theoretically and experimentally. The theoretical work is based on an extension of the classical analysis of Lommel. The experimental work is carried out using an optical diffractometer, and the positions of the axial minima on either side of the geometrical focus are measured. The results of theory and experiment are compared in various receiving planes near the geometrical focal plane.

---

§ 1. INTRODUCTION

THE intensity distributions in the focal plane of a system imaging a point source, with various shapes of aperture, are well known. When the receiving plane is displaced slightly from the focal plane the intensity distribution undergoes many interesting changes which have not been fully investigated. In the case of circular and annular apertures the intensities in various planes have been calculated (Lommel 1886 a) and theoretical intensity charts (isophote diagrams) drawn (Zernike and Nijboer 1949, Linfoot and Wolf 1953, 1956). Recently experimental work has been carried out in these laboratories in an attempt to verify the theoretical intensity distributions in the focal region for circular and annular apertures (Taylor and Thompson 1958 b).

Investigations into the intensity distributions near the focus for apertures bounded by straight edges, e.g. slits and rectangles, have not received much attention although they are of interest not only in light optics but also in the field of microwaves (cf. Mathews and Cullen 1956). Lommel (1886 b) discussed the intensity distributions near the focus for the slit, opaque strip and straight edge. The information he obtained was not sufficient to plot an intensity chart for the region near the focus for a slit aperture, nor did he extend his work to the more general case of a rectangular aperture. The experimental aspect seems to have been neglected apart from the work of Kathavate (1945), who published excellent photographs of the Fresnel diffraction patterns of square apertures showing how the pattern changes with variation in the size of the aperture until a Fraunhofer pattern is reached, and of Duffieux, Tironflet, Guenoche and Lansraux (1944).

In the present paper Lommel's work on the diffraction by a slit aperture is extended and a chart of the intensity near the focus in the error-free diffraction pattern of a slit aperture is obtained. It is shown in §3 of this paper how the intensity distribution in any plane perpendicular to the axis for a rectangular aperture may be calculated easily from the data obtained for the slit aperture. In § 4 experimental work is described which was carried out with the help of the optical diffractometer (Taylor, Hinde and Lipson 1951, Hanson, Lipson and Taylor 1953, Hughes and Taylor 1953); this instrument enables the diffraction patterns of fairly large apertures to be investigated with relative ease; in the present work the patterns of slits up to 7 cm long and squares of side up to 5 cm are used.

The theoretical and experimental results are compared in two ways. Firstly, the positions of the axial minima are measured and compared quantitatively with the theoretical results. Secondly, photographs are obtained in various planes for slit, square and rectangular apertures and are compared qualitatively with the theoretical intensity distributions in these planes.

§ 2. THEORY

2.1. *Rectangular Aperture*

Consider a rectangular aperture of width $2a$ and length $2b$ and centre C, through which passes a train of converging spherical waves of wavelength λ.

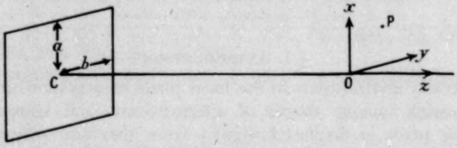

Figure 1. The coordinate system adopted.

O is the geometrical focus of the converging wave; CO $= f$ and P is some general point having rectangular coordinates x, y, z (figure 1).

Let us define four new variables:

$$\left.\begin{aligned} u &= \frac{2\pi}{\lambda}\frac{a^2}{f^2}z, & u' &= \frac{2\pi}{\lambda}\frac{b^2}{f^2}z, \\ v &= \frac{2\pi}{\lambda}\frac{a}{f}x, & v' &= \frac{2\pi}{\lambda}\frac{b}{f}y. \end{aligned}\right\} \qquad \ldots\ldots (2.1)$$

The intensity I_{R} (normalized to unity at the focus) at the point P in the diffraction pattern of a rectangular aperture is given by (see Walker 1904)

$$I_{\mathrm{R}} = \frac{\pi}{2u}\left[U^2{}_{1/2}(u,v) + U^2{}_{3/2}(u,v)\right] \times \frac{\pi}{2u'}\left[U^2{}_{1/2}(u',v') + U^2{}_{3/2}(u',v')\right] \qquad \ldots\ldots (2.2)$$

where $U_{1/2}(u,v)$ and $U_{3/2}(u,v)$ are two of the Lommel functions defined by

$$U_n(u,v) = \sum_{s=0}^{\infty} (-1)^s \left(\frac{u}{v}\right)^{n+2s} \mathrm{J}_{n+2s}(v). \qquad \ldots\ldots (2.3)$$

The J's are Bessel functions of the first kind. Equation (2.2) refers to the general Fresnel case: for the geometrical focal plane (Fraunhofer pattern) $u = u' = 0$ and since in the limit as $u \to 0$

$$\frac{\pi}{2u}\left[U^2{}_{1/2}(u,v) + U^2{}_{3/2}(u,v)\right] = \frac{\pi}{2v}\mathrm{J}^2{}_{1/2}(v) = \left(\frac{\sin v}{v}\right)^2, \qquad \ldots\ldots (2.4)$$

equation (2.2) becomes

$$I_{\mathrm{R}}=\left(\frac{\sin v}{v}\right)^2\left(\frac{\sin v'}{v'}\right)^2. \qquad \ldots\ldots(2.5)$$

2.2. *Slit Aperture*

For a slit length $2a$ and negligible width the variables u' and v' are both zero; equation (2.2) then reduces to

$$I_{\mathrm{S}}=\frac{\pi}{2u}\left[U^2_{1/2}(u,v)+U^2_{3/2}(u,v)\right] \qquad \ldots\ldots(2.6)$$

for the general Fresnel phenomena. I_{S} represents the intensity in the diffraction pattern of a slit with the same normalization as above. For the Fraunhofer case (2.6) reduces to the well-known expression

$$I_{\mathrm{S}}=\left(\frac{\sin v}{v}\right)^2. \qquad \ldots\ldots(2.7)$$

§ 3. NUMERICAL EVALUATION

The expression for the intensity distribution for each of the above examples involves the evaluation of terms of the form

$$\frac{\pi}{2u}\left[U^2_{1/2}(u,v)+U^2_{3/2}(u,v)\right]. \qquad \ldots\ldots(3.1)$$

Lommel (1886 b, p. 604) showed that this type of expression may be evaluated in terms of Fresnel integrals. In fact

$$\left.\begin{aligned} U_{1/2}(u,v)&=\frac{1}{\sqrt{2}}\left[(A-A')\cos\alpha+(B-B')\sin\alpha\right]\\ U_{3/2}(u,v)&=\frac{1}{\sqrt{2}}\left[(A-A')\sin\alpha-(B-B')\cos\alpha\right]\end{aligned}\right\}\text{ for } u\leqslant v \qquad \ldots\ldots(3.2)$$

and

$$\left.\begin{aligned} U_{1/2}(u,v)&=\frac{1}{\sqrt{2}}\left[(A+A')\cos\alpha+(B+B')\sin\alpha\right]\\ U_{3/2}(u,v)&=\frac{1}{\sqrt{2}}\left[(A+A')\sin\alpha-(B+B')\cos\alpha\right]\end{aligned}\right\}\text{ for } u\geqslant v \qquad \ldots\ldots(3.3)$$

where A, B, A', B' are the Fresnel integrals

$$\left.\begin{aligned} A&=\tfrac{1}{2}\int_0^{\sigma}\mathrm{J}_{-1/2}(v)\,dv=\frac{1}{\sqrt{2\pi}}\int_0^{\sigma}\frac{\cos v}{\sqrt{v}}\,dv\\ A'&=\tfrac{1}{2}\int_0^{\delta}\mathrm{J}_{-1/2}(v)\,dv=\frac{1}{\sqrt{2\pi}}\int_0^{\delta}\frac{\cos v}{\sqrt{v}}\,dv\\ B&=\tfrac{1}{2}\int_0^{\sigma}\mathrm{J}_{1/2}(v)\,dv=\frac{1}{\sqrt{2\pi}}\int_0^{\sigma}\frac{\sin v}{\sqrt{v}}\,dv\\ B'&=\tfrac{1}{2}\int_0^{\delta}\mathrm{J}_{1/2}(v)\,dv=\frac{1}{\sqrt{2\pi}}\int_0^{\delta}\frac{\sin v}{\sqrt{v}}\,dv\end{aligned}\right\}. \qquad \ldots\ldots(3.4)$$

Here

$$\sigma = \frac{(u+v)^2}{2u}, \quad \delta = \frac{(u-v)^2}{2u}, \quad \alpha = \frac{(u^2+v^2)}{2u};$$

from (3.2) and (3.3) we have

$$U^2_{1/2}(u,v) + U^2_{3/2}(u,v) = \tfrac{1}{2}[(A \mp A')^2 + (B \mp B')^2], \quad \ldots\ldots (3.5)$$

the upper or lower signs taken according as $u \lesseqgtr v$.

The expression for the intensity in the diffraction pattern of a slit is the simpler and will be considered first. In the second memoir Lommel (1886 b) calculated the value of I along lines perpendicular to the u axis, for $u = 0, 3, 6$, etc., up to and including $u = 30$ at unit intervals of v up to $v = 12$. The calculations do not give sufficient data to make it possible to plot a satisfactory intensity chart; so further values have been computed from (2.6), with u in unit intervals up to $u = 30$ (using Pearcey's (1956) *Tables of the Fresnel Integral*). Figure 2 shows one quarter of the bisymmetrical pattern obtained by reflecting it in the u and v axes. This bisymmetrical pattern shows the lines of equal intensity normalized to unity at the centre: the sloping straight line represents the edge of the geometrical shadow. Along the v axis the intensity distribution represents the Fraunhofer

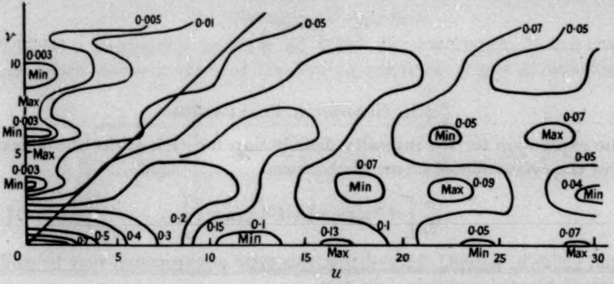

Figure 2. Intensity chart (isophote diagram) near the focus in the error-free diffraction pattern of a slit aperture; the sloping straight line is the edge of the geometrical shadow. Intensity at the origin is normalized to unity.

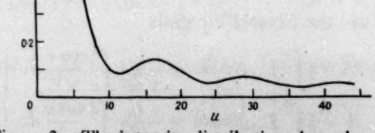

Figure 3. The intensity distribution along the u axis.

diffraction pattern given by equation (2.7) (see also figure 5 (i)). Along the u axis equation (2.6) reduces to

$$(I_S)_{v=0} = \frac{\pi}{2u}\left[U^2{}_{1/2}(u, 0) + U^2{}_{3/2}(u, 0) \right]; \qquad \ldots\ldots(3.6)$$

this function is displayed in figure 3 from which it will be seen that the intensity goes through a series of maxima and minima, the separation of the minima approaching 4π. Quantitative measurements of the positions of these axial minima are described in the next section.

It has already been stated that from the basic set of computations for the intensity in the diffraction pattern of a slit aperture, the intensity distribution in any plane for a rectangular aperture may be calculated. According to (2.2) and (2.6) the intensity $I_R(x, y, z)$ at a point (x, y, z) in space in the diffraction pattern of a rectangular aperture is given by two pairs of parameters u, v and u', v' such that

$$I_R(x, y, z) = I_S(u, v) I_S(u', v') \qquad \ldots\ldots(3.7)$$

where I_S is the expression for a slit given by (2.6). u, v and u', v' are defined by the length of the sides of the rectangle and the value of x, y and z (see (2.1)).

§ 4. EXPERIMENTAL

The optical diffractometer is normally used for the study of optical analogues of x-ray diffraction problems in connection with crystal-structure determination but has recently proved useful in studying various problems in physical optics (Hanson and Taylor 1956, Thompson and Wolf 1957, Thompson 1958, Taylor and Thompson 1958 b).

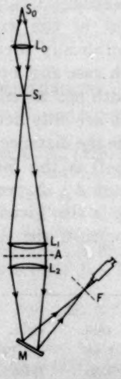

Figure 4. The optical diffractometer.

The instrument is shown diagramatically in figure 4. Light from a mercury-vapour compact source lamp S_0 is focused by a condenser lens L_0 on to a pinhole S_1; the light passing through the pinhole is rendered parallel by a lens L_1 and is brought to a focus at F by a lens L_2. For the convenience of operation a front-silvered optical flat M is used to bring the focal plane F to the same height as the diffracting object A. L_1 and L_2 are identical 152 cm focal length lenses which have been corrected for spherical aberration. A filter, placed over the pinhole, is used to isolate the yellow line of the mercury spectrum (5790 Å). The size of the pinhole used is dependent upon the size of the diffracting object, but is normally no greater than 30 microns in diameter (Taylor and Thompson 1957).

The Fraunhofer diffraction pattern of an object placed in the parallel beam at A is formed in the focal plane F of the lens L_2 and may be viewed through a microscope or recorded photographically on panchromatic microfile film placed at F.

The apparatus has been slightly modified (Taylor and Thompson 1958 a) to enable the camera to be moved through known distances along the axis of the instrument whilst still remaining perpendicular to the axis.

An adjustable aperture was made, consisting of two pairs of parallel straight edges—the two pairs being mutually perpendicular—which could be moved to form precise sizes of slit, square and rectangular apertures. The limitation on the size of these apertures was imposed by the size of the lenses (4 inch diameter).

The first experiments were carried out using slit apertures and the position of the first three *u*-axial minima, obtained on either side of central maxima, were measured. Measurements were made for slit apertures from 3 to 7 cm in length and 0·2 cm wide. Precisely the same positions were obtained if square apertures were used. Photographs were also taken in various planes perpendicular to the axis for each of the three types of aperture, slit, square and rectangular. The results of these experiments are compared with the theoretically predicted results in the next section.

§ 5. COMPARISON OF EXPERIMENTAL AND THEORETICAL RESULTS

The quantitative comparison of the experimentally measured positions of *u*-axial minima with the theoretically predicted ones is given in the table. $2a$ is the length of the slit in each case and a constant width of 0·2 cm was used, although *any* variation in this width had no effect on the positions of the minima since the positions of the minima are only determined by the length of the side equal to $2a$. $z_n (n=1, 2, 3, \text{etc.})$ is the distance of the nth axial minimum from the focus. $\Delta_n = z_n - z_{n-1}$ where $z_0 = 0$ is the focus. A comparison between the observed and calculated values of Δ_1, Δ_2 and Δ_3 is given in the table. The calculated value of Δ_n for n large is also given; this corresponds to a value of u equal to 4π (for a circular aperture the corresponding Δ's are equal, i.e. $\Delta_1 = \Delta_2 = \Delta_3 = \ldots = \Delta_n$).

	Δ_1		Δ_2		Δ_3		Δ_n
$2a$ (cm)	obs.	calc.	obs.	calc.	obs.	calc.	calc.
3	1·05	1·084	1·18	1·179	1·18	1·184	1·189
4	0·60	0·611	0·66	0·663	0·67	0·666	0·669
5	0·37	0·391	0·42	0·422	0·43	0·426	0·428
6	0·25	0·271	0·30	0·295	0·30	0·296	0·297
7	0·19	0·199	0·22	0·217	0·23	0·217	0·219

The agreement shown is seen to be reasonable although the values of Δ_1 are rather low; no great emphasis is placed upon this since the differences are within the experimental error.

Photographs of the intensity distributions in various planes perpendicular to the u axis are shown in figure 5, together with the calculated intensity distributions (dotted lines are the edge of the geometrical shadow) for a slit 2 cm long by 0·2 cm wide. For comparison the distribution in the focal plane is given in figure 5 (i). The intensity at the centre of the pattern is unity. Figure 5 (ii) shows the distribution in the plane $u=11{\cdot}48$; this is the position of the first minimum. It is seen from the intensity chart shown in figure 3 that the maxima and minima along the u axis are not equally spaced, but appear to be arranged in approximately equally spaced pairs. The minima are approximately equally spaced as are the maxima; the planes half-way between minima contain two minima, one on either side of the axis, whilst the intensity at the centre is just less than a maximum. Figure 5 (iii) shows a plane ($u=17{\cdot}71$) containing two minima, one on either side of the maximum. The final figure, 5 (iv), shows the situation at $u=23{\cdot}94$, the second axial minimum. (For figures 5–8 see Plates.)

A similar set of results is shown for a square aperture in figure 6 of side 2 cm; the results are on the same scale as figure 5 and so may be compared directly. In figure 6 (i) $u=u'=11{\cdot}48$, the position of the first minimum. The features shown in the photographs in figure 6 agree very well with the features of the calculated intensity distributions. For comparison figure 7 shows the Fraunhofer diffraction pattern for a square $u=0$ (figure 7 (*a*)) together with photographs of the same planes as shown in figure 6, but taken with a longer exposure. The photographs in figure 7 are reduced to half-size.

Finally in figure 8 a comparison between the theoretical and experimental results is made for a rectangular aperture chosen so that the first axial minimum in one direction coincides with the plane containing two minima, i.e. $u'=11{\cdot}48$ and $u=17{\cdot}71$. The dimensions of the aperture were 2 cm by 2·83 cm (ratio of $1:\sqrt{2}$).

The grain in the photographs in figures 5, 6, 7 and 8 is caused by the enlargement necessarily used because of the smallness of the diffraction patterns (between 1 and 2 mm across).

REFERENCES

DUFFIEUX, M., TIRONFLET, J., GUENOCHE, H., and LANSRAUX, G., 1944, *Ann. Phys., Paris*, **19**, 355.

HANSON, A. W., LIPSON, H., and TAYLOR, C. A., 1953, *Proc. Roy. Soc.* A, **218**, 371.

HANSON, A. W., and TAYLOR, C. A., 1956, Contribution to *Proceedings of the Symposium on Astronomical Optics and Related Topics*, University of Manchester, 1955, Ed. Z. Kopal (Amsterdam : North Holland Publishing Co.).

HUGHES, W., and TAYLOR, C. A., 1953, *J. Sci. Instrum.*, **30**, 105.

KATHAVATE, Y. V., 1945, *Proc. Indian Acad. Sci.*, A, **21**, 188.

LINFOOT, E. H., and WOLF, E., 1953, *Proc. Phys. Soc.* B, **66**, 145.

—— 1956, *Ibid.*, **69**, 823.

LOMMEL, E., 1886 a, *Abh. Bayer. Akad. Wiss.*, **15**, 229.

—— 1886 b, *Ibid.*, **15**, 531.

MATHEWS, P. A., and CULLEN, A. L., 1956, *Proc. Instn. Elect. Engrs, C.*, **103**, 454.

PEARCEY, T., 1956, *Tables of the Fresnel Integral* (Cambridge: University Press).

TAYLOR, C. A., HINDE, R. M., and LIPSON, H., 1951, *Acta Cryst.*, **4**, 261.

TAYLOR, C. A., and THOMPSON, B. J., 1957, *J. Sci. Instrum.*, **34**, 439.

—— 1958 a, *Ibid.*, **35**, 294.

—— 1958 b, *J. Opt. Soc. Amer.*, **48**, 844.

THOMPSON, B. J., 1958, *J. Opt. Soc. Amer.*, **48**, 95.

THOMPSON, B. J., and WOLF, E., 1957, *J. Opt. Soc. Amer.*, **47**, 895.

WALKER, J., 1904, *The Analytical Theory of Light* (Cambridge : University Press).

ZERNIKE, F., and NIJBOER, B. R. A., 1949, Contribution to *Théorie des Images Optiques*, p. 277 (Paris : Edition de la Revue d'Optique).

On Ionic Reactions of Negative μ-Mesons

By P. G. BURKE,[†] F. HAAS[‡], and I. C. PERCIVAL
Department of Physics, University College London

Communicated by H. S. W. Massey; *MS received* 17*th October* 1958,
in revised form 3rd February 1959

Abstract. The threshold rate coefficient for the μ-exchange process $\mathrm{p}\mu+\mathrm{d}^+\rightarrow\mathrm{d}\mu+\mathrm{p}^+$ is calculated taking into account the effects of strong coupling and of reduced masses. The result is smaller by a factor of about 100 than weak coupling approximations, but is still consistent with experiment.

§ 1. Introduction

The catalysis of nuclear fission reactions by negative muons was observed by Alvarez *et al.* (1957) in a liquid hydrogen bubble chamber. At the end of about 0·6% of the stopped muon tracks, secondary muons appeared with energy of about 5·4 Mev, which is that released by the fusion reaction

$$\mathrm{p}+\mathrm{d}\rightarrow{}^3\mathrm{He}+5{\cdot}4\,\text{Mev}.$$

Sometimes gaps of about 1 mm were observed between the end of the stopped muon track and the beginning of the secondary track.

This has been explained by supposing that the mesonic molecular ion $(\mathrm{pd}\mu)^+$ is formed and we shall be concerned with the ionic processes which lead to the formation of this ion. The processes also have an intrinsic value in ionic physics because they accentuate the reduced mass effects which are present when the ions are formed from electrons. The processes are

$$\mathrm{p}\mu+\mathrm{d}^+\rightarrow\mathrm{d}\mu+\mathrm{p}^++135\,\text{ev} \qquad \ldots\ldots(1)$$

$$\mathrm{d}\mu+\mathrm{p}^+\rightarrow\mathrm{d}\mu+\mathrm{p}^+ \qquad \ldots\ldots(2)$$

$$\mathrm{d}\mu+\mathrm{p}^+\rightarrow(\mathrm{pd}\mu)^++h\nu \qquad \ldots\ldots(3)$$

$$\mathrm{d}\mu+\mathrm{pe}\rightarrow(\mathrm{pd}\mu)^++\mathrm{e}^-. \qquad \ldots\ldots(4)$$

There is a small leakage of the proton and deuteron wave function through the Coulomb barrier, which enables the fusion reaction to take place, either with the emission of a γ-ray, and trapping the muon, or again as an Auger transition. In the latter case it is the muon which takes the energy, forming the secondary tracks which are observed.

The deuterium concentration was varied, and the resultant rapid saturation effect has enabled Skyrme (1957) and also Hayashi *et al.* (1957) to obtain relations between the reaction rates and the (competing) decay rate of the muon $4{\cdot}5\times10^5\,\mathrm{sec}^{-1}$. The experiment of Ashmore *et al.* (1958) shows that the lowest limit for the molecule formation rate is $2\times10^5\,\mathrm{sec}^{-1}$.

[†] Now at University of London Computing Centre.
[‡] Now at English Electric Nelson Research Laboratories, Stafford.

§ 2. Reaction Rates

The reaction rates have been calculated by Jackson (1957) and Skyrme (1957) using scaled potentials of the corresponding electronic systems and Born or weak-coupling distorted wave approximations. These might be expected to give an approximate order of magnitude for the reaction rates, but are liable to suffer from two major sources of error which are: (*a*) the neglect of strong coupling between the $p\mu + d^+$ and $d\mu + p^+$ channels, as for the corresponding atomic scattering problems involving proton, deuteron and electron, (*b*) deviation from adiabatic conditions as a consequence of the comparatively large ratio of muon to nucleon mass, as explained in more detail in § 5.

More accurate cross sections may be obtained by taking (*a*) and (*b*) into account. All the reaction rates (1)–(4) may be derived from solutions of the same wave equation over a range of energies with different boundary conditions. We shall be concerned mainly with the zero-energy reaction rate coefficient for the μ-exchange reaction (1).

§ 3. Resonating Group-Structure Method

This method of Wheeler (1937) was applied by Buckingham and Massey (1941) to nuclear collisions of neutrons with deuterons and the present application to reaction (1) has a similar pattern.

When the proton p and deuteron d are far apart, the muon μ may be attached to either p or d. In the first case let $\psi_1(\mathbf{R}_1)$ represent the relative motion of d and the centre of mass of $p\mu$, and in the second case let $\psi_2(\mathbf{R}_2)$ represent the relative motion of p and the centre of mass of $d\mu$. Then the asymptotic form of the wave function representing the whole system is

$$\Psi \sim \phi_1(r_1)\psi_1(\mathbf{R}_1) + \phi_2(r_2)\psi_2(\mathbf{R}_2) \qquad \ldots\ldots(5)$$

where

$$\left.\begin{aligned} \mathbf{r}_1 &= \mathbf{r}_\mu - \mathbf{R}_\mathrm{p}, \qquad \mathbf{R}_1 = \frac{m_\mu \mathbf{r}_\mu + M_\mathrm{p}\mathbf{R}_\mathrm{p}}{m_\mu + M_\mathrm{p}} - \mathbf{R}_\mathrm{d}, \\ \mathbf{r}_2 &= \mathbf{r}_\mu - \mathbf{R}_\mathrm{d}, \qquad \mathbf{R}_2 = \frac{m_\mu \mathbf{r}_\mu + M_\mathrm{d}\mathbf{R}_\mathrm{d}}{m_\mu + M_\mathrm{d}} - \mathbf{R}_\mathrm{p}, \end{aligned}\right\} \qquad \ldots\ldots(6)$$

$\mathbf{R}_\mathrm{x}$ or $\mathbf{r}_\mathrm{x}$ is the position vector of particle x, and m_x or M_x its mass. For the low energies at which reaction (1) is experimentally important, $\phi_1(r_1)$ and $\phi_2(r_2)$ are the ground state wave functions of the hydrogen atoms $p\mu$ and $d\mu$. The notation used for reduced masses is given in table 1.

Table 1. Reduced Masses. 1 mu A.U. = $1{\cdot}88 \times 10^{-25}$ g

1st mass	M_p	M_d	$M_\mathrm{p} + m_\mu$	$M\ + m_\mu$	M_p
2nd mass	m_μ	m_μ	M_d	M_p	M_d
Reduced mass	m_1	m_2	m_1	m_2	$\mathcal{M}$
Value (mu A.U.)	0·899	0·947	6·35	6·03	5·92

In addition

$$\left.\begin{aligned} M_\mathrm{p} + M_\mathrm{d} + m_\mu &= M \\ M^{-1}(M_\mathrm{p} + m_\mu)(M_\mathrm{d} + m_\mu) = \mathcal{M}_2 m_1^{-1} m_\mu &= \mathcal{M}_1 m_2^{-1} m_\mu = a \end{aligned}\right\}. \qquad \ldots\ldots(7)$$

In mu-atomic units (mu A.U.) of mass ($m_\mu = 1{\cdot}88 \times 10^{-25}$ g), length ($a_0 \times m_e m_\mu^{-1} = 2{\cdot}56 \times 10^{-11}$ cm), time (1 A.U. $\times\, m_e m_\mu^{-1} = 1{\cdot}170 \times 10^{-19}$ sec) and energy ($5{\cdot}62 \times 10^3$ ev) the equations satisfied by ϕ_i are

$$\left.\begin{aligned} &\left(-\frac{1}{2m_i}\nabla_{r_i}^{\,2} - \frac{1}{r_i} - \epsilon_i\right)\phi_i(r_i) = 0 \\ &\qquad \phi_i(r_i) = \frac{2}{(4\pi)^{1/2}}\, m_i^{-3/2} \exp(-m_i r_i) \qquad (i = 1, 2) \end{aligned}\right\} \quad \ldots\ldots (8)$$

where $\epsilon_i = -m_i/2$ and $E = E_i + \epsilon_i$ is the total energy of the system. $E_1 = k_1^2/2\mathscr{M}_1$ and $E_2 = k_2^2/2\mathscr{M}_2$ are the kinetic energies of relative motion in channels 1, $\mathrm{p}\mu + \mathrm{d}^+$, and 2, $\mathrm{d}\mu + \mathrm{p}^+$, respectively. In this section $\mathbf{R}_i$ is held constant during integration and differentiation with respect to $\mathbf{r}_i$.

For reaction (1), $E_2 - E_1 = \epsilon_1 - \epsilon_2 = 2{\cdot}39 \times 10^{-2}$ mu A.U. = 135 ev is the difference between the energies of relative motion in the initial and final channels. E_1 corresponds to liquid hydrogen temperatures (4°K) and is of the order of 4×10^{-4} ev. For practical purposes we may put $E_1 = 0$. Then only s waves are significant in channel 1 and by conservation of total angular momentum in channel 2. If the radial parts of these waves are $(4\pi R_1^2)^{-1/2} F_1(R_1)$ and $(4\pi R_2^2)^{-1/2} F_2(R_2)$ respectively, then the simplest trial wave function for the whole system which has the correct asymptotic form is

$$\Psi^{\mathrm{T}} = \frac{1}{(4\pi)^{1/2}}\left[\phi_1(r_1) R_1^{-1} F_1(R_1) + \phi_2(r_2) R_2^{-1} F_2(R_2)\right]. \quad \ldots\ldots (9)$$

In the coordinate systems $(\mathbf{r}_1, \mathbf{R}_1)$ and $(\mathbf{r}_2, \mathbf{R}_2)$ the total Hamiltonian has the form

$$\left.\begin{aligned} H &= \mathrm{K.E} + \frac{1}{R} - \frac{1}{r_1} - \frac{1}{r_2} \\ \mathrm{K.E.} &= -\frac{1}{2\mathscr{M}_1}\nabla_{R_1}^{\,2} - \frac{1}{2m_1}\nabla_{r_1}^{\,2} = -\frac{1}{2\mathscr{M}_2}\nabla_{R_2}^{\,2} - \frac{1}{2m_2}\nabla_{r_2}^{\,2} \end{aligned}\right\} \quad \ldots\ldots (10)$$

where $R = |\mathbf{R}| = |\mathbf{r}_1 - \mathbf{r}_2|$ is the internuclear distance. Multiplying $2(H - E)\Psi^{\mathrm{T}} = 0$ by ϕ_i^* $(i = 1, 2)$ and integrating over $\mathbf{r}_i$ and the angular coordinates $\hat{\mathbf{R}}_i$ we obtain the integro-differential equations

$$\left.\begin{aligned} \left[\frac{d^2}{dR_1^2} - V_1(R_1) + k_1^2\right] F_1(R_1) &= \mathscr{M}_1 a^3 \int_0^\infty K(R_1, R') F_2(R')\, dR' \\ \left[\frac{d^2}{dR_2^2} - V_2(R_2) + k_2^2\right] F_2(R_2) &= \mathscr{M}_2 a^3 \int_0^\infty K^{\mathrm{tr}}(R_2, R') F_1(R')\, dR' \end{aligned}\right\} \quad \ldots\ldots (11)$$

where a is defined by equation (7) and K^{tr} is the transpose of K.

$$V_1(R_1) = 2\mathscr{M}_1 \int \phi_1^2(r_1)\left[\frac{1}{R} - \frac{1}{r_2}\right] dr_1^3$$

$$V_2(R_2) = 2\mathscr{M}_2 \int \phi_2^2(r_2)\left[\frac{1}{R} - \frac{1}{r_1}\right] dr_2^3 \quad \ldots\ldots (12a)$$

$$K(R_1, R_2) = 4(m_1 m_2)^{3/2} R_1 R_2 \times \int_{-1}^{+1} e^{-Q}\left[\frac{1}{R} + m_1 m_2 a\left(\frac{1}{r_1} + \frac{1}{r_2} - \mathbf{r}_1 . \mathbf{r}_2\right) - \tfrac{1}{2}E\right] dx \quad \ldots\ldots (12b)$$

$$Q = m_1 r_1 + m_2 r_2, \qquad x = \hat{\mathbf{R}}_1 . \hat{\mathbf{R}}_2. \quad \ldots\ldots (13)$$

The integration over x is carried out keeping R_1 and R_2 constant. Details of the derivation of a similar kernel are given by Buckingham and Massey (1941).

§ 4. THE KERNEL $K(R_1, R_2)$

This was evaluated by numerical integration over x as a 30×30 matrix, at intervals of 0·25 mu A.U., using a programme for the DEUCE computer which had been prepared for the calculation of nuclear kernels. But as the first few elements in table 2 show, the only significant values of $K(R_1, R_2)$ lie close to the main diagonal. The tabulation is insufficiently fine to follow the rapid variation of the kernel across the diagonal, and as a consequence the equations could not be solved. To tabulate at finer intervals would have involved a prohibitive use of machine time.

Table 2. The Elements of this Table are Proportional to $K(R_1, R_2)$ to one significant figure

R_1 \ R_2	0·25	0·50	0·75	1·00	1·25
0·25	+10000	−600	−100	−8	−1
0·50	−800	+6000	−800	−100	−9
0·75	−100	−1000	+4000	−800	−100
1·00	−10	−200	−1000	+3000	−800
1·25	−1	−10	−200	−1000	+2000

The almost diagonal form of kernel is intermediate between the smoothly varying kernels of nuclear scattering problems and the completely diagonal kernels (or potential functions) which are obtained when the adiabatic approximation is applied to atomic scattering problems. This is a consequence of the mass ratio $m_\mu/M_{\rm P}$ being intermediate between unity, which is the mass ratio for similar nuclear problems, and zero, which is the mass ratio for the adiabatic approximation.

§ 5. REFORMULATION USING THE INTERNUCLEAR COORDINATE R

The effective width of the diagonal ridge of $K(R_1, R_2)$ is very narrow. If the wavelength of internuclear motion is long compared with this width then the kernel K may be replaced† by a potential function without great loss of accuracy, and the integro-differential equations then become differential equations which are usually simpler to solve.

It might be thought that such a replacement would always be equivalent to the adiabatic approximation which is only valid when reduced mass effects are negligible, but this is not the case. In the present problem the difference in wavelength between the two channels is a reduced mass effect. At zero-energy the wavelength in channel 1 is infinite, whilst the wavelength in channel 2 is 11·7 mu A.U., which is comparable with the range of the potential fields (see § 8) so the adiabatic approximation is unsatisfactory.

A reformulation in terms of differential equations which takes account of reduced masses is obtained by choosing a trial function of the form

$$\Psi^{\rm T} = \frac{1}{(4\pi)^{1/2}} [\phi_1(r_1)F_1(R) + \phi_2(r_2)F_2(R)] \qquad \ldots\ldots(14)$$

---

† Those parts of K which arise from the kinetic energy are replaced by differential operators.

where R is the distance between proton and deuteron. Similar coordinate systems have been used for ground states of nuclei, but not for collision problems because of difficulties with the asymptotic form of the wave functions. These difficulties may be overcome for our problem because of the very low energy of collision. The corresponding wavelength is very long in comparison with the width of the ridge of the kernel $K(R_1 R_2)$.

In coordinates (r_1, R) and (r_2, R) the kinetic energy is

$$\begin{aligned} \text{K.E.} &= -\frac{1}{2\mathcal{M}}\nabla_{1,R}^2 + \left(\frac{1}{m_1}-1\right)\nabla_{1,R}\cdot\nabla_{r_1} - \frac{1}{2m_1}\nabla_{r_1}^2 \\ &= -\frac{1}{2\mathcal{M}}\nabla_{2,R}^2 + \left(\frac{1}{m_2}-1\right)\nabla_{2,R}\cdot\nabla_{r_2} - \frac{1}{2m_2}\nabla_{r_2}^2 \end{aligned} \qquad (15)$$

where $\nabla_{i,R}$ $(i=1,2)$ represents differentiation with respect to $\mathbf{R}$ keeping $\mathbf{r}_i$ constant and in this section differentiation with respect to $\mathbf{r}_1$ and $\mathbf{r}_2$ is performed with R held constant.

On multiplying $2(H-E)\Psi^{\mathrm{T}}=0$ by ϕ_i^*, integrating over $\mathbf{r}_i$ and $\hat{\mathbf{R}}$, and substituting analytic forms for ϕ_1 and ϕ_2, the equations for $F_1(R)$ and $F_2(R)$ become

$$\begin{aligned} &\left[\frac{1}{\mathcal{M}}\frac{d^2}{dR^2} - \frac{2}{R} + 2L_1(R) + 2E_1\right]F_1(R) \\ &\quad = -N(R)\left[\frac{1}{\mathcal{M}}\frac{d^2}{dR^2} - \frac{2}{R} + 2E_2\right]F_2(R) - 2M_1(R)F_2(R) + 2\left(1-\frac{1}{m_1}\right)\frac{dN}{dR}\frac{dF_2}{dR} \end{aligned} \qquad \ldots\ldots(16a)$$

$$\begin{aligned} &\left[\frac{1}{\mathcal{M}}\frac{d^2}{dR^2} - \frac{2}{R} + 2L_2(R) + 2E_2\right]F_2(R) \\ &\quad = -N(R)\left[\frac{1}{\mathcal{M}}\frac{d^2}{dR^2} - \frac{2}{R} + 2E_1\right]F_1(R) - 2M_2(R)F_1(R) + 2\left(1-\frac{1}{m_2}\right)\frac{dN}{dR}\frac{dF_1}{dR} \end{aligned} \qquad \ldots\ldots(16b)$$

where

$$\left.\begin{aligned} L_1(R) &= \int \phi_1^2(r_1) r_2^{-1}\, dr_1^3 = \frac{1-\exp(-2m_1R)}{R} - m_1\exp(-2m_1R) \\ L_2(R) &= \int \phi_2^2(r_2) r_1^{-1}\, dr_2^3 = \frac{1-\exp(-2m_2R)}{R} - m_2\exp(-2m_2R) \\ M_1(R) &= \int \phi_1(r_1)\phi_2(r_2) r_1^{-1}\, dr_1^3 \\ &= \frac{4(m_1m_2)^{3/2}}{m_2^2-m_1^2}\left[\frac{2m_2}{m_2^2-m_1^2}\,\frac{\exp(-m_1R)-\exp(-m_2R)}{R} - \exp(-m_2R)\right] \\ M_2(R) &= \int \phi_1(r_1)\phi_2(r_2) r_2^{-1}\, dr_2^3 \\ &= \frac{4(m_1m_2)^{3/2}}{m_2^2-m_1^2}\left[\frac{-2m_1}{m_2^2-m_1^2}\,\frac{\exp(-m_1R)-\exp(-m_2R)}{R} \right. \\ &\qquad\qquad \left. + \exp(-m_1R)\right], \\ N(R) &= \int \phi_1(r_1)\phi_2(r_2)\, dr_1^3 \\ &= \int \phi_1(r_1)\phi_2(r_2/dr_2^3) = \frac{2}{m_2^2-m_1^2}\left[m_2M_2(R) - m_1M_1(R)\right]. \end{aligned}\right\} \qquad \ldots\ldots(17)$$

If the terms in dF_1/dR and dF_2/dR are neglected, the equations (16) become

$$\left[\frac{1}{\mathscr{M}}\frac{d^2}{dR^2}-\frac{2}{R}+\frac{2(L_1-NM_2)}{1-N^2}+2E_1\right]F_1=\frac{2(NL_2-M_1)}{1-N^2}F_2, \quad \ldots\ldots(18\,a)$$

$$\left[\frac{1}{\mathscr{M}}\frac{d^2}{dR^2}-\frac{2}{R}+\frac{2(L_2-NM_1)}{1-N^2}+2E_2\right]F_2=\frac{2(NL_1-M_2)}{1-N^2}F_1. \quad \ldots\ldots(18\,b)$$

§ 6. ASYMPTOTIC FORM

Unlike the trial function (9) of the resonating group-structure method, we show that (14) is not an exact solution of the Schrödinger equation for large R, and corrections to the wave number and amplitude must be applied.

If these corrections were very large, the approximation (14) would be unreliable. In fact the wave number correction is fairly small for reaction (1) and the amplitude correction negligible, but this was not clear until the detailed calculations had been carried out. In this section we are only concerned with these comparatively minor corrections.

Asymptotically the exact solution of the Schrödinger equation in centre-of-mass coordinates $(r_1, \mathbf{R}_1)$ and $(r_2, \mathbf{R}_2)$ has the form

$$\Psi=\Psi_1+\Psi_2 \quad \ldots\ldots(19)$$

where

$$\Psi_i \sim \phi_i(r_i)\int c(\hat{\mathbf{k}}_i)\exp(i\mathbf{k}_i\,.\,\mathbf{R}_i)\,d\hat{\mathbf{k}}_i \quad \ldots\ldots(20)$$

for some function $c(\hat{\mathbf{k}}_i)$ of the angular coordinates of momentum $\mathbf{k}_i$, and $\int d\hat{\mathbf{k}}_i$ represents integration over those coordinates. Changing to the new coordinate system $(\mathbf{r}_i, \mathbf{R})$

$$\exp(i\mathbf{k}_i\,.\,\mathbf{R}_i)=\exp(i\mathbf{k}_i\,.\,\mathbf{R})\times\exp[i(1-m_i)\mathbf{k}_i\,.\,\mathbf{r}_i] \quad \ldots\ldots(21)$$

and the $\phi_i(r_i)$ component of Ψ_i in this system is

$$\int\phi_i^*(r_i)\Psi_i\,d\mathbf{r}_i=\int q_i(\mathbf{k}_i)c(\hat{\mathbf{k}}_i)\exp(i\mathbf{k}_i\,.\,\mathbf{R})\,d\hat{\mathbf{k}}_i \quad \ldots\ldots(22)$$

where

$$q(\mathbf{k}_i)=\int|\phi_i(r_i)|^2\exp[i(1-m_i)\mathbf{k}_i\,.\,\mathbf{r}_i]\,dr_i^3 \quad \ldots\ldots(23)$$

which is independent of $\hat{\mathbf{k}}_i$, from the spherical symmetry of $\phi_i(r_i)$. Therefore

$$\int\phi_i^*(r_i)\Psi_i\,dr_i=q_i(k_i)\int c(\hat{\mathbf{k}}_i)\exp(i\mathbf{k}_i\,.\,\mathbf{R})\,d\hat{\mathbf{k}}. \quad \ldots\ldots(24)$$

For s waves of the exact solution of the Schrödinger equation, it follows that the relation between the asymptotic forms in the two different coordinate systems is

$$F_i(R)\sim q_i(k_i)F_i(R_i). \quad \ldots\ldots(25)$$

Note that the functional forms of $F_i(R)$ and $F_i(R_i)$ are different. $q_i(k_i)$ is the amplitude correction. For the zero-energy scattering

$$q_1(k_1)=q_1(0)=1, \qquad q_2(k_2)=q_2(0{\cdot}537)=0{\cdot}998.$$

Evidently the amplitude correction is negligible in comparison with other approximations, and $F_i(R)$ may be used to calculate reaction rates.

The above analysis applies directly to the exact solution of the Schrödinger equation. But the asymptotic forms of the approximate s wave functions $F_i(R)$

which are solutions of the equation (16) or (18) have wave numbers $k_1'^2$ and $k_2'^2$ given by

$$k_i'^2 = 2\mathcal{M}E_i \qquad \ldots\ldots(26)$$

instead of the correct values given by

$$k_i^2 = 2\mathcal{M}_iE_i. \qquad \ldots\ldots(27)$$

The error in k_i^2 is $2E_i(\mathcal{M}-\mathcal{M}_i)$. When the initial energy of relative motion is zero $E_1=0$, $E_2=2{\cdot}39\times10^{-2}$ and k_2^2 is in error by $5{\cdot}1\times10^{-3}$ mu A.U. only, but even such a small error introduces ambiguities into the calculation of phases.

Consider the complete expansion of Ψ_2 in terms of hydrogenic wave functions of dμ and spherical harmonics *of the internuclear coordinate R*. Then we have just shown that for our particular problem the first term $(4\pi)^{-1/2}\phi_2(r_2)F_2(R)$ is by far the most important when R is large. But the other terms are still present and there is kinetic coupling between the first term and the higher terms in the expansion. If we had used a complete expansion in deriving our equations, then we should have an exact solution of the Schrödinger equation, and since the omission of the kinetic coupling is the only approximation we have made for large R, it must be this omission which causes the error in k_2.

From the asymptotic relation (25) the omitted terms in equation (18) are equal to $(\mathcal{M}^{-1}-\mathcal{M}_2^{-1})d^2F_2/dR^2$, and they may be restored in this form, thereby replacing the reduced mass $\mathcal{M}$ of (26) by the correct reduced mass $\mathcal{M}_2$ of (27). For consistency a similar correction was made for channel 1, although this has no effect on the form of that equation when R is large, and the corrections were made over the whole range of R_1, which might be expected to over-compensate slightly for the error in the kinetic energy, giving

$$\left[\frac{1}{\mathcal{M}_1}\frac{d^2}{dR^2}-\frac{2}{R}+\frac{2(L_1-NM_2)}{1-N^2}+2E_1\right]F_1=\frac{2(NL_2-M_1)F_2}{1-N^2}. \qquad \ldots\ldots(28a)$$

$$\left[\frac{1}{\mathcal{M}_2}\frac{d^2}{dR^2}-\frac{2}{R}+\frac{2(L_2-NM_1)}{1-N^2}+2E_2\right]F_2=\frac{2(NL_1-M_2)F_1}{1-N^2}. \qquad \ldots\ldots(28b)$$

We shall see that the effect of the kinetic energy (K.E.) correction is small for reaction (1), but quite large for the elastic scattering cross sections, including (2).

§ 7. Rate Coefficient and Cross Sections

For a collision above zero energy, let

$$F_{i1}(R_i), \quad F_{i2}(R_2) \qquad (i=1,2) \qquad \ldots\ldots(29)$$

be two arbitrary real linearly independent solutions of the equations, obtained by numerical integration, with asymptotic forms

$$F_{i\mu}(R_i) \sim v_i^{-1/2}[(\cos k_iR_i)C_{i\mu}+(\sin k_iR_i)D_{i\mu}] \qquad (\mu=1,2). \qquad \ldots\ldots(30)$$

This may be put in matrix form

$$F \sim v^{-1/2}[(\cos k\rho)C+(\sin k\rho)D], \qquad \ldots\ldots(31)$$

where

$$F=\|F_{i\mu}\|, \qquad C=\|C_{i\mu}\|, \qquad D=\|D_{i\mu}\| \qquad \ldots\ldots(32)$$

$$v=\operatorname{diag}\{v_1,v_2\}, \qquad k=\operatorname{diag}\{k_1,k_2\}, \qquad \rho=\operatorname{diag}\{R_1,R_2\}. \qquad \ldots\ldots(33)$$

D is non-singular and on postmultiplication by D^{-1} we obtain the special solution

$$\bar{F}=FD^{-1}\sim v^{-1/2}[(\cos k\rho)\mathscr{R}+\sin k\rho] \qquad \ldots\ldots(34)$$

where

$$\mathscr{R}=CD^{-1} \qquad \ldots\ldots(35)$$

is the reactance matrix, which is symmetric. The scattering matrix† S and T matrix are given by

$$S=[I+i\mathscr{R}][I-i\mathscr{R}]^{-1}, \qquad T=I-S \qquad \ldots\ldots(36)$$

where I is the unit matrix, and the cross sections by

$$Q(j\to i)=\pi\hbar^2k_j^{-2}|T_{ij}|^2. \qquad \ldots\ldots(37)$$

For the superelastic collision process (1) at zero energy this analysis is no longer sufficient, since $Q(1\to 2)\to\infty$ as $k_1\to 0$ and the reactance matrix has infinite elements. But the symmetric matrix

$$\mathscr{R}^0=v^{-1/2}\mathscr{R}v^{-1/2} \qquad \ldots\ldots(38)$$

remains finite, and

$$\mathscr{R}^0=C^0D^{0-1} \qquad \ldots\ldots(39)$$

where

$$F\sim(\cos k\rho)C^0+v^{-1}(\sin k\rho)D^0. \qquad \ldots\ldots(40)$$

For reaction (1) the rate coefficient

$$v_1Q(1\to 2)=v_2\pi\hbar^2\mathscr{M}_1{}^{-2}|T^0{}_{21}|^2 \qquad \ldots\ldots(41)$$

remains finite as $v_1\to 0$ where

$$T^0=2i\mathscr{R}^0[I-iv\mathscr{R}^0]^{-1}. \qquad \ldots\ldots(42)$$

Use is made of the inverse matrix $\mathscr{Y}^0=\mathscr{R}^{0-1}$ for which

$$T^0=2i[\mathscr{Y}^0-iv]^{-1} \qquad \ldots\ldots(43)$$

and which is also symmetric.

In internuclear coordinates (r_1, R), (r_2, R) we should apply the normalization correction whereby

$$F_{i\mu}(R)=q(k_i)[(\cos k_iR)C^0{}_{i\mu}+v_i{}^{-1}(\sin k_iR)D^0{}_{i\mu}]. \qquad \ldots\ldots(44)$$

§ 8. SOLUTION OF EQUATIONS

Equations (28) with the K.E. correction and (18) without the K.E. correction were solved numerically out to $R=12$ and $R=16$ respectively, using intervals of 1/16 and 1/8, by an adaptation of the Numerov method to coupled equations.

Table 3. $\mathscr{Y}^0=v^{1/2}\mathscr{R}^{-1}v^{1/2}$ matrices, where $\mathscr{R}$ is the reactance matrix; $\mathscr{Y}^0$ is symmetric for exact solution. Channel 1: pμ+d. Channel 2: dμ+p. Zero relative velocity in channel 1. KE and KC are kinetic energy and kinetic coupling corrections, for which see §§ 6, 8.

Corrections							
KE	KC	Asymptotic	n	$\mathscr{Y}^0{}_{(n)11}$	$\mathscr{Y}^0{}_{(n)12}$	$\mathscr{Y}^0{}_{(n)21}$	$\mathscr{Y}^0{}_{(n)22}$
yes	no	no	1	−0·0331	−0·0170	−0·0207	+0·0475
no	no	no	2	−0·0360	−0·0152	−0·0197	+0·0565
yes	yes	no	3	−0·0342	−0·0158	−0·0151	+0·0852
no	yes	(=0)	4	−0·0373	−0·0156	−0·0163	+0·0663
yes	yes	yes	5	−0·0341	−0·0162	−0·0157	+0·0849

---

† For the theory of scattering matrices see Blatt and Weisskopf (1952).

The comparatively slow electronic computer installed at University College was used. The calculated $\mathscr{Y}^0$ matrices $\mathscr{Y}^0_{(1)}$ and $\mathscr{Y}^0_{(2)}$ respectively are given in table 3.

The marked deviation from symmetry was due to the omission of the first-derivative kinetic term coupling channels 1 and 2, leaving an unsymmetric operator to represent the Hamiltonian. To avoid the solution of the complicated equations (16) these terms were taken into account as a perturbation† on $\mathscr{Y}^0$, with

$$\delta V(v) = \begin{bmatrix} 0 & -2(1-m_1^{-1})\dfrac{dN}{dR}\dfrac{d}{dR} \\ -2(1-m_2^{-1})\dfrac{dN}{dR}\dfrac{d}{dR} & 0 \end{bmatrix}. \quad \ldots.(45)$$

The integrals required for the J-matrices were evaluated by desk computation and although this kinetic coupling (K.C.) correction is small, the corrected matrices $\mathscr{Y}^0_{(3)}$ with the K.E. correction and $\mathscr{Y}^0_{(4)}$ without the K.E. correction show a marked improvement in symmetry which formed a useful check on the computation.

The range of the interaction is large and in order to include the contribution to the $\mathscr{Y}^0_{(3)}$ matrix for $12 < R < 16$ mu A.U. a further (asymptotic) correction was applied with

$$\left.\begin{aligned} \delta V(R) &= -U(R-12)V(R), \\ U(X) &= \begin{cases} 1 & x > 0 \\ 0 & x \leqslant 0 \end{cases} \end{aligned}\right\} \quad \ldots\ldots(46)$$

giving $\mathscr{Y}^0_{(5)}$, which we consider to be the most accurate estimate obtained. The asymptotic correction to $\mathscr{Y}^0_{(4)}$ was negligible. A comparison of $\mathscr{Y}^0_{(3)}$ and $\mathscr{Y}^0_{(5)}$ shows the asymptotic correction in this case to be very small.

The deviation from symmetry of $\mathscr{Y}^0_{(5)}$ is insignificant and a symmetrized $\mathscr{Y}^0_{(5)}$ was used to calculate the rate coefficient for reaction (1) at zero energy, giving

$$v_1 Q(1\to 2) = 5{\cdot}25 \times 10^{-14}\ \text{cm}^3\,\text{sec}^{-1} \quad \ldots\ldots(47)$$

and the cross sections for the reactions 1→1 and 2→2 with the same total energy are

$$Q(1\to 1) = 16{\cdot}2 \times 10^{-20}\ \text{cm}^2, \quad \ldots\ldots(48)$$

$$Q(2\to 2) = 1{\cdot}36 \times 10^{-20}\ \text{cm}^2. \quad \ldots\ldots(49)$$

Table 4. Comparison of Observed and Calculated Rate Coefficients for the Reaction $\text{p}\mu + \text{d} \to \text{d}\mu + \text{p}$

Author	Approximation	$v_1 Q(1\to 2)(\text{cm}^3\,\text{sec}^{-1})$
Alvarez *et al.*	Experiment (see Skyrme 1957)	$> 10^{-14}$
Skyrme	Born	2×10^{-11}
Jackson	Weak coupling	9×10^{-12}
Hayashi *et al.*	Dispersion	$> 2{\cdot}2 \times 10^{-13}$
Present paper	Strong coupling, with reduced mass effects	5×10^{-14}

---

† $\mathscr{Y}^0$ produced more satisfactory results than $\mathscr{R}^0$ as judged by the symmetry test to be described.

The formulation given here neglects the very long range polarization effect. This is effective to first order in the elastic cross sections (48) and (49), but only to second order in the rate coefficient (47).

§ 9. Discussion

Since the calculations described in this paper were completed, the results of Cohen, Judd and Riddell (1958) appeared. Their estimate of the rate coefficient for the exchange reaction (1) at threshold, combined with their calculation of the probability of formation of $(pp\mu)^+$ checks very well with experiment. The rate coefficient (47) is a factor of 4 smaller, but it confirms that strong coupling and reduced mass effects decrease the weak coupling rate coefficient by about two orders of magnitude.

The elastic cross section (49) for collision of $d\mu$ with p^+ is calculated at the same total energy as the exchange reaction. This is outside the energy range required to obtain the millimetre gap in liquid hydrogen, since the kinetic energy of the $d\mu$ atom is soon reduced to thermal energies of about 4×10^{-4} ev and then diffuses at these low energies before forming the $(pd\mu)^+$ molecule.

Acknowledgments

We wish to thank Professor J. M. Cassels for bringing these problems to our attention, Dr. H. H. Robertson for advice in programming the DEUCE computer, Mrs. J. B. G. Wallace for her assistance with the desk computations, and Dr. E. H. S. Burhop, Professor H. S. W. Massey, Mr. L. Castillejo and Dr. M. J. Seaton for helpful discussions.

APPENDIX

Let the pair of coupled equations

$$\frac{1}{M_i}\left(\frac{d^2}{dR^2} + k_i^2\right) F_i(R) = \sum_j V_{ij}(R) F_j(R) \qquad (i, j = 1, 2)$$

have two arbitrary real independent solutions $F_{i_\mu}(R)$, labelled by the variable μ $(=1, 2)$. Then $F(R) = ||F_{i_\mu}(R)||$ satisfies the matrix differential equation

$$M^{-1}\left(\frac{d^2}{dR^2} + k^2\right) F(R) = V(R) F(R)$$

where $M = \text{diag}\{M_1, M_2\}$, and has the asymptotic form

$$F(R) \sim v^{-1/2}[(\cos kR)C + (\sin kR)D],$$

R and d^2/dR^2 being scalar matrices. The remaining matrices are defined in §7. The special solution

$$\bar{F}(R) = F(R)D^{-1} \sim v^{-1/2}[(\cos kR)\mathscr{R} + (\sin kR)].$$

Now suppose

$$\bar{F}^{(t)}(R) = \bar{F}(R) + \delta \bar{F}(R)$$

is an exact solution of the approximate equation

$$M^{-1}\left(\frac{d^2}{dR^2} + k^2\right) F(R) = V^{(t)}(R) F(R)$$

where

$$V^{(t)}(R) = V(R) + \delta V(R).$$

Then by an extension (see Kohn 1948) of the variational principle for $\mathscr{R}$ to two channels with different reduced masses we evaluate the matrix

$$\begin{aligned}\bar{J} &= \int_0^\infty F^{(t)\dagger}\left[M^{-1}\frac{d^2}{dR^2}+M^{-1}k^2-V(R)\right]F^{(t)}\,dR \\ &\simeq \int_0^{R_\infty} F^{(t)\dagger}\left[M^{-1}\frac{d^2}{dR^2}+M^{-1}k^2-V(R)\right]F^{(t)}\,dR \\ &= \int_0^{R_\infty} F^{\dagger}\left[M^{-1}\frac{d^2}{dR^2}+M^{-1}k^2-V(R)\right]\delta F\,dR+\mathcal{O}|\delta F|^2\end{aligned}$$

where $V(R)\simeq 0$ for $R>R_\infty$.

Now

$$\int_0^{R_\infty} F^{\dagger}M^{-1}\frac{d^2}{dR^2}\delta F\,dR=\int_0^{R_\infty}\left(M^{-1}\frac{d^2}{dR^2}\delta F\right)^{\dagger}F\,dR + \left[F^{\dagger}M^{-1}\frac{d}{dR}\delta F-\left(M^{-1}\frac{d}{dR}F\right)^{\dagger}\delta F\right]_{R=R_\infty}.$$

If $V(R)$ is a Hermitian operator

$$\bar{J}\simeq\int_0^{R_\infty}\left\{\left[M^{-1}\frac{d^2}{dR^2}+M^{-1}k^2-V(R)\right]F\right\}^{\dagger}\delta F\,dR + \left[F^{\dagger}M^{-1}\frac{d}{dR}\delta F-\left(M^{-1}\frac{d}{dR}F\right)^{\dagger}\delta F\right]_{R=R_\infty}$$

of which the first term is zero.

But

$$\delta\bar{F}\sim v^{-1/2}(\cos kR)\,\delta\mathscr{R}$$

and so to first order in δF

$$\begin{aligned}\delta\mathscr{R} &= -\bar{J} \\ &= -\int_0^\infty D^{(t)-1\dagger}F^{(t)\dagger}\delta V F^{(t)-1}\,dR \\ &= -D^{(t)-1\dagger}J\,D^{(t)-1}\end{aligned}$$

where

$$J=\int_0^\infty F^{(t)\dagger}\delta V F^{(t)}\,dR.$$

An $\mathscr{R}$ matrix correct to first order in δF is‡

$$\mathscr{R}=\mathscr{R}^{(t)}-\delta\mathscr{R}.$$

The correction term for the $\mathscr{R}^0$-matrix, used at zero energy is

$$\delta\mathscr{R}^0=-D^{0(t)-1\dagger}J\,D^{0(t)-1}$$

where J is calculated using $F^{(t)}$ with asymptotic forms (40).

In practice the $\mathscr{Y}^0=\mathscr{R}^{0-1}$ matrix was used, with correction term

$$\delta\mathscr{Y}^0=C^{0(t)-1\dagger}J\,C^{0(t)-1}$$

and

$$\mathscr{Y}^0=\mathscr{Y}^{0(t)}-\delta\mathscr{Y}^0.$$

---

‡ This has been obtained independently by Dr. M. J. Seaton.

REFERENCES

ALVAREZ, L. W., BRADNER, H., CRAWFORD, F. S., JR., CRAWFORD, J. A., FALK-VARIANT, P., GOOD, M. L., GOW, J. D., ROSENFELD, A. H., SOLOMITZ, F., STEVENSON, M. L., TICHO, H. K., and TRIPP, R. D., 1957, *Phys. Rev.*, **105**, 1127.

ASHMORE, A., NORDHAGEN, R., STRAUCH, K., and TOWNES, B. M., 1958, *Proc. Phys. Soc.*, **71**, 161.

BLATT, J. M., and WEISSKOPF, V. F., 1952, *Theoretical Nuclear Pyhsics* (New York: Wiley).

BUCKINGHAM, R. A., and MASSEY, H. S. W., 1941, *Proc. Roy. Soc.* A, **179**, 123.

COHEN, S., JUDD, D. L., and RIDDELL, R. J., JR., 1958, *Phys. Rev.*, **110**, 1471.

HAYASHI, C., NAKANO, T., NISHIDA, M., SUEKANE, S., and YAMAGUCHI, Y., 1957, *Progr. Theor. Phys., Japan*, **17**, 615.

JACKSON, J. D., 1957, *Phys. Rev.*, **106**, 330.

KOHN, W., 1948, *Phys. Rev.*, **74**, 1763.

SKYRME, T. H. R., 1957, *Phil. Mag.*, **28**, 910.

WHEELER, J. A., 1937, *Phys. Rev.*, **52**, 1083.

The Continuous X-ray Spectrum from Electron-opaque Targets

By N. A. DYSON†
Cavendish Laboratory, Cambridge

Communicated by V. E. Cosslett; MS. received 1st *September* 1958, *in revised form* 9*th December* 1958

Abstract. The angular and energy distributions of the continuous x-ray spectrum have been investigated in the forward hemisphere for accelerating potentials between 6 and 12 kv. The targets were sufficiently thick to bring the incident electrons to rest, and the spectral distributions closely resemble those obtained by earlier workers with massive targets. The angular distributions are greatly influenced by electron scattering, and it is shown that the degree of anisotropy is consistent with multiple scattering and diffusion being usually prevalent even when the electrons have lost only a small proportion of their incident energy.

The absolute efficiency of x-ray production was found to be about 20% greater than expected from the formula of Compton and Allison.

A proportional counter was used for the measurements, and the method is described.

---

§ 1. Introduction

Previous studies of the continuous x-ray spectrum have been confined, with very few exceptions, to conventional x-ray tubes with massive anticathodes, and to the radiations from very thin targets such that a substantial proportion or even the whole of the electron beam is transmitted. The measurements to be described were carried out using a tube with target opaque to electrons but nevertheless sufficiently thin to transmit most of the x-radiation produced. These conditions are those of the projection x-ray microscope (e.g. Cosslett and Nixon 1952, 1953, Nixon 1955), and it is for this reason that the present work was undertaken.

In projection microscopy accelerating voltages of 10 to 20 kv are commonly used, and the present measurements were made in the region of 6 to 12 kv. Spectral and angular distribution curves were obtained with targets of several elements, and the relation between the measurements and earlier work is discussed. A preliminary account of some of the measurements has been given by Cosslett and Dyson (1957). The measurements are related to the data from ordinary tubes in that electron scattering played a large part, and also to more fundamental observations with films transparent to electrons, in that the observations were made in the forward hemisphere.

§ 2. Review of Previous Work

The angular distribution from thin (electron-transmitting) targets has been investigated at moderately low energies by several workers. Kuhlenkampff (1928) made a series of measurements at 16–38 kv using an aluminium target 6000 Å in thickness, and although the target was insufficiently thin to be regarded as a true approach to the 'ideal' condition, the essential features of the angular distribution were observed. It was shown that the intensity in the forward direction and at 180° is minimal, and that the angle of maximum intensity per unit solid angle is a function of the electron energy. For radiation at the high energy limit of the spectrum the maximum would be found at right angles to the forward direction in the case of a vanishingly small electron energy, moving further forward for increasing electron energy. For quanta with energies below the high energy limit the minimum in the forward direction was found to be less marked, and the maximum intensity occurs at a progressively smaller angle (for a given electron energy) as lower quantum energies are approached. The same pattern of behaviour was found by Bohm (1937, 1938) and Honerjager (1940), using thinner targets; it was found that, as the thickness is increased, the minimum in the forward direction becomes less well defined, and the curves become somewhat broader, due to the increasing effects of electron scattering.

---

† Now at the Radiotherapeutic Research Unit, Hammersmith Hospital, London.

The angle of maximum intensity, near the high energy limit, satisfies closely the expression $\beta(1+\sin^2\theta)=\cos\theta$ derived from a formula given by Compton and Allison (1935, p. 114). For an accelerating voltage of 10 kv this yields a value of $68\frac{1}{2}°$.

In the work just described it was deduced that the intensity in the forward direction at the high energy limit would be zero if the target were sufficiently thin, following the theory of Scherzer (1932), which however involved the assumption of small atomic numbers and high electron velocities. Kerscher and Kuhlenkampff (1955) have measured the angular distribution of radiation from an aluminium target 250 Å thick at 34 kv and show that the forward intensity is in fact finite even with target sufficiently thin (0·003 of the electron range in this case) to be regarded as a true approach to the ideal condition. This is in agreement with the calculations of Scheer and Zeitler (1955). Figure 1 of the preliminary communication (Cosslett and Dyson 1957), calculated from the data of Kirkpatrick and Wiedmann (1945), showed this, and also that the forward minimum becomes less marked for higher atomic numbers.

The angular distribution from thick targets, under carefully defined conditions, has been almost completely neglected. Two curves obtained by Oosterkamp and Proper have been published by Botden *et al.* (1952). The data were obtained with a thin electron-opaque gold target in a small tube designed for radiotherapy, using accelerating voltages of 10 and 25 kv. At the higher voltage, the intensity was maximal at about 15° to the forward direction, being about 10% higher in the maximum direction than in the forward direction. This illustrates that electron scattering was not quite obliterating the type of distribution to be expected from an undeviated beam. The absence of such a rise, at 10 kv, was attributed to the effects of target absorption. The measurements were of total radiation, for dosimetric purposes, and no attempt was made to distinguish between the different quantum energies within the spectrum. The ionization method used by these workers tends to emphasize the softer components of the spectrum, and the 'forward' nature of the angular distribution is consistent with this.

Information regarding the energy distribution from massive anticathodes, in the energy range of interest, is available from the work of Kuhlenkampff (1922), for an x-ray tube operated between 7 and 12 kv. The relation $I_\epsilon = AZ(\epsilon_0-\epsilon)+BZ^2$ was found to be closely applicable from the high energy limit ϵ_0 down to about 0·4 ϵ_0, where I_ϵ is the intensity per unit energy interval,

Z the atomic number of the target material, and A and B are constants. These measurements were carried out at approximately 90° to the forward direction.

The second term in this expression for energy distribution predominates only in the immediate vicinity of the high energy limit. The neglect of the second term leaves a very simple expression for the X-ray intensity, and the use of intensity per unit energy (or frequency) interval is then a great advantage. This form of presentation will be used for the experimental results which follow. The relations between the intensities per unit energy, frequency and wavelength intervals respectively are given by

$$I_\epsilon = \frac{1}{h} I_\nu = \frac{\lambda^2}{hc} I_\lambda$$

which follow from the condition that corresponding areas under the three curves must be the same, i.e.

$$I_\epsilon d\epsilon = I_\nu d\nu = I_\lambda d\lambda.$$

For the efficiency of production of continuous X-radiation there is the well-known expression given by Compton and Allison (1935, p. 90):

$$\eta = 1{\cdot}1 \times 10^{-9} ZV \quad (V \text{ in volts}).$$

The calculations of Kirkpatrick and Wiedmann (1945) on the yields to be expected from thick targets give a similar relation, but with a constant of proportionality of $1{\cdot}3 \times 10^{-9}$. It will be shown that this latter value is supported by the present work.

§ 3. EXPERIMENTAL

In the present investigation, the X-ray tube was of the type used in projection microscopy, but as an ultra-fine focus was not needed a single weak magnetic lens was adequate, producing an image of the 'cross-over' of the electron gun with a magnification of the order of unity. The image was about 70 microns in diameter. The electron beam was limited by an aperture to a semi-angle of about 0·005 radian in image space. This was determined more by the need for a narrow electron beam to avoid possible modification of the angular distribution patterns by the convergence of the electrons, rather than by the exigencies of spherical aberration. A drawing of the tube is shown in figure 1 (*a*). The radiation was detected and measured using a proportional counter, to be described below, and figure 1 (*b*) shows a schematic diagram of the electron and X-ray paths.

The target holder consisted essentially of an insulated section in which a disc of target material, 6 mm in diameter, supported by a thin brass aperture, could be fixed. A vacuum seal was ensured by the use of a thin latex ring inserted between the target and the top of the target holder. The section containing the target was insulated from the main body of the target holder, and the target current (usually in the region of 0·05 to 0·1 μA) was measured using a lamp-and-scale galvanometer.

Targets of copper and gold were made by evaporating the metal on to a thin distrene film about 1 mg cm^{-2} thick. The target thicknesses were 0·40 mg cm^{-2} (gold) and 0·67 and 1·46 mg cm^{-2} (copper). (At 12 kv the gold target would allow most of the electrons to be transmitted but with emergent energies too small to affect the measurements). Some measurements were made with aluminium, for which ordinary manufactured foil 0·78 mg cm^{-2} in thickness was used. Beryllium was originally chosen as an example of a light element, but the foils available (2·8 mg cm^{-2}) were of doubtful purity and uniformity. For this reason only a few measurements were made with this material, and absolute measurements were considered unreliable.

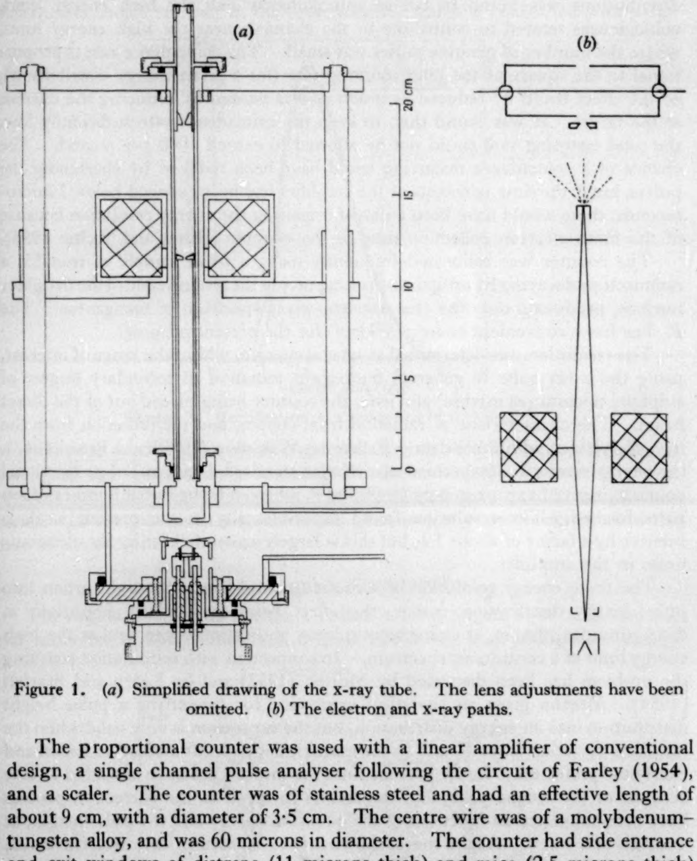

Figure 1. (*a*) Simplified drawing of the x-ray tube. The lens adjustments have been omitted. (*b*) The electron and x-ray paths.

The proportional counter was used with a linear amplifier of conventional design, a single channel pulse analyser following the circuit of Farley (1954), and a scaler. The counter was of stainless steel and had an effective length of about 9 cm, with a diameter of 3·5 cm. The centre wire was of a molybdenum–tungsten alloy, and was 60 microns in diameter. The counter had side entrance and exit windows of distrene (11 microns thick) and mica (2·5 microns thick) respectively.

The gas was a mixture of argon (97½%) and carbon dioxide (2½%), (Arndt, Coates and Crathorn 1954) and flowed continuously through the counter at a rate of about 10 ml. per minute. At 12 kv, the upper limit of quantum energy for most of the measurements, the detection efficiency was in the region of 20%, becoming virtually 100% as the *K* absorption edge of argon (3·2 kv) was approached.

An undesirable effect which becomes important at relatively high counting rates is caused by coincidences between two small pulses. When measuring a continuous X-ray spectrum, the number of pulses near the high energy limit is very much less than at lower quantum energies. Since the maximum of the distributions was found to fall at approximately half the high energy limit, coincidences tended to contribute to the channels near the high energy limit, where the number of genuine pulses was small. The coincidence rate is proportional to the square of the total counting rate (for a given energy distribution), so the effect could be reduced as much as was needed by reducing the current at the target. It was found that, to keep the coincidence rate sufficiently low, the total counting rate could not be allowed to exceed 1000 per second. The chance of a coincidence occurring could have been reduced by shortening the pulses, but if the time constants of the amplifier had been reduced below 3 microseconds, there would have been a risk of impairing the energy resolution because of the finite electron collection time of the counter (Hurst and Richie 1953).

The counter was calibrated frequently using a small sample of iron-55, a radioisotope decaying by orbital electron capture to the ground state of the daughter nucleus, producing only the characteristic X-ray spectrum of manganese. The K_α line has a convenient energy (5·9 kev) for the present purpose.

The resolution was determined at several energies within the range of interest, using the X-ray tube to generate fluorescent radiation in secondary targets of sulphur, calcium (as marble) and iron, the counter being placed out of the direct beam. The characteristic K radiation from copper, and the radiation from the iron-55, yielded additional data. Following Wilkinson (1950) and Fano (1947), the energy resolution (expressed as a relative standard deviation) of proportional counters is given approximately by $(4/3m)^{1/2}$, where m is the initial number of ion pairs formed. The resolution found experimentally in the present work is inferior by a factor of about 1·1, but this is largely accounted for by the electronic noise in the amplifier.

The finite energy resolution of a counting system introduces distortion into pulse height distribution curves, the effect being particularly important at discontinuities, that is, at characteristic lines, absorption edges, and at the high energy limit of a continuous spectrum. In connection with scintillation counting the problem has been discussed by Morton (1952) and by Liden and Starfelt (1954). Morton gives an analytical expression for converting a pulse height distribution into an energy distribution, but the expression is only valid when the standard deviation is small, and so the numerical–graphical method of Liden and Starfelt is preferred. In the present work the method has been extended to take account of the escape peak, and the factors involved in the correction process have been tabulated as functions of the quantum energy and the pulse height, at intervals of 0·4 kev. All the curves shown in the next section have been corrected, or 'rectified', and the process is illustrated here by the curve for aluminium at 10 kv (figure 2). The correction is quite small over most of the spectrum, but is indispensable near the high energy limit.

Secondary emission, and elastic and inelastic back-scattering, are expected to occur at the target. For reliable absolute measurements the secondary electrons should either be collected or an allowance made for those lost. The target holder was such that a large majority of the secondary electrons would in fact be collected, and experiments carried out with a positive bias of 50 volts on the target assembly showed that the loss of secondary electrons amounted to only a few per cent of the incident beam current. Elastic backscattering is known to be small (Paul and Steinwedel 1955), but the same authors show that inelastic backscattering can be considerable. However, correction for these electrons is hardly relevant in the present work, which is concerned with x-ray production in conditions in which electron scattering necessarily plays an integral part. All that is necessary is to arrange for the inelastically scattered electrons either to completely leave the system or to be collected and passed to the galvanometer. In the present arrangement, the great majority are collected, as in the case of the secondary electrons.

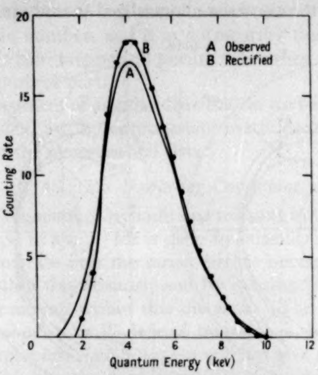

Figure 2. Rectification of a pulse height distribution.

§ 4. Angular Distribution

The angular distribution of the x-radiation from targets of several elements was measured at approximately 6, 8·4, 10, and 12 kv, and usually four energy

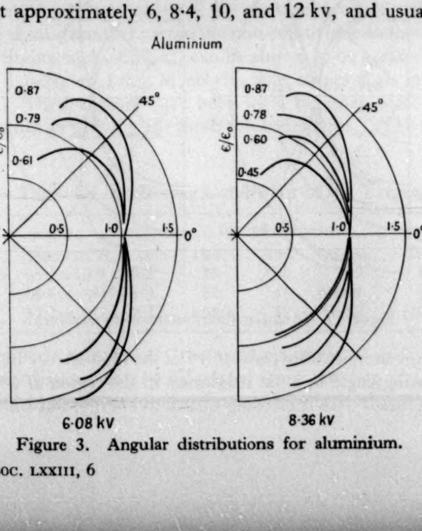

6·08 kV 8·36 kV

Figure 3. Angular distributions for aluminium.

bands within the continuous spectrum were investigated in each case. The angular distributions for aluminium and gold at 6·08 and 8·36 kv are shown in figures 3 and 4. The curves in the upper quadrant show the observed distributions, and the lower curves are corrected for target absorption. Curves obtained with these elements at 10·05 and 12·05 kv were given by Cosslett and Dyson (1957, figures 5 and 6). All the curves are normalized to unity in the forward direction.

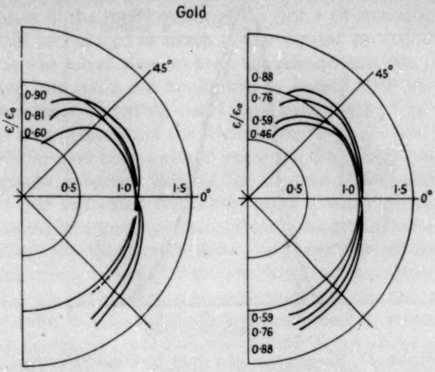

6·08 kv 8·36 kv

Figure 4. Angular distributions for gold.

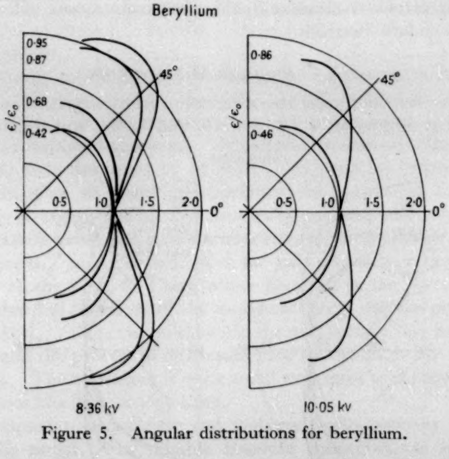

8·36 kv 10·05 kv

Figure 5. Angular distributions for beryllium.

At all quantum energies above about 0·5 of the high energy limit the intensity rises with increasing angle to a flat maximum in the region of 60°. The degree of anisotropy increases with increasing quantum energy, but for a given value of

ϵ/ϵ_0 the variation of anisotropy with kilovoltage is slight. The radiation from aluminium is in general much more anisotropic than that from gold.

Data obtained with a beryllium target at 8·36 and 10·05 kv are shown in figure 5. The anisotropy is seen to be greater than for aluminium, and is about the same as that found with a target of distrene, not illustrated here.

It is clear from these curves that there is a systematic decrease of anisotropy with increasing atomic number, and it is noteworthy that traces of the pattern of behaviour of ideally thin targets still persist even when electron scattering and diffusion play an important part.

The theoretical treatment of angular distribution under the present conditions is prohibitively complex, but by approximate methods it is possible to explain the salient features of the experimental data.

4.1. *The Scattering Conditions*

We shall consider the scattering conditions relevant to the angular distribution curves at $0\cdot 9\,\epsilon_0$, for $\epsilon_0 = 10$ kv. This is done by considering the extent to which the electrons will penetrate into the target before becoming no longer able to produce radiation within this channel, and by relating this to the likelihood of electron scattering occurring within this distance. The curves for $0\cdot 9\,\epsilon_0$ refer in fact to a pulse-channel with ill-defined boundaries, but it will be supposed that quanta with energies less than $0\cdot 9\,\epsilon_0 - \sigma$ will not give rise to any pulse within this channel, where σ is the standard deviation of the pulse height distribution at 9 kev. The relative standard deviation at this energy is about 7%, so it will be supposed that an electron slowed down to below 8·5 kev is unlikely to make any contribution to the channel in question.

The range of electrons in aluminium has been investigated by Lane and Zaffarano (1954) for voltages between 1 and 30 kv, and from their data the expression $V_0^{5/3} - V_t^{5/3} = kt$ may be derived, where $k = 175$ if V_0 and V_t are in kev, and t is in mg cm^{-2}. Writing $V_0 = 10$ kev and $V_t = 8\cdot 5$ kev, it is found that $t_{8\cdot 5}$, the distance in which an electron is slowed down to 8·5 kev from 10 kev, is given by $t_{8\cdot 5} = 6\cdot 4 \times 10^{-2}$ mg cm^{-2}.

The constant of proportionality in the above expression will decrease slowly with increasing atomic number; from the non-relativistic Bethe–Bloch expression (e.g. Paul and Steinwedel 1955), $t_{8\cdot 5}$ can be shown to be greater for gold than for aluminium by a factor of 1·9. In beryllium it is less than in aluminium by a factor of 1·12. These factors have been used together with the experimental data for aluminium to give $t_{8\cdot 5}$ for these three elements. The values are shown in table 1.

Table 1. Scattering Conditions in the Targets

	$t_{8\cdot 5}$ (mg cm^{-2})	n	No. of collisions elas.	inel.	total	ϕ for $t = \frac{1}{2}t_{8\cdot 5}$ Bothe	Blanchard
Beryllium	$5\cdot 7 \times 10^{-2}$	6·2	29	180	209	16½°	23½°
Aluminium	6·4	1·9	32	61	93	33°	41°
Gold	12·2	0·32	61	19	80	(102°)	(80°)

Having obtained values for $t_{8\cdot 5}$, the numbers of elastic and inelastic collisions occurring in this distance can be calculated from the data of Lenz (1954), who gives graphs and expressions for the distance in which an average of one elastic collision is expected, and for the ratio n of inelastic to elastic scattering cross sections. Table 1 shows the values of n for the three elements concerned, and the numbers of collisions of both sorts occurring in the distance $t_{8.5}$.

The total number of collisions occurring in the targets is high, and leads to the somewhat surprising conclusion that we are concerned with either multiple scattering or diffusion, even when considering radiation near the high energy limit, and it is now necessary to find the angle of deviation of the electrons. Emission of a photon can occur at any point along the electron track, and throughout the distance $t_{8.5}$ this will happen with approximately constant probability because the change of electron energy is small. The angle of deviation has therefore been calculated for a distance within the target of one half of $t_{8.5}$.

For multiple scattering, the most probable angle of deviation ϕ is given by the formula of Bothe (quoted by Compton and Allison, 1935, p. 76) and the mean value of $\cos\phi$ is given by Blanchard (1954). Both these expressions have been used to calculate values of ϕ which are shown in the final two columns of table 1.

As the thickness of a scattering foil increases, the distribution of electron flux approaches a form approximately proportional to $\cos^2\phi$, and the most probable angle of scattering tends to a constant value of about 33° (Bothe 1932, Paul and Steinwedel 1955). This condition is known as diffusion, and it is unlikely that the large values of ϕ obtained above for gold mean anything other than that the condition of diffusion has been reached. Aluminium is apparently on the threshold of diffusion; and in the case of beryllium multiple scattering rather than diffusion seems to prevail, although the experimental data is more consistent with the latter, as will be shown in § 4.2.

In the present work the angle of maximum intensity of x-ray emission could not be measured accurately, but was generally about 60°, significantly lower than the value of $68\frac{1}{2}°$ obtained from the theoretical expression quoted earlier. It has been shown (Dyson 1956, pp. 87–89) that this difference is consistent with the predominance of electron diffusion in the target, because if diffusion is assumed to be occurring, the mean angle between the electrons and the observed direction of maximum emission can be shown to be approximately $68\frac{1}{2}°$.

4.2. *The Degree of Anisotropy*

Scheer and Zeitler (1955) have shown that for an ideally thin target, the x-ray intensity at an angle θ to the forward direction can be written in the form

$$\frac{I(\nu, \theta)}{I(\nu, 90)} = F(\theta) + [1 - p(\nu)]G(\theta).$$

where $p(\nu)$ is the polarization, and F and G are functions of angle and electron energy. By two applications of this expression, the ratios of the intensities at any two angles can be determined. If the electrons move in a parallel beam, this can be done immediately; if they are not parallel, but are distributed according to a known law, the calculation is possible in principle but difficult in practice. A preliminary attempt to compare experiment with theory has been made by assuming that all the electrons are moving in their most probable direction, which, for the condition of diffusion, is at 33° to the forward direction.

The anisotropy is defined as the ratio of the intensity in the direction of the maximum (60°) to that in the forward direction. If all the electrons are moving at 33° to the forward direction, the forward radiation is equal to that which would be observed at 33° if the electrons could pass, in the forward direction, through a similar thickness of target without deviation. Further, as the mean angle between the electrons and the observed direction of maximum intensity has been shown to be approximately equal to 68½°, the thin target maximum, it is assumed that the electrons make a maximum contribution to the thick target maximum. So the assumptions amount to the statement that

$$\left(\frac{I_{\max(\alpha=60)}}{I_{(\alpha=0)}}\right)_{\substack{\text{thick}\\\text{target}}} = \left(\frac{I_{\max(\theta=68\frac{1}{2})}}{I_{(\theta=33)}}\right)_{\substack{\text{thin}\\\text{target}}}$$

The calculated values are tabulated in table 2 and compared with the observed values. In the case of beryllium, the calculation is repeated for $\phi=16\frac{1}{2}°$ and $23\frac{1}{2}°$, the values obtained from the multiple scattering formulae of Bothe and of Blanchard. For gold and aluminium the agreement is good, and tends to confirm the relevance of electron diffusion. For beryllium the agreement is reasonable only if the assumption of diffusion is made, and it is not clear why the multiple scattering formulae fail to give a correct prediction of the anisotropy for this element.

Table 2. The Degree of Anisotropy

	observed	calculated
Beryllium	2·0	(4·1) ($\phi=16\frac{1}{2}$)
		(2·7) ($\phi=23\frac{1}{2}$)
		1·8
Aluminium	1·5	1·6
Gold	1·2	1·2

§ 5. ENERGY DISTRIBUTION AND EFFICIENCY OF PRODUCTION

Figures 6 (*a*) and (*b*) show the pulse height distributions for targets of aluminium and gold at the same kilovoltages as were used for the angular distribution measurements. These curves are unrectified and uncorrected for absorption losses or counter efficiency, and the fully corrected curves are shown (as intensity

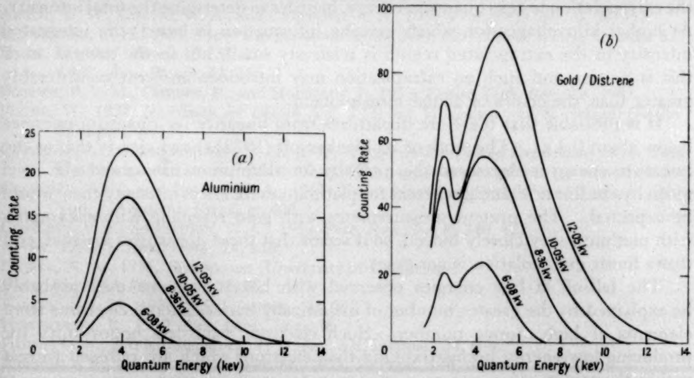

Figure 6. Pulse height distributions from targets of aluminium and gold.

per unit energy interval) in figures 7 (*a*) and (*b*). Similar data were obtained for targets of copper (Cosslett and Dyson 1957). The corrected curves for aluminium and copper are proportional to $\epsilon_0 - \epsilon$ to a high degree of approximation, but in the case of the radiation from gold there is a systematic departure, best represented by a small additional term, essentially independent of accelerating voltage. The energy distributions therefore follow closely the general form of the curves obtained by Kuhlenkampff at right angles to the electron beam.

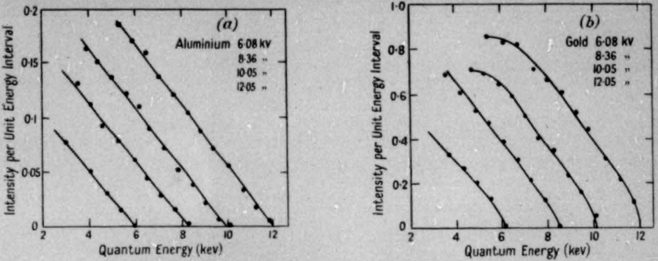

Figure 7. Corrected energy distributions for aluminium and gold. The units are intervals of erg/sterad^{-1} μc^{-1} kev^{-1}.

In all the curves the agreement between the observed and expected positions of the high energy limit and the characteristic peaks is very close and shows that energy measurements of considerable accuracy can be obtained even at these low energies, where the resolution of proportional counter is low.

The intensity measurements are on an absolute basis, and the distribution curves are expressed in intervals of erg sterad^{-1} μc^{-1} kev^{-1}, the mixed units being chosen for practical convenience. The total production within a given range of quantum energy will of course be found by simple integration of the curve between appropriate boundaries.

It is clear that an unequivocal comparison between the present work and the existing data on efficiency of production is not easy, the main difficulty being in the extrapolation to zero quantum energy, in order to determine the total intensity. At higher kilovoltages (on which existing information is based) the integrated intensity in the extrapolated region is relatively small, but in the present work this is not so, and such an extrapolation may introduce an error considerably greater than the errors of actual measurement.

It is probable that there are departures from linearity for quantum energies below about 0·4 ϵ_0. The work of Kuhlenkampff (1922) shows clearly that as the quantum energy is decreased the intensity for aluminium rises above the level given by the linear relation, whereas for platinum there is less intensity than would be expected. The present measurements with gold resemble Kuhlenkampff's with platinum very closely indeed, so it seems that these departures are real, and that a linear extrapolation is not exact.

The fall-off at low energies observed with heavy elements may probably be explained by the greater number of inelastically back-scattered electrons from elements of high atomic number. Such electrons have less opportunity for producing low-energy bremsstrahlung than electrons which are reduced to rest within the target.

To compare the present measurements with existing data we shall arbitrarily extrapolate the curves to zero quantum energy, and calculate the efficiency of production in the forward direction. This is compared with the average efficiency per steradian as deduced from Compton and Allison's expression. These efficiencies are tabulated in table 3. The efficiencies are quoted at 10 kv.

Table 3. Efficiencies per Steradian

	observed	calculated	ratio
Aluminium	$1{\cdot}37\times10^{-5}$	$1{\cdot}15\times10^{-5}$	1·20
Copper	3·44	2·56	1·34
Gold	7·87	6·97	1·13

The ratios in the last column of table 3 have a mean value of 1·22, showing that the efficiencies as calculated here are in excess of Compton and Allison's assessment by about 20%. It is interesting to note that the thick target calculations of Kirkpatrick and Wiedmann referred to earlier give values for efficiency very close to those found here.

It is necessary to emphasize that the extrapolation to zero energy introduces considerable uncertainty, and that the only satisfactory way of presenting the data is as in figure 7, from which the absolute intensity per unit interval in the forward direction, for quantum energies within the observed part of the spectrum, can be reliably obtained.

ACKNOWLEDGMENTS

The author wishes to thank the Department of Scientific and Industrial Research for a maintenance award for the two years during which the experimental work was carried out. The material presented in this paper forms part of a dissertation (Cambridge 1956) entitled ' Physical Problems in Projection X-ray Microscopy ', and a debt of gratitude to Dr. V. E. Cosslett for continued help and supervision, at all stages of the work, is gratefully acknowledged.

REFERENCES

ARNDT, U. W., COATES, W. A., and CRATHORN, A. R., 1954, *Proc. Phys. Soc.* B, **67,** 357.
BLANCHARD, C. H., 1954, Paper I in *Electron Physics, Nat. Bur. Stand. Wash.,* Circular 527.
BOHM, K., 1937, *Physik. Z.,* **38,** 334.
—— 1938, *Ann. Physik,* **33,** 315.
BOTDEN, P. J. M., COMBEE, B., and HOUTMAN, J., 1952, *Philips Tech. Rev.,* **14,** 165.
BOTHE, W., 1932, *Handbuch der Physik,* Vol. 2 (2) (ed. H. Geiger and K. Scheel) (Berlin : Springer), p. 1.
COMPTON, A. H., and ALLISON, S. K., 1935, *X-rays in Theory and Experiment* (New York: Van Nostrand; London: Macmillan). The page numbers refer to the second edition.
COSSLETT, V. E., and DYSON, N. A., 1957, *X-ray Microscopy and Microradiography* (New York : Academic Press), p. 405.
COSSLETT, V. E., and NIXON, W. C., 1952, *Proc. Roy. Soc.* B, **140,** 422.
—— 1953, *J. Appl. Phys.,* **24,** 616.
DYSON, N. A., 1956, *Dissertation* (University of Cambridge).
FANO, U., 1947, *Phys. Rev.,* **72,** 26.
FARLEY, F. J. M 1954, *J. Sci. Instrum.,* **31,** 241.
HONERJAGER, R 1940, *Ann. Phys., Lpz.,* **38,** 33.
HURST, G. S., and RICHIE, R. H., 1953, *Rev. Sci. Instrum.,* **24,** 664.
KERSCHER, R., and KUHLENKAMPFF, H., 1955, *Z. Phys.,* **140,** 632.
KIRKPATRICK, P., and WIEDMANN, L., 1945, *Phys. Rev.,* **67,** 321.

KUHLENKAMPFF, H., 1922, *Ann. Phys., Lpz.*, **69**, 548.
—— 1928, *Ibid.*, **87**, 597.
LANE, R. O., and ZAFFARANO, D. J., 1954, *Phys. Rev.*, **94**, 960.
LENZ, F., 1954, *Z. Naturf.*, **9a**, 185.
LIDEN, K., and STARFELT, N., 1954, *Ark. Fys.*, **7**, 391.
MORTON, G. A., 1952, *Advanc. in Electronics*, **4**, 69.
NIXON, W. C., 1955, *Research*, **8**, 473.
PAUL, W., and STEINWEDEL, H., 1955, *β- and γ-ray Spectroscopy* (ed. K. Siegbahn), (Amsterdam : North Holland Publ.), p. 1.
SCHEER, M., and ZEITLER, E., 1955, *Z. Phys.*, **140**, 642.
SCHERZER, O., 1932, *Ann. Phys., Lpz.*, **13**, 137.
WILKINSON, D. H., 1950, *Ionisation Chambers and Counters* (Cambridge : University Press).

RESEARCH NOTES

A New Class of Materials for Bloembergen-type Masers

By B. BLEANEY
Clarendon Laboratory, Oxford

MS. received 6th February 1959

The operation of a maser of the type proposed by Bloembergen (1956) requires a paramagnetic salt with more than two electronic levels, where there are allowed transitions between levels which are not necessarily consecutively spaced in energy. In general, this has been achieved by the use of a substance where the initial degeneracy of the levels has been lifted by crystal field interactions. For the desired transitions to have adequate intensity it is then necessary that the initial splitting (expressed in frequency units) should be of the same order of magnitude as the applied frequencies. The purpose of this note is to point out that there exists another class of substances where there are four levels degenerate in zero field, which have a linear Zeeman effect, but are not necessarily equally spaced when a magnetic field is applied, and where there are allowed transitions which are not limited to those between adjacent energy levels.

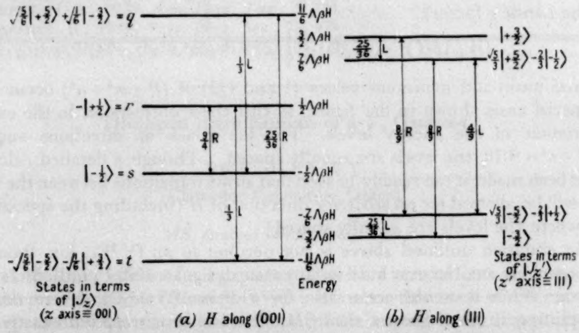
$\sqrt{\frac{5}{6}}|+\frac{5}{2}\rangle+\sqrt{\frac{1}{6}}|-\frac{3}{2}\rangle=q$
$-|+\frac{1}{2}\rangle=r$
$|-\frac{1}{2}\rangle=s$
$-\sqrt{\frac{5}{6}}|-\frac{5}{2}\rangle-\sqrt{\frac{1}{6}}|+\frac{3}{2}\rangle=t$
States in terms of $|J_z\rangle$ (z axis ≡ 001)
$\frac{1}{3}$ L
$\frac{9}{4}$ R
$\frac{25}{36}$ R
$\frac{1}{3}$ L
$\frac{11}{6}\Lambda\beta H$
$\frac{3}{2}\Lambda\beta H$
$\frac{7}{6}\Lambda\beta H$
$\frac{1}{2}\Lambda\beta H$
$-\frac{1}{2}\Lambda\beta H$
$-\frac{7}{6}\Lambda\beta H$
$-\frac{3}{2}\Lambda\beta H$
$-\frac{11}{6}\Lambda\beta H$
Energy
$\frac{25}{36}$ L
$\frac{8}{9}$ R
$\frac{8}{9}$ R
$\frac{4}{9}$ L
$\frac{25}{36}$ L
$|+\frac{3}{2}\rangle$
$\frac{\sqrt{5}}{3}|+\frac{5}{2}\rangle-\frac{2}{3}|-\frac{1}{2}\rangle$
$\frac{\sqrt{5}}{3}|-\frac{5}{2}\rangle-\frac{2}{3}|+\frac{1}{2}\rangle$
$|-\frac{3}{2}\rangle$
States in terms of $|J_{z'}\rangle$ (z' axis ≡ 111)

(*a*) *H* along (001) (*b*) *H* along (111)

Energy levels and allowed transitions within the quartet of levels which form the ground state of an f^1, $^2F_{5/2}$ ion subjected to a cubic (tetrahedral) crystal field, and to a magnetic field (*a*) parallel to an 001 axis, (*b*) parallel to a 111 axis. The symbols R, L denote the sense required when circularly polarized radiation is used to excite the various transitions. The states are given in terms of $|J_z\rangle$, with the z axis along 001 and 111 respectively. Λ is the Landé g-factor ($=\frac{6}{7}$ for f^1, $^2F_{5/2}$).

As a simple example we will take the case of an ion with one f-electron subjected to a cubic (tetrahedral) crystal field whose strength is small compared with that of the spin orbit coupling. This is a situation which could be obtained with a Ce^{3+} ion, $4f^1$, $^2F_{5/2}$, in a suitable crystalline matrix. The ground state of this ion is $J=5/2$, and under the action of a cubic field it splits into a doublet and a quartet, the latter being lower in energy if the cubic field is that due to 4 or 8 charges, as in a tetrahedron or cube. Under the conditions:

spin orbit coupling $\gg$ cubic field splitting $\gg$ Zeeman energy,

the quartet state has a linear Zeeman effect with the splitting shown in the figure when the magnetic field H is directed along one of the cube axes. It will be seen that the levels are not equally spaced and that there are four allowed transitions of which only one is between adjacent levels. These transitions can be induced by an oscillatory field normal to H; the oscillatory field can be either linearly polarized or circularly polarized, but if it is circularly polarized then the sense is different for different transitions. In the diagram transitions which require circularly polarized radiation of the same sense as that generally needed for electrons are labelled R, while those transitions which require the opposite sense are labelled L. Although the system has cubic symmetry, the spacing of the levels is not independent of orientation, and the effect of placing the steady field along the 111 axis is shown in the figure, (*b*). The level spacing is different and there are now five allowed transitions instead of four; the sense of the circularly polarized radiation required for these transitions is again given by the labels, R, L. The relative transition probabilities of the various transitions are shown in the figure for both directions of H; the designation of the states in terms of J_z (z axis $\equiv$ 001 and 111 respectively) is also shown. The unusual circular polarization properties suggest that these substances may be of use in novel gyrator applications.

For an arbitrary direction of the magnetic field H, with direction cosines (l, m, n) to the cubic axes, the energy levels are given by the equation (where Λ is the Landé g-factor)

$$(W/\Lambda\beta H)^2 = (65/36) \pm \frac{1}{9}\{270(l^4+m^4+n^4)-74\}^{1/2}. \quad \ldots\ldots(1)$$

The maximum and minimum values (1 and 1/3) of $(l^4+m^4+n^4)$ occur for the two special cases shown in the figure, so that these correspond to the extremes of variation of the energy levels. For the cones of directions such that $l^4+m^4+n^4=9/10$, the levels are equally spaced. Though a detailed calculation has not been made, it can readily be seen that all six transitions between the various levels will be allowed for an arbitrary direction of H (including the special directions where the levels are equally spaced).

The situation outlined above is not peculiar to an f^1, $^2F_{5/2}$ ion, though the actual numbers are, but may hold for any state designated by Γ_8 in Bethe's (1929) notation. Thus it would occur also for a d^5 ion ($S=5/2$), where the cubic field splitting is much greater than βH; this would correspond exactly to the case above, with $\Lambda=2$ (instead of 7/6 for f^1, $2F_{5/2}$). Unfortunately, the cubic field splitting of d^5 ground states is usually less than 0·1 cm^{-1}, so that the theory developed here is applicable only to rather small magnetic fields. The same difficulty holds for a $4f^7$ ion, where under certain (rather unusual) conditions a Γ_8 state can be lowest in energy. Inspection of Bethe's tables show, however, that Γ_8 quartets occur in all the rare earth ions with Kramers' degeneracy since these have ground states with $J \geqslant 5/2$. Of particular use are likely to be ions of the second half of the lanthanide group, where both J and Λ are largest so that large Zeeman effects can be obtained with small fields. It is also fortunate that the ions with Γ_8 quartet states are the trivalent ions with even atomic number, most of whose isotopes have zero nuclear spin and hence no hyperfine structure.

The problem of obtaining a suitable ion with a Γ_8 quartet as the ground state is that of finding a crystal with cubic symmetry and suitable ratio of the fourth and sixth degree parameters. This problem is being examined theoretically by Dr. B. R. Judd, but two cases where a Γ_8 state is certainly lowest are the ions Ce^{3+}, Sm^{3+} ($J=5/2$) in a cubic (tetrahedral) field. Unfortunately, these have rather small Landé factors ($\Lambda=6/7$ for Ce^{3+}, $2/7$ for Sm^{3+}). One of the few sets of rare earth compounds with overall cubic symmetry is the sequioxides (La_2O_3 etc.) but these have a very complicated structure and it is unlikely that the local symmetry at a lanthanon ion site is cubic. The same is true of the garnets which are being investigated in this laboratory by Dr. W. P. Wolf. The most promising materials at present appear to be CaF_2 (and its isomorphs CdF_2, SrF_2, BaF_2, $SrCl_2$), ThO_2 and MgO, in all of which trivalent ions have been observed to give spectra with cubic symmetry when prepared in certain ways. Baker, Hayes and Jones (1959) have observed the resonance spectrum of Er^{3+} ions with cubic symmetry in CaF_2; unfortunately in this case the ground state is a doublet, but its high g-value (6·78) indicates that Er^{3+}, $4f^{11}$, $J=15/2$, $\Lambda=6/5$; and the ions Nd^{3+}, $4f^3$, $J=9/2$, $\Lambda=8/11$; Dy^{3+}, $4f^9$, $J=15/2$, $\Lambda=4/3$; Yb^{3+}, $4f^{13}$, $J=7/2$, $\Lambda=8/7$, are likely to be of greatest use when economy of magnetic field is desired.

A suitable spin Hamiltonian for Γ_8 states is considered in the following note (Bleaney 1959).

References

Baker, J. M., Hayes, W., and Jones, D. A., 1959, *Proc. Phys. Soc.*, **73**, 942.
Bethe, H. A., 1929, *Ann. Phys., Lpz.*, **3**, 133.
Bleaney, B., 1959, *Proc. Phys. Soc.*, **73**, 939.
Bloembergen, N., 1956, *Phys. Rev.*, **104**, 324.

The Spin Hamiltonian of a Γ_8 Quartet

By B. BLEANEY
Clarendon Laboratory, Oxford

MS. received 6th February 1959

The Zeeman effect of a Γ_8 quartet state in a special case is analysed in the preceding note (Bleaney 1959). It is clear that such effects cannot be represented by a spin Hamiltonian of the normal kind, though it would be useful to find a spin Hamiltonian to represent this situation, using an effective spin $S=\frac{3}{2}$ since there are four levels. Some time ago Dr. A. Abragam pointed out to the writer that it must be possible to find an appropriate spin Hamiltonian using, for example, matrix elements of the form $H_xS_x^3$ etc. To have cubic symmetry, be invariant under inversion through the origin, and give a linear Zeeman effect the spin Hamiltonian must then be of the form

$$\mathscr{H}=g\beta(H_xS_x+H_yS_y+H_zS_z)+f\beta(H_xS_x^3+H_yS_y^3+H_zS_z^3). \qquad \ldots\ldots(1)$$

The matrix elements of this Hamiltonian are then in 1 : 1 correspondence with those of the Zeeman operator $\Lambda\beta\mathbf{H}\,.\,\mathbf{J}$ (where Λ is the Landé g-factor in the notation of Elliott and Stevens (1953)) within the quartet manifold considered in the preceding note, provided we make the following correspondence between the states: either $(q, r, s, t) \equiv (-\frac{3}{2}, +\frac{1}{2}, -\frac{1}{2}, +\frac{3}{2})$ or $(q, r, s, t) \equiv (+\frac{1}{2}, -\frac{3}{2}, +\frac{3}{2}, -\frac{1}{2})$. These form two alternative orders in which the states (designated by $|S_z\rangle$, with the z axis $\equiv$ 001 cubic axis) can be chosen to correspond with the levels q, r, s, t, whose designation in terms of $|J_z\rangle$ is shown in the figure of the preceding note. (The phases shown are chosen so as to obtain a 1 : 1 correspondance between all matrix elements of $\mathscr{H} = \Lambda\beta\mathbf{H} \,.\, \mathbf{J}$ and of the spin Hamiltonian (1)). These two correspondences are completely equivalent alternatives, but the values of g, f are naturally different for the two cases: the former requires $g = 23\Lambda/18$, $f = -10\Lambda/9$, the latter $g = 25\Lambda/6$, $f = -2\Lambda$.

The off-diagonal matrix elements of the spin Hamiltonian (1) are rather tedious to calculate, but their general nature can be seen from equation (2), which is a less elegant form of (1):

$$\begin{aligned}\mathscr{H} = g\beta H_z S_z + f\beta H_z S_z^3 + \beta[\tfrac{1}{2}g + \tfrac{1}{4}f\{3S(S+1)-2\}](H_+S_- + H_-S_+)\\ -(3f\beta/8)S_z(H_+S_- + H_-S_+)S_z + \tfrac{1}{8}f\beta(H_+S_+^3 + H_-S_-^3). \qquad \ldots\ldots(2)\end{aligned}$$

The off-diagonal matrix elements are those between $|S_z = M\rangle$ and $|M \pm 1\rangle$ arising from S_+, S_-; and between $|M\rangle$ and $|M \pm 3\rangle$, arising from S_+^3, S_-^3. The only element of the latter kind is that between the states $|+\frac{3}{2}\rangle$ and $|-\frac{3}{2}\rangle$, and it is this element which is responsible for the ambiguity noted above for the special case considered in the previous note. This is a general feature of the spin Hamiltonian (1), and arises from the fact that the operators with off-diagonal matrix elements generate new states in the cyclic sequence

$$|+\tfrac{3}{2}\rangle \rightarrow |+\tfrac{1}{2}\rangle \rightarrow |-\tfrac{1}{2}\rangle \rightarrow |-\tfrac{3}{2}\rangle \rightarrow |+\tfrac{3}{2}\rangle.$$

By a double cyclic permutation in which the state $|+\frac{3}{2}\rangle$ becomes $|-\frac{1}{2}\rangle$, etc., one finds that the system can again be represented by the spin Hamiltonian (1) but with new values of the parameters g', f' such that $12g = -40g' - 91f'$, $3f = 4g' + 10f'$. The correspondence between the alternative representations

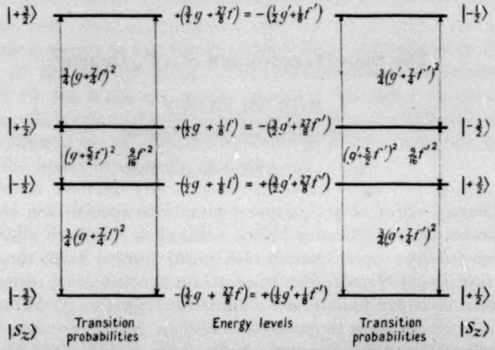
$|+\frac{3}{2}\rangle$
$+(\frac{3}{2}g + \frac{27}{8}f) = -(\frac{1}{2}g' + \frac{1}{8}f')$
$|-\frac{1}{2}\rangle$
$\frac{3}{4}(g + \frac{7}{4}f)^2$
$\frac{3}{4}(g' + \frac{7}{4}f')^2$
$|+\frac{1}{2}\rangle$
$+(\frac{1}{2}g + \frac{1}{8}f) = -(\frac{3}{2}g' + \frac{27}{8}f')$
$|-\frac{3}{2}\rangle$
$(g + \frac{5}{2}f)^2$ $\frac{9}{16}f^2$
$(g' + \frac{5}{2}f')^2$ $\frac{9}{16}f'^2$
$|-\frac{1}{2}\rangle$
$-(\frac{1}{2}g + \frac{1}{8}f) = +(\frac{3}{2}g' + \frac{27}{8}f')$
$|+\frac{3}{2}\rangle$
$\frac{3}{4}(g + \frac{7}{4}f)^2$
$\frac{3}{4}(g' + \frac{7}{4}f')^2$
$|-\frac{3}{2}\rangle$
$-(\frac{3}{2}g + \frac{27}{8}f) = +(\frac{1}{2}g' + \frac{1}{8}f')$
$|+\frac{1}{2}\rangle$
$|S_z\rangle$
Transition probabilities
Energy levels
Transition probabilities
$|S_z\rangle$

Spin states, energy levels (in units of βH) and relative strengths of allowed transitions when H is along the z axis of the spin Hamiltonian (1). The two alternative representations are shown to the right and to the left. It will be seen that the special cases $g + 7f/4 = 0$, $g + 5f/2 = 0$ (and similarly for g', f') correspond to certain transitions having zero probability; in each of these cases a simpler spin Hamiltonian can be found.

is shown in the figure, which gives the energy levels both in terms of g, f and of g', f' for the special case when the steady magnetic field H is along an 001 axis.

The relative intensities of the allowed transitions when the steady magnetic field is along the z axis are also shown in the figure. These transitions can be induced by an oscillatory magnetic field in the 001 plane, but if circularly polarized radiation is used the sense required is different for various transitions. The sense is readily found by observing whether the operator which generates a state of higher energy is associated with $H_+ = H_x + iH_y$ or with $H_- = H_x - iH_y$.

If the steady field is in an arbitrary direction whose direction cosines are (l, m, n) with respect to the cubic axes, the energy levels are given by equation (3)

$$(W/\beta H)^2 = \tfrac{1}{4}(5\gamma^2 + 3\delta^2) \pm \gamma[\gamma^2 + \tfrac{1}{2}\delta^2\{9(l^4 + m^4 + n^4) - 3\}]^{1/2} \qquad \ldots\ldots(3)$$

where $\gamma = g + 7f/4$, $\delta^2 = f(g + 5f/2)$. If the axes are rotated so that H lies along the z' axis of a new coordinate system (x', y', z') where the spin components are now S_z', S_+', S_-' the spin Hamiltonian is found to contain terms in $S_+'^2$, $S_-'^2$. Thus, in general, transitions will be allowed between every pair of levels (here it must be remembered that the spin Hamiltonian for the oscillatory field will also contain such terms). This includes the special directions for H satisfying the relation

$$l^4 + m^4 + n^4 - 3/5 = 2\delta^2/25\gamma^2 \qquad \ldots\ldots(4)$$

where the levels are equally spaced. The cases where H is along 001 or 111 are exceptions where some transitions have zero intensity.

There are three special cases for particular ratios of $f:g$ giving δ or $\gamma = 0$, where the angular variation of the energy levels vanishes. These are:

(*a*) $f = 0$. This is a trivial case, since it corresponds to the terms in S_x^3 etc., vanishing;

(*b*) $g + 5f/2 = 0$. In this case the levels are again equally spaced; transference to the alternative g', f' system shows that it corresponds to $f' = 0$, so that in this system the S_x^3 etc. terms would vanish;

(*c*) $g + 7f/4 = 0$. For this case also $g' + 7f'/4 = 0$, and the levels degenerate into two doublets with energy $W/\beta H = \pm 3g/7$.

Inspection of the figure shows that in these special cases some of the transitions have zero intensity, corresponding to the fact that in each case a simpler spin Hamiltonian exists of the form $\mathscr{H} = g\beta\mathbf{H} \cdot \mathbf{S}$, with $S = \tfrac{3}{2}$ in cases (*a*), (*b*) and $S = \tfrac{1}{2}$ in (*c*).

The spin Hamiltonian (1) is subject to the same limitations as applied to the f^1, ${}^2F_{5/2}$ case considered in the previous note. It is valid only under the condition $E \gg \beta H$, where E is the energy separation between the quartet levels and other levels. The behaviour af the susceptibility is also of interest. At temperatures such that $E \gg kT \gg \beta H$ the susceptibility is isotropic and follows Curie's law $\chi = Np^2\beta^2/3kT$ (apart from a temperature independent term), with $p^2 = \tfrac{5}{8}(5\gamma^2 + 3\delta^2)$ The susceptibility will not be isotropic at temperatures such that $\beta H \sim kT$, and the saturation moment will vary with the direction of the external field, being proportional to the lowest root of equation (3).

If the ion has a non-zero nuclear spin, there will be a hyperfine structure which is also anisotropic. For a rare earth ion, to the approximation that the magnetic hyperfine interaction can be represented by a term $a\mathbf{I} \cdot \mathbf{J}$, and that all matrix elements of the hyperfine structure can be neglected except those within the quartet manifold, one can replace J_x by $(gS_x + fS_x^3)/\Lambda$, etc. This should apply both to the magnetic hyperfine structure and the nuclear electric quadrupole interaction. The latter is not zero in a Γ_8 quartet even with cubic symmetry. This can be verified by considering the quantity $3J_z^2-J(J+1)$ of the f^1 ion discussed in the preceding note; it has the value $+8$ for the states *q*, *t* and -8 for the states *r*, *s*, so that the quadrupole interaction could be determined directly by measurements in a strong magnetic field.

ACKNOWLEDGMENTS

The writer is indebted to a number of people in the Clarendon Laboratory for helpful discussion; in particular to Dr. B. R. Judd, who derived equation (3); and to Professor C. A. Hutchison, whose unpublished results on $[(CH_3)_4N]_2NpCl_6$ drew my attention to this problem.

REFERENCES

BLEANEY, B., 1959, *Proc. Phys. Soc.*, **73**, 937.
ELLIOTT, R. J., and STEVENS, K. W. H., 1953, *Proc. Roy. Soc.* A, **218**, 553.

Paramagnetic Resonance of Impurities in CaF_2

BY J. M. BAKER†, W. HAYES† AND D. A. JONES‡
† Clarendon Laboratory, Oxford
‡ Department of Natural Philosophy, University of Aberdeen

MS. received 24th February 1959

CRYSTALS of CaF_2 were grown from a melt containing iron group (3d) and rare earth (4f) impurities. The specimens were prepared by crystallization from the melt by Stockbarger's technique (Stockbarger 1949) using carefully selected pieces of colourless natural fluorite which were crushed before loading into the graphite crucible. The impurities were introduced by mixing the appropriate amount of salt containing the element required with this powdered fluorite. Where possible fluorides were used but if these were not available 1% PbF_2 was added to the mixture to remove unwanted electro-negative ions. Any excess PbF_2 evaporates from the melt and the resulting crystal certainly contains less than 1 in 10^6 of lead.

The procedure adopted for growing these crystals was as follows. The furnace was evacuated, and when the pressure was less than 5μ the temperature was raised to about 100°c and left under these conditions for 24 hours. This was to ensure thorough drying of the powdered fluorite before it was raised to temperatures at which hydrolysis occurs. The temperature was then increased at a steady rate of 100°c per hour to about 1250°c. At this temperature a stream of oxygen-free nitrogen was passed through the furnace raising the pressure to about 30μ, to avoid undue loss of material due to evaporation. The furnace was then raised to about 40°c above the melting point of fluorite (1380°c) and left at this temperature for an hour or so to ensure complete melting. The crystal was grown by lowering the crucible in the furnace at a rate of 1 mm per hour and when the melt was completely solidified it was cooled to room temperature at about 50°c per hour.

Crystals of CaF_2 belong to the O_h^5 space group. The structure is a regular cubic array of fluorine ions with calcium ions at every other body centre. The spectra of most of the impurities introduced can be explained on the supposition that each impurity ion replaces a calcium ion in the lattice. Resonance measurements on the divalent impurity ions indicate that some are situated in a cubic crystalline field and some are situated in a field of lower symmetry produced by a local lattice distortion. Trivalent impurity ions are in general observed in a field of tetragonal symmetry and there are three distinguishable magnetic centres. When trivalent ions replace Ca^{2+} ions in the lattice charge compensation must occur and Bleaney, Llewellyn and Jones (1956) conclude from measurements on Nd^{3+} and U^{3+} in CaF_2 that charge compensation is achieved by the presence of an extra fluorine ion in a vacant interstitial site next to the impurity ion; the F^- interstitial gives the crystal field its tetragonal component at the impurity ion. This model is supported by x-ray and density measurements of Zintl and Udgard (1939) and of D'Eye and Martin (1957) on similar crystals with large concentrations of trivalent ion. Also, a splitting of the resonance lines by the dipole field of the interstitial F^- ion has been observed in the spectrum of Ce^{3+}. In some cases the trivalent ion occurs in a cubic field; here the charge compensation is presumably remote and does not disturb the surroundings of the impurity ion (see also Low 1958). The radii of the rare earth ions are close to the radius of Ca^{2+} and they are readily incorporated into the lattice; the radii of the iron

Salt mixed with CaF_2 powder	Molar fraction added	 in crystal	Comments
VCl_2	0·01% V	no resonance‡	
Cr_2O_3 B.D.H. Recrystallized	up to 1% Cr	0·0001%	
MnF_2 B.D.H. Purified by crystallization	0·01% Mn	0·001%	see I
$FeSO_4.7H_2O$ B.D.H. Analar	0·01% Fe	no resonance	†Fe^{2+} is non-Kramers
$CoSO_4.7H_2O$ B.D.H. Lab. reagent	0·01% Co	0·0001%	
$NiCl_2.6H_2O$ Hopkins and Williams Analar	0·01% Ni	no resonance	†Ni^{2+} is non-Kramers
CuO B.D.H. Analar	0·01% Cu	no resonance‡	
CeF_3 Thorium Limited	0·01% Ce	0·005%	
PrF_3 ,, ,,	0·01% Pr	no resonance	†Pr^{3+} is non-Kramers
NdF_3 ,, ,,	0·2% Nd	0·01%	see Bleaney, Llewellyn and Jones (1956)
SmF_3 ,, ,,	0·05% Sm	no resonance	may be Sm^{2+} ($J=0$) (see Przibram 1956) but Sm^{3+} has very small g-values
Eu_2O_3 Johnson Matthey	0·01% Eu	0·01%	see I
GdF_3 ,, ,,	0·01% Gd	0·01%	see I
Dy_2O_3 ,, ,,	0·01% Dy	0·0001%	too weak for analysis
Er_2O_3 ,, ,, 'Specpure'	0·01% Er	0·001%	

† Non-Kramers ions contain an even number of electrons and in a crystalline field of rhombic symmetry the degeneracy of the ground state is completely raised.

‡ The fact that no resonance is observed in crystals grown with vanadium and copper in the melt may be due to insufficient intensity.

group ions are less than that of Ca^{2+} and, with the exception of Mn^{2+}, form a solid solution only in small concentration.

A fluorine hyperfine structure is observed in the spectra of iron group ions due to weak covalent bonding of the 3d electrons with the nearest neighbour fluorine ions (cf. Griffiths, Owen and Ward 1953, Tinkham 1956, Hayes 1958). The rare earth ions do not exhibit a resolved fluorine structure of this type because of insufficient bonding of the 4f electrons; in some cases, however, a fluorine satellite structure is observed due to simultaneous transitions of the electron spin and the spin of a neighbouring fluorine nucleus (Baker, Hayes and O'Brien, to be published).

The table contains the molar concentration of impurities added to CaF_2 and the concentrations estimated to be present in the crystal from the intensity of the paramagnetic resonance spectrum. The spectra of Mn^{2+}, Eu^{2+} and Gd^{3+} have already been described (Baker, Bleaney and Hayes 1958, referred to as I). The properties of the resonance spectra of other impurities are outlined below.

Chromium (Cr^{3+}, $3d^3\ {}^4F_{3/2}$; Cr^{2+}, $3d^4\ {}^5D_0$).

A highly anisotropic spectrum was observed at 90°K having rhombic symmetry with two face diagonals z, x and the perpendicular cube edge y as principal axes; there are six possible combinations of this type and six similar centres are observed in the magnetic unit cell. Only one transition is observed for each ion at any field and in zero magnetic field it occurs at $\nu = 0{\cdot}285 \pm 0{\cdot}002\ \mathrm{cm}^{-1}$. We are probably observing the spectrum of Cr^{2+} for which a rhombic distortion will leave singlets as the low lying states.

A fluorine hyperfine structure is observed which has a simple form when the external field is along the z or y axis; in these orientations three lines (width 2G at 20°K) are found (intensity ratio 1 : 2 : 1, overall width 40 gauss in each case) characteristic of interaction with two equivalent fluorines. In other orientations the structure is more complex and indicates an interaction with at least four fluorine ions. A displacement of the small chromium ion along a face diagonal towards the edge of the cube might give (*a*) an overlap of the electron wave function primarily with two fluorine ions and (*b*) rhombic symmetry with the observed principal axes.

Cobalt (Co^{2+}, $3d^7\ {}^4F_{9/2}$).

A spectrum with a resolved fluorine structure was observed at 20°K in crystals grown from a melt containing cobalt. The spectrum has an eight line hyperfine structure suggesting that the paramagnetic ion is probably Co^{2+}, but the symmetry is less than cubic and it has not been found possible to fit the spectrum to a theory of Co^{2+}. V^{2+} would also give an eight line hyperfine structure but we were unable to detect any resonance in a crystal grown from a melt containing vanadium (see table).

Cerium (Ce^{3+}, $4f^1\ {}^2F_{5/2}$).

A spectrum of Ce^{3+} is observed at 20°K. There are three similar ions in the unit cell with axial symmetry about a cube edge and the g-values are

$$g_{\parallel} = 3{\cdot}038 \pm 0{\cdot}003, \quad g_{\perp} = 1{\cdot}396 \pm 0{\cdot}002.$$

These g-values are consistent with a ground state whose admixtures of J_z are of the form $\cos\theta\,|\pm 5/2\rangle - \sin\theta\,|\mp 3/2\rangle$ where $\cos\theta \simeq 0{\cdot}91$.

Erbium (Er^{3+}, $4f^{11}\ {}^4I_{15/2}$).

Three types of spectrum are observed at 20°K: (*a*) An isotropic line with $g = 6{\cdot}78 \pm 0{\cdot}01$. Intensity measurements show that 5% of the erbium ions are responsible for this line and therefore have cubic symmetry. Judd (private communication) has calculated that the ground state in a cubic field is

$$\sqrt{\frac{77}{192}}\left|J_z = \pm\frac{13}{2}\right\rangle - \sqrt{\frac{65}{192}}\left|J_z = \pm\frac{5}{2}\right\rangle - \sqrt{\frac{39}{192}}\left|J_z = \mp\frac{3}{2}\right\rangle + \sqrt{\frac{11}{192}}\left|J_z = \mp\frac{11}{2}\right\rangle$$

for which $g = 6{\cdot}80$. Correction for the breakdown of Russell–Saunders coupling makes $g = 6{\cdot}77$ which is in excellent agreement with the measured value. (*b*) Two sets of three lines from three equivalentions with axial symmetry about a cube edge. Each ion has in one set a line with $g_\parallel = 7{\cdot}76 \pm 0{\cdot}02$, $g_\perp = 6{\cdot}253 \pm 0{\cdot}006$ and in the other set a line with $g_\parallel = 6{\cdot}76 \pm 0{\cdot}02$, $g_\perp = 9{\cdot}11 \pm 0{\cdot}01$; the former line arises from the ground doublet and the latter from an excited doublet of the same ion. Relative intensity measurements at 20°K and 14°K indicate that the excited doublet is about $35k$ above the ground doublet.

The hyperfine structure of ^{167}Er could be measured only for the ground doublet of (*b*); as expected, the hyperfine structure lines have almost the same separation parallel and perpendicular to the symmetry axis (72G and 77G respectively).

ACKNOWLEDGMENTS

We are indebted to the Board of Admiralty for financial support of this work. We would like to thank Professor B. Bleaney and Dr. M. C. M. O'Brien for many helpful discussions.

REFERENCES

BAKER, J. M., BLEANEY, B., and HAYES, W., 1958, *Proc. Roy. Soc.* A, **247**, 141.
BLEANEY, B., LLEWELLYN, P. M., and JONES, D. A., 1956, *Proc. Phys. Soc.* B, **69**, 858.
D'EYE, R. W. M., and MARTIN, F. S., 1957, *J. Chem. Soc.*, **349**, 1847.
GRIFFITHS, J. H. E., OWEN, J., and WARD, I. M., 1953, *Proc. Roy. Soc.* A, **219**, 526.
HAYES, W., 1958, *Disc. Faraday Soc.*, **26**, 58.
LOW, W., 1958, *Phys. Rev.*, **109**, 265.
PRZIBRAM, K., 1956, *Irradiation Colours and Luminescence* (London: Pergamon Press), Ch. 14.
STOCKBARGER, D. C., 1949, *J. Opt. Soc. Amer.*, **39**, 731.
TINKHAM, M., 1956, *Proc. Roy. Soc.* A, **236**, 535, 549.
ZINTL, E., and UDGARD, A., 1939, *Z. anorg. Chem.*, **240**, 50.

Nuclear Magnetic Resonance in Bismuth

BY C. P. FLYNN AND E. F. W. SEYMOUR
Department of Physics, University of Leeds

MS. received 30*th January* 1959, *in final form* 18*th February* 1959

WHILE the rhombohedral structure of solid bismuth causes it to exhibit abnormal electronic properties, including an extremely small electronic specific heat, a large diamagnetic susceptibility, and a large electrical resistivity, liquid bismuth is normal in that its magnetic susceptibility and electrical resistivity are not very different from those of neighbouring elements in the periodic table. Similarly, it would be expected that the conduction electron shift of the nuclear resonance frequency, which depends on the paramagnetic susceptibility of the conduction electrons, would be 'normal' in the liquid but very small in the solid. Using the theoretical expressions given by Knight (1956), and making use of the measured values of the magnetic susceptibility of the liquid and of the electronic specific heat of the solid (Keesom and Pearlman 1955, Ramanathan and Srinivasan 1955), the shifts may be expected to be approximately 1% and 0·1% for the liquid and solid respectively. The value predicted for the liquid is comparable with the observed values (Knight 1956) for solid mercury (2·5%), thallium (1·24%) and lead (1·4%). It should be mentioned that the theoretical values refer to the shift of the resonance in the metal with respect to that of nuclei surrounded only by closed cores of electrons, whereas the quantity measured experimentally is the shift with respect to the resonance in a chosen chemical compound. This introduces an uncertainty in the measured values, which is probably of the order of 0·1% in the cases quoted above.

A search was made in two samples of bismuth for the nuclear magnetic resonance of ^{209}Bi (natural abundance 100%) using a radiofrequency spectrometer (Pound 1952). The first sample consisted of a powder of precipitated bismuth of commercial purity, the main impurity being the oxide, with particle size about 1 μ, and the second of spectrographically standardized bismuth with rather larger particles. The particles were insulated from one another by a viscous silicone oil. The results obtained were substantially the same for the two samples.

No resonance was observed in the solid at any temperature up to the melting point (271°c), probably due to a broadening of the line by interaction of the large ^{209}Bi electric quadrupole moment with the inhomogeneous electric field of the lattice. It is estimated that the line width must be at least 50 oersteds to escape detection. However, on melting the samples a strong signal of width $4{\cdot}2 \pm 0{\cdot}3$ oersteds was observed. The shape was Lorentzian as would be expected if the line width were governed by a spin–lattice relaxation process. The ratio $\nu_{\mathrm{Bi}}/\nu_{\mathrm{H}}$ of the resonance frequency to that of the protons in a glycerine sample in the same magnetic field is given in the table. This ratio was the same for fields of 4100 oersteds and 5750 oersteds. The resonance was observed in the liquid up to a temperature of 320°c, the highest temperature reached, and remained observable on cooling to a temperature 80°c below the normal freezing point, with little change in line width or intensity, and no detectable change in the frequency ratio. At this temperature the signal decreased rapidly in intensity until it became unobservable. The samples were evidently in a supercooled

Sample	$\nu_{\mathrm{Bi}}/\nu_{\mathrm{H}}$	Observer
Bismuth metal[a]	$0{\cdot}162975 \pm 0{\cdot}000012$	Present measurements
Bismuth metal[b]	$0{\cdot}162944 \pm 0{\cdot}000014$	Present measurements
$Bi(NO_3)_3 . 5H_2O$ (0·73N)	$0{\cdot}160693 \pm 0{\cdot}000008$	Present measurements
$Bi(NO_3)_3 . 5H_2O$ (1·45N)	$0{\cdot}160722 \pm 0{\cdot}000014$	Present measurements
$Bi(NO_3)_3 . 5H_2O$[c]	$0{\cdot}16069 \pm 0{\cdot}000016$	Proctor and Yu (1950)
$Bi(NO_3)_3 . 5H_2O$ (0·69N)	$0{\cdot}160696 \pm 0{\cdot}000010$	Ting and Williams (1953)

[a] Precipitated bismuth of commercial purity.
[b] Spectrographically standardized bismuth.
[c] Concentration not stated.

liquid state. This extensive supercooling which has been obtained in many metals when in a finely divided state has been discussed by Turnbull (1950).

A search was also made for the ^{209}Bi resonance in some compounds. No resonance was observed in solid or molten bismuth iodide at temperatures up to 500°c, or in bismuth chloride in acid solution. The apparatus could have detected lines up to 40 oersteds wide in these cases. The resonance in bismuth nitrate dissolved in 25% nitric acid had a line width of $5{\cdot}2 \pm 0{\cdot}5$ oersteds for concentrations from 0·5 N to about 1·0 N, increasing to 14 ± 2 oersteds at 2·1 N concentration. The resonance frequency appeared to increase slightly with concentration. Values are given in the table together with previously observed values. The intensities of the resonances were markedly reduced if the samples were allowed to stand for a few days after the solutions had been made up.

The difference between the frequency ratios in the liquid metal and in the 0·73 N nitrate solution amounts to $1{\cdot}41 \pm 0{\cdot}01_5\%$. This is presumably mainly a conduction electron shift, though it includes a chemical shift the magnitude of which is unknown, but which probably does not exceed about 0·1%, since in salts of neighbouring metals in the periodic table the observed chemical shifts extend over approximately this range. Thus, as expected, the conduction electron shift in the liquid is comparable with the shifts in neighbouring metals in the periodic table.

It has been suggested by Takagi (1956) on the basis of an electron diffraction study of thin bismuth films that the local structure of the liquid changes gradually on supercooling, from a structure where each atom has eight near neighbours (see also Chamberlain 1950 and Hendus 1947), to a rhombohedral or simple cubic structure where each atom has six near neighbours, the change being sensibly complete at 110°c. The appearance of a rhombohedral structure similar to that of the solid would be expected to be accompanied by a marked decrease in the conduction electron shift. Nevertheless, no change was observed in the temperature range of the present measurements, indicating that any structure in the liquid at low temperatures is much more likely to be simple cubic than orthorhombic.

ACKNOWLEDGMENTS

We wish to thank the Royal Society for a grant which assisted this work. One of us (C. P. F.) wishes to thank the Department of Scientific and Industrial Research for a maintenance allowance.

REFERENCES

CHAMBERLAIN, O., 1950, *Phys. Rev.*, **77**, 305.
HENDUS, H., 1947, *Z. Naturf.*, **2 a**, 505.
KEESOM, P. H., and PEARLMAN, N., 1955, *Phys. Rev.*, **96**, 897.
KNIGHT, W. D., 1956, *Solid State Physics*, **2**, 93.
POUND, R. V., 1952, *Progr. Nucl. Phys.*, **2**, 21.
PROCTOR, W. G., and YU, F. C., 1950, *Phys. Rev.*, **78**, 471.
RAMANATHAN, K. G., and SRINIVASAN, T. M., 1955, *Phys. Rev.*, **99**, 442.
TAKAGI, M., 1956, *J. Phys. Soc. Japan*, **11**, 396.
TING, Y., and WILLIAMS, D., 1953, *Phys. Rev.*, **89**, 595.
TURNBULL, D., 1950, *J. Appl. Phys.*, **21**, 1022.

Some Weak Lines in the Paramagnetic Resonance Spectrum of Impure MgO Crystals

By J. H. E. GRIFFITHS and J. W. ORTON
The Clarendon Laboratory, Oxford

MS. received 19th December 1958

RECENTLY several papers have been published on the paramagnetic resonance spectra of 3d transition group ions in single crystals of MgO (Low 1956a, b, 1957a, b, 1958a, b, Wertz and Auzins 1957). (For reference to similar work in other crystals see the table of resonance data by J. W. Orton 1959.) In addition to the fairly intense lines analysed in these papers there is a number of much weaker ones, many of which appear at small values of magnetic field H, and in this note we wish to suggest explanations for two groups of these. The first set of lines may be attributed to 'forbidden' transitions in the spectrum of Fe^{3+} and the second set to Cr^{3+} ions associated with nearest neighbour positive ion vacancies.

1. Fe^{3+}.

Most of the measurements were made at a microwavelength of 3 cm and temperatures of 90°K and 290°K.

MgO has the NaCl structure and the Fe^{3+} ions are found to occur almost entirely in a pure cubic field, since the resonance results can be represented by the spin Hamiltonian:

$$\mathscr{H} = g\beta\mathbf{H}.\mathbf{S} + \tfrac{1}{6}a\{S_x^4 + S_y^4 + S_z^4 - \tfrac{1}{5}S(S+1)(3S^2+3S-1)\}$$

with $S=\frac{5}{2}$, $g=2{\cdot}0037$ and $a=+0{\cdot}0205$ cm^{-1} (290°K) (Low 1956b). At 90°K where the accurate measurements were made $a=0{\cdot}0212$ cm^{-1}. In zero magnetic field the groundstate levels lie at $+a$ (fourfold degenerate) and $-2a$ (twofold degenerate). The cubic field term in the Hamiltonian mixes states with values of M_S differing by 4, i.e. $(\frac{5}{2}, -\frac{3}{2})$ and $(\frac{3}{2}, -\frac{5}{2})$ which causes the transitions $\pm\frac{5}{2}\rightarrow\mp\frac{1}{2}$, $\pm\frac{5}{2}\rightarrow\mp\frac{3}{2}$, $\frac{5}{2}\rightarrow-\frac{5}{2}$ and $\frac{3}{2}\rightarrow-\frac{3}{2}$ to have probabilities different from zero. The positions of the energy levels may be calculated exactly with H along 100 and 111 directions (Kronig and Bouwkamp 1939) but with H in any other direction it is not possible to solve the secular determinant in closed form. Perturbation theory is unreliable in the low field region where these lines occur, so an accurate comparison between theory and experiment is only possible along 100 and 111 axes.

The lines observed correspond to the transitions $\pm\frac{5}{2}\rightarrow\mp\frac{1}{2}$ and $\pm\frac{5}{2}\rightarrow\mp\frac{3}{2}$ which, along a 100 axis, with $1/\lambda=0{\cdot}326$ cm^{-1} and at 90°K should occur in fields of 1197, 1124, and 749, 977 gauss respectively. The observed values for the first two lines were 1195 and 1120 gauss, but with our apparatus it was only possible to make an approximate measurement on the pair in lower field. A check on their positions was made at 1·2 cm wavelength where the theoretical positions were 2005 and 2231 gauss, while the experimental values were found to be 2010 and 2230. Similar agreement was found for measurements with H along 111.

Further evidence that these lines have been correctly interpreted is provided by their anisotropy. The cubic field term in the Hamiltonian has turning values 45° apart, unlike the more usual separation of 90° for terms representing axial symmetry, and both pairs of lines show this behaviour. That they are due to Fe^{3+} is also confirmed by their behaviour on X-irradiation and subsequent annealing. X-irradiation of crystals containing iron removes electrons from Fe^{2+}, thus increasing the intensity of the Fe^{3+} spectrum (Wertz *et al.* 1958) and the low field lines follow the changes in intensity of the allowed transitions quite closely.

Calculation of transition probabilities (for a 100 axis) shows that the $\pm\frac{5}{2}\rightarrow\mp\frac{1}{2}$ pair should have an intensity of 1/400 of that of the (allowed) $+\frac{3}{2}\rightarrow+\frac{1}{2}$ line. The experimental ratio was about 1/300 which is in satisfactory agreement considering the difficulty of such a measurement. Further calculations on the $\frac{5}{2}\rightarrow-\frac{5}{2}$ and $\frac{3}{2}\rightarrow-\frac{3}{2}$ transitions indicate that these lines would have intensities less again by factors of 5 and 25 times respectively, which probably accounts for the fact that they have not so far been observed.

2. Cr^{3+}.

In a paper concerned with the Cr^{3+} ion in MgO Wertz and Auzins (1957) reported three distinct spectra, (i) arising from ions in a purely cubic field, (ii) from ions in an axially symmetric field with 100 axes and (iii) consisting of lines with turning values along 110 type axes, but they did not analyse the third one in detail. We have observed these spectra independently and would like to suggest an interpretation of the last mentioned.

Measurements were made at K band (1·2 cm) and X band (3 cm) and temperatures of 20°K and 90°K. At X band there is a pair of lines, with separation of about 80 gauss, having minima (along a 110 direction) at fields of 1200–1300 gauss. On rotation of the magnetic field in a 100 plane this pair moves to very high field. Along a 100 axis there are two fourfold coincidences at $H\sim1700$ and 1800 gauss, and two other lines at fields of 3000 and 4000 gauss. This system may be attributed to a Cr^{3+} ion in a rhombic field, there being six ions per unit cell (differing only in the orientation of the axes), and fitted by the spin Hamiltonian:

$$\mathscr{H}=g\beta\mathbf{H}.\mathbf{S}+D[S_z^2-\tfrac{1}{3}S(S+1)]+E[S_x^2-S_y^2]$$

with $S=\frac{3}{2}$, $g=1{\cdot}98$, $|D|=0{\cdot}031\pm0{\cdot}002\ \mathrm{cm}^{-1}$, $|E|=0{\cdot}22\pm0{\cdot}01\ \mathrm{cm}^{-1}$, a typical set of axes being: x axis 110, y axis $1\bar{1}0$ and z axis 001.

Energy level diagrams for the x and z axes, calculated from the given Hamiltonian, are shown in figures 1 and 2 respectively, and the observed transitions indicated (by solid arrows). Along the x axis there is only one transition observable at X band (X_1) as the other possible one (X_2) would require a field considerably larger than was available. Both lines were observed along the z axis as indicated. The formulae describing the energy levels along the y axis are essentially similar to those for the x axis except that a term $3E-D$ is replaced by $3E+D$, and, as $D\ll3E$, the spectra for these two axes are nearly identical. This accounts for the occurrence of pairs of lines along a 110 axis, as each 110 type axis is an x axis for one ion and a y axis for another.

At K band the transitions observed were K_1, K_2 (corresponding to X_1, X_2) and K_3. Three other transitions are possible but none of these could be detected with certainty owing to the weakness of this spectrum and the presence of much more intense lines from other iron-group impurities.

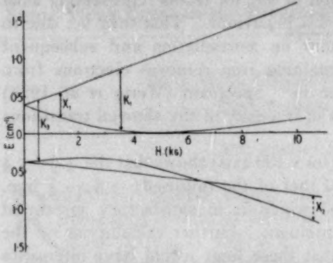

Figure 1. Energy levels for the Cr^{3+} ion in rhombic field with *H* along the *x* axis.

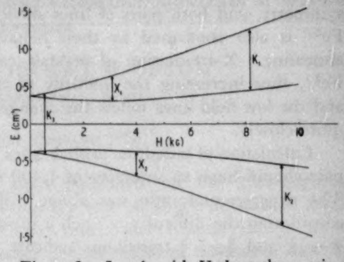

Figure 2. Levels with *H* along the *z* axis.

In all crystals showing the spectrum described above it was found that the number of Cr^{3+} ions concerned was roughly one-half to one-quarter of the number in a purely cubic field. It seems reasonable to assume that the observed rhombic field is produced by a lattice defect near the Cr^{3+} ion, and, if the defects were randomly distributed, this ratio would require a concentration of about one defect to thirty Mg^{2+} ions (an impossibly large figure). There must, therefore, be a strong tendency for association between Cr^{3+} ions and defects which can be explained by assuming the defect to represent an (effective) negative charge, e.g. a positive ion vacancy or monovalent positive ion. The latter possibility was shown to be unlikely by Wertz and Auzins (1957) who had their samples spectroscopically analysed but were unable to detect any suitable monovalent ion.

The most probable model, then, to explain the observed spectrum is that of a positive ion vacancy in the nearest positive ion position, as it provides both charge compensation and the correct crystal field symmetry. The vacancy is closer to the Cr^{3+} ion than in the 100 axial case (ii) which explains the larger splitting found here.

ACKNOWLEDGMENTS

This work was supported by grants from the Admiralty and the Atomic Energy Authority. We should like to thank Dr. J. Owen and Professor J. E. Wertz for much helpful discussion.

REFERENCES

KRONIG, R. DE L., and BOUWKAMP, C. J., 1939, *Physica*, **6**, 290.
LOW, W., 1956 a, *Phys. Rev.*, **101**, 1827.
—— 1956 b, *Proc. Phys. Soc.* B, **69**, 1169.
—— 1957 a, *Phys. Rev.*, **105**, 793.
—— 1957 b, *Ibid.*, **105**, 801.
—— 1958 a, *Ibid.*, **109**, 247.
—— 1958 b, *Ibid.*, **109**, 256.
ORTON, J. W., 1959, *Rep. Progr. Phys.*, **22**, 204 (London: Physical Society).
WERTZ, J. E., and AUZINS, P., 1957, *Phys. Rev.*, **106**, 484.
WERTZ, J. E., AUZINS, P., GRIFFITHS, J. H. E., and ORTON, J. W., 1958, *Discussions of the Faraday Society*, **26**, 66.

Search for the Process $\mu^+ \rightarrow e^+ + \gamma$

BY T. W. O'KEEFFE, M. RIGBY, AND J. R. WORMALD
Nuclear Physics Research Laboratory, University of Liverpool

MS. received 5th February 1959

§ 1. INTRODUCTION

An experimental upper limit for the branching ratio ρ of the process $\mu^+ \rightarrow e^+ + \gamma$, relative to the normal decay mode $\mu^+ \rightarrow e^+ + \nu + \tilde{\nu}$, was determined by Lokanathan and Steinberger (1955), who found $\rho < 2 \times 10^{-5}$. A calculation of this branching ratio, on the basis of the theory of weak interactions taking place through a heavy intermediate meson, has been made by Feinberg (1958) who estimated $\rho \sim 10^{-4}$. The experiment reported here was designed either to establish the existence of the process $\mu^+ \rightarrow e^+ + \gamma$ or to reduce the experimental upper limit of the branching ratio ρ.

§ 2. APPARATUS

The method was to examine the spectrum of positrons, emitted by positive muons decaying at rest, in coincidence with a γ-ray photon at 180°. Since the process for which we were searching is a two-body decay, both the positron and the photon would have an energy 53 MEV, approximately equal to half the rest energy of the muon. The only other processes likely to give coincidences are the radiative decay $\mu^+ \rightarrow e^+ + \nu + \tilde{\nu} + \gamma$ and bremsstrahlung produced either in the target or in adjacent parts of the apparatus by positrons from the usual decay $\mu^+ \rightarrow e^+ + \nu + \tilde{\nu}$. Both these processes could give e^+–γ coincidences, but with both particles having a continuous spectrum with energies less than 53 MEV.

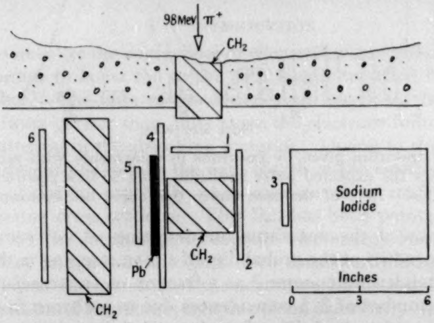

Figure 1. Experimental arrangement.

The arrangement of counters is shown in figure 1. Counters 1 to 6 are of plastic scintillator; the performance of the sodium iodide crystal 6 in. long and 5 in. diameter as an electron spectrometer has already been described (Cassels, O'Keeffe, Rigby and Wormald 1958). A beam of 98 MEV positive pions was slowed down in 10 in. of polyethylene absorber, passed through the monitor counter 1, and stopped in the polyethylene target. Counters 2 and 3 formed a positron telescope arranged so that coincidence events were only obtained if particles entered the sodium iodide crystal within 1 in. of its axis. The photons were detected, after passing through the anti-coincidence counter 4, by pair production in the $\frac{1}{4}$ in. lead converter, the electron pairs giving a coincidence between counters 5 and 6. 1 in. of polyethylene was placed between counters 5 and 6 to reduce the sensitivity of the arrangement to low energy photons.

The experimental procedure was to use 2, 3, 5, 6, $\bar{4}$ quadruple coincidence–anti-coincidence events to open an electronic gate allowing linear pulses from the sodium iodide counter to pass through to a pulse height analyser. The calibration of the linear system was checked periodically by gating with 2, 3 coincidence events, thus giving a spectrum of positrons from normal muon decay.

§ 3. EXPERIMENTAL RESULTS

During the experiment $4{\cdot}7 \times 10^8$ incident pions were recorded and 42 quadruple coincidence events, with a pulse height distribution shown as a histogram in figure 2. The curve shows the expected spectrum of pulses from an arbitrary number of mono-energetic 53 MeV positrons. 78% of the area under this curve lies between the dotted lines. Only three of the observed pulses lie in this range; but since they may well be a part of the continuous background, they can only be used to give an upper limit to the branching ratio ρ.

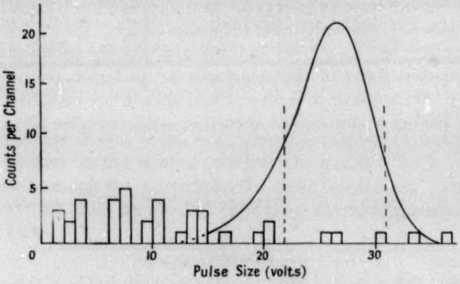

Figure 2. Pulse spectrum given by positrons in coincidence with γ-ray photons. The curve shows the expected pulse spectrum from 53 MeV positrons, on an arbitrary vertical scale. 78% of the area under this curve lies between the dotted lines.

The efficiency of the apparatus for detecting $\mu^+ \rightarrow e^+ + \gamma$ decays is $f_1 f_2 f_3$ where f_1 is the product of the probability of a pion stopping in the target and the solid angle subtended by counter 3 as a fraction of 4π steradians; f_1 was given directly by the number of 2, 3 coincidences due to positrons from normal muon decay and was found to be 1·7%; f_2 is the probability of a photon, at 180° to a positron which enters counter 3, going into the solid angle defined by counter 6; f_2 was estimated to be approximately 70%; f_3 is the efficiency of the γ-ray telescope for detecting 53 MeV photons, estimated to be approximately 30%.

If one assumes that all three of the 'possible' events are due to the $\mu^+ \rightarrow e^+ + \gamma$ decay one obtains a value for the branching ratio $\rho = (2{\cdot}3 \pm 1{\cdot}3) \times 10^{-6}$.

§ 4. Conclusion

The experiment gave no evidence for the existence of the decay mode $\mu^+ \to e^+ + \gamma$; an upper limit to the branching ratio, at the 99% confidence level, is $7{\cdot}5 \times 10^{-6}$. There is, therefore, a considerable discrepancy between the experimental upper limit and Feinberg's estimate of the possible branching ratio which is of the order of 10^{-4}.

Note added in proof. A further experiment with a slightly modified arrangement of the apparatus has yielded similar results, bringing the experimental upper limit to the branching ratio, at the 99% confidence level, to 5.8×10^{-6}.

Acknowledgments

We wish to thank Professor J. M. Cassels for his interest in this work, and Mr. Halliday and the cyclotron crew for providing the pion beam. One of us (T. W. O'K.) is indebted to the Department of Scientific and Industrial Research for a maintenance grant.

References

Cassels, J. M., O'Keeffe, T. W., Rigby, M., and Wormald, J. R., 1958, *Proc. Phys. Soc.*, **72**, 781.

Feinberg, G., 1958, *Phys. Rev.*, **110**, 1482.

Lokanathan, S., and Steinberger, J., 1955, *Phys. Rev.*, **98**, 240.

The Scattering of Fast Charged Particles IV : On the Measurement of the Detour Factor for 10 MeV Electrons and Positrons

By K. PHILLIPS
Research Department, Metropolitan-Vickers Electrical Company, Manchester

MS. received 12*th February* 1959

§ 1. Introduction

In order to measure the energy loss of electrons when passing through matter it is important to know the actual path length travelled by the particles in the absorber. The ratio of the actual path length to the geometrical foil thickness is always greater than unity since the electrons follow a tortuous path due to the scattering in the absorbing material. Owing to this zigzag path it is not always sufficient just to take the path length of the electron as equivalent to the thickness of the foil especially when measurements are being made on the absolute scattering cross sections. This fact has been pointed out by Slawsky and Crane (1939) in an attempt to explain why energy loss measurements of electrons in lead and aluminium foils were consistently larger than predicted by theory. These authors studied the scattering of electrons with energies up to 13·5 MeV in lead and aluminium foils in a cloud chamber. In the measurement on the lead foils the most probable scattering angle was so large that they concluded that the electrons had completely lost their original direction of motion and passage of the electrons through the foils resembled the case of diffusion and could not be compared with theory. For the aluminium foils, however, the values of the path length–foil thickness ratio, t/t_0, calculated from $\theta_{\max}$ were 1·01, 1·04 and 1·10 for foil thicknesses of 0·0025, 0·01 and 0·025 cm respectively. Williams (1940) pointed out that certain errors were introduced by the scattering of electrons in the gas of the cloud chamber and if the square of the ratio of the measured mean scattering angle in the foil to the mean scattering in the gas $(\alpha_f/\alpha_g)^2$ is not large, then the estimation of the ratio t/t_0 is likely to be in error. For the case of the thinnest foil (0·0025 cm thick), used by Slawsky and Crane, α_g is comparable with α_f and little weight can be placed on the figure of 1·01 for t/t_0. The results for the two thicker foils are likely to be somewhat more reliable since the values of $(\alpha_f/\alpha_g)^2$ are about 4 and 10 times greater than for the thinnest foil. The measurement of the ratio $(\alpha_f/\alpha_g)^2$ in the cloud chamber together with the diffusion of the electrons in the foils rather limit the applicability of this technique in the estimation of the detour factor (t/t_0) to low Z materials only. Also an attempt has to be made to reduce the value of α_g by the use of low Z gas fillings at low pressure. This present report describes a method of measuring the detour factor in G5 nuclear emulsions for 10 MeV electrons and positrons and compares the results with theory. Nuclear emulsions in preference to foils are particularly suitable for measurements of this type since they make it possible to follow the track along its complete length.

§ 2. THEORY

The theoretical calculation of the detour factor is by no means a simple matter particularly in moderately thick foils. One obvious difficulty is that the cross section for the scattering of an electron through a given angle is dependent on the energy but owing to the losses caused by radiation and ionization along the path length of the electron its energy is always changing. The two limiting cases which are more amenable to mathematical analysis are when (*a*) the total deviation of the emergent direction is small enough to satisfy the multiple scattering limitation that $\sin\theta \simeq \theta$ and (*b*) when the foil thickness is so large that the problem can be treated as a diffusion problem, see Bethe, Rose and Smith (1938) and Rossi and Greisen (1941).

Consideration of the theoretical problem has been made by Rose (1940) who estimated the detour factor to be

$$t/t_0 = 1 + \sum_1^n a_l(n)\left(\frac{1-\exp(-\nu Q_l)}{\nu Q_l} - 1\right) \qquad \ldots\ldots(1)$$

where n is the number of terms in the series and

$$\nu Q_l = 2\pi K^2 N t_0 l(l+1)\ln(\xi y_1)$$

as deduced from the theory of Williams. The upper limit for y_1 is defined by

$$2 \simeq \pi K^2 n t_0 / {y_1}^2$$

with

$$K^2 = (Ze^2/m_0c^2)(1-\beta^2)^{1/2}/\beta^2$$

where Z, e, $m_0\,c$ and β have their usual meanings and N is the number of atoms per unit volume. For the case of an atomic field of the form

$$V(r) = (Ze^2/r)e^{r/a}$$

where r is the distance from the atom and a is a constant, $\xi = 1{\cdot}21a/\lambda\!\!\!^-$ where $2\pi\lambda\!\!\!^-$ is the wavelength of the incident electron.

The coefficients $a_l(n)$ can be obtained by comparing the series

$$\sec\theta \simeq \sum_0^n a_l(n)\mathrm{P}_n(\cos\theta)$$

and have been tabulated by Rose for n and l from 0 to 5 respectively.

For thin foils equation (1) reduces to $t/t_0 = 1 + \frac{1}{2}\nu Q_l$, instead of the approximate value, $1 + \nu Q_l$, given by Goudsmit and Saunderson (1940).

Yang (1951) calculated the actual path length due to a gaussian multiple scattering distribution of electrons in foils for two separate cases. Firstly, when all the particles are detected regardless of their position and angle of emergence and secondly, only for particles which are travelling in the same direction as they were initially. Case I analysis is obviously applicable in the present experiment and gives the probability that the electron has a path length between $t_0 + \Delta$ and $t_0 + \Delta + d\Delta$ for a foil thickness t_0 in radiation units, as

$$B(v) = 2\pi^{-1/2} v^{-3/2} (u - 3u^9 + 5u^{25} - 7u^{49} + \ldots .) \qquad \ldots\ldots (2)$$

where

$$v = 2w^2 \Delta / t_0 \qquad u = \exp\,(-1/v)$$

for small values of u the higher power terms can be neglected.

The shape of the distribution $B(v)$ is leptokurtic with an average path length increase of

$$(\Delta)_{\mathrm{av}} = t_0{}^2 / w^2 \qquad \ldots\ldots (3)$$

where

$$w^2 = 2p\beta / E_s$$

E_s is the characteristic energy $= m_0 c^2 (4\pi 137)^{1/2} = 21{\cdot}2$ MeV. The radiation length is defined by the equation

$$\frac{1}{x_0} = \frac{4}{137} N r_0{}^2 \left(\frac{Z^2}{A}\right) \ln\,(183\ Z^{-1/3}).$$

This equation only defines individual processes and owing to the fact that the emulsion is heterogeneous it is not permissible to consider the mean values of Z and A in the expression. The correct method is to calculate the mean value of the term $(Z^2/A)\ln\,(183Z^{-1/3})$ and substitute in the equation for $1/x_0$. This method gives a value of 7·085 cm for the radiation length of the emulsion compared with a value less than half this when the mean values of Z and A are used.

§ 3. METHOD OF MEASUREMENT AND RESULTS

The 10 MeV electrons used in this experiment were accelerated by a betatron whilst the positrons were produced by the high energy X-rays impinging on a lead target. The particles were selected by means of a magnetic spectrometer. In order to reduce any distortion effects in the emulsions the particles were projected into the centre of the 400 micron thick G5 plates. Also a low temperature method of development was used. Measurements on the emulsion using the method of Major (1952) showed that the distortion of the tracks in this region was negligible.

The ideal method of measuring the length of the tortuous path of an electron passing through a nuclear emulsion would be to measure the coordinates of every silver grain along the track. This would be very tedious and would be almost a physical impossibility. A simpler and more practical alternative is to count the number of times a known cell length can be laid off along the track for a 1 mm length of emulsion. For a cell length of 40 microns the number is 25 or more. The additional amount is the increase in track length due to the particle's tortuous path. The depth of the track was also measured after it had travelled 1 mm. By using a shrinkage factor of 2·3 and this depth measurement a correction for the inclination of the track was made. Another correction had to be made to take into account the incident angle of the track to the x axis of the plate. This angle was only of the order of 1 or 2 degrees for most tracks and the resulting correction was small.

Measurements along these lines were made on about 70 electron and 80 positron tracks and the respective distributions of the detour factor are shown in figures 1 and 2. The distributions are leptokurtic in shape with a maximum value of t/t_0 between 1·01 and 1·02 for both the electrons and positrons. A statistical analysis of the histograms gives a coefficient of skewness

$$\frac{\text{mean} - \text{median}}{\text{standard deviation}}$$

of approximately $+1{\cdot}8$ indicating a strong positive skewness. There is general agreement with the theoretical curves of Yang, equation (2), normalized at the maximum value, except the number of tracks at the larger value of t/t_0 tend to be larger and also the distribution seems to be shifted to the higher values.

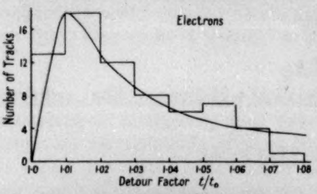

Figure 1. The experimental histogram of the detour factor for electrons compared with the theoretical curve of Yang.

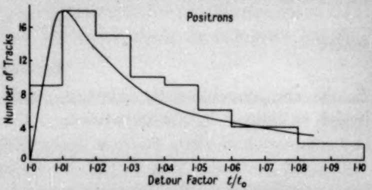

Figure 2. The experimental histogram of the detour factor for positrons compared with the theoretical curve of Yang.

The mean value of the detour factor for the electron and positron experimental distributions was $1{\cdot}02_8$ and $1{\cdot}02_2$ respectively. Both the values are slightly higher than the figure of 1·014 obtained from Yang's formula equation (3). The slight discrepancy seems quite reasonable since Yang only used the simple gaussian for the multiple scattering distribution. Large angle scatters would tend to increase the number having large values of t/t_0. In the present work it is reasonable to expect a 10° scatter on about every tenth track and a 5° scatter on every third track. A 5° scatter at the beginning of a track would increase the detour factor by 1·005 and a 10° scatter by about 1·02. The average value of t/t_0 given by Rose is 1·02, giving a closer agreement with these experimental values. This is probably due to the fact that Rose used the scattering distribution of Williams which will take into account some of the large angle single scatters.

ACKNOWLEDGMENTS

The author wishes to acknowledge the help given to him by Mrs. I. Johnson and to thank Sir Willis Jackson, Director of Research and Education, Metropolitan-Vickers Electrical Co. Ltd., for permission to publish.

REFERENCES

BETHE, H. A., ROSE, M. E., and SMITH, L. P., 1938, *Proc. Amer. Phil. Soc.*, **78**, 573.
GOUDSMIT, S., and SAUNDERSON, J. L., 1940, *Phys. Rev.*, **57**, 24.
MAJOR, J. V., 1952, *Brit. J. Appl. Phys.*, **3**, 309.

Rose, M. E., 1940, *Phys. Rev.*, **58**, 90.
Rossi, B., and Greisen, K., 1941, *Rev. Mod. Phys.*, **13**, 240.
Slawsky, M. M., and Crane, H. R., 1939, *Phys. Rev.*, **56**, 1203.
Williams, E. J., 1940, *Phys. Rev.*, **58**, 292.
Yang, C. N., 1951, *Phys. Rev.*, **84**, 599.

A Measurement of the Spin Correlation Coefficient C_{KP} in p–p Scattering at 382 MeV, for 90° Centre-of-Mass Scattering Angle

By A. ASHMORE, A. N. DIDDENS and G. B. HUXTABLE
Nuclear Physics Research Laboratory, University of Liverpool

MS. received 6*th March* 1959

The coefficient C_{KP} is a measure of the correlation between spin components of the two protons in the scattering plane. It is the expectation value $\langle \boldsymbol{\sigma}_1 . \mathbf{K} \boldsymbol{\sigma}_2 . \mathbf{P} \rangle$ where $\boldsymbol{\sigma}_1$ and $\boldsymbol{\sigma}_2$ are the spins of the incident and target protons; following Wolfenstein (1956) $\mathbf{K}$ and $\mathbf{P}$ are unit vectors in the scattering plane along the directions $\mathbf{p}'-\mathbf{p}$ and $\mathbf{p}'+\mathbf{p}$, $\mathbf{p}$ and $\mathbf{p}'$ being the initial and final momenta of the scattered proton in the centre-of-mass system. A measurement of the coefficient C_{nn} for correlation between the spin components perpendicular to the scattering plane has been made for 382 MeV incident proton energy and 90° centre-of-mass scattering angle (Ashmore, Diddens, Huxtable and Skarsvåg 1958). This experiment did not eliminate any of the five sets of phase shifts for p–p scattering at 310 MeV (Stapp, Ypsilantis and Metropolis 1957). The measurement reported here was made since it seemed likely to distinguish between set 6, which gives a negative value for C_{KP} at 90°, and the other four sets which give positive values.

The correlation coefficient was measured, as previously, by means of a second scattering of both protons from carbon, with analysis in coincidence. For the measurement of C_{KP} the second scattering must be either upwards or downwards in a plane perpendicular to the first scattering. The asymmetry is then defined by the formula

$$e=\frac{UU+DD-DU-UD}{UU+DD+DU+UD} \qquad \ldots\ldots(1)$$

where UU is the number of coincidence counts with both second scattering upwards, DD with both downwards, etc. C_{KP} is related to e by the formula

$$C_{KP}=e/P_1P_2 \qquad \ldots\ldots(2)$$

where P_1 and P_2 are the analysing powers in the second scattering for the two protons.

The experimental arrangement and procedure were almost the same as for the measurement of C_{nn}. To obtain the highest possible counting rate consistent with reasonable energy resolution the first scintillators were made 1 in. square (subtending 3° at the target) and the hydrogen target was increased in diameter from 0·5 to 1·0 in. The size of the beam spot as given for the C_{nn} measurement is in error. It was, in fact, approximately 0·4 in. square for both measurements. The energy resolution in the present measurement was 9·0 MeV, and the angular resolutions in the first and second scattering 1·1° and 3·1°, respectively. All these figures are standard deviations.

The analysing powers of the second scatterings were measured in a double scattering experiment using a carbon first target. On the basis of data from Uppsala, Rochester and Harwell a first scattering angle of 17·2° was used and the polarization in this scattering, after correcting for angular resolution and inelastic scattering, was estimated to be 0·91 ± 0·03. The observed asymmetries for the two sides, corrected for the intensity distribution across the second target, were 0·591 ± 0·014 and 0·578 ± 0·013. After applying a correction for the different contributions from inelastic scattering in the calibration and in the measurement of C_{KP} it was found that

$$P_1 = 0{\cdot}618 \pm 0{\cdot}029, \quad P_2 = 0{\cdot}604 \pm 0{\cdot}028.$$

In the measurement of C_{KP} a beam intensity of about $1{\cdot}3 \times 10^9$ protons per second was used. At this level random coincidences were an acceptably small proportion of the genuine counts. In about 70 hours running a total of 1821 coincidence counts was obtained. After subtracting the estimated number of 46 ± 6 random coincidences in each position, the genuine coincidences were found to be divided between the four positions as shown in table 1. As expected for a centre-of-mass scattering angle of 90° $UU = DD$, and $DU = UD$ within the limits of experimental error.

Table 1. Number of Coincidence Counts for the Four Positions

U U	469 ± 24	*D U*	325 ± 21
D D	495 ± 24	*U D*	348 ± 21

From formula (1), the asymmetry is found to be +0·178 ± 0·027.

A contribution to the asymmetry arises from the geometry of the first scattering, which favours *DU* and *UD* coincidences. By integrating over the first and second scattering angles and over the target the correction was estimated to be +0·057 ± 0·012. Thus the corrected asymmetry is

$$e = +0{\cdot}235 \pm 0{\cdot}03.$$

Then from formula (2) using the values of P_1 and P_2,

$$C_{KP} = +0{\cdot}63 \pm 0{\cdot}10.$$

The phase shift set 6 of Stapp, Ypsilantis and Metropolis (1957), which gives a value of −0·313 ± 0·038, is thus clearly eliminated.

Recently a modified analysis of p–p scattering at 310 MeV has been made (Cziffra, MacGregor, Moravcsik and Stapp 1958), in which the one pion exchange contribution is explicitly included in the scattering amplitude for orbital angular momentum values above the cut-off used in the phase shift analysis. The phase shifts are slightly modified but only sets 1 and 2 give a better fit to the experimental data. These sets now give a best fit for a value of the pion–nucleon coupling constant $g^2 \simeq 14$. It appears that sets 3 and 4 are not separate solutions but merge respectively with sets 1 and 2. The values predicted by the modified phase shifts for C_{nn} and C_{KP} for 90° centre-of-mass scattering angle are given in table 2, with the experimental values. A small relativistic correction given in equation (57) of Stapp (1956) has been added to the calculated value of C_{KP}. The errors in the calculated values were obtained from the error matrix for the original sets of phase shifts.

Table 2. Calculated and Observed Values of C_{nn} and C_{KP}

	Calculated values (310 MeV)		Observed values (382 MeV)
	Set 1	Set 2	
C_{nn}	$+0{\cdot}38 \pm 0{\cdot}08$	$+0{\cdot}61 \pm 0{\cdot}06$	$+0{\cdot}42 \pm 0{\cdot}085$
C_{KP}	$+0{\cdot}44 \pm 0{\cdot}05$	$+0{\cdot}49 \pm 0{\cdot}09$	$+0{\cdot}63 \pm 0{\cdot}10$

Calculated values from Cziffra *et al.* (1958). Observed value of C_{nn} from Ashmore *et al.* (1958), C_{KP} from presnt measurement.

The observed value of C_{KP} is rather high compared with the calculated values, but the difference is not significant and the variation with energy is uncertain. A measurement of C_{nn} at 320 MeV is in progress, but in order to distinguish between the modified phase shift sets 1 and 2 by means of spin correlation a measurement of C_{KP} at a centre-of-mass scattering angle around 45° is probably required, as indicated by Cziffra, MacGregor, Moravcsik and Stapp (1958). This is a difficult experiment but methods of performing it are being investigated.

ACKNOWLEDGMENTS

The authors are indebted to Professor H. W. B. Skinner and Professor J. M. Cassels for their help and encouragement, and to the cyclotron crew for their helpful co-operation. A. N. D. is indebted to C.E.R.N. for the provision of a fellowship and G. B. H. to the Department of Scientific and Industrial Research for the provision of a maintenance grant.

REFERENCES

ASHMORE, A., DIDDENS, A. N., HUXTABLE, G. B., and SKARSVÅG, K., 1958, *Proc. Phys. Soc.*, **72**, 289.
CZIFFRA, P., MACGREGOR, M. H., MORAVCSIK, M. J., and STAPP, H. P., 1958, U.C.R.L. 8510.
STAPP, H. P., 1956, *Phys. Rev.*, **103**, 425.
STAPP, H. P., YPSILANTIS, T. J., and METROPOLIS, N., 1957, *Phys. Rev.*, **105**, 302.
WOLFENSTEIN, L., 1956, *Ann. Rev. Nucl. Sci.*, **6**, 43.

Inter-Electron Collisions and the 'Temperature' of Hot Electrons

BY S. H. KOENIG
IBM Watson Laboratories at Columbia University, New York

MS. received 27th February 1959

IT has been pointed out by several authors (Stratton 1957, Fröhlich 1947, Frölich and Paranjape 1956) that for a sufficiently large density of electrons in the conduction band of a solid, inter-electron collisions will ensure that even in the presence of a large electric field E, the spherically symmetric part of the momentum distribution function will be Maxwellian, characterized by an electron temperature $T_e(E) \geqslant T_0$, the lattice temperature. If the conduction band has many valleys, the population of each will then be determined by the electron temperature and the relative band edge energy of each valley. For equivalent valleys (e.g. unstrained n-Ge), the population of all valleys will be equal and the current j will be collinear with E for all E.

Recently, Paige (1958) and Gibson (1958, private communication) have pointed out that for this condition, the piezoresistance, which is ordinarily proportional to T_0^{-1}, would be proportional to T_e^{-1} for fixed T_0. Paige has measured the electric field dependence of the piezoresistance (~15% for the stress used) for a sample of n-Ge with $2{\cdot}5 \times 10^{15}$ donors cm^{-3} at 77°K. On the assumption that this concentration is sufficiently large so that inter-electron collisions will ensure that an electron temperature may be defined for all carriers, he has interpreted his data as yielding the dependence of T_e on E.

The purpose of this note is to show that the assumption which underlies Paige's interpretation of his experiment is invalid for the quoted carrier density, though from the theoretical estimates (Fröhlich 1947, Fröhlich and Paranjape 1956, Stratton 1957) it is not clear why this should be.

Shibuya (1955) and Sasaki *et al.* (1959) have measured the electric field dependence of the angle ϵ between j and E for suitably oriented 15–20 Ω cm samples. (One would not expect interelectron collisions to play a significant rôle here (Fröhlich 1947, Fröhlich and Paranjape 1956, Stratton 1957, Paige 1958).) Their results, though in qualitative agreement with theory (Shibuya 1955), quantitatively are too *large* by a factor of eight†. This observed enhancement of the anisotropy of the conductivity, they suggest, is due to intervalley transitions which take electrons from the 'hot' valleys to the 'cooler' ones. Since it is the cooler valleys that have the higher mobility, an increase in their population will enhance the anisotropy. (If on the other hand inter-electron scattering were sufficient to maintain all valleys at the same temperature, there would be no anisotropy measured in an experiment of this type, as pointed out earlier.)

We have repeated the Sasaki *et al.* type of experiment on two n-Ge samples of essentially the same size and shape used by Sasaki, cut from a {110} plane approximately 30° from the ⟨100⟩ direction. For this orientation, j and E are coplanar with the sample and ϵ is close to maximum. The carrier concentrations were chosen to bracket the value for Paige's crystal. Figure 1 shows the (j, E) data, figure 2 the anisotropy. The anisotropy for the more impure sample is somewhat less than for the purer sample. (This difference would be reduced if the data were plotted against electron 'temperature' rather than electric field, since for the less pure samples, a given value of E corresponds to a lower mean electron energy because of additional impurity scattering.) The main point is that the anisotropy exists, which in itself demonstrates the invalidity of Paige's assumption. In addition, the magnitude of the anisotropy suggests that for large E the valleys have grossly different populations for zero applied stress, at least by a factor given by the ratio of the observed to the calculated anisotropy angle, ϵ‡.

For the magnitude and orientation of stress that Paige applied, one may calculate a relative valley displacement (Herring 1955)

$$\Delta E = 2\chi\Xi_u/3c_{44} = (9{\cdot}8 \times 10^8 \times 16{\cdot}7)/3 \times 6{\cdot}8 \times 10^{11} \simeq 8 \times 10^{-3}\ \mathrm{ev}.$$

---

† Though the theory is for acoustic scattering only, the order of magnitude of the anisotropy is not strongly dependent on the nature of the scattering. Rather, the results can be obtained by geometrical arguments (similar to those pertaining to figure 8 of Sasaki, Shibuya and Mizuguchi 1958, as long as the mobility tensor can be assumed not much less anisotropic than the mass tensor.

‡ This follows from the same sort of geometric argument referred to in footnote above.

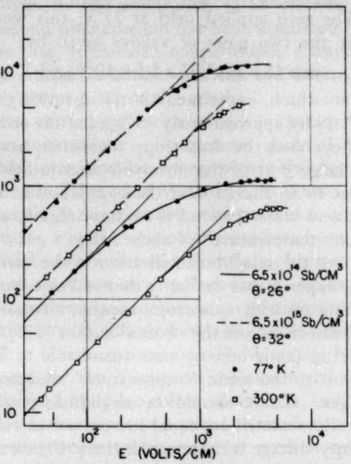

Figure 1. Current density plotted against electric field. The samples are cut from a {110} plane. θ measures the angle between j and the ⟨100⟩ direction.

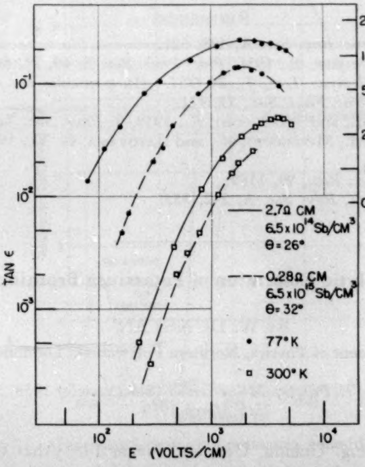

Figure 2. Anisotropy of the conductivity plotted against electric field. ϵ is the angle between the total electric field and the longitudinal current, as determined by measuring the longitudinal conductivity and the voltage transverse to the current flow.

Here χ is the stress, Ξ_u the appropriate deformation potential, and c_{44} the proper elastic constant. For zero applied field at 77°K, this would correspond to a population ratio for the two pairs of valleys given by

$$\exp\,(8\times10^{-3}/77\times8{\cdot}6\times10^{-5})\simeq3{\cdot}3.$$

This population ratio which, experimentally (Paige 1958), in the ohmic region lowers the conductivity by approximately 15%, is of the order of or less than the repopulation of valleys that the anisotropy measurements suggest. It would then appear that a large part of the observed electric field dependence of the piezoresistance is due to an alteration of the population difference of the valleys which is present at zero stress beyond the ohmic region, and is caused by the difference in electron 'temperature' of each valley.

In order to sort out the relative contribution of the various effects, it would be useful to combine experiments similar to that of Paige, but with the stress and electric field not colinear, with anisotropy measurements. For example, if E were along the [100] direction, and the stress along the [110] direction, neglecting inter-electron scattering (as it now appears reasonable to do), the electrons in all the valleys will be at the same 'temperature' measured relative to their respective band edges. There should be negligible piezoresistance for any value of E since all valleys contribute equal current per carrier for this geometry. However an anisotropy voltage will appear in the [010] direction when (and if) there is a population redistribution of the two pairs of equivalent valleys. The magnitude of this voltage would be a direct measure of the population ratio and its variation with E would depend only on ΔE and the electron 'temperature'.

REFERENCES

Fröhlich, H., 1947, *Proc. Roy. Soc.* A, **188**, 521.
Fröhlich, H., and Paranjape, B., 1956, *Proc. Phys. Soc.* B, **69**, 21, 866.
Herring, C., 1955, *Bell Syst. Tech. J.*, **34**, 237. (In particular see equation C3.)
Paige, E. G. S., 1958, *Proc. Phys. Soc.*, **72**, 921.
Sasaki, W., Shibuya, M., and Mizuguchi, K., 1958, *J. Phys. Soc. Japan*, **13**, 456.
Sasaki, W., Shibuya, M., Mizuguchi, K., and Hatoyama, G. M., 1959, *J. Phys. Chem. Solids*, **8**, 250.
Shibuya, M., 1955, *Phys. Rev.*, **99**, 1189.
Stratton, R., 1957, *Proc. Roy. Soc.* A, **242**, 355.

Electrolytic Coloration of Potassium Bromide

By W. DUNSTAN
Department of Physics, Northern Polytechnic, London

Communicated by M. E. Pillow; MS. received 18*th December* 1958, *in revised form* 25*th March* 1959

It is well known (e.g. Uchida, Ueta and Nakai 1951) that the alkali halides may be coloured by electrolysis at moderately high temperatures (of the order of 500°c) using a pointed cathode. The colour associated with the F-centres of the particular crystal employed enters from the negative electrode; if at any stage the field is reversed, the coloration returns to the (new) anode. Also, crystals previously coloured, whether additively or by electrolysis, may be bleached at similar temperatures by the application of an electric field between plane electrodes. This second phenomenon has been discussed by Mott and Gurney (1940) who suppose that, at elevated temperatures, a fraction of the F-centres are dissociated to give negative lattice vacancies and electrons in the conduction band: the latter are swept towards the anode.

Some experiments carried out by the writer on potassium bromide indicate a somewhat different behaviour. Specimens, about 1 cm × 0·4 cm × 0·4 cm, were cut from crystals, some of which were grown in this department, while others were supplied by Messrs. Hilger and Watts Ltd., and were submitted to electrolysis, using a potential difference of 360 volts parallel to the longest dimension. In the majority of cases, a red coloration entered first from the pointed cathode, followed by the blue F-centre tint at a slightly higher temperature (about 525 and 575°c for the two colours in a typical case). Brass, steel, and platinum cathodes were used without producing any variation in the effect. The red colour is least marked in well-annealed crystals, but is never completely absent; portions of specimens which appear entirely blue may however be obtained; one of these was used for the absorption measurements discussed below.

On reversing the field, the blue colour disappears, but the red remains, and cannot be removed, whether plane or pointed electrodes are used, at any temperature up to the melting point. This makes it possible to produce a pure red crystal from one initially containing both colours.

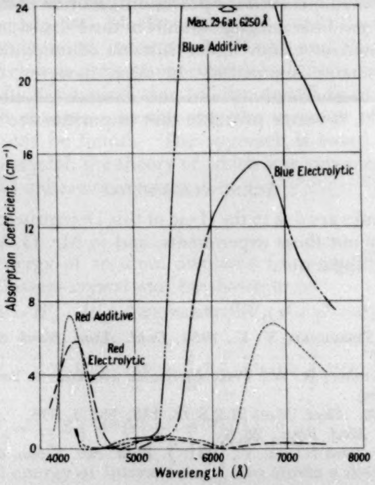

Absorption in coloured potassium bromide.

The writer has occasionally, but not reproducibly, obtained red specimens by heating crystals in potassium vapour at about 550°c; these also cannot be bleached by electrolysis below the melting point. The diagram shows the variation of absorption coefficient with wavelength for both additively and electrolytically coloured red and blue specimens. Applying Smakula's formula, the densities of centres for the former are about $2{\cdot}5 \times 10^{16}$ cm^{-3} for the electrolytically, and $2{\cdot}0 \times 10^{16}$ cm^{-3} for the additively coloured crystals; the last named are seen to have an appreciable F-absorption. Measurements were made using a tungsten source, and a photomultiplier mounted on a constant deviation spectrometer. The maxima are not far from that of the V_1-band (4100 Å), and in this connection it may be mentioned that Kosman and Pisarenko (1957) report the presence of some of the V-bands (but not the V_1) near the cathode after electrolysis of KBr with plane electrodes. The V_1-band is only observed in crystals coloured (e.g. by X-rays) at low (liquid air) temperatures.

The coloration is accompanied by photoconductivity under illumination in the absorption band; for this purpose, mercury violet (4047, 4078 and 4358 Å) light was used. Observations were made at room temperature, in a field of some 300 volt cm^{-1}; the current was recorded with a vibrating reed electrometer. Pisarenko (1957) observed photoconductivity in KBr crystals after electrolysis in the range 4 to 12×10^{-5} cm, but found no change in the absorption spectrum.

Absence of electrolytic bleaching would seem to suggest that the traps associated with the red colour are particularly deep, and hence very largely undissociated at any temperature which may be reached in the solid phase; in this case, however, one would not expect to observe photoconductivity.

The presence of impurities is known to give rise to additional absorption in additively coloured crystals (these are discussed in Section X of the review by Seitz 1954). The small quantities of potassium chloride in the specimens grown by the writer would produce a negligible shift in the F-band; nor do the observed bands show the interconversion under suitable illumination characteristic of possible divalent metallic impurities. In view, however, of the difficulty of explaining both photoconductivity and the absence of electrolytic bleaching on any simple model, it seems probable that impurities are responsible for the effects.

ACKNOWLEDGMENTS

The author's thanks are due to the Head of this Department, Dr. M. E. Pillow, for facilities to carry out these experiments, and to Mr. G. W. Dickson for the construction of the apparatus.

REFERENCES

KOSMAN, M. S., and PISARENKO, V. F., 1957, *Dokl. Akad. Nauk S.S.S.R.*, **115**, No. 4, 693.

MOTT, N. F., and GURNEY, R. W., 1940, *Electronic Processes in Ionic Crystals* (Oxford: University Press).

PISARENKO, V. F., *Dokl. Akad. Nauk S.S.S.R.*, **115**, No. 5, 898.

SEITZ, F., 1954, *Rev. Mod. Phys.*, **26**, 1.

UCHIDA, Y., UETA, M., and NAKAI, Y., 1951, *J. Phys. Soc. Japan*, **6**, 107.

The Zero-Point Energy and Equation of State of Solid Helium at the Absolute Zero

By I. J. ZUCKER†

Wheatstone Physics Laboratory, King's College, London

MS. received 26th January 1959

§ 1.

THE experiments of Dugdale and Simon (1953) have shown that the behaviour of solid helium is dominated by its zero-point energy E_0. The latter is so much larger than the static lattice energy, that even at the absolute zero helium will only solidify under a pressure of 25 atmospheres. Thus even at $T=0°\mathrm{K}$ helium atoms in the solid state are executing vibrations of relatively large amplitude. The assumption that these vibrations are harmonic—the basis of normal lattice dynamics—is no longer true. It is therefore likely that any theoretical treatment which would account for large E_0 might point a way to treating anharmonic vibrations and vice versa.

Several approaches to this problem have been suggested by Born (1951), Domb (1952), Dugdale and MacDonald (1954) and Hooton (1955 a) all of which have been reviewed in an article by Domb and Dugdale (1957). The method described below is a direct approach which finds how the shape of the potential well in which a typical atom of the crystal finds itself varies as the volume of the solid changes. In this way the variation of the lowest energy state with volume may be found. The approach is based on the well-known Einstein model of a crystal, the theory of which was extended by Henkel (1955) to include first order anharmonic terms.

§ 2.

The potential energy of an atom displaced from equilibrium (the classical lattice site) in an Einstein crystal may be shown to be

$$W=W_0+W_2(x^2+y^2+z^2)+W_4(x^4+y^4+z^4) \qquad \ldots\ldots (2.1)$$

where

$$W_0=\frac{1}{2}\Sigma_r\phi(r). \quad W_2=\frac{1}{6}\Sigma_r\left[\phi''(r)+\frac{2}{r}\phi'(r)\right]$$

$$W_4=\frac{1}{72}\Sigma_r\left[\phi^{\mathrm{iv}}(r)+\frac{4}{r}\phi'''(r)\right].$$

$\phi(r)$ is the potential energy of interaction of two atoms a distance r apart, x, y, z are the displacement components of the atom, and Σ_r implies summation over all lattice points. (2.1) is a generalization of Henkel's (1955) result which is now applicable to any central additive potential and for any lattice structure. W_0 represents the static lattice energy, the term involving W_2 is that obtained when normal lattice dynamics is applied to an Einstein crystal, and the term involving W_4 may be considered as the first anharmonic contribution to the potential energy. The problem here is to find the energy levels, in particular the lowest energy level, of an atom vibrating in the potential given by (2.1). The Schrödinger equation is separable in this case, and the problem reduces to finding the eigenvalues of the following one-dimensional anharmonic oscillator equation:

---

† Now at Northampton College of Advanced Technology, St. John Street, London E.C.1.

$$\left(-\frac{\partial^2}{\partial x^2}+\alpha^2x^2+\beta^2x^4\right)\psi=\lambda\psi \qquad \ldots\ldots(2.2)$$

$$\alpha^2=\frac{8\pi^2mW_2}{h^2},\quad \beta^2=\frac{8\pi^2mW_4}{h^2},\quad \lambda=\frac{8\pi^2mE}{h^2},$$

m = mass of atom, h = Planck's constant.

It is well known how the energy levels of (2.2) are obtained if W_4 is treated as a perturbation. It has also been demonstrated by Johns (1958), Henkel (1955) and Zucker (1958) that this particular approach is in many ways more successful than harmonic theories in describing the behaviour of the heavier inert gas solids such as argon, krypton and neon. These solids, however, have E_0 as a small fraction of the total energy. The largest proportion is for neon, the value being about 30%. For helium, however, the fraction is about 90% and the term containing W_4 is no longer a perturbation, indeed it may be larger than W_2. It is thus necessary to find a way of obtaining the eigenvalues of (2.2) which is independent of the sizes of W_2 and W_4.

Coulson and McWeeny (1948) have shown how this can be achieved, the eigenvalues being evaluated to any degree of accuracy in terms of W_2 and W_4. If λ_0 is the lowest eigenvalue it is simple to show that E_0 of the crystal is given by

$$E_0=\frac{3Nh^2}{8\pi^2m}\lambda_0 \qquad \ldots\ldots(2.3)$$

where N = Avogadro's number.

The eigenvalues of (2.2) appear as the latent roots of an infinite matrix. Nearly all the off-diagonal terms, however, are zero. (For the pure harmonic oscillator the matrix is in fact diagonal.) Further the elements depend on an arbitrary parameter γ introduced in the solution of (2.2), which may be chosen for each eigenvalue such that the diagonal terms of the matrix are dominant. The latent roots may then be evaluated by the formula

$$\lambda_i=H_{ii}-\sum_{i\neq j}\frac{H_{ij}H_{ji}}{H_{jj}-H_{ii}}$$

which converges very rapidly to the desired root. The H_{ij} are the matrix elements.

It may be shown that λ_0 is given by the relations

$$\lambda_0=B-\frac{3C^2}{B+12C},\quad B=\frac{3\gamma^2+\alpha^2}{4\gamma},\quad C=\frac{\beta^2}{4\gamma^2} \qquad \ldots\ldots(2.4)$$

and γ is the real root of the cubic

$$\gamma^3-\alpha^2\gamma-3\beta^2=0. \qquad \ldots\ldots(2.5)$$

It is evident that E_0 is easily evaluated as a function of volume since λ_0 depends only on W_2 and W_4. Further since W_2 and W_4 depend simply on $\phi(r)$, the calculation is readily adapted to any central potential chosen. Here two potentials were dealt with. These were

$$\phi(r)=\frac{12\cdot 6}{1-6/12\cdot 4}\left[\frac{6}{12\cdot 4}\exp\left(1-\frac{r}{3\cdot 135}\right)-\left(\frac{3\cdot 135}{r}\right)^{6}\right]\times 10^{-16}\,\mathrm{erg}$$

and

$$\phi(r)=\left[\frac{6\cdot 11}{r^{12}}\times 10^{-10}-\frac{1\cdot 68}{r^{6}}\times 10^{-12}\right]\mathrm{erg}$$

where r is the distance between nearest neighbours in ångströms. The first of these potentials was given by Mason and Rice (1954) and was obtained from high temperature second virial coefficients. The second was given by Hooton (1955 b) and obtained by directly fitting $\phi(r)$ to the experimental values for the crystal lattice energy as a functon of volume given by Dugdale and Simon (1953).

The equation of state at the absolute zero was calculated by differentiating the free energy at $T=0^\circ\mathrm{K}$. This is simply W_0+E_0, hence the equation of state is

$$P=-\left(\frac{\partial W_0}{\partial V}\right)_T-\frac{3\boldsymbol{N}\boldsymbol{h}^2}{8\pi^2 m}\frac{\partial \Lambda_0}{\partial V}. \qquad \ldots\ldots (2.6)$$

This was evaluated in a straightforward manner except that $\partial\lambda_0/\partial V$ was found numerically as no analytic expression for it has yet been obtained. The results of these calculations together with a curve found by de Boer (1948), and the experimental values of Dugdale and Simon (1953) are exhibited in figure 1.

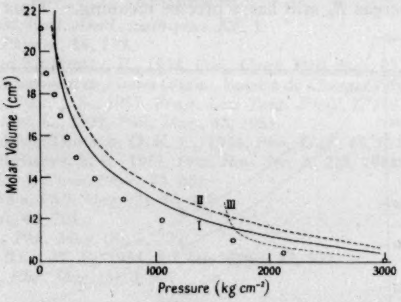

Figure 1. I, theoretical curve 12–6 potential; II, theoretical curve exp-6 potential; III, theoretical curve (de Boer 1948); circles, experimental results (Dugdale and Simon 1953).

The agreement between experiment and the theory presented here is seen to be quite fair. It is also observed that the equation of state in the solid phase depends very much on the intermolecular potential—in great contrast to the equation of state of the gaseous phase. The calculation of de Boer (1948) based on a Debye-type theory breaks down for molar volumes greater than 15 cm³.

It is of course possible to compare the calculated and experimental values of E_0 directly, but it must first be noted how E_0 is found experimentally. Dugdale and Simon (1953) do so by finding the experimental value of the Debye characteristic temperature θ and they then assume that E_0 is $9\boldsymbol{N}\boldsymbol{k}\theta/8$ where $\boldsymbol{k}$ is Boltzmann's constant. This suggests that it is possible to define θ in a way different from the usual. Normally θ is defined in terms of a frequency on the assumption that the harmonic approximation of lattice dynamics is valid. On this basis Domb and Salter (1952) were able to express θ in terms of the sum of the squares of the normal modes of a crystal, which in turn was related to the intermolecular potential. They showed that

$$\theta = \frac{\boldsymbol{hN}}{2\pi\boldsymbol{k}}\left(\frac{10W_2}{3m}\right)^{1/2} \qquad \ldots\ldots(2.7)$$

Further they showed that $9\boldsymbol{Nk}\theta/8$, where θ was expressed as in (2.7), was a good approximation to E_0 for most lattices. It is observed that if W_4 is zero, then E_0 as given by (2.3) is equivalent to that given by (2.7), apart from a numerical factor almost equal to unity, which occurs owing to the different frequency distributions of the Debye and Einstein models. It is evident, however, that if W_2 becomes negative as it will at large volumes, the definition of θ as given by (2.7) fails as θ becomes imaginary. This is exactly what happens for solid helium at molar volumes greater than 15 cm³. None the less experimentally solid helium exists at molar volumes up to 21 cm³, and Dugdale and Simon (1953) show that it is possible to determine a parameter which may be identified as θ at these large volumes. It is thus proposed here to invert the description of Domb and Salter (1952) and to define θ as $8E_0/9\boldsymbol{Nk}$. Obviously for a harmonic crystal this definition and the definition in terms of frequency are equivalent. But this definition is more general, since in the case of a crystal governed by anharmonic forces the original definition of θ in terms of frequency becomes meaningless, whereas E_0 still has a precise meaning. Thus in figure 2 instead of comparing the theoretical and experimental values of E_0, we show the corresponding θ values. For comparison the results given by (2.7) with the Hooton (1955 b) potential are given showing how (2.7) fails at large molar volumes.

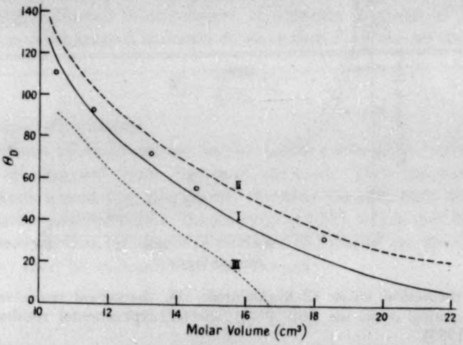

Figure 2. I, theoretical curve 12–6 potential; II, theoretical curve exp-6 potential; III, theoretical curve 12–6 potential, harmonic approximation; circles, experimental results (Dugdale and Simon 1953).

§ 3.

The approach to solid helium described above is a simple way of dealing with an anharmonic crystal. It is unsatisfactory in so far as it is based on the Einstein model of a crystal. Even so the main features of the behaviour of solid helium are described. This is not too surprising if it is remembered that only when more detailed descriptions of the vibrations of crystal atoms are required, as in the case of specific heats, do more accurate theories give better agreement for harmonic crystals. There is no reason to suppose that this is different for anharmonic crystals. The above approach may be applied to hydrogen, deuterium and the helium isotope of mass three. However, some preliminary calculations on the latter have indicated that at the extremely large relative volumes at which the latter exists it is necessary to include the next term in the potential energy. It has been shown that this additional term is

$$W_6(x^6+y^6+z^6), \quad W_6=\frac{1}{2160}\sum_r\left[\phi^{\mathrm{vi}}(r)+\frac{6}{r}\phi^{\mathrm{v}}(r)\right]. \qquad \ldots\ldots(3.1)$$

E_0 for ^{3}He is even larger than for ^{4}He. The stability of the lighter isotope in the solid state is thus even less than that of ^{4}He. It is possible to study the stability of the rare gas solids in general with the above methods, and this will be the subject of a further communication.

ACKNOWLEDGMENTS

The writer is grateful to Professor C. Domb of King's College, London, for many interesting and helpful discussions. The work, was made possible by a maintenance grant from the Department of Scientific and Industrial Research.

REFERENCES

BORN, M., 1951, *Fest. Gott. Akad., math-phys. Kl.*, 1.
DE BOER, J., 1948, *Physica*, **14**, 139.
COULSON, C. A., and MCWEENY, R., 1948, *Proc. Camb. Phil. Soc.*, **43**, 413.
DOMB, C., 1952, *Changement de Phases* (Paris: Société de Chemie Physique), p. 338.
DOMB, C., and DUGDALE, J. S., 1957, *Progr. Low Temp. Phys.*, **2**, 338.
DOMB, C., and SALTER, L., 1952, *Phil. Mag.*, **43**, 1083.
DUGDALE, J. S., and MACDONALD, D. K. C., 1954, *Phil. Mag.*, **45**, 811.
DUGDALE, J. S., and SIMON, F. E., 1953, *Proc. Roy. Soc.* A, **218**, 291.
HENKEL, J. H., 1955, *J. Chem. Phys.*, **23**, 681.
HOOTON, D. J., 1955 a, *Phil. Mag.* (7), **46**, 422.
—— 1955 b, *Ibid.*, **46**, 701.
JOHNS, T. F., 1958, *Phil. Mag.* (8), **3**, 229.
MASON, E. A., and RICE, W. E., 1954, *J. Chem. Phys.*, **22**, 522.
ZUCKER, I. J., 1958, *Phil. Mag.* (8), **3**, 987.

The Grain-boundary Amplifier

BY O. A. WEINREICH, H. MATARÉ AND B. REED
Research Laboratories, Sylvania Electric Products Inc., Bayside, New York

MS. received 12th January 1959

IT has been found experimentally by Pearson (1949) that grain boundaries in n-type germanium show p-type behaviour so that an n–p–n structure is formed. An extensive investigation of the electrical properties of the grain boundaries in germanium was made by Taylor, Odell and Fan (1952), who applied the Schottky barrier theory to the potential formed around the grain boundary region. Later on, Tweet (1955) succeeded in isolating the p-type region from the bulk by doping the bicrystal with gold and measuring the grain boundary 'sheet' conductance in the temperature range from 20° to 100°K.

At these temperatures, levels in the forbidden gap introduced by the gold act as traps for the conduction electrons and the Ge bulk conduction is decreased to negligibly small values compared with the sheet conductance. The latter can be followed up to higher temperatures by applying rectifying contacts to the bulk and ohmic contacts to the grain boundary. In this way it was found that (i) the 'sheet' conductance is only slightly temperature dependent between 2°K and room temperature and (ii) the sheet conductance is fairly independent of impurity type and concentration (Reed, Weinreich and Mataré 1959).

This note describes how the sheet conductance can be modulated by an applied electric field leading to a grain-boundary amplifier; it has a small temperature dependence and works down to the liquid helium temperature range. Figure 1 shows the circuit schematically.

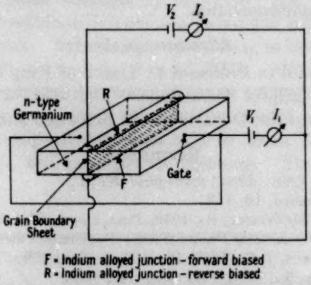
V_2 I_2
R
n-type Germanium
V_1 I_1
Gate
F
Grain Boundary Sheet
F = Indium alloyed junction - forward biased
R = Indium alloyed junction - reverse biased

Figure 1. Grain-boundary field amplifier, schematic.

In terms of field transistor terminology, the forward-biased junction F is the source, the reversed biased junction R is the drain and the contact to the bulk G is the gate.

Figure 2 shows the characteristic of the sheet current: (*a*) at room temperature, (*b*) at 78°K and (*c*) at 4·2°K when modulated at zero, 1·5, 3·0 and 6·0 volts. It can be seen from the curves that even with no field applied the (I, V) characteristic is non-linear, bending downward for higher sheet voltage. This is due to the modulation from the voltage drop along the grain boundary sheet.

As seen from figure 3, the ohmic contact to the grain boundary causes a linear voltage drop along the sheet. The rectifying contacts to the bulk, in contrast, maintain a practically constant potential from the forward-biased junction to the reverse-biased junction, where the voltage drop occurs. Thus at the reverse contact the voltage drop across the sheet acts as a modulating field voltage between bulk and sheet. Therefore the temperature dependence of the sheet conductance must be measured at low sheet voltage. Figure 4, drawn from oscilloscope traces, shows the (I, V) characteristic of the sample in the 0·1 volt range. The conductivity is the same at 300 and 78°K and is decreased by a factor of 2 at 4·2°K. With all other samples measured this factor was less than 2 and thus appears to be an upper limit on account of a possible increase of the contact resistance. The transconductance, which in the sample shown in figure 1 is about 500 micromhos at room temperature, increases with decreasing temperature. It also increases with impurity concentration. With 0·5 ohm cm n-type bi-crystals and appropriate dimensions a transconductance of 3500 micromhos has been obtained. The lower temperature limit of the grain-boundary amplifier is practically unlimited due to the impurity-independent conduction mechanism. The upper temperature limit is probably imposed just as for other semi-conductor devices involving junctions by the thermal injection current proportional to $\exp(-E_g/kT)$ (where E_g is the energy gap) which increases the field current to values that are not negligible compared with the sheet.

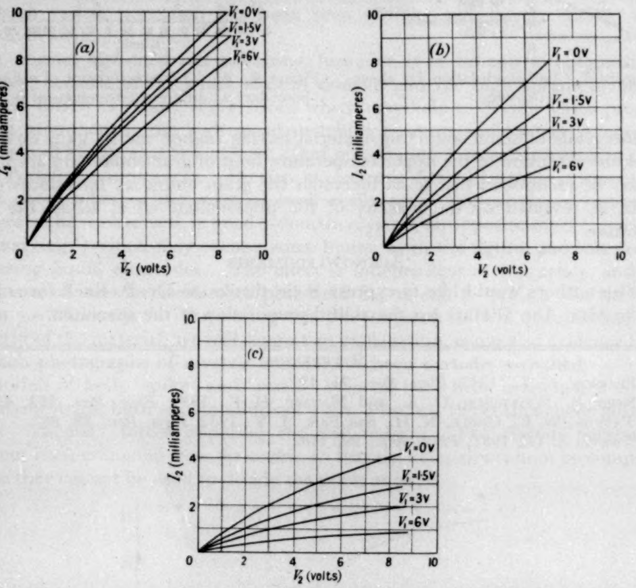

Figure 2. Grain-boundary field effect (*a*) at 300°K, (*b*) at 78°K, (*c*) at 4·2°K.

Our samples have an input resistance of approximately 10^5 ohms at room temperature; we hope in subsequent work to increase this value. At liquid nitrogen and helium temperatures, the input resistance increased to approximately 10^7 ohms. At 78°K and 4·2°K, the power amplification was 21 and 23 dB respectively at a frequency of 1 kc/s. The power gain dropped to half this value at 10 kc/s and approached zero at 50 kc/s. Further investigation is necessary to determine if the frequency limit can be improved by a more favourable geometry.

The detailed mechanism of the grain boundary conduction and its small temperature dependence is not completely understood. It seems probable that the sheet conduction carriers are holes that compensate negative charges in acceptor states at the boundary and that the applied field modulates the width of the space-charge region and the number of available holes.

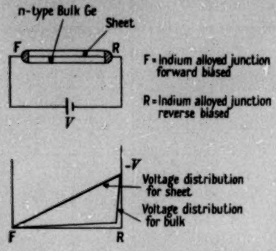
n-type Bulk Ge
Sheet
F
R
F = Indium alloyed junction forward biased
R = Indium alloyed junction reverse biased
V
-V
Voltage distribution for sheet
Voltage distribution for bulk
F
R

Figure 3. Self-modulation by sheet voltage.

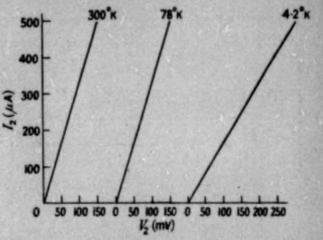

Figure 4. (I, V) characteristics of a Ge grain boundary at different temperatures $(v_1 = 0)$.

Bicrystals of semiconducting material having higher energy gaps obviously allow the extension of the upper temperature limit of grain-boundary amplifiers. It may be mentioned that in Si bicrystals the grain boundary introduces donor levels, as revealed by the polarity of the photovoltaic effect across the grain boundary.

ACKNOWLEDGMENTS

The authors would like to express their thanks to Dr. P. Keck for support and to Mrs. Ann O'Hare for the skilful preparation of the specimen.

REFERENCES

PEARSON, G. L., 1949, *Phys. Rev.*, **76**, 459.
REED, B., WEINREICH, O. A., and MATARÉ, H. F., 1959, *Phys. Rev.*, **113**, 454.
TAYLOR, W. E., ODELL, N. H., and FAN, H. Y., 1952, *Phys. Rev.*, **88**, 867.
TWEET, A. G., 1955, *Phys. Rev.*, **99**, 1182.

LETTERS TO THE EDITOR

Growth of Ferroelectric Hysteresis Loops

Until recently it had been supposed (Merz 1954) that polarization reversal, by an electric field, of c-domain barium titanate crystals occurred by the nucleation of antiparallel domains at a crystal face, followed by forward growth of these as ' spikes '. More recently it has been suggested (Chynoweth 1958) that appreciable sideways movement of these domain walls may subsequently occur, and such radial expansion has been seen (Miller and Savage 1958), with very small switching fields.

In normal *high*-field fast switching, however, it is difficult to obtain direct evidence, because of the small sizes of domain and the high speeds involved. We wish briefly to report observations which may help to decide which process is most prominent in the high-speed switching currents and hysteresis loops.

It is well known that the amount $2Q$ of polarization reversal decreases in time under certain circumstances. Because of electrode difficulties there is sometimes doubt about whether the material itself really ages. But applying sinusoidal voltages we have observed, in good c-domain crystals, an opposite effect (' growth ' or ' unageing ') which may occupy some hours, as in the figure, and this occurs also using liquid electrodes. The effect is independent of frequency, and the initial rate of increase varies with peak field E_m as $\exp(-\gamma/E_m)$. In the case shown $\gamma = 8{\cdot}2$ kv cm^{-1}. Supposing this phenomenon to be a genuine intrinsic property of the material, we will suggest an explanation, using also evidence from our etch photographs of crystals which have been partially switched.

Models of both ' spike ' and ' radial ' reversal have been investigated and in both cases it has been shown (Burfoot 1959, Peacock 1959) that there must be heavy ' viscous ' forces opposing the wall motion. The viscous parameters have not been evaluated *from the models*, so that the velocities cannot be compared and so they cannot be used to decide the point at issue.

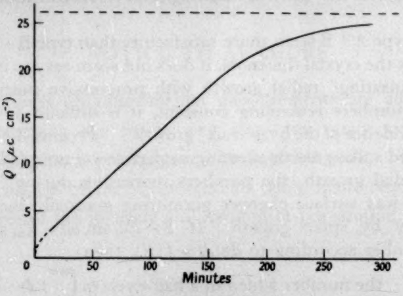

Growth of Q.

If wall energies and depolarizing effects are not too large it is possible (Peacock 1959) to fit the form of the observed switching current curves $i(t)$ for constant field E very successfully, if the nucleation rate R is initially constant and the volume for each domain is proportional to $(t-t_1)^2$ after nucleation at $t=t_1$. The part of $i(t)$ after the rising inflexion is well-fitted by expressions for the effects of over-crowding, and a similar explanation no doubt holds for the later part of the figure; we shall for simplicity discuss only the initial rise. Switching current is always proportional to rate of change of volume of reversed material, so that the required relation, volume $\propto (t-t_1)^2$, may arise either (i) by radial growth at a constant velocity v, regarding the preceding spike growth as effectively providing 'hairline' nuclei while reversing only a negligible amount of polarization or (ii) spike growth with volume proportional to $(t-t_1)^2$ assuming the subsequent radial growth to be slow and to reverse only a negligible amount of polarization.

We lack independent knowledge of the spike and radial velocities. But if we picture a spike as a cone of fixed small angle 2θ in which the walls move radially with velocity v, such a motion is indistinguishable from spike motion through the crystal thickness at velocity $v\theta^{-1}$. Before the cone has passed through the crystal and become truncated, the growth process is creating new wall at the tip in quite a different manner from the process after 'impact' on the far side. But if the viscous force is kv per unit area of wall, it is readily shown that $v=(2EP)/k$ with our assumptions, irrespective of the geometry. Thus if the retardation is of this kind, the motions can both be described in terms of v. Then the current from a single domain is

$$i=\frac{2P}{d}\frac{d\,\mathrm{vol}}{dt}=\frac{2P\pi v^3}{\theta d}t^2$$

until impact, and $4P\pi v^2(t-c)$ thereafter, where c is $\theta d/2v$; since $t=\theta d/v$ at impact, the transition is smooth. Our etch photographs show that 2θ is about $1\frac{1}{2}$°.

During 'growth' the loops are flat-topped; that is, during the high-field part of the sinusoidal E little further switching occurs, though the crystal is by no means fully switched. If the switching current is predominantly due to some growth process B (spike or radial) then the flat tops suggest that growth of each domain is limited, and that either B is regulated by a process A which controls the *number n* of domains, or that the limit on B is progressively lifted by some process C which controls the *volume* switched by each domain. A or C continues in one sense throughout the 'growth' although B reverses continually in succeeding half-cycles.

Processes of type A + B seem more satisfactory than type B + C for if B is spike growth limited by the crystal thickness, it does not seem easy to invoke process C, while if it is 'pulsating' radial growth with progressive pushing back of the limitations, the numbers remaining constant, it is difficult to account for the frequency independence of the hysteresis 'growth'. Process A + B is presumably either (i) nucleated spike growth affecting negligible volume, followed by limited and pulsating radial growth, the numbers increasing during 'growth' of the loop, or (ii) one-way surface changes permitting gradually increasing areas to switch repeatedly by spike growth. If $E=E_\mathrm{m}\sin\omega t=E_\mathrm{m}\sin\phi$, and if A increases the number according to $dn/dt=f(E)$, then

the number added in a half-cycle is $\int_0^{\pi/\omega} f\,dt$

and the number added per second is $\int_0^{\pi} f\,d\phi$,

which is independent of ω, as observed.

In (i) the spikes remain, once grown. In (ii) the regions switched by spike growth must reverse again in the other half-cycle; this may occur at different sites, after coalescence of growing domains. Alternatively, sites may be capable of nucleating domains of either polarity, but our photographs show that spikes grow largely from negative nuclei, so that surface nucleation proceeding in alternate half-cycles is largely on opposite faces of the crystal. If at any instant all domains are of similar size, it would support (ii); in (i), we should expect to see at any instant many sizes of domain, but such an observation would not exclude (ii). We see in fact a range of sizes from 10 microns down to the resolution limit, say $\frac{1}{3}$ micron, many of them clearly coalescences.

Finally, it is clear from our pictures when using evaporated electrodes that the switching time cannot then be divided into parts during which only A or only B takes place. For example, an appreciable proportion of a switched crystal area exhibits 'complete coalescence' when the area as a whole is only 1% reversed, while at 37% reversal the nucleating surface exhibits about 8% of its area as domains under 1 micron in size, 8% as 3 micron domains largely coalesced into rings (Burfoot 1959, figure 4), and 18% completely coalesced.

Queen Mary College,
London, E.1.
19th March 1959.

J. C. Burfoot.
R. V. Peacock†.

Burfoot, J. C., 1959, *Proc. Phys. Soc.*, **73**, 641.
Chynoweth, A. G., 1958, *Phys. Rev.*, **110**, 1316.
Merz, W. J., 1954, *Phys. Rev.*, **95**, 690.
Miller, R. C., and Savage, A., 1958, *Phys. Rev.*, **112**, 755.
Peacock, R. V., 1959, *Ph.D. Thesis*, London University.

† Now at Mullard Research Laboratories, Salfords.

NOTICE TO AUTHORS

Authors of papers on experimental measurements are advised to include information concerning the purity and structure (grain size, homogeneity, degree of working phases present, etc.) of materials used. This should be as complete as the nature of the measurements being made requires and should include the source of the material and method of preparation.

CORRIGENDA

Theory of the Effect of a Magnetic Field on the Absorption Edge in Semiconductors, by R. J. ELLIOTT, T. P. McLEAN and G. G. MACFARLANE (*Proc. Phys. Soc.*, 1958, **72**, 553).

Equation (2.18)	Denominator of first term on right-hand side *should read im.*
Equation (3.3)	*Delete i* from the second term on right-hand side.
Equation (3.4)	Last denominator *should read* $\epsilon_\alpha(0)-\epsilon_V(0)$.
Equation (3.7)	For Z read 2π.
Equation (3.9 *a*)	*Delete* π.
Equations (3.10), (3.11) and (3.12)	*Delete* $\hbar^2$ in denominators of right-hand side.
Equation (3.12)	Last line, for n read $(n+1)$.

The $(2s)^2$ ^1S *State Solution of the Non-relativistic Schrödinger Equation for Helium and the Negative Hydrogen Ion*, by E. HOLØIEN (*Proc. Phys. Soc.*, 1958, **71**, 357).

Some typographical errors have crept into the list of matrix elements of the electronic repulsion energy operator on p. 367.

$\lvert 1s2s \lvert 1s3s \rvert$	$4/8\sqrt{2}$	*should read*	$3/8\sqrt{2}$
$\lvert 2p3p \lvert 1s4s \rvert$	$-17/128\sqrt{30}$	*should read*	$-17/128\sqrt{6}$
$\lvert (3p)^2 \lvert (3d)^2 \rvert$	$431/1280\sqrt{5}$	*should read*	$431/1280\sqrt{15}$
$\lvert 2s4s \lvert 3s4s \rvert$	$9/32$	*should read*	$9/32\sqrt{2}$

$9/128\sqrt{30}$ after the element $(2s4s\lvert(4s)^2)$ is superfluous and *should be deleted.*

Spin–Orbit Coupling and the Extraordinary Hall Effect, by C. STRACHAN and A. M. MURRAY (*Proc. Phys. Soc.*, 1959, **73**, 433).

By an error in printing, the symbol μ which is used for the electronic mass from equation (19) onwards, was replaced in § 2 by m_e. Also in the fifth line from the foot of p. 443 the missing symbol is b.

REVIEWS OF BOOKS

Mechanics, Wave Motion and Heat, by F. W. SEARS. Pp. xiv + 664. (Reading, Mass. : Addison-Wesley Inc., 1958.) 76*s*.

The books from the pen of Professor Sears have gained a wide and good reputation both in Britain and overseas. They are well written, clearly printed and the diagrams usually all that can be desired. The present volume closely follows in the steps of its predecessors although the reviewer feels that he must draw attention to some omissions and minor defects. Routh's rule for moments of inertia is not given and on p. 395 we find a liquid surface represented by a straight line ; the meniscus should be shown, for without it, a rise in a capillary tube becomes an impossibility. The pictorial diagram of a viscometer, on p. 398, is useless for teaching purposes and the calorimeter on p. 516, completely filled with a liquid, is most weird. It is a pity that so many elementary textbooks do not draw a distinction between adiabatic and reversible adiabatic (or isentropic) expansions and the book under review is no exception. It is pleasing, however, to find that the author first defines thermal capacity and then treats specific heat as the thermal capacity per unit mass.

As a strong opponent of the use of the m.k.s. system of units for teaching purposes, the reviewer finds little in this book to cause him to alter his views. Professor Sears appears to prefer the m.k.s. system but to be consistent should not a mole then be the mass in kilogrammes of a substance equal to its molecular weight (or relative molecular mass) ?

Also, on p. 616, Loschmidt's number is given as so many molecules per cubic centimetre ; why not the cubic metre ?

Finally, the reviewer would have preferred the index notation, e.g. cal cm^{-2} sec^{-1} deg^{-1}, to have been used ; it helps so much to appreciate the method of dimensions and is without ambiguity. C. J. SMITH.

Kinetic Theory of Gases, by R. D. PRESENT. Pp. vii + 280. (New York, Toronto, London : McGraw-Hill, 1958.) 60*s*.

This book is designed to provide an introduction to the kinetic theory of gases for undergraduate and beginning postgraduate students of physics, and also for chemists and engineers. The book starts with introductory chapters on distribution functions, the perfect gas law, the discussion of transport phenomena by mean free path methods, and diffusion and the random walk problems. Then there are chapters on the Maxwell–Boltzmann distribution, on the theory of real gases, thermal diffusion and isotope separation, collision dynamics, Brownian motion, the experimental situation, and the Boltzmann equation. Finally a discussion of the calculation of intermolecular forces is given. The book gives a clear and detailed introduction to the subject and should fulfil its purpose well. Occasionally a use of the methods of statistical mechanics would simplify discussions such as that of the imperfect gas, and it is a pity that the discussion of the Boltzmann equation is not fuller ; for having read this book the student will find it very hard to find any book which will develop the theory further in a reasonably straightforward way. Such a fuller discussion would be more valuable than the brief chapter on intermolecular forces. The book is produced up to the usual high standard of this series. S. F. EDWARDS.

An Introduction to Statistical Mechanics, by J. S. R. Chisholm and A. H. de Borde. International series of monographs on physics, vol. II. Pp. ix + 160. (London, New York, Paris, Los Angeles : Pergamon Press, 1958.) 35*s*.

In contrast to most of the many textbooks on statistical mechanics which were published during the last few years the present one is a really comprehensive introduction into the subject which can be used by undergraduate students reading for honours degrees in physics or mathematics. The emphasis is therefore laid on a clear and logically consistent presentation of the fundamental theorems of classical and quantum statistical mechanics and their thermodynamic interpretation. By way of illustration of these theorems useful applications are made to topics chosen from the thermodynamics of gases and solids, the theory of electrons in metals, the theory of radiation and physical chemistry. A knowledge of elementary dynamics, thermodynamics and quantum theory is assumed.

The general theory adopted is that of ' ensembles ' whose members are ' assemblies ' of identical members for which mean values of observable parameters are calculated by an adaptation of the method of Darwin and Fowler. Although this has the advantage that all results can be obtained systematically and with mathematical elegance it seems that for the purpose of undergraduate teaching other approaches would be preferable by which the distribution functions for the various ensembles can be derived in a much simpler way, and which are not restricted to ensembles of assemblies. No indication is given in the book that such other approaches exist and that the study of these more general ensembles is of considerable physical importance.

Nevertheless lecturers and students will, no doubt, in this book find a very useful complement to their lecture courses. R. FÜRTH.

Cosmic Electrodynamics, by J. W. Dungey. Cambridge Monographs on Mechanics and Applied Mathematics. Pp. xi + 183. (Cambridge : University Press, 1958.) 32*s*. 6*d*.

The similarity in titles suggests a comparison between Dungey's book and Alfvén's *Cosmical Electrodynamics*, published in 1950. The resemblance between the books does not, however, go deep. Alfvén's was a pioneer book, with the excitement and also the crudities of the pioneer ; also it was largely devoted to Alfvén's own theories. Dungey's is a more finished article ; he spends a good part of the first few chapters in trampling flat the misconceptions which disfigured early approaches to magnetohydrodynamics, and he is far more eclectic. Unfortunately, at the same time some of the excitement has disappeared.

The topics treated by Alfvén—sunspots, prominences, the sun's corona, cosmic rays, magnetic storms—all feature here, though remarkably little attention is given to Alfvén's own suggestions. Further topics treated include dynamo problems, magnetostatic equilibrium and stability, Dungey's own theory of discharges in an ionized gas, and electrodynamic effects in the ionosphere. Many facets of each topic are treated, and the time available for discussing each is small. Thus, though more comprehensive than earlier books on the subject, Dungey's volume is still only an introduction to it.

Dungey always considers an ionized gas composed of individual particles, not a continuous fluid. Normally he is content to treat the particles statistically, but he is always ready to revert to the effects on individual particles. This makes his presentation the more valuable, but sometimes complicates it.

While not agreeing with Dungey about all the controversial topics discussed, I feel that the book has real value as a solid contribution to a difficult subject. There are defects ; at times the details of an argument tend to obscure the main argument, and one or two minor errors have been allowed to creep in. Also there seem to be one or two gaps in the otherwise full bibliography ; e.g. the important work of Schlüter hardly gets a mention. However, the book represents a real advance on anything earlier on its subject. T. G. COWLING.

Der lichtelektrische Effekt und seine Anwendungen, by H. SIMON and R. SUHRMANN and others. Pp. xii+747. (Berlin, Göttingen, Heidelberg: Springer, 1958.) DM. 97.50.

Photoelectric devices and their associated circuitry are now commonplace, both in scientific research and in a variety of commercial applications. To provide a comprehensive treatise on the subject including basic physical processes, manufacturing details and the numerous applications using photoemissive, photoconductive and photovoltaic cells and image tubes is not an easy task. However, it is attempted in the present volume which benefits by drawing its contributions from several different writers of experience in the field. No current photoelectric device has been omitted as far as one can tell, although emphasis is sometimes a little heavy on some which have been superseded and lacking on others of more recent origin, such as the phototransistor and photodiode employing germanium or silicon.

Some two hundred pages are divided about equally between the discussion of the fundamental characteristics of photoelectric surfaces and those of photoconducting solids. The former includes a detailed discussion of the dependence of photoemission on temperature, crystal structure and surface conditions and there is a brief mention of emission from semiconductors. Discussion of the physical processes in photoconductors is introduced by a brief but lucid treatment of the energy band model for crystalline solids. Although these chapters are followed by detailed descriptions of techniques for preparing photoelectric and photoconductive materials one must remember that recipes are still only effective when joined to ' art ' and ' green fingers ' in making high sensitivity photoemissive layers or solid state devices and that commercial competition often precludes a liberal disclosure of technique.

Perhaps the three major developments in this field in recent years have been photoelectric multipliers, photoelectric image and television pick-up tubes and solid state detectors and image intensifiers. All of these find a place in the text which is interspersed with numerous good plate illustrations and tabulated information on comparative performances of commercial products. Limiting sensitivities of all types of photocell have improved and although only one (Cs–Sb photoelectric surface) has achieved human eye sensitivity this improvement has been reflected in the advances in research thereby made possible, particularly in solid state and nuclear physics. A system briefly referred to is the cascade image intensifier which is of great promise for astronomical and nuclear research applications.

If one has any complaints about the book they are mostly of minor character. The problem of specifying performance amongst a diversity of radiation detectors merits critical discussion in such a text; inclusion of homodyne amplifier-chopped radiation techniques as a means of improving signal to noise ratios would have been useful and a more complete treatment of solar generators would have been welcome. However, these detract little from a very comprehensive and valuable text which should be read both by academic and commercial users of photoelectric apparatus alike. References provided with each chapter are well chosen and the same discrimination is indicated in the adequate subject index. G. F. J. GARLICK.

The Potential Theory of Unsteady Supersonic Flow, by J. W. MILES. Pp. xii + 220. (Cambridge: University Press, 1959.) 45*s*.

This book is an extremely thorough and authoritative account of the field described in its title. Fundamentals, including applications of the appropriate form of the Lorentz transformation, and methods of reduction to steady-flow problems, are especially well treated. Two-dimensional problems, problems of delta wings and quadrilateral wings, as well as of ' slender wings ', ' slender bodies ' and other shapes of low aspect ratio, are very thoroughly discussed by the linearized theory, and there is a final chapter setting out what is known of non-linear solutions. Applications to stability, flutter and gust loading are clearly brought out. The mathematics is treated logically and economically and should not frighten away theoretical engineers or applied mathematicians. Aerodynamicists will be a lot happier for having such a convenient and compendious reference available for all the knowledge on unsteady supersonic flow theory, much of which is of Professor Miles' own gathering. M. J. LIGHTHILL.

An Introduction to Fluid Dynamics, by G. TEMPLE. Pp. xi + 195. (Oxford: University Press, 1958.) 25*s*.

This book, although apparently intended as an introduction to modern fluid dynamics for the degree student, is concerned almost entirely with the theory of an inviscid, incompressible (perfect) fluid. The principal topics discussed are the equations of motion; Bernoulli's theorem with applications to flow through channels; irrotational flow and the dynamical significance of the velocity potential; the complex potential and use of conformal mapping for two-dimensional flow; equivalent distributions of sources, doublets and vortices; the forces exerted by a fluid on a body; and a brief introduction to slender body theory. The analysis is treated throughout with care (and sometimes with a rigour seldom thought worthwhile in applied mathematics), but this occasionally has the effect of making the underlying physical principles difficult to perceive.

A more general criticism is that no account is given of the way in which perfect fluid theory fits into the pattern of modern fluid dynamics of which it is but a part, albeit an important one, or of the conditions under which a perfect fluid is a good approximation to a real fluid which satisfies the different boundary condition of zero slip at a solid boundary. The student can benefit from this book, but as an introduction to modern fluid dynamics, as opposed to the theory of a perfect fluid, it is somewhat deficient. P. G. SAFFMAN.

Materialprüfung mit Röntgenstrahlen (unter besonderer Berücksichtigung der Röntgenmetallkunde), 4th edn, by R. GLOCKER. Pp. vii + 530. (Berlin: Springer, 1958.) DM 61.50.

Books on the theme of X-rays and crystals are apt to possess a pronounced individual flavour and Professor Glocker's book is no exception. Whereas he covers an unusually wide range of topics, he is both most informative and most interesting on those subjects to which his own Institute has largely contributed. The section on the techniques and results of stress measurement by X-rays is outstanding and goes much further than any other account known to the reviewer. Good accounts are also given of X-ray spectroscopic analysis, X-ray physics, single crystal methods, the structure of liquid and amorphous metals, and modern practical techniques such as curved crystal monochromators and small angle scattering. So far as the reviewer can judge, the section on radiography is also very authoritative.

It is a distinct virtue of the book that a determinedly practical outlook is supplemented by a readiness to explain fine points of experimental technique by reference to first theoretical principles. This is particularly evident in the sections on radiography, stress measurement and spectroscopic analysis, and should make these particularly useful for the experimentally inclined reader.

While Professor Glocker has made every effort to be comprehensive, the quality of the treatment inevitably fluctuates. Thus, he is much less thorough and up-to-date in his treatment, for instance, of the structure of cold worked metals, (the concept in this connection of ' frozen heat motion ' is misleading and not generally accepted today), and other subjects such as diffractometer technique, use of the ASTM Index for identification, and textures, are only cursorily treated. The structure of alloy phases is well treated and is up-to-date, as is the brief but informative section on age hardening; but a brief excursion into classical metallurgy such as the section on equilibrium diagrams is too superficial to be of use to the novice, and the equilibrium diagram for the Cu–Zn system which is reproduced is many years out of date.

In summary, then, the book is sufficiently comprehensive and authoritative to be recommended for German readers seeking a single compact source of information. Its uneven quality, however, and concentration on German sources to the virtual exclusion, in some sections, of other work, makes it unsuitable as a general reference book for the English reader, who is already well supplied with outstanding texts such as the books by Barrett and by King and Alexander and the encyclopaedic volume by the Institute of Physics. However, Professor Glocker's book can be strongly recommended for selective reading, most especially for the illuminating section on X-ray stress analysis.

R. W. CAHN.

Introduction to the Design of Servomechanisms, by JOHN L. BOWER and PETER M. SCHULTHEISS. Pp. xi + 510. (London : Chapman and Hall; New York : John Wiley and Sons, 1958.) 104*s*.

This book is remarkable for its approach and attitude to Servomechanism Theory. Drs. Bower and Schultheiss have produced a careful and thorough account of the theoretical background to the subject without losing the reader in an unintelligible maze of differential equations.

They explain the important relationship between experienced guesswork and precise calculation, particularly with reference to the application of the Nyquist and Bode diagram techniques. They emphasize repeatedly the importance of acquiring a ' feeling ' for the subject, and many examples are worked out using probable values of circuit parameters. Sometimes the results are recalculated by other methods (or with slightly different parameter values) so as to indicate the accuracy to be expected in this type of design study.

For those who have found the mathematics of servomechanism theory too formidable, the mathematical introduction should prove invaluable, containing a commonsense approach to the subject of functional transformations, with particular reference to the Fourier integral and to the Laplace transformation theorems. Whenever possible, theoretical conclusions are immediately related to practical examples; mathematical arguments are stated fully and almost conversationally, and are amply illustrated with explanatory diagrams.

A minor criticism of this book is that the many excellent problems following each chapter are not supplied with answers and will therefore be of doubtful value to the private reader. The standard of printing and layout in this volume is exceptionally high. This in itself helps in making the book so very readable.

M. J. DUFF.

Numerical Analysis and Partial Differential Equations, Vol. 5 of *Surveys in Applied Mathematics*, by GEORGE E. FORSYTHE and PAUL C. ROSENBLOOM. Pp. x +204. (London : Chapman and Hall ; New York : John Wiley and Sons, 1959.) 60*s*.

The title of this book, taken at first glance, is somewhat misleading. It comprises, in fact, two essays, one on Numerical Analysis by Forsythe and one on Linear Partial Differential Equations by Rosenbloom. These essays are as unlike in character and approach as it is possible for them to be, and it appears to me that they sit rather ill together in one volume.

The essay by Forsythe is aimed at the scientist, and is excellently put together. Recent Russian work is summarized and their computer development is reviewed. The main contemporary problems in numerical analysis are succinctly stated and the progress so far made towards their solution is discussed. A very useful bibliography is given. My only regret is that more space was not allotted to this essay in order to extend the author's remarks on partial differential equations.

By contrast, Rosenbloom's text is pitched at a far higher mathematical level. He does not set out to expose the basis of his subject in the form of an essay, but to embody, in a logically constructed presentation, recent work both in America and on the Continent. Whilst such a presentation is of undoubted interest to the pure mathematician, and of great value to the University student in mathematics, it is, in the form given, not easily accessible to the practising applied mathematician, and almost totally inaccessible to the general scientist and technologist. Ideas and notations are built up sequentially through the book, and any attempt to ' dip in ' to those subjects of especial interest is doomed to a frustrating search to discover what all the symbols mean. Furthermore, emphasis is largely placed on theorems of the existence of solutions, proofs of uniqueness, and the derivation of general operator methods. The latter have, of course, important applications, particularly in nuclear theory, and it is, no doubt, a relief to know that the use of a chosen mathematical technique will yield a unique answer to the problem studied—under suitably unrealistic conditions. But it all seems an odd approach to a *Survey in Applied Mathematics.* In his essay, Forsythe remarks (p. 11) that there is a tendency in America to use " elementary methods to solve problems rather than advanced analysis "; I do not find this surprising. A. S. DOUGLAS.

Atlas of the Sky, by V. DE CALLATÄY, translated and with a foreword by SIR HAROLD SPENCER JONES. Pp. 157. (London : Macmillan, 1958.) 65*s*.

This book was first published in French in 1955. It has now been translated by Sir Harold Spencer Jones who contributes a foreword. The atlas is unique in the form of its maps, which are ' pseudo-photographs ' showing the main stars and indicating the constellations to which they belong, with an average ' naked eye ' background of smaller stars. Accompanying charts show the constellations in relation to neighbouring constellations and give information on magnitude, etc.

The text accompanying each chart describes some aspect of astronomy related to it and is so planned that, read consecutively in an order suggested by the author, the whole series of texts gives a brief but very clear outline of modern astronomy.

As the translator has said in his foreword " this atlas should prove of great value to the amateur whose interest in astronomy has been aroused by reading some of the excellent popular books . . . . and who wishes to pursue the subject further by studying the sky ". A. C. S.

Free Radicals as studied by Electron Spin Resonance, by D. J. E. INGRAM. Pp. ix +274. (London : Butterworths Scientific Publications, 1958.) 50*s*.

This book is the first to be entirely devoted to this subject. It contains an introductory chapter on free radicals which explains what they are and reviews the older methods of detection. There is a detailed account of the relevant microwave techniques comprising about one quarter of the book. Subsequent chapters discuss stable free radicals, radicals produced by irradiation, radicals produced by polymerization and pyrolysis, inorganic radicals, biradicals and the triplet state and finally biological and medical applications.

There are considerable difficulties in writing this book which Dr. Ingram has in the main successfully overcome. The material is very new and the book has been produced commendably quickly. It is not so long since this reviewer, and perhaps many others, regarded free radical electron resonance as concerned entirely with esoteric chemical compounds such as diphenyl picryl hydrazyl (DPPH) and Chichibabin's hydrocarbon. The subject matter covers a number of fields, physics, chemistry, biology and medicine and no doubt each specialist will feel that the style of presentation is not for him. The physicist will be perturbed at the almost universal use of the word ' probable ' to describe the interpretations. He will also be concerned at the very complicated interpretation required to explain the rather simple spectrum of irradiated Perspex which is presented as a characteristic achievement. The discussion is rather discursive and repetitive although the frequent summaries are a valuable feature.

I suppose that in deference to the folk lore of the subject, it was necessary to include the famous spectrum of Professor Gordy's toenail.

It is rather disconcerting to find that the classic and most familiar hyperfine spectrum, that of DPPH, is given incorrectly on p. 138. The frequency with which the word spectrum occurs where it should be spectra makes one wonder whether this is deliberate.

Dr. Ingram has provided an excellent review of a new and rapidly developing subject which will no doubt stimulate a great deal of interest in it. As a statement of the present state of the art it is particularly valuable. J. G. POWLES.

Landolt–Börnstein Zahlenwerte und Funktionen. 6 Auflage. Band II, Eigenschaften der Materie in ihren Aggregatzuständen. Teil 3. Schmelzgleichgewichte und Grenzflächenerscheinungen. Pp. xi + 535. (Berlin, Göttingen, Heidelberg: Springer, 1956.) DM. 248.

Volume II will appear in seven parts of which this is the third.

Halbleiterprobleme IV, edited by W. SCHOTTKY. Pp. viii + 381. (Braunschweig: Friedr. Vieweg, 1958.) DM. 46.80.

Steric Effects in Conjugated Systems, edited by G. W. GRAY. Pp. viii + 181. (London: Butterworths Scientific Publications, 1958.) 30*s*.

Mechanical Properties of Non-metallic Brittle Materials, edited by W. H. WALTON. Pp. xi + 492. (London: Butterworths Scientific Publications, 1958.) 90*s*.

The Structure and Properties of Porous Materials, edited by D. H. EVERETT and F. S. STONE. Pp. xiv + 389. (London: Butterworths Scientific Publications, 1958.) 60*s*.

Steam Cycles for Nuclear Power Plant, by W. R. WOOTTON. (Nuclear Engineering Monographs.) Pp. vii + 66. (London: Temple Press, 1958.) 10*s*. 6*d*.

Nuclear Reactor Shielding, By J. R. HARRISON. (Nuclear Engineering Monographs.) Pp. viii + 68. (London: Temple Press, 1958.) 10*s*. 6*d*.

Nuclear Reactor Control and Instrumentation, by J. H. BOWEN and E. F. O. MASTERS. (Nuclear Engineering Monographs.) Pp. x + 78. (London: Temple Press, 1959.) 12*s*. 6*d*.

Some Aspects of Analysis and Probability, by I. KAPLANSKY, M. HALL, E. HEWITT and R. FORTET. (Vol. IV of Surveys in Applied Mathematics.) Pp. xi + 243. (New York: John Wiley; London: Chapman and Hall, 1958.) 72*s*.

Fundamentals of Advanced Missiles, by R. B. DOW. Pp. xvi + 567. (New York: John Wiley; London: Chapman and Hall, 1959.) 94*s*.

Guide to the Literature of Mathematics and Physics including related works on Engineering Science, by N. G. PARKE III. Pp. xviii + 436. (New York: Dover Publications, 1958.) $2.49.

Conduction of Heat in Solids, by H. S. CARSLAW and J. C. JAEGER. 2nd Edn. Pp. x + 510. (Oxford: Clarendon Press, 1959.) 84*s*.

Structure Reports: Supplementary Volume and Cumulative Index for 1940–1950, Vol. 14, edited by A. J. C. WILSON. Pp. ix + 215. (Utrecht: N.V. A. Oosthoek's Uitgevers Mij, 1959.) 68*s*.

Dynamics of Flight, by B. ETKIN. Pp. xv + 519. (New York: John Wiley; London: Chapman and Hall, 1959.) 120*s*.

Physical Laws and Effects, by C. F. HIX and R. P. ALLEY. Pp. x + 291. (New York: John Wiley; London: Chapman and Hall, 1958.) 64*s*.

The Geology of Uranium, translated from the Russian. (Suppt. No. 6 of *Atomnaya Energiya*.) Pp. 6 + 128. (London: Chapman and Hall; New York: Consultants Bureau, 1958.) 48*s*.

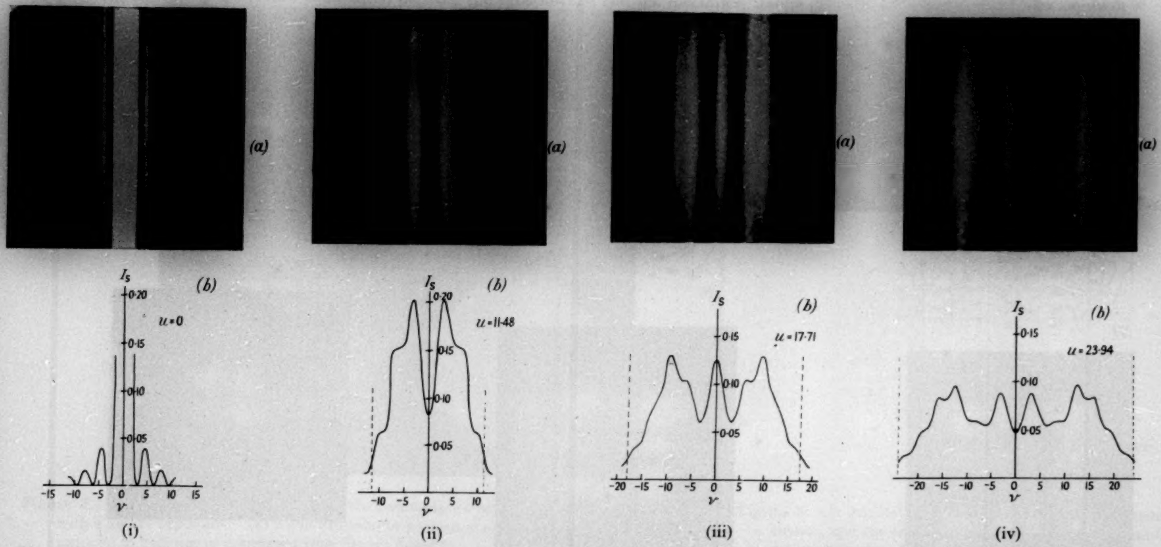

Figure 5. A qualitative comparison between the experimental and the theoretical results for slit apertures for various values of u. In each case (a) is a photograph of the diffraction pattern and (b) is the theoretical intensity distribution.

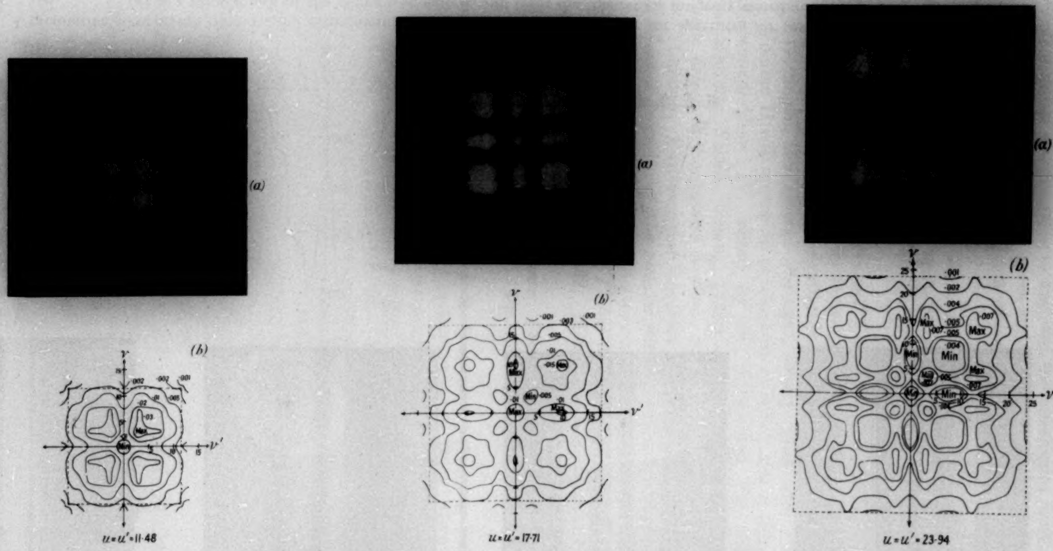

(i) (ii) (iii)

Figure 6. A qualitative comparison between the experimental and the theoretical results for square apertures for various values of u. In each case (a) is a photograph of the diffraction pattern and (b) is the theoretical intensity distribution.

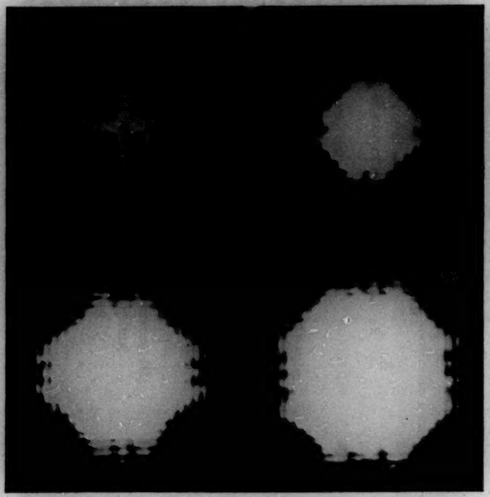

Figure 7. (*b*), (*c*), (*d*) are photographs in the same planes as figure 6 (i), (ii) and (iii), but with a longer exposure. (*a*) is the Fraunhofer pattern at $u=0$. These photographs are reduced to half size as compared with figures 5 and 6.

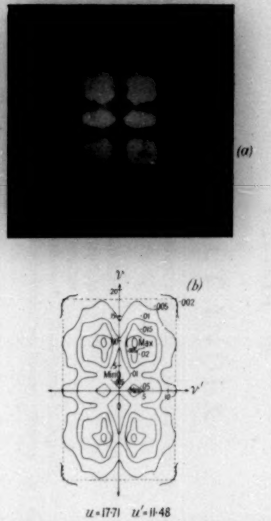

Figure 8. A qualitative comparison between the experimental and the theoeretical results for a rectangular aperture in the plane $u'=11{\cdot}48$, $u=17{\cdot}71$.

PROCEEDINGS OF THE PHYSICAL SOCIETY

1959—VOL. 73.

SUBJECT INDEX

PAGE

Aberration, spherical, and optical frequency response, measurement by automatic recording 465
Absorption bands, lattice, in Si 265
Absorption of light, complete, by thin metal films 40
Absorption, ultrasonic, *see* Ultrasonic absorption
Absorption, *see also* Nuclear magnetic resonance
Acoustic streaming, and measurement of ultrasonic absorption in liquids 354
Alloys, dispersion-hardened and single-domain inclusion theory of magnetic hysteresis (R) 517
Alloys, Heusler, new (R) 520
Alloys, Ni–Fe, 65/35, eddy current losses in (R) 133
Alloys, ordered, vacancy diffusion in 250
Alloys, polycrystalline Ni–Co, Bitter figure examination 14
Alpha-particle bombardment and scintillation of diamond 233
Amplifier, grain-boundary (R) 969
Angular distribution of high energy protons inelastically scattered by light nuclei 881
Argon and krypton, solid and liquid solutions, properties 490
Attachment of slow electrons in air and oxygen (R) 821

Band spectra of MgO and MgOH between 4000 and 3600 Å 244
Band spectra, *see also* Absorption
Beta spectrum of ^{144}Pr and axial vector β-interaction 600
Bismuth telluride, adiabatic and isothermal effects 739
Bitter figure examination of polycrystalline Ni–Co alloys 14

Capture, negative pion, in deuterium 551
Capture, negative pion, in hydrogen 545
Capture, resonance, of neutrons in infinite homogeneous media 561
Carrier concentration, *see* Semiconductors
Cathode glow (R) 822
Cathode glow, polarization of light from (R) 126
Ceramics, ferroelectric, energy loss processes 17
Charge penetration into conductor in equilibrium 869
Collisional relaxation in gases 800
Collisions, inelastic, between heavy systems, distortion 227
Collisions, inter-electron, and temperature of hot electrons (R) 959
Collisions, nuclear, direct interaction with strong coupling 894
Conductivity, electrical, *see* Electrical conductivity
Conductor, charged, charge penetration in equilibrium 869
Copper, effect on work function of tin 807
Copper as impurity in InAs (L) 685
Core polarization, contribution to atomic hyperfine structure and Knight shift of Li and Na 811
Counters, diamond conduction, with small electrode separations 385
Counters, proportional, curves of x-ray spectra, analysis 81
Cross sections, differential, of reactions ^{19}F(α, n)^{22}Na and ^{27}Al(α, n)^{30}P, and neutron spectra (R) 307
Cross sections, electron capture, for protons in helium 201
Cross sections, of hydrogen, 1s–2s electron excitation, variational calculations (R) 515

PAGE
Cross sections for (n, p) and (n, α) reactions with 14·5 Mev neutrons 215
Crystal surface and atom, molecular orbital theory of interaction (L) . . . 323
Crystals, barium titanate, switching, model for 641
Crystals, copper, arsenic content, influence on easy glide (R) 674
Crystals, disordered one-dimensional 413
Crystals of CsI(Tl), particle selection in (R) 523
Crystals, single, determination of principal *g*-values in electron spin resonance . . 788
Crystals, single, nickel, ultrasonic wave propagation in 337
Crystals, single, uniaxial, demagnetizing energy and domain structure . . corr. 325
Crystals, single, wedge-shaped, multiple interference fringes in electron micrographs 45

Decay processes, search for $\mu^+ \to e^+ + \gamma$ (R) 951
Deuteron, photodisintegration at 130 Mev 221
Diamond, scintillation under α-particle bombardment 233
Diamond, semiconducting, thermoelectric power 393
Diffraction by rectangular apertures, intensity distribution near focus . . . 905
Diffusion of boron in germanium (R) 320
Diffusion of copper in germanium, theory 297
Diffusion of phosphorus into silicon under controlled vapour pressure . . . 577
Diffusion, thermal, *see* Thermal diffusion
Digital computer, electronic, lens designing by 777
Discharge, electrodeless, in hydrogen and helium, self-absorption 841
Discharge, oxygen, negative ions in positive column (R) 818
Domain configurations on ferrites 1
Domain structure and demagnetizing energy of uniaxial single crystal . . corr. 325
Domains, ferromagnetic, thermal activation (R) 136

Eddy current losses in 65/35 Ni–Fe (R) 133
Elastic scattering, *see* Scattering
Electrical conductivity of metals 745
Electrolytic coloration of KBr (R) 962
Electron, ejected, in K-shell ionization (R) 681
Electron-opaque targets, continuous X-ray spectrum from 924
Electron pair production in field of (R) 114
Electron–phonon interaction in metals—I : Harmonic approximation . . . 609
Electron–positron pair emission 556
Electron spin resonance, determination of principal *g*-values 788
Electron temperature and inter-electron collisions (R) 959
Electrons, slow, attachment in air and oxygen (R) 821
Energy levels of ^{26}Al 501
Energy levels of ^{18}F 721
Energy levels of ^{15}O, ^{23}Mg and ^{27}Si 727
Equilibrium and non-equilibrium properties of $(n+1)$-state ideal solution . . 25
Evaporation theory of photonuclear reactions 33

Fermi–Thomas potential, angular dependent, for iron 650
Ferrites, domain configurations on 1
Ferroelectric ceramics, *see under* Ceramics
Ferroelectrics, and other oxides, anomalous polarization in 448
Ferromagnetic domain sizes in polycrystalline Si–Fe (L) 694
Ferromagnetic resonance, internal, in nickel 593
Ferromagnetism, *see also* Domains
Films, thin metal, complete absorption of light 40
Fluorides, diatomic, of Si, Ge, Sn and Pb, spectra (R) 317
Freezing, probability of (L) 324
Frequency response, optical, characteristics with spherical aberration, measured by
automatic recording 465
Friction, internal, of annealed copper at low temperatures 95
Fringes, superposition, in white light for length comparison 661

PAGE
Galena, natural, low temperature thermoelectric measurements . . . 49
Gas discharge, arc maintained on isolated metal plate exposed to a plasma . . 508
Gases, collisional relaxation in . . . 800
Gases, thermal relaxation in, analysis of data . . . 273
Germanium devices, 1/*f* noise in . . . 59
Germanium, diffusion of boron in (R) . . . 320
Germanium, diffusion of copper in, theory . . . 297
Germanium, electrical and photoelectric effects for three carriers in magnetic field . 399
Germanium, grain-boundary amplifier (R) . . . 969
Germanium, influence of fast holes on photoelectromagnetic effect in (L) . 692
Guided propagation in slowly varying medium . . . 365
g-value of S-state ions (R) . . . 116

Hall effect, extraordinary, and spin–orbit coupling . . . 433, corr. 976
Hall effect, *see also* Semiconductors (R)
Helium, solid, zero-point energy and equation of state at absolute zero (R) 965
Helium II, quantized growth of turbulence (L) . . . 144
Hydrogen atoms, variability of recombination on metal surfaces (R) 533
Hydrogen chloride, transition $\mathrm{V}^1\Sigma^+ - \mathrm{X}^1\Sigma^+$ (L) . . . 538
Hyperfine structure, atomic, and Knight shift of Li and Na, contribution of core polarization . . . 811
Hysteresis loops, ferromagnetic, growth (L) . . . 973
Hysteresis, single-domain inclusion theory in dispersion-hardened alloys (R) . . 517

Impurities in III–V compounds, behaviour . . . 622
Indium antimonide, n-type, electrical conduction between 2 and 300°K . . 280
Indium antimonide, n-type, oscillatory transverse magnetoresistance effect in (R) . 131
Indium antimonide, p-type, electrical conduction between 100 and 2°K (R) . . 128
Indium arsenide, effects of copper as impurity (L) . . . 685
Interaction, electron–phonon, *see* Electron
Interference filters, limiting band width . . . 480
Interference fringes, multiple, in electron micrographs of wedge-shaped single crystals . . . 45
Interferometric instrument, automatically recording, for measurement of frequency response with spherical aberration . . . 465
Ionization and dissociation by electron impact in fluorine, HF, chlorine and HCl (R) 122
Ionization, K-shell, ejected electron in (R) . . . 681
Ions, S-state, *g*-value (R) . . . 116
Iron, Fermi–Thomas angular dependent potential . . . 650
Iso-butyl bromide, nuclear magnetic resonance absorption in . . . 833

Lattice absorption bands in Si . . . 265
Lattice, calcium fluoride, correction to theory (L) . . . 687
Lengths, comparison by using fringes of superposition in white light . . 661
Lens designing by electronic digital computer . . . 777
Light, white, superposition fringes for comparison of lengths . . . 661
Liquids and aqueous solutions, sonoluminescence measurements from . . 628
Liquids and electrolytes, ultrasonic vibration potentials, phenomenological theory . 345
Liquids, non-ionic, ultrasonic vibration potentials (L) . . . 690
Liquids, reducing effect of superposition approximation . . . 713
Liquids, ultrasonic absorption, measurement by acoustic streaming . . 354
Low temperature measurements, thermoelectric, on natural galena . . 49
Low temperatures, and internal friction of annealed copper . . . 95
Lunar surface, radio observations of (L) . . . 536

Magnetic resonance, *see under* Nuclear, Paramagnetic
Magnetic susceptibility of Ag–Mn solid solutions between 100 and 500°K . . 422
Magnetoresistance, oscillatory transverse, in n-type InSb (R) . . . 131

PAGE
Many-body problem with one-body forces (R) 118
Masers, Bloembergen type, materials for (R) 937
Mesons, mu, cosmic-ray, knock-on electrons from 178
Metal films, *see under* Films
Metal surfaces, recombination of H atoms on (R) 533
Metals, electrical conductivity 745
Metals, electron–phonon interaction—I: Harmonic approximation 609
Metals, noble, optical properties (R) 671
Moiré patterns, calculating (L) 142
Molecular orbital theory of interaction between atom and crystal surface (L) 323
Mu mesons, negative, ionic reactions 912
Muons, −ve, effect of Coulomb field of nucleus on decay rate (R) 314
Muons, +ve and −ve unpolarized, polarization of electrons from decay 169

Neutron spectra and differential cross sections of reactions $^{19}\mathrm{F}(\alpha, \mathrm{n})^{22}\mathrm{Na}$ and $^{27}\mathrm{Al}(\alpha, \mathrm{n})^{30}\mathrm{P}$ (R) 307
Neutrons, resonance capture in infinite homogeneous media 561
Neutrons, scattering, *see* Scattering
Nickel, internal ferromagnetic resonance in 593
Nickel, photodisintegration, competitive processes in 585
Noise, 1/*f*, in germanium devices 59
Nuclear deformation and photodisintegration giant resonances 69
Nuclear magnetic resonance absorption in *iso*-butyl bromide as crystal and as supercooled liquid 833
Nuclear magnetic resonance in bismuth (R) 945
Nuclear reactions, direct interaction with strong coupling 894
Nuclei, light, inelastic scattering of high energy protons, angular distribution 881
Nucleons, high energy, inelastic scattering by complex nuclei—II: Excitation of 4·4 MeV level of $^{12}\mathrm{C}$ (R) 309

Optical model analysis of scattering of 310 MeV protons by carbon 185
Optical properties of noble metals (R) 671

Pair emission, internal, at small angles 556
Pair production in field of electron (R) 114
Paraffins, normal, viscosity 153
Paramagnetic resonance of Fe^{3+} in sapphire at low temperatures (R) 531
Paramagnetic resonance of impurities in CaF_2 (R) 942
Paramagnetic resonance spectrum of impure MgO crystals, weak lines (R) 948
Paramagnetic salts for Bloembergen type maser (R) 937
Particles, fast charged, scattering: detour factor for 10 MeV electrons and positrons (R) 953
Phase shift, unitary, scattering approximation (R) 528
Photodisintegration of deuteron at 130 MeV 221
Photodisintegration of Ni, competitive processes in 585
Photoelectromagnetic effect in Ge, effect of fast holes (L) 692
Photoproduction, π^+ meson, from hydrogen, measurement near threshold 873
Photoprotons, high-energy, from silver 697
Pi$^+$ meson photoproduction from hydrogen, measurement near threshold 873
Pions, negative, capture in deuterium 551
Pions, negative, capture in hydrogen 545
Pions, negative, 98 MeV elastic scattering by hydrogen 856
Polarization, anomalous, in ferroelectrics and other oxides 448
Polarization, lattice screening in polar semiconductors 849
Polarization of light from cathode glow (R) 126
Polarization, longitudinal, of electrons from decay of unpolarized +ve and −ve muons 169
Positrons, *see* Particles
Potassium bromide, electrolytic coloration (R) 962

PAGE
Potential energy function, Wu–Yang (R) . . . 119
Praseodymium 144, β-rays and axial vector β-interaction . . . 600
Propagation, guided, in slowly varying medium . . . 365
Protons, distribution in nuclide ^{12}C (R) . . . 112
Protons, *see also* Angular distribution, Scattering

Radio observations of lunar surface (L) . . . 536
Reactions, ionic, of negative μ-mesons . . . 912
Reactions, parameters, derivation from observations of ultrasonic relaxation . . . 767
Reactions, photonuclear, evaporation theory . . . 33
Reactions ^{27}Al(p, p′)^{27}Al and ^{27}Al(α, p)^{30}Si . . . 793
Reactions ^{39}K(d, p)^{40}K (R) . . . 677
Reactions, ^{24}Mg(^{3}He, α)^{23}Mg (R) . . . 513
Reactions, (γ, n) and (γ, 2n) in ^{141}Pr (R) . . . 110
Reactions, *see also* Cross sections, Nuclear reactions, Stripping
Relaxation, collisional, in gases . . . 800
Relaxation, thermal, in gases, analysis of data . . . 273
Relaxation, ultrasonic, *see* Ultrasonic relaxation
Resonance capture of neutrons in infinite homogeneous media . . . 561
Resonance, ferromagnetic, *see* Ferromagnetic resonance
Resonance, nuclear magnetic, *see* Nuclear magnetic resonance
Resonances, giant, photodisintegration, and nuclear deformation . . . 69

Sapphire, paramagnetic resonance of Fe^{3+} in, at low temperatures (R) . . . 531
Scattering, elastic, low energy, of neutrons by deuterons with Yukawa interaction . 160
Scattering, elastic, of 98 MEV negative pions by hydrogen . . . 856
Scattering, elastic, *see also* Angular distribution
Scattering of fast charged particles: detour factor for 10 MEV electrons and positrons (R) . . . 953
Scattering, inelastic, of high energy nucleons by complex nuclei—II: Excitation of 4·4 MEV level of ^{12}C (R) . . . 309
Scattering, inelastic, of neutrons by thorium . . . 193
Scattering, p–p, spin correlation coefficient at 382 MEV for 90° c.m. scattering angle (R) . . . 957
Scattering, small angle, of 970 MEV protons by carbon . . . 100
Scattering, unitary phase shift, approximation (R) . . . 528
Scattering of 310 MEV protons by carbon, optical model analysis . . . 185
Schrödinger equation, non-relativistic, (2s)^{2} ^{1}S state solution for He and H . corr. 976
Self-absorption in electrodeless discharge in hydrogen and helium . . . 841
Semiconductors, anomalous behaviour in Hall coefficients of SnSe and GeSe (R) . 824
Semiconductors, behaviour of impurities in III–V compounds . . . 622
Semiconductors, effect of magnetic field on absorption edge, theory . . corr. 976
Semiconductors, polar, lattice screening in . . . 849
Semiconductors, polar, theoretical transport coefficients . . . 572
Semiconductors, thermoelectric power of semiconducting diamond . . . 393
Semiconductors, time dependence of excess carrier concentration in presence of surface recombination . . . 54
Semiconductors, *see also* Bismuth, Germanium, Hall effect, Indium
Silicon–iron, polycrystalline, ferromagnetic domain sizes (L) . . . 694
Silicon, lattice absorption bands in . . . 265
Silver, high-energy protons from . . . 697
Sodium chloride, work function . . . 733
Solution, ideal, ($n+1$)-state, equilibrium and non-equilibrium properties . . . 25
Sonoluminescence, measurements from pure liquids and aqueous solutions . . . 628
Spectra of diatomic fluorides of Si, Ge, Sn and Pb (R) . . . 317
Spectra, transition $v^{1}\Sigma^{+}-x^{1}\Sigma^{+}$ in hydrogen chloride (L) . . . 538
Spectra, x-ray, analysis of unresolved proportional counter curves . . . 81
Spectra, *see also* Band spectra, Paramagnetic resonance
Spectrum, x-ray, continuous from electron-opaque targets . . . 924

PAGE
Spin Hamiltonian of a Γ_8 quartet (R) . . . 939
Spin–orbit coupling and extraordinary Hall effect . . . 433, corr. 976
Spin of ^{103}Ru by deuteron stripping (R) . . . 138
Striations, moving, empirical relations for (R) . . . 526
Stripping, deuteron, and spin of ^{103}Ru (R) . . . 138
Stripping reaction, of ^{3}He and α-particles . . . 705
Superconduction, ultrasonic attenuation in superconducting and normal Hg . . . 291
Superposition approximation, liquid, reducing effect of . . . 713
Surface recombination, *see* Semiconductors
Susceptibility, *see* Magnetic susceptibility

Temperature effects, adiabatic and isothermal, of BiTe . . . 739
Thermal diffusion in methanol–carbon tetrachloride mixtures (L) . . . 686
Thermoelectric measurements on natural galena at low temperatures . . . 49
Tin, work function, effect of copper . . . 807
Transport coefficients, theoretical, for polar semiconductors . . . 572
Two-electron wave equation, $(2s)^2\ {}^1S$ state solution . . . corr. 976

Ultrasonic absorption in liquids, measurement by acoustic streaming . . . 354
Ultrasonic attenuation in superconducting and normal Hg . . . 291
Ultrasonic relaxation, derivation of reaction parameters from . . . 767
Ultrasonic velocities in organic solutions . . . 239
Ultrasonic vibration potentials in liquids and electrolytes, phenomenological theory 345
Ultrasonic vibration potentials in non-ionic liquids (L) . . . 690
Ultrasonic wave propagation in nickel single crystal . . . 337

Van der Waals forces . . . 455
Viscosity of normal paraffins . . . 153

Wave propagation, ultrasonic, in nickel single crystal . . . 337
Waves, light, *see also* Diffraction
Work function of sodium chloride . . . 733
Work function of tin, effect of copper . . . 807
Wu–Yang potential energy function (R) . . . 119

X-ray spectrum, continuous, from electron-opaque targets . . . 924
X-ray spectrum, *see also under* Spectra

INDEX TO AUTHORS (WITH TITLES)

PAGE

Allcock, G. R., with Hooton, D. J.: Angular distributions of high energy protons inelastically scattered by light nuclei . . . 881
Anderson, J. C., and Donovan, B.: Internal ferromagnetic resonance in nickel . . . 593
Anderson, J. M., with Vasek, L. J.: Work function of sodium chloride . . . 733
Arthurs, A. M.: Description of ejected electron in K-shell ionization (R) . . . 681
Asanabe, S., and Okazaki, A.: Anomalous behaviour in Hall coefficients of semiconducting compounds SnSe and GeSe (R) . . . 824
Ashmore, A., Diddens, A. N., and Huxtable, G. B.: Measurement of spin correlation coefficient C_{KP} in p–p scattering at 382 MEV, for 90° c.m. scattering angle (R) . . . 957
Astbury, A., Hussain, M., Kemp, M. A. R., Lipman, N. H., Muirhead, H., Voss, R. G. P., and Kirk, A.: Measurement of effect of Coulomb field of nucleus on decay rate of negative muons (R) . . . 314
Azuma, R. E., with Lewis, G. M.: Measurement of π^+ meson photoproduction from hydrogen near threshold . . . 873

Baker, J. M., Hayes, W., and Jones, D. A.: Paramagnetic resonance of impurities in CaF_2 (R) . . . 942
Banbury, P. C., with Nixon, J. D.: Time dependent changes in excess carrier concentrations in presence of surface recombination . . . 54
Barros, F. de S., Forsyth, P. D., Jaffe, A. A., and Taylor, I. J.: Reactions $^{27}Al(p, p')^{27}Al$ and $^{27}Al(\alpha, p)^{30}Si$ . . . 793
Barros, F. de S., Forsyth, P. D., Jaffe, A. A., and Taylor, I. J. : $^{24}Mg(^3He, \alpha)^{23}Mg$ reaction (R) . . . 513
Barrow, R. F., Butler, D., Johns, J. W. C., and Powell, J. L. : Spectra of diatomic fluorides of silicon, germanium, tin and lead (R) . . . 317
Barrow, R. F., with Jacques, J. K. : The transition $v^1\Sigma^+ - x^1\Sigma^+$ in hydrogen chloride (L) . . . 538
Batchelor, R., and Towle, J. H. : Inelastic scattering of neutrons by thorium . . . 193
Batchelor, R., and Towle, J. H. : Neutron spectra and differential cross sections of the reactions $^{19}F(\alpha, n)^{22}Na$ and $^{27}Al(\alpha, n)^{30}P$ (R) . . . 307
Bates, D. R. : Importance of distortion in inelastic encounters between heavy systems 227
Bates, L. F., and Isaac, E. D. : Bitter figure examination of some polycrystalline Ni–Co alloys . . . 14
Batty, C. J. : Optical model analysis of scattering of 310 MEV protons by carbon . . . 185
Batty, C. J., Lock, W. O., and March, P. V. : Small angle scattering of 970 MEV protons by carbon . . . 100
Baumeister, P. W., with Giacomo, P., and Jenkins, F. A. : Limiting band width of interference filters . . . 480
Bell, J. S. : Many-body problem with one-body forces (R) . . . 118
Bleaney, B. : New class of materials for Bloembergen-type masers (R) . . . 937
Bleaney, B. : Spin Hamiltonian of Γ_8 quartet (R) . . . 939
Bloor, D., and Martin, D. H. : Ferromagnetic domain sizes in polycrystalline Si–Fe (L) . . . 694
Bogle, G. S., and Symmons, H. F. : Paramagnetic resonance of Fe^{3+} in sapphire at low temperatures (R) . . . 531
Booker, J., with Yeager, E., and Hovorka, F. : Ultrasonic vibration potentials in non-ionic liquids (L) . . . 690
Brown, G. E., with Nicholson, A. F. : Photodisintegration of deuteron at 130 MEV . . . 221
Burfoot, J. C. : Possible model for switching barium titanate crystals . . . 641
Burfoot, J. C., and Peacock, R. V. : Growth of ferroelectric hysteresis loops (L) . . . 973
Burge, R. E. : Multiple interference fringes in electron micrographs of wedge-shaped single crystals . . . 45
Burke, P. G., Haas, F., and Percival, I. C. : Ionic reactions of negative μ-mesons . . . 912
Butler, D., with Barrow, R. F., Johns, J. W. C., and Powell, J. L. : Spectra of diatomic fluorides of silicon, germanium, tin and lead (R) . . . 317

PAGE

Callaby, D. R., with Lee, E. W., and Troughton, A. G. H. : Eddy current losses in 65/35 Ni–Fe (R) 133
Carte, A. E. : Probability of freezing (L) 324
Carver, J. H., and Turchinetz, W. : Competitive processes in photodisintegration of nickel 585
Carver, J. H., and Turchinetz, W. : Nuclear deformation and photodisintegration giant resonances 69
Carver, J. H., and Turchinetz, W. : (γ, n) and (γ, 2n) reactions in ^{141}Pr (R) 110
Champion, F. C., and Wright, S. B. : Diamond conduction counters with small electrode separations 385
Chester, G. V., and Houghton, A. : Electron–phonon interaction in metals—I: Harmonic approximation 609
Chester, G. V., and Thellung, A. : Electrical conductivity of metals 745
Cohen, M. H., Goodings, D. A., and Heine, V. : Contribution of core polarization to atomic hyperfine structure and Knight shift of Li and Na 811
Cole, G. H. A. : Reducing effect of liquid superposition approximation 713
Coleman, R. F., Hawker, B. E., O'Connor, L. P., and Perkin, J. L. : Cross sections for (n, p) and (n, α) reactions with 14·5 MeV neutrons 215
Cook, A. H., and Richardson, H. M. : Comparison of lengths using fringes of superposition in white light 661
Corngold, N., with Schermer, R. : Resonance capture of neutrons in infinite homogeneous media 561
Coupland, M. J. : Diffusion of phosphorus into silicon under conditions of controlled vapour pressure 577
Craik, D. J., and Griffiths, P. M. : Domain configurations on ferrites 1
Crowther, P., and Raw, C. J. G. : Thermal diffusion in methanol–carbon tetrachloride mixtures (L) 686
Culligan, G., Frank, S. G. F., and Holt, J. R. : Longitudinal polarization of electrons from decay of unpolarized positive and negative muons 169

Dalgarno, A., and Kingston, A. E. : Van der Waals forces 455
Dalton, A. W., Parry, G., and Scott, H. D. : ^{39}K(d, p)^{40}K reaction (R) 677
Davies, R. O. : Equilibrium and non-equilibrium properties of an $(n+1)$-state ideal solution 25
Davies, R. O., and Lamb, J. : Derivation of reaction parameters from observations of ultrasonic relaxation 767
Dean, P. : Disordered one-dimensional crystals 413
Delves, R. T. : Theoretical transport coefficients for polar semiconductors 572
Diddens, A. N., with Ashmore, A., and Huxtable, G. B. : Measurement of Spin correlation coefficient C_{KP} in p–p scattering at 382 MeV, for 90° c.m. scattering angle (R) 957
Dolby, R. M. : Methods for analysing unresolved proportional counter curves of X-ray line spectra 81
Doniach, S. : Lattice screening in polar semiconductors 849
Donovan, B., with Anderson, J. C. : Internal ferromagnetic resonance in nickel 593
Dunstan, W. : Electrolytic coloration of potassium bromide (R) 962
Dyson, N. A. : Continuous X-ray spectrum from electron-opaque targets 924

Edmond, J. T. : Behaviour of some impurities in III–V compounds 622
Edwards, D. N., Frank, S. G. F., and Holt, J. R. : Elastic scattering of 98 MeV negative pions by hydrogen 856
Elcock, E. W. : Vacancy diffusion in order alloys 250
El Khishin, M., with El Nadi, M. : Stripping reaction of ^{3}He and α-particles 705
Elliott, R. J., McLean, T. P., and Macfarlane, G. G. : Theory of effect of magnetic field on absorption edge in semiconductors corr. 976
El Nadi, M., and El Khishin, M. : Stripping reaction of ^{3}He and α-particles 705
Elton, L. R. B., Hiley, B. J., and Price, R. : Distribution of protons in nuclide ^{12}C (R) 112
Emeleus, K. G. : Cathode glow (R) 822
Emeleus, K. G., and Oleson, N. L. : Empirical relations for moving striations (R) 526

PAGE

Evans, J. A. : Evaporation theory of photonuclear reactions 33
Fidone, I., and Stevens, K. W. H. : *g*-value of S-state ions (R) 116
Finlayson, D. M., and Greig, D. : Thermoelectric measurements on natural galena at low temperatures 49
Flack, F. C., with Mason, P., and Parry, G. : Spin of ^{103}Ru by deuteron stripping (R) 138
Flynn, C. P., and Seymour, E. F. W. : Nuclear magnetic resonance in Bi (R) . . 945
Forsyth, P. D., with Barros, F. de S., Jaffe, A. A., and Taylor, I. J. : Reactions ^{27}Al(p, p′)^{27}Al and ^{27}Al(α, p)^{30}Si 793
Forsyth, P. D., with Barros, F. de S., Jaffe, A. A., and Taylor, I. J. : ^{24}Mg(^{3}He, α)^{23}Mg reaction (R) 513
Fox, J. W., Smith, A. C. H., and Smith, E. J. : Variability of recombination of hydrogen atoms on metal surfaces (R) 533
Fox, M., and Tebble, R. S. : Demagnetizing energy and domain structure of uniaxial single crystal . . . . corr. 325
Frank, S. G. F., with Culligan, G., and Holt, J. R. : Longitudinal polarization of electrons from decay of unpolarized positive and negative muons . . . 169
Frank, S. G. F., with Edwards, D. N., and Holt, J. R. : Elastic scattering of 98 MEV negative pions by hydrogen 856
Freeman, N. J. : β-rays of praseodymium-144 and axial vector β interaction . . 600
Fürth, R., and Morris, E. : Charge penetration into conductor in equilibrium . . 869

Garrido, L. M., and Pascual, P. : Unitary phase shift scattering approximation (R) . 528
Gaydon, A. G., with Pesic, D. : Band spectra of magnesium oxide and hydroxide between 4000 and 3600 Å 244
Giacomo, P., Baumeister, P. W., and Jenkins, F. A. : Limiting band width of interference filters 480
Goldring, G. : Internal pair emission at small angles 556
Goldsmid, H. J., Jenns, C. C., and Wright, D. A. : Thermoelectric power of semiconducting diamond 393
Goodings, D. A., with Cohen, M. H., and Heine, V. : Contribution of core polarization to atomic hyperfine structure and Knight shift of Li and Na 811
Greig, D., with Finlayson, D. M. : Thermoelectric measurements on natural galena at low temperatures 49
Griffiths, J. H. E., and Orton, J. W. : Weak lines in the paramagnetic resonance spectrum of impure MgO crystals (R) 948
Griffiths, P. M., with Craik, D. J. : Domain configurations on ferrites 1

Haas, F., with Burke, P. G., and Percival, I. C. : Ionic reactions of negative μ-mesons 912
Haas, F. A., and Robertson, H. H. : Low energy elastic scattering of neutrons by deuterons with Yukawa interaction 160
Hall, D. N., and Lamb, J. : Measurement of ultrasonic absorption in liquids by observations of acoustic streaming 354
Hargreaves, J. K. : Radio observations of lunar surface (L) 536
Harrison, J. A. : Self-absorption in electrodeless discharge in hydrogen and helium 841
Hawker, B. E., with Coleman, R. F., O'Connor, L. P., and Perkin, J. L. : Cross sections for (n, p) and (n, α) reactions with 14·5 MEV neutrons 215
Hayes, W., with Baker, J. M., and Jones, D. A. : Paramagnetic resonance of impurities in CaF_2 (R) 942
Haywood, C. A. : Electron capture cross sections for protons in helium . . . 201
Heastie, R. : Properties of solid and liquid solutions of argon and krypton . . 490
Heine, V., with Cohen, M. H., and Goodings, D. A. : Contribution of core polarization to atomic hyperfine structure and Knight shift of Li and Na . . . 811
Hiley, B. J., with Elton, L. R. B., and Price, R. : Distribution of protons in nuclide ^{12}C (R) 112
Hilsum, C. : Effects of copper as impurity in indium arsenide (L) 685
Hinds, S., and Middleton, R. : Energy levels of ^{26}Al 501
Hinds, S., and Middleton, R. : Energy levels of ^{18}F 721
Hinds, S., and Middleton, R. : Energy levels of ^{15}O, ^{23}Mg and ^{27}Si . . . 727

PAGE

Holøien, E. : $(2s)^2$ ^1S state solution of non-relativistic Schrödinger equation for He and H^- . . . corr. 976

Holt, J. R., with Culligan, G., and Frank, S. G. F. : Longitudinal polarization of electrons from decay of unpolarized positive and negative muons . . . 169

Holt, J. R., with Edwards, D. N., and Frank, S. G. F. : Elastic scattering of 98 MEV negative pions by hydrogen . . . 856

Hooton, D. J., and Allcock, G. R. : Angular distributions of high energy protons inelastically scattered by light nuclei . . . 881

Houghton, A., with Chester, G. V. : Electron–phonon interaction in metals—I : Harmonic approximation . . . 609

Hovorka, F., with Yeager, E., and Booker, J. : Ultrasonic vibration potentials in non-ionic liquids (L) . . . 690

Hum, D. M. : Fermi–Thomas angular-dependent potential for iron . . . 650

Hurd, J. D., Simpson, A. W., and Tredgold, R. H. : Anomalous polarization in ferroelectrics and other oxides . . . 448

Hussain, M., with Astbury, A., Kemp, M. A. R., Lipman, N. H., Muirhead, H., Voss, R. G. P., and Kirk, A. : Measurement of effect of Coulomb field of nucleus on decay rate of negative muons (R) . . . 314

Huxtable, G. B., with Ashmore, A., and Diddens, A. N. : Measurement of spin correlation coefficient C_{KP} in p–p scattering at 382 MEV, for 90° c.m. scattering angle (R) . . . 957

Isaac, E. D., with Bates, L. F. : Bitter figure examination of some polycrystalline Ni–Co alloys . . . 14

Jacques, J. K., and Barrow, R. F. : Transition $v^1\Sigma^+ - x^1\Sigma^+$ in HCl (L) . . . 538

Jaffe, A. A., with Barros, F. de S., Forsyth, P. D., and Taylor, I. J. : Reactions $^{27}Al(p, p')^{27}Al$ and $^{27}Al(\alpha, p)^{30}Si$ . . . 793

Jaffe, A. A., with Barros, F. de S., Forsyth, P. D., and Taylor, I. J. : $^{24}Mg(^3He, \alpha)^{23}Mg$ reaction (R) . . . 513

Jarman, P. : Measurements of sonoluminescence from pure liquids and aqueous solutions . . . 628

Jenkins, F. A., with Giacomo, P., and Baumeister, P. W. : Limiting band width of interference filters . . . 480

Jenns, C. C., with Goldsmid, H. J., and Wright, D. A. : Thermoelectric power of semiconducting diamond . . . 393

Johns, J. W. C., with Barrow, R. F., Butler, D., and Powell, J. L. : Spectra of diatomic fluorides of silicon, germanium, tin and lead (R) . . . 317

Johnson, A. C. J.: Thermal relaxation in gases : New method of analysing experimental data . . . 273

Johnson, F. A. : Lattice absorption bands in Si . . . 265

Jones, D. A., with Baker, J. M., and Hayes, W. : Paramagnetic resonance of impurities in CaF_2 (R) . . . 942

Kail, J. A. E., with Powles, J. G. : Nuclear magnetic resonance absorption in *iso*-butyl bromide as crystal and as supercooled liquid . . . 833

Kelsall, D.: Optical frequency response characteristics in presence of spherical aberration measured by an automatically recording interferometric instrument 465

Kemp, M. A. R., with Astbury, A., Hussain, M., Lipman, N. H., Muirhead, H., Voss, R. G. P., and Kirk, A. : Measurement of effect of Coulomb field of nucleus on decay rate of negative muons (R) . . . 314

Kingston, A. E., with Dalgarno, A. : Van der Waals forces . . . 455

Kirk, A., with Astbury, A., Hussain, M., Kemp, M. A. R., Lipman, N. H., Muirhead, H., and Voss, R. G. P. : Measurement of effect of Coulomb field of nucleus on decay rate of negative muons (R) . . . 314

de Klerk, J. : Ultrasonic wave propagation in Ni single crystal . . . 337

Koenig, S. H. : Inter-electron collisions and ' temperature ' of hot electrons (R) . 959

Koutecký, J. : Comment on T. B. Grimley's paper " The molecular orbital theory of the interaction between an atom and a crystal surface " (L) . . . 323

PAGE

Kuehner, J. A., Merrison, A. W., and Tornabene, S. : Capture of negative pions in hydrogen and deuterium—I : Hydrogen 545
Kuehner, J. A., Merrison, A. W., and Tornabene, S. : Capture of negative pions in hydrogen and deuterium—II : Deuterium 551

Lamb, J., with Davies, R. O. : Derivation of reaction parameters from observations of ultrasonic relaxation 767
Lamb, J., with Hall, D. N. : Measurement of ultrasonic absorption in liquids by observations of acoustic streaming 354
Lee, E. W., Troughton, A. G. H., and Callaby, D. R. : Eddy current losses in 65/35 Ni–Fe (R) 133
Lewis, B. : Energy loss processes in ferroelectric ceramics 17
Lewis, G. M., and Azuma, R. E. : Measurement of π^+ meson photoproduction from hydrogen near threshold 873
Lipman, N. H., with Astbury, A., Hussain, M., Kemp, M. A. R., Muirhead, H., Voss, R. G. P., and Kirk, A.: Measurement of effect of Coulomb field of nucleus on decay rate of negative muons (R) 314
Lloyd, J. L., and Wolfendale, A. W. : Knock-on electrons from cosmic-ray μ-mesons 178
Lock, W. O., with Batty, C. J., and March, P. V. : Small angle scattering of 970 MEV protons by carbon 100
Lokan, K. H. : High-energy photoprotons from silver. 697
Lynn, N. : Variational calculations of the 1s–2s electron excitation cross section of hydrogen (R) 515

McCauley, G. P. : Inelastic scattering of high energy nucleons by complex nuclei—II: Excitation of 4·4 MEV level of ^{12}C (R) 309
Macfarlane, G. G., with Elliott, R. J., and McLean, T. P. : Theory of effect of magnetic field on absorption edge in semiconductors . . . . . corr. 976
Mackinnon, L., and Myers, A.: Ultrasonic attenuation in superconducting and normal mercury 291
McLean, T. P., with Elliott, R. J., and Macfarlane, G. G. : Theory of effect of magnetic field on absorption edge in semiconductors . . . . . corr. 976
March, P. V., with Batty, C. J., and Lock, W. O. : Small angle scattering of 970 MEV protons by carbon 100
Martin, D. H., with Bloor, D. : Ferromagnetic domain sizes in polycrystalline silicon–iron (L) 694
Mason, P., Flack, F. C., and Parry, G. : Spin of ^{103}Ru by deuteron stripping (R) . 138
Mataré, H., with Weinreich, O. A., and Reed, B. : Grain-boundary amplifier (R) . 969
Mendelssohn, K., and Steele, W. A. : Quantized growth of turbulence of He II (L). 144
Merrison, A. W., with Kuehner, J. A., and Tornabene, S. : Capture of negative pions in hydrogen and deuterium—I : Hydrogen. 545
Merrison, A. W., with Kuehner, J. A., and Tornabene, S. : Capture of negative pions in hydrogen and deuterium—II : Deuterium 551
Middleton, R., with Hinds, S. : Energy levels of ^{26}Al 501
Middleton, R., with Hinds, S. : Energy levels of ^{18}F 721
Middleton, R., with Hinds, S. : Energy levels of ^{15}O, ^{23}Mg and ^{27}Si . . . 727
Moffatt, J., and Weeks, G. C. : Pair production in field of electron (R) . . . 114
Mohr, C. B. O. : Direct interaction with strong coupling in nuclear collisions . . 894
Morris, D. P., Preston, R. R., and Williams, I. : Search for new Heusler alloys (R) . 520
Morris, D. P., and Williams, I. : Magnetic susceptibility of Ag–Mn solid solutions between 100° and 500°K 422
Morris, E., with Fürth, R. : Charge penetration into conductor in equilibrium. . 869
Moss, T. S., with Walton, A. K. : Influence of fast holes on photoelectromagnetic effect in Ge (L) 692
Moss, T. S., with Walton, A. K. : Theory of electrical and photoelectric effects for three carriers in magnetic field 399
Muirhead, H., with Astbury, A., Hussain, M., Kemp, M. A. R., Lipman, N. H., Voss, R. G. P., and Kirk, A. : Measurement of effect of Coulomb field of nucleus on decay rate of negative muons (R) 314

PAGE

Murray, A. M., with Strachan, C. : Spin–orbit coupling and extraordinary Hall effect 433, corr. 976
Myers, A., with Mackinnon, L. : Ultrasonic attenuation in superconducting and normal mercury 291

Niblett, D. H., and Wilks, J. : Internal friction of annealed copper at low temperatures 95
Nicholson, A. F., and Brown, G. E. : Photodisintegration of deuteron at 130 Mev 221
Nixon, J. D., and Banbury, P. C. : Time dependent changes in excess carrier concentrations in presence of surface recombination 54

O'Connor, L. P., with Coleman, R. F., Hawker, B. E., and Perkin, J. L. : Cross sections for (n, p) and (n, α) reactions with 14·5 Mev neutrons 215
Okazaki, A., with Asanabe, S. : Anomalous behaviour in Hall coefficients of semiconducting compounds SnSe and GeSe 824
O'Keeffe, T. W., Rigby, M., and Wormald, J. R. : Search for process $\mu^+ \to e^+ + \gamma$ (R) 951
Oleson, N. L., with Emeleus, K. G. : Empirical relations for moving striations (R) 526
Orton, J. W., with Griffiths, J. H. E. : Weak lines in paramagnetic resonance spectrum of impure MgO crystals (R) 948

Parry, G., with Dalton, A. W., and Scott, H. D. : ^{39}K(d, p)^{40}K reaction (R) 677
Parry, G., with Mason P., and Flack, F. C. : Spin of ^{103}Ru by deuteron stripping (R) 138
Pascual, P., with Garrido, L. M. : Unitary phase shift scattering approximation (R) 528
Peacock, R. V., with Burfoot, J. C. : Growth of ferroelectric hysteresis loops (L) 973
Percival, I. C., with Burke, P. G., and Haas, F. : Ionic reactions of negative μ-mesons 912
Perkin, J. L., with Coleman, R. F., Hawker, B. E., and O'Connor, L. P. : Cross sections for (n, p) and (n, α) reactions with 14·5 Mev neutrons 215
Pesic, D., and Gaydon, A. G. : Band spectra of magnesium oxide and hydroxide between 4000 and 3600 Å 244
Phillips, K. : Scattering of fast charged particles : Measurement of detour factor for 10 Mev electrons and positrons (R) 953
Phillips, N. J. : Collisional relaxation in gases 800
Powell, J. L., with Barrow, R. F., Butler, D., and Johns, J. W. C. : Spectra of diatomic fluorides of silicon, germanium, tin and lead (R) 317
Powles, J. G., and Kail, J. A. E. : Nuclear magnetic resonance absorption in *iso*-butyl bromide as crystal and as supercooled liquid 833
Preston, R. R., with Morris, D. P., and Williams, I. : Search for new Heusler alloys (R) 520
Price, R., with Elton, L. R. B., and Hiley, B. J. : Distribution of protons in nuclide ^{12}C (R) 112
Putley, E. H. : Oscillatory transverse magnetoresistance effect in n-type InSb (R) 131
Putley, E. H. : Electrical conduction in n-type InSb between 2° and 300°K 280
Putley, E. H. : Electrical conduction in p-type InSb between 100° and 2°K (R) 128

Rajagopal, A. K. : Correction to theory of calcium fluoride lattice (L) 687
Ralph, J. E. : Scintillation characteristics of diamond under α-particle bombardment 233
Ramachandra Rao, B., and Subba Rao, K. : Investigation of ultrasonic velocities in organic solutions 239
Raw, C. J. G., with Crowther, P. : Thermal diffusion in methanol-carbon tetrachloride mixtures (L) 686
Reed, B., with Weinreich, O. A., and Mataré, H. : Grain-boundary amplifier (R) 969
Richardson, H. M., with Cook, A. H. : Comparison of lengths using fringes of superposition in white light 661
Rigby, M., with O'Keeffe, T. W., and Wormald, J. R. : Search for process $\mu^+ \to e^+ + \gamma$ (R) 951
Robertson, H. H., with Haas, F. A. : Low energy elastic scattering of neutrons by deuterons with Yukawa interaction 160
Robertson, J. C., and Ward, A. : Particle selection in crystals of CsI(Tl) (R) 523
Robson, A. E., and Thonemann, P. C. : Arc maintained on isolated metal plate exposed to plasma 508

PAGE

Rogers, G. L. : Simple method of calculating moiré patterns (L) 142
Schermer, R., and Corngold, N. : Resonance capture of neutrons in infinite homogeneous media 561
Schonland, D. S. : Determination of principal *g*-values in electron spin resonance 788
Schröder, K. : Influence of arsenic content in copper crystals on easy glide at −183°c (R) 674
Scott, H. D., with Dalton, A. W., and Parry, G. : ^{39}K(d, p)^{40}K reaction (R) 677
Seymour, E. F. W., with Flynn, C. P. : Nuclear magnetic resonance in Bi (R) 945
Shepherd, R. S. : Polarization of light from cathode glow (R) 126
Simpson, A. W., with Hurd, J. D., and Tredgold, R. H. : Anomalous polarization in ferroelectrics and other oxides 448
Smith, A. C. H., with Fox, J. W., and Smith, E. J. : Variability of recombination of hydrogen atoms on metal surfaces (R) 533
Smith, E. J., with Fox, J. W., and Smith, A. C. H. : Variability of recombination of hydrogen atoms on metal surfaces (R) 533
Srivastava, S. N., with Varshni, Y. P. : Viscosity of normal paraffins 153
Stacey, F. D. : Objection to single-domain inclusion theory of magnetic hysteresis in dispersion-hardened alloys (R) 517
Stacey, F. D. : Thermal activation of ferromagnetic domains (R) 136
Steele, W. A., with Mendelssohn, K. : Quantized growth of turbulence in He II (L) 144
Stevens, K. W. H., with Fidone, I. : *g*-value of S-state ions (R) 116
Strachan, C., and Murray, A. M. : Spin–orbit coupling and the extraordinary Hall effect 433, corr. 976
Sturge, M. D. : Theory of diffusion of copper in germanium 297
Sturge, M. D. : Diffusion of boron in germanium (R) 320
Subba Rao, K., with Ramachandra Rao, B. : Investigation of ultrasonic velocities in organic solutions 239
Suffczynski, M. : Optical properties of noble metals (R) 671
Symmons, H. F., with Bogle, G. S. : Paramagnetic resonance of Fe^{3+} in sapphire at low temperatures (R) 531

Taylor, I. J., with Barros, F. de S., Forsyth, P. D., and Jaffe, A. A. : Reactions ^{27}Al(p, p′)^{27}Al and ^{27}Al(α, p)^{30}Si 793
Taylor, I. J., with Barros, F. de S., Forsyth, P. D., and Jaffe, A. A. : ^{24}Mg(^{3}He, α)^{23}Mg reaction (R) 513
Tebble, R. S., with Fox, M. : Demagnetizing energy and domain structure of uniaxial single crystal corr. 325
Thellung, A., with Chester, G. V. : Electrical conductivity of metals 745
Thompson, B. J. : Three-dimensional intensity distribution near focus of waves diffracted by slit and rectangular apertures 905
Thompson, J. B. : Negative ions in positive column of oxygen discharge (R) 818
Thompson, J. B. : Attachment of slow electrons in air and oxygen (R) 821
Thonemann, P. C., with Robson, A. E. : Arc maintained on isolated metal plate exposed to plasma 508
Thorburn, R. : Ionization and dissociation by electron impact in fluorine, HF, chlorine and HCl (R) 122
Tornabene, S., with Kuehner, J. A., and Merrison, A. W. : Capture of negative pions in hydrogen and deuterium—I : Hydrogen 545
Tornabene, S., with Kuehner, J. A., and Merrison, A. W. : Capture of negative pions in hydrogen and deuterium—II : Deuterium 551
Towle, J. H., with Batchelor, R. : Inelastic scattering of neutrons by thorium 193
Towle, J. H., with Batchelor, R.: Neutron spectra and differential cross sections of reactions ^{19}F(α, n)^{22}Na and ^{27}Al(α, n)^{30}P (R) 307
Toye, T. C. : Effect of copper on work function of liquid tin 807
Tredgold, R. H., with Hurd, J. D., and Simpson, A. W., : Anomalous polarization in ferroelectrics and other oxides 448
Troughton, A. G. H., with Lee, E. W., and Callaby, D. R. : Eddy current losses in 65/35 Ni–Fe (R) 133

PAGE

Turbadar, T. : Complete absorption of light by thin metal films 40
Turchinetz, W., with Carver, J. H. : Competitive processes in photodisintegration of nickel 585
Turchinetz, W., with Carver, J. H. : Nuclear deformation and photodisintegration giant resonances 69
Turchinetz, W., with Carver, J. H. : (γ, n) and $(\gamma, 2n)$ reactions in ^{141}Pr (R) . . 110

Varshni, Y. P. : Wu–Yang potential energy function (R) 119
Varshni, Y. P., and Srivastava, S. N. : Viscosity of normal paraffins . . . 153
Vasek, L. J., and Anderson, J. M. : Work function of sodium chloride . . . 733
Voss, R. G. P., with Astbury, A., Hussain, M., Kemp, M. A. R., Lipman, N. H., Muirhead, H., and Kirk, A. : Measurement of effect of Coulomb field of nucleus on decay rate of negative muons (R) 314

Walton, A. K., and Moss, T. S. : Influence of fast holes on photoelectromagnetic effect in germanium (L) 692
Walton, A. K., and Moss, T. S. : Theory of electrical and photoelectric effects for three carriers in magnetic field 399
Ward, A., with Robertson, J. C. : Particle selection in crystals of CsI(Tl) (R) . . 523
Watkins, T. B. : $1/f$ noise in germanium devices 59
Weeks, G. C., with Moffatt, J. : Pair production in field of electron (R) . . . 114
Weinmann, A. : Phenomenological theory of ultrasonic vibration potentials in liquids and electrolytes 345
Weinreich, O. A., Mataré, H., and Reed, B. : Grain-boundary amplifier (R) . . 969
Weston, D. E. : Guided propagation in slowly varying medium 365
Wilks, J., with Niblett, D. H. : Internal friction of annealed copper at low temperatures 95
Williams, I., with Morris, D. P. : Magnetic susceptibility of Ag–Mn solid solutions between 100° and 500°K 422
Williams, I., with Morris, D. P., and Preston, R. R. : Search for new Heusler alloys (R) 520
Williams, W. : Adiabatic and isothermal effects in bismuth telluride . . . 739
Wolfendale, A. W., with Lloyd, J. L. : Knock-on electrons from cosmic-ray μ-mesons 178
Wormald, J. R., with O'Keeffe, T. W., and Rigby, M.: Search for process $\mu^+ \rightarrow e^+ + \gamma$ (R) 951
Wright, D. A., with Goldsmid, H. J., and Jenns, C. C. : Thermoelectric power of semiconducting diamond 393
Wright, S. B., with Champion, F. C. : Diamond conduction counters with small electrode separations 385
Wynne, C. G. : Lens designing by electronic digital computer : I. 777

Yeager, E., Booker, J., and Hovorka, F. : Ultrasonic vibration potentials in non-ionic liquids (L) 690

Zucker, I. J. : Zero-point energy and equation of state of solid helium at absolute zero (R) 965

INDEX TO REVIEWS OF BOOKS

PAGE

Aigrain, P., and Englert, F. : *Les semiconducteurs* 325

Ballentyne, D. W. G., and Walker, L. E. Q. : *A dictionary of named effects and laws in chemistry, physics, and mathematics*. 333
Batchelor, G. K. : *G. I. Taylor's scientific papers*. Vol. 1 329
Bohr, Niels : *Atomic physics and human knowledge* 328
Bower, John L., and Schultheiss, Peter M. : *Introduction to the design of servomechanisms* 981
Burgess, E. : *Satellites and space flight* 830

de Callatäy, V. : *Atlas of the sky* 983
Chalmers, A. J. : *Atmospheric electricity* 151
Chisholm, J. S. R., and de Borde, A. H. : *An introduction to statistical mechanics.* International series of monographs on physics, Vol. II. 978
Coker, E. G., and Filon, L. N. G. : *A treatise on photoelasticity* (2nd Edn) 149
Collins, S. C., and Cannaday, R. L. : *Expansion machines for low temperature processes* 831

Duckworth, H. E. : *Mass spectroscopy* : 147
Dungey, J. W. : *Cosmic electrodynamics* 978

Easthope, C. E. : *Three dimensional dynamics—a vectorial treatment* 335
Ehrenberg, W. : *Electric conduction in semiconductors and metals* 334
Eisenbud, L., and Wigner, Eugene P. : *Nuclear structure* 696

Flügge, S. : *Handbuch der Physik*. Vol. 6. *Elasticity and plasticity* 330
Flügge, S. : *Handbuch der Physik*. Vol. 16. *Electric fields and waves* 147
Flügge, S. : *Handbuch der Physik*. Vol. 34. *Corpuscles and radiation in matter:* II 148
Forsythe, George E., and Rosenbloom, Paul C. : *Numerical analysis and partial differential equations* 982
Friedlander, F. G. : *Sound pulses* 329

Gibson, A. F., Aigrain, P., and Burgess, R. E. : *Progress in semiconductors*. Vol. 3. 326
Glocker, R. : *Materialprüfung mit Röntgenstrahlen* (unter besonderer Berücksichtigung der Röntgenmetallkunde) (4th Edn) 981

Hartree, D. R. : *Numerical analysis* (2nd Edn) 149
Hartree, D. R. : *The calculation of atomic structures* 331
Harwood, J. J., Hausner, H. H., Morse, J. J., and Rauch, W. G. : *Effects of radiation on materials* (Report of a Colloquium sponsored by the U.S. Office of Naval Research and the Martin Company of America, March 1957) 152

Ingram, D. J. E. : *Free radicals as studied by electron spin resonance* 983

Koch, J., Dawton, R. H. V. M., Smith, M. L., and Walcher, W. : *Electromagnetic isotope separators and applications of electromagnetically enriched isotopes* 828
Krishnan, R. S. : *Progress in crystal physics* 832
Kroner, E. : *Kontinuumstheorie der Versetzungen und Eigenspannungen* 325

Lanczos, Cornelius : *Applied analysis* 541
Leech, J. W. : *Classical mechanics* 542
Lighthill, M. J. : *An introduction to Fourier analysis and generalised functions* 150

PAGE
Mather, K. B., and Swan, P. : *Nuclear scattering* 696
Miles, J. W. : *The potential theory of unsteady supersonic flow* 980

Newman, F. H., and Searle, V. H. L. : *The general properties of matter* (5th Edn) . 828

O'Connell, D. J. K. : *Stellar populations* 830

Pearson, W. B. : *A handbook of lattice spacings and structures of metals and alloys* . 540
Planck, Max : *Physikalische Abhandlungen und Vorträge.* Vols. I–III 326
Present, R. D. : *Kinetic theory of gases* 977

Raoult, G. : *Les ondes centimétriques* 540

Scheidegger, A. E. : *The physics of flow through porous media* 831
Schön, M., and Welker, H. : *Semiconductors and phosphors* (Proceedings of the International Colloquium 1956 at Garmisch-Partenkirchen) 829
Sears, F. W. : *Mechanics, wave motion and heat* 977
Simon H., and Suhrmann, R. : *Der lichtelektrische Effekt und seine Anwendungen* . 979
Smithies, F. : *Integral equations* 541
Strong, John : *Concepts of classical optics* 543

Temple, G. : *An introduction to fluid dynamics* 980
Tischer, F. J. : *Mikrowellen-Messtechnik* 150

Wilson, J. G., and Wouthuysen, S. A. : *Progress in elementary particles and cosmic ray physics* 332
Wright, W. D. : *The measurement of colour* 333

van der Ziel, A. : *Solid state physical electronics* 544

Printed in England
Taylor & Francis Ltd., Red Lion Court, Fleet Street, E.C.4